GEOLOGICAL SURVEY OF CANADA
COMMISSION GÉOLOGIQUE DU CANADA

PAPER 83-1B
ÉTUDE

This document was produced
by scanning the original publication.

Ce document est le produit d'une
numérisation par balayage
de la publication originale.

CURRENT RESEARCH
PART B

RECHERCHES EN COURS
PARTIE B

GEOLOGICAL INFORMATION
DIVISION
JUIL 18 1983
DIVISION DE L'INFORMATION
GÉOLOGIQUE

Canada

1983

Notice to Librarians and Indexers

The Geological Survey's thrice-yearly *Current Research* series contains many reports comparable in scope and subject matter to those appearing in scientific journals and other serials. All contributions to the Scientific and Technical Report section of *Current Research* include an abstract and bibliographic citation. It is hoped that these will assist you in cataloguing and indexing these reports and that this will result in a still wider dissemination of the results of the Geological Survey's research activities.

Avis aux bibliothécaires et préparateurs d'index

La série Recherches en cours *de la Commission géologique paraît trois fois par année; elle contient plusieurs rapports dont la portée et la nature sont comparable à ceux qui paraissent dans les revues scientifiques et autres périodiques. Tous les articles publiés dans la section des rapports scientifiques et techniques de la publication* Recherches en cours *sont accompagnés d'un résumé et d'une bibliographie, ce qui vous permettra, nous l'espérons, de cataloguer et d'indexer ces rapports, d'où une meilleure diffusion des résultats de recherche de la Commission géologique.*

Technical editing and compilation
Rédaction et compilation techniques
W.C. Morgan
H. Dumych
P.J. Griffin
N.C. Ollerenshaw
M.-F. Dufour

Production editing and layout
Préparation et mise en page
M.J. Kiel
Debby Busby

Typed and checked by
Dactylographie et vérification
Sharon Parnham
Janet Legere
Janet Gilliland
Shirley Kostiew
Murielle Pelletier

GEOLOGICAL SURVEY
PAPER 83-1B

COMMISSION GÉOLOGIQUE
ÉTUDE 83-1B

CURRENT RESEARCH
PART B

RECHERCHES EN COURS
PARTIE B

1983

© Minister of Supply and Services Canada 1983

Available in Canada through

authorized bookstore agents
and other bookstores

or by mail from

Canadian Government Publishing Centre
Supply and Services Canada
Ottawa, Ontario, Canada K1A 0S9

and from

Geological Survey of Canada
601 Booth Street
Ottawa, Ontario, Canada K1A 0E8

A deposit copy of this publication is also available
for reference in public libraries across Canada

Cat. No. M44-83/1BE Canada: $12.00
ISBN 0-660-11391-O Other countries: $14.40

Price subject to change without notice

Geological Survey of Canada – *Commission géologique du Canada*

R.A. PRICE
Director General
Directeur général

J.G. FYLES
Chief Geologist
Géologue en chef

J.C. McGLYNN
Director, Precambrian Geology Division
Directeur/par int. de la Division de la géologie du Précambrien

M.J. KEEN
Director, Atlantic Geoscience Centre,
Dartmouth, Nova Scotia
Directeur du Centre géoscientifique de l'Atlantique, Dartmouth (Nouvelle-Écosse)

A.G. DARNLEY
Director, Resource Geophysics and Geochemistry Division
Directeur de la Division de la géophysique et de la géochimie appliquées

J.A. MAXWELL
Director, Central Laboratories and Technical Services Division
Directeur de la Division des laboratoires centraux et des services techniques

J.S. SCOTT
Director, Terrain Sciences Division
Directeur de la Division de la science des terrains

R.G. BLACKADAR
Director, Geological Information Division
Directeur de la Division de l'information géologique

D.C. FINDLAY
Director, Economic Geology Division
Directeur de la Division de la géologie économique

W.W. NASSICHUK
Director, Institute of Sedimentary and Petroleum Geology,
Calgary, Alberta
Directeur de l'Institut de géologie sédimentaire et pétrolière, Calgary (Alberta)

R.B. CAMPBELL
Director, Cordilleran Geology Division,
Vancouver, British Columbia
Directeur de la Division de la géologie de la Cordillère, Vancouver (Colombie-Britannique)

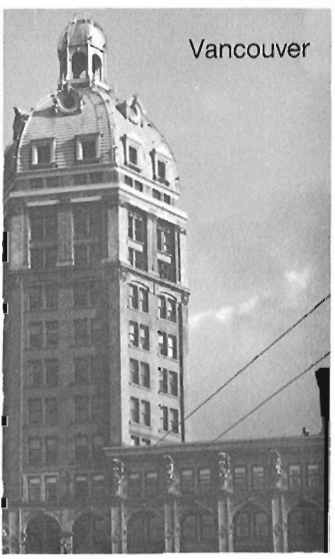

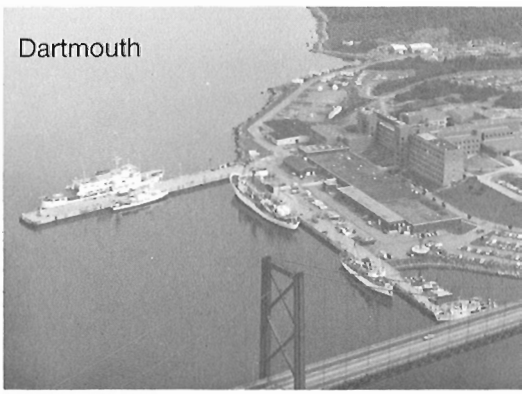

Separates

A limited number of separates of the papers that appear in this volume are available by direct request to the individual authors. The addresses of the Geological Survey of Canada offices follow:

601 Booth Street,
OTTAWA, Ontario
K1A 0E8

Institute of Sedimentary and Petroleum Geology,
3303-33rd Street N.W.,
CALGARY, Alberta
T2L 2A7

Cordilleran Geology Division
100 West Pender Street,
VANCOUVER, B.C.
V6B 1R8

Atlantic Geoscience Centre,
Bedford Institute of Oceanography,
P.O. Box 1006,
DARTMOUTH, N.S.
B2Y 4A2

When no location accompanies an author's name in the title of a paper, the Ottawa address should be used.

Tirés à part

On peut obtenir un nombre limité de "tirés à part" des articles qui paraissent dans cette publication en s'adressant directement à chaque auteur. Les adresses des différents bureaux de la Commission géologique du Canada sont les suivantes:

601, rue Booth
OTTAWA, Ontario
K1A 0E8

Institut de géologie sédimentaire et pétrolière
3303-33rd, St. N.W.,
CALGARY, Alberta
T2L 2A7

Division de la géologie de la Cordillère
100 West Pender Street
VANCOUVER, Colombie-Britannique
V6B 1R8

Centre géoscientifique de l'Atlantique
Institut océanographique de Bedford
B.P. 1006
DARTMOUTH, Nouvelle-Écosse
B2Y 4A2

Lorsque l'adresse de l'auteur ne figure pas sous le titre d'un document, on doit alors utiliser l'adresse d'Ottawa.

SCIENTIFIC AND TECHNICAL REPORTS
RAPPORTS SCIENTIFIQUES ET TECHNIQUES

ECONOMIC GEOLOGY/GÉOLOGIE ÉCONOMIQUE

GEOCHEMISTRY/GÉOCHIMIE

GEOCHRONOLOGY/GÉOCHRONOLOGIE

GEOPHYSICS/GÉOPHYSIQUE

MARINE GEOSCIENCE/ÉTUDES GEOSCIENTIFIQUES DU MILIEU MARIN

MINERALOGY/MINÉRALOGIE

PALEONTOLOGY/PALÉONTOLOGIE

PETROLOGY/PÉTROLOGIE

QUATERNARY GEOLOGY/GÉOLOGIE DU QUATERNAIRE

Inventory Mapping and Stratigraphic Studies/Inventaire cartographique et stratigraphique

Paleoecology and Geochronology/Paléoécologie et géochronologie

Sedimentology and Geomorphology/Sédimentologie et géomorphologie

REGIONAL GEOLOGY/GÉOLOGIE RÉGIONALE

Arctic Islands/Archipel Arctique

Cordilleran Region/Région de la Cordillère

Precambrian Shield/Bouclier précambrien

SCIENTIFIC AND TECHNICAL NOTES
NOTES SCIENTIFIQUES ET TECHNIQUES

DISCUSSIONS AND COMMUNICATIONS
DISCUSSIONS ET COMMUNICATIONS

1.

GEOLOGY OF THE EAST BULL LAKE LAYERED COMPLEX, DISTRICT OF ALGOMA, ONTARIO

EMR Research Agreement 2239-4-175/77

R.S. James[1], P. Born[2], and J. Bigauskas[3]
Precambrian Geology Division

James, R.S., Born, P., and Bigauskas, J., Geology of the East Bull Lake Layered Complex, District of Algoma, Ontario; in Current Research, Part B, Geological Survey of Canada, Paper 83-1B, p. 1-11, 1983.

Abstract

The complex consists of an anorthositic basic rock suite in fault contact with an alkali syenite body. Most of the intrusion recrystallized under lower amphibolite facies metamorphic conditions.

The attitude of isomodal and mineral graded layers and distribution of stratigraphic zones illustrate that the layered basic portion was originally a funnel-shaped basin. These rocks formed as igneous cumulates that crystallized in the order ol+pl, opx, cpx. The stratigraphic section consists of ol-pl cumulates (anorthosites, troctolitic and olivine leuconorites, and olivine norites) overlain by olivine-free rocks with opx and cpx as cumulus minerals (norite, gabbro and leucocratic equivalents).

The syenitic portion consists of very coarse grained alkali syenite underlain abruptly or transitionally by medium grained syenite and intruded by a quartz-bearing facies.

No intrusive relationships between the basic layered rocks and syenite occur. A comagmatic origin from a basaltic parent is doubtful because of their near equal outcrop dimensions.

Résumé

Ce complexe se compose d'une série de roches basiques contenant des anorthosites en contact, par l'entremise d'une faille, avec un massif de syénite alcaline. La majeure partie de l'intrusion a subi une recristallisation dans des conditions de méthamorphisme peu prononcé caractéristique du faciès des amphibolites.

La disposition des couches isomodales et des couches à minéralisation classée et la répartition des zones stratigraphiques indiquent que la partie inférieure litée formait à l'origine un bassin en forme d'entonnoir. Ces roches ont formé des cumulats éruptifs qui se sont cristallisés dans l'ordre suivant: ol+pl, opx, cpx. La coupe stratigraphique présente des cumulats de nature ol-pl (anorthosites, leuconorites à olivines, leuconorites troctolitiques et norites à olivines) recouverts de roches sans olivine accompagnées d'opx et de cpx constituant les minéraux des cumulats (norite, grabbo et équivalents leucocratiques).

La partie de syénite se compose de syénite alcaline à très gros grains qui recouvre, de façon immédiate ou progressive, de la syénite à grains moyens et comprend une intrusion d'un faciès quartzeux.

Il n'existe aucun lien intrusif entre les roches inférieures litées et la venue de syénite. Vu leurs dimensions à l'affleurement à peu près égales, une origine comagmatique en raison de roches basaltiques mères est peu probable.

Introduction

The East Bull Lake Layered Complex is a 36 km^2 elliptical igneous intrusion, located northwest of Sudbury, 30 km north of Massey, Ontario on Highway 535 (NTS 41 J/8). This report considerably supplements the initial geological data published by us (Born and James, 1978). In particular more specific information on the following aspects of the complex are presented: (1) mineralogy of the igneous rock types, (2) a detailed description of the stratigraphy, particularly within the basic, anorthositic portion of the intrusion, and (3) the geology of the syenitic facies. In order to eliminate repetition, readers are referred to our previous publication for more general comments concerning regional geology. This complex is now the site for a major research project by Atomic Energy of Canada Ltd., to assess the suitability of a rock mass of this type for safe, long-term disposal of nuclear fuel wastes.

General Geological Features

The intrusive complex (Fig. 1.1) consists of a syenite body (units CS and MS) in its southern and eastern portions which is separated from the layered, basic rocks (anorthosites, troctolitic and olivine norites, norites and gabbros) in the northern and western part of the complex

[1] Department of Geology, Laurentian University, Sudbury, Ontario, P3E 2C6
[2] Box 531, 165 Frederick Street, Bradford Ontario, L0G 1C0
[3] 3360 Paul Anka Drive, Apt. 809, Ottawa, Ontario, K1V 9S2

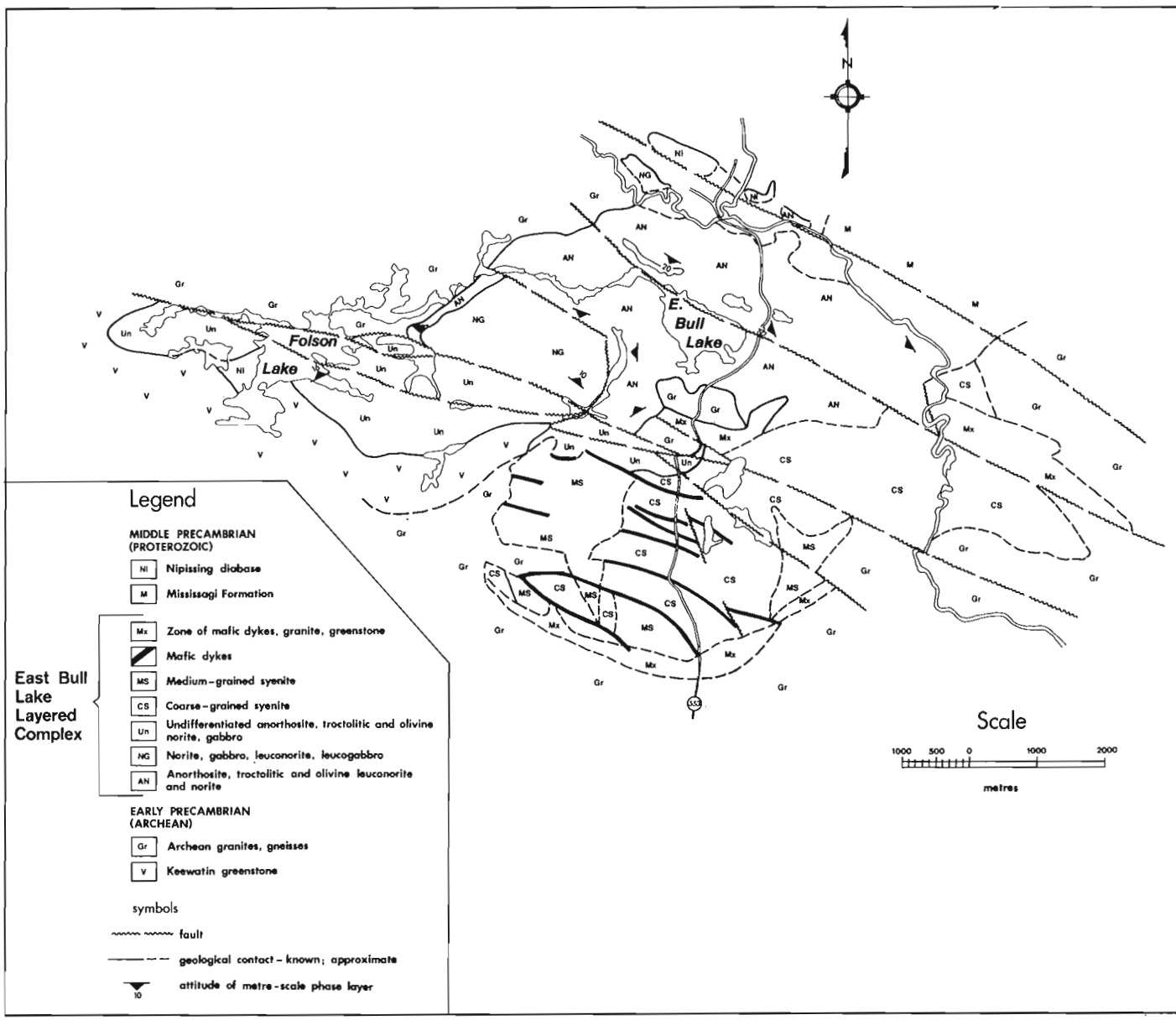

Figure 1.1. *Geology of the East Bull Lake Layered Complex. Field mapping by P. Born and J. Bigauskas.*

(units UN, AN, NG) by a WNW striking fault zone. These two major groups of rocks and the mafic dykes which intrude them make up the East Bull Lake Layered Complex. The basic, leucocratic rock units in the northern and western part of the complex commonly exhibit a recognizable stratigraphy which is in part defined by isomodal and mineral graded layers that range from centimetres to tens of metres in thickness. The distribution of the zones which constitute the stratigraphy of these rocks (see Fig. 1.2) and the strike and gentle dip of the small scale layers at certain horizons in the stratigraphy (Fig. 1.1, 1.2) indicate that the northern portion of the complex has a basin-like morphology. South of the major fault zone in the central and western parts of the complex, the basic rock units dip uniformly to the northwest except at their extreme western margin where the distribution of norite zone rocks suggests the presence of a second basin-like structure (see Fig. 1.2). The similarity in rock types and structure indicates that the layered basic rocks north and south of the major WNW striking fault zone are genetically related. The genetic relationship between these two rock suites and the syenite intrusion on the south side of the major fault is, however, quite unclear. Abrupt faults or unexposed areas characterize the contacts between the two contrasting rock types. The large areal extent of outcrop exposure of the syenite, which is only slightly smaller than that of the layered basic rock suite, at least suggests that the two may not be related by a simple mineral fractionation process from a common basaltic magma source. Mafic dykes are present throughout the entire igneous complex but particularly so in the syenites where they occur as prominent WNW striking units and as a major member of the mixed marginal facies of the syenite intrusion.

Lithological Units of the Layered Complex

In this section, the mineralogy and petrography of the layered basic rock units, the syenites and the mafic dykes are presented in that sequence.

Layered Basic Rock Types

Card and Palonen (1976), Robertson (1976) and Born and James (1978) have referred to these rocks as part of a gabbro-anorthosite suite, and layered bodies such as that at East Bull Lake as gabbro-anorthosite intrusions. Born (1979) pointed out that the term "meta" ought to prefix all such names since the present mineralogy in these rocks is almost entirely metamorphic. Further, he showed from petrographic and petrochemical data that the major igneous minerals which form this rock suite include plagioclase feldspar (An_{80-45}), olivine (Fo_{70-60}), as well as ortho- and clinopyroxene. Combined petrographic data and normative mineralogy from whole-rock chemistry indicate that the order of crystallization was ol+pl, opx, cpx (Born, 1979). Rock types which can form from such a crystallization sequence include anorthosite, troctolite, norite and gabbro. In most samples, however, the original mafic minerals have been replaced by serpentine, talc, or one or more calcic amphiboles. Born (1979) examined a representative suite of specimens chosen from a stratigraphic section through these layered rocks (section A^1-A^{11}, Fig. 1.2). He used colour index, critical replacement textures (described below), composition of relic plagioclase feldspar, and igneous norms for these specimens to estimate their original mineralogy, particularly the type and proportion of mafic minerals in each specimen. As a result of this work, in this paper we present the geology of the layered basic rocks in terms of our best estimate of their original mineralogy. In Table 1.1 the igneous classification scheme we have used is presented; it closely follows the scheme of Hatch et al. (1972) for leucocratic basic igneous rocks. Rocks previously classified as anorthositic gabbros, for example based upon colour index, are identified as troctolitic leuconorites using this scheme, from a knowledge not only of their colour index but also from an estimate of the type and proportions of their mafic minerals. While this scheme is by no means infallible, it is infinitely more informative in terms of conveying to the reader a best estimate of the petrology of the original rock types which form this layered intrusion.

In Figure 1.1, this portion of the layered complex has been divided into three groups. Those rocks south and west of the main fault zone are not known, in terms of their petrography and chemistry, in sufficient detail to subdivide them into more specific groups, and hence are classified as constituting an undifferentiated series of anorthosites, troctolitic and olivine norites and gabbros (unit UN in Fig. 1.1). This group constitutes the Southern Layered Series of Born and James (1978). The Northern Layered Series consists of those basic rocks north of the major WNW striking fault zone. This series can be subdivided into a Lower Layered Series (LLS) which is recognized as ol-pl cumulates (unit AN, Fig. 1.1) and in which both ortho- and

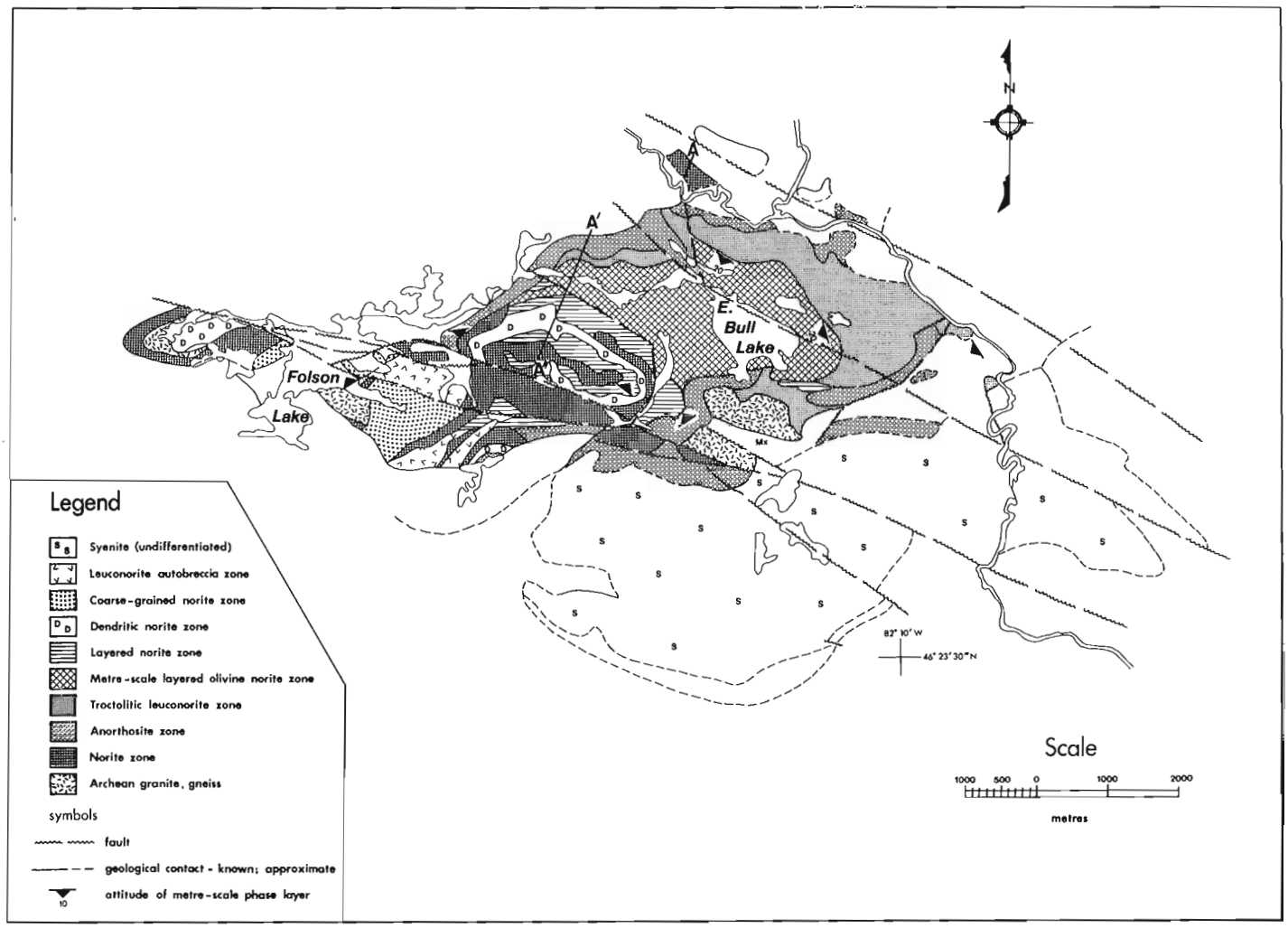

Figure 1.2. *Geology of the basic rocks in the East Bull Lake Complex expressed in terms of eight zones whose distribution is shown in relation to stratigraphy in Figure 1.5.*

Table 1.1

Nomenclature for the basic, anorthositic rock types in the East Bull Lake Layered Complex (after Hatch, Wells & Wells, 1979, p. 341)

Rock type	Modal per cent mafic minerals (C.I.)	Proportion of total mafics		Previously used terminology (Born & James, 1978)
		Olivine	Pyroxene*	
Anorthosite	<10	>50	<50	Anorthosite
Noritic leucotroctolite	10-20	70-50	30-50	Gabbroic anorthosite
Troctolitic leuconorite	20-35	50-30	50-70	Anorthositic gabbro
Olivine norite/ gabbro	35-65	30-10	70-90	Gabbro
Norite/gabbro	35-65	<10	>90	Gabbro
Leuconorite/ leucogabbro	20-35	<10	>90	Anorthositic gabbro

*Terminology assumes opx>cpx except where indicated by gabbro designation of rock types.

clinopyroxene occur as postcumulus phases, and an Upper Layered Series (ULS) in which olivine is absent, orthopyroxene and plagioclase are cumulative phases throughout, and clinopyroxene may form as a cumulus mineral at the highest stratigraphic levels (unit NG, Fig. 1.1).

In Figure 1.1 the rock unit designated as anorthosite, troctolitic leuconorite and olivine norite (AN) represents the ol-pl cumulates which form the LLS. At two localities fresh samples of this rock type have been observed to show cumulus plagioclase and olivine, the latter often showing embayed (resorbed?) margins against orthopyroxene (Fig. 1.3A). Postcumulus clinopyroxene is also common (Fig. 1.3B). Pervasive alteration of these phases is the rule, however; the plagioclase typically is saussuritized and often partially replaced by a near isotropic chlorite (Fig. 1.3D); the olivine most typically is replaced by near colourless randomly oriented laths of tremolite; and the pyroxenes are overgrown by large optically continuous crystals of pale green, pleochroic actinolite normally rimmed by blue-green hornblende (Fig. 1.3C). The pseudomorphic textures of tremolite after olivine, poikilitically enclosed by actinolite after ortho- and clinopyroxene, and the presence of relict cumulus plagioclase have made possible the optical distinction of these ol+pl cumulates of the LLS from those which lack olivine in the ULS. The ULS rocks are identified as norites and gabbros (NG in Fig. 1.1) and plagioclase-rich varieties of these two rock types. Olivine is not observed in either fresh or pseudomorphic form in these rocks and their norms contain quartz rather than olivine unlike analyzed samples from the LLS. Former blocky pyroxene crystals now replaced by actinolite and blue-green hornblende together with saussuritized plagioclase form the main minerals in these rocks.

The pl-px cumulates of the ULS occupy a plateau region in the layered complex. A fault scarp separates them from rocks of the LLS. Born (1979) has shown that the composition of the cores of relict plagioclase varies systematically from near An_{80} at the base of the LLS to An_{45-50} at the top of the ULS. He illustrated that the normative mineralogy of these cumulates becomes progressively depleted in olivine upwards in the sequence and enriched in both ortho- and clinopyroxene. Taken together with the previously reported mineralogical and textural information, these data indicate that the basic rocks north of the WNW trending fault zone form a continuously fractionated suite which appears to be approximately 1 km in true thickness. In a subsequent section, details on the stratigraphy of this part of the complex are presented.

Syenites

The syenite intrusion which forms the southern and eastern portion of the complex consists of a very coarse grained, commonly foliated, alkali syenite and an equally alkaline, massive, medium grained rock of essentially identical mineralogy. Their respective distributions are illustrated in Figure 1.1. Former phenocrysts of an alkali feldspar (sanidine in the Or_{40-50} range is indicated from whole-rock chemistry) now recrystallized almost completely to patch and rod perthite and antiperthite form 70-90 modal per cent of both rock types. In the coarse grained syenite, these feldspars often show a quite marked preferred orientation (foliation) over a distance of 1-2 metres which fades into a much more weakly foliated or even nonfoliated host rock of identical mineralogy. Figure 1.4 illustrates these varieties of coarse grained syenite. Interstitial to the feldspars are irregular to rather equant aggregates of amphibole (both actinolite and blue-green hornblende), epidote, biotite, and small amounts of chlorite, apatite, allanite and zircon. Only the last two phases are considered to be possible relict igneous minerals. Together with quite euhedral crystals of apatite, they (allanite and zircon) are most often found within larger intergrown aggregates of amphibole and epidote. These latter two phases often appear to bear a pseudomorphic relationship to a short stubby relic crystal outline, probably of an alkali rich pyroxene.

Two types of contact relationships have been observed between the coarse- and medium-grained phases of the syenite. At three localities, a sharp contact, near horizontal in attitude, shows the coarse grained syenite overlying the medium grained type. Elsewhere, and much more commonly, abrupt contacts are not observed nor is a sense of stratigraphic relationship obvious. In this case, and on an outcrop scale, a quartz-bearing alkali syenite containing near

10 modal per cent quartz is irregularly intermixed with one of the other two phases of the syenite. These mixed or transitional zones separate homogeneous areas of the other two phases of the syenite.

Mafic Dykes

Saussuritized laths of subhedral plagioclase and blocky to anhedral pyroxene pseudomorphs composed of mixtures of actinolite, blue-green hornblende, and chlorite, constitute the major phases of the dyke rocks. One of the widest dykes is distinguished by abundant saussuritized phenocrysts of plagioclase. Moore and Armstrong (1943) identified this dyke as Matachewan in age. Normally, however, the dykes are not porphyritic. Occasional relict ophitic texture and granophyric intergrowths are present, but they are by no means typical of these rocks. Those dykes which are located at the margins of the syenite body are often narrower, finer grained, and less continuous along strike than those within the central portion of the syenite.

In Figure 1.1 the distribution of these dykes is shown only within the syenite intrusion. They do occur within the layered mafic rocks of the complex and in fact represent a part of the regional NW striking dyke swarm recognized by Moore and Armstrong (1943) as pre-Nipissing diabase in age.

Stratigraphy in the Leucocratic Pl-Ol-Opx-Cpx Cumulates of the Layered Complex

Figure 1.2 is a geological map of the basic rocks of the layered complex expressed in terms of eight recognizable "zones" (Jackson, 1967). Each zone is defined by specific field and petrographic criteria, most often by type of layering or its general absence, and rock types either

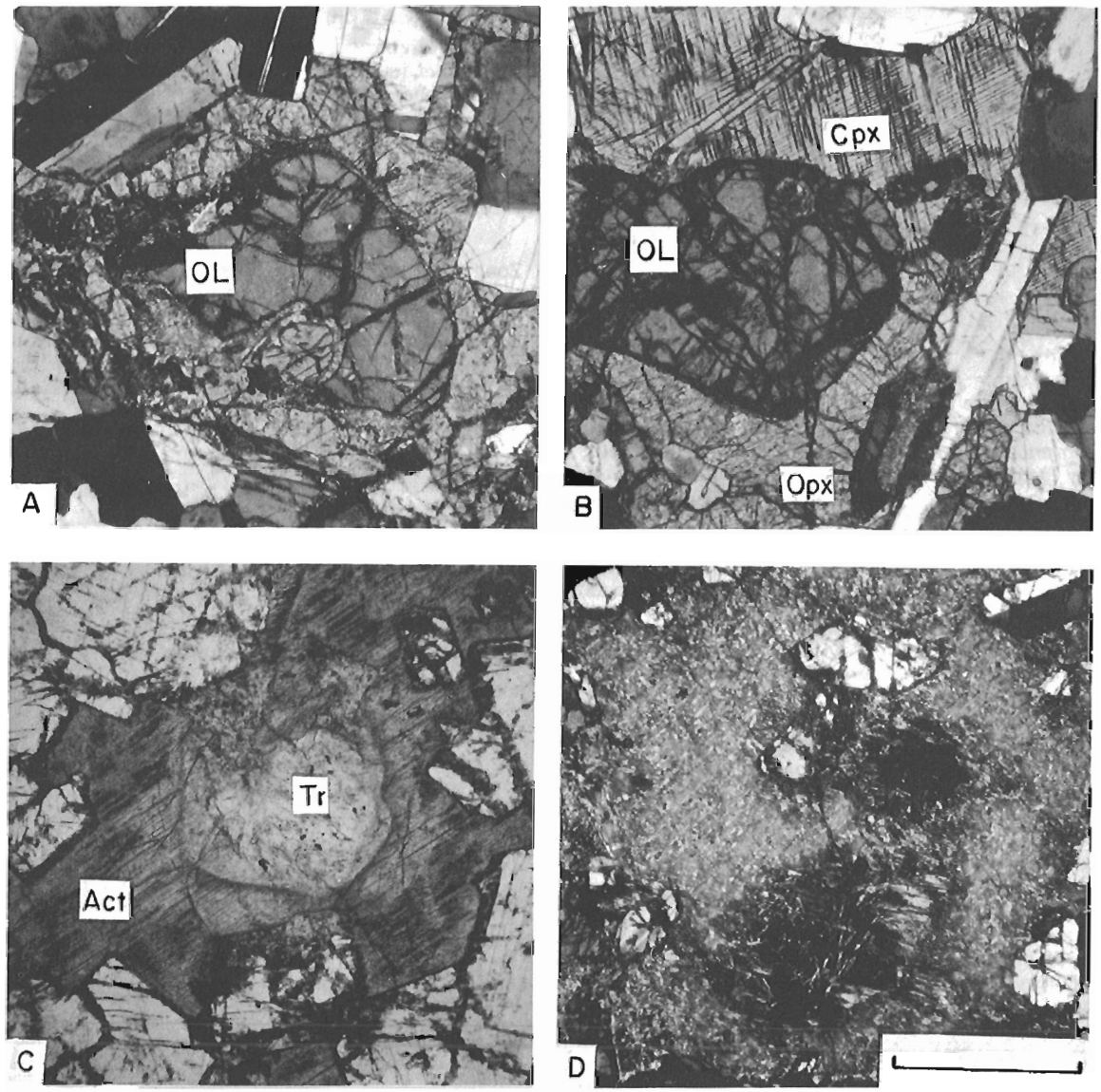

Figure 1.3. *Photomicrographs of fresh and recrystallized olivine-plagioclase cumulates from the East Bull Lake Complex. A: Embayed olivine enclosed by opx in olivine norite. B: Similar textures as in A but here both opx and cpx are present. C: Relict cumulus olivine now replaced by fine grained tremolite (Tr) enclosed by large optically homogeneous crystals of actinolite (Act) which have replaced opx and/or cpx. D: Near isotropic chlorite clusters mark areas of primary cumulus plagioclase feldspar now enclosed by actinolite which replaces one or more pyroxenes. Scale bar for all photos is 1 mm.*

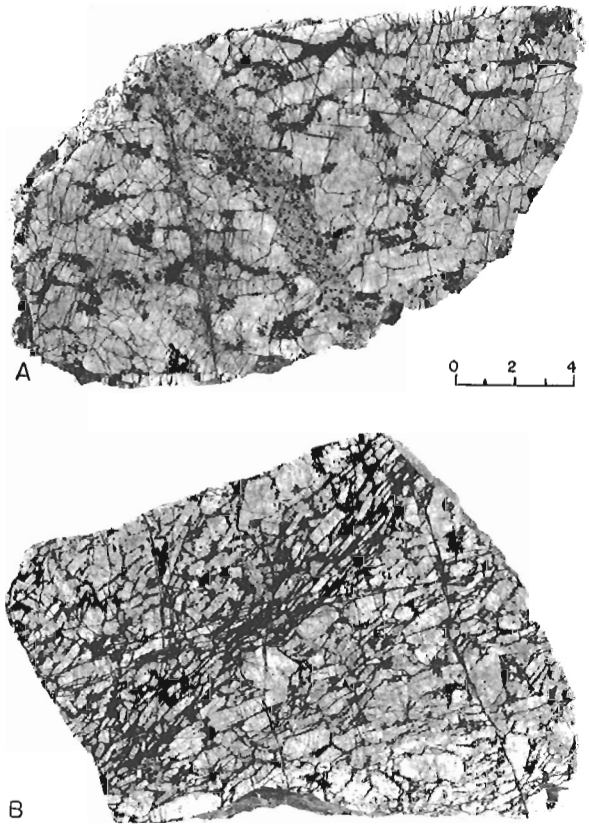

Figure 1.4. *A: Coarse grained alkali syenite from the East Bull Lake Complex. The orientation of the large phenocrysts of pink alkali feldspar define a weak foliation. The sample is cut by a late granophyric dyke. B: This specimen illustrates how, on a very local scale, a very pronounced foliation occurs in the coarse grained syenite. Scale bar in cm.*

individually or in combination. This diagram is a modification of a similar map presented by Born and James (1978). The specific features which characterize each zone are described later in this section.

In Figure 1.5 the stratigraphy of the northern segment of the layered complex for the composite section A-A^{1}-A^{11} located in Figure 1.2 is presented. Nine units are recognized in this section since two zones, the norite and layered norite (zones), are repeated twice and once respectively within this part of the layered series. The rocks of the Lower Layered Series are olivine + plagioclase cumulates and are shown to be divided into zones 2-4 inclusive. The relationship between zone 1 and 2 rocks is unclear. A break in the stratigraphy is certain, however, as the composition of the cumulus feldspar is near 20 mole per cent less calcic in zone 1 norites (An_{55-60}) compared to those in the anorthosites and olivine norites from zone 2. The Upper Layered Series consists of zones 5-9; a 30 metre fault scarp separates these rocks, which are plagioclase + pyroxene cumulates and which occupy a plateau region, from the underlying series.

In plan view the distribution of the zones which form the northern segment of the layered complex (Fig. 1.2) supports our earlier interpretation based upon the attitude of small-scale phase layering, that this portion of the layered complex has a gently dipping basin-like morphology. Major faults have dissected the complex and displacement or discontinuities in the stratigraphy clearly illustrate this fact. Most obvious is the WNW striking fault zone which separates the northern segment suite of rocks from similar basic rocks in the southern segment of the layered complex. This latter series dips for the most part at a shallow angle to the NW and only at its extreme western margin shows structural similarities to the basin-like morphology north of the major fault zone. Within rocks of the northern segment several discontinuities in the "normal" stratigraphy (Fig. 1.5) indicate faults. In Figure 1.2 the anorthosite zone (zone 2) is shown to be the basal unit of the LLS and hence the zone which most often occupies the outer margin of the layered basic rocks in the complex. In the vicinity of the A^{1}-A^{11} section line in Figure 1.2 it is conformably overlain by zones 3 and 4, but immediately to the west across a major WNW striking lineament (fault), it is appreciably thinner and in direct contact with zones 5 and 6. Similarly, immediately east of the ULS plateau rocks and south of East Bull Lake, zone 2 anorthosites are in direct contact with zones 4 and 5 and overlie zone 3. Both of these instances indicate that the stratigraphically lower anorthosites (zone 2) have been thrust upwards into contact with units significantly higher in the stratigraphic section. Finally, the fault drawn along the NE shoreline of East Bull Lake appears to artificially thicken the layered olivine norites of zone 4. It is unclear whether the LLS rocks immediately east and west of this lineament are part of one magmatic cycle or whether the zone 2-4 rocks east of this fault represent a portion of a separate adjacent basin formed by a separate and perhaps older magma pulse.

Specific Features of Individual Zones

Northern Segment of the Layered Complex

Zone 1. Lower norite/gabbro zone: consists of massive medium grained norite/gabbro estimated to form a single homogeneous layer approximately 140 m thick. The composition of relict plagioclase from samples in this unit indicates that it did not form from the same magma pulse from which zones 2-9 crystallized.

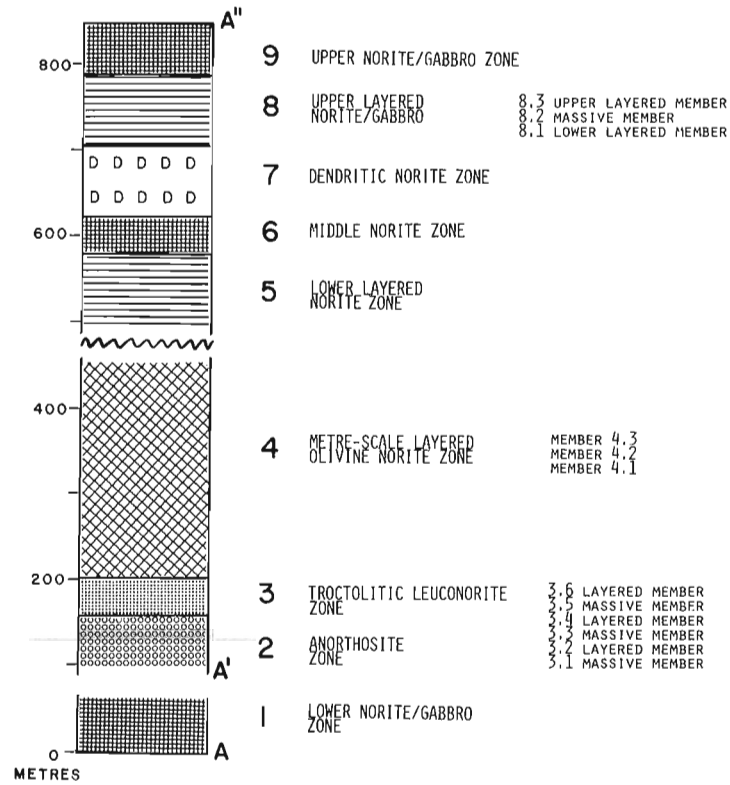

Figure 1.5. *Stratigraphy of the northern segment of the East Bull Lake Layered Complex measured along the section lines A-A^{1}-A^{11} in Figure 1.2.*

Zone 2. Anorthosite zone: decimetre scale (5-17 m thick) isomodal layers of coarse- to very coarse-grained plagioclase-rich rocks such as anorthosite, troctolitic leuconorite and olivine leuconorite are the major rock types in this zone. A few very much thinner (1-4 m) layers of very coarse grained olivine norite are also present. In Figure 1.6, a measured section of this zone is illustrated. Particularly diagnostic features of this zone are the coarse grain size for all rock compositions and the occurrence of anorthosite as a common and relatively abundant rock type. Further, it is the only zone in which elliptical mafic xenoliths, now almost entirely of amphibole, are found. Metre-scale and smaller isomodal layering is not abundant in this zone.

Zone 3. Troctolitic leuconorite zone: this zone is divided into 6 members which are alternately massive and layered as indicated in the typed headings in Figure 1.5 and clearly illustrated in the measured section of this zone presented in Figure 1.6. Decimetre-scale massive layers of medium to coarse grained troctolitic leuconorite form three of the six members of this zone. Groups of mineral-graded layers form the intervening members. These members vary from 2-12 m in thickness and consist of from 4 to 11 graded layers, each of which is 0.1-0.5 m thick. The average (visually estimated) composition of the graded layers appears to be very similar to that of the intervening massive members. In the uppermost mineral graded member (member 3.6) the graded layers rapidly thin from near 10 cm at the base of this member to 4 cm near the contact with zone 4. In Figure 1.7C, small-scale graded and isomodal layers from near the top of zone 3 are illustrated.

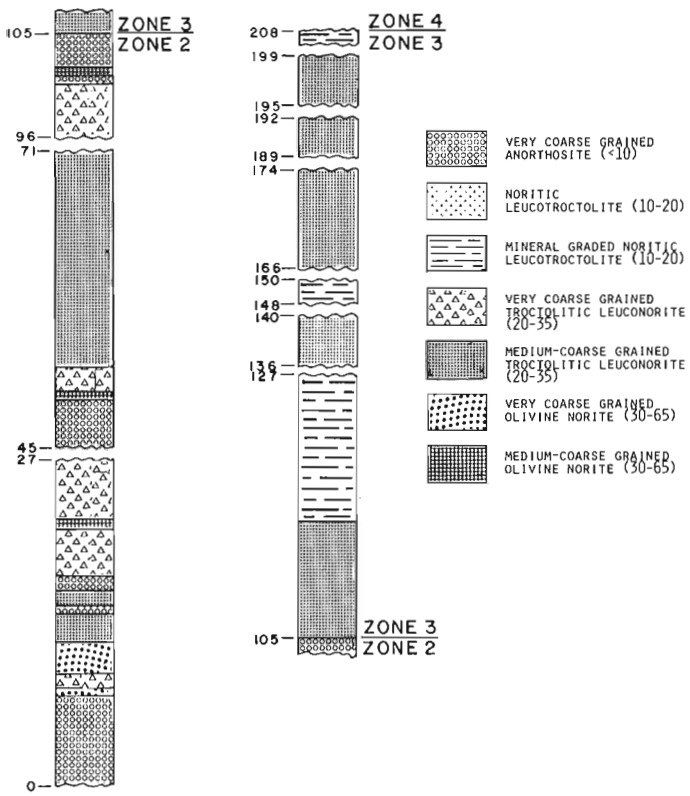

Figure 1.6. *Detailed geology of zone 2 and zone 3. These sections, as well as those presented in Figures 1.8 and 1.9, were measured in the region of the line A^1-A^{11} in Figure 1.2. Height above the base of zone 2 is shown in metres for this diagram.*

Zone 4. Metre-scale layered olivine norite zone: the feature which is distinctive in this zone is the widespread occurrence of metre-scale isomodal layers (0.5-5 m thick; average near 1 m) which generally exhibit sharp regular ratio contacts and which are laterally continuous over minimum distances of 10-30 m. In Figure 1.7A, a typical example of metre-scale isomodal layering from this zone is illustrated; in Figure 1.7B, a relatively uncommon example of a graded layer (in this case reverse grading) from this same zone is shown. Medium- to coarse-grained troctolitic leuconorite, olivine norite and noritic leucotroctolites are the principal rock types which form these layers. In Figure 1.5, this zone is shown to consist of three members and in Figure 1.8, representative sections for each member are illustrated. The middle member (4.2) which is 267 m thick consists of rather equal proportions of troctolitic leuconorite and noritic leucotroctolite whereas the other two members contain all three rock types. Within member 4.2, which is 59 m thick, olivine norite has a clustered distribution as indicated on a small scale in Figure 1.8. Within member 4.3 (76 m thick) it is more evenly distributed and significantly more abundant than in member 4.1. Within this zone there is a clear trend upwards in the section in favour of more melanocratic (pyroxene-rich) rocks of the olivine norite composition.

Zone 5. Lower layered norite zone: a fault scarp marks the boundary between zones 4 and 5. In Figure 1.9 the 61 m section of this zone is shown to consist of alternating isomodal metre-scale layers of norite and leuconorite. These rocks which form the basal zone of the ULS are pl-opx ± cpx cumulates and hence distinctive from the underlying noritic rocks which have modal and normative olivine. The isomodal layering is not as continuous in either vertical or horizontal dimensions compared to that characteristic of zone 4. Further, there exists a clear deficiency of rocks with very low colour indices such as the leucotroctolites and leuconorites in zone 4. This trend towards rocks with a higher proportion of mafic minerals (i.e. pyroxenes) is consistent with the same trend observed in the upper member of zone 4, and continues in all zones of the ULS.

Zone 6. Middle norite zone: is a 50 m thick homogeneous layer of medium- to coarse-grained norite in which no small-scale layering has been observed. Also, unlike zone 7 rocks, it contains none of the harrisitic, crescumulate-like mineral aggregates that typify that zone.

Zone 7. Dendritic norite zone: forms an almost continuous elliptical outcrop pattern in the elevated plateau region of the layered complex. The distinctive feature of this zone is the presence of aggregates of very coarse grained prismatic crystals of amphibole (after olivine and/or pyroxene) and very occasionally plagioclase, forming plumose or dendritic patterns with crystals from 1-6 cm in length. Rosette and frond-like structures are common. These aggregates occur most frequently as ovoid patches 1-20 m in the principal axis dimension, and occasionally as layers 0.2-3 m thick, within massive medium to coarse grained norite. In the Shakespeare-Dunlop Intrusion (James and Harris, 1977) well exposed isomodal layers of these dendritic rock units show the delicate frond-like structures opening upwards from the base of individual layers. Wager et al. (1960) described these harrisitic structures as special types of heteradcumulates in which olivine (or pyroxene) grew upwards into basaltic magma from nuclei that were cumulus crystals lying on top of a crystal mush. Although rapid growth of the mafic

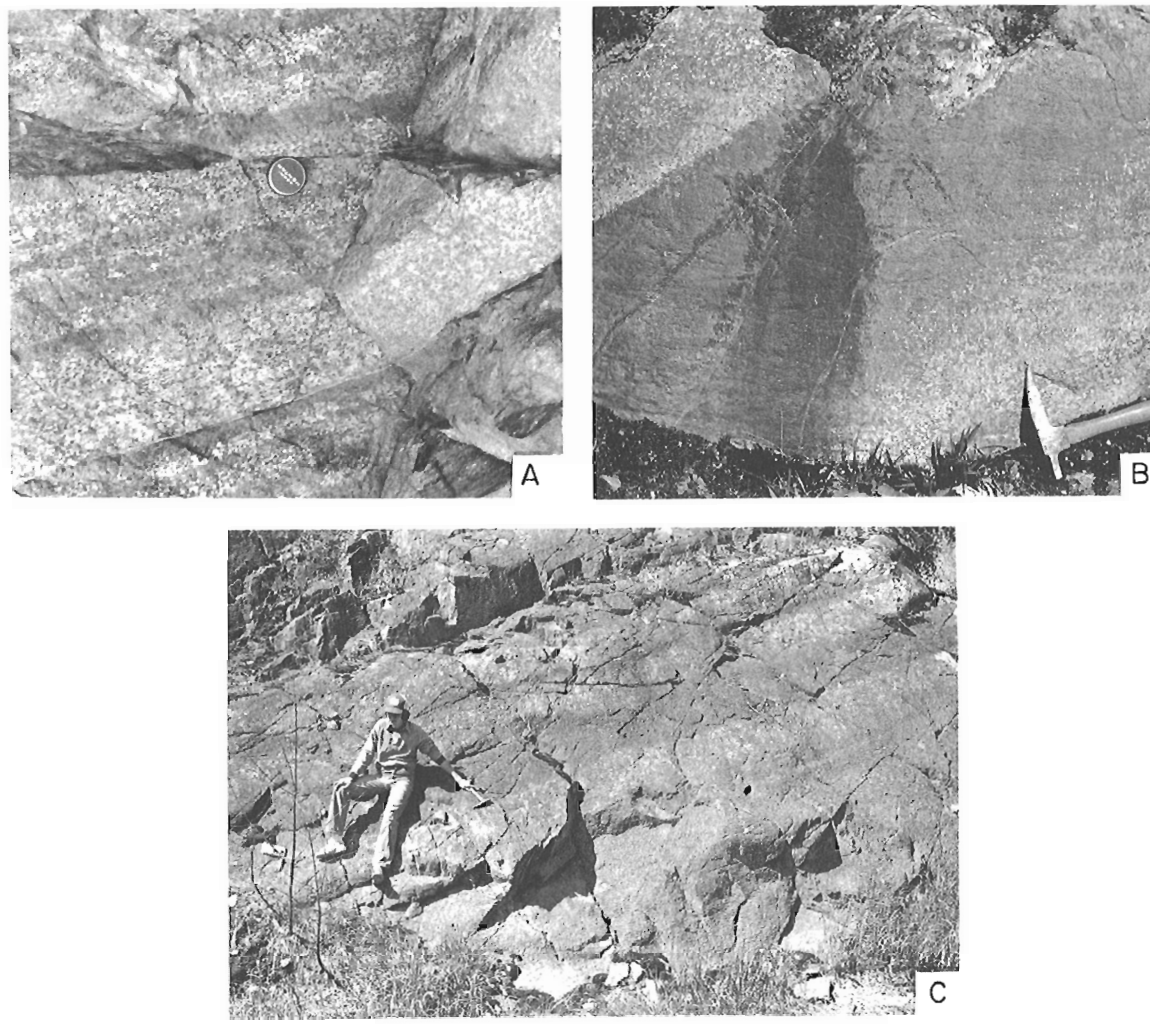

Figure 1.7. *A: Small (centimetre) scale mineral graded layers from the uppermost portion of zone 3. B: A reverse mineral-graded metre-scale layer from zone 4, on Highway 535 adjacent to the lodge on East Bull Lake. C: Typical isomodal metre-scale layers in zone 4 of the northern segment of the layered complex.*

phase is visualized, supersaturation of the melt is not considered to be induced by loss of thermal energy. Rather, as Donaldson (1974) suggests (for peridotitic rock compositions), these structures probably result from either the sudden decrease in the water content of a water-saturated magma or the transition of a water-saturated magma to an unsaturated state by free vapour loss. Rapid crystallization is envisaged, similar to the rates which form spinifex texture in ultramafic lava flows. Similar research by Lofgren (1980) on a much wider range of rock compositions supports Donaldson's explanation of this texture.

Zone 8. Upper layered norite/gabbro zone: this zone has been subdivided into 3 members: in Figure 1.9 the stratigraphy for member 8.1 and 8.3 are illustrated. Like the previous zones of the ULS, norite and leuconorite are the major rock types at this level in the complex. The normative mineralogy of these rocks suggests that modal cpx may equal or exceed opx; hence the dual designation of rock types in naming this zone. The middle member of this zone (8.2) consists of massive norite (15 m thick) and separates the lower and upper members which are illustrated in Figure 1.9 and consist of well formed metre-scale isomodal layers of norite and leuconorite plus groups of thinner mineral graded layers of average leuconorite composition. Like zone 7, this zone forms a near complete elliptical outcrop pattern on the plateau region of the complex.

Zone 9. Upper norite/gabbro zone: forms the uppermost exposed portion of the layered mafic rocks of the igneous complex. It is represented by a 51 m thick section of massive, medium- to coarse-grained norite/gabbro.

Southern Segment of the Layered Complex. The coarse grained norite zone and leuconorite autobreccia zone are observed only within rocks of the southern segment of the layered complex (see Figure 1.2). Our comprehension of the stratigraphy in this part of the complex is not nearly so complete as it is for the northern segment. Born and James (1978) published a tentative stratigraphic column for this part of the complex. Here we draw attention to the leuconorite autobreccia zone which is shown to occur at several localities within the southern segment. This zone consists of irregularly shaped blocks of medium- to coarse-grained norite and leuconorite, 1-10 m in the maximum

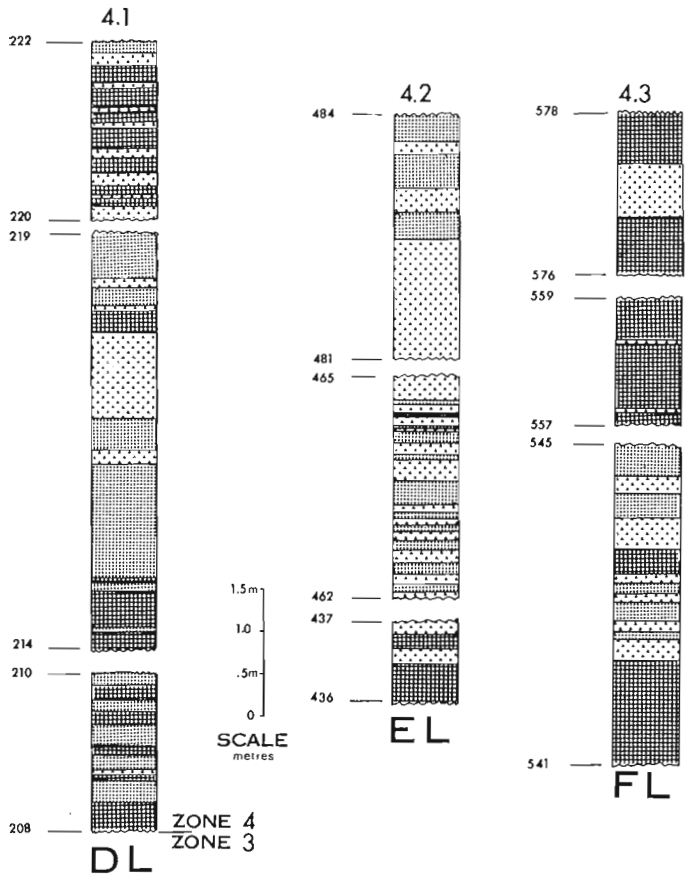

Figure 1.8. *Representative sections of each of the members of zone 4, e.g. members 4.1, 4.2, and 4.3. Height above the base of zone 2 is given in metres as in Figure 1.6.*

dimension, and minor intervening well layered sections of the same rock types. The brecciated portions may represent disrupted layered sequences presumably caused by tectonic instability in the magma chamber. The fact that within these zones, well layered sequences do occur and that zones of this type are recognized at more than one stratigraphic level in the complex suggests that this phenomenon of tectonic instability was a reoccurring one during the evolution of this portion of the intrusion.

Geology of the Syenite Intrusion

A detailed geological map of the syenite intrusion in the layered complex is shown in Figure 1.10. The body covers an area of approximately 20 km^2 and its long axis has an E-W orientation like that of the basic layered rocks to the north. The geology east of the Sable River has been determined by comparing air photo lineation patterns in this region with those for known rock types west of the river.

As in Figure 1.1, coarse- and medium-grained alkali syenite are the two major rock types which form this part of the layered complex and, as stated previously, the medium grained variety occupies the topographically lowest portions of the region to the west of Highway 535 whereas the coarse grained facies tends to dominate the central and eastern parts of the intrusion. The unit designated as the "Transition Zone" in Figure 1.10 contains rock types and structures which mark the contact between these two main varieties of syenite. Within this zone, a medium grained, equigranular, quartz syenite is also present. Aside from the presence of quartz, it is very similar in mineralogy and texture to the medium grained alkali syenite in which it is typically found as irregularly shaped, discontinuous zones with apparent gradational contacts. These features suggest that it is a late differentiate of the magma from which the medium grained syenite crystallized. In a few instances, the contact between the coarse- and medium-grained phases of the syenite intrusion is a sharp, subhorizontal, planar to somewhat irregular, horizon. Normally, however, it is represented by outcrops which consist of irregularly shaped areas of both types of syenite (coarse- and medium-grained) and while contacts are distinct, the precise age relationship between the two phases is unclear due to limited outcrop exposure. Within the coarse grained syenite adjacent to transition zone rocks, numerous features indicate conclusively that the two medium grained varieties of the syenite are intrusive into the older coarse grained type. These features include small to medium veins and stringers of the medium grained syenite within the coarse grained variety, as well as xenocrysts of coarse alkali feldspar and autoliths of the coarse syenite enclosed with sharp form contact by the medium grained facies. At three localities a sharp form contact, tens of metres along strike, between the coarse- and medium-grained phases of the syenite has been observed. At each, the coarse variety overlies the medium grained types and the horizon marking the contact between the two is either horizontal or has a strike near 055° and dip of 5-15 degrees to the southeast. These data are consistent with the observation that the coarse grained syenite occupies much of the central and eastern portion of the intrusion particularly those areas which are topographic highs. The intrusive relationship between the underlying medium grained phases and overlying coarse syenite indicates that the latter phase crystallized first. One way to explain the relationship

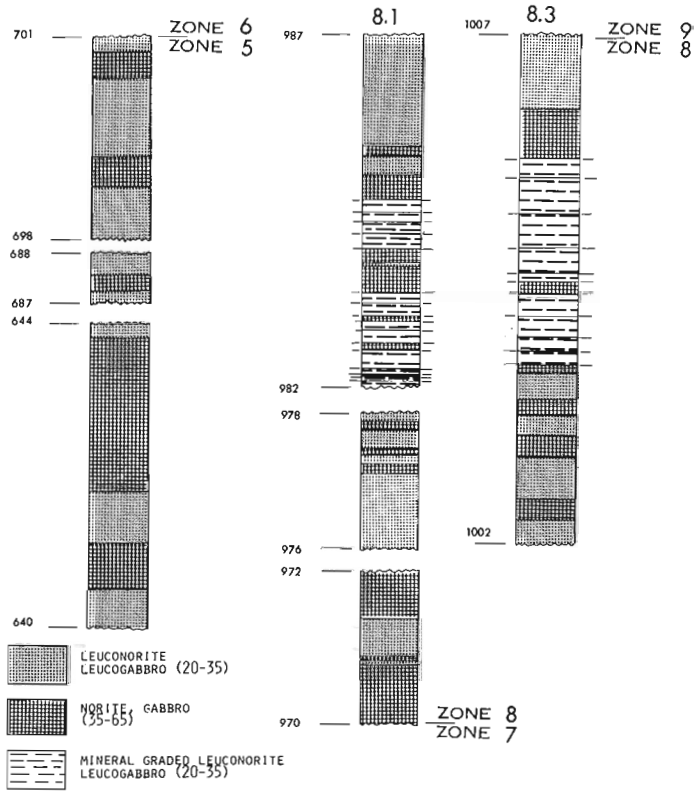

Figure 1.9. *Representative sections of the geology for zone 5 and two of the three members of zone 8 i.e. zone 8.1 and 8.3.*

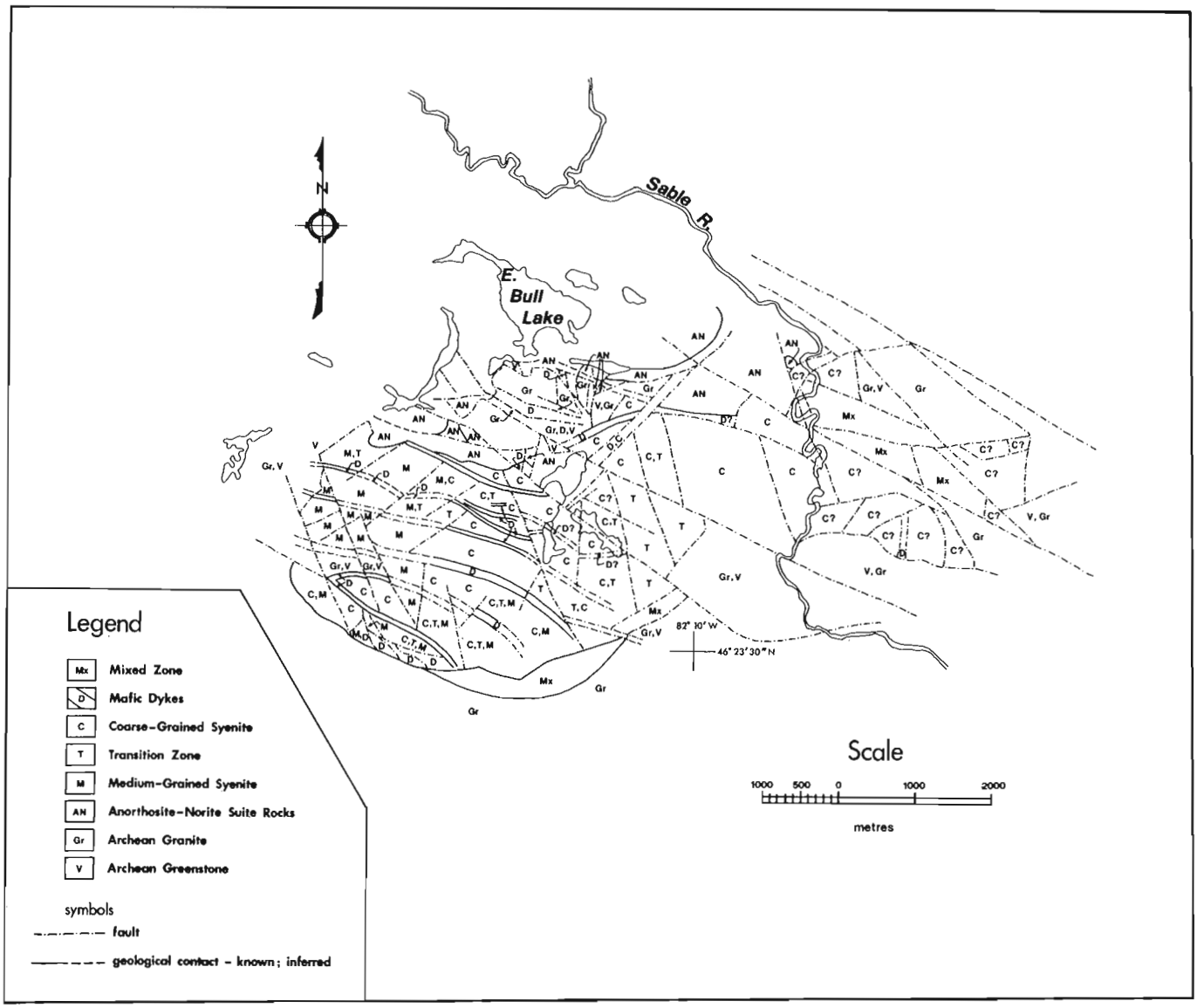

Figure 1.10. *Detailed geology of the syenite intrusion, East Bull Lake Complex. Field relations by J. Bigauskas.*

between the two varieties of syenite is to suggest that the coarse grained type represents part of a roof zone of the intrusion which expanded downward as crystallization proceeded to intersect the rising pile of medium grained syenitic cumulates along the interface described as the transition zone. The preferred orientation of the phenocrysts of alkali feldspar in the coarse grained syenite often defines a weak to very strong foliation which varies from one to the other over a distance of a metre or less. It is not clear to us how this igneous-looking (flow?) fabric can be reconciled with the idea suggested above to explain the origin and distribution of this rock type.

Post-Syenite Dykes

In addition to the syenite dykes and veins which cut the coarse grained syenite of the intrusion, a major set of mafic dykes as well as much less abundant aplite, pegmatite and quartz veins crosscut this pluton.

The petrography of the mafic dykes is summarized in a previous section of this paper. Their detailed distribution within the interior of the syenite body is illustrated in Figure 1.10. These dykes appear to represent part of the WNW striking mafic dyke swarm mapped on a regional scale by Moore and Armstrong (1943) and more recently by GSC geologists for the AECL nuclear fuel waste research program. The latter group reports that the interior dykes can be traced across the syenite – Archean granite/greenstone contact (McCrank et al., 1983). All available information indicates that the dykes postdate the formation of the layered mafic rocks and syenites of the East Bull Lake Complex and predate Nipissing Diabase and metasediments of the Mississagi Formation of the Huronian Supergroup. At the northern and southern margins of the syenite body very closely spaced groups of these dykes contain numerous xenoliths of adjacent syenite, basic anorthositic rocks, as well as granitic and metavolcanic country rock. In Figure 1.10 these areas are shown as "mixed zones" along the

southern margin of the body where scale has not allowed for distinction of individual rock types. In the central portion of the northern margin of the syenite, a complex mixture of mafic and syenitic rocks of the layered complex plus Archean country rock is shown to be intruded by numerous, younger mafic dykes. The field relationships and the absence of a recognizable contact aureole between the syenite and enclosing country rock suggest that this pluton was emplaced tectonically into its present position with accompanying injections of mafic dyke material along its contact.

Numerous veins of granitic aplite and pegmatite, and quartz which postdate the emplacement of the pluton occur throughout the region. Within the East Bull Lake syenite examples of aplite veins cutting mafic (diabase) veins were observed. Distinction between the differentiated quartz-bearing syenite veins which are related in origin to the medium grained alkali syenite of the main intrusion and the regional aplite veins of similar mineralogy is difficult. The association of the former with transition zone rocks and structures is most useful in distinguishing between the two types. Likewise early (related to the magmatic event from which syenites formed) and later (regional) pegmatite and quartz veins are difficult to distinguish. In the case of the quartz veins, it is noted that they are most abundant within the coarse grained facies of the syenite intrusion, suggesting that some at least owe their origin to that magmatic event.

Summary

1. The East Bull Lake igneous complex consists of a layered basic rock suite which is in abrupt fault contact along its southern margin with a (layered?) syenite intrusion of approximately similar size. Neither of these units intrude the other nor do they contain inclusions of the other. Their close proximity and the similarity of their geological relationships to rock units which predate and postdate both of them suggest that they may have a comagmatic origin. Projects now in progress on their petrology and major and trace element geochemistry are designed to test this hypothesis.

2. The layered mafic rock suite shows a systematic variation from anorthosite, troctolitic norite, olivine norite and leuconorite (ol-pl cumulates) in the lower part of the sequence to norites and gabbros (pl-opx-cpx cumulates) in the upper part of the layered section. Most samples are now represented by a metamorphic assemblage in which olivine is replaced by serpentine, talc or tremolite, the cpx and opx phases by actinolite and blue-green hornblende, and plagioclase by saussurite and chlorite. Isomodal and mineral graded, metre-scale phase layering is common throughout the stratigraphy of these rocks. The attitude of this layering and the distribution of the nine zones into which the rocks of the main part of the complex can be subdivided, indicate that the layered mafic rocks initially formed a gently dipping basin-like structure.

3. Coarse- and medium-grained alkali syenite are the two main rock types which form the syenite intrusion. Sanidine and an alkali- and iron-rich clinopyroxene were probably the major primary phases in these syenites which are now represented by a metamorphic assemblage of the type microcline perthite (antiperthite)-actinolite-epidote-biotite. The attitude of the contact or transition zone between the two phases of the syenite is near horizontal. The medium grained variety underlies and locally intrudes the coarse grained syenite which we suggest may have grown from the roof of the intrusion.

4. WNW striking mafic dykes intrude both the mafic and syenitic phases of the complex. They appear to be part of a regional dyke swarm of similar composition reported by Moore and Armstrong (1943). The vast majority of these dykes appear to have an age between post-Archean and pre-Mississagi Formation, although a few are reported to cut sills of Nipissing diabase.

Acknowledgments

We wish to thank the Vantour Family of East Bull Lake for their warm hospitality. S. Cunningham kindly typed this manuscript. Review of the paper by GSC staff has measurably improved its quality, for which we express our thanks.

References

Born, P.
1979: Geology of the East Bull Lake Layered Complex, District of Algoma, Ontario; unpublished M.Sc. thesis, Laurentian University, Sudbury, 147 p.

Born, P. and James, R.S.
1978: Geology of the East Bull Lake layered gabbro anorthosite intrusion, District of Algoma, Ontario; in Current Research, Part A, Geological Survey of Canada, Paper 78-1A, p. 91-95.

Card, K.D. and Palonen, P.A.
1976: Geology of the Dunlop-Shakespeare area, District of Sudbury; Ontario Division of Mines, GR 139, 52 p., Map 2313.

Donaldson, C.H.
1974: Olivine crystal types in harrisitic rocks of the Rhum pluton and in Archean spinifex rock; Geological Society of America, Bulletin, v. 85, p. 1721-1726.

Hatch, F.H., Wells, A.K., and Wells, M.K.
1972: Petrology of the Igneous Rocks; 13th edition, George Allen and Unwin Ltd., London, 551 p.

Jackson, E.D.
1967: Ultramafic cumulates in the Stillwater, Great Dyke, and Bushveld intrusions; in Ultramafic and Related Rocks, ed. P.J. Wyllie; John Wiley, New York, p. 20-38.

James, R.S. and Harris, B.J.
1977: Geology of Shakespeare-Dunlop layered gabbro-anorthosite-intrusion, Ontario; in Report of Activities, Part A, Geological Survey of Canada, Paper 77-1A, p. 411-414.

Lofgren, G.
1980: Experimental studies on the dynamic crystallization of silicate melts, in Physics of Magmatic Processes, ed. R.B. Hargraves; Princeton University Press, Chapter 11, p. 487-551.

McCrank, G.F.D., Stone, D., Kamineni, D.C., Zayachkivsky, B., and Vincent, C.
1983: Regional geology of the East Bull Lake area, Ontario; in Current Research, Part A, Geological Survey of Canada, Paper 83-1A, p. 457-464.

Moore, E.S. and Armstrong, H.S.
1943: Geology of the East Bull Lake area; Ontario Department of Mines, v. 52, pt. 6, p. 1-19, Map 52d.

Robertson, J.A.
1976: Geology of the Massey Area, District of Algoma, Manitoulin and Sudbury, Ontario; Ontario Division of Mines, GR136, 130 p., Maps 2308-2309.

Wager, L.R., Brown, G.M., and Wadsworth, W.J.
1960: Types of igneous cumulates; Journal of Petrology, v. 1, p. 73-85.

2.

ANALYSIS OF STRUCTURE AS A FACTOR CONTROLLING GOLD MINERALIZATION IN NOVA SCOTIA[1]

Project 820013

J.R. Henderson,
Precambrian Geology Division

Henderson, J.R., Analysis of structure as a factor controlling gold mineralization in Nova Scotia; in Current Research, Part B, Geological Survey of Canada, Paper 83-1B, p. 13-21, 1983.

Also in Mines and Minerals Branch, Report of Activities, 1982, Nova Scotia Department of Mines and Energy, Report 83-1, 1983.

Abstract

Quartz veins in the Goldenville Formation comprise three principal varieties: bedding-parallel (¯P), en echelon (EE), and AC veins. The BP and EE veins are contemporaneous and lie in slate beds. They formed early in the strain history of folding at the time of formation of continuous and spaced cleavage during greenschist metamorphism. The AC veins formed in metawacke beds perpendicular to the fold axes late in the folding history.

The BP and EE veins are ubiquitous, but are auriferous only in gold districts in the region The BP veins are not restricted to fold hinge regions and cannot be considered as saddle reefs. Vein fabrics and theoretical considerations support the view that all of the veins are due to hydraulic fracturing and that the fluids producing the fractures were derived locally.

Résumé

Les filons de quartz de la formation de Goldenville se classent en trois catégories principales: filons BP parallèles à la stratification, filons EE en échelon et filons AC. Les filons BP et EE sont contemporains et gisent au sein de couches de schiste Ils ont pris forme au début de la phase de déformation du plissement, lors de la formation d'un clivage continu et espacé au cours de la phase de métamorphisme à l'origine des schistes verts. Les filons AC se sont formés dans des couches de métagrauwacke perpendiculaires aux axes des plis, tard dans l'histoire du plissement.

Les filons BP et EE sont ubiquistes, mais ne contiennent de l'or que dans les zones aurifères de la région. Les filons BP ne sont pas limités aux charnières des plis et ne peuvent pas être considérés comme étant des voûtes anticlinales. L'étude des structures et des textures des filons ainsi que des considérations théoriques viennent appuyer l'hypothèse selon laquelle tous les filons doivent leur origine au phénomène de fracturation hydraulique et que les fluides ayant produit les fractures provenaient de sources locales.

Introduction

The major objective of this study is to investigate the distribution and origin of gold-bearing quartz veins in part of the Cambro-Ordovician Meguma Group in eastern Nova Scotia. The study area (Ecum Secum, Fig. 2.1) lies between 62°00' and 62°30'W., and extends from the Atlantic coastal islands north to the West River-St. Mary's Fault. The area was chosen for study because of its relatively good bedrock exposure and relatively high concentration of gold mines and prospects. The Meguma Terrane east of the Ecum Secum area is currently under investigation by the Nova Scotia Department of Mines and Energy. The part of the study area around Ecum Secum (Fig. 2.2) was mapped in 1982 (this report); in 1983 we plan to extend the mapping north to the West River-St. Mary's Fault, and integrate our mapping with the mapping being done to the east.

E.R. Faribault (1893, 1895a, b, 1896, 1897a, b) mapped the region around Ecum Secum (Fig. 2.2) at 1:63 360 scale, and published detailed maps and sections of Salmon River Gold District (1897c) at 1:3000 scale and Harrigan Cove Gold District (1906) at 1:4800 scale.

Acknowledgments

I am grateful for mapping assistance from Frank Fueten, Jerry Naski, Steve McCollough, Dale Rafuse, Richard Stern, Claudia Stumpp, John Freeland, and Mariette Henderson. I appreciate discussions on Meguma gold deposits with Marcos Zentilli, Ulrich Kretschmar, Craig Miller, Simon Haynes, Duncan Keppie, Brian O'Brien and Paul Smith. I thank Simon Hanmer for reviewing the manuscript.

Regional Geology

The Cambro-Ordovician Meguma Group comprises a lower sandy flysch (Goldenville Formation) and an upper shaly flysch (Halifax Formation). The auriferous quartz veins occur mainly in the Goldenville Formation. The contact between the formations in the Ecum Secum area is conformable and sharp (the contact is not drawn on the structural map, Fig. 2.2). Neither the top of the Halifax nor the base of the Goldenville Formation is exposed in eastern Nova Scotia.

The major fold axial surface traces in Meguma beds curve through a 90 degree arc from the southwestern coast of Nova Scotia to the region east of Ecum Secum (Fig. 2.1). In the Ecum Secum area (Fig. 2.2) the axial traces can be seen to consist of 2-10 km long segments that commonly are offset along their strike in a nonoverlapping, en echelon fashion (e.g. Southern Anticline and Sober Island Syncline). The offset is partly due to northwest-striking sinistral faults (e.g. Sheet Harbour Fault), but may be a primary feature elsewhere (e.g. south of Harrigan Cove and Ecum Secum mines). Note, however, that a 5 km long segment of the Gegogan Harbour Anticline's axial trace south of the Miller Lake mines shows dextral offset east of Liscomb River and

[1] Contribution to Canada-Nova Scotia Co-operative Mineral Program 1981-84. Project carried by Geological Survey of Canada.

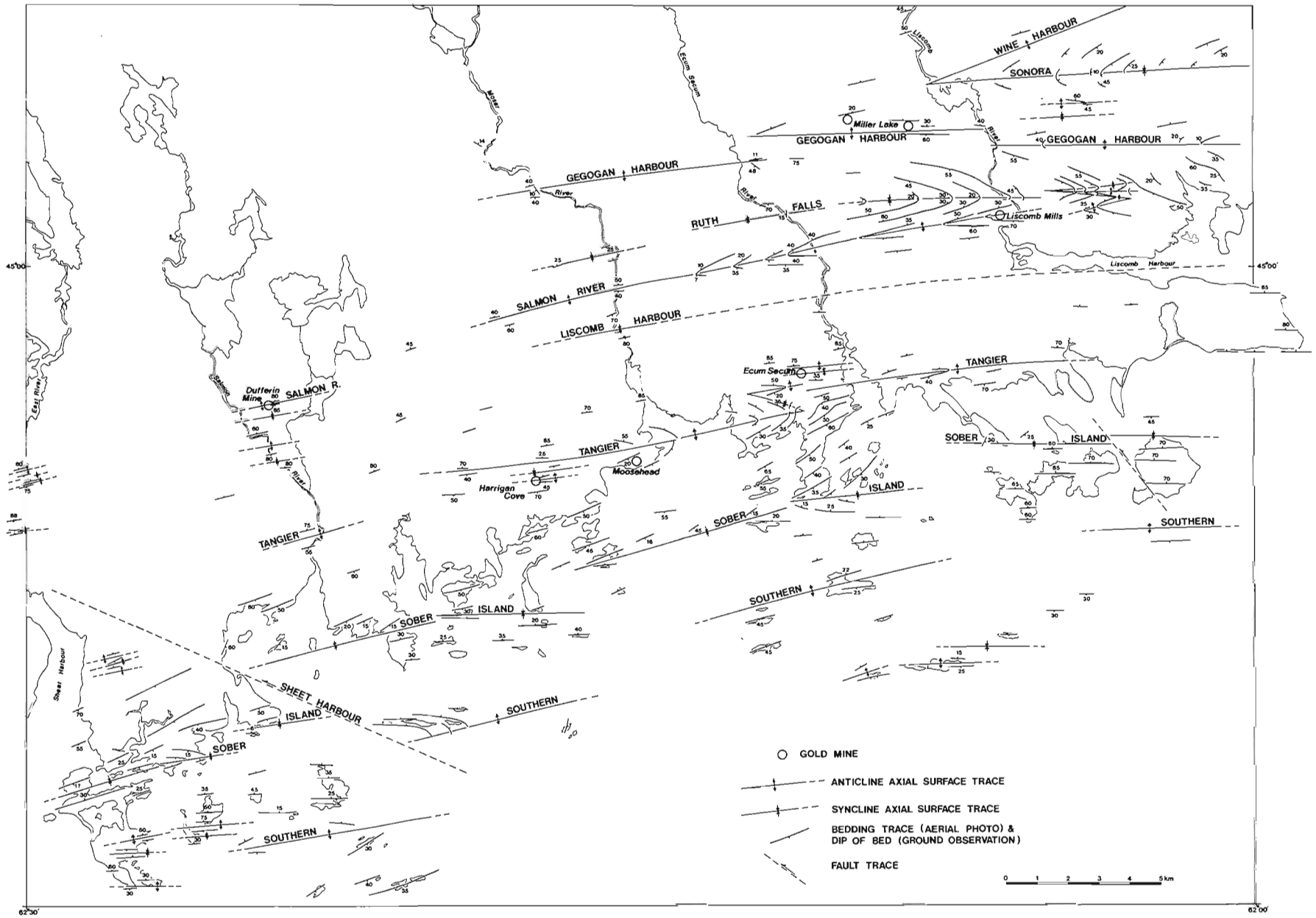

Figure 2.2. *Structural map of the Ecum Secum area.*

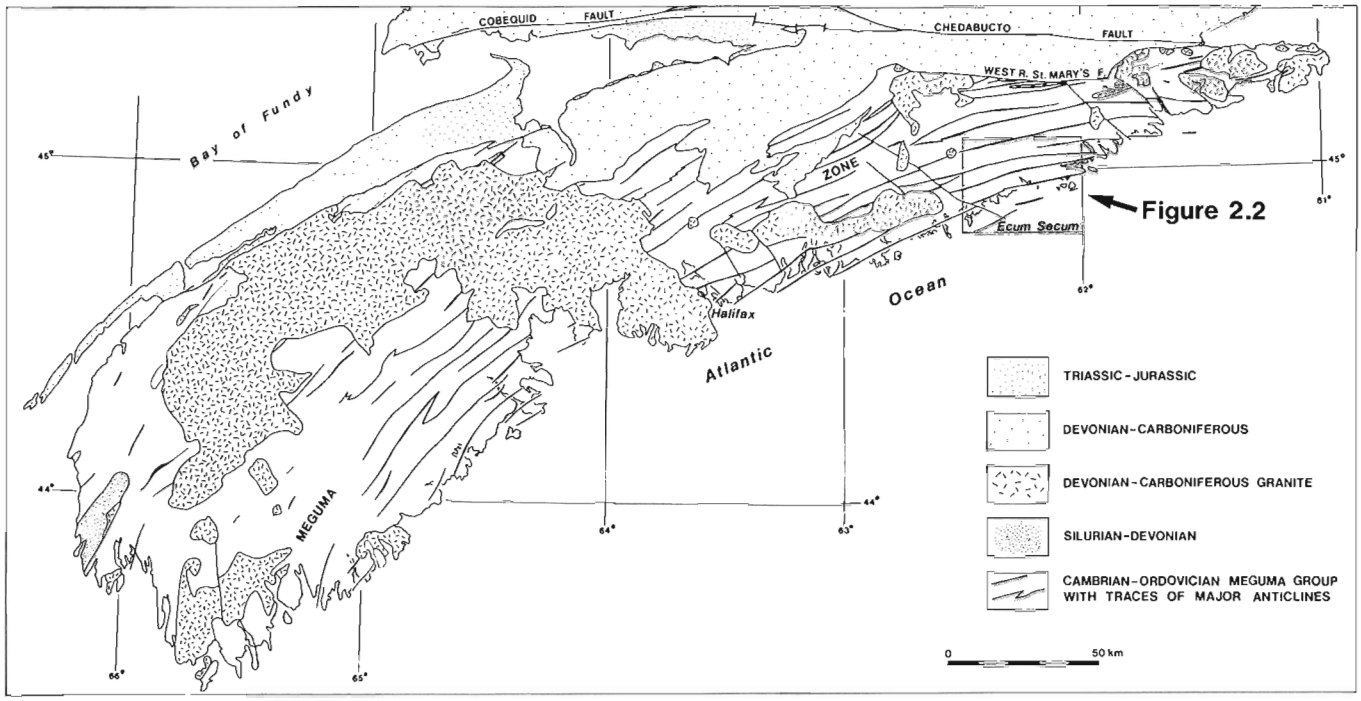

Figure 2.1. *Generalized geological map of southern Nova Scotia showing location of the study area (Ecum Secum).*

sinistral offset near Ecum Secum River. Other folds in the area can be seen to terminate abruptly where conical anticlinal and synclinal axial traces link (e.g. where the Wine Harbour Anticline links with the Sonora Syncline, and where the Salmon River Anticline links with the Ruth Falls Syncline). Within the Ecum Secum area fold limbs are approximately planar and dip 60-70 degrees, fold hinge areas are round to sharp, and axial surfaces are subvertical. The major folds antedate the intrusion of Devonian to Carboniferous granites into Meguma rocks outside of the map area (see Fig. 2.1). The regional metamorphism increases northward from chlorite grade in the area of Figure 2.2 to staurolite grade several kilometres south of the West River-St. Mary's Fault.

Review of Previous Work

Since the discovery in 1860 of auriferous gold veins in slates and arenaceous metawackes of the Meguma Group, numerous authorities have devoted considerable effort to predict the distribution of the deposits and explain their origin. Rickard (1912) provided an annotated bibliography of the important contributions on the subject published from 1862 to 1912; Malcolm (1928) listed a bibliography to 1928, Cameron (1947) provided a bibliography on Nova Scotia gold districts to 1947, and Graves and Zentilli (1982) presented a recent review of the geology of Nova Scotia gold deposits.

According to Faribault (1899) nearly all the rich veins and large bodies of quartz worked for gold in Nova Scotia parallel the bedding planes, and occur at well defined points along anticlinal crests, the centre of an elliptical dome being one of the most favourable places for the occurrence of quartz veins. From the analogy with the gold-bearing saddle reefs of Bendigo, Australia, operated profitably to depths greater than 1200 m, Faribault (1903) argued that in Nova Scotia saddle veins as large and rich in gold as those cropping out at the surface should occur at depth. In order to explain the localization of the veins, Faribault (1899) proposed that slip between thick, competent wacke beds caused fissures to open on the fold limbs along which quartz was deposited ("leg veins"). For anticlines with limbs dipping more than 70 degrees, large bodies of quartz were deposited in openings between the beds at the fold crests ("saddle veins" or "reefs"). He held further that mineralizing solutions were derived locally and that the folding and veining occurred slowly and intermittently. He observed that the quartz in the veins commonly contains minute scales of slate which had been peeled off the walls and subsequently covered by other layers of quartz, giving a laminated structure to the veins. Most of the gold occurs in streaks parallel with the laminations (Faribault, 1899). As early as 1864, Benjamin Silliman Jr., proposed a contemporaneous origin for the veins and folds, and Dawson (1868) noted that the auriferous bedding-parallel quartz veins definitely were not beds, as evident from the way veins branched off into the neighbouring rocks.

Keppie (1976) re-evaluated the anticlinal saddle reef hypothesis of Faribault, and concluded on the basis of a modified concentric fold model that the size of saddle reef veins should increase with the fold tightness (Keppie's "Curvature Index"), and in anticlines of the Goldenville Formation the Curvature Index indicates that saddle reef size should increase with depth.

Recently, Graves and Zentilli (1982) argued on the basis of composition, texture and geometry that the vein minerals were precipitated rapidly from an aqueous fluid which generated hydraulic fractures during greenschist metamorphism. They assumed that the least tectonic stress was vertical at the onset of horizontal compression, and horizontal, bedding-parallel hydraulic fractures formed when the fluid pressure exceeded the least tectonic stress. The

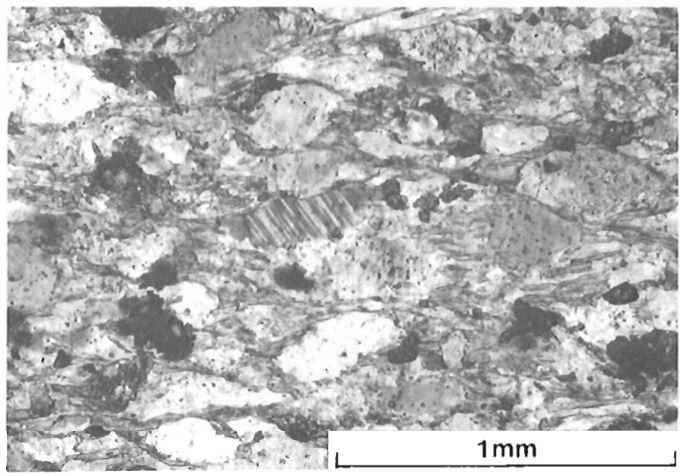

Figure 2.3. *Photomicrograph of metawacke showing continuous cleavage defined by elliptical detrital quartz and feldspar grains, with secondary quartz-mica beards attached to the detrital grains. 2HSA-C22-AC*

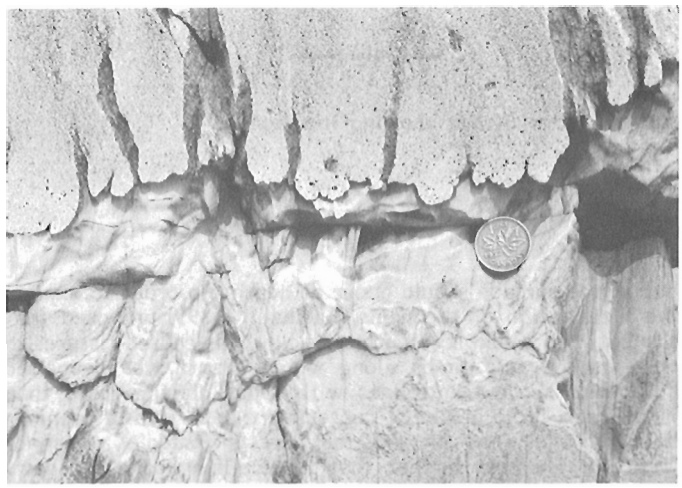

Figure 2.4. *Photograph of metawacke and metasiltstone with vertical spaced cleavage stripes in metawacke and continuous cleavage in siltstone. Bedding is horizontal. GSC 1-20-82*

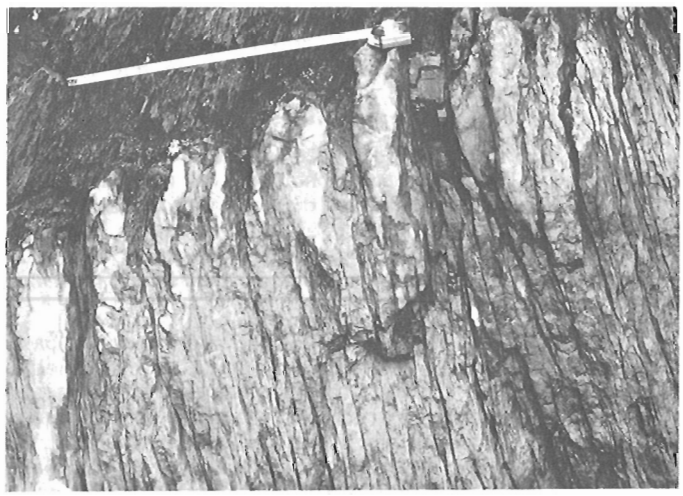

Figure 2.5. *Photograph of metawacke below dark slate showing spaced cleavage stripes (dark) parallel to dewatering sheet traces (light colour with swelling towards top of bed) in metawacke. Note abrupt refraction of slaty cleavage across bedding trace. GSC 203539-H*

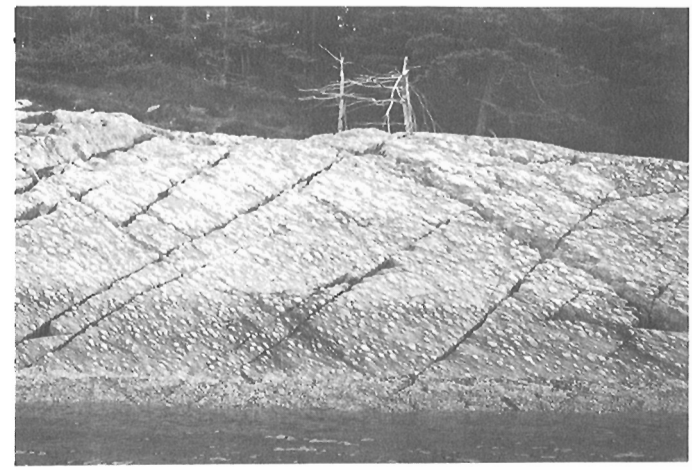

Figure 2.6. *Photograph of an upper surface of a metawacke bed covered with elliptical sand volcanoes. Their maximum elongation is parallel to the spaced cleavage trace. GSC 203683-L*

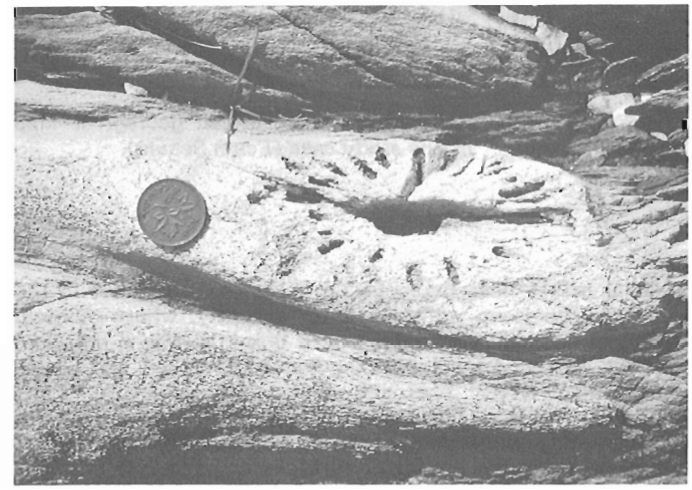

Figure 2.7. *Photograph of a sand volcano on a bedding surface showing radial internal structure and a central vent. Differential erosion of the radial septae and vent probably are due to their higher content of detrital(?) carbonate grains. GSC 203539-N*

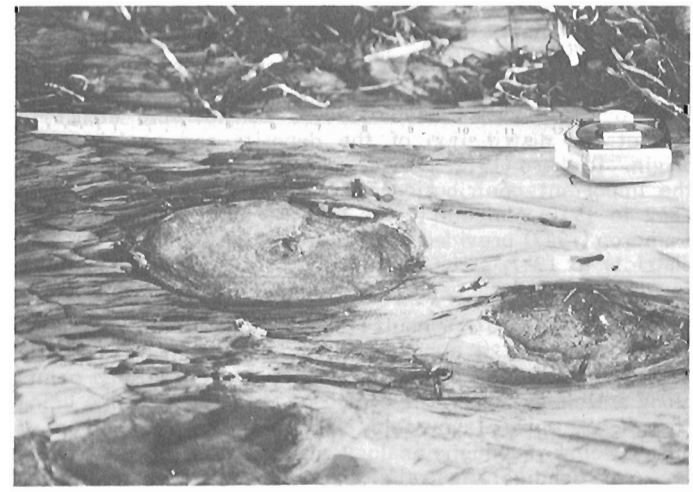

Figure 2.8. *Photograph of sand volcanoes on a horizontal bedding surface showing homogeneous interiors and central vents. GSC 203683-A*

sequence of events proposed by Graves and Zentilli (1982) is 1) vein formation, 2) folding, and 3) cleavage development. Faribault and Keppie directly linked the vein formation and the folding process, whereas Graves and Zentilli believed that the veins antedate the folds and that in some places tight folding of the auriferous quartz veins has produced a mechanical enrichment, by increasing the vein length per chord length of major structures in the fold profile plane.

Bedding-Cleavage Relations in the Ecum Secum Area

Arenaceous metawacke and slate, the principal lithologies of the Meguma Group, exhibit continuous (i.e. slaty, penetrative) cleavage in the Ecum Secum area. In addition, arenaceous metawacke exhibits spaced cleavage parallel to the continuous cleavage. In slates continuous cleavage is defined by parallel alignment of chlorite flakes, and in metawacke continuous cleavage is defined by the planar preferred shape fabric of detrital quartz and feldspar grains as well as parallel alignment of secondary quartz, chlorite and sericite which form "beards" attached to detrital sand grains (Fig. 2.3). Spaced cleavage appears as phyllosilicate-rich seams. The seams vary in width up to several centimetres (Fig. 2.4) and become more closely spaced in the hinge regions of folds. The continuous and spaced cleavages in metawacke beds are parallel in the Ecum Secum area.

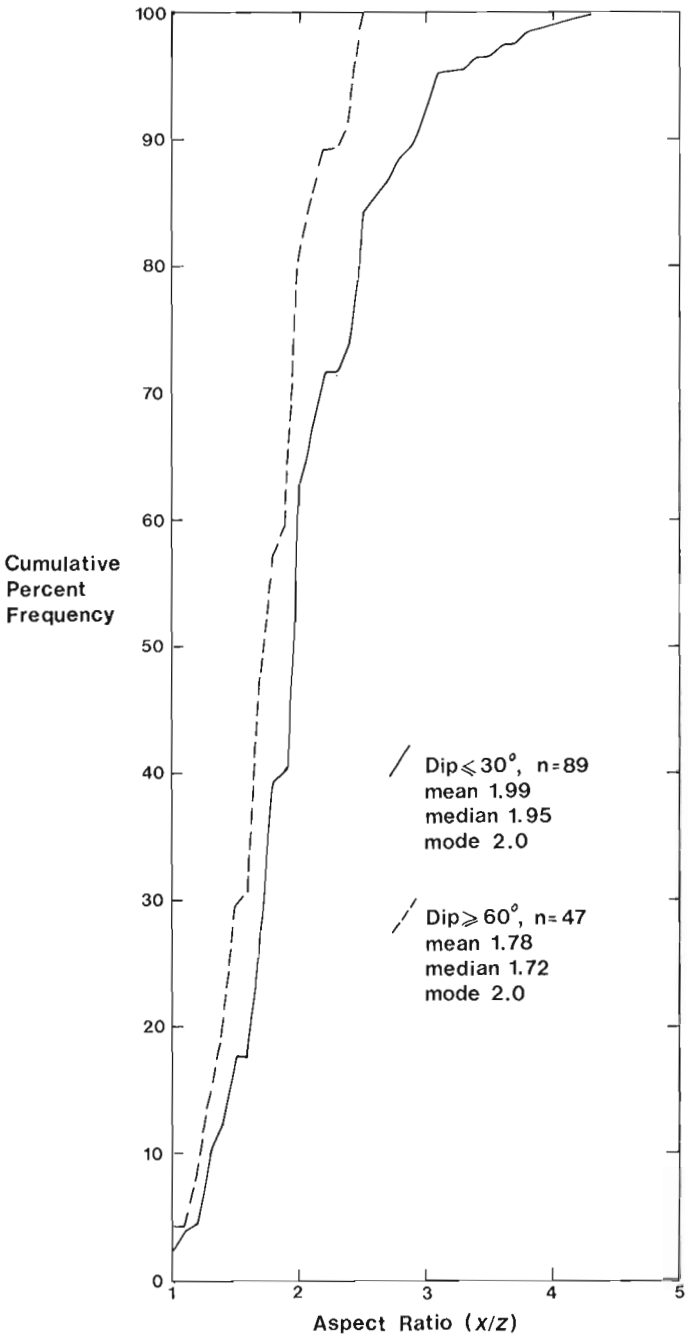

Figure 2.9. *Graph showing sand volcano aspect ratios (X:Z) vs. cumulative per cent frequency measured on bedding surfaces dipping from 0-30°, and 60-90°.*

Figure 2.5 shows typical bedding-cleavage geometries in interbedded metawacke and slate. The bedding surface dipping to the left at 30 degrees shows rounded profiles of sand volcanoes capping dewatering sheets or pipes in the upper part of a metawacke bed. The dewatering structures are penecontemporaneous features formed by the rapid expulsion of water from a "quick" bed, and elutriation of coarse sand upward from the base of a turbidite (Dzulynski and Walton, 1965). The spaced cleavage in the wacke bed, shown by the thin dark stripes, is parallel to the light water-escape structures and dips in the direction opposite to the bedding. The dark slate overlying the metawacke exhibits continuous cleavage dipping more steeply, but in the same direction as the bedding. In Figure 2.5 the two cleavages show an abrupt refraction across the wacke/slate contact; in graded beds on fold limbs the refraction is gradual. In the troughs and crests of folds, cleavages in metawacke and slate are normal to subhorizontal bedding surfaces (e.g Fig. 2.4).

An upper surface of a metawacke bed covered with elliptical sand volcanoes is shown in Figure 2.6. The truncated sand volcanoes exhibit radial, concentric or homogeneous interiors with a small central vent (Fig. 2.7, 2.8). Their maximum elongation is everywhere parallel to the cleavage trace on the bedding surface. On a few bedding surfaces the elliptical structures are aligned en echelon parallel to traces of dewatering sheets, but most commonly the sand volcanoes occur in swarms capping randomly distributed dewatering pipes (e.g. Fig. 2.6). A graph of sand volcano aspect ratio (length:width) vs. cumulative per cent frequency, measured on bedding surfaces dipping less than 30 degrees and more than 60 degrees, is shown in Figure 2.9. The two curves are not significantly different: both indicate a strong unimodal distribution at $\underline{X}/\underline{Z}=2$. The data may be interpreted to suggest that either the principal extension direction for the rocks is parallel to the fold axis and/or that the sand volcanoes were flattened in the cleavage plane when bedding was horizontal and subsequent flexural folding rotated the beds on the fold limbs without appreciable additional distortion of the bedding surface.

Bedding-Cleavage-Vein Relations

Quartz veins (commonly quartz-carbonate-chlorite) are ubiquitous throughout the Goldenville Formation in the map area. Auriferous quartz veins, however, have been found only in the areas of gold mines indicated in Figure 2.2. Exposure is poor in the gold districts, and much of the information on the nature of the auriferous veins must be obtained from the literature; observations on barren quartz veins, on the other hand, are useful to make comparisons with descriptions of auriferous veins made by previous workers.

On the basis of geometry I have distinguished three principal types of quartz veins within the Ecum Secum area: 1) veins lying parallel to bedding planes ("BP" veins), 2) veins lying within slate beds but terminating with short "hooks" extending into adjacent metawacke beds ("EE" veins), and 3) veins lying within metawacke beds in planes approximately normal to the local fold axis ("AC" veins).

Bedding-parallel veins most commonly occur near the top of a slate bed, and at the interface between slate and an overlying metawacke bed. The BP veins may contain several layers of quartz separated by thin laminae of slate, they may be made up of coarse, massive quartz, or they may consist of both layered and boudinaged massive quartz (Fig. 2.10). Commonly, veins with layered quartz also exhibit folded coarse quartz fibres aligned in the plane of the vein, approximately normal to the fold axis (Fig. 2.11). The fibrous quartz veins are found on the limbs and hinges of folds.

En echelon veins occur on the limbs of the large folds in the area. Their intersection with the bedding is subparallel to the fold axis (although one example of two EE veins intersecting bedding parallel to the dip line was seen). Figure 2.12 shows a typical EE quartz vein viewed parallel to its horizontal intersection with bedding. The vein in the figure consists of a two-metre long nearly vertical segment crossing a metre-wide slate bed, and with sharply bent, hook-like terminations in the adjacent metawacke beds. Several other EE quartz veins occur in the same slate bed slightly above and below the vein in the photograph.

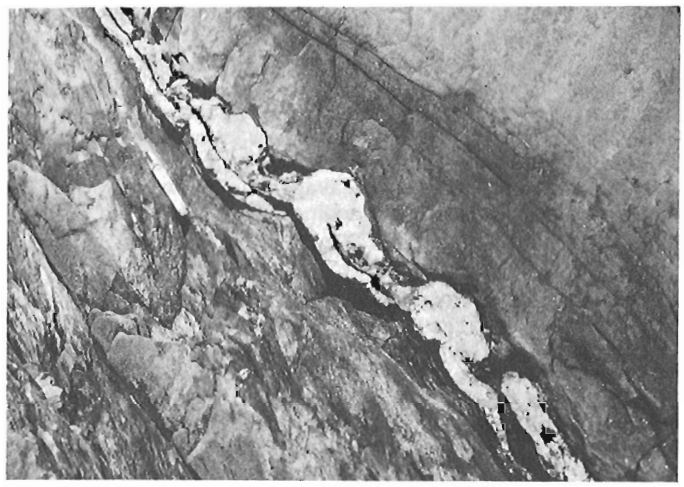

Figure 2.10. *Photograph of a bedding-parallel quartz vein showing both layered fabric and massive quartz "rolls". Viewed parallel to the long axes of the rolls which parallel the local fold axis. GSC 203683-D*

Figure 2.11. *Photograph of a subhorizontal bedding-parallel quartz vein showing quartz extension fibres lying in the plane of the vein. The small fold axes are parallel to the local fold axis in bedding. GSC 203683-E*

In contrast to the BP and EE veins the AC veins are confined to metawacke beds. Quartz veins of this class occur both in limb and hinge areas of folds. Commonly the AC veins occur in single fractures filled with quartz crystals; they also occur as conjugate sets of short en echelon veins that form an acute intersection with the AC plane beyond the termination of a single AC vein. They postdate the folding and record a small amount of E-W extension parallel to the fold axes. The AC veins are deformed by conjugate sets of kink bands in spaced cleavage. The conjugate kink bands record a small amount of E-W shortening (Fig. 2.13).

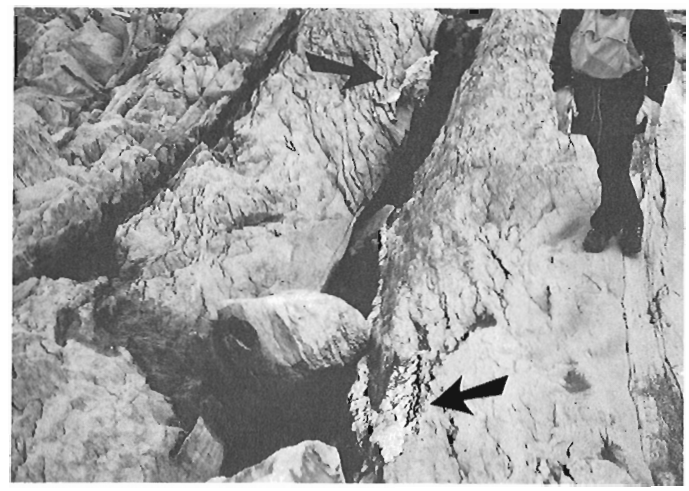

Figure 2.12. *Photograph showing an en echelon quartz vein crosscutting a dark slate bed and terminating with short "hooks" in the bounding metawacke beds (arrows point to hooks). View east parallel to the line of intersection of the vein and bedding. GSC 203539-I*

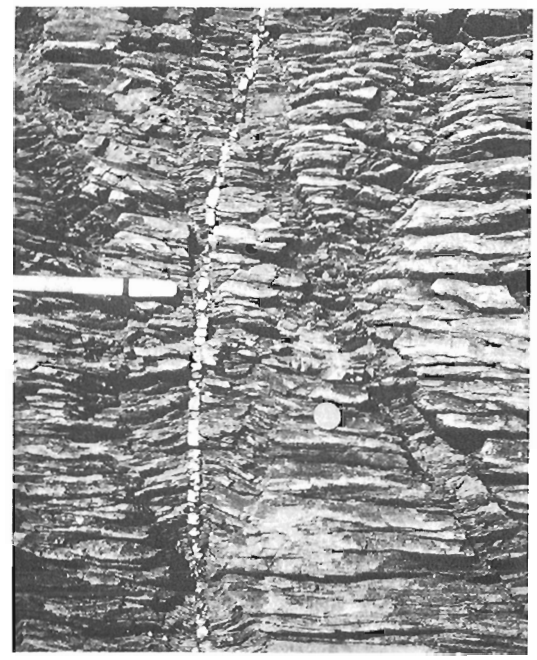

Figure 2.13. *Photograph showing an AC quartz vein. The vertical vein is normal to the spaced cleavage in the horizontal metawacke bed and is offset slightly by a right-hand kink band in the spaced cleavage. Note also the conjugate left-hand kink band. The pen lies parallel to the extension direction (E-W) for the vein and the compression direction for the kink bands. GSC 203683-S*

Interpretation of Bedding-Cleavage-Vein Relations

Figure 2.14 summarizes the geometric features of the principal veins, cleavages and folds in the Ecum Secum area. Parallelism of water escape structures and spaced cleavage on fold limbs, as well as identical aspect ratios of sand volcanoes on fold hinge and limb regions, indicate that: (1) bedding and cleavage were originally perpendicular and (2) the cleavage refraction is due to different distortions in metawacke and slate beds during flexural-shear folding.

The BP and EE veins are auriferous and are contemporaneous in the gold districts; they are older than the AC veins, which are barren. For example, Hedley (1941) and Bell (1948) described contemporaneous BP veins ("leads") and EE veins ("angulars") in the Goldenville and Caribou districts that were particularly auriferous where the two types of veins intersected.

Figure 2.15a represents the bedding-cleavage-vein geometry of EE veins shown in Figure 2.12. The slaty cleavage trace lies in the acute angle between bedding and the EE quartz veins. If the veins as seen now originally formed as en echelon tension gashes at the onset of folding, the geometry shown in Figure 2.15b is obtained by removing a dextral shear strain of 2.75 parallel to the bedding in the slate. This restores the EE vein in Figure 2.15a to an original 45° angle, and also restores the slaty cleavage to a 90° angle with bedding.

The BP veins with parallel lamination and quartz fibre lineation (Fig. 2.10, 2.11) resemble veins described by Ramsay and Huber (in press) as either shear fibre veins or stretched crystal veins wherein the lineations parallel the incremental stretching directions. Given that: (a) the crystal fibres in the BP veins observed in the Ecum Secum area are aligned in the plane of the veins, perpendicular to the fold axis, and (b) that the veins occur in both limb and hinge zones of folds, the BP veins could antedate the folds or have formed early in the strain history of folding.

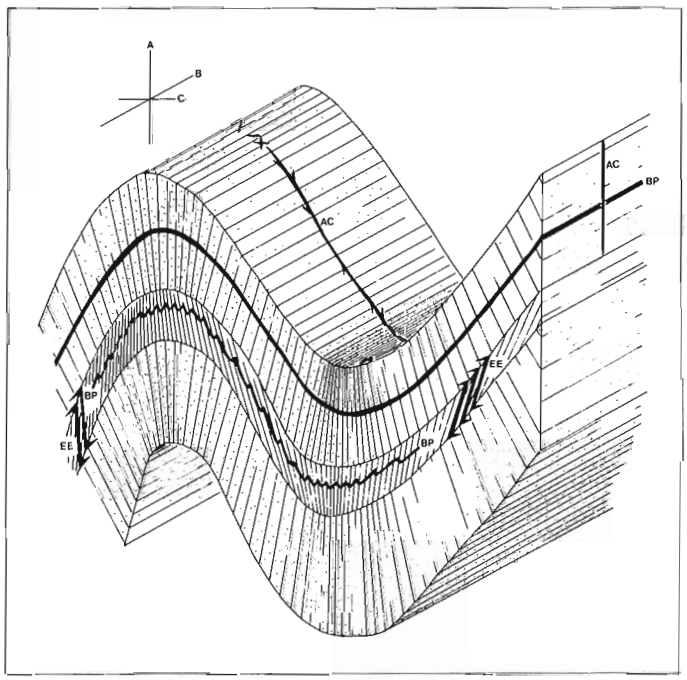

Figure 2.14. *Sketch showing the relationships of the principal veins to folds and cleavages in the Ecum Secum area. Metawacke beds are stippled, slate is in centre and veins are black.*

There are two possible mechanisms: (1) formation of shear fibre veins during pre-fold layer-parallel slip, or (2) modification of hydraulic fracture-fill by layer-parallel slip. It is not yet feasible to unequivocally distinguish between these two possibilities.

Some constraints can be applied: (a) shear fibre vein formation prior to folding can only imply minor layer-parallel slip since removal of the bedding-parallel shear component due to folding restores cleavage to its layer normal position and the EE veins to their initial 45° position, (b) shear fibre vein formation during folding implies major hinge migration, for which there is no evidence, in order to account for BP vein development in the hinge regions of large wavelength folds, and (c) formation of hydraulic BP extension veins could occur either during or prior to folding.

The persistence of the fibre lineation in the fold hinge zones implies that modification of such veins by layer-parallel slip during folding must be accompanied by at least a minor amount of hinge migration. Such hinge migration may only subtly modify the pre-fold cleavage, and may not be detectable from our field data.

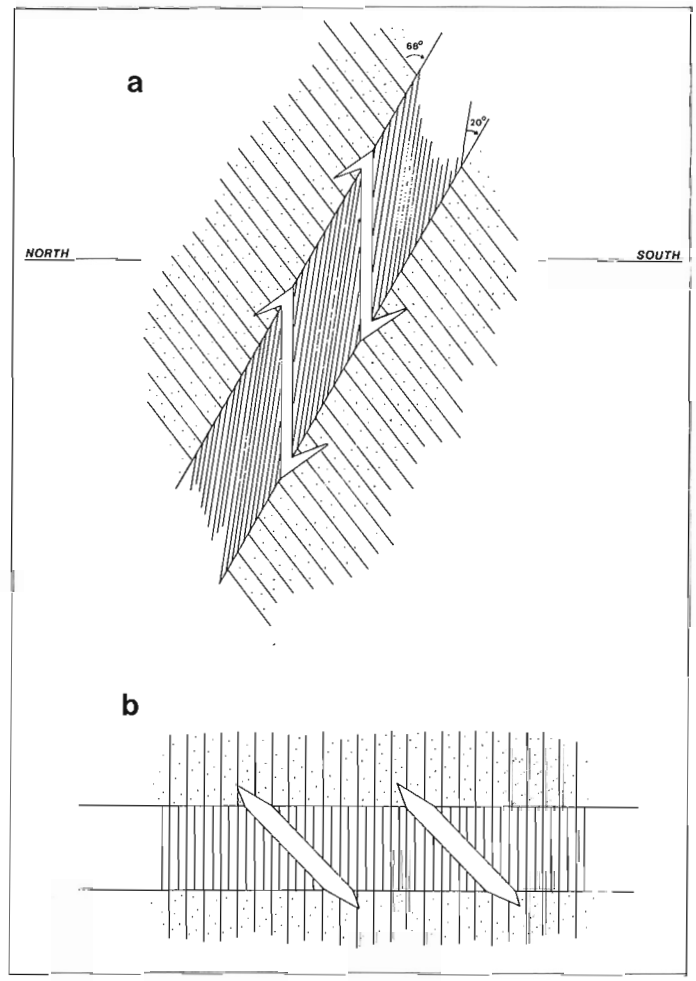

Figure 2.15. *Geometry and origin of en echelon quartz veins. a. Present geometry of en echelon veins, bedding and cleavage in metawacke (stippled) and slate (close-spaced cleavage traces). b. Apparent original geometry of en echelon veins as en echelon tension gashes in slate formed prior to the major folding.*

Table 2.1

Classification of principal veins in the Ecum Secum area

Class	Geometry	Fabric	Relative Age and Mineralization Potential
BP	1. Bedding-parallel, cm-wide veins in slate, commonly folded on much shorter wavelengths than the folds in metawacke beds.	Quartz and chlorite laminae with quartz extension fibres sub-parallel to the vein walls.	Form early in history of folding, commonly auriferous in gold districts
	2. Decimetre-wide between metawacke beds, folded on same wavelength as bedding in metawacke.	Massive quartz with no apparent preferred growth habit.	Form early in history of folding, auriferous in gold districts, distinguished from fibre veins on basis of fabric.
EE	En echelon arrays of veins in slate beds that are discordant to bedding and cleavage and terminate with short hooks in adjacent metawacke beds. EE veins most commonly intersect bedding parallel to the local fold axis.	Massive quartz and chlorite with no preferred growth habit.	Form in extension fractures early in history of folding and after cleavage formation, their present geometry is due to bedding-parallel shear during folding. Aurfierous in gold districts.
AC	Centimetre-wide veins in planes normal to fold axes in metawacke beds.	Quartz crystals normal to vein walls, also massive quartz.	Postdate BP and EE veins, record a period of extension parallel to to fold axes. Barren veins in gold districts.

The local contemporaneity of BP and EE veins, and constraint (a) suggest that BP veins either formed during the final pre-folding strain increment or very early during folding. In either case, BP veins do not correspond to saddle-reef structures.

Support for a hydraulic fracture-fill origin of BP veins is given by the EE veins. Formation of the EE veins as brittle tension-gash features is not associated with significant ductile deformation within the slate units where they occur, and implies that the slates were more brittle than the metawacke beds. These observations may be accounted for by localized high pore fluid pressures within the slate units, which by reducing the effective normal stress term in the modified Coulomb failure criterion (e.g. see Hobbs, Means and Williams, 1976) would enhance brittle behaviour in the slate. Price (in Fyfe, Price and Thompson, 1978) has shown that onset of flexural folding is also enhanced by high pore fluid pressures, and that shearing resistance on bedding surfaces can be reduced to a few tens of bars at more than 10 km depth. At these depths temperatures of around 300°C would be expected to occur, and fluids generated during metamorphic reactions could account for the high pore pressures (e.g. Graves and Zentilli, 1982).

The AC veins are consistent with the hydraulic extension fracture hypothesis also, and indicate that at their stage in the strain history the least tectonic stress was approximately horizontal E-W when the effective normal stress exceeded the tensile strength in metawacke beds.

In order for hydraulic fracturing to occur rocks must lack permeability, and therefore the solutions from which the vein minerals precipitated must be locally derived from slate and/or metawacke.

Table 2.1 summarizes the salient features of the principal vein types in terms of their geometry, fabric, relative age and mineralization potential. In the Ecum Secum area BP and EE veins formed in brittle slate contemporaneously with the cleavage development, and were succeeded by the folding. The AC veins developed in brittle metawacke at a later stage in the deformation when the least tectonic stress was parallel to the fold axes. The conjugate kink bands in spaced cleavage postdate the AC veins in metawacke, and formed when the maximum tectonic stress was parallel to the fold axes. Perhaps the northwest-striking sinistral faults formed under the stress conditions that produced the kink bands.

References

Bell, L.V.
1948: Caribou Mine; in Structural Geology of Canadian Ore Deposits; Canadian Institute of Mining and Metallurgy, Special Volume, p. 927-936.

Cameron, H.L.
1947: Structural control of orebodies in Nova Scotia gold districts; Mining Society of Nova Scotia, Transactions, v. L, p. 1-14.

Dawson, J.W.
1868: Acadian Geology, 2nd Edition; MacMillan, London, 694 p.

Dzulynski, S. and Walton, E.K.
1965: Sedimentary Features of Flysch and Greywackes. Developments in Sedimentology 7; Elsevier Publishing Company, New York, 274 p.

Faribault, E.R.
1893: Gegogan Sheet; Geological Survey of Canada, Map 382.

Faribault, E.R. (cont.)
1895a: Moser's River Sheet; Geological Survey of Canada, Map 551.

1895b: Liscomb River Sheet; Geological Survey of Canada, Map 550.

1896: Tangier Sheet; Geological Survey of Canada, Map 565.

1897a: Sheet Harbour Sheet; Geological Survey of Canada, Map 592.

1897b: Fifteen-mile Stream Sheet; Geological Survey of Canada, Map 607.

1897c: Plan and Section, Salmon River Gold District, Halifax County, Nova Scotia; Geological Survey of Canada, Map 647.

1899: The gold measures of Nova Scotia and deep mining; Journal of the Mining Society of Canada, v. II, p. 119-128.

1903: Deep Gold Mining in Nova Scotia; Government of Nova Scotia, The Commissioner of Public Works and Mines, King's Printer, 16 p.

1906: Plan and Sections, Harrigan Cove Gold District, Halifax County, Nova Scotia; Geological Survey of Canada, Map 945.

Fyfe, W.S., Price, N.J., and Thompson, A.B.
1978: Fluids in the Earth's Crust; Elsevier Scientific Publishing Co.

Graves, M.C. and Zentilli, M.
1982: A review of the geology of gold in Nova Scotia; in Geology of Canadian Gold Deposits; Canadian Institute of Mining, Special Paper No. 24, p. 233-242.

Hedley, P.M.
1941: Geology and structure as related to mining, Guysborough Mines Limited, Goldenville, N.S.; Mining Society of Nova Scotia, Transactions, v. XLIV, p. 251-258.

Hobbs, B.E., Means, W.D., and Williams, P.F.
1976: An Outline of Structural Geology; John Wiley and Sons, Inc., 571 p.

Keppie, J.D.
1976: Structural model for the saddle reef and associated gold veins in the Meguma Group, Nova Scotia; Nova Scotia Department of Mines, Paper 76-1, 34 p.

Malcolm, W.
1928: Gold fields of Nova Scotia; Geological Survey of Canada, Memoir 156, 253 p. (Reprinted in 1976 as Memoir 385.)

Ramsay, J.G. and Huber, M.
- Techniques of Modern Structural Geology, v. 1, Strain Analysis; Academic Press. (in press)

Rickard, T.A.
1912: The domes of Nova Scotia; Canadian Mining Institute, Transactions, v. XV, p. 396-476.

Silliman, B.J., Jr.
1864: On the so-called "barrel quartz" of Nova Scotia; American Journal of Science, 2nd Series, v. 38, p. 104-106.

3.

SELECTED MINERAL ASSOCIATIONS IN RADIOACTIVE OCCURRENCES IN THE GRENVILLE STRUCTURAL PROVINCE: A PROGRESS REPORT

Project 770061

J. Rimsaite
Economic Geology Division

Rimsaite, J., Selected mineral associations in radioactive occurrences in the Grenville Structural Province: a progress report; in Current Research, Part B, Geological Survey of Canada, Paper 83-1B, p. 23-37, 1983.

Abstract

The following mineral associations in leucocratic, melanocratic and mylonitic ore from Bancroft area, Ontario, and radioactive rocks from Mont-Laurier and Baie-Johan Beetz areas, Quebec, are described and related to petrography and evolution of the host rocks:

1. *uranium, thorium and REE-bearing mineral associations in a single grain;*
2. *accumulations of radioactive ore minerals as intergrowths with accessory minerals in or adjacent to ferromagnesian minerals;*
3. *evolution of REE minerals with changing La/Ce ratio, and the relationship between U, Th and REE minerals;*
4. *associations of primary and secondary minerals within altered radioactive ore and accessory minerals;*
5. *radioactive and REE mineral associations in mylonitized quartz-rich rocks.*

Studies of these mineral associations and their textures have suggested possible physico-chemical environments of crystallization, mobilization and redeposition of radioactive and REE minerals. These data contribute to a better understanding of radionuclide behaviour in radioactive occurrences including uranium mill tailings and other nuclear wastes.

Résumé

Le présent rapport décrit les associations minérales suivantes identifiées dans les minerais leucocrates, mélanocrates et mylonitiques de la région de Bancroft (Ontario) et les roches radioactives des régions de Mont-Laurier et de la baie Johan-Beetz (Québec), par rapport à la pétrographie et à l'évolution des roches encaissantes:

1. *associations de minéraux d'uranium, de thorium et des terres rares dans un seul grain;*
2. *accumulations de minerais radioactifs enchevêtrés et de minéraux accessoires dans des minéraux ferromagnésiens ou près de ces derniers;*
3. *évolution des minéraux des terres rares en fonction du changement du rapport La/Ce et lien entre l'uranium, le thorium et les minéraux des terres rares;*
4. *associations de minéraux primaires et secondaires au sein de minerais radioactifs altérés et de minéraux accessoires;*
5. *associations de minéraux radioactifs et de minéraux des terres rares dans des roches mylonitisées riches en quartz.*

L'étude de ces associations minérales et de leurs textures suggère des milieux physiques-chimiques possibles de cristallisation, de mobilisation et de mise en place subséquente pour les minéraux radioactifs et les minéraux des terres rares. Ces données contribuent à une meilleure connaissance du comportement des radionucléides dans les venues radioactives, notamment les résidus d'uranium et d'autres déchets nucléaires.

Introduction

During Grenvillian orogeny and metamorphism, interactions between adjacent diverse sedimentary strata and basic and granitic intrusive rocks resulted in unusual mineral associations (Rimsaite, 1980b). Furthermore, post-tectonic veining and replacement of fractured and mylonitized rocks by anhydrite, calcite, fluorite, gehlenite ($Ca_3AlSiAlO_7$), phyllosilicates, pyrite, quartz, scapolite ($Na_4ClSi_9Al_3O_{24}{\cdot}CaCO_3Si_6Al_6O_{24}$), and tourmaline as well as the development of radioactive and REE-bearing crusts on fractures, also contributed to the diversity of mineral associations.

This paper presents results of mineralogical and chemical studies on specimens collected from radioactive occurrences in the Grenville structural province which were briefly described in preliminary reports by Rimsaite (1978, 1980a,b; 1981a,b; 1982a,b,c) and provides additional illustrations and quantitative analytical data on the following mineral associations:

1. uranium, thorium and rare-earth element (REE)-bearing mineral associations in single grains as a result of sequence of crystallization and replacements (Fig. 3.1);

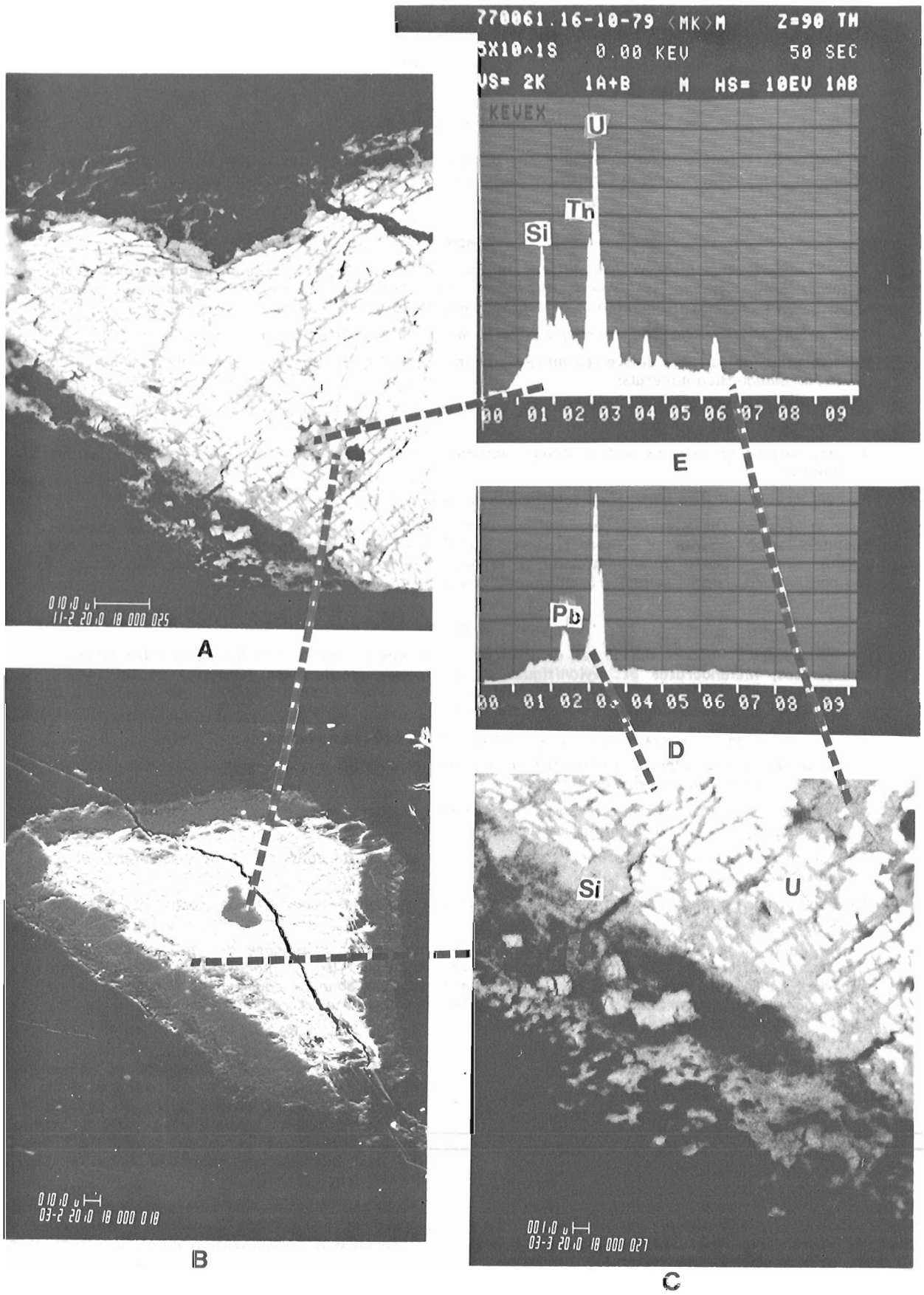
770061.16-10-79 〈MK〉M Z=90 TM
5X10^1S 0.00 KEV 50 SEC
VS= 2K 1A+B M HS= 10EV 1AB
KEVEX
U
Th
Si
00 01 02 03 04 05 06 07 08 09
E
Pb
00 01 02 03 04 05 06 07 08 09
D
A
B
Si
U
C

2. accummulations of radioactive ore minerals and accessory minerals: uraninite, uranothorite, zircon, titanite, magnetite, galena and REE-bearing minerals, in intergrowths clustering adjacent to, or within ferromagnesian minerals (Fig. 3.2, 3.8a);
3. evolution of REE minerals, accompanied by the changing La/Ce ratio, and the relationship between early and late crystallized minerals and between U, Th and REE minerals (Fig. 3.3, 3.5, 3.6; Rimasite 1982b, Fig. 31.4, 31.5c,e,f; 1982c, Fig. 3B,C);
4. associations of primary and secondary minerals within altered radioactive and adjacent accessory minerals, such as uraninite-ilmenite intergrowths (Fig. 3.4; Rimsaite, 1982a, Fig. 3.3a,b);
5. radioactive mineral associations in mylonitized quartz-rich rocks, including the following: pyrite-uraninite-molybdenite; allanite-uraninite-uranothorite-chlorite and titanite-ilmenite-magnetite-pyrite-uranothorite-zircon-secondary and REE-bearing minerals (Fig. 3.5, 3.7, 3.8; Rimsaite, 1982b, Fig. 31.7, 31.8).

General geology of the Bancroft area, Ontario has been described by Hewitt (in Satterly, 1957, p. 5-26) and Satterly (1957), and of the radioactive occurrences north of Mont-Laurier, Quebec by Kish (1977). A review of the geology and sketch maps showing sampling localities and laboratory methods used, namely semiquantitative energy dispersive spectrometric analyses (EDS), optical and scanning electron microscopy (SEM), and X-ray diffraction studies (XRD) have been described by Rimsaite (1978; 1981a,b; 1982a). Tables 3.1 and 3.2 document semiquantitative SEM-EDS analyses of heterogeneous minerals and crusts illustrated in this paper and in Rimsaite, 1982b).

Acknowledgments

The author's mineralogical and petrographic studies were supported by X-ray mineral identification by A.C. Roberts and by scanning electron microscope and energy dispersive spectrometer analyses by G.J. Pringle and D.A. Walker. I gratefully acknowledge these contributions.

Uranium, Thorium and REE-Bearing Mineral Associations in a Single Grain as a Result of Sequence of Crystillization and Replacements (Fig. 3.1, Table 3-1 analyses 2,3)

Replacement of fractured grains of uraninite by uranothorite-like phases has been observed in ore specimens from the Bancroft area, Ontario, and in radioactive rocks north of Mont-Laurier and Baie-Johan-Beetz area, Quebec (Rimsaite, 1980a, Fig. 38.1; 1982a, Table 3.2 analyses 1,6; 1982b, Fig. 31.2c,e,f; 1982c, Fig. 2). As a result of this replacement the following chemical variations occurred within the original grain: in the Si-Th-rich replacing phase, silica increased 14 times and thorium increased five times while uranium and lead decreased about three times (Table 3.1, analyses 2 and 3). Compared with a uranothorite grain in allanite, the uranothorite-like phase that replaces uraninite contains less CaO, SiO_2, ThO_2 and TiO_2, but more PbO, Y_2O_3, FeO and MnO, thus indicating a relationship between chemical composition and sequence and environment of crystallization of uranothorite phases (Table 3.1, analyses 1 and 2).

Grains of uraninite and of uranothorite commonly contain prominent iron-rich rims made up of pyrite, galena, Fe oxides or phyllosilicates. Some rims consist of calcite, fluorite and quartz that contain REE-bearing and radioactive specks and coatings (Rimsaite, 1980a, Fig. 38.2, 3,4c,d,e,f,g; 1982a, Fig. 3.3; 1982c, Fig. 3B,C). On the basis of textural evidence, the thorite-like phase and minerals within the rim and in fractures followed crystallization of host uraninite. The following sequence of crystallization is postulated: uraninite, uranothorite, Fe-rich and REE-rich phases with or without galena, Sr-rich and Sn-rich specks.

The occurrence of such heterogeneous grains and their relationship to the groundmass minerals provide information on the environment and sequence of crystallization. The heterogeneity of the uraninite grains may cause serious problems in the interpretation of isotopic data especially when the interpreter is unaware of Pb-rich rims, mobilization of U and addition of Th. Correlation between chemical composition and X-ray properties, such as Th content in uraninite and its cell edge dimensions, may also cause problems because U and at least part of Th are present in different mineral phases, thorite being amorphous to X-rays.

The uraninites, partly replaced by thorite and rimmed by calcite, fluorite, galena, phyllosilicate, pyrite and REE-bearing bands, commonly crystallize: in biotite or adjacent to biotite bands; in fractures and interstices of feldspar and quartz; and in fractures of hornblende and pyroxene which are filled with anhydrite, calcite, epidote, fluorite, scapolite or tourmaline. These mineral associations indicate there was a close relationship between precipitation of U, Th, REE and B, CO_2, F, M_2O, NaCl, OH and S-bearing phases during late stages of crystallization of radioactive granitoid rocks.

Accumulations of Radioactive Ore Minerals and Accessory Minerals in Intergrowths Clustering in and Adjacent to Ferromagnesian Minerals (Fig. 3.2)

In addition to uraninite and uranothorite grains occurring singly in rock-forming minerals and their fractures, uraninite and uranothorite crystals occur also in intergrowths with accessory minerals in the following associations: zircon, titanite and magnetite (Fig. 3.2); zircon, titanite, allanite, apatite, tourmaline and amorphous REE phases (Rimsaite, 1980a); titanite, zircon with or without apatite and allanite (Fig. 3.5e); monazite, xenotime, zircon, galena, pyrochlore and secondary mineral aggregates: hydroxyl-bastnaesite and kasolite; and anatase, unidentified amorphous Si-U-Y grains and secondary branerite-like aggregates in Baie-Johan-Beetz area (Rimsaite, 1981a, Fig. 17.5A; 1981b, Fig. 4.3A,B,C). Accumulations of accessory minerals commonly occur at the contact zone between biotite schist or metagabbro and microcline pegmatite.

Textures of mineral intergrowths in Figure 3.2 indicate that magnetite crystallized first and was succeeded by zircon, uraninite, uranothorite, titanite, galena, REE-bearing

---

***Figure 3.1** (opposite)*

Backscattered electron images (BEI) of heterogeneous uraninite at various magnifications showing the relationship between U-rich, Th-rich and REE-bearing phases within the radioactive grain and its rim (GSC-203577-U).

A,B,C. Fragments of fractured uraninite (U, white) partly replaced by Si-U-Th-phase (Si, grey) along the edges and fractures. The mottled rim, which contains light grey REE-bearing specks and textural relationships between U and Si-U-Th phases can be seen clearly at the high manification of 3000x in "C", whereas at lower magnification of 300x in "B", the uraninite appears hemogeneous. ED spectrum of REE-bearing specks in a rim of uraninite is shown by Rimsaite (1980a, Fig. 38.4e).

D. Energy dispersive (ED) spectrum of uraninite (line intensities: U > Pb).

E. ED spectrum of Si-U-Th phase: U > Th > Si > Ca = Ti = Fe.

and radioactive rims overgrown on uranothorite and on titanite crystals. In such mineral associations, uranium occurs mainly in uraninite and in uranothorite, and in lesser quantities in zircon and as specks and crusts in radioactive rims on titanite and on uranothorite. Associations of uraninite, pyrochlore and titanite with or without apatite, monazite and galena occur in the Greyhawk mine and in the Silver Crater mine in the Bancroft area (Rimsaite, 1982b).

At the contact zone between metasediments and pegmatite, accumulations of titanite and allanite occur along biotite-rich bands. The uraninite grains occur adjacent to, or in, biotite, titanite and allanite (Fig. 3.5a,b; Rimsaite, 1982b, Fig. 31.5b,e,d,g). In area PP-2 north of Mont-Laurier, Quebec, radioactive biotite schists consist of alternating bands of biotite-allanite and biotite-zircon in quartz-feldspar matrix. Allanite, uraninite and uranothorite grains commonly crystallize at the end of biotite bands, and complex Ti-U-bearing crusts crystallize along the basal fractures of biotite flakes, thus suggesting that biotite bands in the host rock served as an aqueduct for uraniferous solutions.

Figure 3.2. *BEI of an association of radioactive ore minerals: uraninite (U) and uranothorite (Th), and of accessory minerals: magnetite (M), zircon (Zr) and titanite (Ti). The uraninite apparently replaces magnetite and zircon at the northern margin. Zircon has a mottled appearance and is intergrown with uranothorite which is enclosed in a prominent rim having disseminated specks of galena (white) and of radioactive and REE compounds (various shades of grey). Titanite grains are overgrown and traversed along fractures by U-bearing crusts (white). Magnetite is fractured as a result of radiation from the adjacent uraninite. Melanocratic ore, Madawaska mine (GSC 203577-S).*

Table 3.1

Partial semi-quantitative analyses of selected U and Th minerals and crusts from radioactive occurrences in the Bancroft area, Ontario, and north of Mont-Laurier, Quebec

		Oxides weight per cent*											
		SiO_2	TiO_2	Al_2O_3	Total Fe as FeO	MnO	CaO	SO_3	Y_2O_3	PbO	ThO_2	UO_2	Other
Bancroft area, locality "F" (specimens from 1 to 6)**													
1.	Uranothorite	17.7	1.9	1.0	0.0	0.0	3.2	0.4	0.0	1.8	45.4	19.5	
2.	Uranothorite	14.3	0.5	1.4	1.9	0.5	0.4	2.3	1.0	3.9	36.0	19.7	
3.	Uraninite	1.1	0.5	0.6	2.2	0.6	0.4	0.9	0.7	11.3	6.5	63.0	
4.	Uraninite	1.5	0.7	1.0	1.3	0.9	1.1	0.8	1.2	9.5	7.5	65.4	
5.	Coffinite-like	14.9	0.9	2.0	1.9	0.8	0.7	1.4	1.3	3.2	5.0	64.0	K
6.	U-S compound	1.6	0.3	0.2	2.6	0.2	1.6	8.3	0.1	3.1	0.3	14.8	K
7.	U-Ti-Si compound	12.2	19.4	0.2	1.3	0.1	0.7	0.3	0.9	1.2	0.0	42.8	K
8.	U-Si-Ti compound	15.3	6.3	0.2	1.2	0.1	0.0	0.0	3.8	0.0	0.0	51.3	K
Locality TDN-2 north of Mount-Laurier, Quebec (specimens from 10 to 12)**													
9.	Uranite	0.4	0.0	0.0	0.3	0.0	0.0	0.0	0.0	10.8	6.6	73.0	
10.	Inclusion in "9"	9.4	3.0	0.0	20.0	0.0	1.7	0.0	4.3	3.3	18.5	6.6	Na, Nd
11.	Rim on "9"	9.0	1.0	1.5	47.2	0.0	1.4	20.0	1.2	10.3	0.2	1.3	Cr
12.	Crust	6.0	3.7	1.1	49.7	0.3	1.4	27.0	0.9	9.3	1.3	2.2	Cr, Nb,
Locality H-50 north of Mont-Laurier, Quebec (specimens from 13 to 16)**													
13.	Fe-rich thorite	15.4	0.0	1.1	11.1	0.0	0.0	10.0	0.0	4.3	50.4	0.0	
14.	Pb-rich after "13"	6.4	0.0	0.0	3.2	0.0	0.0	18.0	0.0	44.1	27.6	0.0	
15.	Inclusion in "13"	8.1	13.2	1.5	7.4	0.0	1.1	1.6	0.0	2.2	9.4	45.6	Cr
16.	Crust in mica	6.0	7.5	1.0	5.4	0.3	0.8	4.4	0.0	14.7	10.7	34.8	

* Semiquantitative SEM-EDS analysis by G.J. Pringle on spectra collected by D.A. Walker and J. Rimsaite at the SEM Laboratory, Geological Survey of Canada.

** Sample location sketch map published by Rimsaite (1978, Fig. 9.1, 9.2). For notes on analyzed spots see text and Appendix A.

Evolution of REE Minerals Accompanied by Changing La/Ce Ratio, and the Relationship Between U, Th and REE Minerals (Fig. 3.3, 3.5; Rimsaite, 1982b, Fig. 31.4)

The principal REE minerals studied in the Grenville structural province include pyrochlore, xenotime, monazite, allanite and unidentified Si-U-Y grains and amorphous crusts and rims on accessory minerals. The phosphates alter to secondary radioactive and REE-bearing mineral aggregates, including minerals of bastnaesite group that contain similar proportions of REE to those in the original mineral (Rimsaite, 1982a, Table 3.2 analyses 4 and 14; Rimsaite, 1982b). However, REE-bearing rims overgrown on monazite are relatively enriched in light REE, especially La (Rimsaite, 1982b, Fig. 31.4).

Epidote group minerals commonly exhibit zoning and intergrowths of various species. Rimsaite (1967, Plate IX-6) illustrated allanite overgrown by epidote in biotite gneiss north of Cape Smith belt, Quebec. Figure 3.3 presents an example of associations between Ca-rich REE-bearing epidote-allanite (A) which contains disseminated specks of thorite (Th) and overgrowths of a Ca-poor Th-bearing phase (Fig. 3.3a,c,d), and an altered allanite partly replaced by REE and Th-bearing mineral aggregates (Fig. 3.3b,e) from area RTN-2 north of Mont-Laurier, Quebec. In the Bancroft area, REE-bearing mineral aggregates containing La/Ce ratios greater than or equal to 1, crystallize as overgrowths and rims on allanite, on uraninite in allanite and titanite, and in fractures in titanite (Table 3.2, analyses 3, 4, 8 11). The La/Ce ratio in allanite ranges between 0.2 and 0.7. Most of the fine grained REE-rich aggregates are amerphous to X-rays (metamict), but some of them yielded weak X-ray patterns indicating mineral phases of hydroxyl-bastnaesite group (Rimsaite, 1982b). Robinson and Hewitt (in Satterly, 1957) reported the occurences of bastnaesite in the Bancroft area but did not discuss its relationship to other minerals.

All REE-bearing phases studied contain variable quantities of silica and some U and Th, suggesting the presence of Si-bearing REE carbonates probably similar to those recently described by Deliens and Piret (1982).

In addition to fine grained REE-rich mineral aggregates, larger grains containing relatively high proportions of neodymium and samarium crystallize adjacent

to allanite (Fig. 3.5b, Table 2 analysis 15); neodymium-rich phases crystallize adjacent to allanite and in rims on uraninite as for instance in radioactive schists and pegmatites north of Mont-Laurier, Quebec (Table 3.2, analyses 16, 17).

Relatively high proportions of europium (0.8 wt. %) were found in rims on uraninite and in altered allanite (Table 3.2, analyses 2, 11 and 14). The results of semiquantitative analyses confirmed the presence of various REE phases characterized by different proportions of La, Ce, Nd and Sm, and by different La/Ce and Nd/Ce ratios which change with the sequence of crystallization (Rimsaite, 1982b; Van Wambeke 1977).

Heavy REE occur in xenotime, in pyrochlore, in metamict Si-U-Y grains and in Y-P-bearing mineral aggregates and amorphous chemically complex phases that succeeded crystallization of tourmaline in high grade ore at the Madawaska mine. Concentrations of 3 to 8% Y are present in P-bearing mineral inclusions in allanite, uraninite and uranothorite (Table 3.2, analyses 6, 7 and Rimsaite, 1982a, Table 3.2 analyses 1, 2, 7, 9, 26, 27).

REE-bearing minerals and crusts are associated and commonly succeed crystallization of uranium and thorium minerals (Fig. 3.6b,c). REE-bearing crusts occur in fractures of many radioactive rocks after solidification and fracturing of rock-forming and accessory minerals (Rimsaite, 1982c, Fig. 3 and Table 2-III).

Although SEM-EDS analyses indicate the occurrence of numerous REE-bearing chemically different phases, because of small grain size and commonly poor state of crystallization or amorphous nature their identification and characterization is insufficient to justify new mineral species. Nevertheless at the present time, the most useful method for identification and study of these complex REE phases is SEM-EDS analysis.

Associations of Primary and Secondary Minerals in Altered Radioactive and Accessory Minerals (Fig. 3.4; Rimsaite, 1982b, Fig. 31.2d)

In addition to calculated atomic proportions of leached and added ions during alteration and replacements of ore and accessory minerals (Rimsaite, 1982b), this paper documents quantitatively additions and losses of various oxides during alterations (Table 3.1, analyses 4, 5, 6).

Table 3.2

Distribution and relative abundance of radioactive and rare-earth elements in host materials, their inclusions and crusts*

	Bancroft area, Madawaska mine (1 to 11)**										Cheddar granite (12-13)**			Mont-Laurier, PP-2 (14-18)**					TDN-2
	1	2	3	4	5	6	7	8	9	10	11	12	13	14	15	16	17	18	19
SiO_2%	29.7	19.0	4.2	8.6	28.2	6.4	27.7	9.9	21.4	1.5	2.9	20.7	3.8	28.6	19.8	2.2	16.4	6.3	2.1
TiO_2	32.5	6.7	1.7	0.8	0.7	0.5	0.3	0.5	2.4	0.4	1.5	9.4	3.5	0.6	0.3	0.0	1.1	7.8	0.0
Nb_2O_5	2.8	2.6	1.0	0.5	0.0	0.0	0.0	0.0	0.0	0.0	0.0	0.0	0.0	0.0	0.0	0.0	0.0	0.0	0.0
Al_2O_3	2.5	2.4	0.9	1.8	9.7	0.0	3.2	2.5	1.4	0.8	0.6	1.5	0.3	16.5	1.9	0.3	3.9	0.9	0.0
FeO***	3.8	2.7	1.7	2.3	15.2	2.4	8.1	10.7	0.8	0.7	1.3	2.7	0.6	7.7	1.2	0.7	2.3	4.3	0.0
MnO	0.4	0.0	0.1	0.0	1.2	0.1	0.1	0.3	0.0	0.2	0.0	0.0	0.6	0.0	0.0	0.0	0.1	0.3	0.0
MgO	0.4	0.2	0.4	0.2	0.0	0.0	0.3	0.0	0.5	0.1	0.0	0.0	0.0	0.0	0.0	0.0	0.0	0.0	0.0
CaO	28.9	4.2	8.6	4.9	11.7	2.3	3.3	6.0	2.4	0.4	1.5	5.2	6.1	10.1	8.0	8.0	0.8	1.2	4.2
K_2O	0.3	0.0	0.2	0.3	0.0	0.0	0.0	0.2	0.0	0.1	0.0	0.0	0.0	0.0	0.0	0.1	0.0	0.0	0.0
P_2O_5	0.0	0.8	0.0	0.5	0.0	3.0	3.6	0.3	0.0	0.0	0.0	1.8	0.3	0.0	0.0	0.0	2.3	0.8	0.9
Y_2O_3	1.2	2.5	2.3	1.1	0.2	5.9	7.5	0.9	0.0	0.0	0.0	3.4	0.6	0.9	1.6	1.1	5.1	0.5	1.5
Yb_2O_3	0.0	0.0	0.0	0.0	0.0	1.2	2.5	0.6	0.0	0.0	0.0	0.0	0.0	0.0	0.0	0.0	0.0	0.0	0.0
Gd_2O_3	0.0	0.9	0.6	0.7	0.2	1.0	0.4	0.4	0.7	0.6	0.4	0.0	0.1	0.3	2.2	0.4	1.2	0.6	0.0
Tb_2O_3	0.0	0.0	0.0	0.0	0.0	0.0	0.2	0.0	0.0	0.0	0.0	0.0	0.0	0.0	0.0	0.0	0.0	0.0	0.0
Dy_2O_3	0.0	0.0	0.0	0.0	0.0	0.2	0.0	0.0	0.0	0.0	0.0	0.0	0.0	0.0	0.0	0.0	0.0	0.0	0.0
Er_2O_3	0.0	0.0	0.0	0.0	0.8	0.1	0.8	0.3	0.0	0.0	0.0	0.0	0.0	0.0	0.0	0.0	0.0	0.0	0.0
La_2O_3	0.0	4.7	24.2	22.7	6.8	12.2	0.0	10.9	1.7	0.0	29.6	0.0	21.0	3.0	5.8	17.3	0.2	0.7	18.2
Ce_2O_3	0.0	6.3	18.0	17.8	9.9	22.6	1.6	10.8	5.1	0.6	25.1	0.9	24.4	7.9	23.0	27.4	3.4	3.1	27.4
Pr_2O_3	0.0	0.4	0.7	1.3	0.7	2.0	0.0	0.7	0.7	0.3	1.5	0.0	1.1	1.0	3.7	2.7	0.8	0.3	4.2
Nd_2O_3	0.0	1.3	1.7	2.7	1.2	5.6	1.0	1.8	1.8	0.8	2.6	0.0	3.6	3.4	15.3	9.0	1.1	1.0	9.8
Sm_2O_3	0.0	0.2	0.0	0.0	0.0	0.6	0.2	0.0	0.5	0.1	0.0	0.0	0.0	0.4	3.1	0.1	0.3	0.3	0.0
Eu_2O_3	0.0	0.8	0.4	0.2	0.0	0.0	0.0	0.0	0.5	0.0	0.8	0.0	0.3	0.8	0.0	0.0	0.0	0.0	0.0
W_2O_3	0.0	0.0	0.0	0.0	0.0	0.0	0.0	0.4	0.0	0.0	0.0	0.0	0.0	0.0	0.0	0.0	0.0	0.0	0.0
ZrO_2	0.0	0.0	0.0	0.0	0.0	0.0	0.0	0.0	0.0	0.0	0.0	4.3	0.0	0.0	0.0	0.0	0.5	0.2	0.0
PbO	0.0	0.4	0.7	0.3	0.0	0.0	0.0	0.4	0.6	7.2	0.0	0.0	0.0	2.9	0.0	0.2	0.0	4.7	0.2
ThO_2	0.0	7.7	1.0	1.5	1.1	1.1	10.3	1.7	34.2	2.8	0.0	32.8	0.0	1.0	0.3	0.6	32.7	11.7	0.0
UO_2	0.0	19.4	0.3	0.8	0.0	0.7	5.0	0.3	20.9	74.5	0.0	2.5	0.0	3.0	0.1	0.4	21.9	28.5	0.0

* Semiquantitative SEM-EDS analysis by G.J. Pringle on spectra collected by D.A. Walker and J. Rimsaite at the SEM Laboratory, Geological Survey of Canada.
** Sample location sketch map published by Rimsaite (1978, Fig. 9.1, 9.2). For notes on analysed spots see Appendix B.
*** Total iron reported as FeO.

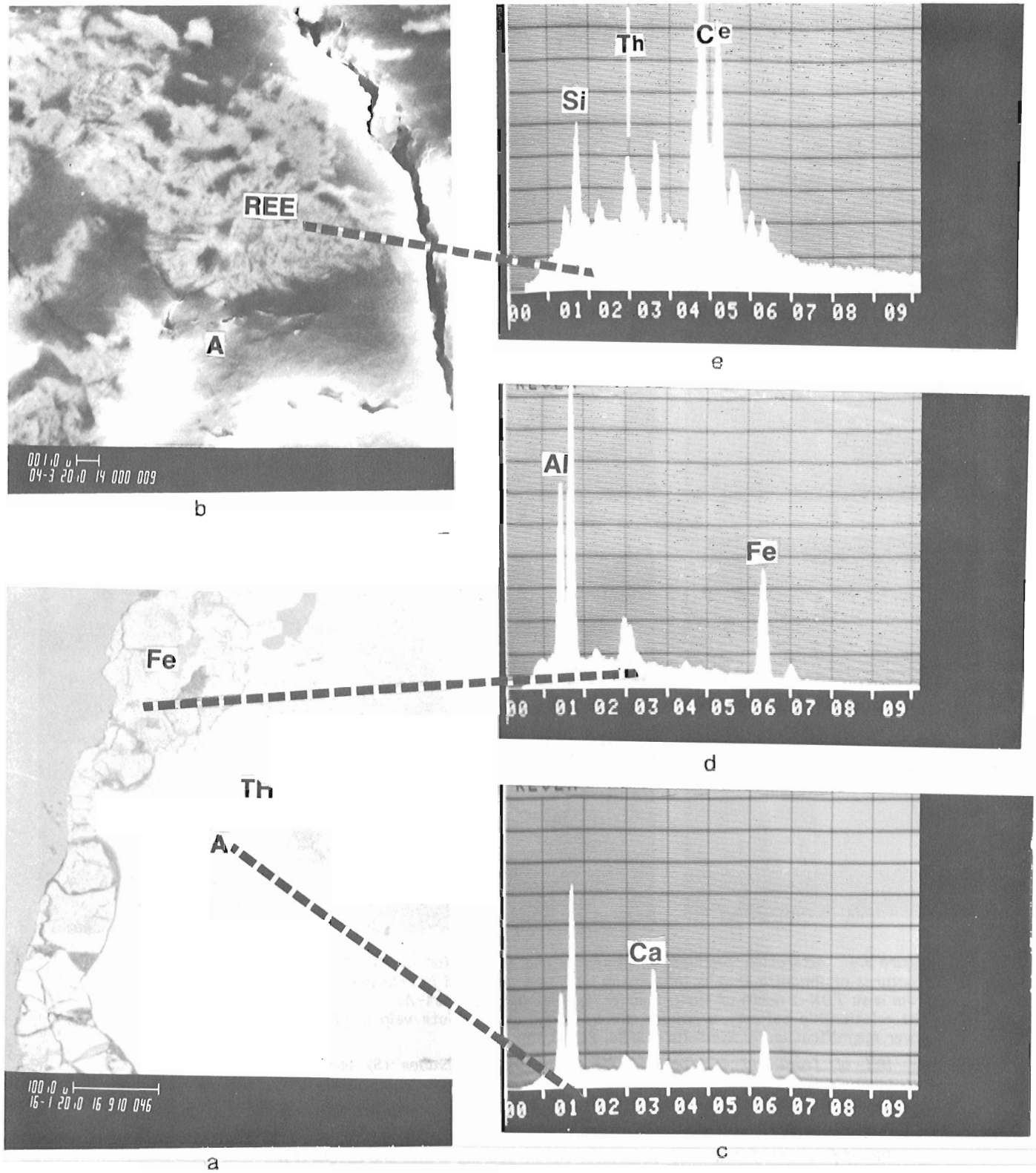

Figure 3.3. *An example of associated, chemically related mineral phases in overgrowths and replacements. The associated minerals are coexistent but not cogenetic. Radioactive REE-bearing mineral associations from area TDN-2 north of Mont-Laurier, Quebec (GSC 203724-D).*

a. BEI of REE-poor allanite, or epidote group mineral (A) which contains thorite inclusions (Th) and overgrowths of radioactive Fe-Th-bearing compound (Fe).

b. BEI of altered allanite (A) partly replaced by amorphous and bastnaesite-hydroxyl-bastnaesite series "REE" aggregates (XRD = 65534, "very poorly crystalline").

c. ED spectrum of epidote group mineral "host allanite" in "a".

d. ED spectrum of Fe-Th-bearing rim on "host allanite" in "a".

e. ED spectrum of poorly crystalline REE-bearing aggregates replacing allanite in "b".

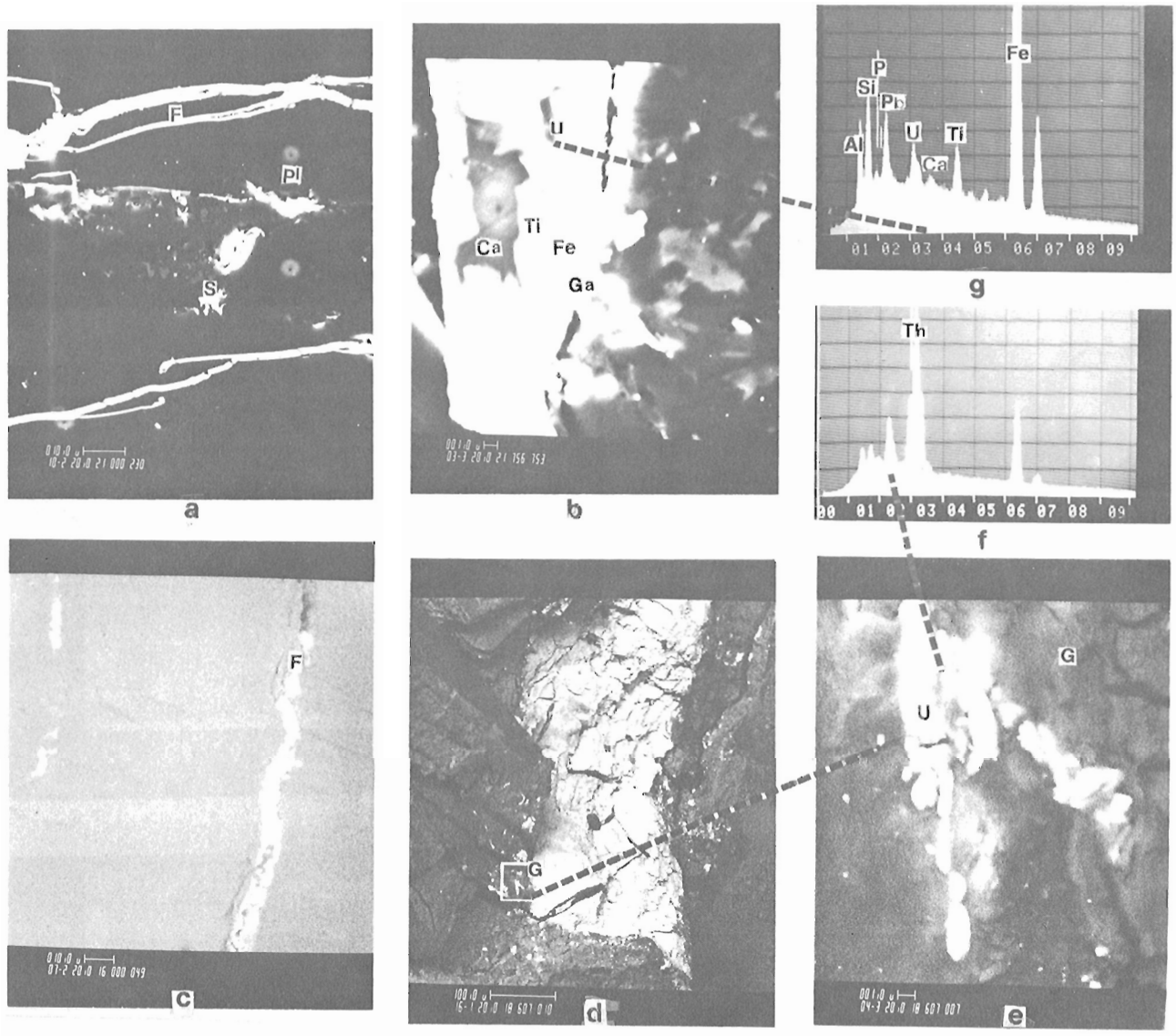

Figure 3.4 *Alteration products of ilmenite and association of Ca, Fe, Ti, Pb and U minerals in fractures of ilmenite that is intergrwon with uraninite and in feldspar in radioactive granitoid rock from area TDN-2 north of Mont-Laurier, Quebec (GSC 203724-A).*
The relationship between uraninite, ilmenite and host epidote vein in plagioclase was illustrated at lower magnification by Rimsaite (1982a, Fig. 3.3b).

a. BEI of fractured plagioclase (Pl) filled with sulphides (S) and with complex Fe-Ti-Ca compounds (F).

b. BEI of ilmenite altered to Ti and Fe oxides that are intergrown with calcite (Ca) and contain disseminated grains of galena (Ga) and U-bearing crusts (U).

c. BEI of fractures filled with radioactive Fe-Ti-bearing crusts and specks (F).

d. BEI of disseminated galena (G) and radioactive specks around thorogummite.

e. BEI of U-rich specks and of galena (G), enlarged from "d".

f. ED spectrum of U-rich specks in "e".

g. ED spectrum of Fe-rich uraniferous crusts in altered ilmenite in "b": Fe > Si > Pb = Al > Ti > P.

During replacement of uraninite crystals by a coffinite-like phase, the uraninite loses about 34 wt. % of its ThO_2, 66% of PbO and gains 100% of SiO_2 and of Al_2O_3, 140% of FeO, 170% of SO_3 and some Ti and K. During further alteration to the unidentified amorphous U-S-bearing phase, the coffinite loses about 77% UO_2, 95% of ThO_2, 92% of Y_2O_3, 90% of SiO_2, 60% of TiO_2; 90% of Al_2O_3, 85% of MnO and gains about 600% SO_3, some Fe, Ca and probably other light elements, such as C, H, OH, O which cannot be detected in ED spectra. It is important to note that the replacement of uraninite by coffinite and by the U-S phase resulted in preferential leaching of Th which to the author's knowledge has not been documented in previous publications. The replacement of uraninite and coffinite by the U-S phase may be cogenetic with crystallization of molybdenite in biotite fractures and in interstices adjacent to the altered grain of uraninite. Although PbO (probably radiogenic Pb) markedly decreased during alteration of uraninite to coffinite, PbO remained unchanged during further replacement by amorphous S-bearing phase, probably due to the strong chemical affinity between Pb and S.

Alteration of the ilmenite portion in uraninite-ilmenite intergrowths from samples collected in radioactive occurrence TDS-2 north of Mont-Laurier, Quebec (Rimsaite, 1982a, Fig. 3.3a,b) involved separation of Fe-rich and Ti-rich phases from the original ilmenite, ilmenite replacement by calcite, and precipitation of galena and of U-bearing phases in coatings (Fig. 3.4b,g). The leached U, Fe and other elements from altered radioactive minerals and associated ilmenite crystallized in fractures of rock-forming minerals (Fig. 3.4a,c,d,e taken from the same polished thin section as in Rimsaite, 1982a, Fig. 3.3a,b, but at higher magnification).

The leaching, migration and reprecipitation of radionuclides derived from altered accessory minerals provide important data on the potential contribution of altered radioactive minerals from granitoid rocks to the formation of other types of uranium deposits. Furthermore, these data on natural behaviour of radioactive and associated elements in altered rocks can be applied to prediction and evaluation of radioactivity hazards in dumps containing uranium mill tailings. It is important to keep in mind that most of the radioactivity and the accessory minerals remain in the tailings. The present study of the behaviour of U, Th, Pb and REE in natural environments indicates that the most stable accessory minerals, such as apatite, xenotime, tourmaline, monazite and zircon alter in hydrous oxidizing and radioactive zones to various secondary minerals and can ultimately be replaced by phyllosilicates and hydroxides, thereby releasing radionuclides from enclosed ratioactive grains and crusts (Rimsaite, 1981a,b; 1982b).

Radioactive and REE Mineral Associations in Mylonitized Quartz-Rich Rocks (Fig. 3.5-3.7)

As can be seen in the geological map of the Bancroft-Haliburton area by the Ontario Department of Mines, map 1957b (Hewitt in Satterly, 1957), the southern part of the Cheddar granite is traversed by east- and northeast-trending fractures and faults. Prominent faults occur also around the Faraday granite and in the Wilberforce area traversing radioactive rocks in the Madawaska, Greyhawk, Bicroft, Dyno and Halo mines. Mylonitized rocks studied include those in the eastern portion of the Cheddar granite containing deformed titanite associated with titanium and iron oxides, zircon, uraninite, uranothorite and secondary radioactive and REE mineral aggregates which are stretched along fractured phenocrysts of plagioclase and microcline perthite and mylonitized quartz veins. Fractured granitoid rocks from the Madawaska mine which contain elongated crystals of allanite with inclusions of rimmed uraninite and uranothorite along veins of mylonitic quartz were also studied. In addition pyrite-rich mylonites from the Halo mine (Fig. 3.5-3.8) were examined. Fractured minerals are also common in radioactive occurrences north of Mont-Laurier, Quebec. In such deformed rocks, fractures in biotite are commonly filled with mobilized U, Ti, Pb, Zr and Fe which precipitated as unidentified chemically complex phases (Fig. 3.7f,g,h). In the deformed rocks, rock-forming and accessory minerals, such as pyroxene, amphibole, plagioclase, biotite, titanite, apatite and uraninite are also fractured and partly replaced by phyllosilicates, carbonates or quartz (Fig. 3.7a,e; Rimsaite, 1982c, Fig. 3A,B,C).

Sulphide-rich samples contain massive and dendritic pyrite, pyrite-chalcopyrite-molybdenite intergrowths and sulphide minerals, commonly pyrite and galena, within accessory minerals and in rims surrounding radioactive minerals (Fig. 3.5, 3.7, 3.8). Deformed grains of allanite and of titanite from the mylonitized zones occur in association with heterogeneous Fe, REE, Th and U minerals. Uranium is present in several mineral species which apparently crystallized before, during and after mylonitization. Uranium-bearing rims on pyrite crystallized after mylonitization (Rimsaite, 1982b, Fig. 31.7a,b,c). A comparison of analyse 7 and 8 in Table 3.1 and analysis 1 in Table 3.2 shows changes in the chemical composition of titanite during reaction with host uraninite in mylonitized pyrite-rich rock. The titanite-uraninite reaction involved addition of uranium to spot "7" (note low Pb/U ratio compared to that in uraninite crystals) and losses of almost all CaO and of significant proportions of SiO_2 and TiO_2. Compared with brannerite-like aggregates from Baie-Johan-Beetz area, Quebec (Rimsaite, 1982a, Table 3.2 analysis 9), the U-Ti-Si phase from Halo mine, Bancroft area, contains more U and Si but less Ti, REE, Fe and no Th. Association between uraninite, uranothorite and overgrowths of galena and uranophane on uraninite provides an example of coexisting U^4 and U^6 phases in the same grain (Rimsaite, 1982c, Fig. 3).

Radioactive bands along the eastern mylonitized edge of the Cheddar granite consist of deformed, partly altered grains of titanite which is in turn partly replaced by chlorite and antase, and contains disseminated specks of uranothorite, uraninite and REE-bearing crusts (Rimsaite, 1982b, Fig. 31.8). The inclusions of uranothorite in the deformed titanite contain less uranium than that in uranothorite from fractured allanite (Table 3.2, analyses 9 and 12). REE-bearing rims on uraninite grain enclosed in titanite and on uraninite enclosed in allanite contain 50.4 and 59.6 wt. % of light REE, or about three times more than in relatively fresh allanite (Table 3.2, analyses 13, 11, 5 respectively). The fresh titanite contains Nb and Y but no REE detecteable by EDS method, and allanite has different proportions on REE which infers that REE in the rims have been derived from an outer source rather than from the host minerals (compare section "3"). A uraninite grain that crystallized within allanite contains less Th than a uraninite grain in biotite (Table 3.2 analysis 10; Table 3.1 analyses 3,4).

In area PP-2 north of Mont-Laurier, Quebec, some radioactive rocks are also fractured and contain pyrite bands overgrown by muscovite filling fractures. In such fractured rocks, biotite is partly replaced by chlorite, and thorite by chlorite and thorobastnaesite (? XRD – 65522).

Uraninite, uranothorite and other inclusions in fractured allanite and in Fe-bearing thorite alter and react with the host, thus producing altered remnants of unusual composition containing REE, U, Th, Ti and other elements (Fig. 3.6b, Table 3.2, analyses 17,18; Rimsaite 1982a, Fig. 3.3f; Table 1, analyses 13,14,15).

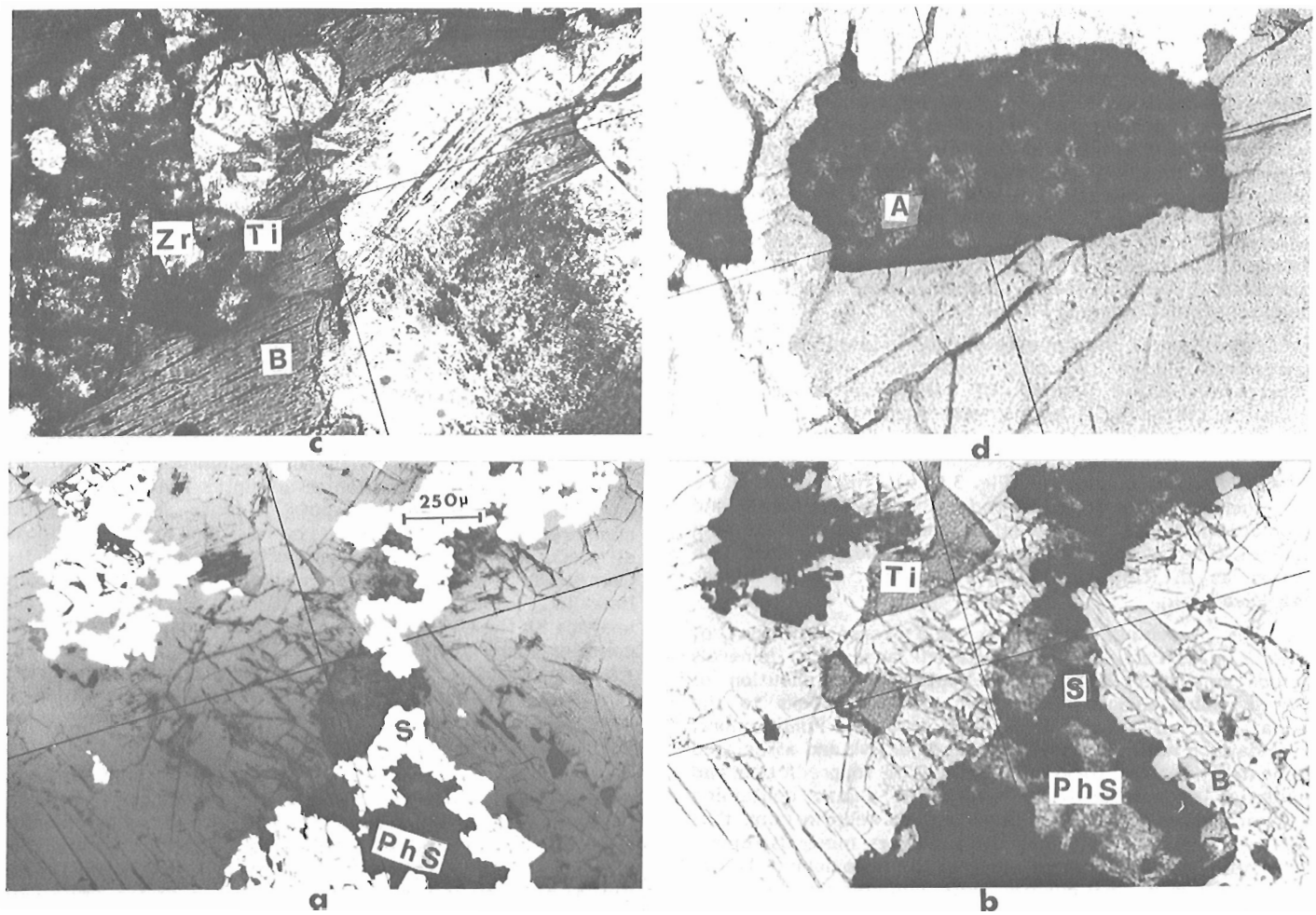

Figure 3.5 *Radioactive mylonitized and hydrid rocks. All photomicrographs are at the same scale as Figure 3.5a. With the exception of "a" which was taken in reflected light, all illustrations were taken in transmitted light.*

a. Sulphides (S) surrounded by phyllosilicates (PhS) in fractures of a mylonitized rock from the Halo mine, Bancroft area, Ontario. Sulphides crystallize after fracturing and engulf earlier-crystallized minerals including uraninite and titanite shown at a higher magnification in backscattered electron images (BEI) by Rimsaite (1982a, Fig. 31.7).

b. The same area as in (a) but photographed in transmitted light. Quartz has partly replaced titanite (Ti) and biotite (B) forming graphic intergrowths.

c. Contact zone between feldspar-quartz pegmatite (right) and recrystallized radioactive biotite schist (B, left) from the Mont-Laurier area, Quebec. Biotite flakes contain prominent pleochroic halos surrounding zircon (Zr), titanite (Ti) and uraninite inclusions (black). This rock contains several types of zircons, similar to those depicted in Rimsaite, 1981b, Fig! 4.4. Preliminary isotope data on an average zircon concentrate yielding point "Z" on the discordia line, indicated a minimum age of 980 Ma for the zircon (Rimsaite, 1982b, Fig. 3.5a,b).

d. Mylonitized radioactive granite in a surface exposure above the Madawaska mine, Bancroft area, contains mylonitized quartz veins and stretched fragments of deformed, radioactive allanite (A). Uraninite, uranothorite and REE-bearing minerals crystallize within allanite crystals and in fractures of adjacent deformed feldspar. Figure 3.6 and Table 3.2 give SEM-EDS analyses of this area, including the distribution of REE, U and Th.

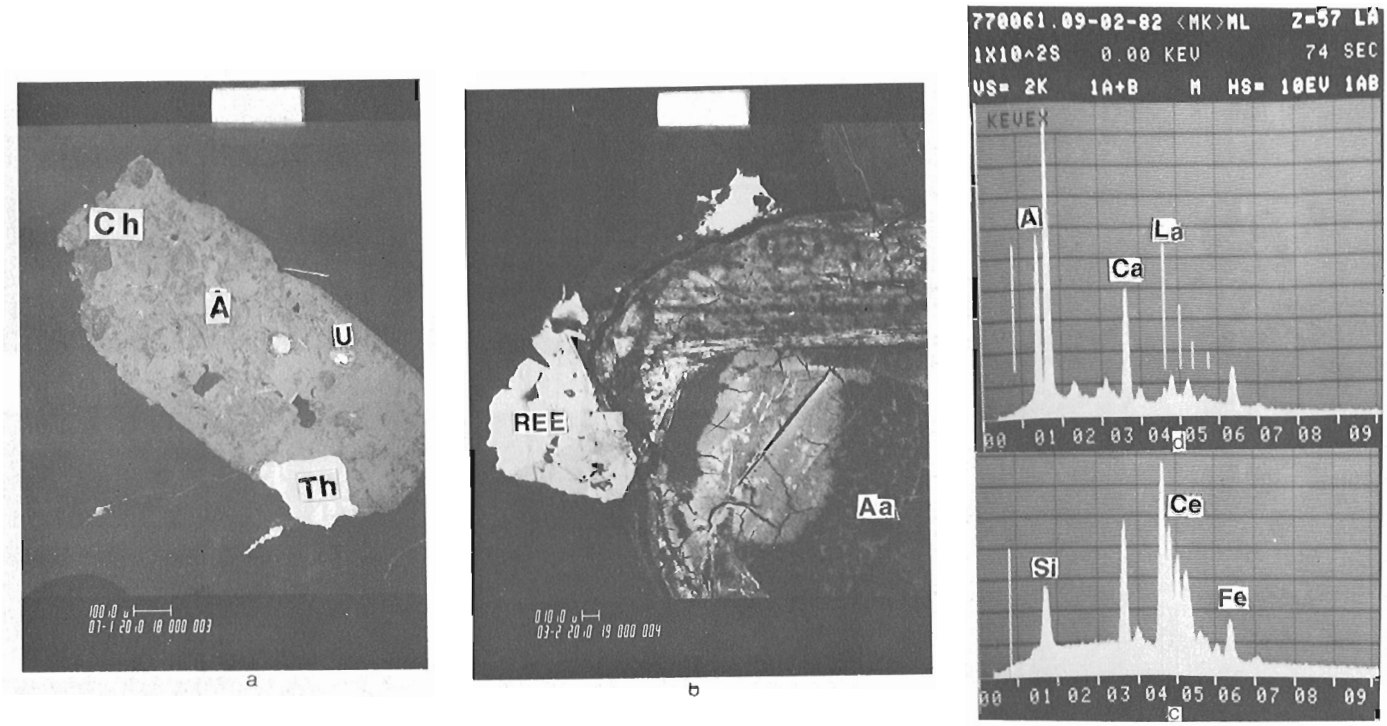

Figure 3.6 *Fresh and altered mineral grains adjacent to, and within allanite (GSC-203724-0).*

a. BEI of allanite (A, grey) with inclusions of uraninite (U), uranothorite (Th) and chlorite (Ch). Inclusions of uraninite and uranothorite are surrounded by REE-bearing rims. The same grain of allanite as in Figure 3.5a.

b. BEI of altered, amorphous allanite (Aa) that contains inclusions of altered uranothorite (Th) and banded Th-REE-bearing rims. Adjacent REE-bearing minerals (REE, white), separated from allanite by fracture, are amorphous to X-rays.

c. ED spectrum of REE-bearing rims on uraninite in (a) with the element line intensities: La > Ce = Ca > Si > Fe.

d. ED spectrum of altered radioactive allanite in (b): Si > Al > Ca > Fe > Ce > La.

Radioactive rocks north of Mont-Laurier, Quebec, fall into two groups. One group is fractured and usually stained red by goethite and iron oxides. It contains predominantly Th with a U/Th ratio of 0.2 or less than 1. The other group contains more U than Th, with a U/Th ratio as high as 4 or more than 1. In the former group, radioactive minerals are altered, oxidized and consist of Fe-bearing thorogummite/thorite (XRD – 65530) which does not contain any uranium detectable by EDS; however, small remnants of altered uraninite inclusions and U-bearing crusts in biotite fractures are present (Table 3.1, analyses 13,15,16; Fig. 3.7f,g). The U-rich group contains uranium in uraninite grains which are commonly enclosed in biotite, in uranothorite and in uranyl-bearing minerals in fractures. In U-rich rocks, thorium is present in uraninite, commonly as a replacing phase, as altered inclusions and crusts filling fractures in uraninite, allanite and titanite, and less frequently as thorite itself (Table 3.1, analysis 10).

The altered and fractured radioactive grains of early crystallization and radioactive and REE-bearing crusts in fractures infer marked leaching, migration and redeposition of radioactive and other elements after fracturing of the rocks.

Summary and Conclusions

Chemical, mineralogical and petrographic studies of radioactive granitoid rocks from the Grenville structural province provided the following additional data on the mode of occurrence, alteration and replacements of radioactive and REE-bearing minerals.

1. Uraninite and uranothorite are present in three types of occurrences: (a) singly in micas, in fractured feldspars, quartz, amphibole and pyroxene rimmed by phyllosilicates, Fe, Pb, Mo sulphides, carbonates, fluorite and REE-bearing bands; (b) in groups associated with zircon allanite, titanite, monazite, xenotime, pyrite, pyrochlore and/or magnetite; or (c) crystallized within accessory minerals, such as zircon, titanite, allanite and phosphates.
2. In some granitoid rocks studied, particularly in mylonitized zones, uranium, thorium and REE occur in early crystallized minerals and in crusts, coatings and in fine grained aggregates which precipitated after fracturing of host rocks.
3. In specimens analyzed here, uraninite crystals contain between 75 and 63 wt. % UO_2; 3 to 8% ThO_2; 7 to 10% PbO; 0 to 1.2% Y_2O_3 and other trace elements in their structure and between 12 and 36% ThO_2; 3 to 38% PbO, and 0 to 7% Y_2O_3, and 0 to 44% of light REE in

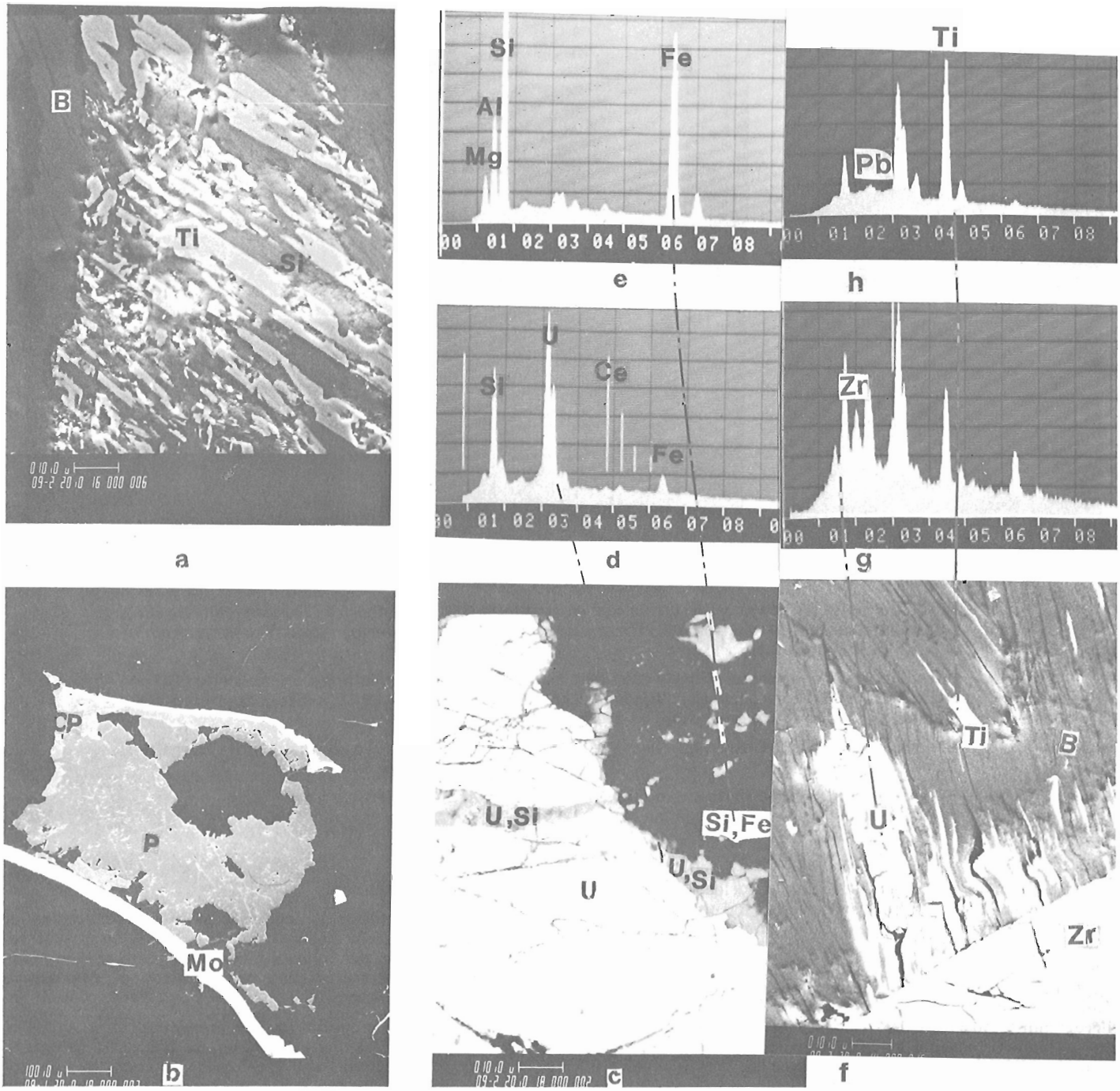

Figure 3.7 *Examples of fractured minerals partly replaced along fractures and edges in mylonitized rocks invaded by sulphides in the Bancroft area. (GSC-203724-Q)*

a. BEI of fractured titanite and anatase (Ti) partly replaced by phyllosilicates (Si).

b. BEI of pyrite (P) that is partly replaced by chalcopyrite (CP) along the edges and overgrown by molybdenite (Mo).

c. BEI of fractured uraninite (U) that is partly replaced by U-Si-bearing phase (U,Si) along fractures and edges.

d. ED spectrum of U,Si-phase in (c): U > Si > Fe > Y > Ce.

e. ED spectrum of Fe-rich rim on uraninite in (c): Si > Fe > Al > Mg > U > Ca > Ti.

f. BEI of fractured biotite (B) adjacent to zircon (Zr) in a fractured rock in the Mont-Laurier area. Chemically complex compounds filling fractures contain mobilized uranium (U), zirconium, titanium (Ti), lead and other ions. In biotite fractures, uranium exceeds thorium content and such U-rich fractures in biotite account for high U/Th ratios in some radioactive rocks in the Grenville structural province (Rimsaite, 1982a, Table 3.1).

g. EDS of U-rich, Pb-Zr-bearing compounds filling fractures in biotite in (f).

h. EDS of Ti-rich, U-bearing compounds in biotite in (f). Semi-quantitative analyses of radioactive and REE-bearing compounds in mineral fractures are given in Table 3.1.

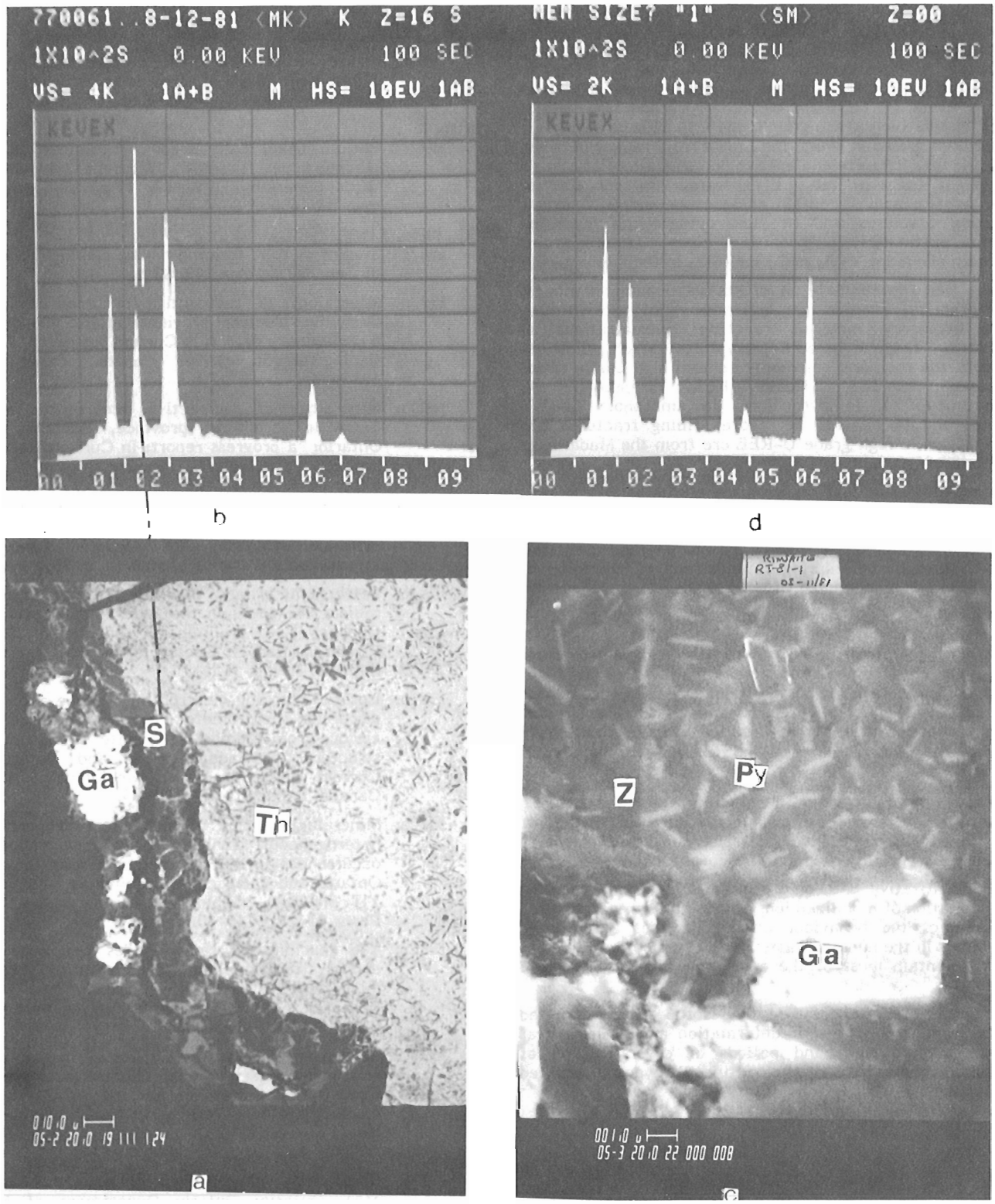

Figure 3.8 *Illustrations of accessory minerals in fractured, pyrite-bearing rocks from the Bancroft area: sulphide-bearing rims on thorite and sulphide blades disseminated in zircon (GSC-203724-I)*

a. BEI of flaky thorite aggregates (Th) overgrown by sulphide-bearing rim (S), including disseminated grains of galena (Ga).

b. EDS of sulphide-bearing rim on thorite-quartz grain in (a): Th > Si > S > Fe.

e. BEI of Fe-S blades (Py) and galena inclusion (Ga, white) in zircon (Z, grey).

d. EDS of S-Ti-bearing rims on zircon in (c): Si > Ti > Fe > S > Nb > U > Th > Al. For identification of element lines in spectra see previous EDS.

replacing phases. Thorite-uranothorite contains between 0 and 20% UO_2; 36 to 50% ThO_2; 0 to 4% PbO, and 0 to 15% UO_2; 0 to 28% ThO_2; and 0 to 44% PbO in replacing phases. Allanite contains between 0.0 and 0.1% UO_2 in the structure of fresh grains and 3% UO_2 in an altered grain; about 1% ThO_2 and of heavy REE and 18% of light REE in relatively fresh grains, and 4 to 16% of light REE in altered grains in which the La/Ce ratio ranges between 0.2 and 0.7. Titanite and apatite do not contain any U, Th and light REE detected in ED spectra. However, titanite and apatite grains contain radioactive and REE crusts coating fractures and in rims overgrowing fractured grains, particularly in mylonitized zones. Titanite grains contain about 1% Y_2O_3 and 3% Nb_2O_5 in their structures.

4. Light REE concentrate in crusts surrounding uraninite, uranothorite, allanite and in fractures of rock-forming and accessory minerals reaching concentrations of 58 wt %. These light REE precipitated after solidification of the rock and commonly contain high La/Ce ratios greater than 1. Heavy REE concentrate in xenotime (50%), in pyrochlore, in amorphous Si-U-Y grains and in mineral aggregates filling fractures and interstices in high grade U-REE ore from the Madawaska mine (8% Y_2O_5).

5. During alteration and replacement of radioactive grains, U and Pb commonly are leached preferenially to Th. However, during certain types and stages of alteration, Th becomes less stable than U and Pb. Marked quantities of Th are leached during replacement of uraninite by coffinite and by an unidentified U-S phase.

6. Most of the REE and Th minerals are metamict or amorphous to X-rays. Therefore, SEM-EDS analysis is the most practical method to detect them and to study their chemical composition. Many unidentified phases of new complex chemical composition have been documented during this study. However, because of small grain size and metamict state, thir detailed characterization to justify new mineral names is not possible at the present time.

7. In radioactive occurrences studied, mineral textures, fracturing, alteration, replacement and redeposition of mobilized U, Th, Pb and REE phases indicate a complex history of crystallization and subsequent alterations.

8. Semiquantitative data on fresh and altered minerals and on migration of mobilized ions along fractures can be used to predict the behaviour of radionuclides and related elements in the nuclear waste and in uranium mill tailings which contain most of the accessory minerals described here.

Studies of stable and radioactive isotopes are warranted to determine the time of deformation and alteration as well as the origin and periods of crystallization of different generations of radioactive, REE and associated sulphide minerals.

References

Deliens, M. and Piret, P.
1982: Bijveetite et lepersonnite, carbonates hydratés d'uranyle et de terres rares de Shiokolobwe, Zaire; Canadian Mineralogist, v. 10, p. 231-238.

Kish, L.
1977: Patibre (Axe) Lake area. Preliminary Report; Ministère des Richesses Naturelles, Service des Gîtes Minéraux, DPV-487, 13 p. and geological map 1:20 000 of DPV-487.

Rimsaite, J.H.Y.
1967: Studies of rock-forming micas; Geological Survey of Canada, Bulletin 149, 82 p.

1978: Mineralogy of radioactive occurrences in the Grenville structural province Ontario and Quebec: a preliminary report; in Current Research, Part B, Geological Survey of Canada, Paper 78-1B, p. 49-58.

1980a: Mineralogy of radioactive occurrences in the Grenville structural province, Bancroft area, Ontario: a progress report; in Current Research, Part A, Geological Survey of Canada, Paper 80-1A, p. 253-264.

1980b: Selected mineral suites and evolution of radioactive pegmatites in the Grenville structural province, Canada; 26e Congrès Géologique International (Paris), Résumés III, p. 999.

1981a: Petrechemical and mineralogical evaluation of radioactive rocks in the Baie-Johan-Beets area, Quebec: a preliminary report; in Current Research, Part A, Geological Survey of Canada, Paper 81-1A, p. 115-131.

1981b: Isotope, scanning electron microscope and energy dispersive spectrometer studies of heterogenesus zircons from radioactive granite in the Grenville structural province, Quebec and Ontario; in Current Research, Part B, Geological Survey of Canada, Paper 81-1B, p. 25-35.

1982a: Mineralogical and petrochemical properties of heterogeneous granitoid rocks from radioactive occurrences in the Grenville structural province, Ontario and Quebec; in Uranium in Granite, ed. Y.T. Maurice; Geological Survey of Canada, Paper 81-23, p. 19-30.

1982b: The leaching of radionuclides and other ions during alteration and replacement of accessory minerals in radioactive rocks; in Current Research, Part B, Geological Survey of Canada, Paper 82-1B, p. 253-266.

1982c: Alteration of radioactive minerals in granite and related secondary uranium mineralizations; in Ore Genesis – The State of Art, ed. G.C. Amstutz, et al.; Springer-Verlag, Berlin, Heidelberg, New York, p. 269-280.

Satterly, J.
1957: Radioactive mineral occurrences in the Bancroft area, Ontario; Ontario Department of Mines, 65th Annual Report, v. 65, pt. 6, 1956, 178 p. and geological map 1957b, Haliburton-Bancroft area.

Van Wambeke, L.
1977: The Karonge rare-earth deposits, Republic of Burundi; Mineralium Deposita, v. 3, p. 373-380.

APPENDIX A

Notes on samples in Table 3.1

1. Uranothorite in allanite (Rimsaite, 1978, Fig. 9.5). Note low concentration of PbO.
2. Uranothorite replacing uraninite (Fig. 3.1, Rimsaite, 1982b, Fig. 31.2c,e,f).
3. Uraninite host to "2". During replacement by uranothorite, the uraninite loses similar proportions of uranium and lead.
4. Uraninite that is being replaced by coffinite and U-S compound (Rimsaite, 1982b, Fig. 31.2d,g). Compare analyses "5" and "6" and note marked losses of Th.
5. Coffinite replacing uraninite "4"; note losses of Pb and Th.
6. Uraninite partly replaced by coffinite alters to an U-S-bearing compound that may contain other additional ions, such as C, H, OH, O or organic matter. Compared with analyses "4" and "5", the uraninite loses U, Th, Y and Mn.
7. Reaction products of uraninite and titanite (Rimsaite, 1982b 31.7b,c,e,f,g). Titanite grain enclosed in uraninite, apparently reacted with U.
8. Rims and U-Si-Ti-Y compounds in fractures of uraninite that contains titanite inclusions "7". Material that moved along fractures contains more Y and Si but less U and Ti than the titanite pseudomorph in "7".
9. Uraninite from mica-rich pegmatite.
10. Iron-thorium-rich inclusion in uraninite. "U". Note abundant Y and Ti.
11. Iron-rich rim on uraninite containing sulphides.
12. Iron-rich crusts between uraninite and biotite grains containing S, Pb and Ti.
13. Fe-bearing thorite.
14. Flaky Pb-S-rich (? galena) aggregates replacing thorite "13".
15. Remnant uraninite in thorite (Rimsaite, 1982a, Fig. 3.3f). The uraninite has been partly replaced by thorite, pyrite and coffinite-like phases. Note abundant Ti.
16. U-Ti-bearing crusts in biotite fractures, Fig. 7f.

APPENDIX B

Notes on analyzed spots in Table 3.2.

Specimens from the Bancroft area are from tourmaline-bearing high grade ore collected underground (spots 1 to 8), from mylonitized rock collected at the surface above the shaft (spots 9, 10, 11), and from eastern edge of Cheddar granite collected in road cuts of highway 648 (spots 12 and 13).

1. Host titanite.
2. Rim on uraninite in titanite "1" (Rimsaite, 1982b, Fig. 31.5).
3. REE-bearing crusts in fractures of titanite "1".
4. Rim on allanite. Note high concentration of La in "3" and "4".
5. Host allanite to "4".
6. Y,P-bearing inclusions in allanite.
7. Amorphous Y,P-bearing groundmass of allanite "5".
8. Allanite and hydroxyl-bastnaesite aggregates along fracture in allanite (Rimsaite, 1982b, Fig. 31.5c).
9. Uranothorite inclusions in allanite.
10. Uraninite inclusion in allanite (Fig. 3.6a). Note relatively low concentration of Th compared to that in other uraninites (Table 1).
11. REE-bearing rim on uraninite "10".
12. Uranothorite inclusion in titanite (Rimsaite, 1982b, Fig. 31.8).
13. REE-bearing rim on uranothorite "12". Specimens from area PP-2 (spots 14 to 18) and from area TDN-2 (spot 19), north of Mont-Laurier, Quebec.
14. Altered allanite containing REE-rich grains near the rim (Fig. 3.6b).
15. Ce, Nd, Sm-rich grain adjacent to allanite "14".
16. Ce, La-rich grain adjacent to allanite "14".
17. Altered inclusion of uranothorite in allanite "14".
18. Altered inclusions of uraninite and titanite in allanite "14".
19. REE-bearing rim on uraninite, similar in chemical composition to "16".

4.

AN INTERIM REPORT ON THE GEOLOGY AND PETROLOGY OF THE MONT SAINT HILAIRE PLUTON, QUEBEC

Project 680071

K.L. Currie
Precambrian Geology Division

Currie, K.L., An interim report on the geology and petrology of the Mont Saint Hilaire pluton, Quebec; in Current Research, Part B, Geological Survey of Canada, Paper 83-1B, p. 39-46, 1983.

Abstract

Mont Saint Hilaire consists of three suites of igneous rocks. The oldest, the Sunrise suite comprises foliated titanaugite-rich melagabbro and jacupirangite, as well as amphibole gabbro and melagabbro. The younger Pain de Sucre suite of biotite trachygabbro, nepheline diorite and nepheline monzonite cuts the older rocks in the form of an external ring dike. The youngest East Hill suite comprises igneous breccia, diatreme-like breccia, and peralkaline syenite and phonolite. Petrochemistry and petrography suggest the two older suites may be related by fractional crystallization or successive partial melting, although a sizeable SiO_2 gap between the suites needs to be explained. The peralkaline rocks seem unlikely to be related to the mafic rocks by either fractional crystallization or liquid immiscibility. They may be a result of remelting of an older alkaline complex.

Résumé

Le mont Saint-Hilaire comprend trois séries de roches ignées. La série Sunrise, la plus ancienne, est composée de jacupirangite et de gabbro mélanocrate feuilletés, riches en titanaugite, de gabbro à amphibole et de gabbro mélanocrate. La série Pain de Sucre, plus récente, est composée de trachygabbro à biotite, de diorite à néphéline et de monzonite à néphéline; elle a la forme d'un filon annulaire externe et recoupe les roches plus anciennes. La série East Hill, la plus récente, se compose de brèches ignées, de brèches en forme de diatrème et de syénite et de phonolite peralcalines. L'analyse pétrochimique et pétrographique suggère que les deux séries plus anciennes pourraient être reliées par la cristallisation fractionnée ou la fusion partielle successive, bien qu'il faudrait expliquer l'important écart observé dans le contenu en SiO_2 dans les deux séries. Les phénomènes de la cristallisation fractionnée ou de l'immiscibilité liquide ne lient probablement pas les roches mafiques aux roches peralcalines. Ces dernières peuvent provenir de la refonte d'un complexe alcalin plus ancien.

Introduction

Mont Saint Hilaire forms a prominent landmark 30 km east of Montreal, a steep, roughly circular massif about 2 km in diameter which rises 350 m above the surrounding lowlands. The mountain consists of alkaline igneous rocks of the Monteregian petrographic province, ranging from gabbroic to dioritic rocks in the west half to peralkaline nepheline syenite and phonolite in the east half. A famous mineral collecting site, the De-Mix quarry (Perrault, 1969), from which many beautiful specimens have been recovered, lies on the northeast flank of the mountain. Despite a voluminous literature on the mineralogy of this site, the geology and petrology of the pluton as a whole remain imperfectly known. The literature is sparse, and generally antiquated, since the only general survey of the complex dates from more than 70 years ago (O'Neill, 1914). Theses by Gold (1963) and Rajasekeran (1966) treated particular aspects of the geology, and their work, together with other relevant work, was summarized by Pouliot (1969). H.M. Aarden mapped and sampled the western half of the pluton during tenure of a research fellowship at Ecole Polytechnique in 1970. I mapped the whole of the mountain in 1971 and 1972 at a scale of 1:6000, using the extensive network of paths, and systematic east-west traverses at intervals of about 100 m. Petrographic and chemical work on my own collections and those of Aarden commenced in 1972. This report summarized the current state of these investigations, which are continuing.

Geology of the Pluton

The Mont Saint Hilaire pluton intrudes calcareous shale, silstone and limestone of the Upper Ordovician Lorraine and Richmond groups (Clark, 1955). A hornfels collar varying in width from 10 to 150 m surrounds the pluton. A pronounced valley extending northward from Lac Hertel (Fig. 4.1) divides the pluton into a western mafic portion, and an eastern salic portion, but detailed mapping summarized in Figure 4.1 shows that the pluton consists of three, rather than two, presumably related, suites of rocks. The oldest suite, here termed the Sunrise suite after a prominent hill northwest of Lac Hertel, comprises melanocratic to ultramafic amphibole-bearing rocks which commonly lack olivine, potassium feldspar and nepheline. The younger Pain de Sucre suite, which locally intrudes the Sunrise suite, comprises more mesocratic and potassic rocks ranging from biotite trachygabbro to nepheline diorite. These rocks consistently contain olivine, nepheline and potassium feldspar. The East Hill suite, which intrudes the other two, consists of leucocratic peralkaline undersaturated rocks ranging from coarse, sodalite-rich syenite and pegmatite through phonolite to various types of igneous breccias. All of the suites exhibit, at least locally, good igneous layering, and a remarkable range of textures. Much of the pluton consists of medium grained massive igneous rock, but indefinite nebulous pegmatitic patches occur in all units, and contacts between units tend to be marked by coarse to pegmatitic zones.

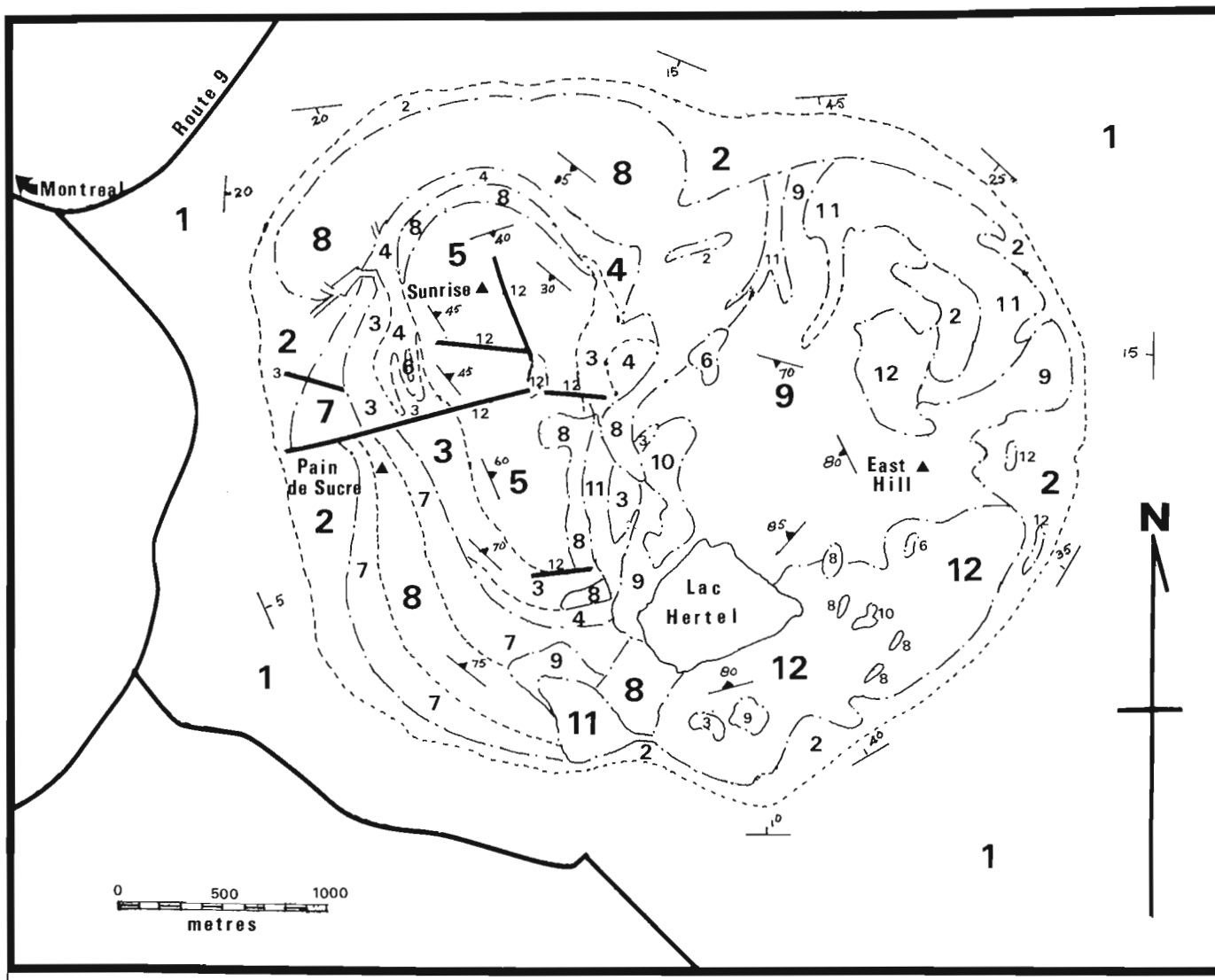

CRETACEOUS

MONT SAINT HILAIRE PLUTON (Units 3-12)

East Hill suite (units 9-12, not necessarily in order of emplacement)

12 Fine grained nepheline syenite, nepheline syenite porphyry and phonolite with trachytoid feldspar, nepheline and sodalite phenocrysts and xenocrysts; locally contains inclusions of units 3-8 and 11; grades to unit 9 by increase in proportion of inclusions

11 Coarse grained peralkaline nepheline syenite and pegmatite with feldspar, nepheline and sodalite phenocrysts; interstitial phonolite

10 Breccia, predominantly of units 2-8 with minor amounts of 9, 11 and 12; fragments well rounded, and locally somewhat altered

9 Igneous breccia; rounded to contorted fragments and xenocrysts of units 3-12 in a trachytoid, opaque-charged matrix similar to 12

Pain de Sucre suite (units 7-8)

8 Nepheline diorite and monzonite; medium- to coarse-grained rocks with tabular to granular plagioclase rimmed by alkali feldspar, interstitial nepheline, and mafic clots containing titanaugite, kaersutite, biotite and olivine

7 Biotite, trachygabbro; lath-like plagioclase with minor alkali feldspar rims, intergrown titanaugite and biotite, olivine and kaersutite

Sunrise suite (suites 3-6)

6 Anorthositic gabbro and leucogabbro; labradorite-rich, foliated titanaugite-magnetite gabbro

5 Amphibole gabbro: strongly foliated coarse grained rocks with minor titanaugite and biotite

4 Amphibole-pyroxene gabbro; moderately to weakly foliated granoblastic rocks with subequal amounts of kaersutite and titanaugite

3 Pyroxene melagabbro and jacupirangite; strongly to moderately foliated medium grained rocks with colour index greater than 60 and abundant magnetite; pyroxenite and perknite

2 Hornfels and metasomatic hornfels; fine grained to aphanitic grey to black quartz-rich, commonly containing abundant dykes

ORDOVICIAN

RICHMOND GROUP

1 Calcareous siltstone and shale, silstone, minor limestone

Strike and dip of bedding

Strike and dip of igneous foliation

Geological contact, defined-approximate, gradational

Geology by K.C. Rajasekeran 1966, H.M. Aarden 1970, K.L. Currie 1971, 1972

Figure 4.1. *Geological map of the Mont Saint Hilaire pluton.*

Description of Units

The Ordovician sedimentary rocks (unit 1) surrounding the Mount Saint Hilaire pluton can be examined in quarries northeast of the mountain, and in rare outcrops elsewhere. At distances of more than 150 m from the pluton the rocks are undisturbed, more or less horizontal, fissile, thin- to medium-bedded calcareous shale and siltstone. In the immediate vicinity of the pluton the sedimentary rocks have been converted to a very tough, homogenous, almost aphanitic grey to black hornfels (unit 2). On the western half of the mountain the contact of hornfels and pluton can be examined on steep rock faces. Where dips can be measured in the hornfels, they are inward toward the pluton, commonly at angles of 15-30°, although local dips are as steep as 70°. The contact is knife sharp. The igneous rocks rarely display any chill zone, and locally appear pegmatitic along the contact. The grade of the hornfels appears no higher than biotite zone within a few metres of the contact, surprisingly low for the margin of a large gabbroic intrusion. On the eastern side of the pluton the contact is poorly exposed, but the grade appears to be even lower, not rising above albite-chlorite zone, although metasomatic phenomena occur in the form of arfvedsonite-bearing hornfels and minute grains of narsarsukite and neptunite which occur as far as 300 m from the contact (Rajasekeran, 1966). In thin section all hornfels specimens consist of a fine grained mosaic of quartz, with varying amounts of albite, muscovite, chlorite, biotite, calcite, and southeast of Lac Hertel, arfvedsonite.

The hornfels collar contains a bimodal dyke suite of green tinguaite similar to unit 12, and mafic to ultramafic dykes similar to units 3 and 5. Hornfels also occurs as large blocks or enclaves in the complex breccia zones north of Lac Hertel, and as inclusions in the igneous breccias of the East Hill suite. High alkali contents of these inclusions suggest that they have been metasomatized (Rajasekeran, 1966).

The Sunrise suite of the pluton (units 3-6) outcrops in an elliptical area elongated from northwest to southeast, at a high angle to the east-west axis of the pluton as a whole. The suite underlies an area about 1700 by 1000 m, truncated to the east and southeast by an intricate maze of breccias of the East Hill suite, and elsewhere by the younger ring intrusion of the Pain de Sucre suite. Rocks of the Sunrise suite can be readily recognized by their melanocratic, moderately to strongly foliated, character. With the exception of some rare (cumulate) anorthositic gabbro, the colour index of the suite exceeds 50, and in some cases approaches 90. Very few of the specimens however, are truly ultramafic (C.I. >90), and the suite is best described as melanocratic gabbro. The most mafic parts of the complex (unit 3) consist of pyroxene melagabbro grading to jacupirangite (titanaugite-magnetite pyroxenite). Rocks of this type form a continuous fringe around the Sunrise sutie, and occur as large inclusions in the East Hill suite. Dykes of similar rocks cut the hornfels collar west of the pluton. In hand specimen the rocks commonly display a felted or trachytoid texture with distinct foliation. They tend to be relatively fine grained (less than 2 mm) and dark brownish black, commonly with rusty tinges. In thin section, pyroxene forms tabular euhedra, which in some specimens are cracked or granulated. The mineral exhibits the pinkish pleochroism, anomalous bluish extinction and low extinction angle typical of titanaugite. Unzoned plagioclase, commonly in the range An_{65-75} with occasional grains of An_{90} according to the Michel-Levy method, forms clusters of interstitial elongate laths noticeably finer grained than the mafic minerals. Trace amounts of olivine occur in only two of 36 sections examined. An amphibole with distinctive brown pleochroism and the optic properties of kaersutite occurs sparsely as adcumulus overgrowths on pyroxene. Opaques, presumed to be titaniferous magnetite, occur as large euhedra, locally reaching 25 per cent by volume. Apatite euhedra tend to be associated with opaques. Sphene occurs in large euhedra only in three specimens, all of which appear to be altered with corrosion of pyroxene, loss of the characteristic pink titanaugite colour, and clouding of feldspar. These observations suggest some deuteric reaction, perhaps

$$3\ CaFeTiSiO_6 + \tfrac{1}{2}O_2 = 3\ CaTiSiO_5 + Fe_3O_4$$

Chemical analyses (Table 4.1) show that this unit is ultrabasic, containing less than 40 per cent SiO_2, more than 5 per cent TiO_2, up to 17 per cent CaO and very high P_2O_5 contents. Presence of fine grained dykes of similar composition demonstrates that these features corresponded to a liquid, although some of the scatter in Figure 4.2 probably results from varying degrees of cumulation of minerals during crystallization of the coarser grained rocks.

The melagabbro grades by increase in the amount of amphibole into amphibole-pyroxene gabbro with roughly equal amounts of amphibole and pyroxene (unit 4). Such rocks form a more or less continuous fringe between the melanocratic gabbro and the amphibole gabbros of unit 5, and locally form the outer fringe of the Sunrise suite. The rocks tend to be more coarse grained and less melanocratic than the melanocratic gabbro. Mesoscopic trachytoid or radiating textures with bluish plagioclase laths up to a centimetre in length are common. In many specimens poikilitic clots of amphibole can be readily identified in hand specimen. Microscopically, the rocks exhibit euhedra of both titanaugite and kaersutite, but the titanaugite euhedra are surrounded by thick mantles of amphibole, and adcumulus (?) amphibole may form large clots up to several centimetres across including pyroxene and plagioclase. Plagioclase occurs in euhedral, unzoned laths. Optical determinations suggest compositions slightly less calcic than the melanocratic gabbro, generally in the range An_{55-65}. A thin selvage of biotite occurs on some amphibole clots, but biotite is rare. Apatite and titaniferous magnetite occur abundantly, in some specimens forming major components, but overall these minerals are less abundant than in the melanocratic gabbro. Chemically the rocks are ultrabasic (Table 4.1) with high contents of TiO_2 and P_2O_5, but the Al_2O_3 and Na_2O contents are noticeably higher than in the melanocratic gabbro, and the CaO and MgO contents marginally lower. No dykes of unit 4 were found during this study, so it cannot be positively stated that these analyses represent liquids.

The most spectacular rocks of the Sunrise suite occur among the amphibole gabbros (unit 5), consisting of plagioclase laths up to 2 cm in length displaying moderate to perfect alignment, with interstitial coal-black amphibole. The most spectacular parts appear on Sunrise hill, but essentially similar, though finer grained and less perfectly foliated rocks form the core of the Sunrise suite. In outcrop, these rocks appear to be fairly typical gabbro, with roughly equal amounts of plagioclase and mafic, and a pronounced ophitic texture. Microscopically the rocks consist of about equal parts of euhedral plagioclase laths (An_{50-60}) and euhedral kaersutite, subordinate augite euhedra rimmed by kaersutite, biotite rims on kaersutite, and magnetite. As with all rocks in this suite, the plagioclase is essentially unzoned, and potassium feldspar, nepheline and olivine are absent. Rocks of very similar mineralogy occur commonly as fine grained dykes in the hornfels west of the Sunrise suite. Chemically the amphibole gabbro resembles other members of the Sunrise suite, although the SiO_2, Al_2O_3 and Na_2O values tend to be slightly higher, and the TiO_2 and MgO values somewhat lower. It is not obvious that variation diagrams against silica are an appropriate way to compare chemical analyses for such ultrabasic analyses, but Figure 4.2 suggests that there are reasonably systematic changes with SiO_2 content, and plots against other variables, such as MgO and CaO, did not significantly reduce the scatter, which probably results from varying degrees of crystal

Table 4.1

Selected chemical analyses of rocks from the Mont Saint Hilaire pluton

	unit 12				unit 11		unit 9				unit 8				
	1	2	3	4	5	6	7	8	9	10	11	12	13	14	15
SiO_2	55.39	59.83	53.78	57.18	57.25	51.65	57.36	54.74	50.39	50.26	53.45	51.47	51.06	51.19	51.70
TiO_2	0.12	0.08	0.29	0.35	0.11	0.19	0.17	0.88	2.40	2.76	2.70	1.17	2.52	2.37	2.73
Al_2O_3	19.56	19.84	21.62	22.51	19.49	15.10	19.32	20.72	19.52	18.29	17.92	24.23	18.37	20.74	17.33
Fe_2O_3	6.07	2.94	2.24	1.69	5.95	1.91	5.22	2.94	2.76	3.32	2.33	1.20	2.42	2.73	2.76
FeO	0.10	0.30	0.51	0.90	0.00	2.32	0.60	1.11	5.62	5.73	6.07	2.20	6.16	4.96	6.20
MnO	0.37	0.26	0.30	0.24	0.42	1.47	0.36	0.28	0.27	0.33	0.25	0.11	0.25	0.26	0.28
MgO	0.21	0.20	0.21	0.34	0.29	2.82	0.13	0.76	2.46	3.02	1.82	1.00	3.02	2.02	3.15
CaO	0.62	0.37	0.64	0.60	0.64	4.43	0.91	1.49	6.51	6.23	4.35	6.71	6.56	6.07	6.60
Na_2O	9.74	8.60	11.52	10.26	11.49	11.88	13.10	9.04	5.52	5.53	5.77	6.31	5.24	5.56	5.02
K_2O	4.53	4.40	5.32	5.30	4.04	2.31	2.31	4.96	2.66	2.41	4.25	2.00	2.52	2.63	2.36
H_2O	2.57	3.14	0.82	0.60	0.51	1.31	0.40	2.84	0.79	1.01	0.51	0.47	0.71	0.71	0.77
CO_2	0.62	0.00	0.71	0.00	0.00	1.40	0.12	0.00	0.10	0.10	0.00	0.11	0.00	0.00	0.00
P_2O_5	0.09	0.02	0.03	0.04	0.00	0.04*	0.00	0.02	0.98	1.01	0.56	2.99	1.15	0.76	1.06

	unit 7				unit 5				unit 4				unit 3			
	16	17	18	19	20	21	22	23	24	25	26	27	28	29	30	31
SiO_2	47.27	48.30	48.39	48.26	41.28	41.56	39.84	41.36	41.42	37.27	36.03	29.94	36.51	37.71	39.56	38.02
TiO_2	3.52	3.37	3.02	3.00	3.85	3.62	4.40	3.59	4.87	5.71	5.71	5.72	6.37	5.70	5.68	5.71
Al_2O_3	17.50	18.59	17.70	20.60	17.91	18.55	16.82	20.07	14.77	17.16	14.11	6.90	14.73	16.54	11.27	12.47
Fe_2O_3	2.97	1.63	3.14	2.49	6.17	3.47	4.30	3.56	6.29	4.87	5.58	10.45	6.65	5.45	6.04	5.57
FeO	6.22	6.84	6.74	6.36	6.89	8.06	8.21	7.23	7.98	8.93	9.85	12.48	7.67	9.45	9.87	10.14
MnO	0.28	0.20	0.29	0.23	0.23	0.22	0.19	0.18	0.30	0.22	0.32	0.35	0.19	0.29	0.24	0.33
MgO	4.78	3.57	3.42	2.69	5.56	6.01	6.51	5.09	4.89	4.67	7.11	10.56	5.93	3.49	7.75	5.88
CaO	9.97	9.29	7.54	7.26	10.42	11.52	12.71	11.21	12.87	15.74	14.82	17.36	17.89	12.43	14.50	13.18
Na_2O	3.36	4.49	5.03	5.47	3.14	3.16	2.90	3.97	2.79	1.73	2.13	0.91	1.23	3.39	1.91	2.33
K_2O	1.63	1.63	2.32	3.09	1.43	1.12	0.90	1.12	0.60	0.30	0.61	0.30	0.10	1.33	0.91	1.22
H_2O	0.81	0.71	0.70	0.59	1.52	1.12	1.11	1.14	0.78	0.71	1.12	1.02	1.02	0.92	1.41	2.53
CO_2	0.41	0.00	0.20	0.11	0.11	0.10	0.49	0.08	0.12	0.00	0.00	0.10	0.00	0.00	0.60	0.00
P_2O_5	1.33	1.34	1.03	0.96	1.52	1.44	1.61	1.39	2.12	2.08	2.60	3.89	1.81	3.26	0.25	2.62

1. Green tinguaite dyke, west of Lac Hertel (specimen #394)
2. Matrix of inclusion-rich nepheline syenite north of Lac Hertel (#419)
3. Olive, fine grained nepheline syenite, south of Lac Hertel (#454)
4. Olive, fine grained nepheline syenite, southeast of Lac Hertel (#451b)
5. Granular white nepheline syenite southwest of Lac Hertel (#71069)
6. Pegmatite sodalite syenite, Dessourdy Quarry (#ES1)
7. Coarse nepheline syenite, west of Dessourdy Quarry (#EX 1)
8. Matrix of igneous breccia north of Lac Hertel (#169)
9. Nepheline diorite northwest of Sunrise hill (#33)
10. Coarse grey nepheline diorite, Pain de Sucre (#58)
11. Very coarse, leucocratic nepheline monzonite, south of Pain de Sucre (#130)
12. Very leucocratic, nepheline-rich diorite northeast of Sunrise hill (#372)
13. Medium grained massive nepheline diorite, south shore of Lac Hertel (#452)
14. Massive nepheline leucodiorite, inclusion, east of Lac Hertel (#480)
15. Coarse nepheline diorite, south of Pain de Sucre (#244)
16. Massive gabbro, bluish, south of Pain de Sucre
17. Massive gabbro, Pain de Sucre
18. Faintly foliated, bluish gabbro with visible biotite, west of Lac Hertel (#13)
19. Gabbro, visible biotite haloes, southeast of Pain de Sucre (#106)
20. Coarse, trachytoid amphibole gabbro, east of Pain de Sucre (#103)
21. Fine grained dyke, north of Pain de Sucre (#119)
22. Fine grained dyke, west of Sunrise hill (#162)
23. Massive, medium grained amphibole gabbro, east side of Sunrise hill (#278)
24. Melagabbro with blotchy, poikilitic amphibole, north of Lac Hertel (#225)
25. Melagabbro with blotchy poikilitic amphibole, east of Sunrise hill (#242)
26. Medium grained, homogeneous melagabbro, southeast of Pain de Sucre (#365)
27. Fine grained, homogeneous pyroxenite or perknite, east of Pain de Sucre (#188b)
28. Fine grained foliated ultramafic, northwest of Lac Hertel (#205)
29. Fine grained dyke, northwest of Pain de Sucre (#220b)
30. Coarse, faintly altered sphene-bearing pyroxenite, southeast of Pain de Sucre (#305)
31. Massive, fine grained black perknite, west of Lac Hertel (#310)

* Analysis includes ZrO_2-2.01; Ce-0.71; La-0.52; Nb-0.92.
Chemical analyses by Rapid Methods Group, Geological Survey of Canada.
Analyses normalized to 100 per cent.

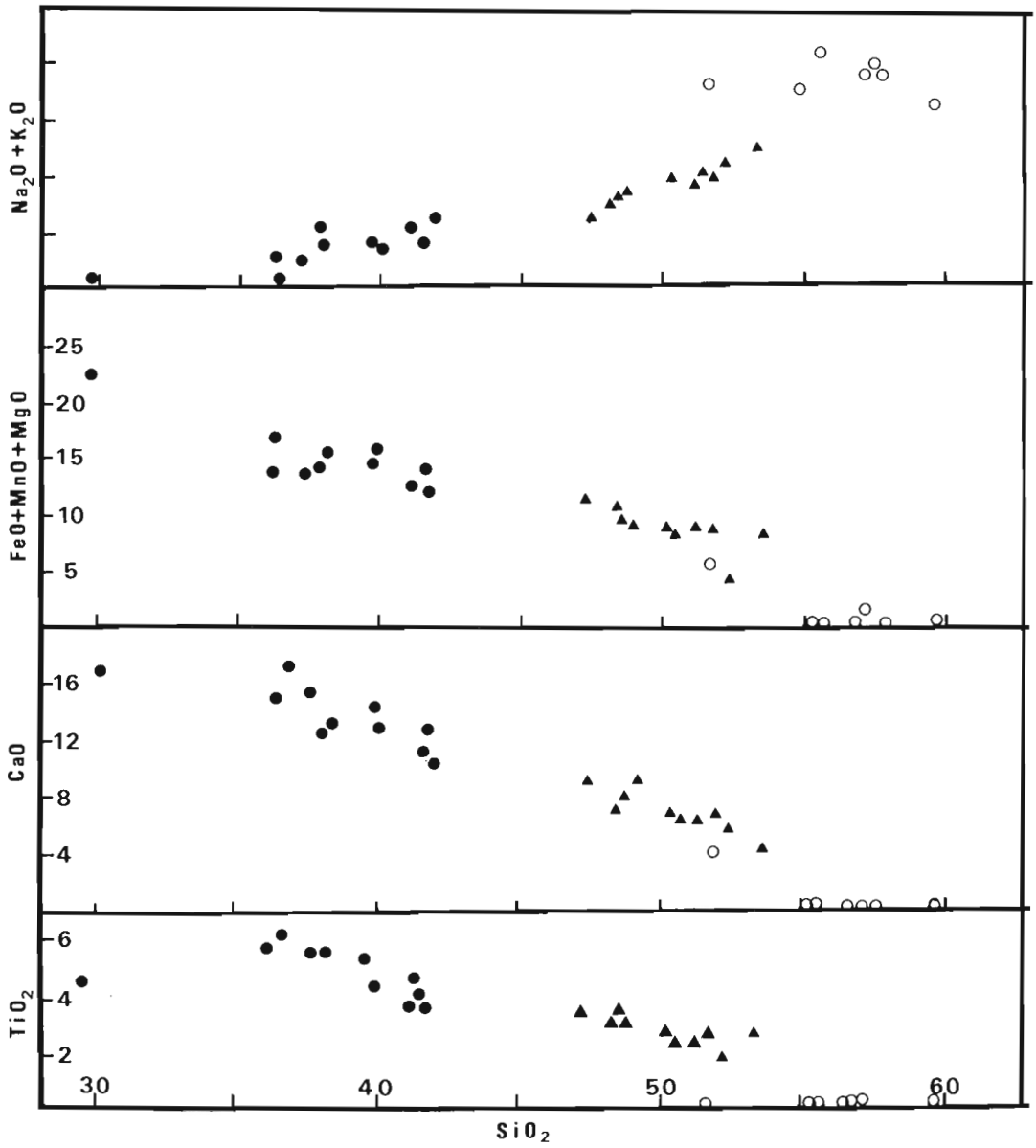

Figure 4.2

Variation of some chemical parameters against SiO_2 for rocks of the Mont Saint Hilaire pluton. Symbols are: solid circles-Sunrise suite, triangles-Pain de Sucre suite, open circles-East Hill suite. Analyses are given in Table 4.1.

accumulation in the coarse grained rocks. Anorthositic gabbros (unit 6) similar in all respects to units 4 and 5 except for a content of plagioclase of 80-85 per cent, form mappable lenticles at two places within the Sunrise suite, and smaller lenticles of calcic plagioclase occur throughout the suite. These occurrences appear to represent extreme examples of crystal accumulation, and hence were not analyzed.

The foliation within the Sunrise suite defines a well-marked pattern, dipping inward at shallow to moderate angles in the northern parts of the suite and at steeper angles to the southeast. The pattern suggests a pipe-like feeder to the north of Lac Hertel, with a scoop-like protrusion to the northwest forming much of the presently visible part of the outcrop.

The Pain de Sucre suite (units 7-8), named from the prominent hill west of Lac Hertel, almost completely encircles the Sunrise suite, forming a high-standing outer ring around the western part of the mountain. The Pain de Sucre suite clearly intrudes the older Sunrise suite on the southern slopes of Sunrise hill, and in the valley north of Lac Hertel, as evidenced by variously assimilated blocks of the older suite in the younger, and dykes of the Pain de Sucre suite cutting the Sunrise suite. Alteration of the older rocks in the form of large euhedra of alkali feldspar occurs along the contact. However dykes of melanocratic gabbro also cut the Pain de Sucre suite, suggesting that the two magmas may have coexisted at depth. No dykes of the Pain de Sucre suite have been found in the hornfels collar of the intrusion, a remarkable observation considering that almost 50 per cent of the contact is between hornfels and rocks of the Pain de Sucre suite.

The older part of the Pain de Sucre suite consists of biotite trachygabbro (unit 7) exposed along the outer edge of the suite in the southwestern part of Mont Saint Hilaire. These rocks are essentially mesocratic, massive, medium- to coarse-grained gabbro, distinguished by low colour index from the melanocratic parts of the Sunrise suite, and by the lack of poikilitic amphibole from the more leucocratic members of that suite. In outcrop the unit rarely shows any foliation, which if present is crude and faint. Microscopically the rocks consist of coarse grained, strongly zoned (from about An_{50-30}) plagioclase with rims of alkali feldspar. Characteristic flesh-coloured titanaugite and biotite occur in about equal amounts as independent but associated euhedral

grains, while magnetite and apatite form the principal accessories. Olivine occurs in accessory amount as partly altered granules. Amphibole locally forms thin selvages on pyroxene. Nepheline does not occur. Chemically the rocks (Table 4.1) exhibit markedly higher SiO_2 contents than the Sunrise suite, along with higher alkali content and lower TiO_2 and MgO contents. They approach the average alkali gabbro of Nockolds (1954), but because of the presence of alkali feldspar, I prefer the name trachygabbro.

The bulk of the Pain de Sucre suite consists of relatively leucocratic coarse grained massive rocks containing significant amounts of nepheline and olivine (unit 8). Traditionally these rocks have been called essexite, or rouvillite in the case of the more nepehline-rich rocks, but the strong objections to these names have been outlined by Gold (1963), and I have elected to term them nepheline diorite and monzonite. In outcrop these rocks are quite variable, ranging from fine grained to pegmatitic within a few metres. Typically, however, they are leucocratic, pale grey, coarse grained rocks with a distinct bluish cast and visible laths of alkali feldspar. Locally textural variations give a crude, vertical to steeply dipping foliation to the rock, but in general the unit is quite massive. In thin section the rocks are dominated by large tabular feldspar laths, often radially arranged, passing gradationally from labradoritic cores through about An_{25} to thick potassium feldspar rims which may be perthitic. Although separate grains of potassium feldspar are rare, the amount of potassium feldspar exceeds plagioclase in many specimens. Nepheline occurs as large interstitial grains, commonly partly to completely altered to cancrinite. Mafic minerals tend to occur as complex polymineralic aggregates involving olivine, titanaugite, kaersutite and biotite. In most rocks titanaugite appears partially replaced by kaersutite and/or biotite, while olivine, although partially altered, seems not to have reacted with other mafic minerals. Magnetite and apatite occur in accessory amounts associated with the mafic clots. Chemically the unit forms a homogeneous group of analyses (Table 4.1) resembling unit 7, but richer in SiO_2 and alkalies and poorer in CaO, FeO and MgO. When plotted on variation diagrams against SiO_2 (Figure 4.2), the trends within the Pain de Sucre suite appear to continue those of the Sunrise suite, but with a marked SiO_2 gap from 41 to 47 per cent. The major minerals, with the exception of alkali feldspar and nepheline, resemble those of the Sunrise suite. The reason for the SiO_2 gap is obscure.

Structurally the Pain de Sucre suite appears to have formed a complete, steeply dipping ring dyke. The portion missing from the southeastern sector can be reconstructed from inclusions in the younger East Hill suite.

The contact between the mafic to intermediate alkaline rocks of the western part of Mont Saint Hilaire and the peralkaline syenites of the eastern part lies in the median valley running north from Lac Hertel, among poorly exposed, complex breccias involving a fragment-charged component (unit 9) which appears to be a hybrid between the mafic alkaline rocks and younger syenites, and a younger suite of diatreme-like breccias which essentially lack igneous matrix (unit 10). The igneous breccia of unit 9 appears to grade continuously into phonolitic to fine grained syenitic rocks (unit 12). Fragments of phonolite and syenite (units 11, 12) occur locally in the breccias, but elsewhere dykes of tinguaite and sodalite pegmatite clearly cut the breccia. One 20 m wide dyke of gabbro, similar to unit 7, cuts breccia north of Lac Hertel. Because of these complex relations, an exact age sequence for the East Hill suite cannot be determined, but all units appear to be of closely similar age.

Igneous breccias (unit 9) form fine grained to aphanitic rocks, charged with myriads of inclusions best seen on weathered surfaces. Inclusions may be stretched and contorted along flow banding, and in many cases appear to be disintegrating. The larger inclusions consist exclusively of older mafic alkaline rocks. The matrix locally show good flow banding, but strong contortion reduces its value for determining structure. In thin section, the matrix consists of trachytoid microlites of sodic plagiclase (albite or oligoclase) charged with minute opaque dust. Pyroxene occurs as equant granules, pale green in rocks most resembling phonolite, and colourless to pale grey in rocks charged with older inclusions. The matrix is charged with cracked and corroded xenocrysts of titanaugite, kaersutite and calcic plagioclase clearly derived from older mafic alkaline rocks. Meaningful chemical analyses from such rocks are difficult to obtain, but one analysis from an unusually homogeneous matrix (Table 4.1) suggests that it represents slightly hybridized peralkaline phonolite. The high TiO_2, MgO and CaO contents probably result from incorporation of older mafic alkaline rocks either as inclusions or by assimilation. The occurrence of a dyke of unit 7 in the breccia suggests that some of the older mafic alkaline rocks remained molten at the time of emplacement of the breccias.

In addition to small inclusions and hybridization, large blocks of mafic alkaline rocks occur as enclaves throughout the igneous breccias, and blocks of phonolite and syenite occur locally. Some of these blocks are readily mappable. Locally the distinction between mafic rocks slightly disrupted by syenitic net veining, and igneous breccia charged with fragments, becomes essentially invisible.

Another phase of brecciation produced rounded fragments of rock densely packed together in a finely granulated matrix (unit 10). This phase of brecciation clearly locally postdates the igneous breccia, for fragments of the latter occur within it. Relations with the peralkaline syenites and phonolites of unit 11 and 12 are less clear, but fragments of such rocks are rare in the breccias, and enclaves of breccia locally appear to be invaded by phonolite. The breccia is highly polymict, containing not only fragments of older alkaline rocks up to 50 m across, but also sizeable blocks of hornfels, and even of little altered sedimentary rocks. Gold (1963) pointed out that unaltered limestone blocks within the breccia contain fossil assemblages ranging in age from Early Ordovician (Trentonian) to Devonian (Helderbergian), compared to the Late Ordovician age of the host rocks at the present level of exposure. These data show that vigorous vertical mixing must have taken place during the generation and emplacement of the breccias, presumably at rather low temperatures in order to preserve the fossils. Such conditions suggest diatreme-like activity, and lend a certain credibility to the traditional view of Mont Saint Hilaire as an eroded volcanic neck (O'Neill, 1914).

The syenitic rocks of Mont Saint Hilaire can be divided into coarse peralkaline syenites and fine grained syenite to phonolite. The coarse grained rocks (unit 11) consist of masses of moderately aligned, tabular alkali feldspar laths with varying proportions of large euhedral nepheline and sodalite, and fine grained interstitial acmitic pyroxene. Pegmatitic patches and schlieren occur locally, commonly richer in sodalite than the surrounding rocks. Coarse grained syenite tends to form a kind of fringe around the eastern side of the Mont Saint Hilaire pluton, but the contacts are very poorly exposed, and the relations of these rocks to the other units are not well defined. Inclusions of the coarse grained syenites occur in the phonolite of unit 12, and well defined, although irregular and discontinuous, dykes of coarse sodalite syenite cut nepheline diorite in the De-Mix quarry. All of the specimens examined contain small but significant amounts of interstitial trachytic matrix similar to unit 12, suggesting that the coarse grained rocks are cumulates from, or cognate xenoliths of, the phonolite and fine grained syenite.

Microscopically, the prominent feldspar laths consist of fine grid perthite, commonly with a thin albitic selvage. The pyroxene is pale green to cinnamon, typical of high acmite content. Nepheline and sodalite look very fresh. About half the specimens contain small euhedra of a distinctive orange biotite, probably close to lepidomelane in such peralkaline rocks (Curtis and Currie, 1981). A large variety of exotic Na-rich silicate minerals have been identified optically and by X-ray in one or more specimens, most commonly eudialyte, catapleiite, lavenite and astrophyllite.

Three chemical analyses of the syenite are given in Table 4.1. The analyses show considerable range in SiO_2, MnO, MgO and CaO, causing Rajasekeran (1966) to give the rocks a variety of names (foyaite, litchfieldite, ditroite and others). The variation probably results mainly from cumulation of various minerals combined with variable metasomatism. The "tawite" (sodalite-rich syenite) of O'Neill (1914) represents very local cumulation of sodalite. Field and petrographic examination show that all these rocks belong to a single unit.

Distinctive olive fine grained syenite and phonolite form a large mass east of Lac Hertel (unit 12). Similar rocks occur widely as deep green, fine grained dykes (tinguaites) both in the hornfels collar, and as a radiating swarm in the Sunrise suite. The rocks consist of a fine grained trachytoid matrix containing large phenocrysts or xenocrysts of feldspar, sodalite and nepheline up to a centimetre across. Some of these rocks have been termed porphyries by other workers, but most of the large crystals appear to be xenocrysts from older rocks. Polycrystalline inclusions of syenite up to 30 cm across also occur, and the phonolite grades to igneous breccia (unit 9) by increase in the number of inclusions and loss of the characteristic colour. Microscopically the rocks consist of a felted mass of alkali feldspar microlites and granular greenish pyroxene. Some specimens contain small amounts of orange biotite. The same "exotic" Na-rich minerals seen in the coarse grained rocks have been identified in phenocrysts. Sodalite, nepheline and natrolite occur interstitially. Large crystals of these minerals are badly cracked, severely altered, and commonly granulated on the edges. They appear to be xenocrysts from slightly older syenites.

Chemically, the phonolites are rather more homogeneous than the syenites (Table 4.1), with extreme Fe^3/Fe^2 ratios (but no oxide in the mode) and lower Na/K ratios than the syenites. The latter may be due to loss of Na by metasomatism, as suggested by arfvedsonite hornfels and the presence of (metasomatic) sodalite in mafic alkaline rocks in contact with the phonolites. When plotted on variation diagrams (Fig. 4.2) the phonolites and syenites show a chemistry distinctly different from that of the older nepheline diorites and monzonites of similar SiO_2 content.

The phonolites exhibit well developed flow banding which converges toward a centre just north of Lac Hertel, that is toward the same region defined by foliation in the mafic rocks. The data would be compatible with a cone sheet type of intrusion dipping inward at angles of 70-80°.

Origin and Development of the Pluton

The Mont Saint Hilaire pluton poses a number of fascinating petrological problems. Before turning to the very difficult problem of explaining the chemical variations, it is instructive to consider the structure of the pluton. Inward dips of strata are common around Monteregian plutons, and Philpotts (1969) proposed an ingenious explanation involving partial melting of the surroundings by the pluton, causing collapse as the hybrid anatectic melt was withdrawn. This explanation seems unlikely to hold at Mont Saint Hilaire because (a) the hornfels collar is of relatively low grade, and (b) there is no evidence of hybridized anatectic melt (such as the norites of Rougement and Mont Bruno). Rajasekeran (1966) reported a 15 cm "granite" sill east of the pluton, but I consider this fenitization feature connected with emplacement of the syenites. I therefore assume that the inward dips represent a partial collapse of the region during or prior to emplacement, so that the Sunrise suite filled a pre-existing or developing void. Similar explanations have been offered for the shape of lopoliths (Carmichael et al., 1974, p. 261). Unlike lopoliths, the layering of the Sunrise suite cannot be due entirely to cumulation, since dykes of similar conposition are abundant. However compositional variation might result from successive additions of magma from a subjacent differentiating magma chamber. On this model the later intrusion of the Pain de Sucre suite as a ring dyke might be explained by renewed subsidence of the central part of the intrusion, forcing magma up the bounding fracture. The Pain de Sucre suite could then exhibit the observed crosscutting relations and a compositional gap due to an indefinite interval of differentiation at depth whose products are not represented at the present level of exposure.

A quite different type of mechanism seems necessary to explain the emplacement of the East Hill suite, which must have been emplaced into a thoroughly disrupted region of older alkaline and country rocks. The initial period of emplacement of igneous breccia apparently involved advance of phonolite magma through thoroughly heated and shattered material, since the large-scale hybridization and assimilation of the mafic alkaline rocks seems to require that they must have been very hot relative to the almost unaffected sedimentary fragments. This initial period of emplacement may have ended catastrophically with explosive venting of gases to the surface and formation of the diatreme-like breccias of unit 10. Finally, phonolite magma seems to have again passively invaded open spaces and enveloped blocks of varying sizes, but with less assimilation than previously.

Geochronological control on this sequence of events must be considered so weak as to be virtually absent. Fairbairn et al., (1963) determined a Rb/Sr age on biotite from "essexite" of 99.5 ± 4 million years. This age seems rather low compared to the roughly 120 Ma ages determined for other Monteregian hills. No data exist to estimate the range in time covered by the three suites of the intrusion. Comparison with other relatively high-level igneous complexes suggests that an intrusion history of 5-10 Ma might be reasonable.

The trends of foliation of both mafic and salic fractions of the Mont Saint Hilaire pluton strongly suggest that they stemmed from a relatively small pipe-like region north of Lac Hertel. Together with confinement of the alkaline rocks to a single pluton, mutual crosscutting relations among the three suites, and evidence that all components were hot at the same time, these relations suggest a single origin for all the alkaline rocks. On the other hand, the petrographic and chemical differences between the three suites are sufficiently large that a unified origin clearly presents problems. Three explanations might be offered to explain the connection of the mafic and salic parts of the pluton, namely (a) differentiation from a single parent by crystal fractionation, (b) differentiation by liquid immiscibility, and (c) presence of separate but cognate magmas.

In support of differentiation by crystal fractionation may be mentioned the more or less regular trends on variation diagrams (Fig. 4.2) in the mafic part of the complex, and the observed similarity of the minerals (titanaugite, kaersutite, plagiclase, magnetite). The significance of crystal fractionation cannot be quantitatively assessed without detailed data on mineral chemistry which are now being collected, but in principle there seems no difficulty in explaining the variation of the mafic rocks in

this way. The cumulates required to cause liquid compositions to pass from melanocratic gabbro to amphibole gabbro must be assumed hidden beneath the present exposure level, and any liquids in the observed SiO_2 gap assumed confined to unexposed regions. There seems to obvious way to pass by crystal fractionation from the nepheline diorite to peralkaline syenite of the same silica content. Very abrupt changes in TiO_2, CaO, MgO, alkali levels and agpaitic index suggest some process other than crystal fractionation. Indeed the extreme ZrO_2, MnO and rare earth element concentrations in the peralkaline rocks suggest that crystal fractionation could not produce the observed volume of syenite from any reasonable volume of initial gabbroic fluid.

One alternative for producing contrasting chemical compositions is liquid immiscibility. Currie (1972) pointed out that empirical criteria suggest that the peralkaline phonolite would be immiscible with nepheline diorite. The apparent coexistence of tinguaite and trachygabbro dykes could be explained in this way. Unfortunately the distribution coefficients for ZrO_2 and rare earths, although imperfectly known, seem to preclude the observed extreme enrichment in the syenitic fraction (Freestone, 1978). Other evidence against immiscibility includes (a) complete lack of textural evidence such as ocelli, presence of the same mineral in two fractions and the like (Ferguson and Currie, 1971), and (b) evidence for hybridization in the igneous breccias.

If the above alternatives are rejected, then more than one magma must be involved. This idea is not incompatible with some versions of either of the two previous mechanisms, and the three possibilities should be considered complementary rather than mutually exclusive. The syenitic fraction might arise by anatexis of deep crustal rocks by heat derived from intrusion of the mafic rocks. This mechanism seems to involve the same difficulties with extreme compositions as the first two. However older alkaline rocks in the general region of Mont Saint Hilaire are well known (Currie, 1970), and a reworking of older alkaline rocks by partial melting may be the most reasonable way to derive aberrant peralkaline rocks, in the same fashion that repeated anatexis of granitoid crust gives rise to peralkaline granites (Collins et al., 1982).

Whatever the mechanism(s), clarification will clearly require data on mineral chemistry and good quality trace element data, as well as sophisticated application of mixing and fractionation models. These data are now being acquired, and will be reported in future applications.

Acknowledgments

This study could not have been made without the notes, maps and specimens of H.M. Aarden, kindly provided by Guy Perrault of Ecole Polytechnique, Montreal. I am also indebted to Gaston Pouliot of Ecole Polytechnique for a lucid introduction to the geology of Mont Saint Hilaire. Ecole Polytechnique provided office and laboratory facilities in 1971-72. The administration of the Gault Donation of McGill University gave permission to map on Mont Sanit Hilaire.

References

Carmichael, I.S.E., Turner, F.J., and Verhoogen, J.
1974: Igneous Petrology: McGraw-Hill Book Company, New York, 739 p.

Clark, T.H.
1955: St. Jean-Beloeil area; Ministère des Richesses Naturelles de Quebec, Geological Report, v. 66.

Colling, W.J., Beams, S.D., White, A.J.R., and Chappell, B.W.
1982: Nature and origin of A-type granites with particular reference to southeastern Australia; Contributions to Mineralogy and Petrology, v. 80, p. 189-200.

Currie, K.L.
1970: An hypothesis on the origin of alkaline rocks suggested by the tectonic setting of the Monteregian Hills; Canadian Mineralogist, v. 10, p. 411-420.

1972: A criterion for predicting liquid immiscibility in silicate melts; Nature Physical Sciences, v. 240, p. 66-68.

Curtis, L.W. and Currie, K.L.
1981: Geology and petrology of the Red Wine Alkaline Complex, central Labrador; Geological Survey of Canada, Bulletin 294, 61 p.

Fairbairn, H.W., Faure, G., Pinson, W.H., Hurley, P.M., and Powell, J.L.
1963: Whole rock age and discordant biotite in the Monteregian igneous province, Quebec; Journal of Geophysical Research, v. 68, p. 6515.

Ferguson, J. and Currie, K.L.
1971: Evidence of liquid immiscibility in alkaline basic dykes from Callander Bay, Ontario; Journal of Petrology, v. 12, p. 561-585.

Freestone, I.C.
1978: Liquid immiscibility in alkali-rich magmas; Chemical Geology, v. 23, p. 115-123.

Gold, D.P.
1963: The relationship between the limestones and the alkaline igneous rocks of Oka and St. Hilaire, Quebec; unpublished Ph.D. thesis, McGill University.

Nockold, S.R.
1954: Average chemical composition of some igneous rocks; Geological Society of America, Bulletin, v. 65, p. 1007-1032.

O'Neill, J.J.
1914: St. Hilaire (Beloeil) and Rougement Mountains, Quebec; Geological Survey of Canada, Memoir 43.

Perrault, G.
1969: Mineralogy at Mont St-Hilaie, P.Q.; in Geology of Monteregian Hills, ed. G. Pouliot; GAC/MAC Annual Meeting Guide Book, p. 103-115.

Philpots, A.R.
1969: Geology of Mount Rougement; in Geology of Monteregian Hills, ed. G. Pouliot; GAC/MAC Annual Meeting Guide Book, p. 77-84.

Pouliot, G.
1969: Notes on the geology of Mont Saint Hilaire; in Geology of Monteregian Hills, ed. G. Pouliot; GAC/MAC Annual Meeting Guide Book, p. 93-102.

Rajasekeran, K.C.
1966: The petrology of the nepheline syenites at Mount St. Hilaire; unpublished Ph.D. thesis, McGill University.

5.

A PRELIMINARY REPORT ON THE GOLD CONTENT OF SULPHIDE SEPARATES FROM SOME CANADIAN BASE-METAL DEPOSITS

Projects 740107, 740043

I.R. Jonasson[1] and D.F. Sangster[2]

Jonasson, I.R. and Sangster, D.F., A preliminary report on the gold content of sulphide separates from some Canadian base-metal deposits; in Current Research, Part B, Geological Survey of Canada, Paper 83-1B, p. 47-52, 1983.

Abstract

Samples of sphalerite, galena, chalcopyrite, pyrite and pyrrhotite separated from ore samples from several Canadian sulphide deposits and occurrences were analyzed for gold, silver, arsenic, antimony, selenium, tellurium and bismuth. There are some interesting distributions and trends within certain mining camps. Arsenic and gold are closely associated in chalcopyrite from the Opemiska-Chibougamau and Matagami regions; selenium is an important accessory. The Abitibi greenstone belt deposits are also enriched in arsenic and gold with minor antimony levels in some samples. Chalcopyrite is the most important mineral host for gold except at Manitou-Barvue where galena is also important. Limited analyses for bismuth in association with gold show it to be unusually abundant in the vein deposits of the Bathurst, N.B. area and in the volcanogenic massive sulphides from Sturgeon Lake and Uchi Lake areas of Ontario. Most other vein deposits carry more antimony than arsenic and are enriched in silver rather than gold.

Résumé

Des échantillons de sphalérite, de galène, de chalcopyrite, de pyrite et de pyrrhotine extraits de minerais provenant de plusieurs venues et gisements de sulfure au Canada ont été analysés afin de déterminer leur teneur en or, en argent, en arsenic, en antimoine, en sélénium, en tellure et en bismuth. On retrouve des répartitions et des tendances intéressantes dans certains camps miniers. L'arsenic et l'or sont étroitement associés dans la chalcopyrite des régions d'Opemiska-Chibougamau et de Matagami; le sélénium est un minéral accessoire important. Les gisements de la zone de roches vertes d'Abitibi sont également riches en arsenic et en or; certains échantillons renferment des quantités mineures d'antimoine. La chalcopyrite est l'hôte minéral le plus important de l'or sauf à Manitou-Barvue où la galène est également importante. L'analyse limitée du bismuth associé à l'or montre que ce minerai est extraordinairement abondant dans les gisements filoniens de la région de Bathurst (N.-B.)et dans les sulfures massifs d'origine volcanique des régions de Sturgeon Lake et d'Uchi Lake en Ontario. La plupart des autres gisements filoniens contiennent plus d'antimoine que d'arsenic et sont riches en argent plutôt qu'en or.

Introduction

In view of the current high interest in locating new sources of gold in Canada, we have published in this preliminary report all data presently available in our files on gold contents of sulphide separates. Samples were gathered from mine sites and surface occurrences by the authors and commodity geologists of the Economic Geology Division. In some cases composite monthly concentrates of zinc, copper or lead sulphides were analyzed; these are indicated in the tables by an asterisk. From most deposits, ore specimens considered typical of the higher grade portions of the sulphide bodies were collected and subjected to physical separation of the constituent base metal sulphides. Various combinations of electromagnetic separation, super-panning and hand picking were employed. Although we aimed for better than 98 per cent purity in separates, this was not commonly achieved in the case of sphalerite- pyrite separations, where cross-contamination of up to 10 per cent was not unusual in fine grained ores. Galena and chalcopyrite separates were generally found to be better than 98 per cent pure by microscope inspection of grain mounts. The presence of sulphosalts was suspected, most commonly in galena separates. To aid in estimating the proportions of sulphosalts and to facilitate interpretation of gold contents measured, analyses are also presented for silver, arsenic and antimony, and for selenium, tellurium and bismuth where available. Since these elements are commonly associated with gold in its deposits, and the last five elements are often implicated in the mechanisms by which gold may be transported and emplaced, these data may also yield a few clues on mechanisms of ore genesis. Readers are invited to make their own interpretations. Information on the average grades for gold and silver in many of the massive sulphide deposits listed can be found in Divi et al. (1980) and Boyle (1979). Reference to such information, in this present work, is to these publications.

The data presented are divided into three separate genetic categories of sulphide deposits:

1. miscellaneous veins;
2. volcanogenic and massive;
3. sediment-hosted.

Within each broad category, deposits are surther subdivided into Archean, Proterozoic and Phanerozoic age groups. Some of these deposits may be misplaced genetically or in time, but the divisions are considered to be the best representation of our current knowledge. Deposits of doubtful classification (e.g., Prairie Creek, Western Nuclear and Sulphide Lake) are marked in the tables by a dagger (†). In general the main problem has been to choose whether a given deposit is a massive sulphide which has been remobilized, or a vein deposit. The decision is particularly difficult when the options are massive sulphide stringer ore or true vein ore; for example, in Louvem, Akasaba and Dunraine deposits of the Val D'or region, Quebec. These particular deposits have been marked with a sharp (#), rather than a dagger.

[1] Resource Geophysics and Geochemistry Division
[2] Economic Geology Division

Methods of Analysis

Gold analyses were carried out by Bondar-Clegg and Co., Ottawa. Samples of sulphide separates or concentrates of 1 to 5 g were subjected to conventional fire-assay treatment and the resultant bead dissolved in aqua regia. Gold was determined by flameless atomic absorption spectrometry following electrothermal volatilization in a graphite furnace. Limit of detection was 5 ng/g for a 5 g sample.

Silver and bismuth was determined in our laboratories by atomic absorption spectrometry following sample decomposition in concentrated HCl (for galena) or by repeated aqua regia attack (for chalcopyrite, pyrite, pyrrhotite, sphalerite and magnetite).

Arsenic and antimony were determined in our laboratories in part by colorimetric methods and in part by flameless atomic absorption methods following concentrated acid decomposition of the samples (as above) and generation of the appropriate metalloid hydride.

Table 5.1

Gold content of some Canadian vein sulphide deposits

Name of occurrence	Location	Host rock	Ore type	Mineral	No.	Au (g/Mg) Range	Au (g/Mg) Arith. mean	Arithmetic mean of some associated elements (g/Mg) Ag	As	Sb	Se	Te	Bi
ARCHEAN													
Severn River	N. Ont.	volcs.	Cu-Zn	sp	1	-	0.015	66	8	54			12
				gn	1	-	0.060	404	1	470			12
Berens River	N. Ont.	volcs.	Pb-Zn	sp	2	5.42 - 8.12	6.77	620	22	340			12
				py	3	0.47 - 88.66	32.70	77	1805	463			<10
North Spirit Lk.	N. Ont.	volcs.	Pb-Zn	sp	1	-	0.350	220	1	150			<10
Wilkinson Lk.	N. Ont.	volcs	Pb-Zn	sp	1	-	18.68		1	25			
Thunder Bay Amethyst Mine	N. Ont.	grnt.	Cu	cp	1	-	0.110		2	1			
				py	1	-	0.100		273	1			
Regan Lk.	Mack.	gnss.(?)	Cu	py	2	-	0.001	7	19	3	5	3	<10
Tommie Lk.	Mack.	grnt.	Cu	py	3	0.04 - 15.74	5.58		87	10			
				cp	3	0.08 - 10.07	3.41		30	58			
				mt	4	0.035 - 1.24	0.46	39	39	24			
Bode Lk.	Mack.	grnt.	Cu	py	5	0.160 - 2.81	0.74						
Louvem #	W. Que.	volcs.	Cu-Zn	sp	2	0.29 - 0.53	0.41		37	3			<10
				cp	1	-	0.14	58	21	5			<10
				py	9	0.22 - 2.36	0.81		310	4			<10
Conigo	W. Que.	volcs.	Cu-Zn	sp	2	0.04 - 0.05	0.05		18	1			
				cp	15	0.11 - 0.74	0.35		41	2			
				py	6	0.10 - 4.00	0.88		714	1			
Louvicourt Goldfields	W. Que.	volcs.	Cu, Au	cp	1	-	67.9	185	8000	6000			<10
				mt	2	3.40 - 4.28	3.84		7	1			
Akasaba #	W. Que.	volcs.	cu, Au	cp	1		5.20		6	2			
				po	3	0.12 - 2.76	1.01		3	2			
				mt	4	0.86 - 7.56	3.27		2	2			
Dunraine #	W. Que.	volcs.	Cu, Au	cp	12	0.11 - 1.33	0.52		12	2			
				py	14	0.15 - 5.64	1.48		247	1			
Opemiska	Que.	meta-gabbr.	Cu, Au	cp*	5	4.30 - 6.40	5.18	87	100	11	69	4	< 8
Patino	Que.	meta-anrs.	Cu, Au	cp*	5	16.0 - 20.0	18.0	81	260	5	62	18	< 8
Campbell-Chibougamau	Que.	meta-anrs.	Cu, Au	cp*	9	4.50 - 31.0	25.6	86	670	2	64	12	< 8
PROTEROZOIC													
Cobalt area (Silverfields)	N. Ont.	seds.	Pb-Zn, Ag	sp	4	0.180 - 0.600	0.34	730	133	398			<10
				po	2	0.001 - 0.090	0.41	20	96	7			<10
Nth. Contact Lk.	N. Sask	volcs.	Cu-Zn	sp	1	-	13.10	300	27	245			<10
Terra Silver Mines	Mack.	seds.	Ag, Cu	sp	1	-	0.13						
				py	3	0.001 - 0.025	0.017				2	2	
				cp	1	-	0.310				27	4	
Norex Prop.	Mack.	seds.	Pb-Zn, Ag	sp	1	-	0.070		8	1			
				cp	2	0.001 - 0.020	0.010		581	1027			
				gn	1		0.020		13400	915			
Icon-Sullivan	Que.	seds.	Cu	cp*	5	0.075 - 0.370	0.270	50	50	1	48	1	< 8
PHANEROZOIC													
Arctic Silver	Yukon	seds.	Pb-Zn, Ag	py	2	12.08 - 38.62	25.35	156	800	2800			116
Keno Hill	Yukon	seds.	Pb-Zn, Ag	gn	2	1.17 - 2.08	1.63	5950	179	4000			<10
Elsa	Yukon	seds.	Pb-Zn, Ag	sp	1	-	0.001	8	5	17	12	1	<10
Galkeno	Yukon	seds.	Pb-Zn, Ag	sp	1	-	1.57	36	3630	25			25
				py	1	-	1.12	312	22100	200			<10
Bluebell	B.C.	seds.	Pb-Zn	gn	3	0.09 - 0.14	0.11		3	290			
PHANEROZOIC													
Keymet	N.B.	volcs.	Pb-Zn	sp	1	-	0.001	110	77	2			<10
				py	1	-	0.030	25	11	300			<10
				gn	2	0.005 - 0.125	0.065	475	3050	550			104
Nigadoo	N.B.	volcs.	Pb-Zn	py	2	-	0.005	120	21	30			155
				cp	1	-	0.020	345	39	10			33
				po	2	-	0.001	265	20	2			310

See Table 5.3 for footnotes

Selenium was determined by Bondar-Clegg and Co. Samples were dissolved in concentrated HNO_3-$HClO_4$ and selenium was determined colorimetrically as the 3.3' diaminobenzidine complex (detection limit for the procedure used was 1 µg/g).

Tellurium was determined by Bondar-Clegg and Co. Samples were dissolved in strong HBr-Bromine solution, extracted into methylisobutylketone and determined by atomic absorption spectrometry (detection limit was 0.5 µg/g for a 1 g sample).

All results are expressed in grams per tonne (g/Mg) i.e., ppm, and are arithmetic means when two or more samples were analyzed.

Discussion

Vein Sulphides

Results are presented in Table 5.1 for sulphide samples from some vein deposits, some of which are known gold occurrences or have been mined for gold. With such a wide variety of deposit settings (host rocks, age, location) it is difficult to draw any general conclusions.

Of the northern Ontario locations, two known gold occurrences, Berens River and Wilkinson Lake (near Beardmore) stand out. Antimony seems to be associated with all of these occurrences.

Little is known about the veins sampled in the Slave Structural Province (N.W.T.); samples were collected from minor occurrences in granitic or gneissic rocks by R.G. Garrett of the Geological Survey of Canada.

Samples from a group of past-producing copper-gold mines, near Val D'or, Quebec, show low to moderate levels of gold in all sulphides (and magnetite). Arsenic would appear to be the most significant associated element in these veins which may be of volcanogenic origin; i.e., stringer ore.

The important gold producers of the Chibougamau area of Quebec are represented by three deposits; Opemiska, Patino and Campbell. A series of monthly composite concentrates of chalcopyrite collected in 1971 provide good average data for these operations. Clearly, chalcopyrite is enriched in gold, moreover a strong relationship between gold, arsenic, and selenium is also apparent from the data of Table 5.1.

A diverse group of Proterozoic deposits includes some districts better known as silver producers. Samples from Silverfields, Terra and Norex were collected from sulphide-rich veins rather than from the more common arsenide-rich veins. Arsenic and antomony are important associate elements; little is known about the distribution and occurrence of the other elements although occurrences of bismuth minerals are known in all three camps.

The silver-rich veins of some Yukon deposits carry low to moderate amounts of gold; all are highly enriched in arsenic and antimony, reflecting the presence of a wide variety of sulphosalts, such as tetrahedrite and freibergite, well known in these deposits (Boyle, 1979, p. 437).

Samples from the Keymet and Nigadoo mines in the Bathurst area of New Brunswick are poor in gold, but rich in silver and bismuth.

Massive Volcanogenic Sulphides

By far the largest group of samples analyzed in this study fall into this category; data are presented in Table 5.2. In general, gold levels for all types of sulphides are low, with a few notable exceptions. Average gold content of most massive sulphide ores is about 1 g/Mg (Boyle, 1979). Data should be viewed for districts or mining camps rather than for single deposits, especially when evaluating which metal sulphide seems to be the most significant host for gold.

Sulphides from occurrences in mixed volcanic-sedimentary lithologies in Slave Province are uniformly poor in gold, but carry moderate amounts of silver. In general arsenic is more prominent than antimony in its association with silver. Insufficient data exist to judge the worth of selenium as an indicator element although it may be important at High Lake (AB zone) which is richer in copper than the other Slave deposits sampled (see Divi et al., 1980).

The deposits of northwestern Ontario (Sturgeon Lake and Uchi Lake areas) are notable for similar gold levels but are much richer in silver and associated arsenic, antimony and bismuth; sulphides from these deposits yielded some of the highest values found for bismuth to date. Pyrite and galena appear to be the most important hosts for gold, silver and bismuth.

Samples of galena from the Geco mine are richest in gold and antimony; one sample of pyrrhotite also has an unusually high gold content.

The few samples from mines in the Timmins area of northern Ontario show little evidence of gold enrichment in sulphide separates, but further sampling is clearly required to confirm this. The data of Divi et al. (1980) indicate very low gold levels in ores from Kidd Creek, Kam Kotia, Jameland and others.

A far more extensive suite of samples, principally in monthly composite concentrate form, is available from deposits in the andesite-rhyolite sequences of the Noranda camp of Quebec. These concentrates date from 1971-72 and are considered to provide a good average data set for these important deposits at that time. A number of conclusions can be drawn from data in Table 5.2. Chalcopyrite (or rather, the copper concentrate and whatever else floats with it) is the most auriferous sulphide at the Normetal, Lac Dufault, Horne and Vauze mines. Chalcopyrite is also richest in arsenic, antimony, selenium and bismuth. It is interesting to note that at the Horne, chalcopyrite and pyrite are by far richest in gold but also the poorest in silver and the associated elements, arsenic, antimony and selenium. However, Horne chalcopyrite is relatively richer in tellurium and probably contains gold tellurides (Boyle, 1979, p. 387).

Massive sulphide separates from the Val D'or camp are typified by the Manitou-Barvue mine for which some composite concentrates were available for analysis. Galena is the most important host for gold with lesser amounts measured in chalcopyrite and pyrite. Arsenic is apparently more abundant than antimony in sulphides from all deposits but distributions are erratic. Minor bismuth is associated with galena from Manitou-Barvue and Coniagas. It is interesting to observe that these deposits are hosted in tuffaceous rocks and other volcanic-derived sediments.

Gold is enriched in chalcopyrite (copper concentrates) from Orchan and Mattagami Lake mines. Arsenic, antimony, selenium and notably, tellurium are associated with gold. Of these, selenium is the most enriched, which is also an uncommon observation. Perhaps the presence of gabbroic sills within these deposits has influenced the levels of tellurium and selenium.

Selenium is also uncommonly high in copper concentrates from the Joutel and Poirier mines, however all sulphides sampled carry very little gold (see Divi et al., 1980).

Of the deposits of Proterozoic age in northern Manitoba and Saskatchewan, samples of pyrite, sphalerite and to a lesser extent, chalcopyrite from Fox Lake, Schist Lake and especially Flin Flon mines are the richest in gold. However, levels are generally lower than for the deposits described above; according to Divi et al. (1980) gold averages about 1 g/Mg in ores from these camps (except Flin Flon, 2.89 g/Mg). This observation also applies to silver levels,

Table 5.2

Gold content of some Canadian massive volcanogenic sulphides

Name of occurrence	Location	Host rock	Ore type	Mineral	No.	Au (g/Mg) Range	Au (g/Mg) Arith. mean	Arithmetic mean of some associated elements (g/Mg) Ag	As	Sb	Se	Te	Bi
ARCHEAN													
Hackett River Camp Lk.	Mack.	meta-rylt.	Pb-Zn	sp	12	0.001 - 0.390	0.070	53	22	179	20	1	< 4
				py	26	0.001 - 3.80	0.24	37	420	87	37	1	< 4
				mt	1	-	0.025		2	13			
Hackett River Jo Zone	Mack.	meta-rylt.	Pb-Zn	sp	1	-	0.14	23	2	16			< 4
				py	1	-	0.55		230	50			
				gn	1	-	0.001		2130	1000			
				po	1	-	0.035		3	4			
Hackett River Watson Lk.	Mack.	meta-rylt.	Pb-Zn	sp	1	-	0.095	44	4	1			587
				py	1	-	0.315		1	1			
				gn	1	-	0.055		1	1			
Hackett River	Mack.	meta-rylt.	Pb-Zn	sp	2	0.09 - 0.16	0.12	63	18	85			18
Trench three	Mack.	meta-rylt.	Pb-Zn	py	3	0.02 - 0.13	0.06		443	2			
Yava Syndicate	Mac.	meta-volcs	Pb-Zn, Cu	py	5	0.035 - 0.405	0.13	49	886	3075			< 4
Agricola Lk.				sp	1		0.05	54	180	3115			< 4
Clinton-Colden Lk.	Mack.	meta-volcs.	Cu-Zn	sp	3	0.080 - 0.230	0.11		1107	70			
				py	1		0.62		1500	70			
				cp	1		0.65		4350	125			
Indian Mt. Lk.	Mack.	meta-rylt.	Pb-Zn	sp	3	0.030 - 0.180	0.12	305	20	420			< 10
Takijuq Lk., 10 zone	Mack.	meta-rylt.	Cu-Zn	sp	4	0.001 - 1.42	0.48	248					
				py	1	-	0.21	29	200	10			
				gn	1	-	0.25	235	1	256			
				mt	1	-	0.16		30	8			
High Lk.	Mack.	meta-rylt.	Cu-Zn	sp	3	0.020 - 2.85	1.00	81	6	2	144	< 1	
				py	4	0.23 - 4.20	1.52	7	87	3			
				cp	6	0.020 - 2.35	0.85	181	6	5	159	1	100
				mt	3	0.28 - 1.84	0.80		5	20			
Spi Lk.	Keew.	meta-volcs.	Cu-Zn, Pb	sp	1	-	0.005	20	2	16			< 25
Mattabi	N. Ont.	tuffs	Cu-Zn	sp	4	0.29 - 1.48	0.82	543	160	2660	17	1	12
				py	3	0.77 - 1.17	0.92	114	5000	100			125
				cp	2	0.055 - 0.21	0.13	560	50	8			140
				gn	1	-	1.14	1610		2000			937
				po	1	-	0.16	750	750	1000			< 10
Sturgeon Lk.	N. Ont.	volcs.	Cu-Zn	sp	2	0.045 - 0.77	0.41	1200	15	4400			79
Falconbridge				py	1	-	0.51	530	40	400			480
South Bay	N. Ont.	volcs.	Cu-Zn	sp	4	0.070 - 0.27	0.17	62	301	735			110
Uchi Lk.				py	3	0.38 - 0.51	0.46	227	3820	35			239
Geco	N. Ont.	meta-seds.	Cu-Zn, Pb	sp	7	0.010 - 0.29	0.14	110	32	50			< 10
				py	5	0.080 - 1.52	0.46	147	218	14			< 10
				cp	2	0.001 - 0.065	0.03	315	6	2	1	1	257
				gn	3	2.25 - 8.73	5.91	147	114	114	730		
				po	1	-	3.30	1020	25	25			< 10
				mt	5	0.18 - 0.36	0.30		69	23			
Willecho	N. Ont.	meta-seds.	Cu-Zn	sp	3	0.075 - 0.12	0.08	240	3	2			88
				py	1	-	0.04	18	57	2			< 10
				po	1	-	0.86	106	46	10			< 10
Kam-Kotia	N. Ont.	ands.	Cu-Zn	sp	1	-	0.001	8	12	2			< 10
				py	1	-	0.35	27	132	2			< 10
Cdn.-Jamieson	N. Ont.	rylt.	Cu-Zn	sp	1	-	0.175	18	74	11			19
				py	1	-	0.22						
Kidd Creek Nth.	N. Ont.	meta-volcs.	Cu-Zn, Ag	sp	3	0.050 - 0.11	0.078	39	300	2	205	1	< 10
				py	1	-	0.015	8	1240	2			< 10
				cp	1	-	0.010	315	280	20			295
Normetal	W. Que.	volcs.	Cu-Zn	sp*	8	0.21 - 0.43	0.32	39	271	14	48	1	12
				cp*	8	8.50 - 11.50	9.50	410	150	183	232	1	52
Lac Dufault	W. Que.	rylt.-ands.	Cu-Zn	sp*	5	0.18 - 0.38	0.30	40	40	12	108	1	86
				cp*	5	2.88 - 9.20	4.70	88	113	15	339	1	118
Delbridge	W. Que.	rylt.	Zn	sp	1	-	0.50	47	4800	820			< 10
Horne	W. Que.	volcs.	Cu, Zn	py*	2	2.00 - 6.75	4.38	4	8	10	10		< 8
				cp*	6	1.12 - 29.80	19.93	37	45	1	260	47	< 8
Vauze	W. Que.	rylt.	Cu-Zn	py	2	0.97 - 2.00	1.48	45	11	2			44
				cp	2	2.34 - 18.81	10.57	195	5	2			35
				po	3	0.15 - 0.38	0.30	40	1	2			13
Gallen	W. Que.	volcs.	Zn	py	1	-	1.16				2	1	
Manitou-Barvue	W. Que.	tuffs	Cu-Pb-Zn	sp*	9	0.20 - 0.51	0.33	300	486	270	22	5	
				py	13	0.040 - 5.22	0.86		265	16			36
				cp*	10	0.15 - 1.44	0.95	65	67	15	380	145	254
				gn*	10	0.40 - 8.42	3.44	450	12050	4600	68	10	35
Coniagas	W. Que.	tuffs	Pb-Zn, Ag	sp	15	0.02 - 1.44	0.34		33	87	2	1	
				py	11	0.05 - 1.44	0.41		1390	74			
				cp	1	-	0.10	37	13				
				gn	5	0.57 - 23.00	11.00		84	900	1	2	104
				mt	1	-	0.002		2	13			
Barvue	W. Que.	tuffs	Cu-Zn	sp	2	0.15 - 0.26	0.20		528	46			
				py	2	0.14 - 0.34	0.24			49			
				cp	1	-	0.21		26	27			

See Table 5.3 for footnotes

Table 5.2 (cont.)

Name of occurrence	Location	Host rock	Ore type	Mineral	No.	Au (g/Mg) Range	Au (g/Mg) Arith. mean	Arithmetic mean of some associated elements (g/Mg) Ag	As	Sb	Se	Te	Bi
Consolidated-Mogadar	W. Que.	volcs.	Cu-Zn	sp	4	0.26 - 2.59	2.01		43	7			
				py	18	0.10 - 3.70	0.74		402	5			
				cp	3	0.35 - 1.26	0.67		35	2			
				po	2	0.03 - 0.36	0.20		11	6			
				mt	1	-	0.24		20	10			
East Sullivan	W. Que.	volcs.	Cu-Zn	cp	2	0.16 - 1.14	0.65		16	1			
Mattagami Lk.	Que.	rylt.	Cu-Zn	sp*	9	0.25 - 0.90	0.62		217	12	201	9	< 8
				py	2	0.38 - 0.77	0.58		1	2			< 10
				cp*	8	5.20 - 8.00	6.52		195	96	537	52	14
				po	2	0.03 - 0.17	0.10		1	2			< 10
Orchan	Que.	rylt.	Cu-Zn	sp*	5	0.25 - 0.66	0.37	33	255	10	116	5	8
				cp*	5	1.50 - 5.72	3.07	202	229	158	345	11	40
Joutel	Que.	rylt.	Cu-Zn	cp*	6	0.07 - 0.37	0.27	94	50	2	412	7	< 8
Poirier	Que.	rylt.	Cu-Zn	sp*	1	-	0.015	6	12	2			< 10
				py	1	-	0.015						
				cp*	4	0.14 - 0.35	0.23	33	19	1	436	33	15
				po	2	0.025 - 0.04	0.33	58	1	2			< 10
Western Nuclear†	N. Sask.	meta-volcs.	Pb-Zn	sp	2	0.60 - 1.00	0.80	57	1800	1500			50
Sulphide Lk.†	N. Sask.	meta-seds.	Cu-Zn	sp	1	-	25.9	20000					
PROTEROZOIC													
Fox Lk.	N. Man.	meta-seds.	Cu-Zn	sp*	2	0.475 - 0.695	0.59	13	350	1220	323	5	< 8
				py	6	0.320 - 3.71	1.07	450	1018	3	198	3	50
				cp	2	0.310 - 5.20	2.76	87		100	321	2	< 8
				po	1	-	0.35	21	20	2			8
Ruttan Lk.	N. Man.	meta-seds.	Cu-Zn, Pb	sp	2	0.035 - 0.090	0.063	48	21	1			31
				py	1	-	0.085	11	69	1			34
				gn	1	-	0.92	6000	1	115			
				po	1	-	0.60		12	1			
Sherridon	N. Man.	meta-seds.	Cu-Zn	sp	5	0.135 - 0.480	0.27	24	1	1			< 10
				py	2	0.135 - 0.415	0.28	17	296	2			< 10
				po	2	0.160 - 0.240	0.20	14	40	2			< 10
Osborne Lk.	N. Man.	meta-seds.	Cu-Zn	sp	1	-	0.010	12	7	2			< 10
				gn	1	-	0.020	121	237	260			336
				po	2	0.040 - 0.17	0.105	18	19	2			< 10
Chisel Lk.	N. Man.	meta-seds.	Cu-Zn, Pb	sp	3	0.005 - 0.205	0.082	23	22	28			< 10
				py	1	-	1.00	8	2750	200			< 10
Schist Lk.	N. Man.	meta-volcs.	Cu-Zn	sp	2	1.01 - 3.06	2.03	64	1203	168			< 10
				py	1	-	3.34	152	9970	400			< 10
Anderson Lk.	N. Man.	meta-volcs.	Cu (Zn)	py	2	0.43 - 0.84	0.64	6	218	2			14
				cp	1	-	0.49	11	106	2			< 10
				po	1	-	0.49	11	145	2			< 10
Stall Lk.	N. Man.	meta-volcs.	Cu (Zn)	py	1	-	0.065	4	1	2			< 10
				po	1	-	0.180		1	1			
Flin Flon	N. Man.	meta-volcs.	Cu-Zn	sp	6	1.72 - 10.10	5.00	71	318	24	152	9	< 10
				py	5	0.56 - 11.30	4.73	22	260	13	133	6	< 10
				cp*	2	0.58 - 1.78	1.18	83	16	2	240	13	< 10
Flexar	N. Sask.	meta-volcs.	Cu (Zn)	py	2	2.37 - 2.58	2.48						< 10
				po	2	0.40 - 0.59	0.49	1	65	2			< 10
Errington	N. Ont.	tuffs	Cu-Zn, Pb	sp	2	0.405 - 0.560	0.48	58	19	31	13	1	< 8
				py	5	0.025 - 2.14	0.63	81					
New Calumet	W. Que.	meta-seds.	Pb-Zn	sp	9	0.015 - 0.790	0.256	485	5	1310	25	1	< 10
				py	3	0.100 - 3.85	1.77	750	4	300			880
				gn	4	0.080 - 1.41	0.72		5	6250			
				mt	4	0.170 - 2.71	1.01		8	750			
Tetrault	Que.	gnss.	Pb-Zn	sp	2	-	0.001	13			44	1	
Hart River	Yukon	volcs.	Cu-Zn	py	1	-	0.14	15	1190	90			30
				po	1	-	0.22	43	82	70			< 10
PHANEROZOIC													
Western (Lynx)	B.C.	volcs.	Pb-Zn, Cu	cp	3	7.00 - 9.50	8.48	144	636	58	8	29	79
				gn	2	0.03 - 31.6	15.8	870					1100
Britannia Beach	B.C.	meta-volcs.	Cu	py	1	-	0.08						
				cp	1	-	0.06						
Key Anacon	N.B.	meta-volcs.	Pb-Zn	sp	3	0.135 - 0.300	0.19	230					< 10
				py	1	-	0.56	7	321	50			< 10
Wedge	N.B.	meta-volcs.	Pb-Zn	py	1	-	0.42						
Heath Steele	N.B.	meta-volcs.	Pb-Zn, Cu	py	2	0.83 - 1.25	1.04	28	266	50			388
				po	1	-	0.53						
Brunswick 12	N.B.	meta-tuffs	Pb-Zn, Cu	py	4	0.015 - 1.17	0.63	27	490	130			100
				po	1	-	0.001						
Austin Brook	N.B.	meta-volcs.	Pb-Zn	py	2	0.001 - 0.120	0.06	10	2230	80			< 10
				po	1	-	0.001						
Buchans	Nfld.	volcs.	Pb-Zn, Cu	sp	1	-	2.25	210					< 10
Weedon	Que.	meta-tuffs	Cu-Zn	sp	1	-	0.02	80	22	66			< 10
				py	2	0.01 - 0.32	0.16	70	250	10			< 10
				gn	1	-	0.001	6	1	2			< 10
Eustis	Que.	volcs.	Cu-Zn	cp*	1	-	0.14	8	1	2	140	7	< 8

See Table 5.3 for footnotes

Table 5.3

Gold content of some Canadian sediment-hosted sulphide deposits

Name of occurrence	Location	Host rock	Ore type	Mineral	No.	Au (g/Mg) Range	Au (g/Mg) Arith. mean	Arithmetic mean of some associated elements (g/Mg) Ag	As	Sb	Se	Te	Bi
PROTEROZOIC													
Nanisivik	Frnk.	carb.	Pb-Zn	sp	4	0.001 - 0.090	0.027	220	4	1	10	10	< 10
				py	1	-	0.001	12	146	2			< 10
Lynx (Long Lk.)	S. Ont.	carb.	Pb-Zn	sp	7	0.001 - 0.030	0.056	55	10	73			< 10
				py	1	-	0.010	44	69	21			< 28
				gn	2	0.280 - 1.07	0.68	1576	18	800			1760
				mt	1	-	0.015		27	73			
PHANEROZOIC													
Anvil (Faro)	Yukon	shle.	Pb-Zn	sp	2	0.055 - 0.105	0.08	108	300	710			< 10
				py	3	0.080 - 2.87	1.33	50	260	65			< 10
				gn	1	-	0.51	817	1460	2000			33
Tom (west zone)	Yukon	shle.	Pb-Zn	gn	1	-	0.001	140	48	300	2	1	< 10
Jersey	B.C.	carb.	Pb-Zn	py	1	-	0.18		87	10			84
				gn	2	0.285 - 0.90	0.59		14	27			
Prairie Creek†	Mack.	carb.	Pb-Zn	sp	2	0.140 - 0.225	0.18	270	850	7000			< 10
				gn	2	0.080 - 0.56	0.32	503	400	4300			< 10

Abbreviations used:

rylt. = rhyolite, volcs. = volcanic rocks, seds. = sediments, gnss. = gneissic rocks, grnt. = granitoid rocks, gbbr. = gabbro, anrs. = anorthosite, carb. = carbonates, shle. = shale.
* signifies sample analyzed was a composite monthly concentrate.
† denotes classification of deposit type in doubt; possibly veins.
# stringer; probably associated with volcanogenic massive sulphide.sp = sphalerite, gn = galena, py = pyrite, po = pyrrhotite, mt = magnetite, cp = chalcopyrite.

except in galena samples. All sulphide separates from Fox Lake and Flin Flon are enriched in selenium; no data are available for the other deposits. Arsenic is most abundant in pyrite separates from all deposits except Stall Lake, from which few samples are available.

Separates of chalcopyrite and galena from Western Mines, B.C. (Lynx deposit) a well-known precious metal producer, are very rich in gold and silver with some arsenic and unusually high levels of bisumth.

Deposits from the Bathurst camp of New Brunswick have been sparsely sampled, mainly for iron sulphides. In general these are poor in gold but carry moderate to high amounts of arsenic. No comparisons can be made, on the basis of our data, with vein deposits in the same camp. The average of Divi et al. (1980) for gold in ores from the Bathurst camp indicate very low levels for the deposits.

Sediment-Hosted Sulphides

None of the occurrences or deposits sampled for sulphides (see Table 5.3) carry more than 2 g/Mg gold; generally average values are an order of magnitude lower. Galena appears to be the prime carrier of trace gold whether deposits are carbonate-hosted or shale-hosted; sampling, however, is insufficiently extensive to be more conclusive. On the other hand, silver is a much more important accessory metal, commonly occurring in galena and usually associated with antimony and arsenic.

Conclusions and Future Work

It is obvious that too few samples from many of the deposits and occurrences listed in the tables have been analyzed for gold to permit useful conclusions to be drawn concerning abundance and distribution between coexisting sulphides. However, our data are generally in harmony with those reported for whole ores (Divi et al., 1980). There is some indication of the existence of persistent geochemical associations between gold and some of the so-called "carrier" elements. Arsenic is commonly associated with gold in most camps and in most massive types; antimony is enriched in veins and especially in deposits hosted wholly or partly in sediments. Although the number of analyses available for bismuth are much fewer, it would seem that volcanogenic massive sulphides are the most enriched, with the possible exception of deposits from the Slave Province for which few data are available.

More comprehensive sampling and analyses are required for selenium and tellurium, especially in the Proterozoic deposits of Manitoba-Saskatchewan. Deposits from the Abitibi greenstone belt appear to be enriched in selenium; measureable levels of tellurium are much rarer by comparison.

One of the original objectives of this project was to make a broad preliminary survey of Canadian sulphide deposits for a wide range of trace elements, including gold. This objective has been largely fulfilled for gold and future work will centre on detailed studies of gold abundance and distribution within the deposits of Noranda and Sturgeon Lake camps.

Acknowledgments

We appreciate the collaboration of our colleagues within the Resource Geophysics and Geochemistry Division and Economic Geology Division. P.J. Lavergne carried out the separations of sulphide minerals, many of which were difficult and slow. We are most grateful.

References

Boyle, R.W.
1979: The geochemistry of gold and its deposits; Geological Survey of Canada, Bulletin 280, 584 p.

Divi, S.R., Thorpe, R.I., and Franklin, J.M.
1980: Use of discriminant analysis to evaluate compositional controls of stratiform massive sulphide deposits in Canada; Geological Survey of Canada, Paper 79-20, 23 p.

6. THE RICHMOND GULF GRAVITY ANOMALY, NORTHERN QUEBEC-NORTHWEST TERRITORIES[1]

Project 770027

R.A. Gibb[2], F.W. Chandler and S. Fogarasi[2]
Precambrian Geology Division

Gibb, R.A., Chandler, F.W., and Fogarasi, S., The Richmond Gulf gravity anomaly, northern Quebec-Northwest Territories; in Current Research, Part B, Geological Survey of Canada, Paper 83-1B, p. 53-56, 1983.

Abstract

Preliminary interpretation of a gravity survey traverse across the Richmond Gulf Graben suggests the presence of a mafic igneous body at depth that could be a large axial dyke, like that found in some inactive failed rifts. This interpretation enhances a hypothesis previously based on geological grounds, that the graben is a failed rift.

Résumé

L'interprétation préliminaire d'un levé gravimétrique en travers du graben de Richmond Gulf suggère la présence d'une masse ignée mafique profonde qui pourrait être un grand filon axial semblable à ceux que l'on retrouve dans certains débuts de fossés tectoniques. Cette interprétation vient appuyer une hypothèse antérieure, fondée sur des motifs géologiques, selon laquelle le graben serait un début de fossé d'effondrement.

Introduction

The 80 km wide Early Proterozoic Richmond Gulf Graben strikes eastward from the Hudson Bay coast (Fig. 6.1, inset a, and 6.2) at about latitude 56°N into the Archean craton of northern Quebec. The graben was first identified as such by Kranck (1951) and interpreted on geological grounds (Chandler and Schwarz, 1980) as a failed rift related to the early rifting phase which led finally to the formation of the Hudson Bay segment of the Circum-Superior Foldbelt. The graben contains less than a kilometre of Early Aphebian pre-graben fluvial arkose and small amounts of basaltic flows, dykes and sills. The graben and its fill are unconformably overlain by several hundred metres of unfaulted Aphebian post-graben carbonate and fine grained clastics equivalent to part of the much thicker Belcher Group that lies 120 km to the west in Hudson Bay (Chandler and Schwarz, 1980; Chandler, 1982). The graben has been mapped

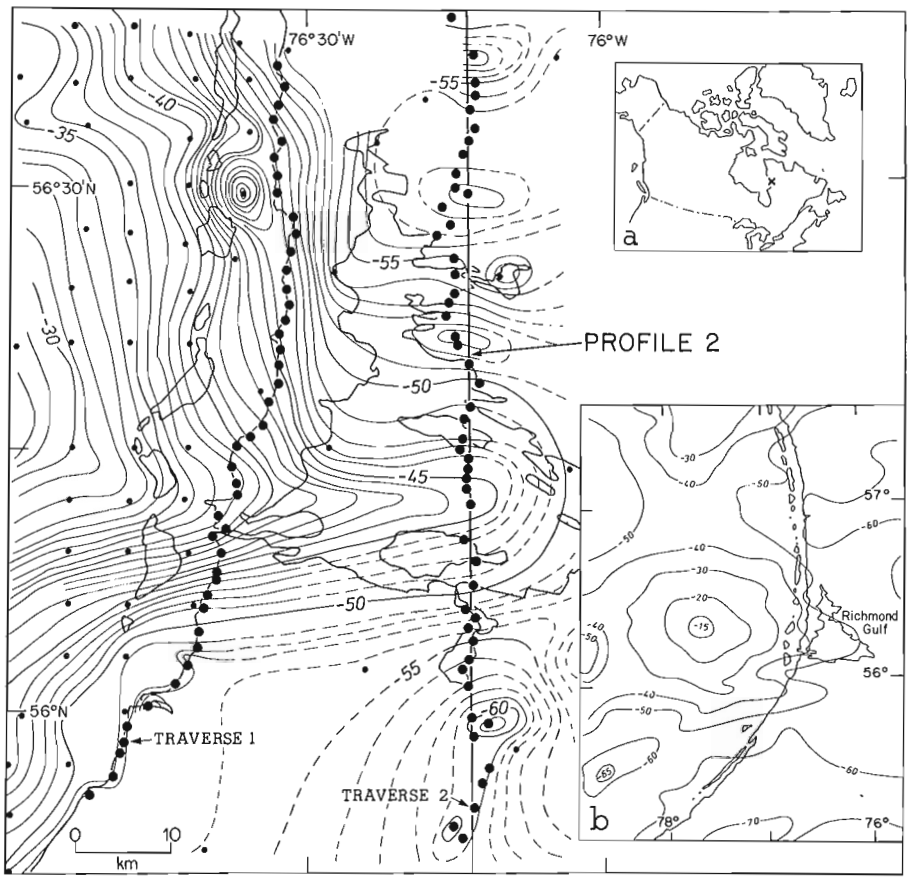

Figure 6.1

Bouguer gravity map of Richmond Gulf Graben showing locations of traverses 1 and 2. Inset a, index map showing location of Richmond Gulf; inset b, regional gravity map of area around Richmond Gulf.

[1] Contribution of the Earth Physics Branch No. 1051

[2] Gravity, Geothermics and Geodynamics Division, Earth Physics Branch, Department of Energy, Mines and Resources, Ottawa, K1A 0Y3

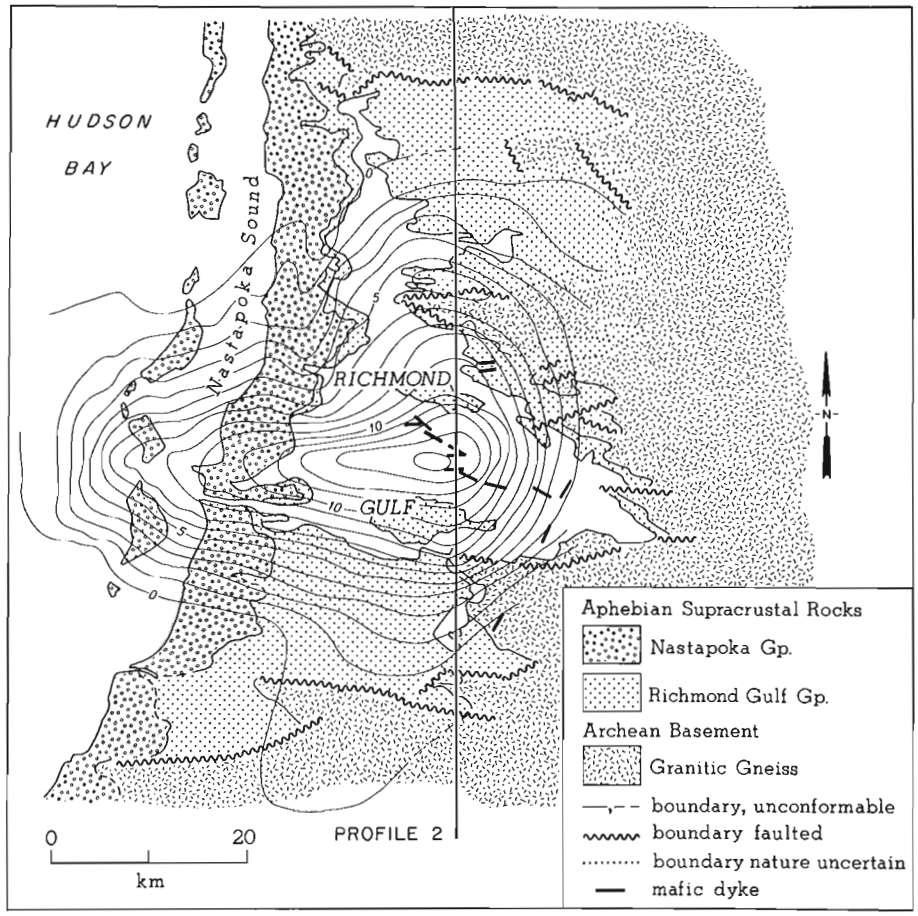

Figure 6.2

Residual gravity anomaly and geology, Richmond Gulf Graben.

at a scale of 1:50 000 (Chandler, 1979; Chandler et al., 1982) and the surrounding Archean gneisses at a scale of 1:1 000 000 (Eade, 1966; Stevenson, 1968).

When a failed rift becomes inactive, gabbroic magma at depth may crystallize as an axial dyke or dykes, each at least 10 km wide. If not exposed these dykes can be recognized from a resultant positive gravity anomaly aligned along the graben axis (Burke, 1977). Earlier regional gravity data (Tanner and McConnell, 1970; Mukhopadhyay and Gibb, 1981) show that a positive element of the gravity field projects eastward into the Richmond Gulf Graben (Fig. 6.1, inset b). Several basaltic dykes, up to 35 m wide, tend to be concentrated along and parallel to the axis of the graben. Because they do not cut the overlying mioclinal carbonates they are probably related to graben development, and imply that basaltic magma had access to the axial zone of the graben. For these reasons it was thought that a thick axial dyke like those noted by Burke (1977) might lie at depth along the axis of the graben. If one could be reasonably inferred from the local gravity pattern the interpretation of the graben as a failed rift would be more soundly based. Accordingly two detailed gravity traverses were made across the graben.

Gravity Survey

Two north-south detailed gravity traverses, one along the Hudson Bay coast and the other 25 km inland (Fig. 6.1, traverses 1 and 2) were planned and observed by personnel of the Earth Physics Branch to augment existing regional gravity data. Both traverses are approximately 100 km long with stations spaced at intervals of 2 km. A LaCoste and Romberg geodetic gravimeter (No. G278) was used for all observations. The traverses were tied to a local gravity base station previously established by ties to a station of the National Gravity Net at Great Whale River. Topographic maps (scale 1:50 000) were used for horizontal control. Elevations were obtained by barometer with frequent control ties to sea level and to a local geodetic bench mark. The adjusted observed gravity values are accurate to ± 0.1 mgal, horizontal positions to ± 50 m and elevations to ± 3 m. Bouguer anomalies were computed using a uniform density of 2.67 g/cm^3 and are accurate to ± 1 mgal. Terrain corrections were not computed but station positions were selected as far as possible from the vicinity of cliffs to minimize the effects of high relief.

Richmond Gulf Gravity Anomaly

The Bouguer anomaly contour pattern (Fig. 6.1 and inset b) suggests that the Richmond Gulf gravity anomaly, although appearing as a bulge on the large circular positive anomaly to the west, probably has an independent source whose gravity effect could be isolated as a residual anomaly for interpretations. A graphical regional anomaly map was prepared simply by connecting contours north and south of the Richmond Gulf anomaly following the circular trends of the large anomaly. The regional anomaly contour values were then subtracted from superimposed Bouguer anomaly values at contour intersections to yield residual anomalies. The residual anomaly (Fig. 6.2) has an amplitude of 14 mgal and an easterly trend. It is centred approximately over the graben in the southern part of Richmond Gulf and overlaps the gulf to the west and northeast.

Interpretation

The densities of Nastapoka Group and Richmond Gulf Group rocks are listed in Table 6.1. Aphebian carbonate (2.84 g/cm^3), fine grained clastic rocks (2.56 g/cm^3) and

Table 6.1

Rock densities, Richmond Gulf

Group and/or formation	Major lithology	Range in thickness (m)	Number of samples	Mean density (g/cm^3)
Nastapoka Group				
	basalt	up to 107*	3	2.81
	quartzite	up to 50	4	2.56
	dolomite	up to 100	10	2.84
Sills				
	diabase	up to 50	6	2.82
Richmond Gulf Group				
Qingaaluk Formation	arkose	up to 600	10	2.61
Persillon Formation	basalt	up to 70	8	2.76
Pachi Formation	arkose	up to 500	8	2.69
Archean Basement				
	granitic gneiss		40**	2.65

* From Parks (1949) at latitude 55°57.5'N

** Samples provided by A. Ciesielski, Geological Survey of Canada

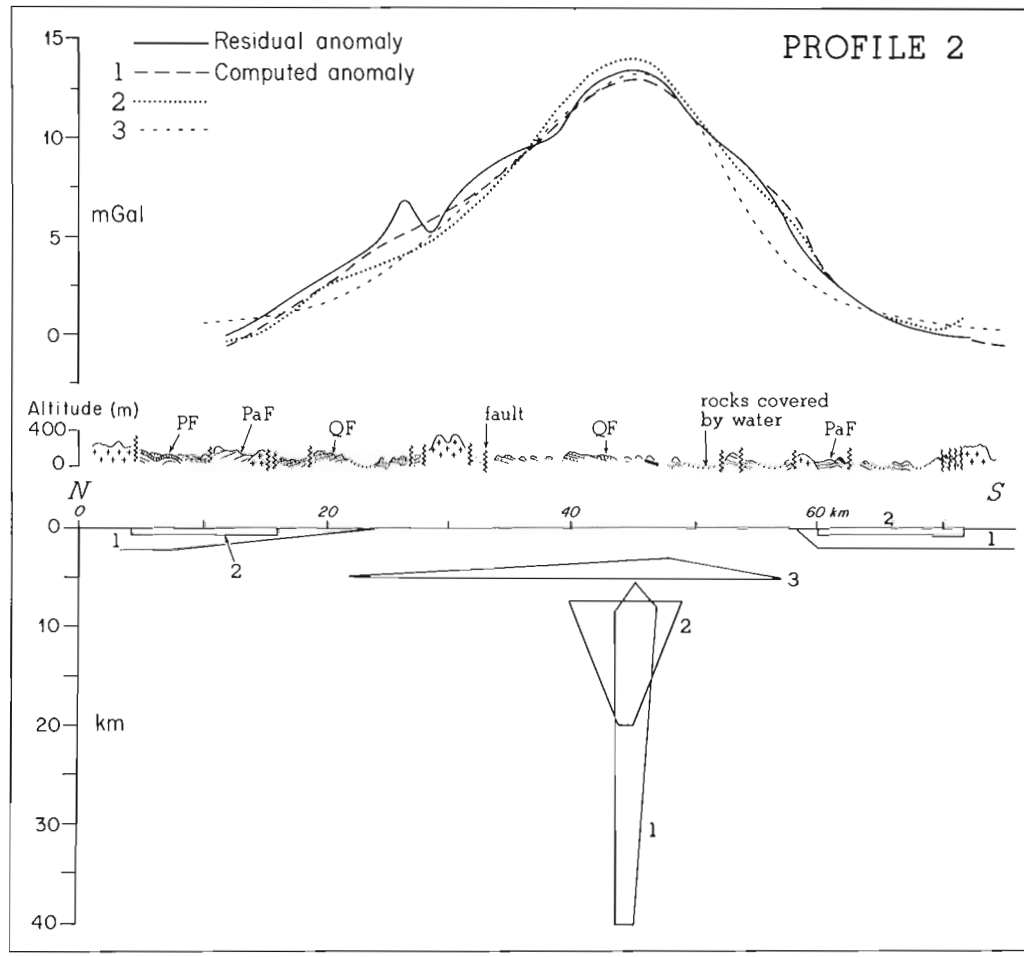

Figure 6.3

Gravity profile 2, geological cross-section of Richmond Gulf Graben, and computed anomalies derived from models 1, 2 and 3. Legend: Archean basement (crosses); Pachi Formation, PaF, with bedding shown (lines); Persillon Formation, PF (open dots); Qingaaluk Formation, QF (lines with dots); sills (solid black).

basalt (2.81 g/cm^3) of the Nastapoka Group, which postdate graben formation, have a mean density of 2.77 g/cm^3 (weighted according to maximum thickness). Although they are denser than the Archean basement rocks (2.65 g/cm^3) they are an unlikely source of the residual anomaly because they are only about 250 m thick at most and are restricted in outcrop to the western coastal cuesta. Maximum downwarp of the Richmond Gulf Group sediments, which predate graben formation, occurs in the axial part of the graben (Chandler, 1982) where the gravity anomaly peaks. However, these rocks have a weighted mean density of 2.64 g/cm^3 and were derived from the Archean basement granitic rocks and are clearly not the source of the anomaly. A source related to the graben is nevertheless indicated by confinement of the anomaly within the northern and southern bounding faults of the graben, and by the correlation of the anomaly axis with the diabase dyke swarm and mafic sills in southern Richmond Gulf (Chandler, 1982).

The most likely source of the anomaly is considered to be a dense mafic intrusive body perhaps related to graben formation and perhaps related both spatially and compositionally to the axial diabase dykes. In the absence of additional reliable controls on the depth and shape of the body, three possible models were investigated. Density contrasts of 0.2 g/cm^3 and 0.25 g/cm^3 suggested by the presumed mafic composition of the body were assigned to two deep models (1 and 2) and to a shallow model (3) respectively. Although the anomaly is more suitable for three-dimensional interpretation, all the models investigated are two-dimensional interpretations of profile 2 (Fig. 6.1, 6.2, 6.3) and therefore must be considered as preliminary.

The first model (Fig. 6.3, model 1) considered is a dyke-like body extending from a depth of 5.4 km to the base of the crust (taken as 40 km, cf. Mukhopadhyay and Gibb, 1981). The body is about 40 km long and strikes east-west. It diminishes in width towards the west from a maximum width near profile 2 of about 3.5 km. In the second model (Fig. 6.3, model 2), it is assumed that crustal density increases with depth so that any density contrast between the body and the lower crust below an arbitrary depth of 20 km is insignificant. The disturbing mass was therefore limited by this depth. This restriction results in a wider funnel-shaped body (top width 9 km, base width 1 km). The top of the body is at a depth of 7 km. The disturbing mass is concentrated higher in the crust in the third model (Fig. 6.3, model 3) between depths of 3 and 5 km. The body is much wider (34 km) and has an almost tabular shape. However, because 1:1 000 000 scale maps by Eade (1966) and Stevenson (1968) suggest moderate to steep foliation in granitic basement rocks, model 3 is tentatively considered less likely than models 1 and 2.

In both deep models the flanks of the anomaly (up to 3 mgal mismatch) can be fitted by the presence of low density surface masses (density contrast -0.05 g/cm^3) on either side of the anomalous body (see Fig. 6.3). These surface layers are up to 2 km thick and may correspond to the arkoses of the Richmond Gulf Group preserved by faulting and/or to low density phases in the granitic basement, or to a combination of both effects. All models could represent a mafic intrusive body related to graben formation in the gulf area and perhaps related compositionally and physically, as a feeder body, to the axial dyke swarm. All bodies widen landward from the coast and lie along the graben axis. The gravity anomaly terminates landward within the gulf suggesting that the intrusive mass pinches out eastwards. Continental breakup and formation of the ancient Superior margin have been dated at about 2.1 Ma by Burke and Dewey (1973) who used the Molson dykes of northern Manitoba and the Ungava dykes of northern Quebec, with ages of 2.0 Ma (I.F. Ermanovics, personal communication, 1983) and 2.15 Ma (Fahrig and Wanless, 1963) respectively, to date these events. If the axial body and Richmond Gulf dykes are comagmatic and related to continental breakup, both should have an age in the range 2.0 to 2.15 Ma.

References

Burke, K.
1977: Aulacogens and continental breakup; Annual Reviews of Earth and Planetary Sciences, v. 5, p. 371-396.

Burke, K. and Dewey, J.F.
1973: Plume-generated triple junctions: key indicators in applying plate tectonics to old rocks; Journal of Geology, v. 81, p. 406-433.

Chandler, F.W.
1979: Geology of the Aphebian supracrustal rocks, Lac Guillaume Delisle, Quebec; Geological Survey of Canada, Open File 600, two bedrock geological maps, scale 1:50 000.

1982: The structure of the Richmond Gulf Graben and the geological environments of lead-zinc mineralization and of iron-manganese formation in the Nastapoka Group, Richmond Gulf area, New Quebec – Northwest Territories; in Current Research, Part A, Geological Survey of Canada, Paper 82-1A, p. 1-10.

Chandler, F.W. and Schwarz, E.J.
1980: Tectonics of the Richmond Gulf area, Northern Quebec – a hypothesis; in Current Research, Part C, Geological Survey of Canada, Paper 80-1C, p. 59-68.

Chandler, F.W., Ciesielski, A., and St. Michel, R.
1982: Geological map of the southern margin of the Richmond Gulf Graben, New Quebec; Geological Survey of Canada, Open File 840, scale 1:50 000.

Eade, K.E.
1966: Fort George River and Kaniapiskau River (west half) Map-areas, New Quebec; Geological Survey of Canada, Memoir 339, 82 p.

Fahrig, W.F. and Wanless, R.K.
1963: Age and significance of diabase dyke swarms of the Canadian Shield; Nature, v. 200, p. 934-937.

Kranck, E.H.
1951: On the geology of the east coast of Hudson Bay and James Bay; Acta Geographica, Societas Geographica Fenniae, v. 11, p. 1-71.

Mukhopadhyay, M. and Gibb, R.A.
1981: Gravity anomalies and deep structure of eastern Hudson Bay; Tectonophysics, v. 72, p. 43-60.

Parks, T.
1949: A report on the geology of the Nastapoka Group of sediments (Hudson Bay) with its contained lead and zinc bearing strata; unpublished B.A.Sc. thesis, University of Toronto.

Stevenson, I.M.
1968: A geological reconnaissance of Leaf River Map-area, New Quebec and Northwest Territories; Geological Survey of Canada, Memoir 356, 112 p.

Tanner, J.G. and McConnell, R.K.
1970: The gravity field in the Richmond Gulf – Fort Chimo area, Quebec; Earth Physics Branch, Gravity Map Series nos. 7-10, 48, 9 p.

7.

OBSERVATIONS ON THE NATURE AND ORIGIN OF MAGNETIC TOTAL FIELD AND VERTICAL GRADIENT ANOMALIES OVER THE GOLDENVILLE FORMATION IN NOVA SCOTIA[1]

Project 820013

Richard A. Stern[2] and J.R. Henderson
Precambrian Geology Division

Stern, R.A. and Henderson, J.R., Observations on the nature and origin of magnetic total field and vertical gradient anomalies over the Goldenville Formation in Nova Scotia; in Current Research, Part B, Geological Survey of Canada, Paper 83-1B, p. 57-65, 1983.

Also in Mines and Minerals Branch, Report of Activities, 1982, Nova Scotia Department of Mines and Energy, Report 83-1, 1983.

Abstract

Fluctuations in magnetite content of metaturbidites in the Goldenville Formation produce total magnetic field and vertical magnetic gradient anomalies that are detectable with a portable magnetic gradiometer. A ground magnetic survey carried out over bedrock as well as till-covered bedrock shows that some magnetic anomalies in the total field and vertical gradient are sufficiently characteristic to permit correlations to be made from profile-to-profile across the 6 km width of the study area. Matching anomalies in overlapping parts of adjacent profiles enabled the construction of a composite magnetic and lithological section of 2.3 km in total. Magnetite is the only strongly magnetic mineral detected, and is found in some sandy metawacke beds in amounts of less than one weight per cent. Slate beds as well as some metawacke beds do not contain magnetic phases. Detailed analysis of the magnetism in the Goldenville Formation may be useful for stratigraphic subdivision of the monotonous metaturbidites, lithofacies analysis, and provenance studies.

Résumé

Les fluctuations du contenu en magnétite des métaturbidites de la formation de Goldenville produisent des anomalies du champ magnétique total et du gradient magnétique vertical qui peuvent être détectées par un gradiomètre magnétique portatif. Un relevé magnétique au sol, mené à bien au-dessus d'affleurements ainsi qu'au-dessus de zones couvertes de till, démontre que certaines anomalies du champ total et du gradient vertical sont suffisamment caractéristiques pour permettre la corrélation de profil à profil sur une largeur de 6 km de la région étudiée. Une section magnétique et lithologique composée d'une épaisseur totale de 2,3 km a été construite en faisant correspondre les anomalies de parties chevauchantes de profils voisins. La magnétite est le seul minéral fortement magnétique détecté et on en trouve moins de un pour cent en poids dans certains lits de métagrauwacke arénacée. Les lits de schiste et certains lits de métagrauwacke ne contiennent pas de phases magnétiques. L'analyse détaillée du magnétisme de la formation de Goldenville peut servir à établir la subdivision stratigraphique des métaturbidites monotones, l'analyse du lithofaciès et les études de provenance.

Introduction

Recent aeromagnetic total field and vertical gradient surveys of parts of Nova Scotia (Geological Survey of Canada, 1982a,b) indicate the presence of linear magnetic anomalies over the Goldenville Formation of the Meguma Group. Some of these magnetic anomalies are several hundreds of metres wide and extend for more than 30 km parallel to the strike of bedding. They indicate that characteristic magnetic horizons may be used to subdivide the Goldenville Formation. In May, 1982 a two-year program was begun to map the Meguma Group in the Ecum Secum-Liscomb area of Nova Scotia (Henderson, 1983) from the Atlantic coast to the West River-St. Mary's Fault between 62°00'W and 62°30'W (Fig. 7.1). An aeromagnetic total field and vertical gradient survey was flown over the map area in September 1982 by the Geological Survey of Canada. In order to evaluate the forthcoming aeromagnetic data, a program of ground magnetic profiling was carried out using a portable magnetic gradiometer. The principal objectives were: (1) to determine the cause of the aeromagnetic responses over the Goldenville Formation, and (2) to determine whether the portable gradiometer could be useful in defining and correlating marker beds by recognizing small magnetic features not resolved by an aeromagnetic survey.

The study area (Fig. 7.2) consists of Crooks, Goose, and Barren islands which were selected because of their abundant shoreline outcrop and relatively treeless, till-covered interiors. The area is entirely in the Goldenville Formation on the south limb of the Sober Island Syncline where the beds dip north at 60 to 70 degrees (Fig. 7.2). The Goldenville Formation consists of greenschist grade sandy metawacke and slate composing a metaturbidite succession. The formation is estimated to be 5.6 km thick (Faribault, quoted in Taylor, 1967). In the late 19th and early 20th centuries more than 35 million grams of gold were recovered mainly from stratabound quartz veins in the Goldenville Formation (Graves and Zentilli, 1982).

Acknowledgments

We are grateful for the advice and support of Les Kornik throughout the study. Steve McCollough provided invaluable assistance in carrying out all aspects of magnetic and lithological data collection and machine profiling. We thank Ken Buchan, Peter McGrath, John B. Henderson and Les Kornik for reviewing the manuscript.

---

[1] Contribution to Canada-Nova Scotia Co-operative Mineral Program 1981-84. Project funded and carried by Geological Survey of Canada.

[2] Department of Earth Sciences, University of Waterloo, Waterloo, Ontario, N3L 3G1.

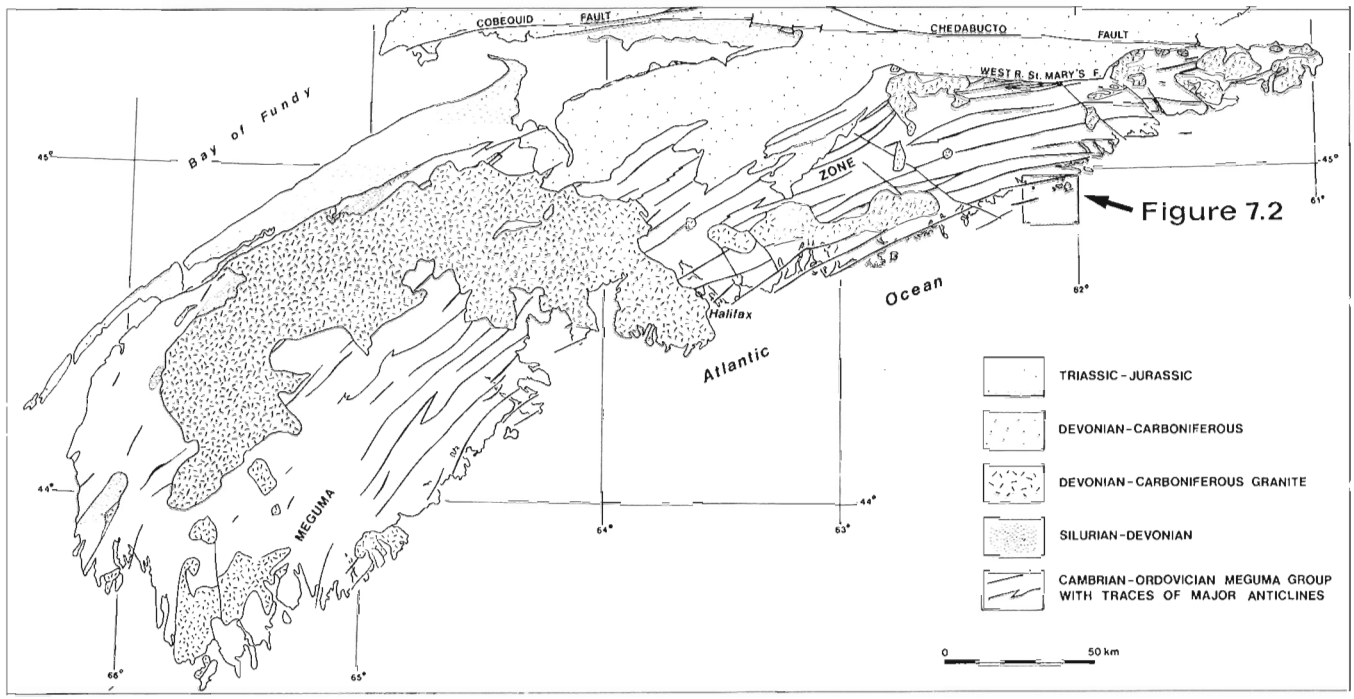

Figure 7.1. *Generalized geological map of southern Nova Scotia. The area shown in Figure 7.2 is outlined.*

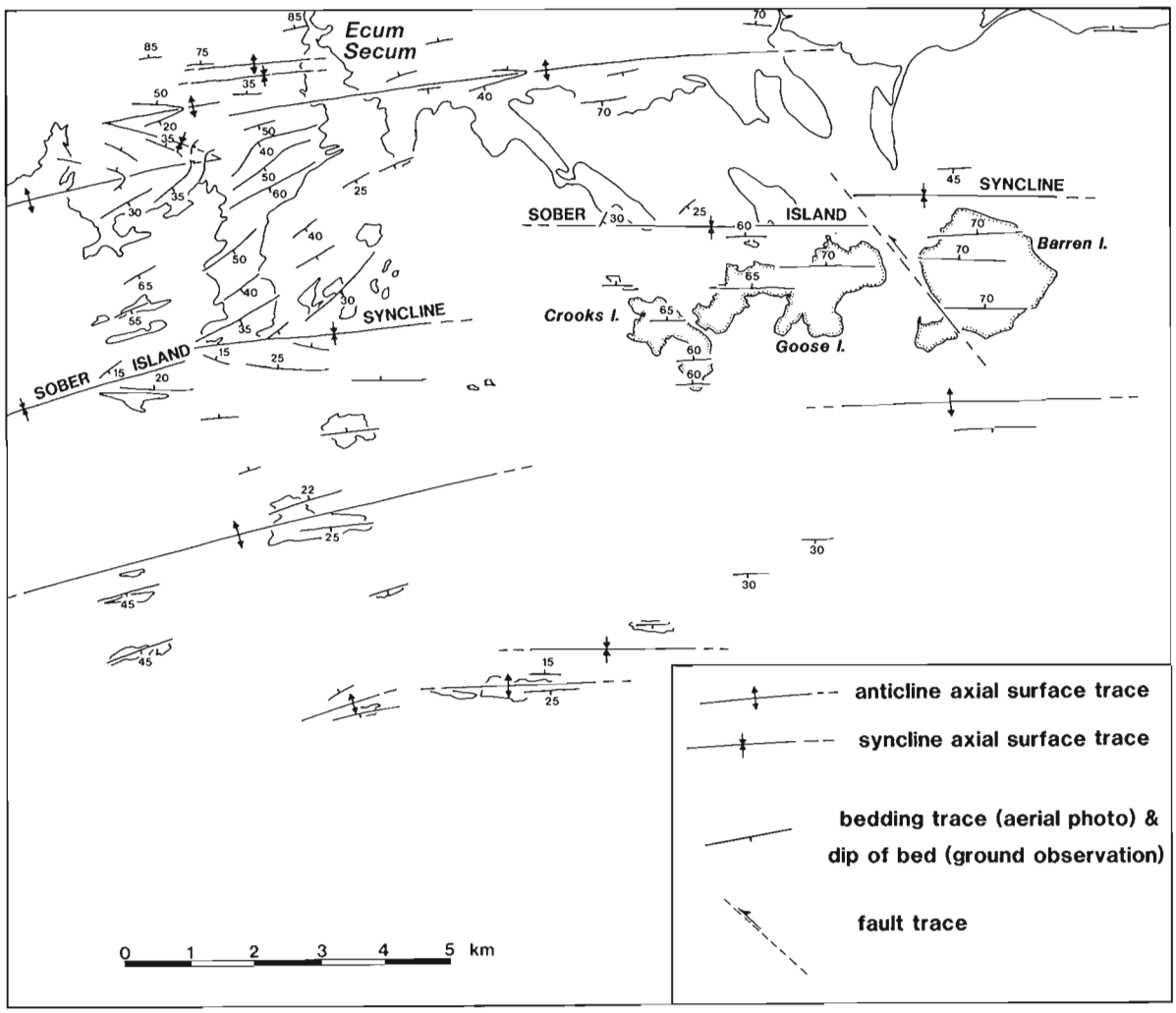

Figure 7.2. *Structural geological map of the area south of Ecum Secum showing the location of Crooks, Goose and Barren islands.*

Gradiometer Survey

Nine ground magnetic profiles were made over the survey area to determine the magnetic character of a typical Goldenville sequence of rocks. Total magnetic field and vertical magnetic gradient measurements were taken at two-metre intervals along north-south lines using a one-man, portable gradiometer. For the purpose of comparison, the lines were run both across areas of good shoreline exposure and across mainly till-covered inland areas.

The measuring system consisted of an EDA PPM-500 Vertical Magnetic Gradiometer, an EDA PPM-400 Base Station Magnetometer to monitor diurnal variations in the magnetic field, and a Hewlett-Packard HP-85 micro-computer for machine profiling of the magnetic data with a preprogrammed tape supplied by EDA Instruments, Inc.

The PPM-500 Vertical Magnetic Gradiometer (Fig. 7.3) has two total magnetic field sensors, located one metre apart on a vertically held pole. The sensors are simultaneously energized, and the difference in the total magnetic field between the upper and lower sensors divided by the sensor separation of one metre yields the vertical magnetic gradient in gammas per metre. The readings are retained in a built-in memory. The results of the vertical gradient survey are shown in Figure 7.4. The total magnetic field reading obtained from the upper sensor is retained as the total magnetic field value. The results of this survey are shown in Figure 7.5.

Results

The magnetic profiles (Fig. 7.4, 7.5) show that the Goldenville Formation has distinctive magnetic horizons that can be traced from profile-to-profile across the three islands. Profiles A, C, E, F, G and I are over coastal sections of excellent bedrock exposure; profiles B, D, and H are over till-covered inland areas with a few bedrock ridges of metawacke. The affect of thin till cover on the magnetic response of the beds appears to be negligible in the survey area. Dashed correlation lines in Figures 7.4 and 7.5 connect similar points between the profiles. This ability to correlate magnetically between profiles resulted in the identification of a 400 m sinistral offset of magnetic markers between profile lines F and G (Fig. 7.4, 7.5). This is interpreted as offset across a fault near the west shore of Barren Island. Brecciated rocks occur along the strike of the inferred fault zone and support the interpretation.

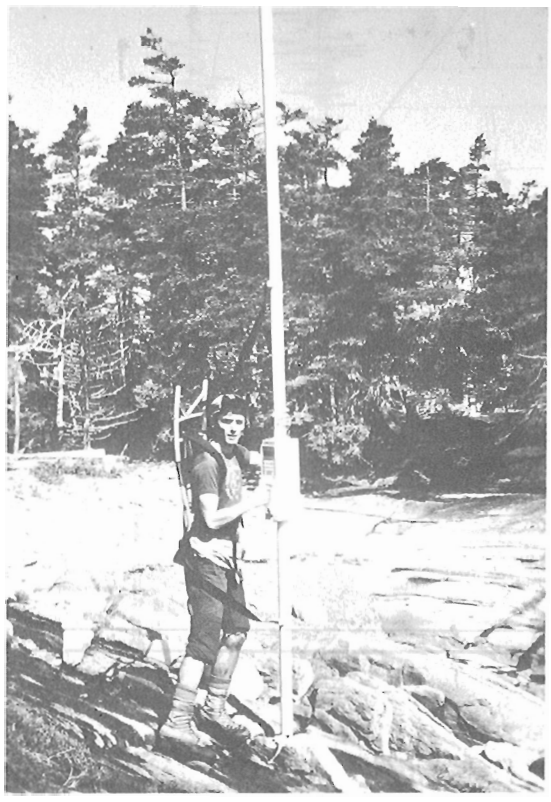

Figure 7.3. *The EDA PPM-500 Vertical Magnetic Gradiometer in operation over an outcrop of the Goldenville Formation on Goose Island. GSC 203683-V.*

Relationships Between Magnetics and Lithology

Stratigraphic sections of 2300 m combined thickness were measured in order to determine the relationship between the rocks and their magnetic signature. The total section was divided into five subsections, located across beach profiles A, C, E, G and I, that were also surveyed with the gradiometer (Fig. 7.4, 7.5). The beds were classified according to the classical Bouma (1962) turbidite sequence: massive, graded division A; plane parallel laminated division B; ripple bedded division C; upper parallel laminated division D; pelitic division E.

The relationships between magnetic response and lithology are illustrated in Figure 7.6 where a 170 m stratigraphic interval, present, at least in part, in all profiles, has been identified and correlated across the study area by matching magnetic vertical gradient and total field profiles. In Figure 7.6 the magnetic profiles over the 170 m interval have been superimposed for comparison. The corresponding parts of lithological subsections C, E, and G, are placed below the magnetic profiles so that the beds responsible for the magnetic variations can be identified.

The following generalizations can be made about the magnetic characteristics of the Goldenville Formation with reference to Figure 7.6:

1. The total magnetic field values increase as the proportion and volume of Bouma A, B, and C divisions (metawacke) increases.
2. The contact of large metawacke units with slate (Bouma D and E divisions) commonly is marked by a change from negative magnetic gradients (slate) to positive gradients (metawacke); the metawacke-slate contact is close to the zero gradient crossover.
3. Some sequences of interbedded metawacke and slate possess smooth magnetic gradient profiles that lie near the zero gradient level, and the two lithologies are indistinguishable magnetically.

In summarizing the relationships between lithology and magnetic signature, it can be seen that metawacke very commonly shows high total magnetic field values and positive vertical gradient anomalies, whereas slate shows low total field values, and, where adjacent to metawacke, shows negative vertical gradient anomalies.

Causes of Magnetic Anomalies

McGrath (1970) attributed the aeromagnetic anomalies associated with the Goldenville Formation to magnetite in sandy metawacke beds. In order to verify this finding in the study area and to investigate further the magnetic character of the Goldenville Formation, heavy mineral analyses and magnetic susceptibility measurements were performed on metawacke samples from three locations, representing high negative, high positive, and zero vertical magnetic gradient anomalies. Figure 7.7 shows the three sample sites, G-1, G-2, and I-1 located on their stratigraphic subsections.

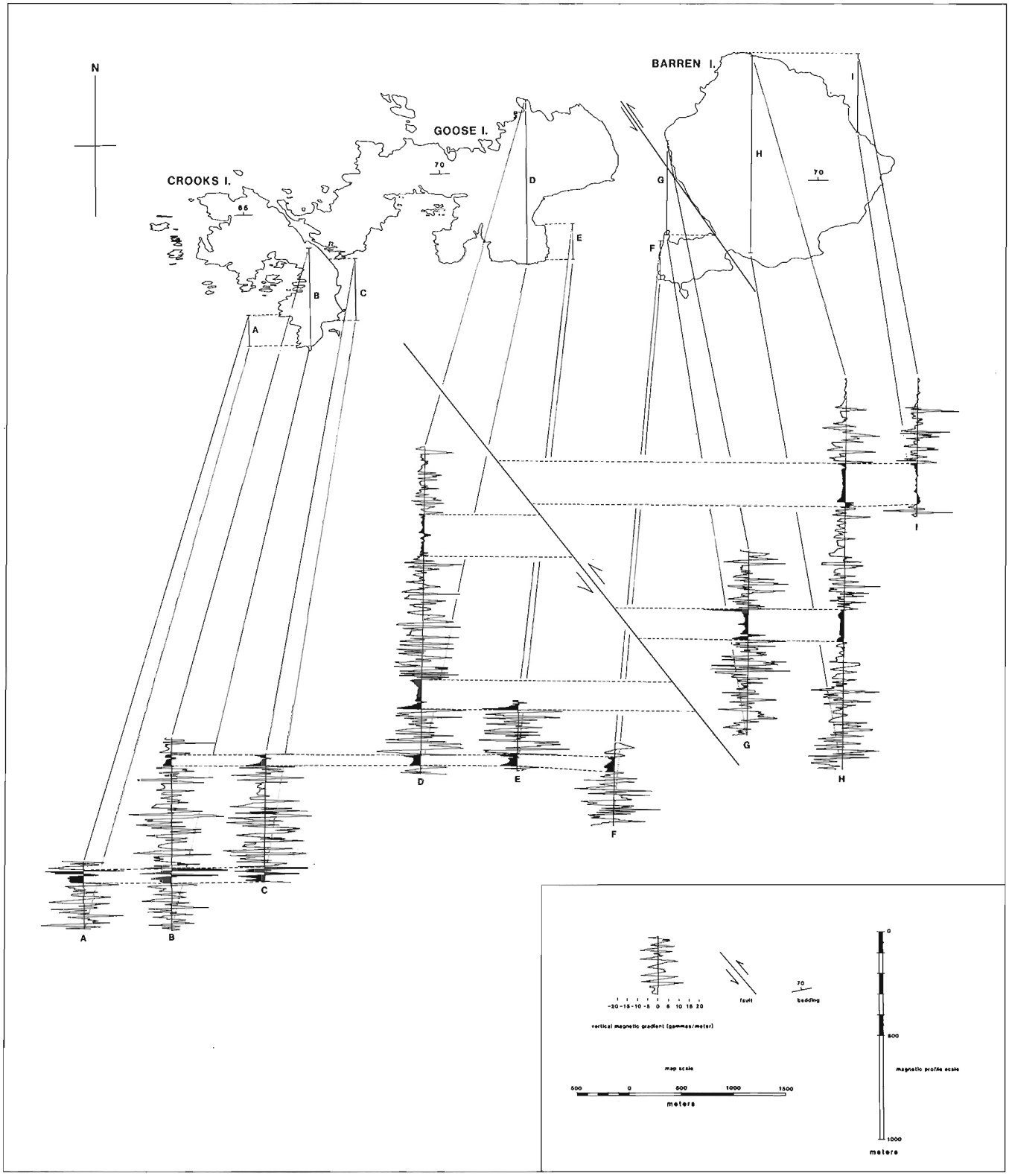

Figure 7.4. *Correlation diagram showing vertical magnetic gradient profiles A-I and their location on the three islands. Profiles A, C, E, F, G, and I were run over shoreline outcrops and are projected onto N-S lines; the inland profiles B, D and H were run along N-S lines. Dashed lines connect correlative magnetic intervals between the profiles. Note the left-hand offset of the correlative intervals across an inferred fault between profiles F and G.*

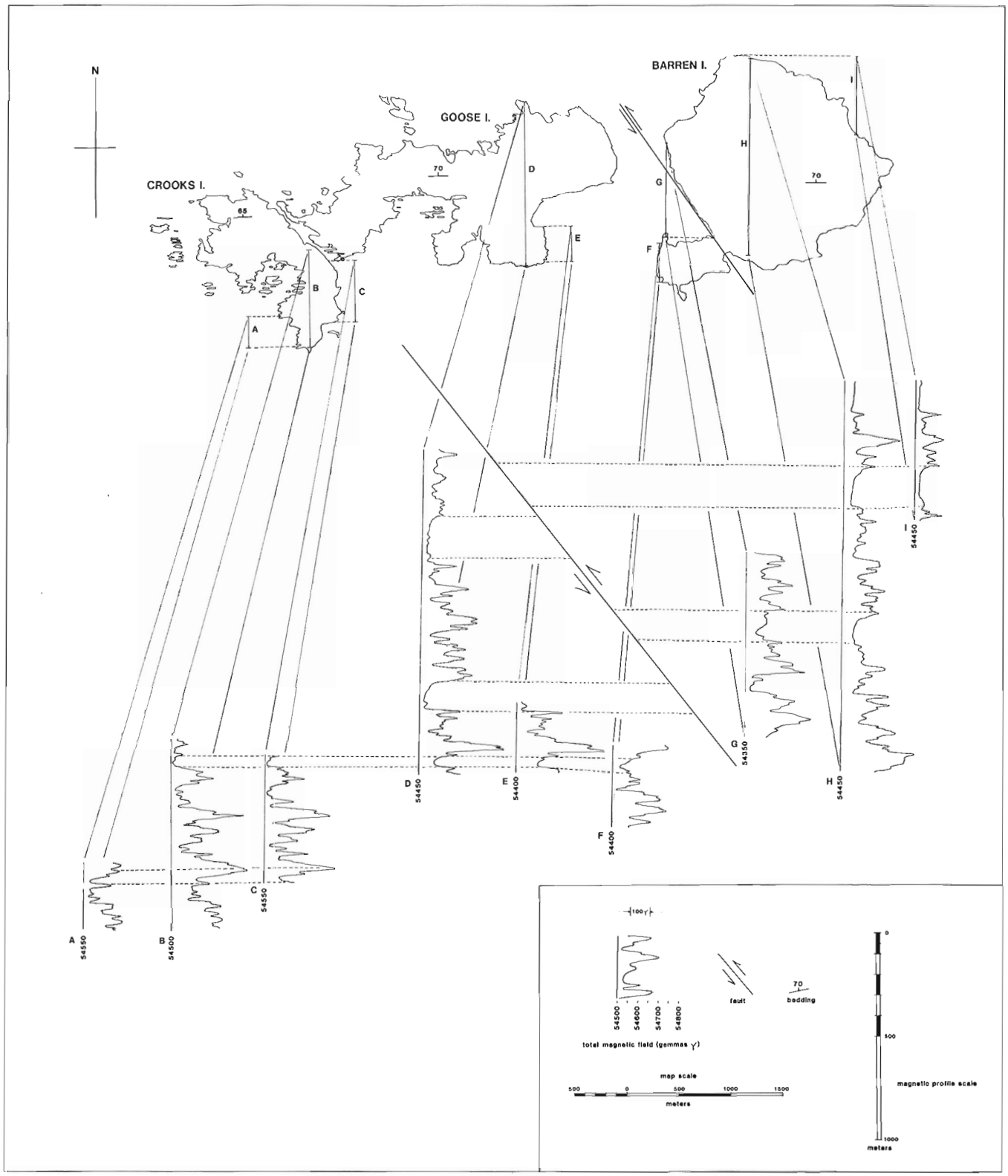

Figure 7.5. *Correlation diagram showing total magnetic field profiles A-I and their locations on the three islands. Dashed tie lines connect correlative magnetic intervals between profiles, and are the same correlations as those of Figure 7.4.*

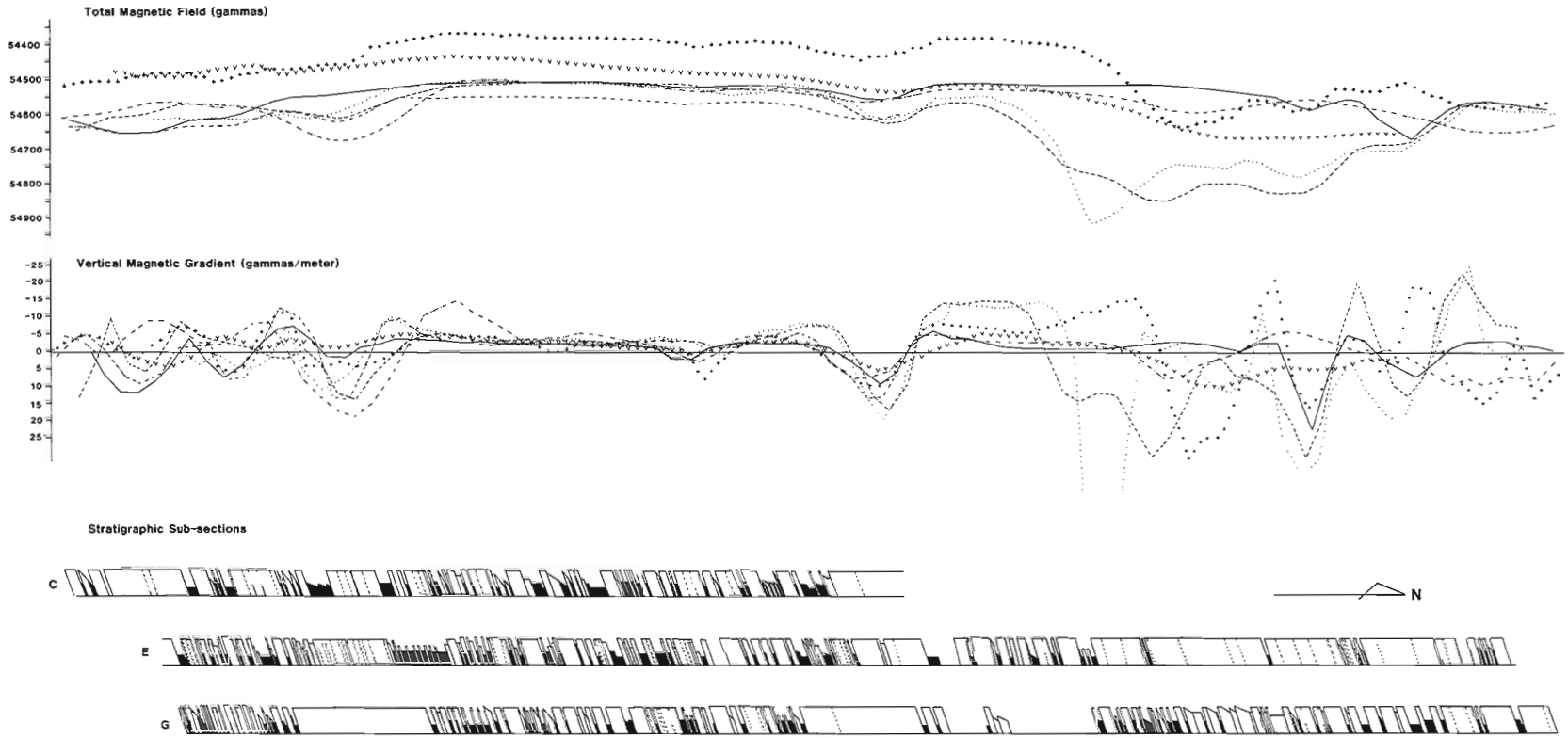

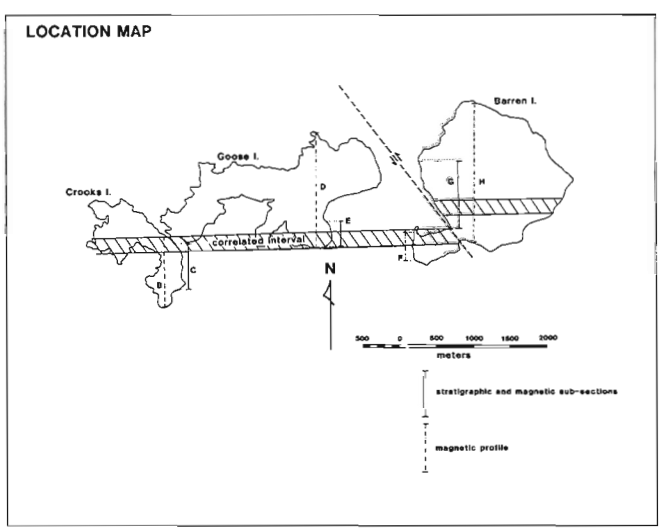

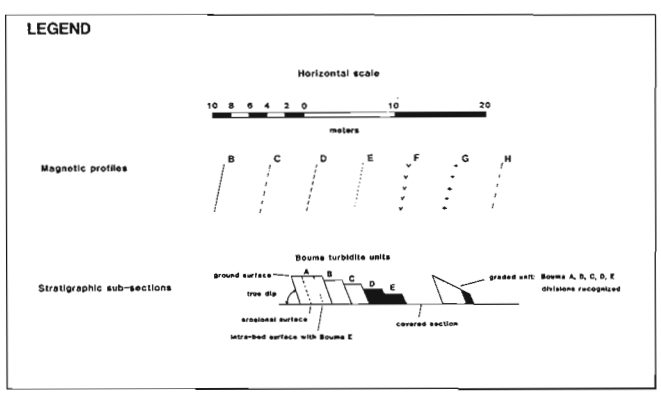

Figure 7.6. *Magnetic correlation diagram showing a 170 m interval of the Goldenville Formation. Magnetic profiles B-H are overlapped for comparison. Note that positive gradient and total magnetic field values increase downward in the figure. Equivalent parts of stratigraphic subsections C, E and G are aligned below the profiles in order to compare the magnetic responses with the lithologies.*

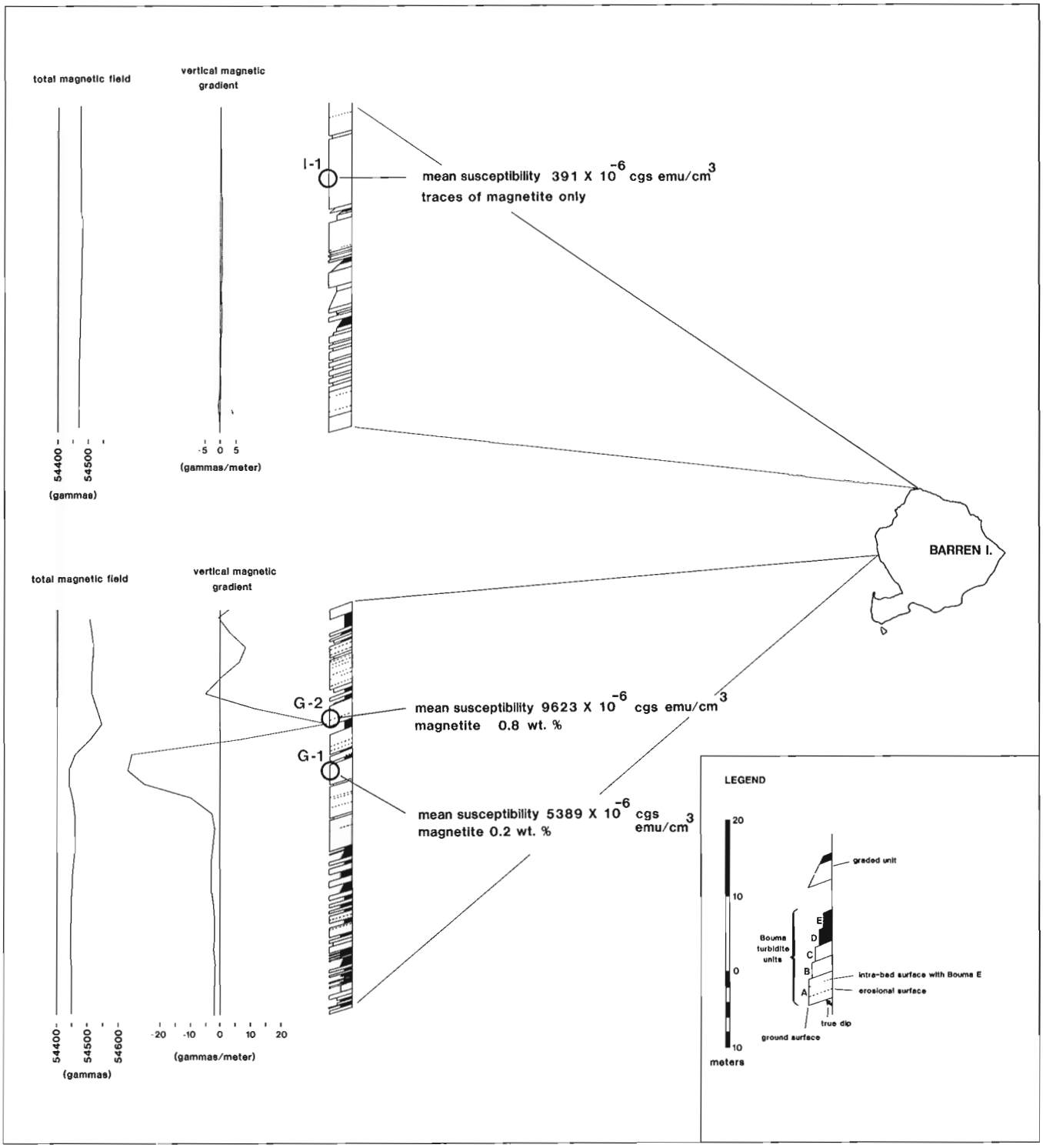

Figure 7.7. *Diagram showing the location of magnetic susceptibility sample sites G-1, G-2, and I-1 on their lithological subsections. Total magnetic field and vertical gradient profiles are placed beside them for comparison. The vertical gradient anomaly between G-1 and G-2 is due to a susceptibility contrast caused by a four-fold difference in magnetite concentration. No magnetic anomalies are produced by low or uniform magnetite concentrations, e.g. the lithological subsection of Profile I adjacent to sample site I-1.*

Beside each subsection the corresponding total magnetic field and vertical magnetic gradient profiles are drawn. The results of the heavy mineral analyses are shown in Table 7.1.

Magnetic anomalies (both total field and vertical gradient) are caused by small variations in magnetite concentration between adjacent beds or groups of beds. Metawacke sample G-1 has a magnetite concentration of 0.2 weight per cent which results in a low mean susceptibility (5389×10^{-6} cgs emu/cm^3), a correspondingly low total magnetic field value and a high negative magnetic gradient. Metawacke sample G-2 has a magnetite concentration of 0.8 weight per cent, a higher mean susceptibility (9623×10^{-6} cgs emu/cm^3), a higher total magnetic field value, and a high positive magnetic gradient. The variation in magnetic susceptibility between samples G-1 and G-2, caused by a four-fold difference in magnetite concentration, produces the vertical magnetic gradient and total field anomalies recorded at the sample sites.

Adjacent slate and metawacke beds commonly produce a vertical magnetic gradient anomaly, with slates being characterized by negative gradients and metawackes by positive gradients. This observation and the heavy mineral analyses of samples G-1 and G-2 indicate that some metawackes are magnetite-rich in comparison to slates, and cause the magnetic anomalies. Sites G-1 and G-2 (Fig. 7.7) show that it is also possible to produce a magnetic anomaly between two metawacke units with different magnetite contents.

Where there is no susceptibility contrast between beds, no magnetic anomalies are created. For example, metawacke sample I-1 in Figure 7.7 is almost barren of magnetite, which has resulted in a very low susceptibility of 391×10^{-6} cgs emu/cm^3 and a low total field value recorded at the sample site. These metawacke beds are similar to slates in terms of their magnetic signature and produce a flat magnetic response.

Table 7.1

Heavy mineral analyses

Heavy Minerals[2]	Sample Sites[1] G-1	G-2	I-1
magnetite[3]	0.2 wt.%	0.8 wt.%	trace
hematite[4]	trace amounts as alteration of magnetite		
other[5]	0.1 – 0.2 wt.% epidote >> titanite > zircon		

[1] See Figure 7.7 for location of sample sites.

[2] Heavy minerals were extracted by crushing and seiving of the samples, followed by immersion in bromoform (specific gravity 2.85) and methylene iodide (s.g. 3.32) to concentrate the heavy mineral fraction. Further separation of the minerals was done on the basis of magnetic character with the use of a hand magnet and a Frantz electromagnetic separator. Mineral identification under the binocular microscope was confirmed by X-ray diffraction analysis. All size fractions of the crushed rock were analyzed magnetically, thus the mineral weight percentages are true whole-rock percentages.

[3] Magnetite (Fe_3O_4) was removed with hand magnet and with the Frantz magnetic separator set at 0.1A.

[4] Hematite (Fe_2O_3) was removed with the Frantz magnetic separator set at 0.25A.

[5] Fraction of the sample that was not removed with the Frantz magnetic separator set at 0.25A.

Sedimentological Interpretations Based on Magnetic Profiles

The direct relationship between magnetite concentration, mean susceptibility, and the production of magnetic anomalies may provide information on Goldenville sedimentology. For example, the vertical magnetic gradient profiles (Fig. 7.4) show an overall trend from larger, closely spaced anomalies in the bottom half of the section to smaller, more widely spaced anomalies toward the top. This trend may be seen best in profiles D and H which cross a large portion of the total section. Accompanying this upward smoothing of the vertical magnetic gradient profile is a decrease in the average value of total magnetic field readings (Fig. 7.5). These trends are interpreted as resulting from progressively less magnetite variability between beds, accompanied by an overall decrease in magnetite concentrations in metawacke upsection. There is no apparent increase in the proportion of slate upsection, so this possible cause of the decreasing total magnetic field values may be ruled out. These variations in magnetite concentration which appear to be on the kilometre-scale may cause the aeromagnetic anomalies over the Goldenville Formation.

Magnetic profiles may be useful in the recognition of sedimentary cycles within the Goldenville Formation. For example, Walker (1978) shows that thickening-upward and coarsening-upward facies sequences characterize submarine fan progradation. Since the total magnetic field values are directly proportional to the amount of metawacke present, the recognition of Walker's (1978) facies sequences (that involve increases in the proportion of sand) may be accomplished by looking at the variation in the total magnetic field values. For example, the progressive increase in the total magnetic field intensity from bottom to top (left to right) in Figure 7.6 corresponds to an increase in the number and thickness of metawacke beds. This may be interpreted as part of a thickening-upward and coarsening-upward cycle, typical of fan progradation. Reference back to the total field profiles for the whole study area (Fig. 7.5) indicates that similar cycles may be present on the scale of 100-200 m in all profiles, but are most noticeable in profile H. These cycles show a progressive upsection increase and abrupt decrease in magnetic intensity. The total magnetic field profiles may provide a rapid method by which sedimentary cycles such as these can be recognized.

Additional information on sedimentology may be gained by using the magnetic profiles to correlate beds or turbidite flow units between outcrops, thereby providing a basis to measure lateral variations in sedimentological features. Such variations would normally be difficult to measure because there is no method by which to correlate monotonous turbidite sequences in the absence of marker horizons. The lithological profiles in Figure 7.6 show that groups of beds with a distinctive lithological character, such as dominantly sand, tend to persist as far as 4 km parallel to strike, but that individual beds are not persistent.

Conclusions

The results of this ground magnetic study of part of the Goldenville Formation may be summarized as follows:

1. Magnetite-bearing metawacke beds in contact with metawacke or slate beds with less magnetite produce total magnetic field and vertical gradient anomalies.
2. A portable gradiometer is useful for tracing magnetic marker horizons between isolated outcrops by matching total magnetic field and vertical magnetic gradient profiles.

3. Total magnetic field profiles may detect coarsening-upward cycles within the Goldenville Formation. Vertical gradient and total field profiles may also reveal progressive vertical and lateral changes in magnetic mineral concentration that may be useful in facies modelling and provenance studies.

References

Bouma, A.H.
1962: Sedimentology of Some Flysch Deposits; Elsevier Publishing Co., Amsterdam, 168 p.

Graves, M.C. and Zentilli, M.
1982: A review of the geology of gold in Nova Scotia; in Geology of Canadian Gold Deposits; Canadian Institute of Mining, Special Paper No. 24, p. 233-242.

Geological Survey of Canada
1982a: Experimental colour compilation (high resolution aeromagnetic residual total field), parts of 11D/13, 11D/14, Nova Scotia; Geological Survey of Canada, Map C 20,335 G.

1982b: Experimental colour compilation (high resolution aeromagnetic vertical gradient), parts of 11D/13, 11D/14, Nova Scotia; Geological Survey of Canada Map C 40,076 G.

Henderson, J.R.
1983: Analysis of structure as a factor controlling gold mineralization in Nova Scotia; in Current Research, Part B, Geological Survey of Canada, Paper 83-1B, Report 2.

McGrath, P.H.
1970: Aeromagnetic interpretation Appalachia, New Brunswick and Nova Scotia; in Report of activities, Part A, Geological Survey of Canada, Paper 70-1A, p. 79-82.

Taylor, F.C.
1967: Reconnaissance geology of Shelbourne map-area, Nova Scotia; Geological Survey of Canada, Memoir 349, 83 p.

Walker, R.G.
1978: Deep-water sandstone facies and ancient submarine fans: models for exploration for stratigraphic traps; American Association of Petroleum Geologists Bulletin, v. 62, no. 6, p. 932-966.

8.

OXYGEN ISOTOPE VARIATIONS IN PERMAFROST, TUKTOYAKTUK PENINSULA AREA, NORTHWEST TERRITORIES

Project 680047

J. Ross Mackay[1]
Terrain Sciences Division

Mackay, J.R., Oxygen isotope variations in permafrost, Tuktoyaktuk Peninsula area, Northwest Territories; in Current Research, Part B, Geological Survey of Canada, Paper 83-1B, p. 67-74, 1983.

Abstract

Oxygen isotope variations in permafrost in the Tuktoyaktuk Peninsula area, Northwest Territories, are used in conjunction with other data to provide a range of estimates for the $\delta^{18}O$ values of ice in post-Hypsithermal lake bottom taliks, modern ice-wedge ice, and ground ice of pre-late Wisconsinan age. Some estimates are given for the rate of growth of permafrost in recently drained lakes; the freezing rate at the end of a decade can be less than 0.1 mm•h^{-1}. The freezing rates are so slow that the effects of oxygen isotope fractionation should be considered in the interpretation of oxygen isotope variations at sites with both closed and open system freezing.

Résumé

Les variations des isotopes d'oxygène dans le pergélisol de la région de la péninsule de Tuktoyaktuk (Territoires du Nord-Ouest) et d'autres données permettent d'obtenir une gamme d'estimations pour les valeurs de δO^{18} de la glace dans les tabétisols des fonds lacustres post-hypsithermiques, de la glace remplissant les fentes de gel contemporaines et les hydrolaccolithes (glace dans le sol) antérieurs au Wisconsinien supérieur. Quelques estimations sont données pour le rythme de croissance du pergélisol dans les lacs récemment drainés; le taux de congélation à la fin d'une décennie peut être inférieur à 0,1 mm/h^{-1}. Les vitesses de congélation sont si faibles qu'il faudra tenir compte du fractionnement des isotopes d'oxygène lors de l'interprétation des variations des isotopes d'oxygène dans les endroits caractérisés par le phénomène de congélation se manifestant aussi bien en système ouvert que fermé.

Introduction

Oxygen isotope variations ($^{18}O/^{16}O$) in natural systems have been widely used in the interpretation of past climatic conditions in environments ranging from polar ice caps to the tropics. Since the oxygen isotope variations depend primarily upon the condensation temperature of the precipitation, the $\delta^{18}O$ values for ice in permafrost help to give an indication of the conditions when precipitation occurred, provided there have been no major isotopic changes between the time of precipitation and subsequent freezing. Although there has been a great deal of research on oxygen isotope variations for glacier ice, far less is known about permafrost ice. Stuiver et al. (1976, 1981) have used oxygen isotope ratios effectively in the study of Antarctic permafrost. Michel (1982) and Michel and Fritz (1978, 1980, 1981, 1982a) have reported in detail on oxygen isotope ratios at "Illisarvik" (Fig. 8.1), an experimental drained lake site (Mackay, 1981a); the Dempster Highway; and at several sites in Mackenzie valley. Other studies are also available for the Tuktoyaktuk Peninsula area (Mackay, 1972; Mackay and Lavkulich, 1974; Fujino and Kato, 1978; Kato and Fujino, 1981). In addition to the preceding published data, some two hundred analyses are also available to the writer. This paper discusses the oxygen isotope variations for a number of ice types that occur in the Tuktoyaktuk Peninsula area, using both published and unpublished sources.

Active Layer Ice

The suprapermafrost water in the thawed active layer in summer will be derived mainly from snowmelt, rainfall, and the thaw of active layer ice frozen the previous winter. Because the thickness of the active layer varies by about 10 to 20% from year to year, the water released by basal thaw of the active layer in one summer may be water that froze several winters previously. To complicate matters, ice lenses in the active layer may contain water that migrated upwards in the previous winter from the top of permafrost (Parmuzina, 1978; Cheng, 1982; Mackay, 1983). On a volume basis, however, the ice (water) in the active layer should reflect approximately the proportions of snowmelt and rain that enter the groundwater system for the year under investigation. In the Tuktoyaktuk Peninsula area, where there is both downward freezing from the ground surface and upward freezing from the late summer frost table, isotope fractionation may occur (Michel and Fritz, 1981, 1982a; Michel, 1982). The $\delta^{18}O$ values for active layer waters at Illisarvik and Site 1 (Fig. 8.1) are mainly in the -18 to -20 ‰ range (Fujino and Kato, 1978; Michel and Fritz, 1980, 1981, 1982a; Michel, 1982). The range of -18 to -20 ‰ is more positive than that for winter snowfall and more negative than that for summer rain, thus showing an averaging of the two principal water sources.

Aggradational Ice

The top of permafrost is commonly ice rich because the permafrost table has risen at some time in the past to incorporate within it basal ice formerly at the bottom of the active layer (Cheng, 1982). Such ice is referred to as aggradational ice (Brown and Kupsch, 1974). Aggradational ice should reflect the isotopic composition of the basal active layer ice at the time when the ice was incorporated into permafrost. Furthermore, there may be an addition of water from the subjacent permafrost. During the Hypsithermal period, which lasted from about 8500 to 5500 BP (Ritchie and Hare, 1971), the active layer thickened. The Hypsithermal permafrost table (base of active layer) can be seen as a widespread thaw unconformity along many coastal exposures such as at Garry, Pelly, and Hooper islands (Mackay, 1975).

[1] Department of Geography, University of British Columbia, Vancouver, British Columbia V6T 1W5

Aggradational ice has formed, following the close of the Hypsithermal, above the thaw unconformity. A $\delta^{18}O$ value of -25.3 ‰ was obtained for one sample of aggradational ice at Hooper Island and -26.1 ‰ for Garry Island. These values are more negative than present active layer ice.

Modern Ice-Wedge Ice

The source water for ice-wedge ice is derived mainly from snowmelt in May and June. Although some hoar crystals may grow in the ice-wedge cracks during the temperature reversal of winter to summer, most of the crack infilling is from snowmelt in May and early June. At Illisarvik (Fig. 8.1) Michel and Fritz (1981) found a fairly constant value of -22.5 ‰ at two ice-wedge sites. At a third site, massive ice, interpreted as ice-wedge ice (Michel, 1982), had extremely uniform oxygen-18 contents of -24 to -25 ‰. Near Tuktoyaktuk, nine samples collected by V.N. Rampton at Site 1 (Fig. 8.1) showed a range of from -23.3 to -26.3 ‰. In summary, analyses from four and possibly five modern ice wedges were mainly in the range of -22 to -26 ‰.

Relict Ice-Wedge Ice

At Hooper Island organic matter from a former active layer just above the Hypsithermal thaw unconformity has been dated at 8765 ± 230 years BP (GX-4352). A sample of ice from a large ice wedge, whose top was truncated by the thaw unconformity, gave a value of -32.3 ‰, which is much more negative than that of modern ice-wedge ice.

Pingo Ice

With the exception of small pingos, most pingo ice cores have several ice types. The bulk of the core can be segregated ice, intrusive ice formed from the freezing of bulk water, or any combination of the two types. In addition, dilation-crack ice (tension-crack ice, Brown and Kupsch, 1974) is commonly the main ice type beneath the summit of pingos with craters. Ice wedges may also penetrate into the ice core. The ice encountered in a drill core can therefore contain one or more of the following ice types: segregated ice, intrusive ice, dilation-crack ice, and ice-wedge ice. For example, Fujino and Kato (1978) give a $\delta^{18}O$ range of -22.2 to -26.0 ‰ for pingo ice at the top of Peninsula Point Pingo near Site 1 (Fig. 8.1), southwest of Tuktoyaktuk, but the ice was ice-wedge ice. Michel and Fritz (1980, 1981) discussed the isotopic composition (-18 to -28 ‰) of ice in several holes drilled in the top of a pingo near Illisarvik, and infer that some of the ice is injection ice frozen from bulk water.

Massive Ice

In the Tuktoyaktuk Peninsula area, tabular ice-rich sections, here termed "massive ice" are commonly encountered at varying depths below the ground surface. The origin of the massive ice is uncertain. Probably most of the ice is segregated ice (Mackay, 1971, 1973; Rampton and Mackay, 1971; Rampton, 1974, 1982; Gell, 1976; Kato and Fujino, 1981), although some buried glacier ice may also be present. In general, the stratigraphic sequence, from the ground surface downwards is: a reworked clayey glacial till; massive ice; and sands and gravels, commonly interlayered with ice. An excellent exposure of massive ice (Fig. 8.2) occurs about 5.5 km southwest of Tuktoyaktuk at Site 1 (Fig. 8.1). Three samples (collected by V.N. Rampton) from near the top of the ice yielded $\delta^{18}O$ values of -31.1, -30.3, and -31.9 ‰. Fujino and Kato (1978) and Kato and Fujino (1981) collected numerous samples from the massive ice shown in Figure 8.2, the analyses of which fall within the range of -27.9 to -30.9 ‰. The preceding values are similar to those for ice collected from Pleistocene sediments in other areas, namely: -28.7 and -30.5 ‰ for ice in an ice cellar in Tuktoyaktuk and -29.9, -31.7, and -32.2 ‰ for massive ice in the Eskimo Lakes area Site 2 (Fig. 8.1).

In the spring of 1973 and 1974 a drilling program was carried out by the Geological Survey of Canada at the Involuted Hill site, 15 km northeast of Tuktoyaktuk (Fig. 8.1).

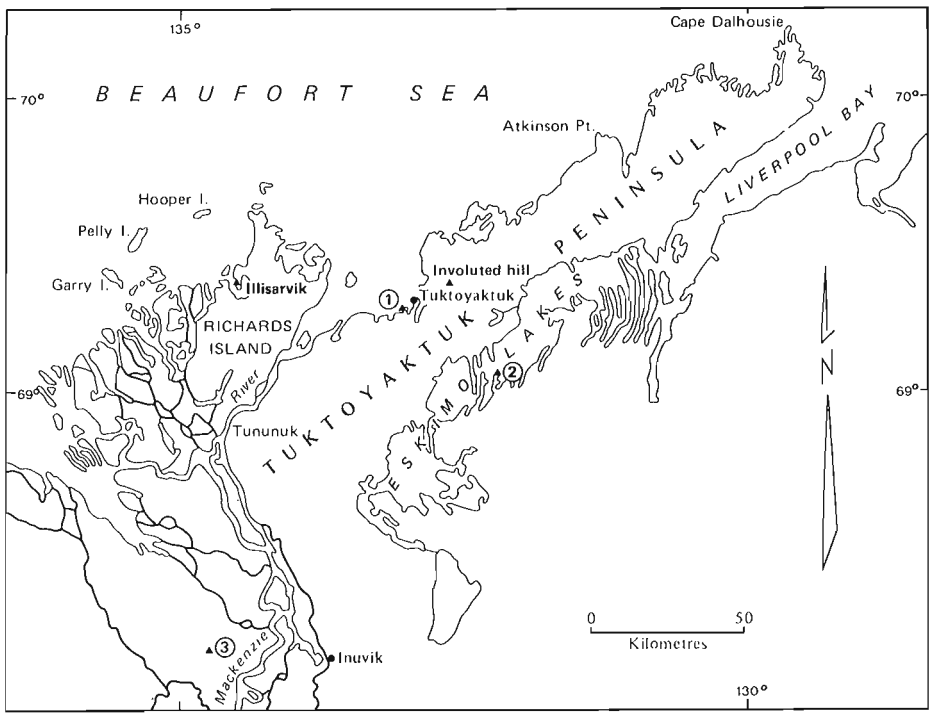

Figure 8.1
Location map.

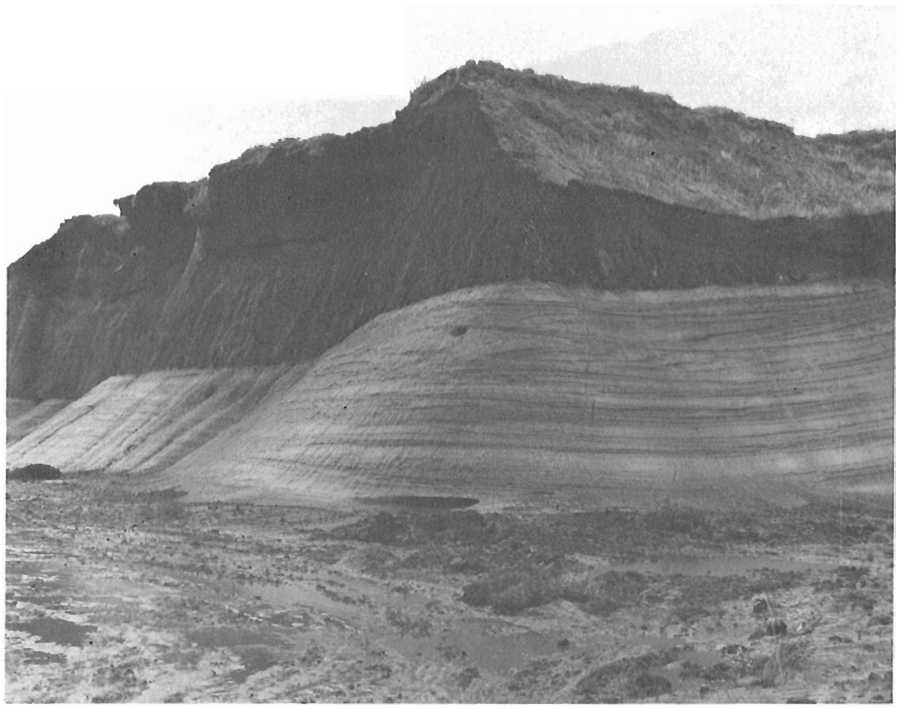

Figure 8.2

Massive ice at Site 1 (Fig. 8.1) southwest of Tuktoyaktuk. The thickness of ice exposed in the slump face is about 5 to 7 m. A stony clay with some pond sediments overlies the ice.

The massive ice appears to be similar to that of the ice shown in Figure 8.2. Samples (collected by V.N. Rampton and W.J. Scott) have been analyzed for oxygen isotope ratios and water quality. The $\delta^{18}O$ values for the massive ice lie mainly between -31 and -35 ‰, whereas those of the underlying sand are more positive and are mostly between -27 and -31 ‰ (Fig. 8.3). Because there is no sharp discontinuity of the oxygen isotope ratios in passing downwards from the massive ice to the underlying sands, a common water source is implied.

Garry Island Terraces

Three unglaciated terraces, 12 to 14 m above sea level, flank the northeast side of Garry Island. The terraces lie beyond the limits of late Wisconsinan glaciation (Mackay et al., 1972). The 15 m-thick terrace sands and gravels overlie an icy silt; $\delta^{18}O$ values for drill core samples (courtesy Imperial Oil Limited) from the icy silt yielded: -30.8 ‰ at 15.2 m; -31.4 ‰ at 21.3 m; and -30.8 ‰ at 30.5 m. The range of values is similar to that of the massive ice in the Tuktoyaktuk area.

Glacially Deformed Pleistocene Sediments

Glacially deformed Pleistocene sediments (Fig. 8.4) which lie beyond the limit of late Wisconsinan glaciation are abundant at Garry, Pelly, and Hooper islands (Mackay et al., 1972). Three samples from Garry Island have yielded $\delta^{18}O$ values of -24.0, -24.9, and -31.8 ‰. Because the beds have been greatly deformed by extensive shearing and faulting, the stratigraphic relationship of the beds, even though less than 100 m apart, is uncertain. At Hooper Island, $\delta^{18}O$ values for an icy clay were -28.2, -29.5, -29.6, and -30.5 ‰. One sample from Pelly Island had a $\delta^{18}O$ value of -30.2 ‰.

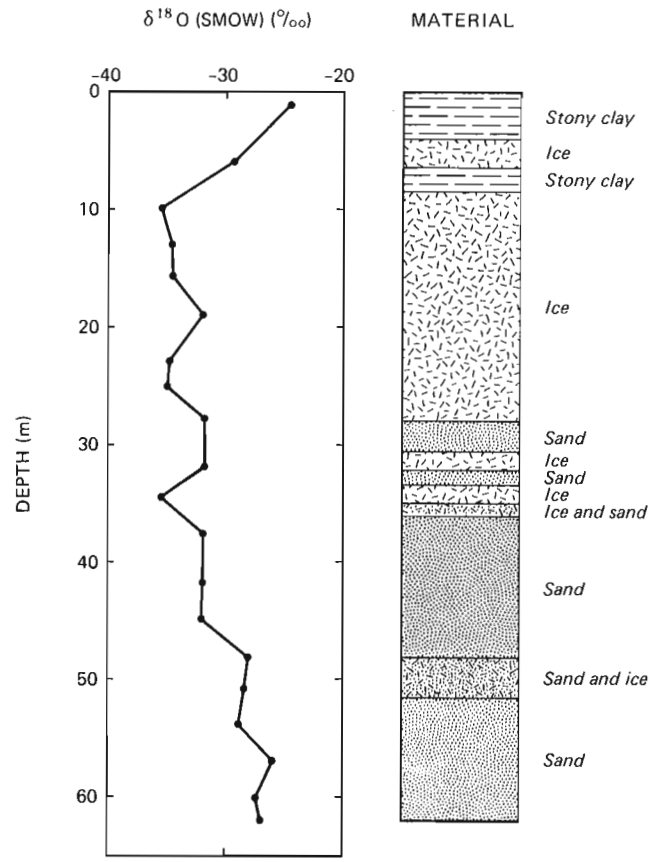

Figure 8.3. *Oxygen isotope ratios and the stratigraphy for a drillhole at the Involuted Hill site, just to the northeast of Tuktoyaktuk (Fig. 8.1).*

Figure 8.4. *Glacially deformed Pleistocene sediments at Garry Island, NWT. About 2 m of slumped debris overlies the nearly vertical, high ice-content beds. The arrow points to one collection site with* $\delta^{18}O$ *of -24.9 ‰.*

Grey and Brown Sand

In the western part of Tuktoyaktuk Peninsula and adjacent Richards Island, the sequence, from top to bottom, is commonly a clayey diamicton, a brown sand, a grey sand, and an ice-rich silty clay (Fyles et al., 1972). The sequence is well exposed at Hooper Island. A single sample from the brown sand gave a $\delta^{18}O$ value of -27.5 ‰ and one from the underlying grey sand, a more positive value of -20.6 ‰.

Lake Bottom Taliks

Oxygen isotope ratios are available from a number of lake bottom taliks which either are in the process of freezing through or else froze through at some time in the past. At the Involuted Hill site (Fig. 8.1) where permafrost is aggrading, a drill core sample gave a $\delta^{18}O$ value of -16.2 ‰ at a depth of 14.5 m where permafrost was 20.5 m deep. At a depth of 21.5 m, just below permafrost, the $\delta^{18}O$ value was -28.8 ‰ (Mackay and Lavkulich, 1974). The difference of 12.6 ‰ is too great to explain by fractionation alone, and the value of -28.8 ‰ may represent that of an older and colder water source. On the west side of Garry Island, lacustrine sediments containing twigs and shells have been radiocarbon dated at 9730 ± 160 years BP (GSC-575). The lacustrine sediments, exposed at about 8 to 11 m elevation, are underlain by beach gravels. Towards the bottom of the section, and 4 m above sea level, a horizontal layer of segregated ice yielded a $\delta^{18}O$ value of -16.4 ‰. As the geometry of the site shows that the ice layer came from what was once the sublake talik, the relatively high positive value can be attributed to the former presence of lake water not much different from that of the present (cf. Michel, 1982; Michel and Fritz, 1982a). At Pelly Island, a sample from a depth of 26 m at the edge of a large, recently drained lake gave a value of -19.2 ‰, a much more positive value than that of the adjacent Pleistocene sediments. At Hooper Island, reticulate vein ice on the edge of an old lake basin gave a $\delta^{18}O$ value of -26.5 ‰ whereas that for vein ice beneath the former basin talik was -17.7 ‰.

Oxygen Isotope Variations in Modern Water

A few $\delta^{18}O$ values for modern water may be helpful in interpreting values for permafrost ice. On 15 June 1970, samples of Mackenzie River and Liard River water were collected at their confluence at Fort Simpson, NWT. The mean of six Mackenzie River samples was -17.4 ‰ and that of six Liard River samples was -21.3 ‰ (Krouse and Mackay, 1971). When the Mackenzie and Liard river waters became fully mixed 500 km downstream the mean was -20.2 ‰. Hitchon and Krouse (1972) reported a somewhat similar range for the entire Mackenzie River drainage basin in summer. In March 1974, samples of lake ice from three Mackenzie Delta lakes at Site 3 (Fig. 8.1) were collected from the top, middle, and bottom of the lake ice at each lake (samples collected by W.A. Adams and N.B. Snow). The results were similar with a grand mean of -16.9 ‰ and a range from -15.5 to -18.2 ‰. A sample of near surface lake ice at Garry Island gave a $\delta^{18}O$ value of -15.2 ‰. On 3 August 1972, water samples were collected from 23 large and small lakes in the eastern half of Tuktoyaktuk Peninsula (analyses by H.R. Krouse). The range of $\delta^{18}O$ values was from -8.1 to -19.1 ‰ and the mean was -12.8 ‰. The more positive values may be due to fractionation from evaporation.

Mackenzie Valley

Oxygen isotope data that have been obtained from lower Mackenzie valley (Hume River and Norman Wells area) are included here, because the data complement that reported for the Tuktoyaktuk Peninsula area. Hume River flows into the left (west) bank of Mackenzie River at about 66°02'N midway between Sans Sault Rapids to the south and Fort Good Hope to the north. In 1973 a drilling program was carried out at a permafrost site 8 km west from the mouth (McRoberts, 1973), and water samples from ice-rich core sections were made available to the writer by E.C. McRoberts and N.R. Morgenstern. The material was a frozen silty clay. Values of $\delta^{18}O$ were: -22.4 ‰ at 2.6 m; -24.4 ‰ at 5.2 m; -23.0 ‰ at 6.1 m; -30.2 ‰ at 15.2 m; -30.7 ‰ at 33.5 m; and -30.6 ‰ at 42.7 m. It is clear that between a depth of 6.1 and 15.2 m, there was a rapid change from a $\delta^{18}O$ value of -23.0 to -30.2 ‰. The shift can probably be explained in terms of the postglacial history of the area, an observation also made by Michel and Fritz (1978) for similar changes elsewhere in Mackenzie valley. With the retreat of the ice lobe, which occupied the Mackenzie Plain in late Wisconsinan time, a large lake was impounded in the area through which lower Hume River now flows (Mackay and Mathews, 1973). A major meltwater system, feeding into the lake via Mountain River, built an extensive compound delta into the lake and later into its shrunken successors. Deltaic and floodplain sediments, yielding 11 000 to 11 500 year radiocarbon dates, accumulated on the floor of the basin at this stage. The lacustrine deposits beneath may date in part from the ice-dammed phase. Draining of the lake was nearly complete by about 6000 years ago. It seems likely, therefore, that the high negative values in the silty clay (-30.2 to -30.7 ‰) below 15.2 m represent entrapped glacial meltwater, whereas the more positive values (-22.4 to -24.4 ‰) nearer to the surface represent later deposition in warmer waters. To what extent permafrost aggradation may have contributed to negative values by fractionation is unknown.

In the spring of 1972, twelve frozen samples were obtained from a drilling site near Norman Wells at depths of from 1 to 6.4 m. The $\delta^{18}O$ values had a mean of -20.4 ‰ with a range of -19.0 to -22.8 ‰. The values are similar to present Mackenzie River water in June at Norman Wells and suggest a warm surface water source compatible with present suprapermafrost groundwater in the area.

Discussion

A summary of the oxygen isotope ratios for ice in the active layer and permafrost in the Tuktoyaktuk Peninsula area is given in Table 8.1. An interpretation of the ratios in terms of the past climatic environment is dependent upon a variety of factors such as the history of the groundwater prior to freezing and oxygen isotope fractionation during the freezing period. The ice in the active layer and modern ice-wedge ice reflect contemporary conditions. In some ice types, fractionation effects may be present.

When water freezes, the ice is enriched in $\delta^{18}O$ in comparison to that of the water from which it froze (O'Neil, 1968; Suzuoki and Kimura, 1973; Michel, 1982). Laboratory experiments have shown that when the freezing rate of water is rapid, little to no fractionation will occur, but if the freezing rate is relatively slow, such as 2 $mm \cdot h^{-1}$ and there is mixing, fairly complete fractionation may occur (Suzuoki and Kimura, 1973). Michel (1982) has carried out laboratory experiments on saturated and unsaturated soils and found that in order for fractionation to proceed, the rate of advancement of the freezing front must be very slow.

Table 8.1

Values for $\delta^{18}O$ for the Tuktoyaktuk Peninsula area. See text for the number of samples involved

Description	$\delta^{18}O$ in ‰
Lake water in mid-summer, Tuktoyaktuk Peninsula	-8 to -19
Lake ice, Mackenzie Delta and Garry Island	-15 to -18
Lake bottom taliks, post-Hypsithermal freezing	-16 to -20
Active layer ice, Tuktoyaktuk Peninsula	-18 to -20
Mackenzie River water near Delta, late June	-20
Pleistocene grey sand, Hooper Island	-21
Ice-wedge ice, modern, Tuktoyaktuk Peninsula	-22 to -26
Pleistocene icy brown sand, Garry Island	-24 to -25
Sand below massive ice, Involuted Hill	-27 to -31
Pleistocene brown sand, Hooper Island	-27
Massive ice, Tuktoyaktuk area	-28 to -35
Pleistocene icy clay, Hooper and Garry Islands	-28 to -31
Relict ice wedge, pre-Hypsithermal, Pelly Island	-32

The freezing rate of saturated soils with minimal ice segregation in the Tuktoyaktuk Peninsula area is known for a number of recently drained lakes. The depth (z) to which permafrost can grow in time (t) can be approximated by Stefan's solution, given a step change in temperature and a number of simplifying assumptions (Johnston, 1981):

$$z = \sqrt{\frac{-2kTt}{Q}} = b\sqrt{t} \qquad (1)$$

where z is depth of freezing,
k is the thermal conductivity of the frozen soil,
T is the temperature in 0°C,
t is time,
Q is volumetric latent heat, and
b is a constant.

Stefan's solution will overestimate the depth of freezing because the contribution of heat conduction from the unfrozen zone below permafrost is ignored. The freezing rate is:

$$\frac{dz}{dt} = \frac{b}{2\sqrt{t}} \qquad (2)$$

Combining equations 1 and 2:

$$\frac{dz}{dt} = \frac{b^2}{2z} \qquad (3)$$

The value of b for four recently drained lakes (Mackay, 1979) and the middle of Illisarvik (Mackay, 1981a) ranges from about 25 mm•h$^{-½}$ to 45 mm•h$^{-½}$ for saturated silts to fine sands with little excess ice. Substitution of these values for b into equations 2 and 3 shows that the freezing rate for most aggrading permafrost after about 10 years would be less than 0.1 mm•h^{-1}. When segregated or injection ice develops, the freezing rate will be much slower than at sites where little excess ice is growing. Therefore, when permafrost has been aggrading for much longer than 10 years in the Tuktoyaktuk Peninsula area and segregation or injection ice is forming, the freezing rates should be much less than 0.01 mm•h^{-1}. If permafrost were aggrading in an area without a step change in temperature (equation 1) following lake drainage, the freezing rate would be much slower. In view of the fact that most permafrost growth has probably been in response to a gradual decrease in temperature below 0°C, and permafrost may be well over 500 m in depth, freezing rates could be much slower than 0.001 mm•h^{-1}.

Under natural conditions of permafrost growth, there can be every possible gradation between open system freezing and closed system freezing because of variations in soil type, groundwater, and talik geometry. In the Tuktoyaktuk Peninsula area, closed system freezing is a common occurrence. At Illisarvik, for example, a closed system talik is now present (Burgess et al., 1982). Stuiver et al. (1981) have estimated the effects of oxygen isotope fractionation for the freezing of a 165 m closed system section in Antarctica, assuming a well mixed subpermafrost water reservoir and homogeneous sediments. Fractionation has undoubtedly occurred in hundreds if not thousands of closed system taliks which have frozen through at some time in the past in the Tuktoyaktuk Peninsula area.

The oxygen isotope ratios for intrusive ice grown from a subpingo water lens should show the effects of fractionation. Some of the water lenses exceed 2 m in depth and as freezing rates can be much slower than 0.05 mm•h^{-1}, fractionation should occur.

Michel (1982) and Michel and Fritz (1981, 1982a, 1982b) reported on fractionation of the active layer at Illisarvik with two-sided (downwards and upwards) freezing. The rates of freezing at their active layer drillhole sites are unknown, but at Garry Island (Mackay, 1974, 1981b) comparable sites have rates estimated at 0.15 to 0.03 mm•h^{-1} depending upon the active layer thickness, snow cover, and amount of ice segregation. With respect to ice wedges, although fractionation may take place in the freezing of water in ice-wedge cracks, the crack widths are commonly no more than several millimetres, a width that is normally far less than that of the sample, so fractionation effects would not be observed. Fractionation effects might well be noted in the dilation crack ice of pingos, however, because some cracks are at least 20 cm wide.

The $\delta^{18}O$ values for the massive ice in the Tuktoyaktuk Peninsula area (Rampton, 1974, 1982) and the Pleistocene icy clay of Hooper and Garry islands suggest a glacier water source. For example, the $\delta^{18}O$ values of about -30 ‰ are in the same range as that reported for mid to late Wisconsinan ice of the Devon Island ice cap (Paterson et al., 1977). By way of contrast, taliks that have frozen through in the past few thousand years, can commonly be recognized by much more positive oxygen isotope ratios than that of the surrounding material.

Conclusions

The oxygen isotope variations for ice in permafrost in the Tuktoyaktuk Peninsula area, Northwest Territories, range from about -15 to about -35 ‰. The most positive values are associated with the post-Hypsithermal freezing of lake bottom taliks where the sublake-bottom porewater, prior to freezing, may have had $\delta^{18}O$ values not much diferent from those of present lake waters. The most negative values are associated with the pre-late Wisconsinan freezing of waters with a very cold source, possibly glacial meltwaters. The extent of fractionation accompanying freezing is dependent, in part, upon the rate of freezing. In the Tuktoyaktuk Peninsula area, where a step temperature change occurs from positive to negative, when a lake bottom becomes exposed to subaerial conditions by rapid lake drainage, the freezing rate at the end of a decade can be less than 0.1 mm•h^{-1}. The rate should be very much slower for a gradual temperature change and for freezing at depth in thick permafrost. Therefore, fractionation effects should be widespread.

Acknowledgments

The fieldwork upon which this paper is based has been supported by the Geological Survey of Canada; the Polar Continental Shelf Project (Department of Energy, Mines and Resources); and the Natural Sciences and Engineering Research Council of Canada. Logistic help has been given by the Inuvik Scientific Resource Centre. The writer would like to thank: W.A. Adams, E.C. McRoberts, N.R. Morgenstern, V.N. Rampton, W.J. Scott, N.B. Snow, and Imperial Oil Limited for help in obtaining samples; H.R. Krouse for carrying out some analyses; and F. Michel for suggesting improvements to the manuscript.

References

Brown, R.J.E. and Kupsch, W.O.
1974: Permafrost terminology; National Research Council Canada, Associate Committee on Geotechnical Research, Technical Memorandum No. 111, 62 p.

Burgess, M., Judge, A., Taylor, A., and Allen, V.
1982: Ground temperature studies of permafrost growth at a drained lake site, Mackenzie Delta; Proceedings of the Fourth Canadian Permafrost Conference (Calgary, Alberta), ed. H.M. French; National Research Council of Canada, Associate Committee on Geotechnical Research, p. 3-11.

Cheng, G.
1982: The forming process of thick layered ground ice; Academia Sinica, v. 25, no. 7, p. 777-788.

Fujino, K. and Kato, K.
1978: Determination of oxygen isotopic concentration in the ground ice of a tundra area; Joint Studies on Physical and Biological Environments in the Permafrost, Alaska and North Canada, July to August 1977. ed. S. Kinosita; Hokkaido University, Sapporo, Japan, Institute of Low Temperature Science, p. 77-83.

Fyles, J.G., Heginbottom, J.A., and Rampton, V.N.
1972: Quaternary geology and geomorphology, Mackenzie Delta to Hudson Bay; 24th International Geological Congress (Montreal), Guidebook, Excursion A-30, 23 p.

Gell, W.A.
1976: Underground ice in permafrost, Mackenzie Delta-Tuktoyaktuk Peninsula, N.W.T.; unpublished Ph.D. thesis, University of British Columbia, Vancouver, 258 p.

Hitchon, B. and Krouse, H.R.
1972: Hydrogeochemistry of the surface waters of the Mackenzie River drainage basin, Canada. III. Stable isotopes of oxygen, carbon and sulphur; Geochimica et Cosmochimica Acta, v. 36, p. 1337-1357.

Johnston, G.H. (editor)
1981: Permafrost Engineering Design and Construction; John Wiley, Toronto, 540 p.

Kato, K. and Fujino, K.
1981: Oxygen isotopic composition of massive ice at Tuktoyaktuk, North Canada: Joint Studies on Physical and Biological Environments in the Permafrost, North Canada, July to August 1980 and February to March 1981, ed. S. Kinosita; Hokkaido University, Sapporo, Japan, Institute of Low Temperature Science, p. 13-20.

Krouse, H.R. and Mackay, J.R.
1971: Application of $H_2{}^{18}O/H_2{}^{16}O$ abundances to the problem of the lateral mixing in the Liard-Mackenzie River system; Canadian Journal of Earth Sciences, v. 8, p. 1107-1109.

Mackay, J.R.
1971: The origin of massive icy beds in permafrost, western arctic coast, Canada; Canadian Journal of Earth Sciences, v. 8, p. 397-422.

1972: Offshore permafrost and ground ice; Canadian Journal o˙ Earth Sciences, v. 9, p. 1550-1561.

1973: Problems in the origin of massive icy beds, western arctic, Canada; Permafrost, The North American Contribution to the Second International Conference (Washington, D.C.), National Academy of Sciences, p. 223-228.

1974: Measurement of upward freezing above permafrost with a self-positioning thermistor probe; in Report of Activities, Geological Survey of Canada, Paper 74-1, Part B, p. 250-251.

Mackay, J.R. (cont.)
1975: Relict ice wedges, Pelly Island, N.W.T. (107 C/12); in Report of Activities, Geological Survey of Canada, Paper 75-1, Part A, p. 469-470.

1979: Pingos of the Tuktoyaktuk Peninsula area, Northwest Territories; Géographie physique et Quaternaire, v. 23, p. 3-61.

1981a: An experiment in lake drainage, Richards Island, Northwest Territories: a progress report; in Current Research, Part A, Geological Survey of Canada, Paper 81-1A, p. 63-68.

1981b: Active layer slope movement in a continuous permafrost environment, Garry Island, Northwest Territories, Canada; Canadian Journal of Earth Sciences, v. 18, p. 1666-1680.

1983: Downward water movement into frozen ground, western arctic coast, Canada; Canadian Journal of Earth Sciences, v. 20, p. 120-134.

Mackay, J.R. and Lavkulich, L.M.
1974: Ionic and oxygen isotopic fractionation in permafrost growth; in Report of Activities, Geological Survey of Canada, Paper 74-1, Part B, p. 255-256.

Mackay, J.R. and Mathews, W.H.
1973: Geomorphology and Quaternary history of the Mackenzie River Valley near Fort Good Hope, N.W.T., Canada; Canadian Journal of Earth Sciences, v. 10, p. 26-41.

Mackay, J.R., Rampton, V.N., and Fyles, J.G.
1972: Relic Pleistocene permafrost, western arctic, Canada; Science, v. 176, p. 1321-1323.

McRoberts, E.C.
1973: Stability of slopes in permafrost; unpublished Ph.D. thesis, University of Alberta, Edmonton, 370 p.

Michel, F.A.
1982: Isotope investigations of permafrost waters in northern Canada; unpublished Ph.D. thesis, University of Waterloo, Waterloo, Ontario, 424 p.

Michel, F.A. and Fritz, P.
1978: Environmental isotopes in permafrost related waters along the Mackenzie Valley corridor; Proceedings Third International Conference on Permafrost (Edmonton, Alberta), National Research Council Canada, v. 1, p. 207-211.

1980: Laboratory and field studies to investigate isotope effects occurring during the formation of permafrost, Part II; Waterloo Research Institute, University of Waterloo, Waterloo, Ontario; Department of Energy, Mines, and Resources, Earth Physics Branch, Open File 80-11, 139 p.

1981: Laboratory and field studies to investigate isotope effects occurring during the formation of permafrost, Phase III; Waterloo Research Institute, University of Waterloo, Waterloo, Ontario; Department of Energy, Mines, and Resources, Earth Physics Branch, Open File 81-5, 57 p.

1982a: Significance of isotope variations in permafrost waters at Illisarvik, N.W.T.; Proceedings of the Fourth Canadian Permafrost Conference (Calgary, Alberta), ed. H.M. French; National Research Council of Canada, Associate Committee on Geotechnical Research, p. 173-181.

Michel, F.A. and Fritz, P. (cont.)
1982b: Laboratory and field studies to investigate isotope effects occurring during the formation of permafrost, Part IV; Waterloo Research Institute, University of Waterloo, Waterloo, Ontario; Department of Energy, Mines, and Resources, Earth Physics Branch, Open File 82-5, 83 p.

O'Neil, J.R.
1968: Hydrogen and oxygen isotope fractionation between ice and water; Journal of Physical Chemistry, v. 72, p. 3683-3684.

Parmuzina, O. Yu.
1978: Cryogenic texture and some characteristics of ice formation in the active layer (in Russian); Problemy Kriolitologii, no. 7, p. 141-164. Translation in Polar Geography and Geology, July-September 1980, p. 131-152.

Paterson, W.S.B., Koerner, R.M., Fisher, D., Johnsen, S.J., Clausen, H.B., Dansgaard, W., Bucher, P., and Oeschger, H.
1977: An oxygen-isotope climatic record from the Devon Island ice cap, arctic Canada; Nature, v. 266, p. 508-511.

Rampton, V.N.
1974: The influence of ground ice and thermokarst upon the geomorphology of the Mackenzie-Beaufort Region; in Research in Polar and Alpine Geomorphology, Proceedings 3rd Guelph Symposium on Geomorphology, ed. B.D. Fahey and R.D. Thompson; Geo Abstracts, University of East Anglia, Norwich, England, p. 43-59.

Rampton, V.N. (cont.)
1982: Quaternary geology of the Yukon coastal plain; Geological Survey of Canada, Bulletin 317, 49 p.

Rampton, V.N. and Mackay, J.R.
1971: Massive ice and icy sediments throughout the Tuktoyaktuk Peninsula, Richards Island, and nearby areas, District of Mackenzie; Geological Survey of Canada, Paper 71-21, 16 p.

Ritchie, J.C. and Hare, F.K.
1971: Late-Quaternary vegetation and climate near the arctic tree line of northwestern North America; Quaternary Research, v. 1, p. 331-342.

Stuiver, M., Yang, I.C., and Denton, G.H.
1976: Permafrost oxygen isotope ratios and chronology of three cores from Antarctica; Nature, v. 261, p. 547-550.

1981: Oxygen isotope ratios of Antarctic permafrost and glacier ice; Dry Valley Drilling Project, Antarctic Research Series, American Geophysical Union, v. 33, p. 131-139.

Suzuoki, T. and Kimura, T.
1973: D/H and $^{18}O/^{16}O$ fractionation in ice-water systems; Mass Spectroscopy, v. 21, p. 229-233.

9. # RECONNAISSANCE VEGETATION STUDIES ON WESTERN VICTORIA ISLAND, CANADIAN ARCTIC ARCHIPELAGO

Project 760058

S.A. Edlund
Terrain Sciences Division

Edlund, S.A., Reconnaissance vegetation studies on western Victoria Island, Canadian Arctic Archipelago; in Current Research, Part B, Geological Survey of Canada, Paper 83-1B, p. 75-81, 1983.

Abstract

Reconnaissance observations of the flora and plant communities of western Victoria Island suggest that surficial materials strongly influence the flora. The widespread calcareous glacial deposits support a variety of calciphilous plant communities and flora. All three broad arctic ecosystems (Low, Mid, and High Arctic) occur on western Victoria Island. The Low Arctic ecosystem is the most extensive, occurring along the southwest coast of Prince Albert Peninsula, coastal areas of Diamond Jenness Peninsula and up Kuujjua River valley, and most of Wollaston Peninsula; dwarf shrubs dominate most plant communities and vegetation cover is nearly continuous. The High Arctic ecosystem is restricted to northern Victoria Island and to areas above 500 m in Shaler Mountains and parts of Diamond Jenness Peninsula. The Mid Arctic ecosystem occurs mainly in central Prince Albert and Diamond Jenness peninsulas. Around Minto Inlet rare tree-sized (2 to 5 m-high) thickets of willow occur in some sheltered valleys and along river terraces. The vegetation of western Victoria Island is compared with calciphilous vegetation of the southern Queen Elizabeth Islands, Banks, Somerset, and Prince of Wales islands, and with vegetation on noncalcareous surficial materials of north-central District of Keewatin. Several bioclimatic zones are suggested, including an extension of the 'mini-forest zone' from the Queen Elizabeth Islands and an erect shrub limit and an erect shrub-forest limit in wetlands.

Résumé

L'étude préliminaire de la flore et des associations végétales de l'ouest de l'île Victoria suggère que les matériaux de surface influent grandement sur la flore. Les vastes dépôts glaciaires calcaires supportent une gamme d'associations végétales et de plantes calcicoles. Les trois grands écosystèmes arctiques (Bas-Arctique, Arctique moyen, Extrême-Arctique) se manifestent dans l'ouest de l'île Victoria. L'écosystème du Bas-Arctique est le plus vaste; on le trouve le long de la côte sud-ouest de la péninsule Prince-Albert, dans les régions côtières de la péninsule Diamond Jenness et en amont de la vallée de la rivière Kuujjua, ainsi que dans la plus grande partie de la péninsule Wollaston; des arbustes nains dominent la plupart des associations végétales et la couverture végétale y est presque continue. L'écosystème de l'Extrême-Arctique est limité à la partie nord de l'île Victoria et aux régions des monts Shaler et de certaines parties de la péninsule Diamond Jenness situées à une altitude supérieure à 500 m. L'écosystème de l'Arctique moyen se rencontre surtout dans la partie centrale des péninsules Prince-Albert et Diamond Jenness. On trouve de rares halliers de saules (2 à 5 m de haut) dans certaines vallées abritées et le long de terrasses fluviatiles autour de l'inlet Minto. L'auteur compare la végétation de l'ouest de l'île Victoria à la végétation calcicole de la partie sud des îles Reine-Élisabeth et des îles Banks, Somerset et Prince-de-Galles et à celle des dépôts de surface non calcaires de la partie nord-centrale du district de Keewatin. Elle propose plusieurs zones bioclimatiques, notamment une extension de la "zone de la micro-forêt" à partir des îles Reine-Élisabeth, et des limites des zones d'arbustes droits et de forêts d'arbustes droits dans les marécages.

Introduction

During the summer of 1982 Terrain Sciences Division, Geological Survey of Canada, initiated a Quaternary mapping project on western Victoria Island, west of 110°W (87 D, F-H; 88 A, B; parts of 77 B, C, F, G; 78 B). As part of this group, I studied the flora of the area and the relationships between plant communities and surficial materials. Fieldwork was done from three camps: Cape Wollaston, with J-S. Vincent; Natkusiak Peninsula, with D.A. Hodgson and J. Bednarski; and near Mount Bumpus, Wollaston Peninsula, with D.R. Sharpe and M.F. Nixon (Fig. 9.1). During the latter part of July and early August we conducted helicopter traverses to the three areas while based at Holman (Fig. 9.1), and in August I conducted detailed studies of plant communities around Holman.

The extensive calcareous tills, ice contact and glaciofluvial deposits, which cover most of western Victoria Island (Fyles, 1963), provide an opportunity to study calciphilous plant communities on chemically and texturally similar substrates over an elevation interval of more than 500 m and along a 550 km north-south transect, from Richardson Islands along the south coast to Peel Point in the northwest (Fig. 9.1).

The glacial deposits are derived from the dominantly calcareous bedrock of Victoria Island described by Thorsteinsson and Tozer (1962). Noncalcareous extrusive basalt lava flows occur in the central Shaler Mountains; where this type of rock outcrops, the weathering products are predominantly felsenmeer. Only rarely (in local pockets) does the weathered basalt form the gravel and sand required to support vascular plants; well vegetated sites in areas underlain by basalt commonly are veneered by calcareous till.

Arctic Ecosystems

Low, Mid, and High Arctic ecosystems (Polunin, 1951; Young, 1971) occur on western Victoria Island. The Arctic ecosystem begins at the limit of coniferous trees and ends in the region where climate no longer permits plants to survive.

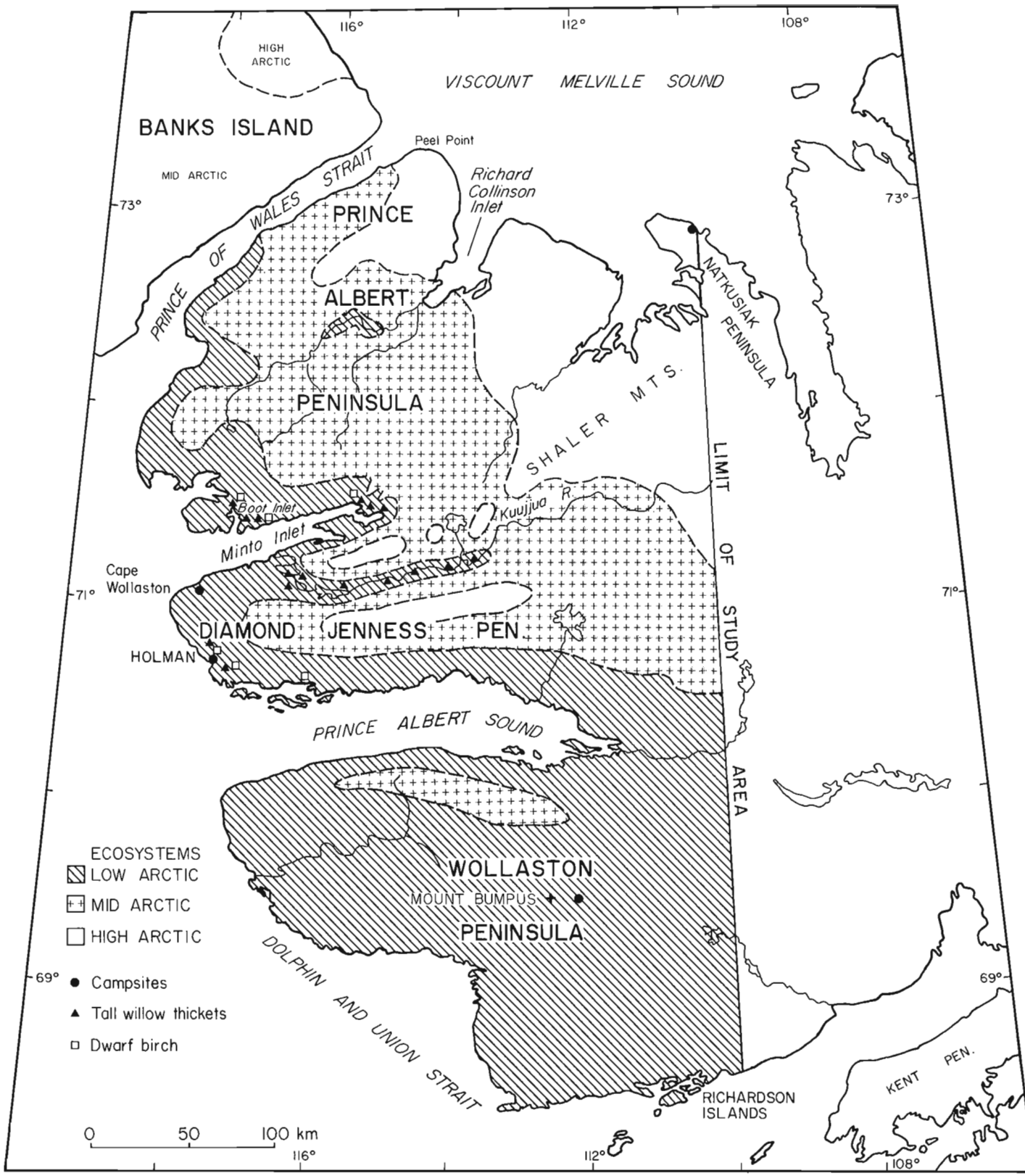

Figure 9.1. *Western Victoria Island showing arctic ecosystems, locations of campsites and of tree-size willows and dwarf birch.*

The progression from Low to High Arctic ecosystems is marked by a decrease in species diversity, major changes in the life form of the plant communities, and a decrease in the per cent plant cover (Fig. 9.2). In describing the ecosystems of western Victoria Island, the two extremes High and Low Arctic ecosystems – are compared and contrasted and then the intermediate Mid Arctic ecosystem is described.

High Arctic Ecosystem

The High Arctic ecosystem is dominant in the Queen Elizabeth Islands north of the map area (Edlund, 1983a). On western Victoria Island it occurs along the north coast and farther south at high elevations in Shaler Mountains, Prince Albert Peninsula, and Diamond Jenness Peninsula (Fig. 9.1). The flora and plant communities in these areas are comparable to those on southern Melville Island (Edlund, 1982b), southern Bathurst Island (Edlund, 1983b), Cornwallis Island (Edlund, 1982c), and Prince of Wales and northern Somerset Island (Woo and Zoltai, 1977). Flora of this ecosystem is the least diverse found on western Victoria Island (less than 100 vascular species), and continuous plant cover is restricted to lower slopes and wetlands.

The vascular component of the plant communities at all but the wettest sites is dominated by dwarf shrub communities which commonly have less than 25% cover but locally reach 50% cover. The calciphile **Dryas integrifolia** (mountain avens) is the most common dwarf shrub, although arctic willow **(Salix arctica)** is also common in many communites. Two of the most common herbaceous associates are purple saxifrage, **Saxifraga oppositofolia,** and the sedge **Carex rupestris,** both calciphiles.

Continuous vegetation is generally confined to moist lower slopes and lowlands found locally near the north coast. Sedge meadows with a large grass component are common on these wet areas but are relatively low in graminoid abundance and general diversity, as are other herbaceous species. Arctic willow is common on raised moss hummocks in these wet meadows.

Low Arctic Ecosystem

The Low Arctic ecosystem on western Victoria Island is found on Wollaston Peninsula and northwards along the coast, up Kuujjua River valley, to southwestern Prince Albert Peninsula (Fig. 9.1). The rich flora (from 150 to more than 200 vascular species) is found in communities that have a nearly continuous vegetation cover on all but the coarsest and driest materials. **Dryas,** including **D. integrifolia** and **D. punctata,** is again a major component of the vascular plant stratum of the plant communities on well to moderately drained materials, with arctic willow a common dwarf shrub associate. Herbaceous associates include a variety of legumes, such as **Oxytropis, Hedysarum,** and **Astragalus,** as well as **Artemisia, Potentilla, Kobresia, Carex,** and various grass species.

The wetlands are generally continuously vegetated with dense and diverse sedge meadows having an abundance of graminoid species and a substantial component of shrubs. The shrub component includes several dwarf shrubs as well as thickets of semi-erect and erect shrubs, commonly willows, which reach 25 to 50 cm in height and may form a nearly continuous low canopy. Heaths, such as **Cassiope tetragona** (arctic heather) and to a lesser extent **Vaccinium uliginosum** (blueberry), **Rhododendron lapponicum** (Lapland rosebay), **Arctostaphylos rubra,** and **A. alpina** (bear berry), occur with dwarf willow on raised hummocks in wet sedge meadows and on sheltered slopes. Dwarf birch **(Betula glandulosa)** occurs locally in this ecosystem as well, generally in sheltered locations (Fig. 9.1).

An unusual feature within this zone is the presence of sites with tree sized willows in the Minto Inlet area (Fig. 9.1). Willows as high as 1.5 m have been reported near Holman (Porsild, 1955; T. Washburn, personal communication, 1982); tall willows have been noted in a river valley near the head of Minto Inlet (Peterson et al., 1981). Nevertheless, it was surprising to see the size of the felt-leaved willow **(Salix alaxensis)** in many sheltered valleys around Minto Inlet, Boot Inlet, along terraces of Kuujjua River and dunes near its mouth (Fig. 9.3), as well as in extremely sheltered niches near Holman (Fig. 9.1). They form thickets, 1.5 to 5 m in height, with trunk diameters of 5 to 12 cm. Other erect willow species, such as **S. lanata** spp. **Richardsonii** (Porsild and Cody, 1980), which usually grow no higher than 0.25 m elsewhere on Victoria Island, also reach heights of up to 1 m in some of these sheltered valleys. The rich arctic herbaceous flora found nearby or as an understory to the thickets, is similar to the flora of communities near treeline, 400 km to the south.

The dense thickets have developed from shoots from a relatively few willows; preliminary tree ring analysis shows that the largest shoots are 50 years old. Numerous dead trunks, similar in size to the willow shoots sampled, were found within the thickets, but so too were new suckers. Thus, in some places, present day conditions are suitable for continued growth of the thickets.

The willow thickets represent vegetational and floristic oases. They probably form as a result of the special microclimatological conditions prevailing in some deep valleys where steep walls, composed of dark gabbro, absorb and reradiate heat into the valleys. One afternoon (August 1, 1982), at a site at the head of Minto Inlet, a temperature difference of more than 20°C existed between the plateau (1°C) and valley floor (22°C). Protection from winds, availability of nutrients and moisture, as well as deep snow conditions during winter probably also contribute to the unique flora at these special sites.

Mid Arctic Ecosystem

The Mid Arctic ecosystem occurs on central Prince Albert Peninsula, and at moderate elevations in Shaler Mountains and on Diamond Jenness Peninsula, and in a small area of northern Wollaston Peninsula (Fig. 9.1). As in the Low Arctic ecosystem, dwarf shrubs, particularly **Dryas** species, dominate all but the wettest areas. The diversity is less than 150 species, however, and fewer types of legumes are associated with these communities than is the case for the Low Arctic ecosystem. Common associates are several **Oxytropis, Kobresia,** and **Carex** species, **Pedicularis lanata,** and **Parrya arctica** – all of which are also common in the Low Arctic ecosystem. But the rich diversity of Low Arctic herbs is absent.

Wetlands are characterized by sedge meadows in which the woody component consists of prostrate shrubs, primarily **Salix arctica,** but do include other dwarf shrubs such as **S. reticulata** and **S. polaris. Cassiope** is the only heath species, growing in sheltered spots. Species of willow that are normally semi-erect and erect are present, but in this zone they usually take on a prostrate form. The exceptions occur locally where some gnarled individual branches of **Salix lanata** and **S. alaxensis** reach about 25 cm in height.

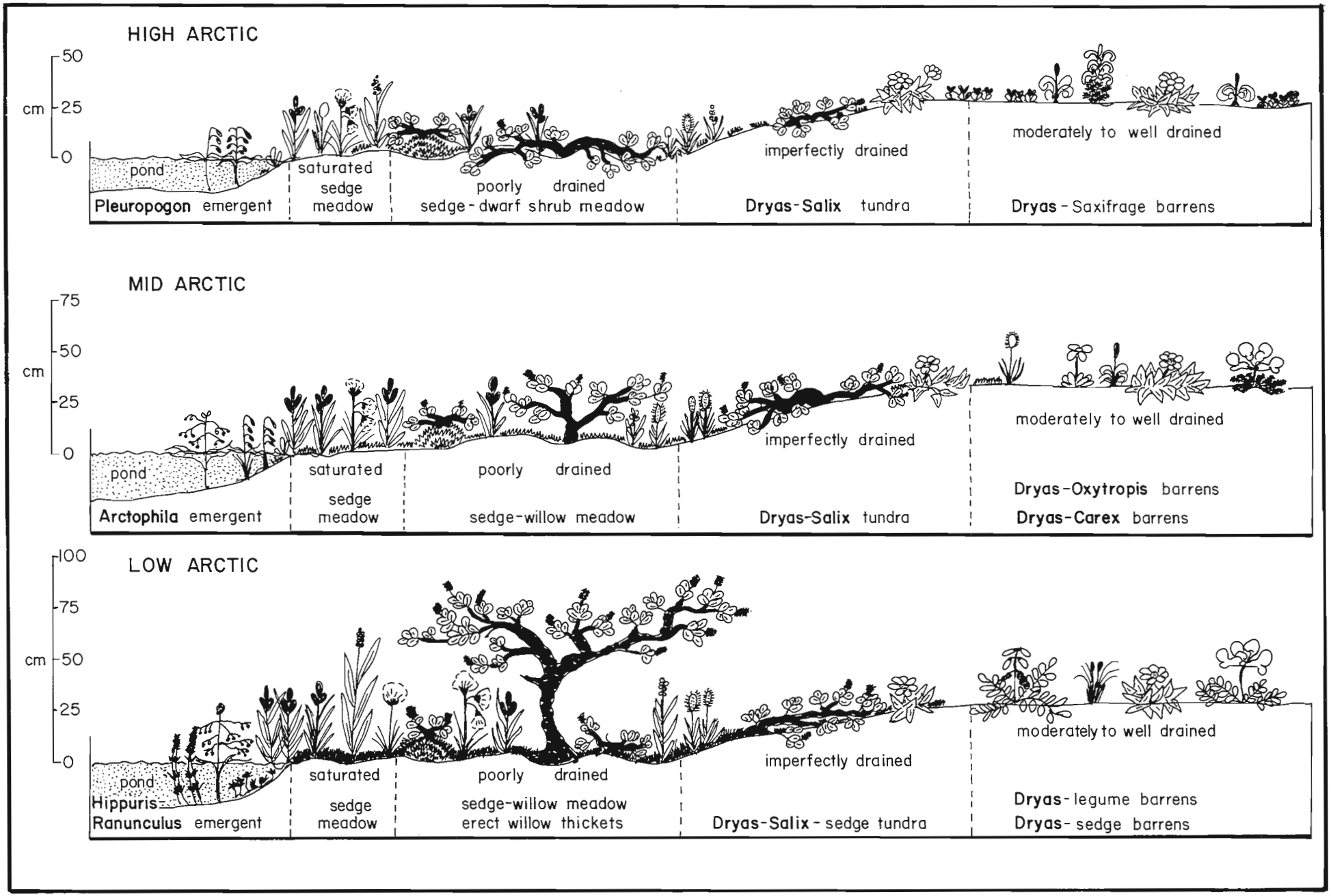

Figure 9.2. *Catena showing plant communities of the Low, Mid, and High Arctic ecosystems on the different moisture regimes of calcareous deposits of Victoria Island.*

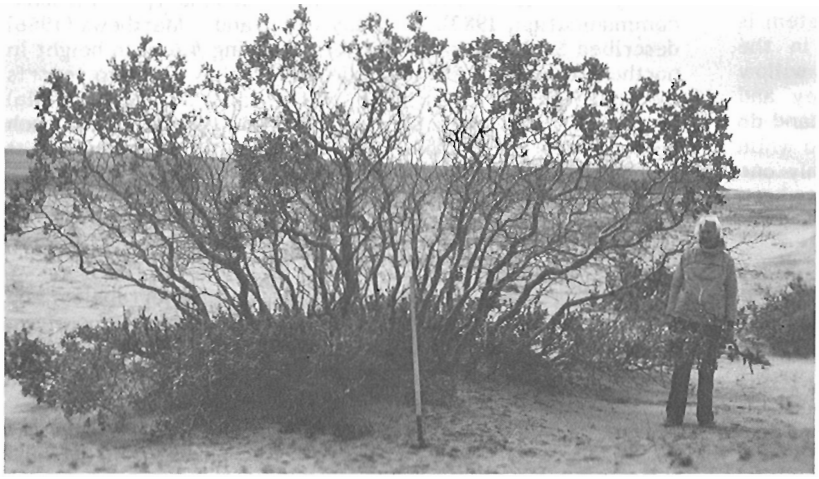

Figure 9.3

*An erect willow (**Salix alaxensis**) thicket on deflated sands along the north bank of Kuujjua River, 20 km from its mouth, on Diamond Jenness Peninsula. (203642-D, courtesy of J-S. Vincent).*

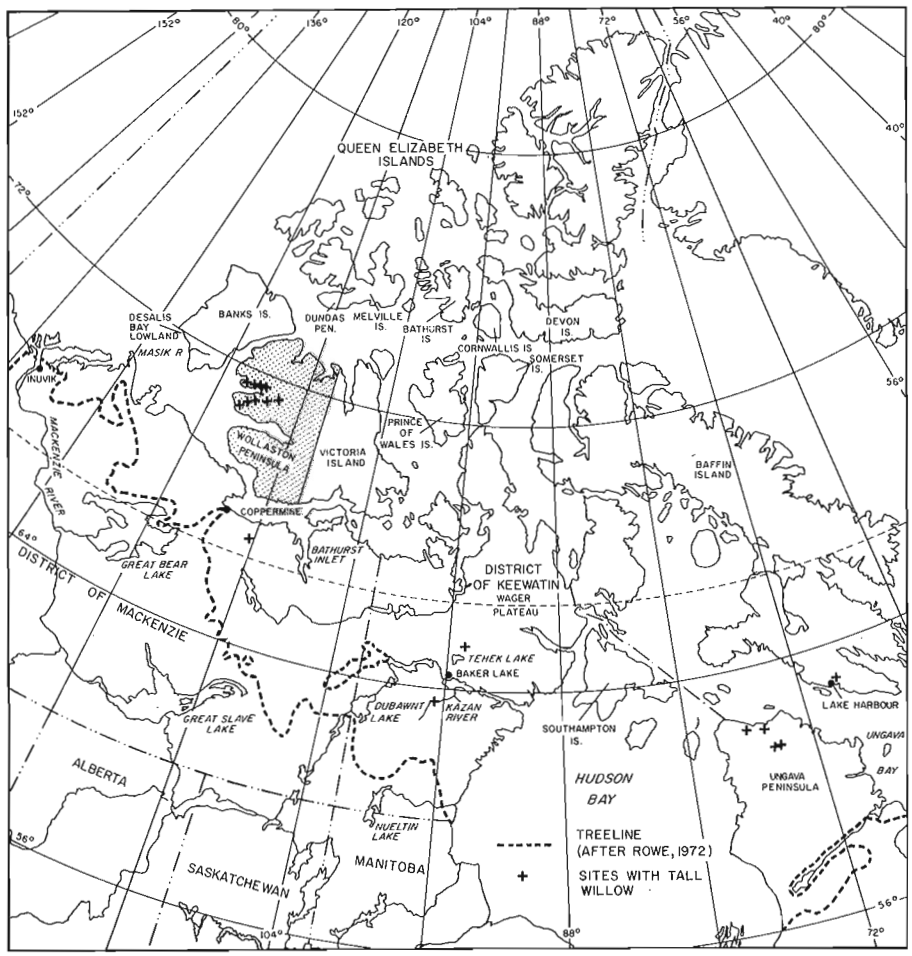

Figure 9.4

Location of tall willows in northern Canada and their proximity to treeline.

Comparisons with other Areas in the Canadian Arctic (Fig. 9.4)

Western Victoria Island is floristically similar to Banks Island to the west. Banks Island, like Victoria Island, is largely blanketed by calcareous glacial deposits (Vincent, 1982), although on Banks till masks neutral to weakly acidic bedrock. Banks Island, therefore, is also vegetated by calciphilous plant communities, predominantly **Dryas integrifolia,** barrens, and wet sedge meadows (Vincent and Edlund, 1978), and is characterized by all three arctic ecosystems. On western Victoria Island, which extends farther south than Banks Island, the Low Arctic ecosystem is more extensive; on Banks Island, it occurs only in the southernmost part of the island and the only low willow thickets are found primarily in Masik River valley and De Salis Bay lowland (Fig. 9.4). Nowhere on Banks Island do willows attain heights seen in the Minto Inlet area, and while dwarf birch is locally common on Victoria Island, only one clump on a south-facing slope in Masik River valley has been reported on Banks Island (Kuc, 1970).

On Banks Island, the Mid Arctic ecosystem is dominant whereas on western Victoria Island Mid Arctic-type vegetation is much less common. The High Arctic ecosystem on Banks Island is confined to the northeastern plateau (Fig. 9.1) and the foggy, low lying northwest coast adjacent to the permanent ice pack whereas on western Victoria Island it occurs on the northern coast and in mountainous areas.

The High Arctic plant communities of northwestern Victoria Island are most similar to those of the southern part of Dundas Peninsula, Melville Island (Edlund, 1982b), north of the study area, which is also covered by calcareous till probably derived from materials from Victoria Island (Hodgson et al., in press). Similar plant communities also develop on Bathurst and Cornwallis islands on materials derived from local, moderately calcareous bedrock. Woo and Zoltai (1977) found similar communities on calcareous substrates on Prince of Wales Island and northern Somerset Island.

The flora and plant communities of western Victoria Island are quite different from those found on materials derived from noncalcareous rocks of the Canadian Shield. In north-central District of Keewatin, south of the study area, the Low Arctic communities are dominated by heath species such as **Cassiope tetragona** (heather) and **Ledum palustre** ssp. **decumbens,** (Labrador tea) and commonly possess a thick, nearly continuous carpet of foliose, squamulose, and fruiticose lichens, particularly **Cladonia** and **Alectoria** species, and mats of mosses such as **Rhacomitrium** and **Polytrichum** (Edlund, 1982a). A similar dense and diverse cryptogamic stratum is not present on the calcareous gravels of Victoria and Banks islands; neither are heath-dominated communities common, but species characteristic of heath are found locally in hummocky wetlands and in areas having wet, snowpatch conditions where the local reducing environment of the soil results in a lowered pH (6.8 to 7.2). In spite of these distinctions, which include a general lack of overlapping dominant species, physiognomic similarities exist between the plant communities on western Victoria Island and northern District of Keewatin. The Low Arctic ecosystem in both regions has nearly continuous vegetation, and the vascular plant stratum of all but the wettest soils is dominated by dwarf shrubs. For example, on the highest parts of Wager Plateau (Edlund, 1982a) of northern Keewatin (Fig. 9.4) the vascular plant stratum is dominated by dwarf shrubs, similar to that on Wollaston Peninsula, Victoria Island. At lower elevations surrounding Wager Plateau, semi-erect willows, particularly **Salix phylicifolia** and **S. alaxensis,** and dwarf birch (**Betula**) appear generally with less than 10% cover; in the southern part of the plateau around Tehek Lake (north of Baker Lake), dwarf shrubs are a major ground cover, and in sheltered valleys and along some river terraces, thickets of willow up to 80 cm in height are found. This physiognomy similar to that found in the Low Arctic ecosystem of Victoria Island.

Within the Low Arctic ecosystem, to find willow thickets of a comparable size to those in the Minto Inlet area, one must look farther afield (Fig. 9.4). The Bathurst Inlet and Tree River areas south of Victoria Island, not far from treeline, harbour such thickets in some sheltered valleys (W. Blake, Jr. and B.G. Craig, personal communication, 1983). Tree-sized willows are also found south of Baker Lake in the Kazan River area of Keewatin, between Ford Lake and Thirty Mile Lake (A.N. LeCheminant, personal communication, 1983). Maycock and Matthews (1966) described **Salix alaxensis** thickets reaching 4.6 m in height in northern Ungava Peninsula, Quebec and they refer to reports by J.D. Soper of 3.7 m-high willow (probably **S. plainfolia**) near Lake Harbour, southern Baffin Island. All such communities are extremely local and rare. It appears that the occurrence of the willow "forests" at Minto Inlet are the northernmost ones known in North America.

Bioclimatic Zones

Victoria Island has several zones of biogeographical and bioclimatological importance. The High Arctic ecosystem, which extends across the Queen Elizabeth Islands to the north, has its southern limit on Victoria Island. The High Arctic ecosystem on Victoria Island lies entirely within the richest subzones of the High Arctic, where dwarf shrubs are the major vascular plants (Edlund, 1983a). Farther north, in the Queen Elizabeth Islands, dwarf shrubs are no longer dominant. The boundary between the zone where dwarf shrubs are dominant and that where dwarf shrubs occur only locally may be thought of as a 'mini-forest line'. The northermost limit of dwarf woody species is the 'mini-treeline'.

All of Victoria Island lies well within the 'mini-forest zone'. Dwarf shrubs are dominant on moderately to well drained substrates. They are absent from plant communities only in areas where local snowbeds persist well into mid and late July; in such places, the communities are floristically similar to those seen farther north above the 'mini-treeline'.

This concept of broad bioclimatic zonation of the ecosystems can be applied to other parts of Victoria Island as well. The southern boundary of the High Arctic ecosystem is, in effect, the limit of erect and semi-erect shrubs – an 'erect shrub limit'. Throughout the Mid Arctic ecosystem, erect and semi-erect shrub species are locally present in poorly drained areas but are less than 25 cm high and have low percentages of cover. In the Low Arctic ecosystem, the semi-erect and erect shrubs of the low shrub forest zone generally reach 0.5 m high and commonly form thickets on poorly drained, sheltered sites; these represent a local erect shrub forest. The tree-sized willow thickets in valleys around Minto Inlet represent isolated tall willow-forest zones in an area far removed from treeline.

Further research may tie these biogeographical observations with climatological parameters, possibly coincident with isotherms such as the mean July isotherms, as suggested by Edlund (1983a) for the central Queen Elizabeth Islands.

Acknowledgments

Excellent field support was provided by the Polar Continental Shelf Project and R. Frost, pilot with Quasar helicopters. Special thanks are given to my colleagues, J. Bednarski, D.A. Hodgson, F.M. Nixon, D.R. Sharpe, and J-S. Vincent who allowed me to work from their field camps, provided useful discussions about the surficial materials, and brought plant observations and samples from areas I personally did not visit. I wish to thank D.R. Sharpe and J.V. Matthews, Jr. who critically reviewed this report.

References

Edlund, S.A.
1982a: Plant communities on the surficial materials of north-central District of Keewatin; Geological Survey of Canada, Paper 80-33, 20 p.

1982b: Vegetation of Melville Island, District of Franklin: eastern Melville Island and Dundas Peninsula; Geological Survey of Canada, Open File 852.

1982c: Vegetation of Cornwallis, Little Cornwallis, and associated islands, District of Franklin; Geological Survey of Canada, Open File 857.

1983a: Bioclimatic zonation in a High Arctic region: central Queen Elizabeth Islands; in Current Research, Part A, Geological Survey of Canada, Paper 83-1A, p. 381-390.

1983b: Vegetation of the Bathurst Island area, Northwest Territories; Geological Survey of Canada, Open File 888.

Fyles, J.G.
1963: Surficial geology of Victoria and Stefansson Islands, District of Franklin; Geological Survey of Canada, Bulletin 101, 38 p.

Hodgson, D.A., Vincent, J-S., and Fyles, J.G.
Quaternary geology of central Melville Island, Northwest Territories; Geological Survey of Canada, Paper 83-16. (in press)

Kuc, M.
1970: Vascular plants from some localities in the western and northern parts of the Canadian Arctic Archipelago; Canadian Journal of Botany, v. 48, no. 11, p. 1931-1938.

Maycock, P.F. and Matthews, B.
1966: An Arctic forest in the tundra of northern Ungava, Quebec; Arctic v. 19, p. 114-144.

Peterson, E.G., Kabzems, R.D., and Levson, V.M.
1981: Terrain and vegetation along the Victoria Island portion of a Polar Gas combined pipeline system; Report of Polar Gas Environmental Program (Toronto); 136 p. plus appendices. Prepared by Western Ecological Services (B.C.) Ltd.

Polunin, N.
1951: The real Arctic: suggestions for its delimitation, subdivision and characterization; Journal of Ecology, v. 39, p. 308-315.

Porsild, A.E.
1955: The Vascular Plants of the Western Canadian Arctic Archipelago; National Museum of Canada, Bulletin 135, 226 p.

Porsild, A.E. and Cody, W.J.
1980: Vascular Plants of Continental Northwest Territories, Canada; National Museum of Canada, Ottawa, 667 p.

Rowe, J.S.
1972: Forest Regions of Canada; Department of the Environment, Canadian Forestry Service Publication No. 1300, 172 p.

Thorsteinsson, R. and Tozer, E.T.
1962: Banks, Victoria and Stefansson Islands, Arctic Archipelago; Geological Survey of Canada, Memoir 330, 83 p.

Vincent, J-S.
1982: The Quaternary History of Banks Island, N.W.T., Canada; Géographie physique et Quaternaire, v. XXXVI, no. 1-2, p. 209-232.

Vincent, J-S. and Edlund, S.A.
1978: Extended legend to accompany preliminary surficial geology maps of Banks Island, Northwest Territories; Geological Survey of Canada, Open File 577.

Woo, V. and Zoltai, S.C.
1977: Reconnaissance of the soils and vegetation of Somerset and Prince of Wales Islands, N.W.T. Northern Forest Research Center, Information Report NOR-X-186, 127 p.

Young, S.B.
1971: The vascular flora of St. Lawrence Island, with special reference to floristic zonation in the arctic regions; Contributions from the Gray Herbarium of Harvard University, No. 201, p. 11-115.

10.

ASPECTS OF THE ROCKNEST FORMATION, ASIAK THRUST-FOLD BELT, WOPMAY OROGEN, DISTRICT OF MACKENZIE

Project 810021

J.P. Grotzinger[1] and P.F. Hoffman
Precambrian Geology Division

Grotzinger, J.P. and Hoffman, P.F., Aspects of the Rocknest Formation, Asiak Thrust-Fold Belt, Wopmay Orogen, District of Mackenzie; in Current Research, Part B, Geological Survey of Canada, Paper 83-1B, p. 83-92, 1983.

Abstract

Field study of the Rocknest Formation during 1981 and 1982, and laboratory study during the fall of 1982 has produced several interesting findings which are summarized in this report. Topics are: 1) subdivision of Rocknest Formation into ten informal members, 2) Rocknest shelf cyclicity and paleogeography, 3) shelf-to-slope transitions, 4) paleoclimate, and 5) evidence of possible microbial remnants in stromatolite bioherms of the Odjick/Rocknest transition beds. Future fieldwork is outlined.

Résumé

Le rapport présente les résultats intéressants d'études de la formation de Rocknest entreprises sur le terrain en 1981 et 1982, et en laboratoire en automne 1982. Les sujets comprennent 1) la subdivision en dix niveaux officieux de la formation de Rocknest, 2) la cyclicité et la paléogéographie du plateau de Rocknest, 3) les transitions de plateau à talus, 4) le paléoclimat et 5) des preuves de la présence possible de restes de microbes dans les biohermes de stromatolites des couches de transition d'Odjick et de Rocknest. Un aperçu des travaux sur le terrain à venir est présenté.

Introduction

The Rocknest Formation is a 1.9 Ga carbonate terrace that formed on a passive continental margin, exposed in the Asiak Thrust-Fold Belt and autochthonous basins (Fig. 10.1) of Wopmay Orogen (Hoffman, 1980). In 1981, a three-year project was initiated to investigate the evolution of the Rocknest carbonate shelf and document: 1) shelf-to-basin transitions, 2) slope, shelf-edge, and cyclic shelf-interior facies, 3) stromatolite types present and environmental and/or biological controls on their distribution, and 4) similarities and differences between the Rocknest and Phanerozoic carbonate shelf sequences. This study is part of a broader project designed to study the externides of Wopmay Orogen (Hoffman et al., 1983).

In 1982, sections were measured at the southern and northern ends of the thrust-fold belt, and at present a total of 28 sections have been measured in the Redrock Lake (86 G), Point Lake (86 H), Takijuq Lake (86 I), Hepburn Lake (86 J), Coppermine (86 O), and Kikerk Lake (86 P) map areas. The information in this report is based on fieldwork completed during 1981 and 1982, and laboratory work completed during the fall of 1982.

Subdivision of Rocknest Formation into Informal Members

The Rocknest shelf-interior facies comprises interstratified argillaceous dololutite and stromatolitic dolomite arranged in cyclic, shoaling-upward sequences 1-10 m thick. The cycles can be grouped into distinct sets, or members, 10-450 m thick, based on variations in the relative proportion of argillaceous dololutite to stromatolitic dolomite.

The Rocknest Formation was previously subdivided into five informal members (Grotzinger, 1982) that were used as stratigraphic markers for 1:50 000 scale mapping of selected areas within Asiak Thrust-Fold Belt during the 1981 field season (Tirrul, 1982). However, recent 1:50 000 scale mapping during the 1982 field season (Hoffman et al., 1983) has shown that a more detailed stratigraphic breakdown is required to best show variations in structural level and style. It is proposed here that the Rocknest Formation be subdivided into ten informal members according to key beds, and variations in the ratio of argillaceous dololutite to stromatolitic dolomite in successive groups of shoaling-upward cycles.

Figure 10.2 illustrates the ten informal members of the Rocknest Formation in Asiak Thrust-Fold Belt. These members are shelf-interior facies and occur in the autochthon and all thrust panels which expose the Rocknest Formation except for the "X" thrust sheet (Fig. 10.1) which exposes shelf-edge and slope facies. Correlations between shelf-interior sections and shelf-edge sections are obscured by abrupt facies changes across thrust "X". However, in structural panels exposed east of thrust "X", members, many cycles, and even single beds are laterally continuous for over 200 km along strike (see Fig. 10.3).

Basal Member

The Basal member is the thickest (100-500 m) and most complex. Its base coincides with the base of the Rocknest Formation which is marked by the first metre-thick bed of dolomite above the highest green shale and siltstone of the Odjick Formation. This basal bed contains discrete or coalesced bioherms of small digitate stromatolites that branch divergently (Fig. 10.4a). The bulk of the member is characterized by shoaling-upward, argillaceous dololutite-to-stromatolitic dolomite cycles. Stromatolites at tops of cycles in the lower part of the member are commonly linked hemispheroids, contiguous or isolated, but tops of cycles in the upper part of the member are capped by dark, cherty, cryptalgal tufa sheets that often contain microdigitate stromatolites (Fig. 10.4b). The uppermost two cycles of the Basal member have **Conophyton** bioherms (Fig. 10.4c) except in the thrust sheet to the east of thrust "X", and in the northeastern corner of the autochthon. The same two cycles can be recognized in most areas, making them very reliable stratigraphic markers. The contact between the top of the upper **Conophyton**-bearing cycle and the base of the succeeding cycle is used as the boundary between the Basal member and the overlying Lower Shale member, and as one boundary in a three-fold subdivision of the Rocknest Formation on 1:250 000 scale maps.

[1] Department of Geological Sciences, Virginia Tech., Blacksburg, Va., 24061

Lower Shale Member, 30-80 m thick

The lower part of the Lower Shale member comprises shale-dominated cycles with thin cryptalgalaminite caps. Upwards in the member, cycles are more stromatolitic and the uppermost cycles are dominated by dark, cherty, cryptalgal tufa with microdigitate stromatolites. The boundary between the Lower Shale member and overlying Intraclastic member coincides with the contact between the uppermost of these cycles and the lowest cycle of the Intraclastic member.

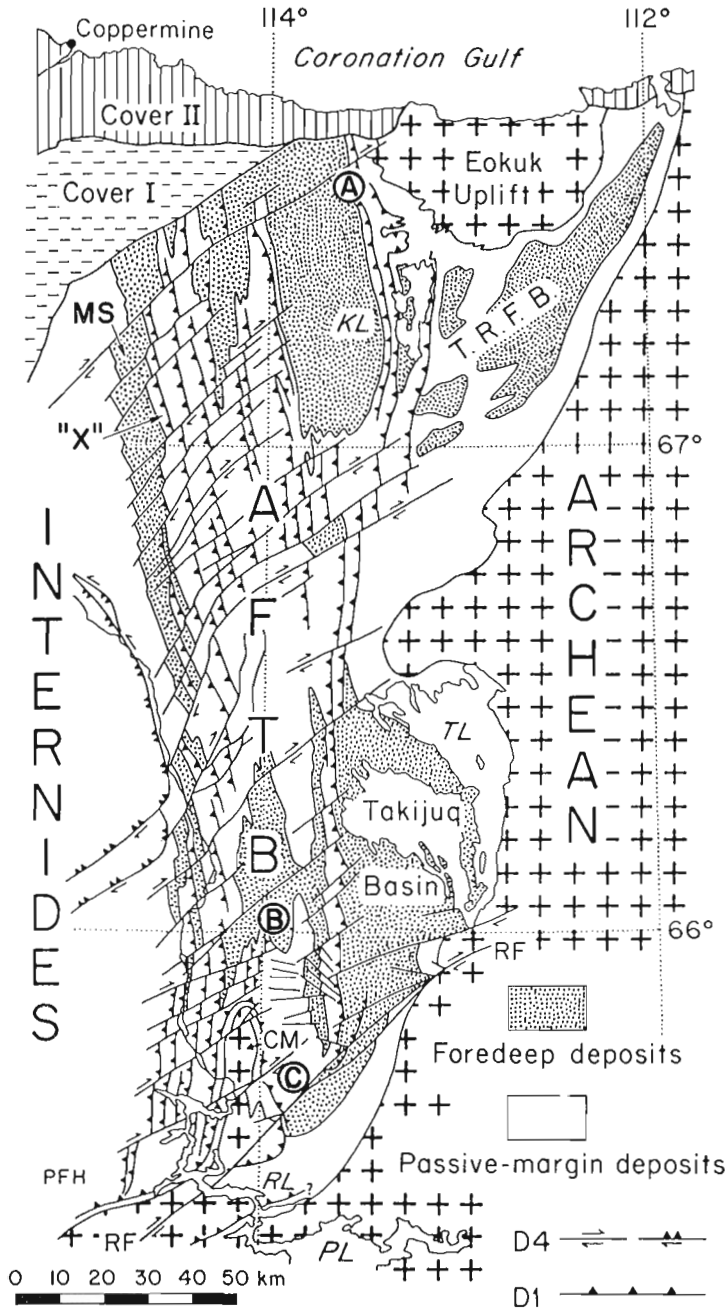

Figure 10.1. *The externides of Wopmay Orogen showing location of syncline "M" (MS), thrust "X" ("X"), and measured sections (A, B, C) of Figures 10.2 and 10.3. AFTB, Asiak Fold-Thrust Belt; TRFB, Tree River Fold Belt; CM, Carousel Massif; RF, Redrock Fault; KL, Kikerk Lake; TL, Takijuq Lake; RL, Redrock Lake; PL, Point Lake. Adapted from Hoffman et al. (1983, Fig. 60.1).*

Intraclastic Member, 20-100 m thick

The lowest cycle of the Intraclastic member has argillaceous dololutite that passes upwards into a very distinct, laterally continuous bed of dolomitic, isolated, columnar stromatolites with furcate branching. This bed is sharply overlain by a noncyclic interval of dolomitic, partially linked, strongly elongate, pseudocolumnar stromatolites. The lower part of the member passes gradationally upwards into dolomitic, crossbedded intraclast grainstone/packstone that generally fines upwards into planebedded to crossbedded dolarenite grainstone/packstone with interbeds of dolomitic, crossbedded intraclast grainstone/packstone. The top of the Intraclastic member is gradational with the base of the Thrombolitic member and the boundary is placed at the base of the first argillaceous or stromatolitic bed above the uppermost metre-thick bed of intraclast grainstone/packstone.

Thrombolitic Member, 50-110 m thick

The Thrombolitic member comprises at least 17 cycles, several of which contain very distinctive stromatolite and thrombolite (Fig. 10.4d) beds that make superb markers for testing the potential of long distance cycle correlation (Fig. 10.3). In particular, a light, cherty, **Conophyton**-bearing bed occurs just below the upper boundary of the member, which is placed at the base of the first metre-thick interval containing cream, crosslaminated dolosiltite and dolarenite grainstone with nodular white chert. This boundary is also used for 1:250 000 scale maps.

Pink Chert Member, 10-70 m thick

The Pink Chert member contains interstratified sequences of very distinctive reddish-pink dolosiltite with nodular pink chert, and cream, crosslaminated dolosiltite and dolarenite (ooid-intraclast) packstone. Both lithologies exhibit wave-ripple crosslaminae draped by cryptalgalaminite. The upper boundary of the Pink Chert member is placed at the base of the lowest metre-thick interval of argillaceous dololutite above the uppermost cream dolosiltite with nodular white chert.

Domal Stromatolite Member, 30-100 m thick

The base of this member has one or two cycles dominated by thick intervals of argillaceous dololutite that pass upward into thin cryptalgalaminite caps containing uncommon domal stromatolites. These first cycles are succeeded by stromatolite-dominated cycles containing abundant linked, very closely spaced domes, and cycle caps with dark, cherty cryptalgal tufa sheets that often contain microdigitate stromatolites. Although stromatolite-dominated cycles are typical of the middle and upper parts of the member, bases of cycles in the middle part of the member frequently contain argillaceous dololutite which is uncommon at bases of cycles in the upper part of the member. The upper boundary of the Domal Stromatolite member occurs at the top of the uppermost cycle containing stromatolites below the lowest metre-thick interval of argillaceous dololutite.

Red Shale Member, 20-100 m thick

The Red Shale member consists entirely of argillaceous dololutite and dolosiltite, with intercalated beds of intraclast packstone, intraclast/ooid packstone, and dolarenite packstone with large intraclast rip-ups. Wavy cryptalgalaminite also occurs at the tops of shale-dominated cycles. The top of this member grades into the overlying Thin member and the boundary is at the top of the lowest stromatolitic bed that is succeeded by several argillaceous dololutite-to-stromatolitic dolomite cycles.

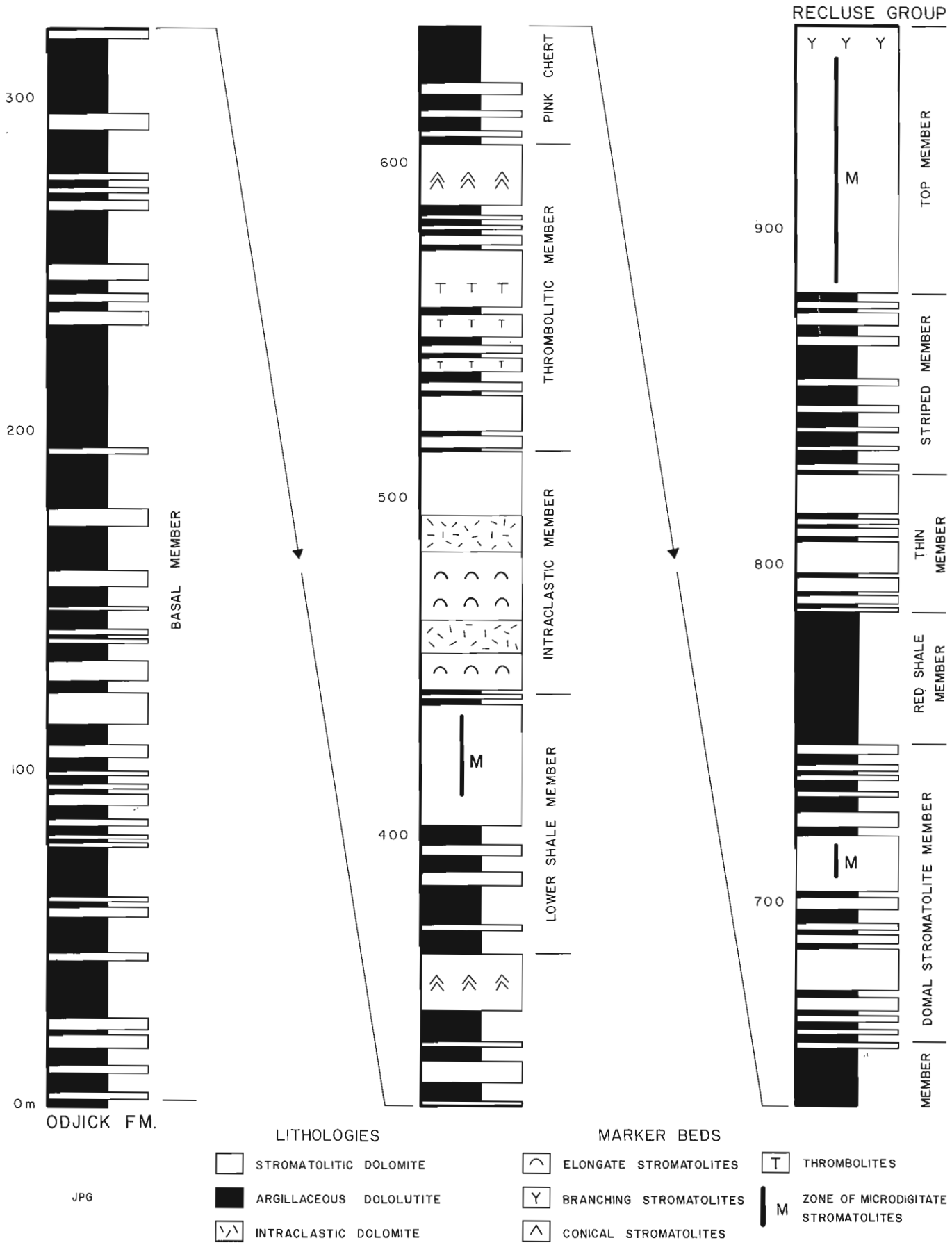

Figure 10.2. *The ten informal members of the Rocknest Formation, section (A), northern Asiak Fold-Thrust Belt.*

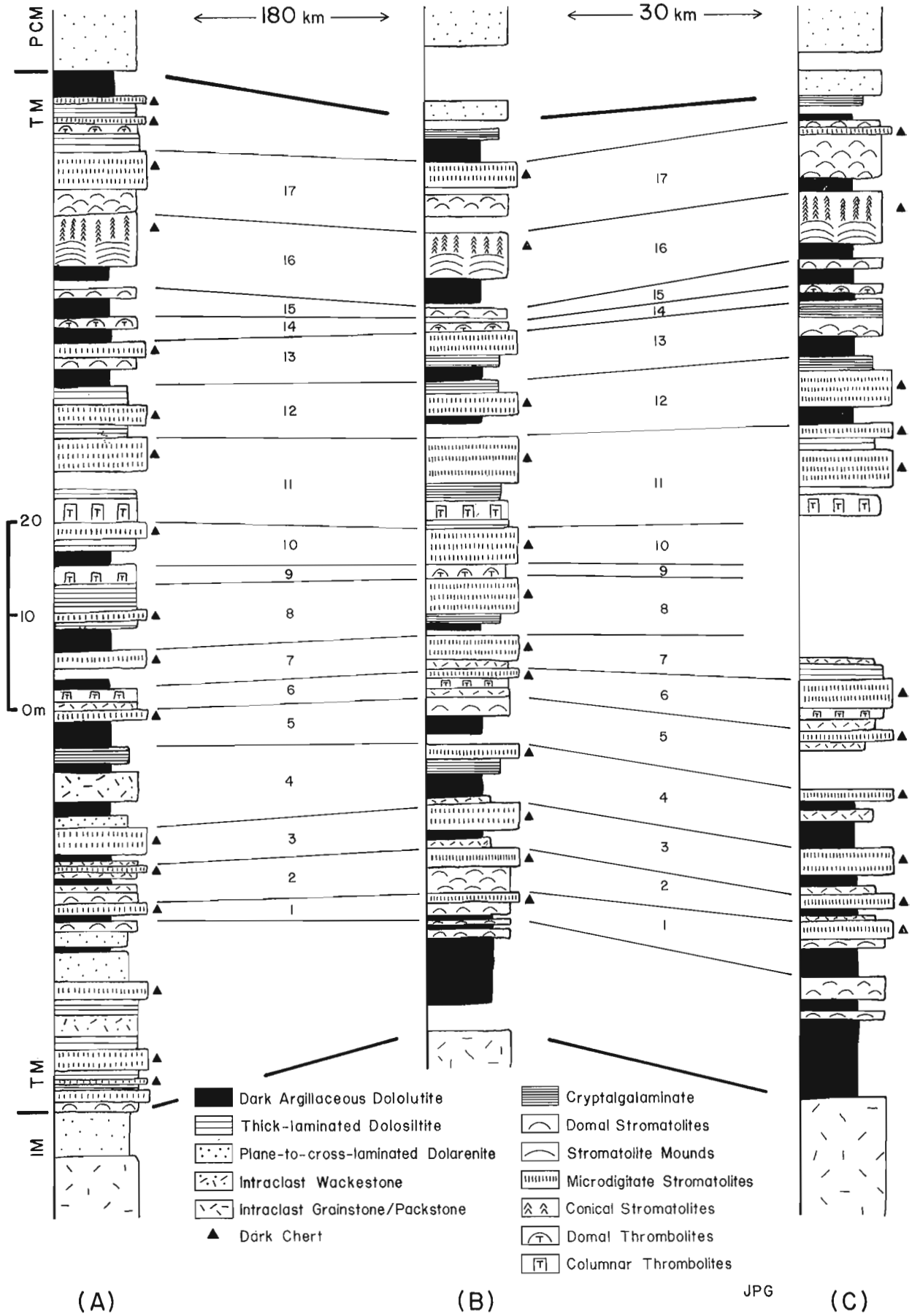

Figure 10.3. *Correlation of 17 cycles in Thrombolitic member (TM). IM, Intraclastic member; PCM, Pink Chert member. Location of sections shown in Figure 10.1.*

Thin Member, 10-30 m thick

The lower part of the Thin member comprises several cycles which become progressively more stromatolite-dominated toward the upper part of the member. The cycle caps in the upper part of the member frequently have cherty, cryptalgal tufa sheets with uncommon microdigitate stromatolites. Locally, these uppermost cycles also contain the columnar stromatolite **Conophyton** that passes upwards into **Baicalia**-like stromatolites, or less commonly, branching conical stromatolites resembling **Jacutophyton** that pass up into **Baicalia**-like stromatolites. These cycles resemble those described by Serebryakov (1976), and Jackson (1982). The upper boundary of the Thin member is placed at the top of the uppermost sequence of stromatolite-dominated cycles below the lowest metre-thick interval of argillaceous dololutite of the overlying Striped member.

Striped Member, 30-70 m thick

The lower part of the Striped member comprises shale-dominated cycles with intercalated beds of intraclast packstone and intraclast/ooid packstone. Cycle caps are relatively thin and stromatolitic. Upwards, cycles become stromatolite-dominated and the upper boundary of the Striped member is placed at the top of the uppermost cycle containing over 0.5 m of argillaceous dololutite.

Top Member, 60-150 m thick

The Top member is mostly stromatolitic except for a few beds of argillaceous dololutite in cycles at the base of the member. The member typically comprises a large number of cycles that contain small, linked to unlinked stromatolites at bases that pass upward into dark, cryptalgal tufa sheets that characteristically are not cherty, in contrast to the cryptalgal tufa sheets found in other members below. Furthermore, in many locations the cryptalgal tufa sheets dominate cycles and it becomes difficult to identify successive cycles, which may consist entirely of amalgamated cryptalgal tufa sheets. The upper part of this member is very distinct. It consists of several successive biostromes containing a diverse assemblage of branching columnar stromatolites that bear a resemblance to such forms including **Gymnosolen, Minjaria** and **Tungussia.** Although this interval of columnar stromatolites is present in every structural panel which exposes the Rocknest Formation except for the "X" thrust sheet, stromatolite forms in the biostromes vary considerably both vertically on the scale of a metre or two, and laterally on the scale of tens of kilometres. The upper boundary of the Top member coincides with the top of the Rocknest Formation which conformably underlies the Tree River Formation everywhere except in the northeastern corner of the autochthon where the contact is an erosional disconformity. Typically, the uppermost metre or two of stromatolitic dolomite contains small lenses of quartzose sandstone and siltstone which are developed between stromatolite columns. Above this zone, siliciclastic sediments blanket the carbonates and the upper boundary is placed at the top of the uppermost stromatolite bed.

Rocknest Shelf Cyclicity and Paleogeography

The asymmetric, shoaling-upward cycles of the Rocknest Formation have been described and interpreted by Hoffman (1975). Here, their relationship to the members is briefly discussed and analyzed from the standpoint of the implications this relationship may have for evaluating longer term variations in sea level during Rocknest deposition, and reconstructions of Rocknest shelf paleogeography.

The cycles comprise asymmetric, argillaceous dololutite-to-stromatolitic dolomite sequences, 1-10 m thick, and represent the progradation of stromatolitic tidal flats across muddy lagoons (Hoffman, 1975). They have striking lateral continuity; the 17 cycles of the thrombolitic member can be traced for over 200 km parallel to depositional strike (see Fig. 10.1, 10.3). The continuity of cycles across depositional strike has not yet been tested and may provide the key for understanding the mechanism of cyclicity. The cycles are typical of all members in the Rocknest Formation, except for the Intraclastic member, in which cycles have not been recognized, if present. A cycle with the complete range of component facies contains: 1) basal transgressive intraclastic lag lying on and derived from the top of preceding cycle, overlain by 2) reddish or greenish argillaceous dololutite with wave ripples, salt casts and synaeresis cracks, overlain by 3) thickly laminated tan dolosiltite and edgewise conglomerate, overlain by 4) stromatolitic or thrombolitic dolomite boundstone in which synoptic relief decreases upwards, overlain by 5) cryptalgalaminite with salt casts and rare gypsum casts, overlain by 6) dark, cherty, cryptalgal tufa with microdigitate stromatolites, salt casts, and rare gypsum casts. It is important to note that this is not an "ideal cycle" and the application of such an abstraction to cycle analysis should be avoided. A cycle with all the components listed above may be typically found within the Domal Stromatolite member or the Thrombolitic member, but is not typical of the Red Shale member or Top member which may, respectively, contain cycles that have no stromatolitic tops or argillaceous bases. Instead, a more useful concept for cycle analysis and classification utilizes end-members. Between end-members, development of component facies ranges from shale-dominated in which stromatolitic tops may be poorly developed or absent, to stromatolite-dominated in which shale bases may be poorly developed or absent. An intermediate cycle has all six component facies and represents rapid submergence of the shelf, followed by progradation and shoaling to sea level. Accordingly, shale-dominated cycles represent complete submergence of the shelf followed by incomplete shoaling to sea level before the next submergence increment, and stromatolite-dominated cycles represent incomplete submergence of the shelf followed by complete shoaling to sea level. These relationships indicate that complete shoaling of the shelf to sea level was not required to induce the next submergence increment, suggesting that the mechanism involved was allocyclic rather than autocyclic.

The transition from one member to the next is marked by a change in the ratio of lower components to upper components in cycles. For example, the transition from the Red Shale member to the Thin member is characterized by the gradual appearance of upper components and disappearance of lower components within a set of successive cycles. The top of the first cycle in which a stromatolitic bed occurs provides the upper boundary for the Red Shale member. These transitions from members in which cycles are dominated by the lower components (e.g. Red Shale member) to members in which cycles are dominated by the upper components (e.g. Thin member) constitute the basis for defining longer term variations in relative sea level on the Rocknest shelf. It is suggested that members containing primarily shale-dominated cycles represent times when relative sea level was higher over the platform-interior, in contrast with members containing primarily stromatolite-dominated cycles that were deposited during times when the platform was aggraded and relative sea level was very low.

Data collected during the 1981 and 1982 field seasons suggest that the Rocknest shelf had three north-trending facies belts, approximately parallel to structural strike; a western reefal rim and peritidal flat complex, a central fine

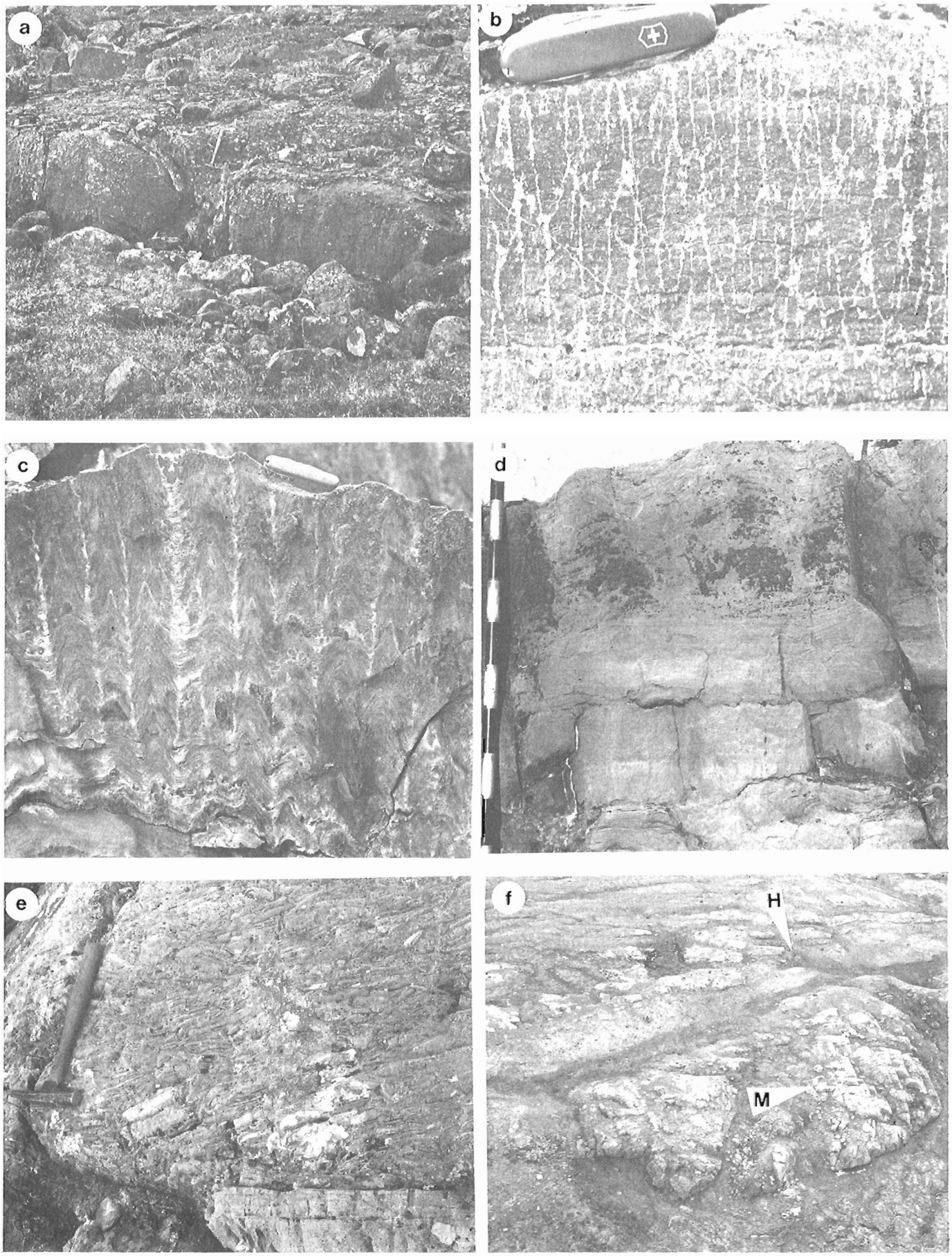
a
b
c
d
e
f
H
M

grained mixed terrigenous/carbonate lagoonal belt, and an eastern terrigenous clastic-dominated shoreline paralleling the exposed craton. The eastern clastic shoreline may be represented by terrigenous sediments in the upper Western River Formation or overlying Burnside River Formation (Goulburn Group, Kilohigok Basin), exposed near Rockinghorse Lake and Contwoyto Lake, 30-100 km east of the preserved Rocknest platform. Furthermore, the cycles most likely formed by west to east progradation of tidal flats from the reefal rim toward the centrally located lagoon. This hypothesis will be tested during the 1983 field season by conducting detailed studies of facies changes within cycles across depositional strike. Features that would support the suggested paleogeographic configuration include 1) evidence of westward stratigraphic thinning, or pinch-out of argillaceous dololutite (lagoonal facies) within cycles, indicating a centrally located lagoon, and 2) lateral transition of argillaceous dololutite to more siliciclastic-rich and coarser grained sediments to the east, indicating a clastic-dominated shoreline to the east of the lagoon. If valid, the hypothesis predicts that the reefal rim and peritidal flat complex should have been narrowest during periods of shale-dominated cyclic deposition (e.g. Red Shale member), and broadest during periods of stromatolite-dominated cyclic deposition (e.g. Top member). Such a paleogeographic configuration is similar to that proposed for the Cambrian of the Canadian Cordillera (Aitken, 1978).

Shelf-to-slope Transitions

Facies

The exposed shelf-edge and slope facies of the Rocknest Formation occur exclusively in the syncline "M" (Fig. 10.1) where the west limb exposes down-slope facies, and the east limb exposes both shelf-edge and up-slope facies. Shelf-edge reefal facies are characterized by algal boundstone sheets composed of strongly elongate, partially linked mounds with up to 2 m of synoptic relief. Channel deposits composed of trough crossbedded intraclast/ooid grainstone are locally well developed, but generally uncommon indicating that the stromatolite reefal rim was a very continuous, wave resistant structure.

Back-reef facies comprise thick, laterally continuous sheet-like bodies of crossbedded intraclast/ooid grainstone and low relief, strongly elongate, partially linked stromatolites. Locally, back-reef facies are overlain by peritidal facies containing spectacular examples of tepee antiform structures up to 1 m in width. The tepees contain giant silica and dolomite pseudomorphs of botryoidal aragonite that are attached to, and diverge downwards from the undersides of buckled plates (Grotzinger and Read, in press; Hoffman et al., 1983, Fig. 60-2).

Reefal-foreslope deposits are characterized by very thinly bedded, graded dolarenite/dolosiltite rhythmites with intercalated, flat-bottomed lensoidal bodies of vertically packed intraclasts. These sequences are associated with large **Conophyton** bioherms in which individual cones may have up to 1 m of synoptic relief. Locally, the bioherms contain isolated, branching **Conophyton** stromatolites resembling **Jacutophyton.** These deposits are very similar to those described by Hoffman (1974) for similar depositional settings in the Pethei Group of Athapuscow Aulacogen.

Upper-slope facies comprise thick sequences of graded, thickly laminated dolarenite and dolosiltite rhythmite with massive or laminated dololutite. Locally these deposits exhibit large-scale slump folding associated with concave-up slump scars and brecciated rhythmites. Breccia units may also be developed independently(?) of slumping as isolated lenses containing platy rhythmite clasts within otherwise undisturbed rhythmite. Breccias containing clasts derived from the shelf-edge do not occur as part of the upper-slope facies.

Lower-slope facies are restricted to a very thin panel, usually less than 100 m thick, on the west limb of syncline "M" where they are characterized by abundant resedimented platy rhythmite breccia units which commonly contain shelf-derived talus blocks. Individual breccia units generally fine upward and are amalgamated, or separated by thinly laminated dolosiltite/dololutite beds. Internally, the clasts are both matrix and self supported, and are oriented parallel to bedding although they are locally imbricated in an upslope direction (Fig. 10.4e). These deposits are similar to debris flows described by Cook and Taylor (1977) and probably have a similar origin.

West of syncline "M" the Recluse Group directly overlies the Odjick Formation indicating a stratigraphic pinch-out of the Rocknest Formation. At that location the Odjick Formation is of continental rise facies (Hoffman, 1973) indicating substantial water depth. The pinch-out of the Rocknest Formation can be explained by either nondeposition due to sediment starvation farther up on the slope, dissolution of sediment below the carbonate compensation depth, or a combination of both. Although the level of the carbonate compensation depth during Rocknest deposition cannot be evaluated, it seems reasonable to assume that carbonate dissolution may not have been important because of the preservation of periplatform talus aprons down to depths of several kilometres adjacent to modern carbonate platforms (Bathurst, 1975; Mullins and Neumann, 1979). More likely, sediment starvation had the greatest effect on the ultimate thickness of sediment deposited on the Rocknest slope and on the position of the stratigraphic pinch-out. Sediment starvation was probably related to local drowning and backstepping of the reefal rim during evolution of the shelf-edge (see below), and to the landward sediment transport effect of likely onshore directed paleotradewinds (Hoffman et al., 1983) during Rocknest deposition.

Relationship of Shelf-Edge to Structure

For most of the distance along syncline "M", the Rocknest shelf-to-slope transition occurs between its east and west limbs. Because of this coincidence between structural strike of syncline "M" and trend of the Rocknest facies change, it is inferred that the strike of the syncline is parallel to the general trend of the shelf-edge. However, locally along strike in the eastern panel, upper-slope facies

Figure 10.4. *(opposite)*

a. Discrete bioherms of digitate stromatolites in basal bed of Rocknest Formation.

b. Microdigitate stromatolites.

c. ***Conophyton.***

d. Partially linked columnar thrombolites in cycle 6, Thrombolitic member, section (B). Dark where cryptalgal "clots" are selectively silicified, imparting a splotchy appearance to the bed. Thrombolites overlie intraclast grainstone/packstone (middle of figure), and domal stromatolites (bottom of figure). Jacobs staff marked in decimetre intervals.

e. Resedimented, platy rhythmite breccia sharply overlying undisturbed rhythmite, west limb of syncline "M". Clasts are imbricated upslope.

f. Megabreccia block (M), east limb of syncline "M". Stratigraphic facing (arrow) of host sediments (H) is from top left to bottom right; in block, from centre to centre right. Block is approximately 50 m wide.

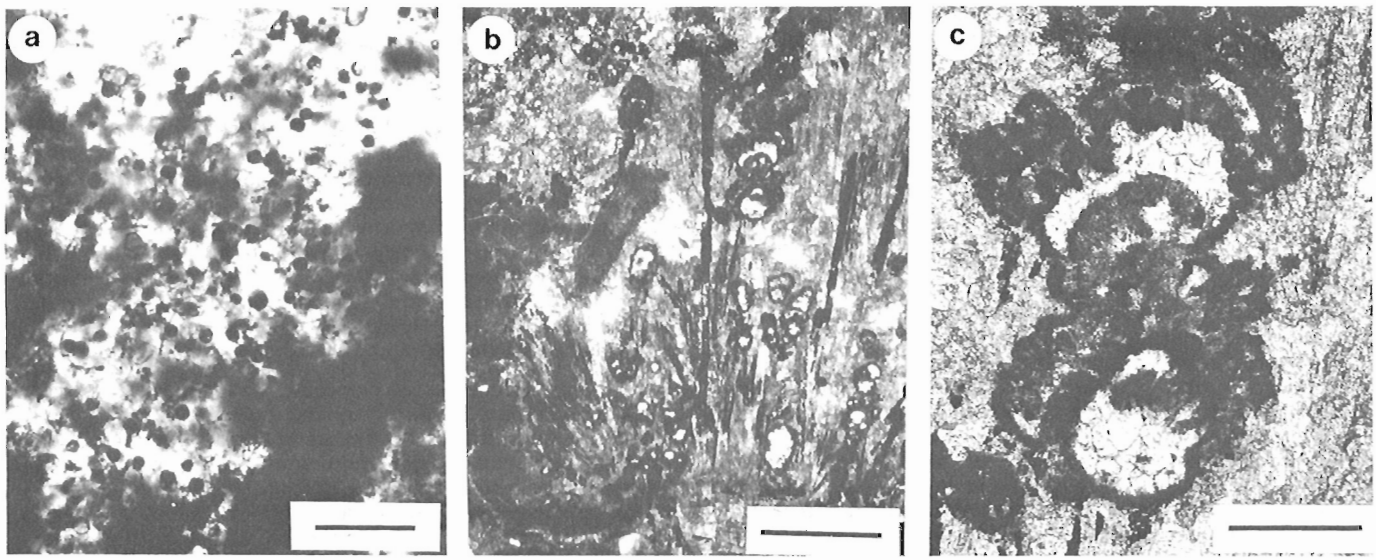

Figure 10.5.

a. Thin section photomicrograph of microbial(?) spheres and filaments in dolomitized aragonite marine cement, Odjick/Rocknest transition beds. Scale bar is 10 microns.

b. Thin section photomicrograph of fibrous dolomite neospar after upward divergent, botryoidal aragonite cement. Precursor fibres (prominent, weakly divergent vertical fabric) are outlined by thin hematitic coatings and inclusion trains. Note the ***Renalcid****-like microcolumnar structures. Scale bar is 3 mm.*

c. Thin section photomicrograph of ***Renalcid****-like microcolumnar structure with superimposed, upward-branching inflated chambers. Hematitic coatings outline chambers which are enclosed in turbid dolomite neospar, and filled with clear dolomite neospar. Scale bar is 1 mm.*

are exposed rather than shelf-edge facies. This variation in the distribution of upper-slope facies versus shelf-edge facies along the eastern limb of syncline "M" could be explained by either of the following: 1) the shelf had an irregular margin with promontories coinciding with areas of preserved shelf-edge facies and embayments coinciding with areas of preserved upper-slope facies, or 2) the distribution of facies is structurally controlled. Even though the former explanation seems possible by analogy with modern rimmed shelves which are known to be irregular (Maxwell, 1968; Purdy et al., 1975), the latter explanation is more likely for this case. Facies changes along the east limb of syncline "M" occur over transcurrent faults which postdate and segment the syncline. Although they are dominantly strike-slip faults, a small component of dip-slip (up to 200 m) can be demonstrated for some areas with good stratigraphic control (Tirrul, personal communication, 1983). Since the dip of the Rocknest Formation on the east limb of syncline "M" is generally 60 degrees west, a dip-slip component of 200 m on a transcurrent fault would produce a 240 m separation of the Rocknest Formation perpendicular to the shelf-edge. In syncline "M", upthrown blocks would tend to show more seaward facies relative to downthrown blocks which would tend to show more landward facies. In Holocene reefal rims, facies changes are very abrupt between the reefal rim and upper slope and often occur on the order of tens to hundreds of metres (Longman, 1981). Thus, vertical offsets along transcurrent faults could account for the observed distribution of facies along strike in the east limb of syncline "M".

Evolution of Shelf-Edge

Along the east limb of syncline "M", the Rocknest Formation shows several general features of shelf-edge evolution. In the early stages of rim development, reefal facies prograded out over upper-slope carbonates and upper-slope clastics of the underlying Odjick Formation. This was followed by the progradation of back-reef facies and peritidal facies over reefal facies. Subsequent to the initial stage of progradation, the shelf-edge entered a period of aggradation during which a reefal rim was established and vertically built up as shown by the uninterrupted deposition of up to 600 m of shelf-edge sediments. Progradation and aggradation of the rim was recorded downslope by deposition of only 200 m of rhythmite and slope/shelf-edge breccias on argillaceous siltstones of the Odjick Formation, preserved in the west limb of syncline "M".

At the end of this stage of shelf-edge development, construction was interrupted and terminated along the length of the margin as shown by the abrupt deposition of thinly laminated dololutite and black shale over reefal facies. This event of shelf-edge drowning occurred locally and was associated with backstepping of the reefal rim to a position not exposed, but which must lie palinspastically between the present outcrop on the east limb of syncline "M", and the outcrop of the next thrust sheet to the east where there is no evidence for drowning and the Rocknest Formation attains its greatest thickness of over 1 km.

After backstepping, the reefal rim began another aggradational phase that persisted until the terminal drowning of the entire platform. During this stage a steep escarpment was constructed as shown by the occurrence of huge, allochthonous shelf-edge derived blocks up to 40 m in length that fell onto the earlier drowned rim (see Fig. 10.4f). More commonly, drowned rim deposits are overlain by thickly laminated, graded rhythmites and resedimented rhythmite breccias containing shelf-edge derived talus blocks. The drowned rim was a terrace that acted as a trap and probably prevented most sediment from being transported over its edge and down the main slope into the basin, thus starving

the main slope of sediment. This interpretation is supported by the very thin section of slope deposits in the west limb of syncline "M", which contains an upper starved-slope unit of laminated dololutite (10-20 m thick) that sharply overlies a lower unit (100 m) of graded rhythmites and platy rhythmite breccias containing shelf-edge derived talus blocks. The lower unit was probably deposited during upbuilding of the older, drowned rim; the upper unit was probably deposited as "background" sediment during upbuilding of the younger, backstepped rim. The main slope must have been a zone of bypassing during upbuilding of the older rim as shown by the occurrence of shelf-edge derived blocks in down-slope deposits of the west limb of syncline "M", which are not present in up-slope deposits of the east limb. At the time of rim backstepping, the average inclination of the slope was probably 4-7 degrees (Hoffman et al., 1983).

In general, evolution of the Rocknest shelf margin was very similar to the evolution of Phanerozoic rimmed shelves, involving stages of progradation, aggradation, backstepping, and drowning (Read, 1982). The principles involved behind the evolution of the Rocknest platform margin may have been similar to those operative on the modern margin of the Bahamas where similar features are currently being produced (Schlager and Camber, 1982).

Paleoclimate

The Rocknest Formation was previously interpreted to have been deposited in a humid paleoclimatic setting (Hoffman, 1975). This interpretation was based in part on comparison of Rocknest cryptalgal tufas and microdigitate stromatolites at the tops of shoaling-upward cycles with algal tufa crusts currently being formed in fresh/brackish water supratidal ponds on Andros Island, Bahamas. Hoffman (1975) noted that Rocknest cryptalgal tufas, like Bahamian algal tufas, most likely formed by direct precipitation of carbonate in algal mats and cited the development of palisade structure with preserved filament molds as evidence for this. However, additional field and petrographic studies have recently shown that the most likely carbonate cement precipitated in Rocknest cryptalgal tufas was not calcite (predicted for humid climate), but dolomitized aragonite (predicted for semiarid to arid climate). Evidence for aragonite precipitation in Rocknest cryptalgal tufas includes square and feathery terminations of precursor acicular crystals, replaced by neospar mosaics containing anhedral, randomly oriented (optically) dolomite crystals with ragged boundaries and abundant inclusions (Grotzinger and Read, in press). In regard of this new information, the Rocknest cryptalgal tufas are reinterpreted to have formed by the direct precipitation (biologically influenced?) of aragonite to form lithified crusts on tidal flats, under semiarid climatic conditions. More evidence for a semiarid setting is discussed below and includes preservation of abundant pseudomorphs after halite, rare pseudomorphs after gypsum and possibly anhydrite, vadose pisolites associated with laminated scalloped surfaces, and tepee structures filled with pseudomorphs after botryoidal aragonite.

Pseudomorphs after halite are common within peritidal cyclic sediments of the Rocknest Formation. They are best preserved as displacive cubic crystal casts in "detrital" carbonate mud interlaminae of cryptalgal tufas in the upper parts of cycles, and as skeletal hopper casts in argillaceous dololutites in lower parts of cycles. Less commonly, displacive halite casts occur in muddy layers of stromatolitic facies within cycles. Displacive halite casts in cryptalgal tufas are 0.05-3.0 mm wide and filled with muddy host sediment or early diagenetic chert. Skeletal hopper crystal casts in argillaceous dololutites are up to 5 cm wide and show no evidence of silica replacement. In both cases, crystal faces tend to be oriented subparallel to bedding. In contrast to the abundance of halite casts, crystal casts after gypsum or anhydrite are rare. However, well preserved swallow-tail, rosette cluster, and lozenge-shaped casts after gypsum occur in a few cycles capped by cryptalgal tufa sheets. These pseudomorphs are now preserved as coarse, brown ankeritic dolomite, which similarly fills associated globular masses that may have been anhydrite.

Other features in the Rocknest Formation that are diagnostic of semiarid climates are tepee structures, vadose pisolites associated with cryptalgal tufas, and inorganic cement crusts on scalloped surfaces (Purser and Loreau, 1973; Scholle and Kinsman, 1974; Assereto and Kendall, 1977). Tepee structures in the Rocknest Formation occur in back-reef peritidal and cyclic peritidal settings. Those of back-reef peritidal origin are large (up to 1 m) and locally filled with silica and dolomite pseudomorphs after downward-diverging botryoidal aragonite (Grotzinger and Read, in press); tepees found in cyclic peritidal settings are small (up to 20 cm) and occur in cryptalgal tufa sheets at tops of cycles, associated with broken plates of cryptalgal tufa that are coated by later generations of tufa. Less commonly, these features are associated with scalloped surfaces, outlined by finely laminated fibrous cement, and filled with irregular-shaped pisolites. These pisolite-filled surfaces are overlain by isopachous linings of additional laminated, fibrous cement.

Possible Microfossils in the Odjick/Rocknest Transition Beds

Well preserved microbial remnants(?) occur in dolomite/hematite stromatolite bioherms of the Odjick/Rocknest transition beds. Bioherms (up to 30 cm thick) are lenticular units (50 cm x 10 m) enclosed within green and red shales, siltstones and pebbly sandstones. The siliciclastic sediments contain crossbedding, hummocky storm deposits, lenticular channel deposits, and lack desiccation features suggesting deposition on a subtidal, shallow shelf. Stromatolitic layers in bioherms are flat, irregular to wavy, and locally form low, sharp-crested peaks with 1-4 mm relief. In plan, stromatolites are 1-5 cm long, and strongly elongate. Laminae are 0.01-0.1 mm thick and consist of alternating layers or mixtures of dolomite and hematite. Some layers contain detrital, rounded quartz grains (up to 2.5 mm) and rare dolomite intraclasts.

Stromatolitic layers are interbedded with and pass laterally into layers of noemorphic, acicular carbonate characterized by mosaics of anhedral, turbid, randomly oriented (optically) dolomite crystals with ragged boundaries. Acicular cement fans contain well preserved precursor crystal fibres of aragonite that are outlined by very thin synsedimentary hematite coatings and inclusions (Fig. 10.5b). The possible microfossils occur within dolomite neospar cement layers; well preserved forms include spheres (2-20 microns) and filaments (1-2 microns wide, 4-20 long) outlined by hematite (Fig. 10.5a), and questionable microcolumnar structures made of upward-branching inflated chambers (Fig. 10.5b,c) that resemble the Paleozoic alga **Renalcis**. Microcolumnar structures are 0.2-4.0 mm tall and 0.06-0.9 mm wide; component chambers are 0.08-0.24 mm high and 0.06-0.9 mm wide, with walls 0.016-0.026 mm thick. Walls often have isopachous, extremely fine, fibrous fringes on their outer sides and show no obvious pigmentation gradients. Spheres and filaments are not usually associated with microcolumnar structures, and typically occur as geopetal "sediment" in primary voids within stromatolitic layers, now filled with neomorphic dolomite cement. Filaments appear to have been torn and eroded from stromatolitic laminae. Spheres may also have been a component of the stromatolitic laminae, although this is less certain.

Future Work

The final season for field study of the Rocknest Formation is planned for 1983. Investigations will focus on detailed studies of the complex reefal rim and flanking facies belts, and on east-west facies changes within the cycles at the northern end of the thrust-fold belt.

Acknowledgments

Jean David, Mark Daynecka, Greg Eiche, Karen Pelletier, and Janien Schwarz were superb assistants in the field. Rein Tirrul is gratefully acknowledged for excellent tips on where to measure sections. J. Fred Read visited in the field and provided advice, encouragement, and stimulating discussions.

J.P.G. thanks the Geological Survey of Canada for the opportunity to study the Rocknest Formation, and also for logistical support. Additional logistical support was provided by the Geology Office, Department of Indian and Northern Development, N.W.T., and additional financial support for J.P.G. was provided by a Geological Society of America Grant 2992-82, and a Grant-in-Aid from Sigma Xi, the Scientific Research Society.

References

Aitken, J.D.
– Revised models for depositional grand cycles, Cambrian of the southern Rocky Mountains, Canada; Canadian Petroleum Geologists, Bulletin, v. 26, no. 4, p. 515-524.

Assereto, R.L.A.M. and Kendall, C.G.St.C.
1977: Nature, origin and classification of peritidal tepee structures and related breccias; Sedimentology, v. 24, p. 153-210.

Bathurst, R.G.C.
1975: Carbonate Sediments and the Diagenesis; Elsevier, Amsterdam, 658 p.

Cook, H.E. and Taylor, M.E.
1977: Comparison of continental slope and shelf environments in the Upper Cambrian and Lowest Ordovician of Nevada; in Deep-Water Carbonate Environments, ed. H.E. Cook and P. Enos, Society of Economic Paleontologists and Mineralogists, Special Publication 25, p. 51-82.

Grotzinger, J.P.
1982: A preliminary account of the internal stratigraphy of the Rocknest Formation, foreland thrust-fold belt of Wopmay Orogen, District of Mackenzie; in Current Research, Part A, Geological Survey of Canada, Paper 82-1A, p. 117-118.

Grotzinger, J.P. and Read, J.F.
– Evidence for aragonite precipitation, early Proterozoic (1.9 B.Y.) Rocknest Formation, N.W.T., Canada; Geology. (in press)

Hoffman, P.F.
1973: Evolution of an early Proterozoic continental margin: the Coronation geosyncline and associated aulacogens of the northwestern Canadian Shield; The Royal Society of London, Philosophical Transactions, Series A, v. 273, p. 547-581.

1974: Shallow and deepwater stromatolites in Lower Proterozoic platform-to-basin facies change, Great Slave Lake, Canada; American Association of Petroleum Geologists, Bulletin, v. 58(5), p. 856-867.

1975: Shoaling-upward shale-to-dolomite cycles in the Rocknest Formation, Northwest Territories; in Tidal Deposits, ed. R.N. Gisburg; Springer-Verlag, Heidelberg, p. 257-265.

Hoffman, P.F. (cont.)
1980: Wopmay Orogen: a Wilson Cycle of early Proterozoic age in the northwest of the Canadian Shield; in The Continental Crust and Its Mineral Resources, ed. D.W. Strangway; Geological Association of Canada, Special Paper 20, p. 523-549.

Hoffman, P.F., Tirrul, R., and Grotzinger, J.P.
1983: The externides of Wopmay Orogen, Point Lake and Kikerk Lake map areas, District of Mackenzie; in Current Research, Part A, Geological Survey of Canada, Paper 83-1A, p. 429-435.

Jackson, M.J.
1982: Correlations of stromatolites between northern Australia and U.S.S.R.; in Abstracts of Papers, International Association of Sedimentologists, Hamilton, p. 161.

Longman, M.W.
1981: A process approach to recognizing facies of reef complexes; in European Fossil Reef Models, ed. D.F. Toomey, Society of Economic Paleontologists and Mineralogists, Special Publication 30, p. 9-40.

Maxwell, W.G.H.
1968: Atlas of the Great Barrier Reef; Elsevier, Amsterdam, 258 p.

Mullins, H.T. and Neumann, A.C.
1979: Deep carbonate bank margin structure and sedimentation in the northern Bahamas; Society of Economic Paleontologists and Mineralogists, Special Publication 27, p. 165-192.

Purdy, E.G., Pusey, C.W., and Wantland, K.F.
1975: Continental shelf of Belize – regional shelf attributes in Belize Shelf – Carbonate Sediments, Clastic Sediments, and Ecology, ed. K.F. Wantland and W.C. Pusey; American Association of Petroleum Geologists, Studies in Geology, no. 2, p. 1-39.

Purser, B.H. and Loreau, J.P.
1973: Aragonitic, supratidal encrustations on the Trucial Coast, Persian Gulf; in The Persian Gulf, ed. B.H. Purser; Springer-Verlag, Heidelberg, p. 343-376.

Read, J.F.
1982: Carbonate platforms of passive (extensional) continental margins: types, characteristics and evolution; Tectonophysics, v. 81, p. 195-212.

Schlager, W. and Camber, O.
1982: Depositional, erosional and by-pass slopes on carbonate platforms; in Abstracts of Papers, International Association of Sedimentologists, Hamilton, p. 179.

Scholle, P.A. and Kinsman, D.J.J.
1974: Aragonite and high-Mg calcite caliche from the Persian Gulf – a modern analog for the Permian of Texas and New Mexico; Journal of Sedimentary Petrology, v. 44, no. 3, p. 904-916.

Serebryakov, S.N.
1976: Distribution of stromatolites in Riphean deposits of the Uchur-Maya region of Siberia; in Stromatolites, ed. M.R. Walter; Elsevier, Amsterdam, p. 613-634.

Tirrul, R.
1982: Frontal thrust zone of Wopmay Orogen, Takijuq Lake map area, District of Mackenzie; in Current Research, Part A, Geological Survey of Canada, Paper 82-1A, p. 119-122.

11. # MINERALOGICAL, PETROCHEMICAL AND PETROGRAPHIC-TEXTURAL STUDIES OF ORE GRADE AND LOWER GRADE RADIOACTIVE ROCKS FROM THE BANCROFT AREA, ONTARIO: PROGRESS REPORT 2

Project 770061

J. Rimsaite
Economic Geology Division

Rimsaite, J., Mineralogical, petrochemical and petrographic-textural studies of ore grade and lower grade radioactive rocks from the Bancroft area, Ontario: progress report 2: in Current Research, Part B, Geological Survey of Canada, Paper 83-1B, p. 93-108, 1983.

Abstract

Results of rapid chemical, spectrographic, scanning electron microscope and neutron activation analyses for U are discussed in relation to metamorphism, recrystallization, replacement textures and mineralization of hybrid rocks collected at mine sites in the Bancroft area. The samples represent the following:

1. *gneisses, migmatites and granitoid rocks in and adjacent to the Faraday granite;*
2. *Cheddar granite, mylonite and surrounding gneisses with sedimentary textures;*
3. *pegmatite and adjacent high grade metamorphic rocks surrounding Halo mine;*
4. *selected ore specimens from the Madawaska, Greyhawk, Bicroft and Halo mines, and their relation to petrographic-textural characteristics and ore and accessory mineral associations.*

Relicts of diverse metasedimentary rocks, porphyroblastic and anatectic textures, impregnations, mylonitization and alteration account for the mineralogical and petrochemical diversity of the hybrid rocks. With a few exceptions which contain radioactive accessory minerals, most of the metasediments contain less than 4 ppm U and are unlikely sources for the uranium mineralization.

Résumé

Le présent rapport décrit les résultats de l'analyse chimique rapide, de l'analyse spectrographique, de l'analyse au microscope électronique à balayage et de l'essai par activation de neutrons de roches hybrides provenant de mines dans la région de Bancroft (Ontario). Ces analyses ont été effectuées en vue de déterminer la teneur en U des roches et les résultats sont présentés en fonction du métamorphisme, de la recristallisation, des textures de remplacement et de la minéralisation. Les échantillons comprennent:

1. *des gneiss, des migmatites et des roches granitoïdes du granite de Faraday et adjacents à ce dernier;*
2. *du granite de Cheddar, de la mylonite et des gneiss environnants à textures sédimentaires;*
3. *de la pegmatite et des roches adjacentes à degré de métamorphisme élevé, trouvées aux environs de la mine Halo;*
4. *des échantillons choisis de minerais provenant des mines Madawaska, Greyhawk, Bicroft et Halo et leur lien avec les caractéristiques pétrographiques-texturales et les associations de minerais et de minéraux accessoires.*

Les résidus de diverses roches métasédimentaires, les textures porphyroblastiques et anatectiques, les imprégnations, la mylonitisation et l'altération expliquent la diversité minéralogique et pétrochimique des roches hybrides. Sauf quelques rares exceptions qui contiennent des minéraux accessoires radioactifs, la plupart des métasédiments renferment moins de 4 ppm d'U et ne seraient probablement pas la source de la minéralisation uranifère.

Introduction

The Bancroft area is famous for its occurrences of alkaline and silica-deficient rocks which host a great variety of rare minerals. Although the area has been studied by many prominent geologists, mineralogists and petrologists since 1910, and many theories have been proposed, there is no unanimous opinion concerning the origins of these minerals and rocks (Adams and Barlow, 1910; Goldich and Kniser, 1939; Chayes, 1942; Fyson et al., 1979; Lumbers, 1980).

General geology and descriptions of uranium mines can be found in Satterly (1957), Hewitt (1967) and Masson and Gordon (1981) who also provided geological maps with mining localities. On the basis of the above maps, uranium deposits are situated in pegmatites transecting metasediments and metagabbro which surround granite-syenite bodies, namely the Faraday granite, Cheddar granite and Moak Lake granite (Satterly, 1957).

The purpose of this study is to attempt to define differences and similarities between ore grade specimens and adjacent lower grade specimens on the basis of the author's mineralogical and petrographic studies, supported by chemical analyses. I spent 1 to 3 days in 1977, 1979 and 1981 collecting representative samples of diverse rocks in and around the mines. Short accounts discussing textures and alteration of radioactive ore and accessory minerals, illustrated in backscattered electron micrographs have been published (Rimsaite, 1978, 1980a, b, 1981, 1982a, b, 1983).

Table 11.1

Partial chemcial analyses of selected metasediments, migmatites, hybrid granitoid rocks and ore grade samples from the Bancroft area, Ontario *,**

	Faraday granite and adjacent migmatites						Cheddar granite, metasediments					Halo mine		Madawaska mine		ore	GH***	B***	Halo
	1	2	3	4	5	6	7	8	9	10	11	12	13	14	15	16	17	18	19
SiO_2%	71.9	74.9	56.4	68.9	74.7	74.3	73.8	55.7	54.9	74.1	53.3	80.6	36.2	50.3	55.7	64.8	45.4	59.9	47.4
TiO_2	0.2	0.3	0.9	0.2	0.9	0.2	0.1	0.4	1.6	0.2	0.9	0.1	0.9	0.3	1.6	1.9	2.0	1.0	0.1
Al_2O_3	14.4	12.1	16.2	15.0	4.6	12.3	13.7	8.6	21.8	13.7	12.6	11.1	13.4	1.6	6.0	7.9	11.1	16.1	7.7
Fe_2O_3	1.6	1.4	4.6	0.9	9.0	2.1	0.2	1.6	3.0	0.3	2.1	(0.3)	2.9	6.7	4.1	5.6	6.7	1.1	(17.0)
FeO	0.5	1.0	4.3	0.4	3.4	0.4	0.2	3.4	7.7	0.1	4.9	ND	5.0	10.9	6.3	5.9	8.0	2.3	ND
MnO	0.0	0.0	0.1	0.1	0.1	0.0	0.0	0.2	0.1	0.0	0.2	0.0	0.6	0.8	0.5	0.2	0.3	0.2	0.1
MgO	0.0	0.7	3.6	0.2	0.2	0.2	0.0	7.6	2.1	0.1	4.4	0.1	7.1	4.7	4.7	4.5	5.3	1.7	1.8
CaO	1.0	0.7	1.6	1.3	0.6	1.0	0.3	14.6	0.2	0.8	10.7	0.9	18.7	17.8	11.5	0.1	9.8	7.7	1.1
Na_2O	4.9	5.3	5.4	4.8	1.4	4.0	3.6	1.5	0.4	3.9	0.9	3.3	0.6	1.8	1.9	0.0	3.4	6.4	1.7
K_2O	4.4	1.5	5.5	5.9	1.4	4.8	6.4	5.0	5.1	5.6	6.4	2.4	0.9	0.3	2.5	4.1	1.0	2.3	0.1
H_2O	0.3	0.3	1.0	0.3	0.6	0.4	0.4	0.5	3.5	0.2	1.0	0.4	1.4	0.5	2.1	1.8	1.9	0.4	0.7
Cl	.04	.04	.09	.03	.02	.05	.05	.06	.24	.02	.12	.01	.03	.04	.03	.04	.11	.06	.22
F	.02	.12	.39	.06	.03	.46	.01	.04	.14	.02	.17	.00	.06	.17	.18	.23	.14	2.00	.19
P_2O_5	.05	.01	.20	.05	.05	.05	.02	.16	.09	.02	.20	.01	.17	.10	.06	.02	.30	.20	.06
CO_2	.40	.10	.10	.90	.10	.00	.00	1.30	.00	.20	.00	.00	5.00	.50	.00	.00	1.80	.30	.09
S	.00	.00	.00	.00	.00	.00	.00	.00	.02	.00	1.00	.41	.18	1.40	.08	.20	.03	.10	9.60
Ba	.05	.01	.10	.06	.02	.01	.04	.11	.04	.04	.13	.04	.01	.01	.04	.02	.01	.03	.01
Ni	.00	.00	.01	.01	.01	.00	.00	.00	.01	.00	ND	ND	ND	.01	ND	ND	.01	ND	ND
Rb	.01	.01	.05	.03	.00	.01	.03	.01	.02	.03	.02	.01	.00	.01	.04	.04	.01	.01	.01
Sr	.01	.01	.03	.02	.01	.01	.02	.02	.01	.02	.03	.03	.03	.08	.09	.00	.02	.05	.00
Zn	.01	.01	.02	.01	.01	.00	.00	.01	.01	.00	.01	.00	.01	.03	.02	.04	.01	ND	.05
Zr	.04	.09	.00	.01	1.22	.08	.03	.01	.02	.00	.01	.01	.01	.23	.06	.01	1.20	.50	.02
U ppm	1.8	3.7	1.7	3.2	167	5.4	25.1	2.9	5.6	4.4	2.7	2.5	8.7	10290	450	4800	4470	3100	f5000
Th ppm	ND	ND	ND	ND	ND	ND	ND	ND	ND	ND	10.	7.	11.	8600	294	331	3000	920	1195

* Chemical and emission spectrographic analyses by the staff of the Central Laboratories and Technical Services Division, Geological Survey of Canada.

** Uranium (ppm) determined by neutron activation analysis by Atomic Energy of Canada, Ltd. Thorium (ppm) determined by X-ray fluorescence analysis by Bondar-Clegg & Co., Ltd.

*** Sample locations and mines symbols are the same as those on sketch map (Rimsaite, 1978, Fig. 9.2). Location of mines are indicated on the Ontario Department of Mines geological map 1957b, Haliburton-Bancroft area (Satterly, 1957). See Appendix for description of samples.

Brackets indicate total iron reported as Fe_2O_3. ND = not determined.

This report contains petrographic descriptions and selected chemical analyses of the following suites:

1. gneisses, migmatites and granitoid rocks in and adjacent to the Faraday granite;
2. Cheddar granite, mylonite and surrounding gneisses;
3. pegmatite and adjacent high grade metamorphic rocks surrounding Halo mine;
4. selected examples of ore grade specimens from the Madawaska, Greyhawk, Bicroft and Halo mines; these are discussed in relation to petrographic-textural characteristics and ore and accessory mineral associations of individual specimens.

All rocks consist essentially of the same mimerals, differing mainly in proportion and textural relationships between the rock-forming and accessory minerals. Thus emphasis was placed on the relict sedimentary textures, on the type, intergrowths and replacements of feldspars and on alteration of minerals in mylonitized rocks using already established techniques for studies of alteration (Rimsaite, 1967, 1974). Nineteen selected chemical analyses are presented in Table 11.1. Petrographic descriptions of chemically analyzed specimens are given in the Appendix.

Acknowledgments

The petrographic-textural studies were supported by neutron activation analyses for U by Atomic Energy of Canada Limited; X-ray fluorescence determinations of Th by Bonder-Clegg and Company Ltd.; rapid chemical and emission spectrographic analyses by the staff of the Analytical Chemistry Section, Geological Survey of Canada; and scanning electron microscope (SEM) and energy dispersive spectrometer (EDS) analyses by D.A. Walker of the Geological Survey of Canada. I am grateful for this analytical support. My sincere thanks are due to J. Kerswill for his assistance in the field in 1977 and 1979, and to the Staff of the Madawaska uranium mine for thier guidance at the mine site.

Gneisses, Migmatites and Granitoid Rocks in and Adjacent to the Faraday Granite

(Fig. 11.1, 11.2; Table 11.1, analyses 1-5)

The Faraday granite is heterogeneous and consists of fine- and coarse-grained pegmatitic granitoid and syenitic phases. It contains xenoliths of surrounding invaded metagabbro, biotite-hornblende gneiss, migmatite and other metasediments. The petrographic-textural characteristics of specimens collected along the western, eastern and southern edges of the granite and from its central portion in road cuts along Highway 500 as well as underground in the Madawaska mine (Rimsaite, 1978, Fig. 9.2, localities A, F) are correlated with their chemical compositions. All specimens consist essentially of the same rock-forming minerals but differ in proportions, size and type fo quartz, feldspars, ferromagnesian and accessory minerals, and the degree of deformation and alteration that the assemblages have undergone. The metasedimentary schists consist of quartz-feldspar mosaics with variable amounts of biotite and amphibole. Accessory magnetite, pyrite, titanite, apatite, zircon and calcite commonly occur in biotite-amphibole layers as disseminated grains or in intergrowths with one another. In biotite-hornblende schists and gneisses, collected underground in the Madawaska mine, the biotite-rich varieties contain abundant radioactive titanite, apatite, and zircon grains which produce marked pleochroic haloes in biotite. Radioactive titanite, apatite and zircon may contain some radioactive elements in their structure, but their radioactivity more commonly results from minute uraninite and uranothorite inclusions and crusts that contain secondary uranyl-bearing mineral aggregates. Rocks containing radioactive accessory minerals have elevated uranium values of between 6 and 18 ppm. The hornblende-rich varieties studied contain weakly radioactive accessory minerals, resulting in very faint pleochroic haloes or the absence of haloes. Calcite crystallized late in the sequence of crystallization. It occurs as interstitial patches around and within fractures partly replacing biotite and adjacent feldspar grains (Fig. 11.1a). Locally some biotite bands and adjacent feldspars are entirely replaced by calcite-sericite-muscovite aggregates and speckled clay-like and oxide minerals, thus indicating that biotite-rich bands acted as aqueducts for alteration fluids in otherwise compact and apparently fresh rock.

Schists grade into gneisses and migmatites in which biotite flakes lose their preferential orientation, and relatively uniform equigranular textures change to porphyroblastic and poikilitic textures with grain sizes showing marked variations ranging from a few microns to several centimetres. Primary banding, such as Na-rich oligoclase-bearing bands, microcline-and/or quartz-rich bands have been retained in banded gneisses (Fig. 11.1a, c). Mafic minerals and leucocratic minerals, mainly quartz and feldspars, are segregated into bands in migmatite and into composite crystals and porphyroblasts in gneisses and pegmatites. In the eastern, central and southern portions of the Faraday granite, the segregation of minerals into coarse grained porphyroblasts takes place in the following order: (1) patches of poikilitic magnetite commonly overgrown by titanite, apatite ± zircon; (2) segregations of composite plagioclase grains (similar to those in Rimsaite, 1967, Fig. IV-12, V-13, 14) and of porphyroblastic microcline, which invades and partly replaces plagioclase along the edges (Fig. 11.1d) and ultimately forms poikilitic porphyroblasts showing heterogeneous distribution of mineral inclusions, perthitic lamellae and interrupted twinning (Rimsaite, 1967, Fig. IV-11, VIII-22); and (3) hornblende and associated accessory minerals segregated into coarse patches reaching several centimetres in size. Quartz segregates into vugs and veinlets of quartz neosome, locally engulfing all earlier formed (paleosome) portions of the rock or individual minerals (Fig. 11.1d). Quartz also forms myrmekitic intergrowths with amphibole and biotite (Fig. 11.1c).

In schists, gneisses and migmatites west of the Faraday granite, feldspars are nonperthitic or contain only very fine grained specks or thin lamellae of alkali feldspar (Rimsaite, 1967, Fig. II-6).

Banded gneisses contain several types and generations of zircon which were concentrated for isotopic analyses of Pb, Th and U (Fig. 11.1b). The clear prismatic zircon of type 1 (type "S-2" according to the classification of Pupin, 1980), appears to be the youngest. It contains a few opaque inclusions, exhibits concentric zoning and occurs in quartz-feldspar bands, commonly as disseminated crystals within quartz grains. Zircon of type 2 is more complex. It consists of older fragments of zircon overgrown by clear rims, similar to zircon of type 1. The third type of zircon consists of crushed, fragmented zircon grains. Zircon varieties "2" and "3" are associated with ferromagnesian minerals and commonly form inclusions in biotite, or are attached to magnetite-titanite intergrowths. They may also occur as paleosome remnants in fractures of mylonitized quartz (Fig. 11.2d). Although truly radioactive zircons have been encountered in the Bancroft area, most zircons contain radioactive inclusions and uranyl-bearing crusts (Rimsaite, 1981).

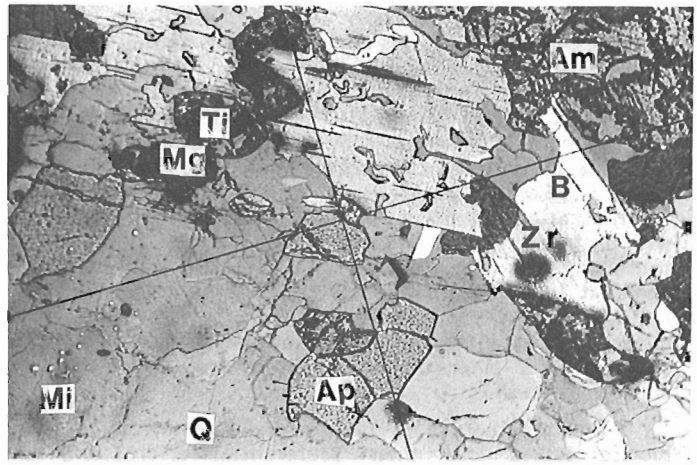

c

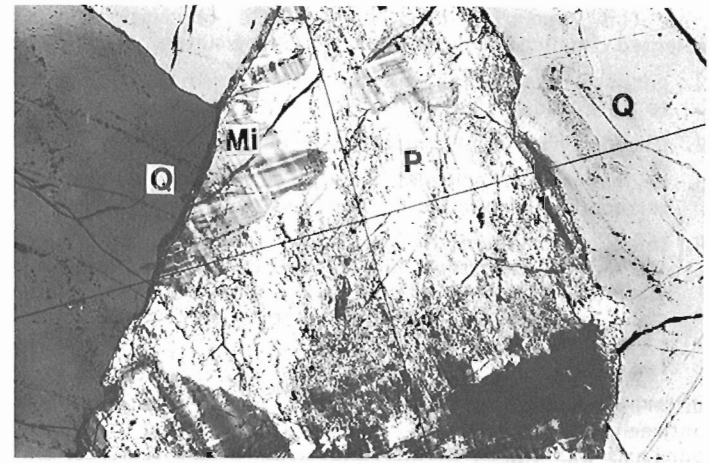

d

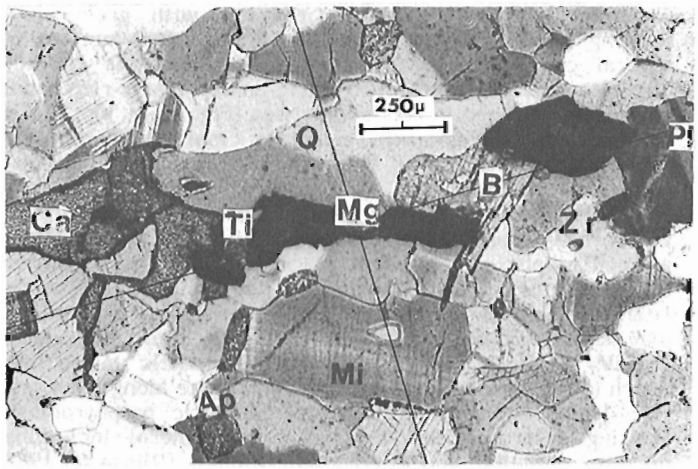

a

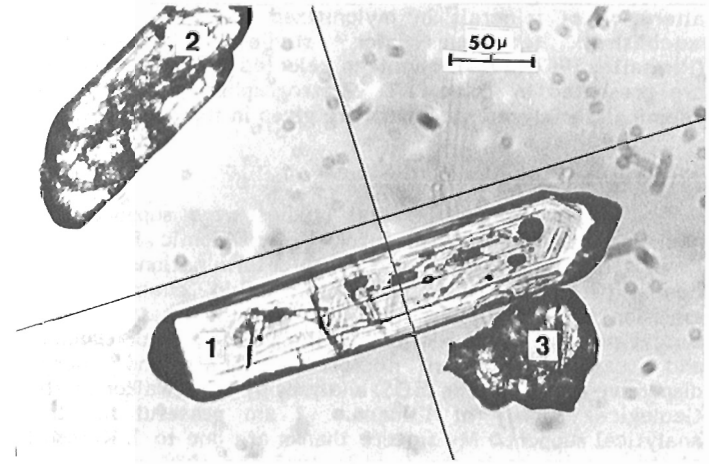

b

a. *Migmatite at the NW edge of the Faraday granite, south of Baptiste Lake, showing a mosaic texture of quartz (Q), microcline (Mi), biotite (B), apatite (Ap), titanite associated with magnetite (Ti, Mg, opaque), calcite (irregular patches in fractures), and zircon in biotite and quartz (Zr).*

b. *Three types of zircon grains separated from migmatite in (a) for isotopic studies of U, Th and Pb: (1) clear, long zoned prisms; (2) red zoned composite prisms with rounded edges; (3) irregular fragments.*

c. *Migmatite at the SE edge of the Faraday granite, about 2.5 km north of Bancroft. Dark bands of migmatite are made up of green amphibole (Am), biotite with prominent pleochroic haloes surrounding zircon inclusions (B, Zr) titanite with magnetite crusts (Ti, Mg) and apatite (Ap) in quartz-microcline-oligoclase matrix. Quartz veins invade the migmatite (Q) and microcline recrystallized to porphyroblastic grains near vein quartz (Mi).*

d. *Feldspar-rich plaeosome remnants (P), partly replaced by fresh microcline (Mi: twinned) in neosome quartz (Q). Coarse grained patches in Faraday granite 5 km north of Bancroft along Highway 500.*

Figure 11.1. *Textures of migmatites and neosome quartz veins in and around Faraday granite, Bancroft area. All photomicrographs were taken in transmitted light with partly crossed nicols of 60 using the same magnification for a, c, d, shown in (a).*

At the contact between granitoid pegmatite, metagabbro as well as metasediments [the latter consisting of fine grained fluorite-calcite aggregates and impure limestones made up of a fine grained mosaic of calcite and quartz (5-20 microns in size) and disseminated phlogopite, pyrite, poikilitic diopside and titanite, calcite, fluorite, hornblende, pyroxene, phologopite and titanite] have been recrystallized to coarse grained porphyroblasts resulting in grain size increases up to several hundred times. Furthermore, at the contact with granitoid rocks, the porphyroblastic ferromagnasian minerals are metasomatic and differ in chemical composition from their equivalents in metasediments and metagabbro away from the contact. Thus, porphyroblastic amphibole in granitoid pegmatite contains more K, Na, and F tha hornblende from migmatite, and the biotite from radioactive pegmatite contains more Fe, F, Li and Rb than biotite from the migmatite (Rimsaite, 1982a, Table 3.1, analyses 8, 10, 11, 12; 1978). In areas adjacent to impure limestone and other sediments, anhydrite, calcite, scapolite and tourmaline occur in fractures and as overgrowths in ferromagnesian minerals. At the contact between pegmatite and various metasediments, the contact zone crystallized from several sources and commonly consists of porphyroblastic ferromagnesian minerals, interstitial and porphyroblastic feldspars and interstitial fluorite, calcite and tourmaline (Fig. 11.3).

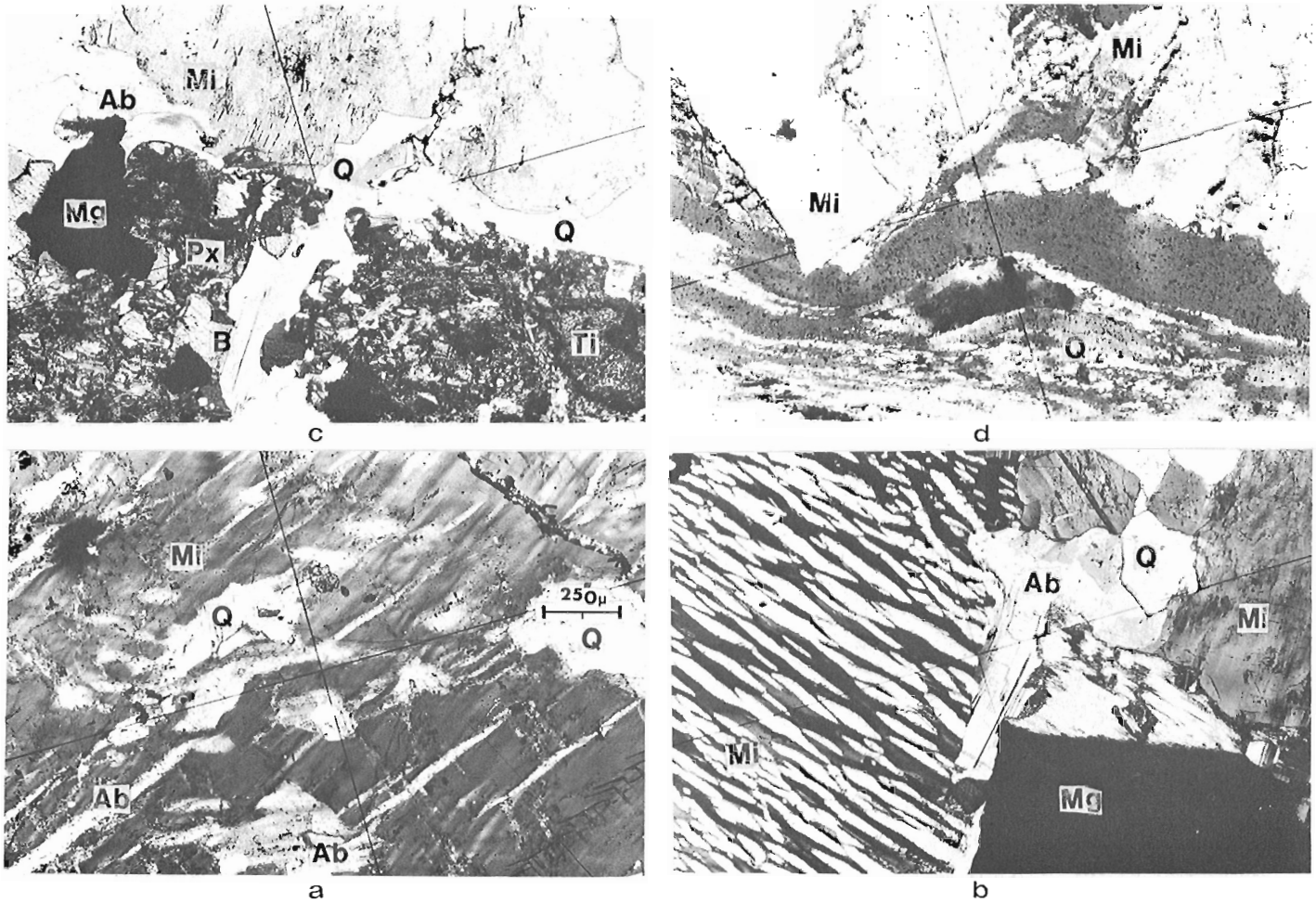

a. *Deformed microcline perthite (Mi) with bent albite lamellae and stretched inclusions of albite (Ab) and quartz (Q). Faraday granite.*

b. *Microcline perthite (Mi, black and white) invaded by albite (Ab) along interstices and fractures, adjacent to magnetite (Mg) and quartz (Q). Lamellar perthite with prominent albite component and albite overgrowths commonly occurs in the Cheddar granite.*

c. *Fractured Faraday granite showing deformed patches of pyroxene (Px), replaced by biotite (B), titanite (Ti), magnetite (Mg) and small specks of phyllosilicates, and remnant microcline-perthite (Mi) partly replaced by albite patches (Ab) in vein quartz (Q).*

d. *Deformed Cheddar granite in road cuts of Highway 648, showing fractured microcline perthite adjacent to veins of mylonitic quartz (Q). Mylonite zones contain deformed titanite-magnetite bands which can be radioactive and REE-bearing (Rimsaite, 1982b, Fig. 31.8).*

Figure 11.2. *Textures of fractured and mylonitized Faraday and Cheddar granites. All photomicrographs were taken in transmitted light and partly crossed nicols, at the same magnification as in (a).*

Granitoid pegmatites adjacent to the Faraday granite are composed of perthitic microcline which has deformed albitic lamellae and/or organ pipe-like and botryoidal replacement perthites (Fig. 11.2a, b). In such replacement perthites, the albite component varies between 20 and 80 volume per cent of the host microcline. In strongly mylonitized granitoid rocks, the perthitic lamellae seem to fade and gradually disappear. Such waning perthitic lamellae may commonly be replaced by fine grained alteration products or, alternatively, perthitic albite may be segregated into discrete grains of well-twinned checkerboard albite. Some granitoid pegmatites contain both older generation waning perthites and fresh recrystallized interstitial microcline and albite. In mylonitized rocks, ferromagnesian minerals also underwent various stages of deformation and alteration. They commonly recrystallized to mineralogically complex aggregates, and consist of irregular remnant patches of the original pyroxene and/or amphibole, biotite, chlorite, magnetite, titanite, apatite and fine grained iron oxides and clay. Locally, fine grained nontronite aggregates replace pyroxene and amphibole. Mylonitized rocks containing partly altered ferromagnesian minerals are commonly stained red by iron oxides which precipitated along fractures and deformed perthitic lamellae of feldspars and in mylonitic quartz (Fig. 11.2c, d).

In hybrid granitoid rocks, accessory minerals such as magnetite, titanite, apatite and zircon also increase in size and can form local segregations, obviously affecting the local chemical composition of their host rocks (Table 11.1, analyses 1-5). Some chemical variations, such as sodium and potassium contents in banded gneisses, can be accounted for

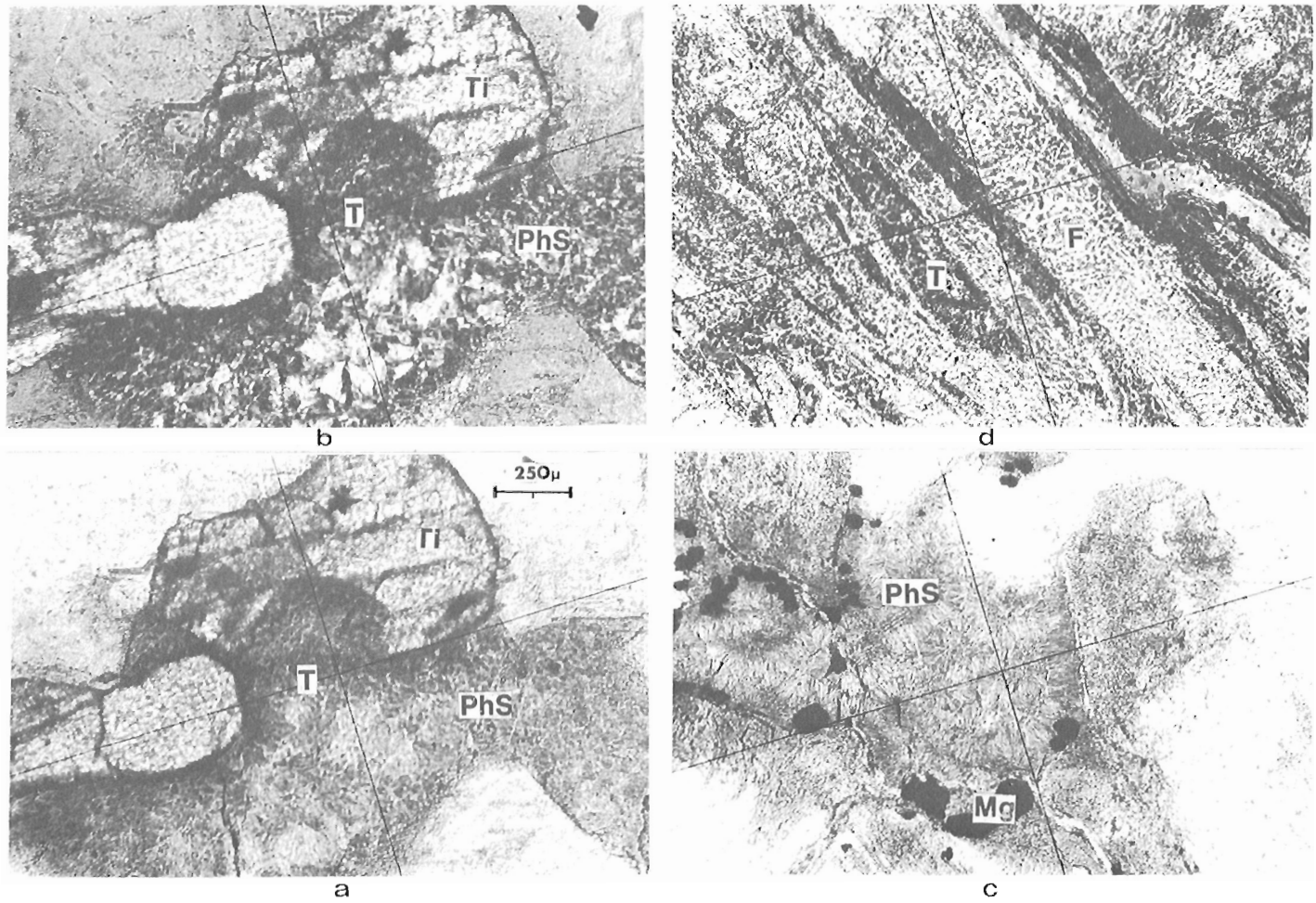

a. *Tourmaline (T) partly altered to phyllosilicates (PhS) surrounds fragments of titanite (Ti).*

b. *The same tourmaline fragments and radiating phyllosilicates as in (a) photographed with crossed nocols.*

c. *Radiating phyllosilicate aggregates and magnetite specks (opaque) after tourmaline in fractured rocks around the Halo mine.*

d. *Tourmaline rims (T) in feldspar fractures (F). Feldspar and tourmaline alter to fine grained phyllosilicates giving this rock a speckled appearance.*

Figure 11.3. *Altered tourmaline in fractured rocks from the Halo mine, Bancroft area. All photomicrographs were taken in transmitted light at the same magnification as in (a).*

by the original differences in sodic and potassic feldspars in the metasediment (Table 11.1, analyses 1, 2). Other differences result from the hybrid character of the rock or from metasomatic alterations, including redistribution of K and Na feldspar components during perthitization and in waning perthites. Specimens of the Faraday granite and associated rocks commonly contain more plagioclase than potassic feldspar, a feature that is also reflected in their K and Na chemistry. The occurrence of segregated, deformed and recrystallized quartz, of porphyroblastic, perthitic and recrystallized feldspars and the complex evolution of zircons and other accessory minerals (Fig. 11.4) all indicate remobilization and redistribution of mafic, leucocratic and accessory components in the rocks examined. Textures of the hybrid rocks indicate apparent interactions and genetic links between metasediments, metagabbros, migmatites, granitoid rocks and mylonites. The mylonites are enriched in vein quartz which could have been derived from the original silica-rich layers and/or from segregated quartz grains during porphyroblastic growth of hornblende, pyroxene and feldspars (Fig. 11.2d).

Cheddar Granite, Mylonite and Surrounding Gneisses and their Relict Sedimentary Textures
(Table 11.1, analyses 6-10)

Specimens of Cheddar granite were collected in road cuts in the northeastern portion of the granite. Contact rocks between the granite, mylonitized granite and metasediments were collected between the eastern edge of the Cheddar granite and the road to Dyno mine (Rimsaite, 1978, Fig. 9.2). Cheddar granite is leucocratic. It contains very few ferromagnesian silicates and exhibits marked variations in grain size and in quartz, microcline, plagioclase and accessory mineral content. The Cheddar granite is made up dominantly of microcline perthite. The perthite records a marked mobility of alkalies, indicated by variations in the abundance, shape and size of the perthitic albite component. In mylonitized and deformed areas along the eastern portion of the Cheddar granite, the organ pipe-like perthite, similar to that in Figure 11.2b, has segregated into vein perthite (Fig. 11.2a) and migrated towards the edges of the host microcline, forming prominent albite rims.

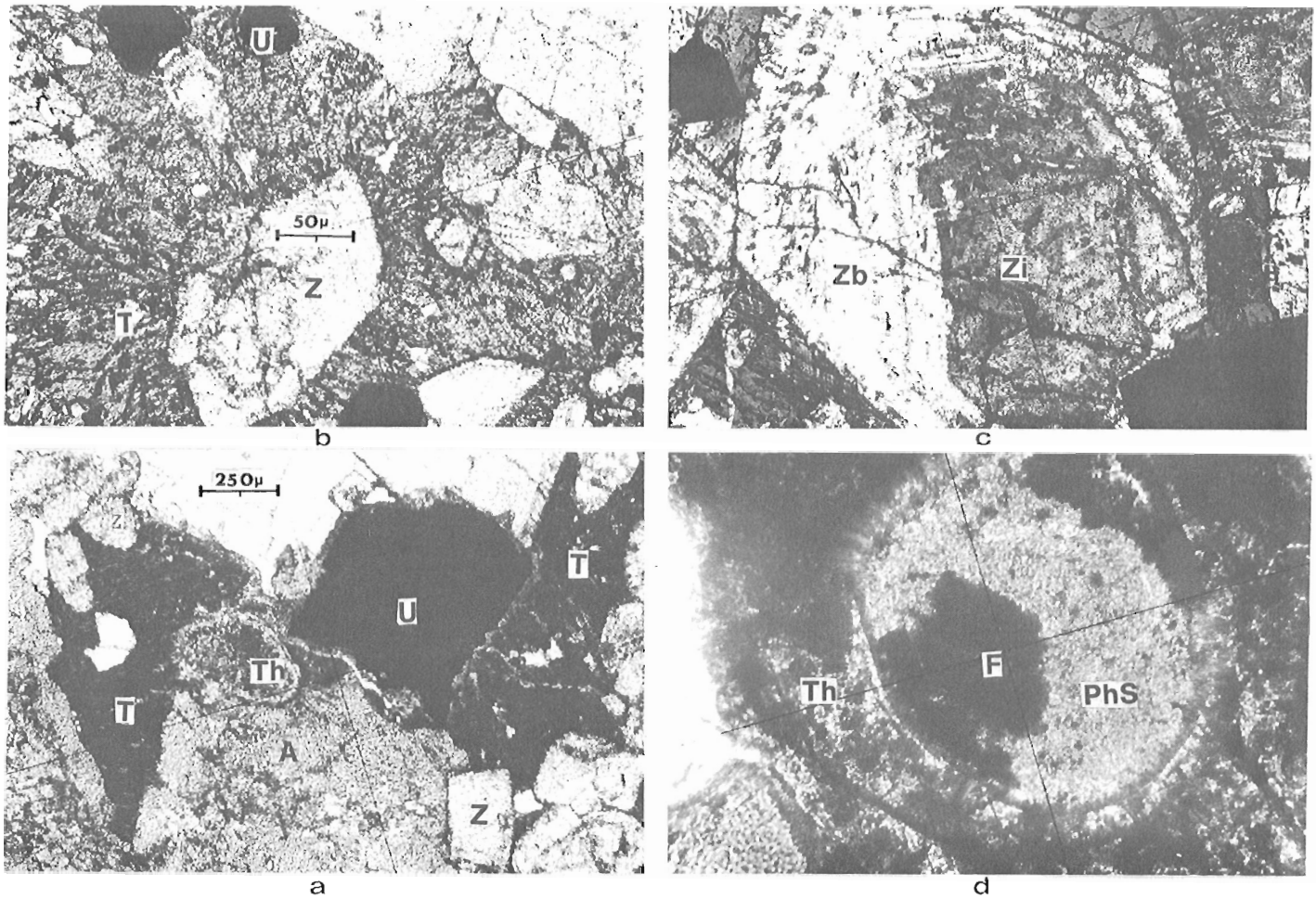

a. *Anhedral patches of tourmaline (T) filling interstitial spaces between uraninite (U), uranothorite (Th), allanite (A) and zircon (Z).*

b. *Poikilitic tourmaline contains numerous inclusions of zircon (Z), uranothorite and uraninite (U), and REE-bearing compounds in fractures. Backscattered electron micrographs of uraninite and uranothorite and of their complex rims are given by Rimsaite (1980a, Fig. 38.4 and REE in tourmaline in Table 38.1).*

c. *Zoned birefringent zircon (Zb) overgrown on irregular core of isotropic zircon (Zi) which infer periodical growths of zircon zones under different environmental conditions alternating with destruction of the zircon preceeding further growth.*

d. *Speckled grain of uranothorite (Th) containing oval-shaped inclusion of phyllosilicate aggregates (PhS) associated with purple fluorite (F) which represents residual pegmatite liquids enclosed in the uranothorite.*

Figure 11.4. *Interstitial poikilitic tourmaline in a high grade ore from the Madawaska mine. Figure b, c, d were photographed at the same magnification shown in (b). All photomicrographs were taken in transmitted light with partly crossed nicols.*

Fresh microcline, albite and checkerboard albite crystallized within and around the margins of apparently older porphyroblastic microcline perthite. Mylonitized veins of speckled quartz, healed by clear quartz, engulf older (paleosome) feldspathic portions of the rock as well as accessory minerals, such as zircon, titanite, allanite, apatite and iron oxides (Rimsaite, 1983, Fig. 3.5, 3.6). In mylonitized zones, quartz was crushed to very fine grained mylonite, whereas other rock-forming and accessory minerals were deformed, fractured and in part recrystallized to fine grained aggregtes (Fig. 11.2c, d). The deformed titanite grains, in addition to chlorite and recrystallized iron oxides, contain grains, patches and crusts of radioactive and REE-bearing minerals (Rimsaite, 1982b, Fig. 31.8d-f).

Contact rocks between granitoid pegmatites and metasediments contain relicts of fine grained mineral aggregates from the original sediment as well as porphyroblastic minerals apparently formed at the expense of the sediment.

Four types of metasediments and their remnant textures having small grain size (1-20 microns) were encountered in this study: 1. fluorite-quartz-calcite aggregates; 2. impure limestone, consisting of calcite, quartz, phlogopite, pyrite, remnant clay and commonly small porphyroblasts of diopside (20-50 microns in size); 3. limy arkosic quartzite; and 4. Al-rich sediments which consisted of quartz and clay layers. As a result of regional and thermal metamorphism and emplacement of adjacent granitoids,

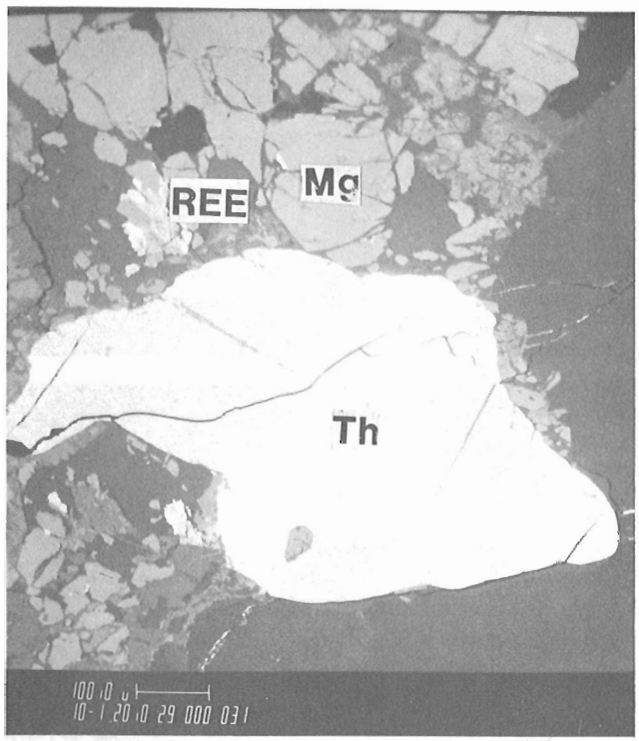

a

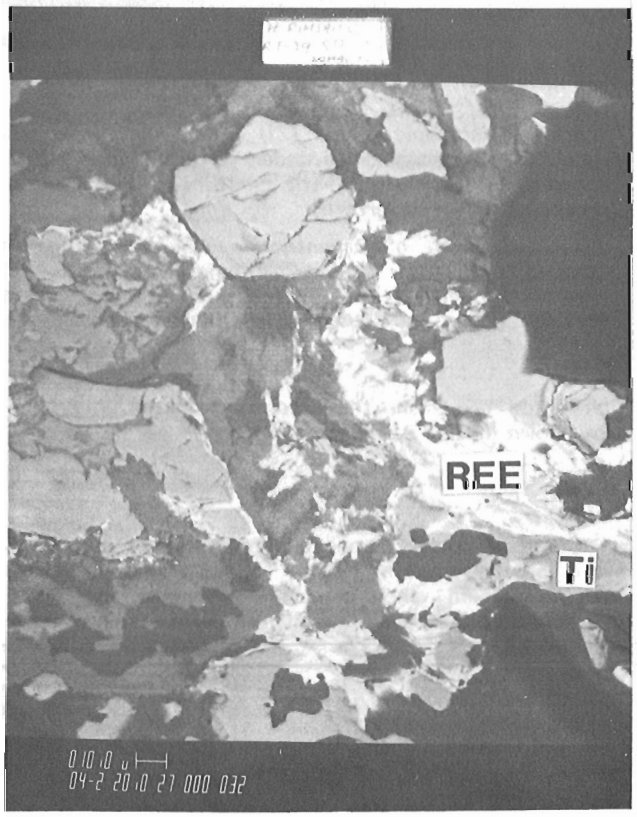

b

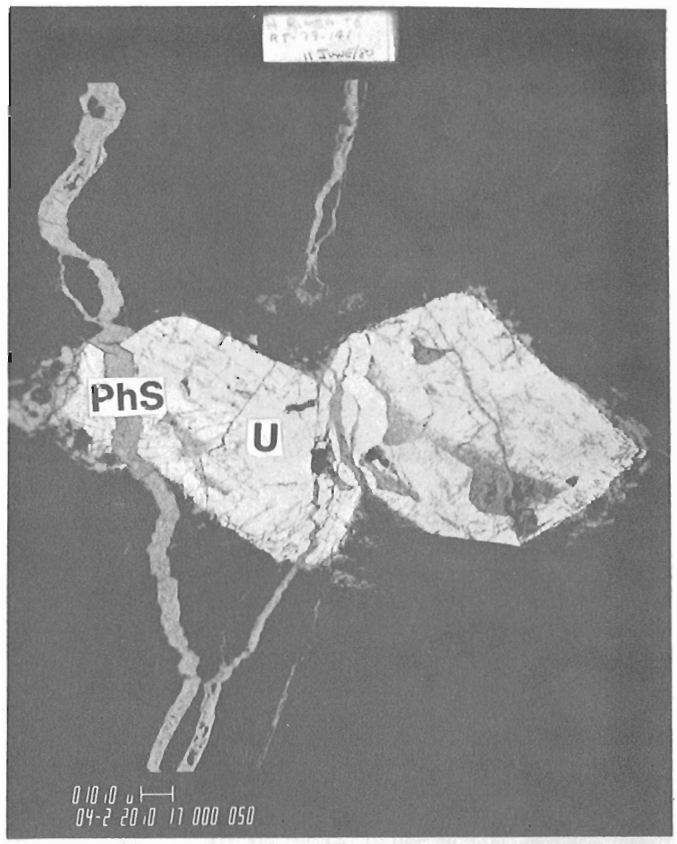

c

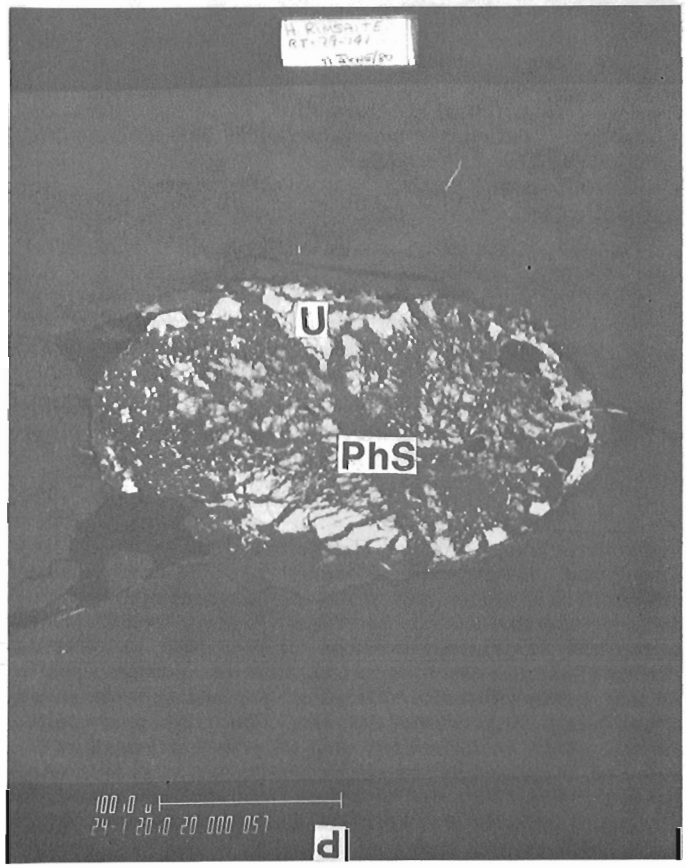

d

these fine grained metasediments recrystallized to coarse grained monomineralic zones; porphyroblastic mineral assemblages and banded gneisses. They include coarse grained quartz-fluorite-calcite zones; phlogopite, biotite, hornblendite bands; medium- to coarse-grained calcite marbles with or without porphyroblastic pyroxene, amphibole, biotite and feldspar, as well as accessory anhydrite, cordierite, epidote, scapolite, titanite and allanite; banded quartz-feldspar-pyroxene-hornblende-biotite gneiss; quartz-oligoclase-microcline gneiss containing accessory biotite, hornblende, calcite, titanite, magnetite, apatite and zircon; and quartz-biotite-garnet or quartz-biotite-garnet-sillimanite gneiss with accessory microcline, kyanite, zircon, wollastonite and secondary muscovite and calcite.

The heterogeneous and patchy appearance of the porphyroblasts, as well as the relict fine grained and poikilitic textures indicate a sedimentary origin for these rocks. Furthermore, chemical compositions of porphyroblastic pyroxene and amphibole also reflect the composition of the parent Si-Al-Na-K-Ca-Fe-S-bearing sediments. The Ca-Fe-rich amphiboles differ from the Mg-rich amphiboles in metamorphic rocks apparently derived from metagabbro and mafic volcanics (Rimsaite, 1974, Table 2).

At the contact with granitoids, alkalic feldspars and residual pegmatitic-hydrothermal liquids penetrated the adjacent metasediments causing metasomatic effects. The Ca-Fe-rich pyroxene and hornblende, and locally biotite, have altered to blue-green alkali pyroxene and hornblende, and to F-rich biotite porphyroblasts (Rimsaite, 1982a, Table 3.1, analyses 10, 12). In addition to alkali pyroxene and hornblende, the contact zones of metamorphic rocks adjacent to alkali pegmatite contain coarse grained allanite, apatite, titanite and tourmaline, all of which crystallized along melanocratic portions of the metasediment and/or in feldspar fractures of the granitoid pegmatite (Fig. 11.3). At the contact zone, metasomatic pyroxene, amphibole, biotite, allanite, titanite, zircon and magnetite are common hosts for U, Th and REE minerals (Table 11.1, analysis 8, nonmineralized rock; analyses 15, 16 mineralized rocks).

Sillimanite gneisses reflect the chemical composition of the original Al-rich parent rocks and contain more Al than the adjacent Cheddar granite as well as the mylonite and metasomatic pyroxene-bearing rocks (Table 11.1, analyses 6-10). The radioactive accessory minerals which produced prominent pleochroic haloes in biotite apparently account for 5.6 ppm U in the sillimanite gneiss (Table 11.1, analysis 9).

***Figure 11.5** (opposite)*

Fractured radioactive and accessory minerals which crystallized before deformation and fine grained radioactive and REE mineral aggregates which crystallized after mylonitization as coatings on fragmented accessory minerals. Eastern edge of mylonitized Cheddar granite. (GSC 203577-O, 203414-R)

a. *BEI* of fractured magnetite (Mg, grey) and uranothorite (Th) in mylonitic granite. Mineral aggregates containing La, Ce, Nd, Ca and Si (REE) crystallized as crusts on fragmented accessory minerals.*

b. *SEI** of titanite fragments (Ti, dary grey) overgrown by mottled clay-like aggregates containing Ca, Ce, La, Si (REE).*

c. *BEI of fractured uraninite (U) which is traversed by a fracture filled with phyllosilicates (PhS).*

d. *BEI of uraninite which has been crushed to fine grained fragments (white, U) and in part replaced by phyllosilicates (black, PhS).*

* *backscattered electron image*
** *secondary electron image*

The mylonitized eastern edge of the Cheddar granite contains characteristic albitized microcline perthites and variable concentrations of titanite and allanite crystals along veinlets of mylonitic quartz. The fractured accessory minerals contain radioactive mineral inclusions and crusts which account for variable uranium values in the mylonitized Cheddar granite (4.4 to 25.1 ppm U, Table 11.1, analyses 6, 7, 10).

Pegmatite and Adjacent High Grade Metamorphic Rocks Surrounding Halo Mine
(Table 11.1, analyses 11, 12, 13, Fig. 11.3, 11.5, 11.6).

Metasediments surrounding the Halo deposit consist of high grade garnet-pyroxene-bearing gneisses which locally retain fine grained sedimentary layers of limy arkosic quartzite and of impure fluorite-bearing limy sediments. Fine grained calcite-fluorite rocks contain 7.2-7.5 ppm U (Rimsaite, 1978). Banded metasediments composed of quartzitic, arkosic and biotite-oligoclase layers contain poikilitic garnet and tourmaline porphyroblasts. They vary in grain size from 10 microns in arkosic layers to several centimetres in layers containing porphyroblastic garnet. Such metasediments contain abundant grains of zircon and apatite which produce prominent pleochroic haloes in ginger-red biotite and apparently account for 8.3 ppm U in the rock. Proportions of mica, pyroxene, tourmaline and apatite vary. Some layers consist dominantly of tourmaline, others of mica and apatite or of pyroxene, titanite and tourmaline in a groundmass of oligoclase, albite, microcline, fluorite, scapolite and quartz. In mylonitic zones, biotite, pyroxene, titanite, tourmaline, feldspars and quartz are deformed and fractured. Titanite and associated tourmaline are stretched along the fractures. Deformed tourmaline grains recrystallized to acicular aggregates and ultimately lost birefringence and pleochroism and altered to phyllosilicates. Fractured titanite has been altered to Fe and Ti oxides as well as phyllosilicates and contains specks, patches and coatings of radioactive and REE-bearing minerals (Fig. 11.3, 11.4, 11.5). In mylonitic zones, biotite and pyroxene have a shredded appearance. They consist of the original unaltered remnants, red bands coated by red iron oxides and striated bands intergrown with needle-like quartz (Fig. 11.6).

The deformed feldspars lose their perthitic component which may be replaced by bands of tourmaline and by fine grained speckled oxides and clay (Fig. 11.3d). The deformed and altered accessory minerals commonly contain uranyl- and REE-bearing mineral aggregates, introduced after deformation, which account for elevated U values of some mylonitized host rocks (8.7 to 99 ppm U). Metapyroxenite and quartz-feldspar pegmatite at the entrance to the abandoned Halo mine contain only 2.7 and 2.5 ppm U (Table 11.1, analyses 11, 12). The metapyroxenite consists of pyroxene, alkali hornblende, titanite and apatite in a groundmass of microcline and scapolite. The leucocratic pegmatite cuts metapyroxenite and is made up of mylonitized quartz, deformed microcline and patchy albite, partly altered to white mica. The adjacent pyroxene-scaplite gneiss consists mainly of pyroxene and amphibole with less abundant apatite, magnetite, pyrite and titanite in a groundmass of calcite and scapolite (Table 11.1, anlayses 11, 12, 13). Although mafic constituents in gneiss samples 11 and 13 are similar, the dominantly calcite-scapolite groundmass in sample 13 apparently considerably reduced the silica and alkali contents. At the Halo mine, pyroxene and amphibole are similar in chemical composition to Ca-Fe amphiboles from metasediments and migmatites adjacent to the Faraday and Cheddar granite (Fig. 11.6d) and thus differ from Mg-rich amphiboles from greenstones (Rimsaite, 1974, Table 2). The presence of xenoliths rich in ferromagnesian minerals, interstitial calcite, fluorite, sulphides, sulphates and of

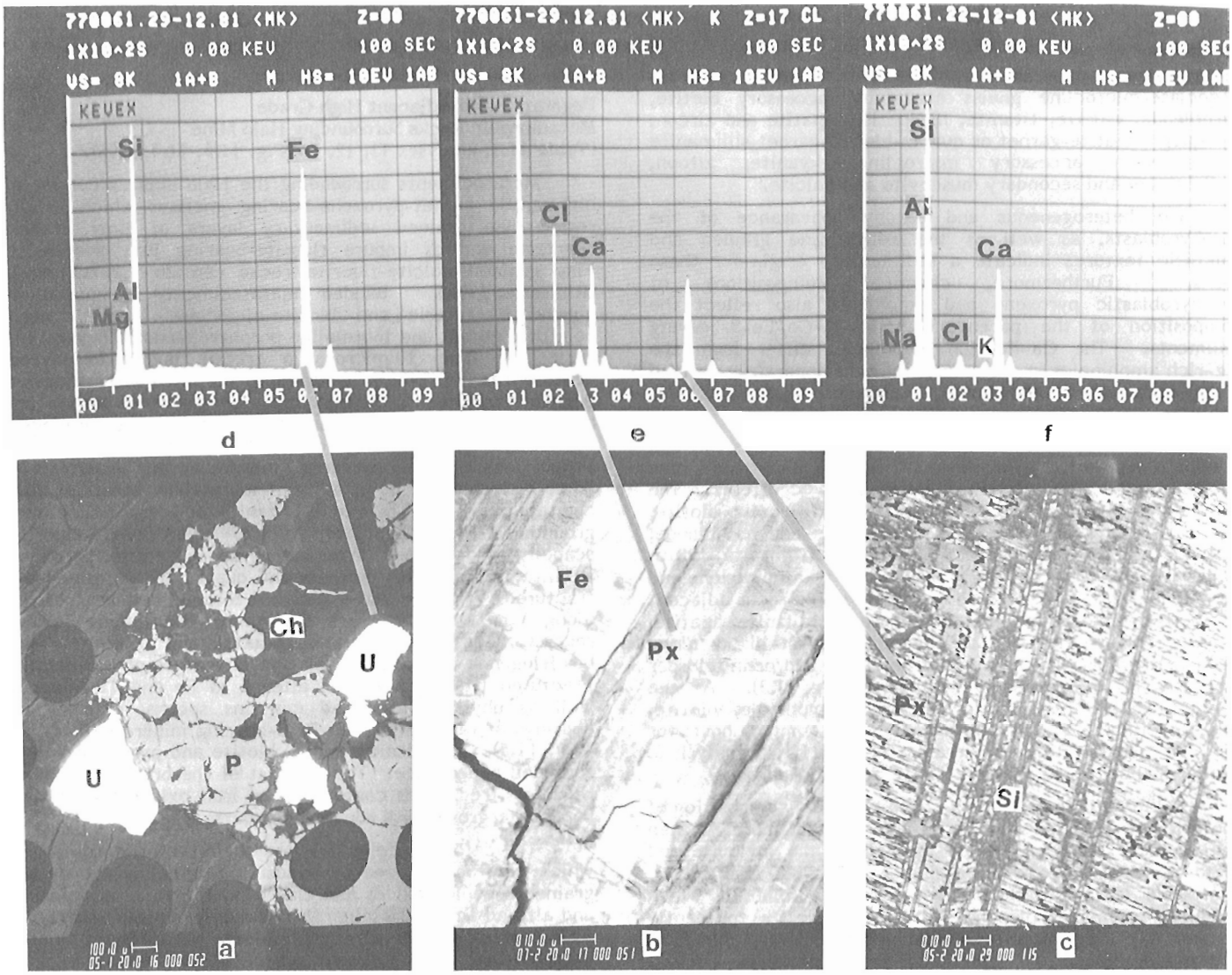

a. *BEI of fractured pyrite (P) which crystallized in red phyllosilicate groundmass (Ch) filling mylonitized quartz. Pyrite enclosed uraninite grains (U) which are surrounded by Fe-rich silicate rims (Table 11.1, rock analysis 19).*

b. *BEI of coarse grained pyroxene (Px) impregnated with Si with altered lamellae coated by red iron-rich crusts (Fe).*

c. *BEI of shredded pyroxene (Px) impregnated with needle-like silica (Si, dark grey).*

d. *ED* spectrum of iron-rich rims on uraninite in "a" (Si>Fe>Al=Mg>K, Ca, S).*

e. *ED spectrum of fresh portions of pyroxene in "b" (Si>Ca>Fe>Al>Mg>K>Cl).*

f. *ED spectrum of scapolite (Si>Al>Ca>Cl>Na>K; Table 11.1, rock analysis 13).*

**ED spectrum = energy dispersive spectrum.*
Elements listed in order of decreasing intensities of element lines.

Figure 11.6. *Alteration of minerals in mylonitic zones. Examples from Halo mine. (GSC 203724-S)*

quartz veins, markedly alter chemical composition of the host granitoid rocks. Because the xenoliths may be derived from different sources and some elements, such as F and Cl can come from various minerals, namely fluorite, mica, apatite and/or scapolite, petrochemical interpretation should be made in conjunction with petrographic studies of individual samples (Table 11.1 and the Appendix with petrographic notes). Considering the complexity and diversity of mineral associations, a grouping of samples for statistical studies would require careful selection of samples.

Selected Examples of Ore Grade Specimens from the Madawaska, Greyhawk, Bicroft and Halo Mines (Table 11.1, analyses 14-19, Fig. 4-8)

To illustrate differences and/or similarities between the ore grade and lower grade rocks, a few examples of low grade specimens (0.3-400 ppm U) are discussed first. The lowest U values (less than 0.6 ppm) came from metagabbro, coarse grained fluorite-calcite rock, phlogopite and anhydrite (Rimsaite, 1978, Table 9.1 and this study). Uranium values < 4 ppm were obtained on hornblende and on biotite concentrates, on leucocratic quartz-microcline pegmatite (1.8 ppm U) and on hornblende-oligoclase and pyroxene-microcline gneisses which contain nonradioactive or weakly radioactive accessory minerals (1.8 and 3.1 ppm U, Table 11.1). Gneisses and pegmatites which contain radioactive apatite, titanite and zircon yielded U values between 4 and 20 ppm, and rocks showing 20 to 400 ppm U contained some primary and/or secondary uranium minerals, commonly disseminated in zircon, titanite, apatite and allanite, and as coatings on micas. The fine grained sedimentary calcite-fluorite rocks contained higher U values than coarse grained fluorite-bearing marbles (7.5 and 0.3 ppm respectively). These examples show that impure limestones, fluorite and anhydrite-bearing metasediments and paragneisses do not show marked enrichments of uranium. However, this 7.2 ppm differences between the uranium content in recrystallized rock (0.3 ppm U) and in fine grained calcite-fluorite metasediment (7.5 ppm U) although small, may be significant. Likewise, the presence of strongly radioactive accessory minerals which produce prominent pleochroic haloes in host biotite and could possibly be precursors of uranium mineralization, warrants more detailed studies using a scanning electron microscope (SEM) and an energy dispersive spectrometer (EDS) to determine the origin of radioactivity and to determine whether or not radioactive elements are actually in the structure of accessory minerals or whether they are present as coatings and inclusions.

Ore Grade Specimens from the Madawaska Mine (>400 ppm U)

The ore grade specimens include a great variety of hybrid rocks and uncommon mineral assemblages (Rimsaite, 1978, 1980a, b, 1982a). However, high grade ore commonly occurs at the contact zone between different rock types and is made up dominantly of accessory minerals which contain inclusions of uraninite, uranothorite and REE-bearing mineral aggregates (Fig. 11.4). The U, Th and REE-bearing ore, in addition to oxides listed in Table 11.1, contains the following elements determined by emission spectrography without commonly used enrichment procedures; B = 0.2% (present in tourmaline); Ba = 0.02% (present in barian celestite, Fig. 11.7); Ce = 3%; La = 2%; Yb = 0.015%; Y = 0.15% (REE mainly in allanite, in rims surrounding uraninite and in fractures and interstices (Fig. 11.4; Rimsaite, 1982b, Fig. 31.4, 31.5); Sr = 0.5%; Th = 0.5%; U = 0.7%; Zr > 2%.

Melanocratic ore is made up predominantly of pyroxene, alkali amphibole and less abundant biotite in a groundmass of feldspars, quartz and/or anhydrite, calcite, scapolite and fluorite. In chemical and mineralogical compositions it resembles metasomatic pyroxenites formed at the contact between metasediments, metagabbro and quartz/feldspar pegmatite. The presence of anhydrite and calcite affects the chemical composition of the ore by reducing ("diluting") the content of silica, alumina and alkalies (Table 11.1, analysis 14). Titanite and coarse grained, zoned zircon, commonly intergrown with uranothorite and uraninite are prominent accessory minerals in the ore. The melanocratic ore contains almost equal amount of uraninite and uranothorite, the U/Th ratio being close to 1, and small quantities of Ce (0.11%), La (0.06%) and mainly radiogenic Pb (0.5%: in radioactive minerals and as galena in rims and crusts).

The contact zone between metapyroxenite and microcline pegmatite resembles the high grade uranium ore in chemical and mineralogical compositions, but, in addition to abundant accessory and ore minerals, it contains portions of less mineralized pyroxenite and of pegmatitic microcline which had replaced allanite (Table 11.1, analysis 15, Fig. 11.7; Rimsaite, 1982b, Fig. 31.5a, b). This contact rock contains organ pipe-like microcline perthite, similar to that in the Faraday granite (Fig. 11.2b), abundant zircon and apatite. It exhibits evidence of alteration of pyroxene and of migration of REE in aqueous solutions into pyroxene fractures now filled with REE and chlorite (Fig. 11.7). At the contact with the mineralized zone, the common Ca, Fe-clinopyroxene has recrystallized to patches of iron oxide and to wollastonite (Fig. 11.7a).

An example of metamorphic-metasomatic ore is a mylonite which consists dominantly of coarse grained recrystallized biotite and mylonitized quartz (Table 11.1, analysis 16). It is similar in chemical composition to the garnet-sillimanite-biotite gneiss but contains more Mg, Rb, F and S due to the presence of abundant biotite and some molydbenite, and the absence of sillimanite. The uraninite, titanite, zircon and molybdenite crystallize adjacent to, or within biotite. Molybdenite postdates mylonitization and crystallization of uraninite. The latter is fractured and altered to coffinite and to an unidentified Th-poor U-S compound (Rimsaite, 1982b, Fig. 31.2; 1983, Table 3.1, analyses 4, 5, 6). The high U/Th ratio of 10 is accounted for in part by the presence of Th-poor altertion products, namely coffinite and U-S compounds in this sample. Similar biotite-rich mylonitized rocks, having the high U/Th ratio have also been encountered in the Halo mine.

Other ore grade and lower grade mylonitic rocks studied contain variable proportions of mylonitic quartz and deformed plagioclase and microcline. In the mylonites, quartz may exceed 50% (SiO_2 = 84.5%) and albite content commonly exceeds that of microcline. Uraninite and uranothorite grains occur in bands along the deformation zones and are commonly associated with coarse grained zircon (Fig. 11.3b), allanite, titanite and apatite. Most of the ore and accessory minerals crystallized before deformation. This is evident from their fractured and deformed appearance and retrograde alterations to phyllosilicates, oxides and other fine grained aggregates. The latter generation of radioactive and REE-bearing minerals precipitated on the surfaces and fractures of the fragmented accessory minerals during and after deformation (Fig. 11.5). Mylonitized and deformed rocks are commonly stained red by iron oxides which precipitated along deformed perthitic and twinning lamellae in feldspars and in fractures of mylonitized quartz and in other minerals. Mylonitized rocks contain erratic distributions of radioactive and accessory minerals and thus show marked variations in uranium values, from 4 ppm to ore grade.

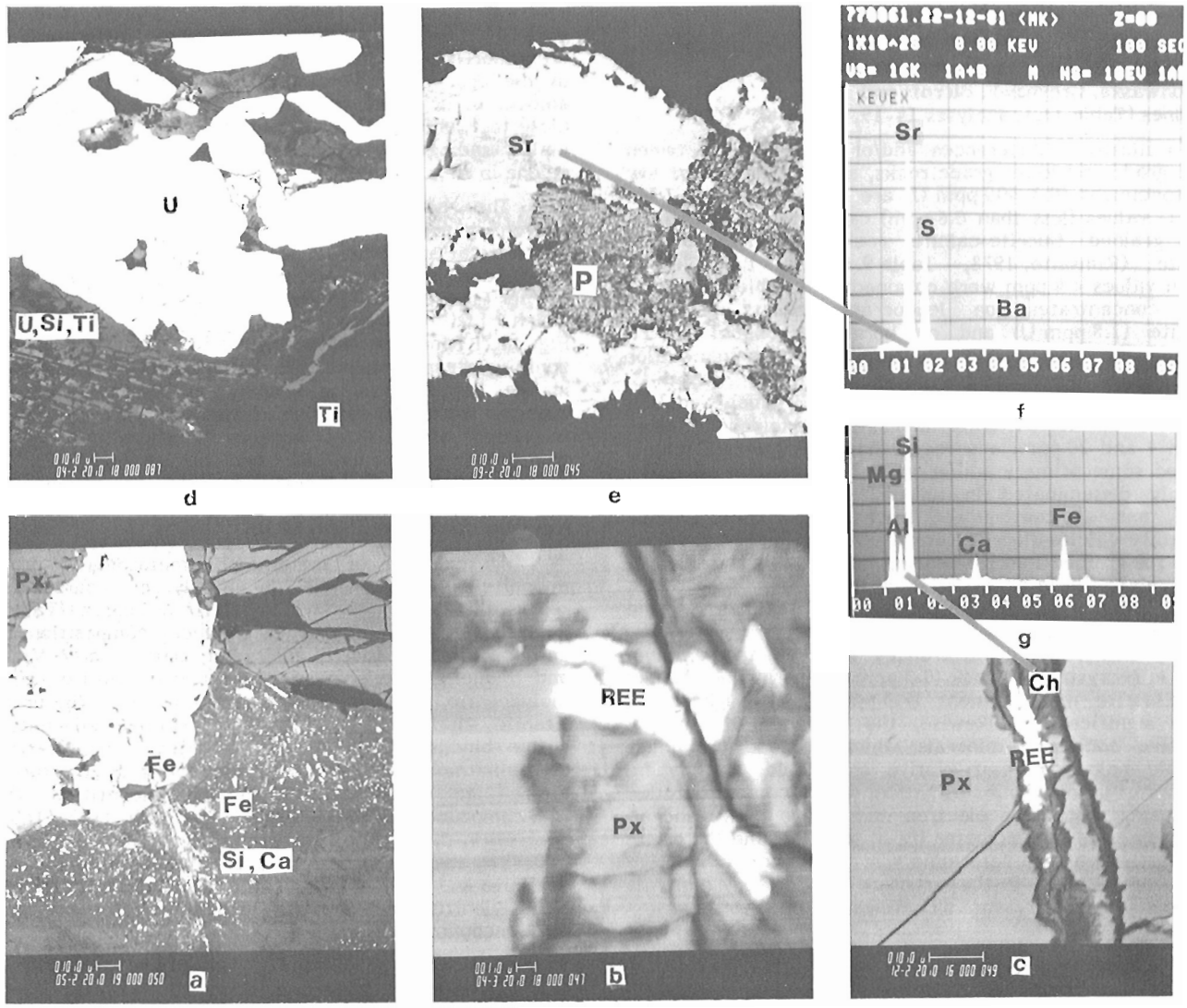

a. *BEI of Ca-Fe-rich pyroxene (Px) which altered to Si, Ca phase (Si,Ca) and to iron oxide (Fe). Iron crystallized as iron oxide patches and as small specks in a Si, Ca phase.*

b. *BEI of mobilized REE which crystallized along fractures of deformed pyroxene (Px).*

c. *BEI of fractures in pyroxene (Px) which are filled with chlorite (Ch) and REE-bearing mineral aggregates (REE).*

d. *BEI of uraninite (irregular, white, U), surrounded by Si,U,Ti-bearing rims (Si,U,Ti) in shredded titanite (Ti).*

e. *BEI of remnant oxidized pyrite (P) surrounded by barian celestite (Sr).*

f. *ED spectrum of the barian celestite in "e" (Sr>S>Ba).*

g. *ED spectrum of chlorite which fills fractures in pyroxene in "c" (Si>Mg>Fe>Al>Ca).*

Figure 11.7. *Alterations at the mineralized contact zone between pyroxene gneiss and microcline pegmatite (Table 11.1, analysis 15; GSC 203724-R).*

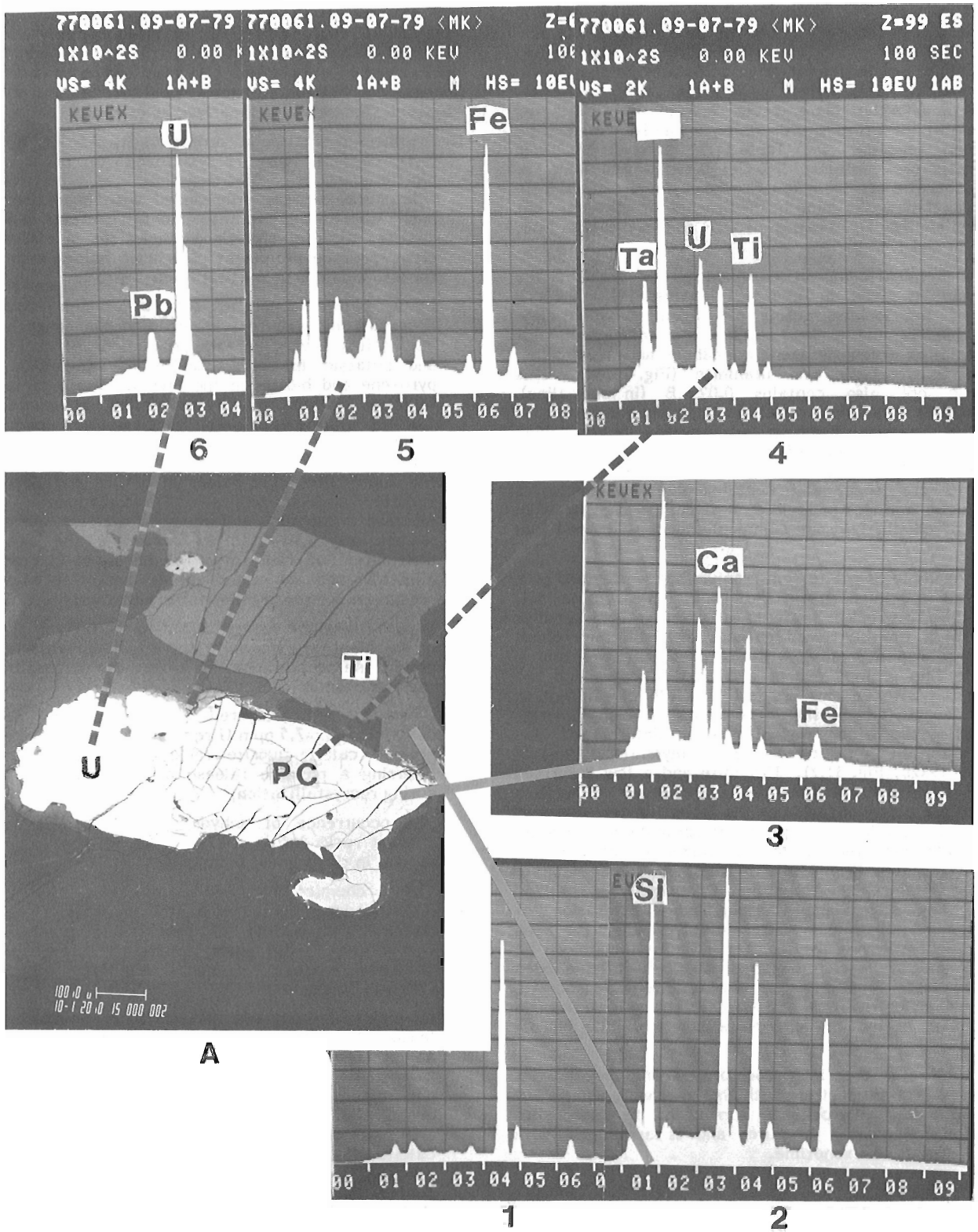

1. *A BEI of titanite (Ti), pyrochlore (PC), and uraninite (U). ED spectrum of niobian TiO_2 in the rim surrounding uraninite-pyrochlore intergrowths in "A" (Ti>Fe>Nb>Ca>Si>U).*
2. *ED spectrum of titanite in "A" (Ca>Si>Ti>Fe>Al).*
3. *ED spectrum of pyrochlore at the margin in "A" (Nb>Ca>U>Ti>Ta>Fe).*
4. *ED spectrum of another spot in pyrochlore in "A" (Nb>U>Ti>Ta = Ca).*
5. *ED spectrum of Fe-rich rim on uraninite-pyrochlore intergrowths in "A" (Si>FE>S = Pb, Al>U>Nb = Ca>Ti>Mg>Mn)*
6. *ED spectrum of uraninite in "A" (U>Pb)*

Figure 11.8. *Titanite-pyrochlore-uraninite association in leucocratic ore from the Bancroft mine (Table 11.1, analysis 18; GSC 203532-J).*

Melanocratic ore from the Greyhawk mine consists mainly of pleochroic dark green to brown amphibole and brown biotite in a matrix of albite, microcline, calcite and quartz. Albite crystallized in large composite patches and is stained red by iron oxides. Titanite, zircon, apatite, uraninite and uranothorite occur around the edges of hornblende at the contact with albite or calcite. In addition to oxides reported in Table 11.1 (analysis 17) this melanocratic ore contains 0.2% Ce; 0.1% La and 0.1% Pb. The melanocratic ore from the Greyhawk mine differs from that at the Madawaska mine in the absence of anhydrite, but both have similar U/Th ratios of 1.2 and 1.4 (Table 11.1, analyses 14 and 17).

The chemical composition of leucocratic ore from the Bicroft mine is given in Table 11.1 (analysis 18). The ore consits of interlocking grains of oligoclase, microcline perthite, quartz and a few patches and intergrowths of apatite-calcite; green pyroxene-amphibole and tourmaline; and titanite-pyrochlore and uraninite (Fig. 11.8). This leucocratic ore also contains 0.02% B (in tourmaline), 0.03% Ce, 0.01% La, and a relatively high concentration of F due to the presence of interstitial fluorite. It has a high U/Th ratio of > 3. Uraninite is also present in prominent rims of calcite and fluorite (Rimsaite, 1980a, Fig. 38.3b). Some leucocratic ore specimens contain blue peristerite, a recrystallized albitic oligoclase antiperthite having thin lamellae of alkalic feldspar commonly speckled by red iron oxides.

An example of pyrite-rich uranium ore is provided by a mylonitized specimen from the Halo mine (Table 11.1, analysis 19). This rock is made up of coarse grained lamellar albite with a few scattered patches of fresh microcline, calcite and scapolite along with shredded pyroxene, and is altered to fine grained quartz and phyllosilicates and red bands coated with Fe-rich crusts (Fig. 11.7b, c) adjacent to mylonitic quartz and pyrite. The latter Fe-rich minerals apparently invaded the mylonite after deformation and crystallized in fractures in mylonitic quartz (Rimsaite, 1982b, Fig. 31.7). Uraninite and a few deformed grains of titanite crystallized along the edges of massive pyrite and are partly engulfed by the latter. A few grains of magnetite and pyrrhotite occur in intergrowths with pyrite. The uraninite and pyrite have crystallized in red iron-rich silicate aggregates (Fig. 11.6). The fine grained silicate aggregates which replace and stain all previously crystallized silicates may have been derived from lateration of ferromagnesian minerals or, alternatively, could have been emplaced accompanying pyrite. This rock contains much Fe in pyrite and in Fe-rich phyllosilicates which have been introduced after brecciation to the originally leucocratic rock. This mylonitic rock has a relatively high U/Th ratio of >4, similar to that in leucocratic ore from the Bicroft mine.

The Nb-Ta ore in pyrochlore-bearing pegmatities consists of albite antiperthite with the K-bearing component being muscovite. Pyrochlore, surrounded by muscovite, crystallized in feldspar fractures and is associated with uraninite, apatite and xenotime.

Summary and Conclusions

The mineralogical, petrochemical and petrographic-textural studies described here cover a variety of metasediments, metaggabro, hybrid contact rocks and granitoid rocks in the Bancroft area, Ontario. The purpose of the study was to attempt to determine significant similarities and differences between ore grade specimens and lower grade rocks.

On the basis of relict sedimentary textures and mineralogy, four types of metasediments have been distinguished and their transformation into coarse grained hybrid rocks at the contact with granitoid rocks is described. Changes due to prograde and retrograde metamorphism and metasomatism can be summarized as follows:

1. Argillitic quartzite, according to its Al, Fe, alkali and H_2O content, was recrystallized to porphyroblastic biotite-quartzite, biotite-garnet or biotite-garnet-sillimanite gneisses interbanded with quartzitic layers. Such high grade metasediments contain radioactive apatite, titanite, and zircon inclusions in biotite. The latter produce prominent pleochroic haloes and account for 6 to 8 ppm U in the host rock;
2. Limy arkosic quartzite with a variable content of accessory minerals recrystallized to banded gneisses and migmatites having varying proportions of quartz, sodic and potassic feldspars, Ca-Fe-rich amphibole and/or pyroxene and biotite in the layers. The amphibole-rich varieties contain weakly radioactive or nonradioactive apatite, titanite and zircon which account for ⩽4 ppm U in the rock. On the other hand biotite-rich varieties contain radioactive accessory minerals which produce prominent pleochroic haloes in biotite and account for elevated uranium values of ⩾4 to 25 ppm. Scanning electron microscope and energy dispersive spectrometer studies are warranted to determine the nature and distribution of radioactive elements in the accessory minerals and to assess their potential as possible precursors for the uranium mineralization;
3. Impure limestone recrystallized to marble and pyroxenite or amphibolite; pyroxenite and amphibolite derived from greenstone contain more Mg than those derived from limy metasediments;
4. Fine grained, layered calcite-fluorite sediments containing 7.2-7.5 ppm U recrystallized to U-poor coarse grained calcite-fluorite rocks having 0.3 ppm U, thus inferring a possible release of approximately 7 ppm U during recrystallization;
5. The occurrence of anhydrite and scapolite in hybrid contact rocks infers the presence of gypsum, salt and calcite in the original sediments;
6. The chemically and mineralogically diverse metasediments contained all the ingredients required to produce the variety of hybrid and granitoid rocks encountered in this study, apparently through partial to complete anatexis, a thesis originally suggested by Chayes (1942);
7. Examples of ore grade rocks include: melanocratic and leucocratic ore; contact rocks between metapyroxenite and/or metasediments; feldspar-quartz pegmatites which in addition to U and Th minerals contain abundant REE and other accessory minerals; metasomatic biotite-quartz-uranite-molybdenite ore; and various mylonitized ore specimens. The presence of abundant anhydrite, calcite, fluorite, scapolite, zircon, molybdenite, pyrite, allanite, apatite, monazite, xenotime and titanite contributes to the diversity of petrographic ore types and their petrochemical compositions;
8. Scapolite, anhydrite, fluorite, calcite and fine grained iron oxide stains on feldspars and other minerals have been encountered in ore grade and lower grade specimens having U values from 2.7 to 10 000 ppm, thus the presence of these minerals is not restricted to ore grade specimens;
9. Mylonitic rocks have been affected by retrograde metamorphism. This has resulted in redistribution of alkalies in feldspars, and the rocks are characterized by erratic distribution of U, Th and REE minerals which both predate and, in part, postdate the period of deformation;

10. Although most rocks that retain sedimentary textures, mineral concentrates and coarse grained granite pegmatites yielded low U values ($\lesssim$4 ppm), some metasediments which contain radioactive accessory minerals, namely fluorite-calcite-phlogopite rocks (7.5 ppm U) and biotite-hornblende gneisses ($\gtrsim$4-25 ppm U), could have been precursors for U-Th mineralization. However, further enrichment by 20 to 100 times would have been necessary to yield ore grade material;

11. Anatectic contact rocks made up of metasedimentary and pegmatitic components are favourable hosts for U, Th and REE mineralization, particularly where they have been modified and enriched by secondary mineralization in some mylonitized zones.

References

Adams, F.D. and Barlow, A.E.
1910: Geology of Haliburton and Bancroft Areas, Ontario; Geological Survey of Canada, Memoir 6, 419 p.

Chayes, F.
1942: Alkaline and carbonate intrusives near Bancroft; Geological Society of America, Bulletin, v. 53, p. 449-512.

Fyson, W.V., Baer, A.J., Habib, M.K., and Culshaw, N.
1979: Structural fabric and uranium distribution in shear zones near Cardiff, Ontario; in Geoscience Grant Program, Summary of Research 1978-1979, ed. E.G. Pye, Ontario Geological Survey, Miscellaneous Papers MP 87, p. 11-12.

Goldich, S.S. and Kniser, J.H.
1939: Perthite from Tory Hill, Ontario; American Mineralogist, v. 24, no. 7, p. 407-427.

Hewitt, D.F.
1967: Uranium and thorium deposits in southern Ontario; Ontario Department of Mines, Mineral Resources Circular, no. 4, 76 p.

Lumbers, S.B.
1980: Geology of Renfrew County, southern Ontario; Ontario Geological Survey, Open File Report 5282.

Masson, S.L. and Gordon, J.B.
1981: Radioactive mineral deposits of the Pembroke-Renfrew area: Ontario Ministry of Natural Resources, Ontario Geological Survey, Mineral Deposits Circular 23.

Pupin, J.P.
1980: Zircon and granite petrology; Contributions to Mineralogy and Petrology, v. 73, p. 207-220.

Rimsaite, J.H.Y.
1967: Optical heterogeneity of feldspars observed in diverse Canadian rocks; Schweizerische Mineralogische and Petrographische Mitteilungen, v. 47, no. 1, p. 61-76.

Rimsaite, J.
1974: Mineral assemblages and low-grade metamorphic-metasomatic alterations in an Archean greenstone belt, Malartic, Quebec; Canadian Mineralogist, v. 12, p. 520-526.

1978: Mineralogy of radioactive occurrences in the Grenville Structural Province Ontario and Quebec, a preliminary report; in Current Research, Part B, Geological Survey of Canada, Paper 78-1B, p. 49-58.

1980a: Mineralogy of radioactive occurrence in the Grenville Structural Province, Bancroft area, Ontario; a progress report; in Current Research, Part A, Geological Survey of Canada, Paper 80-1A, p. 253-264.

1980b: Selected mineral suites and evolution of radioactive pegmatities in the Grenville Structural Province, Canada; 26e Congrés Géologique International (Paris), Résumés III, p. 999.

1981: Isotope, scanning electron microscope and energy dispersive spectrometer studies of heterogeneous zircons from radioactive granites in the Grenville Structural Province, Quebec and Ontario; in Current Research, Part B, Geological Survey of Canada, Paper 81-1B, p. 25-35.

1982a: Mineralogical and petrochemical properties of heterogeneous granitoid rocks from radioactive occurrences in the Grenville Structural Province, Ontario and Quebec; in Uranium in Granites, ed. Y.T. Maurice, Geological Survey of Canada, Paper 81-23, p. 19-30.

1982b: The leaching of radionuclides and other ions during alteration and replacement of accessory minerals in radioactive rocks; in Current Research, Part B, Geological Survey of Canada, Paper 82-1B, p. 253-266.

1983: Selected mineral associations in radioactive occurrences in the Grenville Structural Province; a progress report; in current Research, Part B, Geological Survey of Canada, Paper 83-1B, report 3.

Satterly, J.
1957: Radioactive mineral occurrences in the Bancroft area, Ontario; Ontario Department of Mines, 65th Annual Report, v. 65, pt. 6, 1956, 178 p.

APPENDIX

Description of samples in Table 11.1

1. Migmatite south of Baptiste Lake, west of Faraday granite: granular mosaic of quartz, microcline and plagioclase with disseminated crystals of biotite, apatite, titanite magnetite and zircon, and a few patches of calcite interbanded with quartz-rich layers (Fig. 11.1a). Several types of zircon crystals were concentrated for isotopic studies (Fig. 11.1b).
2. Bands adjacent and similar to "1" but containing more plagioclase, less microcline, and biotite flakes in parallel layers. Titanite-magnetite-apatite intergrowths form disseminated spots, >1 mm in size. Biotite in some layers contains zircon inclusions and is partly replaced by calcite.
3. Gneiss below Faraday granite. Similar to "2" but contains more mafic minerals: hornblende, biotite and magnetite which is overgrown by titanite. Bands rich in plagioclase and mafic minerals alternate with bands rich in microcline and perthite.
4. Contact between Faraday granite and gneiss. Similar to "1" but contains coarser grains of microcline perthite, twinned plagioclase, quartz and rare biotite.
5. Fractured pegmatite in Faraday granite: deformed microcline perthite with patches of albite and quartz; fractured and altered pyroxene and plagioclase-rich paleosome are engulfed and partly replaced by microcline and quartz and by veins of mylonitized quartz (Fig. 11.1d, 11.2). Locally accumulations of zircon grains occur in mylonite.
6. Cheddar granite: characteristic lamellar microcline perthite (replacement perthite, similar to that in Fig. 11.2); quartz veinlets and accessory apatite, magnetite and titanite.
7. Cheddar granite, fractured (Fig. 11.2d): deformed flame-perthite associated with mylonitized quartz veins. A few patches of plagioclase-rich paleosome, titanite grains and associated iron oxides occur along and within mylonitic quartz veins.
8. Contact between Cheddar granite and pyroxene gneiss; mafic minerals: pyroxene and associated amphibole are partly replaced by microcline, flame-perthite and accessory apatite and titanite. A few calcite patches replace pyroxene.
9. Sillimanite gneiss adjacent to Cheddar granite: bands rich in biotite alternate with biotite-sillimanite layers and mylonitized quartz veins. Locally porphyroblastic garnets replace all other minerals.
10. Deformed Cheddar granite: similar to "7" but locally contains radioactive patches and veinlets of fractured titanite stretched between deformed microcline perthite and plagioclase porphyroblasts and veins of mylonitized quartz. The titanite is associted with magnetite, pyrite, zircon, hematite, uraninite, uranothorite and REE-bearing aggregates (Rimsaite, 1982b, Fig. 31.8d, e, f, g).
11. Metagabbro near Adit 1 at the Halo mine: green pyroxene grains associated with dark green amphibole in a matrix of poorly twinned microcline. Abundant grains of apatite, titanite and patches of scapolite, black and red iron oxides adjacent to and in fractures of pyroxene and feldspar.
12. Pegmatite associated with "11": mainly coarse grained microcline perthite and mylonitized quartz enclosing remnants of altered plagioclase grains.
13. Pyroxene-amphibole-scapolite rock: pyroxene grains associated with amphibole in a groundmass of scapolite crystals containing patches of calcite.
14. Radioactive pyroxenite near contact with granite pegmatite: mainly coarse grained, fractured pyroxene with anhydrite, calcite, feldspar and quartz filling fractures. Radioactive and accessory minerals: uraninite, uranothorite, titanite, apatite, allanite, zircon, magnetite and pyrite adjacent to, and in fractures of, pyroxene. In addition to oxides in Table 11.1, this sample contains 0.11% Ce, 0.06% La and 0.5% Pb.
15. Contact between pyroxene-rich rock and microcline pegmatite made up of Ca-Fe-rich pyroxene, plagioclase, allanite which is partly replaced by microcline, titanite with inclusions of uraninite and REE-bearing crusts in fractures, zircon, apatite and tourmaline overgrown on titanite and allanite (Rimsaite, 1982b, Fig. 31.5a, b, e, f).
16. Biotite-rich portion of quartz mylonite. Uraninite grains occur in biotite and local molybdenite crystallized around uraninite and in biotite fractures. Uraninite grains altered to coffinite and to amorphous U-S compound (Rimsaite, 1982b, Fig. 31.2d).
17. Mafic ore from Greyhawk mine, similar to "15" but contains more plagioclase, hornblende partly replaced by biotite, calcite, apatite and no anhydrite. Uraninite, uranothorite, titanite, apatite, zircon and magnetite adjacent to pyroxene and amphibole.
18. Leucocratic ore from Bicroft mine: a few remnants of green pyroxene, rimmed by dark green amphibole, and partly replaced by quartz, fluorite and calcite, occur in a groundmass of plagioclase and microcline perthite. Uraninite enclosed in phyllosilicate aggregates occurs along the margins of pyroxene, which is altered to nontronite, and in interstices between plagioclase and microcline. Locally, uraninite occurs in intergrowths with pyrochlore, and amphibole is rimmed by tourmaline. This ore also contains 0.02% B, 0.03% Ce and 0.01% La.
19. Pyrite-rich ore from Halo mine: Pyrite invades mylonitized pyroxene-plagioclase-bearing rock along fractures and engulfs uraninite and other minerals. Pyrite occurs in a Fe-rich phyllosilicate which replaces pyroxene and lamellar feldspars. Depending on iron content and degree of oxidation, phyllosilicate aggregates range from green, through orange to bright red. Dendritic pyrite occurs in fractures of mylonitized quartz (Rimsaite, 1982b, Fig. 31.7).

12.

CARTOGRAPHIE D'UNE PARTIE DE LA SOUS-PROVINCE ARCHÉENNE D'UNGAVA À LA HAUTEUR DE POSTE-DE-LA-BALEINE, QUÉBEC

Project 800005

A. Ciesielski
Division du Précambrien

Ciesielski A., Cartographie d'une partie de la sous-province archéenne d'Ungava à la hauteur de Poste-de-la-Baleine, Québec; in Current Research, Part B, Geological Survey of Canada, Paper 83-1B, p. 109-119, 1983.

Résumé

La région de Poste-de-la-Baleine a été cartographiée à 1/125 000 au cours des étés de 1980 et 1981. Les sédiments protérozoïques le long de l'arc Nastapoka reposent en discordance sur le socle granitique. Il s'agit de formations carbonatées et détritiques recouvertes par des coulées de basalte. Le socle archéen est formé de granodiorites relativement homogènes enclavant divers types d'ultrabasiques, de métabasites, de métasédiments et de gneiss orthodérivés. La déformation comprend au moins trois phases; la direction moyenne des foliations a été établie à N280°.

Abstract

The Poste-de-la-Baleine (Great Whale) region was mapped at the scale of 1:125 000 during the 1980 and 1981 summer seasons. Proterozoic sediments discordant on the basement along the Nastapoka Arc are composed of carbonates, sandstones and volcanics at the top. The homogenous granodiorites which constitute the basement contain numerous inclusions of ultrabasics, metabasites, metasediments and orthogneisses. Foliation trending N280° was measured in the most recent of three phases of deformation.

Introduction

Entrepris à l'été 1980, le présent projet porte sur la cartographie à 1/125 000 de la partie nord de la coupure SNRC 33, de la Grande Rivière à l'axe formé par le golfe de Richmond et le lac à l'Eau Claire. Les travaux ont débuté sur la côte de la baie d'Hudson entre le 55° et 56° de latitude nord et ont fourni l'occasion d'effectuer une reconnaissance du territoire. Les travaux de l'été 1981, bénéficiant d'un support héliporté, ont permis la cartographie systématique de la région de Poste-de-la-Baleine, entre le lac Fagnant et le golfe de Richmond (fig. 12.1). On a pu ainsi dresser la carte des sédiments protérozoïques au sud du golfe (Chandler et coll., 1982; Ciesielski et coll., 1983a) et tracer deux profils de gravité pour le compte de la Direction de la physique du globe (Gibb, Chandler, et Fogarasi, 1983). Une série de forages de surface, entrepris dans le but de procéder à des études de paléomagnétisme, a également été exécutée pour le compte de M. E. Schwarz sur une île du secteur est du golfe de Richmond.

Les travaux se répartissent selon trois bases différentes:

1. Cartographie du socle granitique à l'échelle de 1/125 000 et 1/250 000
   - Lac Bienville (non complétée)
   - Lac à l'Eau Claire (non complétée)
   - Côte est de la baie d'Hudson
   - Région de Poste-de-la-Baleine et du golfe de Richmond
2. Cartographie des sédiments protérozoïques à l'échelle de 1/150 000 et 1/100 000
   - Golfe de Richmond
   - Îles Manitounuk
   - Côte est de la baie d'Hudson et Grande Île
3. Cartographie des roches volcano-sédimentaires à l'échelle de 1/50 000
   - Lacs Fagnant et Denys
   - Lac <<Brézolles>> (non complétée)
   - Lac Burton (non complétée)

Travaux antérieurs

Les premiers travaux géologiques dans la partie sud de l'arc Nastapoka (baie d'Hudson) ont été effectués par Bell en 1877 et par Low en 1886-1888 et 1898-1899. Depuis, plusieurs gîtes métallifères ont été découverts dans la région de la Grande rivière de la Baleine et de nombreuses sociétés minières y ont jalonné des terrains à caractère lithologique varié, notamment les carbonates le long de la côte entre le passage de Manitounuk et le golfe de Richmond (dépôts de plomb-zinc), les métasédiments du lac Burton (oxides de fer) et les volcanites du lac <<Brézolles>> à l'est du lac Bienville (prospection des sulfures). La société Great Whale Iron Mines a réalisé les travaux les plus importants dans la région du lac Fagnant de 1957 à 1960 (Scofield, 1960). Au cours de la même période, MM. K. Eade (1966) et I.M. Stevenson (1968) procédaient, respectivement, à une reconnaissance géologique au millionième de la moitié sud et nord de la région comprise entre la rivière Eastmain (52° lat. N) et de la fosse d'Ungava (zone de Cape-Smith et Wakeham Bay). Parallèlement, des travaux importants avaient lieu au golfe de Richmond (Woodcock, 1960), au lac à l'Eau Claire (Kranck et Sinclair, 1963; Bostock, 1969) et dans la région du lac Fagnant (Sabourin, 1961). Plus récemment, la société Uranerz a effectué une importante campagne d'exploration de l'uranium au golfe de Richmond en 1977 et 1978. M. F.W. Chandler, pour sa part, a dressé la carte de la partie nord et centre du golfe en 1977 et 1978, et de la partie sud en 1981 (Chandler et Schwarz, 1980; Chandler et coll., 1982); MM. Schwarz et Fujiwara (1981) procédaient dans un même temps à des travaux de paléomagnétisme dans la même région. Les formations volcano-sédimentaires du lac Fagnant ont également fait l'objet de trois projets d'études supérieures durant la campagne de 1980, (Mercier, 1981; Mercier et Ciesielski, 1983, sous presse; Geoffroy, sous presse). Enfin la société Hydro-Québec procède depuis plusieurs années à différentes expertises géologiques de surface en vue de l'exploitation éventuelle de la Grande rivière de la Baleine.

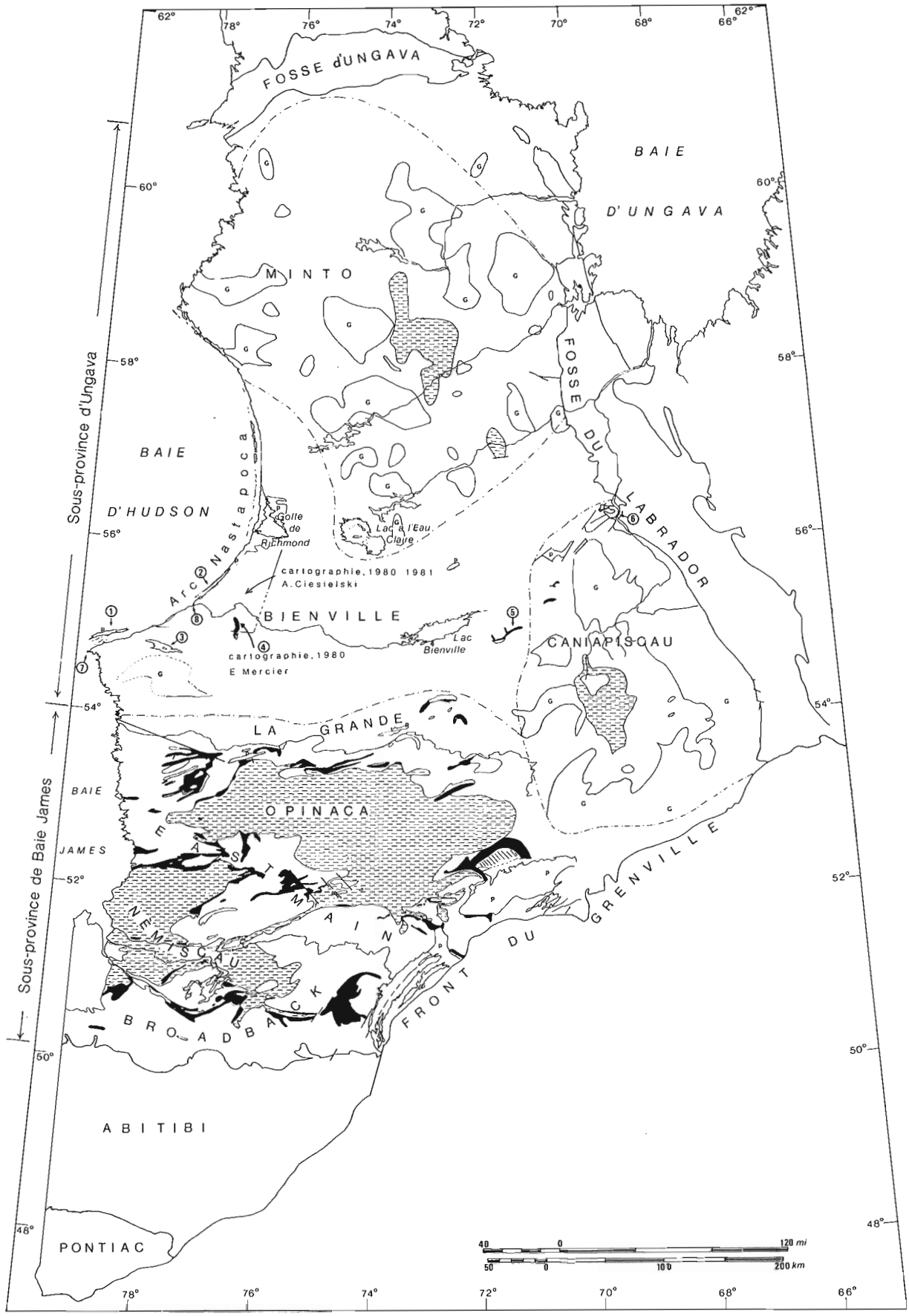
FOSSE d'UNGAVA
BAIE D'UNGAVA
MINTO
FOSSE DU LABRADOR
BAIE D'HUDSON
Arc Nastapoca
Golfe de Richmond
Lac à l'Eau Claire
cartographie, 1980 1981
A.Ciesielski
BIENVILLE
Lac Bienville
cartographie, 1980
E Mercier
CANIAPISCAU
LA GRANDE
OPINACA
EASTMAIN
NEMISCAU
BROADBACK
FRONT DU GRENVILLE
ABITIBI
PONTIAC
BAIE JAMES
Sous-province d'Ungava
Sous-province de Baie James
62°
60°
58°
56°
54°
52°
50°
48°
78°
76°
74°
72°
70°
68°
66°
120 mi
200 km

LÉGENDE

ARCHÉEN DU QUÉBEC

Échelle: 1/3 000 000

APHÉBIEN

Arc Nastapoka
Sakami
Fosse du Labrador — p — Roches volcaniques et sédiments peu métamorphisés

ARCHÉEN

Minto et Caniapiscau — G — Roches plutoniques et enclaves ortho-et paradérivées au faciès des granulites (G) et petits bassins métasédimentaires

Bienville — Roches plutoniques et enclaves orthodérivées au faciès des amphibolites

La Grande
Eastmain
Broadbacket — Roches volcanosédimentaires au faciès des schistes verts roches plutoniques

Opinaca
Némiscau — Roches métasédimentaires au faciès des amphibolites

PROVINCE ARCHÉENNE DU LAC SUPÉRIEUR AU QUÉBEC

SOUS-PROVINCE D'UNGAVA

- DOMAINE DU LAC MINTO (1)
- DOMAINE DU LAC BIENVILLE (2)
- DOMAINE DU LAC CANIAPISCAU (1)

(1) roches plutoniques au faciès des granulites et métasédiments
(2) roches plutoniques au faciès des amphibolites

SOUS-PROVINCE DE LA BAIE JAMES

- ZONE DE LA GRANDE RIVIÈRE (1)
- BASSIN DE LA RIVIÈRE OPINACA (2)
- ZONE DE LA RIVIÈRE EASTMAIN (1)
- BASSIN DU LAC NEMISCAU (2)
- ZONE DE LA RIVIÈRE BROADBACK (1)

(1) roches plutoniques et volcano-sédimentaires
(2) roches métasédimentaires

SOUS-PROVINCE D'ABITIBI-PONTIAC

- NON SUBDIVISÉE

Figure 12.1
Toponymie

1 – Grande île
2 – îles Manitounuk
3 – Lac Burton
4 – Lacs Fagnant et Denys
5 – Lac <<Brézolles>>
6 – Lac Cambrien
7 – Pointe Louis-XIV
8 – Poste-de-la-Baleine

Figure 12.1. *Carte géologique simplifiée du Québec montrant les subdivisions qui ont été effectuées dans l'Archéen selon les différentes lithologies en place. D'après Avramtchev et Marcoux 1979, modifiée.*

Géologie générale

Archéen du Québec

Les roches archéennes de la province du lac Supérieur au Québec peuvent être classées selon trois régions principales

- sous-province d'Ungava, au nord
- sous-province de la baie James, au centre
- sous-province d'Abitibi-Pontiac, au sud

On peut encore subdiviser ces grands ensembles de la façon suivante (fig. 12.1):

a. sous-province d'Ungava

- domaine du lac Bienville, au sud
- domaine du lac Caniapiscau, à l'est
- domaine du lac Minto, au nord

b. sous-province de la baie James (du sud au nord)

- zone volcano-plutonique Broadback
- bassin méta-sédimentaire Nemiscau
- zone volcano-plutonique Eastmain
- bassin méta-sédimentaire Opinaca
- zone volcano-plutonique La Grande

La sous-province d'Abitibi-Pontiac ne fera pas ici l'objet d'une étude puisque beaucoup de travaux y ont déjà été menés (par exemple, Gélinas et coll., 1982; Dimroth et coll., 1982; Goodwin, 1977a, b).

Les subdivisions effectuées à l'intérieur de la sous-province d'Ungava sont basées sur les travaux de Stevenson (1968), Eade (1966) et sur les travaux de reconnaissance et de cartographie partiqués par l'auteur en 1980, 1981 et 1982. On a différencié le domaine du lac Bienville des deux autres parce que son contenu en enclaves du faciès des granulites est moins important, sauf pour la seule zone de granulites qui se situe au sud-ouest de la région. L'existence des deux bassins sédimentaires dans les domaines Caniapiscau et Minto semble due au hazard et n'entre pas dans les critères de différenciation. En outre, il est possible que le complexe de Caniapiscau soit bordé au nord-ouest par une série de reliquats volcaniques et par une série de failles à orientation NE-SW. La limite entre le complexe de Bienville et la zone volcano-plutonique La Grande est définie par les intrusifs tardi-tectoniques en contact avec les séries volcano-sédimentaires mais dont la limite nord demeure inconnue. Les subdivisions reconnues dans la sous-province de la baie James sont conformes aux lithologies présentes et sont basées, entre autres, sur les travaux de Sharma (1977), Schumacher et Fouque (1978) et Marchand (1981). On peut d'ailleurs consulter à cet effet les titres des publications pertinentes dans Veilleux (1980). Les deux bassins sédimentaires se détachent nettemment du reste et on note que les roches volcaniques sont, soit en contact avec la bordure des bassins, soit noyées dans des masses plutoniques. À première vue, il n'existe pas de différences marquées entre ces deux types de distributions. En outre, il est probable qu'il existe une relation structurale entre les zones volcaniques de la rivière Eastmain et de la Grande Rivière et qu'elles soient liées directement à la déformation des deux bassins sédimentaires qui représentent plus de la moitié de la surface lithifiée de la sous-province.

À partir des informations prises sur le terrain dans la région de Poste-de-la-Baleine et le long de la côte est de la baie James (travaux de l'été 1982), on peut différencier le domaine plutonique du lac Bienville des deux autres en ce qu'il ne contient pratiquement pas d'enclaves de roches de compositions dioritique et gabbroique dans le faciès des granulites. En effet, la région à l'ouest et au centre du lac à l'Eau Claire par exemple, et celle située immédiatement à l'est de la fosse du Labrador et au sud de la

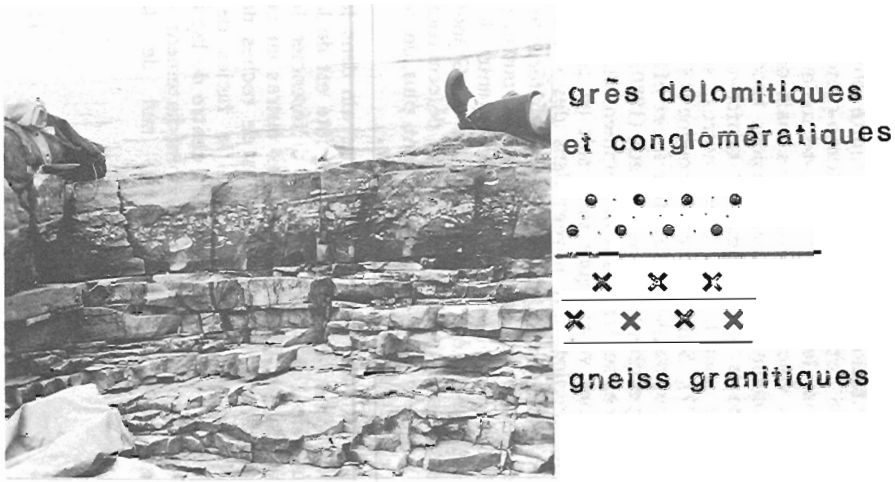

Figure 12.2. *Contact discordant des sédiments du groupe de Nastapoka (Protérozoïque) sur les gneiss granitiques archéens, 5 km au nord de Poste-de-la-Baleine. A noter, la fracturation horizontale au contact.*

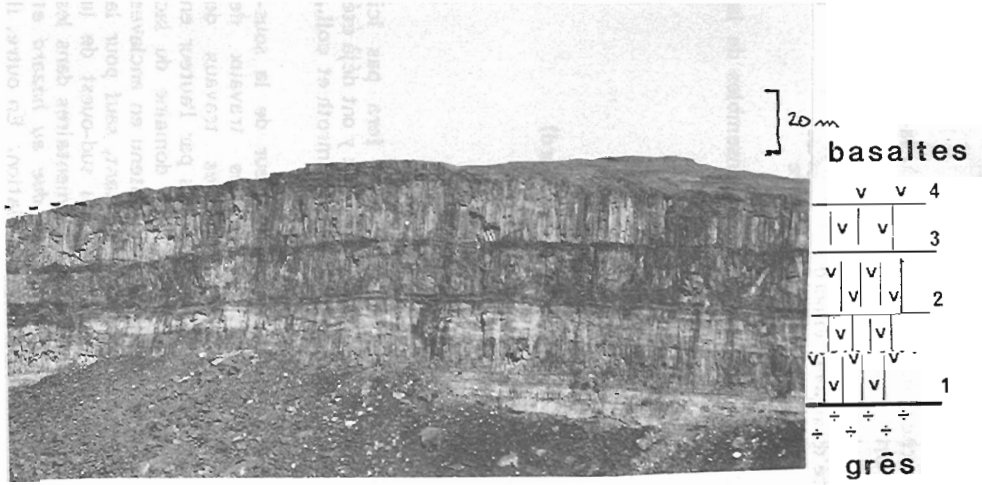

Figure 12.4. *Séquence volcanique comprenant quatre contacts de coulées distincts. On note un changement dans la taille des débits prismatiques au milieu de la coulée nº 1.*

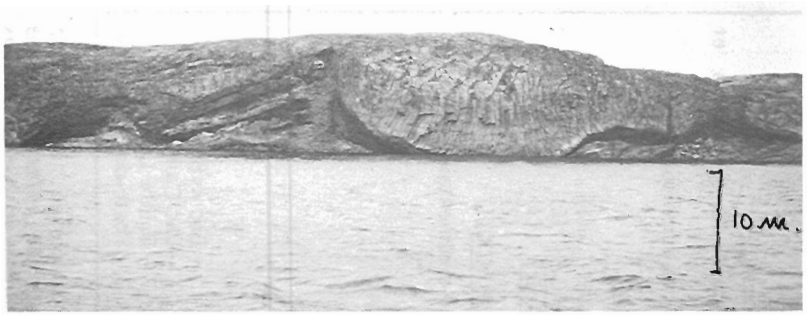

Figure 12.3. *Coulée volcanique mise en place sur des reliefs accidentés. A noter, les débits prismatiques.*

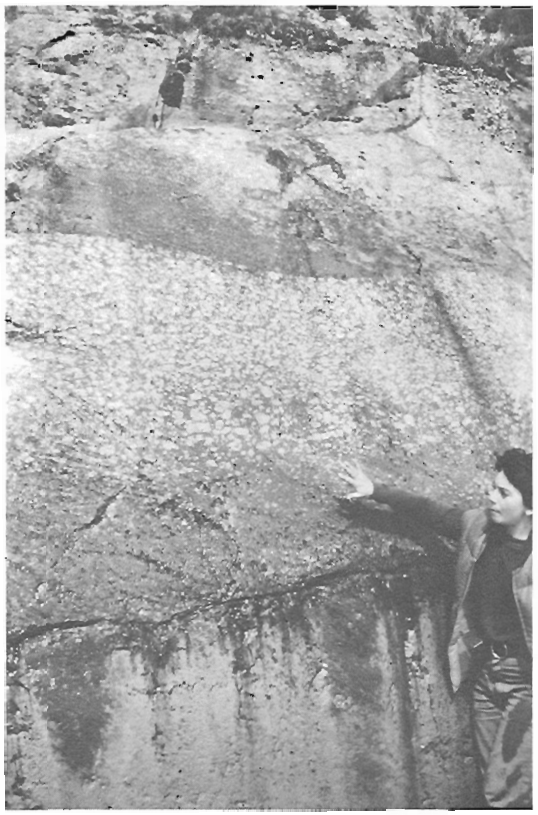

Figure 12.5.

Cumulat de plagioclase flottant au sommet des zonations minéralogiques à l'intérieur de coulées, à l'embouchure de la Petite rivière de la Baleine.

rivière Larch, 57°35' de latitude N (travaux de terrain en 1976 par l'auteur pour le compte du ministère de l'Énergie et des Ressources du Québec, Ciesielski et Clark, sous presse), contient une proportion notable de roches dioritiques massives ou foliées de couleur verte à chinopyroxène, hornblende, biotite et plagioclase; ces dernières passent graduellement à des roches plus basiques et même ultrabasiques, le tout recoupé par une granodiorite a pyroxènes et repris par des granites tardi-tectoniques. Ces phénomènes de différenciation n'ont jamais été observés dans le domaine du lac Bienville. On reconnaît donc dans ce dernier plusieurs types de lithologies qui s'apparentent, soit:

a. - aux granodiorites à enclaves de Poste-de-la-Baleine et de la baie James,
   - aux granodiorites à petits phénocristaux du lac Bienville, ou
   - aux granodiorites à phénocristaux en bordure du domaine du lac Bienville au sud, le long de la Grande Rivière;

b. - aux gneiss leucocrates de la région du lac <<Brézolles>> (à l'est du lac Bienville),
   - aux gneiss leucocrates de la côte est de la baie James, ou
   - aux gneiss leucocrates associés aux roches volcano-sédimentaires de la Grande Rivière (Ciesielski et Marchand, 1983b).

Le domaine plutonique du lac Bienville et sa couverture volcano-sédimentaire d'âge protérozoique

La couverture protérozoique Dans toute la région située au nord de la zone volcano-plutonique de la Grande Rivière, on retrouve deux grands ensembles géologiques très distincts. Le socle cristallin d'une part, et une couverture volcano-sédimentaire d'autre part, cette dernière étant restreinte principalement à la côte le long de l'arc Nastapoka et formant une bande étroite longue de plusieurs centaines de kilomètres (Ciesielski et coll., 1983a). Dans le bassin du golfe de Richmond, situé au centre de l'arc, on observe le groupe de "Richmond Gulf" de nature principalement volcano-détritique mis en place sur le socle cristallin et ayant subséquement subi l'effet d'une série de failles à orientation est-ouest, de façon à former un graben recouvert à son tour en discordance par le groupe Nastapoka principalement volcano-carbonaté et détritique (Chandler, 1982; Chandler et coll., 1982). Ce dernier s'étend vers le sud sur les îles Manitounuk, jusqu'à la Grande Île et comporte des changements de faciès latéraux importants. Enfin, il faut mentionner les plaquages gréseux entre le lac Bienville et le lac Cambrien qui présentent une filiation génétique et probablement tectonique avec le groupe de Sakami de la Grande Rivière. Au sud de la Petite rivière de la Baleine, le groupe Nastapoka se décrit de la façon suivante: carbonates à cherts sulfureux, stromatolites variés contenant des passages grèseux microconglomératiques et bréchiques, des structures entrecroisées, des intraclastes, etc. Le contact avec les gneiss granitiques est marqué par des fractures sub-horizontales et par un grès microconglomératique à cailloux de dolomie et de quartz aplatis (fig. 12.2). Le long de la côte, les carbonates forment de minces chapelets d'îles ainsi que des lambeaux discordants de petites dimensions dont les contacts avec les gneiss sont souvent marqués par des failles (Ciesielski et coll., 1983a). Les séquences détritiques comprennent des grès de composition variable, des argillites et des quartzites. Les structures sédimentaires y sont nombreuses et bien développées. On note le long des îles Manitounuk des changements de faciès latéraux très importants qui résultent en la transformation en masses lenticulaires des séquences détritiques. Si on sépare les roches volcaniques de ces séquences, on retrouve un horizon de cherts bréchiques contenant, par endroits, des dolomies grèseuses à stromatolites.

Les roches volcaniques gisent en contact normal avec les sédiments sous-jacents. On a pu noter que la mise en place des coulés s'est produite sur des reliefs très irréguliers par endroits (fig. 12.3) et que le contact est marqué par une brèche sédimentaire riche en dolomie; d'ailleurs, au sud de la péninsule de Manitounuk, on note la présence d'une mégabrèche de roche dolomitique au contact entre les quartzites et les laves.

Les lithologies volcaniques se présentent sous forme de coulées basaltiques d'une vingtaine de mètres d'épais ayant un débit prismatique relativement prononcé. La roche est aphanitique, de couleur verte, et porphyrique par endroits. Sur le versant nord de l'embouchure de la Petite rivière de la Baleine, la séquence comporte au moins quatre coulées distinctes (fig. 12.4). On en a d'ailleurs dénombré beaucoup plus le long d'une coupe du golfe de Richmond; il s'agit de coulées qui s'avèrent susceptibles d'être relevées et portées sur carte sur toute la longueur du groupe de Nastapoka. Certaines séquences présentent des structures de cumulats (fig. 12.5) où des mouvements intramagmatiques dus, entre autres aux différences de densités, ont provoqué la formation de structures diapiriques. L'altération caractérise certains sommets de coulées; la roche devient alors rouge-brun et un grand nombre de vésicules et d'agates font leur apparition. Les sédiments à l'intérieur de coulées trouvés à plusieurs endroits n'ont généralement pas plus de 2 m d'épaisseur et se composent de pélites, de cherts de couleur rouge ou verte, de brèches et de grauwackes volcanogéniques (Ciesielski et coll., 1983a). Les brèches de sommets de coulées sont pratiquement inexistantes, elles n'ont d'ailleurs été décrites qu'à un endroit au sud de Boat Opening. Il n'existe aucun indice qui permette de reconnaître la direction de déplacement des coulées. Des flexures dans le débit prismatique (fig. 12.6) se dirigeant grossièrement vers l'est-nord-est sont plutôt reliées à des irrégularités sur les surfaces de coulées. Les reliefs sous les coulées, quant à eux, ne permettent pas non plus d'établir l'origine puisqu'on ne possède de renseignements que sur deux de leurs dimensions.

La déformation touche peu les sédiments protérozoïques de l'arc Nastapoka. Elle se limite à une série de fractures à orientation est-ouest, postérieures à la sédimentation et à la mise en place du groupe de "Richmond Gulf". Il s'agit de fractures synchrones avec l'intrusion de deux familles de dykes de diabases suivant des orientations de N300° et N30° dans le golfe de Richmond (Chandler, 1982). Ces orientations se retrouvent également au sud du secteur de Poste-de-la-Baleine où l'on remarque des orientations de N330° et N40°. Une phase de fracturation postérieuse au groupe de Nastapoka vient coiffer le tout selon une orientation est-ouest grossière et représente sans doute l'effet d'une réactivation des réseaux de fractures du socle déjà existants.

Le socle archéen L'ensemble cristallin se divise en deux: les reliquats de zones volcano-sédimentaires et les granitoïdes gneissiques qui constituent la quasi-totalité du territoire. En règle générale, il s'agit d'une roche de composition granodioritique à grains moyens, de couleur gris-vert. La foliation est bien développée, ainsi que l'indiquent les données du secteur de Poste-de-la-Baleine illustrées à la figure 12.7. Les plis, trouvés en grand nombre, se dirigent souvent dans toutes les directions et présentent des dimensions et géométries variables souvent associées à des enclaves basiques allongées aux dimensions métriques. Du point de vue des lithologies, on remarque des enclaves de composition dioritique ou gabbroïque, des amphibolites, des paragneiss et des ultrabasiques. Les pegmatites roses

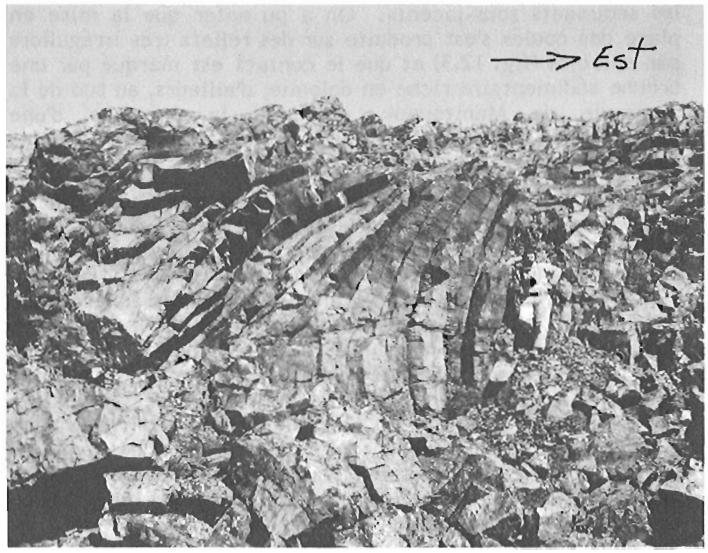

Figure 12.6. *Flexure du débit prismatique au sud des îles Manitounuk.*

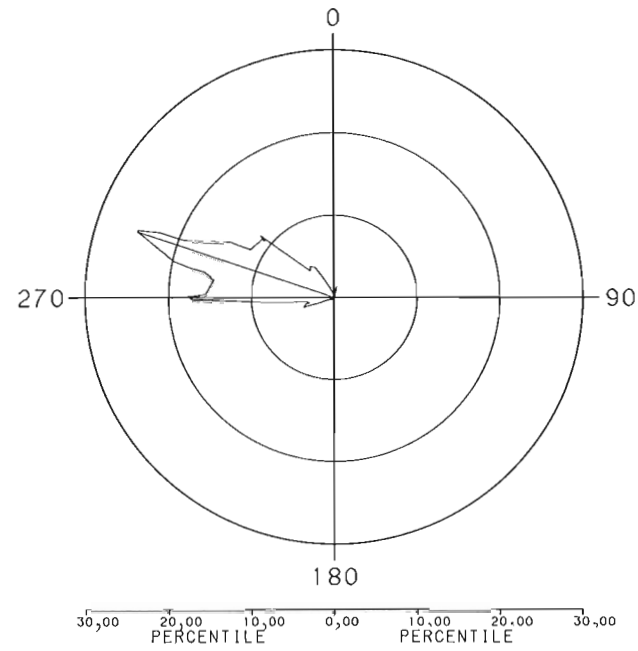

Figure 12.7. *Diagramme de fréquence des orientations des foliations dans la région de Poste-de-la-Baleine, sur 230 mesures.*

Figure 12.8. *Dyke basique différencié et repris à angle par l'avant-dernière phase de foliation F_2; le litage métamorphique S_2 est parallèle au mur du dyke.*

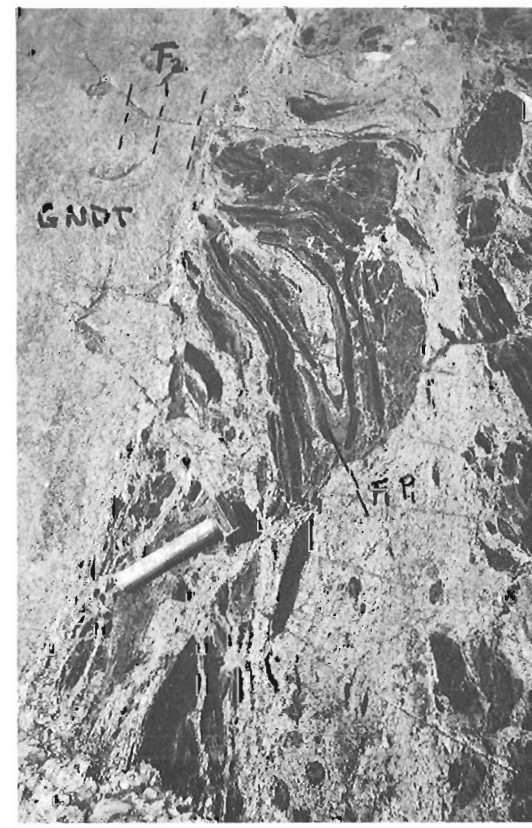

Figure 12.9. *Métabasites foliées et plissées en F_1 et P_1, puis repris par la phase de granitisation (granodiorite) et foliées en F_2.*

associées à de petites masses de granites roses recoupent la granodiorite de base à maints endroits. Un aperçu sommaire des relations chronologiques est donné au tableau 12.1.

Le socle a été divisé en secteurs nord et sud représentant respectivement la partie allant du golfe de Richmond à la Grande Île et la partie allant de la pointe Louis-XIV à la la Grande Rivière (fig. 12.1, reconnaissance et cartographie de la côte est de la baie James, effectuées en août 1982 par l'auteur). Là où la mer a nettoyé les affleurements, le long de la côte, les enclaves et les structures dans les granodiorites se remarquent nettement mieux qu'à l'intérieur des terres. On remarque d'emblée que le secteur sud a subi plus de déformation; en outre, il contient plus d'enclaves métabasiques et ultrabasiques et deux types différents de granodiorites qui se distinguent très bien l'un de l'autre en ce que l'un est mésocrate et très déformé et l'autre, de nature plus granitique, est leucocrate et moins déformé; ce dernier porte d'ailleurs des traces de structures de fluage encore très apparentes. L'augmentation de la déformation dans le secteur sud est lié à la présence

Tableau 12.1

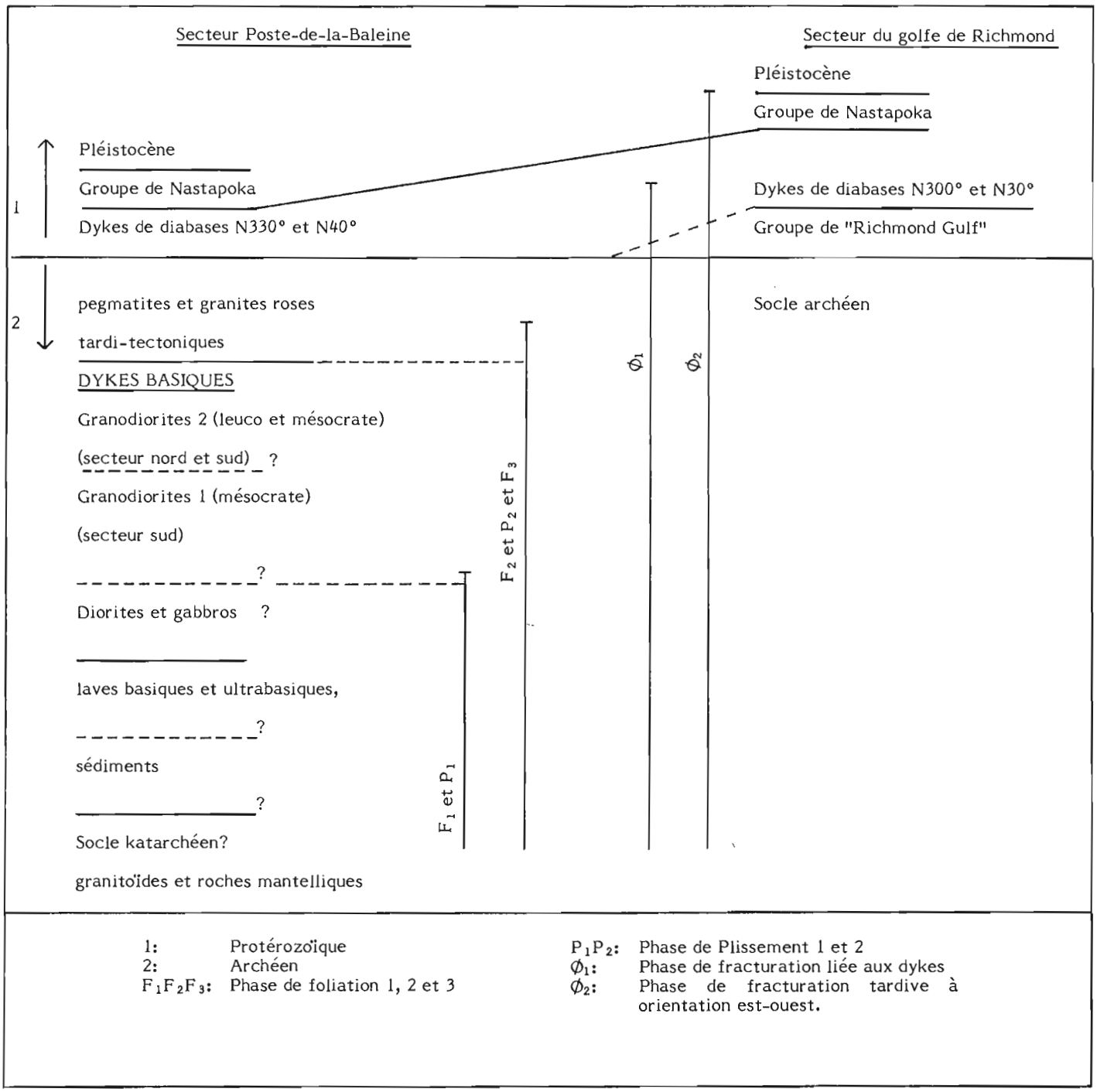

d'un grand bloc de granulite situé dans le sud-ouest du domaine du lac Bienville (fig. 12.1). On peut classer les différents types d'enclaves selon qu'ils représentent:

1. d'anciens dykes basiques repris par la foliation F_2 et différenciés par le métamorphisme (fig. 12.8)
2. des métabasites foliées et plissées en F_1 et P_1, puis recoupées par la granodiorite et foliées en F_2 (fig. 12.9 et 12.10)
3. des ultrabasites massives reprises par la granodiorite et foliées en F_2 (fig. 12.11)
4. des métasédiments légèrement migmatisés, foliés et plissés en F_1 et P_1, puis repris par la granodiorite et F_2 (fig. 12.12).

La déformation a marqué les granodiorites selon deux phases, l'une à orientation de N280°, soit la phase dominante du secteur nord, et l'autre à orientation pratiquement nord-sud (fig. 12.13) dont les traces sont plutôt effacées dans le secteur de Poste-de-la-Baleine et du golfe de Richmond mais qui devient néanmoins la phase principale dans la région

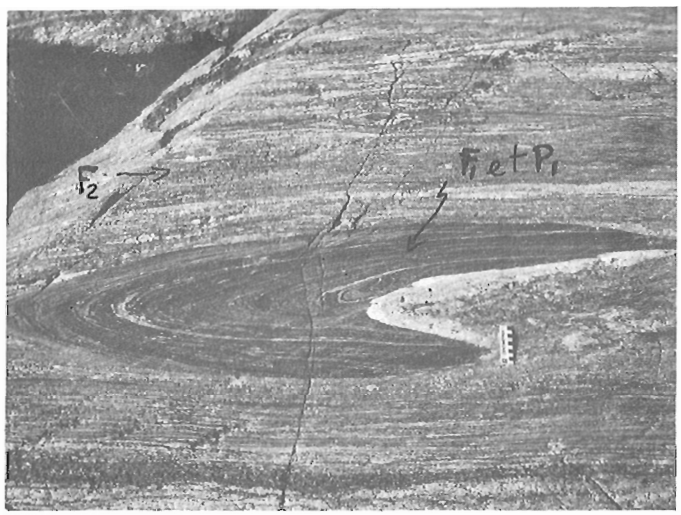

Figure 12.10. *Métabasites homogènes foliées et plissées en F_1 et P_1, puis repris par la granodiorite mésocrate (secteur sud) et foliées en F_2.*

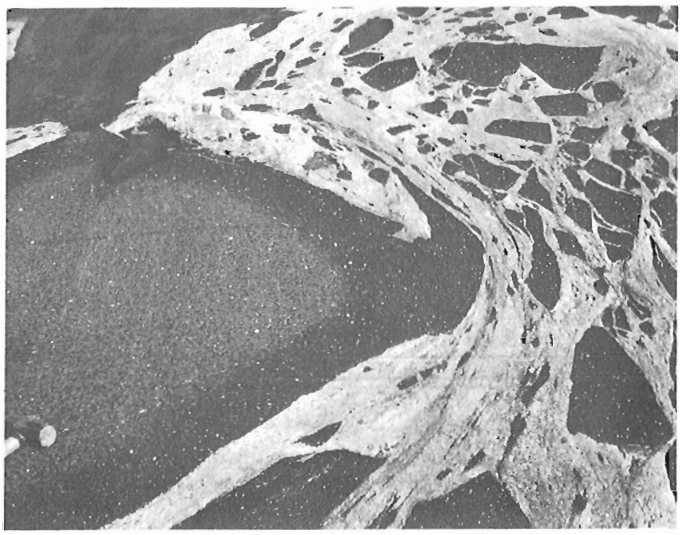

Figure 12.11. *Ultrabasites massives reprises par la granodiorite leucocrate (secteur sud). A noter, les structures de fluage donnant une rotation dextre.*

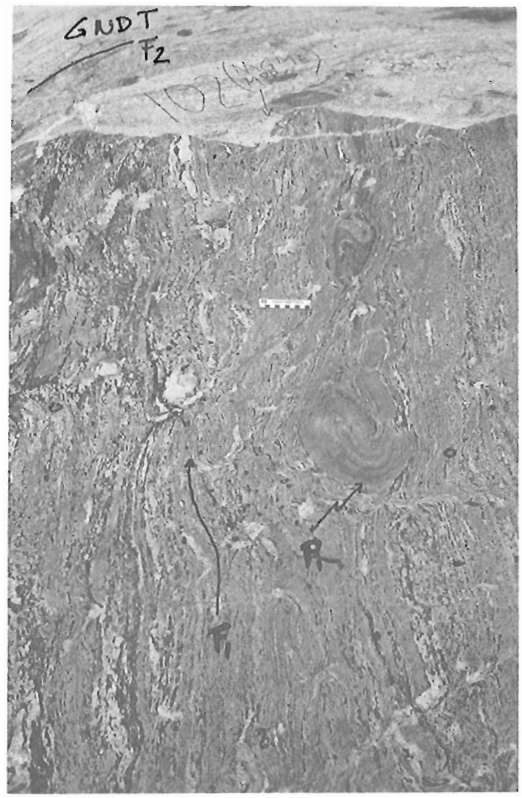

Figure 12.12. *Métasédiments ou roches apparentées légèrement migmatisées, foliées et plissées par une première phase F_1 et P_1, puis recoupées par la granodiorite leucocrate (secteur sud) et reprises par F_2.*

du domaine du lac Minto (Stevenson, 1968; Taylor, 1982). Les pegmatites et granites roses tardifs ne sont pratiquement pas touchés par les foliations. Les plis P_2 liés à la phase de foliation F_2 sont trés marqués dans les zones d'hétérogénéité de compétence, c'est-à-dire là où l'on remarque la présence de dykes et d'enclaves. Quand elles sont isolées, les enclaves allongées se présentent souvent sous forme de grand plis à plongements et à traces axiales très variables. L'étude des champs d'enclaves du secteur sud révèle l'existence de plis à faibles plongements marqués par d'anciens dykes foliés, étirés puis plissés (fig. 12.14). En outre, la granodiorite du secteur sud se distingue par de grands plis à plongements verticaux, où les discordances internes dues à la foliation sont nombreuses (fig. 12.15).

Quant à l'origine des différentes types d'enclaves, seul les dykes basiques antérieurs aux phases F_2 et P_2 et les métasédiments offrent une réponse satisfaisante. Les métabasites et les ultrabasiques peuvent être affilieés à des phases de volcanisme antérieures au Kénoréen, ou à des complexes basiques différenciés, mais peuvent aussi représenter des roches mantelliques jouant un rôle dans la différenciation acide primaire. Il est impossible de retracer un socle acide primaire sur lequel les protolithes des métasédiments et des métabasites se seraient déposés. La distinction de deux types de granodiorites dans le secteur sud empêche l'établissement d'une chronologie relative. Il est cependant tout à fait probable que la granodiorite leucocrate, moins déformée et plus granitique, soit intrusive dans celle de nature nettement plus mésocrate et gneissique. Il est à noter que l'on retrouve les même types d'enclaves basiques dans les deux granodiorites.

Les ensembles volcano-sédimentaires sont très restreints dans le domaine du lac Bienville. En effet, ces lithologies disparaissent au nord de la Grande Rivière. Deux petits reliquats ont cependant résisté à l'érosion et ont d'ailleurs fait l'objet d'études; l'une, détaillée, porte sur la bande Fagnant-Denys à l'est de Poste-de-la-Baleine, l'autre, de type reconnaissance, porte sur la bande du lac <<Brézolles>> située à 60 km à l'est du lac Bienville (fig. 12.1). Cette dernière se compose essentiellement de métatufs au faciès des amphibolites, à inclinaison verticale et en contact à un endroit avec des micaschistes et, de façon plus systématique, avec des métatonalites typiques sans relation chronologique claire. La bande Fagnant-Denys, pour sa part, fait depuis longtemps l'objet d'études plus détaillées en raison de son potentiel en minerai de fer (Scofield, 1960; Sabourin, 1961; Mercier, 1981; Mercier et Ciesielski, sous presse). Il s'agit d'une série synclinale comportant un groupe sédimentaire riche en fer à la base, et un groupe volcanogénique au sommet, le tout présentant un faciès des amphibolites et schistes verts. Des séries conglomératiques surmontées d'amphibolites et d'ultrabasites (Ciesielski, sous presse). caractérisent le sud de la bande. La bande Fagnant-Denys n'est pas partout en contact direct avec les granodiorites du domaine du lac Bienville. Ces dernières en sont séparées à certains endroits par des pegmatites blanches ou roses intrusives; sur le terrain, aucune relation chronologique ne saute aux yeux et l'on pourrait croire que les séries volcano-sédimentaires flottent en quelque sorte sur les granodiorites. Les datations effectuées (Lowdon, 1960) donnent 2 555 millions d'années (K/Ar) pour les métasédiments et 2 625 millions d'années (K/Ar) pour les pegmatites qui les recoupent. Ces âges contradictoires mesurés sur les muscovites ne semblent pas d'une grande fiabilité; par contre, des datations effectuées sur des pegmatites habituellement tardi-tectoniques repousseraient

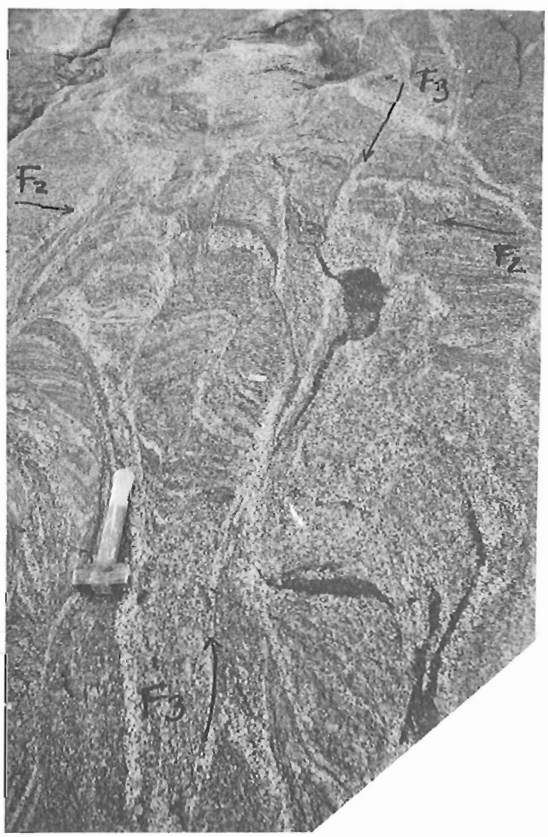

Figure 12.13. *Granodiorite du secteur nord ayant subi l'effet de deux foliations, F_2 étant antérieure à F_3.*

Figure 12.14. *Pli dans un champ d'enclaves basiques du secteur sud marqué par un dyke basique folié, étiré puis plissé en F_2 et P_2.*

Figure 12.15. *Discordance interne de foliation dans les granodiorites 1 du secteur sud. Il s'agit d'une forte augmentation locale de la déformation, même affleurement que dans la fig. 12.14.*

sensiblement l'âge du réajustement du socle archéen. D'autre part, au sud, des contacts de type intercalé entre les granodiorites et les métaconglomérats, ainsi qu'une rotation rapide de 60° des foliations vers le nord, peuvent indiquer un rapport de type intrusif syntectonique. Des études plus détaillées déjà entreprises fourniront éventuellement d'autres éléments de réponse.

Conclusions

Quelques questions importantes se posent auxquelles, il faut espérer, les recherches en cours sauront répondre, notamment en ce qui a trait à la nature:

- du chimisme des divers types de granodiorites du domaine du lac Bienville; leurs affiliations génétiques et les comparaisons possibles avec d'autres granitoïdes plus réçents;
- du chimisme et de l'origine des enclaves basiques, ultra-basiques et métasédimentaires; leurs genèses et leurs rapports aux granodiorites;
- du rôle de la déformation et de sa signification dans le cadre de la genèse des grandes étendues de granodiorites; et
- du rapport tectonique et génétique existant entre le domaine du lac Bienville et la sous-province de la baie James.

Remerciements

Les travaux dans la région de la baie d'Hudson n'ont été rendus possibles que grâce à l'aimable collaboration des gens de l'Hydro-Québec, du Centre d'Études Nordiques (CEN) de l'Université Laval et de la Société de Développement de la Baie James (SDBJ) stationnés à Poste-de-la-Baleine et LG-2, et plus spécialement grâce à l'aide exceptionnelle apportée sur le terrain par MM. S. Payette, C. Locat et P. Marchand, P. Geoffroy, R. St-Michel, C.M. Hamel, P. Diver, P. Byrne (cuisinier), R. Pritchard (pilote d'hélicoptère) et C. Côté. L'auteur apprécie en outre les judicieuses interventions de M. F.W. Chandler (CGC) lors d'une lecture du manuscript et M. K.D. Card (CGC) pour le dessin de la carte géologique.

Bibliographie

Avramtchev, L. et Marcoux, P.
1979: Carte géologique du Québec, Édition Provisoire, 1/1 500 000, ministère de l'Énergie et des Resources du Québec, B-1348.

Bell, R.
1877: Report on an exploration of the east coast of Hudson's Bay; Geological Survey of Canada, Report of Progress, 1877-78.

Bostock, H.H.
1969: The clearwater complex (New Quebec); Geological Survey of Canada, Bulletin 178, 63 p.

Chandler, F.W.
1982: The structure of the Richmond Gulf Graben and the geological environments of lead-zinc mineralization and of iron manganese formation in the Nastapoka Group, Richmond Gulf area, New Quebec – Northwest Territories; in Current Research, Part A, Geological Survey of Canada, Paper 82-1A, p. 1-10.

Chandler, F.W. and Schwarz, E.J.
1980: Tectonics of the Richmond Gulf area, Northern Quebec – a hypothesis; in Current Research, Part C, Geological Survey of Canada, Paper 80-1C, p. 59-68.

Chandler, F.W., Ciesielski, A., and St. Michel, R.
1982: Geological map of the southern margin of the Richmond Gulf Graben, New Quebec; Geological Survey of Canada, Open File, Map 840, Scale 1:50,000.

Ciesielski, A.
– Géologie de la bande Fagnant-Denys, sous-province archéenne d'Ungava, Québec. (sous presse)

Ciesielski, A. et Clark, T.
– Géologie et géochronologie du socle adjacent à la fosse du Labrador, côte est et ouest, 57° lat. N. (sous presse)

Ciesielski, A. et Marchand, P.
1983b: Géologie révisée de la région LG2-Duncan (1/50 000), baie James, Québec; Commission géologique du Canada, Dossier public 934.

Ciesielski, A., St. Michel, R., et Hamel, C.M.
1983a: Géologie d'une portion sud de l'arc Nastapoka, baie d'Hudson, Québec; Commission géologique du Canada, Dossier public 896.

Dimroth, E., Imreh, L., Rocheleau, M., and Goulet, N.
1982: Evolution of the south-central part of the Archean Abitibi Belt, Québec. Part I stratigraphy and paleogeographic model; Canadian Journal of Earth Sciences, v. 19, p. 1729-1758.

Eade, K.E.
1966: Fort George river and Kaniapiskau river (west half) map-areas, New Quebec; Geological Survey of Canada, Memoir 339, 84 p.

Gélinas, L., Mellinger, M., and Trudel, P.
1982: Archean mafic metavolcanics from Rouyn-Noranda district, Abitibi Greenstone Belt, Quebec. I. Mobility of the major elements; Canadian Journal of Earth Sciences, v. 19, p. 2258-2275.

Geoffroy, P.
– Mémoire de Maîtrise, Université du Québec à Montréal (sous presse)

Gibb, R.A., Chandler, F.W., and Fogarasi, S.
1983: The Richmond Gulf gravity anomaly; in Current Research, Part B, Geological Survey of Canada, Paper 83-1B.

Goodwin, A.M.
1977a: Archean basin – craton complexes and the growth of Precambrian Shields; Canadian Journal of Earth Sciences, v. 14, p. 2737-2759.

1977b: Archean Volcanism in Superior Province, Canadian Shield; Geological Association of Canada, Special Paper 16, p. 205-241 (1977).

Kranck, S.H. and Sinclair, G.W.
1963: Clearwater Lake, New Quebec; Geological Survey of Canada, Bulletin 100.

Low, A.P.
1888: Report on explorations in James Bay and country east of Hudson Bay, drained by the Big Great Whale and Clearwater rivers; Geological Survey of Canada, Annual Report, III J, 1887-88.

1900: Report on an exploration of east coast of Hudson Bay from Cape Wolstenholme to the south end of James Bay; Geological Survey of Canada, Annual Report (n.s.), XIII D.

Lowdon, J.A.
1960: Age determinations by the Geological Survey of Canada. Report 1: Isotopic Ages; Geological Survey of Canada, Paper 60-17, 51 p.

Marchand, P.
1981: Rapport géologique de synthèse, 1978 à 1980 pour la région Duncan LG-2. Baie James Québec, SDBJ (Société de Développement de la Baie James.)

Mercier, E.
1981: Métavolcanites et métasédiments archéens du N.E. de la province du lac Supérieur (Bouclier Canadien) Québec, Canada; Mémoire de D.E.A. inédit, Université des Sciences et Techniques de Lille, 59 p.

Mercier, E. et Ciesielski, A.
– Un reliquat de ceinture volcano-sédimentaire dans la sous-Province archéenne d'Ungava, Québec. (sous presse)

Sabourin, R.J.E.
1961: Rapport préliminaire sur la région des lacs Denys et Fagnant (Nouveau Québec); dans Rapport RP nº 469; ministère des Richesses naturelles du Québec, 9 p.

Schumacher, F. et Fouque, J.P.
1978: Carte géologique au 1/250 000 du Permis S.E.S., SERU Nucléaire, Eldorado Nucléaire, SDBJ (Société de Développement de la Baie James).

Schwarz, E.J. and Fujiwara, Y.
1981: Paleomagnetism of the Circum-Ungava Fold Belt II: Proterozoic Rocks of Richmond Gulf and Manitounuk Islands; in Proterozoic Basins of Canada, F.H.A. Campbell, editor; Geological Survey of Canada, Paper 81-10, p. 255-267.

Scofield, L.M.
1960: Report of the magnetite deposits of great Whale Iron Mines Limited; Private report to Belcher Mining Corporation Limited, 10 p.

Sharma, K.N.M.
1977: Région de la Grande Rivière; ministère des Richesses naturelles du Québec, Rapport géologique 184.

Stevenson, I.M.
1968: A geological reconnaissance of Leaf River map-area, New Quebec and Northwest Territories; Geological Survey of Canada, Memoir 356, 112 p.

Taylor, F.C.
1982: Reconnaissance geology of a part of the Canadian Shield, Northern Quebec and Northwest Territories; Geological Survey of Canada, Memoir 399.

Veilleux, P.P.
1980: Catalogue du fichier géologique au 1 août 1980; ministère de l'Énergie et des Ressources du Québec, DPV 766.

Woodcock, J.R.
1960: Geology of the Richmond Gulf area New Quebec; Proceedings of the Geological Association of Canada, v. 12, p. 21-40.

13.

A KINEMATIC STUDY OF MYLONITIC ROCKS IN THE OMINECA-INTERMONTANE BELT TECTONIC BOUNDARY IN EAST-CENTRAL BRITISH COLUMBIA

C.J. Rees[1] and Filippo Ferri[2]

Rees, C.J. and Ferri, F., A kinematic study of mylonitic rocks in the Omineca-Intermontane belt tectonic boundary in east-central British Columbia; in Current Research, Part B, Geological Survey of Canada, Paper 83-1B, p. 121-125, 1983.

Abstract

The contact between the Omineca and Intermontane belts in east-central British Columbia is a shear zone marked by mylonitic rocks. The sense of shear is from west to east as determined from rotated feldspar megacrysts and asymmetry of shear band foliation in orthogneiss of the footwall (Omineca Belt).

Overthrust strata of the Intermontane Belt include the Mississippian to Lower Permian Antler Formation and overlying Triassic and Lower Jurassic sedimentary and volcanic rocks. Major displacement occurred in Early to Middle Jurassic time.

Résumé

La surface de contact entre les zones d'Omineca et d'Intermontane dans la partie est-centrale de la Colombie-Britannique est une zone de cisaillement caractérisée par la présence de mylonite. La direction ouest-est du cisaillement est déterminée à partir de macrocristaux tournés de feldspath et de l'asymmétrie de la foliation cisaillée dans l'orthogneiss de la lèvre inférieure (zone d'Omineca).

Les couches charriées de la zone d'Intermontane comprennent la formation d'Antler, du Mississippien au Permien inférieur, recouverte par des roches sédimentaires du Trias et du Jurassique inférieur. Un déplacement important a eu lieu du Jurassique ancien au Jurassique moyen.

Introduction

In the Quesnel Lake area in east-central British Columbia, the boundary between the Omineca Belt and the Intermontane Belt (Fig. 13.1) is marked by mylonitic rocks (Campbell, 1971; Rees, 1981). The Intermontane Belt west of this shear zone comprises Upper Paleozoic ophiolitic rocks (Montgomery, 1978), overlain by Triassic and Lower Jurassic sedimentary and volcanic rocks (Campbell and Campbell, 1970). The Omineca Belt east of the shear zone comprises Upper Proterozoic and Paleozoic clastic metasedimentary rocks and bodies of orthogneiss of uncertain age (Campbell and Campbell, 1970).

The boundary was metamorphosed in the Middle Jurassic; isograds transect it near Crooked Lake to the southeast (Campbell and Campbell, 1970) and within the study area. Tectonic emplacement of the hanging wall (Intermontane Belt) and formation of the mylonites occurred during or after deposition of the youngest, Lower Jurassic

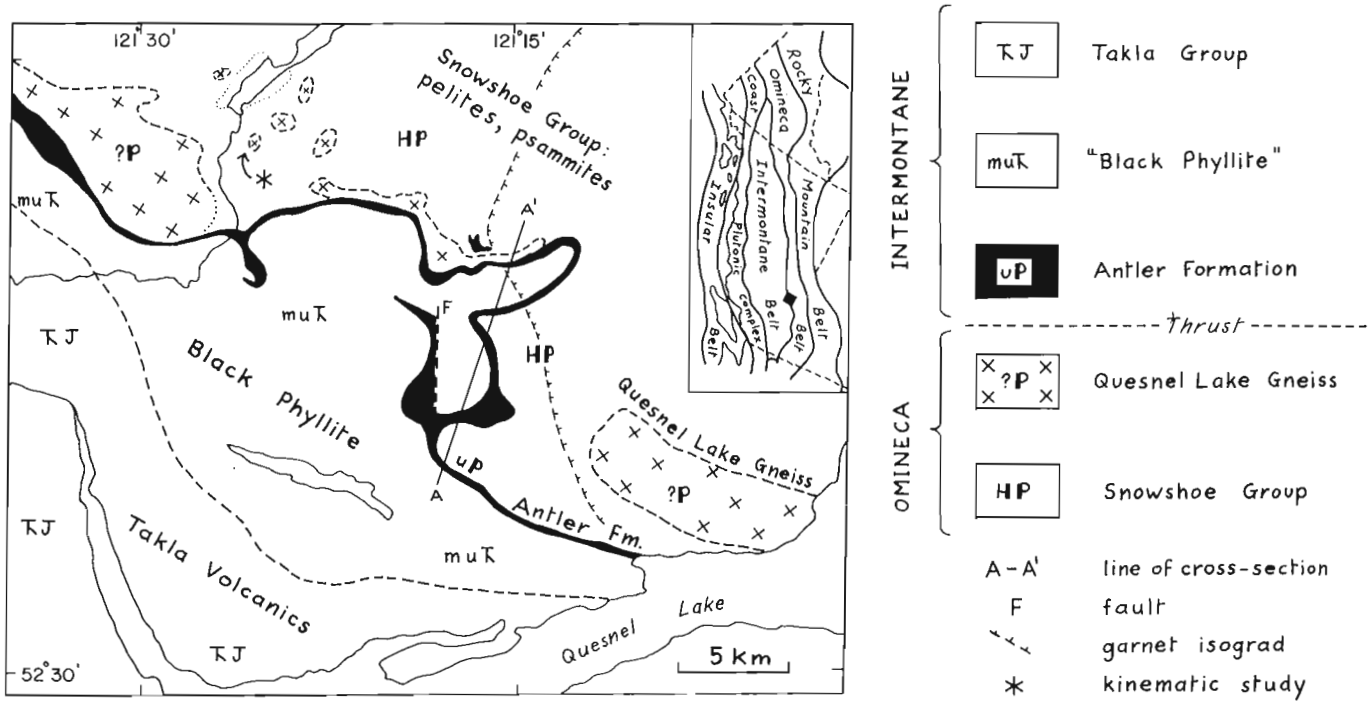

Figure 13.1. *Simplified geological map of the study area, incorporating some information from Campbell (1978) and Struik (1983). Inset shows the location of the area in the Canadian Cordillera.*

[1] Department of Geology, Carleton University, Ottawa, K1S 5B6
[2] Department of Geology and Geophysics, University of Calgary, Calgary, T2N 1N4
Ottawa-Carleton Centre for Geoscience Studies, Publication 20-83

rocks, and prior to Middle Jurassic metamorphism and deformation. The geometry of the shear zone and metamorphism associated with it have been obscured by later deformations and metamorphism, although previous workers have recognized 'early' east-verging isoclinal structures (Montgomery, 1978; J.S. Getsinger, personal communication, 1983) that may be coeval with overthrusting.

This paper presents some kinematic evidence from the footwall (Omineca Belt) orthogneiss indicating that shearing was easterly directed.

General Geology

The Intermontane Belt consists of the Antler Formation and overlying unnamed Triassic and Jurassic sedimentary and volcanic units (Fig. 13.1). The Mississippian to Lower Permian Antler Formation (Campbell, 1978; Struik, 1983) forms the base of the hanging wall, and comprises mainly foliated and banded greenstone, and locally meta-ultramafic schist. The latter contains no relict olivine but dominantly contains either talc or antigorite, with porphyroblasts of magnesite. Trace element geochemistry (also Campbell, 1971; Hall-Beyer, 1976) indicates that the greenstone was derived from ocean-floor tholeiitic basalt. Outside the study area chert beds are interlayered with the greenstone (Struik, 1981), and cumulate structures are preserved in the meta-ultramafite (Montgomery, 1978).

The Antler greenstone is overlain (probably stratigraphically) by an unnamed Triassic unit of grey to black graphitic siltite and phyllite. These rocks are probably contemporaneous with, and laterally transitional to the Upper Triassic to Lower Jurassic Takla Group volcanic and volcaniclastic rocks which crop out in the southwest part of the area. Volcanic rocks are dominated by alkalic augite porphyry basalt (Bailey, 1978; Morton, 1976). Between these and the Triassic black argillite is a zone of volcaniclastic rocks ranging from very coarse debris flows to laminated grey-green lithic sandstones and siltstones.

The Omineca Belt is underlain by the Snowshoe Group (as designated by Struik, 1982, 1983) and the Quesnel Lake Gneiss. The Snowshoe Group is probably time-correlative with Kaza Group, Cariboo Group and Black Stuart Group rocks to the east in the Cariboo Mountains, and if so ranges from Hadrynian to upper Paleozoic, but the lithological successions are not directly comparable, hence the distinction. Most of the Snowshoe rocks are thinly bedded pelitic to psammitic metasediments; some are more massive coarse grained 'gritty' psammite and feldspathic conglomerate. Carbonate rocks are uncommon, and no mafic metavolcanics have been confidently identified.

The Quesnel Lake Gneiss consists of several bodies of granitoid orthogneiss that apparently intrude Snowshoe Group rocks (Struik, personal communication, 1983), although contacts with the metasediments are rarely clear because of strong deformation. The gneiss bodies vary in composition, texture and probably in age; they could be Paleozoic (R.L. Armstrong, personal communication). Northwest of Quesnel Lake, the gneiss is granitic with megacrysts of potassium feldspar; it lies in the footwall adjacent to the shear zone and exhibits mylonitic texture and structures.

Structure and Metamorphism

The formation of the mylonite and related structures are ascribed to phase one (D1), although there may be an earlier pre-Jurassic deformation. Regional folding of the mylonitic foliation (Fig. 13.2) is correlated with second phase southwest-verging folds (here ascribed D2) that dominate the structural culmination of the Cariboo Mountains to the east (Struik, 1981; Murphy and Journeay, 1982; Murphy and Rees, 1983). Open folds and ubiquitous, generally upright crenulation cleavage which trend 130° are ascribed to the third phase of deformation (D3).

Metamorphic grade increases from lower greenschist in the northwest to at least lower amphibolite in the southeast part of the study area. The mylonitic rocks are annealed (also Campbell, 1971) rather than marking localized retrogression; the garnet isograd transects a major second-phase fold closure with Triassic phyllite in the core (Fig. 13.1). This indicates that the peak of metamorphism postdates both the emplacement of the hanging wall, and the D2 folding. Metamorphic conditions during the D1 mylonitization have not yet been ascertained.

Kinematic Analysis

This study was done on an exposure of Quesnel Lake Gneiss on the upward facing limb of a major southwest-verging D2 fold (indicated by an asterisk in Fig. 13.1). The mylonitic layering in the gneiss is subhorizontal, and two roughly orthogonal vertical joint sets are parallel and perpendicular to the finite extension direction (097°) in this foliation, indicated by strongly aligned potassium feldspar megacrysts and quartz ribbons (Fig. 13.3). Those joint faces parallel to the lineation thus display very closely the XZ plane of the finite strain ellipsoid; the other joint set faces display the YZ plane (Fig. 13.4). Seven XZ surfaces each of about (50 cm)^2 were examined (Fig. 13.5); the length, width, and angle between the long axis and the mylonitic foliation were measured for each megacryst considered to have behaved as a rigid inclusion during shearing. Smaller or

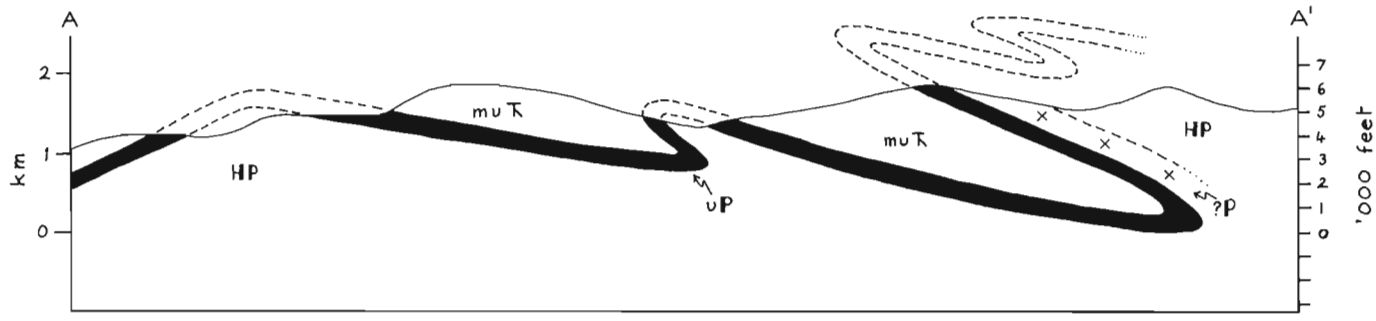

Figure 13.2. *Geological cross-section through the area, showing the predominance of southwesterly-verging, tight overturned D2 folds. The upright open fold in the southwest is D3. The kinematic study was done on an exposure of Quesnel Lake Gneiss downplunge to the northwest of this section, on the upward facing limb of a D2 fold, as indicated by cleavage-bedding relationships in nearby metasediments.*

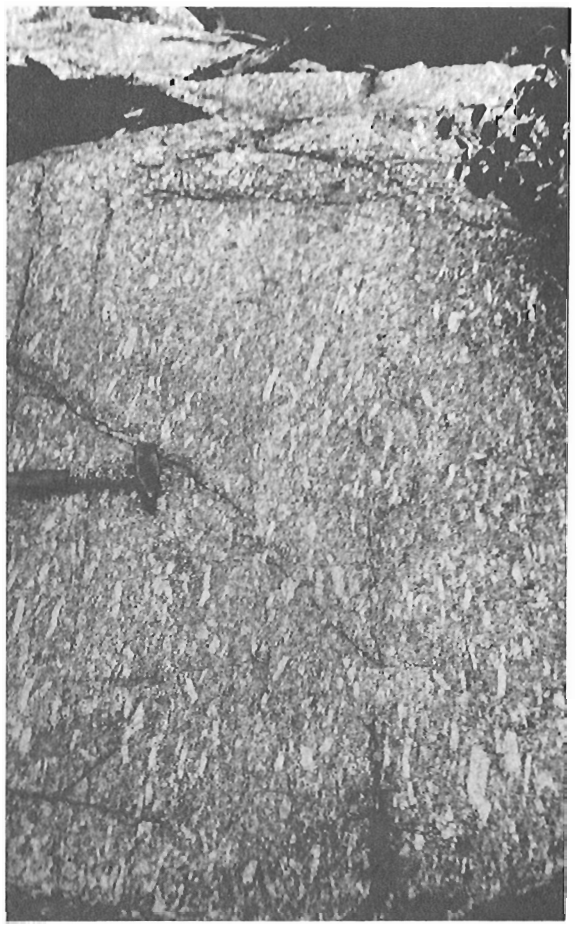

Figure 13.3. *Surface of exposure showing finite extension lineation in foliation (XY) plane, marked mainly by potassium feldspar megacrysts.*

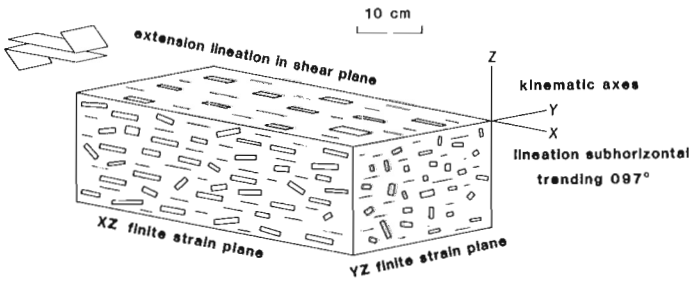

Figure 13.4. *Schematic diagram showing arrangement of exposure surface and vertical joint faces with respect to finite strain axes.*

strongly comminuted feldspars were ignored as in effect they behaved as part of the 'matrix'. A total of 504 measurements are plotted in Figure 13.6. The finite angle of rotation (Ø) generally increases as the axial ratio (R) increases. This is generally a reflection of the relative stability of these originally randomly oriented inclusions in simple shear: the more inequant the megacryst, the more likely it is to have rotated close to the flow plane. Even megacrysts with low R tend to lie with their long axis nearly parallel to the mylonitic flow plane. The overall distribution with respect to Ø is illustrated in the rose diagram in Figure 13.7, which is oriented parallel to the XZ plane, looking north; three to four

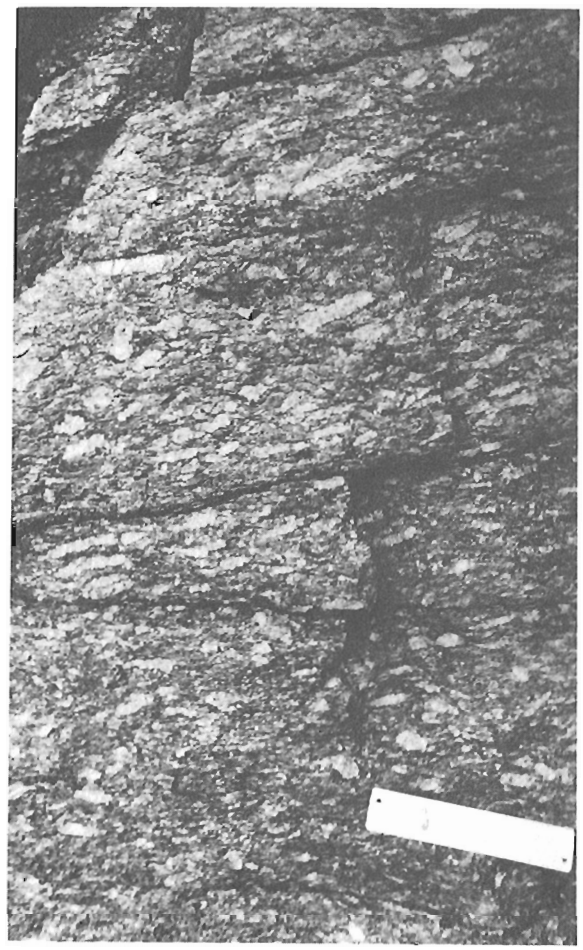

Figure 13.5. *Typical XZ surface, looking north. Scale is 15 cm long. Long axes of megacrysts lie approximately in this plane, and most are inclined at a low angle to the mylonitic foliation. Three to four times as many dip west as east.*

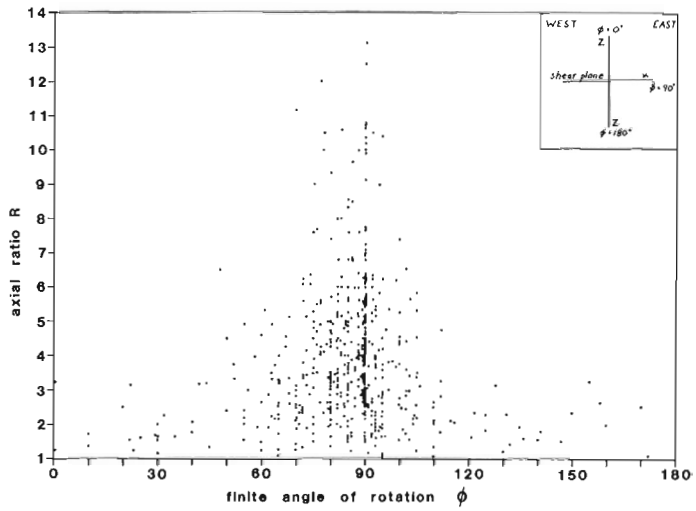

Figure 13.6. *Finite angle of rotation (Ø) of megacrysts in XZ plane in relation to their axial ratio (R). Note that the more equant inclusions (R<3) have little orientation bias; this is compatible with simple shear accompanied by a component of pure shear flattening.*

times as many dip west as east. If the orientation bias reflects rotation during progressive simple shear, it implies west over east shearing parallel to the mylonitic flow plane.

The comparatively high number of megacrysts in the range between $\emptyset = 90°$ and $\emptyset = 115°$ is explicable in terms of a simultaneous component of pure shear flattening parallel to the shear zone (Ghosh and Ramberg, 1976).

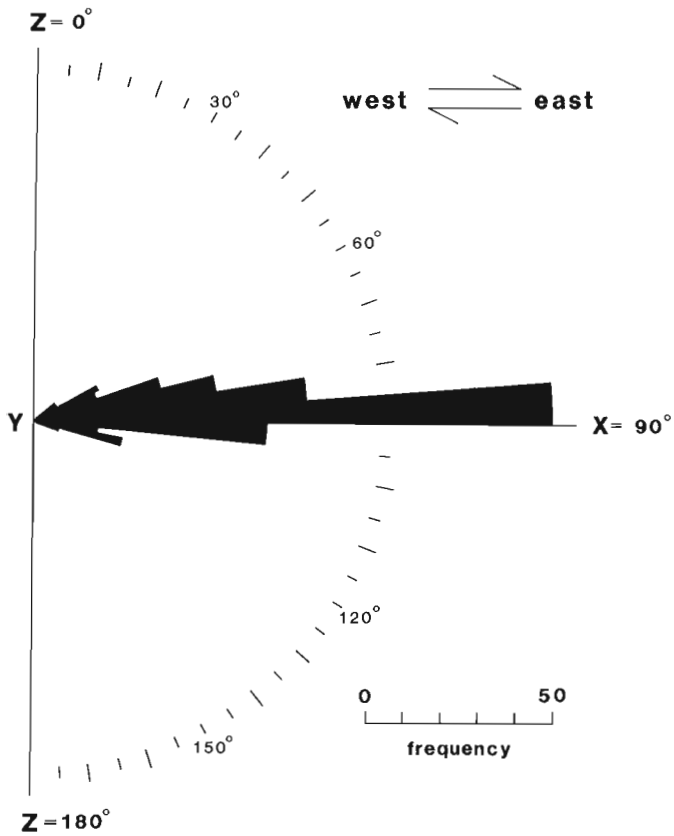

Figure 13.7. *Rose diagram illustrating orientation distribution of megacrysts in XZ, looking north.*

In at least two separate places in the same exposure (XZ planes of the finite strain ellipsoid) a discrete ductile shear zone about 12 cm thick marks a discontinuity in the shear strain (Fig. 13.8). The shear zone consists of many fine, parallel micaceous layers which are the metamorphic derivative of highly strained potassium feldspar, and milky white quartz. For about 50 cm below it, megacrysts, quartz ribbons and micas define a fabric that is not parallel to the shear zone and the general mylonitic foliation elsewhere, but inclined at about 20°, dipping west. This fabric represents the XY plane of finite strain after a relatively small amount of progressive simple shear; that it dips west implies rotation to the east.

Another useful kinematic indicator is shear band foliation, which forms during mylonitization after a strong anisotropy has been produced (White et al., 1980). It is generally inclined at 30 ± 5° to the plane of shear (Fig. 13.9), in a position corresponding to 120° in Figure 13.7. Moderately well developed shear bands have been identified in the Quesnel Lake Gneiss. They indicate a sense of shear consistent with the other observations. The shear bands seem to propagate from the corners of the feldspar porphyroclasts and extend for a few centimetres before attenuating into the shear plane. That they are not pervasive and do not crenulate the mylonitic layering demonstrates that they are synkinematic and not a superimposed cleavage or kink feature.

Attempts to deduce the sense of shear in mylonitic rocks from other parts of the boundary in the study area have been unsatisfactory. To the southeast where the metamorphic grade is higher, feldspars in the Quesnel Lake Gneiss were ductile and there is no systematic orientation distribution; megacrysts have been rounded by dynamic recrystallization and their long axes are parallel to the mylonitic foliation. Several quartz c-axis fabric diagrams have been produced, mainly from quartz-rich mylonitic metasediments, but the fabric patterns are ambiguous.

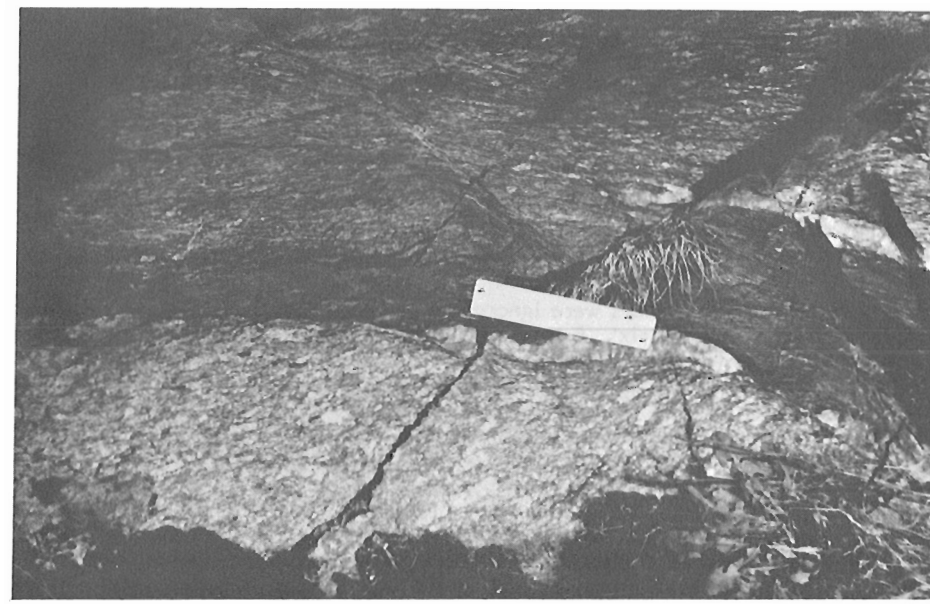

Figure 13.8

XZ face showing discrete ductile shear zone below which the XY plane of finite strain dips 15 to 20 west (see text).

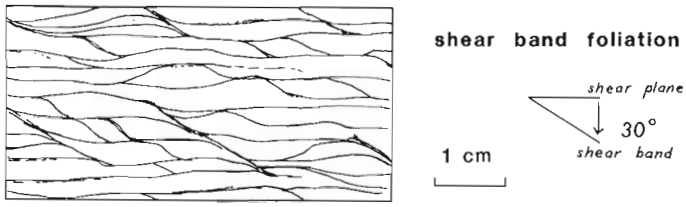

Figure 13.9. *Sketch diagram of shear band foliation indicating dextral shear. This sense of asymmetry is seen in the Quesnel Lake Gneiss in the XZ plane of finite strain, looking north.*

Concluding Remarks

Several kinematic indicators in a mylonitized orthogneiss from the area of the Omineca-Intermontane tectonic boundary imply a west over east sense of shear. This is consistent with the geological evidence that the Intermontane Belt has been transported eastwards on a flat fault over continental margin sedimentary rocks (cf. Campbell et al., 1973; Montgomery, 1978). The displacement occurred in Early to Middle Jurassic time and predates southwesterly-directed folds (also Struik, 1981) and the Middle Jurassic peak of regional metamorphism.

The determined displacement vector has only limited regional application because the mylonitic contact rocks have been folded non-coaxially at least twice and so have sustained some rotation. Elsewhere, mylonitic stretching directions are northeast or southeast. More observations are needed to establish the regional sense of shear.

Acknowledgments

The authors gratefully acknowledge funding from the Natural Sciences and Engineering Research Council of Canada through operating grant A2693 to R.L. Brown. Part of the study is the subject of a B.Sc. Thesis (Carleton University, 1982) by F. Ferri and continuing research on this problem is part of a doctoral thesis by C. Rees of Carleton University.

References

Bailey, D.G.
1978: The geology of the Morehead Lake area, south-central British Columbia; unpublished Ph.D. thesis, Queen's University, Kingston, Ontario, 198 p.

Campbell, K.V.
1971: Metamorphic petrology and structural geology of the Crooked Lake area, Cariboo Mountains, British Columbia; unpublished Ph.D. thesis, University of Washington, Seattle, U.S.A., 192 p.

Campbell, K.V. and Campbell, R.B.
1970: Quesnel Lake map-area, British Columbia (93A); in Report of Activities, Part A, April to October, 1969, Geological Survey of Canada, Paper 70-1, p. 32-35.

Campbell, R.B.
1978: Quesnel Lake, British Columbia; Geological Survey of Canada, Open File 574.

Campbell, R.B., Mountjoy, E.W., and Young, F.G.
1973: Geology of McBride map-area, British Columbia; Geological Survey of Canada, Paper 72-35, 104 p.

Ghosh, S.K. and Ramberg, H.
1976: Reorientation of inclusions by combination of pure shear and simple shear; Tectonophysics, v. 34, p. 1-70.

Hall-Beyer, B.M.
1976: Geochemistry of some ocean-floor basalts of central B.C.; unpublished M.Sc. thesis, University of Alberta, Edmonton, 103 p.

Montgomery, S.L.
1978: Structural and metamorphic history of the Lake Dunford map-area, Cariboo Mountains, British Columbia: ophiolite obduction in the southeastern Canadian Cordillera; unpublished M.Sc. thesis, Cornell University, Ithaca, New York, U.S.A., 170 p.

Morton, R.L.
1976: Alkalic volcanism and copper deposits of the Horsefly area, central British Columbia; unpublished Ph.D. thesis, Carleton University, Ottawa, 196 p.

Murphy, D.C. and Journeay, J.M.
1982: Structural style in the Premier Range, Cariboo Mountains, southern British Columbia: preliminary results; in Current Research, Part A, Geological Survey of Canada, Paper 82-1A, p. 289-292.

Murphy, D.C. and Rees, C.J.
1983: Structural transition and stratigraphy in the Cariboo Mountains, British Columbia; in Current Research, Part A, Geological Survey of Canada, Paper 83-1A, p. 245-252.

Rees, C.J.
1981: Western margin of the Omineca Belt at Quesnel Lake, British Columbia; in Current Research, Part A, Geological Survey of Canada, Paper 81-1A, p. 223-226.

Struik, L.C.
1981: A re-examination of the type-area of the Devonian-Mississippian Cariboo Orogeny, central British Columbia; Canadian Journal of Earth Sciences, v. 18, p. 1767-1775.

1982: Snowshoe Formation (1982), central British Columbia; in Current Research, Part B, Geological Survey of Canada, Paper 82-1B, p. 117-124.

1983: Bedrock geology of Spanish Lake and parts of adjoining map-areas, central B.C.; Geological Survey of Canada, Open File 920.

White, S.H., Burrows, S.E., Carreras, J., Shaw, N.D., and Humphreys, F.J.
1980: On mylonites in ductile shear zones; Journal of Structural Geology, v. 2, p. 175-187.

14.

A SUMMARY OF Rb-Sr ISOTOPE STUDIES IN THE ARCHEAN HOPEDALE BLOCK AND THE ADJACENT PROTEROZOIC MAKKOVIK SUBPROVINCE, LABRADOR: REPORT 5

Project 780025

N.K. Grant[1], F.R. Voner[2], M.S. Marzano[3],
M.H. Hickman[1] and I.F. Ermanovics,
Precambrian Geology Division

Grant, N.K., Voner, F.R., Marzano, M.S., Hickman, M.H., and Ermanovics, I.F., A summary of Rb-Sr isotope studies in the Archean Hopedale block and the adjacent Proterozoic Makkovik Subprovince, Labrador: report 5; in Current Research, Part B, Geological Survey of Canada, Paper 83-1B, p. 127-134, 1983.

Abstract

Rb-Sr isotope study of thirteen whole-rock suites of Archean and Proterozoic rocks from Hopedale block and Makkovik Subprovince shows that the crustal history began about 3115 Ma ago. We tentatively recognize younger crustal segments that formed 2920 Ma ago, from which Kanairiktok intrusives were derived at 2832 ± 178 Ma.

In Makkovik Subprovince the Island Harbour granites range in age from 1843 ± 90 to 1794 ± 71 Ma. These ages overlap with the 1847 ± 87 Ma age for Kanairiktok shear zone mylonites. The Island Harbour granodiorites from inland localities to the southwest are contaminated with Archean rocks in Makkovik Subprovince and their initial $^{87}Sr/^{86}Sr$ ratios imply a crustal contribution to their source. In contrast, the Island Harbour granites of Striped Island were derived from a mantle source.

The sills of Striped Island are 1635 ± 47 Ma old. An undeformed northeast trending Kikkertavak dolerite dyke from Hopedale block is 1206 ± 120 Ma.

Résumé

La datation aux isotopes de Rb-Sr de 13 séries de roches entières archéennes et protérozoïques du bloc de Hopedale et de la sous-province de Makkovik révèle que l'histoire de la croûte a commencé il y a environ 3 115 millions d'années. Dans la partie sud-est du bloc archéen, on identifie provisoirement des segments de croûte formés il y a 2 920 millions d'années, à partir desquels les roches intrusives de Kanairiktok ont été dérivées il y a 2 832 ± 178 millions d'années.

Dans la sous-province de Makkovik, les granites d'Islands Harbour datent de 1 843 ± 90 millions à 1 794 ± 71 millions d'années. Ces âges chevauchent celui des mylonites de la zone de cisaillement de Kanairiktok, datant de 1 847 ± 87 millions d'années. Les granodiorites d'Island Harbour au sud-ouest sont contaminées par des roches archéennes dans la sous-province de Makkovik; leurs rapports Sr^{87}/Sr^{86} initiaux laissent croire qu'elles ont été formées à partir de la croûte. Par opposition, les granites d'Island Harbour dans l'île Striped proviennent du manteau.

Les filons-couches de l'île Striped datent de 1 635 ± 47 millions d'années. Un filon non déformé de dolérite de Kikkertavak, orienté nord-est et provenant du bloc de Hopedale, date de 1 206 ± 120 millions d'années.

Introduction

The Rb-Sr geochronology summarized here is based on samples collected in July, 1980. Some details of this work are reported by Marzano (1981). Sample suites were collected from all rock units recognized during the first two years of Project 780025.

The fourth report on the project (Ermanovics et al., 1982) presented conclusions reached after four years' work on the Hopedale block, and gives the geological framework for the geochronological results. The authors recognized two stages of Archean deformation (Ermanovics et al., 1982, p. 153).

> "Stage one – the Hopedalian – resulted in NW-trending planar structures and SE-plunging linear structures in volcanic rocks (Hunt River belt and Weekes amphibolite) and in already poly-deformed tonalites and granodiorites (Maggo gneiss). . . . . Stage two – the Fiordian – resulted in NNE-SSW planar structures and mainly NE-plunging linear structures. This deformation has a sinistral shear sense as evidenced by the deflection of Hopedalian structures; it followed the deposition of Florence Lake volcanics and the emplacement of Kanairiktok intrusions. . . . .
>
> In the southern part of Hopedale block these Archean rocks and structures were deformed during the early Proterozoic and formed the Makkovik Subprovince. Deformation is associated with syn- and post-kinematic phases of the Island Harbour granite. . . . . Initially deformation was dominated by strain of pure shear type with formation of poorly defined NE-trending zones of ductile simple shear. The boundary between Archean Nain Province and Proterozoic Makkovik Subprovince is defined in rocks of Nain Province along Kanairiktok Bay where one such zone of ductile shear coincides with an amphibole isograd of Proterozoic age."

All ages quoted are based on $\lambda^{87}Rb = 1.42 \times 10^{-11} y^{-1}$, and all uncertainties are quoted to two standard deviations.

[1] Department of Geology, Miami University, Oxford, Ohio 45056, U.S.A.
[2] Department of Geology, Marietta College, Marietta, Ohio 45750, U.S.A.
[3] Mobil Oil, 1250 Poydras Building, New Orleans, Louisiana 70113, U.S.A.

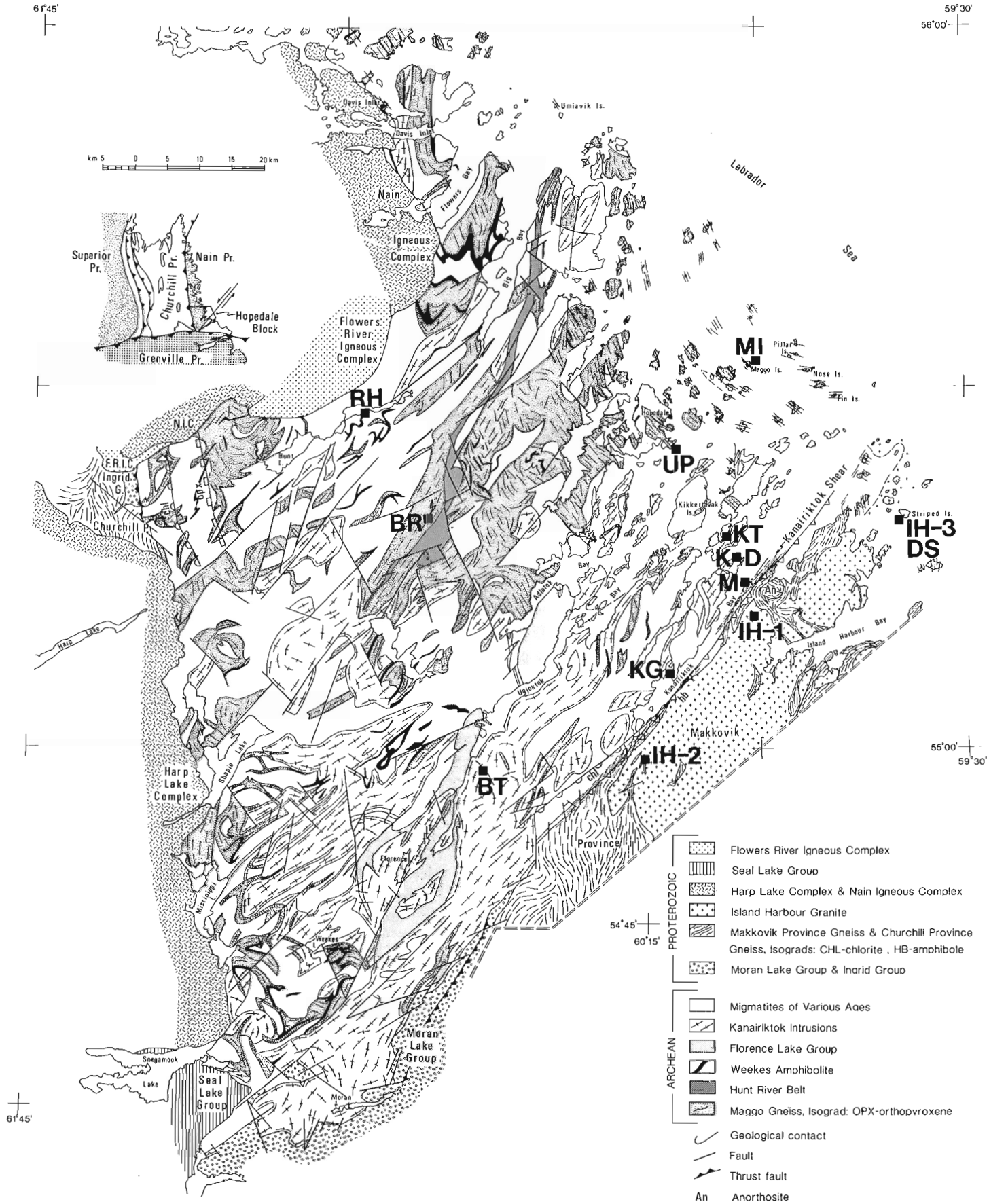

Figure 14.1. *Locations of the sample suites. The map is from Ermanovics et al. (1982).*

Acknowledgments

We are grateful to A. Davidson and J.C.M. Roddick for reviewing the manuscript. We thank the Geological Society of America, Sigma Xi and Tenneco Inc. for grants to Marzano and Voner, and the Geological Survey of Canada for supporting this work in the field.

Archean Rocks of the Nain Province

Hopedale Trend

Maggo Gneiss Three suites of rocks (MI, UP, KG, Fig. 14.1) were collected from the Maggo gneisses that are characterized by the Hopedalian structural trend. This trend is the end product of a polyphase tectonic history that includes possibly two metamorphisms, the last at upper amphibolite facies. Some parts of the Maggo gneiss have been reoriented to the Fiordian structural trend during later lower amphibolite facies metamorphism. Other parts, although affected by this metamorphism, have retained the Hopedalian trend. The three suites described here are from gneisses that have retained the Hopedalian structural trend.

The rock suite (MI) from the northeastern side of Maggo Island (Fig. 14.1) was collected from layered tonalitic gneisses in an assemblage which includes concordant amphibolitic to ultrabasic lenses, and concordant and discordant pegmatite sheets. This age is 2704 ± 74 Ma, with an initial $^{87}Sr/^{86}Sr$ ratio of 0.7035 ± 2 (Fig.14.2a).

The second suite (UP) comes from Uivak Point (Fig. 14.1), and is a collection of two phases of the Maggo gneiss of which the more leucocratic variety appears to be younger. The gneisses are tonalitic, are weakly layered and enclose concordant amphibolite sheets and slightly discordant pegmatites. Rocks from this suite and those from Maggo Island show traces of retrograde adjustment to upper greenschist facies conditions. The age of Uivak Point suite is 3022 ± 110 Ma, with an initial $^{87}Sr/^{86}Sr$ ratio of 0.7019 ± 2 (Fig. 14.2b).

The third suite (KG), from the northern shore of the southwestern end of Kanairiktok Bay (Fig. 14.1), is of layered tonalitic to dioritic gneisses. Its age is 3025 ± 102 Ma, with an initial $^{87}Sr/^{86}Sr$ ratio of 0.7002 ± 12 (Fig. 14.2c).

Fiord Trend

Maggo Gneiss Ermanovics et al. (1982) concluded that the main rock types having the Fiordian trend are reoriented and reworked equivalents of Hopedalian rocks. This younger deformation was accompanied by epidote-amphibolite facies metamorphism. Widespread intrusion of tonalite-granodiorite (Kanairiktok intrusions, Fig. 14.1) preceded the deformation.

Strongly layered gneisses (BR), exposed in a river bed east of the Hunt River belt (Fig. 14.1), range from granodiorite through tonalite to amphibolite. The rocks, particularly the amphibolites, are more strongly affected by retrograde greenschist facies metamorphism than the felsic gneisses. A suite containing all rock types gave an age of 3226 ± 106 Ma, with an initial $^{87}Sr/^{86}Sr$ ratio of 0.7000 ± 8 (Fig. 14.3a). The relationship of these gneisses to the volcanogenic rocks of the Hunt River belt is problematical (cf. Jesseau, 1976); the amphibolite gneisses may be derivatives of the Hunt River rocks, or they may be unrelated and either older or younger.

The second suite (RH) comes from a bedrock trench cut in weakly layered and strongly retrograded gneisses exposed on a hill at an abandoned radar station east of the Hunt River (Fig. 14.1). Epidote, clinozoisite, and penninite are abundant

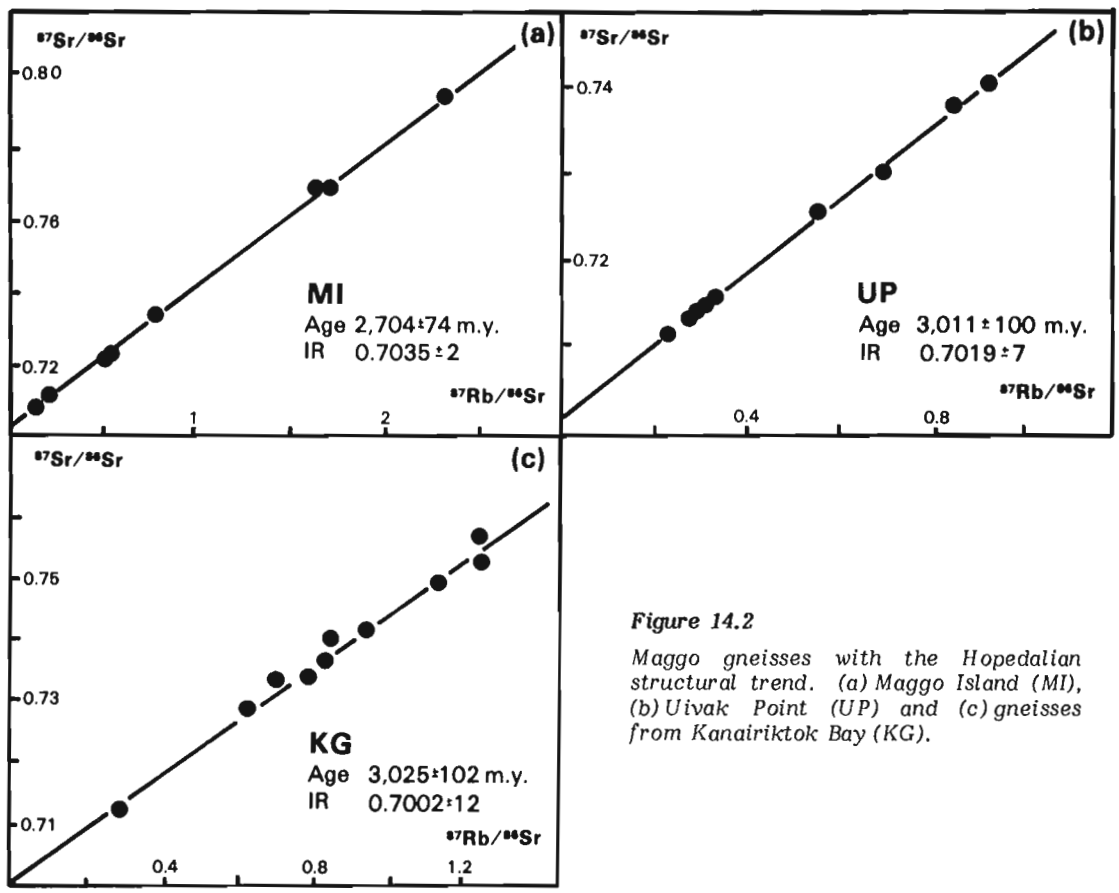

Figure 14.2

Maggo gneisses with the Hopedalian structural trend. (a) Maggo Island (MI), (b) Uivak Point (UP) and (c) gneisses from Kanairiktok Bay (KG).

Table 14.1

Sample Suite Fig. 14.1	Lithology	Structural Domain	Age in Ma and initial $^{87}Sr/^{86}Sr$ Ratios (This Work)	Other ages in Ma and Footnotes
UP	Maggo gneiss	Hopedalian	3011 ± 110 0.7019 ± 2	ca. 3050, U-Pb zircon (1)
KG	Maggo gneiss	Hopedalian	3025 102 0.7002 ± 12	
MI	Maggo gneiss	Hopedalian	2704 ± 74	(2)
BR	Maggo gneiss	Fiordian	3226 ± 106 0.7000 ± 8	
KT	Kanairiktok intrusion	Fiordian	2832 ± 178 0.7019 ±	ca. 2820, U-Pb zircon (3)
K	Kanairiktok intrusion	Fiordian	2762 ± 118 0.7030 ± 4	
BT	Kanairiktok intrusion	Fiordian	2453 ± 232 0.7043 ±	1860 ± 60 hornblende K-Ar (4)
IH-1	Island Harbour granite	Late synkinematic Makkovikian	1843 ± 90 0.7043 ± 3	
IH-2	Island Harbour granite	Late synkinematic Makkovikian	1974 ± 71 0.7044 ± 3	
IH-3	Island Harbour granite	Post kinematic Makkovikian	1805 ± 42	
M	Mylonite	Kanairiktok shear zone; post Island Harbour granite	1847 ± 87 0.7070 ± 5	
DS	Diorite dykes and sills	Post Island Harbour granite and the Kanairiktok shear zone	1635 ± 47 0.7027 ± 3	ca. 1640 ± 59, Rb-Sr whole-rock (5)
D	Kikkertavak diabase dykes	Post Fiordian in Nain Province	1206 ± 120 0.7074 ± 5	ca. 2200 ± 55 Rb-Sr whole-rock (6)
RH	Maggo	Fiordian	No age regression possible gneiss (see Fig. 14.3b)	

(1) The preliminary U-Pb zircon discordia age for three zircon fractions is ca. 3050 Ma; two additional zircon fractions lie beneath this discordia. All the zircons are small and rounded, and those that define the discordia age are zoned (W.D. Loveridge, personal communication, 1982). The zircons are clearly disturbed and the isotopic data may reflect both the timing of high grade metamorphism and possibly some evidence for an older premetamorphic age.

(2) Maggo gneisses with discordant mica-bearing pegmatites which may be younger than Fiordian deformation.

(3) Discordia U-Pb zircon age, preliminary data (W.D. Loveridge personal communication, 1982).

(4) GSC, K-Ar 3224 (R.D. Stevens, personal communication, 1982). The hornblende was obtained from the unaltered central part of an amphibolite xenolith whose margins and the host Kanairiktok intrusive were sheared to chlorite-epidote grade.

(5) B.J. Fryer, Memorial University of Newfoundland, personal communication, 1982.

(6) The younger age strengthens the correlation of part of the Kikkertavak dyke swarm in the Archean Hopedale block with the Harp dykes which also intrude the Harp Lake Complex (Emslie, 1980). The older age is of a layered, plagioclase porphyry, gabbroic diabase (B.J. Fryer, personal communication, 1982).

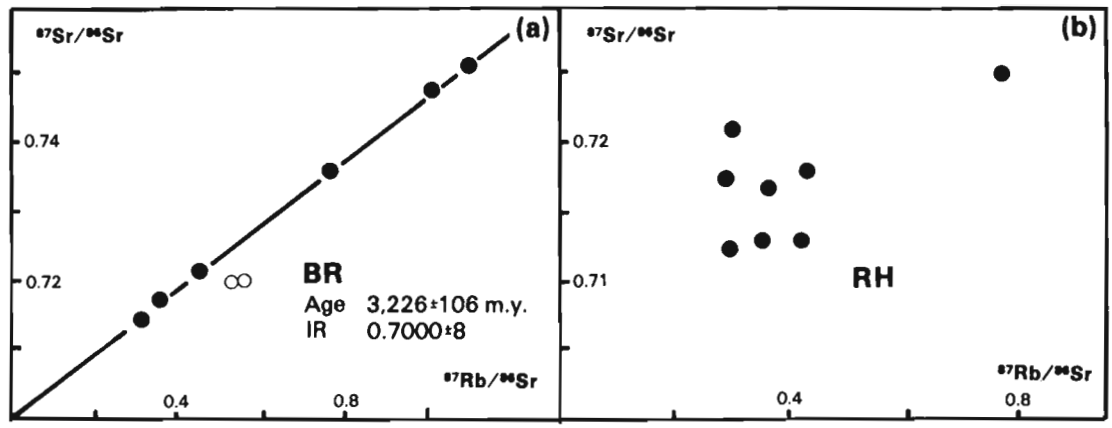

Figure 14.3. *Maggo gneisses with the Fiordian structural trend. (a) Layered gneisses from west of the Hunt River belt (BR), and (b) retrograded gneisses from the abandoned radar station (RH). In all cases the age regressions are based only on the samples shown as solid circles. Open circles identify isotopically disturbed samples.*

in these rocks, in some of which plagioclase is completely altered. Some samples from this locality contain as much as 20 per cent chloritized hypersthene and diopside. The Rb-Sr isotope systematics of the suite are strongly disturbed and are not suitable for age regression (Fig. 14.3b).

Kanairiktok Intrusions The Kanairiktok intrusions, of tonalite to granodiorite composition, were emplaced as pre- and syn-kinematic plutons relative to the regional epidote-amphibolite facies metamorphism accompanying the formation of the Fiordian structures. The intrusions are associated with widespread migmatite development and metasomatic differentiation. A late chlorite-epidote metamorphism of possible Proterozoic age affects much of the map area and is particularly noticeable in the Kanairiktok intrusive rocks.

A suite from one of the most northeasterly intrusions (KT), comes from an island (informally named Diorite Island) immediately north of the entrance to Kanairiktok Bay (Fig. 14.1). The homogeneous tonalites possess a moderately steep northeasterly plunging linear fabric characteristic of the Fiordian trend, and are penetrated by 0.5-2 cm epidote- and chlorite-filled fractures. The age of this suite is 2832 ± 178 Ma, with an initial $^{87}Sr/^{85}Sr$ ratio of 0.7030 ± 4 (Fig. 14.4b).

The second suite (K) was collected from the northern shore of Kanairiktok Bay, close to the entrance to the Bay (Fig. 14.1). As at Diorite Island, the rocks are not layered, and also show the effects of retrograde greenschist facies metamorphism associated with shearing along the northern shore of Kanairiktok Bay. The age of this suite is 2763 ± 118 Ma, with an initial $^{87}Sr/^{86}Sr$ ratio of 0.7030 ± 4 (Fig. 14.4b).

The third suite (BT) comes from the head of Ugjoktok Bay (Fig. 14.1); it contains rocks that are distinct from the others both in composition (granodiorite) and in their deformed textures. Strongly flattened and elongaged biotite aggregates characterize these rocks, which also show the effects of greenschist retrogression. The range in Rb-Sr ratios of this suite is extremely limited, and the age is 2453 ± 232 Ma, with an initial $^{87}Sr/^{86}Sr$ ratio of 0.7043 ± 8 (Fig. 14.4c). The difference between this age and those for the other Kanairiktok suites, and the high initial $^{87}Sr/^{86}Sr$ ratio, suggest that this age reflects partial metamorphic resetting during the Proterozoic (Table 14.1).

Discussion of the Results for the Archean Rocks

It is far from clear how the Rb-Sr ages for the Maggo gneisses relate to the geological framework. For instance, the youngest age (MI, 2704 ± 74 Ma) comes from Maggo gneisses with Hopedalian trend, and the oldest (BR, 3227 ± 206 Ma) from Maggo gneisses adjacent to the Hunt River belt with Fiordian trend. The conventional view is that Rb-Sr isochrons in high grade gneisses reflect the timing of metamorphic events. In this connection we emphasize the differences between the two assemblages of Maggo gneisses. Near the Hunt River belt they are part of a terrane lacking the variety of younger mica-bearing pegmatites present on Maggo Island, possibly younger than Fiordian deformation. By themselves these observations do not address the question of the genetic relationship between the Maggo gneisses adjacent to the Hunt River belt and those on Maggo Island, but they do provide the context for the conclusion that the Maggo Island gneisses analyzed by us record a 2700 Ma old metamorphism, even though structural observations have led to the conclusion that the gross features of these gneisses were formed during the oldest of the structural events preserved in the Hopedale block (Ermanovics et al., 1982). From the same point of view the survival of a 3226 ± 106 Ma-old age for the gneisses adjacent to the Hunt River belt means that the bulk of our studied samples (see Fig. 14.2 for exceptions, which lie beneath the isochron) do not reflect the youngest Archean metamorphism and deformation associated with the Fiordian trend.

The question of the genetic connection between the different regions of Maggo gneisses can be assessed through the relationships between the ages and the initial $^{87}Sr/^{86}Sr$ ratios as on the strontium evolution diagram (Fig. 14.5). The Archean rocks show the inverse correlation between the ages and the initial $^{87}Sr/^{86}Sr$ ratios to be expected of a terrane modified during an extended history of metamorphic and anatectic events. The intersection of this correlation with the evolution line for the reference mantle, here taken to be the bulk Earth (Zindler et al., 1982), implies that the Archean rocks separated from the mantle 2900 to 3100 Ma ago. This conclusion is not sensitive to the assumption that the Archean subcontinental mantle under the Hopedale block was chemically and isotopically equivalent to the bulk Earth (see McCulloch and Compston, 1981, for an example of the recognition of Archean depleted mantle), or to the assumption that the Hopedale block rocks have behaved isochemically during their crustal history. For example, the

extreme assumption that the Hopedale block was underlain in Archean times by mantle equivalent to the most depleted mantle now detected under mid-oceanic ridges, would increase the estimate of the mantle extraction ages by a maximum of 120 Ma. Archean mantle of such depleted type has not yet been recognized. Similarly, the influence of Rb metasomatism on the crustal residence times for the Hopedale rocks must be negligible in view of the low initial $^{87}Sr/^{86}Sr$ ratios for the BR and KG suites. The only process which could significantly increase the crustal residence times of the Maggo gneisses beyond 3100 Ma would be the regional open-system exchange of the strontium in the gneisses with strontium in some nonradiogenic reservoir, an extreme hypothesis which we cannot justify for the Hopedale rocks. These considerations cause us to conclude that the Rb-Sr geochronology of the Archean gneisses does not support the speculation that the Hopedale dykes may be analogous to the Saglek dykes of northern Labrador and the Ameralik dykes of West Greenland which are emplaced into very early Archean rocks (Ermanovics et al., 1982).

The only elaboration which we consider possible for the crustal history of the Maggo gneisses is that they come from two crustal segments, with slightly different mantle extraction times (Fig. 14.5). The older segment is defined by the gneisses from west of the Hunt River belt (BR) and Uivak Point (UP) to the northwest with a crustal extraction age of 3115 Ma, defined by the intersection of the evolution line joining these two suites and the mantle evolution line. The younger segment is defined by the suites from Kanairiktok Bay (KG), Maggo Island (MI) and the Kanairiktok intrusives (KT, K, BT) to the southeast with a mantle extraction age of 2920 Ma. The data suggest that the tonalitic to granodioritic magmas of the Kanairiktok intrusives were derived from the younger crustal segment. Their subsequent emplacement around 2800 Ma is reflected in the agreement between our results and a U-Pb zircon age of 2830 Ma (Table 14.1) for the tonalites of Diorite Island. Very low Rb/Sr ratios in some of these tonalites, which in the case of the KT suite are too low to account for the initial $^{87}Sr/^{86}Sr$ ratio within the age of the Earth (Fig. 14.5), probably reflect the origin of these rocks as plagioclase cumulates.

Proterozoic Rocks of the Makkovik Subprovince

Island Harbour Granites

All the gneisses of the Nain Province were intruded by the Kikkertavak gabbro and diabase dykes, probably during the Proterozoic. To the east of Kanairiktok Bay these gneisses and dykes were deformed and metamorphosed to upper greenschist or lower amphibolite facies. This new structural fabric is used to define the Proterozoic Makkovik Subprovince. The Island Harbour granites are late synkinematic and postkinematic intrusions within the gneisses. Mylonites of the major Kanairiktok shear zone occur along the eastern shore of Kanairiktok Bay. The shear zone cuts the Island Harbour granites and has downgraded the earlier Proterozoic metamorphism.

Three suites were collected from the Island Harbour granites, two (IH-1, IH-2) from inland localities, and one (IH-3) from Striped Island to the northeast (Fig. 14.1). Both inland localities consist of weakly foliated granites and granodiorites which include enclaves of gneissic rocks. The IH-1 suite gives an age of 1843 ± 90 Ma, with an initial $^{87}Sr/^{86}Sr$ of 0.7044 ± 3 (Fig. 14.6a). The IH-2 suite gives an age of 1794 ± 71 Ma, with an initial ratio of 0.7044 ± 3 (Fig. 14.6b). Both suites include samples which lie above these isochrons, and which have late Archean model ages. One is a gneissic tonalite, the others appear to be mineralogically and chemically similar to the granodiorites and are presumed to be contaminated with Archean rocks.

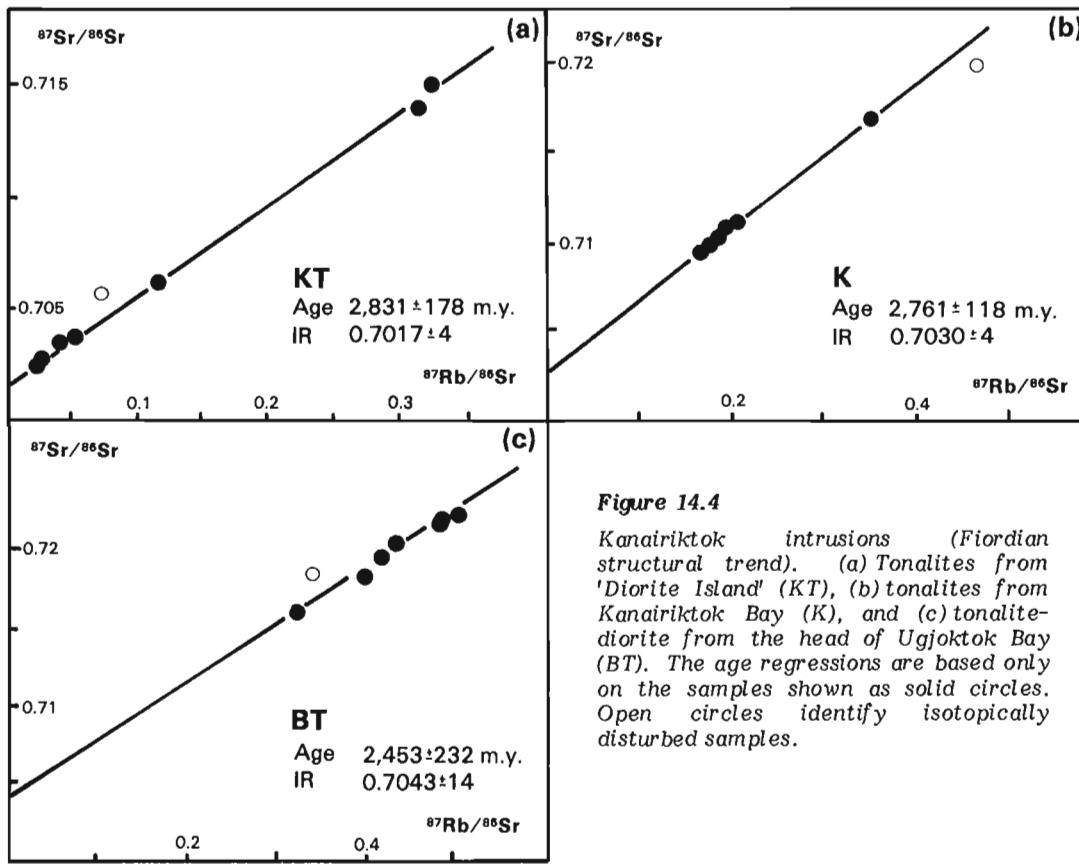

Figure 14.4

Kanairiktok intrusions (Fiordian structural trend). (a) Tonalites from 'Diorite Island' (KT), (b) tonalites from Kanairiktok Bay (K), and (c) tonalite-diorite from the head of Ugjoktok Bay (BT). The age regressions are based only on the samples shown as solid circles. Open circles identify isotopically disturbed samples.

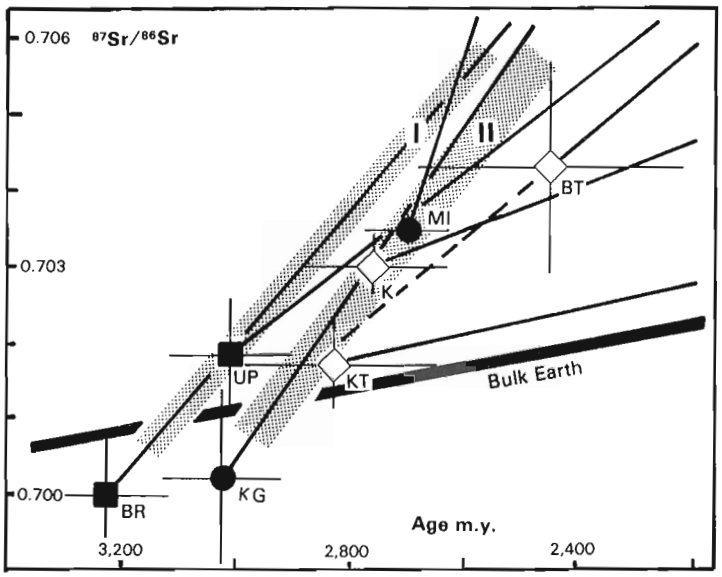

Figure 14.5. *The relations between the ages and initial $^{87}Sr/^{86}Sr$ ratios for the Archean rocks, compared with reference mantle with a bulk Earth Rb-Sr ratio. The choice of a depleted mantle with Rb-Sr ratios less than that of the bulk Earth does not significantly change the implications of this diagram (see the text for a further discussion of this point). The stippled lines (I, II) mark the two crustal segments tentatively identified in the text.*

The Island Harbour granite on Striped Island consists of two phases. The oldest is a massive coarse porphyritic granite, the youngest a medium grained grey granite which is intrusive into the first. The age of a suite (IH-3) based on both phases is 1805 ± 42 Ma, with an initial $^{87}Sr/^{86}Sr$ of 0.7020 ± 15 (Fig. 14.6c). A second suite (DS) from Striped Island was collected from the subhorizontal diorite sills conspicuous on the island and elsewhere. Their age is 1635 ± 47 Ma, with an initial ratio of 0.7027 ± 3 (Fig. 14.7a; cf. Table 14.1).

Kanairiktok Shear Zone Mylonites

A suite (M) of mylonites sampled from a single locality on the southwestern side of a small island off the southern shore of Kanairiktok Bay (Fig. 14.1) has given an age of 1847 ± 87 Ma, with an initial $^{87}Sr/^{86}Sr$ of 0.7074 ± 5 (Fig. 14.6d). Two of the eight samples lie above this isochron, perhaps on a subparallel line, and show that strontium isotope homogenization in the mylonite at the time of its formation was achieved only locally within chemically and isotopically distinct rock volumes.

Kikkertavak Dykes

The name Kikkertavak is applied to all undeformed northeast-trending gabbroic and diabase dykes that cut the youngest structural fabric (Fiordian) in the Archean Nain Province. Ermanovics et al. (1982) have postulated that Kikkertavak dykes represent several generations of early (pre-Island Harbour granite) and late Proterozoic basic dykes.

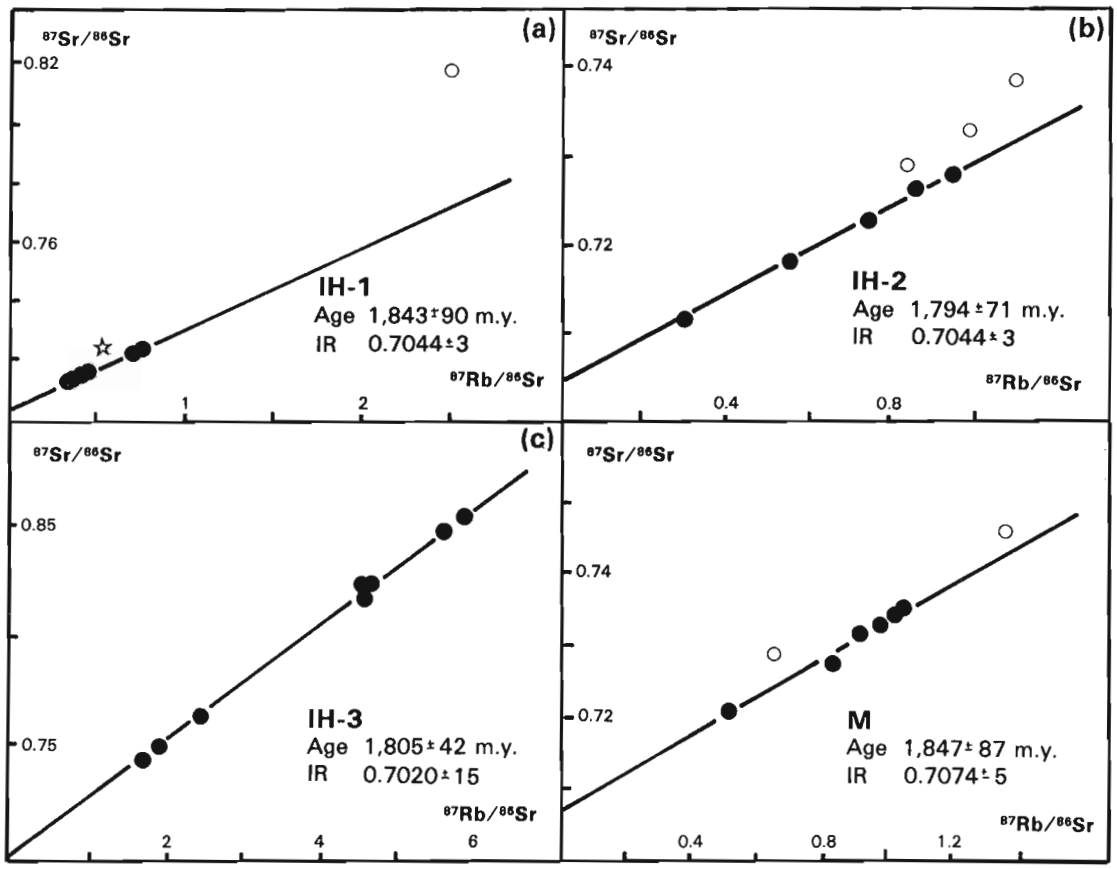

Figure 14.6. *Island Harbour granites. (a) Inland granodiorite (IH-1), the star is a foliated tonalite xenolith and the open circle is a contaminated granodiorite; (b) inland granodiorite (IH-2), the open circles are contaminated granodiorites; (c) Striped Island granite (IH-3), and (d) Kanairiktok shear zone mylonites. The age regressions are based on samples shown as solid circles only.*

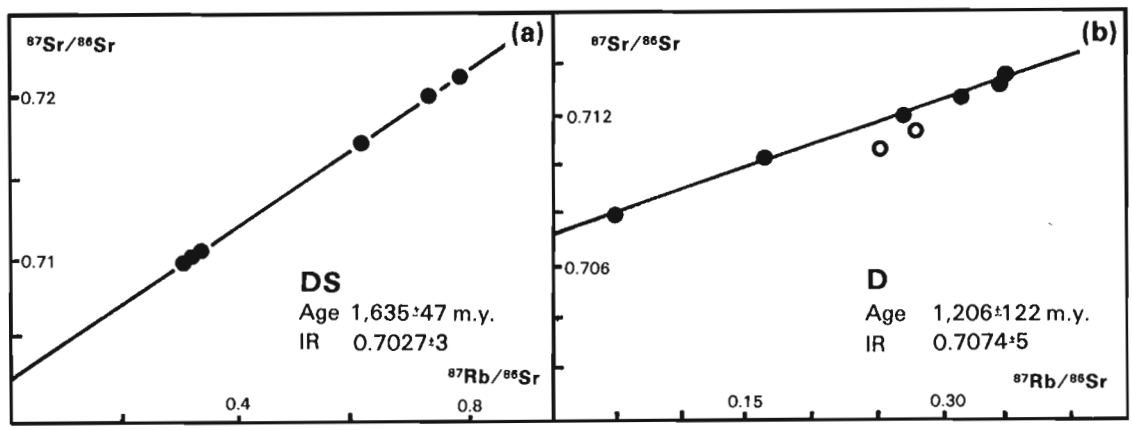

Figure 14.7. *Late intrusives. (a) Striped Island diorite sill (DS) that intrudes the Island Harbour granite, and (b) diabase dyke (D) from the western side of Kanairiktok Bay in Nain Province. The open circles are samples interpreted as having been contaminated by nonradiogenic Kanairiktok tonalite. The age regressions are based only on the samples shown as solid circles.*

A diabase dyke (D) was sampled from a small island off the northern shore of Kanairiktok Bay, where the northern contact of the more than 20 m wide dyke is exposed (Fig. 14.1). The dyke is undeformed except for chlorite- and epidote-filled fractures which are mostly a few millimetres wide. Minor deuteric alteration has affected the plagioclase and the clinopyroxene. The age of this dyke is 1206 ± 120 Ma, and the initial $^{87}Sr/^{86}Sr$ is 0.7074 ± 5 (Fig. 14.7b). Two samples lie under this isochron and appear to be contaminated with nonradiogenic Kanairiktok tonalite which is intruded by the dyke at this locality.

An age of 2200 ± 55 Ma was obtained from a layered gabbroic diabase located on the south side of Cross Island immediately east of Kikkertavak Island (Fig. 14.1), (B.J. Fryer, Memorial University of Newfoundland, personal communication, 1983). Both this and the younger age confirm the original hypothesis that the Kikkertavak 'swarm', comprises more than one generation of dykes.

Discussion of the Results for the Proterozoic Rocks

The ages for the Island Harbour granites and the Kanairiktok shear zone mylonites are indistinguishable within the limits of uncertainties, indicating that the shearing and granite emplacement are closely related in time. The ages also provide a minimum estimate for the age of the structural fabric of the Proterozoic Makkovik Subprovince which predates both the Kanairiktok shear zone and the Island Harbour granites. The results confirm the identification of Archean rocks in the Makkovik Subprovince (Ermanovics et al., 1982), because the two inland suites of granodiorite include a gneiss xenolith and contaminated granodiorites (Fig. 14.6a, b) with model ages in the range 2300-3100 Ma. This crustal contribution to the inland granodiorites can be recognized in two ways. The uniform initial $^{87}Sr/^{86}Sr$ ratios of the granodiorites are elevated above the ratio (0.7027) for contemporaneous mantle with a bulk Earth Rb/Sr ratio, and this difference together with the uniformity of the initial ratios implies that the crustal contribution has been efficiently homogenized, probably in the source region of the granodiorities. The presence of Archean gneiss xenoliths and granodiorities in samples with varied and anomalously high initial $^{87}Sr/^{86}Sr$ ratios implies that the granodiorite magmas have been locally contaminated late in their magmatic history, perhaps close to their present structural level.

The initial $^{87}Sr/^{86}Sr$ ratio for the Striped Island granite (0.7020 ± 15) and the intrusive diorite sills (0.7027 ± 3) are indistinguishable from a mantle with a bulk Earth Rb/Sr ratio; we conclude that these rocks are magmatically unrelated to the inland granodiorities and were derived from a mantle source over the period 1805 to 1635 Ma ago.

The initial $^{87}Sr/^{86}Sr$ ratio of the undeformed Kikkertavak diabase dyke (0.7074 ± 5) is unusually but not uniquely high for continental basalts. Like other continental basalts with high initial ratios the data may not constrain the isotopic character of the mantle under the Hopedale block 1206 Ma ago, but rather reflect contamination during the ponding of basic magma in or at the base of continental crust. Such ponding may be reasonably inferred from the widely recognized equilibration of nearly all basaltic magmas to low pressure conditions.

References

Emslie, R.F.
1980: Geology and petrology of the Harp Lake Complex, central Labrador: An example of Elsonian magmatism; Geological Survey of Canada, Bulletin 293, 136 p.

Ermanovics, I.F., Korstgård, J.A., and Bridgwater, D.
1982: Structural and lithological chronology of the Archean Hopedale block and adjacent Proterozoic Makkovik Subprovince, Labrador; Report 4; in Current Research, Part B, Geological Survey of Canada, Paper 82-1B, p. 153-165.

Jesseau, C.W.
1976: A structural, metamorphic and geochemical study of the Hunt River supracrustal belt, Nain Province, Labrador; unpublished M.Sc. thesis, Memorial University of Newfoundland.

Marzano, M.S.
1981: Rb-Sr whole rock geochronology of six rock suites from the Hopedale Block, Nain Province, Labrador, Canada; unpublished M.Sc. thesis, Miami University, Ohio.

McCulloch, M.T. and Compston, W.
1981: Sm-Nd age of Kambalda and Kanowna greenstones and heterogeneity in the Archaean mantle; Nature, v. 294, p. 322-326.

Zindler, A., Jagoutz, E., and Goldstein, S.
1982: Nd, Sr and Pb isotopic systematics in a three component mantle; a new perspective; Nature, v. 298, p. 519-523.

15.

GEOCHEMISTRY AND HYDROTHERMAL ALTERATION STUDIES OF THE WHITING CREEK STOCKWORK MOLYBDENUM DEPOSIT, TAHTSA LAKE AREA, BRITISH COLUMBIA

Project 740081

M.D. Goodz[1], I.R. Jonasson and R.M. Cann[2]
Resource Geophysics and Geochemistry Division

Goodz, M.D., Jonasson, I.R. and Cann, R.M., Geochemistry and hydrothermal alteration studies of the Whiting Creek stockwork molybdenum deposit, Tahtsa Lake area, British Columbia; in Current Research, Part B, GeologicalSurvey of Canada, Paper 83-1B, p. 135-144, 1983.

Abstract

The Whiting Creek deposits on Sibola Peak, B.C. are subdivided into two major zones. A copper-molybdenum porphyry-type deposit, referred to as the "Creek Zone", is within the Whiting Creek granodiorite. The "Ridge Zone" molybdenum stockwork deposit, discussed in this paper, is associated with and alkali-calcic series granite ("quartz porphyry") which has been bisected by monzonitic intrusive rocks. Diamond drilling by the Saskatchewan Mining and Development Corp. has indicated approximately 40 000 000 tonnes of 0.10 per cent molybdenite and 0.17 per cent chalcopyrite.

Mineralized zones of the quartz porphyry contain molybdenite in veinlets and quartz stockworks with or without pyrite and chalcopyrite. Supergene enrichment is evidenced by the presence of ferrimolybdite. Lateral and vertical hydrothermal alteration is exhibited by a quartz-sericite-pyrite (phyllic) assemblage. Sericite with minor K-feldspar and kaolinite have formed at the expense of plagioclase. No ferromagnesian minerals are present.

Differentiation of a granitic magma has resulted in enrichment of SiO_2, K_2O, Al_2O_3, F, Rb and Mo, and depletion of TiO_2, total Fe, MgO and MnO. Depletion of Na_2O and CaO is probably due to hydrothermal alteration.

The main geological and lithochemical features of the Ridge Zone at Whiting Creek are typical of a stockwork molybdenum deposit of the Climax transitional-type.

Résumé

Les gisements de Whiting Creek du mont Sibola (C.-B.) sont subdivisés en deux zones majeures. Un gisement de type cuivre-porphyre à molybdène, soit celui de "Creek Zone", git au sein de la granodiorite de Whiting Creek. Le présent rapport traite du gisement de molybdène "Ridge Zone", de type stockwerk; ce dernier est associé à un granite calco-alcalin ("porphyre quartzifère") qui a été coupé en deux par des roches monzonitiques intrusives. Les forages au diamant effectués par la Saskatchewan Mining and Development Corporation indiquent la présence d'environ 40 millions de tonnes de minerai d'une teneur de 0,10 % en molybdénite et de 0,17 % en chalcopyrite.

Des zones minéralisées dans le porphyre quartzifère contiennent de la molybdénite en petits filons et des stockwerks de quartz avec ou sans pyrite et chalcopyrite. La présence de ferromolybdite indique qu'il y a eu enrichissement secondaire. Un assemblage de quartz-séricite-pyrite (phyllique) témoigne de l'action de l'altération hydrothermique latérale et verticale. La séricite, ainsi que de petites quantités de feldspath potassique et de kaolinite ont été formées aux dépens du plagioclase. Il n'y a pas de minéraux ferromagnésiens.

La différenciation d'un magma granitique a eu pour résultat l'enrichissement en SiO_2, en K_2O, en Al_2O_3, en F, en Rb et en Mo, et l'appauvrissement en TiO_2, en Fe, en MgO et en MnO total. L'appauvrissement en Na_2O et en CaO résulte probablement de l'altération hydrothermique.

Les éléments géologiques et lithochimiques principaux du gisement Ridge Zone à Whiting Creek sont caractéristiques d'un gisement en stockwerk de molybdène de type Climax transitoire.

Introduction

Regional geological mapping of the Tahtsa area was conducted by Hedley (1935) and Duffell (1959). Copper-molybdenum mineralization at Whiting Creek (Fig. 15.1) was discovered in 1964 by Kennco Explorations Western Ltd. In 1979, Saskatchewan Mineral Development Corporation (SMDC) gained control of the property and carried out further drilling and exploration in the area. Nineteen diamond-drill holes, coupled with extensive geochemical sampling and geophysical surveys, have outlined a large, low grade molybdenum deposit, the Ridge Zone (Cann, 1982; Goodz, 1982) within granitoid rocks of the Sibola Stock.

During the 1981 field season, an area of 1.5 X 0.5 km centred on the Ridge Zone was mapped at a scale of 1:50 000. Detailed studies of petrography and major and minor element chemistry were made on 37 surface rock samples, and 26 core samples from four diamond-drill holes.

General Geology

The general geology and geological formations of the Sibola Peak area are given in Figure 15.2 and Table 15.1 respectively. The most significant feature in terms of areal extent, is the Hazelton Group which comprises an andesitic

[1] Geology Department, Carleton University, Ottawa
[2] Saskatchewan Mining Development Corp., Saskatoon

pyroclastic assemblage of green crystal lapilli and lithic tuffs of early to middle Jurassic age. These rocks have been deformed into broad open folds and have been regionally metamorphosed to greenschist facies.

Rocks of the Hazelton Group were intruded by three pulses of the Bulkley intrusions at 70, 76 and 82 Ma (Carter, 1982). These late Cretaceous intrusions are composed of a series of granodiorite to quartz monzonite zoned stocks with later crosscutting dyke swarms of magmatic differentiates. At Whiting Creek, the compositionally zoned Sibola stock is dated at 78-82 Ma (M. Rebagliati, personal communication). It is represented by a biotite-hornblende granodiorite (GRDR). Within and peripheral to the GRDR stock are plugs of "quartz porphyry" (QPP) which host the molybdenum mineralization of the Ridge Zone. The rocks contain 5 to 15 per cent corroded quartz "eyes" and 5 to 15 per cent variably sericitized plagioclase phenocrysts; sericitization varies from none to complete. The groundmass consists of quartz, K-feldspar and sericite (-kaolinite) giving the unit the appearance of a quartz-plagioclase porphyritic rhyolite. Molybdenite is present in both veinlets and quartz stockworks. Locally, disseminated and vein pyrite content exceeds 1 to 2 per cent.

Table 15.1
Table of Formations

CENOZOIC		
Quaternary		
Recent and Pleistocene	Glacial debris:	till, gravel, sand
Unconformity		
MESOZOIC		
Late Cretaceous	Bulkley intrusion: (70-84 Ma)	hornblende feldspar porphry, monzonite porphyry, quartz porphyry, granodiorite-quartz diorite
Intrusive Contact		
Early to Middle Jurassic	Hazelton Group	andesitic pyroclastic rocks

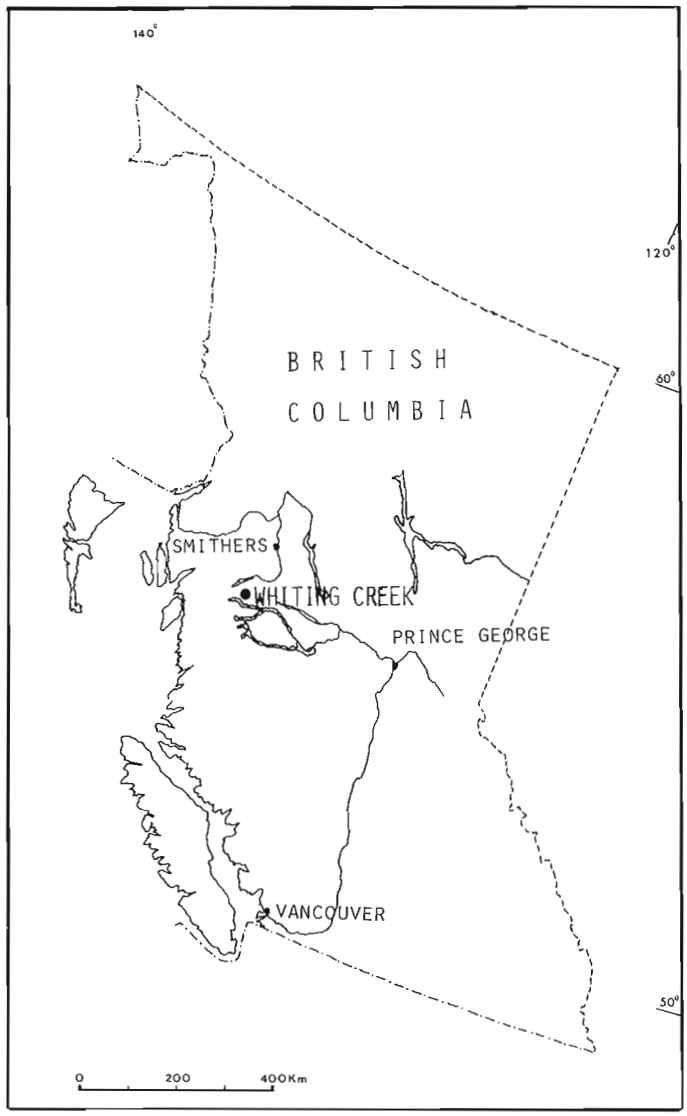

Figure 15.1. *Location map of the Whiting Creek deposits.*

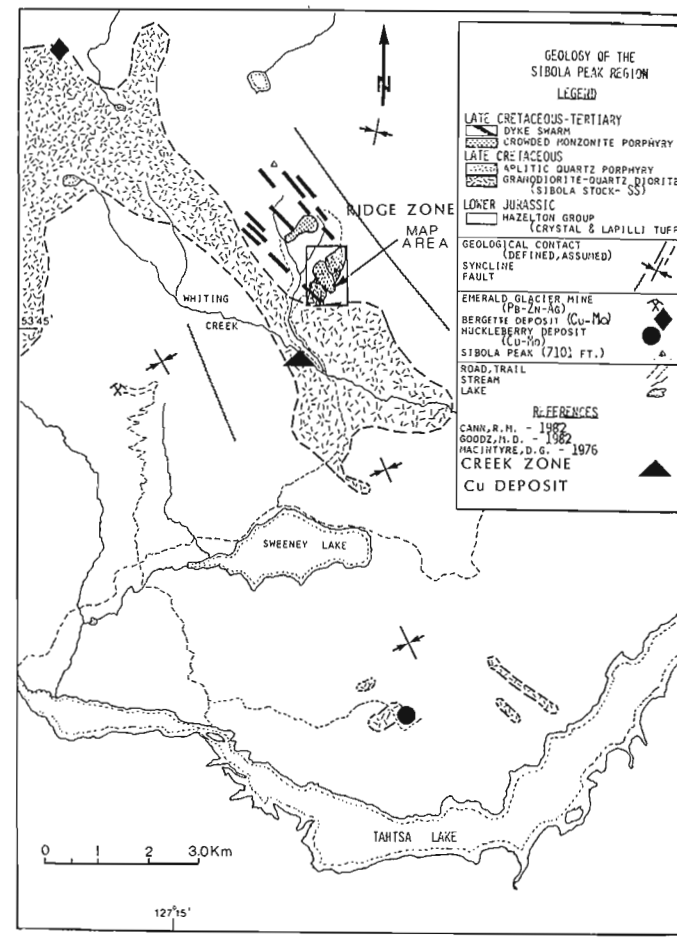

Figure 15.2. *General geology of the Sibola Peak area.*

Late northwest-trending dyke swarms have been localized in part by faults. One such dyke swarm of porphyritic monzonite (MZPP) incises and separates what was once a single mineralized QPP plug. A post-ore northwest trending dyke swarm of hornblende-feldspar porphyry (HFP) is the youngest unit in the map area.

Detailed geology of the Ridge Zone and sample locations are shown in Figures 15.3 and 15.4

Alteration

Only the phyllic alteration facies, as defined by Lowell and Guilbert (1970), was identified in the mineralized QPP. From observation of the degree of sericitization of feldspar, a qualitative scale (none-weak-fair-moderate-strong-complete) was developed to assess the extent of alteration. This interpretation, shown in Figure 15.5, yields a symmetrical zoning pattern across the pluton. Comparison of the alteration zoning with the distribution of molybdenite and pyrite suggests that this exposed "plan view" is within the pyllic alteration zone. Phenocrysts of plagioclase are replaced by mattes of sericite with minor K-feldspar and kaolinite. Sericitization of the matrix is slightly more intense adjacent to quartz veinlets. Drillhole samples exhibiting nil to fair sericitization, little pyrite, and unaltered K-feldspar phenocrysts suggest that either these rocks are unaltered or that a higher temperature potassic alteration core may exist at depth. Supergene alteration has resulted in weak limonitic staining and the formation of ferrimolybdite along Mo-rich veins.

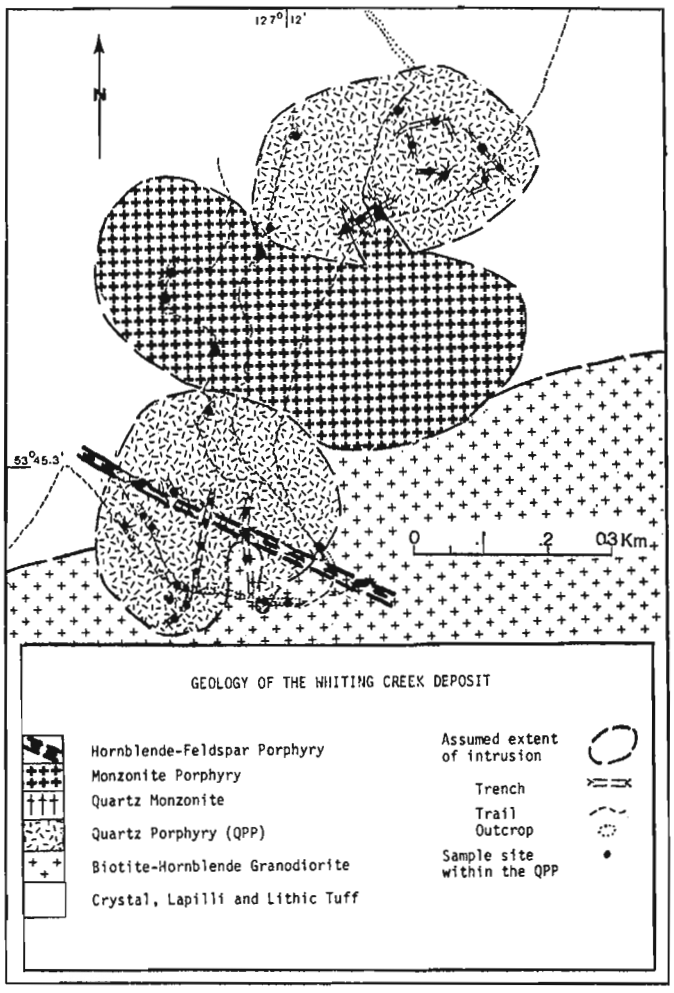

Figure 15.3. *Detailed geology of the Whiting Creek "Ridge Zone" molybdenum deposit.*

Table 15.2
Whole Rock Analyses of Bulkley Intrusions in the Whiting Creek area

	GRDR[1]	QPP[2]	MZPP[3]	HFP[4]
	Weight per cent			
SiO_2	65.2	80.1	65.7	62.7
TiO_2	0.51	0.14	0.53	0.66
Al_2O_3	15.8	11.4	15.6	16.7
Fe[5]	4.2	1.3	3.9	5.3
MgO	1.8	0.31	1.8	2.5
CaO	2.8	0.09	2.1	3.2
Na_2O	3.2	0.16	3.1	3.4
K_2O	3.6	4.3	3.4	2.7
	Parts per million			
Rb	70	84	90	70
Sr	350	51	430	500
Mo	3	218	8	4
Cu+Zn	301	34[6]	608	134
W	3	20	4	2
F	380	370	400	420

1. Granodiorite, 2 analyses
2. Quartz porphyry, 19 analyses
3. Monzonite porphyry, 5 analyses
4. Hornblende-feldspar porphyry, 3 analyses
5. Total Fe content = Fe_2O_3 + FeO
6. Cu = 20 ppm, Zn = 14 ppm
7. The GRDR and MZPP units are differentiated by texture, quantity of visible quartz and degree of alteration, using SMD (Mining) Co. nomenclature even though columns 1 and 3 indicate they may be of similar composition.

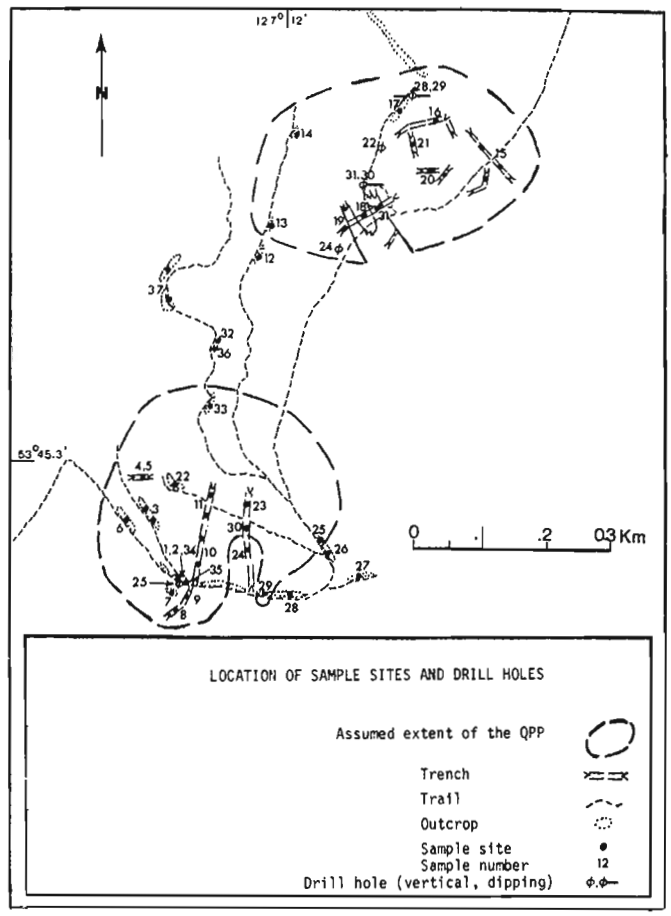

Figure 15.4. *Sample and drill hole location map.*

The phyllic alteration appears to be symmetrically distributed between the two QPP bodies, supporting the concept of a single pluton that was later intruded by MZPP. The degree of sericitization (Fig. 15.5) is not coincident with the development of the quartz stockwork which is reflected in the variation of SiO_2 content of the QPP shown in Figure 15.6. Selection of samples of chemical analyses was restricted to specimens showing the least surface bleaching and quartz stockwork development; however high silica values are representative of stockwork-rich specimens.

Lithochemistry of the deposit

Major, minor, and trace element content of QPP was investigated in order to: (1) relate zoning patterns of major oxides and trace elements to hydrothermal alteration and mineralization; (2) chemically identify highly altered and weathered rocks; (3) define a suitable model of magma genesis and classify the type of deposit based on characteristic chemical features.

Major oxide analyses by X-ray fluorescence(XRF) and minor and trace element analyses by atomic absorption spectrometry (AAS), colourimetry and ion-selective electrode were performed on 33 samples. Data are listed in Appendices 15.1 and 15.2

Major Element Chemistry

Although relatively unaltered rocks were prefered for chemical analysis, it is apparent that no rocks have escaped some degree of hydrothermal or supergene alteration. Consequently, only the mean values derived from all analyses will be compared with average data of similarly altered plutons taken from the literature. Comparison of chemistry of samples containing the least silica with degree of alteration, had a poor correlation. The two least silica-rich specimens (03 and 08) were clearly associated with moderate alteration, had irregular Fe, Mg and Ti contents, and thus were excluded from consideration for reasons of Fe-Mg contamination. It is believed that the sample numbers on analyzed specimens 35 and 36 were interchanged, hence these analyses have also been excluded.

There is no obvious correlation between Na_2O content and K_2O, SiO_2, or degree of alteration. Due to alteration of plagioclase, Sr depletion has contributed to the "positive" Rb/Sr ratio of 1.64, (i.e., greater than 1).

Minor Element Chemistry

Minor element analyses (Appendix 15.2) show the altered QPP contains only trace amounts of tungsten, copper, zinc, lead and silver. In many samples, tungsten values exceeded those of copper. Figure 15.10 show only those areas of greater than 0.05 per cent Mo, even though

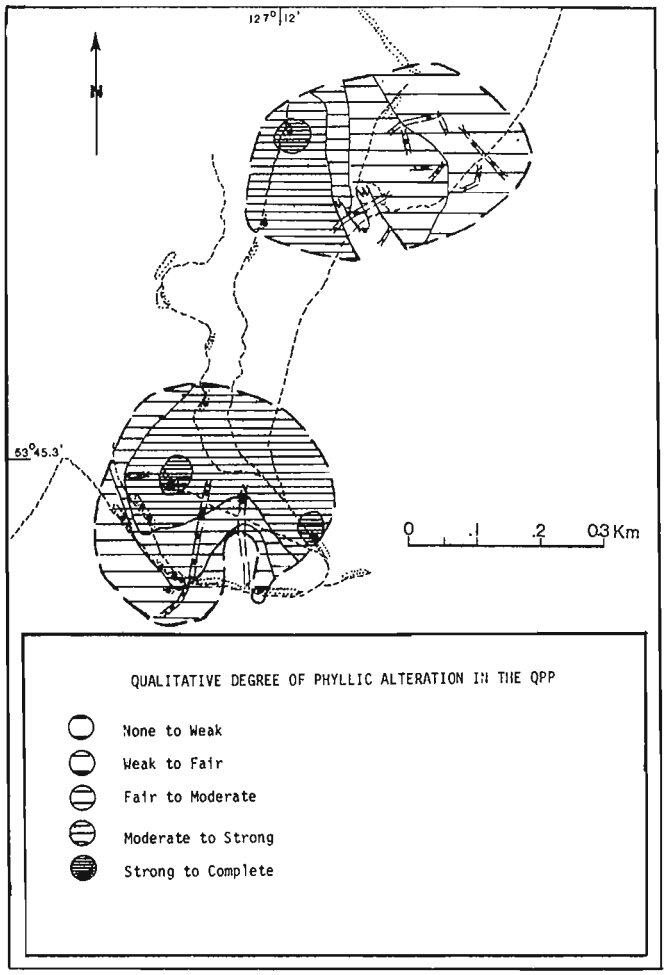

Figure 15.5. *Qualitative degree of phyllic alteration across the quartz porphyry.*

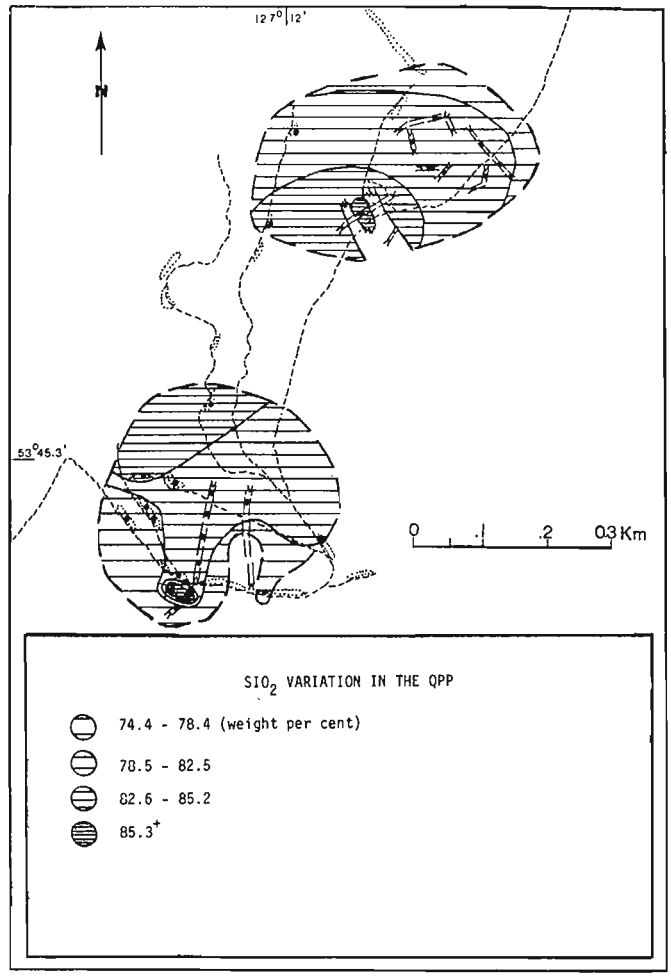

Figure 15.6. *Variation of K_2O across the QPP.*

molybdenite was observed to be present in all the specimens. Mo/Cu values average 10.9. Fluorine content averages 0.04 per cent and high fluorine concentrations coincide with those of molydenum and potassium (Fig. 15.7, 15.9, 15.10).

Average values of the chemistry of the various "differentiates" of the Bulkley intrusions in the Whiting Creek area are given in Table 15.2. CIPW norm calculations for the QPP yield average normative quartz and corundum contents of 64 and 6.6 per cent respectively. These may be compared with values of less than 30 and 3.0 per cent respectively, for all the other intrusive phases. The average ratio of orthoclase to albite calculated from petroraphic and oxide studies of the QPP is 15:1, compared with 1:1 to 1:2 for the other intrusives.

Major element analyses suggest the QPP is a silica- and potassium-rich, peraluminous rock, depleted in Ca, Na, Ti, Mn, Fe and Mg. Westra and Keith (1981) suggested that Si, K and Al enrichment and Ti, Fe, Mn and Mg depletion may be the direct result of differentiation of a granitic magma; Na and Ca depletion being a result of hydrothermal alteration.

Whiting Creek

General characteristics (Westra and Keith, 1981) of tectonic setting, petrography, and chemistry of calc-alkaline and Climax-type stockwork molybdenum deposits, are given in Table 15.3. The chemical data listed for Whiting Creek are average values for the altered QPP.

Important similarities between Whiting Creek and the Climax-type are observed for the cogenetic granite rock type, major oxide content, "positive" (i.e., greater than one) Rb to Sr ratio and the trace element assemblage.

Major, minor, and trace concentrations appear to be slightly lower than those values quoted for unaltered rocks by Westra and Keith (1981); slight depletion due to hydrothermal and supergene alteration may explain these values. Lower K_2O and trace concentrations, regional tectonic setting and low grade and tonnage figures are similar to those of the calc-alkaline type.

A Climax "transitional-type" deposit model has been suggested for those Climax-type deposits having characteristics similar to the calc-alkaline type. The Whiting Creek deposit is considered to be of this type primarily because of the chemistry of the cogenetic igneous rocks. Chemical analyses of altered granite rocks from a Climax- and transitional-type deposit are listed in Table 15.4 for comparison with the mean composition of the altered QPP. The chemistry of the QPP is more similar to, or intermediate between, that of the transitional-type and Climax-type intrusions. Lower Na and Ca contents are most likely due to more extensive hydrothermal alteration.

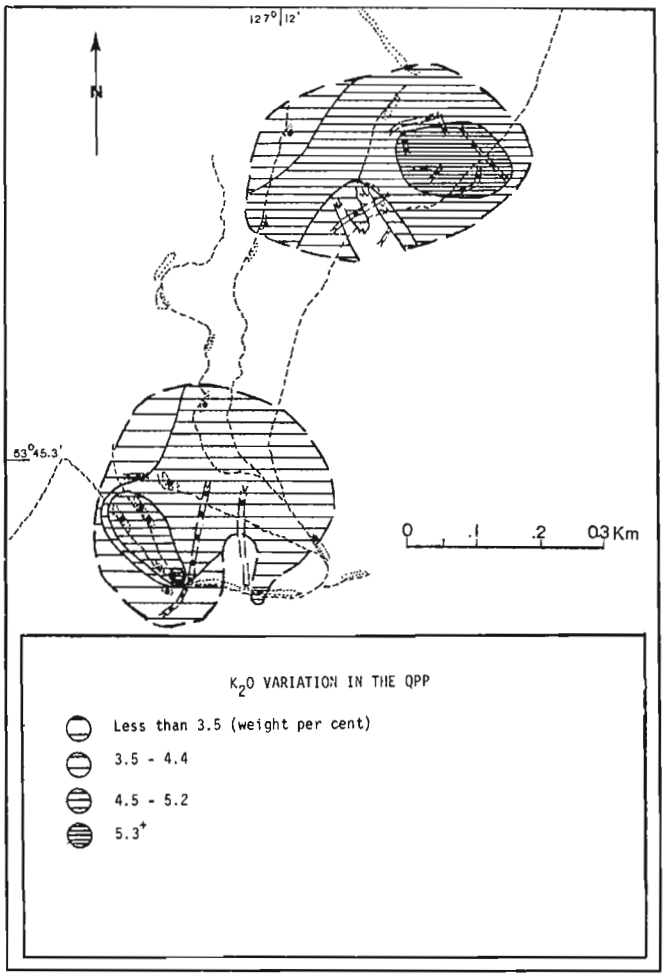

Figure 15.7. Variation of K_2O across the QPP.

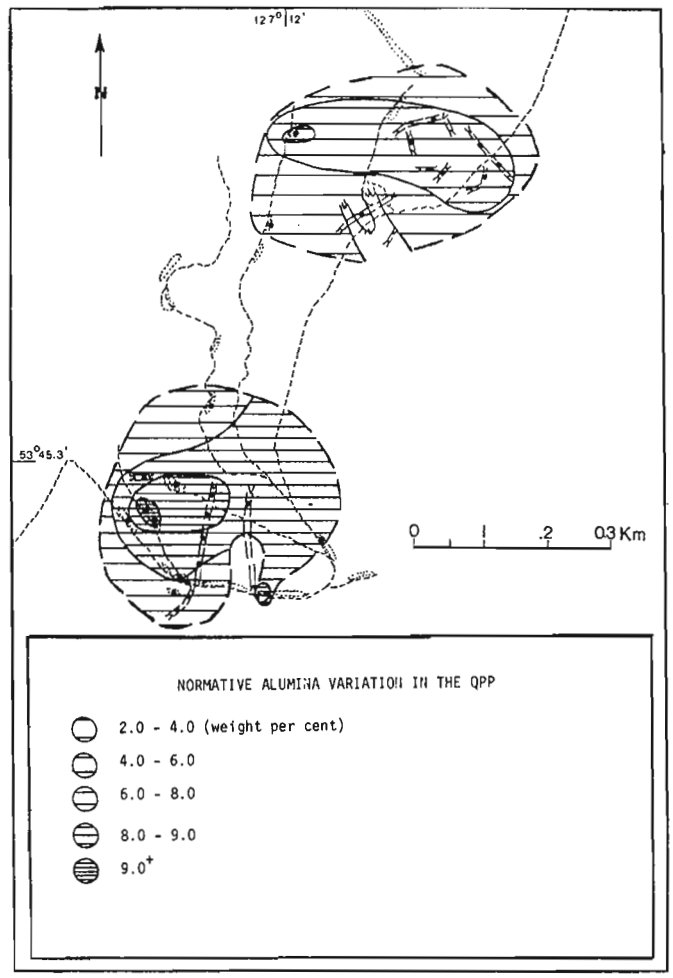

Figure 15.8. Variation of normative corundum across the QPP.

The Glacier Gulch Mo deposit, Smithers, British Columbia, is considered by Westra and Keith (1981) to be a Climax transitional-type stockwork deposit. This deposit, situated 100 km due north of Whiting Creek, is set in a rhyolitic plug which has been intruded by monzonitic intrusions. These rocks are also part of the Bulkley intrusions.

The general similarities in the lithologies, chemisty, and tectonic setting between Glacier Gulch and Whiting Creek, imply that these two deposits may have formed by similar processes.

Conclusion

The "QPP" is an altered granitic rock characterized by an apparent enrichment of SiO_2, Al_2O_3, and K_2O, and depletion of Na_2O, CaO, TiO_2, MnO, total Fe, and MgO. There is an anomalous enrichment of F, Rb, Mo, and W with respect to Sr and Cu.

Intensity of phyllic alteration is not coincident with either the zone of maximum quartz stockwork development or mineralization. There appear to be direct correlations between K_2O, normative Al_2O_3, F and Mo concentration. Normative corundum content is unrelated to the degree of alteration, suggesting that the original melt was peraluminous.

Lithogeochemical zoning supports the possibility that there was originally a single pluton, bisected by a younger intrusion, rather than two separate plugs representing separate apophyses of a larger pluton at depth.

On the other hand, variations of Mo, K_2O, F and Al_2O_3 suggest two centres of mineralization. Multiple phases of mineralization may possibly explain the presence of more than one molybdenite zone.

Mineralogical and textural evidence for the presence of a core potassic alteration zone was not directly observed. Widespread phyllic alteration and associated extensive barren pyrite zones may be peripheral to the core of the hydrothermal system. It follows that if this is the centre of the system, it is likely that either the potassic zone remains undiscovered or the hydrothermal event was too weak to produce the potassic zone and associated mineralization.

Table 15.3

General Characteristics of Stockwork Molybdenum Deposits

Deposit type	Calc-alkaline stock and plutonic type[1]	Alkali-calcic, Climax type[1]	Whiting Creek[2]
Tectonic Setting	Compressive continental plate margin	Subduction-related continental back-arc spreading environment	Continental volcanic arc regime with possible local rifting[3]
Cogenetic igneous rocks	Quartz monzonite Granodiorite	Rhyolite Granite	Granite
Porphyry texture	Yes and no	Yes	Yes
Sio_2%	<70	≥75	80
K_2O%	<4	>5	4.3
TiO_2%	0.1 - 0.2+	<0.2	0.14
F%	0.1 - 0.25	0.5 - 2	0.04
Rb ppm	100 - 350	200 - 800	84
Sr ppm	100 - 800	<125	51
Rb/Sr	<1	>1	1.64
F/Cl	low	high	?
Nb ppm	20	25 - <200	?
Important elements	Mo-Cu-(W)	Mo-F-W-Sn	Mo-Cu-F-(W)
Multiple ore shells	none	Common	?
Max. Mo content in million tonnes	0.3 - 1.6	2.0	~0.24
MoS_2% in ore zone	0.2 - 0.25	0.2 - 0.49	~0.2
Examples	Kitsault, Endako	Climax, Urad-Henderson Mount Hope[4] Glacier Gulch[4]	

[1] Relatively unaltered rocks (Westra and Keith, 1981)
[2] Altered quartz porphyry
[3] D.G. MacIntyre (1976)
[4] Climax transitional-type

Alternatively, the alteration and mineralization might be the result of a late-stage event. This interpretation would imply that there might exist a much larger deposit at depth which may be offset by the MZPP intrusion.

Lithogechemical data suggest that potassium and fluorine may be useful as pathfinder elements for molybdenum mineralization in Climax transitional-type deposits. However, before these chemical trends can be used authoritatively, sample density should be increased and vertical zonation patterns studied.

Acknowledgments

We are grateful to the staff of Saskatchewan Mining and Development Corporation, and in particular to Mark Rebagliati, for their co-coperation in allowing us to carry out this study at the Whiting Creek Property. We also acknowledge the helpful comments and criticism of M. Rebagliati during the preparation of this article, and latterly, those of W.D. Sinclair (GSC). Chemical analyses were made in the laboratories of Bondar Clegg and Co., Ottawa, and of the Geochemistry Subdivision, GSC, Ottawa. Facilities of the Geology Department, Carleton University, Ottawa were used for petrographic studies. These studies formed part of a B.Sc. dissertion of one of the authors (M.D.G.) at Carleton University.

Table 15.4
Chemical Analyses of Altered Granite Rocks

	1 Climax type	2 Transitional type	3 Whiting Creek
		Weight per cent	
SiO_2	77.50	77.10	80.07
Al_2O_3	10.10	11.30	11.42
Fe_2O_3	0.86	0.20	0.50
FeO	0.26	0.30	0.84
MgO	0.07	0.50	0.31
MnO	NA	0.01	0.01
CaO	0.40	0.50	0.09
Na_2O	0.31	0.60	0.16
K_2O	7.30	8.60	4.26
TiO_2	0.38	0.04	0.14
		Parts per million	
Rb	550	NA	84
Sr	140	NA	51
F	NA	400	370

1. Southwest mass of Climax stock – potassic and phyllic alteration, Climax, Colorado (White et al., 1981)
2. Strongly altered rhyolite porphyry, Mount Hope, Nevada (Mutschler et al., 1981)
3. Quartz-sericite alteration, quartz porphyry, Whiting Creek, British Columbia

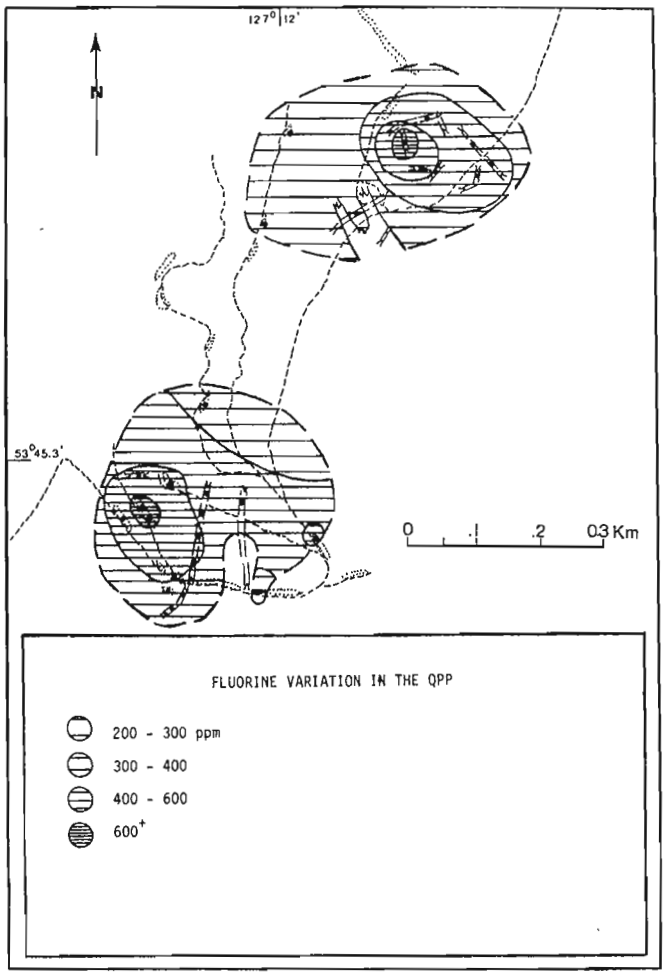

Figure 15.9. Variation of fluorine across the QPP.

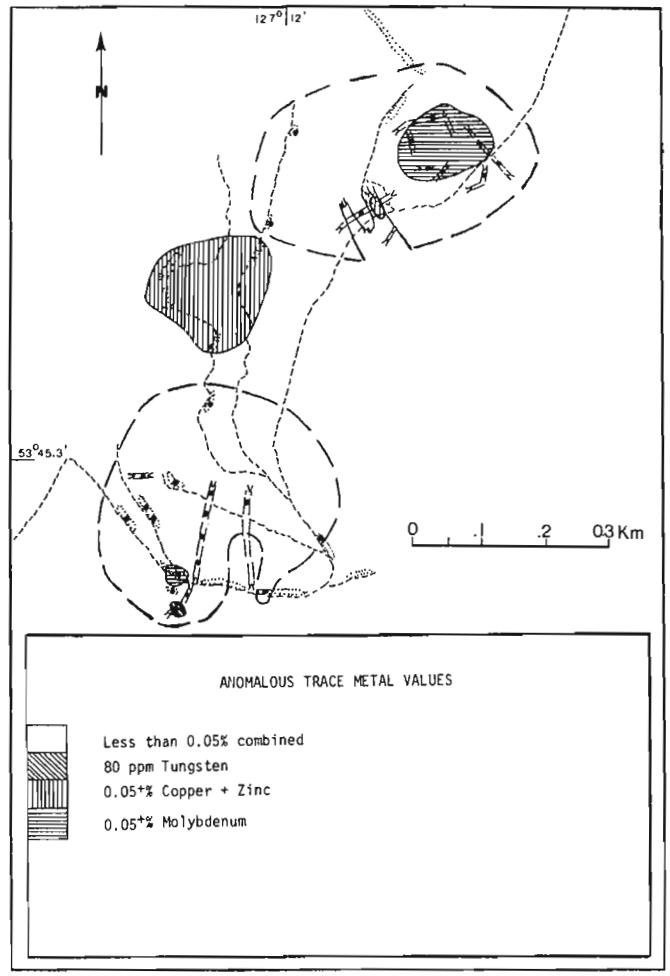

Figure 15.10. Variation of Mo-W across the QPP and Cu-Zn in the MZPP.

References

Cann, R.M.
1982: Geological map of Whiting Creek (WHIT 1-6); SMD Mining Company Limited Map.

Carter, N.C.
1982: Porphyry copper and molybdenum deposits, West-Central British Columbia; British Columbia Ministry of Mines, Energy and Petroleum Resources, Bulletin 64, 150 p.

Duffell, S.
1959: Whitesail Lake map-area, British Columbia; Geological Survey of Canada, Memoir 229, 119 p.

Goodz, M.
1982: Geochemistry and hydrothermal alteration zoning of the Whiting Creek stockwork molybdenum deposit, Tahtsa Lake area, British Columbia; Unpublished B.Sc. thesis, Carleton University, Ottawa.

Hedley, M.S.
1935: Tahtsa-Morice area, coast district, British Columbia; Geological Survey of Canada, Map 367A.

Lowell, J.D. and Guilbert, J.M.
1970: Lateral and vertical alteration - mineralization zoning in porphyry ore deposits; Economic Geology, v. 65, p. 373-408.

MacIntyre, D.G.
1976: Evolution of upper Cretaceous volcanic and plutonic centres and associated prophyry copper occurrences, Tahtsa Lake area, British Columbia; Unpublished Ph.D. thesis, University of Western Ontario, London.

Mutschler, F.E., Wright, E.G., Ludington, S., and Abbott, J.T.
1981: Granite molybdenite systems; Economic Geology, v. 76, p. 874-897.

Westra, G. and Keith, S.B.
1981: Classification and genesic of stockwork molybdenum deposits; Economic Geology, v. 76, p. 844-873.

White, W.H., Bookstrom, A.A., Kamilli, R.J., Gangster, M.W., Smith, R.P., Ranta, D.E., and Steininger, R.C.
1981: Character and origin of Climax-type molybdenum deposits; Economic Geology, Seventy-Fifth Anniversary Volume, p. 270-316.

Appendix 15.1

Major and minor element analyses - by XRF

Sample Number	Rock Type	SiO_2 %	TiO_2 %	Al_2O_3 %	Total Fe%	MgO %	CaO %	Na_2O %	K_2O %	Rb ppm	Sr ppm
01	QPP	79.4	0.09	12.0	1.2	0.30	0.08	0.2	4.59	90	50
02	QPP	76.6	0.13	13.4	1.6	0.19	0.08	0.3	5.93	110	50
04	QPP	82.7	0.09	11.5	0.6	0.19	0.08	0.1	3.26	70	30
05	HFP	61.2	0.64	17.5	5.0	2.83	3.54	3.2	2.41	80	490
06	QPP	78.4	0.09	12.8	1.2	0.46	0.11	0.2	4.52	90	40
07	QPP	85.3	0.14	8.8	0.9	0.29	0.12	0.2	2.32	40	60
09	QPP	86.0	0.13	7.8	0.9	0.38	0.10	0.2	2.61	40	50
10	QPP	80.6	0.09	10.8	1.5	0.31	0.10	0.0	3.70	80	50
11	QPP	79.8	0.09	12.6	1.3	0.29	0.07	0.1	3.54	90	50
12	MZPP	66.9	0.51	15.3	3.8	1.60	2.41	2.9	3.35	210	470
13	QPP	82.5	0.09	9.5	1.1	0.21	0.13	0.3	4.73	80	50
14	QPP	81.4	0.09	11.4	0.7	0.14	0.08	0.0	4.03	60	40
15	QPP*	78.2	0.11	11.7	1.7	0.31	0.10	0.2	5.53	90	50
16	QPP*	78.6	0.10	11.4	1.9	0.27	0.09	0.3	4.88	90	40
18	QPP	86.0	0.08	7.4	0.7	0.24	0.09	0.3	3.89	70	70
19	MZPP	66.2	0.53	15.9	4.0	1.72	2.79	3.4	2.94	30	510
21	QPP	77.1	0.11	12.0	2.0	0.34	0.10	0.2	5.38	110	30
22	QPP	78.9	0.12	13.1	0.7	0.37	0.09	0.0	4.12	100	30
23	QPP	81.3	0.08	11.8	0.6	0.11	0.07	0.2	4.53	80	60
24	GRDR	65.4	0.51	15.7	4.2	1.83	2.53	3.0	4.13	100	320
25	QPP	79.0	0.25	12.2	1.2	0.34	0.09	0.2	3.83	80	80
27	HFP	65.2	0.61	16.3	4.1	2.06	2.66	4.1	2.84	70	520
28	GRDR	65.0	0.51	15.9	4.3	1.75	3.09	3.3	3.08	40	390
29	QPP	74.4	0.40	13.5	3.0	0.44	0.09	0.0	4.41	110	50
30	HFP	61.7	0.73	16.2	6.4	2.48	3.41	2.9	3.80	70	500
31	MZPP	64.6	0.49	15.7	3.9	1.86	1.63	3.4	3.28	50	450
32	MZPP	63.9	0.63	16.1	4.4	2.18	2.14	3.3	2.82	80	490
33	QPP	83.1	0.08	9.3	1.0	0.22	0.09	0.0	4.22	60	80
37	MZPP	67.1	0.50	15.0	3.4	1.78	1.37	2.6	4.49	80	220

Notes

1. * Least altered samples.
2. Analyses of samples 03, 08, 35, 36 are not included for reasons given in text.

Appendix 15.2

Trace element analyses

Sample Number	Rock Type	Zn	Cu	Mo	W	F
			Parts per million			
01	QPP	11.6	12	108	16	410
02	QPP	12.1	14	56	4	330
03	QPP	14.9	25	27	20	680
04	QPP	15.6	6	76	8	410
05	HFP	53.5	40	5	1	410
06	QPP	10.6	10	80	16	410
07	QPP	16.6	10	154	8	330
08	QPP	14.2	26	4	80	330
09	QPP	11.9	10	27	8	330
10	QPP	7.9	9	286	24	410
11	QPP	7.4	19	61	16	380
12	MZPP	88.0	1380	4	1	440
13	QPP	13.3	67	36	4	220
14	QPP	22.8	17	40	8	250
15	QPP	9.0	20	407	24	330
16	QPP	36.9	42	862	24	330
18	QPP	12.0	27	865	20	220
19	MZPP	54.8	124	3	1	330
21	QPP	14.7	24	500	1	760
22	QPP	14.3	9	70	16	410
23	QPP	10.9	9	569	24	300
24	GRDR	37.0	420	1	1	380
25	QPP	11.5	13	33	12	410
27	HFP	61.1	60	5	4	440
28	GRDR	45.6	99	5	1	380
29	QPP	15.1	41	44	32	250
30	HFP	50.0	137	3	1	410
31	MZPP	28.0	438	9	4	410
32	MZPP	54.8	223	17	1	500
33	QPP	9.9	15	55	4	220
35	QPP	22.7	90	4	20	250
36	MZPP	22.1	48	137	16	200
37	MZPP	64.7	584	138	12	330

Notes: Analyses of Zn, Cu and Mo by AAS, W by colorimetry and F by ion-selective electrode

16.

THE P-T CONDITIONS OF LATE-STAGE DIAGENESIS AND LOW GRADE METAMORPHISM IN THE TACONIC BELT OF THE GASPE PENINSULA FROM FLUID INCLUSIONS: PRELIMINARY RESULTS

EMR Research Agreement 134-4-82

Shafiul Islam[1] and Reinhard Hesse[1]
Precambrian Geology Division

Islam, S. and Hesse, R., The P-T conditions of late-stage diagenesis and low grade metamorphism in the Taconic Belt of the Gaspé Peninsula from fluid inclusions: preliminary results; in Current Research, Part B, Geological Survey of Canada, Paper 83-1B, p. 145-150, 1983.

Abstract

In diagenetic and low grade metamorphic terrains of the Taconic Belt of the Gaspé-Peninsula four types of fluid inclusions were observed in vein quartz from ac-joints: 1) CH_4-inclusions; 2) two-phase H_2O-inclusions; 3) three-phase liquid H_2O, liquid CO_2 and vapour CO_2 inclusions and 4) four-phase H_2O, CO_2 (L + V) and salt (solid) inclusions. Correlation between maturation zones (established by pyrobitumen reflectance and illite crystallinity), fluid compositions and homogenization temperatures T_H of water-rich inclusions is as follows.

Late diagenetic zone: H_2O, CH_4: T_H generally below 200°C.

Anchimetamorphic zone: $H_2O \pm CO_2$; T_H generally between 200 and 270°C (but as low as 130°C).

Epimetamorphic zone: $CO_2 + H_2O$; $CO_2 + H_2O$ + salt crystal; H_2O, T_H up to 320°C (but as low as 150°C).

The water-rich fluids are generally low salinity (1.5 equiv. wt. %) NaCl-brines or $CaCl_2$-brines (up to 8% salinity). Minimum subsurface pressures at the time of entrapment determined from CH_4 inclusions ranged from 620 to 780 bars.

Résumé

Dans des terrains diagénétiques et faiblement métamorphisés de la zone du Taconique de la péninsule de Gaspé, on a identifié, à partir des joints ac, quatre types d'inclusions fluides dans un filon de quartz: 1) inclusions de CH_4; 2) inclusions de H_2O à deux phases; 3) inclusions de H_2O liquide, de CO_2 liquide et de CO_2 gazeux à trois phases et 4) inclusions de H_2O, de CO_2 (L et G) et de sel (solide) à quatre phases. La corrélation établie entre les zones de maturation (déterminées à partir de la réflectance des pyrobitumes et de la cristallinité de l'illite), les compositions des fluides et les températures d'homogénéisation (T_H) des inclusions riches en eau est la suivante:

Zone épidiagénétique: H_2O, CH_4; T_H généralement inférieure à 200°C.

Zone anchimétamorphique: $H_2O \pm CO_2$; T_H généralement entre 200 et 270°C (mais peut atteindre 130°C).

Zone épimétamorphique: $CO_2 + H_2O$; $CO_2 + H_2O$ + cristal de sel; H_2O, T_H jusqu'à 320°C (mais peut atteindre 150°C).

Les fluides riches en eau sont généralement des saumures de NaCl de faible salinité (1,5 % en poids correspondant) ou des saumures de $CaCl_2$ dont la salinité peut atteindre 8 %. Les pressions minimales en subsurface au moment du piégeage, déterminées à partir des inclusions de CH_4, variaient de 620 à 780 bars.

Introduction

Fluid inclusion analyses provide a suitable tool to establish temperatures and pressures of diagenetic and metamorphic reactions involving the growth of new mineral phases. Information can also be obtained on the chemical composition of the pore fluids from which minerals grew. Where thermal maturation levels have been established with indicators such as organic matter reflectance and/or illite cyrstallinity, fluid inclusion data may be used to calibrate maturation levels in terms of subsurface paleotemperatures and paleopressures. Under favourable conditions paleo-geothermal gradients may be derived (e.g. Mullis, 1979).

In this study fluid inclusions in vein quartz were analyzed for an area whose regional patterns of thermal maturation have previously been established using pyrobitumen reflectance and illite crystallinity (Islam et al., 1982). Samples were collected from ac-joints at 16 localities in Cambro-Ordovician deep-water turbidite sequences of the Taconic Belt, Gaspé Peninsula (Fig. 16.1). The quartz is typically massive, "milky" vein quartz, but at a few localities well developed prismatic crystals were found. The stretched fibrous variety called "Fadenquarz" by Mullis (1979) was also sampled, but rarely gave successful results. For microthermometry of the phase transitions in the inclusions a heating and freezing stage developed at the U.S. Geological Survey was used.

Acknowledgment

A.E. Williams-Jones at McGill University and an anonymous reviewer commented on a first draft of this paper.

[1] Department of Geological Sciences, McGill University, 3450 University Street, Montreal, Quebec, H3A 2A7

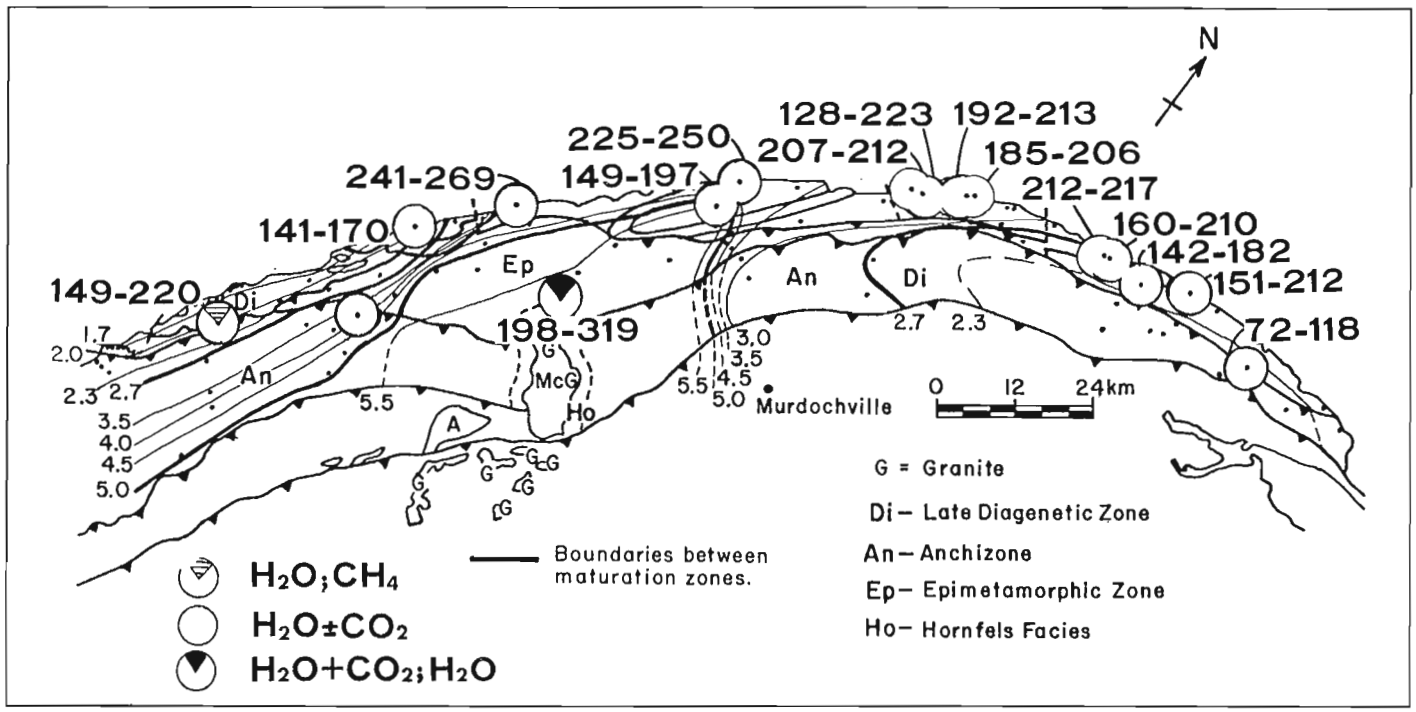

Figure 16.1. *Isoreflectance map for the Taconic Belt of Gaspé Peninsula with homogenization temperatures in °C from fluid inclusions. Isoreflectance lines are in per cent reflected light measured on asphaltic pyrobitumen under oil (Islam et al., 1982).*

Types of Inclusions

Generally more than one kind of inclusion is present in a given sample. The following four types of inclusions were observed, various combinations of which occur together in the same sample as will be discussed in the section on regional distribution:

1) methane inclusions;
2) two-phase water-rich inclusions;
3) three-phase water-carbon dioxide inclusions containing a liquid and a gaseous CO_2 phase;
4) four-phase H_2O-CO_2-salt inclusions containing H_2O liquid, CO_2 liquid, CO_2 vapour and a salt crystal.

Identification of these different types of inclusions is based on the following phase transitions determined microthermometrically:

1) Methane inclusions (Fig. 16.2a)

These are nearly pure supercritical methane inclusions. Cooling the inclusions below the critical temperature for methane (-82.45°C) leads to separation into a liquid and a gaseous phase, which rehomogenize to liquid when heated. The exact homogenization temperature during heating gives information on contaminants (higher aliphatic hydrocarbons such as C_2H_6, C_3H_8 etc.; CO_2; N_2; etc.) or, if the methane is pure, on the density of the supercritical CH_4 fluid. Admixtures of higher hydrocarbons and CO_2 raise the homogenization temperature above the critical point, N_2 depresses it. The presence or absence of these components must, therefore, be verified by other methods, e.g. Raman spectroscopy. Methane-rich inclusions (more than 95 vol. % CH_4) with homogenization temperatures below the critical point usually contain less than 1 mol % ethane or propane (Mullis, 1979). These inclusions can therefore be used to determine an isochore for methane. From this the pressure of entrapment can be determined using the PVT diagram of Zagoruchenko and Zhuravlev (1970) if an independent temperature measurement is available. The minimum temperature of formation is obtained from the homogenization temperature of water-rich inclusions in the same sample, assuming that both the methane-rich and water-rich inclusions formed under the same P-T conditions. Mullis (1979) was able to distinguish up to four successive generations with eight episodes of inclusion growth using zoned crystals, and to ascribe individual methane-rich or water-rich inclusions to a designated generation. This lead to interesting conclusions about the pressure oscillations during joint opening and the regional cooling history after the peak of the last Alpine heating event.

In the present study homogenization temperatures for methane-rich inclusions range from -84.1 to -81.4°C (homogenization to liquid). The detailed composition of these inclusions has not yet been identified. However, temperatures above the critical point of -82.45°C as obtained in four cases (-81.4, -81.5, -81.5, and -82.1°C) are most likely due to contamination by small concentrations of higher molecular weight hydrocarbons. Inclusions giving temperatures below the critical point can be assumed to contain more or less pure supercritical CH_4 fluid as in Mullis' example. From these data minimum pressures of formation are obtained with the aid of homogenization temperatures of water-rich inclusions from the same sample (see below). Minimum pressures range from 620 to 780 bars.

2) Two-phase Water-rich Inclusions (Fig. 16.2b)

Three groups of inclusions were found within this type, in terms of initial melting temperatures of the frozen sample. Samples were frozen to temperatures below -80°C and then heated slowly. (i) In the common group thawing

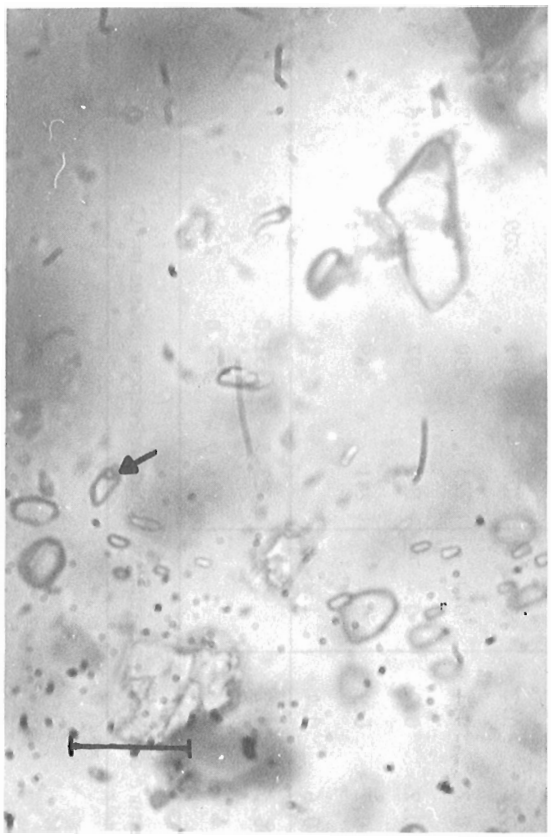

Figure 16.2a. *One-phase supercritical methane inclusions. Two-phase water-rich inclusion (arrow) at lower left hand side. Sample no. CC-77. Scale bar is 30 microns.*

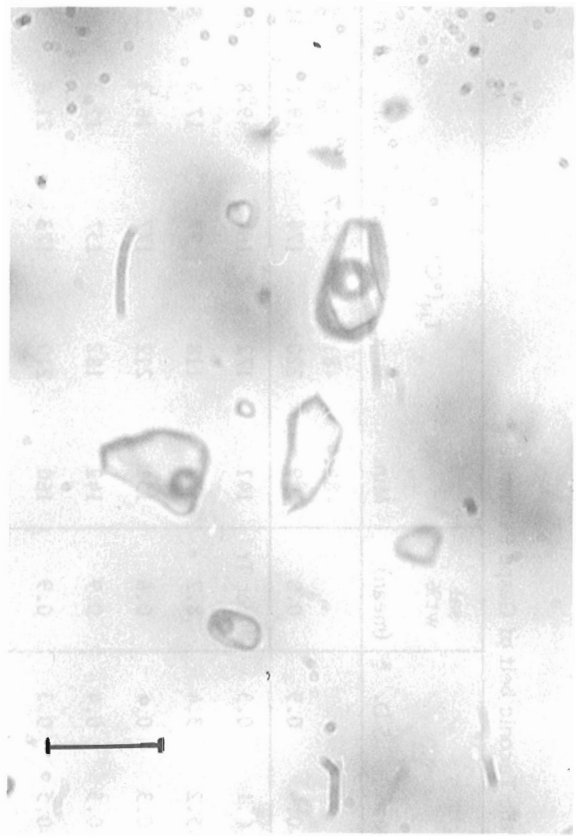

Figure 16.2b. *Two-phase water-rich inclusions (vapour bubble surrounded by liquid water). Sample no. CC-77. Scale bar is 30 microns.*

starts between -20.4 and -2.6°C (Table 16.1). In NaCl brines melting starts at the eutectic temperature of -20.8°C. In practice this is often difficult to measure because the first sign of thawing may occur well above the eutectic point. This is particularly true for the low-salinity brines studied which will yield only minute amounts of liquid at the eutectic. Observed final melting temperatures range from -3.4 to + 0.1°C indicating salinities between 0 and 1.4% (Table 16.1). These represent NaCl equivalents, since from microthermometric data alone it is difficult to identify other salts, except divalent chlorides. (ii) In one sample initial thawing occurred between -37.7 and -34.8°C (mean -36.1°C) indicating the presence of $CaCl_2$ in aqueous solution which has a eutectic minimum at -49.8°C. In $MgCl_2$ solutions the minimum occurs at -33.6°C, too high for the observed inclusions, but in the NaCl-$MgCl_2$ system it is depressed to -35°C, in NaCl-$CaCl_2$ mixtures to -52.0°C (Crawford, 1981). Final melting in this sample occurred between -10.2 and -0.5°C. Thus, the fluid is probably a $CaCl_2$ or $CaCl_2$-NaCl brine with a salinity of 8.2 wt% (mean, Table 16.1). (iii) The third group of water-rich inclusions is represented by another single sample which has initial melting temperatures ranging from -1.4 to + 0.5°C (mean -0.8°C and a final melting temperature of 0.0°C with 3 (out of 19) measurements giving values as high as +0.7 and +0.8°C. Among the water-rich inclusions this is the sample with the lowest salinity. In a few cases where final thawing above +0.15°C was observed, this is probably a kinetic effect.

Upon heating, the liquid and vapour phases of these water-rich inclusions homogenize to liquid without prior decrepitation. Measured homogenization temperatures for the low salinity fluids range from +128 to +269°C, which are interpreted as minimum temperatures of entrapment. The $CaCl_2$ brine yielded exceptionally low temperatures of 72 to 118°C. These data must be corrected for salinity if actual formation temperatures and pressures are higher than the minimum values and salinities are appreciable (Crawford, 1981). However, estimated salinities are generally low (less than 1.5 equiv. wt %, except for the $CaCl_2$ brine) and, therefore, no salinity correction is required.

3) Three-phase Water-carbon Dioxide Inclusions

At room temperature these consist of liquid water (occupying the space at the outer rim of the inclusion), liquid CO_2 and vapour-phase CO_2 (at centre, Fig. 16.2c,d). Frozen to below -120°C CO_2 melting occurs upon slow heating between -56.7 and -56.4°C. Therefore the vapour phase of these three-phase inclusions contains almost pure CO_2 with virtually no admixture of CH_4. Values above -56.6°C, the final melting temperature of pure CO_2, are probably due to kinetic effects. As decrepitation commonly occurs in CO_2-rich inclusions, bulk homogenization cannot be observed and the minimum temperature of formation cannot be determined. However, homogenization of the two CO_2 phases occurs before decrepitation, in the samples studied +23.5 and +29.5°C, in one case at +31.0°C.

4) Four-phase H_2O-CO_2 Salt Inclusions

These consist of liquid water, liquid CO_2, CO_2 vapour and an unidentified salt crystal. In one case two different salt crystals were observed which both appear to be genuine precipitates from the fluid trapped (Fig. 16.2c) rendering this a five-phase inclusion. Melting behaviour of the salt crystals has not been tested in order not to decrepitate the inclusions.

Table 16.1

Microthermometric data for fluid inclusions from the Taconic belt of Gaspé Peninsula

Sample no.	Type	T_I(°C)					T_F(°C)				sal wt%	T_H(°C)				
		Min.	Max.	Mean	S.D.	n	Min.	Max.	Mean	S.D.	(mean)	Min.	Max.	Mean	S.D.	n
	CH_4											-84.4	-81.4	-82.7	1.6	5
C.C.77	H_2O	-19.1	-12.1	-15.2	3.1	37	-1.3	-0.1	-0.4	0.9	0.8	149	220	174	19.0	31
TR-13		-1.4	+0.5	-0.8	0.3	20	0.0	+0.8	+0.1	0.3	0 or Tr	141	172	164	9.8	20
MA-51		-39.5	-34.8	-36.1	1.1	18	-10.2	-0.5	-5.2	3.4	8.2	72	118	97	17.5	8
LE-53		-20.4	-11.0	-16.4	3.2	27	-0.5	-0.1	-0.3	0.3	0.6	151	212	177	16.3	22
FP-58		-12.0	-3.2	-5.5	2.6	20	-1.2	-0.1	-0.5	0.4	0.9	142	182	157	12.3	20
GE-1	H_2O	-11.9	-3.8	-9.1	2.9	13	-1.0	-0.2	-0.5	0.3	0.9	160	210	173	21.6	5
GE	±	-10.2	-3.1	-6.6	5.0	2	-0.4	-0.2	-0.3	0.1	0.2	212	217	213	2.4	4
PV-4	CO_2	-20.2	-8.0	-14.9	4.6	15	-3.4	-0.2	-0.9	0.9	1.4	192	213	205	7.8	15
PV-6		-15.9	-2.6	-8.1	5.9	10	-1.2	-0.1	-0.4	1.9	0.8	185	206	200	7.5	12
GV		-16.3	-12.1	-13.9	2.0	4	-0.8	-0.1	-0.3	0.2	0.6	128	223	190	36.0	8
GV-45		-16.9	-13.8	-14.9	1.4	5	-0.4	-0.1	-0.2	0.2	0.5	207	212	209	2.4	4
GM-10		-20.2	-8.2	-12.8	4.8	15	-0.5	-0.1	-0.2	0.1	0.4	225	250	235	12.6	3
AP-33		-16.2	-11.5	-13.8	2.2	28	-0.4	+0.1	-0.2	0.2	0.4	149	197	166	16.1	16
EM-11		-15.1	-13.8	-14.5	0.6	6	-0.3	-0.1	-0.2	0.1	0.4	241	269	251		3
SM-20		-16.4	-11.1	-13.9	2.2	12	-1.0	-0.2	-0.6	0.4	1.1					
CC-73	CO_2	-56.7	-56.4	-56.6	0.1	9	-56.6	-56.0	-56.5	0.2		23.5	31.0	28.8		20
	H_2O											198.0	319.0	259.0		2

T_I = Initial melting temperature in °C; T_F = Final melting temperature in °C; T_H = Temperature of homogenization of liquid and vapour phases in °C.

Figure 16.2c. *Five-phase CO_2-rich inclusion at centre with two salt crystals. Water is in outer rim, CO_2 vapour bubble at centre surrounded by liquid CO_2. The salt crystals have not been identified. The other inclusions visible on this photomicrograph are water-rich. Sample no. CC-73. Scale bar is 40 microns.*

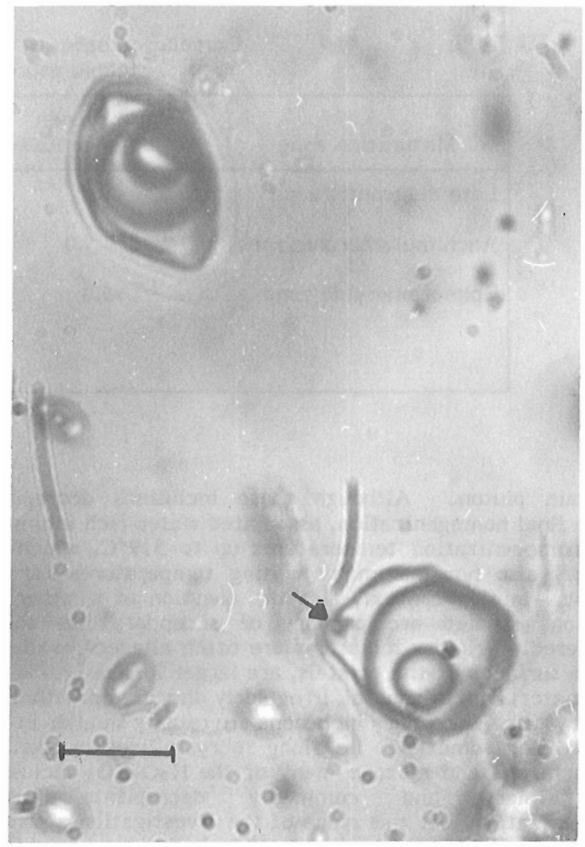

Figure 16.2d. *CO_2-rich inclusions, one of which contains a salt crystal (arrow). Sample no. CC-73. Scale bar is 20 microns.*

Regional Distribution of Homogenization Temperatures and Inclusion Compositions

Since all the samples studied contain water-rich inclusions which did not decrepitate before homogenization of the liquid and vapour phases during heating, a sufficiently large number of homogenization temperatures was obtained (Fig. 16.1) whose distribution can be compared to the thermal maturation map produced from isoreflectance lines and illite crystallinity isopleths for the study region (Islam et al., 1982).

Temperatures in the three maturation zones show significant overlap, which is not surprising considering the fact that these are temperatures of fluid entrapment which are not restricted to the time of maximum heating. In order to identify data which correspond to the peak heating episode only, a more detailed study is required using zoned crystals, which should lead to establishing fluid inclusion generations and from this to deduce the postorogenic cooling history of the region.

In the late diagenetic zone homogenization temperatures are generally below 200°C except at one locality where two single measurements gave values slightly above 200°C (204 and 212°C), whereas the mean is 177°C. In comparison Mullis' (1979) findings from the Swiss Alps give minimum temperatures for the late diagenetic zone above 200°C, but this includes the low grade anchizone.

In the anchizone temperatures below 200°C were observed at four localities. In three of these, inclusions with the highest homogenization temperatures lie above 200°C, but not above 270°C as Mullis found for the medium- to high-grade anchizone in the Swiss Alps. Again, this discrepancy is probably explained most easily by assuming that entrapment in the Gaspé samples took place significantly after the peak heating event of the Taconic Orogeny. Also, for the same temperature of entrapment pressure differences can lead to variable homogenization temperatures for different regions, if the entrapment temperature is higher than the homogenization temperature (i.e. higher than the minimum temperature of formation). An alternative explanation for the relatively low homogenization temperatures is that the maturation level determined by pyrobitumen reflectance may be too high compared to vitrinite reflectance. This problem requires further study.

In the late diagnetic zone CH_4 inclusions and H_2O inclusions occur together. The water-rich inclusions are low salinity, NaCl-dominated pore waters with one exception (St. Maurice section, Sample MA-51) where a $CaCl_2$ or CaCl-NaCl mixed brine is present. In the anchizone two phase water-rich inclusions with low salinities are the only type observed. Inclusions containing free CO_2 phases are restricted to hydrothermal veins of the epizonal aureole surrounding the Acadian intrusion of the McGerrigle

Table 16.2

Correlation between maturation zones, homogenization temperatures and fluid compositions

Maturation zone	Pyrobitumen reflectance Ro%	Illite crystallinity° Δ2θ	Homogenization temperature °C	Fluid composition
Late diagenetic zone	<2.7	>0.43	72-212	CH_4, H_2O
Anchimetamorphic zone	2.7-5.0	0.24-0.43	128-269	$H_2O \pm CO_2$
Epimetamorphic zone	>5.0	<0.24	149-319	$CO_2 + H_2O$
				$CO_2 + H_2O +$ salt, H_2O

Mountain pluton. Although these inclusions decrepitate before final homogenization, associated water-rich inclusions gave homogenization temperatures up to 319°C, which are probably also not maximum heating temperatures for the epizone. In this context, also the question of whether the inclusions studied are primary or secondary has to be considered. Primary inclusions are often aligned parallel to growth surfaces of the crystals, are larger in size (20-30 μm in diameter) and, in general, irregularly distributed within the host crystals. Secondary inclusions are usually smaller in size (10 μm) and sometimes lie along recrystallized cracks. In the anchizone and epizone many of the H_2O-CO_2 inclusions are primary and commonly decrepitate before homogenization. At this stage of the investigation a general statement on the nature of the inclusions would be premature.

This correlation of CH_4 and H_2O inclusions with the late diagenetic zone, of $H_2O \pm CO_2$ inclusions with the anchizone, and of CO_2-H_2O inclusions with the epizone repeats the general shift in composition with increasing grade observed in the Alps (Mullis, 1979). In the Alps, however, methane was still found in the low- and medium-grade anchizone. CH_4 results from the cracking of higher hydrocarbons and requires low oxygen fugacity or high pressure to remain stable. In this study CH_4 was found to disappear with increasing temperature within the anchizone. Possible sources of carbon for the CO_2 in fluid inclusions from the anchizone are (i) decarbonation reactions in carbonate-rich sediments or (ii) oxidation of carbonaceous material or graphite. Ziegenbein and Johannes (1980), however, suggest that graphite reacts only very sluggishly with a fluid phase at temperatures below 700°C.

References

Crawford, M.L.
1981: Phase equilibria in aqueous fluid inclusions; in Short Course in Fluid Inclusions: Application to Petrology, ed. L.S. Hollister, and M.L. Crawford; Mineralogical Association of Canada, p. 75-100.

Islam, S., Hesse, R., and Chagnon, A.
1982: Zonation of diagenesis and low-grade metamorphism in Cambro-Ordovician flysch of Gaspé-Peninsula, Quebec Appalachians; Canadian Mineralogist, v. 20, p. 155-167.

Mullis, J.
1979: The system methane-water as a geologic thermometer and barometer from the external part of the Central Alps; Bulletin de Minéralogie, v. 102, p. 526-536.

Zagoruchenko, V.A. and Zhuravlev, A.M.
1970: Thermophysical properties of gaseous and liquid methane; Israel Program, Scientific Translations, Jerusalem.

Ziebenbein, D. and Johannes, W.
1980: Graphite in C-H-O fluids: an unsuitable compound to buffer fluid composition at temperatures up to 700°C; Neues Jahrbuch für Mineralogie, Monatshefte 1980, Heft 7, p. 289-305.

17.

SELWYN PLUTONIC SUITE AND ITS RELATIONSHIP TO TUNGSTEN SKARN MINERALIZATION, SOUTHEASTERN YUKON AND DISTRICT OF MACKENZIE

Project 790044

R.G. Anderson
Cordilleran Geology Division, Vancouver

Anderson, R.G., Selwyn plutonic suite and its relationship to tungsten skarn mineralization, southeastern Yukon and District of Mackenzie; in Current Research, Part B, Geological Survey of Canada, Paper 83-1B, p. 151-163, 1983.

Abstract

Two northwest-trending, coeval, mid-Cretaceous (K-Ar isotopic age range: 77-96 Ma) plutonic belts in the southeastern Selwyn Mountains are characterized by the presence or absence of hornblende as an essential mineral. The northeastern belt comprises granite or granodiorite with common or abundant hornblende. The southwestern belt consists of granite with common biotite, minor muscovite and little or no hornblende. Plutons in either belt may be: small or large; composite or homogeneous; massive, lineated or foliated; megacrystic or equigranular. Inclusion mineralogy and the abundance and type of intraplutonic dykes differ for each group.

Tungsten skarns are associated with some plutons lacking hornblende. Satellitic intrusions near, or marginal phases within, these plutons contain combinations of andalusite, garnet, tourmaline and/or muscovite apparently as primary accessory minerals. Geochemistry for these phases in the Mactung pluton indicates they are also anomalously rich in tungsten (8-12 ppm).

Résumé

Deux zones plutoniques contemporaines orientées nord-ouest, datant du Crétacé moyen (la datation isotopique au K/Ar donne un âge variant de 77 à 96 millions d'années) dans le sud-est des monts Selwyn, sont caractérisées par la présence ou l'absence de hornblende comme minéral essentiel. La zone au nord-est renferme du granite ou de la granodiorite; la hornblende y est commune ou abondante. La zone au sud-ouest est formée de granite avec de la biotite et de petites quantités de muscovite; la hornblende y est rare ou absente. Les plutons des deux zones peuvent être petits ou grands; composites ou homogènes; massifs, linéaires ou feuilletés; macrocristallins ou isogranulaires. La minéralogie des inclusions et l'abondance et le genre de filons intraplutoniques varient dans chaque groupe.

Des skarns riches en tungstène sont associées à certains plutons dépourvus de hornblende. Des inclusions satellites près de ces plutons, ou des phases marginales à l'intérieur de ceux-ci, contiennent des combinaisons d'andalousite, de grenat et de tourmaline ou de muscovite, ou des deux, comme minéraux accessoires primaires. La géochimie de ces phases dans le pluton Mactung indique qu'il s'agit aussi de phases anormalement riches en tungstène (8 à 12 ppm).

Introduction

Posttectonic, mid-Cretacrous plutons are widespread in northern British Columbia and eastern and central Yukon. Dick and Hodgson (1982), Dick (1979, 1980), Dawson and Dick (1978) among others, emphasized the importance of country rocks in the localization of extensive tin and tungsten skarns near these plutons.

This report summarizes 1981 (see also Anderson, 1982) and 1982 field observations on part of the Selwyn plutonic suite in southeastern Selwyn Mountains (NTS 105I, O) where plutons with tungsten skarns and barren plutons are represented (Fig. 17.1, Table 17.1). Two northwest-trending plutonic belts are defined. The northeastern belt comprises granite and granodiorite plutons with hornblende as an essential mafic silicate (O'Grady batholith, northern and central South Nahanni plutons). The southeastern belt consists of granite and granodiorite plutons, some with tungsten skarns, which contain little or no hornblende (Mactung, CLEA, Mount Wilson, Pelly River, southern South Nahanni, LENED, CAC, RUDI and Flat Lake plutons). Results from this and other work suggest regional setting and essential and accessory mineralogy of a pluton and its marginal or satellitic phases are important guides in exploration for tungsten skarns in the southeastern Selwyn Mountains.

Geology of the Plutons

Hornblende-free and hornblende-bearing plutons are described on the basis of the presence and distribution of phases, lithology, essential and accessory mineralogy, inclusion type and abundance, interphase and external intrusive relations and intraplutonic and satellitic intrusions.

Plutons Without Hornblende and Associated With Tungsten Skarns

CLEA Pluton. Tungsten skarns at the CLEA property occur near a small (0.3 km^2), massive to weakly foliated, composite biotite granite pluton (Fig. 17.1, 17.2a, 17.3a) described by Tompson (1978) and Godwin et al. (1980).

Equigranular and coarsely megacrystic phases are most extensive compared with subordinate aplitic and pegmatitic dykes and tourmaline-quartz veins (Fig. 17.2a, 17.3a). Equigranular biotite granite outcrops along the northern and eastern margins of the pluton. It is homogeneous, massive, medium grained, and equigranular to seriate. Alkali feldspar megacrysts (2-5 cm long) generally account for less than 1 to 2 per cent of the rock. Coarse grained round patches of smoky grey quartz are distinctive. The coarsely megacrystic phase forms the southern half of the pluton and consists of 5 to 10 per cent, euhedral, massive to faintly foliated alkali

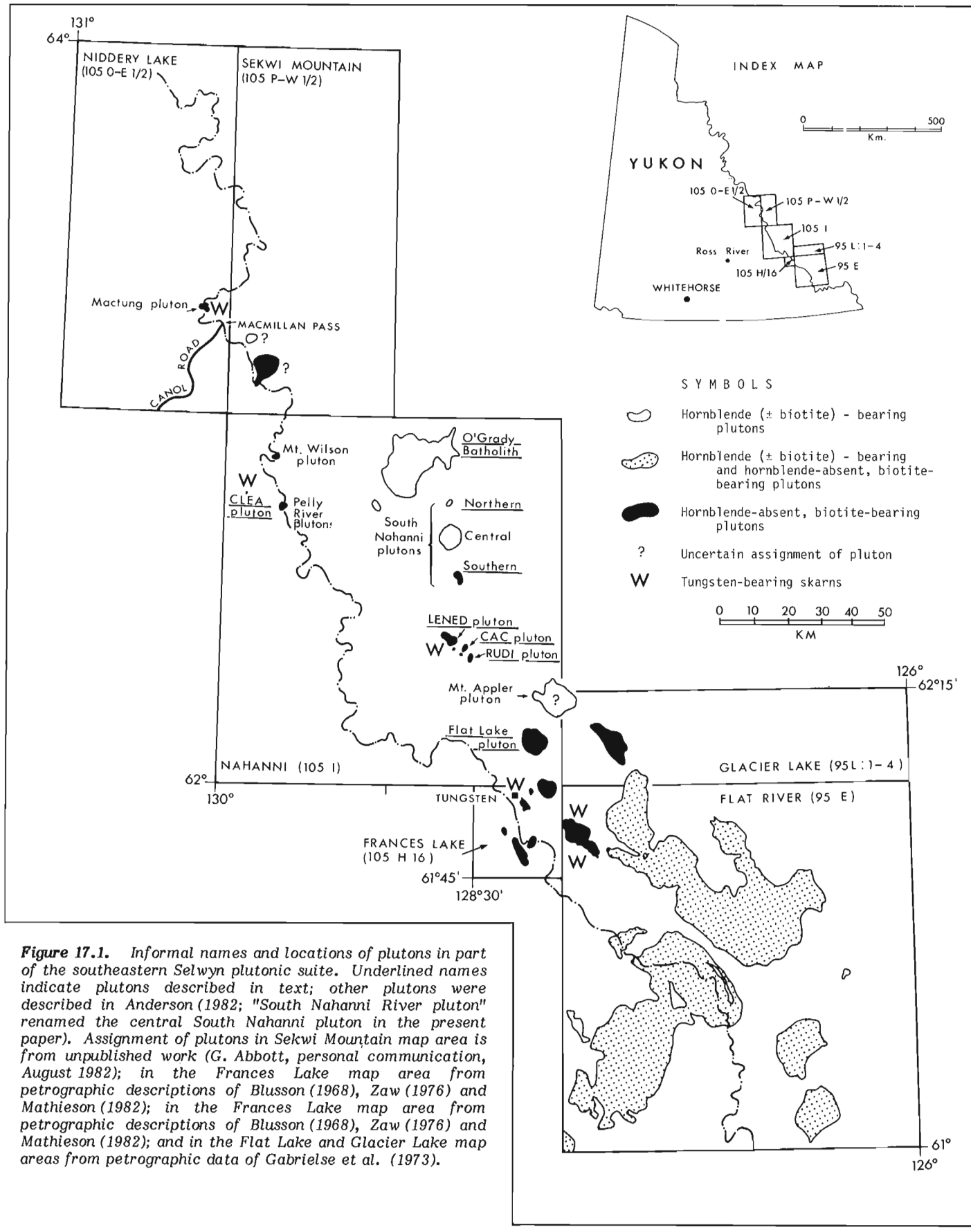

Figure 17.1. *Informal names and locations of plutons in part of the southeastern Selwyn plutonic suite. Underlined names indicate plutons described in text; other plutons were described in Anderson (1982; "South Nahanni River pluton" renamed the central South Nahanni pluton in the present paper). Assignment of plutons in Sekwi Mountain map area is from unpublished work (G. Abbott, personal communication, August 1982); in the Frances Lake map area from petrographic descriptions of Blusson (1968), Zaw (1976) and Mathieson (1982); in the Frances Lake map area from petrographic descriptions of Blusson (1968), Zaw (1976) and Mathieson (1982); and in the Flat Lake and Glacier Lake map areas from petrographic data of Gabrielse et al. (1973).*

Table 17.1

Compilation of some field and petrographic characteristics of the southeastern Selwyn plutonic suite

PLUTON (area)	ASSOCIATED WITH W SKARNS	COMPOSITE OR HOMOGENEOUS	PHASES	COMPOSITION	ABUNDANCE AND SIZE OF MEGACRYSTS	FABRIC	MAFIC MINERALS	ACCESSORY MINERALS	SATELLITIC AND INTRAPLUTONIC DYKES	INCLUSION TYPE AND ABUNDANCE
					Plutons Without Hornblende					
Mactung (2.9 km^2)	yes	composite	equigranular, megacrystic, fine-grained, satellitic intrusions	granite, granodiorite	megacrystic phase (7-20%; 1-2 cm long)	massive	biotite, muscovite	muscovite, garnet, tourmaline, apatite, zircon, allanite	peraluminous granite (which contains garnet and muscovite) and aplitic granite	biotite diorite (rare)
CLEA (0.3 km^2)	yes	composite	equigranular, coarsely megacrystic	granite (both phases)	equigranular phase (<2%; 3-5 cm long); coarsely megacrystic phase (5-10%; 5-8 cm long	massive or faintly foliated megacrysts	biotite	muscovite, tourmaline, zircon, allanite	aplite, pegmatite, tonalite	hornfels (common); fine-grained mafic inclusions (rare)
LENED (12.3 km^2)	yes	composite	equigranular, coarsely megacrystic,	granite (all phases)	equigranular phase (<1% to <<1%; ? cm long); coarsely megacrystic phase (3-7%; 3-5 cm long, up to 7-10 cm long)	massive or weakly lineated or foliated megacrysts	biotite ±muscovite	muscovite, apatite, zircon	aplite, felsic porphyry	fine-grained biotite diorite (rare or absent)
CAC (1.9 km^2)	yes	composite	equigranular, coarsely megacrystic, satellitic intrusions	granite	coarsely megacrystic phase (3-10%; 3-5 cm long)	massive	biotite	muscovite apatite, zircon, ±garnet, ±tourmaline, ±andalusite especially in satellitic plutons	peraluminous granite (contains muscovite+garnet+ andalusite); aplite	fine-grained biotite diorite (rare to absent)
RUDI (4.7 km^2)	yes	composite	equigranular, coarsely megacrystic, satellitic intrusions	granite	equigranular phase (<1% to <<1%; 2-3 cm long); coarsely megacrystic phase (3-5%; 2-5 cm long)	massive; rare mafic schlieren near contacts	biotite	muscovite, garnet, tourmaline, (especially in peraluminous intrusions	peraluminous granite (contains muscovite+garnet+ tourmaline); aplite	fine-grained biotite diorite (rare)
Mount Wilson (2.1 km^2)	no	composite	equigranular, megacrystic, satellitic intrusions	granite and granodiorite	megacrystic (5-10%; 1-2 cm long)	massive	biotite	apatite, zircon, monazite	coarsely megacrystic granite	biotite-rich, polymictic mafic diorite (1-5%)
Pelly River (5.4 km^2)	no	composite	equigranular, megacrystic, coarsely megacrystic	granite and granodiorite	megacrystic and coarsely megacrystic phases (5-15%; 2 cm x 1 cm, up to 4 cm x 2 cm)	massive or foliated (megacrystic phase); massive (coarsely megacrystic and equigranular phases)	biotite	apatite, zircon, allanite, monazite, muscovite (secondary)	aplite, porphyry, lamprophyre	fine-grained biotite diorite
Southern South Nahanni (5.4 km^2)	no	homogeneous	coarsely megacrystic	granite	7-15%; 3-5 cm long	massive or faintly foliated megacrysts	biotite, rare hornblende	allanite, zircon, apatite	aplite, porphyry	fine-grained, mafic biotite diorite (rare)
Flat Lake (47.6 km^2)	no	homogeneous	megacrystic	granite	5-7%; 1 cm x 1 cm	massive	biotite,	allanite, zircon, apatite, hornblende, clinopyroxene	aplite	mafic, biotite porphyroblastic or fine-grained biotite-hornblende diorite (uncommon)
					Plutons With Hornblende					
O'Grady Batholith (270 km^2)	no	composite	marginal (equigranular and coarsely megacrystic), transitional, crowded megacrystic	granite	crowded megacrystic phase (40-60%; 0.5-1 cm); transisitional phase (3-5%; 0.5-1 cm); marginal phase (absent or 5-15%; 0.5-2 cm long)	massive (marginal and crowded megacrystic phases) or foliated (transitional phase)	hornblende ±biotite ±clinopyroxene	magnetite, titanite, apatite, zircon, allanite, tourmaline	aplite, pegmatite, rare porphyry	fine-grained hornblende diorite (marginal phase, 1-3%; transitional and crowded megacrystic phases, <1 to <<1%)
Northern South Nahanni (2.0 km^2)	no	homogeneous	equigranular	granodiorite	none	massive; locally intensely fractured	biotite > hornblende	allanite, zircon, apatite	aplite, mafic porphyry	mafic, polymictic hornblende-biotite diorite (<1 to 2%)
Central South Nahanni (37.5 km^2)	no	homogeneous	equigranular	granodiorite	none	massive	biotite > hornblende	apatite, zircon, allanite, tourmaline	porphyry, aplitic granite	mafic, polymictic hornblende- and biotite-rich diorite (1-5%)

a) CLEA Pluton

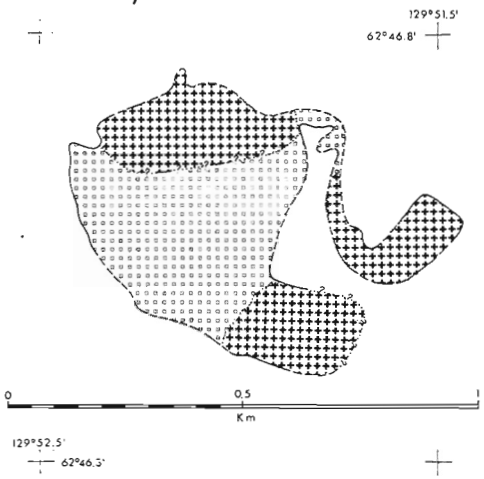

LEGEND

- peraluminous garnet-tourmaline-muscovite-biotite granite (CAC and Rudi plutons)
- coarsely megacrystic biotite granite
- megacrystic biotite granite
- equigranular biotite granite
- equigranular hornblende-biotite granite or granodiorite
- equigranular, leucocratic, fine or fine- to medium-grained granite
- zone of common, leucocratic aplite and alaskite intrusions (O'Grady batholith)
- crowded megacrystic phase (O'Grady batholith)
- transitional phase (O'Grady batholith)
- marginal phase (O'Grady batholith)
- 45 mineral or mafic schlieren foliation
- 30 mineral lineation
- accessory hornblende± clinopyroxene in host or inclusion
- geological contact: defined, approximate, gradational, inferred
- alteration zone (northern South Nahanni pluton)

LENED Pluton

CAC Pluton

RUDI Pluton

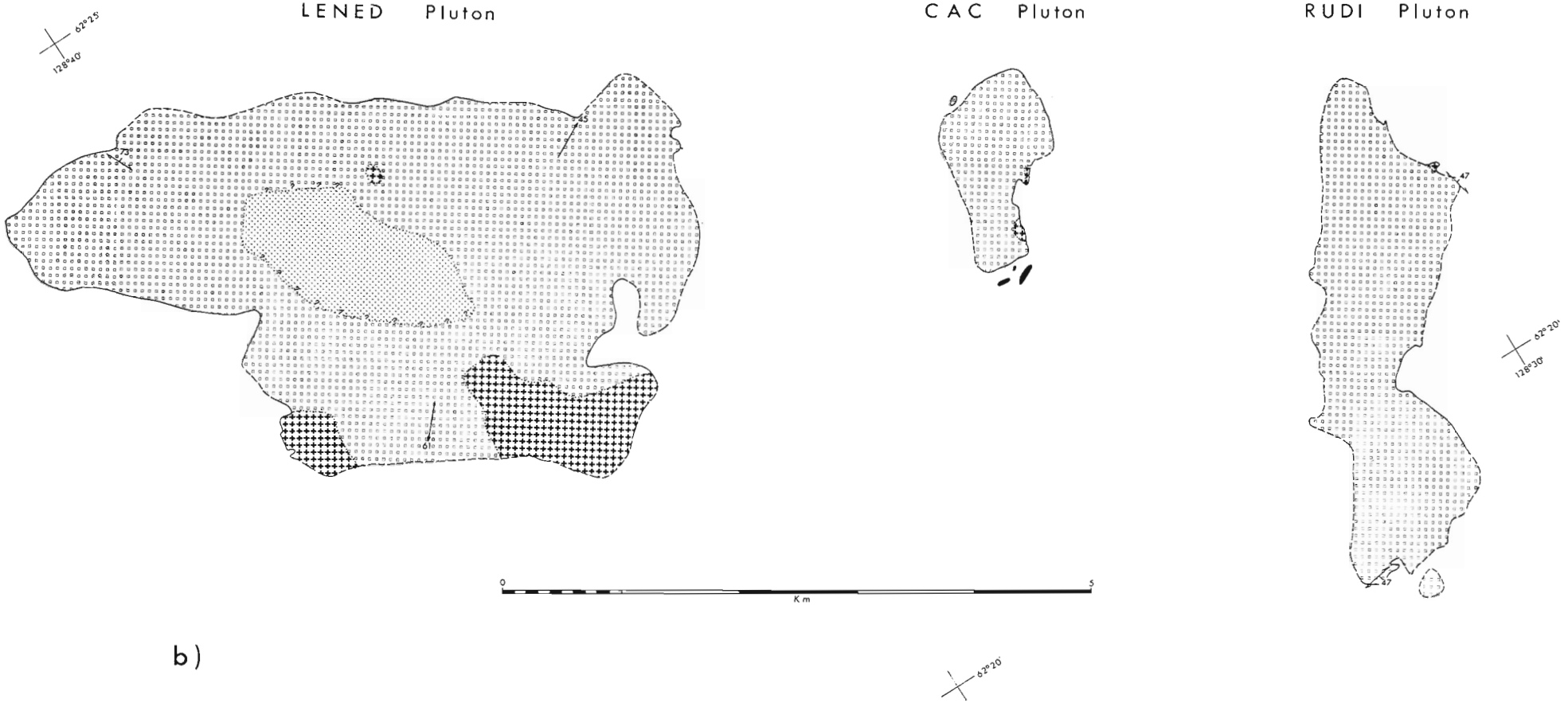

b)

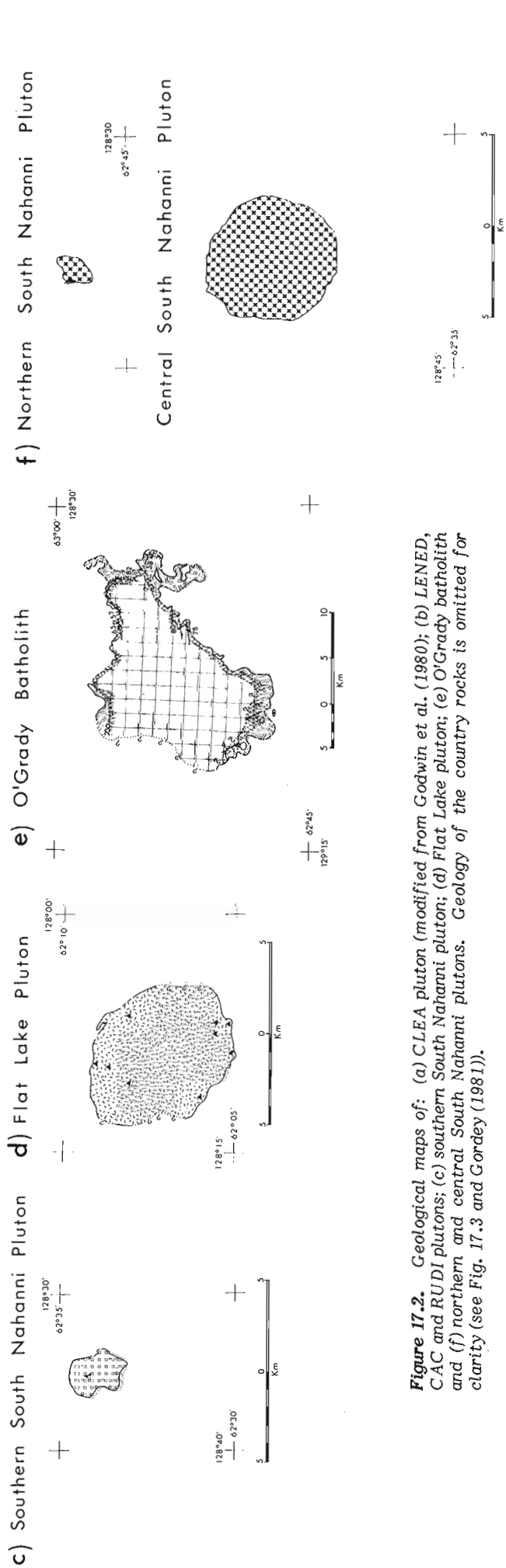

Figure 17.2. Geological maps of: (a) CLEA pluton (modified from Godwin et al. (1980); (b) LENED, CAC and RUDI plutons; (c) southern South Nahanni pluton; (d) Flat Lake pluton; (e) O'Grady batholith and (f) northern and central South Nahanni plutons. Geology of the country rocks is omitted for clarity (see Fig. 17.3 and Gordey (1981)).

feldspar megacrysts (5-8 cm long) set in a medium grained biotite granite groundmass identical to the equigranular phase. Aplitic fine- to medium-grained, muscovite-tourmaline-biotite granite occurs locally along the eastern and southeastern margins.

Fine grained, mafic inclusions are rare or absent and are restricted to the northeastern part of the pluton. Hornfels inclusions occur in the equigranular phase within a few metres of its intrusive contact.

The equigranular phase is gradational with the coarsely megacrystic phase (Tompson, 1978, Fig. 17.3a). Near the contact, in the equigranular phase, are rare zones (1-3 m wide) of abundant, crudely aligned, large alkali feldspar megacrysts. They may be dykes, but they are not defined by distinct margins. Randomly oriented, coarse megacrysts also form metasomatic "aureoles", 1-3 m wide, in the equigranular phase around these zones. At the contact between the two phases, irregular, gently west-dipping units of megacryst-rich and megacryst-free granite interdigitate. No analogous equigranular "zones" were observed in the coarsely megacrystic phase south of the contact. These relationships (Fig. 17.3a) suggest late growth of alkali feldspar megacrysts mainly in the southern part of the pluton, in isotopic disequilibrium with the equigranular groundmass (Godwin et al., 1980).

In the southern part of the pluton, the coarsely megacrystic phase extends to the covered contact with the scheelite-bearing skarn (Godwin et al., 1980). Varieties of pelitic and calc-silicate hornfels of possible Silurian age (Godwin et al., 1980; Tompson, 1978; correlated with unit OSpt of Gordey (1981)) form the remainder of the country rock adjacent medium- to coarse-grained granite.

Tourmaline-bearing, biotite (± muscovite) granite aplite dykes, pegmatitic seams and pods and late quartz veins intrude both phases and the scheelite-bearing skarns (Fig. 17.3a). Locally, two or more generations of aplite dykes are developed.

LENED, CAC, and RUDI Plutons. Important tungsten skarns on the LENED, CAC and RUDI properties (Dick, 1980) are associated with a northwest-trending zone of similar plutons, three of which are described together (Fig. 17.1, 17.2b, 17.3b, Table 17.1).

The LENED (12.3 km^2), CAC (1.9 km^2) and RUDI (4.7 km^2) plutons are small, massive, commonly composite stocks that consist of a predominant coarsely megacrystic phase, a subordinate equigranular phase and, in the LENED pluton, an extensive, heterogeneous, finer grained, more leucocratic phase. A homogeneous, medium grained biotite granite forms the equigranular phase and the groundmass of the coarsely megacrystic phase. Alkali feldspar megacrysts are euhedral to subhedral, tabular grains 2 to 5 cm long (rarely 7 to 13 cm long and 2 cm wide) and constitute 3 to 10 per cent (locally 15 to 20 per cent) of the rock. Lineation or foliation of the megacrysts occurs rarely near intrusive contacts. Rare megacrysts exhibit inner, concentric zones of fine grained mafic silicates. Biotite is the essential mafic; muscovite occurs in a few places as an accessory mineral.

The finer grained leucocratic phase in the LENED pluton is heterogeneous. Biotite granite in the northwest is massive, leucocratic, equigranular and medium grained. Fine- to medium-grained, equigranular to seriate, leucocratic biotite granite in the southeast contains rare alkali feldspar, quartz, and biotite phenocrysts. As with the Mactung pluton (Anderson, 1982), the finer grained leucocratic phase occurs near the centre of the pluton; in the LENED pluton, however, the finer grained leucocratic phase does not underlie the topographically highest point in the pluton.

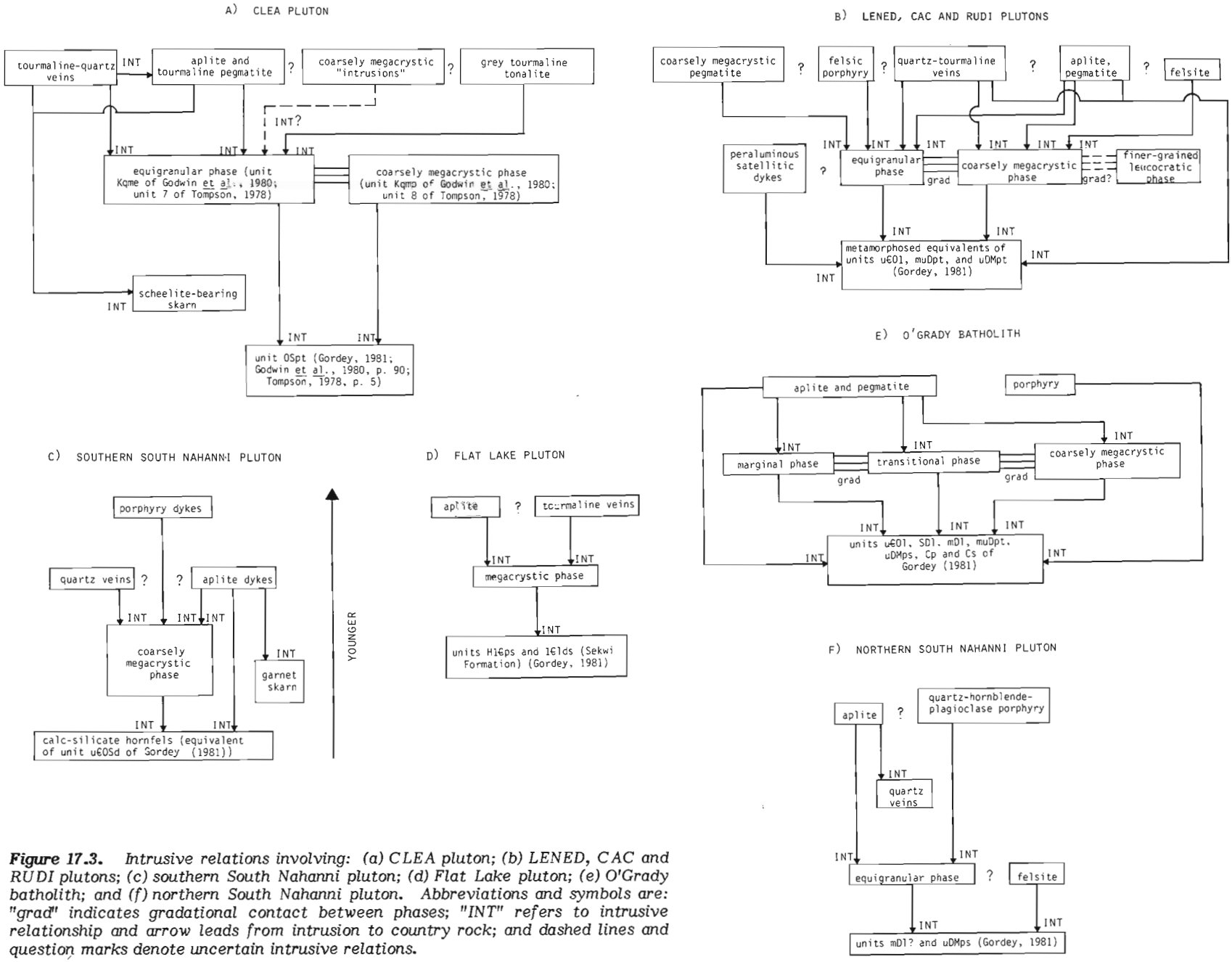

Figure 17.3. *Intrusive relations involving: (a) CLEA pluton; (b) LENED, CAC and RUDI plutons; (c) southern South Nahanni pluton; (d) Flat Lake pluton; (e) O'Grady batholith; and (f) northern South Nahanni pluton. Abbreviations and symbols are: "grad" indicates gradational contact between phases; "INT" refers to intrusive relationship and arrow leads from intrusion to country rock; and dashed lines and question marks denote uncertain intrusive relations.*

Fine grained, round (3-15 cm long), mafic inclusions of biotite diorite, biotite porphyry diorite and rare, thinly layered diorite are common near plutonic margins and constitute less than 1 per cent of the rock. Megacrysts are present in some inclusions.

Megacryst size, shape and abundance in the coarsely megacrystic phase diminish across gradational contacts with the equigranular phase. The transition may occur within 20-40 cm to several tens of metres from a plutonic margin or may occur locally within a phase producing heterogeneous intervals. In some places, "zones" (dykes?) of aligned, coarse alkali feldspar megacrysts occur within the equigranular phase (cf. CLEA pluton). Within the equigranular and coarsely megacrystic phases, apophyses of different grain size or composition but similar texture probably represent later intrusive pulses in the earlier phase. Unlike the Mactung pluton (Anderson, 1982), intrusive relations between the finer grained leucocratic and coarsely megacrystic phases are not known.

Equigranular and coarsely megacrystic phases intrude: greenish brown, spotted phyllite; white to grey marble, carbonaceous limestone and marble and diopside- and garnet-bearing calc-silicate hornfels; and rusty to brownish black andalusite hornfels. They are the contact metamorphosed equivalents of units HlCp, uCOl and muDpt and uDMps of Gordey (1981; Fig. 17.3b). Intrusive contacts are steep and discordant or rarely subconcordant. Layering in the hornfels dips away from the pluton.

Leucocratic and biotite (± tourmaline ± muscovite) granite aplite dykes and subordinate felsic porphyry, grey biotite felsite and tourmaline-bearing pegmatite dykes and intrusions intrude the plutons (Fig. 17.3b). They are particularly common near intrusive contacts. Distinctive leucocratic, locally miarolitic, pyrite-bearing muscovite aplite dykes intrude calc-silicate and scheelite-bearing skarns. Biotite granite satellitic intrusions invade pelitic and calc-silicate hornfels near the CAC and RUDI plutons. They contain some or all of the accessory minerals muscovite, garnet, andalusite and tourmaline, and some are miarolitic. These paraluminous dykes seem to distinguish plutons associated with extensive tungsten skarns (cf. Mactung pluton; Table 17.1 and Anderson, 1982). Tourmaline-quartz veins occur in equigranular and coarse grained phases and hornfels around all three plutons.

Barren Plutons Without Hornblende

Southern South Nahanni Pluton. The southern South Nahanni pluton is a north northwest-trending, oval body (5.4 km^2) consisting of massive, coarsely megacrystic biotite granite (Fig. 17.1, 17.2c, 17.3c). The rocks are massive to weakly foliated or lineated and medium to coarse grained. Euhedral to subhedral megacrysts (average size 3 to 5 cm x 1 cm; rarely 7 cm x 2 cm) constitute 7 to 15 per cent of the coarsely megacrystic phase. Locally, they impart a faint to moderate foliation or lineation to the massive, medium grained biotite granite host. Generally, biotite is the sole mafic silicate, but hornblende occurs as an additional essential ferromagnesian mineral in the east central part.

Within 100 m of some intrusive contacts, megacrysts decrease in size and abundance leaving a leucocratic, medium grained, equigranular rock. In the central part of the pluton, the coarsely megacrystic phase is intruded by two generations of melanocratic, medium grained, inclusion-bearing, mafic granodiorite apophyses. Inclusions are generally rare or absent, reach lengths of 30 cm, and consist of round, megacryst-bearing, fine grained, biotite diorite.

Except for the uncommon equigranular contact zones, the coarsely megacrystic phase extends to intrusive contacts with diopside- and garnet-bearing calc-silicate and pelitic hornfels (metamorphosed equivalents of unit uCOSd of Gordey (1981); Fig. 17.3c). Subconcordant, shallowly inclined intrusive contacts along the southern, northern and northwestern margins dip radially outwards. In the west and east, the contacts are steep and discordant and adjacent country rock layering is steeply dipping. Thin (1-10 cm wide) tourmaline-garnet skarns are developed along intrusive contacts in places along the pluton's southern margin. At one locality, coarser grained garnet skarn cuts across thinly layered diopside hornfels and both are intruded and disaggregated by a leucocratic aplite dyke (see Fig. 17.6). Timing of this skarn relative to contact metamorphism is similar to that envisioned for the Cantung skarns (Mathieson, 1982; Zaw, 1976).

Porphyritic dykes with phenocrysts of quart, alkali feldspar, plagioclase, biotite and clinopyroxene intrude the coarsely megacrystic phase and country rock near the southern margin. Aplite dykes invaded the pluton at least two or three times. They are common at intrusive contacts between the pluton and country rocks. Along the eastern margin, a thin aplite separates the coarsely megacrystic phase from the diopside-bearing calc-silicate hornfels.

Flat Lake Pluton. The oval Flat Lake pluton (47.6 km^2) is a homogeneous, massive, medium grained megacrystic biotite granite (Fig. 17.1, 17.2d, 17.3d). Subhedral megacrysts (0.5 to 1 cm square) form 5 to 20 per cent of the rock. Distinctive clinopyroxene and hornblende are widespread accessory minerals within 1 to 3 km of the intrusive contact.

Widespread but rare mafic inclusions (up to 1 m long) consist of fine grained, equigranular or porphyroblastic(?) biotite-hornblende diorite.

The Flat Lake pluton changes from megacrystic to seriate or equigranular (i.e., sparingly megacrystic) within a few hundred metres of its margin, but remains medium grained. Marble and tremolite calc-silicate hornfels (metamorphosed equivalents of the lCIds unit (Sekwi Formation; Gordey, 1981), with a "swiss cheese" texture, and rarer garnet-diopside skarns are developed locally along the pluton's southern and northern margin. Creamy white quartzite, rusty meta-arkose and brownish green phyllite of the HlCps unit (Gordey, 1981) form the country rock along most of the pluton margin (Fig. 17.3d).

Thin, irregular aplite dykes and rare tourmaline veins and fracture coatings occur in the megacrystic phase.

Plutons With Hornblende

O'Grady Batholith. The O'Grady batholith is the largest (270 km^2) northernmost hornblende-bearing pluton in the Nahanni map area (Fig. 17.1). It comprises three phases, namely a predominant, crowded megacrystic granite core (which underlies about 80 per cent of the batholith), and subordinate transitional and marginal granite phases arranged concentrically around the core (Fig. 17.3e). The marginal and transitional phases are most extensive along the southwestern, northwestern and northeastern margins where the batholith's intrusive contacts are subhorizontal or dip gently outward. Along the steep. outward-dipping eastern contacts. The transitional and marginal phases are less important. There, the transitional phase may predominante along some intrusive contacts and the marginal phase forms 1 to 10 m thick subhorizontal apophyses which extend up to 0.5 km into the country rock. Overburden obscures the distribution of the transitional and marginal phases along much of the batholith's western margin.

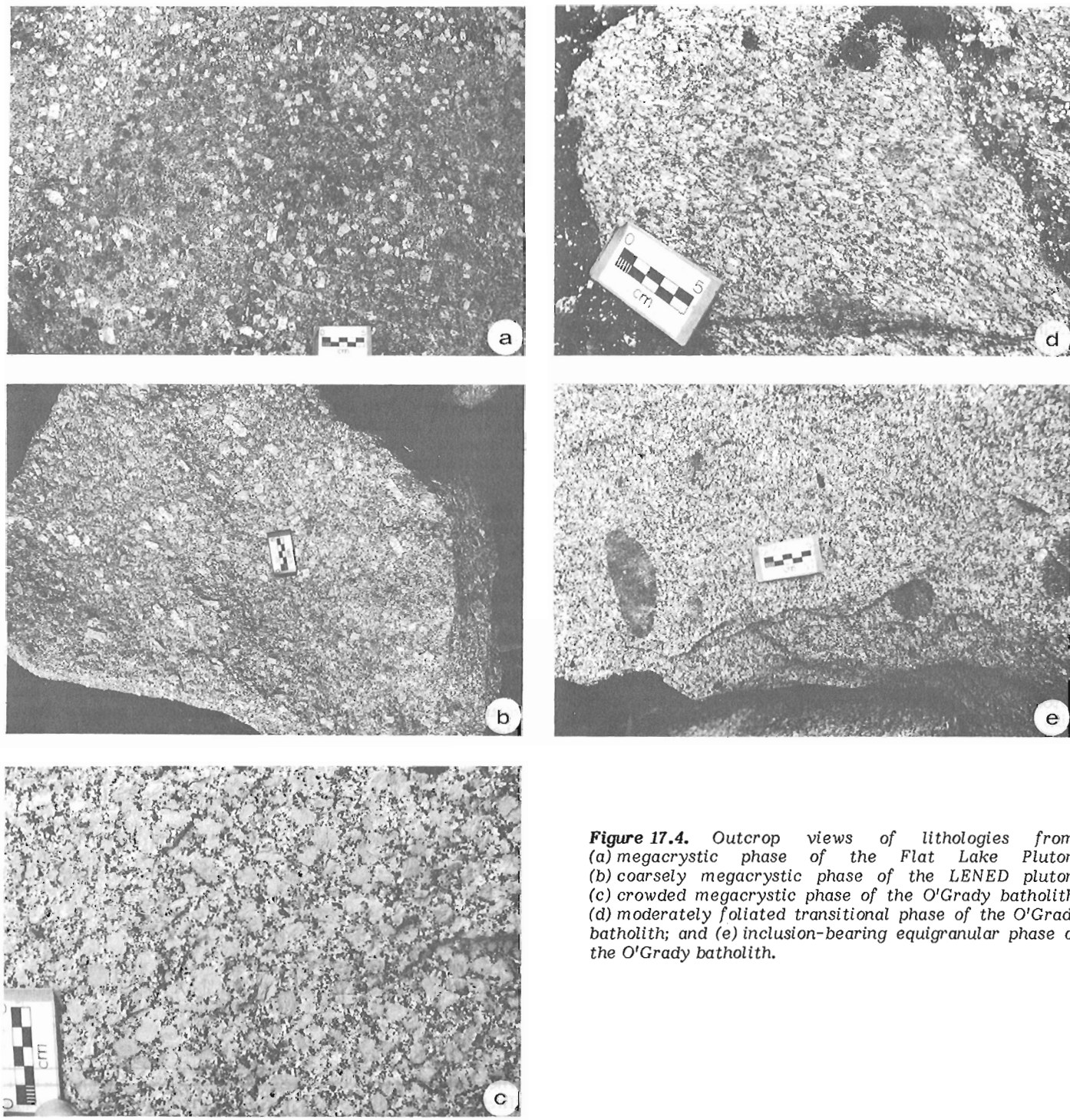

Figure 17.4. *Outcrop views of lithologies from: (a) megacrystic phase of the Flat Lake Pluton; (b) coarsely megacrystic phase of the LENED pluton; (c) crowded megacrystic phase of the O'Grady batholith; (d) moderately foliated transitional phase of the O'Grady batholith; and (e) inclusion-bearing equigranular phase of the O'Grady batholith.*

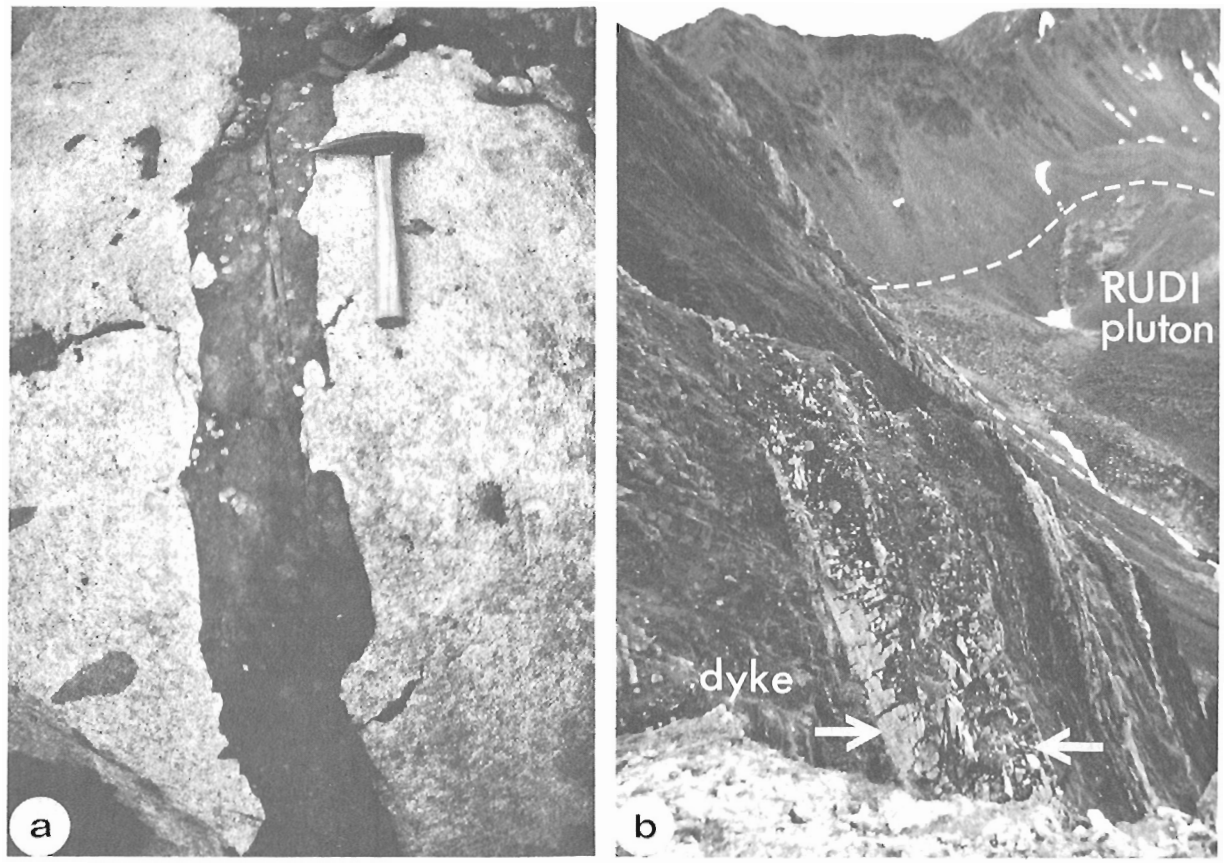

Figure 17.5. *Distinctive dykes in plutons with hornblende and plutons without hornblende, respectively: (a) aphanitic mafic andesite dyke in central South Nahanni pluton; and (b) satellitic tourmaline-garnet-muscovite-biotite granite dyke (outlined by arrows) along northern margin of RUDI pluton viewed from northwest.*

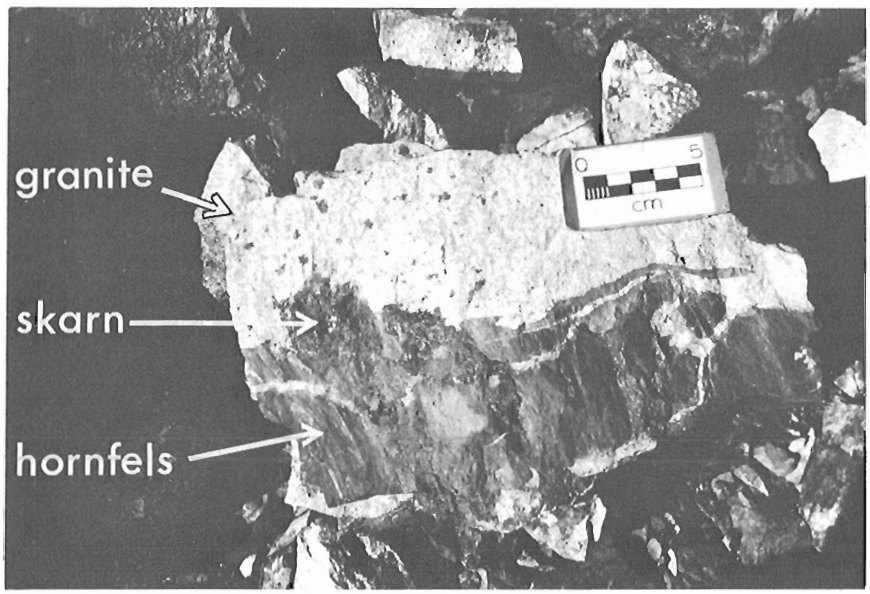

Figure 17.6

Talus block near southern margin of southern South Nahanni pluton. Sequential development of diopside-rich, layered calc-silicate hornfels, discordant garnet-rich skarn and aplitic granite intrusion are shown. Coarse grained dark minerals in granite are garnet xenocrysts incorporated from skarn.

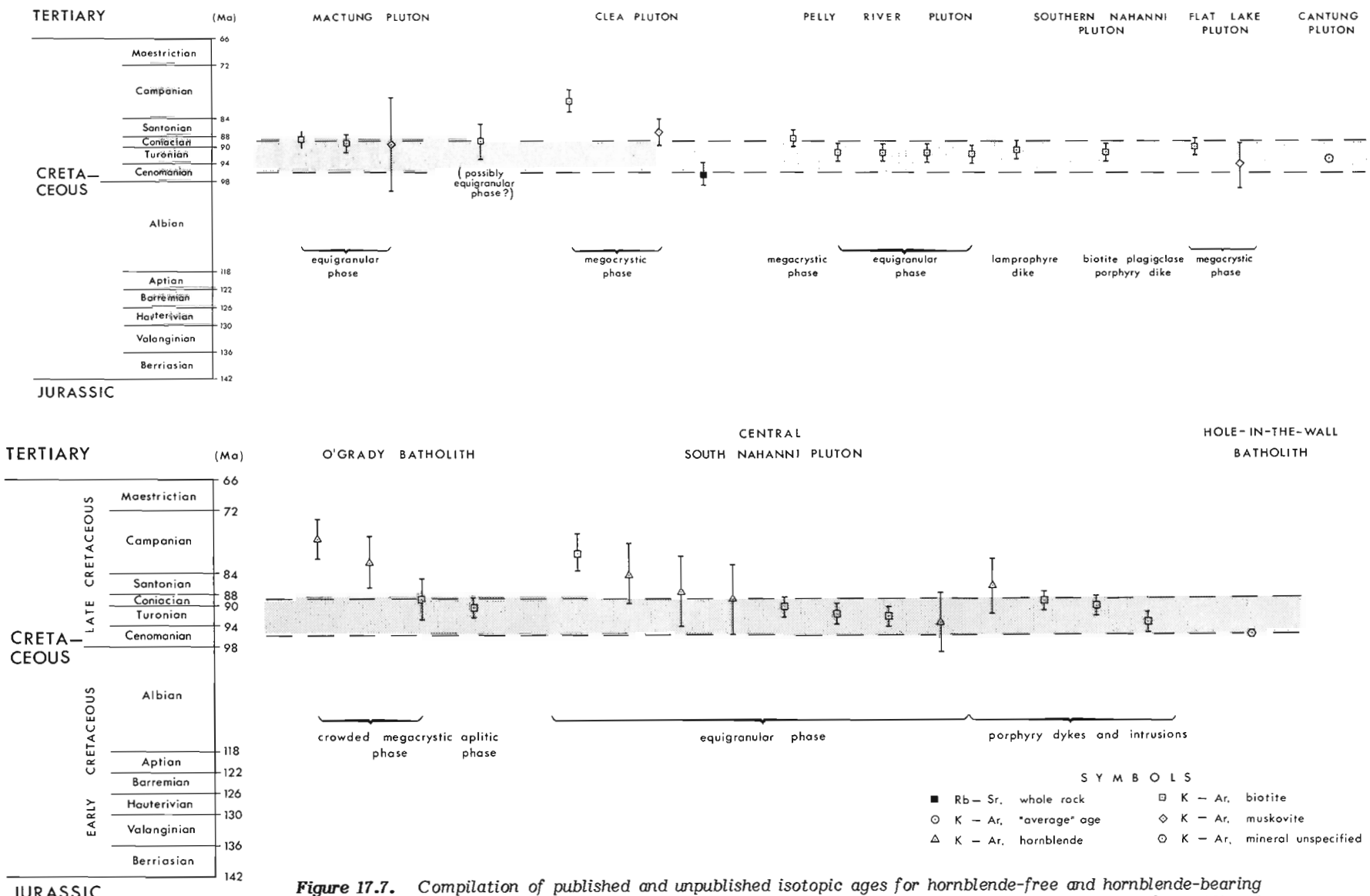

Figure 17.7. *Compilation of published and unpublished isotopic ages for hornblende-free and hornblende-bearing members of the southeastern Selwyn plutonic suite and time scale of Armstrong (1978). Sources for published isotopic ages given in Anderson (1982, Fig. 45.2) and all ages are consistent with new decay constants (Steiger and Jäger, 1977). Unpublished K-Ar isotopic ages are (R.D. Stevens, personal communication, 1982): Mactung pluton, 88.5 ± 2.0 Ma (Bi), 88.6 ± 2.0 Ma (Bi), 89.7 ± 10.5 Ma (Musc); Pelly River pluton, 88.2 ± 2.0 Ma (Bi), 91.3 ± 2.0 Ma (Bi), 91.5 ± 1.9 Ma (Bi), 91.7 ± 2.0 Ma (Bi), 91.9 ± 2.0 Ma (Bi), 91.0 ± 2.0 Ma (Bi; dyke); southern South Nahanni pluton, 91.4 ± 2.0 Ma (Bi; dyke), Flat Lake pluton, 90.1 ± 2.0 Ma (Bi), 94.0 ± 5.3 Ma (Musc); (Bi; dyke); and central South Nahanni pluton, 80.2 ± 3.6 Ma (Bi), 84.2 ± 5.9 Ma (Hb), 87.7 ± 6.9 Ma (Hb), 89.1 ± 6.8 Ma (Hb), 90.6 ± 2.0 Ma (Bi), 91.9 ± 2.0 Ma (Bi), 92.3 ± 2.0 Ma (Bi), 93.4 ± 5.8 Ma (Hb), 86.7 ± 5.4 Ma (Hb; dyke), 89.5 ± 1.9 Ma (Bi; dyke), 90.4 ± 2.0 Ma (Bi; dyke), 93.4 ± 2.0 (Bi; dyke). Abbreviations are: Bi = biotite: Musc = muscovite; Hb = hornblende. Shaded interval (89-96 Ma) is time of intrusion of southeastern Selwyn plutonic suite predicted by Godwin et al. (1980).*

The three main phases of the O'Grady batholith are distinguished by grain size, abundance and shape of alkali feldspar megacrysts, abundance and habit of biotite, and inclusion content.

The crowded megacrystic phase is composed mainly of randomly arranged subhedral (square) or anhedral (round) alkali feldspar megacrysts (40-60% of the rock). Their coarse grain size (0.5-1 cm) and light greenish grey colour also distinguish them from smaller, round white plagioclase and subhedral hornblende, euhedral titanite and subhedral magnetite in the finer grained groundmass (Fig. 17.4c). Generally, hornblende and clinopyroxene are the predominant and only ferromagnesian silicates; anhedral patches of biotite occur in a few places as an alteration product of hornblende.

The crowded megacrystic phase grades over a few tens of metres to a seriate or equigranular, medium grained transitional phase. Compared with the crowded megacrystic phase, alkali feldspar grains in the transitional phase are smaller, more euhedral, tabular and faintly to strongly aligned in a steep, radially outward dipping foliation (Fig. 17.2, 17.3d). Megacryst content locally reaches 40 per cent. Plagioclase is subordinate and anhedral. Biotite is sparse, but well formed as are hornblende, titanite and magnetite. Reduced abundance of megacrysts makes the transitional phase more mafic than the crowded megacrystic phase.

Abrupt gradational contacts between the transitional and marginal phases are marked by a change to the equigranular, massive texture of the latter phase (Fig. 17.3e). Megacrysts are absent or rare (1-2%) and biotite is common, widespread and euhedral to subhedral. Hornblende, titanite and magnetite are widespread and the equigranular subphase of the marginal phase is the most mafic unit in the batholith. A megacrystic variety of the marginal phase (5-15% megacrysts), occurs sporadically in the northwestern and southwestern parts, but grades inward to equigranular rock.

Round to elongate, randomly oriented mafic inclusions are widespread but their abundance varies with the host. The marginal phase contains most inclusions (1-3%; Fig. 17.3e); inclusions are rare or absent in the transitional and megacrystic phases. Inclusions (5 cm to 50 m long) are commonly fine grained, biotite- and/or hornblende-bearing diorite. Other interesting varieties are "igneous-looking" hornblende-plagioclase porphyry, porphyroblastic(?) biotite or hornblende porphyry and inclusions which are layered or contain smaller and fine grained inclusions. Subhedral alkali feldspar megacrysts occur in some inclusions; in a few places, the megacrysts cross the host rock-inclusion boundary. Calc-silicate and rusty, layered pelitic hornfels inclusions, particularly common near the margins of the batholith, are megacryst-free. Oblate, medium grained tourmaline-rich clots are distinctive inclusions (up to 7% of the rock) in the east central transitional phase. Along part of the northeastern margin, a small, heterogeneous zone of equigranular phase stockworks and agmatite contain abundant angular, fine grained mafic inclusions.

O'Grady batholith intrudes metamorphosed equivalents of units uCOdl, SDl, mDl, muDpt, uDMps, Cp and Cs of Gordey (1981; see Fig. 17.3e). Andalusite ± biotite is developed in pelitic rocks of appropriate composition and along the southern part of the eastern lobe of the batholith, and garnet-diopside hornfels but apparently no skarn (cf. Einaudi and Burt, 1982, p. 745) is produced from impure carbonate. Tourmaline-bearing calc-silicate hornfels occurs as far as 1 km north of the northern margin of O'Grady batholith.

Tourmaline-bearing, rarely miarolitic, aplite and granite pegmatite dykes are widespread, especially in the immediate country rock. Some intrusions are associated with subparallel mafic (tourmaline-rich) schlieren in the granitic host. Layered aplite and interlayered aplite and pegmatite intrusions occur mainly in the western part of the batholith. Aplitic and medium grained, leucrocratic, tourmaline-bearing granite intrusions are abundant in the crowded megacrystic phase in the central western part (see Fig. 17.2e). One of the highest tungsten values (18 ppm) for samples from the O'Grady batholith was determined from an alaskite dyke in the west central part (Garrett, 1971 and unpublished data). This may account for the anomalously high tungsten (and fluorine) stream sediment and water values that characterize drainage in the western third of the batholith (Goodfellow, 1982). Satellitic and rare biotite-plagioclase porphyry dykes occur along its northeast margin and probably are fine grained equivalents of the equigranular marginal phase at that locality.

Northern South Nahanni Pluton

Northern South Nahanni pluton forms a small, oblong intrusion (2.0 km^2; Fig. 17.1, 17.2f, 17.3f) consisting of massive, homogeneous, equigranular and medium grained granodiorite. Biotite is ubiquitous; hornblende is common (2-5%) in the north but absent in the east and south.

Randomly oriented, round, mafic inclusions form less than 1 or 2 per cent of the equigranular phase and range from 3 to 15 cm long. Fine grained, hornblende-biotite diorite, hornblende-plagioclase porphyry, and biotite porphyry diorite inclusions were recognized.

Except for thin fine grained felsite contact zones, the northern South Nahanni pluton is texturally homogeneous. In the north, the pluton intrudes light to dark grey, medium to thin bedded marble with black chert fragments parallel to bedding (unit mDl? of Gordey, 1981) and dark grey to black siliceous shale and chert (unit uDMps of Gordey, 1981).

Steep, closely spaced, subparallel rusty fractures are well developed in the centre of the pluton. A small, intensely altered zone, with small, uncommon sphalerite-pyrite-arsenopyrite veins in the granodiorite and country rock, occurs along part of the northwest contact (west of the pyrite-chalcopyrite-arsenopyrite ± sphalerite skarn on the PR property). This mineralization and arsenopyrite-rich skarns on the HILLMAN showing to the north (K. Dawson, personal communication, 1983) probably explain anomalously high arsenic values in stream sediment and water samples collected northwest of the pluton (Goodfellow, 1982).

Uncommon aplite and rare quartz-hornblende-plagioclase porphyry dykes intrude the granodiorite. Bluish to greenish grey felsite and fine grained biotite plagioclase porphyry dykes invade the country rock (Fig. 17.3f).

Petrography

Presence or absence of essential, euhedral or subhedral hornblende is a field criterion for subdividing the southeastern Selwyn plutonic suite. Other petrographic criteria that distinguish the two plutonic types include biotite habit and type and abundance of accessory minerals.

Biotite occurs in hornblende-bearing and hornblende-free plutons as euhedral to subhedral, tabular grains. In hornblende-bearing plutons it is devoid of inclusions or contains uncommon, fine grained apatite, and has pale yellowish brown to dark chocolate brown pleochroism. In contrast, biotite in hornblende-free plutons contains common,

fine grained, round zircon inclusions (and possibly monazite?; cf. Mittlefehldt and Miller, 1983, Fig. 7, p. 118) surrounded by radiation-damage haloes. Pleochroism is a distinctive pale yellowish brown to rusty or reddish brown.

Accessory minerals in the Selwyn plutonic suite include magnetite, titanite, muscovite, monazite, garnet, andalusite, tourmaline, zircon, allanite, chlorite, sericite, epidote and calcite. Opaque minerals are absent or rare except in the O'Grady batholith, where euhedral magnetite with euhedral titanite distinguishes it from other hornblende-bearing plutons. Muscovite occurs as medium grained, ragged anhedra (probably secondary) in alkali feldspar and biotite, and as subhedral grains (primary?) in aplitic granites. Whatever its texture or origin, muscovite occurs as a common accessory mineral only in plutons without hornblende. Monazite is rare and is also recognized only in plutons lacking hornblende. Inclusion-free euhedra of garnet and andalusite distinguish the satellitic or marginal phases of tungsten skarn-asociated plutons. Interstitial tourmaline, subhedral to euhedral zircon and allanite and chlorite, epidote, sericite and calcite (alteration products of the ferromagnesian minerals and plagioclase) are ubiquitous in plutons with or without hornblende.

K-Ar Geochronometry

Most of the published (see Anderson, 1982 for compilation) and unpublished (Archibald, 1980, 1981; this study, see Fig. 17.7) K-Ar isotopic ages for plutons with or without hornblende range from 88-96 Ma, the approximate time interval postulated by Godwin et al. (1980) for intrusion of the Selwyn plutonic suite. Aplite, lamprophyre and porphyry dykes yield coeval K-Ar isotopic ages (87-93 Ma) and indicate that the intrusion of the suite must be earlier. U-Pb (zircon) and Rb-Sr isotopic studies are underway to determine intrusion ages for members of the Selwyn plutonic suite.

Geochemistry

Preliminary geochemistry for plutons described by Anderson (1982) and for a few samples from other plutons collected by Gordey and others (in reconnaissance mapping of the Nahanni map area (Gordey, 1981)) indicate different geochemical affinities for the hornblende-bearing and hornblende-free plutons. Hornblende-bearing plutons, compared with peraluminous hornblende-free plutons, are less evolved (SiO_2 < 70%, higher MgO, CaO), metaluminous (molar $Al_2O_3/(CaO + Na_2O = K_2O)$ < 1.07), diopside-normative (or normative corundum < 1%) and have higher TiO_2/Zr ratios. Both types ahve low Fe_2O_3/FeO (<0.4) and Na_2O/K_2O (<1). Some geochemical criteria for I- and S-type granitoids (proposed by Chappell and White (1974) and Kwak and White (1982) among others) apply to the hornblende-bearing ("I-type") and hornblende-absent ("S-type") plutons although other field, petrographic and geochemical criteria are more equivocal.

Tungsten geochemistry for samples of tourmaline-muscovite-garnet-biotite granite (which forms marginal or satellitic phases in the Mactung pluton (Anderson, 1982)) shows they are richer in tungsten (8-12 ppm) compared with samples from other phases or plutons of hornblende-absent type (1-2 ppm W) and hornblende-bearing plutons (1-2 ppm W). These tungsten-rich peraluminous satellitic or marginal phases distinguish hornblende-free plutons associated with tungsten skarns form barren plutons.

Summary

In the Nahanni (105I) and southeastern Niddery Lake (105O) map areas, plutons with or without hornblende constitute the northwest-trending, mid-Cretaceous (older than 93 Ma) southeastern Selwyn plutonic suite. Different geographic position, composition, mineralogy, inclusions, intraplutonic dykes and related mineralization characterize each variety (Table 17.1). Coarse megacrysts occur in several plutons with large tungsten skarns (CLEA, LENED, CAC and RUDI plutons) and one which is apparently barren (southern South Nahanni pluton). Smoky grey quartz phenocrysts or patches in marginal or fine grained leucocratic phases characterize the Mactung, CLEA and LENED plutons. Hornblende-bearing, fine grained, mafic inclusions occur in plutons with essential hornblende and two plutons (southern South Nahanni and Flat Lake plutons) which generally lack hornblende. Mafic lamprophyrye or porphyritic dykes with hornblende or clinopyroxene occur in hornblende-free (Pelly River and southern South Nahanni) plutons and hornblende-bearing (northern and central South Nahanni) plutons, but are more common in the latter variety and absent in plutons with tungsten skarns.

This twofold subdivision may be extended to northwest on the basis of reconnaissance mapping of plutons in the Sekwi Mountain map area (105P; G. Abbott, personal communication, August 1982) and to the southeast (Mount Appler pluton (Mako, 1981, p. 87), Frances Lake map area (105H; Blusson, 1968), and Glacier Lake (95L) and Flat River (NTS 95E) map areas (Gabrielse et al., 1973)) on the basis of published petrography (Fig. 17.1).

Hornblende-free plutons with tungsten-rich, satellitic intrusions or marginal phases, containing some or all of apparently primary, widespread accessory minerals garnet, andalusite, muscovite and tourmaline, are associated with larger tungsten skarns (Mactung, CLEA and LENED-CAC-RUDI). Blusson (1968, p. 20) also reported garnet and tourmaline as rare accessory minerals in plutons around Tungsten, Northwest Territories.

Acknowledgments

Amax of Canada, Ltd., Union Carbide Exploration, Ltd. and Placer Development, Ltd. kindly allowed access to their properties and drill core information and provided logistical support. The able field asistance of L. Duchene and D. Humer is also gratefully acknowledged.

References

Anderson, R.G.
1982: Geology of the Mactung pluton in Niddery Lake map area and some of the plutons in Nahanni map area, Yukon Territory and District of Mackenzie; in Current Research, Part A, Geological Survey of Canada, Paper 82-1A, p. 299-304.

Archibald, D.A.
1980: Description and K-Ar geochronology of the intrusive rocks, LENED property, N.W.T.; unpublished Union Carbide company report.

1981: Preliminary report on the K-Ar geochronology and petrography of intrusive rocks, Selwyn Mountains, N.W.T. and Y.T.; unpublished Union Carbide company report, 31 p.

Armstrong, R.L.
1978: Pre-Cenozoic Phanerozoic time scale--Computer file of critical dates and consequences of new and in-progress decay-constant revisions; in Contributions to the Geological Time Scale, ed. G.V. Cohee, M.F. Glaessner and H.D. Hedberg, American Association of Petroleum Geologists, Studies in Geology, no. 6, p. 73-91.

Blusson, S.L.
1968: Geology and tungsten deposits near the headwaters of Flat River, Yukon Territory and southwestern District of Mackenzie, Canada; Geological Survey of Canada, Paper 67-22, 77 p.

Chappell, B.W. and White, A.J.R.
1974: Two contrasting granite types; Pacific Geology, v. 8, p. 173-174.

Dawson, K.M. and Dick, L.A.
1978: Regional metallogeny of the northern Cordillera: tungsten and base metal-bearing skarns in southeastern Yukon and southwestern Mackenzie; in Current Research, Part A, Geological Survey of Canada, Paper 78-1A, p. 287-292.

Dick, L.A.
1979: Tungsten and base metal skarns in the northern Cordillera; in Current Research, Part A, Geological Survey of Canada, Paper 79-1A, p. 259-266.

1980: A comparative study of the geology, mineralogy and conditions of formation of contact metasomatic mineral deposits in the norhteastern Canadian Cordillera; unpublished Ph.D. thesis, Queen's University, 471 p.

Dick, L.A. and Hodgson, C.J.
1982: The MacTung W-Cu(Zn) contact metasomatic and related deposits of the northeastern Canadian Cordillera; Economic Geology, v. 77, p. 845-867.

Einaudi, M.T. and Burt, D.M.
1982: Introduction – Terminology, classification, and composition of skarn deposits; Economic Geology, v. 77, p. 745-754.

Gabrielse, H., Blusson, S.L., and Roddick, J.A.
1973: Flat River, Glacier Lake and Wrigley Lake map-areas, District of Mackenzie and Yukon Territory; Geological Survey of Canada, Memoir 366, 421 p.

Garrett, R.G.
1971: Molybdenum and tungsten in some acid plutonic rocks of southeast Yukon Territory; Geological Survey of Canada, Open File 51, 5 p.

Godwin, C.I., Armstrong, R.L., and Tompson, K.M.
1980: K-Ar and Rb-Sr dating and the genesis of tungsten at the Clea tungsten skarn property, Selwyn Mountains, Yukon territory; Canadian Institute of Mining and Metallurgy, Bulletin, v. 73, no. 821, p. 90-93.

Goodfellow, W.D.
1982: Regional stream sediment and water geochemistry of the Nahanni map area (NTS 105I), Yukon and Northwest Territories (National Geochemical Reconnaissance Map NGR 51-1981); Geological Survey of Canada, Open File 868.

Gordey, S.P.
1981: Geology of Nahanni map area, Yukon Territory and District of Mackenzie; Geological Survey of Canada, Open File 780.

Kwak, T.A.P. and White, A.J.R.
1982: Contrasting W-Mo-Cu and W-Sn-F skarn types and related granitoids; Mining Geology, v. 32, p. 339-351.

Mako, D.A.
1981: The geology and genesis of the stratiform zinc-lead-barite mineralization of the Vulcan property, Selwyn Basin, Northwest Territories, Canada; unpublished M.Sc. thesis, University of Wisconsin-Madison, 180 p.

Mathieson, G.A.
1982: The Cantung E-zone scheelite skarn ore-body, Tungsten, N.W.T. Canada: A revised genetic model; unpublished M.Sc. thesis, Queen's University, 156 p.

Mittlefehldt, D.W. and Miller, C.P.
1983: Geochemistry of the Sweetwater Wash Pluton, California: Implications for "anomalous" trace element behaviour during differentiation of felsic magmas; Geochemica et Cosmochimica Acta, v. 47, p. 109-124.

Steiger, R.H. and Jäger, E.
1977: Subcommission on geochronology: Convention on the use of decay constants in geo- and cosmochronology; Earth and Planetary Science Letters, v. 36, p. 359-362.

Tompson, K.M.
1978: Geology of the Clea tungsten deposit, Yukon Territory; unpublished B.Sc. thesis, University of British Columbia, 32 p.

Zaw, U.K.
1976: The Cantung E-zone orebody, Tungsten, Northwest Territories, a major scheelite skarn deposit; unpublished M.Sc. thesis, Queen's University, 327 p.

18. UN RELIQUAT DE ZONE VOLCANO-SÉDIMENTAIRE DANS LA SOUS-PROVINCE ARCHÉENNE D'UNGAVA, QUÉBEC

Project 800005

Eric Mercier[1] et André Ciesielski
Division géologique du Précambrien

Mercier, E. et Ciesielski, A., Un reliquat de zone volcano-sédimentaire dans la sous-province archéenne d'Ungava, Québec; in Current Research, Part B, Geological Survey of Canada, Paper 83-1B, p. 165-175, 1983.

Résumé

Une séquence métamorphique affleurant sur 30 km² et noyée dans un socle de métagranodiorite se compose:

- *du groupe de Mac Isaac, à la base, qui présente le cycle complet de roches sédimentaires, caractéristiques de certaines zones vertes du sud de la province du lac Supérieur; et*
- *du groupe de Fagnant, qui repose en discordance sur le précédent et correspond au début d'un cycle volcanogénique.*

Ces roches ont subi les effets de deux phases de plis isoclinaux survenus au début et à la fin du paroxysme du métamorphisme, ainsi que d'une granitisation tardi-tectonique.

Abstract

A 30 km² metamorphic sequence outcrops in a basement of metagranodiorite and consists of:

- *at the base, the Mac Isaac Group, showing the complete cycle of sedimentary rocks characteristic of certain green zones in the south of the Superior Province*
- *above, the Fagnant Group surmounts it unconformably and marks the beginning of a volcanogenic cycle.*

The climax of metamorphism occurred between two phases of isoclinal folds, and is followed by late tectonic granitization.

Introduction

La sous-province archéenne d'Ungava se caractérise par une absence presque totale de formations volcano-sédimentaires (zones vertes) typiques des régions méridionales de la province du lac Supérieur, soit le Sud de l'Ontario, l'Abitibi et la baie James (Stevenson, 1968; Eade, 1966). Le domaine du lac Bienville (fig. 18.1), essentiellement granitique, est caractérisé par une quasi-absence d'enclaves au faciès des granulites (Herd, 1978), et par la présence de quelques lambeaux de zones vertes semblables à celles que l'on retrouve au sud, le long de la Grande Rivière (Sharma, 1976; Franconi, 1978). Les zones archéennes de la province du lac Supérieur présentent une forme généralement allongée et sont en contact avec des ensembles gneissiques ortho-et para-dérivés aux relations chronologiques parfois obscures, et avec des granitoïdes syn- et tardi-tectoniques sécants. On y reconnaît toutes les compositions de roches volcaniques dominées par des éléments basiques et intermédiaires (Wilson et Morrice, 1977; Dimroth et coll., 1982; Goodwin, 1977a), le tout surmonté de formations sédimentaires de compositions variées contenant des horizons ferrifères de type BIF (banded iron formation) caractéristiques de l'Archéen, ainsi que des conglomérats mono-et polymictes à galets granitoïdes (Baragar et McGlynn, 1976; Goodwin, 1977b).

Le métamorphisme à l'intérieur des zones atteint le faciès à amphibolites, mais avec une dominance au schistes-verts, tandis qu'à l'extérieur des zones, les gneiss paradérivés atteignent souvent le faciès à granulites à orthopyroxènes. Dans la sous-province de la baie James, les faciès tufacés dominent souvent, en particulier dans la zone de la Grande Rivière où les séquences volcaniques se situent stratigraphiquement tantôt au-dessus, tantôt en-dessous des sédiments (Franconi, 1978). On a remarqué que les sédiments intra-volcaniques diffèrent fortement des sédiments appartenant aux grands bassins sédimentaires d'Opinaca et de Némiscau (fig. 18.1) en ce qu'ils s'avèrent nettement plus alumineux, plus arkosiques, ou volcano-dérivés. En outre, la forme allongée des zones vertes n'est pas nécessairement originale; en effet, ces dernières sont plutôt périphériques et tributaires de la déformation des bassins sédimentaires. On y reconnaît au moins deux phases de plis, les plans axiaux de la dernière phase s'orientant souvent dans le sens de la longueur. Des reliquats de zones volcano-sédimentaires reconnus au nord de la Grande Rivière, trois se situent immédiatement à l'est du lac Bienville, et le plus important, à quelque 60 km à l'est de Poste-de-la-Baleine. Ce dernier, dont il est ici question, à déjà fait l'objet d'études visant à déterminer son potentiel économique (Gregory, 1958). La bande volcano-sédimentaire (foliation orientée à N280°) du lac Fagnant (fig. 18.1) est noyée dans un ensemble plutonique de composition granodioritique qui compose la presque totalité du domaine du lac Bienville (Ciesielski, 1983, ailleurs dans le présent volume). Le métamorphisme des enclaves basiques contenues dans ces granodiorites atteint un degré plus élevé que celui subi par les formations volcano-sédimentaires du lac Fagnant; en effet, ces enclaves se révèlent de nature respectivement fin amphibolite, mi-amphibolite et fin schiste vert. Ce reliquat de zone verte se distingue de ceux situés le long de la Grande Rivière du fait que, proportionnellement, il renferme plus de formations de fer (BIF) et de métaconglomérats à cailloux granitiques; en outre le rapport des roches volcaniques aux roches sédimentaires est beaucoup plus petit. Cette mini zone, bien qu'identique du point de vue du métamorphisme à d'autres bandes volcaniques, pourrait effectivement correspondre à un milieu passablement différent de ceux qui ont prévalu au sud, le long de la Grande Rivière où les phases pyroclastiques sont dominantes.

[1] Laboratoire de géologie structurale, Université des Sciences et Techniques de Lille, 59665 Villeneuve-d'Ascq. France

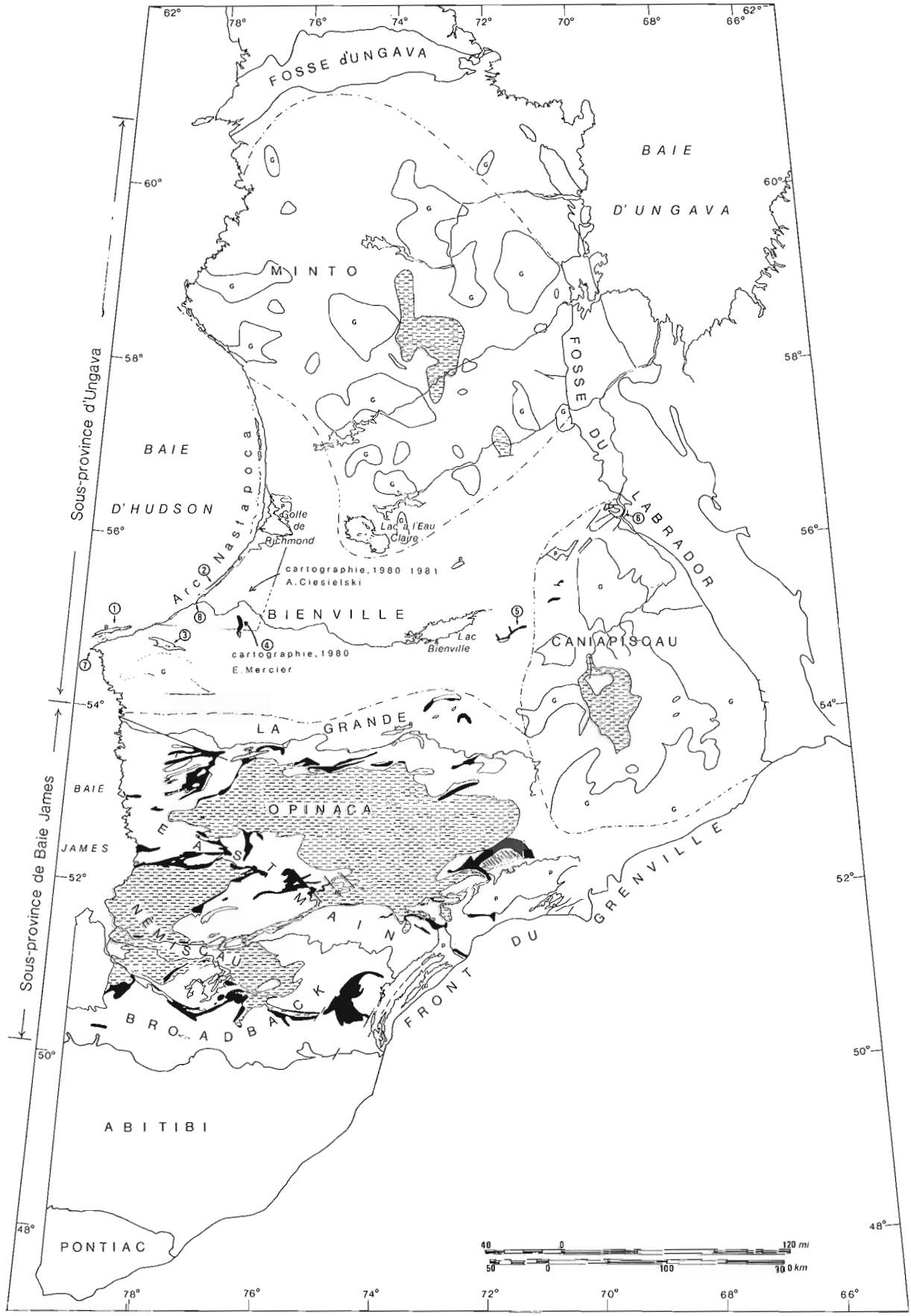

Figure 18.1. *Carte géologique simplifiée de l'Archéen du Québec, montrant la position des différents sous-ensembles tels qu'établis selon les différentes lithologies et variations structurales impliquées. D'après Avramtchev et Marcoux 1979, modifiée.*

Le milieu granitique

Les travaux de Sabourin (1961) et Eade (1966) ont permis de distinguer deux types de granitoïdes dans le milieu géologique de la bande du lac Fagnant.

Les gneiss granitiques

Il s'agit de roches souvent massives, de couleur gris vert, à grains moyens et à foliation discrète. L'étude miscroscopique montre une texture granoblastique à quartz, plagioclase (An_{22}), biotites vertes, hornblende (édenite), microcline rare, épidote, sphène et symplectiques à biotite et quartz et à épidote et plagioclase. La composition est celle d'une granodiorite. Le contact entre les gneiss granitiques et les séries volcano-sédimentaires est concordant à l'échelle de l'affleurement, par ailleurs, la foliation normalement orientée à N 280° dans les granodiorites va tourner à N 320° sur une distance de 500 m en approchant du contact. Ce dernier n'est pas recoupé par des pegmatites mais est souvent occupé par une roche différente de composition monzonitique (adamellite) et syntectonique. Vu la présence de conglomérats étirés à la base des séries volcano-sédimentaires, on pourrait croire à l'origine stratigraphique de ce contact, toutefois la présence de contacts caractérisés par des alternances de granodiorites, ou de monzonite et métasédiments, ainsi que des galets de conglomérats ayant une composition différente de celle de la roche granitique adjacente, semble indiquer qu'il ne s'agit pas d'un conglomérat de base, mais que le contact est plutôt d'origine tectonique.

Les granites massifs

Ces roches occupent les zones de contact ou recoupent les séries volcano-sédimentaires loin à l'intérieur de la bande du lac Fagnant. Il s'agit de roches sub-alcalines à monzonitiques accompagnées de toute la gamme de roches intermédiaires. Le pôle subalcalin est représenté par un leucogranite rose à gros grains (5 mm) de quartz, microcline, épidote ainsi que de la muscovite et du plagioclase rare. La texture est granoblastique.

Le pôle monzonite est représenté par un granite fin (1 mm), rosâtre, moucheté de vert. Il se compose de quartz, plagioclase abondant, microcline, biotite souvent chloritisée et myrmékites. Sa texture est aussi granoblastique. Ces deux types de granites syngénétiques tardifs présentent un contact sécant lorsqu'il s'agit de granites d'origine tardi-tectonique, et on observe sur plus d'un kilomètre en arrière du contact, des filons de pegmatites à quartz, microcline, muscovite et tourmaline qui recoupent la foliation (exceptionnellement on observe des boudinages). Près de ce même contact, les amphibolites ont subi une recristallisation non orientée et le granite contient des enclaves décimétriques et hectométriques de métavolcanites et métasédiments. Les monzonites présentent des contacts concordants quand elles sont d'origine syntectoniques. Il s'agit ici d'un faciès de bordure qui diffère de la masse des granodiorites dans laquelle est noyée la bande du lac Fagnant. Ces phénomènes de granitisation des contacts se retrouvent ailleurs dans l'A chéen et surviennent lorsqu'il y a rencontre, soit à petite ou à grande échelle, de roches acides ou intermédiaires et basiques.

D'autre part un échantillon de pegmatites sécantes a livré un âge de 2 625 millions d'années et un métasédiment a donné 2 555 millions d'années, (Lowdon, 1960). Ces âges sont contradictoires et on devrait d'ailleurs s'attendre à ce que les pegmatites soient plus jeunes. La méthode utilisée, soit celle du K/Ar sur muscovite, permet d'obtenir un âge de stabilisation de la croûte plutôt qu'un âge thermique de métamorphisme puisque la température de fermeture du système K/Ar sur muscovite est de l'ordre de 350°C.

Lithostratigraphie des métavolcanites et métasédiments

La série lithostratigraphique est donnée à la figure 18.3. On remarque que les deux types de schistes décrits par Gregory (1958) et Sabourin (1961), élevés ici au rang de "groupe", sont divisés respectivement en trois et en deux couches qui non seulement servent d'unité cartographique (fig. 18.2) mais sont également désignées par leur constituant principal. (Dans la nomenclature de Hedberg (1976) ces "couches" correspondent à des "zones".)

Le groupe de Mac Isaac

La couche des amphibolites à grenats Cette couche, épaisse de 400 m, repose sur les gneiss granitiques; elle se compose essentiellement d'amphibolites vert sombre ou bleu clair à foliation nette et cassure brillante, ponctuées de nombreux grenats plurimillimétriques. On observe aussi de rares niveaux de micaschistes sombres, riches en grenats, et des niveaux de quartzites blancs de quelques centimètres à plusieurs mètres d'épaisseur, particulièrement nombreux vers le sommet de la couche.

Les amphibolites vertes ont une texture nématoblastique. La paragnèse est constituée de hornblende (hastingsite magnésienne), biotite (souvent chloritisée), quartz, plagioclase (An_{40}), cummingtonite ss et grenat (almandin) riche en inclusions.

Les amphibolites bleu clair (moins abondantes) ont une texture nématoblastique à diablastique. On y observe de la cummingtonite sl (limite cummingtonite ss et grunérite), des grenats (almandin) riches en inclusions et de rares feldspaths et biotites.

Les micaschistes sombres ont une texture granoblastique. On y observe de la biotite, du quartz, du plagioclase (An_{20}), du grenat (almandin), quelques gédrites, des chlorites magnésiennes et des cordiérites plus ou moins altérées. Les quartzites, souvent très purs, ont une texture granoblastique polygonale.

Les éléments susceptibles d'indiquer la nature originelle des constituants de cette couche sont rares.

Quelques structures en coussins dans des amphibolites situées 10 km plus au sud et corrélées par Sabourin (1961) avec l'unité ici dénommée groupe de Mac Isaac, indiquent une nature orthodérivée. L'examen de lames minces révèle que les contacts entre les quartzites et les amphibolites (fig. 18.4) sont systématiquement progressifs et semblent donc d'origine sédimentaire. Dans ces quartzites, on peut observer des lits alternants de micaschistes de 1 à 10 cm, qui peuvent représenter d'anciens dépôts gréso-pélitiques (turbidites?).

Le niveau ferrifère Cette couche, épaisse de 10 m au nord et de 150 m au sud, se compose d'un quartzite finement lité (1 mm) alternativement blanc (quartzite pur) et noir (quartzite à magnétite). À la base, on observe dans les lits noirs, des grenats poecilitiques (almandins) et de la cummingtonite (limite cummingtonite ss et grunérite). Le phénomène de la tectonique ne permet pas, à lui seul, d'expliquer l'ampleur de la variation d'épaisseurs.

Il appert que ce niveau a un type de gisement (couche à tendance lenticulaire au passage d'une série à dominante volcanique à une série à dominate sédimentaire), une minéralogie (quartz et magnétite), un faciès lithologique (finement lité), et un âge (archéen) qui le rapproche fortement des minéraux de type "Algoma" (Gross, 1965). Ces minerais sont considérés comme spécifiques aux zones volcanosédimentaires d'âge archéen.

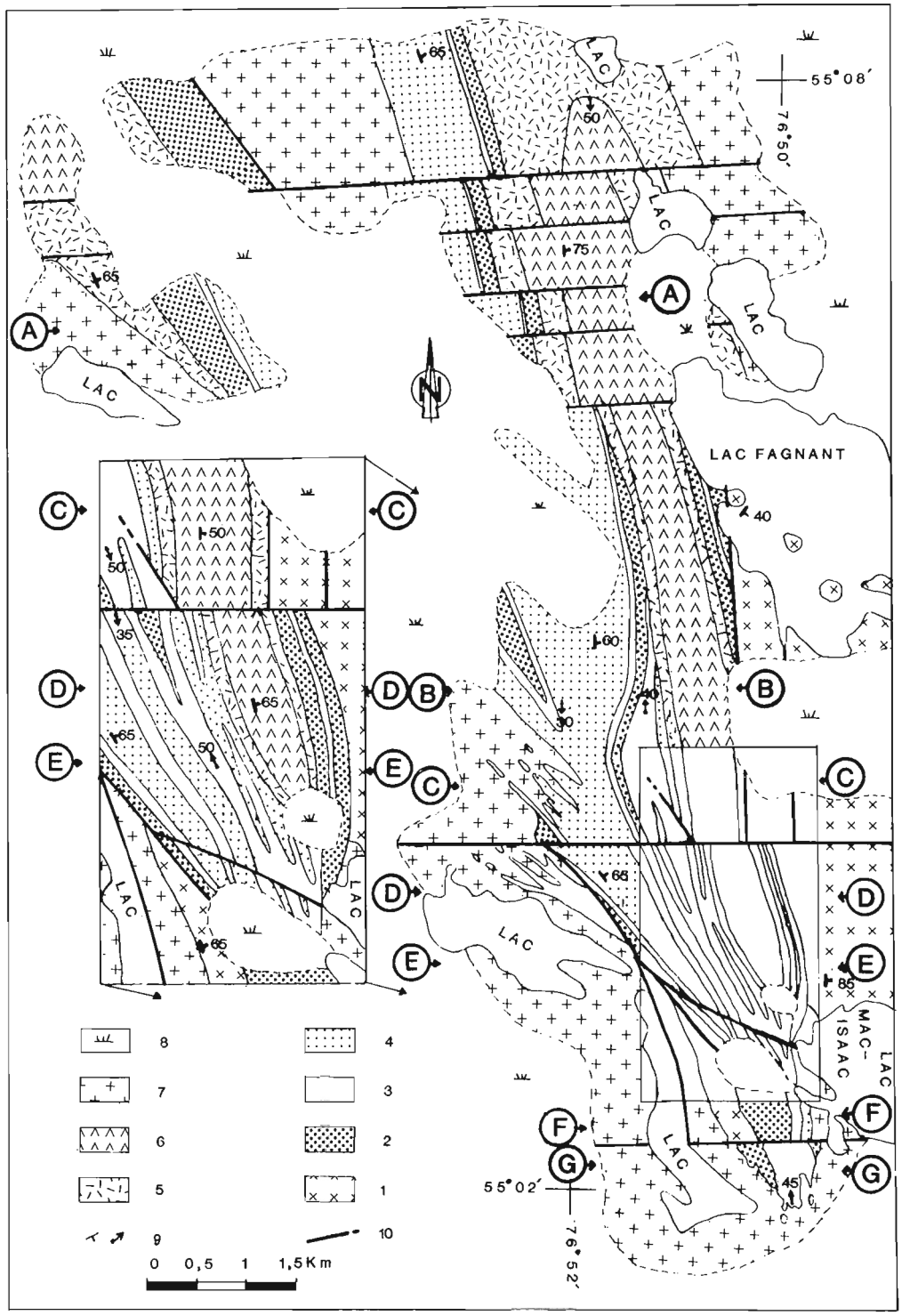

Figure 18.2. *Carte géologique de la région du lac Fagnant (1 à 8: unités cartographiques).*
1. gneiss granitiques; 2. couche des amphibolites à grenats; 3. niveau ferrifère; 4. couche des micaschistes; 5. couche des amphibolites litées; 6. couche des amphibolites massives ou à coussins; 7. granites massifs; 8. Quaternaire: sables fluvio-glaciaires et marécages; 9. foliation S_2 et plongement axial des plis P_2; 10. failles. L'emplacement des coupes de la figure 18.6 est indiquée.

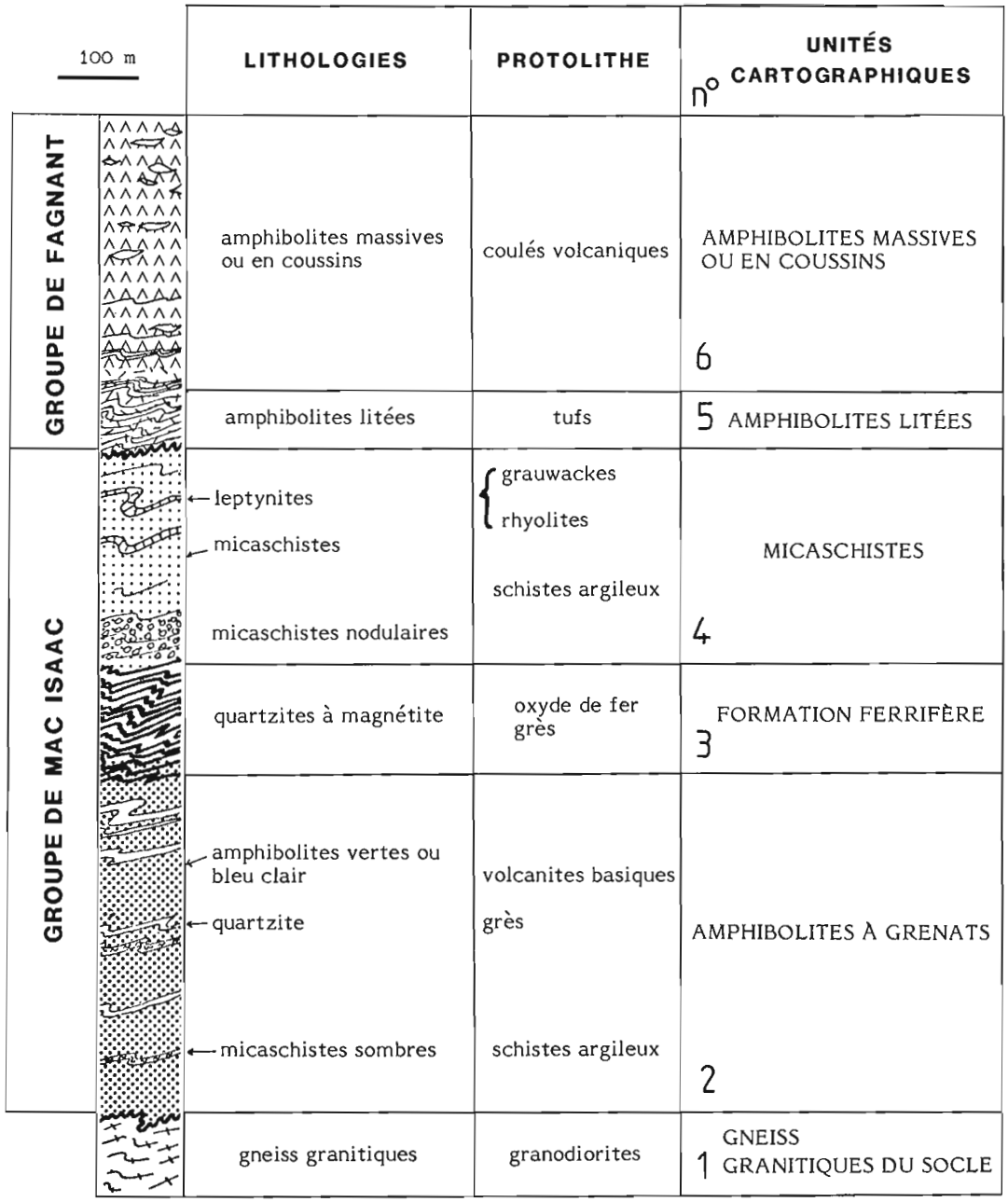

Figure 18.3. *Colonne lithostratigraphique des métavolcanites et métasédiments de la région du lac Fagnant. Le style tectonique, isoclinal très pincé, empêche toute évaluation précise des épaisseurs qui ne sont données qu'à titre d'information. Une partie de la nature originelle de la série est hypothétique du fait de la double origine possible (ortho- et para-) de certaines des roches concernées.*

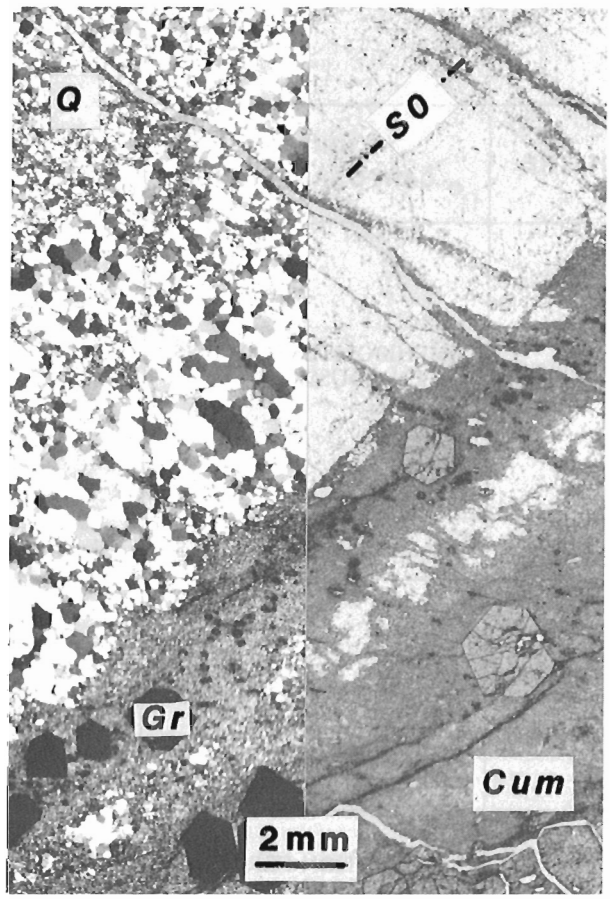

Figure 18.4. *Microphotographie (LN, LP) d'un contact sédimentaire maintenant composé d'un quartzite (Q) et d'une amphibolite à cummintonite (Cum) et grenat (Gr) prélevée dans la couche des amphibolites à grenats du groupe Mac Isaac.*

La couche des micaschistes Cette couche épaisse de 250 m repose sur la précédente sans niveau de transition. Elle se compose, à la base (20 m), de micaschistes noduleux dorées ou violets puis, dans le reste de la série, de micaschistes noir mat ou jaune doré associés à quelques niveaux (1 à 10 m) de leptynites massives à yeux millimétriques et à des bancs métriques de quartzites.

Tous les micaschistes sont de texture granoblastique et se composent de quartz, de feldspath altéré, de biotite et parfois de grenat poecilitique, de muscovite, de chlorite magnésienne et de tourmaline. Les micaschistes noduleux contiennent également, des nodules poecilitiques de cordiérite altérée et des aiguilles de sillimanite. Les micaschistes violets possèdent en plus de la muscovite, de l'andalousite en grandes bandes, de la cordiérite et de la sillimanite. Les quartzites, très purs, ont une texture granoblastique.

Les leptynites sont également de texture granoblastique. Selon le cas, les yeux se composent de quartz ou de plagioclase. Dans ce dernier cas, on observe alors des grains polycristallins de hornblende qui ponctuent un fond composé, dans les deux cas, de quartz, de feldspath et de biotite très rare.

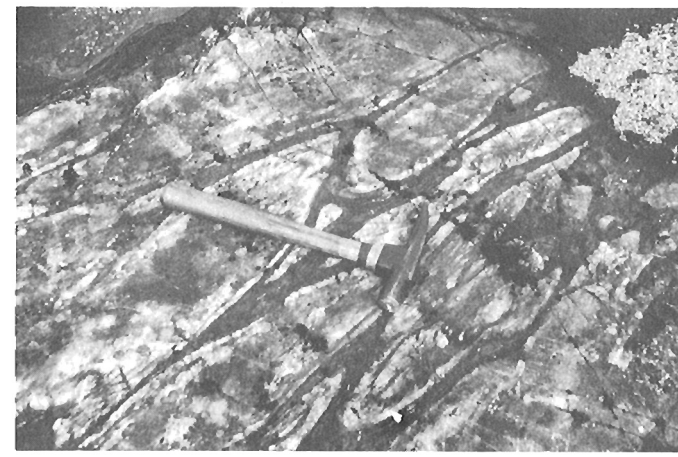

Figure 18.5. *Structure en coussins dans la couche des amphibolites massives ou en coussins (groupe de Fagnant).*

S'il est aisé d'attribuer une origine détritique (pélites, alumineuses à la base, et grès) au reste de la zone, l'origine des leptynites, elle, est plus délicate à établir. Les auteurs estiment que les leptynites aux yeux en quartz pourraient être des métarhyolites, et les autres, des métagrauwackes.

Le groupe de Fagnant Le groupe repose sur le précédent grâce à une discordance cartographique peu marquée dont la signification fera plus loin l'objet d'une discussion.

La couche des amphibolites litées Cette couche épaisse de 1 000 m au nord et de 20 m au sud se compose d'amphibolites massives à cassure terne au niveau de laquette on observe des lits (1 cm à 1 mm) alternativement vert clair et vert franc.

L'examen des lames minces révèle une texture lépidoblastique aux composants suivants: hornblende dans les lits vert franc et hornblende, plagioclase, et biotite dans les lits vert clair.

Il ne peut s'agir, ici, d'autre chose que d'une ségrégation minérale originelle qui correspond; vraisemblablement, à la mise en place rythmique de particules de laves basiques. Cette couche s'avèrerait donc un méta-tuf et la diminution d'épaisseur observée vers le sud correspondrait à un éloignement du site éruptif.

La couche des amphibolites massives ou en coussins Cette couche sans limite tranchée avec la précédente se compose, sur au moins 300 m d'épaisseur, d'amphibolites massives à foliation discrète et à patine terne d'un vert brun sombre.

Des coussins étirés (mieux conservés vers le haut où les bordures figées sont dégagées par l'érosion) sont pourtant visibles (fig. 18.5).

L'examen des lames minces révèle une texture nématoblastique aux composants suivants: hornblende, plagioclase altéré, dont quelques microlites corrodés (An_{50-55}), et des amas de carbonate. Au sommet de la couche, la texture devient diablastique et l'amphibole est une actinote, associée ici à des granules d'épidote.

Ces roches étaient, probablement dans leur totalité, des coulées basiques d'origine, au moins en partie, sous-aquatiques.

Histoire structurale

L'anomalie magnétique provoquée par le niveau ferrifère a limité le nombre des mesures prise; ces dernières n'ont d'ailleurs pu être réalisées qu'à l'aide d'une méthode astronomique adaptée de Dassié (1979). En conséquence, le présent rapport ne comprend pas de stéréogrammes.

Les métavolcanites et métasédiments se présentent en un vaste synclinorium à axe orienté du nord au sud, et que l'on peut reconnaître sur une carte à sa forme en éventail.

Les deux groupes, bien que séparés par une discordance, présentent les mêmes éléments structuraux. La discordance est donc précoce par rapport aux phases synschisteuses. La simplicité cartographique de cette discordance (le groupe de Fagnant repose pourtant sur la couche des amphibolites à grenats, sauf au sud-ouest de son affleurement principal) indique qu'elle recouvre une déformation à géométrie simple (basculement ou larges plis).

Les structures macroscopiques

Dans les affleurements des deux groupes, la foliation dominante S_2 a une attitude relativement constante: direction nord-sud et pendage de 60° à 80° vers l'est. Cette foliation représente le plan axial des plis P_2 isoclinaux, d'ordre kilométrique, visibles sur la carte (fig. 18.2). Ces plis ont des plongements axiaux de 45°, alternativement vers le nord et vers le sud. Comme le plan axial est constant, cette variabilité peut s'expliquer par des hétérogénéités dans les déformations et par une géométrie initiale complexe de la surface plissée (déjà plissée par la phase 1: voir plus loin). Cette particularité implique l'absence de cylindrisme sur une grande distance dans la structure (fig. 18.6). Il est à remarquer que cette fluctuation d'axe n'a que de faibles manifestations cartographiques et se distingue par son style très pincé. La confrontation de la carte (fig. 18.2) et de la colonne lithostratigraphique (fig. 18.3) suppose, au moins pour le groupe de Mac Isaac, l'existence de plis P_1 antérieurs, isoclinaux et d'ordre kilométrique repris par les plis P_2 (fig. 18.9). Ces deux générations de plis ne se recoupent pas sur la carte, ils sont donc coaxiaux (Ramsay, 1967).

Le terrain est découpé par des failles verticales qui engendrent une morphologie spécifique. Les failles directionnelles sont interrompues par les failles transverses sans être décollées. La fracturation d'orientation nord-sud a donc eu lieu dans des panneaux déjà isolés par des accidents à orientation est-ouest.

Les structures mésoscopiques et microscopiques

La foliation S_2, souvent parallèle à S_1, fait généralement preuve d'une grande force de pénétration: ce caractère s'atténue dans les coeurs des plis de la phase 2, notamment au sud du terrain étudié (fig. 18.7), et dans les niveaux compétents (niveau ferrifère, amphibolitiques du groupe de Fagnant...). On peut alors observer, à l'affleurement ou sur lame mince, selon la position géographique et la compétence, des éléments planaires antérieurs à S_2. Les figures 18.7 et 18.8 illustrant deux échelles d'observation, montrent que S_2 a valeur de clivage de type "strain slip" par rapport à une surface métamorphique S_1 et ceci, aussi bien dans les roches du

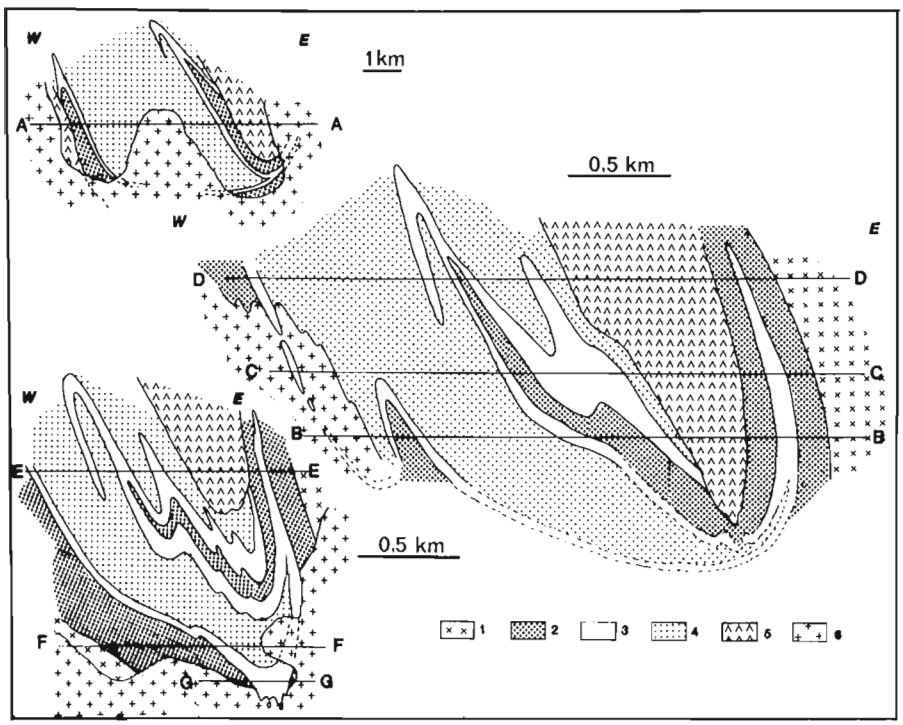

Figure 18.6. *1. gneiss granitiques; 2. couche des amphibolites à grenats; 3. niveau ferrifère; 4. couche des micaschistes; 5. groupe de Fagnant; 6. granites massifs.*

Ces coupes structurales schématiques et interprétatives (localisées sur la figure 18.2) résultent de la confrontation de la carte géologique (fig. 18.2) avec la colonne lithostratigraphique (fig. 18.3) une fois le rejet des failles annulé.

La méthode de représentation choisie, soit un regroupement en trois schémas et en sept coupes, utilise une hypothèse cylindrique qui n'a pas été totalement vérifiée sur le terrain. De plus, la très importante fluctuation des plongements axiaux (avec, notamment, un important ensellement d'axe entre les coupes D et E) explique qu'il n'y ait pas de correspondance directe entre l'altitude des coupes sur la figure et leur position sur la carte.

Cette interprétation suppose l'existence, au moins dans le groupe de Mac Isaac, d'une phase de plissement d'ordre kilométrique antérieure à la phase 2 qui a déterminé les plis F_2 et la surface S_2, soit les éléments largement dominants de l'affleurement. On constate que dans cette reconstitution, le style des plis F_1 est plus pincé que celui des plis F_2 (observation que confirme, à une échelle plus réduite, la figure 18.9 et l'étude microstructurale qui montre que S_1 fait preuve d'une plus grande force de pénétration que S_2).

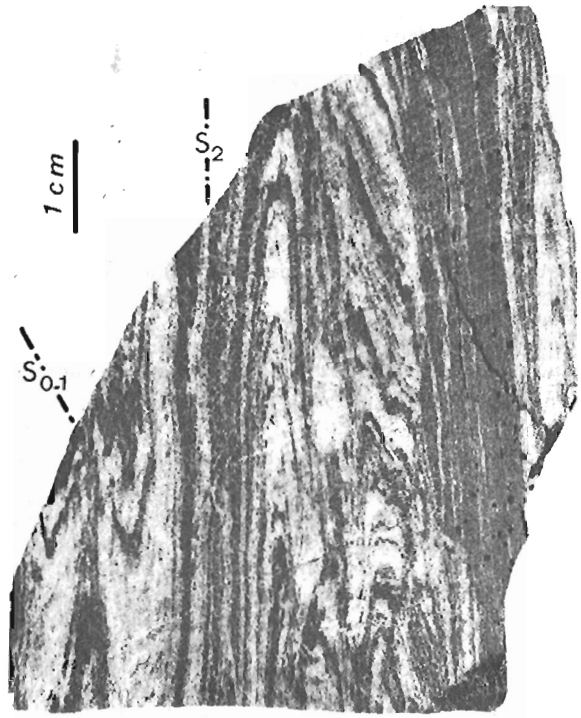

Figure 18.7. *Echantillon du niveau ferrifère. La surface S_2 a valeur de "strain slip" macroscopique par rapport à S_{0-1} qui est transposée.*

groupe de Mac Isaac que du groupe de Fagnant. Parfois, les bandes de "strain-slip" sont suffisamment espacées pour que l'on observe (fig. 18.9) des plis de plan axial S_2 associés qui reprennent des plis de plan axial S_1 isoclinaux et, à cette échelle, également coaxiaux aux premiers.

Le fait que la foliation S_2 a pénétré moins profondément que S_1 dans les roches compétentes, semble indiquer que la foliation des gneiss granitiques est assimilable à S_1 (auquel elle est systématiquement parallèle au sud du terrain étudié où S_1 est facilement mesurable); la migmatitisation aurait donc eu lieu après la foliation S_1. La surface S_2 subit parfois l'effet de kinks (plis en chevrons) centimétriques ou de plissotements de plan axial vertical et de direction est-ouest. Cette phase tardive (phase 3) de compression à orientation nord-sud est peut-être la cause de la fracturation systématique et parallèle à S_2 (à valeur de joint de tension) observée dans les niveaux compétents du groupe de Fagnant.

La cristallogenèse et le métamorphisme

Trente-huit pointés à la microsonde permettent, bien que n'étant pas statistiquement représentatifs, de préciser la nature des principaux minéraux*. Les plagioclases sont de type An_{17} au plus et les cordiérites sont magnésiennes à 65 %. Les biotites se divisent en deux groupes: dans les micaschistes, elles sont très alumineuses et le rapport entre le Fe et le Mg se rapproche de 1; dans les amphibolites, elles sont moins alumineuses et le rapport entre le Fe et le Mg varie entre 2,5 et 5; les amphiboles sont (cf. II) des gédrites, des grunérites et cummungtonites, ou des hastingsites et hastingsites magnésiennes; les grenats sont almandins à plus de 80 %.

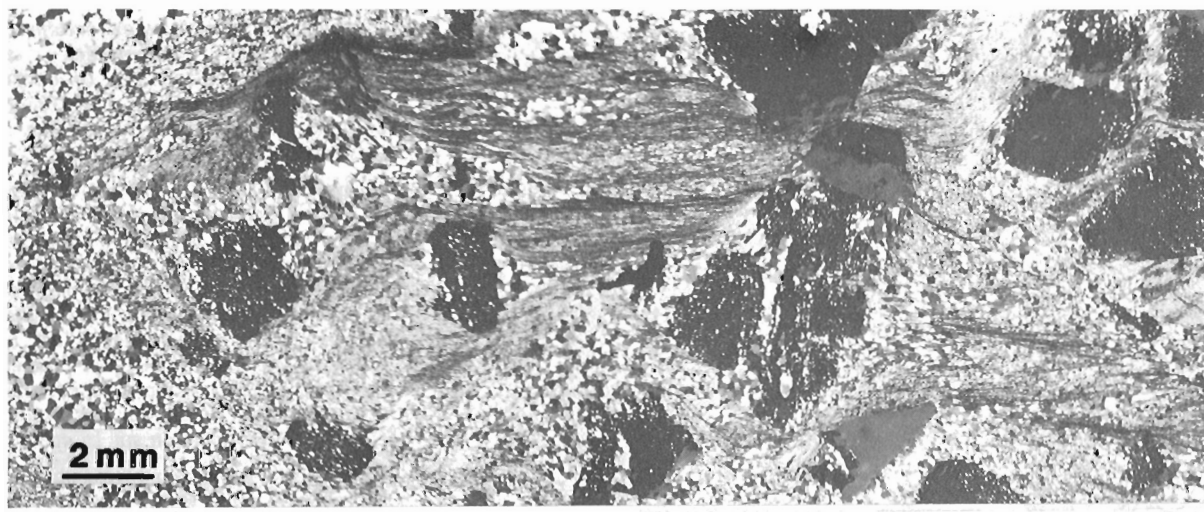

Figure 18.8. *Microphotographie (LP) et interprétation d'un michaschiste à biotite (Biot) et grenat (Gr). La foliation S_2, représenté par les biotites, transpose une foliation S_1 qui n'est visible qu'à l'état de relique.*

* Les résultats des analyses sont disponibles de l'auteur (E.M.).

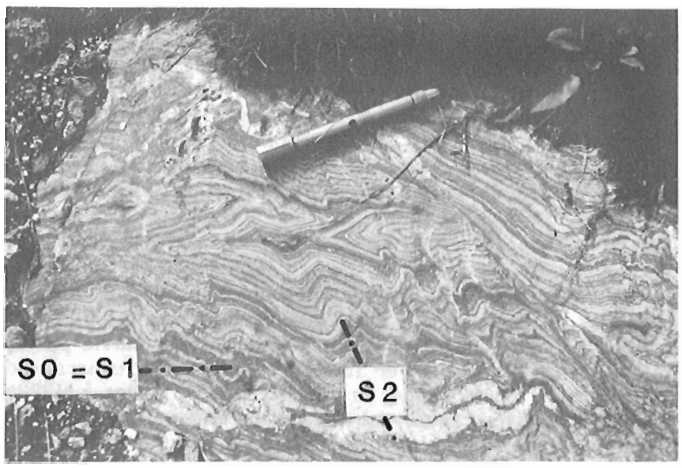

Figure 18.9. *Affleurement du niveau ferrifère. Les plis de plan axial S_1 sont repris par des plis de plan axial S_2 coaxiaux aux premiers.*

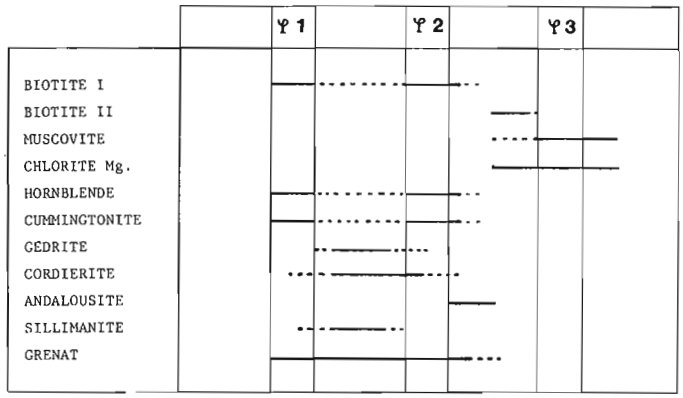

Figure 18.10. *Chronologie relative de la croissance des minéraux de métamorphisme. Trait continu: période de croissance certaine; pointillés: période de croissance maximum. Pour l'établissement de ce tableau, on a supposé que le métamorphisme était continu entre les phases 1 et 2.*

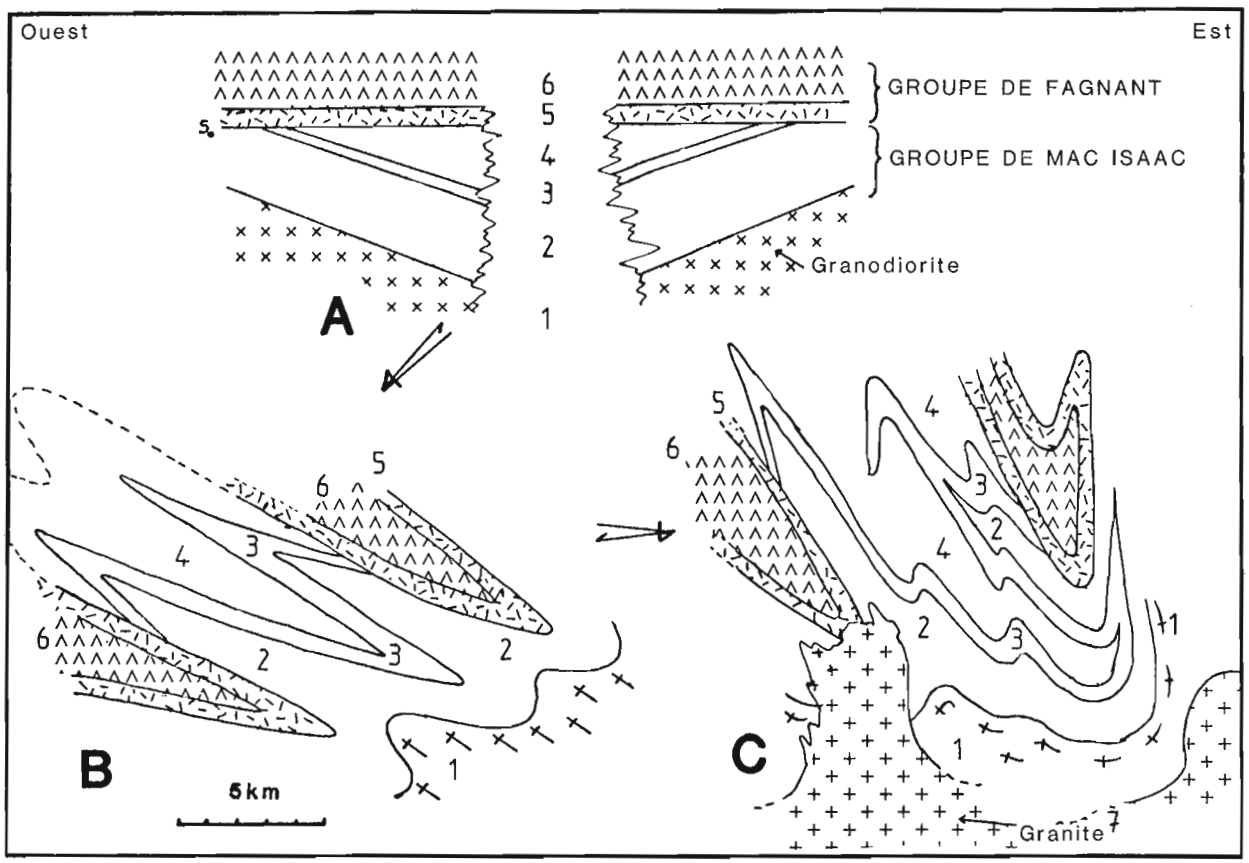

Figure 18.11. *Reconstitution schématique des évènements dans la région du lac Fagnant; 1 à 6: unités cartographiques représentées à la figure 18.3.*

A – mise en place des deux cycles volcano-sédimentaires sur un socle de granodiorite; la discordance entre les cycles n'est pas liée à une phase importante.

B – première phase synschisteuse; plis et foliation (S_1), généralités.

C – deuxième phase synschisteuse, les plis sont moins amples et la foliation S_2, moins pénétrante, ne touche pas les métagranodiorites (gneiss granitiques). La montée granitique prend fin à la phase 2.

B–C Le métamorphisme (faciès des amphibolites) chevauche dans le temps les deux phases synschisteuses et atteint son paroxysme au cours de l'interphase.

En utilisant les critères géométriques, on observe que la croissance des minéraux de plus haut grade (cordiérite, sillimanite, gédrite) n'a eu lieu qu'entre les phases 1 et 2. De plus, de très nombreux grenats sont contemporains de cette période intermédiaire (par exemple, les grenats de la fig. 18.8). Par ailleurs, on n'observe aucune trace de rétromorphose entre ces deux phases. De toute évidence, il est donc probable que le métamorphisme est continu et qu'il a atteint son paroxysme entre les phases 1 et 2 (la coaxialité des plis liés à ces deux phases qui suggère une logique commune vient appuyer cette hypothèse).

La figure 18.10, basée sur cette hypothèse, suggère une évolution du métamorphisme d'abord prograde, avec un paroxysme entre les phases 1 et 2, puis elle devient rétrograde et se poursuit, peut-être, par la cristallogenèse des minéraux synchrones et postérieurs à la phase 3.

Les paragenèses synchrones des phases 1 et 2, dans presque toutes les roches étudiées, indiquent le faciès des amphibolites. Seul le sommet du groupe de Fagnant (coeur du synclinal) se trouve dans le faciès des schistes verts (actinote accompagnée d'épidote).

Des calculs au géothermomètre (31), par la méthode des coefficients de partage, ont été effectués sur des roches du groupe de Mac Isaac. Les abaques de Ferry et Spear (1978), Thomson (1975) et Perchuk (1969) ont été utilisées et fournissent des résultats convergents. L'interprétation de ces températures est délicate (Schoneveld, 1978); il en ressort cependant que la majorité des résultats se situent entre 530 et 600°C mais, les échantillons prélevés sur les coupes F et G de la figure 18.6 (soit à la base de l'édifice tectonique) ont livré des températures de 570 à 670°C, proches de la température d'anatexie des roches pélitiques hydratées. Comme la présence de gneiss granitiques à proximité de ces affleurements (cf. II) atteste du fait qu'une anatexie a eu lieu, on peut se permettre de relier à cette phase de métamorphisme la migmatisation, même faible, des gneiss granifiques, soit un phénomène qui s'est produit après la phase 1.

Conclusions

La géologie de la région du lac Fagnant se distingue de celle de son cadre granitique général. En effet, on y observe une série volcano-sédimentaire archéenne constituée de deux ensembles à épaisseurs originelles inconnues et actuellement plissés et métamorphisés.

Le premier ensemble (group de Mac Isaac), enclavé dans un socle de gneiss granitiques (métagranodiorites), est constitué, de bas en haut, par:

- des volcanites basiques associées à quelques sédiments détritiques (turbidites?);
- un niveau biseauté de grès à magnétite (minerai de fer "Algoma"); ou
- des sédiments détritiques associés à des volcanites acides (?).

Le deuxième ensemble (groupe de Fagnant) repose en discordance sur le premier et est constitué de volcanites basiques, la nature du sommet demeurant inconnue.

Cette série a été déformée par deux phases successives de plis synschisteux coaxiaux et isoclinaux, observées à petite échelle et déduites à grande échelle. Un métamorphisme sans doute continu et synchrone à ces phases de plis a atteint son paroxysme entre ces dernières. Il a provoqué la transformation de la plus grande partie de la série au faciès des amphibolites; la base atteignant la quasi anatexie et le sommet restant dans le faciès des schistes verts. À la fin de la deuxième phase plicative, un complexe granitique (peut-être issu d'une fusion partielle de la masse encaissante) a été mis en place. Une phase mineure (synchrone avec le refroidissement ?) et une fracturation à grande échelle termine l'histoire tectonique de la région. Cette histoire (fig. 18.11), aussi bien sur le plan stratigraphique, que structural ou métamorphique, suit le même cours que celle des zones volcano-sédimentaires archéennes situées au sud et sud-ouest de la province du lac Supérieur (Baragar et McGlynn, 1976). Il est certain que les métavolcanites et métasédiments de la région du lac Fagnant font partie des restes d'une zone volcano-sédimentaire archéenne typique mais, si tel est le cas, son évolution métamorphique et structurale n'est peut-être pas identique à celle suivie par le milieu granitique comme en font foi les orientations nord-sud des foliations de la bande du lac Fagnant et celles à N280° des granodiorites ainsi que les différentes intensités de métamorphisme relevées. Il est probable que l'érosion a fait disparaître d'autres ensembles volcano-sédimentaires de la région, toutefois les grandes différences existant entre le domaine du lac Bienville (granitique) au nord et la sous-province de la baie James (volcano-sédimentaire) au sud, sont surtout attibuables à un régime tectonique différent et à une granitisation plus développée que celle observée dans le sud de la région. D'ailleurs la compréhension du phénomène de la granitisation (lato sensu) est une condition sine qua non à l'élaboration d'un modèle satisfaisant de l'évolution de l'Archéen.

Remerciements

Les auteurs adressent leurs remerciements à M. I.M. Stevenson qui a facilité la venue de M. Mercier sur le terrain, ainsi qu'à MM. Mansy, Raoult et St-Onge de la Commission géologique du Canada pour avoir accepté de relire, en tout ou en partie, le manuscrit.

Bibliographie

Avramtchev, L. et Marcoux, P.
1979: Carte géologique du Québec, Édition provisoire, 1/1 500 000, ministère de l'Énergie et des Ressources du Québec, B-1348.

Baragar, W.R.A. and McGlynn, J.C.
1976: Early Archean basement in the Canadian Shield: a review of the evidence. Geological Survey of Canada, Paper 76-14, 20 p.

Ciesielski, A.
1983: Cartographie d'une partie de la sous-province archéenne d'Ungava à la hauteur de Poste-de-la-Baleine, Québec; dans Recherches en cours, partie B, Commission géologique du Canada, Étude 83-1B.

Dassié, J.
1979: Astronav: Programme de calcul de la position des astres; Micro-Systèmes, 5, p. 107-117; 6, p. 103-109.

Dimroth, R., Imreh, L., Rocheleau, M., and Goulet, N.
1982: Evolution of the south-central part of the Archean Abitibi Belt, Québec. Part I: Stratigraphy and paleogeographic model; Canadian Journal of Earth Sciences, v. 19, p. 1729-1758.

Eade, K.E.
1966: Fort George river and Kaniapiskau river (west half) map-areas, New Quebec; Geological Survey of Canada, Memoir 339, 84 p.

Ferry, J.M. and Spear, F.S.
1978: Experimental calibration of the partitioning of Fe and Mg between biotiote and garnet; Contributions to Mineralogy and Petrology, v. 66, p. 113-117.

Franconi, A.
1978: La bande volcanosédimentaire de la rivière Eastmain Inférieure (ouest de la long. 76°15'); Rapport géologique final, ministère des Richesses naturelles du Québec, DRV 574.

Goodwin, A.M.
1977a: Archean basin – craton complexes and the growth of Precambrian shields; Canadian Journal of Earth Sciences, v. 14, p. 2737-2759.

1977b: Archean Volcanism in Superior Province, Canadian Shield; in Volcanic Regimes in Canada, ed. W.R.A. Baragar, L.C. Coleman and J.M. Hall; Geological Association of Canada, Special Paper 16, p. 205-214.

Gregory, A.F.
1958: Geology of iron occurrence, deposit "A" Great Whale Iron Mines Limited, near Great Whale, Quebec; Private report to Great Whale Iron Mines Limited, 14 p.

Gross, G.A.
1965: Geology of Iron deposits in Canada. Volume I. General Geology and Evaluation of Iron Deposits; Geological Survey of Canada, Economic Geology Report no. 22, 181 p.

Hedberg, H.
1976: Guide stratigraphique international: Doin éd. Paris, 233 p.

Herd, R.K.
1978: Notes on metamorphism in New Quebec; in Metamorphism in the Canadian Shield, Geological Survey of Canada, Paper 78-10, p. 79-83.

Lowdon, J.A.
1960: Age determinations by the Geological Survey of Canada. Report 1: Isotopic Ages; Geological Survey of Canada, Paper 60-17, 51 p.

Perchuk, L.L.
1969: The effect of temperature and pressure on the equilibrium of natural iron – magnesium minerals; International Geology Review, v. 11, no. 8, p. 875-901.

Ramsay, J.G.
1967: Folding and Fracturing of Rocks; McGraw-Hill, New York, 568 p.

Sabourin, R.J.E.
1961: Rapport préliminaire sur la région des lacs Denys et Fagnant (Nouveau-Québec); ministère des Richesses naturelles du Québec, Rapport RP nº 469, 9 p.

Schoneveld, C.
1978: Syntectonic growth of garnets: discussion of a new model proposed by M.J. de Wit; Geological Journal, v. 13, Part 1, p. 37-46.

Sharma, K.N.M.
1976: Région de la Grande Rivière; ministère des Richesse naturelles du Québec, Rapport géologique nº 184.

Stevenson, I.M.
1968: A geological reconnaissance of Leaf River map area, New Quebec and Northwest Territories; Geological Survey of Canada, Memoir 356, 112 p.

Thompson, A.B.
1975: Mineral reactions in pelitic rocks: II. Calculation of some P-T-X (Fe-Mg) phase relations; American Journal of Science, v. 276, p. 425-454.

Wilson, H.D.B. and Morrice, M.G.
1977: The volcanic sequence in Archean Shields; in Volcanic Regimes in Canada, ed. W.R.A. Baragar, L.C. Coleman and J.M. Hall; Geological Association of Canada, Special Paper 16, p. 356-374.

19.

GEOLOGY AND ALTERATION CHARACTERISTICS OF Cr-SPINEL IN DUNITE AT MT. SYDNEY-WILLIAMS, CENTRAL BRITISH COLUMBIA

EMR Research Agreement 65-4-82

Peter J. Whittaker[1] and David H. Watkinson[1]
Economic Geology Division

Whittaker, P.J. and Watkinson, D.H., Geology and alteration characteristics of Cr-spinel in dunite at Mt. Sydney-Williams, central British Columbia; in Current Research, Part B, Geological Survey of Canada, Paper 83-1B, p. 177-184, 1983.

Abstract

Detailed mapping of the Mt. Sydney-Williams ultramafic massif has given information on structure and Cr-spinel mineralization. Zones of layered dunite within host harzburgite outline a faulted synform – antiform structure. Within dunite some layers contain centrally located, disseminated Cr-spinel laminae. Large dunite pods, on the order of 100 m long, are connected to dyke-like dunite bodies which contain only accessory disseminated Cr-spinel. Skeletal textures and magnetite-ferritchromit rims suggest extensive alteration; translucent unaltered cores are rarely observed. Spinels are generally variable in composition and are usually aluminum-rich. Serpentinization has produced low sulphur minerals such as heazlewoodite and Ni-Fe alloy. These are associated with chrome-spinel seams in layered dunite.

Résumé

La cartographie détaillée du massif ultramafique du mont Sydney-Williams a fourni des renseignements sur la structure et la minéralisation en spinelle chromifère. Des zones de dunite stratifiée au sein de l'harzburgite encaissante tracent une structure synforme-antiforme faillée. Certaines couches au sein de la dunite contiennent des lames disséminées et centralisées de spinelle chromifère. De grandes lentilles de dunite, longues de 100 m, sont reliées à des masses de dunite en forme de filon qui ne contiennent que des spinelles chromifères accessoires disséminées. Des textures squelettiques et des bords de magnétite-ferrite-chromite laissent supposer qu'il y a eu altération poussée; on observe rarement des noyaux transluscides non altérés. La composition des spinelles est généralement variable; elles sont habituellement riches en aluminium. La serpentinisation a produit des minéraux faibles en soufre comme la heazlewoodite et un alliage de Ni-Fe. Ces derniers sont associés à des filons de spinelle chromifère dans la dunite stratifiée.

Introduction

Mt. Sydney-Williams is located 92 km northwest of Fort St. James, British Columbia, and rises to an elevation of 1877 m (Fig. 19.1). The Mt. Sydney-Williams area is 44 km south-southwest of the ultramafic massif of the Mitchell Range (Whittaker, 1982), and is underlain by tectonized harzburgite and minor dunite. The Mt. Sydney-Williams massif has been obducted into Permian Cache Creek Group metasedimentary rocks (Armstrong, 1949). Adjacent to the ultramafic massif, Cache Creek Group rocks consist of metamorphosed schistose argillites and andesitic volcanics (Little, 1947).

Cache Creek Group metasedimentary and metavolcanic rocks are folded into open anticlines and synclines with northwest-trending axial planes. The Pinchi Fault, 30 km to the east and also striking northwest, separates the Cache Creek Group from Upper Triassic Takla Group metasedimentary and metavolcanic rocks. The Cache Creek Group and enclosed ultramafic rocks have been metamorphosed to upper greenschist facies.

Field Relationships of Ultramafic Rocks

Harzburgite

Tectonite harzburgite forms 85 to 90 per cent of the outcrop area at Mt. Sydney-Williams (Fig. 19.1). It is penetratively deformed with several planar to ribbony foliations. Olivine constitutes 50 to 60 per cent of the rock with orthopyroxene making up the balance. Orthopyroxene is coarse grained, anhedral and elongate. Olivine neoblasts form elongate patches or clots with very fine grained polygonal texture. Such textures formed during solid state flow in high strain environments (Nicolas and Le Pichon, 1980; Calon, 1973). Elongation of olivine clots parallels that of orthopyroxene porphyroclasts and together they define the tectonite fabric. Such textures have elsewhere been interpreted as having developed in the upper mantle near moving plate boundaries (Nicolas et al., 1980; Nicolas et al., 1982). Harzburgite in Mt. Sydney-Williams massif is more olivine-rich than harzburgite of the Mitchell-Range ultramafic massif (Whittaker, 1982) which has 50 to 60 per cent orthopyroxene. The development of tectonite fabric, however, is much stronger in the Mitchell Range.

Dunite Pods

Serpentinized dunite occurs throughout Mt. Sydney-Williams massif as irregularly shaped, deformed pods (Fig. 19.1, 19.2) and as layers.

Dunite pods range in size from 2 to 500 m (Fig. 19.2) and were mapped on both Mt. Sydney-Williams and on Pinchi Mountain northeast of Fort St. James. Pods may be ovoid, or have sigmoidal form reflecting ductile shear. Deformed dunite pods consist of very fine grained recrystallized olivine which has mosaic or polygonal texture. Pods are virtually monomineralic with accessory sub- to euhedral Cr-spinel which is fine to medium grained. Tectonite fabric (foliation) is only weakly developed in monomineralic dunite pods. This may be due to extensive recrystallization and grain size reduction as olivine underwent strain. Brittle shear zones, up to 10 cm wide, have sharp boundaries within dunite and develop deeply weathered (5 to 7 cm) grooves with friable, platy texture. In larger dunite pods (greater than 10 m) zones of brittle shear may be as wide as 2.5 m and within these zones foliation may be highly variable.

[1] Department of Geology, Carleton University, Ottawa, Ontario, K1S 5B6

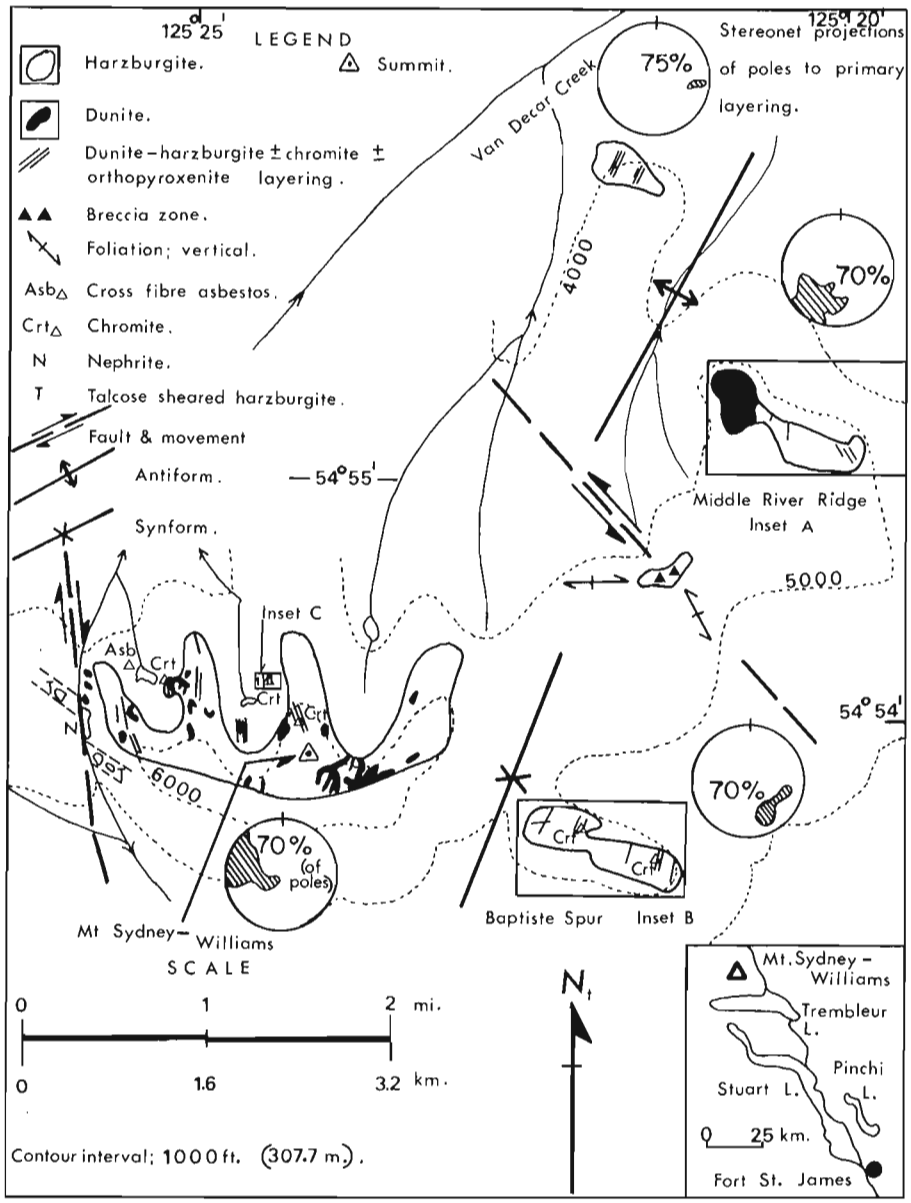

Figure 19.1

Geology of the Mt. Sydney-Williams ultramafic massif.

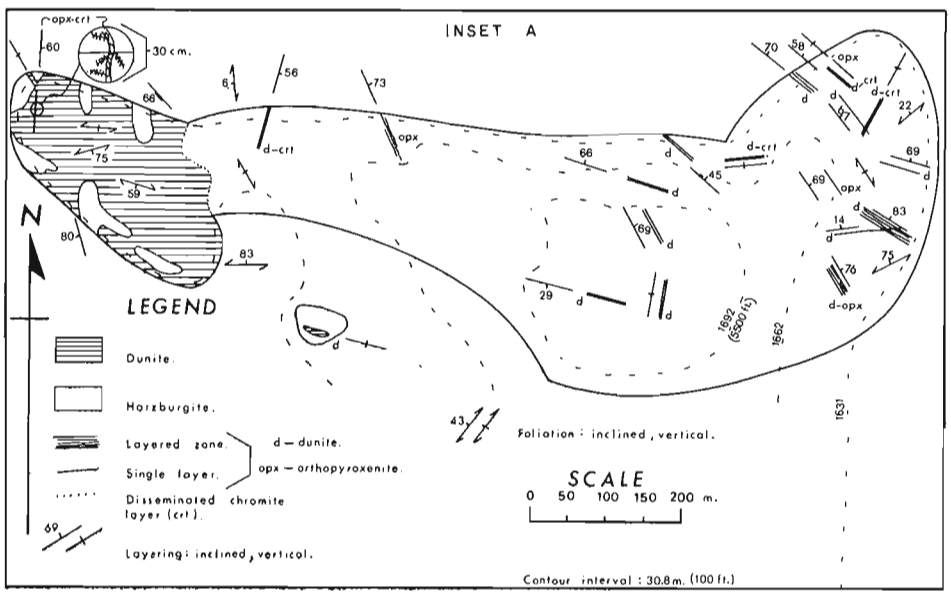

Figure 19.2

Middle River Ridge (for location see Fig. 19.1, inset A).

This variable foliation, which may be curviplanar, tends to isolate spheroids of less intensely foliated dunite and results in outcrops with spheroidal weathering structures. Individual spheres are 10 to 25 cm in diameter and may also be ovoid. Contacts between dunite pods and enclosing harzburgite are sharply defined and are accentuated by recessive weathering of dunite. Foliation planes are abruptly refracted at these sharp contacts with deflections of up to 24 degrees.

Dunite in Layered Zones

Dunite in layered zones (Fig. 19.1-19.4) exhibits textures similar to those in dunite pods. Olivine is very fine grained and polygonal having recrystallized during deformation. Dunite layers range in thickness from 3-5 cm up to 25-30 cm and are separated by layers of harzburgite of variable thickness. Layered zones are generally planar with both sharp and gradational contacts against harzburgite or they may be folded as at Baptiste Spur (Fig. 19.3). Layered zones both at Pinchi Mountain and at Mt. Sydney-Williams are usually subconcordant with the tectonite foliation. Gradational contacts are developed over 1 to 2 cm and have serrated to lobate texture. In some cases flame-like structures are defined by tongues of dunite penetrating harzburgite, as was also observed at Murray Ridge (Whittaker and Watkinson, 1981). Orthopyroxene phenocrysts may become incorporated in dunite layers (Fig. 19.5) and exhibit embayed resorption textures. Dunite layers in layered zones of Mt. Sydney-Williams massif host disseminated Cr-spinel (Fig. 19.4) either as accessory disseminated grains or as single-grain thick, chain-like laminae, usually discontinuous but traceable for the length of the dunite layer.

Also occurring within dunite layers are monomineralic orthopyroxenite layers which are commonly centrally located. Orthopyroxene is coarse grained, sub- to anhedral and may occur with accessory Cr-spinel and rarely with subhedral bottle-green diopside which locally forms websterite patches. Orthopyroxenite layers also occur individually in harzburgite and may be either concordant or discordant to dunite layered zones.

Dunite Dyke-Like Bodies

In the southeastern part of the massif (Fig. 19.1) and on Pinchi Mountain, crosscutting dyke-like bodies of dunite were mapped. These tend to strike parallel or subparallel to the tectonite fabric with variable dips of 45-90°. On both Pinchi Mountain and Mt. Sydney-Williams the roots of dunite dyke-like bodies begin from the zones of irregularly shaped dunite pods, usually 50 m or wider. At Mt. Sydney-Williams the headwall of east cirque provides a vertical section of a dunite pod with numerous dunite dyke-like bodies emanating from it. These bodies range in thickness from 1 to 4 m; most are subvertical but some dip 45 degrees. These two dyke sets appear to be contemporaneous, are not crosscutting and form stockworks 10 to 15 m wide.

Textures within dunite bodies are similar to those in dunites described previously. The texture is uniformly very fine grained and equigranular across the width of these bodies. Chilled margins are absent. In some cases detached and openly folded apophyses of dyke structures may also be traced to a common dunite pod indicating that these features are pre- and synkinematic. Dunite dykes represent a process that was continuous throughout mantle deformation and for some time after.

Within some dunite dykes harzburgite xenoliths, 5 to 10 cm in size, show only minor displacements of 1 to 10 cm from wallrock. In some cases larger xenoliths are autobrecciated forming subangular to ovoid fragments. Development of these could be accounted for by in situ resorbtion. Long dimensions of harzburgite xenoliths are parallel to the foliation in adjacent wallrock harzburgite which also parallels the strike of dykes.

Structure

Layered dunite zones define a broad antiform-synform pair offset by left-lateral faulting. The fault zone is an area of brecciated harzburgite in the central part of Middle River Ridge (Fig. 19.1). Stereo plots of poles to layering in four domains within the map area help to define a synform in the southern part of Mt. Sydney-Williams massif and an antiform in the northern part (Fig. 19.1). Fold-axis trends parallel the overall foliation in a north-northeasterly direction. This direction is oblique to the northwesterly trend of fold axes in the enclosing Cache Creek Group and could therefore be related to earlier mantle deformation.

Silicate Minerals

Serpentinization is ubiquitous throughout the Mt. Sydney-Williams massif and all silicate minerals are altered to various degrees. Olivine and orthopyroxene in harzburgite, and olivine alone in dunite exhibit 75-100 per cent serpentinization. Lizardite is the common serpentine mineral with minor talc + magnetite + chlorite ± brucite. Ribbony lizardite defines moderately to well-developed mesh texture. Some relict olivine cores in dunite layers have exsolved skeletal, translucent brown spinel in planar arrangement within the olivine.

Field Distribution of Chromium Spinel

Occurrences of Cr-spinel at Mt. Sydney-Williams are unlike the generally podiform chromitite described from the Mitchell Range ultramafic massif (Whittaker, 1982). At the former site Cr-spinels which form disseminated and massive laminae occur only within dunite layers which are part of larger layered zones. In mineralized dunite layers, disseminated Cr-spinel forms 45 to 95 per cent of individual laminae which pinch and swell from 0.5 to 2.0 cm thick. These laminae may be discontinuous, are usually concordant with layering and are centrally located in the dunite layer (Fig. 19.5A). Medium grained, sub- to euhedral Cr-spinel also forms irregular patches from 1 to 15 cm in size which are aligned parallel to the dunite layers (Fig. 19.5B).

Discordant seams of Cr-spinel occur at Pinchi Mountain, and at Middle River Ridge, Mt. Sydney-Williams massif (Fig. 19.2). At Pinchi Mountain Cr-spinel is medium grained and forms 95 per cent of a 2 m long, gently folded layer. The layer varies from 1 to 3 cm thick and is oriented at an acute angle to the tectonite fabric and layered zones. Cr-spinel at Middle River Ridge has developed in fractures which are acute to a more prominent and central fracture (Fig. 19.2). Cr-spinel is medium grained and sub- to euhedral.

All disseminated to massive Cr-spinel occurring within dunite layers have 0.5-1.5 mm silicate reaction rims (Fig. 19.5C,D) which may completely or partially surround single grains or enclose aggregates of several medium grained subhedra. In some Cr-spinel grains, lobate embayments result from encroachment of reaction-rim material. Reaction rims appear to form at the expense of both the original silicate and spinel grains suggesting that dunite layers were conduits for late, chemically aggressive solutions.

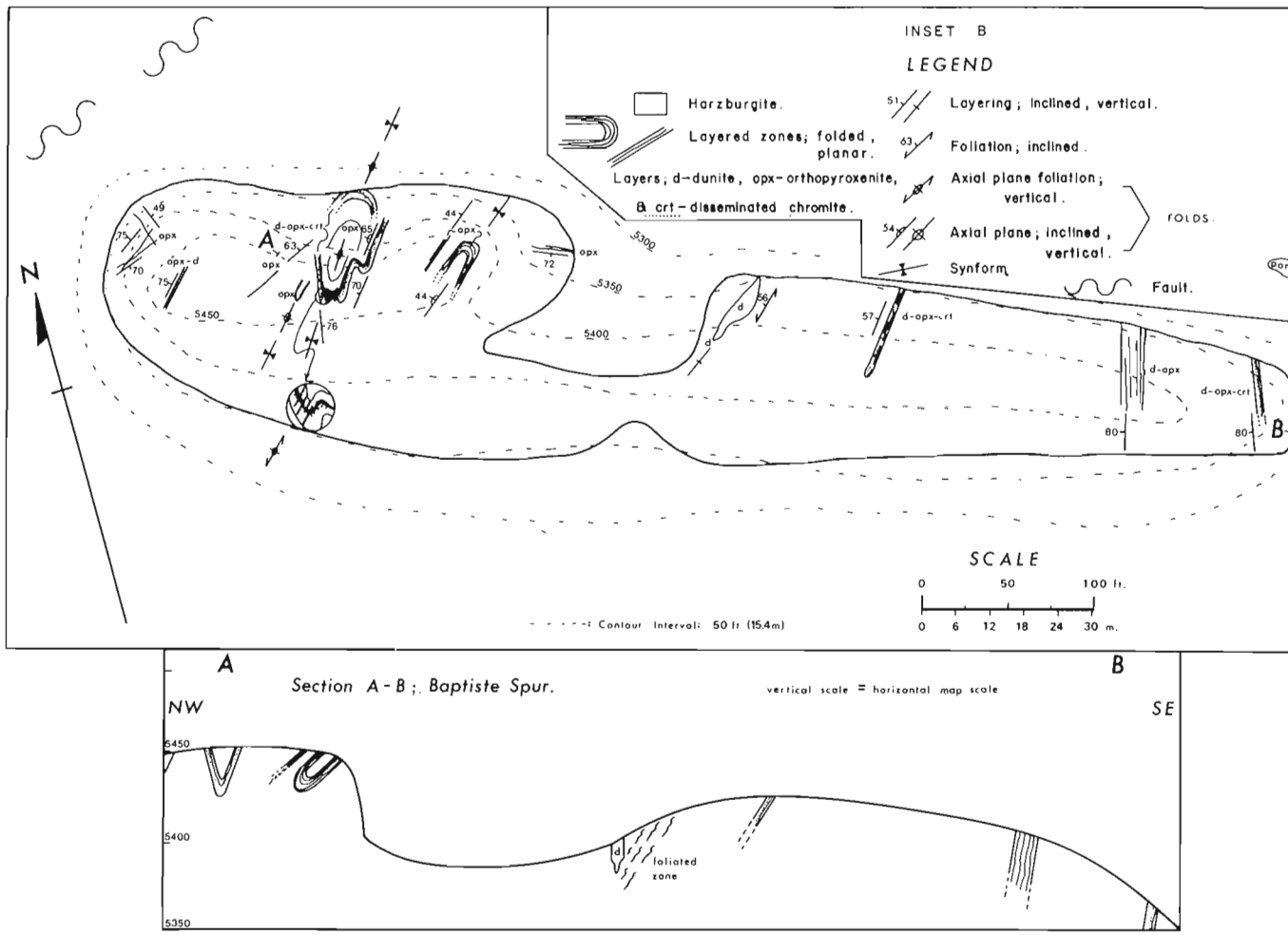

Figure 19.3. *Baptiste Spur (for location see Fig. 19.1, inset B).*

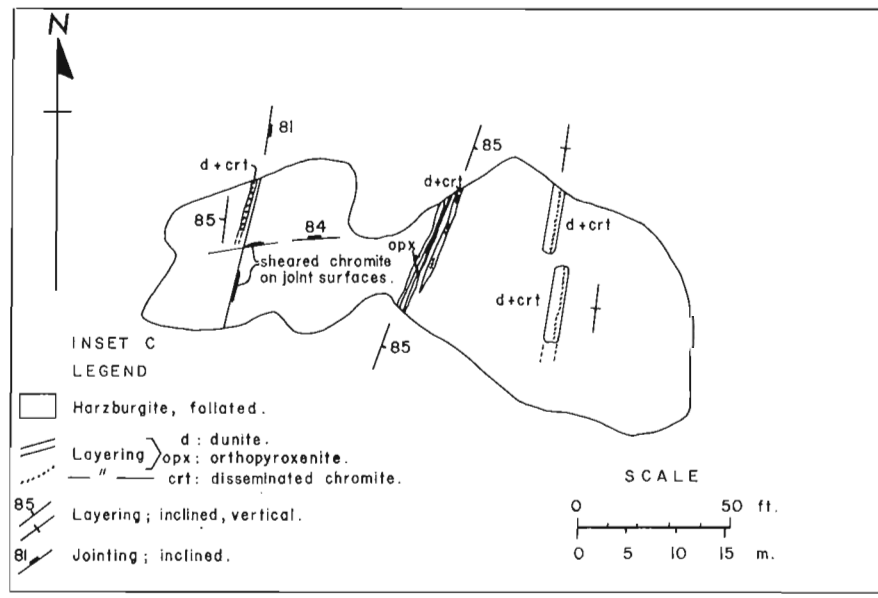

Figure 19.4. *Dunite and Cr-spinel layering in the central massif (for location see Fig. 19.1, inset C).*

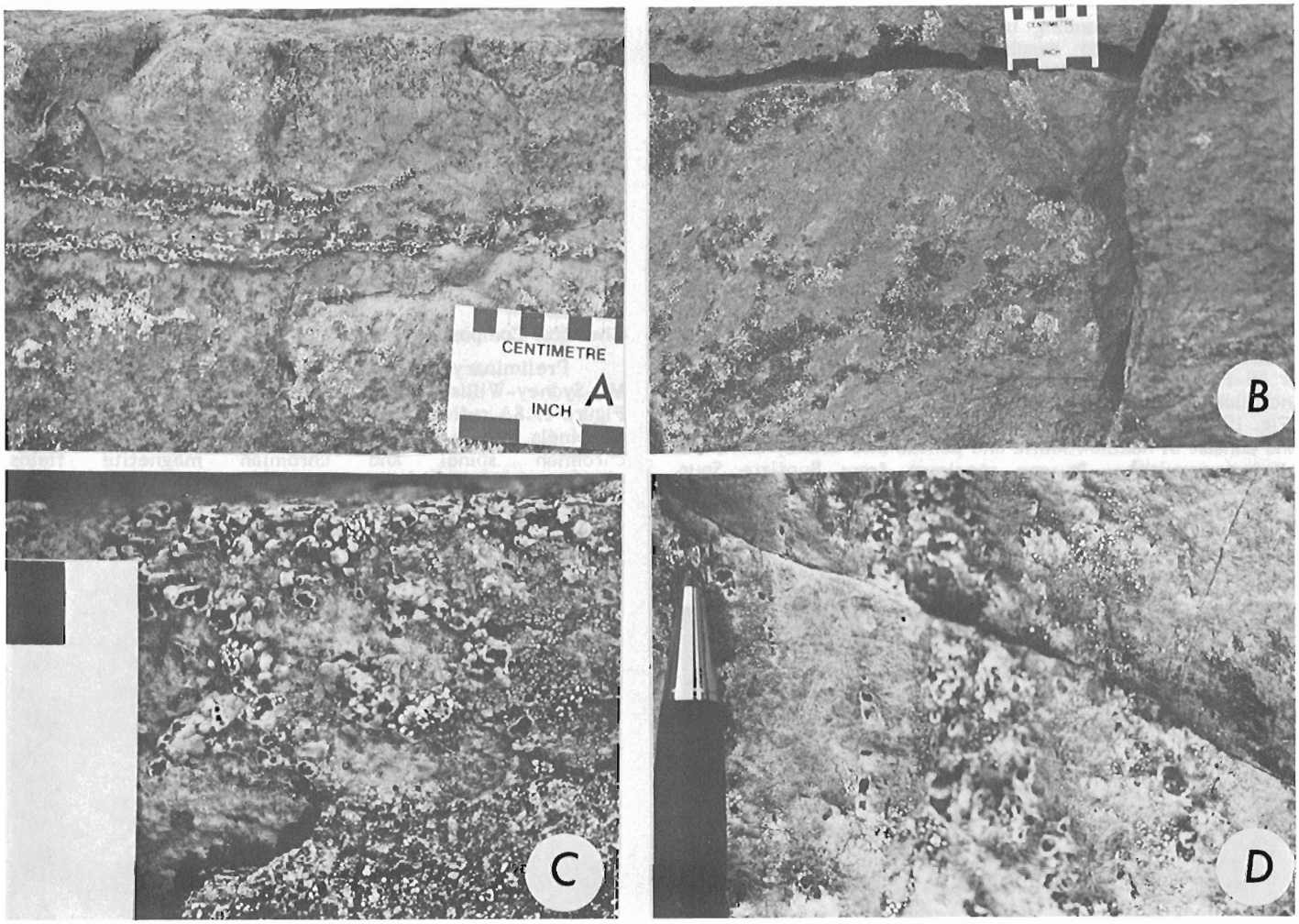

Figure 19.5

A. Disseminated Cr-spinel laminae centrally located in dunite layer.

B. Patchy disseminations of Cr-spinel in dunite layer, vertical plane.

C,D. Pale chlorite-serpentine reaction rims around black Cr-spinel in fine grained dunite.

At Baptiste Spur evidence exists for two distinct generations of Cr-spinel. Earliest Cr-spinel seams have been folded with the dunite layer and so predate ductile deformation (Fig. 19.6A). The later generation has developed in the axial plane foliation of the fold structure, but only within the dunite layer (Fig. 19.6B).

Extensive development of reaction rims and multi-stage Cr-spinel mineralization in dunite strongly suggests that dunite bodies were zones of solution migration. Round xenoliths of harzburgite in dunite dyke structures are also compatible with this hypothesis.

Cross-fibre asbestos is well developed in 1 to 3 cm wide brittle fractures that strike east-west (Fig. 19.1) as described by Armstrong (1949). Additional field work has shown them to be restricted to west cirque.

Petrography of Spinels and Sulphides

Cr-spinel in layered zones from Mt. Sydney-Williams (Fig. 19.3, 19.4) occur as both single grains and as constituents in disseminated to massive seams. In all cases observed reaction rims which surround single chromite grains and net-textured aggregates consist of serpentine (lizardite) and chlorite. Most grains are completely altered but some spinels retain primary Cr-spinel cores. Grains that are completely or partially altered retain their original subhedral to euhedral form.

Cr-spinel cores can form up to 25 per cent of the total grain and are not always at the original grain centre (Fig. 19.7A). Original cores are irregularly shaped and have serrated borders with surrounding altered spinel. Compared to areas of altered spinel, cores have few or no silicate inclusions. Where present though, primary anhedral silicate inclusions are round with smooth borders. In transmitted light, spinels have dark reddish brown to pale brown colour with moderate translucency.

Partial and complete alteration of Cr-spinel leads to development of mottled skeletal textures (Fig. 19.7A,B). Silicate inclusions are numerous and form up to 50 per cent of the altered areas. In reflected light altered skeletal-dendritic spinel is mottled pale grey and white. Microprobe analyses indicate higher Fe in white areas than in the pale grey patches. Dependable analyses are difficult to obtain because of the intimate development of silicate inclusions.

Opaque areas can be directly correlated to areas of white reflectance corresponding to ferritchromit and magnetite. This is similar to results obtained by Stumpfl and Rucklidge (1982) for altered spinels in dunite pipes of the Bushveld Complex.

Sulphides and alloys are usually present with altered spinels in dunite layers. They commonly occupy fractures in original spinels and occur at the junction of two or more grains (Fig. 19.8A,B). Secondary sulphide inclusions (those in fractures in spinel) and groundmass sulphides are present both as mono- and polyphase grains. Polyphase sulphides occur as secondary anhedral grains both in fractures in spinel and the groundmass between spinel grains (Fig. 19.7B). In some grains up to three co-existing sulphide phases occur. The most abundant sulphide is Ni_3S_2 (heazlewoodite) based on qualitative energy dispersive microprobe analysis. This phase or Ni-Fe alloy forms the host for smaller anhedral sulphide inclusions which are cream-coloured round to ovoid blebs (Fig. 19.7B). These inclusions are various Ni-Fe-S phases, and consist of heazlewoodite and pentlandite usually in Ni-Fe alloy (awaruite). In one specimen from Baptiste Spur disseminated secondary sulphides form approximately 1 to 2 modal per cent of the spinel seam.

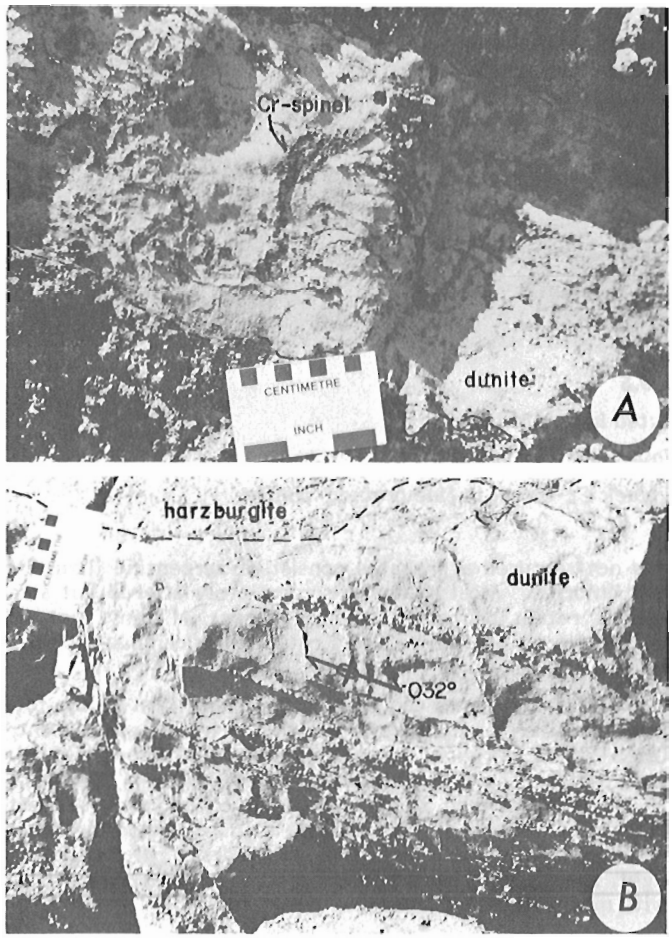

Figure 19.6

A. Folded early Cr-spinel laminae in folded dunite, Baptiste Spur.

B. Cr-spinel parallel to foliation in limb of folded dunite layer, Baptiste Spur.

Secondary sulphides in the groundmass are most concentrated and largest adjacent to altered Cr-spinel grains and become sparser and smaller away from them. This distribution may represent a primary concentration of sulphides around Cr-spinel grains as documented in the Bushveld complex (Hiemstra, 1979). Alternatively, secondary sulphides may have formed from diffusion of metals originally in solid solution in Cr-spinel and olivine (Stumpfl and Tarkian, 1976). This process is favoured since it could have occurred during serpentinization and does not rely on primary magmatic processes. Available sulphur during serpentinization would stabilize the metal cations as secondary sulphides using spinels as nucleation sites.

Chemical Composition of Spinels

Preliminary electron microprobe data on spinels from Mt. Sydney-Williams area are given in Figure 19.8A and B. Figure 19.8A reflects the generally Fe, Al-rich compositions of spinels from layered dunite. Most compositions are in the chromian spinel and chromian magnetite fields

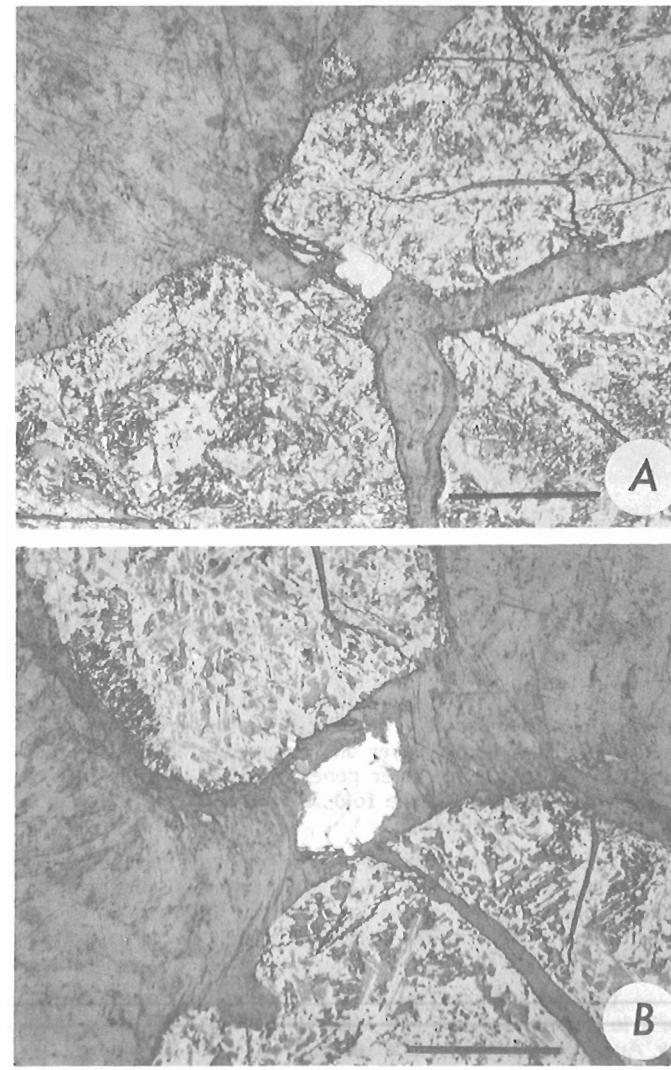

Figure 19.7

A. Cr-spinel with alteration textures and secondary Ni-sulphide (heazlewoodite).

B. Skeletal alteration texture after Cr-spinel and secondary polyphase grain of pentlandite rimmed by thin veneer of magnetite, all enclosed by heazlewoodite.

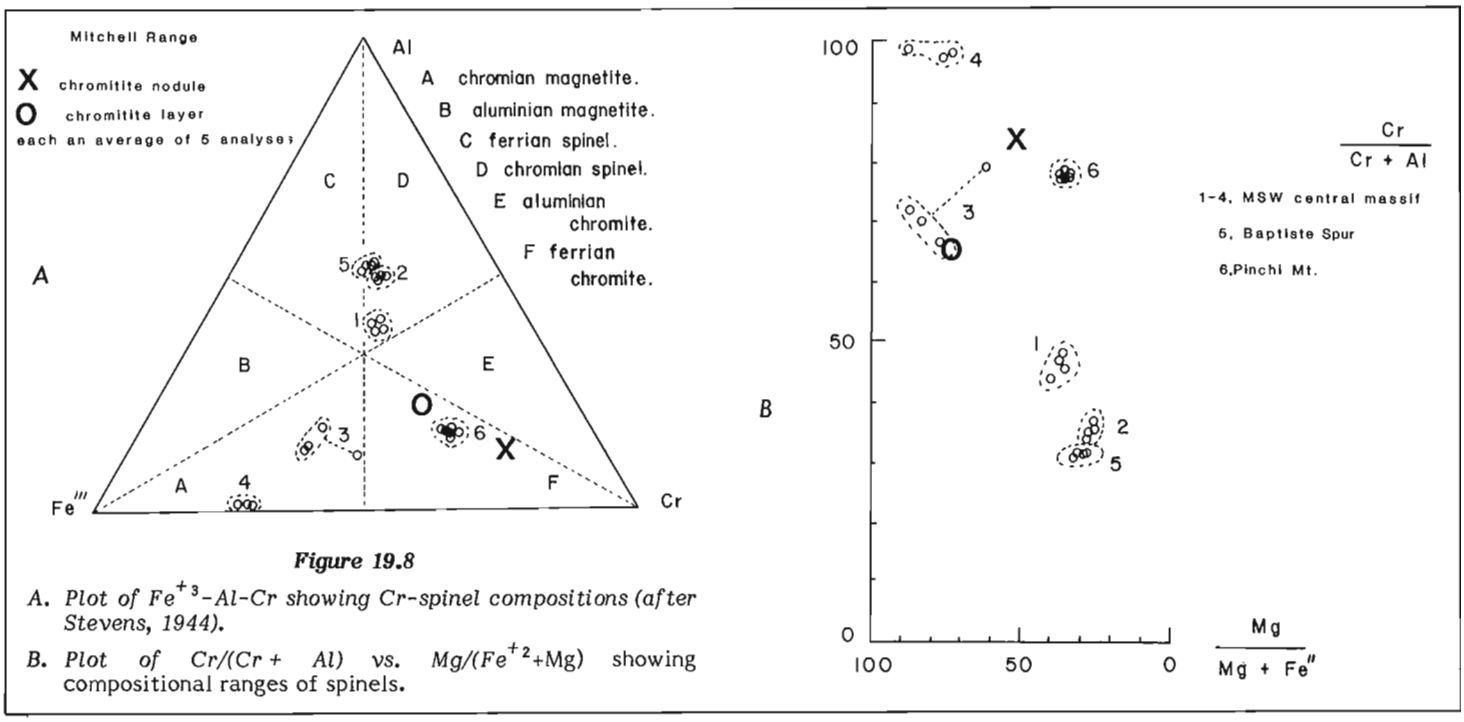

Figure 19.8

A. Plot of Fe^{+3}-Al-Cr showing Cr-spinel compositions (after Stevens, 1944).

B. Plot of Cr/(Cr + Al) vs. Mg/(Fe^{+2}+Mg) showing compositional ranges of spinels.

(Stevens, 1944). The trend from chromian spinel to chromian magnetite corresponds to analyses of unaltered cores to altered rims. Rims have skeletal texture, are opaque and contain both high total iron and ferric iron. In many areas magnetite overgrowths enclose skeletal textured rims and represent final alteration related to serpentinization (Bliss and MacLean, 1975). Magnetite rim analyses plot in field "4" in Figure 19.8A and B.

The compositional range defined by analyses from unaltered spinel cores and altered spinel rims is again shown in Figure 19.8B in fields 1, 2, 3, 5, and 6. The trend is one of decreasing Cr, Mg and increasing Al, Fe. Field "6" (Pinchi Mountain) plots close to compositions of Mitchell Range chromitite.

It is evident from the range of compositions and textures that pre-serpentinization spinels (before development of chromian magnetite rims) in dunite layers are different from most other chromites. Relict core compositions reflect generally Cr-Mg poor compositions compared to chromite of the Mitchell Range, with altered-skeletal areas further impoverished in Cr-Mg. This suggests a paucity of Cr-Mg, balanced primarily by Al in spinels.

Discussion and Conclusions

Spinel and sulphide textures indicate an environment within dunite layers where solutions were mobile and chemically aggressive during mantle deformation. That solution migration and serpentinization were pre-obduction is indicated by the presence of unserpentinized norite dykes that intrude the altered ultramafic rocks but do not cut the enclosing country rocks. Thus serpentinization occurred prior to obduction, probably in suboceanic mantle. Initial alteration of Cr-spinel is associated with Fe-rich solutions which formed the opaque (Fe-rich) ferritchromit and magnetite rims. If original Cr-spinel had only a few silicate inclusions (about 5 modal per cent) then a substantial amount of the constituents of primary Cr-spinel has been removed and its place taken by silicates. This is shown by the abundance (25 to 30%) of fine silicate inclusions occupying interstices in skeletally textured Cr-spinel pseudomorphs. Continued element mobility and metasomatism is suggested by the growth of anhedral Fe-Ni sulphide grains within the groundmass and in fractures in Cr-spinel (Eckstrand, 1975). The environment must also have been one of low sulphur fugacity to stabilize these elements as alloys and low-sulphur sulphides. Textural relations show that Cr-spinel grains acted as nuclei for sulphides. Sulphur was concentrated in dunite layers by migrating solutions, primarily during serpentinization. Discrete euhedral to subhedral inclusions of Ni-Fe-S, Ni-Fe alloy, PGM sulphides and PGM alloys have been described in unaltered chromite from other localities (Talkington et al., 1982; Whittaker and Watkinson, 1981; Pritchard et al., 1981). These in addition to Ni, Fe and other cations from altered silicate groundmass minerals could contribute to the growth of observed secondary sulphides and alloy.

All Cr-spinels from Mt. Sydney-Williams dunite layers are altered, whether layers are planar or folded and whether they are pre- or post-deformation. This strongly suggests a period of mantle metasomatism which was pre-, syn-, and post-deformational and mostly confined to monomineralic dunite layers.

In further support of the conclusion that intense metasomatic processes alter spinels, sulphides and silicates, and in particular produce monomineralic dunite layers are the dunite pipes in the Bushveld Complex, South Africa. Several workers at the Driekop dunite pipe (Peyerl, 1982; Schiffries, 1982) and at the Onverwacht and Mooihoek pipes (Stumpfl and Rucklidge, 1982; Cameron and Desborough, 1964) suggested an origin involving post-magmatic metasomatism involving chloride-rich solutions. At Mt. Sydney-Williams evidence exists for late migration of solutions which may have been chloride-rich, possibly connate seawater. In addition, CO_2 is known from inclusions in mantle olivine (Roedder, 1965). With the availability of chloride and CO_2 in an upper oceanic mantle environment, Ni and Fe could be transported from altered Cr-spinel and silicates to reprecipitate as low "S" sulphides and awaruite under low fS_2 conditions (cf. Eckstrand, 1975). For dunite layers at Mt. Sydney-Williams, serpentinization was an effective mechanism for concentrating Ni with Fe and S or as Ni-Fe alloy. Cr-spinel-bearing laminae in these dunite layers represent the zone of most concentrated Ni mineralization and solution migration.

Acknowledgments

The authors would like to extend thanks to P. Jones for assistance in the field, to Z. Johan BRGM-CNRS, France for arranging access to their electron microprobe for some analyses, and to J.M. Duke (GSC) for many helpful discussions. Financial support for field work from the Geological Survey of Canada (EMR Research Agreement 65-4-82) to D.H. Watkinson is gratefully acknowledged.

References

Armstrong, J.E.
1949: Fort St. James map-area, Cassiar Coast Districts, British Columbia; Geological Survey of Canada, Memoir 252, 210 p.

Bliss, N.W. and MacLean, W.H.
1975: The paragenesis of zoned chromite from central Manitoba; Geochimica et Cosmochimica Acta, v. 39, p. 973-990.

Calon, T.J.
1973: A study of the alpine-type peridotites in the Steve-Koli nappe complex, central Swedish Caledonides, with special reference to the Kittelfjall peridotite; Ph.D. thesis, University of Leiden, Leiden, Nederland, 236 p.

Cameron, E.N. and Desborough, G.A.
1964: Origin of certain magnetite-bearing pegmatites in the eastern part of the Bushveld Complex, South Africa; Economic Geology, v. 59, p. 197-225.

Eckstrand, O.R.
1975: The Dumont Serpentinite: A model for control of nickeliferous opaque mineral assemblages by alteration reactions in ultramafic rocks; Economic Geology, v. 70, p. 183-201.

Hiemstra, S.A.
1979: The role of collectors in the formation of the platinum deposits in the Bushveld Complex; Canadian Mineralogist, v. 17, p. 469-482.

Little, H.W.
1947: The ultrabasic and associated rocks of the Middle River Range, British Columbia; Ph.D. thesis, University of Toronto, Toronto, Canada, 98 p.

Nicolas, A. and Le Pichon, X.
1980: Thrusting of young lithosphere in subduction zones with special reference to structures in ophiolitic peridotites; Earth and Planetary Science Letters, v. 46, p. 397-406.

Nicolas, A., Boudier, F., and Bouchez, J.L.
1980: Interpretation of peridotite structures from ophiolitic and oceanic environments; American Journal of Science, v. 280A, The Jackson Volume, p. 192-210.

Nicolas, A., Rabinovicz, M., and Vigneresse, J.L.
1982: Modelling of oceanic spreading centres based on structural studies in ophiolites; in Ophiolites and Ocean Lithosphere, Abstracts, Geological Society of London, November 1982, p. 10.

Peyerl, W.
1982: The influence of the Driekop dunite pipe on the platinum-group mineralogy of the UG-2 chromitite in its vicinity; Economic Geology, v. 77, no. 6, p. 14321438.

Pritchard, H.M., Potts, P.J., and Neary, C.R.
1981: Platinum group element minerals in the Unst chromite, Shetland Isles; Transactions of the Institute of Mining and Metallurgy, Section B, v. 90, p. B186-B188.

Roedder, E.
1965: Liquid CO_2 inclusions in olivine-bearing nodules and phenocrysts from basalts; American Mineralogist, v. 50, p. 1746-1782.

Schiffries, C.M.
1982: The petrogenesis of a platiniferous dunite pipe in the Bushveld Complex: Infiltration metasomatism by a chloride solution; Economic Geology, v. 77, no. 6, p. 1439-1453.

Stevens, R.E.
1944: Compositions of some chromites of the western hemisphere; American Mineralogist, v. 26, p. 1-34.

Stumpfl, E.F. and Rucklidge, J.G.
1982: The platiniferous dunite pipes of the eastern Bushveld; Economic Geology, v. 77, no. 6, p. 1419-1431.

Stumpfl, E.F. and Tarkian, M.
1976: Platinum genesis: New mineralogical evidence; Economic Geology, v. 71, p. 1451-1460.

Talkington, R.W., Watkinson, D.H., Whittaker, P.J., and Jones, P.
1982: The petrological significance of platinum-group minerals and other solid and fluid inclusions in chromite of ophiolitic and stratiform complexes; in Ophiolites and Ocean Lithosphere, Abstracts, Geological Society of London, November 1982, p. 32.

Whittaker, P.J.
1982: Chromite occurrences in ultramafic rocks in the Mitchell Range, central British Columbia; in Current Research, Part A, Geological Survey of Canada, Paper 82-1A, p. 239-245.

Whittaker, P.J. and Watkinson, D.H.
1981: Chromite in some ultramafic rocks of the Cache Creek Group, British Columbia; in Current Research, Part A, Geological Survey of Canada, Paper 81-1A, p. 349-355.

20.

PRELIMINARY EVIDENCE FOR LATE WISCONSINAN CLIMATIC FLUCTUATIONS FROM POLLEN STRATIGRAPHY IN BURIN PENINSULA, NEWFOUNDLAND

Project 690064

T.W. Anderson
Terrain Sciences Division

Anderson, T.W., Preliminary evidence for Late Wisconsinan climatic fluctuations from pollen stratigraphy in Burin Peninsula, Newfoundland; in Current Research, Part B, Geological Survey of Canada, Paper 83-1B, p. 185-188, 1983.

Abstract

Preliminary pollen studies were carried out on a 5 m-long Livingstone core obtained from a lake in southernmost Burin Peninsula, southeastern Newfoundland. Sandy, stony clay (till) is overlain by gyttja which records a shrub-tundra landscape dating to 13 400 BP. Within the gyttja is a 7 cm-thick silty clay layer which discriminates a reversion to herb tundra. Conditions returned to shrub tundra thereafter (until 10 700 BP at least). Inferred vegetative and climatic changes are tentatively correlated with Late Wisconsinan fluctuations of the North Atlantic polar front.

Résumé

Des études palynologiques préliminaires ont été entreprises sur une carotte de 5 m de la formation de Livingstone, provenant d'un lac dans l'extrémité sud de la péninsule de Burin, au sud-est de Terre-Neuve. Du gyttja, qui témoigne d'un paysage de toundra à broussailles datant de 13 400 ans, recouvre de l'argile sableuse et pierreuse (till). Le gyttja renferme une couche d'argile limoneuse de 7 cm d'épaisseur qui indique qu'il y a eu réversion à la toundra à herbes. Par après, le paysage est redevenu de la toundra à broussailles (au moins jusqu'à 10 700 ans avant l'ère actuelle). Les modifications végétales et climatologiques présumées sont provisoirement reliées aux fluctuations du front polaire sévissant dans l'Atlantique Nord durant le Wisconsinien supérieur.

Introduction

The surficial geology and Quaternary history of Burin Peninsula, southern Newfoundland, were initially reported on by Grant (1975) and later in more detail by Tucker (1979). From these studies, a generally consistent sequence of late Quaternary events has emerged for the region (Grant, 1975, 1977; Tucker and McCann, 1980). An overall chronology for these events, however, is still lacking. Mapping has shown that there were two complete glaciations of Burin Peninsula by Newfoundland-centred ice during pre- and Early Wisconsinan time. A period of marine inundation of presumed Middle Wisconsinan age affected the western extremity of the peninsula. A later ice advance partly covered Burin Peninsula from an offshore source to the southeast. Its ice-marginal position was clearly recognized just inland from the northwest coast of south Burin (Tucker and McCann, 1980). The latest glaciation to affect the area occurred probably during Late Wisconsinan time when Newfoundland-centred ice reached either the top of the peninsula (Grant, 1977) or perhaps somewhat farther south (Tucker and McCann, 1980). In either case, southernmost Burin Peninsula, except perhaps for a small upland ice cap, has apparently remained ice free since late Middle Wisconsinan time, i.e., since about 30 000 years or more.

To test this hypothesis, eight lake sites were cored in 1982 in southern Burin Peninsula, the adjacent Harbour Breton-Hermitage area, and the Codroy Lowland on the southwest coast, which are believed by Grant (1977) to lie beyond the limit of Late Wisconsinan ice (Fig. 20.1). It was hoped that southern Burin Peninsula, in particular, might yield some of the earliest palynological records and radiocarbon dates on the Late Wisconsinan and possibly confirm whether or not this area was ice free since late Middle Wisconsinan time. While the record obtained is not as lengthy as was hoped, it did provide evidence of significant insight into Late Wisconsinan climatic fluctuations.

This report summarizes preliminary findings on a lake site located 6 km southwest of Lawn on the south coast. (Fig. 20.1). No previous pollen studies have been undertaken in southern Burin Peninsula.

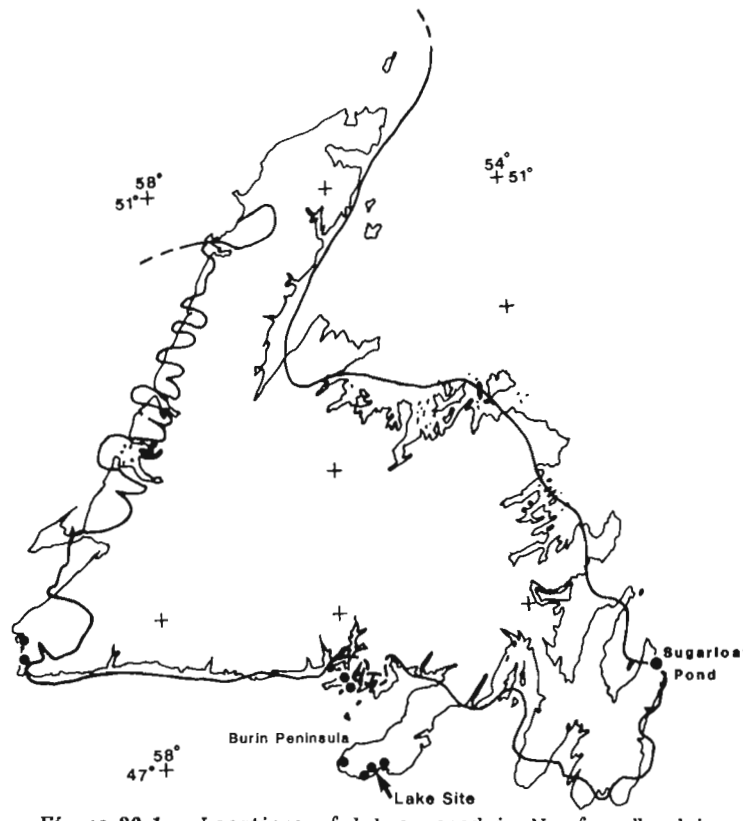

Figure 20.1. *Locations of lakes cored in Newfoundland in 1982 (closed circles) and Macpherson's (1982) Sugarloaf Pond. The heavy line is the inferred limit of Late Wisconsinan ice from Grant (1977).*

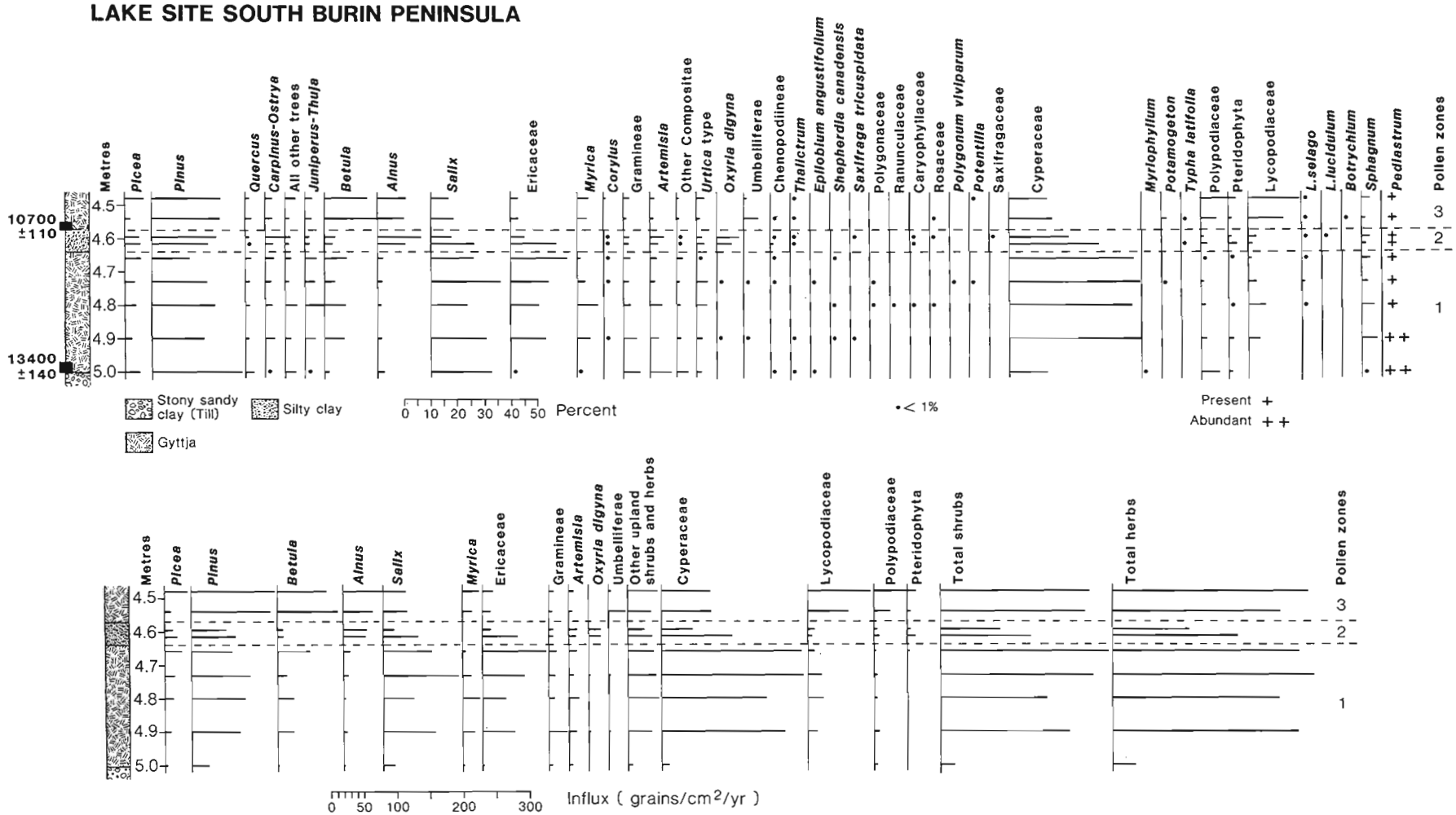

Figure 20.2. *Abbreviated pollen percentage and influx diagrams for the lowermost sediments in a lake from southern Burin Peninsula, Newfoundland.*

Site Description

The lake (46°55'10"N; 55°36'45"W) lies on the upland plateau 2 km inland from the south coast of Burin Peninsula. It is at an elevation of about 114 m a.s.l. and has a maximum depth of 3.2 m in the centre. The bedrock in the area is mostly Precambrian volcanics with bodies of granite and gneisses of the same age (Baird, 1954).

Burin Peninsula falls within the Avalon Boreal Forest Region of Rowe (1972). The vegetation of southern Burin Peninsula consists mainly of dwarf shrub heath, grasses, sedges, and conifer clumps, especially in wet depressions and along the coast. Arctic-alpine species such as **Diapensia lapponica, Vaccinium uliginosum, Empetrum eamesii,** and **Carex bigelowii** are common as this area is one of the colder parts of the island (Damman, 1976). Blanket bog peatland is the dominant surface material because of the climatic conditions; the southern Burin Peninsula experiences the highest recorded mean annual rainfall and fog occurrences in eastern Newfoundland (Wells, 1981).

A 5 m-long (7.5 cm diameter) Livingstone core was obtained from the centre of the lake from two aluminum boats bolted together in raft fashion. The core bottomed into stiff, noncalcareous, stony, sandy clay believed to be till. The mineral substrate is overlain by 5 m of detrital gyttja. Within the gyttja is a silty clay layer (4.57-4.64 m) with minor pebbles. This clay layer, like the basal clay, is noncalcareous. Two radiocarbon dates were obtained for the gyttja: 13 400 ± 140 BP (GSC-3559) from immediately above (4.97-5.00 m) the basal sandy clay and 10 700 ± 110 BP (GSC-3572) from immediately above (4.55-4.57 m) the silty clay bed. The apparent sedimentation rate is 0.015 cm/year between the dated horizons. This rate, however, may not be applicable to the silty clay layer which probably accumulated rapidly. The same sedimentation rate was extrapolated into the gyttja above the clay layer to obtain pollen influx up to 4.48 m.

Pollen Analysis

Methods

Sediment samples of 1 cm^3 from the core interval 4.48 to 5.0 m were spiked with a measured volume of **Eucalyptus** pollen suspension prior to chemical processing. The samples were treated with HF and KOH followed by acetolysis. Counts of 220 or more fossil tree, shrub, and herb pollen, excluding aquatics, provided the basic pollen sum for the percentage calculations. **Eucalyptus** pollen was also counted, and the ratio of **Eucalyptus** counted to that added gave an estimate of the concentration of fossil pollen and spores in each sample; pollen concentrations (grains/cm^3) divided by the sediment accumulation rate produced pollen influx (grains/cm^2/year).

Results

Abbreviated percentage and influx diagrams are shown in Figure 20.2. **Pinus, Salix,** Cyperaceae, Ericaceae and, to a lesser extent, **Betula, Alnus,** and Lycopodiaceae dominate the spectra. **Betula** ranged between 14 and 22 µm which is the size range for shrub birch according to Macpherson (1982). Arboreal pollen of **Picea, Pinus, Quercus,** and other hardwoods is considered exotic and is attributed to long distance transport from boreal-like forests in the southern New England States at this time (Davis, 1981).

The diagrams are tentatively divided into three pollen assemblage zones which correspond more or less with the sediment changes. Zone 1 (5.0-4.64 m), the **Salix**-Cyperaceae-Ericaceae zone, is characterized by an initial high in **Artemisia** followed by maximum percentages and influx rates of **Salix,** Ericaceae, and Cyperaceae. **Betula** and **Myrica** increase upward to peak values and then decline. Total shrub and herb pollen influx rates increase about eight-fold above the lowermost sample from less than 50 grains/cm^2/year to almost 200 and 300 grains/cm^2/year, respectively.

Zone 2 (4.64-4.58 m), the **Oxyria digyna-Alnus** zone, is based on two analyses from the clay band. **Oxyria digyna** reaches maximum percentages (8%) and influx rates (close to 20 grains/cm^2/year). Interestingly, **Alnus** (mostly **A. crispa** type) and **Artemisia** also increase to peak values. On the other hand, **Salix,** Ericaceae, and Cyperaceae decline gradually, **Betula** attains a minimum, while **Myrica** is absent altogether. Influx of shrub pollen drops more than three-fold from the previous zone but significantly less in the case of the herbs. The overall lower influx rates in this zone may be partly an artifact of a higher sedimentation rate during deposition of the clay band. Average pollen concentrations in the clay compared with those from the gyttja above and below indicate the clay layer had accumulated almost twice as rapidly as the gyttja.

Zone 3 (4.57-4.48 m) is the **Betula**-Lycopodiaceae zone. **Betula** increases five-fold on a percentage basis and more than ten-fold in influx from the previous zone. **Salix,** Ericaceae, and Cyperaceae are significantly lower and **Myrica** reappears after being absent in the previous zone. The other major change is the sudden increase in Lycopodiaceae and Polypodiaceae (**Dryopteris** type) spores. Total shrub and herb pollen influx estimates increase again in this zone from minimum values in the preceding zone to values comparable to those in Zone 1.

Vegetation and Climatic Inferences

Several inferences can be made with respect to changes in vegetation and climate from the abbreviated pollen stratigraphy. The dominance of **Salix,** Ericaceae, and herbs in Zone 1 indicates that shrub tundra vegetation characterized the area around the lake at 13 400 BP and for some time after this date. Initially, the vegetation consisted of willow and herbs (Cyperaceae, Gramineae, **Artemisia**), the influx rates of which were extremely low (less than 50 grains/cm^2/year). Once a herb mat of sedges, clubmosses (Lycopodiaceae), ferns (Polypodiaceae), and **Sphagnum** moss developed, shrub plant seedlings such as the heaths (Ericaceae), **Myrica,** and **Shepherdia canadensis** became established as the dominant vegetation around the lake. **Oxyria digyna, Polygonum viviparum, Epilobium angustifolium,** one or more **Urtica** species, saxifraga (**Saxifraga tricuspidata**), and composites (Compositae) apparently were common, presumably in the upland areas.

The decrease of **Betula, Salix,** Ericaceae, and Cyperaceae, absence of **Myrica,** and corresponding increases in **Oxyria digyna** and **Artemisia** denote a change in vegetation of major proportion from shrub tundra in Zone 1 to herb tundra in Zone 2. **Oxyria digyna** was more widespread at this time than at any time previously. **Oxyria digyna** presently occurs more often in moist gravelly arctic and alpine habitats where snowbanks persist well into the summer months (Porsild and Cody, 1980). Its prominence in Zone 2 is indicative of a sudden shift to cooler climatic conditions sometime after 13 400 BP but prior to 10 700 BP, the age of the upper boundary of Zone 2. With possibly a decrease in the shrub plant cover deduced from the greater than three-fold decline in total shrub pollen influx at this time (Fig. 20.2), open-ground areas had increased and herbs such as **Oxyria digyna, Saxifraga tricuspidata,** and **Artemisia** became more abundant.

Zone 3 marks the re-establishment of shrub vegetation based on a five-fold increase in shrub **Betula,** return of **Myrica,** continued high values of **Salix** and **Alnus,** the decline of **Artemisia,** and disappearance of **Oxyria digyna.**

Clubmosses and ferns expanded to greater proportions than in Zone 2 and apparently were even more widespread than in Zone 1. Total shrub and herb pollen influx rates increase to those of Zone 1 primarily on account of the increase in shrub birch.

The complete disappearance of **Oxyria digyna** and decrease in **Artemisia** implies climatic conditions had become less severe by about 10 700 BP. This probably represents the beginning of the postglacial warming trend associated with widespread deglaciation. Evidence from elsewhere (Macpherson, 1982) indicates that rapid amelioration of the climate occurred after 9000 BP.

Discussion and Conclusions

The pollen stratigraphy in this study is almost identical to the basal record at Sugarloaf Pond, Avalon Peninsula, some 300 km to the northeast (Macpherson, 1982). There too a shrub-tundra sequence is documented with an intervening herb interval, similarly dominated by **Oxyria digyna.** Unlike this site, however, the equivalent interval at Sugarloaf Pond falls entirely within the basal inorganic sediments for which chronological control is not feasible. The Burin Peninsula study, thus extends the known Late Wisconsinan chronology of southeastern Newfoundland an additional 4000 years.

The sediment sequence and vegetation changes inferred in this study may best be explained on the basis of fluctuations of the North Atlantic polar front during Late Wisconsinan time (Ruddiman and McIntyre, 1973). The polar front retreated northward after reaching its southernmost limit at the time of the Late Wisconsinan maximum. By about 13 000 BP, it had been displaced well to the North Atlantic resulting in climatic warming in the more southerly regions (Ruddiman and McIntyre, 1981). Gyttja deposition starting at 13 400 BP at this lake site, reflects this period of climatic amelioration. Prior to this date, conditions apparently were not ideal for organic sedimentation even though southernmost Burin Peninsula may have been largely ice free during Late Wisconsinan time. It is conceivable that the area was blanketed by a perennial snow cover and the lake was probably frozen on a year-round basis at the time of the Late Wisconsinan maximum. By 13 400 BP, favourable climatic conditions had been achieved, the permanent snow and frozen-lake conditions possibly gave way to a more seasonal situation with freezing and thawing, and a distinct aquatic biota suddenly had flourished in the lake. This is borne out by the abundance of the planktonic alga, **Pediastrum,** and presence of the submersed aquatic, **Myriophyllum,** in the basal-most gyttja (Fig. 20.2).

Gyttja sedimentation, however, was evidently interrupted just prior to 10 700 BP by a period of silty clay deposition. The clay layer is a reflection of a rejuvenated glacial-type climate in Late Wisconsinan time. The clay bed presumably was derived from erosion of open-ground areas which had increased as a result of the reduced plant cover and cooler climate inferred for this time. This climatic deterioration is tentatively correlated with the readvance of North Atlantic polar water between 10 000 and 11 000 years ago (Ruddiman and McIntyre, 1981). In this connection, it is significant that Grant (1969) has dated a major readvance of Newfoundland ice at 10 900 BP.

Further dating below the clay layer seems desirable in order to substantiate correlation with the Late Wisconsinan events of the North Atlantic. More paleoenvironmental studies are needed to determine the intensity of the climatic oscillations.

Acknowledgments

W. Blake, Jr. and the Geological Survey of Canada Radiocarbon Laboratory are thanked for providing the radiocarbon dates. D.R. Grant and R.J. Mott reviewed the manuscript and provided constructive criticism which greatly improved the paper.

References

Baird, D.M. (compiler)
1954: Geological map of Newfoundland; Newfoundland Geological Survey, scale: 1" = 12 miles.

Damman, A.W.H.
1976: Plant distribution in Newfoundland especially in relation to summer temperatures measured with the sucrose inversion method; Canadian Journal of Botany, v. 54, p. 1561-1585.

Davis, M.B.
1981: Quaternary history and the stability of forest communities; in Forest Succession: Concepts and Application, ed. D.C. West, H.H. Shugart, and D.B. Botkin; Springer-Verlag, New York, p. 132-153.

Grant, D.R.
1969: Surficial deposits, geomorphic features, and Late Quaternary history of the terminus of the northern peninsula of Newfoundland and adjacent Quebec-Labrador; Maritime Sediments, v. 5, p. 123-125.

1975: Glacial features of the Hermitage-Burin Peninsula area, Newfoundland; in Report of Activities, Part C, Geological Survey of Canada Paper, 75-1C, p. 333-334.

1977: Glacial style and ice limits, the Quaternary stratigraphic record, and changes of land and ocean level in the Atlantic Provinces, Canada; Géographie physique et Quaternaire, v. XXXI, p. 247-260.

Macpherson, J.
1982: Postglacial vegetational history of the eastern Avalon Peninsula, Newfoundland, and Holocene climatic change along the eastern Canadian seaboard; Géographie physique et Quaternaire, v. XXXVI, p. 175-196.

Porsild, A.E. and Cody, W.J.
1980: Vascular plants of continental Northwest Territories, Canada; National Museum of Natural Sciences, National Museum of Canada, Ottawa, 667 p.

Rowe, J.S.
1972: Forest regions of Canada; Department of Fisheries and Environment, Canadian Forestry Service, Publication 1300, 172 p.

Ruddiman, W.F. and McIntyre, A.F.
1973: Time-transgressive deglacial retreat of polar water from the North Atlantic; Quaternary Research, v. 3, p. 117-130.

1981: The North Atlantic Ocean during the last deglaciation; Palaeogeography, Paleoclimatology, Palaeocology, v. 35, p. 145-214.

Tucker, C.M.
1979: Late Quaternary events on the Burin Peninsula, Newfoundland; unpublished Ph.D. thesis, McMaster University, Hamilton, Ontario, 282 p.

Tucker, C.M. and McCann, B.
1980: Quaternary events on the Burin Peninsula, Newfoundland and the islands of St. Pierre and Miquelon, France; Canadian Journal of Earth Sciences, v. 17, p. 1462-1479.

Wells, E.D.
1981: Peatlands of eastern Newfoundland; distribution, morphology, vegetation, the nutrient status; Canadian Journal of Botany, v. 59, p. 1978-1997.

21.

INTERPRETATION OF A GRAVITY PROFILE OVER A CONTACT ZONE BETWEEN AN ARCHEAN GRANODIORITE AND THE YELLOWKNIFE SUPERGROUP USING AN INTERACTIVE COMPUTER PROGRAM WITH PARTIAL AUTOMATIC OPTIMIZATION

Project 700015

P.H. McGrath[1], John B. Henderson, and F.M. Lindia[2]
Precambrian Geology Division

McGrath, P.H., Henderson, J.B., and Lindia, F.M., Interpretation of a gravity profile over a contact zone between an Archean granodiorite and the Yellowknife Supergroup using an interactive computer program with partial automatic optimization; in Current Research, Part B, Geological Survey of Canada, Paper 83-1B, p. 189-194, 1983.

Abstract

An interactive computer program with partial automatic optimization is described that is used to calculate the anomalies of 2½-D model sources. As an example, a gravity profile is presented across an Archean basin margin complex involving granitoid, metavolcanic and metasedimentary rocks at Yellowknife. On the basis of the gravity model it is shown that the volcanics, which outcrop only at the margin of the basin, extend to a depth of 2 to 3 km (depth determinations are shown to be very sensitive to the density contrasts used) and are continuous for a distance of about 15 km into the basin below the metasediments which occupy the main part of the basin. Within the basin an inverse relationship between the modelled thickness of the metasedimentary block and its grade of metamorphism is explained by the occurrence of nearer surface intrusive granitoid plutons in the high grade zone.

Résumé

Le présent rapport décrit un programme interactif avec optimisation automatique partielle qui sert à calculer les anomalies des sources de modèles à 2½-D. À titre d'exemple, les auteurs présentent un profil gravimétrique transversal d'un complexe marginal de bassin archéen à Yellowknife, qui est composé de roches granitoïdes, métavolcaniques et métasédimentaires. Le modèle gravimétrique montre que les roches volcaniques, qui affleurent seulement sur le bord du bassin, s'étendent sur une profondeur de 2 à 3 km (la détermination de la profondeur est très susceptible aux contrastes de densité utilisés) et sur une distance approximative de 15 km, sous les métasédiments qui remplissent une grande partie du bassin. Au sein du bassin, une relation inverse entre l'épaisseur donnée par le modèle et le degré de métamorphisme est expliquée par la présence, plus près de la surface, de plutons granitoïdes dans la zone de métamorphisme élevé.

Introduction

The use of computers to assist in the interpretation of gravity and magnetic data is well established. One of the earliest papers promoting this concept was published by Talwani et al. (1959). This approach consists of approximating the proposed geological model with 2-dimensional right polygonal bodies. By simplifying the geological model in this manner, it is possible to rapidly compute the associated gravity or magnetic anomaly from the appropriate mathematical expressions. Subsequently, using available geological constraints, adjustments can be made to the parameters of the idealized model so that the resultant calculated profile is brought into closer agreement with the measured anomalies. On this basis it is often possible to exclude certain geological options as well as to predict modifications to the original geological model. On the other hand, the validity of the predictions can sometimes be tested in light of other geological and/or geophysical data. To this extent, it is possible to reduce the ambiguity problem which is inherent in all potential field interpretations.

More recently, Shuey and Pasquale (1973), Rasmussen and Pedersen (1979), and Cady (1980) have published end corrections for the Talwani-Heirtzler mathematical expressions (Talwani and Heirtzler, 1964) to handle models of finite strike length – the 2½-dimensional case. Also, Ogawa and Hiroji (1976), Enmark (1981), and Wells (1979) have published interactive computer graphics software which, by improving the dialogue between man and machine, provides a friendlier interpretational environment. In the present paper an application based on the software developed for 2-D bodies at the Atlantic Geoscience Centre by Wells is presented. The program was modified to handle the 2½-D case, and to permit partial automatic optimization of the model fit. The interpretation was performed interactively on a Tektronix Graphics Terminal (model 4013) which is connected with a 9600 baud line to EMR's Cyber at the Computer Science Centre, 588 Booth Street, Ottawa.

Model

Mathematical expressions have been published for 2-, 2½- and 3-D models. The application of the 2-D Talwani-Heirtzler equations is restricted to causative bodies with large strike lengths. On the other hand, the use of 3-D models requires more complex software which increases the calculation costs, and creates problems in presenting the models in such a way that the iterative process of interpretation can be easily monitored. Hence the n-sided, 2½-D polygonal model (Fig. 21.1) was adopted for our interpretational problems. Such models have many of the advantages of 3-D models without the added complications of complexity and presentation.

The XZ plane, and the calculated and observed anomalies (Fig. 21.1) are viewed on a graphics terminal. The software permits continuous man/computer dialogue. Changes to the model are made iteratively, either manually using the video display cursor, or automatically by the computer using an optimization routine.

The expression used for the gravity anomaly produced by the finite strike length n-sided polygonal model was published by Rasmussen and Pedersen (1979, equation 8, page 753), and for the magnetic anomaly by Shuey and Pasquale (1973, equation 19, page 510).

[1] Resource Geophysics and Geochemistry Division.
[2] Department of Geology, Carleton University, Ottawa, Ontario.

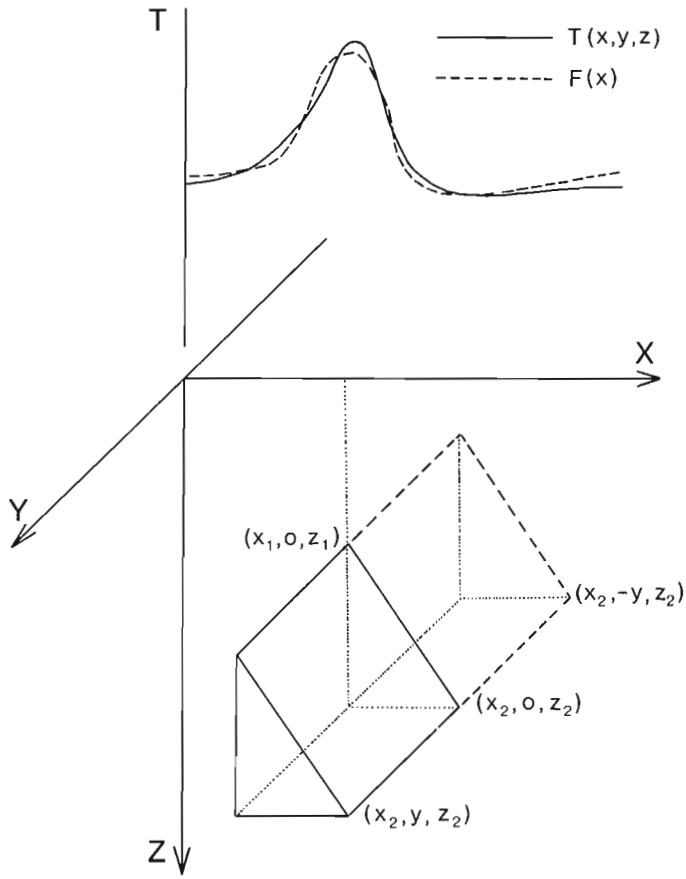

Figure 21.1. *N-sided 2½-D body with associated gravity profile along the x axis of an orthogonal co-ordinate system; the y axis parallels the strike of the body, and the z axis is positive down. The xz plane and the calculated, T(x,y,z), and observed, F(x), anomalies are viewed on the graphics terminal screen.*

Optimization

The objective is to obtain an idealized model such that the differences, $f_i(x)$, between the observed and calculated anomaly profiles are minimized, where

$$f_i(x) = F_i(x) - T_i(x,y,x_1,z_1x_2,z_2.....) \quad (1)$$

and $F_i(x)$ and $T_i(x,y,x_1z_1,x_2,z_2,.....)$ are the ith observed and calculated data points. An accepted method of curve-fitting is by least squares, where

$$R = \sum_{i=1}^{N} f_i(x)^2 \quad (2)$$

and it is necessary to determine values for the body points $x_1,z_1,.....$, such that R is a minimum. Y is the half-strike length of the body and N is equal to the number of observations. It is also to be noted that equations (1) and (2) are nonlinear with respect to the body points.

The nonlinear least squares method selected to solve this problem was developed by Powell (1965). In applying this method it was decided that only one or two body points would be allowed to move at a time under control of the algorithm. Thus the complexity of the software and amount of computer memory was reduced, which is always a concern in the time-sharing mode. Also, by restricting the changes in the model to a series of finite increments, the interpreter is better able to contain the model within reasonable geological constraints, yet is free to test ideas and to explore obvious conflicts between the observed and the resultant calculated anomalies as the interpretation proceeds, hence taking full advantage of operating in a time-sharing environment.

The Powell algorithm requires an input model which produces a reasonably good approximation of the observed anomaly, otherwise the method will fail. Also, any body points in which one of the co-ordinates is zero cannot be moved under control of this algorithm. An acceptable model for optimization is normally obtained by trial and error manual adjustments of an initial model using the video terminal cursor.

During optimization, the algorithm proceeds by generating a correction vector, d, from partial derivatives of the function, $f_1(x)$, with respect to the body points concerned by finite differences. A one-dimensional search is made for a minimum value of R in the direction d, i.e. we determine λ such that $R(\epsilon_i + \lambda d)$ is a minimum, where ϵ_i is the initial estimate of the ith body point. The search is iterative and continues until either a minimum value of R is determined or a pre-defined number of iterations has taken place.

Under a separate software option the Powell algorithm can also be used to determine estimates of the density or magnetization contrasts for the various bodies if no other source for this information is available. Again, zero values for these parameters are unacceptable.

An Application to a Geological Problem of the Partial Automatic Optimization Modelling Procedure Using Gravity Data

In low relief terranes such as the Slave Province the extent of steeply dipping geological units in the third dimension is commonly difficult to determine. In the Slave, the complexly deformed and metamorphosed, sediment-dominated, Archean Yellowknife supracrustal rocks occur in several irregular areas normally bounded by intrusive granitoid rocks, although basement gneisses and granitoid rocks that are basement to the Yellowknife rocks are locally preserved (Henderson, 1981, p. 226). Where present, the less abundant metavolcanic rocks tend to occur at the margins of the supracrustal areas between the metasediments and the granitoid rocks, facing toward the metasediments. The traditional stratigraphic interpretation of Archean supracrustal successions such as these, but developed elsewhere in granite-greenstone terranes where metavolcanic rocks dominate over metasedimentary rocks, is that the supracrustal rock remnants represent parts of originally much more extensive basins that have been preserved as synclinal keels; the implication being that the metavolcanic rocks exposed at the surface and separated by metasediments are, or at least were at one time, continuous at depth (i.e. Windley, 1981). In the Slave Province, on the other hand, it has been suggested that the areas underlain by supracrustal rocks represent remnants of fault bounded basins in which most of the volcanism was restricted to the basin margin fault zones while the main part of the basin was filled with greywacke-mudstone turbidites derived from the granitoid basement rocks and mainly felsic volcanic rocks on the uplifted basin margins (McGlynn and Henderson, 1970; Lambert, 1977; Henderson, 1981). According to this interpretation, the metasediments in the central part of the basin were deposited directly on granitoid basement and so there is little reason to suppose there was a continuous mafic volcanic layer from one side of the basin to the other. There is no directly observable evidence apparent of such a layer at the present erosion level, such as the occurrence of mafic volcanics in the cores of major anticlinal structures or around plutons in the central part of the basin, but as a test of the

model it was thought an investigation to see if there is any geophysical expression of a hypothetical mafic layer would be in order.

One of the best preserved of these supracrustal basin remnants occurs in the southern Slave Province east of Yellowknife. There parts of two opposite margins have well preserved mafic metavolcanic successions, the central metasedimentary part has a minimal number of granitic intrusions, and there is good evidence that at least some of the bounding granitoid rocks are older than the adjacent Yellowknife metavolcanic and metasedimentary units (Fig. 21.2). In addition, in the immediate Yellowknife area regional gravity surveys have been supplemented by more closely-spaced gravity data. This allows the possibility of attempting to determine if the major mafic metavolcanic succession at Yellowknife can be traced eastwards into the basin below the metasediments with presently available data.

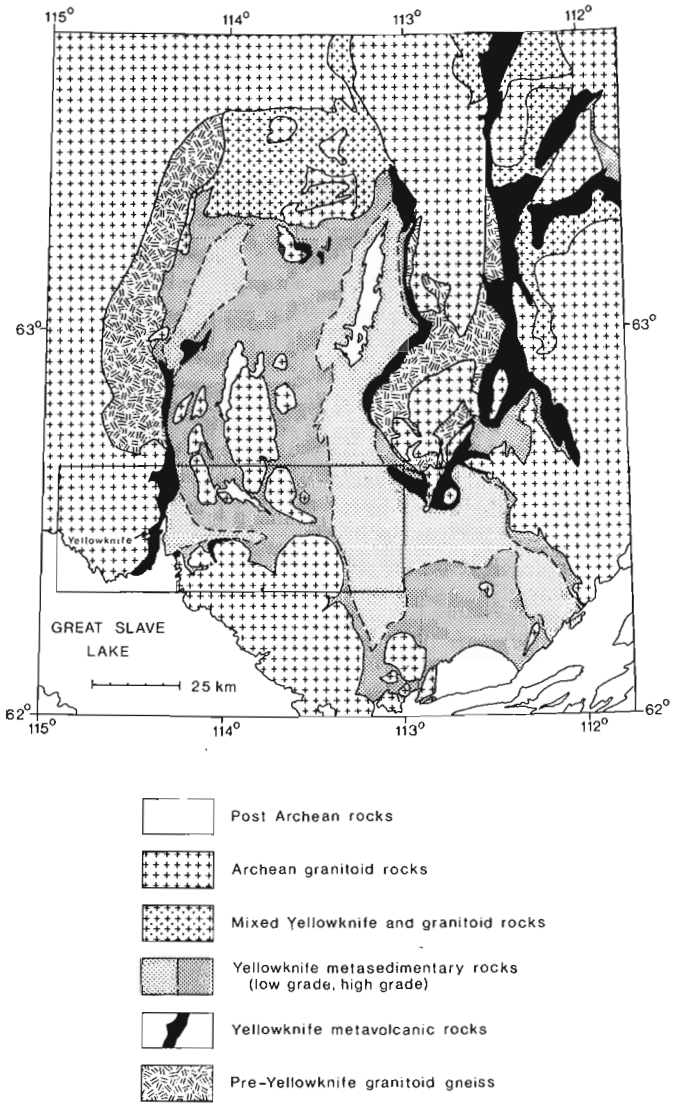

Figure 21.2. *Remnant of an Archean basin in the southern Slave Province filled mainly with greywacke-mudstone turbidites of the Yellowknife Supergroup, but with thick, predominantly mafic volcanic sequences exposed at the margins. Basement to the Yellowknife supracrustal rocks is locally preserved. Area outlined is that shown in Figure 21.3. After McGlynn (1977).*

A profile through Yellowknife (Fig. 21.3) was selected for gravity modelling purposes that is more or less orthogonal to the regional Bouguer gravity anomaly contours (Earth Physics Branch, 1969) but includes part of the bordering intrusive Defeat granodiorite west of Yellowknife, the major sequence of Kam metabasalt and meta-andesite that occurs at the margin of the supracrustal basin, and the metagreywacke-mudstone turbidites of the Burwash Formation that constitute the main basinal fill. The profile extends over halfway across the basin. Within the basin the profile passes between two granitoid units that intrude the Burwash metasediments, the Prosperous Granite to the north, and the Defeat Plutonic Suite to the south.

Structurally the area is very complex. A major synclinal axis occurs under and parallel to Yellowknife Bay with mainly steeply dipping to locally overturned Kam metavolcanics on the west limb and mainly refolded Burwash metasediments on the eastern limb, although minor metavolcanic units thought to be equivalent to the Kam metavolcanics (Henderson, 1970) occur to the east in an anticlinal structure adjacent to the Defeat plutonic complex. In addition, a series of post-Archean sinistral faults occur in the Yellowknife Bay area.

The profile is located within the northern part of the area recently modelled in three dimensions by Gibb and Thomas (1980), in which they proposed the Kam metavolcanics extend southeast of Yellowknife Bay under Great Slave Lake. Unfortunately, the area covered by their closely-spaced array of gravity stations does not include a geologically suitable transect across the basin margin without the added complications of major intrusive granites.

Gravity values along the profile, ABCD, (Figs. 3 and 4) were determined at one kilometre spacing by interpolation of the regional gravity data (Earth Physics Branch, 1969). These data were used in the interpretation without modification since it was apparent from inspection of the regional gravity map that the profile could be entirely explained in terms of changes related to the surface geology, and that anomalous gradients due to other sources were not present in the data.

The initial model consisted of a granodiorite body extending from the west to 22.3 km along the profile, a metavolcanic body from 22.3 to 30 km, and a metasedimentary body from 30 km to beyond the east end of the profile. The granodiorite was assumed to underlie the metavolcanic and metasedimentary bodies. The contacts between the bodies were originally assumed to be vertical, and depth extents of 7 km were assigned to the volcanic and metasedimentary bodies. The strike length of the volcanic body was considered as infinite while that of the metasedimentary body was estimated as 10 km on the basis of the known geology (Fig. 21.3).

The density data used for the modelling were similar to those used by Gibb and Thomas (1980) in their study of the area. The density used for the Kam metavolcanics was 2.90 ± 0.10 gm/cm^3, for the Burwash metasediments, 2.74 ± 0.03 gm/cm^3, and for the Defeat granodiorites, which occur both west of and within the basin south of the profile, 2.64 ± 0.02 gm/cm^3. In addition, Kretz et al. (1982) determined a similar average density of 2.64 gm/cm^3 for a pluton of the Prosperous Granite which occurs north of the profile within the basin. The mean granite-granodiorite density of 2.64 gm/cm^3 was arbitrarily chosen as a reference or background density to which the densities of the metavolcanic and metsedimentary bodies were contrasted, thus simplifying the model to two bodies. Mean density contrasts of 0.26 gm/cm^3 and 0.10 gm/cm^3 were used for the metavolcanic and metasedimentary bodies respectively. A value of -59 mGal was used as the zero reference for the calculated model since it is a representative value of the gravity field over the granite-granodiorite terrane.

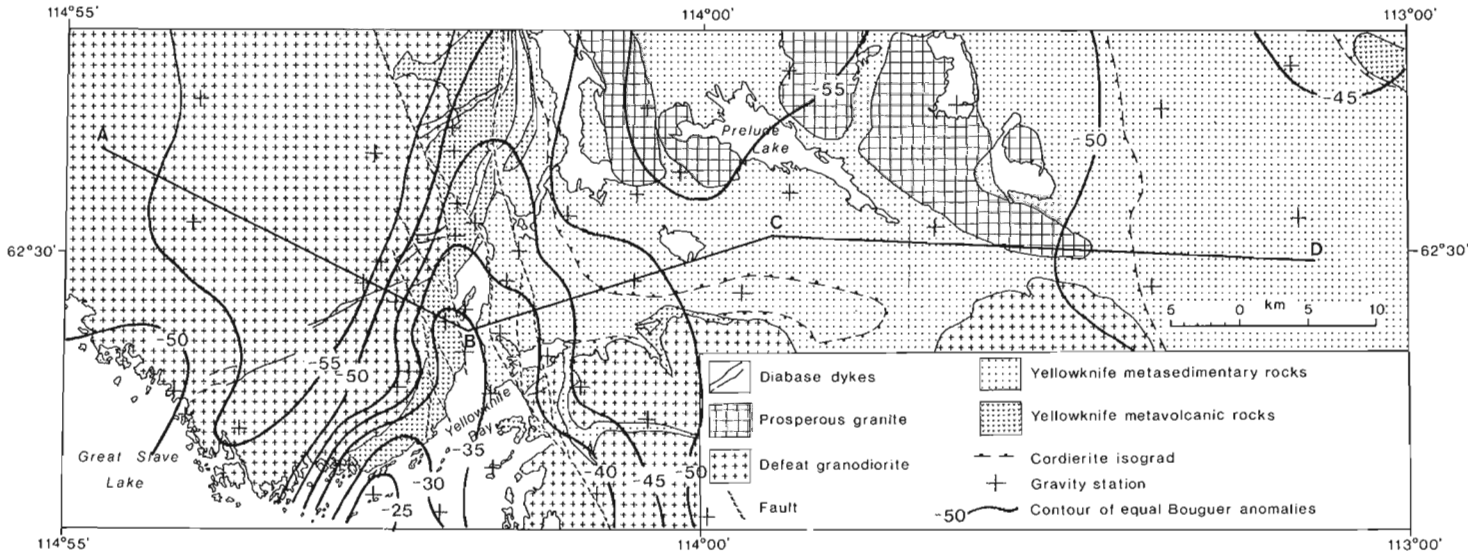

Figure 21.3. *Location of gravity profile (ABCD) across the margin of the Yellowknife basin and superimposed Bouguer gravity field. After Henderson (1976) and Earth Physics Branch (1969).*

During the preliminary stages of the iterative procedure of interpretation, modifications to the body parameters were performed by trial and error. Once the general outline of the model had been chosen, the main part of the interpretation was continued to a best-fit model by movement of the body points under control of the automatic optimization algorithm. The density contrasts, strike lengths and surface definition of the bodies were used to constrain the curve-fitting.

Results

The results of gravity modelling along the section through Yellowknife are shown in Figure 21.4a where both the gravity profile determined from the regional gravity data and the profile calculated from the optimized gravity model are shown. Immediately below the gravity profiles the best-fit model is shown at equal vertical and horizontal scale.

This best-fit model indicates that the block of metavolcanics tapers gently eastward into the basin below the metasediments but doesn't extend beyond 15 km of its main area of outcrop west of Yellowknife Bay. It has a nearly horizontal lower contact at a depth of about 2.75 km. The metasediments to the east have a thickness (not stratigraphic) of 3.5 km at the eastern end of the profile in the central part of the basin but thin to less than 2 km in the area of highest metamorphic grade, as outlined in both Figures 21.3 and 21.4 by the cordierite isograd. Both the metasediments and the metavolcanics are assumed to be underlain by rocks of similar density to the intrusive granodiorite west of Yellowknife.

In Figure 21.4b the gravity model is shown with about a 6 fold vertical exaggeration. In addition to the model calculated using the average densities of the rocks involved, two supplementary models were also calculated using the standard deviations of the density data as limits so as to maximize and minimize the contrast between the supracrustal rocks and the granitic rocks. This procedure has had little effect on the general shape of the models, but it does have a significant effect on the thickness of the various blocks, indicating that the model is rather sensitive to the density contrasts used.

Discussion

The gravity model presented appears to be geologically reasonable. The question originally asked as to whether or not there is a layer of mafic metavolcanics below the metasediments appears to be answered in the negative. Using the densities of the rocks exposed at the surface and assuming the supracrustal basin is underlain by granitoid rocks of similar density to those that occur adjacent to the basin and are known to intrude it, it does not seem possible that a dense mafic layer could exist today below the metasediments. This, of course, is not proof that such a layer never existed at any time during the evolution of the basin, but if such a layer ever did exist there is no evidence that any part of it has been preserved below the metasediments in that part of the basin covered by the profile.

The volcanics are modelled as a wedge-shaped block thinning away from the margin of the basin. There is geological evidence south of the profile that mafic metavolcanics occur some 15 km east of the margin as relatively thin units adjacent to the granodiorite intrusions in the basin (Fig. 21.2). The wedge-shaped block is probably a reasonable approximation of the section across the synclinal structure through Yellowknife Bay. The mafic metavolcanics occur on the west limb of the structure but since they are thinning into the basin they are not seen again at the surface on the east limb until they reappear in the core of the anticline that rims the granitic intrusion to the southeast. The late faults through Yellowknife Bay, which are at a moderate angle to the trend of the volcanics and the profile, no doubt have distorted the picture but probably not to an excessive degree.

In the model (Fig. 21.4) there is a dome in the granitic rocks beneath the metasediments that corresponds to the higher grade metamorphic zone east of Yellowknife in Figure 21.3. The prediction that the granitoid rocks occur closer to the surface in this part of the profile is reasonable, particularly since large plutons are exposed both north and south of the profile (Fig. 21.2). Indeed, the profile just crosses the end of one of these plutons, although this is not indicated in the model as none of the gravity stations occur on the granite in the vicinity of this part of the profile.

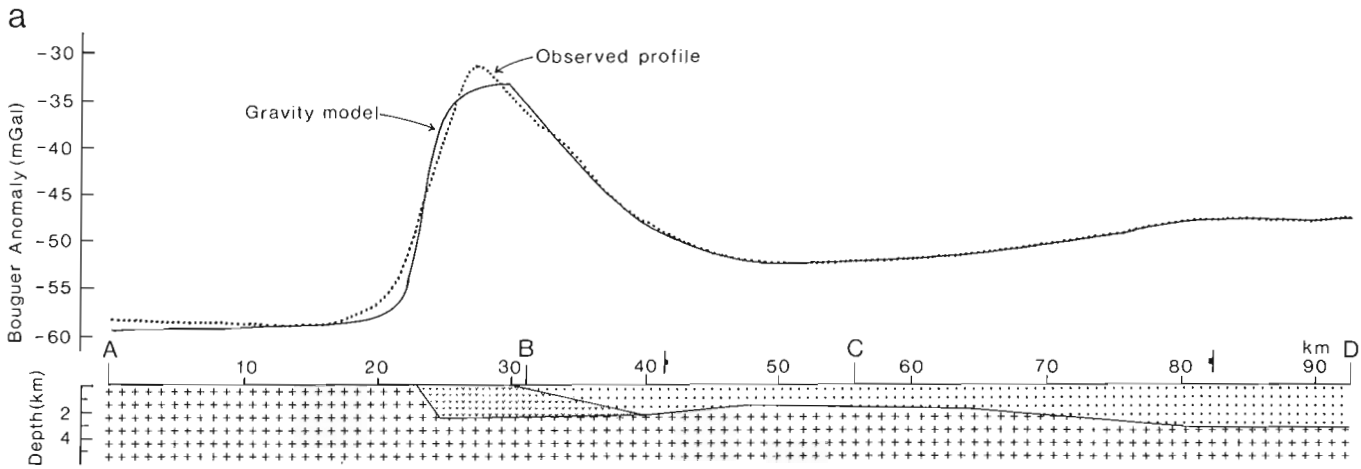

Figure 21.4a. *The Bouguer gravity anomaly along the profile ABCD (shown in Figure 21.3) together with the calculated anomaly based on the model shown below the profile at equal horizontal and vertical scales. Unit patterns for granitoid, metavolcanic, and metasedimentary rocks correspond to the legend in Figure 21.3. The model, whose gravity profile is closely similar to the observed profile, predicts that the basin-margin volcanic sequences do not extend into the central part of the basin and that the thickness of metasediments relative to granitoid rocks thins in the vicinity of C. The latter region approximately corresponds to the pluton cored thermal ridge indicated in both this figure and Figure 21.3 by the cordierite isograd symbols.*

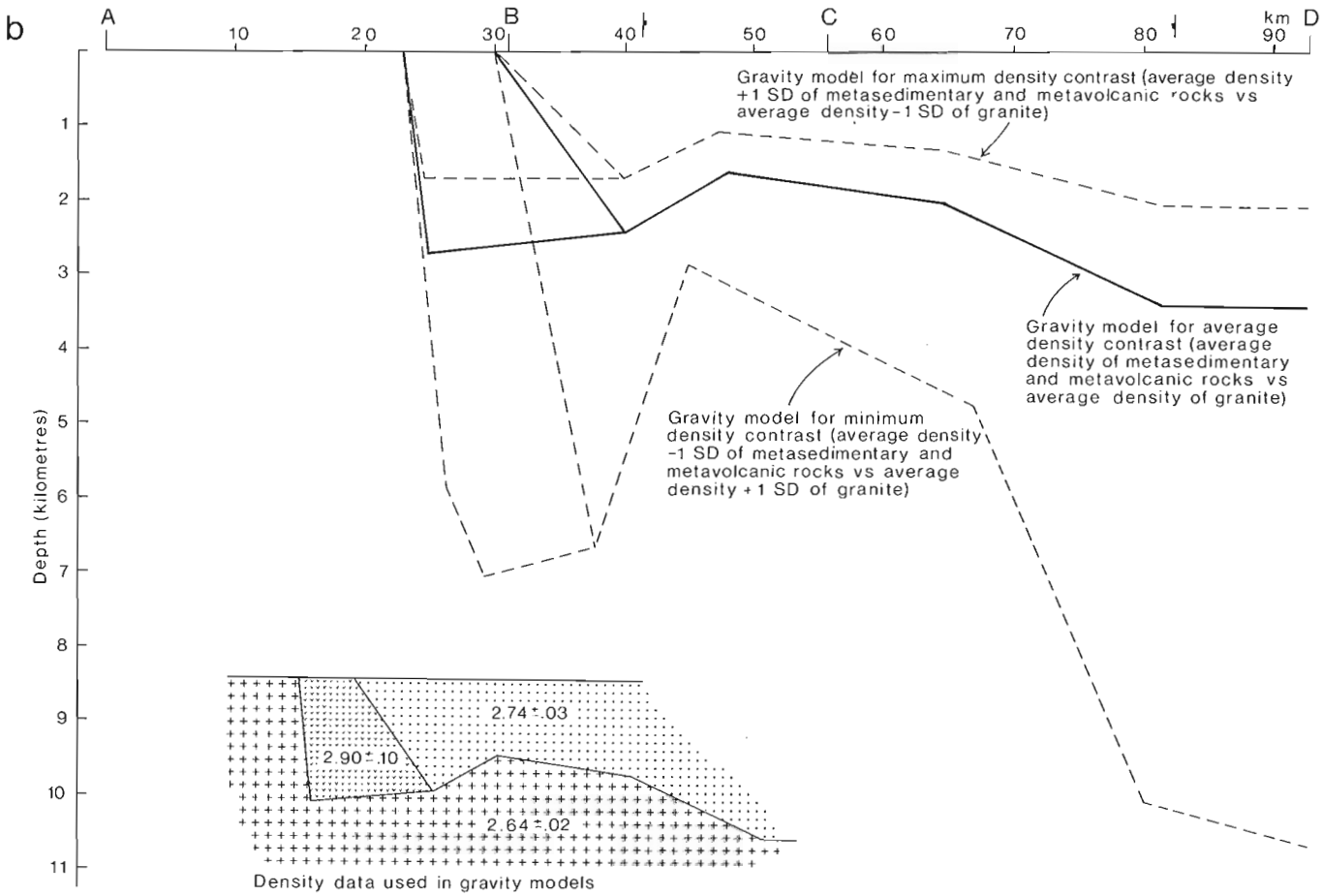

Figure 21.4b. *The same model is presented with 6 times vertical exaggeration. The density values used for the model with their standard errors are shown in the inset. Two other models are shown using maximum and minimum density estimates to provide maximum and minimum density contrast between the supracrustal rocks (metasediments and metavolcanics) and the granitoid rocks. The basic shape remains about the same, but depth estimates are strongly affected by small variations in density contrast.*

The part of the profile traversing the metavolcanics and immediately adjacent metasediments is more or less coincident with the northernmost profile of Gibb and Thomas (1980) based on their 3-D gravity model south and southeast of Yellowknife Bay. The configuration of their blocks differs considerably from that suggested here, but again, they found no reason to extend the volcanics eastward beneath the metasediments into the basin. They suggested a depth of about 4.5 km for the volcanics (Gibb and Thomas, 1980, profile P1, Fig. 5, p. 1512), which is considerably more than the 2.75 km suggested in this model. They imposed a limitation that all blocks have vertical sides, which may explain the difference in the two depth estimates.

Finally, it is probably worth making two observations with regard to the maximum and minimum density contrast models shown in Figure 21.4b. Obviously the interpreted depths are very sensitive to the densities used for the model bodies. This underscores the need to obtain adequate numbers of density measurements so that proper statistical average densities can be calculated. Secondly, some caution should be exercised with regard to the reliability of the interpretation at depth since it is based on density measurements on surface or near surface materials. Furthermore, it is likely that the lower contacts of the metavolcanic and metasedimentary units with the underlying intrusive bodies are gradational, hence the depths shown in Figure 21.4b should probably be considered only as minimum estimates.

The software was developed in Fortran IV for EMR's Cyber computer. A listing will be provided by the authors on request, however the Tektronix Inc. graphics software which is an integral part of the program cannot be included. Also, at present, no user manual is available.

Acknowledgments

We thank R.T. Haworth, who initiated the software development at the Atlantic Geoscience Centre, Dartmouth, Nova Scotia, and who demonstrated the method at a workshop at the Geological Survey in Ottawa; and T.M. Gordon, who modified the original computer code for use on the Cyber at the Computer Science Centre in Ottawa. We also wish to thank the critical readers, M.D. Thomas (Earth Physics Branch) and J.A. Percival (GSC) for their suggestions.

References

Cady, J.W.
1980: Calculation of gravity and magnetic anomalies of finite length right polygonal prisms; Geophysics, v. 45, no. 10, p. 1507-1512.

Earth Physics Branch
1969: Rae, Northwest Territories; Earth Physics Branch, Department of Energy, Mines and Resources, Gravity Map Series No. 90.

Enmark, T.
1981: A versatile interactive computer program for computation and automatic optimization of gravity models; Geoexploration, v. 19, p. 47-66.

Gibb, R.A. and Thomas, M.D.
1980: Correlation of gravity anomalies with Yellowknife Supergroup rocks, North Arm, Great Slave Lake; Canadian Journal of Earth Sciences, v. 17, p. 1506-1516.

Henderson, J.B.
1970: Stratigraphy of the Yellowknife Supergroup, Yellowknife Bay-Prosperous Lake area, District of Mackenzie; Geological Survey of Canada, Paper 70-26.

Henderson, J.B. (cont.)
1976: Yellowknife and Hearne Lake map areas; Geological Survey of Canada, Open File 353.

1981: Archean basin evolution in the Slave Province, Canada; in Precambrian Plate Tectonics, ed. A. Kroner, Elsevier, Amsterdam, p. 213-235.

Kretz, R., Garrett, D., and Garrett, R.G.
1982: Na-K-Li geochemistry of the Prestige pluton in the Slave Province of the Canadian Shield; Canadian Journal of Earth Sciences, v. 19, p. 540-554.

Lambert, M.B.
1977: Anatomy of a greenstone belt, Slave Province, Northwest Territories; in Volcanic Regimes in Canada, ed. W.R.A. Baragar, L.C. Coleman, and J.M. Hall, Geological Association of Canada, Special Paper 16, p. 331-340.

McGlynn, J.C.
1977: Geology of Bear-Slave Structural Provinces, District of Mackenzie; Geological Survey of Canada, Open File 445.

McGlynn, J.C. and Henderson, J.B.
1970: Archean volcanism and sedimentation in the Slave Structural Province; in Symposium on Basins and Geosynclines of the Canadian Shield, ed. A. Baer, Geological Survey of Canada, Paper 70-40, p. 31-44.

Ogawa, K. and Hiroji, T.
1976: Magnetic interpretation using interactive computer graphics; Report of Technical Research Center, Japan Petroleum Development Corp., no. 3, p. 19-39.

Powell, M.J.D.
1965: A method for minimizing a sum of squares of nonlinear functions without calculating derivatives; Computer Journal, v. 7, p. 303-307.

Rasmussen, R. and Pedersen, L.B.
1979: End corrections in potential field modeling; Geophysical Prospecting, v. 27, no. 4, p. 749-760.

Shuey, R.T. and Pasquale, A.S.
1973: End corrections in magnetic profile interpretation; Geophysics, v. 38, no. 3, p. 507-512.

Talwani, M. and Heirtzler, J.R.
1964: Computation of magnetic anomalies caused by two-dimensional structures of arbitrary shape; in Computers in the Mineral Industries, ed. G. Parks, Stanford University, p. 464-480.

Talwani, M., Worzel, J.L., and Landisman, M.
1959: Rapid gravity computations for two-dimensional bodies with application to the Mendocino Submarine Fracture Zone; Journal of Geophysical Research, v. 64, p. 49-59.

Wells, I.
1979: MAGRAV Users Guide – a computer program to create two-dimensional gravity and/or magnetic models; Geological Survey of Canada, Open File 597.

Windley, B.F.
1981: Precambrian rocks in the light of the plate-tectonic concept; in Precambrian Plate Tectonics, ed. A. Kroner, Developments in Precambrian Geology 4; Elsevier, Amsterdam, p. 1-20.

22.

A NEW ZLICHOVIAN (EARLY DEVONIAN) SPECIES OF THE RUGOSE CORAL GENUS *ZELOLASMA* FROM THE EIDS FORMATION OF ELLESMERE ISLAND, NORTHWEST TERRITORIES

Project 680093

Alan E.H. Pedder and Gary P. Smith[1]
Institute of Sedimentary and Petroleum Geology, Calgary

Pedder, A.E.H. and Smith, G.P., A new Zlichovian (Early Devonian) species of the rugose coral genus ***Zelolasma*** *from the Eids Formation of Ellesmere Island, Northwest Territories; in Current Research, Part B, Geological Survey of Canada, Paper 83-1B, p. 195-200, 1983.*

Abstract

Zelolasma*, sensu stricto, is known from the Pragian of Tadzhikistan, late Pragian or early Zlichovian of New South Wales, early Zlichovian of Ellesmere Island, and Dalejan of Taymyr. Reported occurrences in the late Lochkovian of Salair and the Dalejan or Eifelian of Gansu have yet to be substantiated. Forms resembling* ***Zelolasma****, but differing from it by lacking discrete adaxial septal fragments, are known from the Ludlow Series of New South Wales and the Upper Silurian (Ludlow or Pridolian equivalent) of the southern Urals.*

Zelolasma apsidiferum *sp. n. is described from high strata of the Eids Formation, 20.5 km west of the head of Sor Fiord, southwestern Ellesmere Island. The type horizon of the new coral is in the* ***Polygnathus dehiscens*** *Zone, which spans the Pragian/Zlichovian boundary. However, the age of the type stratum is judged to be early Zlichovian, rather than late Pragian, because it overlies probable Zlichovian brachiopods, as well as spores dated approximately as middle Emsian (equivalent to late Zlichovian).*

Résumé

Le ***Zelolasma****, au sens strict, a été identifié dans le Pragien du Tadzhiskistan, le Pragien récent ou le Zlichovien ancien de la Nouvelle-Galles du Sud, le Zlichovien ancien de l'île Ellesmere et le Dalejan de Taymyr. La présence de ce fossile dans le Lochkovien récent de Salair et dans le Dalejan ou l'Eifélien du Gansu n'a pas encore été vérifiée. Des formes semblables, qui diffèrent du* ***Zelolasma*** *par l'absence de fragments septaux adaxiaux discrets, ont été identifiées dans la série de Ludlow en Nouvelle-Galles du Sud et dans le Silurien supérieur (équivalent au Ludlowien ou au Pridolien) des montagnes de l'Oural du Sud.*

Les auteurs décrivent une nouvelle espèce, ***Zelolasma apsidiferum****, qui provient des couches supérieures de la formation de Eids, à 20,5 km à l'ouest du sommet du fjord Sor dans le sud-ouest de l'île Ellesmere. L'horizon type du nouveau corail est la zone de* ***Polygnathus dehiscens****, qui embrasse la limite du Pragien et du Zlichovien. Toutefois, le stratotype daterait du Zlichovien ancien plutôt que du Pragien récent puisqu'il recouvre des brachiopodes d'origine probablement zlichovienne, ainsi que des spores datant de l'Emsien moyen environ (équivalent au Zlichovien récent).*

Introduction

With the exception of some Upper Devonian corals illustrated by Embry and Klovan (1971, 1972) from Banks Island, all of the Devonian corals previously figured or described from the Canadian Arctic Archipelago have derived from either the Blue Fiord or Bird Fiord formations. Much of the Eids Formation, especially in the type area of southwestern Ellesmere Island, consists of poorly exposed, fine grained, clastic sediments, that either lack or have few megafossils. Known shelly faunas of the formation have come from limestone members exposed on west central Ellesmere Island (Trettin, 1978) and from calcareous shales near the top of the formation, 20 to 35 km west of the head of Sor Fiord (Jones and Smith, 1980).

Corals from the upper limestone member of the Eids Formation near Vesle Fiord, west central Ellesmere Island, have been identified by one of us (Pedder, in Trettin, 1978, p. 114) as **Favosites** sp., **Thamnopora** sp., **Pseudamplexophyllum** sp. n., **Xystriphyllum** sp. and **Stringophyllum** sp. n. It is hoped that this probable Pragian assemblage will be described in the future. The present work describes and names the only rugose coral so far collected from the Eids Formation of southwestern Ellesmere Island.

Acknowledgments

We are grateful to D.C. McGregor and T.T. Uyeno, both of the Geological Survey of Canada, for identifying spores and conodonts that help date the new coral. L. Sherwin, of the Geological Survey of New South Wales, kindly allowed Pedder to examine a coral, collected by him in New South Wales, that has a bearing on the distribution of **Zelolasma**. A.I. Lavrusevich, of the Tadzhikskiy Gosudarstvennyy Universitet, Dushanbe, also aided our assessment of the distribution of **Zelolasma** by sending photographs of a specimen from Tadzhikistan.

Biostratigraphy

The type horizon of **Zelolasma apsidiferum** is in a stratigraphic unit comprising 4 m of dark grey, very thin-bedded, argillaceous limestone. Abundant favositid and alveolitid corals constitute most of the fauna. The top of the unit is 30.9 m stratigraphically below the contact between the Eids and overlying Blue Fiord formations. The thickness of the Eids Formation in its type area is not known precisely. McLaren (1963, p. 318) estimated it to be "not less than 1,000 feet", and the Panarctic ARCO et al. Blue Fiord E-46 well, which was located about 20 km WNW of the type

[1] Department of Geological Sciences, McGill University, Montréal, Quebec, H3A 2A7

locality of **Zelolasma apsidiferum**, spudded in the Eids Formation and drilled 480.4 m before entering the underlying Cape Phillips Formation (Mayr et al., 1978, p. 393). These data suggest that the **Zelolasma apsidiferum**-bearing unit is more than 400 m above the base of the Eids Formation.

A widely distributed, late Pragian to early Zlichovian conodont, **Polygnathus dehiscens** Philip and Jackson, has been recovered from near the top of the Eids Formation at GSC loc. C-12504 (Uyeno and Klapper, 1980, p. 83), which is about 8 km east of the type locality of **Zelolasma apsidiferum.** Field work by one of us (Smith) indicates that the type horizon of the new coral is stratigraphically above the horizon of GSC loc. C-12504.

The **Zelolasma apsidiferum**-bearing unit is 27 m above beds that yielded the brachiopod fauna of Jones and Smith's (1980) locality G. Forms identified from this locality are **Cortezorthis maclareni** Johnson and Talent, **Parapholidostrophia sorensis** Jones, **Phragmostrophia** sp., **Parachonetes**? sp., **Carinagypa aseptata** Johnson, **Trigonirhynchia** sp. aff. **T. occidens** (Walcott), **Athyrhynchus loriei** Jones, **Atrypa** sp. aff. **A. aspiformis** Lenz, and **"Fimbrispirifer" scheii** (Meyer). A Zlichovian age is suggested by this assemblage.

Conodonts (GSC loc. C-86753) and spores (GSC loc. 97206) have been isolated from 78.7 m below the unit bearing **Zelolasma apsidiferum** by T.T. Uyeno and D.C. McGregor. The conodont fauna is small. A 983 g sample from C-86753 yielded only **Belodella** sp., **Panderodus** sp., and a single fragment of a Pa unit of a **Pandorinellina** sp., indicating an Early or Middle Devonian age. The spore assemblage is much more abundant and diverse. McGregor (personal communication, September 1982) provided the following floral list: cf. **Archaeozonotriletes varius** Nadler, ?**Convolutispora** sp., **Dibolisporites echinaceus** (Eisenack) Richardson, cf. **Dictyotriletes emsiensis** (Allen) McGregor, **Punctatisporites** sp., **Retusotriletes antiquus** Naumova ex Kedo, **R. rotundus** (Streel) Streel, and **Verruciretusispora dubia** (Eisenack) Richardson and Rasul. This assemblage includes several undescribed species which distinguish it from other known assemblages. It is approximately dated as middle Emsian.

Zelolasma apsidiferum occurs low in the apparent range of **Polygnathus dehiscens** in the area, which is from some level high in the Eids Formation to 141 m above the base of the Blue Fiord Formation (Uyeno and Klapper, 1980, p. 83). Our interpretation of the occurrence of probable Zlichovian brachiopods and spores (middle Emsian is roughly equivalent to late Zlichovian) below the apparent range of **Polygnathus dehiscens,** is that this range is significantly less than the full range of the taxon. That is, it is a teilzone. Nevertheless, we recognize that although **Zelolasma apsidiferum** is probably Zlichovian, it must be very early Zlichovian, because possibly as much as 600 m of overlying Eids and Blue Fiord strata are also of Zlichovian age (Table 8.1 and Figures 8.2, 3 of Uyeno and Klapper, 1980).

Systematic Paleontology

Family COLUMNARIIDAE Nicholson, 1879

Subfamily TROPIDOPHYLLINAE Pedder, 1983

Genus **Zelolasma** Pedder, 1964

Zelolasma Pedder, 1964, p. 364, 365.

Type species. **Diphyphyllum gemmiforme** Etheridge, 1902, p. 253-255, Pl. 37, fig. 1; Pl. 39, figs. 1, 2; Pl. 40, fig. 1. "Cave Limestone-Middle Devonian"; holotype from Taemas Bridge road, north bank of Murrumbidgee River, Parish of Warroo, County Murray, New South Wales, Australia (Hill, 1940b, p. 259). The type stratum is now assigned to the Cavan Limestone, and is either late Pragian or early Zlichovian. Pedder (in Pedder et al., 1970, p. 232-234, Pl. 44, figs. 1, 3, 6; Pl. 46, fig. 17, text-fig. 10) has monographed the species with a full synonymy, and new illustrations of typical examples of it have been published by Hill (1981, Fig. 180, 1a, b).

Diagnosis. Fasciculate genus of tropidophyllinid corals.

Description. Corallum fasciculate, locally subcerioid or weakly catenoid. Increase marginarial, multiple and parricidal in type species, single and nonparricidal in others.

Corallite walls thin. Septa radially arranged. Major septa withdrawn from the axis, so that they are only a little longer than the minor septa. Peripheral ends of septa smooth and straight or only slightly sinuous. Inner parts of the septa are more sinuous, and may be distinctly undulant and carinate. Adaxial terminations of the septa are commonly spinose. Spiniform septal fragments are present in the tabularium. At certain levels, septa become dilated and generally somewhat fusiform. Carination increases at these levels. Trabeculae are finely monacanthate and typically slightly divergent.

Dissepimentarium narrow, consisting of one to mostly not more than a few rows of dissepiments. Despite being narrow, the dissepimentarium is commonly exsert in mature corallites. The shape of the dissepiments is variable, many are either rhomboid or arched, but none is a true horseshoe dissepiment. Tabulae are broad and some are quite complete. They form essentially flat tabularial surfaces.

Assigned species. **Diphyphyllum gemmiforme** Etheridge (1902); **Cylindrophyllum planivesiculosum** Chernyshev (1941); **Zelolasma apsidiferum** sp. n.; ?**Zelolasma cystosa** (an apparent nomen nudum listed by Qin and Gan, 1976).

Distribution. Pragian **Farabophyllum intermedium** Zone of the upper Turkparida Suite, Magian River Basin, Tadzhikistan (Lavrusevich, 1971, p. 85-87, Pl. 4, figs. 1a-v). Late Pragian or early Zlichovian **Polygnathus dehiscens** Zone of the Cavan Limestone, Yass Shelf, New South Wales (type occurrence). Late Pragian or early Zlichovian **Polygnathus dehiscens** Zone of the upper Garra Beds, Molong High, New South Wales (Hill, 1942, p. 183; part of Pl. 6, fig. 6; Strusz, 1965, p. 534, 535, Pl. 72, fig. 7; text-fig. 5). Early Zlichovian part of the **Polygnathus dehiscens** Zone of the upper Eids Formation of southwestern Ellesmere Island (this paper). Dalejan Nganasanskie Beds of central Taymyr (Chernyshev, 1941, p. 11, 12, 53, Pl. 1, figs. 4, 5; Kravtsov in Besprozvannykh et al., 1975, p. 60, Pl. 13, figs. 2a, b).

Reports of the genus in the late Lochkovian Pettsevskiy (Peetz) Horizon of the Salair (Elkin et al., 1982, p. 67, 68), and in the Dalejan or Eifelian Lure Formation near Diebu, Gansu Province (Qin and Gan, 1976, listed on Figure 5), are unsupported by either illustrations or descriptions.

Remarks. The genus has been put into synonymy with **Acinophyllum** McLaren (1959, p. 22, 23) by Birenheide (1978, p. 87), and questionably into **Disphyllum** de Fromentel (1861, p. 302, 303) by Ivanovskiy (1976, p. 187). The six known species of **Acinophyllum** are all from the Eastern Americas Realm and have been studied in detail by Oliver (1976, p. 53-68, Pls. 8-29). They differ from species of **Zelolasma** in having flanged carinae and consistently inwardly inclined dissepimentarial surfaces, and their tabularia lack spiniform septal fragments. An acceptable interpretation of **Disphyllum** has been given by Hill (1981, p. 264-266). **Disphyllum** differs from **Zelolasma** in lacking spiniform septal fragments and in having less undulant and carinate septa and longer major septa. Its dissepimentaria are rarely everted as those of **Zelolasma** are.

Since the inception of the genus **Zelolasma**, several species and forms have been transferred from other genera to it, with varying degrees of certainty. Of these corals, only **Cylindrophyllum planivesiculosum** Chernyshev is retained in **Zelolasma**, sensu stricto.

Disphyllum praecox Hill (1940a, p. 398, 399, Pl. 11, figs. 15-17) from the Silverdale Formation (Ludlow age), near Yass, New South Wales, was questionably assigned to **Zelolasma** by Pedder (1964, p. 365) and by McLean (1976, p. 188, 189). A specimen of a somewhat similar form, from the Upper Silurian on Yamashla River, west slope of the southern Urals, which was described and figured by Soshkina (1937, p. 63, 64, Pl. 17, figs. 1, 2) as **Acervularia luxurians** var. **breviseptata** Weissermel, and refigured by Ivanovskiy and Shurygina (1975, Pl. 13, figs. 4a, b) as **Acervularia** ?sp., was considered to be a species of **Zelolasma** by Lavrusevich (1971, p. 85), and to be a possible member of the genus by McLean (1976, p. 188). Both of these forms are, indeed, similar to **Zelolasma**, sensu stricto, but lack signs of any spiniform septal fragments in their tabularia.

Thamnophyllum abrogatum Hill (1940b, p. 260, 261, Pl. 10, figs. 4a, b) from the Cavan Limestone (Late Pragian or early Zlichovian), in the Taemas region of New South Wales, was referred to **Zelolasma** by Pedder (1964, p. 365; in Pedder et al., 1970, p. 234). This assignment, however, is not satisfactory, because of the strongly dilated septa, coarse monacanths and small presepiments that are present in the coral. It would seem that a new genus is required for **Thamnophyllum abrogatum**, but the available material of the species is limited – at present, only two specimens are known to us.

Thamnophyllum curtum Hill (1940b, p. 261, 262, Pl. 10, figs. 5a, b), from the Zlichovian part of the Taemas Limestone of the Taemas and Wee Jasper areas of New South Wales, has also been placed in **Zelolasma** by Pedder, at first without qualification (Pedder, 1964, p. 365) and later with doubt (in Pedder et al., 1970, p. 234, 235). This and the form identified as a new species of **Zelolasma** by Pedder (1964, p. 365), and as cf. **Zelolasma** sp. by Philip and Pedder (1968, p. 1034), from a level now known to be Dalejan, in the Mount Frome Limestone, near Mudgee, New South Wales, are here considered more likely to be members of the subfamily Spongonariinae than of the subfamily Tropidophyllinae.

Similarities between **Zelolasma gemmiforme** and **Hexagonaria mayendorfi** Le Maître (1952, p. 59, 60, Pl. 5, figs. 1-3), from the "Emsien inférieur" (?Zlichovian), between Beni Abbès and Kerzaz is southern Algeria, were noted by Pedder (1964, p. 365). They are probably responsible for Hill's (1981, p. 280) record of the possible occurrence of **Zelolasma** in the Lower Devonian of Algeria. However, the Algerian species is entirely cerioid, and exterior calicular views, shown in Figure 1 of Le Maître's Plate 5, indicate that it has long major septa.

Schlueteria verrucosa Soshkina (1952, p. 100, Pl. 40, fig. 138, text-fig. 118), from the Voronezh, Evlanova and Liven Horizons (all Frasnian) of the Russian Platform, was removed to **Zelolasma** by Spasskiy (1977, p. 63). We agree with Rozkowska and Fedorowski's (1972, p. 291) decision to place it in the genus **Disphyllum.**

Spasskiy (1977, p. 63) also removed **Schlueteria lyskovensis** Ermakova (1957, p. 163-165, Pl. 2, fig. 2; Pl. 2 [two plates numbered 2], figs. 3-5; Pl. 3, figs. 1, 2), from subsurface beds of the upper Voronezh Horizon (Frasnian) of the Russian Platform, to **Zelolasma.** Illustrations of the internal morphology of the holotype of this species have not been published, but good thin sections of a paratype show that at least part of the type series should be assigned to the genus **Peneckiella.**

A coral, of probable Ludlow age, from the Mirrabooka Formation of the Cheesemans Creek region, in east central New South Wales, was listed as **Disphyllum** cf. **praecox** Hill by Sherwin (1971, p. 215) and subsequently referred questionably to **Zelolasma** by McLean (1982, p. 20). Through the kindness of L. Sherwin, Pedder has been able to examine this coral. It has a narrow, discontinuous and inwardly sloping dissepimentarium and long thin major septa, and is not **Zelolasma**, as the genus is interpreted in this paper.

Zelolasma apsidiferum sp. n.

Plate 22.1, Figures 1-7

Type series. Holotype, GSC 71260; paratype GSC 71261. Both from 30.9 to 34.9 m below top of the Eids Formation; early Zlichovian part of the **Polygnathus dehiscens** Zone. Southwestern Ellesmere Island, recessive beds above first bluff, near the convergence of two small creeks, 20.5 km west of the head of Sor Fiord; 77°18'N latitude, 85°17'W longitude. Collected by Gary P. Smith, August 1978 (Field no. DA27).

Diagnosis. Dendroid species of **Zelolasma** with marginarial nonparricidal increase. Adult corallites have a mean diameter of 5.0 to 6.5 mm, and 17x2 or 18x2 septa.

Description. Corallum irregularly shaped, dendroid, with the tendency for groups of three or four corallites to be attached to each other and aligned like links in a chain. Corallites attain a maximum mean diameter of 5.0 to 6.5 mm. Their direction of growth changes every centimetre, or so, with the result that long, longitudinal thin sections are difficult to obtain. Increase is marginarial and nonparricidal; normally only one offset is produced at a time. The type material is embedded in matrix, transverse sections suggest that septal furrows and interseptal ridges are variable.

The outer corallite wall is continuous and mostly 0.06 to 0.1 mm thick (total observed range 0.03 to 0.13 mm). It normally embeds the septal bases, but, in places, is continuous with them. Arrangement of the septa is radial. Minor septa just project from the dissepimentarium; major septa are only slightly longer than the minor septa, and normally extend only about one half of the distance to the axis. The full septal count of 17x2 or 18x2 is acquired as the corallite diameter enlarges from about 3.3 to 3.5 mm. Most of the septa are thin and only slightly undulant; some are more strongly undulant; a few, particularly at levels where the septa are dilated, bear zig-zag carinae. Adaxial ends of the septa may be slightly spinose. Short, spiniform septal fragments are present in parts of the tabularia. Typically, they are confined to an intertabularial space and do not penetrate the overlying tabula. Trabeculae are fine monacanths that are only slightly divergent.

In early stages, the narrow dissepimentarium is inwardly inclined and comprises a single row of small globose dissepiments. In later stages, the dissepimentarium increases only a little in width, but develops everted dissepimentarial surfaces. In the mature dissepimentarium many of the dissepiments are rhomboid, or almost symmetrically arched and additional vessicles may be added on either side of the high point of the dissepimentarium. An internal wall, typically 0.05 to 0.15 mm thick and formed by sclerenchymal thickening of the inner surface of the dissepimentarium, is present in many corallites. Tabular are broad, many are complete. Tabularial surfaces are mostly flat or slightly concave, a few are sloping or slightly convex.

Remarks. Compared with the new species, **Zelolasma planivesiculosa** (Chernyshev) is larger (adult corallite diameter 6 to 8 mm), has more numerous (19 x 2 or 20 x 2) and more strongly differentiated septa (major septa almost twice as long as minor septa), and has tabularial surfaces that tend to be broadly convex, rather than flat or concave.

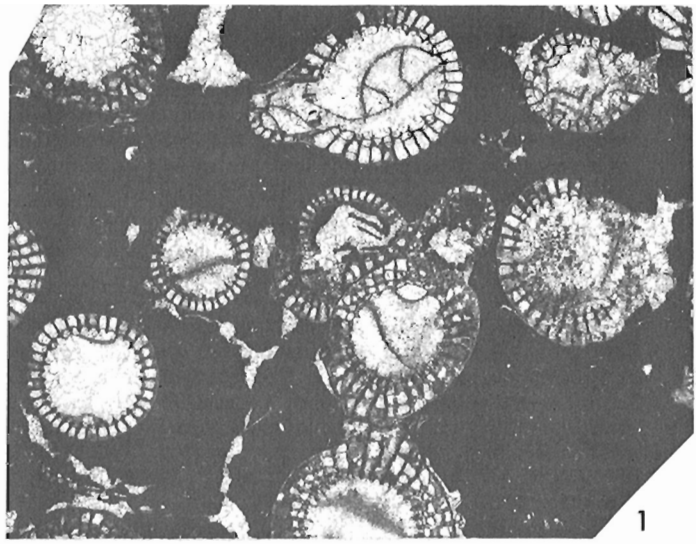

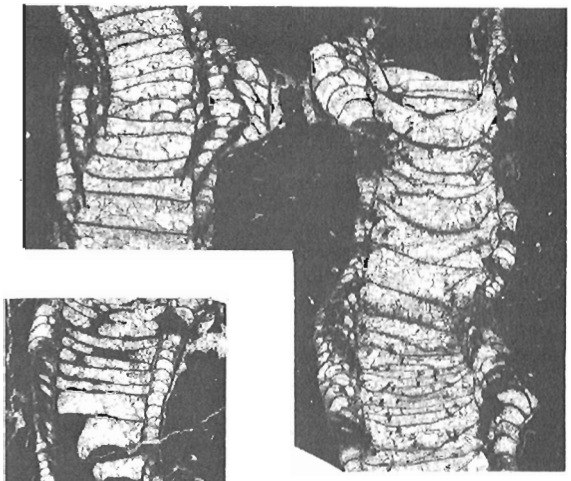

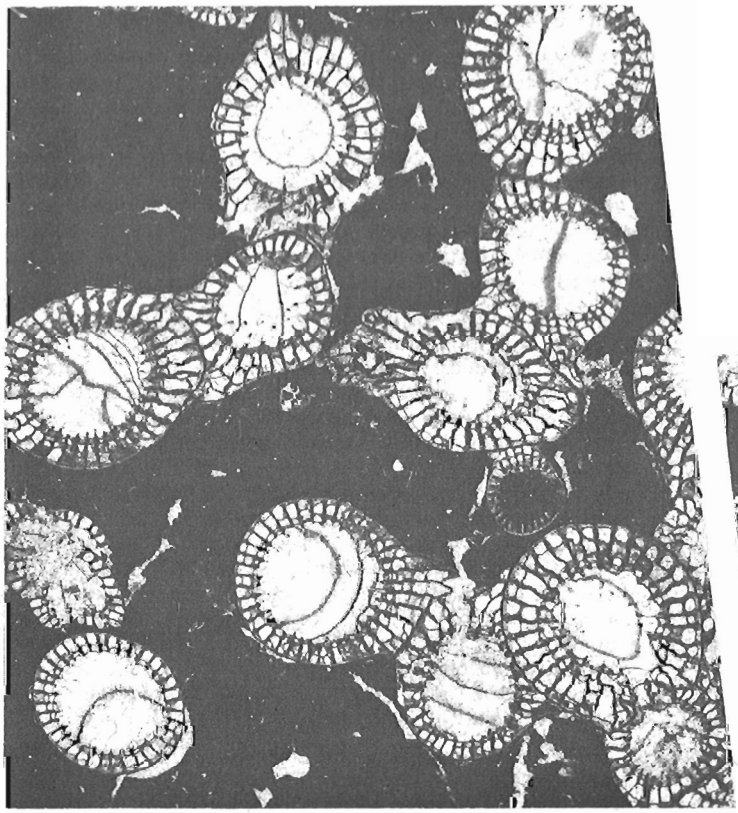

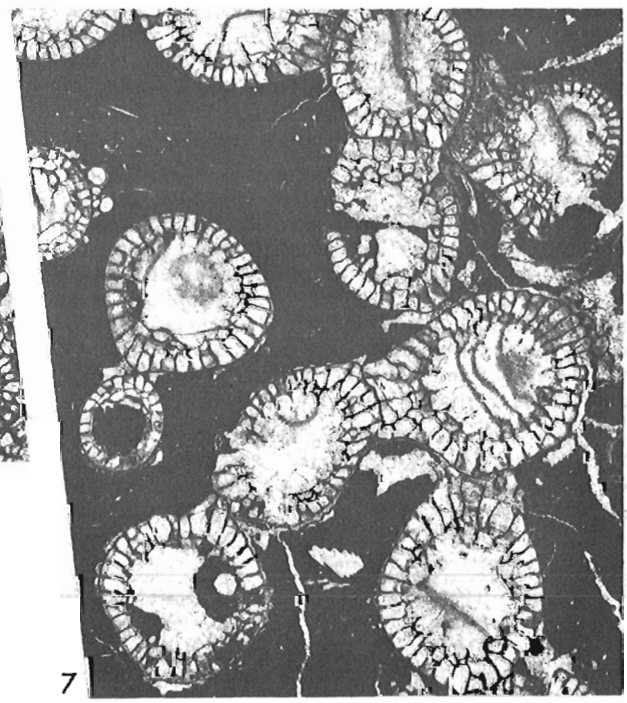

Plate 22.1

Figures 1-7. **Zelolasma apsidiferum** sp. n.
Holotype, GSC 71260
1, 6, 7. Transverse thin sections, X4.
2-5. Longitudinal thin sections, X4.

Zelolasma gemmiforme (Etheridge) is not likely to be confused with the new species. Its corallites are larger with diameters of as much as 15 mm, and have as many as 26 x 2 septa. Its septa are more carinate, and the mode of increase in **Z. gemmiforme** is multiple and parricidal, whereas in **Z. apsidiferum** it is neither multiple nor parricidal.

The trivial name of the new species is Latin, **apsis, -idis**, meaning arch, and the suffix **fer, -a, -um**, meaning to bear or carry. It refers to the arch-like dissepiments of the species.

References

Besprozvannykh, N.I., Dubatolov, V.N., Kravtsov, A.G., Latypov, Yu. Ya., and Spasskiy, N.Ya.
1975: Devonskie rugozy Taymyro-Kolymskoy provinstii; Akademiya Nauk SSSR, Sibirskoe Otdelenie, Instituta Geologii i Geofiziki, Trudy, vyp 228, 172 p.

Birenheide, R.
1978: Leitfossilien. No. 2. Rugose Korallen des Devon; Gebruder Borntraeger, Berlin, Stuttgart, vi+265 p.

Chernyshev, B.B.
1941: Siluriyskie i nizhnedevonskie korally basseyna reki Tarei (yugo-zapadnyy Taymyr); in Paleontologiya Sovetskoy Arktiki, vyp. 5, ed. D.V. Nalivkin; Arkticheskogo Nauchno-Issledovatel'skogo Instituta, Trudy, tom 158, p. 9-64.

Elkin (Yolkin), E.A., Gratsianova, R.T., Zheltonogova, V.A., and Kim, A.I.
1982: Osnovnye biostratigraficheskie rubezhi i podrazdeleniya nizhnego i srednego devona na zapade Altae-Sayanskoy oblasti i ikh korrelyatsiya; in Biostratigrafiya pogranichnykh otlozheniy nizhnego i srednego devona. Trudy polevoy sessii Mezhdunarodnoy podkomissii po stratigrafii devona. Samarkand, 1978, ed. B.S. Sokolov and M.A. Rzhonsnitskaya; Vsesoyuznyy Nauchno-Issledovatel'skiy Geologicheskiy Institut (VSEGEI), Leningrad, p. 65-80.

Embry, A.F. and Klovan, J.E.
1971: A Late Devonian reef tract on northeastern Banks Island, N.W.T.; Bulletin of Canadian Petroleum Geology, v. 19, no. 4, p. 730-781.

1972: Absolute water depth limits of Late Devonian paleoecological zones; Geologische Rundschau, Band 61, Heft 2, p. 672-686.

Ermakova, K.A.
1957: Novye vidy devonskikh korallov rugoza iz tsentral'nykh oblastey Russkoy platformy; in Voprosy stratigrafii, fatsiy i fauny paleozoya Russkoy platformy i kaynozoya severnogo Kavkaza, ed. E.K. Shutsky; Vsesoyuznyy Nauchno-Issledovatel'skiy Geologo-Razvedochnyy Neftyanoy Institut (VNIGNI), Trudy, vyp. 8, p. 160-191.

Etheridge, R., Jr.
1902: Additions to the Middle Devonian and Carboniferous corals in the Australian Museum; The Australian Museum, Records, v. 4, no. 7, p. 253-262.

Fromentel, E. de
1861: Introduction à l'étude des polypiers fossiles; F. Savy, Paris, 357 p.

Hill, D.
1940a: The Silurian Rugosa of the Yass-Bowning district, N.S.W.; The Linnean Society of New South Wales, Proceedings, v. 65, pts. 3, 4, p. 388-420.

Hill, D. (cont.)
1940b: The Lower Middle Devonian rugose corals of the Murrumbidgee and Goodradigbee Rivers, N.S.W.; The Royal Society of New South Wales, Journal and Proceedings, v. 74, pt. 3, p. 247-276.

1942: Middle Palaeozoic rugose corals from the Wellington district, N.S.W.; The Royal Society of New South Wales, Journal and Proceedings, v. 76, pt. 3, p. 182-189.

1981: Treatise on invertebrate paleontology. Part F. Coelenterata. Supplement 1. Rugosa and Tabulata, ed. Curt Teichert; The Geological Society of America and the University of Kansas Press, Boulder and Lawrence, v. 1, p. i-xl, 1-378, v. 2, p. i, ii, 379-762.

Ivanovskiy, A.B.
1976: Ukazatel' rodov rugoz; Akademiya Nauk SSSR, Sibirskoe Otdelenie, Instituta Geologii i Geofiziki, Trudy, vyp 217, 256 p.

Ivanovskiy, A.B. and Shurygina, M.V.
1975: Reviziya rugoz Urala; Akademiya Nauk SSSR, Sibirskoe Otdelenie, Instituta Geologii i Geofiziki, Trudy, vyp 218, 68 p.

Jones, B. and Smith, G.P.
1980: Lower Devonian brachiopods from the Eids Formation, southwest Ellesmere Island, Arctic Canada; Journal of Paleontology, v. 54, no. 4, p. 675-695.

Lavrusevich, A.I.
1971: Rannedevonskie rugozy Zeravshano-Gissara; in Novye Dannye po Geologii Tadzhikistana, vyp. 1, ed. V.V. Loskutov; Tadzhikskiy Gosudarstvennyy Universitet im V.I. Lenina, Dushanbe, p. 75-133.

Le Maître, D.
1952: La faune du Dévonien inférieur et moyen de la Saoura et des abords de l'Erg el Djemel (Sud-Oranais); Matériaux pour la carte géologique de l'Algérie, série 1, Paléontologie, no. 12, 171 p.

Mayr, U., Uyeno, T.T., and Barnes, C.R.
1978: Subsurface stratigraphy, conodont zonation, and organic metamorphism of the Lower Paleozoic succession, Bjorne Peninsula, Ellesmere Island, District of Franklin; in Current Research, Part A, Geological Survey of Canada, Paper 78-1A, p. 393-398.

McLaren, D.J.
1959: A revision of the Devonian coral genus **Synaptophyllum** Simpson; Geological Survey of Canada, Bulletin 48, p. 15-33.

1963: Southwestern Ellesmere Island between Goose Fiord and Bjorne Peninsula; in Y.O. Fortier et al., Geology of the north-central part of the Arctic Archipelago, Northwest Territories (Operation Franklin); Geological Survey of Canada, Memoir 320, p. 310-338.

McLean, R.A.
1976: Aspects of the Silurian rugose coral fauna of the Yass region, New South Wales; The Linnean Society of New South Wales, Proceedings, v. 100, pt. 3, p. 179-194.

1982: Rugose corals; in The Silurian System in New South Wales, ed. J.W. Pickett; Geological Survey of New South Wales, Bulletin 29, p. 20, 21.

Oliver, W.A., Jr.
1976: Noncystimorph colonial rugose corals of the Onesquethaw and Lower Cazenovia Stages (Lower and Middle Devonian) in New York and adjacent areas; United States Geological Survey, Professional Paper 869, 156 p.

Pedder, A.E.H.
1964: Two new genera of Devonian tetracorals from Australia; The Linnean Society of New South Wales, Proceedings, v. 88, pt. 3, p. 364-367.

Pedder, A.E.H., Jackson, J.H., and Philip, G.M.
1970: Lower Devonian biostratigraphy in the Wee Jasper region of New South Wales; Journal of Paleontology, v. 44, no. 2, p. 206-251.

Philip G.M. and Pedder, A.E.H.
1968: Stratigraphical correlation of the principal Devonian limestone sequences of eastern Australia; in International Symposium on the Devonian System. Calgary, 1967, ed. D.H. Oswald; Alberta Society of Petroleum Geologists, Calgary, v. 2, p. 1025-1041.

Qin, Feng and Gan Yiyan
1976: The Palaeozoic stratigraphy of western Qin Ling Range (Chinese with English abstract); Acta Geologica Sinica 1976, no. 1, p. 74-97.

Różkowska, M. and Fedorowski, J.
1972: Genus **Disphyllum** de Fromentel (Rugosa) in the Devonian of Poland and its distribution; Acta Palaeontologica Polonica, v. 17, no. 3, p. 265-340.

Sherwin, L.
1971: Stratigraphy of the Cheesemans Creek district, New South Wales; The Geological Survey of New South Wales, Records, v. 13, pt. 4, p. 199-237.

Soshkina, E.D.
1937: Korally verkhnego silura i nizhnego devona vostochnogo i zapadnogo sklonov Urala; Akademiya Nauk SSSR i Vsesoyuznyy Institut Mineral'nogo Syr'ya Nktp, Paleozoologicheskogo Instituta, Trudy, tom 6, vyp. 4, 155 p.

1952: Opredelitel' devonskikh chetyrekhluchevykh korallov; Akademiya Nauk SSSR, Paleontologicheskogo Instituta, Trudy, tom 39, 127 p.

Spasskiy, N.Ya.
1977: Devonskie Rugozy SSSR (sistematika, stratigraficheskoe i geograficheskoe znachenie); Izdatel'stvo Leningradskogo Universiteta, Leningrad, 344 p.

Strusz, D.L.
1965: Disphyllidae and Phacellophyllidae from the Devonian Garra Formation of New South Wales; Palaeontology, v. 8, pt. 3, p. 518-571.

Trettin, H.P.
1978: Devonian stratigraphy, west-central Ellesmere Island, Arctic Archipelago; Geological Survey of Canada, Bulletin 302, 119 p.

Uyeno, T.T. and Klapper, G.
1980: Summary of conodont biostratigraphy of the Blue Fiord and Bird Fiord formations (Lower-Middle Devonian) at the type and adjacent areas, southwestern Ellesmere Island, Canadian Arctic Archipelago; in Current Research, Part C, Geological Survey of Canada, Paper 80-1C, p. 81-93.

23. *STEUSLOFFINA CUNEATA* (STEUSLOFF), 1895, FROM ANTICOSTI ISLAND, QUEBEC

Project 720072

M.J. Copeland
Institute of Sedimentary and Petroleum Geology, Ottawa

*Copeland, M.J., **Steusloffina cuneata** (Steusloff), 1895, from Anticosti Island, Quebec; in Current Research, Part B, Geological Survey of Canada, Paper 83-1B, p. 201-204, 1983.*

Abstract

***Steusloffina cuneata** (Steusloff), 1895, an ostracode species previously recorded from Ordovician rocks of the circum-Baltic region, is reported for the first time from strata at Cape Henry, Anticosti Island, Quebec. Although several ostracode genera from this general stratigraphic interval show intercontinental relationships between northern Europe and Anticosti Island, this is the first specifically similar ostracode common to both regions.*

Résumé

***Steusloffina cuneata** (Steusloff), 1895, espèce d'ostracode déjà décrite dans les roches ordoviciennes de la région péribaltique, a été identifiée pour la première fois dans les couches situées au cap Henri dans l'île d'Anticosti (Québec). Bien que plusieurs genres d'ostracodes de cet intervalle stratigraphique général établissent qu'il existe une relation entre l'Europe du Nord et l'île d'Anticosti, il s'agit ici néanmoins du premier ostracode commun aux deux régions.*

Introduction

Species of the genus **Steusloffina** occur throughout the Baltic region of Europe (Sarv, 1960; Netskaya, 1966; Schallreuter, 1968; Sarv, 1968; Hessland and Adamczak, 1974; Põlma, Sarv and Hints, 1977; Siveter, 1982; etc), the eastern Canadian Arctic (Teichert, 1937a,b; Copeland, 1977), the southwestern District of Mackenzie, Canada (Copeland, 1974), east-central Alaska (Berdan, personal communication, 1983), and eastern New York, U.S.A. (Ruedemann, 1901; Berdan, personal communication, 1983). They are generally of early Middle to late Late Ordovician age, although a questionable steusloffinid species has been reported from strata as young as late Llandovery in Estonia (Netskaya, 1966).

The type species, **Steusloffina ulrichi** Teichert, 1937, based on an incomplete carapace from Melville Peninsula, District of Franklin, is of late Middle Ordovician age. This species is also recorded from strata of similar age at Silliman's Fossil Mount, Baffin Island (Copleland, 1977) and, as **Aechmina acuminata** Teichert, 1937, may occur in Washington Land, North Greenland (Teichert, 1937b). Hessland (in Hessland and Adamczak, 1974) also reported an undated specimen of **Steusloffina** from Ellesmere Island in the Warthin collection, Poughkeepsie, New York. **S. cuneata** (Steusloff), morphologically very similar to **S. ulrichi** but having greater L/R valve overlap, has previously been known to occur only in Upper Ordovician strata of the Baltic region (for synonymy see Schallreuter, 1968, p. 138). Other previously described steusloffinid species are less similar to **S. ulrichi.**

Stratigraphy

Recently, several well preserved carapaces of **Steusloffina cuneata** (Steusloff) were recovered from a sample (GSC loc. 62156) of weathered shale about 6 m above biohermal beds at Cape Henry, on the west side of Ellis Bay, Anticosti Island, Quebec (Copeland, 1981, Fig. 5). The question arises as to the Late Ordovician or Early Silurian age of these strata (Fig. 23.1). Some workers consider strata above the bioherms to be Silurian (e.g. McCracken and Barnes, 1981), whereas others are of the opinion that at least several metres (up to 15?) of Ordovician rock (much of member 6 of the Ellis Bay Formation, as interpreted by Bolton, 1972) are present in this interval. For a full discussion of this problem refer to various papers in Lespérance (1981).

The collection under consideration comes from within the **Euprimitia gamachei** subzone of the **Jonesites semilunatus** zone (Copeland, 1973). Ostracodes occurring with **Steusloffina cuneata** in this collection are generalized 'bythocyprids' of no particular stratigraphic importance. There are, moreover, no tetradellids or beyrichiids, so that the exact age of the collection is in doubt (Copeland, 1981). Elswhere on Anticosti Island strata in this interval bear **Euprimitia gamachei** Copeland and **Schmidtella** sp. (Nowlan, 1982).

All previous workers have considered **Steusloffina cuneata** (Steusloff) to be of Late Ordovician age (Siveter, 1982, p. 122, Table 1). Most specimens were recovered from drift boulders (Geschiebe) throughout the Baltic region, but Sarv (1960), Pranskevicius (1972), and Siveter (1982) have recorded this species from Fla to F2 (Nabala, Vorms, Pirgu and Porkuni stages) of Estonia, Fla to Flc of Latvia (Ul'st, Gailite and Yakovleva, 1982), and the Fla and Flb Stages in the Berzini borehole of southwestern Latvia (Põlma, Sarv and Hints, 1977). Henningsmoen (1954, p. 76) recorded **S. cuneata** from Etage 5b (Upper **Dalmanitina** Series) of the Oslo region of Norway. These occurrences are generally associated with the **Amorphognathus ordovicicus** conodont zone. A species of **Tetradella** (an ostracode genus restricted on Anticosti Island to the Ordovician) occurs with **S. cuneata** throughout its range in Estonia. Also, **Foramenella,** another tetradellid genus present in Ordovician strata of Anticosti Island, occurs with **S. cuneata** throughout much of the Flc Stage of Estonia. Species of these tetradellid genera occur in members 1 to 5 of the Ellis Bay Formation (terminology of Bolton, 1972) and are of Gamachian (post Richmond-Late Ordovician) age.

From the literature it is not possible to determine accurately the youngest occurrence of **S. cuneata** in the Baltic region. Most authors only indicate that it occurs there in one or more stage(s) of the Late Ordovician. Siveter (1982) commented that the Ordovician-Silurian boundary may be more precisely defined on the basis of ostracodes in North America than in northern Europe. This leaves us with the following possibilities: a) **S. cuneata** may have been one of the few ostracode species that survived the Ordovician-Silurian glacio-eustatic regime (at least in North America); b) the Ordovician-Silurian systemic boundary in northern Europe, if less well defined than in North America, may overlap the youngest occurrence of **S. cuneata;** c) the conodont zone of **Oulodus? nathani** on Anticosti Island may

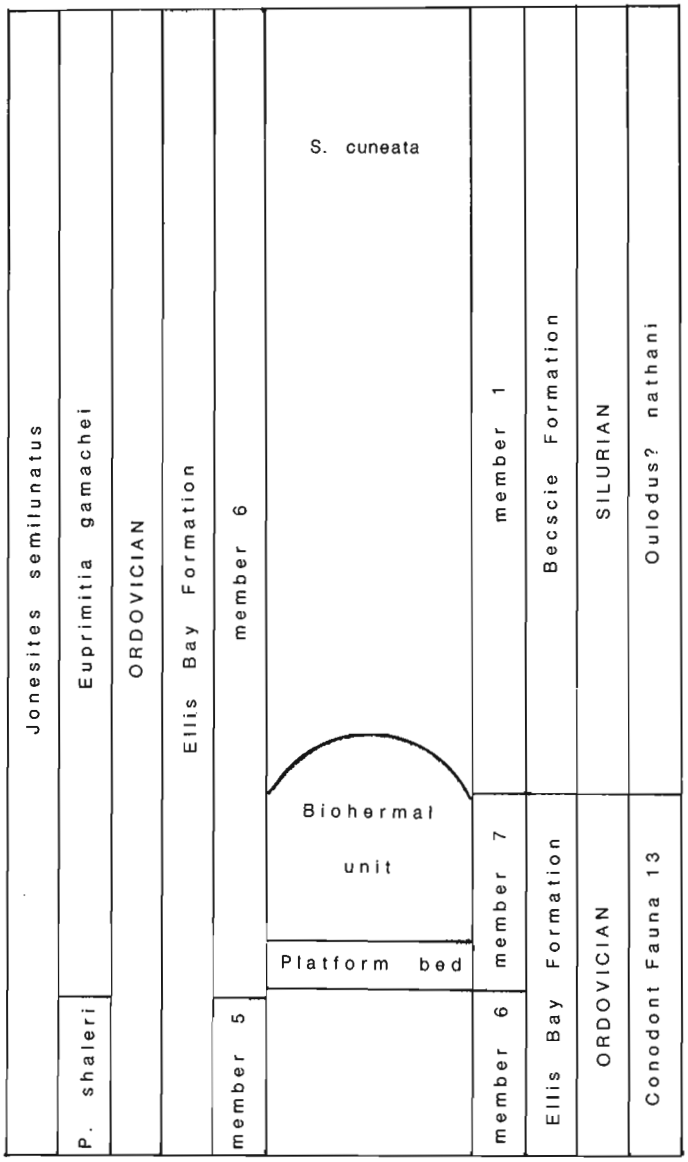

Figure 23.1. *Terminology used for about 11 m of strata in the vicinity of the biohermal unit at Cape Henry, Anticosti Island, Quebec, showing the relative position of the collection containing* ***Steusloffina cuneata*** *(Steusloff) about 6 m above the biohermal unit. Zonation and terminology on the left follow Bolton (1972) and Copeland (1973), those on the right follow McCracken and Barnes (1981) and Barnes, Petryk and Bolton (1981).*

be, in part, latest Ordovician. Evidence from other phyla (i.e. brachiopods and graptolites) occurring in this interval on Anticosti Island may clarify this problem.

Paleontology

Hessland and Adamczak (1974) presented a detailed discussion of the morphology of **S. cuneata.** They concluded that the genus **Steusloffina** belonged within the Order Podocopida and, possibly, the Suborder Metacopa. This taxonomy is followed here. The lectotype of **S. cuneata** was figured by Schallreuter (1968, Fig. 12).

Genus **Steusloffina** Teichert, 1937
Type Species **Steusloffina ulrichi** Teichert, 1937
Steusloffina cuneata (Steusloff), 1895
Figure 23.2

Description: Strongly preplete. Dorsal margin long, epicline, slightly arched near mid length, caused by low median dorsal swelling. Anterdorsal corner somewhat angular, may be produced into a short, blunt acroidal projection on immature specimens; posterodorsal corner actue, narrowly rounded. Anterior margin broadly rounded, meeting dorsal margin at about 100 degrees.

Lateral surface with strong, slightly posteriorly inclined spine near mid height of valve and 3/5 greatest length of valve from anterior margin. Discrete, randomly oriented papillae present, especially in posterior and ventral portions of valve.

Left valve overreaches right valve at anterodorsal and posterodorsal corners and overlaps right valve around entire free margin, particularly in the mid ventral region where the left valve forms a "bow-shaped projection". Median dorsal swelling of left valve slightly higher than that of right valve above the sunken hinge.

Measurements of 9 carapaces (in mm):

GSC type number	L.	H.	W. (Excluding lateral spines)	Figure
Hypotype 73015	1.15	0.6	0.55	23.2-1
Hypotype 73016	1.1	0.65	0.6	23.2-2
Hypotype 73017	1.0	0.55	0.45	23.2-3
Hypotype 73018	1.1	0.5	0.5	23.2-4
Hypotype 73019	1.2	0.65	0.6	23.2-5
Hypotype 73020	1.1	0.6	0.6	23.2-6
Hypotype 73021	1.2	0.6	0.6	23.2-7
Hypotype 73022	1.15	0.6	0.6	23.2-8
Hypotype 73023	1.2	0.6	0.6	unfigured

Number of specimens studied. 15.

Types. Hypotypes, GSC 73015-73023.
Occurrence. Cape Henry, Anticosti Island, Quebec (GSC loc. 62156), about 6 m above the biohermal unit near the base of member 6, Ellis Bay Formation (stratigraphy following Bolton, 1972).

Remarks. **S. cuneata** has a strongly preplete outline and a lateral spine on each valve supposedly typical of other species of the genus. It differs from other **Steusloffina** species in having more pronounced L/R overlap, especially anteriorly, and a broader "bow-shaped projection". Specimens of **S. cuneata** figured by several authors (e.g. Hessland and Adamczak, 1974) appear to lack evidence of lateral spines. J.M. Berdan (personal communication, 1983) reported that specimens of **Steusloffina** from Alaska and New York State also lack lateral spines. One carapace of **S. cuneata** from Anticosti Island (now destroyed) was sectioned longitudinally through both spine bases. The carapace wall was complete beneath the hollow spine without any apparent connection between the spine and the interior of the carapace. Thus, loss of the spine would not result in perforation of the domicilium. The spines, therefore, may have served protective, balancing, and/or buoyancy functions. Also, from the number of specimens reported to occur without spines or indication of spine bases, it is possible that, if the spine broke off in an early instar, it might not have been regenerated in subsequent instars. Throughout successive moults the circular impression of the spine base might have been progessively eliminated until, by maturity, all evidence of the attachment area of the spine could have been obliterated.

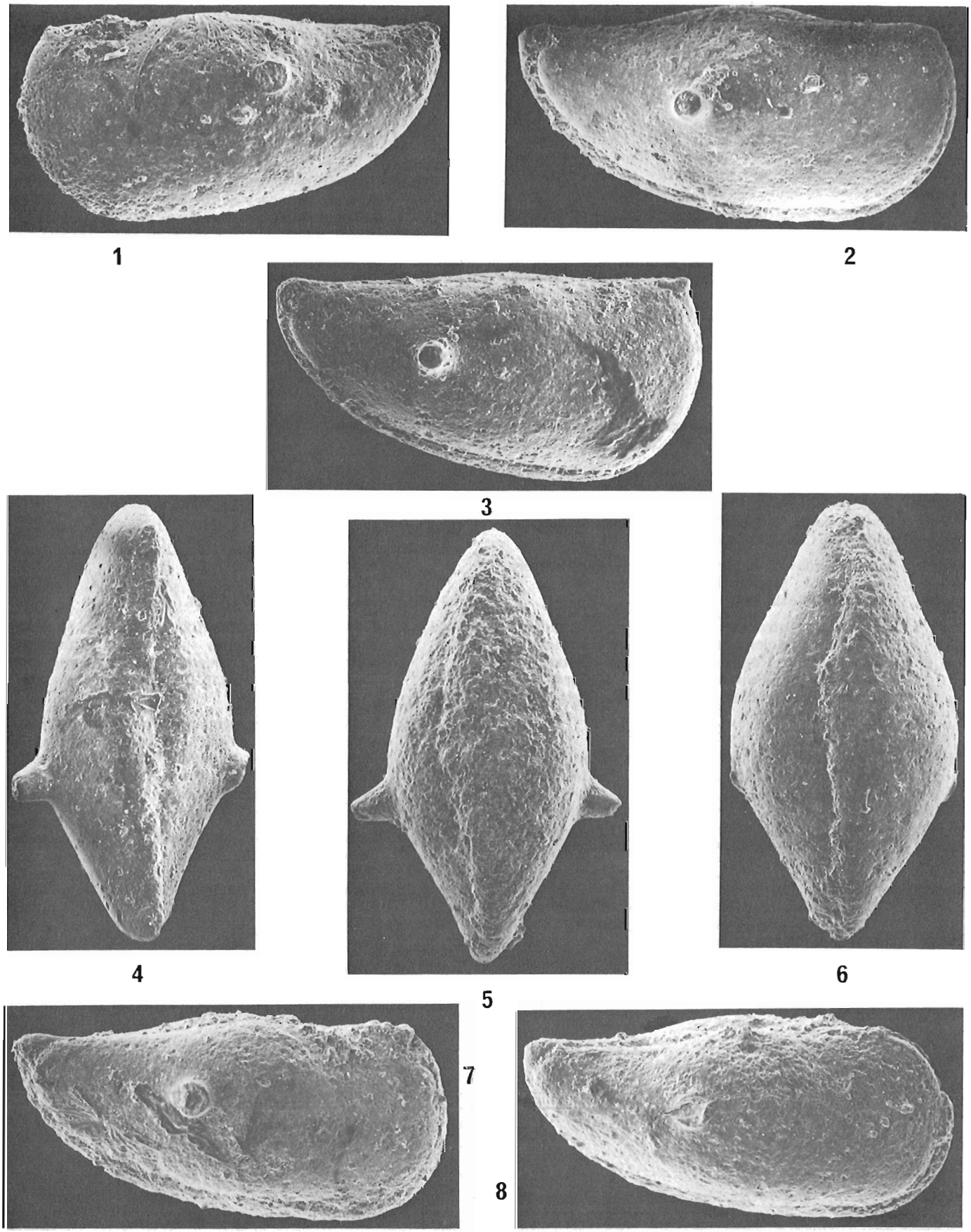

1. *Left lateral view, carapace, X68, hypotype, GSC 73015.*
2. *Right lateral view, carapace, X75, hypotype, GSC 73016.*
3. *Right lateral view, carapace, X79, hypotype, GSC 73017.*
4. *Dorsal view, carapace, X75, hypotype GSC 73018.*
5. *Ventral view, carapace, X69, hypotype, GSC 73019.*
6. *Ventral view, carapace, X76, hypotype, GSC 73020.*
7. *Right lateral view, carapace, X67, GSC 73021.*
8. *Right lateral view, carapace, X70, GSC 73022.*

Figure 23.2. ***Steusloffina cuneata*** *(Steusloff), 1895 Cape Henry, Anticosti Island, Quebec, about 6 m above the biohermal unit of the Ellis Bay Formation.*

This may be shown by the prominent lateral spines on immature specimens of **S. cuneata** illustrated by Schallreuter (1968, Fig. 13). Most specimens of **S. cuneata** from Anticosti Island appear to be adults that have retained the spines, broken at varying lengths from the carapace wall (either naturally or broken during preparation of the sample). Whether the spines on the Anticosti Island specimens were more robust than those on specimens from the Baltic area, or the individuals existed in a lower energy environment and thus were less prone to spine beakage, is conjectural.

References

Barnes, C.R., Petryk, A.A., and Bolton, T.E.
1981: Anticosti Island, Québec; in Field Meeting, Anticosti – Gaspé, Québec, 1981, Lespérance, P.J., ed.; IUGS Subcommission on Silurian stratigraphy, Ordovician-Silurian Boundary Working Group; v. I – Guidebook, p. 1-24.

Bolton, T.E.
1972: Geological map and notes on the Ordovician and Silurian litho- and biostratigraphy, Anticosti Island, Québec; Geological Survey of Canada, Paper 71-19.

Copeland, M.J.
1973: Ostracoda from the Ellis Bay Formation (Ordovician), Anticosti Island, Quebec; Geological Survey of Canada, Paper 72-43.

1974: Middle Ordovician Ostracoda from southwestern District of Mackenzie; Geological Survey of Canada, Bulletin 244.

1977: Ordovician Ostracoda, Southeastern District of Franklin; in Geology of Ordovician rocks, Melville Peninsula and Region, Southeastern District of Franklin, Bolton, T.E., Sanford, B.V., Copeland, M.J., Barnes, C.R. and Rigby, J.K.; Geological Survey of Canada, Bulletin 269, p. 77-97.

1981: Latest Ordovician and Silurian ostracode faunas from Anticosti Island, Québec; in Field Meeting, Anticosti – Gaspé, Québec, 1981, Lespérance, P.J., ed.; IUGS Subcommission on Silurian stratigraphy, Ordovician-Silurian Boundary Working Group; v. II – Stratigraphy and Paleontology, p. 185-195.

Henningsmoen, G.
1954: Upper Ordovician ostracods from the Oslo Region, Norway; Norsk Geologisk Tidsskrift, v. 22, no. 1-2, p. 69-108.

Hessland, I. and Adamczak, F.
1974: On the taxonomic position of **Steusloffina** Teichert (Ostracoda); Geoscience and Man, v. VI, p. 59-64.

Lespérance, P.J. (editor)
1981: Field meeting, Anticosti – Gaspé, Québec, 1981: v. I – Guidebook; v. II – Stratigraphy and Paleontology; IUGS Subcommission on Silurian Stratigraphy, Ordovician-Silurian Boundary Working Group; Département de Géologie, Université de Montréal.

McCracken, A.D. and Barnes, C.R.
1981: Conodont biostratigraphy across the Ordovician-Silurian boundary, Ellis Bay Formation, Anticosti Island, Québec; Field Meeting, Anticosti-Gaspé, Québec, 1981, Lespérance, P.J., ed; IUGS Subcommission on Silurian Stratigraphy, Ordovician-Silurian Boundary Working Group; v. II – Stratigraphy and Paleontology, p. 61-69.

Netskaya, A.I.
1966: Ostracodes of the Ordovician and Silurian deposits of the USSR (Families Schmidtellidae, Rectellidae, Longisculidae, and some new species of other families); Transactions of the All-Union Scientific Research Institute for Oil and Geological Prospecting (VNIGRI), v. 251.

Nowlan, G.S.
1982: Conodonts and the position of the Ordovician-Silurian boundary at the eastern end of Anticosti Island, Québec, Canada; Canadian Journal of Earth Sciences, v. 19, no. 6, p. 1332-1335.

Põlma, L., Sarv, L., and Hints, L.
1977: The subdivision of the Ordovician in the Berzini boring (Southeast Latvia); Eesti Nsv Teaduste Akadeemia, Toimetised, Keemia, v. 26, no. 2, p. 113-121.

Pranskevičius, A.
1972: South Baltic Silurian Ostracoda; Department of Geology under the Council of Ministers of Lithuanian SSR, Lithuanian Scientific-Research Geological Survey Institute, Transactions, v. 15.

Ruedemann, R.
1901: Trenton conglomerate of Rysedorph Hill Rensselaer Co. N.Y. and its fauna; New York State Museum, Bulletin 49, p. 3-114.

Sarv, L.
1960: On the stratigraphic distribution of ostracods in the Ordovician of the Estonian S.S.R.; Ensv Teaduste Akadeemia Geoloogia Instituudi Uurimused V, p. 237-244.

1968: Development of Ordovician ostracodes of the East Baltic; Proceedings of the International Paleontological Union, XXIII International Geological Congress, p. 203-210.

Schallreuter, R.
1968: Ordovizische Ostracoden mit geradem Schlossrand und konkavem Ventralrand; Wissenschaftliche Zeitschrift der Ernst Moritz-Arndt-Universitat Greifswald, Jahrgang XVII, 1968; Mathematisch-naturwissenschaftliche Reihe NR. 1/2, p. 127-152.

Siveter, D.J.
1982: Late Ordovician and Early Silurian ostracodes from the Oslo Region, Norway; in IUGS Subcommission on Silurian Stratigraphy, Field Meeting, Oslo Region 1982, Worsley, D., ed.; Paleontological Contributions from the University of Oslo, no. 278, p. 121-128.

Teichert, C.
1937a: Ordovician and Silurian faunas from Arctic Canada; Museum de Minéralogie et de Géologie de l'Université de Copenhague, Communications Paléontologiques, no. 59.

1937b: A new Ordovician fauna from Washington Land, North Greenland; Meddelelser om Grønland; Kommissionen for Videnskabelige Undersøgelser i Grønland, v. 119, no. 1.

Ul'st, R.Zh., Gailite, L.K., and Yakovleva, V.I.
1982: Ordovician of Latvia; Ministry of Gas Industries of USSR; All Union Scientific Research Institute of Marine Geology and Geophysics, 294 p.

24.

STRATIGRAPHIC SUBDIVISION OF THE HEIBERG FORMATION, EASTERN AND CENTRAL SVERDRUP BASIN, ARCTIC ISLANDS

Project 750083

Ashton F. Embry
Institute of Sedimentary and Petroleum Geology, Calgary

Embry, A.F., Stratigraphic subdivision of the Heiberg Formation, eastern and central Sverdrup Basin, Arctic Islands; in Current Research, Part B, Geological Survey of Canada, Paper 83-1B, p. 205-213, 1983.

Abstract

The Heiberg Formation, an Upper Triassic-Lower Jurassic sandstone-dominant unit in the Sverdrup Basin, is divided into three members, named in ascending order, Romulus, Fosheim, and Remus. The Romulus Member consists of interbedded sandstone, siltstone and shale with the lithologies arranged in coarsening-upward cycles of delta front origin. The Fosheim Member consists mainly of fine- to medium-grained sandstone with thin interbeds of carbonaceous siltstone, shale and coal. The member contains both fining-upward and thin, coarsening-upward cycles and is of delta plain origin. The Remus Member consists almost entirely of very fine- to medium-grained sandstone of beach and nearshore marine origin. The Romulus and Fosheim members represent the progradation of a major deltaic complex into the Sverdrup Basin in the Norian to Sinemurian, followed by delta destruction and transgression in the Pliensbachian and Toarcian (Remus Member).

Résumé

La formation de Heiberg dans le bassin de Sverdrup date de la période s'étendant du Trias supérieur au Jurassique inférieur et est dominée par des grès; on la divise en trois niveaux, notamment en ordre ascendant: Romulus, Fosheim et Remus. Le niveau de Romulus se compose de grès, de pélite et de schiste argileux interstratifiés, disposés en cycles où les matériaux deviennent grossiers vers le haut; il résulte d'une mise en place en milieu de front deltaïque. Le niveau de Fosheim comprend surtout des grès à grains fins à moyens avec de minces couches interstratifiées de pélite carbonatée, de schiste argileux et de charbon. Il contient des cycles de matériaux qui deviennent fins vers le haut ainsi que des cycles étroits où les grains deviennent grossiers vers le haut; dans ce cas, la mise en place a eu lieu dans une plaine deltaïque. Le niveau de Remus se compose presque entièrement de grès à grains dont la dimension varie de très fine à moyenne provenant d'un milieu de plage ou de littoral marin. Les niveaux de Romulus et de Fosheim représentent la progradation d'un important réseau deltaïque vers le bassin de Sverdrup, du Norien au Sinémurien, suivie par la destruction du delta et la transgression durant le Pliensbachien et le Toarcien (niveau de Remus).

Introduction

The stratigraphic framework for the Mesozoic succession in the Sverdrup Basin of arctic Canada was established by Heywood (1957), Tozer (1956, 1961, 1963a, 1963b), Souther (1963), Greiner (1963) and Tozer and Thorsteinsson (1964) from reconnaissance field studies done in the 1950's and was summarized by Tozer (1970). Following that reconnaissance over one hundred wells have penetrated Mesozoic strata in the Sverdrup Basin and more detailed stratigraphic and sedimentologic studies of surface exposures have been done by scientists of the Geological Survey of Canada (e.g. Balkwill, in press). The wealth of new surface and subsurface data has led to a revision of the stratigraphic nomenclature system, so that recently recognized stratigraphic relationships of the Mesozoic succession can be adequately described.

Numerous new stratigraphic units, both formations and members, have been delineated from both surface and subsurface studies. Many of these units have direct applicability to petroleum exploration in the Sverdrup Basin because they are established, or potential, reservoir, source or seal strata. In the interest of making these new units available for stratigraphic and petroleum related studies as quickly as possible, a series of short papers will be published in "Current Research" in 1983 and 1984, which will name and describe the new Mesozoic units in an expanded lexicon style. An appendix giving the tops of the units in selected wells will accompany each paper, so that regional correlation of the units will be understood.

This paper and a companion paper (Embry, 1983) describe the new stratigraphic units proposed for the Heiberg Formation/Group, a sandstone-dominant interval of Late Triassic and Early Jurassic age which contains significant oil and gas reserves. The regional stratigraphy, sedimentology and petroleum geology of the Heiberg Formation/Group have been described by Embry (1982) and the new stratigraphic units used in that analysis are formally defined in this paper and in Embry (1983).

Heiberg Formation

Previous Work

The Heiberg Formation was defined by Souther (1963) from studies completed during Operation Franklin in 1955. He established a type section at the southwestern end of Buchanan Lake on east-central Axel Heiberg Island where the formation is 1422 m thick. At that locality the sandstone-dominant Heiberg lies between two shale-siltstone units, the Blaa Mountain Formation below, and the Savik Formation above. Souther (1963) recognized two informal members in the type Heiberg Formation. The lower member consists of interbedded very fine- to fine-grained sandstone, siltstone and shale with ripple crosslamination and burrows common throughout. The upper member also consists of interbedded sandstone, siltstone and shale but is distinguished from the lower member by thicker and coarser grained sandstone units, a higher content of carbonaceous material in the shales and siltstones, the occurrence of thin coal seams, and the relative scarcity of burrows.

During Operation Franklin the Heiberg Formation was also examined by Tozer (1963b, c) on southwestern Ellesmere Island and west-central Axel Heiberg Island; by Glenister (1963) on southeastern Axel Heiberg Island; by McLaren (1963) on northern Cornwall Island; and by Greiner (1963) on central Cornwall Island.

Subsequent to Operation Franklin, Tozer (1961, 1963a) examined the Heiberg Formation on Ellesmere and Axel Heiberg islands and found that the uppermost 50 to 100 m of the formation consists of massive sandstone, characterized by thin, ferruginous layers which occasionally contain burrows and marine fossils. Tozer (1963a) assigned these strata to the Borden Island Formation, a Lower Jurassic ferruginous sandstone unit first recognized on Borden Island on the western edge of the Sverdrup Basin. Tozer (1963a) assumed that the Borden Island Formation of Ellesmere and Axel Heiberg islands was also of Early Jurassic (Sinemurian) age and rested unconformably on the Upper Triassic Heiberg sandstones.

Fricker (1963) described the Heiberg Formation in the Strand Fiord area of west-central Axel Heiberg Island. He noted that the formation was divisible into two members, similar to those described by Souther (1963) for the type section.

Nassichuk and Christie (1969) studied the Heiberg Formation in the vicinity of the head of Tanquary Fiord on northern Ellesmere Island. They mapped two informal members throughout the area. The lower member consists of interbedded sandstone, siltstone and shale with all lithologies containing abundant carbonaceous material. The upper member consists almost entirely of massive sandstone.

Balkwill (in press) describes the outcropping Heiberg Formation of Cornwall and Amund Ringnes islands and also includes descriptions of two subsurface sections (Amund Central Dome H-40, Linckens Island P-46). On Cornwall Island Balkwill (in press) divided the Heiberg Formation into two informal members. The lower member, which conformably overlies the Blaa Mountain Formation, consists of interbedded sandstone, siltstone and shale, commonly arranged in coarsening-upward cycles. The upper member consists of massive to crossbedded, fine- to coarse-grained sandstone with only thin, widely spaced intervals of carbonaceous siltstone, shale and coal. On eastern Cornwall Island pebbly and glauconitic sandstones, which contain Toarcian ammonites, overlie the Heiberg and were assigned by Balkwill (in press) to the Jaeger Formation (member B). On western Cornwall Island similar strata overlie the Heiberg but, in that area, Pliensbachian fossils occur in the strata. Because of this, these strata were assigned to the Borden Island Formation by Balkwill (in press). Stratigraphically higher ferruginous sandstones, which contain Toarcian ammonites, were assigned to the Jaeger Formation. The first shale unit overlying this essentially continuous succession of sandstone (which includes the Heiberg, Borden Island, and lower portion of the Jaeger Formation), was placed in the Jaeger Formation (member C).

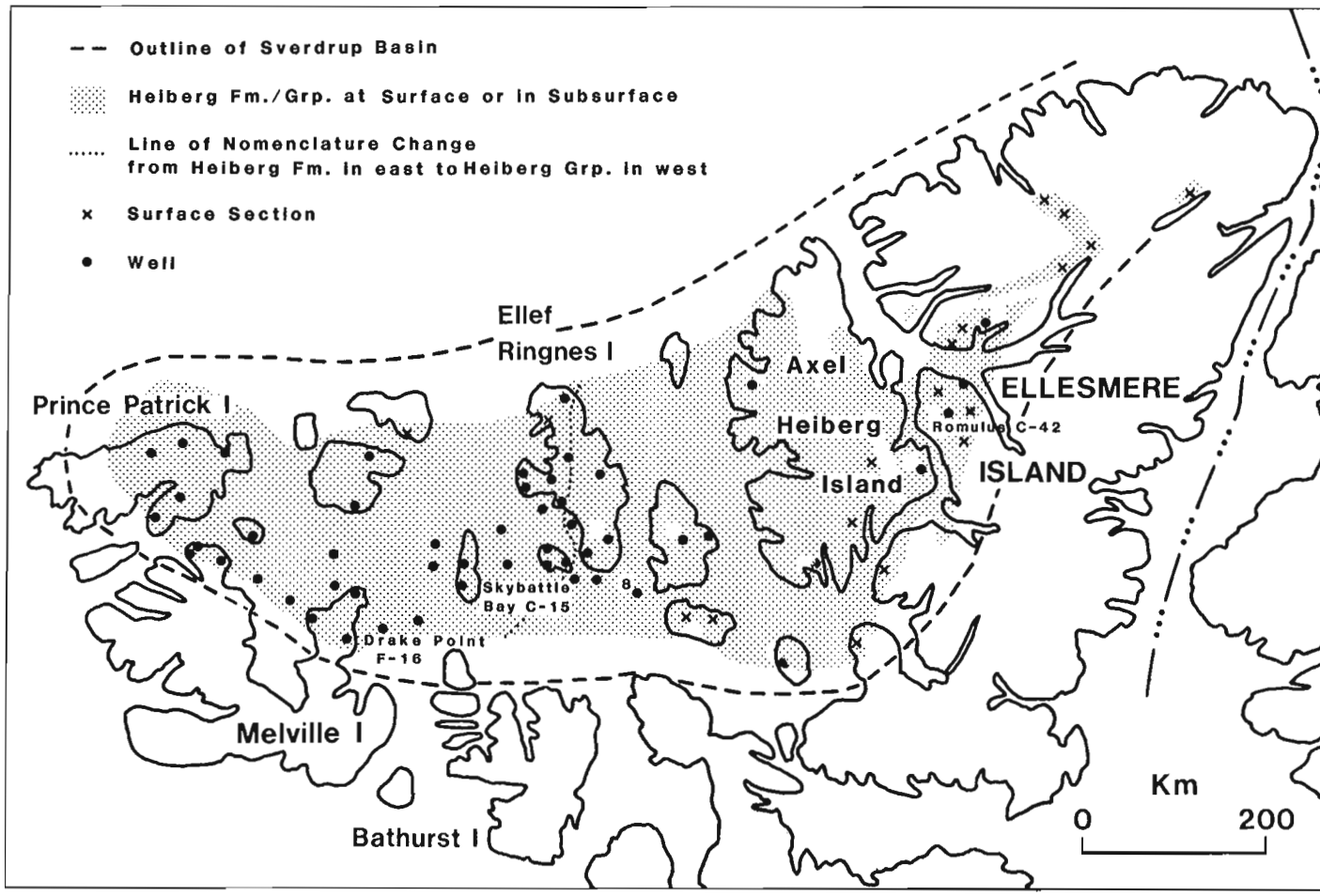

Figure 24.1. *Distribution of Heiberg Formation/Group and control points. Key to numbered wells listed in appendix: 1. Romulus C-42, 2. Neil 0-15, 3. May Point H-02, 4. Graham C-52, 5. Sherwood P-37, 6. Mid Fiord J-53, 7. Amund Central Dome H-40, 8. Linckens Island P-46, 9. Hoodoo Dome H-37.*

To the north, on Amund Ringnes Island, for both the surface and subsurface sections, Balkwill (in press) recognized a lower Heiberg Formation and an upper Heiberg Formation-Borden Island Formation (undivided). These strata are overlain by shale and siltstone of the Savik Formation. Balkwill (in press) includes a comprehensive discussion on the problem of objectively differentiating a Borden Island Formation from the Heiberg Formation in the eastern and central Sverdrup Basin. He suggests that the nomenclatural system be revised following a basin wide stratigraphic and sedimentologic study.

Present Work

I have recently completed a regional study of the Upper Triassic/Lower Jurassic stratigraphic interval in the Sverdrup Basin (Embry, 1982) and, following Balkwill's suggestion, I have revised the stratigraphic nomenclature for the interval. Souther's (1963) original definition of the Heiberg Formation (sandstone-dominant unit between two shale-siltstone units) has been applied to all of the available surface and subsurface sections (Fig. 24.1). This has provided a consistent and objective determination of the Heiberg Formation over the entire area and it circumvents the problem discussed by Balkwill (in press) of differentiating a Borden Island Formation from the Heiberg Formation.

The shale-siltstone units which bound the Heiberg Formation have been renamed. The underlying shale is referred to the Barrow Formation (Embry, 1982) and the overlying shale-siltstone unit is placed in the Jameson Bay Formation (Embry, 1982). The contact of the Heiberg with the Barrow is placed at the base of the first sandstone unit which is at least 4 m thick and above which sandstone units are common. The upper contact of the Heiberg Formation is placed at the top of the highest sandstone unit, above which shale and siltstone are the dominant lithologies.

Figure 24.1 illustrates the extent of the Heiberg Formation and the available surface and subsurface control. In the western Sverdrup Basin the Heiberg has been given group status and five formations are recognized (Embry, 1982, 1983). The line of nomenclature change (Fig. 24.1) follows the eastern limit of two mappable shale-siltstone units which allow a five-fold subdivision of the Heiberg in the west.

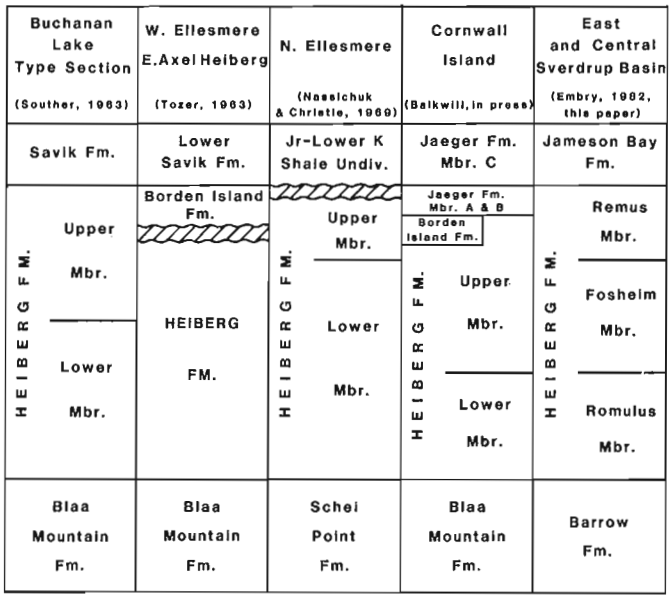

Figure 24.2. *Heiberg Formation nomenclature, past and present.*

In the eastern and central Sverdrup Basin, where the Heiberg has formation status, three new members are now delineated in the formation. Each of the members consists of a distinctive suite of lithologies which is recognizable in both surface and subsurface sections. The three new members are, in ascending order: Romulus, Fosheim, and Remus. They are formally defined herein. The type sections for these three new stratigraphic units are in the Panarctic Romulus C-42 well on Fosheim Peninsula, west-central Ellesmere Island (Fig. 24.1) at 79°51'05"N, and 84°22'42"W.

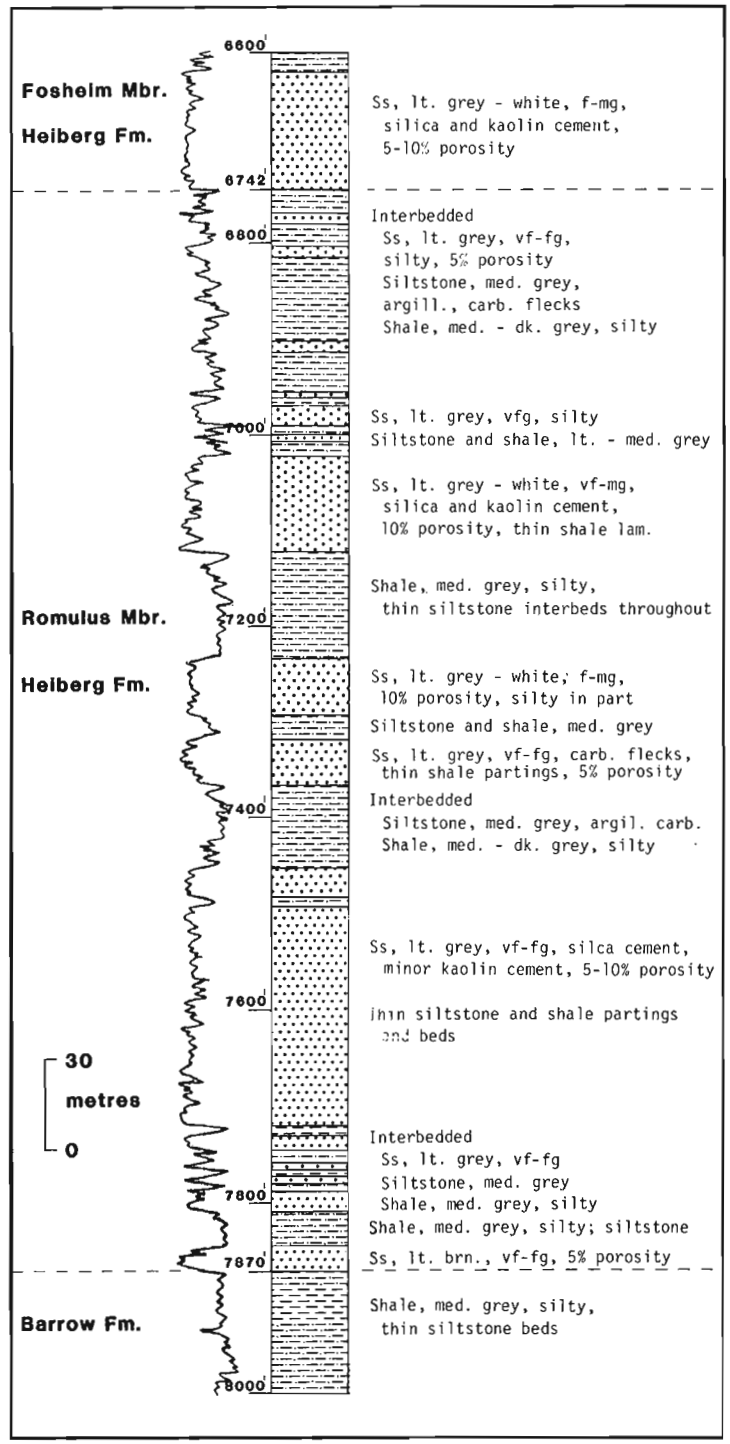

Figure 24.3. *Lithology and gamma ray curve of type section of Romulus Member, Romulus C-42 well.*

The Romulus C-42 well was spudded on January 28, 1972 and was abandoned on July 25, 1972 at a total depth of 4554 m. The elevation of the K.B. is 160 m.

Subsurface type sections were chosen because chip samples (3 m intervals) from the Romulus C-42 well are available for study at the Institute of Sedimentary and Petroleum Geology in Calgary, Alberta. Subsurface type sections are, therefore, far more accessible to interested geologists than are remote surface sections in the Arctic Islands.

Figure 24.2 illustrates the present nomenclature for the Heiberg Formation in the eastern and central Sverdrup Basin and compares it with the nomenclature used by previous workers.

Romulus Member

Definition

The Romulus Member of the Heiberg Formation consists of interbedded, very fine- to fine-grained sandstone, siltstone and shale. The type section is in the Romumuls C-42 well, between 2055.5 m (6742 ft) and 2400 m (7870 ft), and the member is 344.5 m thick (Fig. 24.3). The member is named after Romulus Lake which lies 13 km west of the Panarctic Romulus C-42 well site.

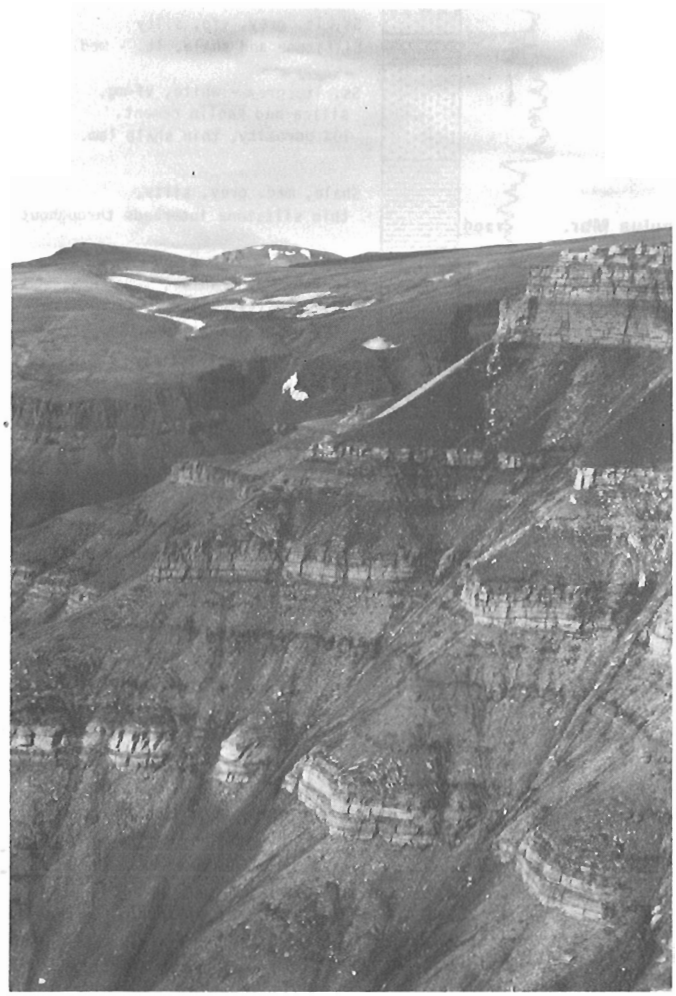

Figure 24.4. *Interbedded sandstone, siltstone and shale of Romulus Member, Raanes Peninsula, Ellesmere Island. Contact with Fosheim Member at base of sandstone in upper right.*

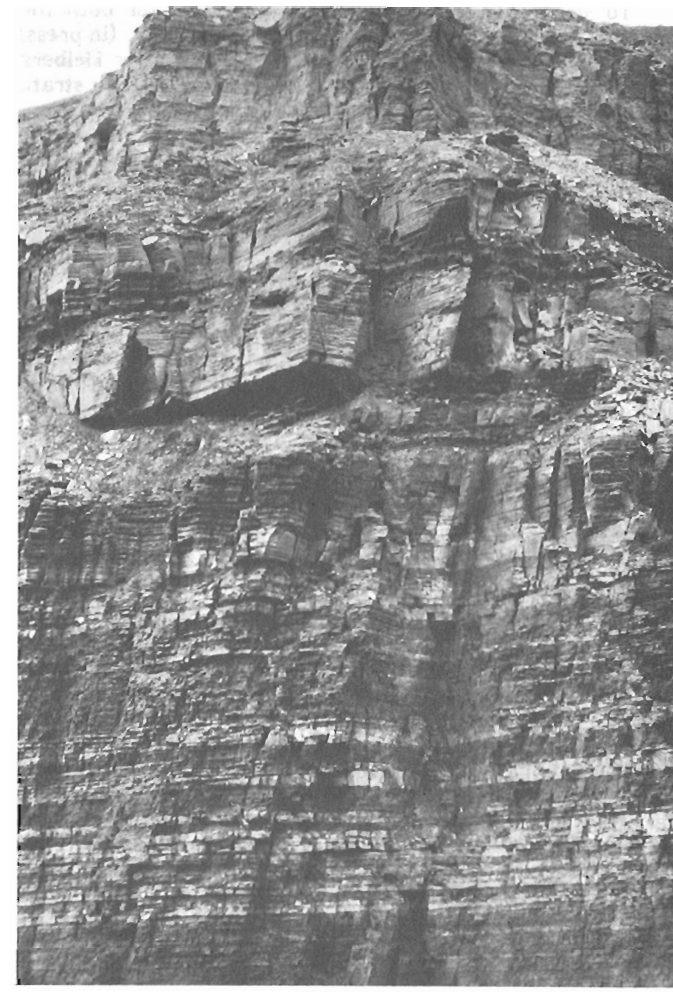

Figure 24.5. *Interbedded shale, siltstone and sandstone overlain by sandstone unit, Romulus Member, Raanes Peninsula, Ellesmere Island.*

Synonyms

1. Lower portions of lower member of Heiberg Formation of Souther (1963).
2. Lower member of Heiberg Formation of McLaren (1963) and Balkwill (in press).
3. Basal portion of lower member of Heiberg Formation of Nassichuk and Christie (1969).

Boundaries

The contact of the Romulus Member with the underlying Barrow Formation is placed at the base of the first thick sandstone unit (>4 m) above which sandstone is relatively common. The upper contact with the Fosheim Member of the Heiberg Formation is placed at the base of the sandstone unit above which carbonaceous siltstone, shale and coal are common and argillaceous intervals seldom exceed 10 m in thickness. Both contacts are conformable.

Lithology

The Romulus Member consists of interbedded sandstone, siltstone and shale with the lithologies commonly arranged in coarsening-upward cycles between 5 and 50 m thick (Fig. 24.4, 24.5). Shales and siltstones are light to medium grey and commonly exhibit parallel lamination.

Ripple crosslamination and burrows occur in siltstone beds. Thin, pelecypod coquinas are present within some thick shale units. The argillaceous intervals vary in thickness from 5 to 100 m.

Sandstone units are up to 60 m thick and consist mainly of very fine- to fine-grained quartzose sandstone. The most common sedimentary structures are ripple crosslamination and burrows. Thin shale laminations and flasers occur throughout the sandstone units and many individual sandstone beds have sharp, basal contacts. The flasers consist of red, silty shale and are one of the most characteristic features of the member.

In most areas sandstone is the predominant lithology and comprises between 60 and 80 per cent of the member. However, in the southwestern Ellesmere – southern Axel Heiberg area, shale and siltstone dominate the member and sandstone units are thinner and more widely spaced.

Distribution and Thickness

The Romulus Member has the same areal extent as the Heiberg Formation (Fig. 24.1) and varies in thickness from 50 m on the basin margin to 400 m in the basin centre.

Age

Macrofossils are rare within the Romulus Member but have been reported from southwest Ellesmere Island (Tozer, 1961), Wolf Fiord, southeastern Axel Heiberg Island (Glenister, 1963), and Cornwall Island (McLaren, 1963; Balkwill, in press). In all cases a Norian (Late Triassic) age was indicated for the member. Palynological study also indicates a Norian age for the member over its extent (unpublished GSC paleontological reports).

Environment of Deposition

The lithologies, fossil content, cyclicity, and stratigraphic relationships of the Romulus Member are all compatible with a delta front origin for the member (Balkwill, in press; Embry, 1982).

Fosheim Member

Definition

The Fosheim Member of the Heiberg Formation is a sandstone-dominant unit which contains thin interbeds of carbonaceous shale, siltstone and coal. The type section for the member is in the Panarctic Romulus C-42 well, between 1535 m (5034 ft) and 2055.5 m (6742 ft), and it is 520.5 m thick (Fig. 24.6). The name is taken from Fosheim Peninsula where the Romulus C-42 well is located.

Synonyms

1. Upper portion of lower member and most of upper member of type Heiberg Formation (Souther, 1963).
2. Upper member of Heiberg Formation of McLaren (1963) and Balkwill (in press).
3. Lower member of Heiberg Formation of Nassichuk and Christie (1969) with the exception of the basal portion.

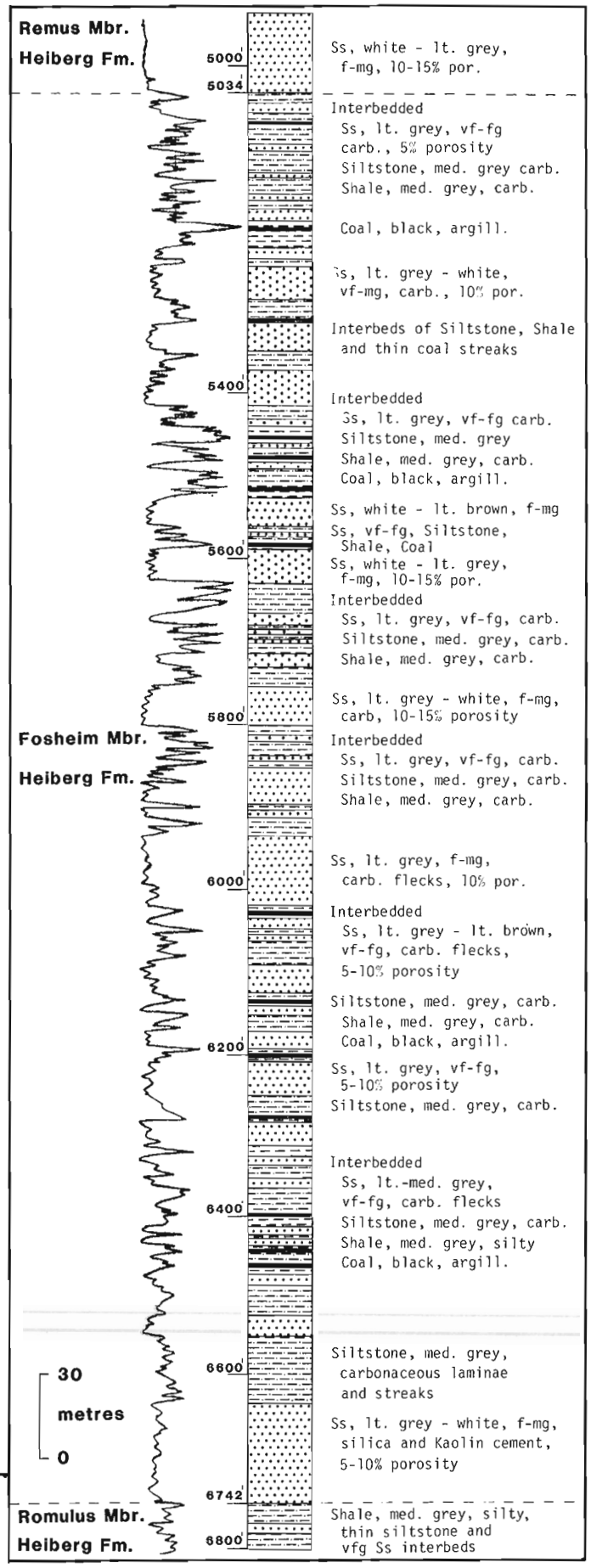

Figure 24.6. *Lithology and gamma ray curve of type section of Fosheim Member, Romulus C-42 well.*

Boundaries

The contact of the Fosheim Member with the underlying Romulus Member is placed at the base of the first sandstone unit above which carbonaceous shale and siltstone and coal are relatively common. The upper contact of the Fosheim Member with the Remus Member is placed at the top of the highest carbonaceous shale and siltstone unit, above which sandstone is nearly continuous to the top of the Heiberg Formation.

Lithology

The Fosheim Member consists mainly of fine- to medium-grained, quartzose sandstone, with thin interbeds of carbonaceous shale, siltstone and coal. In the Cornwall-Ringnes islands area of the central Sverdrup Basin, sandstone commonly comprises over 90 per cent of the member. To the east, on Axel Heiberg and western Ellesmere, sandstone content is usually between 60 and 90 per cent.

In central Sverdrup Basin, sandstone occurs in units up to 100 m thick. The sandstone is fine- to medium-grained, but contains chert pebbles and conglomerate bands along the southern basin margin. Carbonaceous material is very common and is concentrated along bedding planes. In outcrop, the sandstone usually appears to be massive, but trough and planar crossbeds are sometimes discernable with sets up to 3 m thick. Units of dark grey, carbonaceous shale and siltstone with thin coal seams occur throughout the member. These units seldom exceed 5 m in thickness and many are widely spaced.

In the eastern Sverdrup Basin, where shale and siltstone are more common, the Fosheim Member has a characteristic striped appearance in outcrop (Fig. 24.7). Both fining-upward and coarsening-upward cycles are common within the member. Fining-upward cycles are up to 15 m thick. They consist of a basal scour surface, fine- to medium-grained, crossbedded sandstone in the lower portion; very fine grained, horizontally bedded and ripple crosslaminated sandstone in the middle; and carbonaceous shale and siltstone, with parallel lamination and root markings, in the upper portion.

The coarsening-upward cycles range in thickness from 2 to 10 m. The cycles display an upward gradation from carbonaceous, silty shale at the base, through siltstone in the middle, to ripple crosslaminated and massive sandstone at the top (Fig. 24.8). The upper portion of the sandstone commonly contains root markings and/or burrows.

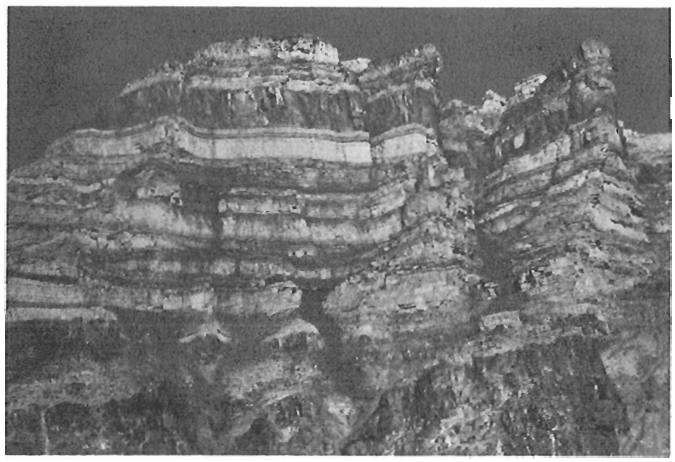

Figure 24.7. *Section of Fosheim Member in the Yelverton Pass area of northern Ellesmere. Striped appearance is characteristic of member.*

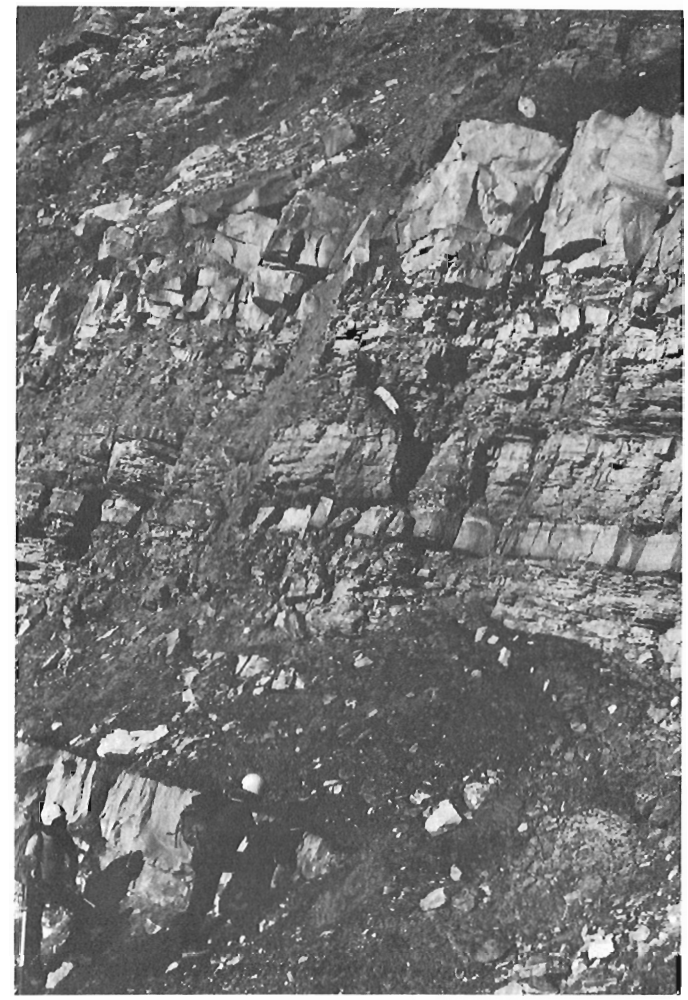

Figure 24.8. *Coarsening-upward cycle of bay-fill origin, Fosheim Member.*

Also present in the Fosheim Member of the eastern Sverdrup Basin are lenticular, massive, fine- to medium-grained sandstone units up to 20 m thick and 500 m wide.

Distribution and Thickness

The Fosheim Member has the same areal extent as the Heiberg Formation and ranges in thickness from 10 m on the basin margin to over 800 m in the basin centre [see Fig. 10 in Embry (1982) for an isopach map of the member].

Age

The only marine macrofossil obtained from the Fosheim Member is a Norian pelecypod in the lower portion of the member at Buchanan Lake (Souther, 1963). The overlying Remus Member has yielded late Pliensbachian ammonites. Because the contact between the Fosheim and Remus members is conformable and no unconformities have been recognized within the Fosheim Member it is inferred that the Fosheim Member contains strata of Norian, Hettangian, Sinemurian and early Pliensbachian age. Palynological studies (unpublished GSC reports) indicate a Late Triassic to Early Jurassic age for the member, which is compatible with the above inference. Also, the Fosheim Member is laterally equivalent to the Maclean Strait, Lougheed Island and King Christian formations of the Heiberg Group which range in age from Hettangian to Pliensbachian (Embry, 1982, 1983).

Environment of Deposition

The lithologies, cycles and stratigraphic relationships of the Fosheim Member are compatible with a deltaic plain origin (Embry, 1982). Sandstones are of channel and crevasse-splay origin, whereas the siltstone, shale and coal formed in interdistributary bay, marsh, swamp and lake environments.

Remus Member

Definition

The Remus Member of the Heiberg Formation consists almost entirely of very fine- to medium-grained sandstone and is characterized by a near-absence of shale and siltstone interbeds. The type section is in the Panarctic Romulus C-42 well, between 1436 m (4711 ft) and 1535 m (5034 ft), and the member is 99 m thick (Fig. 24.9). The member is named after Remus Creek which is 20 km northwest of the Romulus C-42 well.

Synonyms

1. Uppermost portion (100 m) of the upper member of the type Heiberg Formation (Souther, 1963).
2. Uppermost portion of the Heiberg Formation and the Borden Island Formation of Tozer (1963a).
3. Upper member of Heiberg Formation of Nassichuk and Christie (1969).
4. Uppermost Heiberg Formation, Borden Island Formation and lower portion of Jaeger Formation (members A and B) of Balkwill (in press).

Boundaries

The Remus Member conformably overlies the Fosheim Member with the contact placed at the top of the highest carbonaceous shale and siltstone bed above which sandstone is nearly continuous to the top of the Heiberg Formation. The contact of the Remus Member with the overlying Jameson Bay Formation is also conformable, and is placed at the top of the highest sandstone unit above which shale and siltstone are the predominant lithologies.

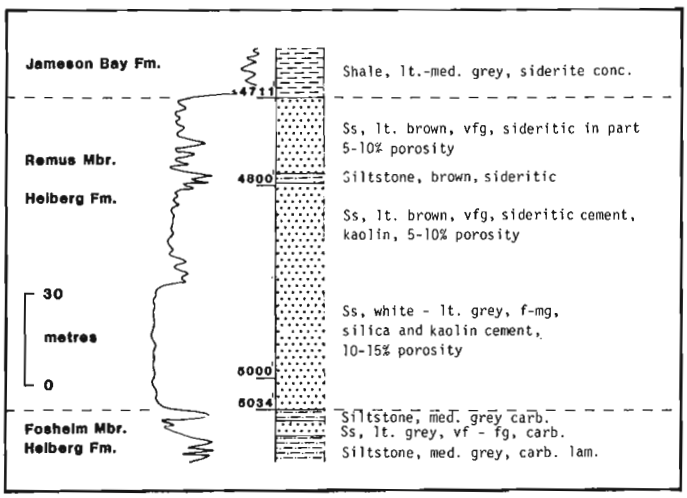

Figure 24.9. *Lithology and gamma ray curve of type section of Remus Member, Romulus C-42 well.*

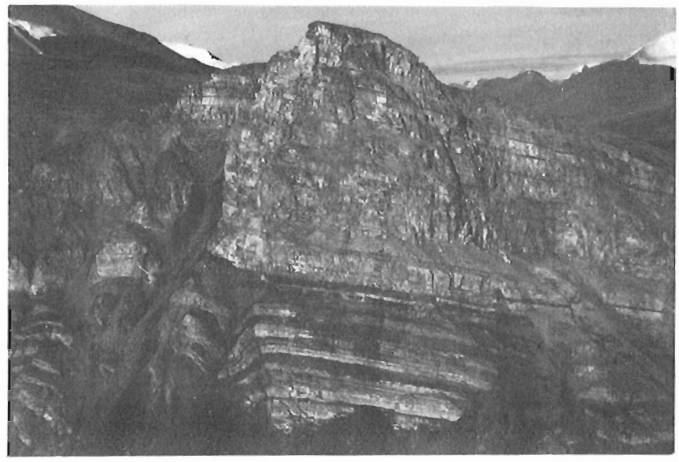

Figure 24.10. *Massive sandstone of Remus Member at Yelverton Pass, northern Ellesmere Island. The member is about 200 m thick and the contact with the Fosheim Member is placed at the top of the highest, dark weathering, shale-siltstone unit.*

Lithology

The Remus Member consists almost entirely of very fine- to medium-grained sandstone which is commonly massive in appearance. Thin, sideritic sandstone units, which commonly contain burrows and fossils, are present and are most common in the upper portion of the member. Red weathering ironstone bands up to 50 cm thick are also characteristic of the member at many localities.

On the southern margin of the basin, chert pebbles occur in pebbly sandstone beds or in thin conglomerate bands and pods. Glauconite is locally present and is most common in the upper portion of the member. Shale and siltstone interbeds, when present, are thin and usually occur near the top of the member.

Distribution and Thickness

The Remus Member has the same areal extent as the Heiberg Formation and ranges in thickness from 5 to 220 m. It is in the 30 to 100 m range over most of its extent.

Age

Late Pliensbachian ammonites occur in the lower portion of the member on western Ellesmere Island and eastern Axel Heiberg Island (Frebold, 1975; unpublished GSC data). On Cornwall Island, strata now assigned to the Remus Member, contain Pliensbachian pelecypods and Toarcian ammonites (Balkwill, in press). The overlying Jameson Bay Formation contains Toarcian ammonites (Tozer, 1963a). From these data the Remus Member is assumed to be Pliensbachian to Early Toarcian in age.

Environment of Deposition

The Remus Member is interpreted to represent strand plain and nearshore deposits of a destructive delta on the basis of the well sorted, quartzose nature of the sandstone, the near-absence of argillaceous units, the presence of burrows, marine fossils and glauconite, and the widespread occurrence of the sandstone (Embry, 1982).

References

Balkwill, H.R.
– Geology of Amund Ringnes, Cornwall and Haig-Thomas islands, District of Franklin; Geological Survey of Canada, Memoir 390. (in press)

Embry, A.F.
1982: The Upper Triassic - Lower Jurassic Heiberg Deltaic Complex of the Sverdrup Basin; in Arctic Geology and Geophysics, ed. A.F. Embry and H.R. Balkwill; Canadian Society of Petroleum Geologists, Memoir 8, p. 189-217.

1983: The Heiberg Group, western Sverdrup Basin; in Current Research, Part B; Geological Survey of Canada, Paper 83-1B, report 46.

Frebold, H.
1975: The Jurassic faunas of the Canadian Arctic, Lower Jurassic ammonites, biostratigraphy and correlations; Geological Survey of Canada, Bulletin 243.

Fricker, P.E.
1963: Geology of the Expedition Fiord area, west central Axel Heiberg Island, Canadian Arctic Archipelago; McGill University, Axel Heiberg Island Research Reports, Geology No. 1.

Glenister, B.F.
1963: Localities on southern Axel Heiberg Island; in Y.O. Fortier et al., Geology of the north-central part of the Arctic Archipelago, Northwest Territories (Operation Franklin); Geological Survey of Canada, Memoir 320, p. 472-481.

Greiner, H.R.
1963: Jaeger River, eastern Cornwall Island; in Y.O. Fortier et al., Geology of the north-central part of the Arctic Archipelago, Northwest Territories (Operation Franklin); Geological Survey of Canada, Memoir 320, p. 533-537.

Heywood, W.W.
1957: Isachsen area, Ellef Ringnes Island, District of Franklin, Northwest Territories; Geological Survey of Canada, Paper 56-8.

McLaren, D.J.
1963: Mount Nicolag, Cornwall Island; in Y.O. Fortier et al., Geology of the north-central part of the Arctic Archipelago, Northwest Territories (Operation Franklin); Geological Survey of Canada, Memoir 320, p. 529-533.

Nassichuk, W.W. and Christie, R.L.
1969: Upper Paleozoic and Mesozoic stratigraphy in the Yelverton Pass region, Ellesmere Island, District of Franklin; Geological Survey of Canada, Paper 68-31.

Souther, J.G.
1963: Geological traverse across Axel Heiberg Island from Buchanan Lake to Strand Fiord; in Y.O. Fortier et al., Geology of the north-central part of the Arctic Archipelago, Northwest Territories (Operation Franklin); Geological Survey of Canada, Memoir 320, p. 426-448.

Tozer, E.T.
1956: Geological reconnaissance, Prince Patrick, Eglinton and western Melville Islands, Arctic Archipelago, Northwest Territories; Geological Survey of Canada, Paper 55-2.

1961: Triassic stratigraphy and faunas, Queen Elizabeth Islands, Arctic Archipelago; Geological Survey of Canada, Memoir 316.

1963a: Mesozoic and Tertiary stratigraphy, western Ellesmere Island and Axel Heiberg Island, District of Franklin; Geological Survey of Canada, Paper 63-30.

1963b: Northwestern Bjorne Peninsula; in Y.O. Fortier et al., Geology of the north-central part of the Arctic Archipelago, Northwest Territories (Operation Franklin); Geological Survey of Canada, Memoir 320, p. 363-370.

1963c: South side of Strand Fiord; in Y.O. Fortier et al., Geology of the north-central part of the Arctic Archipelago, Northwest Territories (Operation Franklin); Geological Survey of Canada, Memoir 320, p. 448-456.

1970: Geology of the Arctic Archipelago, Mesozoic; in Geology and Economic Minerals of Canada, ed. R.J.W. Douglas; Geological Survey of Canada, Economic Geology Report 1, p. 574-583.

Tozer, E.T. and Thorsteinsson, R.
1964: Western Queen Elizabeth Islands, Arctic Archipelago; Geological Survey of Canada, Memoir 332.

Appendix

Selected well tops, Heiberg Formation, eastern and central Sverdrup Basin
(location of wells shown on Figure 24.1)

Panarctic Romulus C-42	
Remus Member	1436 m (4711 ft)
Fosheim Member	1535 m (5034 ft)
Romulus Member	2055.5 m (6742 ft)
Barrow Formation	2400 m (7870 ft)
Gulf Neil 0-15	
Fosheim Member	spud
Romulus Member	357 m (1170 ft)
Barrow Formation	609 m (1997 ft)
Panarctic May Point H-02	
Remus Member	2515.5 m (8251 ft)
Fosheim Member	2582 m (8470 ft)
BP Graham C-52	
Remus Member	1360 m (4460 ft)
Fosheim Member	1415 m (4640 ft)
Romulus Member	1472.5 m (4830 ft)
Barrow Formation	1519.5 m (4984 ft)
Imperial Sherwood P-37	
Remus Member	631 m (2070 ft)
Fosheim Member	665 m (2180 ft)
Romulus Member	1116.5 m (3662 ft)
Barrow Formation	2476 m (8122 ft)
Horn River Mid Fiord J-53	
Remus Member	1452 m (4762 ft)
Fosheim Member	1491.5 m (4892 ft)
Romulus Member	1770 m (5806 ft)
Panarctic Amund Central Dome H-40	
Remus Member	313 m (1026 ft)
Fosheim Member	362 m (1188 ft)
Romulus Member	1365 m (4478 ft)
Barrow Formation	1811.5 m (5942 ft)
Sun Linckens Island P-46	
Remus Member	980 m (3215 ft)
Fosheim Member	1010.5 m (3314 ft)
Romulus Member	1460.5 m (4790 ft)
Barrow Formation	1570 m (5150 ft)
Panarctic Hoodoo Dome H-37	
Remus Member	2301.5 m (7549 ft)
Fosheim Member	2353.5 m (7720 ft)
Romulus Member	2807.5 m (9208 ft)
Barrow Formation	3244 m (10640 ft)

25. THE LAKE HAZEN FAULT ZONE, ELLESMERE ISLAND: A TRANSPRESSIONAL UPTHRUST?

Project 730051

A.K. Higgins[1] and N.J. Soper[2]
Institute of Sedimentary and Petroleum Geology, Calgary

Higgins, A.K. and Soper, N.J., The Lake Hazen fault zone, Ellesmere Island: a transpresssional upthrust?; in Current Research, Part B, Geological Survey of Canada, Paper 83-1B, p. 215-221, 1983

Abstract

Observations on well-exposed sections of the Lake Hazen fault zone around the head of Tanquary Fiord, northern Ellesmere Island, suggest a model of development involving basement upthrusts controlled by tectonic transpression, with a small amount of dextral strike-slip. Large displacements, whether strike-slip or dip-slip, need not be invoked.

Résumé

Des observations le long de sections bien exposées de la zone faillée de Lake Hazen, près du sommet du fjord Tanquary dans le nord de l'île Ellesmere, suggèrent un modèle de formation comprenant des soulèvements du socle rocheux contrôlés par la transpression tectonique, avec de petits rejets horizontaux vers la droite. Il n'est pas nécessaire de faire appel aux déplacements importants, qu'ils soient horizontaux ou verticaux.

Introduction

The Lake Hazen fault zone trends east-northeast across northern Ellesmere Island (Fig. 25.1). It is traceable for almost 400 km from Hare Fiord in the west via Tanquary Fiord and Lake Hazen to the coast of the Lincoln Sea near Alert, and in its eastern part forms the southern margin of the Grantland Mountains (Christie, 1964; Nassichuk and Christie, 1969; Trettin, 1971; Trettin et al., 1972; Miall, 1979). It consists of a series of en echelon reverse faults, which cut both the lower Paleozoic sediments of the Hazen Trough, deformed by the mid-Paleozoic Ellesmerian orogeny, and their upper Paleozoic-Mesozoic cover of Sverdrup Basin sediments. Locally faults affect the early Tertiary Eureka Sound Formation (Miall, 1979). The fault deformation is ascribed to the main phase of the Eurekan orogeny (post-middle Eocene, pre-early Miocene: Trettin and Balkwill, 1979).

The dip-slip component of displacement on the faults is upwards on the north side and Nassichuk and Christie (1969, p. 24) described them as "steep, north-dipping mountain front thrusts", bordering the Grantland Uplift with an estimated vertical displacement of 1-2 km. Subsequent workers have generally accepted this interpretation, but recently larger displacements have been proposed, as is currently fashionable. Håkansson and Pedersen (1982) have erected a mobilistic model for northern Ellesmere Island and North Greenland in which several hundred kilometres of strike-slip displacement are proposed on the Lake Hazen fault zone and its supposed continuation in North Greenland, the Harder Fjord fault zone (Higgins et al., 1981). Since stratigraphic and structural features can be matched across the Harder Fjord fault zone without the necessity for any strike-slip displacement (authors' observations), and since the Tanquary structural high (Nassichuk and Christie, 1969; Wilson, 1976) crosses the Lake Hazen fault zone with a few kilometres offset only (Fig. 25.1), this interpretation can be ruled out. More serious consideration must be given to the thin-skinned model of Osadetz (1982), as this is based on fieldwork in the vicinity of Tanquary Fiord and Ekblaw Lake. He proposed that the component faults of the Lake Hazen fault zone are low-angled thrusts, rooting in a décollement near the base of the Grant Land Formation and having dip-slip displacement of many tens of kilometres.

An invitation to join the GSC party based at Tanquary Fiord in 1982 enabled the authors to map selected parts of the Lake Hazen fault zone in more detail than had been previously possible, with a view to deciding between the thin-skinned and upthrust interpretations. Observations were made on four well-exposed sections in the fault zone around the head of Tanquary Fiord: east of Bent Glacier; between Rollrock Lake and Ekblaw Lake; at Mount Timmia; and at Mount Thompson (Fig. 25.1). This paper is a preliminary report on our findings which, in our view, support a model which involves upthrusts associated with limited dextral transpression.

Bent Glacier

In the vicinity of Bent Glacier on the north side of Tanquary Fiord (Fig. 25.1), the published 1:250 000 scale geological map (Thorsteinsson and Trettin, 1971) shows several fault-bounded wedges of Sverdrup Basin sediments in fault contact with lower Paleozoic Grant Land Formation to the north. A section across the Bent Glacier fault zone is shown in Figure 25.2a. The main fault is clearly exposed east of Bent Glacier and dips north at 35-53°, with Grant Land Formation in the hanging wall. The footwall is composed of Carboniferous-Permian limestones of the Nansen Formation inclined a little more steeply than the fault and probably inverted, in a slice or 'horse' which has a maximum thickness of 300 m. The Nansen is in fault contact with sandstones and shales of the Triassic-Jurassic Heiberg Formation (mainly Fosheim Member with dolerite sills), which is clearly inverted, dipping northwest at 45°, and forms a wedge with a maximum thickness of about 800 m. Another poorly exposed reverse fault separates the Heiberg Formation from Mesozoic formations in the steeply inverted limb of a southward verging asymmetric syncline. From a consideration of the altitude of the mid-Paleozoic unconformity north and south of the fault zone, the vertical displacement is estimated to be 3.5 km.

Rollrock Lake and Ekblaw Lake

A branch of the Lake Hazen fault zone runs along the north side of Rollrock valley (Fig. 25.1) as shown on the maps by Nassichuk and Christie (1969) and Wilson (1976).

[1] Geological Survey of Greenland, Øster Voldgade 10, DK-1350 Copenhagen K, Denmark.
[2] Department of Geology, University of Sheffield, Sheffield S1 3JD, U.K.

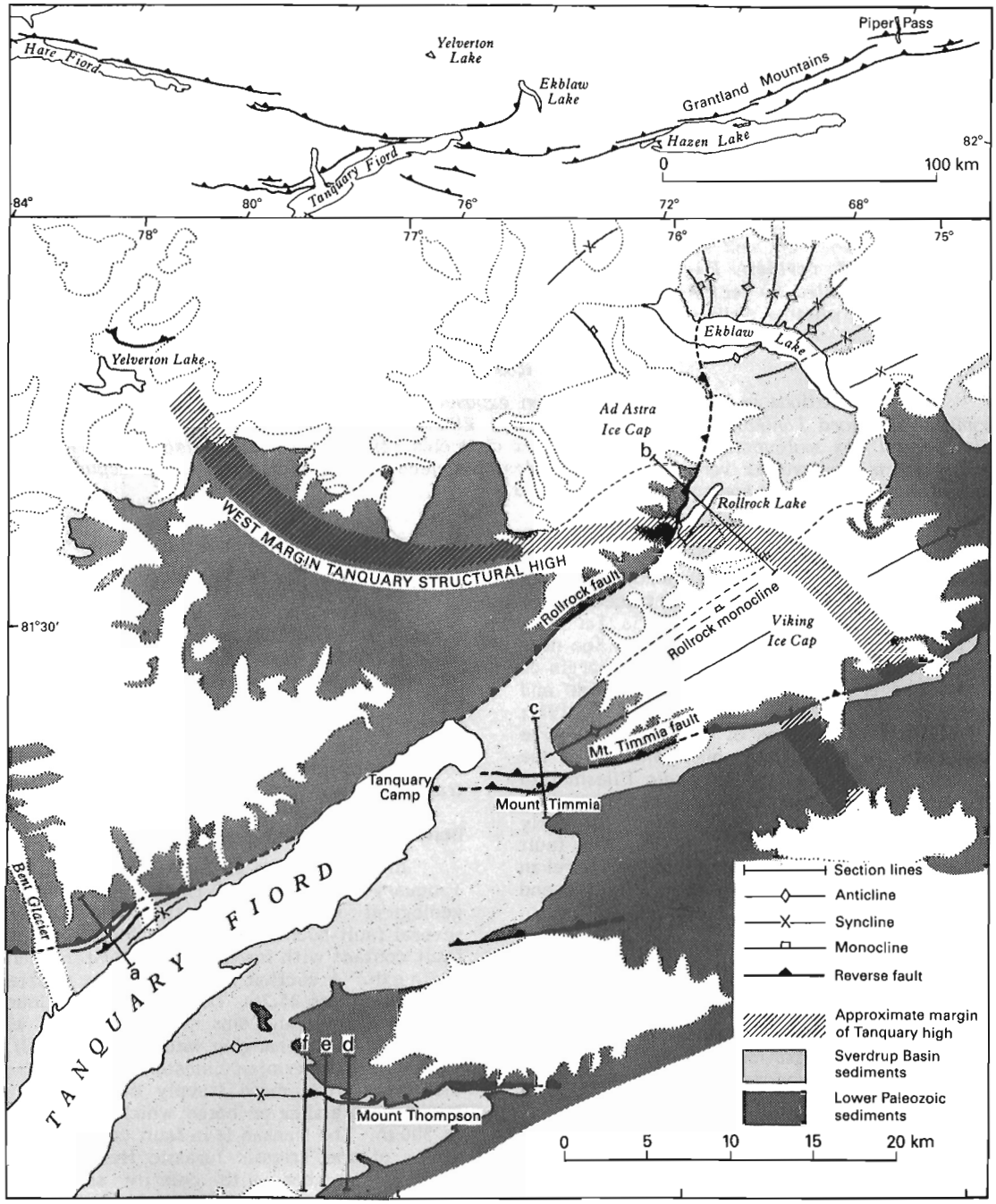

Figure 25.1. *Sketch map of the area around the head of Tanquary Fiord showing main structural elements, and location of the cross-sections of Figure 25.2. The west boundary of the Tanquary structural high coincides approximately with the erosional limit of the Upper Carboniferous-Lower Permian Belcher Channel Formation, which here unconformably overlies the lower Paleozoic basement. Farther east, the basement is overlain in some areas by the Upper Triassic-Lower Jurassic Heiberg Formation and in others by a thin Lower Permian Sabine Bay Formation, in turn overlain by the Heiberg. The limit has been adapted from the preliminary geological map by Mayr et al. (1982), but our interpretation involves projection across several large areas of non-exposure. Inset at top shows en echelon elements of Lake Hazen Fault Zone.*

Osadetz (1982) has shown that towards Ekblaw Lake this fault trace swings from northwest to north. The fault is best exposed on the north side of Rollrock Lake (Fig. 25.3), while at Ekblaw Lake it dies out into a monocline. We therefore refer to it here as the 'Rollrock fault', rather than the 'Ekblaw Lake thrust', the term introduced by Osadetz (1982).

At Rollrock Lake the main reverse fault, dipping northwest at angles between 30° and 62°, carries lower Paleozoic rocks in the hanging wall (Grant Land Formation) and climbs up-sequence into the Sverdrup Basin cover, which here on the Tanquary structural high consists of Heiberg Formation resting directly on Grant Land Formation (Figs. 25.2b, 25.3). The Sverdrup basin sequence in the footwall consists of Permo-Carboniferous to Cretaceous sediments preserved in a conspicuous monocline, which has a maximum limb dip of 70°. The fault cuts up-sequence through late Jurassic and Cretaceous sediments. Interposed between the lower and upper plates is a 'horse' of Heiberg Formation, and again, as at Bent Glacier, this is inclined to the northwest and inverted. The vertical displacement on the fault zone in this area is estimated to be about 2.5 km.

The fault swings northwards beneath the Ad Astra Ice Cap and reappears to cross the west end of Ekblaw Lake. Osadetz (1982) showed his 'Ekblaw Lake thrust' terminating here against a fault which displaces it above the present erosion level. Our mapping indicates that stratigraphic separation on the Rollrock fault diminishes northwards and on the northern side of Ekblaw Lake it dies out into the vertical limb of a north-northwest trending monocline. The displacement is also taken up on a further monocline some 6 km to the west, and the series of open folds mapped by Osadetz to the east, which are responsible for the spectacular inverted topography north of Ekblaw Lake.

Mount Timmia

A main branch of the Lake Hazen fault zone passes through Mount Timmia, northeast of Tanquary Camp at the head of Tanquary Fiord (Fig. 25.1), and was first shown on the map by Nassichuk and Christie (1969). Osadetz (1982) mapped a single thrust here, inclined at about 15°, and regarded this as important evidence in favour of a thin-skinned interpretation for the fault zone. Our more detailed mapping shows there to be, in fact, two reverse faults at Mount Timmia (Fig. 25.2c). The main fault, which east of

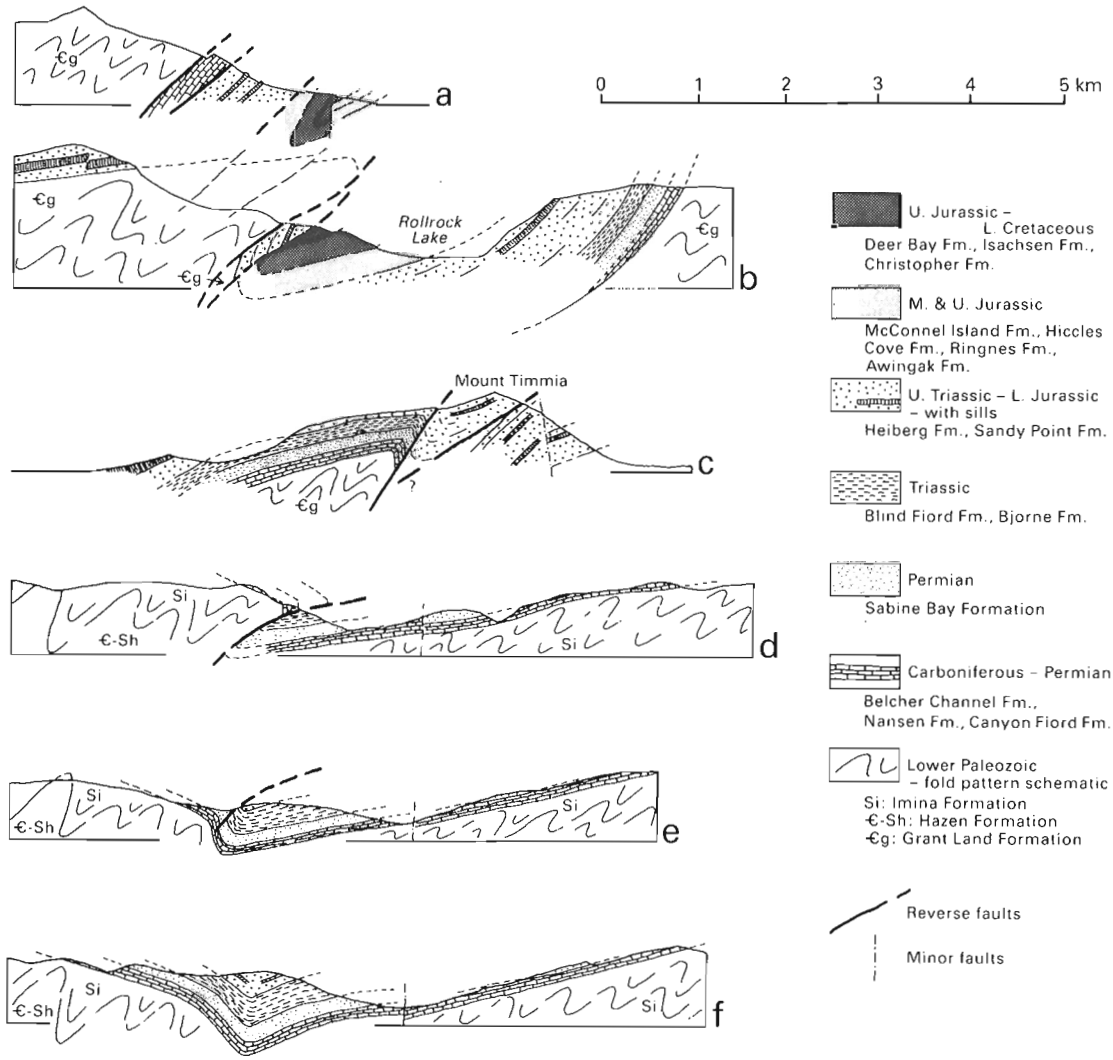

Figure 25.2. *Sketch cross-sections (see Fig. 25.1 for location): (a) East of Bent Glacier; (b) Rollrock Lake; (c) Mount Timmia; (d), (e) and (f) Mount Thompson.*

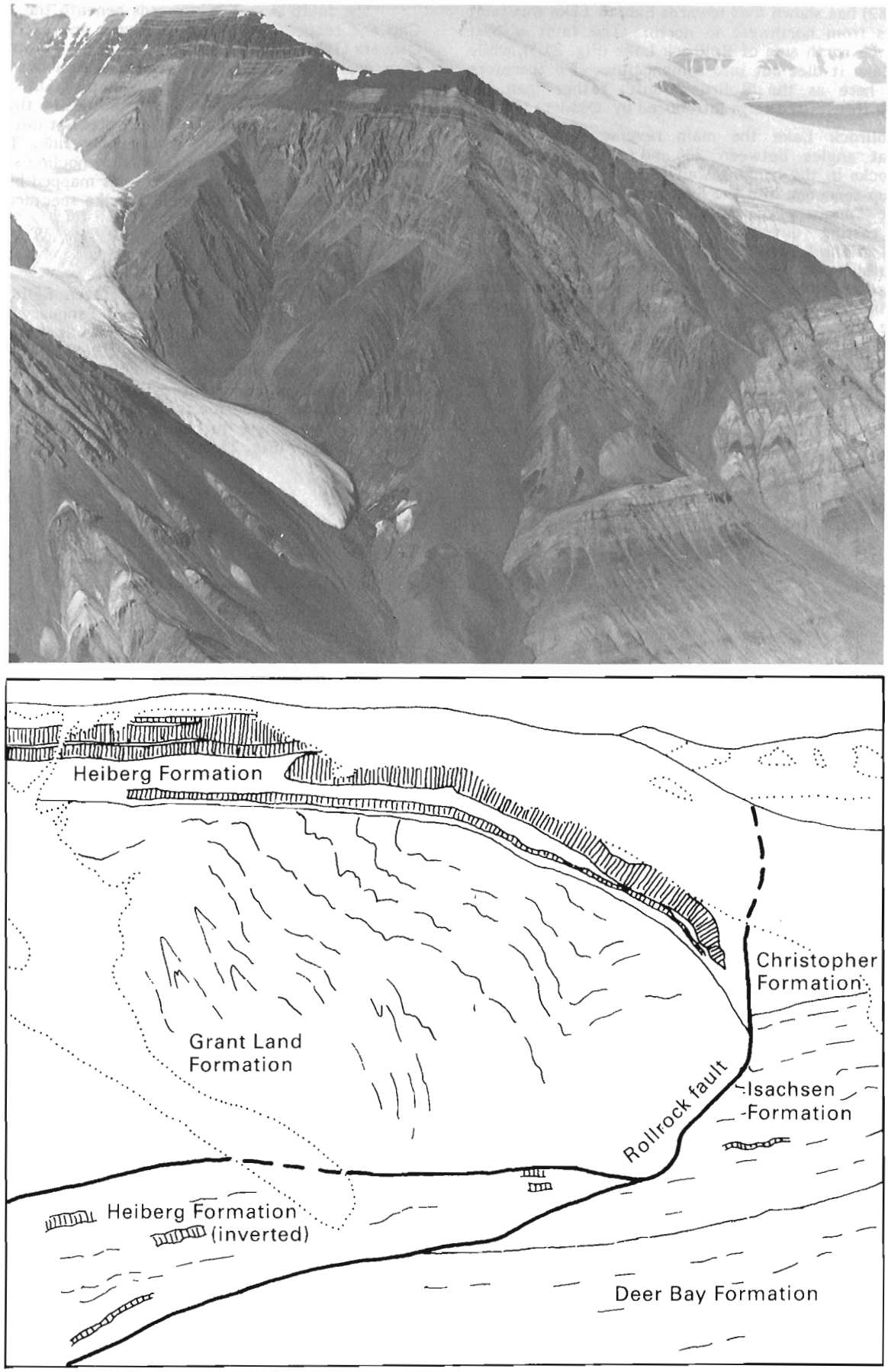

Figure 25.3. *The Rollrock fault north of Rollrock Lake. Folded Grant Land Formation and unconformably overlying Heiberg Formation in the hanging wall are faulted against Mesozoic formations in the footwall. Note wedge of inverted Heiberg Formation at left – see also Figure 25.2b.*

Mount Timmia emplaces lower Paleozoic Grant Land Formation over Sverdrup Basin cover, climbs westward into the cover in the hanging wall and bifurcates into northern and southern branches, which are inclined northwards at 55° and 35° respectively (Fig. 25.2c). The southern branch cuts down-sequence locally in the footwall.

Mount Thompson

Sixteen kilometres south of Tanquary Camp, the 1:250 000 scale geological map by Thorsteinsson and Trettin (1971) shows a reverse fault in the Mount Thompson area passing westwards into a major syncline in Sverdrup Basin sediments. Our detailed mapping confirms this basic interpretation.

The fault plane dips north at low angles of 20-25°, subparallel to the bedding of the sediments in the footwall, and along strike follows the same stratigraphical level for 7 km before cutting rapidly up-sequence in the hanging wall to die out in the steep common limb of an east-west trending fold pair. Three cross-sections of the structure in the transition from reverse fault to fold are shown in Figure 25.2d, e, f.

Discussion

Osadetz (1982) stated that the thrust faults in the Tanquary Fiord – Ekblaw Lake area generally dip at angles of less than 15°, and this appears to be one of the reasons for his adoption of a thin-skinned interpretation for the Lake Hazen fault zone. We do not wish to discuss here each point on which our respective interpretations differ, but it is necessary to emphasize that our direct observations of the fault planes show them to have extremely variable and commonly steep inclinations. As described briefly above, and shown in Figure 25.2, the main faults at Bent Glacier are inclined at 35-55°, at Rollrock Lake 30-62°, at Mount Timmia 35-55°, and only at Mount Thompson can a thrust fault be traced for an appreciable distance with a rather uniform dip of less than 25°. East of the Tanquary Fiord area, a dip of 60° was observed on a part of the Lake Hazen fault zone east of Piper Pass (Fig. 25.4), and this concurs with the report by Miall (1979) that the main thrust fault is steeply dipping to near vertical between Lake Hazen and Piper Pass (Fig. 25.1).

Our overwhelming impression is that when one or both walls of the faults are in Sverdrup Basin cover rocks then the inclination is variable, commonly steep as a fault cuts up-section or follows a surface in steeply inclined strata, but locally following gently inclined bedding in certain units (particularly the Fosheim Member of the Heiberg Formation). When entirely within previously folded lower Paleozoic rocks the faults are difficult to discern, but when visible or inferred from aerial photographs, they appear to cross pronounced topography with little deflection, suggestion steep inclinations (H.P. Trettin, personal communication). A few direct observations of fault traces in Grant Land Formation indicate dips in excess of 60°, and we infer that the faults could well steepen with depth, as required by an upthrust interpretation.

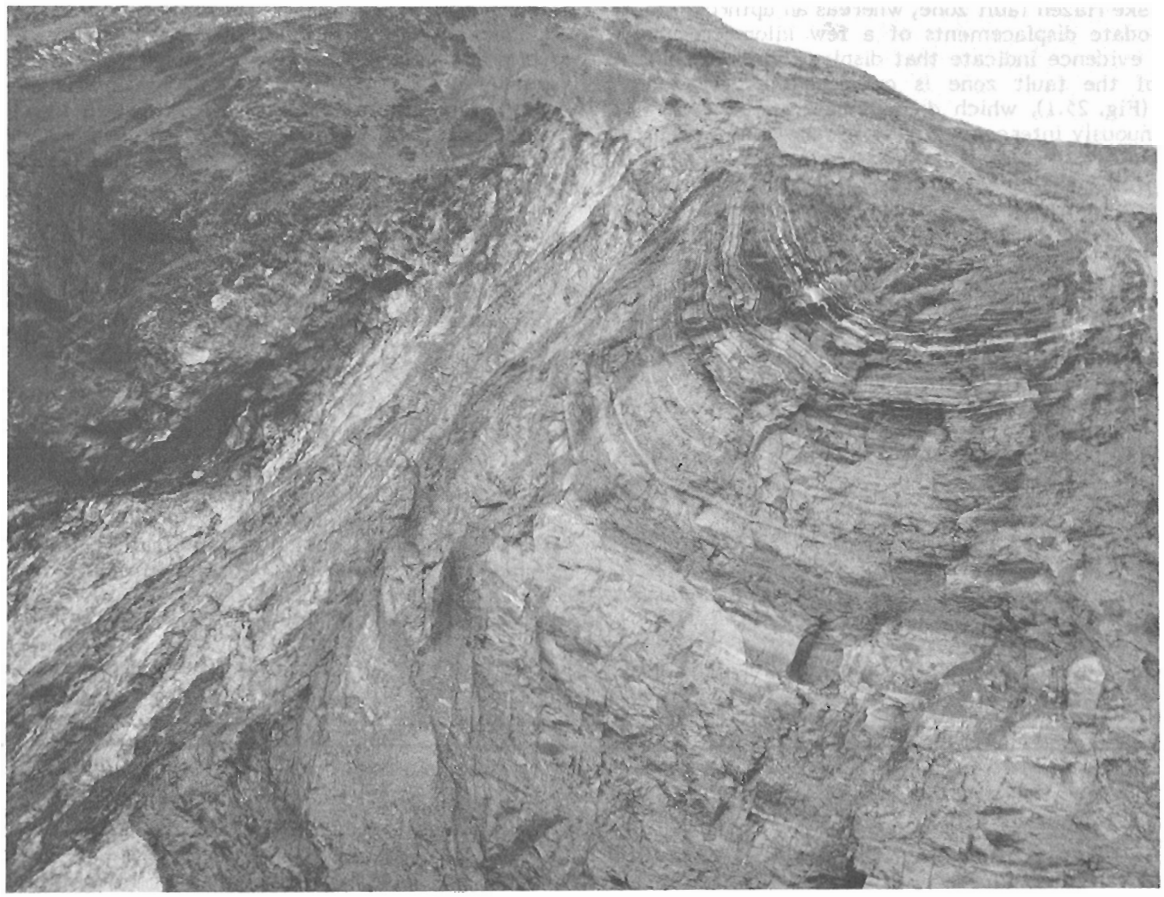

Figure 25.4. *Part of the Lake Hazen fault zone east of the southern end of Piper Pass. The fault plane dips northwards at 60°. Grant Land Formation in the hanging wall is faulted against Permian sandstones (Trold Fiord Formation).*

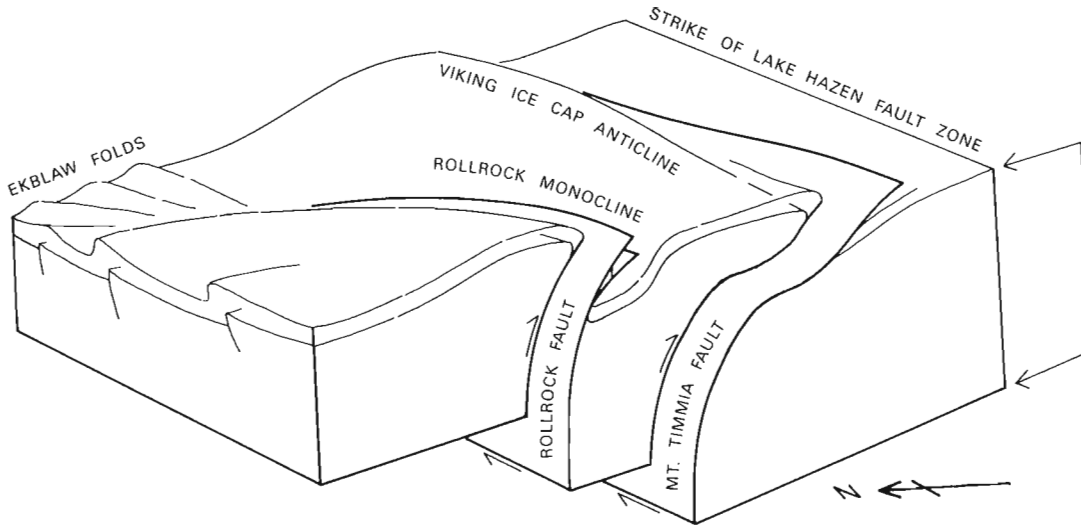

Figure 25.5. *Schematic block diagram showing the geometry of the Rollrock and Mount Timmia faults, associated folds, and inferred displacements, according to a transpresssional upthrust interpretation. The Viking Ice Cap anticline and Rollrock monocline are regarded as 'roll-over' structures associated with displacement on the Mount Timmia staircase fault plane.*

Substantial dip-slip displacement, in the order of tens of kilometres, is implicit in Osadetz' thin-skinned interpretation of the Lake Hazen fault zone, whereas an upthrust model can accommodate displacements of a few kilometres only. Two lines of evidence indicate that displacements are small. The whole of the fault zone is composed of en echelon dislocations (Fig. 25.1), which die out laterally and do not form a continuously interconnected network. The manner in which the faults terminate is not easy to discern when both the hanging wall and footwall are in lower Paleozoic strata. When in Sverdrup Basin cover the faults are seen to lose stratigraphic separation and pass into folds, as described above for the Mount Thompson and Rollrock faults. Displacement is transferred in this manner from one fault to the next, and clearly only a few kilometres of displacement can be so accommodated. Secondly, a simple bed-length comparison across the Rollrock and Mount Timmia faults and their associated folds indicates basement shortening of 7-8 km along a 34 km cross-strike section. The profile on which this construction is based (the front face of Fig. 25.5) lacks adequate topographic control, and there are problems connected with balancing sections across tectonic zones which involve both upthrust displacements and strike-slip, but it is clear that it is not necessary to invoke large dip-slip displacements to explain the structures.

The en echelon pattern of the individual dislocations which make up the fault zone in the Tanquary Fiord – Ekblaw Lake area suggests that a component of dextral strike-slip accompanied the upthrust displacements. Notably, the trace of the Rollrock fault curves northwards as the displacement dies out, as described above. Stratal shortening across the zone of monoclines and open folds into which the fault passes at Ekblaw Lake (Fig. 25.1) is a little more than one kilometre, indicating that a strike-slip component is present, but not great.

A model which involves basement upthrusts controlled by tectonic transpression, as developed for example by Sylvester and Smith (1976) for part of the San Andreas fault zone, can account for the observed structures and inferred displacements on the Lake Hazen fault zone in the area studied (Fig. 25.5), although in our case the displacements are relatively small. We envisage that southeast facing drape monoclines developed in the cover sequence above the upthrusts and that their steep limbs were subsequently disrupted and locally inverted by continued displacement on the reverse faults, together with footwall imbrication. The essentially monoclinal nature of the Lake Hazen fault zone seems to persist along the southern frontal scarp of the Grantland Mountains, at least as far as Piper Pass, with a thin veneer of steeply inclined cover sediments resting unconformably on the lower Paleozoic rocks and passing southeast into the Lake Hazen syncline (cf. Miall, 1979).

More detailed analysis of these structures must await preparation of a suitable topographic base map for the Rollrock Lake and Ekblaw Lake areas, which is currently in hand.

Acknowledgments

We thank the Geological Survey of Canada, and especially H.P. Trettin, for providing the opportunity to visit northern Ellesmere Island and for logistical support during the 1982 field season. Our investigations have been greatly helped by discussions in the field with H.P. Trettin, U. Mayr, and K.G. Osadetz. A.K.H. publishes with the permission of the Director of the Geological Survey of Greenland.

References

Christie, R.L.
1964: Geological reconnaissance of northeastern Ellesmere Island, District of Franklin; Geological Survey of Canada, Memoir 331.

Higgins, A.K., Friderichsen, J.D., and Soper, N.J.
1981: The North Greenland fold belt between central Johannes V. Jensen Land and eastern Nansen Land; Rapport Grønlands Geologiske Undersøgelse 106, p. 35-45.

Håkansson, E. and Pedersen, S.A.S.
1982: Late Paleozoic to Tertiary tectonic evolution of the continental margin in North Greenland; in Arctic geology and geophysics, Proceedings of the Third International Symposium on Arctic Geology, A.F. Embry and H.R. Balkwill, ed.; Canadian Society of Petroleum Geologists, Memoir 8, p. 331-348.

Mayr, U., Trettin, H.P., and Embry, A.F.
1982: Preliminary geological map and notes, part of Tanquary Fiord map-area, District of Franklin; Geological Survey of Canada, Open File 835.

Miall, A.D.
1979: Tertiary fluvial sediments in the Lake Hazen intermontane basin, Ellesmere Island, Arctic Canada; Geological Survey of Canada, Paper 79-9.

Nassichuk, W.W. and Christie, R.L.
1969: Upper Paleozoic and Mesozoic stratigraphy in the Yelverton Pass region, Ellesmere Island, District of Franklin; Geological Survey of Canada, Paper 68-31.

Osadetz, K.G.
1982: Eurekan structures of the Ekblaw Lake area, Ellesmere Island, Canada; in Arctic geology and geophysics, Proceedings of the Third International Symposium on Arctic Geology, A.F. Embry and H.R. Balkwill, ed.; Canadian Society of Petroleum Geologists, Memoir 8, p. 219-232.

Sylvester, A.G. and Smith, R.R.
1976: Tectonic transpression and basement-controlled deformation in San Andreas fault zone, Salton Trough, California; American Association of Petroleum Geologists, Bulletin, v. 60, p. 2081-2102.

Thorsteinsson, R. and Trettin, H.P.
1971: Geology, Tanquary Fiord, District of Franklin; Geological Survey of Canada, Map 1306A.

Trettin, H.P.
1971: Geology of lower Paleozoic formations, Hazen Plateau and southern Grant Land Mountains, Ellesmere Island, Arctic Archipelago; Geological Survey of Canada, Bulletin 203.

Trettin, H.P. and Balkwill, H.R.
1971: Contributions to the tectonic history of the Innuitian Province, Arctic Canada; Canadian Journal of Earth Sciences, v. 16, p. 748-769.

Trettin, H.P., Frisch, T.O., Sobczak, L.W., Weber, J.R., Niblett, E.R., Law, L.K., DeLaurier, J.M., and Witham, K.
1972: The Innuitian Province; in Variations in tectonic styles in Canada, R.A. Price and R.J.W. Douglas, ed.; Geological Association of Canada, Special Paper 11, p. 83-179.

Wilson, D.G.
1976: Studies of Mesozoic stratigraphy, Tanquary Fiord to Yelverton Pass, northern Ellesmere Island, District of Franklin; in Report of Activities, Part A; Geological Survey of Canada, Paper 76-1A, p. 449-451.

26.

NEW DALEJAN (EARLY DEVONIAN) RUGOSE CORALS FROM THE BLUE FIORD FORMATION OF SOUTHWESTERN ELLESMERE ISLAND, NORTHWEST TERRITORIES

Project 680093

A.E.H. Pedder
Institute of Sedimentary and Petroleum Geology, Calgary

Pedder, A.E.H., New Dalejan (Early Devonian) rugose corals from the Blue Fiord Formation of southwestern Ellesmere Island, Northwest Territories; in Current Research, Part B, Geological Survey of Canada, Paper 83-1B, p. 223-236, 1983.

Abstract

The family Columnariidae Nicholson, 1879, is revised, so that it comprises the subfamilies Columnariidae Nicholson, 1879, Hexagonariinae Bul'vanker, 1958, Paradisphyllinae Jell, 1969, Utaratuiinae Spasskiy, Kravtsov and Tsyganko, 1975, Spongonariinae Crickmay, 1962, and Tropidophyllinae subfam. n.

Stereophyllum** Schluter, 1889, is likely to be a synonym of **Digonophyllum** Wedekind, 1923. However, **Digonophyllum**, which is a widely used generic name, is retained on the grounds that **Stereophyllum** appears to be a nomen oblitum. **Aulacophyllum** Milne Edwards and Haime, 1850, and its probable synonym **Pinnatophyllum** Grabau, 1922, are discussed, because of similarities between them and a new genus **Thoulelasma.

***Digonophyllum primitivum confertum** subsp. n. (Family Cystiphyllidae) and **Thoulelasma loewei** gen. et sp. n. (Family Halliidae) are described from high in the **inversus** Zone in the Sor Fiord section. **Paraspongonaria delicata** gen. et sp. n. (Family Columnariidae) is described from the same horizon and locality, as well as from the overlying **serotinus** Zone near Vendom Fiord. Newly prepared type material of **Paraspongonaria sverdrupi** (Loewe, 1913) is figured from the Zlichovian (Early Devonian) Db Series of Schei (1903; 1904) in the vicinity of Goose Fiord.*

Résumé

L'auteur modifie la famille Columnariidae Nicholson, 1879, de façon à ce qu'elle comprenne les sous-familles Columnariidae Nicholson, 1879, Hexagonariinae Bul'vanker, 1958, Paradisphyllinae Jell, 1969, Utaratuiinae Spasskiy, Kravtsov et Tsyganko, 1975, Spongonariinae Crickmay, 1962 et Tropidophyllinae subfam. n.

Stereophyllum** Schluter, 1889, est probablement synonyme de **Digonophyllum** Wedekind, 1923. Toutefois, le nom générique **Digonophyllum**, très répandu, a été conservé puisque **Stereophyllum** semblerait être un **nomen oblitum**. **Aulacophyllum** Milne Edwards et Haime, 1850 et son synonyme probable, **Pinnatophyllum** Grabau, 1922, sont étudiés en raison de leur ressemblance avec le nouveau genre **Thoulelasma.

*L'auteur décrit les coraux **Digonophyllum primitivum confertum** subsp. n. (famille des Cystiphyllidae) et **Thoulelasma loewei** gen. et sp. n. (famille des Halliidae) qui proviennent des couches supérieures de la zone **d'inversus** dans la coupe du fjord Sor. Il décrit les coraux **Paraspongonaria delicata** gen. et sp. n. (famille des Columnariidae) provenant du même horizon et de la même localité et de la zone susjacente de **serotinus** près du fjord Vendom. Il considère que le matériel type nouvellement préparé de **Paraspongonaria sverdrupi** (Loewe, 1913) provient de la série Db de Schei (1903; 1904) datant du Zlichovien (Dévonien ancien); cette série se situe près du fjord Goose.*

Introduction

The Blue Fiord Formation of Sor Fiord region is of considerable importance to the Devonian coral biostratigraphy of arctic Canada. This is due partly to the richness of the coral faunas in the formation, and partly to the refined correlation that has been achieved by conodont studies between the Blue Fiord Formation and the standard Lower Devonian sequence of Czechoslovakia (Uyeno and Klapper, 1980).

Although most of the coral species that occur in the Blue Fiord Formation have not been made known, **Zonophyllum sorense, Mesophyllum ellesmerense, M. kirki, Taimyrophyllum nolani baumannense** and **Cavanophyllum uyenoi** have been described from the Zlichovian part of the formation, and **Lekanophyllum pustulosum** has been established on material from the Dalejan part of the formation (Pedder and McLean, 1982; Pedder, 1982b). The present paper adds to the Dalejan fauna of the formation by describing **Digonophyllum primitivum confertum** subsp. n., **Thoulelasma loewei** gen. et sp. n. and **Paraspongonaria delicata** gen. et sp. n.

For reasons evident in the systemmatic paleontology section, it is necessary to consider carefully three poorly known genera, **Stereophyllum, Aulacophyllum** and **Pinnatophyllum**, that are not used in the paper, because of similarities between them and junior genera that are used. It is also necessary to revise the family Columnariidae, because study of newly acquired representatives of relevant genera shows that none of the previously proposed classifications of these genera is satisfactory.

I am grateful to David Worsley, University Paleontological Museum, Oslo, for arranging the loan of material collected by Per Schei on the Second Norwegian Arctic Expedition in the "Fram", and for permission to prepare new thin sections from it. Without this help, it would not be certain that the species described by Loewe (1913) as **Cyathophyllum sverdrupi** is also a species of the new genus **Paraspongonaria.**

Systematic Paleontology

Family CYSTIPHYLLIDAE Milne Edwards and Haime, 1850
Subfamily DIGONOPHYLLINAE Wedekind, 1923

Genus **Stereophyllum** Schlüter, 1889

Stereophyllum Schlüter, 1889, p. 339 (p. 81 in reprints).
not **Stereophyllum** Grabau, 1917, p. 199 (nomen nudum).
nor **Stereophyllum** Soshkina, 1937, p. 19, 20, 88, 89 (homonym replaced by **Astrictophyllum** Spasskiy, 1971, p. 24).

Type species. **Cyathophyllum goldfussi** Milne Edwards and Haime, 1851, p. 363, Pl. 2, figs. 3, 3a. Devonian, Eifel region, Germany. This is a homonym of **Cyathophyllum goldfussi** Castelnau, 1843, p. 47, Pl. 21, fig. 2 (=upper fig. 1; there is no labelled fig. 2), an unrecognisable species, believed to be from the Onondaga Limestone, near Buffalo, New York (Bassler, 1950, p. 133). Stumm (1949, p. 20) renamed **Cyathophyllum goldfussi** Milne Edwards and Haime **Plasmophyllum eifelense**, but according to Birenheide (1964, p. 19), it is a junior subjective synonym of the lectotype of **Cyathophyllum limbatum** Quenstedt, 1879, p. 465. This lectotype was chosen by Birenheide himself, and is reposited in the Geological Museum, University of Tübingen, where it is numbered Coe 3/158/37. It has been figured by Quenstedt (1881, Pl. 158, two views designated fig. 37) and Birenheide (1964, Pl. 23, figs. 105a, b), and appears to be only the distal part of the corallum. Quenstedt recorded the species as coming from Gerolstein; Birenheide noted that, to the time of his writing, authentic in-place specimens had been found only in the Gees trilobite horizon, Ahrdorf Schichten (Eifelian), in the Gerolstein and Prüm synclines of Germany.

Remarks. For present purposes, and in the absence of any contrary evidence, the species-level systematic treatment accorded to **Cyathophyllum limbatum** Quenstedt, 1879, and **Plasmophyllum eifelense** Stumm, 1949, by Birenheide (1964, p. 19-21) is accepted. However, his generic determination, which placed these species in **Plasmophyllum** Dybowski, 1873, is rejected, because, as Weyer (1971) pointed out, he and others wrongly interpreted **Plasmophyllum**, by regarding **Cyathophyllum goldfussi** Milne Edwards and Haime, 1851, and not **Cystiphyllum brevilamellatum** McCoy, 1850, as its type species.

In the light of Birenheide's revision, **Cyathophyllum limbatum** Quenstedt is a recognisable species, especially on the bases of Birenheide's (1964, Pl. 21, figs. 99a-101c; Pl. 22, figs. 102a-103; Pl. 23, figs. 105a-106; Pl. 24, figs. 113-116) and Ma's (1956, Pl. 63, figs. 1-3, 5a-c) figures. Clearly, Quenstedt's species is neither **Cyathophyllum** nor **Plasmophyllum** (see Hill, 1981, p. 255, 297 for these genera), but is **Stereophyllum** Schlüter, 1889, and is also probably **Digonophyllum** Wedekind, 1923, as that genus was defined by McLean (1976b, p. 14, 15).

Stereophyllum Schlüter was proposed conditionally, but like other names erected before 1961, is not invalid for this reason [International Code of Zoological Nomenclature, Articles 15, 17(8)]. On the other hand, it seems probable that it is technically a nomen oblitum and should not be used without direction from the International Commission on Zoological Nomenclature [I.C.Z.N., Article 23(b)(ii)].

Arguments for regarding **Stereophyllum** Schlüter as a nomen oblitum are: 1) Fifty-one years elapsed between publication of the name in 1889 and subsequent mention of it in primary zoological literature by Lang, Smith and Thomas (1940, p. 123), who, incidentally, regarded it as an objective synonym of **Plasmophyllum**. 2) Wedekind, his students, and Ma (1937) all had occasion to use **Stereophyllum** within the fifty year period after 1889, but did not do so. 3) Two coral workers, Grabau (1917) and Soshkina (1937) proposed homonyms of **Stereophyllum** for other Devonian corals during the same period.

Genus **Digonophyllum** Wedekind, 1923

Stereophyllum Schlüter, 1889, p. 339 (p. 81 in reprints) (nomen oblitum-see above).
Digonophyllum Wedekind, 1923, p. 27.

Type species. **Digonophyllum schulzi** Wedekind, 1923, p. 27, Fig. 1. Nohner Schichten (early Eifelian); Nohn, Hillesheim Syncline, Eifel region, Germany. This species is regarded (Birenheide, 1964, p. 45) as a junior subjective synonym of **Actinocystis pseudoorthoceras** Schulz, 1883, p. 240, 241 (84, 85), Pl. 22, figs. 3, 4. The holotype of **Digonophyllum pseudoorthoceras** is also from the Nohner Schichten, near Nohn.

Diagnosis. Solitary digonophyllinid corals with septal crests that are dilated to contiguity in early stages. In late stages of most species, septal dilation is confined to the periaxial region. Septal apparatus bilaterally symmetrical about the cardinal/counter plane. Discrete septal carinae absent or rare.

Remarks. The present concept of **Digonophyllum** is very close to McLean's (1976b, p. 14-18), but is slightly broader in that it admits to the genus corals like **Pseudozonophyllum primitivum** Kravtsov, in which most of the subcalicular part of the corallum is filled with skeleton. Development of horizontal skeletal elements is much retarded in such forms. Similar discoid species, such as **Combophyllum multiradiatum** Meek, **Palaeocyclus kirbyi** Meek and **Glossophyllum clebroseptatum** Kravstov, and others that are discoidal in early stages, for example **Glossophyllum discoideum** Soshkina, continue to be excluded from **Digonophyllum** even though there is no appropriate genus for them.

Digonophyllum primitivum (Kravtsov, 1963)

Pseudozonophyllum primitivum Kravtsov, 1963, p. 29, 30, Pl. 8, figs. 2-4v; Pl. 9, figs. 1a-3b; Pl. 10, figs. 1a, b.

Pseudozonophyllum primitivum Kravtsov; Kravstov in Besprozvannykh et al., 1975, p. 99, 100, Pl. 39, figs. 2a-v.

Remarks. The holotype and figured paratypes originally were said to have come from unit 4 of the Early Devonian Tareya Suite, 40 to 45 km above the mouth of Tareya River, central Taimyr, U.S.S.R. In terms of the stratigraphic scheme proposed for the area by Cherkesova et al. (1968), they are from the Yunkhodsk Beds. Lane (1974, p. 721) interpreted conodonts that Kuz'min (1967) had described from the Yunkhodsk Beds, as including **Icriodus taimyricus** and "in all probability" **Polygnathus dehiscens.** These species indicate an early Zlichovian age for the Yunkhodsk Beds.

The genus **Pseudozonophyllum** and its three syntypic species - **P. halli, P. logani** and **P. clarkei** - were established by Wedekind (1924, p. 25-29) on lower Middle Devonian material from the Eifel area of Germany. **Pseudozonophyllum halli,** which became the type species of the genus by designation of Lang, Smith and Thomas (1940, p. 110), and **P. logani** have identical type stratum and locality in the lower Nohn Schichten, in a railway cutting near Ahütte in the Hillesheim Syncline (Birenheide, 1968, p. 15, 18), and are likely to be conspecific. Birenheide (1964, p. 21) also considered them to be junior subjective synonyms of the species named **Cyathophyllum antilimbatum** by Quenstedt (1879, p. 467; 1881, Pl. 158, two views designated fig. 40). **Pseudozonophyllum clarkei** is possibly another synonym of **Cyathophyllum antilimbatum,** but the precise stratigraphic and geographic origin of the unfigured type specimen are unknown, and the specimen is lost (Birenheide, 1968, p. 5). On the basis of Wedekind's (1924, figs. 28-33) figures of **Pseudozonophyllum halli** and **P. logani,** and Birenheide's (1964, Pl. 4, figs. 5-7; Pl. 5, fig. 16; Pl. 17, figs. 82, 83; Pl. 18, figs. 84, 85) illustrations of **Cyathophyllum antilimbatum,** the

type species of **Pseudozonophyllum** appears to have relatively few septal spines that are not fused appreciably in adult stages to form lamellar septa. As such, it is a species of **Cystiphylloides** Chapman (1893, p. 46), as that genus was interpreted by McLean (1976b, p. 3-10) and by Pedder and McLean (1982, p. 63-65). In contrast, Kravtsov's (1963, Pl. 8, fig. 4b) excellent illustration of a transverse section through the distal part of the holotype of **Pseudozonophyllum primitivum** shows abundant and well formed, although largely contiguous, septal crests.

Digonophyllum primitivum confertum subsp. n.

Plate 26.1, figures 1-5

Type series. Holotype, GSC 71183, GSC loc. C-12472. Paratype, GSC 71184, GSC loc. C-12472.

Diagnosis. Subspecies of **Digonophyllum primitivum** Kravstov distinguished by its smaller size (maximum diameter <20 mm in **D. primitivum confertum**; >30 mm in **D. primitivum primitivum**), narrower septal crests (about 60 major septa at 17 mm diameter in **D. primitivum confertum**; 54 major septa at 32 mm diameter in **D. primitivum primitivum**) and almost totally suppressed horizontal skeletal elements.

Description. Corallum ceratoid to trochoid, with maximum known length and diameter of about 30 mm and 18 mm, respectively. Exterior smooth except for extremely faint septal furrows and interseptal ridges. Growth rings subdued; rejuvenescences not evident on exterior surface of corallum. Calice about as deep as it is wide, with rounded, or rounded to subconical base.

Septal apparatus is so strongly developed that it excludes horizontal skeletal elements from all but the most distal part of the corallum. Peripherally and periaxially it comprises laterally contiguous monacanthate septal crests, arranged pinnately in the cardinal quadrants, and radially in the counter quadrants. Adaxially, the septal crests normally fuse with septal crust which fills the axial region of the corallum. Locally, below rejuvenescences of the skeletal apparatus, septal crust may be absent; figure 3 depicts a transverse section cut from such a level. The cardinal septum is situated on the convex side of the corallum. In transverse sections, minor septal crests appear as triangular wedges, confined to the peripheral region of the corallum. Major septal crests are of variable length, but even the shortest are considerably longer than the minor septal crests. There are about 52 major septal crests at a diameter of 9 mm, and about 60 at maturity (16-20 mm diameter).

Some specimens have neither dissepiments nor tabulae; others have a few small, peripherally situated dissepiments in the distal part of the corallum.

Remarks. The distinctive form of the new subspecies is not likely to be confused with either the nominate subspecies, or any other described species.

The name of the subspecies is the Latin adjective, **confertus**, meaning compressed, dense, crowded, etc., a reference to the septal morphology of the subspecies.

Occurrence. Known only from very high beds of the **inversus** Zone (Dalejan) of the Blue Fiord Formation, Sor Fiord section, southwestern Ellesmere Island.

Family HALLIIDAE Chapman, 1893
Subfamily HALLIINAE Chapman, 1893

Remarks. The question as to whether the Halliinae would be better assigned to the Plasmophyllidae Dybowski (1873, p. 340) is not given serious consideration here, because it cannot be properly answered without revision of several genera based on Silurian material from Europe.

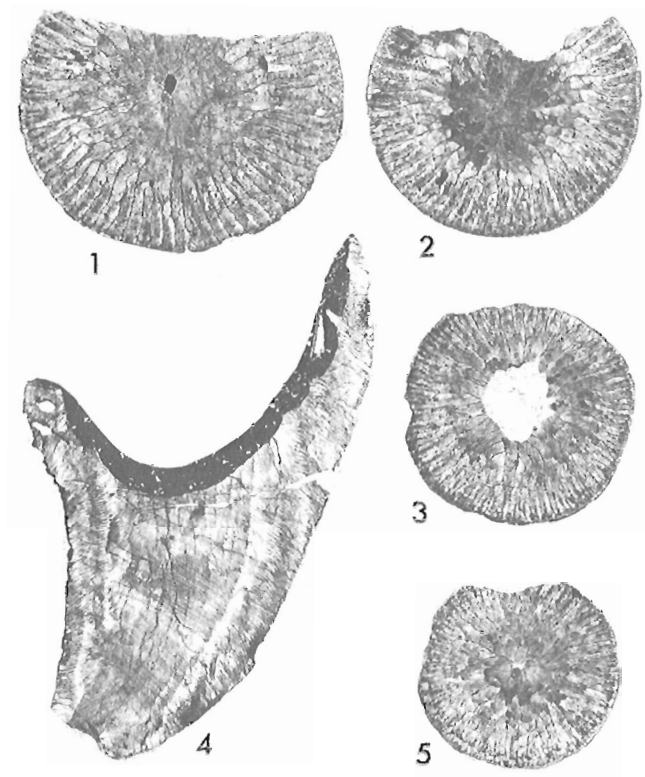

Plate 26.1

Figures 1-5. **Digonophyllum primitivum confertum** subsp. n.

1-3, 5. Holotype, GSC 71183, series of transverse thin sections, X3; GSC loc. C-12472.
4. Paratype, GSC 71184, longitudinal thin section, X3; GSC loc. C-12472.

Genus **Aulacophyllum** Milne Edwards and Haime, 1850

Aulacophyllum Milne Edwards and Haime, 1850, p. lxvii.
?**Pinnatophyllum** Grabau, 1917, p. 199 (nomen nudum).
?**Pinnatophyllum** Grabau, 1922, p. 13, 66.
?**Pinnatophyllum** Grabau ms. Bassett, 1935, p. 444.

Type species of **Aulacophyllum**. **Caninia sulcata** d'Orbigny, 1850, p. 105. Devonian; "Etats-Unis, failles de l'Ohio (Cincinnati), lac Erié". A lectotype for this species was chosen when Thevenin (1906, p. 196) wrote "ils (Milne Edwards and Haime) en ont décrit et figuré le type (Polyp. foss. des terr. paléoz., 1851, p. 355, Pl. VI, fig. 2)". Thevenin (1906, Pl. 21, figs. 29, 30) published beautiful figures of the exterior of this specimen and in the following year (Thevenin 1907, p. 89) stated that the specimen came from "l'Ohio". It is believed to have come from the Eifelian part of the Jeffersonville Limestone at the Falls of the Ohio, Louisville, Kentucky, or from bluffs on the north side of the Falls of the Ohio, which are in Indiana.

Type species of **Pinnatophyllum**. **Cyathophyllum scyphus**; authorship not specified, presumed to be Rominger, 1877, p. 103, Pl. 35, two right hand specimens of lower tier. Devonian, lower beds of Hamilton Group; Long Lake, north of Alpena, Michigan. According to Stumm (1951, card 70; 1963, p. 148), these specimens are from the lower part of the Genshaw Formation (Givetian). The upper specimen on Rominger's plate has been refigured, and chosen as lectotype, by Stumm (1963, Pl. 3, figs. 6, 7).

Diagnosis. Inadequately known ceratoid to trochoid halliid corals with long narrow cardinal fossula on convex side of corallum, and weakly to moderately well developed alar fossulae. Cardinal septum short. Septa in cardinal quadrants pinnately arranged; septa in counter quadrants radially arranged and, on the whole, shorter than those of the cardinal quadrants. Type species has few dissepiments and short minor septa. It is assumed that the septa are dilated in early stages and that during ontogeny the dilation decreases from periphery to axis, first in counter quadrants and later in cardinal quadrants (Stumm, 1963, p. 140, 141). It is also assumed that incomplete tabulae form broadly arched tabularial floors (Hill, 1981, p. 259). Fine septal structure is not known, but Thevenin's (1906, Pl. 21, fig. 29) excellent figure of the exterior of the lectotype of **Aulacophyllum sulcatum** shows no sign of either carinae, vepreculae, or denticles on the septa.

Remarks. Topotypic specimens of **Aulacophyllum sulcatum** are heavily silicified and interior structures have not been made known. Any interpretation of the genus must be tentative until this situation is rectified. The provisional interpretation adopted here is based largely on Stumm's (1965, p. 29) monography of the type species, with the reservation that specimens identified doubtfully by Stewart (1938, p. 31, Pl. 5, figs. 4-6) as **Odontophyllum convergens** (Hall), and accepted into the synonymy of **Aulacophyllum sulcatum** by Stumm, are likely to be specimens of **Hallia insignis** Milne Edwards and Haime.

The lectotype and paralectotype of **Pinnatophyllum scyphus** are unprepared silicified specimens. Figures of the lectotype show a narrow cardinal fossula, situated on the convex side of the corallum, enclosing a thin, moderately short, cardinal septum. Arrangement of the septa and development of alar fossulae are the same as in **Aulacophyllum sulcatum.**

Transverse and longitudinal sections of specimens, identified as **Aulacophyllum scyphus** (Rominger), have been figured from the Ferron Point Formation (also Givetian) of Alpena County, Michigan, as well as from the lower Genshaw Formation. Those from the Ferron Point Formation (Stumm, 1963, Pl. 8, figs. 2-5) appear to match the lectotype, whereas those from the Genshaw Formation (Stumm, 1963, Pl. 7, fig. 1; Pl. 8, figs. 6, 7) do not. This is surprising, because the latter come from roadside ditches at the south end of Long Lake, which must be close to the type locality. Transverse sections of the Ferron Point material reveal distinct pinnate symmetry and greater adaxial septal dilation in the cardinal quadrants than in the counter quadrants. The only longitudinal section of the Ferron Point material shows elevated tabularial surfaces. In contrast, Stumm's figures of Genshaw material display little evidence of either fossulae or septal dilation. Furthermore, tabularial surfaces are distinctly depressed in the distal part of the figured longitudinal section.

Grabau did not figure or formally describe **Pinnatophyllum** in 1922, but his brief statement on page 66 satisfies articles 11, 12 and 16 of the International Code of Zoological Nomenclature, which are the only requirements necessary to validate a genus-group name published before 1931. This is a point of note, because Bassett (1935, p. 444-446) published excerpts from a manuscript by Grabau, that purport to establish **Pinnatophyllum** as a new genus, based on **P. dundeense** Grabau ms. from the Eifelian Dundee Limestone of Michigan. The assumption, made here, that **Pinnatophyllum** Grabau, 1922, and **Pinnatophyllum** Grabau in Bassett, 1935, are conceptually the same, despite differences in type species, is supported by the inclusion of a form called **Pinnatophyllum scyphus** from the Traverse Group, which is presumed to be **Cyathaophyllum scyphus** Rominger, 1877, in **Pinnatophyllum** Grabau in Bassett, 1935.

Bassett's (1935, Pl. 34, figs. 1-4) illustrations include good figures of transverse and longitudinal thin sections of **Pinnatophyllum dundeense.** The transverse section reveals prominent cardinal and alar fossulae, a cardinal septum that is short but longer than the adjacent major septa, and strong dilation of all septa in the cardinal quadrants. It also shows the septa of the cardinal quadrants to be pinnate about the cardinal/counter plane, and those of the counter quadrants to be radial in arrangement. The longitudinal section shows a narrow dissepimentarium with numerous small dissepiments, and a flat to slightly elevated tabularium. In the proximal region of the corallite, septa of both quadrants appear to be strongly dilated.

Genus **Thoulelasma** nov.

Type species. **Thoulelasma loewei** sp. n.

Diagnosis. Trochoid to ceratoid halliid corals with a moderately long cardinal fossula situated on the convex side of the corallum. Alar fossulae not developed. Septa of cardinal quadrants pinnate about a cardinal septum that is shorter than the neighboring major septa on either side of it. Septa radially arranged in counter quadrants. In early stages, septa inside the outermost row of dissepiments are dilated by coating with apparently structureless stereome; typically, the dilation is sufficient to bring adjacent septa in lateral contact with each other. In subsequent ontogeny, septal dilation is lost progressively in the usual halliid manner, that is, it reduces first in the counter quadrants. Trabeculae are fine and apparently monacanthate. Immediately inside the periphery, trabeculae make angles of more than 70° with the horizontal. This angle decreases progressively toward the axis, as far as the inner dissepimentarium, and then increases abruptly, before decreasing again, in the area of transition from dissepimentarium to tabularium. In late stages, some fibre fascicles project from the sides of the unthickened septa to form very short vepreculae. At first, the dissepimentarium typically comprises a single row of somewhat rhomboid shaped dissepiments; as septal dilation decreases, many rows of normal dissepiments are added. At maturity, tabularial surfaces are more or less flat, except for the depression in the cardinal fossula.

Remarks. Unprepared, but freely weathered silicified specimens of **Aulacophyllum** suggest that this essentially Eastern North Americas Realm genus does not have the same vepreculae-producing trabecular structure as **Thoulelasma.** In any event, the genera are distinguished by the absence of alar fossulae in **Thoulelasma.**

Moravophyllum, erected by Kettnerová (1932, p. 27-30, 79-81) for Givetian species from Czechoslovakia, is similar to **Thoulelasma,** but, in adult stages, has much finer septa that show no tendency to become vepreculate.

Bethanyphyllum was proposed by Stumm (1949, p. 18) before the interior morphology of the type species, which is **Cyathophyllum robustum** Hall (1877, Pl. 22, figs. 1-9, 14), was known. Since Stumm's proposal, thin sections of the type lot of **Bethanyphyllum robustum** have been prepared. W.A. Oliver, Jr. has kindly made available photographs of these and other sectioned specimens in his collection from the Givetian Centerfield Formation of New York. On the basis of these photographs, **Bethanyphyllum** is distinguished from **Thoulelasma** in having much more pronounced vepreculae and a periaxially elevated tabularium that forms a calical boss.

Houershanophyllum Yu and Liao in Kong and Huang (1978, p. 54) is based on **H. involutum** Yu and Liao in Kong and Huang (1978, p. 54, Pl. 17, figs. 1a-f) from the Eifelian Longdongshui Formation of Guizhou Province, China. Septal microstructure is not visible in published figures of the type species, and in the translation of the Kong and Huang (1978)

available to the present author, it is said, only, that the septa are "composed of feathery fascicles". The Canadian species most resembling **H. involutum** is **Zaphrentis mcfarlanei** Meek (1867, p. 83, Pl. 11, figs. 2-2b) from the Eifelian Hume Formation of northwestern District of Mackenzie. This species has coarse monacanthate trabeculae that are directed inwards from the periphery at a low angle to the horizontal. For the purpose of the present paper, this is assumed to be the essential trabecular morphology of **Houershanophyllum.** Other differences between **Houershanophyllum involutum** and **H. mcfarlanei,** and **Thoulelasma loewei,** are that the septa in the first two species are commonly, adaxially, both dilated and rotated somewhat, at maturity.

Oliver and Pedder's (1979) record of **Glossophyllum** in the Zlichovian (Dalejan Stage was not available when the work was prepared) of their area 1, which is western and arctic Canada and Alaska combined, was based on the initial identification of **Thoulelasma loewei** as a species of **Glossophyllum.** Birenheide (1978, p. 82-84) considered **Glossophyllum** Wedekind (1924, p. 76, 77) to be a junior synonym of **Ceratophyllum** Gurich (1896, p. 163). Both genera are based on inadequately known type species and cannot be used with certainty at present (Pedder, 1982a, p. 562-564). Provided Birenheide's interpretation of the genera is correct, it can be seen from his illustrations (Birenheide, 1978, Pl. 11) that **Thoulelasma** has a different early ontogeny, longer septa at maturity and a flatter tabularium.

The generic name is derived from the Greek words, **thoule,** meaning farthest north, and **elasma,** a plate. The elision is deliberate.

Thoulelasma loewei gen. et sp. n.

Plate 26.1, figures 6-10; Plate 26.1, figures 11-20

Glossophyllum; Oliver and Pedder, 1979, p. 240 (in part; column 1 occurrence only).
Glossophyllum; Pedder, 1982a, p. 564 (in part; Ellesmere Island specimens only).
Glossophyllum sp. nov.; Pedder and McLean, 1982, p. 80.

Type series. Holotype, GSC 68839, GSC loc. C-12473. Paratypes, GSC 68840-68843, GSC loc. C-12473; GSC 68844, GSC loc. C-12472.

Diagnosis. Only known species of **Thoulelasma.**

Description. Corallum solitary, mostly ceratoid, less commonly trochoid. Length of largest specimen (GSC 68842) before preparation, 9.5 cm measured over the exterior of the most convex part of the corallum, 7.5 cm measured from proximal tip to the centre of the plane enclosed by the lip of the calice. Greatest diameter 3.9 cm. Adult calice 2.0 to 2.5 cm deep and bell-shaped. Unabraided exterior surfaces of the corallum bear narrow, shallow septal furrows, broad, flat interseptal ridges and fine growth rings. Typically, reductions of diameter due to rejuvenescences are small.

A distinct cardinal fossula, that normally extends a little more than one half of the distance from the periphery to the axis of the coral, is situated slightly to one side of the line of greatest convex curvature of the corallum. In the cardinal quadrants, septa are pinnately arranged about the cardinal/counter plane. In the counter quadrants the arrangement is radial. Despite these differences, and because the cardinal fossula does not reach the axis, alar fossulae are either not present, or are extremely indistinct. Major septa are long, and many extend to the axial region, especially on the upper surfaces of certain tabularial surfaces. The cardinal septum, although prominent, is shorter than neighboring major septa. The counter septum is normally longer than the major septa next to it. In early stages of development, minor septa are mostly about one third to two fifths as long as the major septa; in later ontogeny, their length increases to about half that of the major septa. Minor septa are commonly much reduced, or absent, in the cardinal fossula, especially in early stages. The earliest pattern of septal development is not known. At a diameter of 8 to 9 mm there are about 26 major septa, and at 12 mm diameter there are about 30 major septa. At 15 mm diameter the number of major septa has increased to about 33. At 20 and 25 mm diameter the numbers of major septa are about 40 and 45, respectively. In these early stages, some or all of the septa inside the outermost dissepiments are dilated. Commonly the dilation is sufficient to fill all but the most peripheral region of the corallum. If the degree of septal dilation is less, it is invariably greater in the cardinal than in the counter quadrants. Much of the early dilation of the septa is caused by apparently structureless stereome. Where adjacent septa are not contiguous, stereome extends over dissepimentarial surfaces between neighboring septa. As the diameter increases beyond 25 mm, septal dilation ceases to be more pronounced in the cardinal quadrants, and in both pairs of quadrants is confined to the tabularium. At 30 mm diameter there are 48 or 49 major septa. The full adult count of 50 to 54 major septa is attained at a diameter of about 35 mm. At maturity, there is virtually no septal dilation, even in the tabularium.

Fine septal structure is partly obscured by recrystallization. Trabeculae are apparently finely monacanthate, and are unusual, in that some fibre fascicles project from the plane of the septum, where there is no stereome, to produce incipient vepreculae. Because they are so short, the vepreculae are seen best in longitudinal sections, such as the one shown in figure 10. Next to the periphery, the trabeculae are vertical, or nearly so. Adaxially they become progressively more inwardly inclined in the dissepimentarium, but return to a more erect attitude in the outer tabularium.

A single row of small rhomboid shaped dissepiments appears as the corallum attains a diameter of 3 to 5 mm. Globular, inwardly inclined dissepiments are added as the corallum enlarges, so that, at maturity, the dissepimentarium typically comprises 15 to 20 rows of dissepiments. Some of the inner dissepiments are elongate, although most are small. The transition from dissepimentarium to tabularium is not well defined. Tabulae are vesicular, sinuous as viewed in longitudinal section, or flat; only very rarely are they complete. Tabularial surfaces tend to be elevated around the margin of the tabularium, and are either flat or somewhat depressed axially and periaxially.

Remarks. **Thoulelasma loewei** bears some resemblance to a form described as **Aulacophyllum sulcatum** d'Orbigny by Lavrusevich (1971b, p. 48, 49, Pl. 10, figs. 1a-3b), from the Lochkovian Kshtut Horizon of Tyan' Shan, as well as to the species **Desmophyllum densatoseptatum** Goryanov in Bul'vanker et al. (1968, p. 30, Pl. 12, figs. 1a-v), from the Pragian Talbulak Horizon of the same region, and **Aulacophyllum trizonatum** Hill (1942, p. 160, Pl. 3, figs. 10-12), from Dalejan levels in the Sulcor Limestone of New South Wales.

Aulacophyllum sulcatum of Lavrusevich (1971b) and **Desmophyllum densatoseptatum** are likely to be conspecific. They are larger (diameter as much as 6.0 cm in **A. sulcatum**) than **Thoulelasma loewei,** and have a relatively narrower dissepimentarium with no more than ten rows of dissepiments. Their cardinal fossula is longer and more profoundly affects the tabularial morphology. In both forms, counter septa are weakly pinnate about a shortened counter septum. Fine septal structure has not been figured or described in any of the Tyan' Shan material, but does not appear to be vepreculate.

Aulacophyllum trizonatum is also larger (greatest observed diameter 5.0 cm) than **Thoulelasma loewei,** and has a narrower dissepimentarium, comprising less than ten rows of dissepiments. Unlike **T. loewei,** its counter septum is much shorter than the major septa on either side of it, and its tabularium is strongly elevated to form a prominent calicular boss. The septal microstructure of **A. trizonatum** has not yet been described, but is dissimilar from that of **T. loewei,** in that it does not seem to produce vepreculae.

The trivial name of the new species is a patronym dedicated to Stephan Loewe, in recognition of his work on Per Schei's Devonian corals from Ellesmere Island.

Occurrence. Known only from very high beds of the **inversus** Zone (Dalejan) of the Blue Fiord Formation, Sor Fiord section, southwestern Ellesmere Island.

Family COLUMNARIIDAE Nicholson, 1879

Remarks. Classifications by Pickett (1967), Jell (1969), Birenheide (1978) and Hill (1981) of **Disphyllum** and related Devonian genera differ remarkably. Large collections, not available to previous authors, of several key genera, including **Planetophyllum, Utaratuia, Zelolasma** and **Tropidophyllum,** have been studied in connection with the present work. These studies suggest that none of the classifications alluded to above is entirely satisfactory. Appraisal of all the family- and genus-group names involved is neither possible, nor within the scope of this article. Nevertheless, seven measures regarding family-level classification are adopted, which lead to a new classification of the Columnariidae.

These measures are: 1) The family Columnariidae, which in Birenheide's (1978) work was demoted to subfamily rank within the Cyathophyllidae, is retained at full family rank. 2) The family Disphyllidae, which in Hill's (1981) classification stands apart from the Columnariidae, is merged in the Columnariidae. 3) The subfamily Spongonariinae, which was apparently overlooked by Birenheide (1978) and was regarded by Hill (1981) as a subfamily of the Disphyllidae, is transferred to the Columnariidae. 4) The family Utaratuiidae, which was proposed on the mistaken belief that its type genus is a colonial cystimorph (see Pedder and McLean, 1982) is relegated to subfamily rank within the Columnariidae. 5) A new subfamily is proposed for **Spongonaria**-like genera that have arched dissepiments or dissepimentarial surfaces. Genera referred to this subfamily had been assigned, previously, to the Phillipsastreidae by Pickett (1967), to the Disphyllinae of the Phillipsastraeidae by Jell (1969), to the Zaphrentinae and Neocolumnariinae of the Cyathophyllidae by Birenheide (1978), and to the Spongonariinae of the Disphyllidae by Hill (1981). 6) The subfamily Paradisphyllinae, which was assigned to the Phillipsastraeidae by Jell (1969), was synonymised with the Cyathophyllinae in the Cyathophyllidae by Birenheide (1978), and classified in the Disphyllidae by Hill (1981), is removed to the Columnariidae. 7) The Marisastridae, which was demoted to a subfamily of the Phillipsastraeidae by Jell (1969), merged in the Columnariinae of the Cyathophyllidae by Birenheide (1978), and placed under the Hexagonariinae of the Disphyllidae by Hill (1981), is synonymised with the Hexagonariinae, and tentatively retained as a subfamily of the Columnariidae. Jell (1969) placed the type genus of the Hexagonariidae in the Disphyllinae of the Phillipsastraeidae.

The subfamily classification of the Columnariidae that emerges from these measures is as follows.

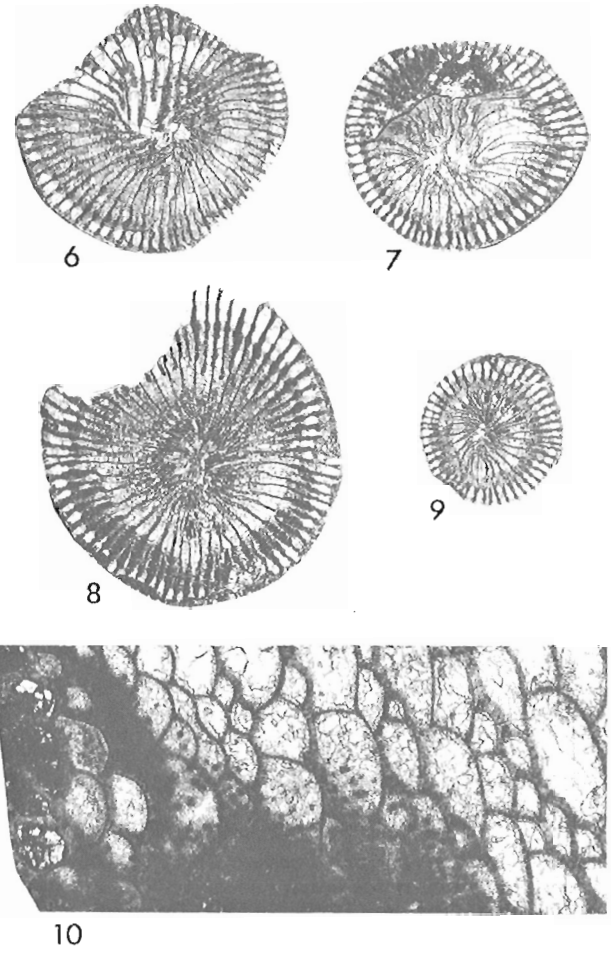

Plate 26.1 (cont.)

Figures 6-10. **Thoulelasma loewei** gen. et sp. n.

6, 7, 9. Paratype, GSC 68843, series of transverse thin sections of a specimen with early rejuvenescence, X2; GSC loc. C-12473.
8. Paratype, GSC 68842, transverse thin section, X2; GSC loc. C-12473.
10. Paratype, GSC 68841, part of longitudinal thin section showing incipient vepreculae, X10; GSC loc. C-12473.

Figures 11-20. **Thoulelasma loewei** gen. et sp. n.

11, 14, 16. Paratype, GSC 68841, two transverse and a longitudinal thin section, X2; GSC loc. C-12473.
12, 17. Holotype, GSC 68839, transverse and longitudinal thin sections, X2; GSC loc. C-12473.
13, 20. Paratype, GSC 68842, longitudinal and transverse thin sections, X2; GSC loc. C-12473.
15. Paratype, GSC 68840, transverse thin section, X2; GSC loc. C-12473.
18, 19. Paratype, GSC 68844, longitudinal and transverse thin sections, X2: GSC loc. C-12472.

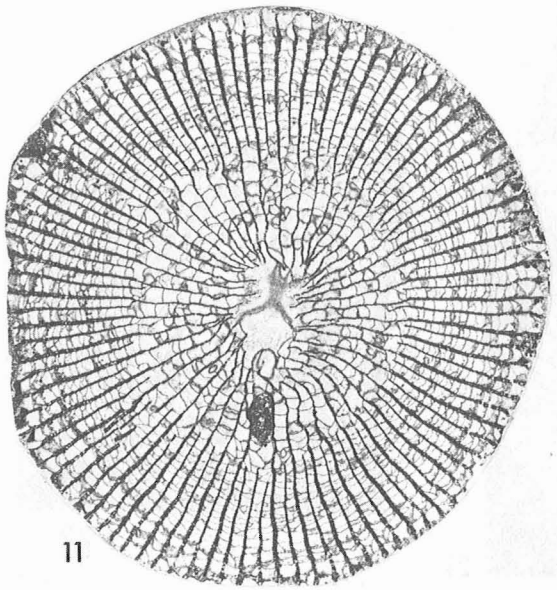

11

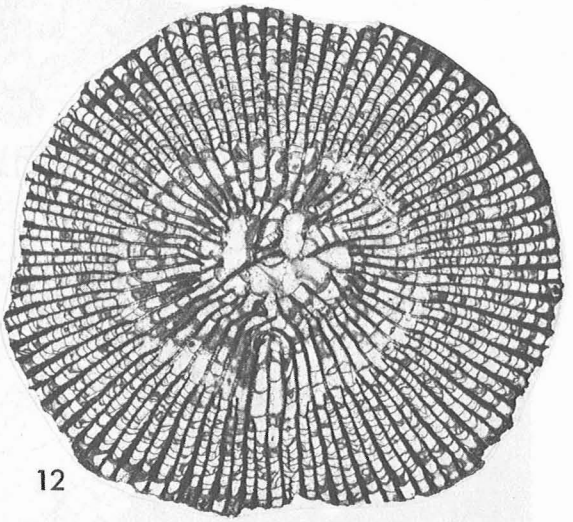

12

13

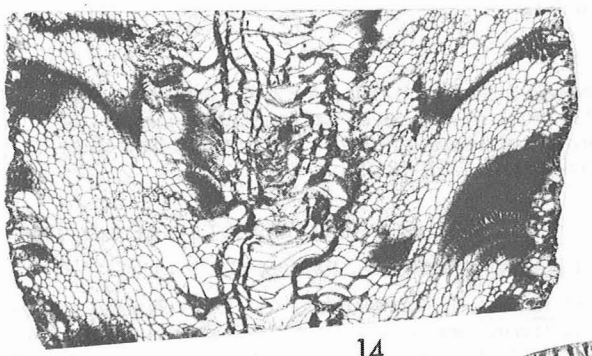

14

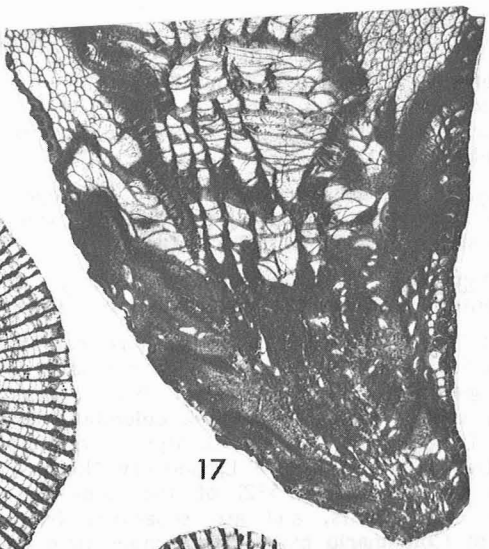

17

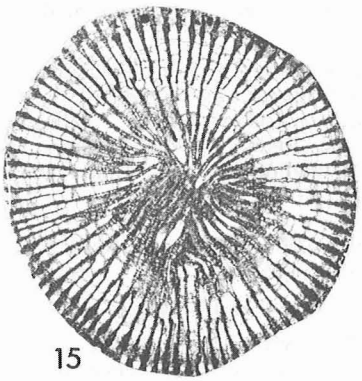

15

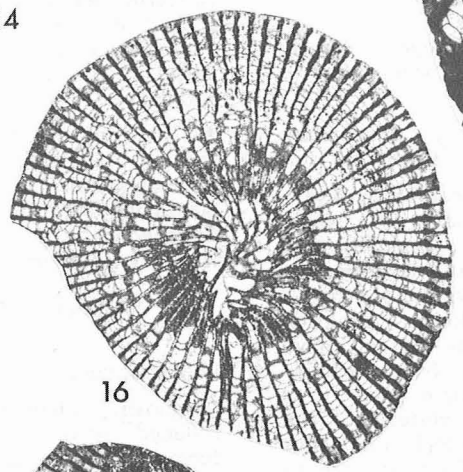

16

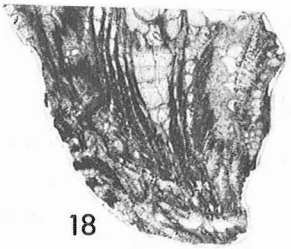

18

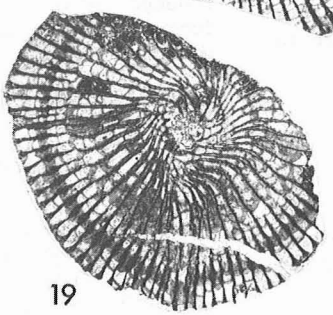

19

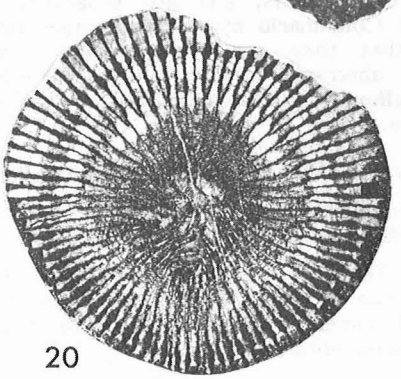

20

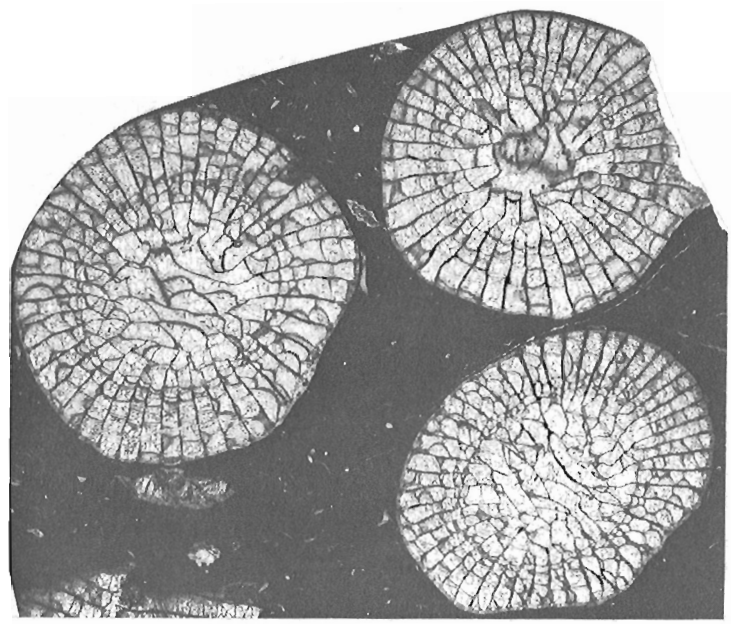

21

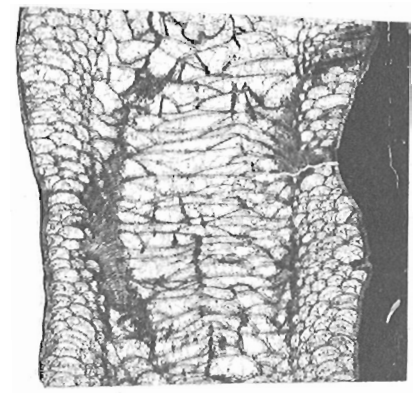

22

Plate 26.1 (cont.)

Figures 21, 22. **Paraspongonaria sverdrupi** (Loewe) gen. n.

Paratype?-previously unprepared specimen, Paleontological Museum, Oslo, A 12097, transverse and longitudinal thin sections, X3; Db Series of Schei (1903; 1904), now believed to be a Zlichovian part of the Blue Fiord Formation; Vestre Borgen, Goose Fiord, southwestern Ellesmere Island. Collected by Per Schei, geologist on the second Norwegian Polar Expedition, 1898-1902.

Subfamily COLUMNARIINAE Nicholson, 1879

Columnariadae Nicholson, 1879, p. 17, 18.
Disphyllidae Hill, 1939, p. 224.
Columnariidae Hill, 1939, p. 240 (correction of original spelling).

Diagnosis. Columnariidae with well developed, lightly carinate major septa, and small dissepiments forming flat to inwardly sloping dissepimentarial surfaces.

Assigned genera. **Columnaria** Goldfuss, **Disphyllum** deFromentel, **Pseudocampophyllum** Ivanovskiy, **Disphyllia** He.

Remarks. The species **Spongophyllum pax**, named by Smith (1945, p. 56, 57, Pl. 11, figs. 6a-c) on the basis of a single boulder specimen from Peace River, British Columbia, and the very similar form, **Columnaria columbia**, described by Norford (1962, p. 28, 29, Pl. 10, figs. 1, 2; Pl. 11, fig. 1; Pl. 12, fig. 1) from the late Llandovery Nonda Formation (Norford et al., 1966, p. 512) of the same region, have elongate dissepiments, and are separated from definite species of **Columnaria** by a considerable time gap. It is possible that they are phylogenetically closer to the seemingly aberrant, Middle Silurian, entelophyllid genus **Strephophyllum** Lavrusevich (1971a, p. 77), than they are to **Columnaria.**

Subfamily HEXAGONARIINAE Bul'vanker, 1958

Hexagonariidae Bul'vanker, 1958, p. 178.
Marisastridae Różkowska, 1965, p. 261, 262.

Diagnosis. Tentatively recognized subfamily of the Columnariidae with long, strongly carinate, slightly fusiform septa, and numerous small dissepiments that form gently arched dissepimentarial surfaces.

Assigned genera. **Hexagonaria** Gürich (includes **Marisastrum** Różkowska), **Hapolothecia** Frech, **Spinophyllum** Wedekind.

Subfamily PARADISPHYLLINAE Jell, 1969

Paradisphyllinae Jell, 1969, p. 67.

Diagnosis. Columnariidae with variably carinate and fusiforme septa, numerous small dissepiments forming gently arched to prominently everted dissepimentarial surfaces, and a tabularium that is commonly differentiated into an inner series of elevated plates, and an outer series of downturned and depressed plates.

Assigned genera. **Paradisphyllum** Strusz, **Radiastraea** Stumm (possibly a polyphyletic genus as currently interpreted) **Tipheophyllum** Hill, **Gurievskiella** Zheltonogova, **Martinophyllum** Jell and Pedder, **Ivdelephyllum** Spasskiy, **Xystrigona** Yu, **Xystriphylloides** Yu, Liao and Deng, **Xiangzhouphyllum** Yu and Kuang.

Subfamily UTARATUIINAE Spasskiy, Kravtsov and Tsyganko, 1975 [1]

Utaratuiidae Spasskiy, Kravtsov and Tsyganko, 1975, p. 171.

Diagnosis. Columnariidae with considerably to greatly reduced major septa and moderately large dissepiments forming a moderately wide and inwardly sloping dissepimentarium.

Assigned genera. **Utaratuia** Crickmay, ?**Breviseptophyllum** Ermakova.

Subfamily TROPIDOPHYLLINAE nov.

Diagnosis. Columnariidae with adaxially withdrawn and variably carinate septa formed of subparallel to weakly divergent monacanths. Adaxial terminations of septa are commonly dilated and spinose; short, isolated septal spines are also commonly developed on tabularial surfaces. Dissepimentarium slightly to moderately everted at some levels, even in forms having only one row of dissepiments. Tabulae broad, commonly quite, or almost, complete.

Assigned genera. **Tropidophyllum** Pedder (1971, p. 374-376) (type genus), **Zelolasma** Pedder, **Variseptophyllum** Kong.

Remarks. Corals interpreted as primitive species of **Zelolasma** are known from rocks of Ludlow age in New South Wales and the western slopes of the southern Urals, and from Middle or Upper Silurian beds in the Kolyma River regions of northeast Soviet Union (references given by McLean, 1976a, p. 187, 188). These would be the oldest known members of the family Columnariidae, if the British Columbian species, currently referred to **Columnaria**, are members of the Entelophyllidae, as discussed in the remarks concerning **Columnaria**.

Subfamily SPONGONARIINAE Crickmay, 1962

Spongonariinae Crickmay, 1962, p. 2.

Diagnosis. Columnariidae with septa that are thin, notably in the outer dissepimentarium, and vary considerably in length. If present in the tabularium, septa there are typically undulant, or largely reduced to discrete, ribbon-like fragments. Septa are also commonly undulant in the inner dissepimentarium, and in one genus (**Exilifrons**) bear mostly weak, zig-zag carinae. Dissepiments large relative to size of corallite, forming inwardly sloping to flat, or only slightly arched, dissepimentarial surfaces.

Assigned genera. **Spongonaria** Crickmay, **Planetophyllum** Crickmay, **Exlifrons** Crickmay (includes **Pinyonastraea** Merriam), **Paraspongonaria** gen. n.

Remarks. Crickmay proposed the Spongonariinae as a subfamily of the Silurian family Acervulariidae, and diagnosed it simply as "acervulariids with diminished septa". The proposal was not supported by discussion of any kind, nor was indication given as to whether any genus, other then the newly erected **Spongonaria**, was to be included in the subfamily.

Subsequently, the family-group name was abandoned by its author (Crickmay, 1968, p. 1), and has been overlooked or disregarded by most other workers, exceptions being Hill (1981, p. 276-280), who regarded it as a subfamily of the Disphyllidae, and Pedder and McLean (1982, p. 76), who placed it in the Cyathophyllidae, used in a broad sense.

Systematic treatment of the type genus has also varied considerably since it was first erected. Latypov (in Besprozvannykh et al., 1975, p. 42) is the only worker to have both accepted it as a valid genus and retained it in its original family. Jell (1969, p. 70, misspelled **Spongaria**) regarded it as a doubtful representative of the Phillipsastraeidae, broadly interpreted. Birenheide (1978, p. 90) questionably synonymized it with **Disphyllum** in the subfamily Columnariinae and family Cyathophyllidae, broad sense. Kong and Huang (1978, p. 61, 62) recognized it as a valid genus in the family Columnariidae, but included in it a form, identified as **Spongonaria parallexa** (Glinski), that seems certain to be a columnariinid.

Genus **Paraspongonaria** nov.

New genus 34; Oliver and Pedder, 1979, p. 242.

Type species. **Paraspongonaria delicata** sp. n.

Diagnosis. Phaceloid to locally subcerioid genus of spongonariinid corals with adaxial ribbon-like septal fragments and a narrow dissepimentarium of two or more rows of dissepiments.

Description. Corallum phaceloid; corallites cylindrical, locally in contact, although the growth form is never cerioid. Budding marginarial and nonparricidal.

Outer wall thin, but continuous. Septa radially arranged, smooth and thin. Trabeculae, if present, exceedingly slender. Major septa lamellar in the dissepimentarium and the outer region of the tabularium, reduced to ribbon-like fragments adaxially. Minor septa lamellar in the dissepimentarium, mostly absent from the tabularium, represented locally there by rare ribbon-like fragments.

Dissepimentarium narrow. Outer dissepiments moderate size, flat lying, or only slightly inwardly inclined; inner dissepiments smaller and more steeply inclined. Tabularium well differentiated from the dissepimentarium, comprises peripheral tabellae, and axial and periaxial tabulae.

Remarks. **Paraspongonaria** is closely allied to **Spongonaria** Crickmay (1962, p. 2) and probably also to **Planetophyllum** Crickmay (1960, p. 4). The first of these genera is typified by **Spongonaria filicata** Crickmay (1962, p. 2, 3, Pl. 1, figs. 1, 2; Pl. 3, figs. 6, 7), whose type horizon is known now to be in the Zlichovian/Dalejan Landry Formation of the Mackenzie Mountains, northwestern District of Mackenzie. The type and only named species of the second genus is **Planetophyllum planetum** Crickmay (1960, p. 4, Pl. 1, figs. 1-5) from the Zlichovian/Dalejan Fitzgerald Formation of northeastern Alberta. Differences between these genera and **Paraspongonaria** are that **Spongonaria** is cerioid, and **Planetophyllum** is solitary, lacks septal fragments and has a discontinuous dissepimentarium, typically comprising only a single row of dissepiments.

In addition to the type species, **Cyathophyllum sverdrupi** Loewe (1913, p. 11, Pl. 1, fig. 3; Pl. 2, figs. 4a, b) from Schei's (1903; 1904) Db Series (now considered to be Zlichovian, Blue Fiord Formation) of the Goose Fiord region of southwestern Ellesmere Island, is referred to the new genus. It is refigured in Plate 26.1, figures 21 and 22 of the present work.

The name **Paraspongonaria** is compounded from the Greek prefix **para-**, meaning close to, and the genus name **Spongonaria**.

Paraspongonaria delicata sp. n.

Plate 26.1, figures 23-30

Phaceloid species of **Spongonaria**; Pedder and McLean, 1982, p. 59.

Spongonaria(?) sp. nov. (phaceloid form); Pedder and McLean, 1982, p. 80.

Type series. Holotype, GSC 68648, GSC loc. C-12473. Paratype, GSC 68649, GSC loc. C-76823.

Diagnosis. Species of **Paraspongonaria** in which adult corallites have diameters of 8.5 to 10.0 mm, 16x2 to 20x2 septa, abundant septal fragments, and a narrow dissepimentarium, mostly comprising two or three rows of dissepiments.

Description. Corallum large, consisting of many free and loosely attached, long cylindrical corallites, produced by nonparricidal, marginarial budding. Corallites normally produce only one offset at a time; new corallites rapidly enlarge to their full adult diameter of 8.5 to 10.0 mm. Adult calice about 5 mm deep, with steep sides and a broad, low calical boss. Exteriors of corallites bear fine growth rings. Septal furrows and interseptal ridges are not visible on most corallites. Where they are present, the septal furrows are finer than the growth rings, and the interseptal ridges are flat.

The outer wall is consistently only 0.05 to 0.25 mm thick. Apart from some dilation at the periphery, the septa, which are radially arranged and number 16x2 to 20x2 in

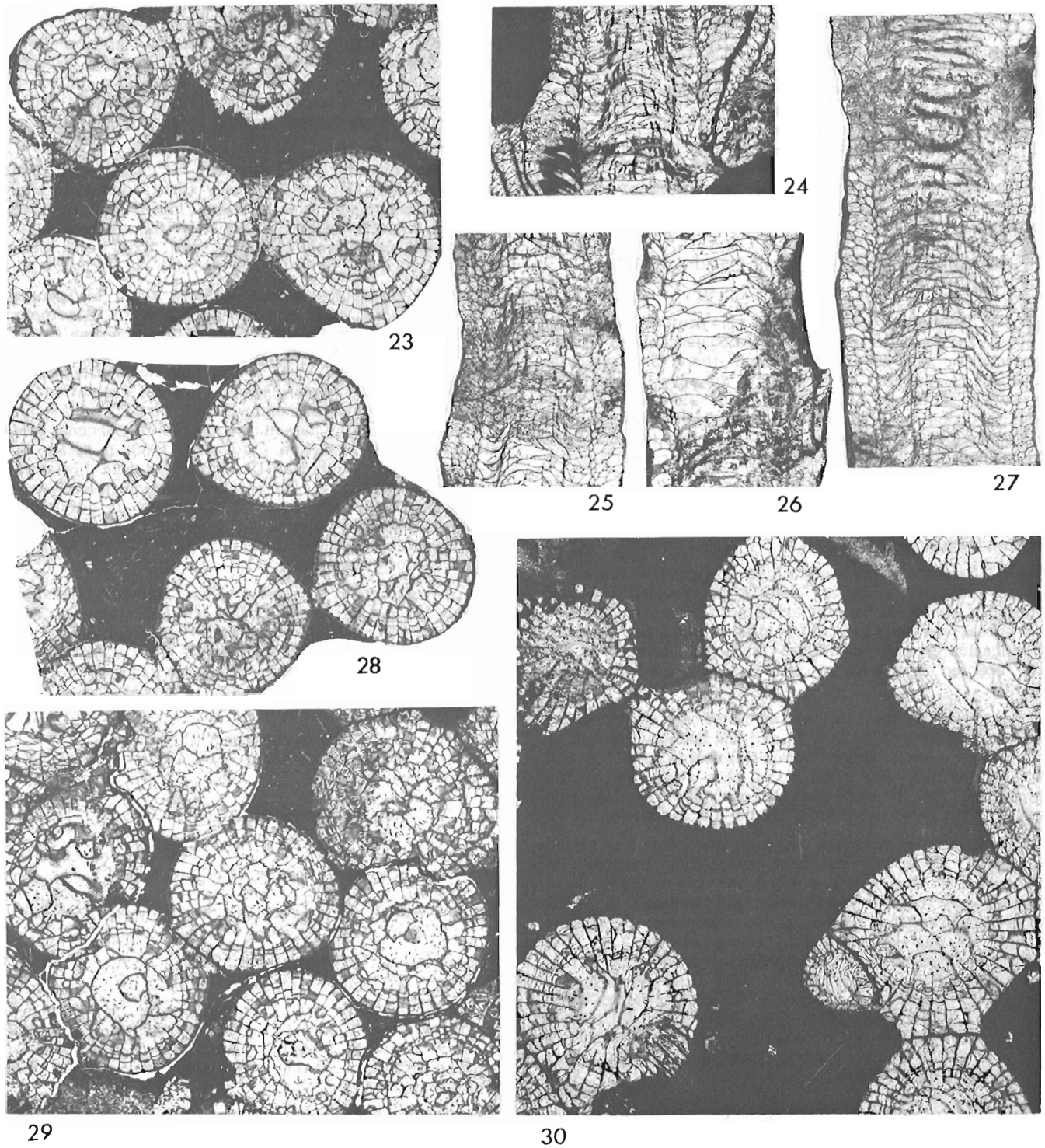

Plate 26.1 (cont.)

Figures 23-30. **Paraspongonaria delicata** gen. et sp. n.

23, 25-29. Holotype, GSC 68648, three transverse and three longitudinal thin sections, X3; GSC loc. C-12473.
24, 30. Paratype, GSC 68649, longitudinal and transverse thin sections, X3; GSC loc. C-76823.

mature corallites, are extremely thin and lack carinae. Most major and minor septa are continuous lamellae in the dissepimentarium; a few are withdrawn from the periphery, or have gaps in them. Minor septa typically only just penetrate the tabularium. The lamellar parts of the major septa are a little longer than the minor septa. Most of the ribbon-like septal fragments in the tabularium are remnants of major septa. The longest septal remnants pierce ten or more tabularial surfaces. Third order septa, represented by low ridges, occur in some corallites. Fine septal structure is not well preserved in the type series. Trabeculae, if present, are extremely fine.

Dissepiments appear early in the development of an offset, and in fully grown corallites, are generally arranged in two or three rows. Locally, this number is reduced to one, or increased to four, rarely as many as five rows. Outer dissepiments are flatter and larger than the innermost ones, which may be very small and steeply inclined towards the axis. Diameter of adult tabularium normally between 7 and 8 mm. Tabularia and dissepimentaria are clearly differentiated from each other. The predominantly incomplete tabulae form broadly elevated tabularial surfaces with sharply rounded peripheral shoulders.

Remarks. **Paraspongonaria sverdrupi** is a similar, slightly older Zlichovian species. It differs from **P. delicata** in being larger (corallite diameter as much as 14.5 mm), having more septa (as many as 22x2). Furthermore, the septa are less fragmented.

The trivial name is the Latin adjective, **delicatus,** meaning dainty, delicate, etc., and refers to the fine skeletal structure of the coral.

Occurrence. **Serotinus** and possibly the topmost **inversus** Zones (Dalejan), Blue Fiord Formation, Sor Fiord and Vendom Fiord regions of southern Ellesmere Island.

Locality Register

GSC loc. C-12472. Blue Fiord Formation, 905.9-908.0 m above base of section, 154.6-157.7 m below top of formation; Dalejan (incoming of **Polygnathus serotinus** 915.9 m above base of section). Sor Fiord section, southwestern Ellesmere Island, District of Franklin; base of section 77°17'12"N latitude, 85°07'00" W longitude; top of section 77°15'48"N latitude, 85°03'30"W longitude. Collected by A.E.H. Pedder, 1971. **Favosites** sp. cf. **F. goldfussi** sensu Jell and Hill (1970) infested with **Streptindytes** sp., **Digonophyllum primitivum confertum** Pedder, **Thoulelasma loewei** Pedder, biaxial crinoid ossicles.

GSC loc. C-12473. Blue Fiord Formation, 911.6-914.0 m above base of section, 148.6-151.0 m below top of formation; Dalejan (incoming of **Polygnathus serotinus** 915.9 m above base of section). Same section as above., Collected by A.E.H. Pedder, 1971. **Stellarispongia aspera** Rigby, **Favosites** sp., **Mariusilites** sp., **Lekanophyllum pustulosum** Pedder and McLean, **Thoulelasma loewei** Pedder, **Paraspongonaria delicata** Pedder, **Warrenella franklini praefranklini** Brice transverse form, **Ozarkodina** sp., **Pelekysgnathus** sp. nov., single axis and biaxial crinoid ossicles [conodonts (GSC loc. C-12474) collected and identified by Gilbert Klapper from 0.3 m above base of C-12473].

GSC loc. C-76823 and C-76831 (two numbers assigned to same collection). Blue Fiord Formation, 311 m above base of upper siltstone and carbonate member, 58 m below top of upper siltstone and carbonate member (i.e. 58 m below top of formation and base of Strathcona Fiord Formation); Dalejan, **serotinus** Zone. Northwest side of Vendom Fiord, 6.3 km from mouth, southern Ellesmere Island, District of Franklin; 77°32'30"N latitude, 83°45'30"W longitude. Collected by R.F. Roblesky, 1977. **Favosites** sp., **Alveolites** sp., **Roemeripora** sp., **Paraspongonaria delicata** Pedder, **Athyrhynchus sverdrupi** (Meyer), **Atrypa** sp., **Warrenella** sp., **Orthonychia** sp., ostracode and trilobite fragments, single axis and biaxial crinoid ossicles.

References

Bassett, C.F.
1935: Stratigraphy and paleontology of the Dundee Limestone of southeastern Michigan; Geological Society of America Bulletin, v. 46, p. 425-461.

Bassler, R.S.
1950: Faunal lists and descriptions of Paleozoic corals; Geological Society of America, Memoir 44, 315 p.

Besprozvannykh, N.I., Dubatolov, V.N., Kravtsov, A.G., Latypov, Yu. Ya., and Spasskiy, N. Ya.
1975: Devonskie rugozy Taymyro-Kolymskoy provinstii; Akademiya Nauk SSSR, Sibirskoe Otdelenie, Instituta Geologii i Geofiziki, Trudy, vyp. 228, 172 p.

Birenheide, R.
1964: Die "Cystimorpha" (Rugosa) aus dem Eifeler Devon; Senkenbergischen Naturforschenden Gesellschaft, Abhandlungen, 507, p. 1-120.

1968: Die Typen der Sammlung Wedekind aus der Gattung **Plasmophyllum** (Rugosa; Mitteldevon); Senckenbergiana lethaea, Band 49, p. 1-37.

1978: Leitfossilien. No. 2. Rugose Korallen des Devon; Gebrüder Borntraeger, Berlin, Stuttgart, 265 p.

Bul'vanker, E.Z.
1958: Devonskie chetyrekhluchevye korally okrani Kuznetskogo basseyna; Vsesoyuznyy Nauchno-Issledovatel'skiy Geologicheskiy Institut (VSEGEI), Leningrad, text 212 p. and atlas.

Bul'vanker, E.Z., Goryanov, V.B., Ivanovskiy, A.B., Spasskiy, N. Ya., and Shchukina, V. Ya.
1968: Novye predstaviteli chetyrekhluchevykh koral-lovykh polipov SSSR; in Novye vidy drevnikh rasteniy i bespozvonochnykh SSSR, vyp. 2, chast' 2, ed. B.P. Markovskiy; Vsesoyuznyy Nauchno-Issledovatel'skiy Geologicheskiy Institut (VSEGEI), Izdatel'stvo "Nedra", Moskva, p. 14-45, 304-343.

Castelnau, F. de
1843: Essai sur le systéme silurien de l'Amérique septentrionale; P. Bertrand, Parix, xv+56 p.

Chapman, E.J.
1893: On the corals and coralliform types of Palaeozoic strata; Royal Society of Canada, Proceedings and Transactions, v. 10, section 4, p. 39-48.

Cherkesova, S.V., Patrunov, D.K., Smirnova, M.A., Kuz'min, A.M., Kravtsov, A.G., and Nekhorosheva, L.V.
1968: Tareyskiy nizhnedevonskiy opornyy razrez (Tsentral'nyy Taymyr); Nauchno-Issledovatel'skiy Institut Geologii Arktiki, Uchenye Zapiski, Paleontologiya i Biostratigrafiya, vyp. 22, p. 5-35.

Crickmay, C.H.
1960: The older Devonian faunas of the Northwest Territories; Evelyn de Mille Books, Calgary, 21 p.

1962: New Devonian fossils from western Canada; Evelyn de Mille Books, Calgary, 16 p.

1968: Lower Devonian and other coral species in northwestern Canada; Evelyn de Mille Books, Calgary, 9 p.

Dybowski, W.N.
1873: Monographie der Zoantharia sclerodermata rugosa aus der Silurformation Estlands, Nord-Livlands und der Insel Gotland, nebst einer Synopsis aller palaeozoischen Gattungen dieser Abtheilung und einer Synonymik der dazu gehörigen, bereits bekannten Arten; Archiv für die Naturkunde Liv-, Ehst-und Kurlands, Ser. 1, Band 5, p. 257-414.

Grabau, A.W.
1917: New genera of corals of the Family of Cyathophyllidae (abstract); Geological Society of America, Bulletin, v. 28, p. 199.

1922: Palaeozoic corals of China. Part 1; Tetraseptata; Palaeontologia Sinica ser. B, v. 2, fascicle 1, p. 1-76.

Gürich, G.
1896: Das Palaeozoicum des Polnischen Mittelgebirges; Imperatorskago S.-Peterburgskago Mineralogicheskago Obshchestva, Zapiski, ser. 2, chast' 32, p. i-iv, 1-539.

Hall, James
1877: Illustrations of Devonian fossils: Gasteropoda, Pteropoda, Cephalopoda, Crustacea and corals of the Upper Helderberg, Hamilton and Chemung Groups; Geological Survey of the State of New York, Albany, 7 p. (imprint, 1876).

Hill, D.
1939: The Devonian rugose corals of Lilydale and Loyola, Victoria; Royal Society of Victoria, Proceedings, new ser., v. 51, p. 219-256.

1942: The Devonian rugose corals of the Tamworth district, N.S.W.; Royal Society of New South Wales, Journal and Proceedings, v. 76, p. 142-164.

1981: Treatise on invertebrate paleontology. Part F. Coelenterata. Supplement 1. Rugosa and Tabulata, ed. Curt Teichert; Geological Society of America, Inc. and the University of Kansas, Boulder and Lawrence, v. 1, p. i-xl, 1-378, v. 2, p. i, ii, 379-762.

Jell, J.S.
1969: Septal microstructure and classification of the Phillipsastraeidae; in Stratigraphy and Palaeontology. Essays in honour of Dorothy Hill, ed. K.S.W. Campbell; Australian National University Press, Canberra, p. 50-73.

Jell, J.S. and Hill, D.
1970: The Devonian coral fauna of the Point Hibbs Limestone, Tasmania; Royal Society of Tasmania, Papers and Proceedings, v. 104, p. 1-16.

Kettnerová, M.
1932: Paleontologické studie z celechovického devonu. Cást IV. Rugosa. Práce geologicko-palaeontologického ústavu Karlovy university v Praze za rok 1932, p. 1-97.

Kong, Lei and Huang, Yun-ming
1978: Tetracoralla; in Atlas of the Paleontology of the southwestern regions of China, v. 1. Cambrian to Devonian (in Chinese), Geological Science Research Institute, Hubei and other institutions eds. ; Geological Publishing House, Peking, p. 35-161, 739-759.

Kravtsov, A.G.
1963: Rannedevonskie chetyrekhluchevye korally s reki Tarei (Tsentral'nyy Taymyr); Nauchno-Issledovatel'skiy Institut Geologii Arktiki, Uchenye Zapiski, Paleontologiya i Biostratigrafiya, vyp. 3, p. 5-49.

Kuz'min, A.M.
1967: Pervaya nakhodka konodontov v nizhnedevonskikh otlozheniyakh Tsentral'nogo Taymyra; Nauchno-Issledovatel'skiy Institut Geologii Arktiki, Uchenye Zapiski, Paleontologiya i Biostratigrafiya, vyp. 20, p. 52-57.

Lane, H.R.
1974: **Icriodus taimyricus** (Conodonta) from the Salmontrout Limestone (Lower Devonian), Alaska; Journal of Paleontology, v. 48, p. 721-726.

Lang, W.D., Smith, S., and Thomas, H.D.
1940: Index of Palaeozoic coral genera; British Museum (Natural History), London, 231 p.

Lavrusevich, A.I.
1971a: Rugozy rannego silura Zeravshano-Gissarskoy gornoy oblasti; Upravleniya Geologii Soveta Ministrov Tadzhikskoy SSR, Trudy, Paleontologiya i Stratigrafiya, vyp. 3, p. 38-136.

1971b: Nekotorye rugozy iz pozdnesiluriyskikh i rannedevonskikh otlozheniy Tsentral'nogo Tadzhikistana; Upravleniya Geologii Soveta Ministrov Tadzhikskoy SSR, Trudy, Paleontologiya i Stratigrafiya, vyp. 4, p. 33-52, 123-135.

Loewe, S.
1913: Die devonischen Korallen von Ellesmereland; in Report of the Second Norwegian Arctic Expedition in the "Fram" 1898-1902, Videnskabs-Selskabet i Kristiania, v. 4, no. 30, p. 1-23.

Ma, T.Y.H.
1937: On the seasonal growth in Palaeozoic tetracorals and the climate during the Devonian period; Palaeontologia Sinica, ser. B, v. 2, fascicle 3, 96 p.

1956: A reinvestigation of climate and the relative positions of continents during the Devonian; Research on the past climate and continental drift, v. 9, National Taiwan University, Taipei, China (World Book Co. Ltd.), 116 p.

McLean, R.A.
1976a: Aspects of the Silurian rugose coral fauna of the Yass region, New South Wales; The Linnean Society of New South Wales, Proceedings, v. 100, p. 179-194.

1976b: Middle Devonian cystiphyllid corals from the Hume Formation, northwestern Canada; Geological Survey of Canada, Bulletin 274, 80 p.

Meek, F.B.
1867: Remarks on the geology of the valley of Mackenzie River, with figures and descriptions of fossils from that region, in the Museum of the Smithsonian Institution, chiefly collected by the late Robert Kennicott, Esq.; Chicago Academy of Sciences, Transactions, v. 1, p. 61-114.

Milne Edwards, H. and Haime, J.
1850: A monograph of the British fossil corals. Part 1. Introduction and chapters I-VII; The Palaeontographical Society, London, lxxxv+71 p.

1851: Monographie des polypiers fossiles des terrains palaeozoïques; Archives du Muséum d'Histoire Naturelle, tome 5, 502 p.

Nicholson, H.A.
1879: On the structure and affinities of the "tabulate corals" of the Palaeozoic period with critical descriptions of illustrative species; William Blackwood and Sons, Edinburgh and London, 342 p.

Norford, B.S.
1962: **Columnaria pax** (Smith) and the Silurian **Columnaria columbia** n. sp. from British Columbia; Geological Survey of Canada, Bulletin 92, p. 25-30.

Norford, B.S., Gabrielse, H. and Taylor, G.C.
1966: Stratigraphy of Silurian carbonate rocks of the Rocky Mountains, northern British Columbia; Bulletin of Canadian Petroleum Geology, v. 14, p. 504-519.

Oliver, W.A., Jr. and Pedder, A.E.H.
1979: Rugose corals in Devonian stratigraphical correlation; in The Devonian System, eds. M.R. House, C.T. Scrutton and M.G. Bassett; Special Papers in Palaeontology 23, p. 233-248.

Orbigny, A. d'
1850: Prodrome de paléontologie stratigraphique universelle des animaux mollusques et rayonnés; Victor Masson, Paris, tome 1, lx+394 p.

Pedder, A.E.H.
1971: Lower Devonian corals and bryozoa from the Lick Hole Formation of New South Wales; Palaeontology, v. 14, p. 371-386.

1982a: **Chostophyllum**, a new genus of charactophyllid corals from the Middle Devonian of western Canada; Journal of Paleontology, v. 56, p. 559-582.

1982b: New Zlichovian (Early Devonian) rugose corals from the Blue Fiord Formation of Ellesmere Island; Geological Survey of Canada, Paper 82-1C, p. 71-82.

Pedder, A.E.H. and McLean, R.A.
1982: Lower Devonian cystiphyllid corals from North America and eastern Australia with notes on the genus **Utaratuia**; Geologica et Palaeontologica 16, p. 57-110.

Pickett, J.
1967: Untersuchungen zur Familie Phillipsastreidae (Zoantharia rugosa); Senckenbergiana lethaea, Band 48, p. 1-89.

Quenstedt, F.A.
1878-1881: Petrefactenkunde Deutschlands. Band 6. Korallen (Röhren- und Sternkorallen); Fues's Verlag, Leipzig, p. 1-144 (1878), 145-624 (1879), 625-912 (1880), 913-1094 (1881), atlas (1881).

Rominger, C.
1877: Lower Peninsula, 1873-1876, accompanied by a geological map. Part II. Palaeontology. Fossil corals; Geological Survey of Michigan, v. 3, pt. 2, 161 p. (imprint 1876).

Różkowska, M.
1965: Marisastridae n. fam. and **Marisastrum** n. gen. (Devonian corals); Acta Palaeontologica Polonica, v. 10, p. 261-266.

Schei, P.
1903: Preliminary report on the geological observations made during the Second Norwegian Polar Expedition of the "Fram"; Royal Geographical Society, London, 9 p.

Schei, P. (cont.)
1904: Preliminary account of the geological investigations made during the Second Norwegian Polar Expedition in the "Fram". Appendix 1, p. 455-466; in Otto Sverdrup; New Land. Four years in the arctic regions, v. 2; Longmans, Green and Co., London, New York and Bombay, xii+504 p.

Schlüter, C.
1889: Anthozoen des rheinischen Mittel-Devon; Geologischen Specialkarte von Preussen und den Thüringischen Staaten, Abhandlungen, Band 8, Heft 4, p. i-x, 259-465 (reprint pagination 1-207).

Schulz, E.
1883: Die Eifelkalkmulde von Hillesheim. Nebst einem palaeontologischen Anhang; Königlich Preussischen geologischen Landesanstalt und Bergakademie zu Berlin, Jahrbuch, Abhandlungen, 1882, p. 158-250 (reprint pagination 1-94).

Smith, S.
1945: Upper Devonian corals of the Mackenzie River region, Canada; Geological Society of America, Special Paper, no. 59, viii+126 p.

Soshkina, E.D.
1937: Korally verkhnego silura i nizhnego devona vostochnogo i zapadnogo sklonov Urala; Akademiya Nauk SSSR i Vsesoyuznyy Institut Mineral'nogo Syr'ya Nktp, Paleozoologicheskogo Instituta, Trudy, tom 6, vyp. 4, 155 p.

Spasskiy, N.Ya.
1971: Dva novykh devonskikh roda kolonial'nykh tetrakorallov Uralo-Tyan'shan'skoy provintsii; Leningradskogo Ordenov Lenina i Trudovogo Krasnogo Znameni Gornogo Instituta im G.V. Plekhanova, Zapiski, tom 59, vyp. 2, Paleontologiya, p. 23-25.

Spasskiy, N.Ya., Kravtsov, A.G., and Tsyganko, V.S.
1975: Kolonial'nye tsistimorfy; in Drevnie Cnidaria, Tom 1, ed. B.S. Sokolov; Akademiya Nauk SSSR, Sibirskoe Otdelenie, Instituta Geologie i Geofiziki, Trudy, vyp. 201, p. 170-172 (imprint 1974).

Stewart, G.A.
1938: Middle Devonian corals of Ohio; Geological Society of America, Special Paper, no. 8, vii+120 p.

Stumm, E.C.
1949: Revision of the families and genera of the Devonian tetracorals; Geological Society of America, Memoir 40, 92 p.

1951: Type invertebrate fossils of North America (Devonian). Division 1. Unit 1-F. Tetracoralla. Part A; Wagner Free Institute of Science, Philadelphia, cards 1-88.

1963: Corals of the Traverse Group of Michigan. Part XI, **Tortophyllum, Bethanyphyllum, Aulacophyllum,** and **Hallia**; University of Michigan, Contributions from the Museum of Paleontology, v. 18, p. 135-155.

Stumm, E.C. (cont.)
1965: Silurian and Devonian corals of the Falls of the Ohio; Geological Society of America, Memoir 93, ix+184 p. (imprint 1964).

Thevenin, A.
1906-1907: Dévonien; in Types du prodrome de paléontologie stratigraphique universelle de d'Orbigny; Annales de Paléontologie, tome 1, p. 170-172, 193-196 (1906); tome 2, p. 89 (1907).

Uyeno, T.T. and Klapper, G.
1980: Summary of conodont biostratigraphy of the Blue Fiord and Bird Fiord formations (Lower-Middle Devonian) at the type and adjacent areas, southwestern Ellesmere Island, Canada Arctic Archipelago; in Current Research, Part C, Geological Survey of Canada, Paper 80-1C, p. 81-93.

Wedekind, R.
1923: Die Gliederung des Mitteldevons auf Grund von Korallen; Gesellschaft zur Beförderung der gesamten Naturwissenschaften zu Marburg, Sitzungsberichte, 1922, No. 4, p. 24-35.

1924: Das Mitteldevon der Eifel. Eine biostratigraphische Studie. 1 Teil. Die Tetrakorallen des unteren Mitteldevon; Gesellschaft zur Beförderung der gesamten Naturwissenschaften zur Marburg, Schriften, Band 14, Heft 3, vii+93 p.

Weyer, D.
1971: Nomenklatorische Bemerkungen zum Genus **Plasmophyllum** Dybowski, 1873 (Anthozoa, Rugosa, Silur); Berichte der geologischen Gesellschaft in der Deutschen Demokratischen Republik für das Gesamtgebiet der geologischen Wissenschaften, Reihe A, Geologie und Paläontologie, Band 16, Heft 1, p. 13-17.

27.

ANDRADITE GARNET IN ALTERED BASALT FROM BORUP FIORD, ELLESMERE ISLAND, NORTHWEST TERRITORIES

Project 680064

Koichi Tazaki[1]
Institute of Sedimentary and Petroleum Geology, Calgary

Tazaki, K., Andradite garnet in altered basalt from Borup Fiord, Ellesmere Island, Northwest Territories; in Current Research, Part B, Geological Survey of Canada, Paper 83-1B, p. 237-242, 1983.

Abstract

Mineral chemistry and paragenesis of cavity-filling andradite garnet, epidote and prehnite in altered basalt collected from Borup Fiord, Ellesmere Island are described.

The garnet is idiomorphic to sub-idiomorphic and dark brown to amber coloured. The ferrian garnet part contains more than 30.0 per cent Fe_2O_3 and less than 1.0 per cent Al_2O_3. The birefringent rim of the garnet contains more than 8.0 per cent Al_2O_3. Epidote occurs as euhedral to subhedral cavity fillings and a replacement of plagioclase. All analyses of epidote range from Ps_{17} to Ps_{36}. Euhedral prehnite usually forms overgrowths on epidote in the cavities. The ferrian prehnite contains less than 8.0 per cent Fe_2O_3. There are two equilibrium temperatures calculated from coexisting garnet and epidote. These results suggest that the various mineralization stages were preserved metastably in the same specimen. The garnet and associated cavity-filling minerals may have been produced during local hydrothermal alteration of the Esayoo basalt in the Borup Fiord region.

Résumé

Le présent rapport décrit la chimie et la paragénèse de l'andradite, de l'épidote et du prehnite qui remplissent les creux du basalte altéré recueilli au fjord Borup, dans l'île Ellesmere.

Le grenat est idiomorphe à subidiomorphe, de couleur brun foncé à ambrée; la partie ferrique contient plus de 30 % de Fe_2O_3 et moins de 1 % de Al_2O_3. Le bord biréfringent du grenat contient plus de 8 % de Al_2O_3. L'épidote se présente sous forme de remplissages automorphes à subautomorphes des creux et comme minéral de remplacement du plagioclase. Toutes les analyses de l'épidote varient de Ps_{17} à Ps_{36}. Des excroissances automorphes de prehnite sont souvent trouvées sur l'épidote recouvrant les creux. La prehnite ferrique contient moins de 8 % de Fe_2O_3. Deux températures d'équilibre ont été calculées à partir du grenat et de l'épidote coexistants. Ces résultats suggèrent que les diverses étapes de minéralisation ont été conservées de façon métastable dans le même échantillon. La formation du grenat et des minéraux de remplissage associés a peut-être eu lieu lors de l'altération hydrothermale locale du basalte d'Esayoo dans la région du fjord Borup.

Introduction

Boulders of garnet-bearing, altered basalt were collected by P. Moore, in 1979, from the toe of a glacier near Borup Fiord (lat. 80°55'N; long. 83°00'W), on Ellesmere Island in the Canadian Arctic (Fig. 27.1).

This paper is an analysis of the chemistry of the cavity-filling garnet, epidote and prehnite in the basalt, and presents hypotheses concerning their mode of formation, their mineralization temperature and paragenesis.

The geology of the west central area of Ellesmere Island has been discussed by Thorsteinsson (1974). According to him, this region consists of upper Carboniferous to Triassic sedimentary sequences composed mainly of limestone, chert, siltstone and sandstone (Fig. 27.2). This area is geosynclinally folded and the axis of the geosyncline trends northeast. In the northern part, upper Carboniferous to lower Permian sediments of the Nansen Formation, composed of limestone, minor sandstone, siltstone, chert and dolomite, are overlain by the upper Permian Degerböls Formation. The latter is composed of limestone, cherty limestone, and chert. These sediments are overlain by Triassic rocks composed mainly of shale and sandstone in the southern part of the area.

The Esayoo Formation, which consists of interlayered basalt and agglomerate, is the only volcanic rock formation in this area, and ranges in thickness from 30 to 300 m. As the formation overlies the Nansen Formation and underlies lower Permian rocks, Thorsteinsson (1974) considered the Esayoo Formation to be Early Permian.

Although it is far from any outcrop of the Esayoo Formation, the boulder of garnet-bearing, altered basalt examined in this study is considered to have been derived from the Esayoo, because of its lithologic and petrographic similarity to rocks of that formation exposed near the upper reaches of the boulder-bearing glacier (Fig. 27.2). Also, no other volcanics are known to occur in this region.

Petrography

The Borup Fiord samples are from boulders of dark to light green, fine grained, altered basalt, which have many ovoidal or orbicular cavities ranging up to 3 cm in diameter. The cavities are usually filled with dark brown or amber coloured andradite garnet, epidote, prehnite and calcite, with minor quartz and dusty iron oxides. Chlorite is also rarely present.

[1] On leave from Institute for Thermal Spring Research, Okayama University Misasa, Tottori-Pref., JAPAN 682-02

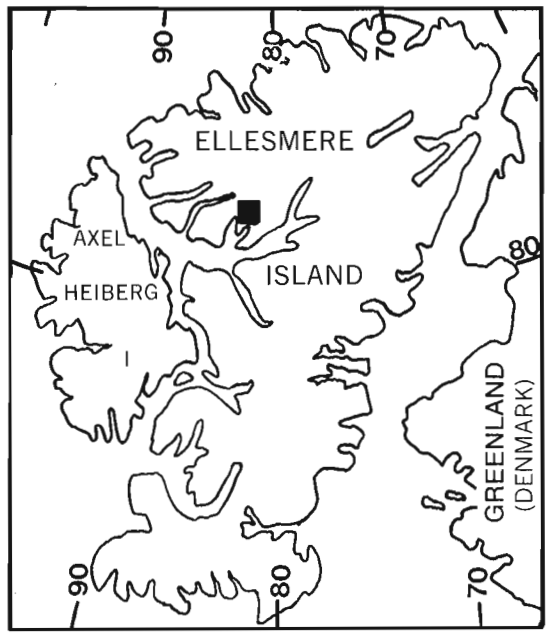

Figure 27.1. *Locality map of sampling point. The solid square is the area shown in Figure 27.2.*

In the weakly altered, dark greyish part, basaltic texture is well preserved. Sparse cavities are also filled with garnet and other Ca-silicate minerals. Metasomatic epidote bands, about 10 mm wide, separate the weakly altered from the heavily altered parts where carbonation predominated.

Thin sections reveal that the weakly altered parts contain a well preserved texture of finely crystalline, aphyric basalt. Laths of plagioclase needles smaller than 0.1 mm are altered to albite. Mafic minerals (presumably originally clinopyroxene) are also decomposed and have recrystallized into iron oxides, chlorite and epidote. In heavily altered parts, basaltic texture is obscure. Calcite and epidote minerals are predominant. Plagioclase laths are altered to albite + calcite, whereas mafic minerals have recrystallized to epidote + calcite + iron oxides.

Cavity-filling minerals

Andradite garnet is the main and characteristic mineral filling cavities. Garnet fills not only orbicular, but also large, lenticular cavities up to 3 cm wide. The garnet is idiomorphic to subidiomorphic and dark brown (fresh) to amber (weakly altered) coloured. Garnet cores commonly include epidote, prehnite and calcite. Another common cavity-filling mineral is epidote. Small cavities are, in some cases, essentially filled with epidote.

Calcite, quartz, prehnite and chlorite are subordinate to rare cavity-filling minerals.

Thin section observations reveal three major mineral assemblages of cavity filling:

Ia. Garnet – epidote – prehnite – calcite – quartz – iron oxides ± chlorite
Ib. Garnet – epidote – prehnite – quartz – iron oxides
II. Garnet – epidote – calcite – quartz – iron oxides
III. Epidote – iron oxides

A mineral assemblage of type Ia is illustrated in Figure 27.3. Idiomorphic garnet, about 4 mm in width, occupies the centre of the cavity. The rim bordering the garnet crystal is less than 200 µm wide and is optically anisotropic and birefringent. The periphery of the cavity is a reaction zone composed mainly of fine grained epidote and dusty iron-oxides. Plagioclase is completely replaced by epidote pseudomorphs. Chlorite is also present sporadically. In most cases, idiomorphic epidote crystals grew from the edge radially towards the centre of the cavity. Clusters of prehnite crystals grew on the epidote layer. Quartz and a small amount of calcite are present in the interstices between the garnet and prehnite crystals.

Electron-backscattering images reveal that the mineralogic composition of the andradite garnet is homogeneous, except for the aluminous birefringent rim. The idiomorphic prehnite is zoned, with a ferric core fringed by an aluminous rim. The idiomorphic to subidiomorphic epidote shows a reverse trend from aluminous in the core to ferrian in the rim (Fig. 27.4). The mineral assemblage of type Ib is found in partly resorbed garnet in which the core is replaced by iron-free prehnite.

Figure 27.5 shows an example of the mineral assemblage of type II. In this case, calcite occurs in the core of the garnet. The birefringent rim of garnet is also present. A reaction zone composed of epidote and dusty iron oxides surrounds the cavity. Idiomorphic epidote crystals grew inwards from the edge of the cavity. Interstitial quartz is present between garnet and epidote crystals.

In the type III mineral assemblage, epidote is the main constituent and garnet is not present (Fig. 27.6). An aggregate of dusty iron oxides suggests the decomposition of the garnet into epidote and iron oxides.

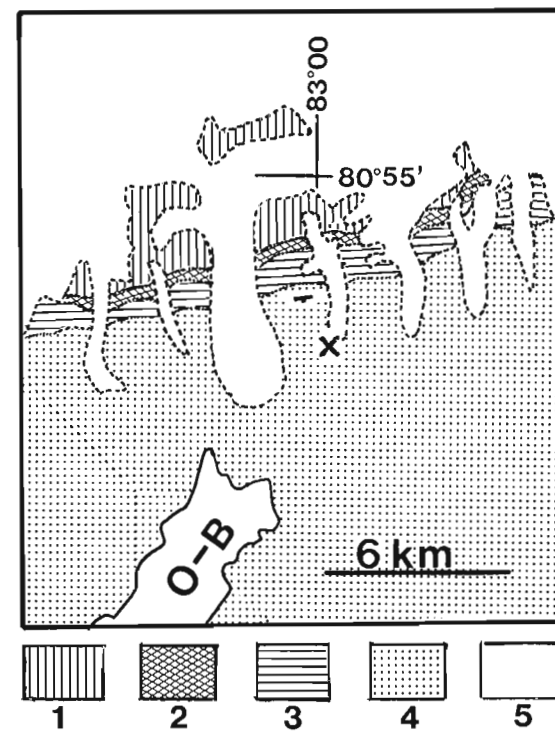

Figure 27.2. *Geological map of the study area, simplified after Thorsteinson (1969). O-B = Oobloyah Bay; X = sampling point; 1 = Nansen Formation (Upper Carboniferous and lower Permian); 2 = Esayoo Formation (Lower Permian, basalt); 3 = Degerbols Formation (Upper Permian); 4 = Triassic formations; 5 = Glacier.*

Mineral chemistry

The cavity filling minerals, garnet, epidote, and prehnite, were analyzed by electron probe microanalyzer. Representative analyses of these minerals are listed in Tables 27.1 and 27.2.

Garnet Spot analyses of garnet reveal that the chemical composition of the ferrian garnet is homogeneous, with no distinct zoning. The transitional, birefringent rim shows sharp and abrupt changes in Al and Fe contents. MgO seems to increase a little in the birefringent zone but this trend is not unequivocal. The ferrian garnet part contains more than 30.0 per cent Fe_2O_3 and less than 1.0 per cent Al_2O_3. Preliminary analyses suggest that MnO and MgO are less than 0.3 and 0.1 per cent respectively and, therefore, were omitted in routine analyses.

The birefringent zones, less than 200 μm in width, are enriched in Al_2O_3 and contain from 8.0 to 10.4 per cent, while the inner parts of exceptionally broad birefringent rims rarely have less than 7.0 per cent Al_2O_3.

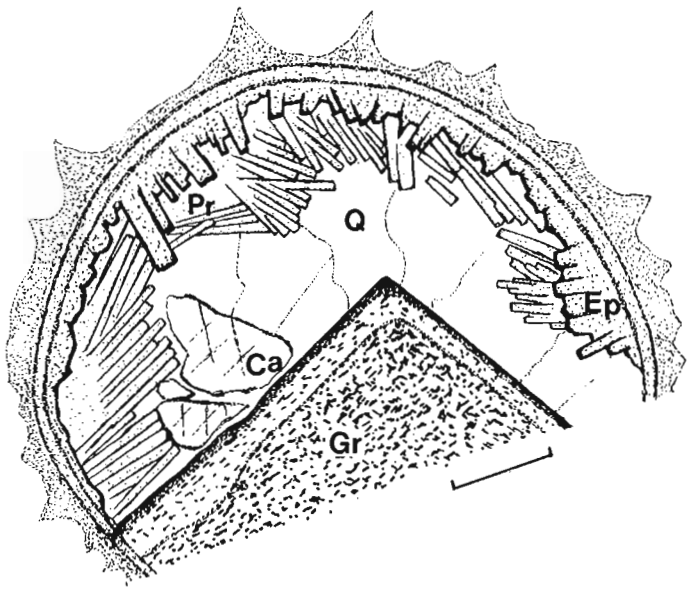

Figure 27.3. *Occurrence of cavity-filling minerals. Gr = garnet; Ep = epidote; Pr = prehnite; Q = quartz; Ca = calcite. Scale bar is 1.2 mm.*

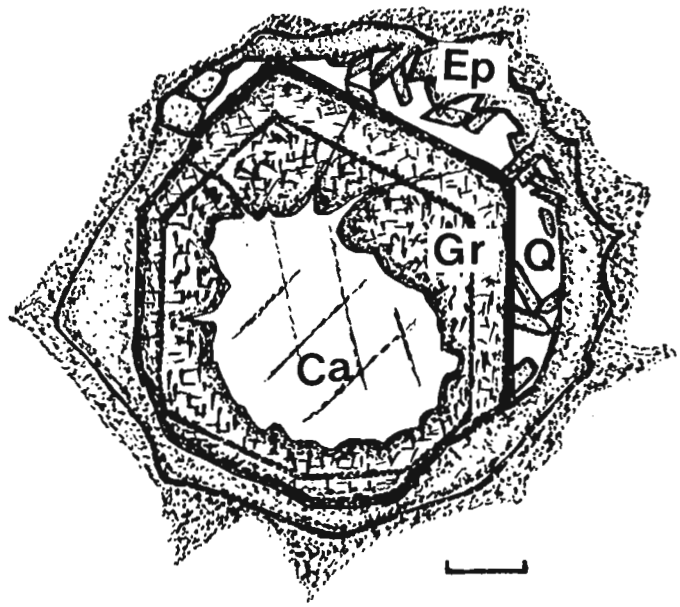

Figure 27.5. *Occurrence of resorbed garnet. Gr = garnet; Ep = epidote; Q = quartz; Ca = calcite. Scale bar is 0.4 mm.*

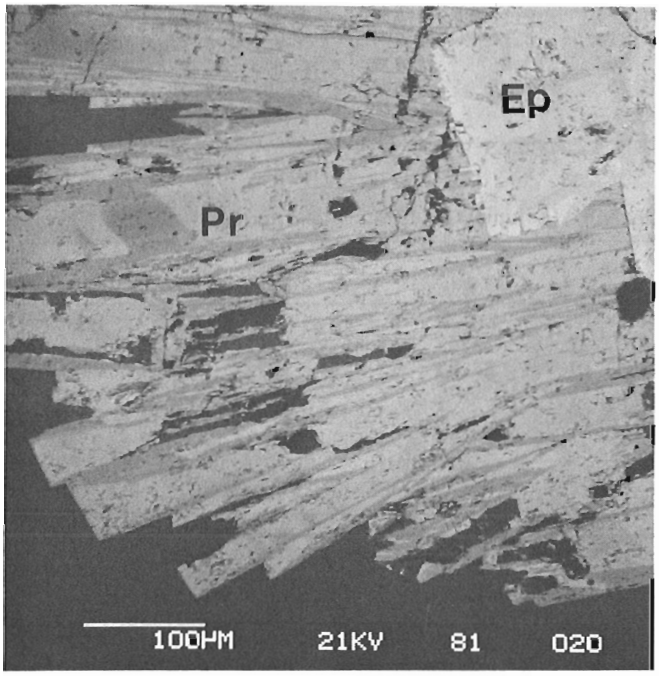

Figure 27.4. *Electron-backscattering image of epidote and prehnite. Ep = epidote; Pr = prehnite. Brighter parts of crystals are more enriched in iron.*

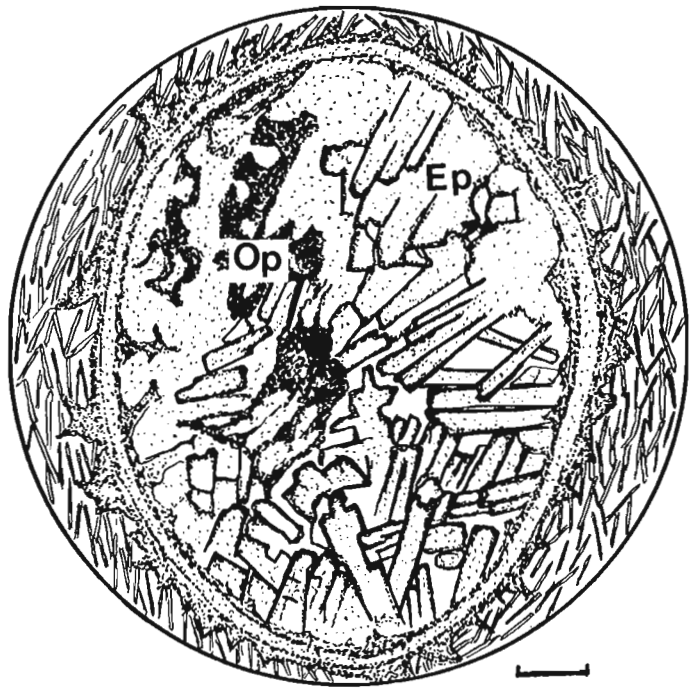

Figure 27.6. *Occurrence of epidote. Ep = epidote; Op = opaque iron oxides. Scale bar is 0.4 mm.*

$Fe^{3+}/(Fe^{3+} + Al)$ of the ferrian garnet ranges from 0.97 to 1.0, which corresponds to 97 to 100 per cent andradite. $Fe^{3+}/(Fe^{3+} + Al^{3+})$ of the birefringent rim generally ranges from 0.52 to 0.60, rarely from 0.68 to 0.75. All analyses of garnet, plotted in terms of Al, Fe^{3+} and Ca ratio in Figure 27.7, are on the low Ca side of the ideal andradite-grossular join, suggesting the existence of minor ferrous iron, possibly in a small component of almandine.

Epidote Epidote shows a variety of habits as a constituent in cavity reaction rims. It occurs as euhedral to subhedral cavity fillings and as a replacement of plagioclase crystals. As previously stated, electron backscattering images show the compositional zoning in the relatively large crystals, more than 100 μm in length, to be from alumina-rich cores to iron-rich rims. Total iron, as Fe_2O_3 of the analyzed epidote, ranges from 8.5 to 17.6 per cent, whereas Al_2O_3 ranges from 20 to 27 per cent. All analyses of epidote plotted in Figure 27.7 are scattered between Ps_{17} to Ps_{36}.

Prehnite Euhedral prehnite crystals are up to several 100 μm long and usually form overgrowths on epidote crystals in the cavities. In places prehnite occurs in the cores of garnet crystals. Euhedral prehnite shows distinct compositional zoning from iron-rich core to iron-poor rim. This relationship is the opposite to that of epidote. The ferrian prehnites contain from 4.8 to 7.9 per cent Fe_2O_3, whereas prehnites in the cores of garnet crystals have Fe_2O_3 contents less than 1.0 per cent.

Discussion

Mineral assemblages of the present cavity fillings are characteristic of low temperature skarns or hydrothermal alteration. The cavity-filling garnet is usually present as subidiomorphic to idiomorphic monocrystals and the chemical composition of the cores is homogeneous, which suggests crystallization from fluid or vapour under stable physico-chemical conditions. Abrupt compositional change from andradite to grandite at the rim may reflect a change in

Table 27.1

Representative analyses of garnet (per cent oxides)

Sample No.	1	2	3	4	5	6	7	8	9	10	11
Grain	3-1-2	2-2-3	1-1-2	2-1-6	2-1-3	2-3-4	2-3-3	2-1-1	2-2-7	4-1-3	1-1-4
SiO_2	35.26	35.19	35.61	35.37	35.46	35.55	35.99	36.65	36.91	36.77	37.36
Al_2O_3	0.07	0.16	0.24	0.33	0.55	5.22	7.02	8.93	9.89	9.92	10.41
Fe_2O_3	32.26	31.91	32.02	32.18	31.37	25.23	23.34	20.19	18.49	18.36	17.96
CaO	31.94	32.41	32.65	32.21	32.52	32.47	33.00	33.58	33.45	33.71	34.18
Total	99.53	99.67	100.52	100.09	99.90	98.47	99.35	99.35	98.74	98.76	99.91
					Structure formula (O = 24)						
Si	5.989	5.972	5.986	5.971	5.987	5.941	5.814	5.929	5.984	5.992	5.993
Al	0.014	0.033	0.046	0.065	0.109	1.028	1.359	1.703	1.890	1.905	1.968
Fe^{3+}	4.124	4.075	4.051	4.088	3.985	3.173	2.885	2.458	2.256	2.252	2.124
Ca	5.813	5.893	5.881	5.826	5.884	5.815	5.809	5.821	5.812	5.779	5.875
Total	15.940	15.973	15.964	15.950	15.965	15.957	15.867	15.911	15.942	15.928	15.960
$Fe^{3+}/(Fe^{3+}+Al^{3+})$	1.00	0.99	0.99	0.98	0.97	0.75	0.68	0.59	0.54	0.54	0.52

Table 27.2

Representative analyses of epidote (columns 1-9) and prehnite (columns 10-13) (per cent oxides)

Sample No.	1	2	3	4	5	6	7	8	9	10	11	12	13
Grain	4-1-4	1-1-1	2-1-1	4-1-3	2-1-2	2-2-7	2-2-6	1-1-4	2-2-5	4-1-2	2-1-1	4-1-1	1-1-1
SiO_2	37.50	37.68	37.67	37.15	39.23	38.43	37.41	37.66	37.61	41.81	42.11	42.83	44.11
Al_2O_3	20.06	21.72	22.87	22.75	22.32	24.51	25.10	21.72	27.23	18.98	19.51	21.44	24.66
Fe_2O_3	17.60	15.23	14.81	14.80	13.72	12.26	11.62	10.02	8.46	7.90	6.93	4.78	0.30
CaO	22.58	22.65	22.96	22.51	20.88	23.15	23.33	23.62	23.19	25.85	25.76	26.37	26.77
Total	97.74	97.28	98.31	97.21	96.15	98.35	97.46	93.02	96.49	94.54	94.31	95.42	95.84
						Structure formula							
					(O = 12.5)						(O = 22)		
Si	3.034	3.034	2.997	2.989	3.148	3.024	2.972	3.131	2.980	5.982	6.011	5.993	6.033
Al	1.912	2.061	2.145	2.157	2.111	2.274	2.351	2.129	2.543	3.200	3.281	3.536	3.976
Fe^{3+}	1.071	0.923	0.887	0.896	0.828	0.726	0.695	0.627	0.505	0.774	0.744	0.504	0.031
Ca	1.957	1.954	1.957	1.941	1.795	1.952	1.986	2.104	1.969	3.960	3.939	3.953	3.923
Total	7.974	7.972	7.986	7.983	7.882	7.976	8.004	7.991	7.997	13.916	13.975	13.986	13.963
$Fe^{3+}/(Fe^{3+}+Al^{3+})$	0.36	0.30	0.29	0.29	0.28	0.24	0.23	0.23	0.17	0.19	0.18	0.13	0.01

these conditions during crystallization. The irregular and complex zoning in epidote and prehnite suggests rapid crystallization under metastable conditions.

Paragenetic relations, therefore, can only be postulated for the surface equilibrium among garnet, epidote and prehnite.

Kitamura (1975) measured Al-Fe partitioning between grandite garnet and epidote from contact metasomatic deposits. He found that the partition coefficient, $K' = (Al/Fe^{3+})$ garnet / (Al/Fe^{3+}) in M3 of epidote, is generally in a range from 1.7 to 10.0 and mineral pairs formed under relatively high temperature have smaller partition coefficients. The compositional relations of coexisting epidote and garnet have also been calculated by Bird and Helgeson (1980). They proposed a tentative temperature-composition diagram. $Fe^{3+}/(Fe^{3+} + Al^{3+})$ and Al/Fe^{3+} values for several coexisting pairs of garnet rim and epidote rim in the present cavity-fillings are listed in Table 27.3. $Fe^{3+}/(Fe^{3+} + Al^{3+})$ values for the garnets range from 0.52 to 0.59 while those of coexisting epidote range from 0.23 to 0.29. The K' values range from 2.2 to 4.9. It is noteworthy that mineral pairs 4-1-3 and 2-1-1 are accompanied by ferrian prehnite and the temperatures of coexisting garnet and epidote deduced from Bird and Helgeson (1980) are less than 200°C. Meanwhile, mineral pairs 1-1-4 and 2-2-7 are devoid of prehnite and temperatures are estimated to be 500-550°C. Average K' value is 4.6 in the former and 3.3 in the latter.

The upper stability limit of prehnite defined by Liou (1971) and Strens (1968) is insensitive to pressure and is about 400°C. Recently, Kerrick and Ghent (1978) calculated that the upper stability limit of prehnite has a significant negative slope at higher pressures and the upper stability limit of 1-2 kbar extends up to more than 500°C. Consequently, the upper stability limit of prehnite is still controversial. However, the upper stability limit of ferrian prehnite is suspected to be lower than that of iron-free prehnite (Coombs et al., 1977). It is reasonable that the calculated temperature of mineral pairs without prehnite is higher than that of prehnite-bearing mineral assemblages.

The paragenetic mineral pairs 2-2-7 and 2-1-1, however, coexist in the same thin section.

These contradictions lead to the assumption that there could have been an evolution in the chemistry of the fluid from which the cavity-filling minerals crystallized and that the various mineralization stages were preserved metastably in the same specimen.

In this regard, the mineral assemblage of type III, epidote-iron oxides, suggests decomposition of andradite garnet under lower temperature or higher CO_2 conditions (Taylor and Liou, 1978).

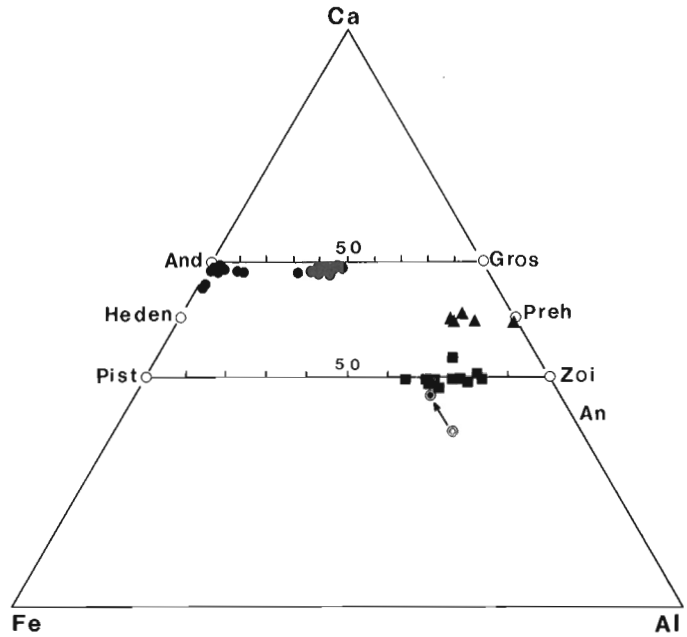

Figure 27.7. *Fe^{3+}-Al-Ca plot of analyses. Solid circles = garnet; solid triangles = prehnite; solid squares = epidote; circle with dot = heavily carbonated basalt; double circle = weakly carbonated basalt.*

The type III mineral assemblage also coexists with type II or type I mineral assemblages in the same specimen. These occurrences would support the above mentioned assumption.

In carbonate-bearing, cavity-free basalt from the Esayoo Formation, epidote and calcite are ubiquitous in the groundmass but garnet is absent. It is conceivable that, in these rocks, the introduction of carbonate took place prior to the formation of garnet.

One of the weakly altered samples of Esayoo basalt contains 9.0 per cent total iron oxides, 10.4 per cent MgO, 10.6 per cent CaO, and 4.5 per cent total alkalies, whereas heavily carbonated basalt contains 9.7 per cent total iron oxides, 8.0 per cent MgO and more than 13 per cent CaO (H.P. Trettin, unpublished data).

Carbonation transformed the chemical composition of basalt making it easier to yield the epidote solid solution, as shown in Figure 27.7. Moreover, the formation of andradite is restricted to H_2O-rich fluid at temperatures below 400°C (Taylor and Liou, 1978).

Table 27.3

Partition of Elements

Grain No.	Garnet		Epidote		K*
	$Fe^{3+}/(Fe^{3+}+Al^{3+})$	Al/Fe^{3+}	$Fe^{3+}/(Fe^{3+}+Al^{3+})$	$(Al/Fe^{3+})M3$	
4-1-3	0.54	0.84	0.29	0.17	4.9
2-1-1	0.59	0.69	0.29	0.16	4.3
1-1-4	0.52	0.93	0.23	0.21	4.4
2-2-7	0.54	0.84	0.24	0.38	2.2

*partition coefficient = (Al/Fe^{3+}) garnet /(Al/Fe^{3+}) in M3 of epidote

Coombs et al., (1977) described various occurrences of andradite and intermediate grandite garnet in low grade metamorphic rocks, of prehnite-pumpellyite and pumpellyite-actinolite facies, from southern New Zealand. They estimated conditions of formation involving temperatures of 300 to 400°C, or less, at pressures up to a few kilobars.

In the Borup Fiord region, neither regional metamorphic nor plutonic rocks are known to date.

The infiltration of high temperature, H_2O-rich fluid may have caused the precipitation of andradite-grandite garnet, and associated cavity-filling minerals, by means of metasomatic reactions between the fluid and the altered basalt, along the rims of cavities, under hydrothermal or shallow burial conditions, where oxygen fugacity was relatively high, although the heat source is uncertain.

Conclusions

1. There are three major mineral assemblages of cavity filling minerals:
   - Ia. Garnet – epidote – prehnite – calcite – quartz – iron oxides ± chlorite
   - Ib. Garnet – epidote – prehnite – quartz – iron oxides
   - II. Garnet – epidote – calcite – quartz – iron oxides
   - III. Epidote – iron oxides
2. Temperatures calculated from coexisting garnet and epidote are twofold: prehnite-bearing assemblages with temperatures less than 200°C, and prehnite-free assemblages with temperatures ranging from 500° to 550°C. These results lead to the assumption that the various mineralization stages were preserved metastably in the same specimen, as physico-chemical conditions changed during mineralization.
3. Carbonation of basalt transforms the chemical composition of basalt so as to more readily produce epidote solid solution. The subsequent infiltration of high temperature, H_2O-rich-fluid may have caused the precipitation of andradite garnet.
4. It is concluded that the garnet and associated cavity filling minerals may have been produced during local hydrothermal alteration of the Esayoo basalts, in the Borup Fiord region.

Acknowledgments

The writer is grateful to E.D. Ghent and B. Rutherford of the University of Calgary for use of the electron microprobe analyzer; to G.P. Michael of the Institute of Sedimentary and Petroleum Geology for scanning electron microscopy; and to H.P. Trettin of the same Institute for permission to use unpublished chemical analyses of the Esayoo basalt. The writer also wishes to thank W.W. Nassichuk for providing samples of the garnet-bearing Esayoo Formation, and D.W. Morrow, T. Frisch and W.R.A. Baragar for reading the manuscript.

This study was carried out by the writer during his visit to the Institute of Sedimentary and Petroleum Geology. The writer expresses his gratitude to the Department of Energy, Mines and Resources, Canada, and the Ministry of Education of Japan, for supporting his visit to Canada, which made the study possible.

References

Bird, D.K. and Helgeson, H.C.
1980: Chemical interaction of aqueous solutions with epidote feldspar mineral assemblages in geologic systems. I. Thermodynamic analysis of phase relations in the system $CaO - FeO - Fe_2O_3 - Al_2O_3 - SiO_2 - H_2O - CO_2$; American Journal of Science, v. 280, p. 907-941.

Coombs, D.S., Kawachi, Y., Houghton, B.F., Hyden, G., Pringle, I.J., and Williams, J.G.
1977: Andradite and andradite-grossular solid solutions in very low-grade regionally metamorphosed rocks in southern New Zealand; Contributions to Mineralogy and Petrology, v. 63, p. 229-245.

Kerrick, D.M. and Ghent, E.D.
1978: P-T-X CO_2 relations of equilibria in the system. $CaO - Al_2O_3 - SiO_2 - CO_2 - H_2O$; in "Korzhinskii Memorial Volume".

Kitamura, K.
1975: Al - Fe partitioning between garnet and epidote from the contact metasomatic deposits of the Chichibu Mine, Japan; Economic Geology, v. 70, p. 725-738.

Liou, J.G.
1971: Synthesis and stability relations of prehnite, $Ca_2Al_2Si_3O_{10}(OH)_2$; American Mineralogist, v. 56, p. 507-531.

Strens, R.G.J.
1968: Reconnaissance of the prehnite stability field; Mineralogical Magazine, v. 36, p. 864-867.

Taylor, B.E. and Liou, J.G.
1978: The lowest-temperature stability of andradite in C-O-H fluids; American Mineralogist, v. 63, p. 378-393.

Thorsteinsson, R. (comp.)
1969: Greely Fiord West, District of Franklin; Geological Survey of Canada, Map 1311A.

Thorsteinsson, R.
1974: Carboniferous and Permian stratigraphy of Axel Heiberg Island and western Ellesmere Island, Canadian Arctic Archipelago; Geological Survey of Canada, Bulletin 224.

28.

STRUCTURAL SUBDIVISIONS OF THE GRENVILLE PROVINCE IN THE PARRY SOUND – ALGONQUIN REGION, ONTARIO

Project 760061

N.G. Culshaw, A. Davidson, and L. Nadeau[1]
Precambrian Geology Division

Culshaw, N.G., Davidson, A., and Nadeau, L., Structural subdivisions of the Grenville Province in the Parry Sound – Algonquin region, Ontario; in Current Research, Part B, Geological Survey of Canada, Paper 83-1B, p. 243-252, 1983.

Abstract

Domains and subdomains in southwestern Grenville Province, geologically distinct and bounded by tectonic zones, represent at least four, major, superincumbent crustal segments stacked during deep-seated, northwest-directed ductile thrusting. Internal tectonic zones in some segments may reflect earlier phases of a similar history.

Résumé

Des domaines et des sous-domaines dans le sud-ouest de la province de Grenville, géologiquement distincts et limités par des zones tectoniques, représentent au moins quatre grands segments lithosphériques superposés empilés lors d'une période de charriage ductile survenu en profondeur et orienté vers le nord-ouest. Des zones tectoniques internes dans certains segments pourraient refléter des phases antérieures d'une histoire semblable.

Introduction

Earlier reconnaissance mapping in the southwestern Grenville Province established a tectono-metamorphic framework for the Parry Sound region based on the recognition that continuous, curviplanar zones of highly deformed gneiss and mylonite (tectonic zones) lie between terranes with distinctive lithologies, metamorphism and structural signatures (domains and subdomains: Davidson et al., 1982). Consideration of features at various scales associated with tectonite zones, including the generally southeast-plunging well developed stretching lineation, mesoscopic kinematic indicators and juxtaposition of different rock assemblages at different metamorphic grades in adjacent domains, led to the hypothesis that the entire crustal section has evolved by way of stacking segments or blocks of crust through repeated northwest-directed ductile thrusting that occurred deep in the crust. Tectonite zones are thereby interpreted to be the loci of greatest displacements.

Fieldwork in 1982 extended mapping eastward into the western part of Algonquin Park (Fig. 28.1). The concept of domains separated by zones of high strain remains a useful one for preliminary analysis. However, the former boundary between Muskoka and Algonquin domains (Davidson and Morgan, 1981, Fig. 41.2) has been modified, and Algonquin Domain in part divided into subdomains (Fig. 28.2). Relationships between all these subdomains will be reviewed and discussed after outlining both their distinctions and similarities. A further result of this summe 's work has been the verification of the tectonic nature of the northwest boundary of the Central Metasedimentary Belt. It is apparent that northwest-directed ductile thrusting within zones at moderate to low angle, previously demonstrated to be so important in the vicinity of Parry Sound, also shaped the overall structural pettern in the south and west Algonquin region. Intra-domain structures are overprinted, but it is as yet unclear which of the older structures are an early manifestation of ductile thrusting and which reflect and entirely older history.

Muskoka Domain

Parts of Muskoka Domain, namely the northwestern lobes that form Seguin and Moon River subdomains, are synformal and bounded by continuous tectonite zones (Davidson et al., 1982). The Seguin subdomain changes structural character southeastward, widening several-fold and merging with tracts of as yet unknown extent that lie north and west of the Central Metasedimentary Belt (Fig. 28.2). The southeast widening of this subdomain is also accompanied by gradual lithological and metamorphic changes. In its northwest synformal lobe, migmatitic quartzofeldspathic gneisses, commonly containing mafic blocks and silvers and generally of undecipherable protolith, are the dominant rocks. In the wider southeastern part, tracts of orthogneiss in amphibolite facies display varying degrees of migmatization and are separated by zones of migmatitic gneiss of obscure origin. Buff-weathering hypersthene-bearing gneisses in granulite facies, some of which are nonretrograded equivalents of amphibolite facies orthogneisses, are widespread but of subordinate importance. The amphibole facies rocks are mainly grey, carry hornblende and/or biotite and have tonalitic to granodioritic composition; K-feldspar-rich varieties are present locally.

In its northwest and central parts Seguin subdomain is comparable to Moon River subdomain, being a synformal structure with axes at all scales parallel to the gently

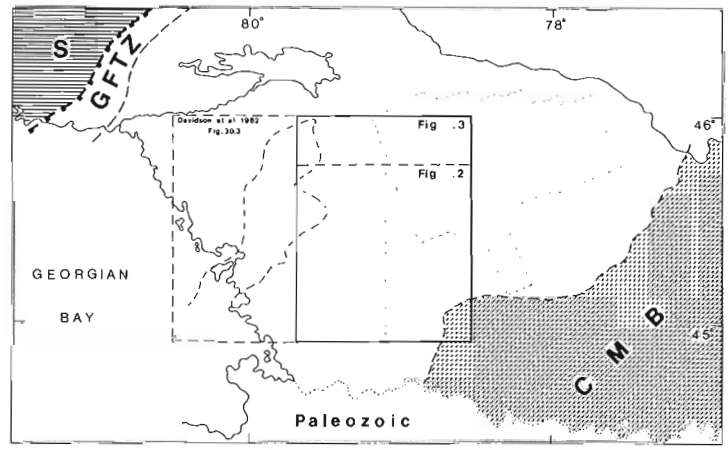

Figure 28.1. *Location map; S – Southern Province, GFTZ – Grenville Front Tectonic Zone, CMB – Central Metasedimentary Belt.*

[1] Department of Geology Carleton University Ottawa, K1S 5B6

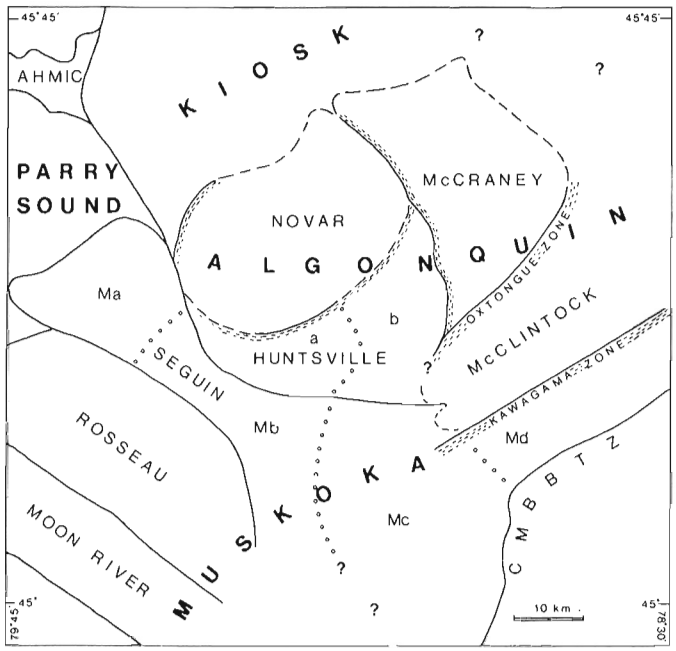

Figure 28.2. *Lithostructural subdivisions in the western Algonquin region. CMBBTZ – Central Metasediment Belt boundary tectonic zone. Areas represented by stereoplots in Figure 28.4 and 28.5 are shown.*

southeast-plunging stretching lineation (Fig. 28.3, 28.4). Where it widens into the southeast part of Muskoka Domain, a set of large-scale folds, absent to the northwest, are coaxial with the stretching lineation. This lineation, however, swings easterly in the southeastern extremity of this domain, where patches of nonretrograded granulite facies rocks are the most common. Perhaps the constriction of the central part of Seguin subdomain can be explained by syntectonic uplift in Rosseau subdomain and western Algonquin Domain (Novar subdomain). The northwestward disappearance of large internal folds and of preserved granulite facies rocks, coupled with the regional swing in the lineation trend, may possibly be related to transition from a root zone of orthogneiss previously deformed and metamorphosed in granulite facies to a northwest-directed migmatite nappe formed under amphibolite facies conditions.

Tectonic Boundary of the Central Metasedimentary Belt

It has been suggested previously that the presence of 'tectonoclastic gneiss' along the northwestern boundary of the Central Metasedimentary Belt indicates that it was the locus of deep-seated dislocation, and that the Metasedimentary Belt has moved as a block with respect to the underlying rocks in the Central Gneiss Belt (Davidson and Morgan, 1981). It is now known that the boundary west of Haliburton (Fig. 28.3) is a broad zone characterized by gneisses with strongly developed tectonic features, including straight gneiss, tectonic schist and mylonite (for terminology, see Davidson et al., 1982, p. 177), distributed in closely spaced, sinuous and laterally merging belts, within which tectonically modified rocks typical of the Central Gneiss Belt are interleaved with Metasedimentary Belt lithologies, notably marble and calc-silicate gneiss. The Boshkung Lake and Logan Lake zones of Schwerdtner and Mawer (1982) belong to this boundary zone. As has been found in the tectonic zones between domains and subdomains to the west and northwest, blocks and slivers of metagabbroic, ultramafic and anorthositic rock are present. On the map the boundary zone is as much as 10 km wide, and although its true thickness is less (~3 km?), judging by the prevalence of gently southeast-dipping structures (Fig. 28.5), it is nevertheless a zone of major proportions. Within the boundary zone, individual belts of more intensely tectonized rock (Fig. 28.6) are replete with evidence for northwest-directed tectonic transport parallel to the ubiquitous stretching lineation (Fig. 28.4). Examples of kinematic indicators include rotated feldspar porphyroclasts (Fig. 28.6C), a large-scale, subhorizontal shear zone in which both straight gneiss and tectonic schist have been produced, shear band foliation (Fig. 28.6B), drag folds with axes at high angles to the lineation, and narrow, southeast-dipping schist bands across which pegmatites have been displaced.

As suggested earlier (Davidson and Morgan, 1981), the gneisses in which coarse, rounded feldspar grains and small pegmatitic aggregates (Fig. 28.6C, E, F), and various types of metabasite 'lumps' are so common are not coarse clastic metasedimentary rocks, as has been suggested for similar rocks northwest along the same boundary (Lumbers, 1980). It can be demonstrated in several places that the scattered distribution of large feldspars in such rocks is due to disaggregation of syntectonic pegmatite, a finding already reported for tectonites in the Parry Sound region (Davidson et al., 1982) and in accord with the much earlier tectonic interpretation of Adams and Barlow (1910) for 'conglomerate gneiss' in the Central Metasedimentary Belt boundary zone.

An interesting feature of the amphibolite facies rocks of the tectonite zones, observed in thin sections, is the ubiquity of microcline in contrast to the dominance of orthoclase in the less strained and structurally underlying rocks of southeastern Muskoka Domain. This feature may be attributed to the catalytic effect of shearing on the ordering process in K-feldspar (Smith, 1974).

Algonquin Domain

Prevalence of granulite facies metamorphism and irregularity of structural trend, contrasting strongly with adjacent regions, formed the basis for outlining Algonquin Domain (Davidson and Morgan, 1981). The southern boundary of this domain has now been revised such that the domain is now separated from the Central Metasedimentary Belt by a northeastward extension of Muskoka Domain. Algonquin and Muskoka domains are separated by a planar zone of gneissic tectonites, the Kawagama zone (Fig. 28.2), that contains numerous inclusions of different types of metabasite and slivers of granulite. Structural trends of both domains swing into parallelism along this southeast-dipping zone (Fig. 28.3, 28.5); granitoid and pelitic gneisses along the southeast margin of Algonquin Domain become increasingly attenuated and mylonitized. Relationship between the two domains is complicated and at present unresolved in the neighbourhood of Dorset (Fig. 28.3), but farther west there is a major change from the flaggy granulite terrane around Huntsville southward to migmatitic rocks in Muskoka Domain. This boundary passes northwestward into the tectonite zone that marks the edge of Seguin subdomain. On its northern side, Algonquin Domain merges with Kiosk Domain across an as yet poorly defined zone beyond which northeast-trending structures prevail. Slivers of anorthositic gneiss occur at this boundary south of Burk's Falls.

Four subdomains are so far identified within Algonquin Domain, each characterized by its own lithological assemblage and structural pattern. They are bounded by zones of straight gneiss – zones of highly flattened, flaggy or thinly layered gneiss and granulite that follow regular trends through otherwise less regularly structured terranes

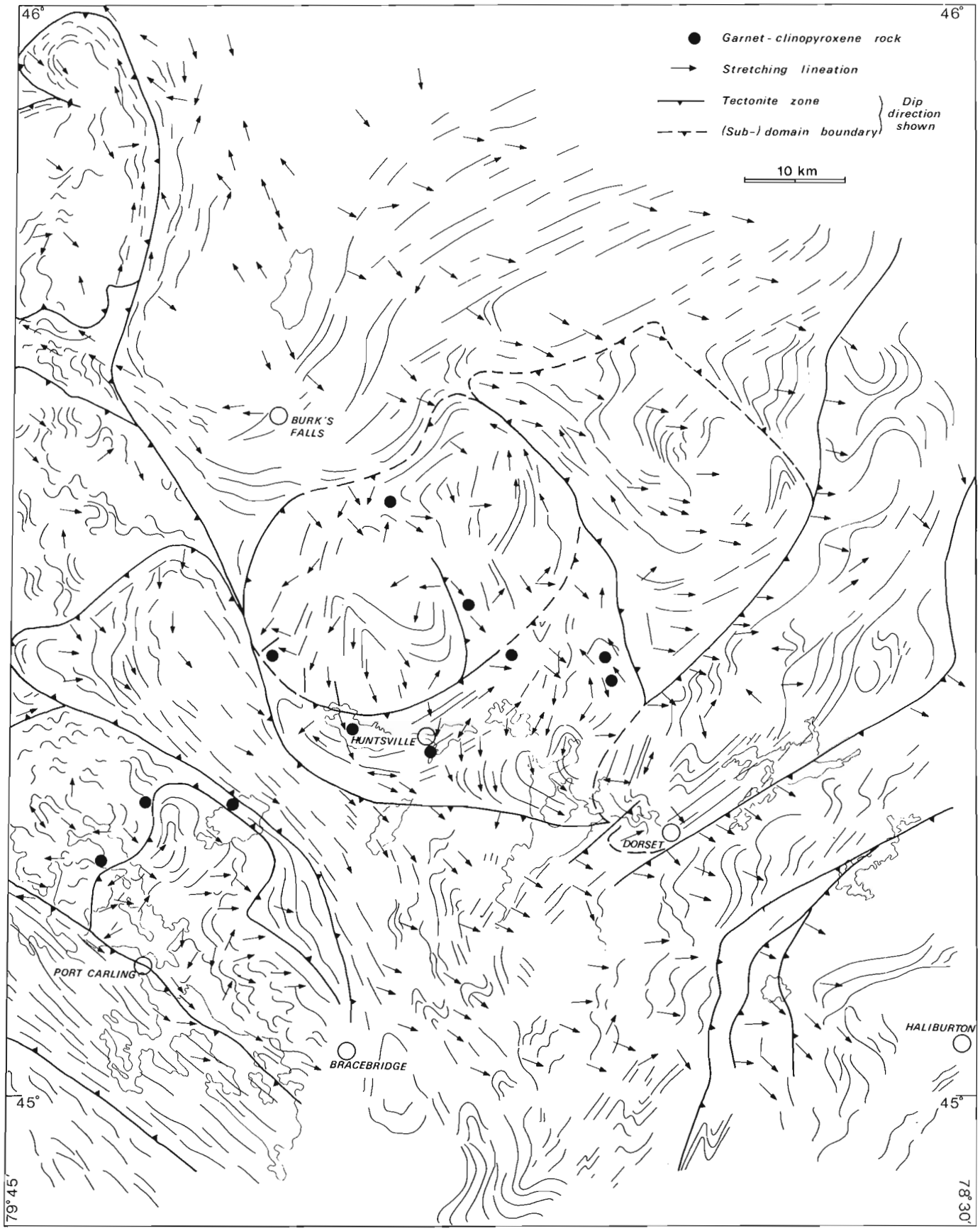

Figure 28.3. *Structural trends in the western Algonquin region.*

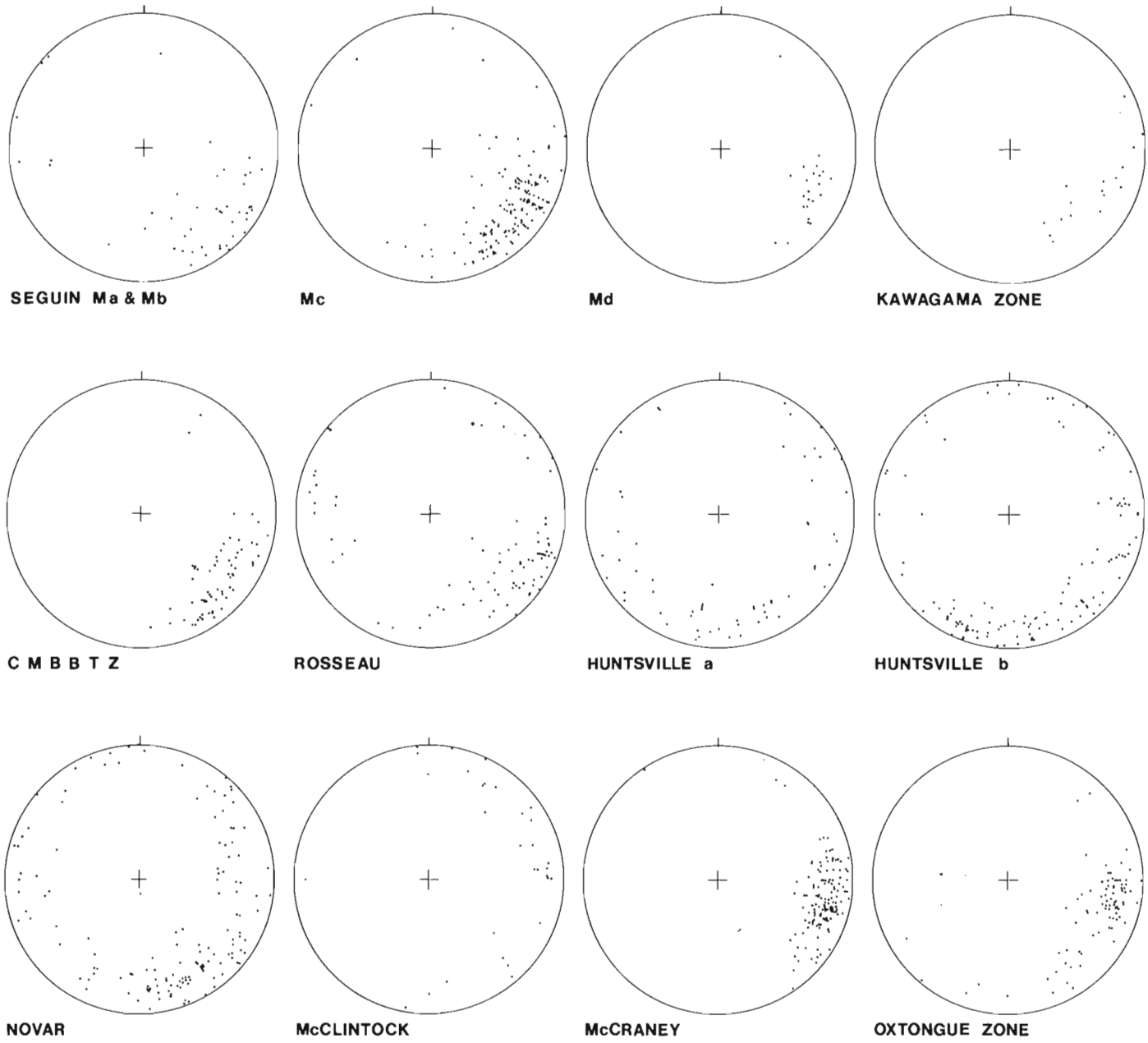

Figure 28.4. *Equal area, lower hemisphere plots of stretching lineations for the areas given in Figure 28.2.*

(Fig. 28.3), in the same manner as the internal tectonite zone in Rosseau subdomain (Davidson et al., 1982, Fig. 30.3). The more coarsely structured gneissic and migmatitic tectonites typical of the boundaries around Seguin and Moon River subdomains and at the edge of the Central Metasedimentary Belt are absent. Features of the various subdomains in Algonquin Domain are outlined below.

Novar Subdomain

A high proportion of orthogneissic rocks, ranging widely in composition, characterizes this subdomain. Hornblende-rich garnetiferous meta-quartz diorite is a common type in the northwest part; well preserved metagabbro, variously flattened, pink, megacrystic granitoid orthogneiss and dark gneissic charnockite occur elsewhere. Narrow septa of supracrustal gneiss lie between different metaplutonic phases locally and include aluminous varieties (perthite-plagioclase-sillimanite-garnet-corundum-magnetite-spinel). In places the different orthogneisses have the form of thick sheets folded around southeast-plunging axes. The Novar subdomain assemblage contrasts strongly with that of Seguin subdomain (migmatitic gneisses); the adjacent part of Kiosk Domain has a higher proportion of metasedimentary gneiss, including graphite-bearing and sillimanite-rich varieties.

Huntsville Subdomain

Separated from Novar subdomain by a straight-layered tectonic zone, Huntsville subdomain contains a notable proportion of metasedimentary gneiss and granulite, including pelitic gneiss with graphite, pyrite, pink garnet and minor

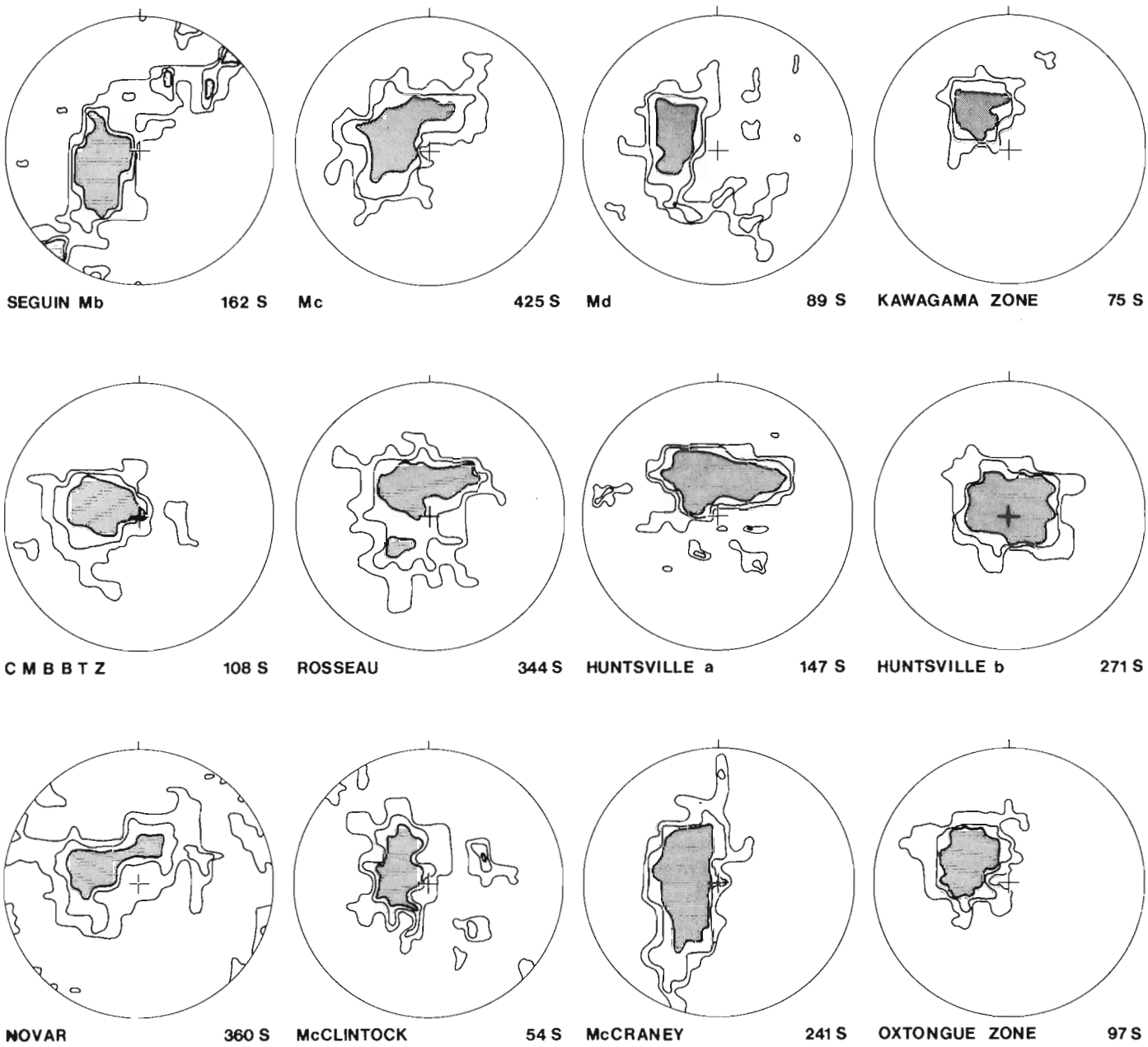

Figure 28.5. *Orientations of planar structures in the same areas as Figure 28.4. Equal area, lower hemisphere plots are contoured with intervals ranging from 1.1 – 1.9, 2.0 – 5.6 and 3.1 – 10.3% per 1% area.*

sillimanite in zones that can be traced for several kilometres (Davidson, 1982). Between metasedimentary gneiss belts lie elongate masses of highly flattened granitoid orthogneiss, commonly containing thin, lenticular augen of granular feldspar. A large mass of fine grained charnockitic orthogneiss in the eastern part of this subdomain is associated with a body of metagabbro within which are found rocks rich in garnet and pyroxene that look like eclogite. Shallow south- to east-dipping layering, within which intrafolial isoclines are common, is warped about 100 metre scale open folds.

McCraney Subdomain

An east- to northeast-dipping belt of flaggy, highly attenuated, dominantly quartzofeldspathic gneisses lies between the two subdomains just described and McCraney subdomain. Internally, quartzofeldspathic gneiss is abundant, particularly in the western part of this subdomain. The rocks vary from pink to pale green, are fine- to very fine-grained and commonly display quartz ribbons. Some grade to granitoid orthogneiss with K-feldspar augen, but others are interlayered with biotite-hypersthene gneiss and pelitic gneiss and contain in excess of 50 per cent quartz, suggesting

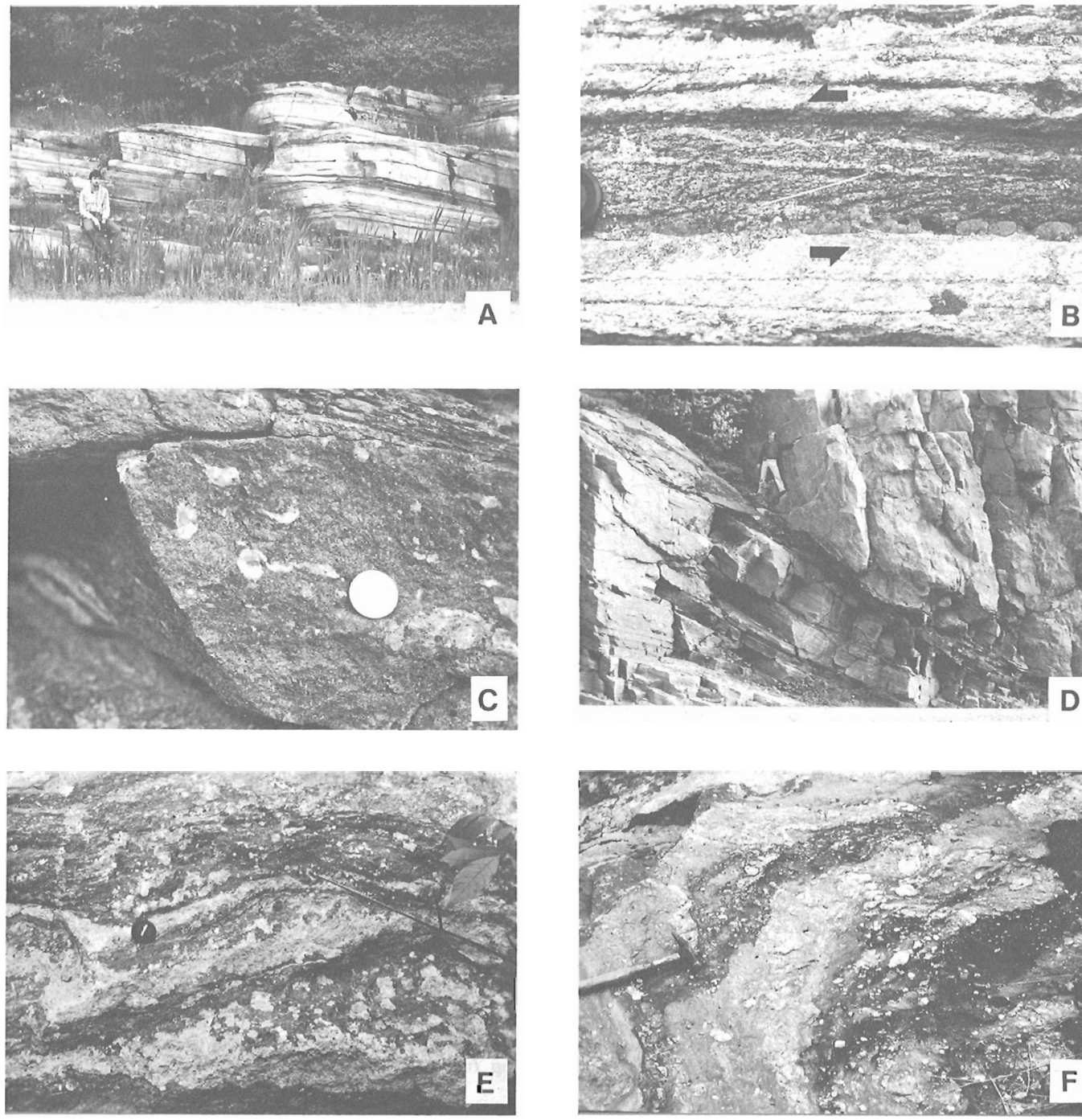

Figure 28.6. *Tectonic features in the Central Metasedimentary Belt boundary tectonic zone. All photographs are from roadcuts on Highway 35 northwest of Haliburton.*

A. Straight gneiss. GSC 203958-U.
B. Shear band foliation (parallel to white line) in a biotite-rich layer from straight gneiss illustrated in A. Shear sense is indicated by arrows. GSC 203958-T.
C. Feldspar augen with sigmoidal tail in 'tectonoclastic gneiss'. Coin is 2.3 cm in diameter. GSC 203958-W.
D. Large-scale sinistral shear of an upper, less deformed block over low-dipping straight gneiss. A tectonic schist horizon lies in the shear plane between the two blocks. GSC 203958-S.
E. Feldspar porphyroclasts in schistose tectonite formed by disaggregation of pegmatite. GSC 203958-X.
F. Porphyroclasts and isolated pegmatite fragments dispersed in schistose tectonite. GSC 203958-G.

a sedimentary origin. Mafic rocks are subordinate. The internal structure is one of intermediate to large scale folds coaxial with the east-southeast stretching lineation (Fig. 28.4, 28.5).

McClintock Subdomain

Bounded to the northwest and southeast by the Oxtongue and Kawagama straight belts respectively, McClintock subdomain, poorly known to date, appears to be in large part underlain by charnockitic orthogneiss of both monzonitic and granitic affinity. Metasedimentary gneisses in granulite facies form narrow, sinuous layers between orthogneiss masses and display northwest-verging recumbent folding that also involves flattened orthogneiss sheets. Some apparently homogeneous olive-brown granulites, previously tentatively mapped as a phase of the 'Algonquin batholith' (Schwerdtner and Lumbers, 1980), are interpreted to be of supracrustal origin in that they are intimately interlayered with pelitic gneiss and locally with calc-silicate gneiss and marble.

Metamorphism

An initial estimation of the distribution of granulite facies rocks in the western Algonquin region, based on field observations and limited thin section study, is given in Figure 28.7. Parry Sound Domain granulites are in part retrograded along the eastern margin, and the bounding gneissic tectonites display amphibolite facies assemblages. To the east, however, hypersthene-bearing assemblages occur on both sides of tectonic boundaries and, in addition, are present in many straight gneisses within the subdomain boundary zones in Algonquin Domain. In Figure 28.7, areas shown by the lightly ruled pattern indicate sporadic occurrences of hypersthene-bearing rocks, many of which show evidence of incomplete retrogression (growth of secondary hornblende and/or biotite, recrystallization of perthite to microcline and oligoclase). In southeastern Muskoka Domain, for example, a core of hypersthene-bearing orthogneiss is surrounded by an irregular zone in which patches of 'green rock' occur within otherwise pink and grey gneisses lacking hypersthene. Metamorphic hypersthene occurs locally in various rock types that form elongate masses within and parallel to the Kawagama zone. In much of Algonquin Domain, retrogression is limited to late, narrow shear zones and to margins of late pegmatite dykes. Some nonretrograded granulites are anhydrous (quartz-perthite-plagioclase-garnet-augite-hypersthene), but most in addition contain biotite and/or hornblende that do not show a replacement relationship with the anhydrous mafic silicates.

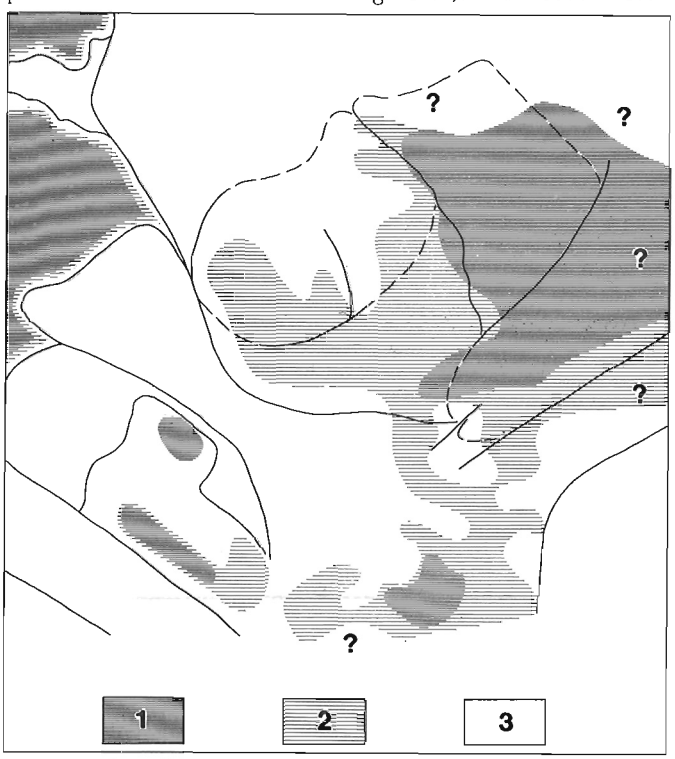

Figure 28.7. *Distribution of metamorphic facies. 1 – granulite facies, 2 – amphibolite facies with subordinate patches of granulites facies, in part retrograded, 3 – amphibolite facies.*

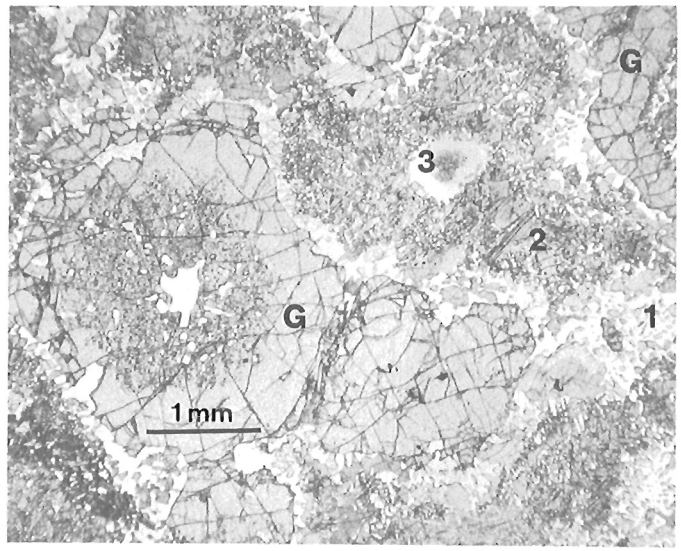

Figure 28.8. *Photomicrograph (plane light) of pseudo-eclogitic metagabbro, Novar subdomain. G – garnet, 1 – matrix plagioclase with fine hypersthene and amphibole, 2 – clinopyroxene with plagioclase laths, 3 – plagioclase knot with altered corundum core.*

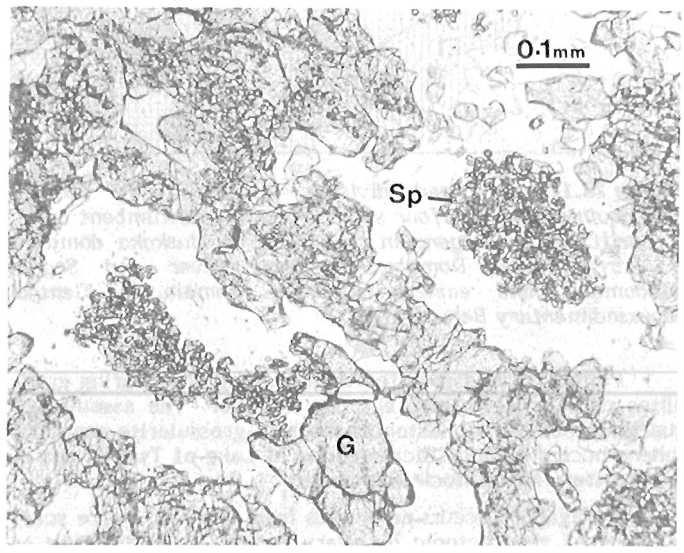

Figure 28.9. *Photomicrograph (plane light) of pseudo-eclogitic metagabbro, Novar subdomain, showing detail of spinel clusters (Sp) in the cores of plagioclase knots. G – garnet.*

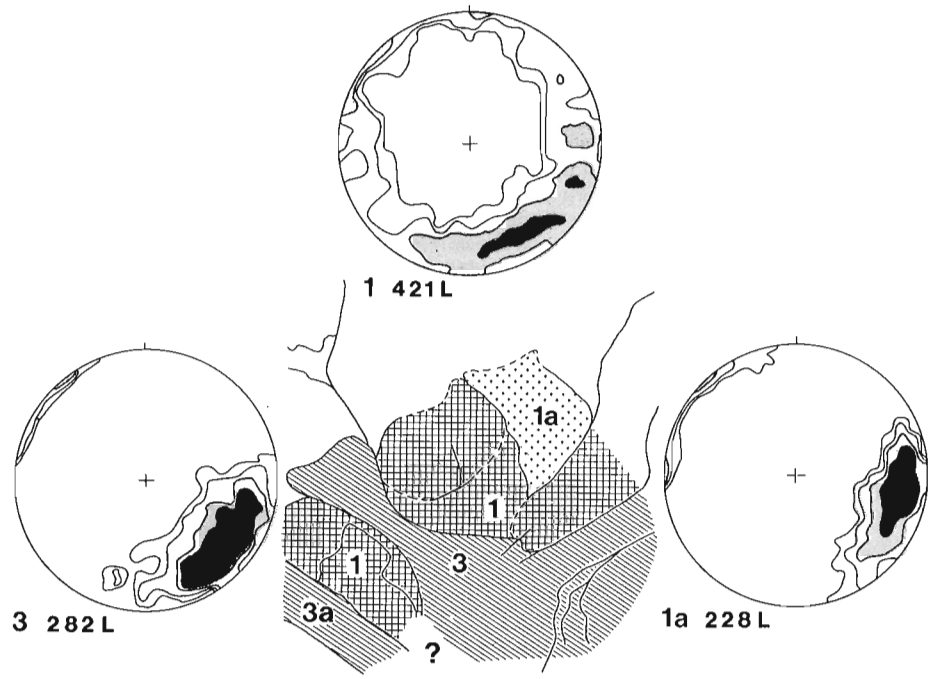

Figure 28.10

Synoptic diagram of orientations of stretching lineations. Data from area 3a (Moon River subdomain) are not included. Equal area, lower hemisphere plots are contoured at 0.5, 1.0, 2.0 and 4.0% per 1% area.

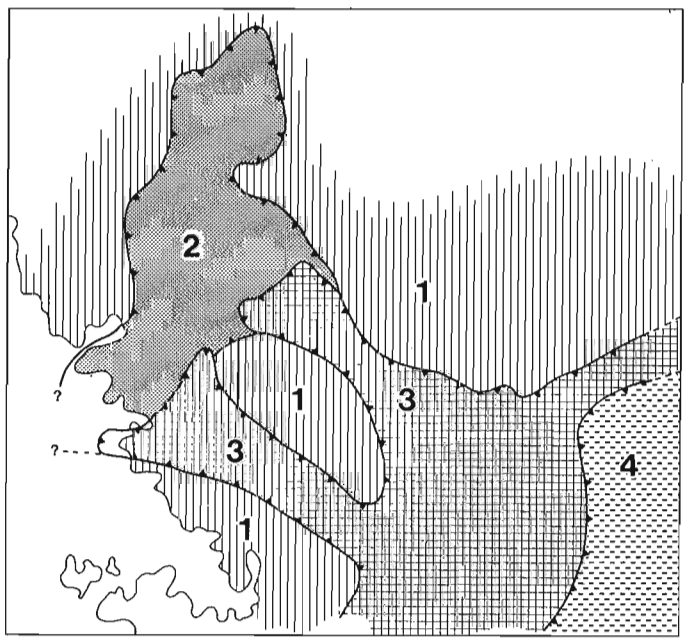

Figure 28.11. *Proposed division of the Parry Sound – Algonquin region into four structurally superincumbent units. 1 – Britt, Kiosk, Algonquin and parts of Muskoka domains, 2 – Parry Sound Domain, 3 – Moon River and Seguin subdomains and eastern Muskoka Domain, 4 – Central Metasedimentary Belt.*

Pelitic rocks associated with hypersthene-bearing granulites contain sillimanite but not kyanite. The assemblage quartz-orthoclase-wollastonite-diopside-grossularite-scapolite-sphene occurs in calc-silicate gneiss at Lake of Two Rivers in northeastern McClintock subdomain.

Metagabbro occurs as masses from 1 to 100 metre scale in many of the tectonic boundary zones. It also occurs as bodies of several km^2 outcrop are within subdomains. Much of the metagabbro has coronitic texture (see Davidson et al., 1982, p. 186 and Fig. 30.4A), though commonly advanced to such a degree that the original ophitic texture has been all but destroyed. Hydration of such rocks has produced varieties of amphibolite. Within some metagabbro bodies, however, complete recrystallization under relatively dry conditions has produced massive, medium to pale green pyroxene-rich granulite, studded with garnet, that looks like eclogite (locations shown in Fig. 28.2). Thin sections show that these rocks contain appreciable quantities of plagioclase, however, both as a fine grained, granular matrix and as lamellar intergrowths with clinopyroxene (Fig. 28.8). Garnets have spongy cores with inclusions of quartz, plagioclase, rutile and mafic silicates. Granular hypersthene and pale amphibole are present in the matrix. Some of these rocks show small white or green knots on weathered surfaces that prove to be fine aggregates of corundum and/or spinel in the cores of granular plagioclase patches (Fig. 28.9). These rocks are texturally similar to the sapphirine-bearing metabasite previously described from near Arnstein (Davidson et al., 1982, p. 188).

All gradations have been observed between weakly coronitic to pseudo-eclogitic metagabbro. This gradation is accompanied by a decrease in the amount of plagioclase in the rock and a corresponding reduction of its anorthite content from about An_{60} to about An_{40}. Ca and Al from anorthite presumably contribute to the formation of garnet and clinopyroxene, with excess Al being taken up as corundum, spinel or sapphirine. Instability of the anorthite component of plagioclase is the first step toward the disappearance of plagioclase required to produce a true eclogite. In Algonquin Domain, pseudo-eclogitic metagabbro of the type described above is the product of granulite facies metamorphism, likely isofacial with the pervasive regional metamorphic grade. Pseudo-eclogitic metagabbro within metabasite inclusions in amphibolite grade gneissic tectonites of domain boundary zones, therefore, indicates derivation either from a lower crustal level or from laterally adjacent terranes in which granulite facies metamorphism had been formerly established.

Structural Framework

Perusal of Figure 28.3, 28.4, 28.5 reveals that structural patterns vary from one domain or subdomain to another. The stereoplots serve to emphasize the generally moderate to low dips of planar elements and low plunges of stretching lineations. Linear elements in particular are concentrated in the southeast quadrant for Seguin subdomain, eastern Muskoka Domain, and for the Kawagama and Central Metasedimentary Belt boundary tectonic zones. Those of Novar, Huntsville and McClintock subdomains of Algonquin Domain and of Rosseau subdomain of Muskoka Domain, on the other hand, are more widely dispersed; McCraney subdomain and the Oxtongue zone have an easterly plunging linear element. These three groupings are summarized in Figure 28.10.

Given the similarity in structural pattern (as well as lithological and metamorphic attributes) between Rosseau subdomain and much of Algonquin Domain, and the continuity and inward dip of the boundary around Seguin subdomain and its extension south of Algonquin Domain, it seems logical to equate Rosseau subdomain as an extension of Algonquin Domain buried by the Seguin synformal lobe. Rosseau subdomain and Algonquin Domain thus constitute part of a lower structural unit on which the Seguin lobe lies. By the same token, Go Home subdomain, lying southwest of the Moon River lobe, belongs to the same lower structural unit (Fig. 28.11; see Davidson et al., 1982, p. 189). Interpretation from marginal structural relationships that Parry Sound Domain lies structurally between the lower unit and the Moon River and Seguin lobes of Muskoka Domain is corroborated by gravity modelling of the positive Bouguer anomaly associated with Parry Sound Domain (see Lindia et al., 1983). Identification of a major southeast-dipping tectonic zone at the east side of Muskoka Domain leads to identification of the Central Metasedimentary Belt as a structurally higher unit lying above Muskoka Domain. The Grenville crust in the Parry Sound – Algonquin region is thus envisaged as embracing four, major, superincumbent structural units. Where preserved, kinematic indicators in the bounding tectonite zones suggest an overall northwesterly direction for tectonic transport, that is, up the regional lineation. A working model thus involves northwestward stacking of large crustal slices with major shear zones along the slice interfaces.

Algonquin Domain contains several internal blocks bounded by curviplanar tectonic zones, expressed at the surface as belts of highly attenuated gneisses equivalent to those in the adjacent subdomains. Similar zones in other parts of the lower structural unit, such as the internal tectonite zone in Rosseau subdomain, shown in Fig. 28.3, and a zone of straight gneiss and mylonite in Britt Domain, have already been described (Davidson et al., 1982). Characteristic of many of these zones, particularly in Algonquin Domain, is that the straight gneisses themselves contain granulite facies mineral assemblages and do not usually have the blocky tectonite ('tectonoclastic gneiss') component found at the boundaries between higher structural units. Rocks of the tectonite zones above the lower structural unit have amphibolite assemblages, although syndeformational hypersthene is present in some minor shears in Parry Sound granulites near the base of the overlying Moon River subdomain (S.K. Hanmer, personal communication, 1983). Truncation of the internal Rosseau subdomain tectonite zone by the Moon River boundary suggests an earlier tectonic history within the lower structural unit. Presence of pseudo-eclogitic metagabbro blocks in amphibolite facies tectonite zones points to an earlier metamorphic history. Occurrence of this rock type in Algonquin Domain apparently in equilibrium with metamorphic assemblages both within subdomains and in their bounding straight gneisses supports the hypothesis that internal tectonite zones in the lower structural unit have an earlier origin. Truncation of subdomain structure by the internal tectonite zones (e.g. between Novar and Huntsville subdomains) suggests the presence of even earlier structure, but the extent to which this may have been subsequently modified is not known.

The Algonquin region has been characterized as the site of a ridge-shaped batholith of variously modified and different plutonic rocks, originally emplaced in Middle Precambrian supracrustal rocks, unroofed, and overlain by Late Precambrian supracrustals (Grenville Supergroup of the Central Metasedimentary Belt) that have a coarse clastic basal unit (Schwerdtner and Lumbers, 1980). These authors state that "Most of the tectonic and metamorphic features now preserved in the batholith and the surrounding rocks were formed during late high-rank metamorphism when the batholith was reactivated and became diapiric toward the overlying supracrustal rocks." (ibid., p. 167). In the western Algonquin region a significant proportion of the rock assemblage is of undoubted supracrustal origin. In addition, structural patterns are more readily interpreted as representing a series of southeast-inclined lobes or slices that may subsequently prove worthy of being termed nappes. In the Central Metasedimentary Belt boundary tectonic zone, northwesterly tectonic transport of the overlying structural unit is the reverse of what would be expected if the Algonquin batholith behaved diapirically with respect to the Grenville Supergroup. The role that diapirism, of whatever order, may have played in the tectonic history within the confines of Algonquin Domain seems to be of subordinate importance in explaining the rock distribution, metamorphism and fundamental structure outlined above. Despite the abundance of metaplutonic rock, the term batholith conveys the wrong impression of this exceedingly complex terrane.

References

Adams, F.D. and Barlow, A.E.
1910: Geology of the Haliburton and Bancroft areas; Geological Survey of Canada, Memoir 6, 419 p.

Davidson, A.
1982: Graphite occurrences in the Algonquin region, Grenville Province, Ontario; Geological Survey of Canada, Open File 870.

Davidson, A. and Morgan, W.C.
1981: Preliminary notes on the geology east of Georgian Bay, Grenville Structural Province, Ontario; in Current Research, Part A, Geological Survey of Canada, Paper 81-1A, p. 291-298.

Davidson, A., Culshaw, N.G., and Nadeau, L.
1982: A tectono-metamorphic framework for part of the Grenville Province, Parry Sound region, Ontario; in Current Research, Part A, Geological Survey of Canada, Paper 82-1A, p. 175-190.

Lindia, F.M., Thomas, M.D., and Davidson, A.
1983: Geological significance of Bouguer gravity anomalies in the region of Parry Sound Domain, Grenville Province; in Current Research, Part B, Geological Survey of Canada, Paper 83-1B, Report 30.

Lumbers, S.B.
1980: Geology of Renfrew County, southern Ontario; Ontario Geological Survey, Open File Report 5282, 118 p.

Schwerdtner, W.M. and Lumbers, S.B.
1980: Major diapiric structures in the Superior and Grenville provinces of the Canadian Shield; in The Continental Crust and its Mineral Deposits, ed. D.W. Strangway; Geological Association of Canada, Special Paper 20, p. 149-180.

Schwerdtner, W.M. and Mawer, C.K.
1982: Geology of the Gravenhurst region, Grenville Structural Province, Ontario; in Current Research, Part B, Geological Survey of Canada, Paper 82-1B, p. 195-207.

Smith, J.V.
1974: Feldspar Minerals, v. 2; Springer-Verlag, Heidelberg, 690 p.

29. STRUCTURE CROSS-SECTIONS ACROSS ASIAK FORELAND THRUST AND FOLD BELT, WOPMAY OROGEN, DISTRICT OF MACKENZIE

Project 810021

R. Tirrul
Precambrian Geology Division

Tirrul, R., Structure cross-sections across Asiak Foreland Thrust and Fold Belt, Wopmay Orogen, District of Mackenzie; in Current Research, Part B, Geological Survey of Canada, Paper 83-1B, p. 253-260, 1983.

Abstract

Two structure cross-sections across Asiak Foreland Thrust and Fold Belt display a lower structural level characterized by folded Odjick-Rocknest formation imbricates on a sole thrust 100-300 m above Archean basement, and an upper level dominated by tight chevron folds of the Recluse Group. Minimum shortening estimates are consistently above 40 per cent, indicating that the northern Rocknest shelf edge has been translated no less than 47 km toward the craton. Numerous reversals of vergence, and the lack of change in average structural level across its width suggest that the active belt was a wedge of low taper.

Résumé

Deux coupes transversales de la zone de chevauchement et de plissement des avant-pays Asiak montrent un niveau structural inférieur caractérisé par des structures imbriquées plissées de la formation de Odjick-Rocknest sur un plan de chevauchement situé de 200 à 300 m au-dessus du socle archéen, ainsi qu'un niveau supérieur dominé par des plis en chevron serrés du groupe de Recluse. On estime le taux de raccourcissement minimal généralement à 40 %, ce qui indique que la marge nord du plateau de Rocknest a été charriée sur au moins 47 m en direction du craton. De nombreux changements de vergence et l'absence d'une modification du niveau structural moyen en travers de la largeur de la zone suggèrent que cette zone active était un coin faiblement effilé.

Introduction

Asiak Foreland Thrust and Fold Belt of Wopmay Orogen is a wedge of late Aphebian supracrustal rocks which has been detached from its basement, shortened and translated eastward with respect to the Slave Craton during the first of three major compressional events to affect the orogen. Termed the 'Calderian orogeny', (Hoffman and Bowring, 1983), it is interpreted to record the collision of a west-facing passive continental margin with a microcontinent between 1.90 and 1.885 Ga (Hoffman, 1980; Hoffman and Bowring, 1983).

The establishment and interpretation of the geometry of Asiak Thrust-Fold Belt is a major focus of the current project, presently in its third and final year. Mapping is now sufficiently advanced to enable the construction of comparatively well constrained structure cross-sections across the entire foreland. Discussion in this report centres around two composite cross-sections at 66°N and 67°30'N, located in Figure 29.1. Previous accounts of Asiak Thrust-Fold Belt structural features include Tirrul (1982) and Hoffman et al. (1983). Stratigraphic aspects are discussed in Grotzinger and Hoffman (1983) and references contained therein.

Acknowledgments

It is a pleasure to thank Jean David, Mark Daynecka, Greg Eiché and Karen Pelletier for mapping assistance. Paul Hoffman, John Grotzinger and Marc St-Onge have made important contributions to the data and ideas presented here.

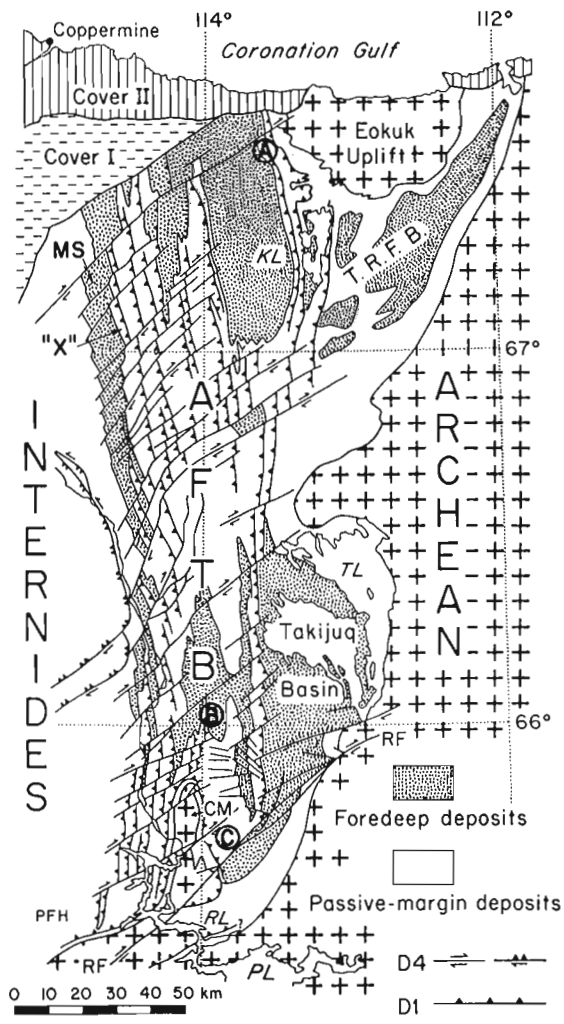

Figure 29.1. *The externides of Wopmay Orogen, showing the location of cross-sections in Figure 29.2. AFTB, Asiak Fold-Thrust Belt; TRFB, Tree River Fold Belt; CM, Carousel Massif; RF, Redrock Fault; KL, Kikerk Lake; TL, Takijuq Lake; RL, Redrock Lake; PL, Point Lake.*

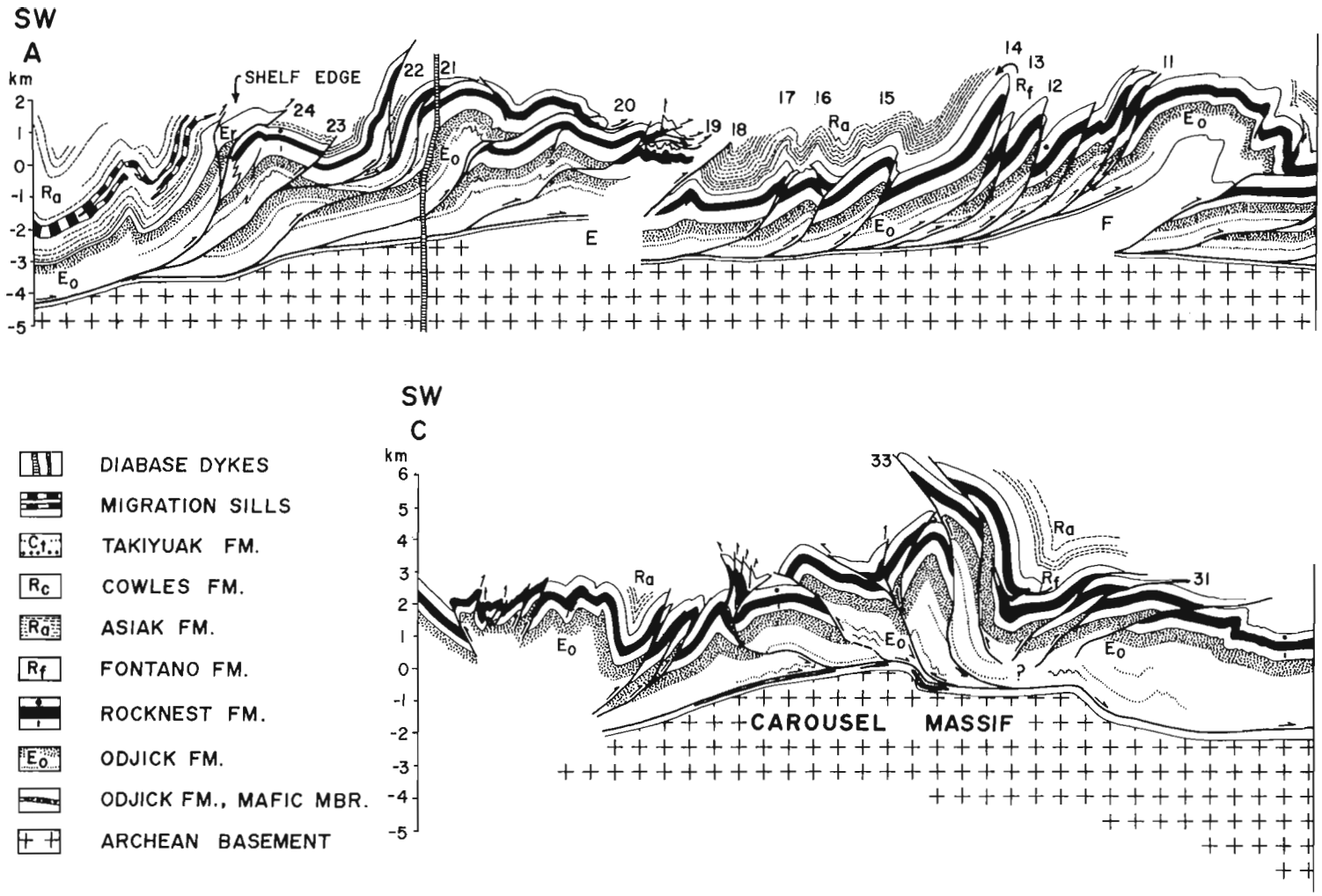

Figure 29.2. *Composite cross-sections across Asiak Thrust and Fold Belt. Data has been liberally projected into the sections from both north and south of the lines located in Figure 29.1. Numbers and letters refer to features discussed in the text. 'Fontano Fm.' includes the Tree River Formation.*

Cross-Section Limitations and Assumptions

(a) Basement Depth

The major limitation on the construction of unique sections remains our inability to define basement profiles. Comparison of Carousel Massif (St-Onge et al., 1982; Hoffman et al., 1983) with other Calderian anticlinoria exposed at higher structural levels raises the possibility that the latter are underlain by basement culminations, but of unknown depth and configuration. The basement surface does not have a uniform slope.

Basement depth determination based on magnetic anomaly modelling has been unsuccessful in spite of excellent published 1:50 000 aeromagnetic maps of the entire fold belt. This is partly due to the magnetic contribution from units above the basement, and partly because useful basement anomalies have not been recognized. Over much of the area, the signature of the Mackenzie diabase dyke swarm overwhelms other components, making accurate anomaly partitioning difficult. In regions of comparatively high (but greenschist) metamorphic grade, beds of lower Odjick Formation contain concentrations of metamorphic magnetite and are responsible for the most prominent anomalies.

(b) Odjick Stratigraphy

Compounding the basement depth problem is the lack of distinctive marker beds within the Odjick Formation. Odjick stratigraphy is well known locally, or for incomplete sections, but a detailed regional internal stratigraphy has yet to be resolved. Total formation thickness is known only from the autochthon where it is 750 m thick but generally poorly exposed. It is asumed to increase westward to 1.4 km at the shelf edge, according to minimum thicknesses of exposed sections.

(c) Penetrative Strain

The amount, type, and distribution of penetrative strain must be accounted for in any restorable cross-section. North of 67°N, and west of Tree River Fold Belt, homogeneous

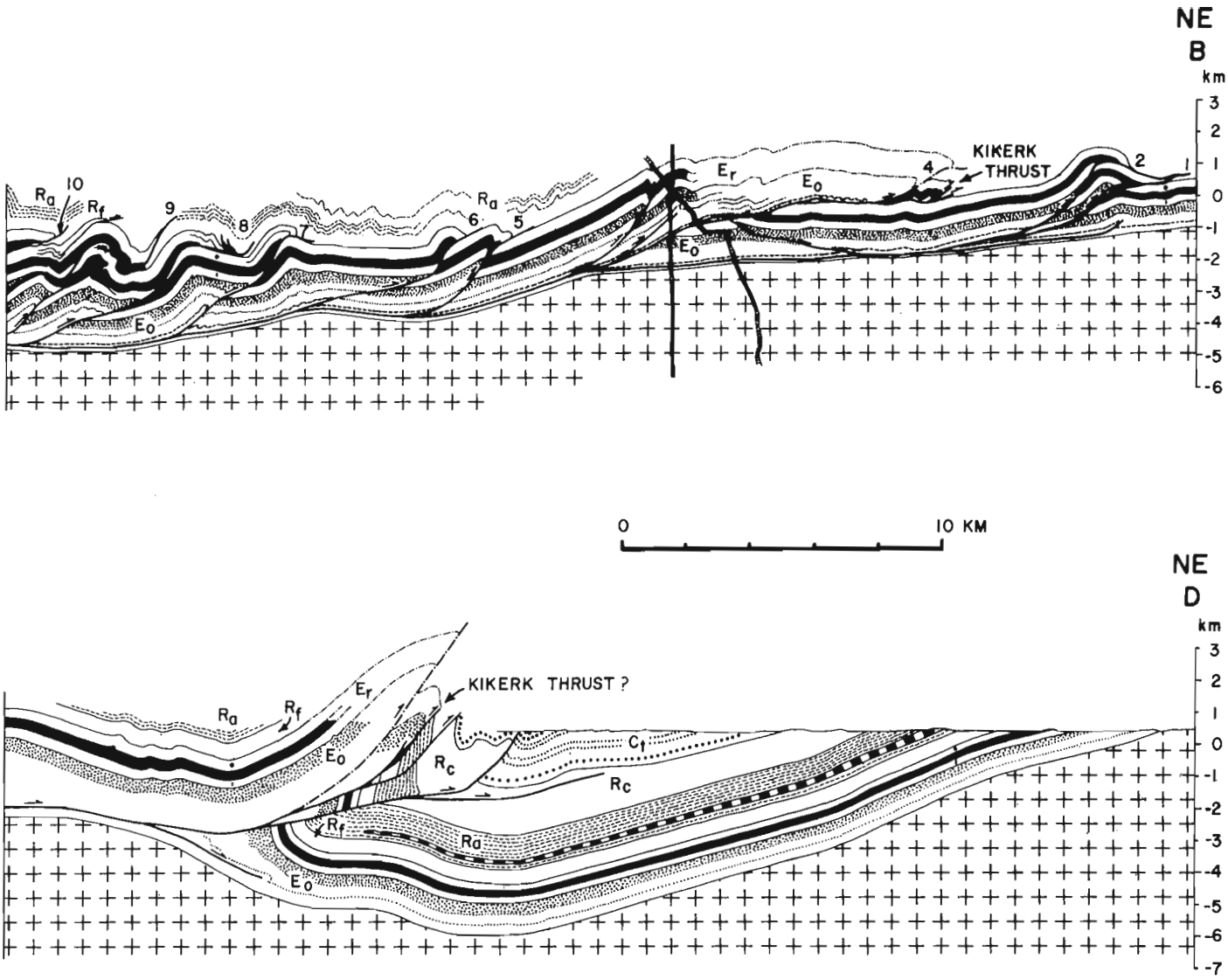

strain of Rocknest members with high dolomite/dololutite ratio is low ($X/Z \leq 1.2$). This is shown by excellent preservation of primary textures and structures (Grotzinger and Hoffman, 1983), by the weak development of cleavage, by mesoscopic dolomite fold profiles which approach class 1B (concentric) folds, and by the small variation in member thickness as measured in the field and on plunge projections irrespective of bedding attitude. For example, the thickness of Rocknest members 3 to 10 measured at two adjacent localities (immediately east and west of thrust 23, Fig. 29.2) where bedding is at low (65-51°W dips) and high (19-38°E dips) angles to local axial surfaces was found to be 329 and 333 m respectively (Grotzinger, unpublished data) indicating no significant fold 'flattening' (Ramsay, 1967).

The bulk of the Odjick Formation is cleaved semipelite with numerous small-scale folds that vary from class 1C through 3, negating the possibility of accurate bed-length 'balancing'. Accordingly, the area of Odjick shown on section segments 5-10, 11-17 and 19-24 (Fig. 29.2, section A-B) corresponds to that required to match the bed length of Rocknest member 3 and minimum stratigraphic thicknesses of 1.0, 1.0 and 1.4 km respectively. The geometry of thrusts which stack Odjick is largely inferred. It is recognized that some of the shortening represented by thrusts at the Rocknest level may be taken up by penetrative strain and folding at lower levels.

Rocknest Formation dolomite around Carousel Massif and probably farther north, shows moderate penetrative strain as determined from deformed oolites and **Conophyton** cross-sections. Axial ratios X/Z in the cross-section plane range from 1.18-1.61 (X subvertical) on gently dipping panels. The distribution of the strain and its timing with respect to fold development is not known, so it has not been incorporated into estimates of shortening outlined below.

Thrust Slip Estimates

Despite the absence of seismic and well data, slip on many Asiak thrusts is defined. These faults include folded thrusts 1, 2, 7, 8, 9 and 20 (Fig. 29.2, Section A-B) where

Figure 29.3. *Geological map of Carousel Massif area, simplified from unpublished 1:50 000 maps, showing structural levels depicted on Figure 29.4. See Figure 29.2 for an explanation of stratigraphic symbols. 1. transcurrent fault; 2. normal fault; 3. oblique-slip fault; 4. thrust fault; 5. basal décollement; 6. plunging anticline; 7. plunging syncline; 8. projected structural level, Figure 29.4. 1-7 are inferred where dashed.*

hangingwall and footwall cutoffs of the same stratigraphic level are exposed in the transport direction. Reliable minimum estimates can be made for faults such as Kikerk thrust (Fig. 29.2, Section A-B) where the location of footwall cutoffs can be confidently inferred. The situation of the later thrust along the southeastern flank of Eokuk uplift is particularly fortunate. Here upright, open Tree River folds are orthogonal to, and fold Calderian structures, exposing hangingwall 'flats' of Kikerk thrust for about 4.5 km in the transport direction. This enables a firm minimum slip estimate of 8 km for Kikerk Thrust and trailing imbricate 4 to be made.

Somewhat less reliable, but extensively incorporated into the sections are structure projections. Where plunge is 15-30° (Rocknest folds between 7 and 10, Section A-B, and much of Section C-D), the projections are rigorous. Where plunge is shallower (between thrusts 14 and 20), projections are semiquantitative.

In the absence of other criteria, thrust strike length was used to constrain slip. Elliot (1976) shows average slip gradients of 0.14 km/km strike length for the southern Canadian Rockies; gradients higher than 0.3 are common in the Wyoming Overthrust Belt (Dixon, 1982). Gradients were arbitrarily limited to 0.2 for section A-B. (If a thrust terminates 10 km from the section line it was limited to 2 km slip). Even so, the slip and geometry of thrusts 10 and 18 are hard to define. If slip is large, then much of the volume at E and F may be occupied by Epworth Group rocks, rather than basement.

Carousel Structure

To demonstrate the use of projections and to document relations around Carousel Massif described by Hoffman et al. (1983) a summary map and detailed projection are presented (Fig. 29.3, 29.4). In this area, data from traverses A-R, located in Figure 29.3, have been stacked according to local fold plunge, which varies from 0-30°N, and after correction for transcurrent and normal fault offset. Rocknest fold profiles along A-B, at H and at K are rigorous projections. The procedure is justified by the fact that variations of Rocknest bed length with stratigraphy are local and non-cumulative, and because the area of Odjick is compatible with its observed thickness and Rocknest bed length. Exceptions include thrust 33 where there is a large mismatch of cutoffs and the Odjick beneath thrust 31, (Fig. 29.4) which is anomalously thick. It is not clear whether this thickening is stratigraphic or tectonic.

The structure on the crest of the massif can be viewed as a 'triangle zone' where Epworth Group imbricates have been wedged between a forward décollement and multiple back thrusts. The position of the massif beneath the imbricates and folded décollement invites the idea that the basement itself occupies part of the 'triangle zone'. By this model the massif is a basement ramp fold riding on a thrust(s) which merges with the basal décollement to the east, in a geometry analogous to that observed in the Rocky Mountain Foothills. This predicts about 8 km of slip, equal to the aggregate of the back thrust set, for any proposed basement thrust. However, careful mapping of the synclinal cores of second-order basement folds (Fig. 29.1) of Carousel Massif shows continuity of basal Odjick stratigraphy with no evidence of thrusting. The folds are apparently buckles or manifestations of basement shears which do not break the sedimentary cover, and are probably unrelated to the back thrust set.

Minimum Shortening Estimates

Bed length shown on section A-B from the Rocknest shelf edge to the frontal thrust, a distance of 68 km, is 115 km (41 per cent shortening). This is thought to be a minimum estimate because conservative values of slip have been applied to thrusts of unknown displacement. The southern section does not extend to the shelf edge, but here too the shortening is similar: 75 km of bed-length over a section length of 43 km represents 43 per cent shortening. These values are intermediate when compared with younger thrust-fold belts which range from about 10 per cent (Southern Zagros) to 65 per cent (Foothills and Front Ranges, southern Canadian Rockies).

The Active Belt: A Wedge of Low Taper?

The growth of any thrust-fold belt occurs by the sequential initiation of foreland imbricates or folds at the deformation front, contemporaneously with shortening and thickening of the entire belt. The active belt develops a stable taper, defined by basal décollement and erosional profile, which is a reflection of the ratio of the yield strength of the wedge to that of the décollement (Chapple, 1978; Davis et al., 1983; Stockmal, in press). Where the ratio is comparatively high, a steep taper develops, resulting in a crude internal 'tectonic stratigraphy' where, on average, progressively older units are exposed toward the hinterland. With postorogenic uplift, this feature is accentuated. It is well displayed in the southern Canadian Rockies, for example, where the average erosional level ranges from Paleogene at the deformation front to the Proterozoic of Purcell Anticlinoria.

One of the first order characteristics of Asiak Thrust-Fold Belt is the absence of a progressive increase in average erosional level toward the hinterland along any transect across the Rocknest shelf. In this regard the belt is similar to the Jura (Pierce, 1966) or the southern Zagros Mountains (Huber, 1977) which have very weak detachments, and suggests that Asiak Thrust and Fold Belt was a wedge of lower taper.

Common reversals of vergence exemplified by the back thrusts of Carousel Massif also imply a wedge of low taper. Normally, the forward slope of maximum stress trajectories (Chapple, 1978; Stockmal, in press) combined with (on average) gently dipping bedding favours forward thrusts with a shallow dip. With an increase in the ratio of rock strength to décollement strength, the trajectories flatten, increasing the likelihood of failure by low angle back thrusting. This occurs at shallow depths in the toe regions of fold belts, where cohesion is an important component of rock strength, or for belts sliding on a weak décollement.

Why should the pelite of the basal décollement be significantly weaker than that of the rest of the stratigraphic succession? There is no stratigraphic evidence for the occurrence of evaporites within the lower Odjick. One possibility is that the position of the décollement is to some degree controlled by metamorphic grade. Qualitative indicators of grade (cleavage intensity, growth of syntectonic chlorite, red to green transitions and appearance of metamorphic magnetite) suggest that metamorphic grade is partly related to structural depth. Does the position of the décollement coincide with a transition from frictional to ductile sliding mechanisms, or to an increase in pore fluid pressure related to dehydration reactions? Future work will include detailed studies of exposed detachment surfaces, as well as a systematic survey of metamorphism in the externides.

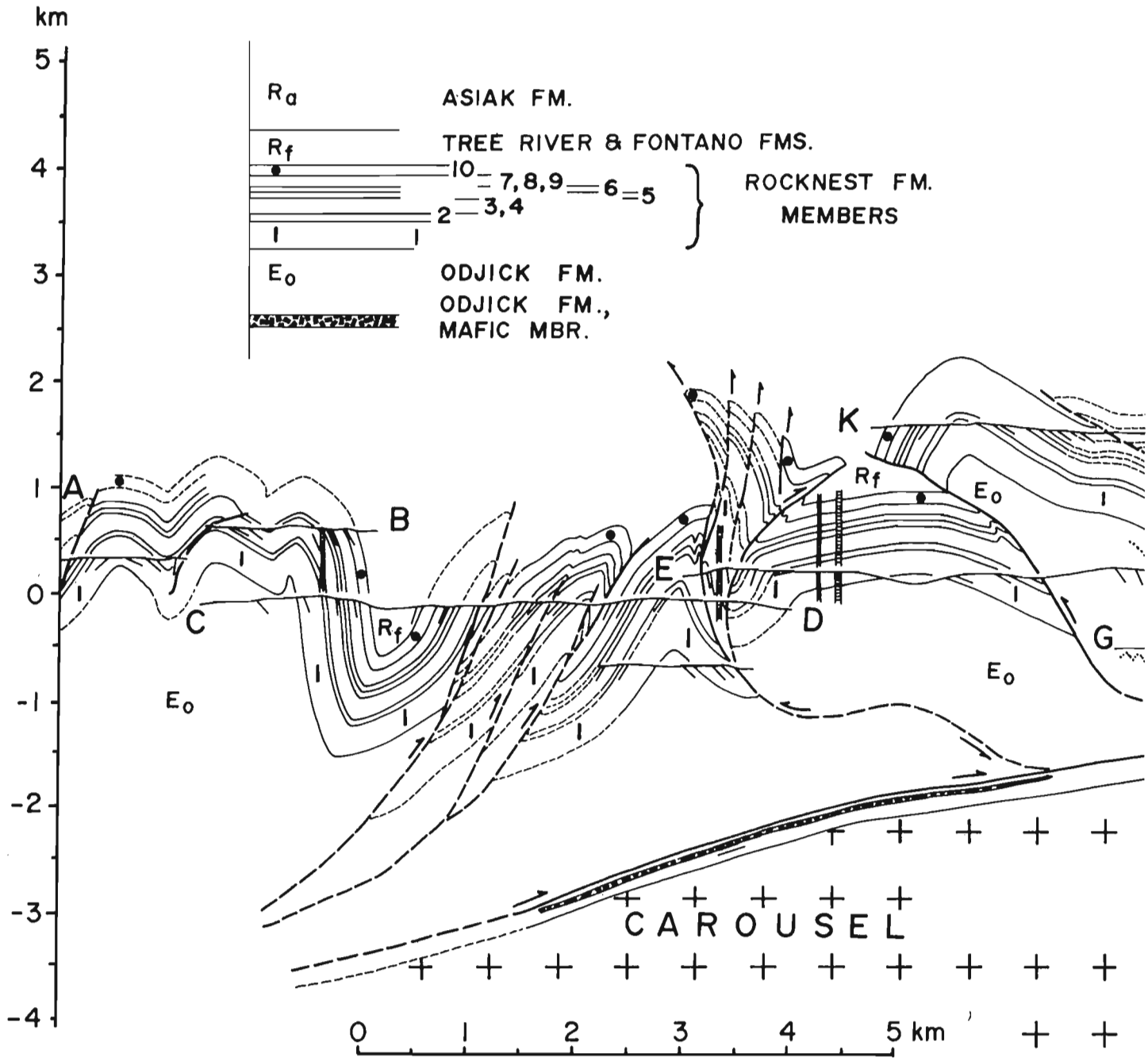

Figure 29.4. *A composite plunge projection of structure at the north end of Carousel Massif. Contacts are dashed where no down-plunge information is available. Rocknest members 2, 3, 4 and 5 are combined to make the middle, bold unit shown on Figure 29.3. See text for discussion.*

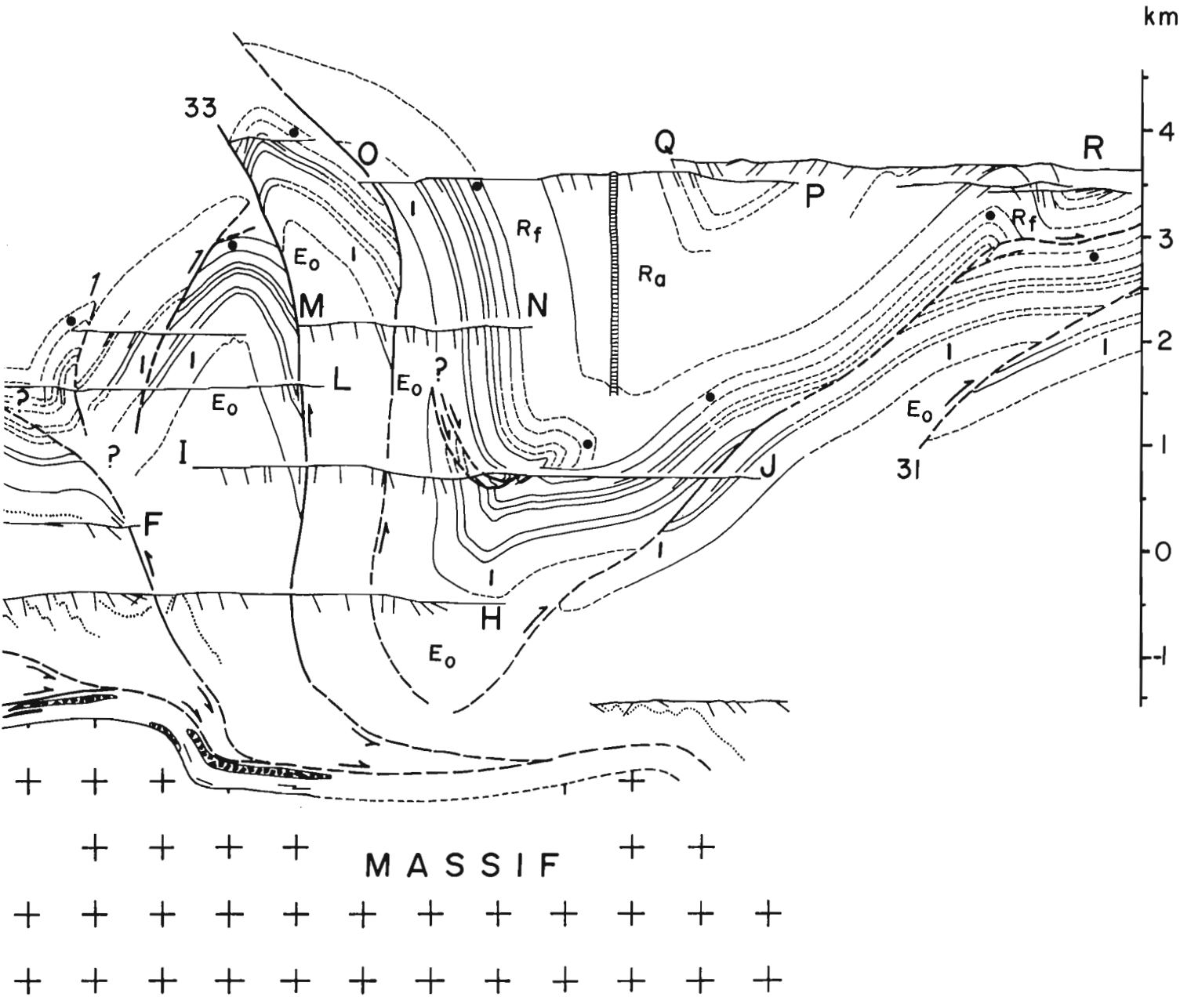
km
4
3
2
1
0
-1
33
O
Q
R
P
R_f
R_a
E_o
M
N
L
I
J
F
H
?
31
MASSIF

References

Chapple, W.M.
1978: Mechanics of thin-skinned fold-and-thrust belts; Geological Society of America, Bulletin, v. 89, p. 1189-1198.

Davis, D., Suppe, J., and Dahlen, F.A.
1983: Mechanics of fold-and-thrust belts and accretionary wedges; Journal of Geophysical Research, v. 88, no. B2, p. 1153-1172.

Dixon, J.S.
1982: Regional structural synthesis, Wyoming salient of Western Overthrust Belt; American Association of Petroleum Geologists, Bulletin, v. 66, no. 10, p. 1560-1580.

Elliot, D.
1976: The energy balance and deformation mechanisms of thrust sheets; Royal Society of London, Philosphical Transactions, Series A, v. 283, p. 289-312.

Grotzinger, J.P. and Hoffman, P.F.
1983: Aspects of the Rocknest Formation, Asiak Thrust-Fold Belt, Wopmay Orogen, District of Mackenzie; in Current Research, Part B, Geological Survey of Canada, Paper 83-1B, Report 10.

Hoffman, P.F.
1980: Wopmay Orogen: a Wilson cycle of early Proterozoic age in the northwest of the Canadian Shield; in The Continental Crust and Its Mineral Resources, ed. D.W. Strangway; Geological Association of Canada, Special Paper 20, p. 523-549.

Hoffman, P.F. and Bowring, S.A.
1983: A short-lived 1.9 Ga continental margin and its destruction, Wopmay Orogen, northwest Canada; Geology.

Hoffman, P.F., Tirrul, R., and Grotzinger, J.P.
1983: The externides of Wopmay Orogen, Point Lake and Kikerk Lake map areas, District of Mackenzie; in Current Research, Part A, Geological Survey of Canada, Paper 83-1A, p. 429-435.

Huber, H.
1977: Geological cross sections south-central and south-west Iran, 1:500 000; Tehran, National Oil Company of Iran, Exploration and Production Affairs.

Pierce, W.G.
1966: Jura tectonics as a decollement; Geological Society of America, Bulletin, v. 77, p. 1265-1276.

Ramsay, J.G.
1967: Folding and Fracturing of Rocks: New York, McGraw-Hill, 568 p.

St-Onge, M.R., King, J.E., and Lalonde, A.E.
1982: Geology of the central Wopmay Orogen (Early Proterozoic), Bear Province, District of Mackenzie: Redrock Lake and the eastern portion of Calder River map areas; in Current Research, Part A, Geological Survey of Canada, Pper 82-1A, p. 99-108.

Stockmal, G.S.
– Modeling of large-scale accretionary wedge deformation; Journal of Geophysical Research. (in press)

Tirrul, R.
1982: Frontal thrust zone of Wopmay Orogen, Takijuq Lake map area, District of Mackenzie; in Current Research, Part A, Geological Survey of Canada, Paper 82-1A, p. 119-122.

30.

GEOLOGICAL SIGNIFICANCE OF BOUGUER GRAVITY ANOMALIES IN THE REGION OF PARRY SOUND DOMAIN, GRENVILLE PROVINCE, ONTARIO[1]

Project 760061

F.M. Lindia[2], M.D. Thomas[3] and A. Davidson
Precambrian Geology Division

Lindia, F.M., Thomas, M.D., and Davidson, A., Geological significance of Bouguer gravity anomalies in the region of Parry Sound Domain, Grenville Province, Ontario; in Current Research, Part B, Geological Survey of Canada, Paper 83-1B, p. 261-266, 1983.

Abstract

Regional gravity surveys supplemented by closely spaced observations along selected traverses outline a 35 mGal amplitude positive anomaly coinciding with Parry Sound Domain of the Central Gneiss Belt, Grenville Province. Quantitative two- and two-and-a-half-dimensional modelling of the anomaly, constrained by data obtained from several hundred density measurements and surface geological boundaries, indicates that Parry Sound Domain has overall bowl-shaped geometry. Depths to the bottom are generally 5 km or so in the northeastern and southwestern sections of the domain, but may plunge to a maximum of 13 km in the central region.

An important result of the gravity modelling, as far as the tectonic history of the region is concerned, is that Parry Sound rocks extend as southeastward-thinning wedges beneath Seguin and Moon River subdomains, thus supporting geological arguments that the latter units are superposed on Parry Sound Domain.

Résumé

Des levés gravimétriques régionaux complétés par des observations rapprochées le long de cheminements choisis tracent une anomalie positive de 35 mGal qui coïncide avec le domaine de Parry Sound de la zone centrale de gneiss de la province de Grenville. Des modèles quantitatifs à 2 dimensions et à 2,5 dimensions de l'anomalie, limités par les données provenant de plusieurs centaines d'observations de la densité et par des limites géologiques de surface, indiquent que la géométrie globale du domaine de Parry Sound présente la forme d'un bol. Les profondeurs sont généralement de 5 km dans les sections nord-est et sud-ouest du domaine mais peuvent atteindre un maximum de 13 km dans la partie centrale.

Le modèle gravimétrique a donné un résultat important en ce qui concerne l'histoire tectonique de la région: les roches de Parry Sound s'étendent en forme de coins amincis en direction sud-est sous les sous-domaines de Seguin et de Moon River. Ce résultat vient appuyer la notion selon laquelle ces dernières unités recouvrent le domaine de Parry Sound.

Introduction

In contrast to surrounding structural domains within the Central Gneiss Belt of the Grenville Province, Parry Sound Domain (Fig. 30.1) is unique for its abundance of relatively mafic rocks, associated in part with sizeable bodies of anorthosite (Davidson and Morgan, 1981; Davidson et al., 1982). In addition, much of the domain is characterized by granulite or retrograde granulite facies metamorphism, whereas the metamorphic grade of adjacent domains is largely amphibolite facies. The domain boundary comprises a series of tectonite zones that truncate structural trends and metamorphic facies. Petrological and structural data suggest that Parry Sound Domain has been transported northwestward over the adjacent Britt Domain from a position deep within the crust (Davidson et al., 1982). Likewise, Moon River and Seguin subdomains may have been emplaced by northwestward ductile thrusting onto the southeastern margin of Parry Sound Domain. These two subdomains are presently separated by Rosseau subdomain, but may at one time have belonged to a single sheet.

Important information from the point of view of tectonic modelling is the deep crustal structure of Parry Sound Domain. Whether the domain 'bottoms out' or has a narrowing deep root separating Britt Domain from the eastern structures (Davidson et al., 1982) could be critical evidence in determining its tectonic history. Fortunately, a means toward answering this question is provided by a 35 mGal amplitude positive gravity anomaly (Fig. 30.1) that coincides with Parry Sound Domain, reflecting the dense nature of its ubiquitous mafic rocks.

Generally, the zone of steep gravity gradient that outlines the Parry Sound gravity high lies within the domain boundaries, but where the domain is next to Moon River and Seguin subdomains, the gradients follow paths that are convex toward the southeast and invade the two subdomains. This gravity contour configuration suggests that Parry Sound Domain is present beneath the subdomains, which, if true, would substantiate the interpreted structural superposition.

With these problems in mind, one of the authors (F.M.L.) undertook a gravity study of the Parry Sound region as a subject for a B.Sc. thesis (Department of Geology, Carleton University). The results of this study, summarized here, are drawn from the thesis (Lindia, 1983).

Acknowledgments

The authors thank R.A. Gibb, Earth Physics Branch, and P.H. McGrath, Geological Survey of Canada, for reviewing the manuscript, and D.W. Halliday, Earth Physics Branch, for his contribution to the gravity surveys carried out in the summer of 1982.

---

[1] Contribution of the Earth Physics Branch No. 1054

[2] Department of Geology, Carleton University, Ottawa, Ontario, K1S 5B6
[3] Earth Physics Branch, 1 Observatory Crescent, Ottawa, Ontario, K1A 0Y3

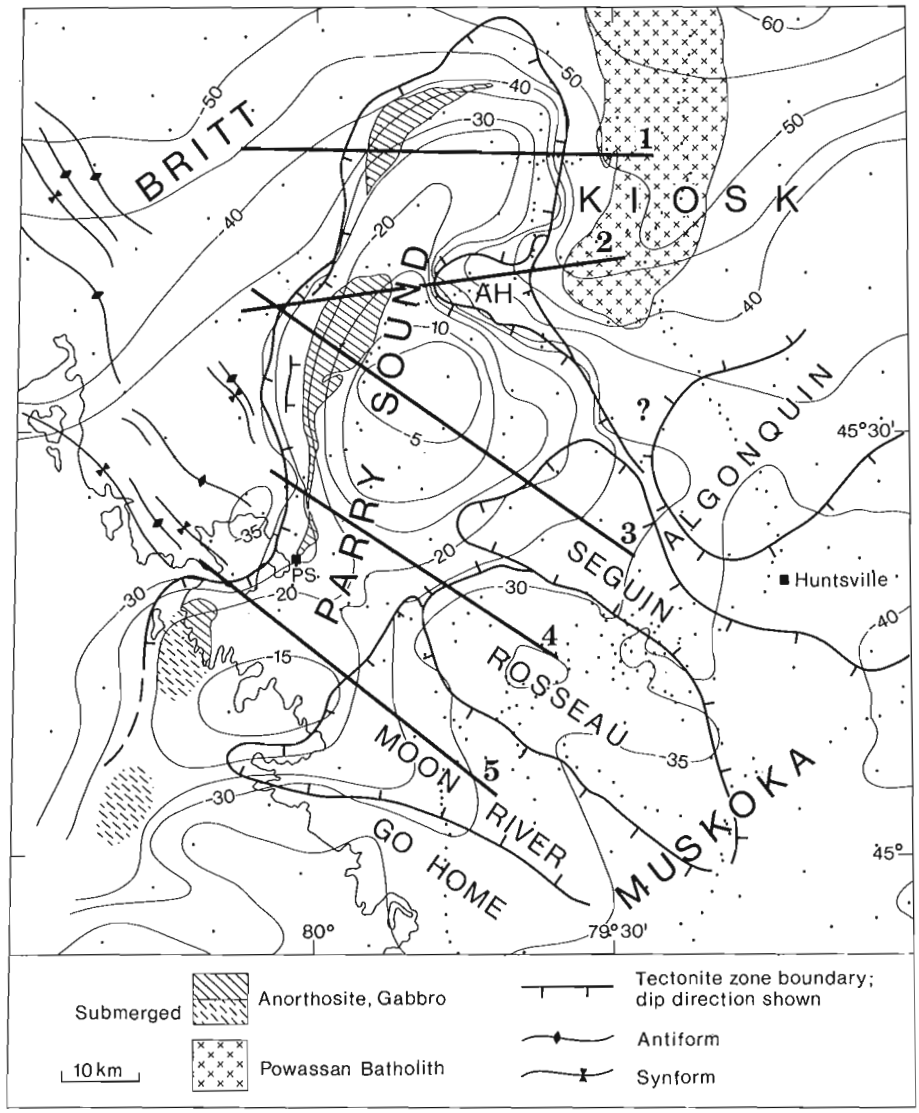

Figure 30.1

Geological map outlining tectonic domains/subdomains in the Parry Sound region, Grenville Province; AH, Ahmic subdomain. Tick marks indicate dip directions of tectonite zones. A Bouguer gravity anomaly map, contour interval 5 mGal, is superposed; small dots indicate gravity stations. Locations of 5 profiles used in modelling (Fig. 30.2) are indicated. PS, Parry Sound.

Geology

The following description of the geology of the region is extracted from the reports of Davidson and Morgan (1981) and Davidson et al. (1982). Parry Sound Domain is located approximately halfway between the Grenville Front and the Central Metasedimentary Belt, within a region of the Grenville Province designated the Central Gneiss Belt (Wynne-Edwards, 1972). The domain extends north-northeasterly from the shores of Georgian Bay for approximately 100 km, and ranges in width from about 20 to 40 km. For ease of reference, the western boundary is defined as that section extending from Georgian Bay to the northern tip of the domain, the eastern boundary is that section separating the domain from Kiosk Domain and the southeastern boundary is that section between Parry Sound Domain and Muskoka Domain (Fig. 30.1). One more or less continuous tectonite zone forms the entire western and eastern boundaries. Dips recorded from the tectonite zone along the western boundary are directed inward and undulate between 10 and 50°, averaging around 30°, while inward dips along the eastern boundary are considerably steeper, attaining 70° in places. The shape of the western boundary is interrupted by a prominent incursion around the nose of the roughly triangular Ahmic subdomain. The eastern boundary of the latter is itself marked by a tectonite zone that merges northward and southeastward with the tectonite zone bounding Parry Sound Domain. The southeastern boundary, with Muskoka Domain, is the most irregular in shape and also the most complex in that the tectonite boundary dips both inward and outward with respect to Parry Sound Domain. Inward dips are associated with the boundary along Rosseau subdomain and probably that along Go Home subdomain, while outward dips characterize the boundaries between Parry Sound Domain and Moon River and Seguin subdomains. The outward dips, the truncation of Parry Sound Domain structure and the indented nature of the northwestern margins of the subdomains with respect to Parry Sound Domain, together, strongly suggest that Moon River and Seguin subdomains overlie portions of the southeastern margin of Parry Sound Domain, with the contact between considered to be a zone of ductile thrusting (Davidson et al., 1982).

Within the interior of Parry Sound Domain, relatively mafic rocks dominate in a very complex assemblage ranging from mafic to feldspathic gneiss, and including hypersthene-bearing metaplutonic rocks, mainly metagabbro, metadiorite and metatonalite. Narrow layers of marble trace out the dominantly northerly structural grain of the domain. Structural trends in the western part of the domain are generally more continuous and occur in well layered supracrustal gneiss in amphibolite facies that encloses major bodies of gabbroic anorthosite. In the eastern part of the

domain, trends are more irregular and are truncated along the eastern and southeastern boundaries; rocks in the eastern part are entirely in granulite or retrograde granulite facies.

Britt Domain is a complex of highly deformed quartzofeldspathic gneisses, migmatites and younger granitoid plutonic rocks in amphibolite facies. Kiosk Domain includes such metaplutonic rocks as metamonzonite and metaquartz monzonite, individual intrusions of which are separated by layered gneiss. The Powassan Batholith lies close to the eastern margin of the north part of Parry Sound Domain and is relatively undeformed. Preliminary studies farther east indicate that alternating zones of amphibolite facies gneiss and of hypersthene-bearing granulite developed from highly flattened plutonic rocks are characteristic of Kiosk Domain (Davidson et al., 1982). Muskoka Domain consists of four northwest-trending subdomains. The synformal Moon River and Seguin subdomains are very similar and consist largely of migmatitic gneisses in amphibolite facies. Go Home and Rosseau subdomains are also described as having much in common (Davidson et al., 1982) and both contain granulite facies locally, most obvious in metaplutonic rocks. The latter subdomains are distinctly different from Moon River and Seguin subdomains.

Rock Densities

Rock densities were determined on 772 samples collected throughout the study area. The variety of rock types is considerable, not only throughout the study area, but also within domains and subdomains. In spite of the variations, an attempt was made to assign the rocks to one or other of the following categories: gneiss, granulite, migmatite, igneous rocks, tectonite, anorthosite, and marble. A further subdivision of several of these categories was required to accommodate mafic and leucocratic varieties. The gneiss category includes schists and pelitic gneisses, as well as quartzofeldspathic gneisses. The igneous category includes all rocks having obvious relict igneous textures; gabbros, diorites and granitoids fall in this category. Included in the migmatite category are swirly structured rocks in which irregular leucosomes occur in recrystallized parent material of metasedimentary and/or metaplutonic origin. The granulite category includes rocks that display an even-sized granular mineral texture formed by high temperature metamorphism. The tectonite category includes all rock types that have undergone very pronounced tectonism such as mylonites.

The range of densities and mean density of each category, and of leucocratic and mafic subgroups, where applicable, are listed in Table 30.1. In Table 30.2 comparable data for the various domains and subdomains are presented. The range of densities for both lithological categories and domains/subdomains are all quite large. This arises in large part from the layered nature of many of the rock types with its associated changes in mineralogy. Estimation of mean densities of large units of terrace having several rock types is an extremely uncertain exercise. Ideally, weighted mean densities would improve the situation, but geological maps showing adequate detail are not available. Under these circumstances, simple arithmetic means provide a reasonable approximation.

The mean densities of the Britt, Kiosk and Algonquin domains are virtually identical (Table 30.2), and the mean density of 2.73 g/cm^3 has been assigned to them for the purpose of gravity modelling; this is regarded as a background density against which other mean densities are compared. The most noticeable difference from background density is provided by the denser rocks of Parry Sound Domain; this domain has a positive contrast of 0.12 g/cm^3. The subdomains of Muskoka Domain are all marginally more positive than background density, Moon River subdomain having a contrast of 0.03 g/cm^3, and Go Home, Rosseau and Seguin subdomains having contrasts of 0.02 g/cm^3. The Ahmic subdomain, although described as having a rock assemblage closely similar to that of Britt Domain and having a possible link with that domain beneath Parry Sound Domain (Davidson et al., 1982), has a moderately high negative contrast of 0.08 g/cm^3. The Powassan Batholith of Kiosk Domain also has a negative contrast, in this case 0.05 g/cm^3.

Table 30.1

Densities of individual rock types

Rock type	No. samples	Density range (g/cm^3)	Mean density (g/cm^3)
Gneiss			
Leuco	292	2.57 – 2.87	2.68
Mafic	241	2.61 – 3.49	3.02
Igneous			
Leuco	37	2.59 – 2.73	2.66
Mafic	30	2.78 – 3.00	2.90
Migmatite			
Leuco	35	2.61 – 2.82	2.68
Mafic	9	2.66 – 3.06	2.84
Granulite			
Leuco	15	2.61 – 2.87	2.74
Mafic	42	2.65 – 3.25	2.89
Anorthosite	22	2.68 – 3.07	2.78
Tectonite	41	2.60 – 3.14	2.75
Marble	8	2.68 – 3.07	2.75

Table 30.2

Densities within each domain subdomain

Domain/ subdomain	No. samples	Density range (g/cm^3)	Mean density (g/cm^3)
Britt	161	2.59 – 3.16	2.73
Parry Sound	305	2.57 – 3.49	2.85
Ahmic	27	2.60 – 2.74	2.65
Muskoka			
Moon River	59	2.59 – 3.10	2.76
Rosseau	95	2.58 – 3.13	2.75
Seguin	39	2.59 – 3.00	2.75
Go Home	17	2.60 – 3.03	2.75
Algonquin			
Kiosk	69	2.59 – 3.11	2.72

Gravity Surveys

Prior to 1982, regional gravity coverage in the area was provided by stations having an average spacing of about 10 km. Closer spacing of 1-2 km was available along certain highways and in the vicinity of the Skeleton Lake impact

structure (Waddington and Dence, 1979), but very few of these stations were located across the anomaly associated with Parry Sound Domain. In order to improve the control on the gravity field, especially in regions where belts of steep gradients are associated with boundaries of the domain, several gravity profiles with station spacing generally 2 km or less were surveyed in the summer of 1982. Two profiles comprising a total of 51 stations were established in the northeastern part of Parry Sound Domain, one crossing the entire domain and Ahmic subdomain, and another traversing the eastern boundary to the north of Ahmic subdomain. Another profile with similar station spacing was surveyed across Go Home, Moon River and Rosseau subdomains in an attempt to improve the definition of a positive gravity feature associated with the Moon River subdomain. A total of 74 stations was measured along, and in the general area of this profile. Traverses were selected to be as perpendicular as possible to the various geological boundaries, but the orientations of roads were ultimately the controlling factor in determining the profile paths.

Gravity station elevations, critical to the accuracy of the gravity anomalies, were controlled wherever possible by benchmarks, but otherwise were obtained by altimetry. Elevations obtained by the latter method are estimated to have an accuracy better than ±5 metres, corresponding to an error of slightly less than 1 mGal in a gravity anomaly. Terrain corrections were not computed, but are unlikely to exceed 1 mGal. Bouguer anomalies are estimated to be accurate to within ±2 mGal.

Interpretation of Gravity Anomalies

The positive gravity anomaly associated with Parry Sound Domain is saddle-shaped, characterized by two domal culminations; one with an amplitude relative to background of 35 mGal is located in the central part of the domain, and a smaller one with an amplitude of about 20 mGal is centred near the coast of Georgian Bay in the southwestern part of the domain (Fig. 30.1). Between the two culminations, immediately southeast of Parry Sound, the amplitude of the anomaly diminishes to about 15 mGal. Here, also, the width of the anomaly is reduced in harmony with that of Parry Sound Domain which is reduced to less than 20 km. Farther northeast where the domain is at its widest, about 40 km, the gravity anomaly attains maximum amplitude. The gradients outlining the anomaly are, for the most part, located within the boundaries of Parry Sound Domain, indicating that the mutual contacts of the domain and surrounding rocks are inward-dipping. However, along the southeastern boundary of the domain the gradients continue uninterrupted from the domain into the neighbouring Moon River and Seguin subdomains of Muskoka Domain, strongly suggesting that Parry Sound rocks are present at no great depth below these subdomains. The picture furnished by gravity anomalies accords with the idea that these subdomains overlie Parry Sound Domain.

The gravity anomaly is largely symmetrical with respect to the axis of Parry Sound Domain, but steeper gradients are noted along the eastern margin north of Ahmic subdomain and around the steeply westward-plunging nose of Ahmic subdomain itself. These steeper gradients probably reflect the greater dips of the tectonite zones along this particular boundary, but may also, in part, arise from a larger density contrast associated with the relatively low density rocks of Ahmic subdomain (2.65 g/cm^3) and Powassan Batholith (2.68 g/cm^3: Lindia, 1983). Closely spaced gravity observations traversing the Parry Sound Domain-Ahmic subdomain boundary, and three new observations located in the interior of the subdomain indicate that this boundary controls the path of gravity contours. Previously, without the added control, contours could be drawn across the northern boundary of the subdomain at an highly oblique angle and could thus be interpreted in terms of structure other than the boundary.

The positive gravity lobes on the southeast side of the Parry Sound gravity high that coincide with Moon River and Seguin subdomains were originally thought by one of the authors (A.D.) to reflect buried Parry Sound rocks, but it remained an open question as to whether these subdomains might themselves have a positive influence on the gravity field. Measurements, though, suggest very little or no difference in mean densities of the various subdomains (Table 30.2), and hence no expected significant gravity effect. However, the mean density of Moon River subdomain is very slightly higher (by 0.01 g/cm^3), and a detailed gravity traverse across Go Home, Moon River and Rosseau subdomains does suggest that Moon River subdomain makes a small positive contribution to the gravity field. This conjecture is based on the observation that the maximum value along the profile is almost coincident with the main synformal axis. The concept of a synformal geometry for Moon River subdomain is, therefore, apparently supported by the gravity data. The geometry of gravity contours also indicates that buried Parry Sound rocks make a considerable positive contribution to the positive lobe.

Gravity Models

Models for five gravity profiles across Parry Sound Domain are shown in Figure 30.2; the northernmost two are well controlled by two of the new gravity traverses established in 1982. Profile locations are shown in Figure 30.1. All models have been constrained using the mapped geological boundaries and the simple arithmetic mean densities listed in Table 30.2. The cross-sections of the various component bodies are either two-dimensional (infinite strike length) or two-and-one-half-dimensional (limited strike length: Shuey and Pasquale, 1973) according to the dimensions of the body in question. Modelling was accomplished using an interactive computer program designed for use on a graphics terminal (Wells, 1977).

Base level gravity values for all profiles, equated with 0 mGal for modelling, were determined from the gravity field over Britt Domain, the mean density of which was used as a background value. For Profiles 2 through 5 base levels are relatively easy to determine because the gravity field is relatively flat, generally ranging between -30 and -35 mGal (Fig. 30.1). However, selection of base level for Profile 1 is complicated by a northeast-trending gradient that merges with the Parry Sound high along the northern extremity of the western boundary of Parry Sound Domain. No attempt was made to separate the two gravity features, and thus base level for Profile 1 is somewhat more speculative. In the following discussion of the various profiles and their interpreted models, all amplitudes quoted are relative to the respective base levels assumed for Britt Domain.

Model 1. Profile 1 runs east-west from Britt Domain through the northernmost part of Parry Sound Domain into Kiosk Domain; the amplitude of the anomaly is about 20 mGal. Parry Sound Domain is modelled as a symmetrical bowl-shaped body having a maximum depth of about 6 km (Fig. 30.2). Close to the surface, both inward-dipping contacts dip gently (~10°) from the boundary positions, but at depths approaching 1 km they steepen abruptly (~55° on west, ~35° on east). On the east side of the domain, a body corresponding to the Powassan Batholith has been modelled. This has a maximum depth of 5 km and is separated from Parry Sound rocks by a wedge of gneissic rocks approximately 5 km wide. The western boundary dips 45° westward. A triangular prism of Britt Domain adjacent to Parry Sound Domain with a density contrast of +0.05 g/cm^3 relative to

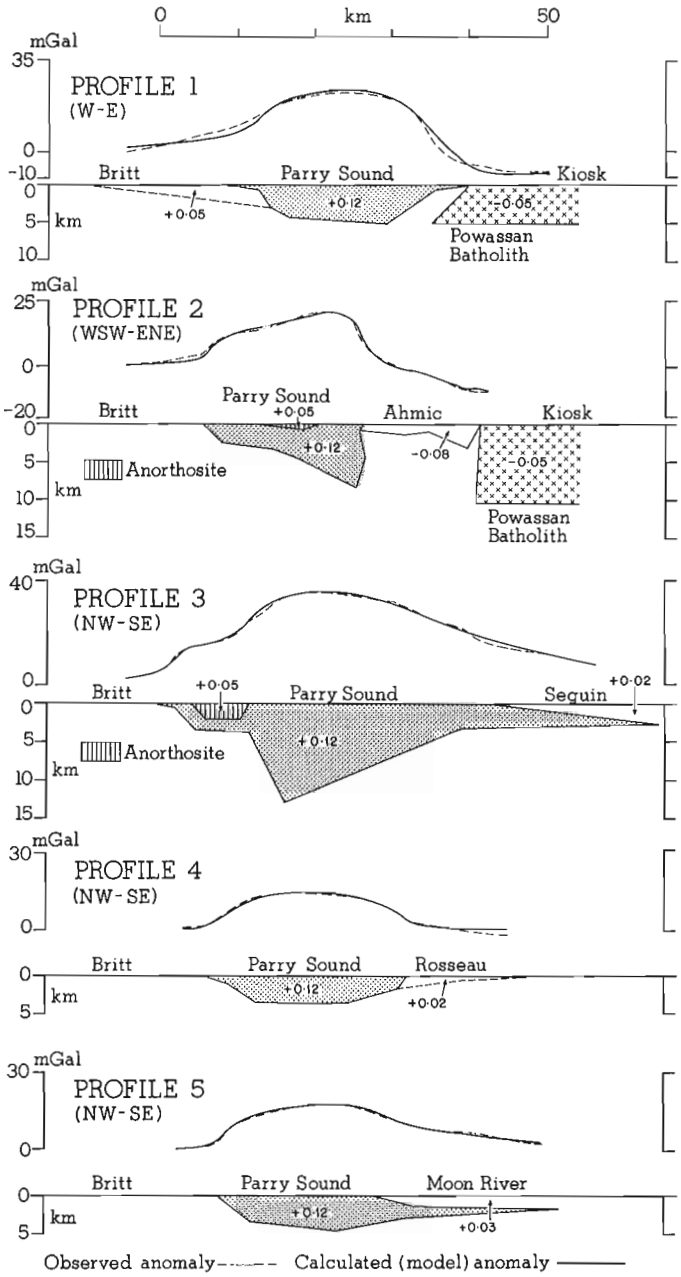

Figure 30.2. *Two- and two-and-one-half dimensional models interpreted from 5 gravity profiles crossing Parry Sound Domain (see Fig. 30.1 for locations). Density contrasts of bodies are in units of g/cm^3.*

the rest of Britt Domain has been included in the model. This addition allowed a better fit between the observed and model gravity curves. A geological explanation is that this particular area has an abundance of pelitic gneisses with densities in the range 2.75 to 2.80 g/cm^3.

Model 2. Profile 2 extends from Britt Domain east-northeastward across Parry Sound Domain, Ahmic subdomain and Kiosk Domain. It has an amplitude of roughly 20 mGal, equivalent to that of Profile 1, though being closer to the main culmination of the anomaly a greater amplitude would have been expected. The lack of increase is attributed to the enhancement of Profile 1 amplitude by the regional gradient in Britt Domain. In the model (Fig. 30.2) Parry Sound Domain has an asymmetrical basin-shape with the deepest part, attaining a depth of 8 km, located very close to the eastern edge of the domain. The steeply dipping eastern boundary, grossly vertical but dipping inward at about 60° in the uppermost kilometre, is consistent with dips observed in the tectonite zone at the surface. A small body of anorthosite that crops out in the western part of Parry Sound Domain has also been included in the model; this has a maximum depth of about 1 km. Without this body the Parry Sound body could be modelled as having a small subsidiary western root attaining a depth of about 3.5 km. Ahmic subdomain is modelled as an elongate prism that increases in thickness from about 1 to 3 km west to east, and has a gently antiformal lower boundary. The geological nature of the lower boundary is unknown, but geometrically it is difficult to fit it into the regional pattern of tectonites. A narrow wedge of gneissic rocks separates Ahmic subdomain from the Powassan Batholith that is modelled as having a depth of about 10 km and a vertical western boundary.

Model 3. Profile 3 runs from Britt Domain southeastward across Parry Sound Domain and Seguin subdomain, and crosses the peak of the gravity high; it has an amplitude of about 35 mGal. Parry Sound Domain has the general form of a reasonably symmetrical inverted triangle with a maximum depth of 13 km (Fig. 30.2). The sharp-pointed root would be diminished if there were a concentration of denser rocks southeast of the small anorthosite body; gabbroic rocks are present in this area, but a more representative density sample is required before any conclusions in this regard can be made. The anorthosite mapped in the western part of the domain has a maximum interpreted depth of 2 km; exclusion of the block from the model results, as in Model 2, in a subsidiary root close to the northwestern margin. An important feature of Parry Sound Domain is the wedge-shaped tongue on the southeast side that extends southeastward beneath Seguin subdomain for just over 20 km, diminishing from an initial thickness of roughly 3 km.

Model 4. Profile 4 crosses, from northwest to southeast, Britt Domain, Parry Sound Domain and Rosseau subdomain, it has an amplitude of about 15 mGal. The model (Fig. 30.2) is relatively simple and has a symmetrical bowl-shaped Parry Sound Domain with a maximum depth of about 3.5 km. The contact with Rosseau subdomain is steep and northwestward dipping (~55°) in harmony with dip information obtained from the tectonite zone forming the mutual boundary at the surface. The northwestern boundary dips inward at 18° near the surface, and at about 35° below a depth of 1 km. Rosseau subdomain is modelled as a thin wedge, maximum thickness of about 2 km, that dies out southeastward. From geological considerations, it is unlikely that the lower boundary of the wedge does in fact represent the lower boundary of Rosseau subdomain, and considering the small density contrast, a discrete boundary may not exist at all; rather, a gradual change in density may be more realistic.

Model 5. Profile 5 extends from Britt Domain southeastward across Parry Sound Domain to Moon River subdomain and has a maximum amplitude of 20 mGal. Parry Sound Domain is once again a bowl-shaped body attaining, in this instance, a maximum thickness of 4.7 km (Fig. 30.2). The southeast side of the Parry Sound body extends approximately 25 km southeastward as a wedge beneath Moon River subdomain, mimicking the situation in Model 3.

Discussion

Density studies and gravity modelling have provided new information regarding the subsurface form of Parry Sound Domain, and on the nature of the western boundary and depth extent of the Powassan Batholith. A configuration for

the Ahmic subdomain has also been obtained. Perhaps the most important result of the gravity study is the geophysical affirmation that denser rocks, probably in continuations of Parry Sound Domain, extend southeastward in the form of narrowing wedges beneath Moon River and Seguin subdomains. This is in accord with the proposal of Davidson et al. (1982) that these subdomains have been emplaced above Parry Sound Domain by northwestward ductile thrusting. A minimum amount of 25 km lateral transport is suggested by the gravity models. Another important result that strengthens geological interpretation is the northwestward-dipping boundary modelled between Parry Sound Domain and Rosseau subdomain; dips recorded in the boundary tectonite zone are northwestward at about 50°. A steep boundary between Parry Sound Domain and Ahmic subdomain, evident in tectonite zones and dipping toward Parry Sound Domain, has also been obtained in the gravity modelling. Powassan Batholith has been modelled with steep sides and decreases in thickness from about 10 km near Ahmic subdomain to roughly 5 km only 15 km farther north.

With the exception of Model 2, and ignoring the wedges that protrude beneath Muskoka Domain, the gross cross-section of Parry Sound Domain is relatively symmetrical and attains a maximum thickness of about 13 km. This answers the question regarding 'bottoming out' of the domain (Davidson et al., 1982). The geometry is consistent with an idea that, following thrust emplacement of Parry Sound Domain in its present position, the great mass of dense rocks reacted to gravitational forces by downwarping. All of this probably occurred deep in the crust, according to mineral assemblages in tectonites that indicate upper amphibolite facies. An even deeper provenance, of at least around 30 km depth (Davidson et al., 1982), is indicated for rocks of Parry Sound Domain. At such depths the rocks may have been more mobile and able to respond to vertical overburden pressures. The greater dips recorded in tectonite zones along the eastern boundary represent a departure from symmetry and are difficult to explain by a simple sagging model. However, the rocks in the adjacent Ahmic subdomain and Kiosk Domain are lighter than peripheral rocks elsewhere around the Parry Sound Domain boundary, and it is possible that these reacted to lithostatic pressures by diapiric movements that dragged up the eastern boundary of the domain and significantly increased dips of associated tectonite zones.

A noteworthy feature of the Parry Sound gravity high is the saddle located where the Parry Sound Domain narrows significantly. The saddle indicates a sympathetic thinning of the domain. This takes place immediately northwest of Rosseau subdomain; another pinching of Parry Sound gravity high occurs northwest of Go Home subdomain. Both Go Home and Rosseau subdomains are antiformal structures that trend northwestward. It is tentatively suggested that the antiformal doming observed in the subdomains continues along strike northwestward beneath Parry Sound Domain and suggested by the pattern of gravity contours is a consequence of arching about northwest trending axes. Britt Domain is characterized by a structural pattern in which large scale folds have axes that plunge gently to the southeast (Davidson et al., 1982). These axes may link beneath Parry Sound Domain with structures of Go Home and Rosseau subdomains. Another domal structure that may cross beneath Parry Sound Domain is one related to the domal Ahmic subdomain. Significantly, the western boundary of Parry Sound Domain, opposite Ahmic subdomain, is concave outward. Ahmic subdomain has been linked tentatively with Britt Domain, based on similarities in rock assemblages. Density measurements do not support such a correlation, but do not necessarily rule it out.

References

Davidson, A. and Morgan, W.C.
1981: Preliminary notes on the geology east of Georgian Bay, Grenville Structural Province, Ontario; in Current Research, Part A, Geological Survey of Canada, Paper 81-1A, p. 291-298.

Davidson, A., Culshaw, N.G., and Nadeau, L.
1982: A tectono-metamorphic framework for part of the Grenville Province, Parry Sound region, Ontario; in Current Research, Part A, Geological Survey of Canada, Paper 82-1A, p. 175-190.

Lindia, F.M.
1983: An interpretation of the Bouguer anomaly field in the Parry Sound area, Ontario; unpublished B.Sc. thesis, Carleton University.

Shuey, R.T. and Pasquale, A.S.
1973: End corrections in magnetic profile interpretation; Geophysics, v. 38, p. 507-512.

Waddington, E.D. and Dence, M.R.
1979: Skeleton Lake, Ontario – evidence for a Paleozoic impact crater; Canadian Journal of Earth Sciences, v. 16, p. 256-263.

Wells, I.
1977: MAGRAV users guide: A computer program to create two-dimensional gravity and/or magnetic models; Bedford Institute of Oceanography Computing Services Technical Memorandum No. 85, unpublished report (also available as Open File 597, Computer Science Centre, EMR, Ottawa).

Wynne-Edwards, H.W.
1972: The Grenville Province; in Variations in Tectonic Styles in Canada, ed. R.A. Price and R.J.W. Douglas; Geological Association of Canada, Special Paper No. 11, p. 263-334.

31. DIATOMS FROM THE SOUTHERN BEAUFORT SEA

Project 720078

Sigrid Lichti-Federovich
Terrain Sciences Division

Lichti-Federovich, S., Diatoms from the southern Beaufort Sea; in Current Research, Part B, Geological Survey of Canada, Paper 83-1B, p. 267-271, 1983.

Abstract

Qualitative floristic analysis of 30 offshore summer phytoplankton samples from the southern Beaufort Sea resulted in the systematic enumeration of 40 genera comprising 135 diatom taxa. Positive correlation is suggested between cryophilic diatom distribution and sea ice proximity as well as between the relative frequency determinations of ***Thalassiosira baltica*** *and decreased salinities caused by the freshening influence of the Mackenzie estuarine system.*

Résumé

L'analyse qualitative de la flore de trente échantillons de phytoplancton prélevés l'été dans le sud de la mer de Beaufort a mené à l'énumération systématique de 40 genres composés de 135 taxons de diatomées. Il y aurait une corrélation positive entre la répartition des diatomées cryophiles et la proximité de la glace de mer ainsi qu'entre la fréquence relative de ***Thalassiosira baltica*** *et la réduction de la salinité causée par l'apport d'eau douce du réseau estuarien du Mackenzie.*

Introduction

Phytoplankton offshore samples from the southern Beaufort Sea were investigated with the principle objective of furnishing a scanning electron illustrative account of diatoms and augmenting earlier diatom enumerations from this area. This is the second report initiated by examination of the same sample material. The first one (Lichti-Federovich, 1982) documents an identifiable correlation between the distribution pattern of teratological forms of **Chaetoceros** and the freshwater diatom component of the Mackenzie sediment plume and proposes salinity stress as likely causal factor for the occurrence and distribution of these morphological aberrants. The current report, aside from focusing on systematic enumeration, discusses the apparent relationship between some distributional aspects and environmental parameters.

Material and Methods

The following information has been referred to in a previous report (Lichti-Federovich, 1982).

The phytoplankton samples were collected during a cruise of **CSS Hudson** between August 26 and September 22, 1970. Floristic analysis is based on 200 µm mesh vertical and horizontal net hauls from 30 open water stations located within the southern Beaufort Sea (Fig. 31.1, 31.2). Horizontal hauls were taken from the surface metre of water, whereas the sampling depth of the vertical hauls was standardized to 200 m and up. The main purpose for this collection was to provide sample material for distributional studies of certain foraminiferal species (Vilks et al., 1979). Sample preparation for diatom analysis followed the method outlined in Lichti-Federovich (1981).

Systematic listing of the Beaufort Sea diatoms (Table 31.1) is presented in alphabetical order as to genera and species with information relating to ecological preferences and environmental parameters. These data have been abstracted from various reference sources too numerous to mention. The term "lesser affinity" denotes a taxon's infrequent occurrence with regard to certain environmental parameters as inferred from the literature.

Results and Discussion

At the outset, some of the limitations that likely have influenced the results of this investigation should be stated. Aside from restrictions imposed by non-uniformity or discontinuity in phytoplankton distribution due to hydrographic conditions and size selective zooplankton predation, species enumeration and distributional representation are severely limited by the small sample size. Further restraints are introduced by the method of collection which permits only partial retention of the phytoplankton population with selective bias towards the larger species. It also should be emphasized that the taxonomic list comprises species of a single sampling only, thus excluding taxa of seasonal or successional occurrence.

The systematic account of the Beaufort Sea phytoplankton collections represents 135 diatom taxa within 40 genera. Aside from phytoplankton investigations in the western part of the Beaufort Sea, with Point Barrow, Alaska, as their focal point (Bursa, 1963; Horner, 1973), only two taxonomic floristic studies fall within the area of investigation. The first one relates to a single vertical net plankton haul in ice northwest of the Alaska-Yukon International Boundary at 70°20'N, 140°20'W yielding only 14 diatoms (Mann, 1925). In contrast, a three year phytoplankton study by Hsiao et al. (1977) reflects closer spatial agreement with regard to regional distribution of sampling stations. Differences from the current study, however, include a lower total number of sampling locations (21) and significantly higher ratios of inshore to offshore sampling sites and ice to open water stations. In general, and with due consideration to the above differences, comparison of their phytoplankton list with the enumerations recorded in Table 31.1 suggests reasonable accord.

Qualitative floristic analysis of the diatom populations from the Beaufort Sea offshore samples as recorded here, discloses compositional heterogeneity reflecting local and regional differences. Nevertheless, collective assessment of the general nature of the diatom flora as abstracted from the numerically dominant taxa common to all or most sampling stations – i.e. **Thalassiosira baltica, Chaetoceros atlanticus, Chaetoceros decipiens, Rhizosolenia styliformis, Coscinodiscus centralis,** and **Thalassionema nitzschioides** – stresses its arctoboreal character. The arctic nature of this

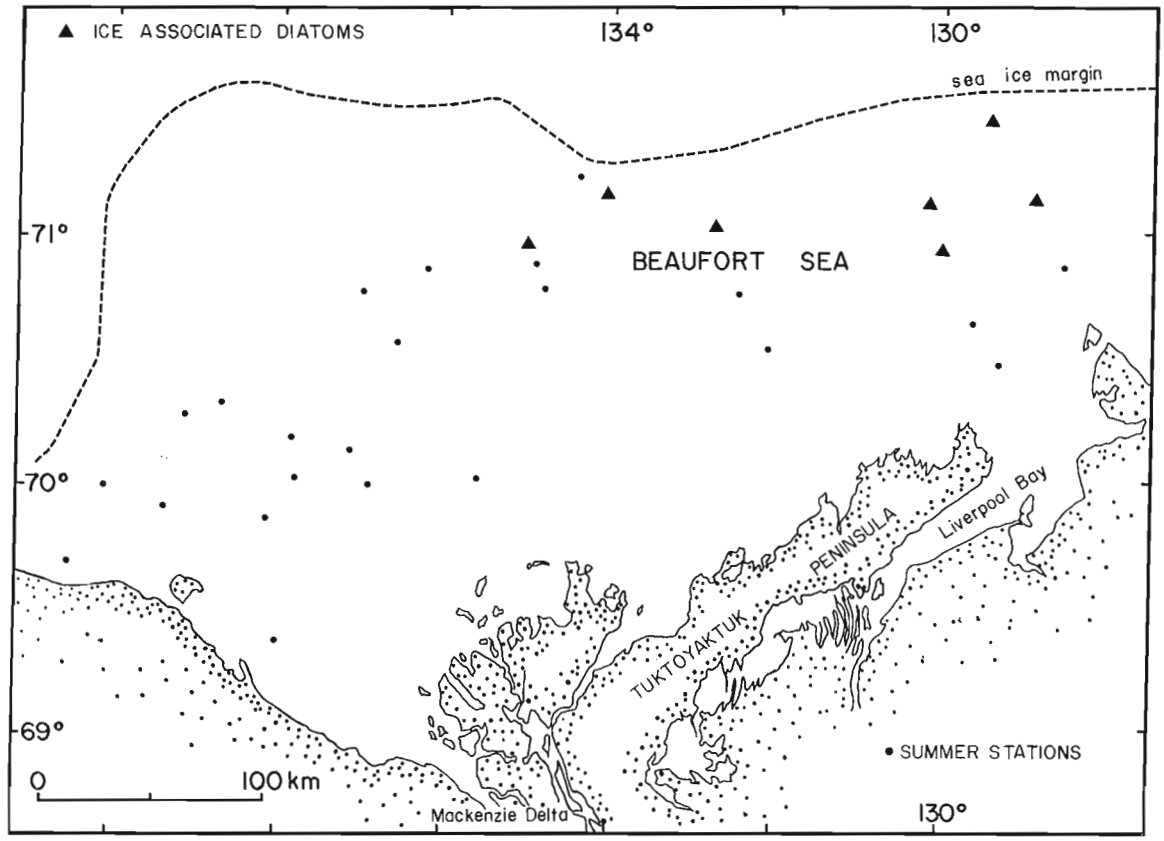

Figure 31.1. *Occurrence and distribution of ice associated diatoms.*

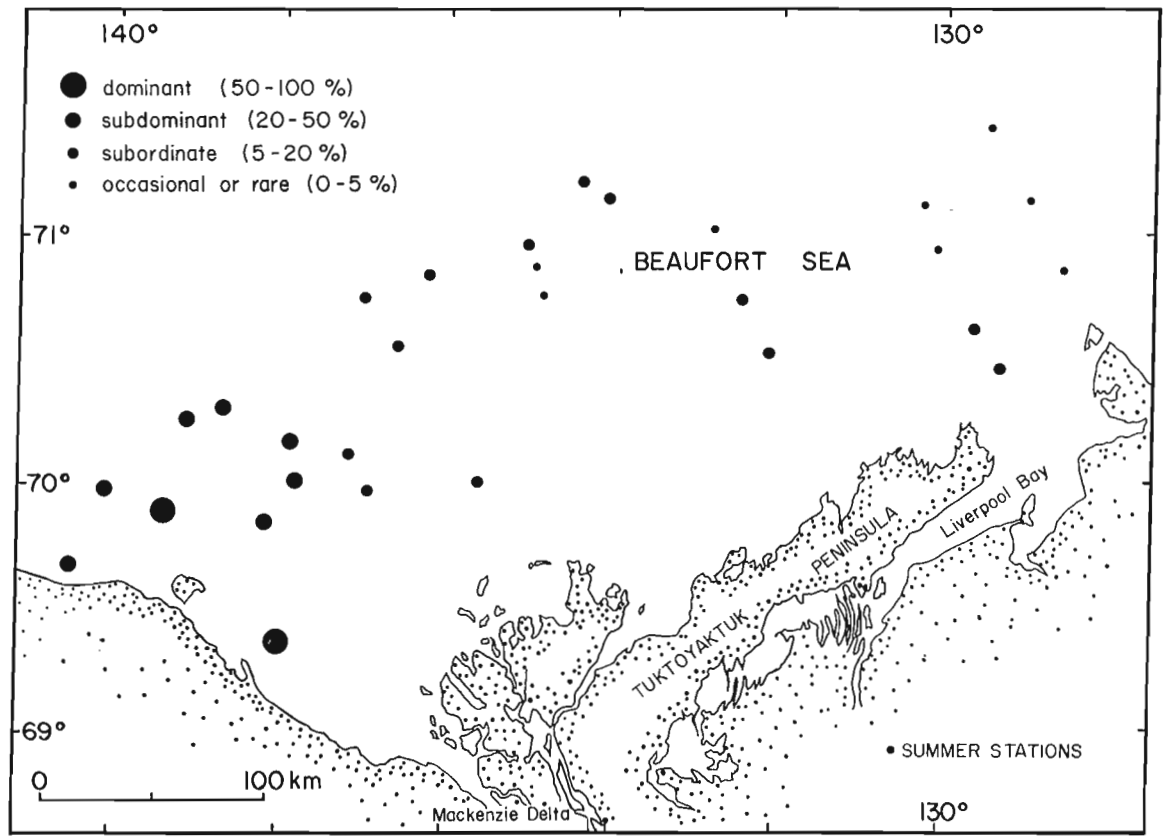

Figure 31.2. *Relative abundance distribution of* ***Thalassiosira baltica*** *(Grun.) Ostf.*

Table 31.1

List of diatom taxa from the southern Beaufort Sea

Climatic/ geographic affinity				Mode of living				General salinity rating			
cosmopolitan	temperate	boreal	arctic	ice-associated	littoral	neritic	oceanic	fresh	brackish	marine	
											BACILLARIOPHYTA
											CENTRALES
											ACTINOCYCLUS Ehrenberg 1837
							x			x	**A. curvatulus** Jan. in A.S. et al.
											ACTINOPTYCHUS Ehrenberg 1841
	o	x				x				x	**A. undulatus** (Bail.) Ralfs in Pritch.
											ASTEROMPHALUS Ehrenberg 1845
		x					x			x	**A. robustus** Castr.
											BACTERIASTRUM Shadbolt 1853
x						x	x			x	**B. delicatulum** Cl.
											BIDDULPHIA S.F. Gray 1821
		x	o		o	x	o		x	x	**B. aurita** (Lyngb.) Bréb. et God.
											CHAETOCEROS Ehrenberg 1844
		x	x				x			x	**C. atlanticus** Cl.
		x	o				x			x	**C. borealis** Bail.
x		x	x			x				x	**C. compressus** Laud.
		x	x				x			x	**C. concavicornis** Mang.
		x	o				x			x	**C. convolutus** Castr.
		x	o				x			x	Δ **C. decipiens** Cl.
	x	x	x				x			x	**C. densus** Cl.
x		x				x				x	**C. diadema** (Ehr.) Grun.
			x			x	x			x	Δ **C. furcellatus** Bail.
	x					x				x	**C. lorenzianus** Grun.
			x			x	x			x	**C. mitra** (Bail.) Cl.
		x	o			x				x	Δ **C. socialis** Laud.
		x	o			x				x	**C. teres** Cl.
		x				x			x		Δ **C. wighami** Brightw.
											COSCINODISCUS Ehrenberg 1838
x					x					x	**C. argus** Ehr.
x		x				o	x			x	**C. centralis** Ehr.
		x	x			o	x			x	**C. curvatulus** Grun. in A.S. et al.
		x	x			o	x			x	**C. curvatulus** var. **kariana** Cl. et Grun.
		x	x				x			x	**C. curvatulus** var. **minor** (Ehr.) Grun.
					x	x	x			x	**C. divisius** Grun.
		x	x		x				x	x	**C. lacustris** Grun. in Cl. et Grun.
		x	x		x				x	x	**C. lacustris** var. **hyperborea** (Grun.) Rattr.
		x	x		x				x	x	**C. lacustris** var. **septentrionalis** (Grun.) Rattr.
x							x			x	* **C. marginatus** Ehr.
x			x				x			x	* C. oculus-iridis Ehr. var. **borealis** (Bail) Cl.
		x	x			x					**C. radiatus** Ehr.
											CYCLOTELLA Kützing 1833
									x		Δ **C. caspia** Grun.
								x			**C. comta** (Ehr.) Kütz.
								x			**C. stelligera** Cl. et Grun.
								x	x		**C. striata** (Kütz.) in Cl. et Grun.
											MELOSIRA Agardh 1824
			x	x	x	x				x	Δ **M. arctica** (Ehr.) Dickie in Pritch.
								x			* Δ **M. granulata** (Ehr.) Ralfs in Pritch.
								x			Δ **M. islandica** O.M.
								x			**M. italica** (Ehr.) Kütz.
	x	x	x			x			x	x	**M. moniliformis** (Müll.) Ag.
											M. sulcata (Ehr.) Kütz.
											M. sulcata var. **biseriata** (Grun.) Per. et Per.
											M. sulcata fo. **coronata** Grun. in V.H.
											M. sulcata fo. **radiata** (Grun.) Per. et Per.
											POROSIRA E. Jørgensen 1905
											Δ **P. glacialis** (Grun.) Jørg.
											RHIZOSOLENIA Ehrenberg 1841
											R. hebetata Bail. fo. **semispina** (Hens.) Gran
											R. styliformis Brightw.
											SKELETONEMA Greville 1865
											Δ **S. costatum** (Grev.) Cl.
											T. anguste-lineata (A.S.) Fryx. et Hasle
											T. antarctica Comb.
											Δ **T. baltica** (Grun.) Ostf.
											T. bioculata (Grun.) Ostf.
											T. constricta Gaard.
											T. decipiens (Grun.) Jørg.
											T. eccentrica Cl.
											Δ **T. gravida** Cl.
											T. hyalina (Grun. in Cl. et Grun.) Grun.
											Δ **T. nordenskioldi** Cl.
											T. spp.
											T. auxospores
											PENNALES
											ACHNANTHES Bory 1822
											Δ **A. taeniata** Grun. in Cl. et Grun.
											ACTINELLA Lewis 1864
									x		**A. punctata** Lewis
											AMPHIPRORA Ehrenberg 1840
											A. gigantea var. **septentrionalis** (Grun.) Cl.
											AMPHORA Ehrenberg 1840
											A. angusta var. **ventricosa** (Greg.) Cl.
											A. lineolata Ehr.
											Δ **A.** sp.
											ANOMOEONEIS Pfitzer 1871
											A. exilis (Kütz.) Cl.
											ASTERIONELLA Hassal 1855
											Δ **A. formosa** Hass.
											CALONEIS Cleve in Cleve et Grove 1891
											C. sectilis (A.S. in A.S. et al.) Cl. var. **boryana** (Pant.) Cl.
											COCCONEIS Ehrenberg 1838
											C. scutellum Ehr.
											C. scutellum var. **stauroneiformis** Rabh.
											DIATOMA De Candelle 1805
											Δ **D. elongatum** (Lyngb.) Ag.
											DIMEREGRAMMA Ralfs in Pritchard 1861

o = indicates lesser affinity

Previously recorded species

* = Mann, 1925

Δ = Hsiao et al., 1977

Table 31.1 (cont.)

Climatic/ geographic affinity				Mode of living				General salinity rating			
cosmopolitan	temperate	boreal	arctic	ice-associated	littoral	neritic	oceanic	fresh	brackish	marine	
x	x				x					x	**D. minor** (Greg.) Ralfs
											DIPLONEIS Ehrenberg 1840
x					x					x	**D. incurvata** (Greg.) Cl.
		x	x		x					x	Δ **D. litoralis** (Donk.) Cl.
			x	x	x					x	Δ **D. litoralis** var. **clathrata**
											(Østr.) Cl.
			x		x					x	**D. oestrupii** Hust.
x					x				x	x	Δ **D. smithii** (Bréb. in
											Wm. Smith) Cl.
x										x	**D. vacillans** (A.S. in
											A.S. et al.) Cl.
											EUNOTIA Ehrenberg 1837
								x			Δ **E.** spp.
											FRAGILARIA Lyngbye 1819
								x			**F.** sp.
											GOMPHONEMA Agardh 1824
					x					x	**G. exiguum** Kütz.
			x	x	x					x	**G. exiguum** var. **arcticum**
											(Grun. in V.H.) Cl.
		x	x	x	x					x	**G. exiguum** var. **pachycladum**
											(Bréb. in Bréb. et God.) Cl.
			x	x	x					x	**G. groenlandicum** Østr.
			x		x					x	Δ **G. kamtschaticum** Grun.
								x	x		**G. olivaceum** (Lyngb.) Desm.
											GYROSIGMA Hassall 1845
											G. sp.
											LICMOPHORA Agardh 1827
					x					x	**L. gracilis** (Ehr.) Grun.
					x					x	**L. gracilis** var. **anglica**
											(Kütz.) Perag. et Perag.
											Δ **L.** spp.
											NAVICULA Bory 1822
			x	x						x	* **N. algida** Grun.
								x	x		**N. anglica** Ralfs in Pritch.
											var. **subsalsa** (Grun.) Cl.
x					x					x	**N. cancellata** Donk.
x					x					x	**N. cancellata** var. **apiculata**
											(Greg.) Perag. et Perag.
								x			**N. cryptocephala** Kütz.
x				x	x					x	Δ **N. directa** (Wm. Smith)
											Ralfs in Pritch.
x					x					x	**N. dissipata** Hust.
											in A.S. et al.
x					x					x	**N. forcipata** Grev.
x					x					x	**N. forcipata** var. **spatiata** Østr.
			x	x						x	**N. gelida** Grun.
			x	x						x	**N. novadecipiens** Hust.
								x			**N. pupula** Kütz.
			x							x	**N. retusa** Bréb.
x									x		Δ **N. salinarum** Grun in
											Cl. et Möll.
			x							x	**N. semistriata** Østr.
		x	x						x	x	**N. spicula** (Hickie) Cl.
		x	x	x	x					x	Δ **N. subinflata** Grun
											in Cl. et Möll.
			x	x	x					x	**N. transitans** Cl.
			x	x	x					x	**N. transitans** var. **derasa**
											(Grun. in Cl. et Grun.) Cl.

Climatic/ geographic affinity				Mode of living				General salinity rating			
cosmopolitan	temperate	boreal	arctic	ice-associated	littoral	neritic	oceanic	fresh	brackish	marine	
			x	x						x	* **N. trigonocephala** Cl.
			x	x						x	**N. valida** Cl. et Grun.
			x			x				x	Δ **N. vanhoeffenii** Gran
											N. spp.
											NITZSCHIA Hassall 1845
x		x			x	x			x	x	Δ **N. closterium** (Ehr.) Wm. Smith
			x							x	**N. curta** (V.H.) Hasle
			x	x						x	**N. cylindrus** (Grun.) Hasle
			x	x		x				x	Δ **N. frigida** Grun.
			x			x				x	**N. grunowii** Hasle
			x							x	**N. hybrida** Grun. in Cl. et Grun.
			x	x						x	**N. laevissima** Grun. in
											Cl. et Möll.
	x									x	**N. lanceolata** Wm. Smith
			x	x						x	**N. lecointei** V.H.
			x	x						x	**N. lineata** Hasle
			x	x						x	**N. polaris** Grun. in Cl. et Möll.
		x				x	x			x	Δ **N. seriata** Cl.
		x				x	x			x	**N. seriata** fo. **obtusa** Hasle
											N. sp.
											PINNULARIA Ehrenberg 1840
			x	x						x	* **P. quadratarea** (A.S.) Cl.
			x	x						x	**P. quadratarea** var. **bicontracta**
											(Østr.) Heid. in Schmidt et al.
			x	x						x	**P. quadratarea** var. **constricta**
											(Østr.) Heid. in Schmidt et al.
			x	x						x	**P. quadratarea** var. **stuxbergii**
											(Cl. in Cl. et Grun) Cl.
											PLEUROSIGMA Wm. Smith 1852
	x				x					x	**P. angulatum** (Quck.) Wm. Smith
	x									x	Δ **P. strigosum** Wm. Smith
											RHAPHONEIS Ehrenberg 1844
		x							x	x	**R. amphiceros** (Ehr.) Ehr.
		x							x	x	**R. surirella** (Ehr.) Grun. in
											Cl. et Möll.
											STAURONEIS Ehrenberg 1841
								x			**S. phoenicenteron** (Nitzsch.) Ehr.
											STENONEIS Cleve 1894
			x							x	* **S. inconspicua** (Greg.) Cl.
											var. **baculus** (Cl.) Cl.
											SYNEDRA Ehrenberg 1830
			x	x						x	Δ **S. hyperborea** Grun. var.
											rostellata Grun.
x					x				x	x	**S. tabulata** (Ag.) Kütz. var.
											fasciculata (Lyngb.) Hust.
											S. sp.
											TABELLARIA Ehrenberg 1840
								x			Δ **T. fenestrata** (Lyngb.) Kütz.
								x			Δ **T. flocculosa** (Roth) Kütz.
											THALASSIONEMA Grunow 1881
						x				x	Δ **T. nitzschioides** (Grun.) V.H.
											THALASSIOTHRIX Cleve et
											Grunow 1880
						x	x			x	**T. longissima** Cl. et Grun.
											in Cl. et Möll.

flora finds expression in associational affinity with the bipolar cold water form **Nitzschia cylindrus.** Further studies, however, are needed to delineate seasonal and successional changes.

Although a definite causal relationship is lacking, examination of some distributional aspects does suggest a more than tentative correlation with certain environmental parameters. Proximity to the polar sea-ice margin, for example, is demonstrated by the distributional pattern of ice-linked elements which only occur in diatom associations from sample stations located near the margin of polar ice (Fig. 31.1). Aside from **Porosira glacialis,** an important cryoplanktonic species, common and often abundant in antarctic sea ice (Krebs, 1977), it is the occurrence of the bipolar taxon **Thalassiosira antarctica,** a recognized indicator of ice border proximity (Hasle and Heimdal, 1968), which characterizes these diatom assemblages. This specific correlation appears to be further substantiated by the significant component in these assemblages of arctic endemics such as **Navicula algida, N. trigonocephala, N. valida, N. transitans, N. transitans** var. **derasa,** and **N. subinflata** which have been previously recorded from various ice dominated environments in the Beaufort Sea (Mann, 1925; Fukushima, 1965; Meguro et al., 1967; Horner, 1976; and Hsiao, 1980).

Distribution data and relative frequency ratings of **Thalassiosira baltica** suggest a close approximation to salinity (Fig. 31.2). Predominance of this brackish water taxon at sampling stations located within the Mackenzie River discharge area indicates a direct relationship to lowered salinities. According to Cholnoky (1968), **Thalassiosira baltica** can also be found abundantly in the plankton of certain inland waters. Its brackish affinity is clearly demonstrated by the following occurrences: Baltic, Dutch coastal waters, Gulf of Finland, Gulf of Bothnia, and Gulf of Maine, among others. Delineation of the region of estuarine influence and detrital deposition is further supported by the distribution data of the allochthonous freshwater diatom component and by the distribution pattern of planktonic aberrants (Lichti-Federovich, 1982, Fig. 23.3, 23.4).

In conclusion, it should be stated that continuing phytoplankton research in the Beaufort Sea is duly merited. Aside from emphasis on economic considerations relating directly to primary productivity, biocoenotic investigations also assist paleoenvironmental interpretation. By extrapolation from present day environments, qualitative and quantitative floristic determinations such as abundance and distributional data, seasonal and successional patterns, phytosociological groupings, and phytogeographical zonations aid interpretation of thanatocoenoses and provide a valid basis for the elucidation of paleo-oceanographic conditions. Furthermore, the imminence of future environmental changes, caused by offshore petroleum exploration for example, justifies a thorough documentation of the current diatom floras of the Beaufort Sea.

Acknowledgments

This diatom analytical study was made on phytoplankton samples provided by G. Vilks, Atlantic Geoscience Centre. The manuscript was read by S.I.C. Hsiao, Department of Fisheries and Oceans. I extend my thanks to both.

References

Bursa, A.
1963: Phytoplankton in coastal waters of the Arctic Ocean at Point Barrow, Alaska; Arctic, v. 16, no. 4, p. 239-262.

Cholnoky, B.J.
1968: Die Ökologie der Diatomeen in Binnengewassern; Verlag J. Cramer, Lehre, 699 p.

Fukushima, H.
1965: Preliminary report on diatoms from coloured sea ice in Point Barrow, Alaska; Antarctic Record, v. 24, p. 31-35.

Hasle, G.R. and Heimdal, B.R.
1968: Morphology and distribution of the marine centric diatom **Thalassiosira antarctica** Comber; Journal of the Royal Microscopical Society, v. 88, no. 3, p. 357-369.

Horner, R.A.
1973: Biology and ecology of phytoplankton and ice organisms in coastal waters near Barrow, Alaska; in National Technical Information Service (Report) AD 770 155; Institute of Marine Science, University of Alaska, 75 p.

1976: Sea ice organisms; Oceanography and Marine Biology, An Annual Review, v. 14, p. 167-182.

Hsiao, S.I.C.
1980: Quantitative composition, distribution, community structure and standing stock of sea ice microalgae in the Canadian Arctic; Arctic, v. 33, no. 4, p. 768-793.

Hsiao, S.I.C., Foy, M.G., and Kittle, D.W.
1977: Standing stock, community structure, species composition, distribution, and primary production of natural populations of phytoplankton in the southern Beaufort Sea; Canadian Journal of Botany, v. 55, no. 6, p 685-694.

Krebs, W.N.
1977: Ecology and preservation of neritic marine diatoms, Arthur Harbor, Antarctica; unpublished Ph.D. thesis, University of California, Davis; University Mircofilms International, Ann Arbor, Michigan, 202 p.

Litchi-Federovich, S.
1981: Contribution to the diatom flora of Arctic Canada: Report 2. Arctic representatives of the genus **Navicula;** in Current Research, Part A, Geological Survey of Canada, Paper 81-1A, p. 57-62.

1982: Contribution to the diatom flora of Arctic Canada: Report 3. On the occurrence of **Chaetoceros** spp. fo. **clavipes** in the southern Beaufort Sea; in Current Research, Part B, Geological Survey of Canada, Paper 82-1B, p. 169-171.

Mann, A.
1925: The marine diatoms of the Canadian Arctic Expedition 1913-1918; in Report of the Canadian Arctic Expedition 1913-1918, Volume 4, Botany; F.A. Acland, Ottawa, p. 1-33.

Meguro, H., Ito, K., and Fukushima, H.
1967: Ice flora (bottom type): A mechanism of primary production in polar seas and the growth of diatoms in sea ice; Arctic, v. 20, no. 2, p. 114-133.

Vilks, G., Wagner, F.J.E., and Pelletier, B.R.
1979: The Holocene marine environment of the Beaufort Shelf; Geological Survey of Canada, Bulletin 303, p. 1-43.

32.

A SHALLOW SEISMIC SURVEY ON THE INTERTIDAL FLATS AT PANGNIRTUNG, BAFFIN ISLAND, NORTHWEST TERRITORIES

Project 790034

S.E. Pullan, J.A. Hunter, and R. Gilbert[1]
Resource Geophysics and Geochemistry Division

Pullan, S.E., Hunter, J.A., and Gilbert, R., A shallow seismic survey on the intertidal flats at Pangnirtung, Baffin Island, Northwest Territories; in Current Research, Part B, Geological Survey of Canada, Paper 83-1B, p. 273-277, 1983.

Abstract

A hammer seismic survey was conducted along selected lines across the intertidal flats at Pangnirtung, Baffin Island, in an attempt to delineate the bedrock surface beneath the sediments. The results indicate that bedrock drops off steeply from shore where the flats are narrow, whereas it forms a supporting platform beneath the extensive flats at the mouth of the Duval River. Approximately 30 m of sediment lie above this bedrock platform. There is some evidence of boulders or groups of boulders buried in these sediments, but the density of these cannot be estimated.

Résumé

Une étude sismique au marteau a été entreprise le long de cheminements choisis en travers de l'estran à Pangnirtung (île de Baffin) en vue de tracer la surface du socle rocheux sous les sédiments. Les résultats indiquent que le socle plonge abruptement à partir du rivage, là où l'estran est étroit; d'autre part, il forme une plate-forme de soutènement sous la vaste étendue d'estran à l'embouchure de la rivière Duval. Environ 30 m de sédiments recouvrent cette plate-forme. Des gros blocs ou des groupes de gros blocs sembleraient exister sous les sédiments mais il est impossible d'estimer leur densité.

Introduction

A hammer seismic survey was conducted along two lines across the intertidal flats at Pangnirtung, Baffin Island, in July 1982, as the first stage in a co-operative research program between the Geological Survey of Canada and the Department of Geography at Queen's University. The objective of this program is to evaluate the origin and development of the intertidal flats, especially with respect to tidal processes, the action of sea ice, and the changes in sea level which have occurred through the Holocene Epoch. The geophysical results presented here define the bedrock topography and set the stage for the recovery of cores through the sediments to be used in stratigraphic and paleo-environmental study.

Intertidal flats are found all around the shores of Pangnirtung Fiord. They are generally less than 200 m wide except at the mouth of the Duval River at Pangnirtung where they reach a maximum width of 600 m (Fig. 32.1). The intertidal surface is characterized by the presence of large boulders and a prominent boulder barricade near the outer edge. Biological and sedimentary environments of the intertidal flats were described by Aitken and Gilbert (1981), Gilbert and Aitken (1981), and McCann et al. (1981).

Survey Operations

The seismic source used in this survey was a 7.3 kg sledge hammer striking a steel plate firmly set on the ground surface. Where standing water did not drain from the surface of the flats, the hammer was used directly on the top of boulders. The data were recorded on a Nimbus 1210F 12-channel engineering seismograph and stored on cassette tape in the field using the Nimbus G742S digital tape recorder. In the office, the tape recorder was linked to an Apple II microcomputer and the records were transferred to floppy disk to allow further interpretation and display through the computer (Hunter et al., 1980).

The intertidal flats did present some operational difficulties. It was only possible to work during low tide, and even then there were large pools of standing water especially near the boulder barricade at the end of line 2. The geophones (4.5 Hz) were in waterproof marsh cases, but the records deteriorated rapidly when the goephone/cable connections got wet. These connections had to be made temporarily waterproof with a covering of silica caulking compound before useable data could be collected in this environment.

In order to map the detailed structure of the bedrock surface beneath the tidal flats, the "optimum offset" shallow reflection technique (Hunter et al., 1982) was used. This method involves recording an initial expanded spread shot, from which an optimum offset between source and receiver is chosen. This offset is one at which the bedrock reflection can be observed without interference from either shallower events or surface waves. Using the individual channel "memory hold" feature of the Nimbus 1210F, records of common offset data can be produced. Periodically, other expanded spread reflection and/or refraction records are shot to provide velocity information.

Results

The "optimum offset" sections along lines 1 and 2 are shown in Figures 32.2 and 32.3 respectively. These records were obtained with one or two hammer blows per trace, a 3 m spacing between traces, and a 150 Hz low-cut filter setting on the instrument. The water-saturated sediments were an excellent transmitter of high frequencies, and even with this relatively low filter setting, the predominant energy on these records is in the 300-500 Hz range. This, along with negligible interference from either ground roll or a ground-coupled air wave, made it possible to map bedrock reflections from depths of less than 30 m.

[1] Department of Geography, Queen's University, Kingston, Ontario K7L 3N6

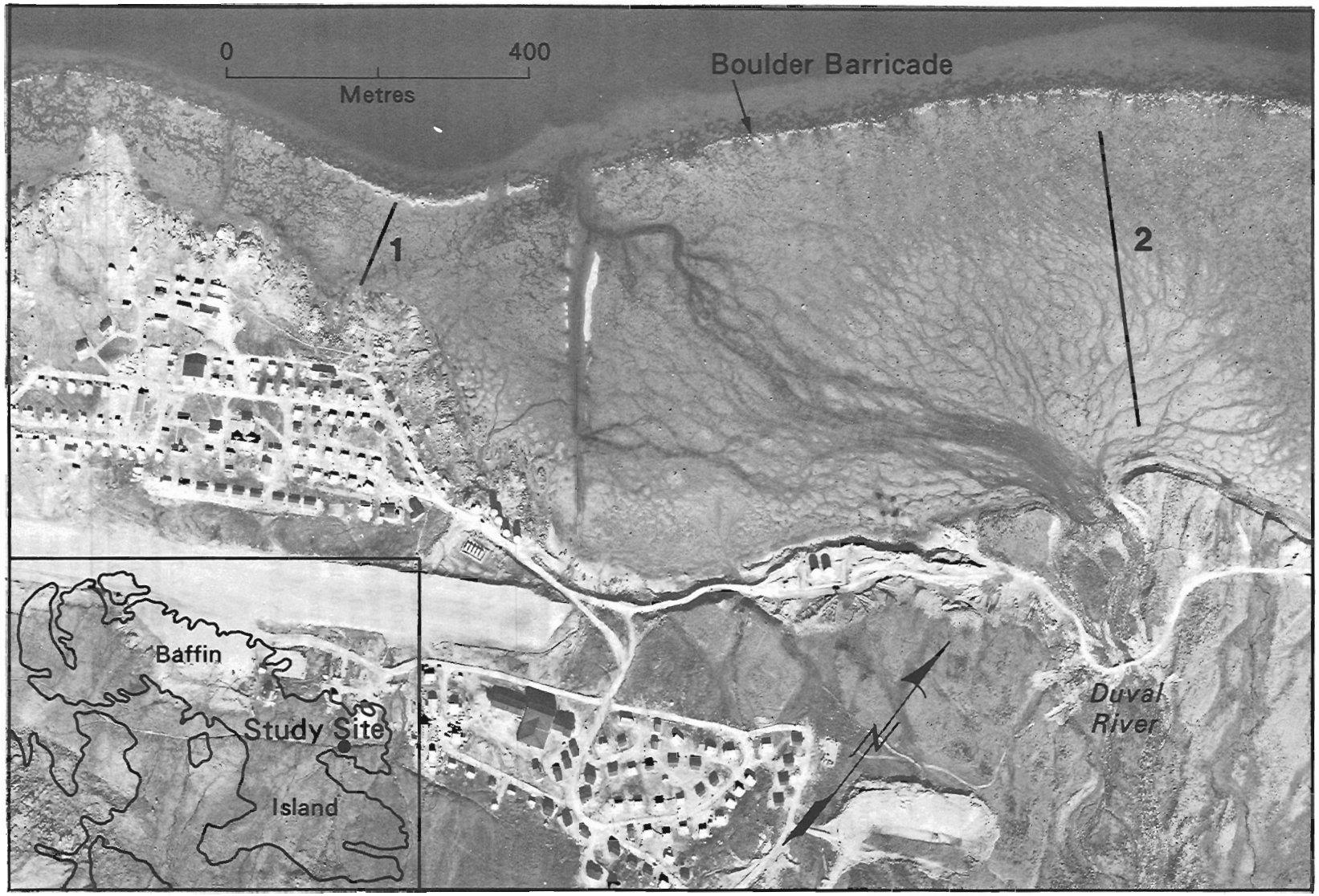

Figure 32.1. *Portion of air photograph A24493-54 taken on August 20, 1976, showing the intertidal flats and seismic lines 1 and 2 in the vicinity of Duval River and the Hamlet of Pangnirtung, Baffin Island.*

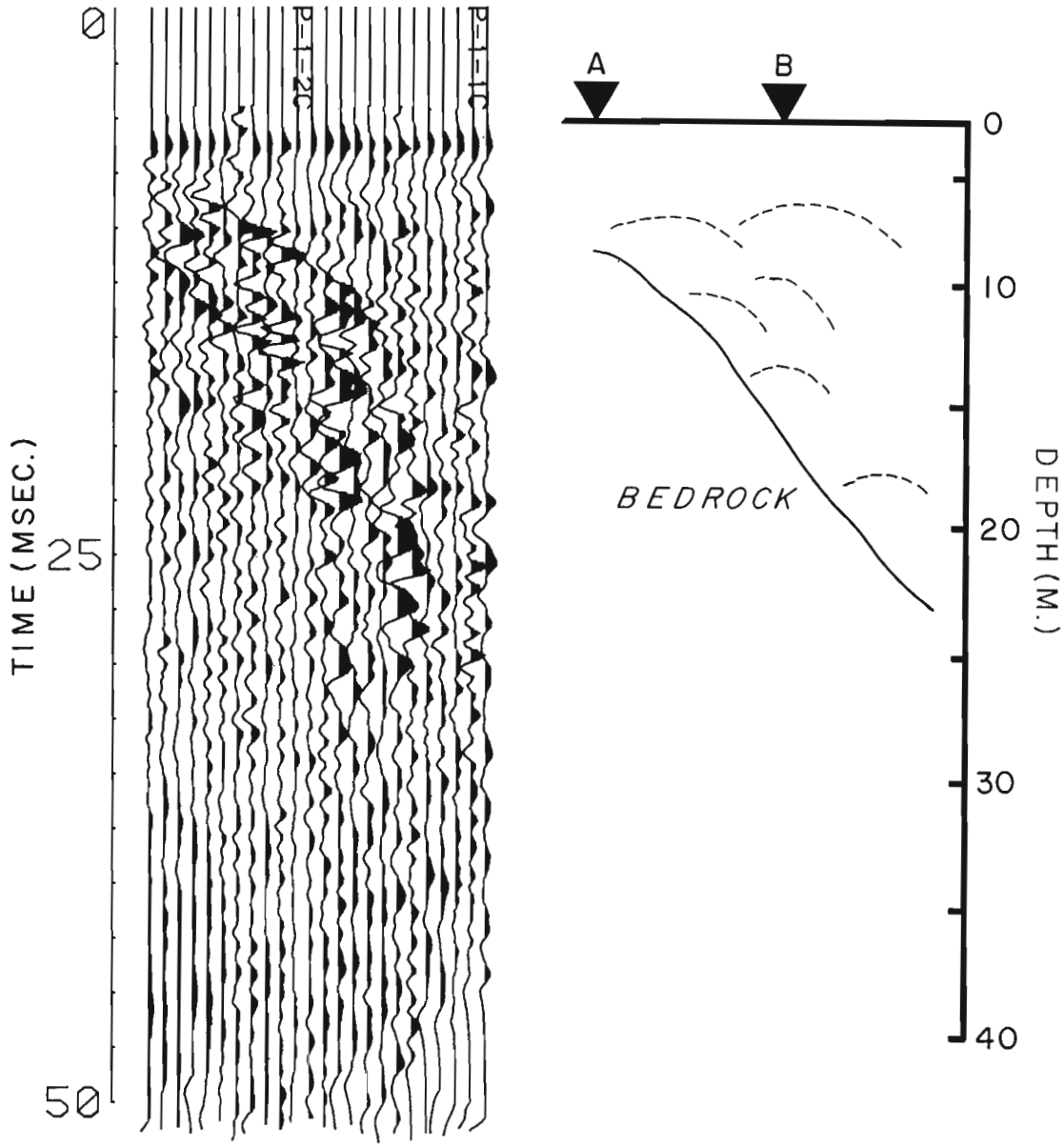

Figure 32.2. *Common offset section along line 1 from shore (at left) towards the boulder barricade. The offset between source and receiver was 9 m along this line. There is a 3 m spacing between traces, and the total length of the section is 70 m. An automatic gain control with a sampling window of 8 ms has been applied to these records.*

At the right of the figure is a schematic interpretation of the section with a non-linear depth scale that has been calculated assuming an average velocity of 1700 m/sec above bedrock. The arrows above this interpreted section mark the positions where expanded spread reflection and refraction records were shot perpendicular to the line. The dashed curved lines represent possible diffraction events.

Reversed expanded reflection and refraction spreads were shot perpendicular to these optimum offset sections at the positions (A to E) indicated in Figures 32.2 and 32.3, and were used to obtain the interpreted sections shown along with the data. The refraction data indicated consistent velocities of 1700 m/sec for the surface layer, and from this information the time scale of the optimum offset sections has been converted to a non-linear depth scale. It is evident from the reversed spreads that there is considerable variability in elevation of the bedrock surface perpendicular to the sections presented here (i.e. approximately parallel to the shoreline). For example, the refraction data from E (Fig. 32.4) indicate that there is an elevation change of 6 or 7 m along the spread length of 80 m. Thus, the bedrock profiles along lines 1 and 2 can only be considered to represent bedrock topography beneath the flats in a most general sense.

Along line 1 where the intertidal flats are quite narrow (130 m wide), bedrock drops off steeply from shore. Under the boulder barricade the wedge of sediments is more than 20 m thick.

The picture is quite different, however, beneath line 2 across the wide zone of the flats. Here a bedrock plateau exists beneath the centre of the intertidal zone, and there is a broad bedrock high (a knob? or ridge?) shoreward of the

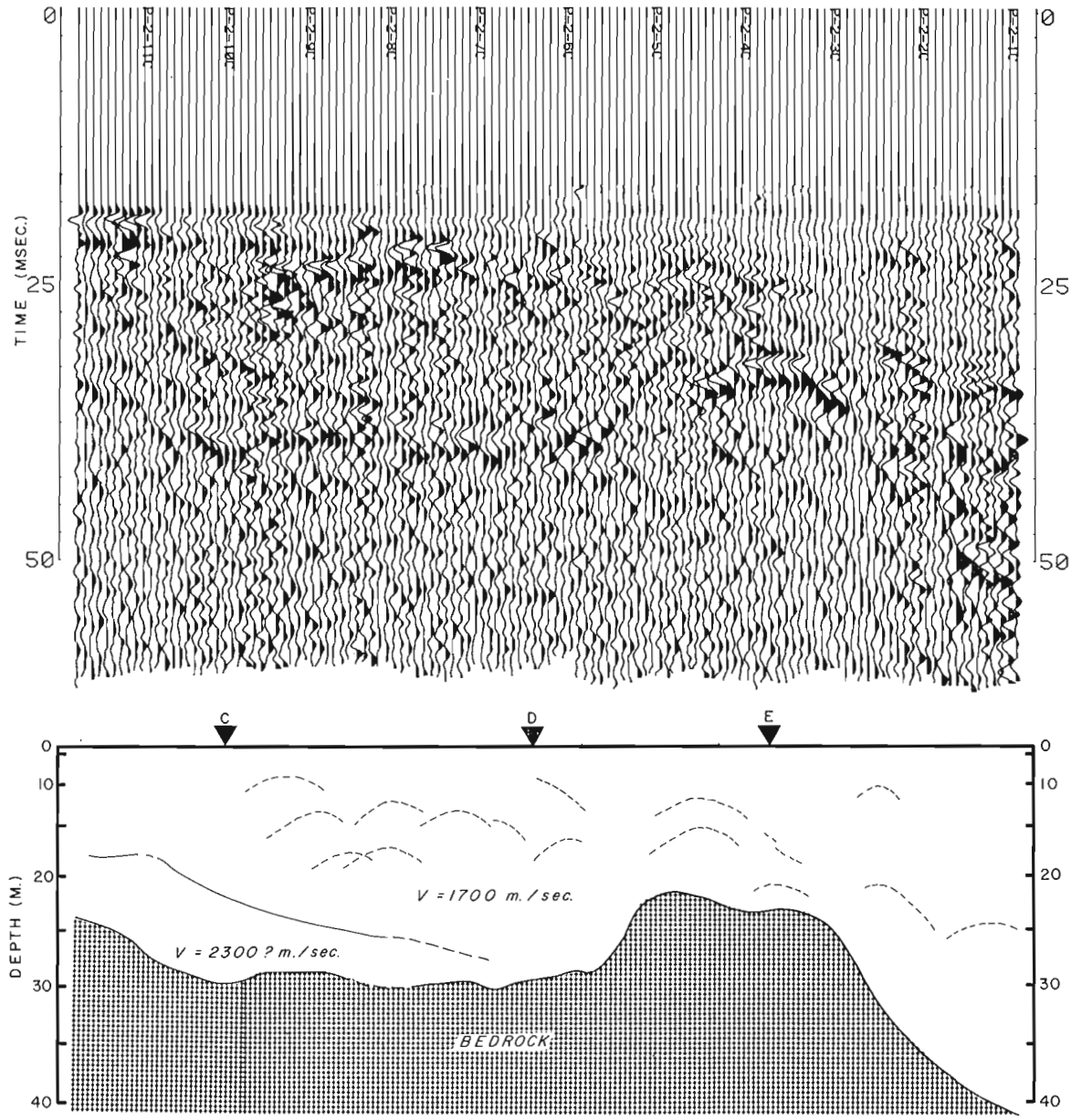

Figure 32.3. *Common offset section along line 2 from shore (at left) towards the boulder barricade. The offset in this case was 30 m and the total length of the section is 390 m. Otherwise the comments accompanying Figure 32.2 apply also to this figure.*

steep drop-off into the fiord. Under the boulder barricade at the end of line 2, the sediment thickness is estimated to be of the order of 50-60 m. At the shoreward end of this profile there is some evidence of stratification in the sediments above bedrock (see Fig. 32.3). This is tentatively interpreted as the top of a wedge of coarser sediments from Duval River, deposited perhaps during a period of lower sea level. For example, evidence presented by Dyke (1979) indicated sea level at Pangnirtung Fiord was some 10 m below present about 3000 years B.P. It is also possible that the shallow reflection comes from a permafrost zone in the sediments, but this is considered unlikely in view of the warm surface water temperatures in this region of the fiord which may exceed 6°C during the open water season (Gilbert, 1978). The velocity of 2300 m/sec that is given for this layer is based on a single reflection record. It would, however, support either of the interpretations suggested above.

One question that it was hoped the seismic data might address was whether the boulders are confined to the surface of the intertidal flats or are scattered throughout the sediments. On the records obtained in this survey there is considerable energy return from within the sedimentary layer (though this has been disguised somewhat in the sections presented here by the automatic gain control that has been applied to the data). On the interpreted sections are indicated possible diffraction events which may be caused by buried boulders, or groups of boulders.

SUMMARY

The results of the hammer seismic survey conducted on the intertidal flats at Pangnirtung in 1982 indicate that bedrock drops off steeply from shore where the flats are narrow, whereas it forms a supporting platform beneath the

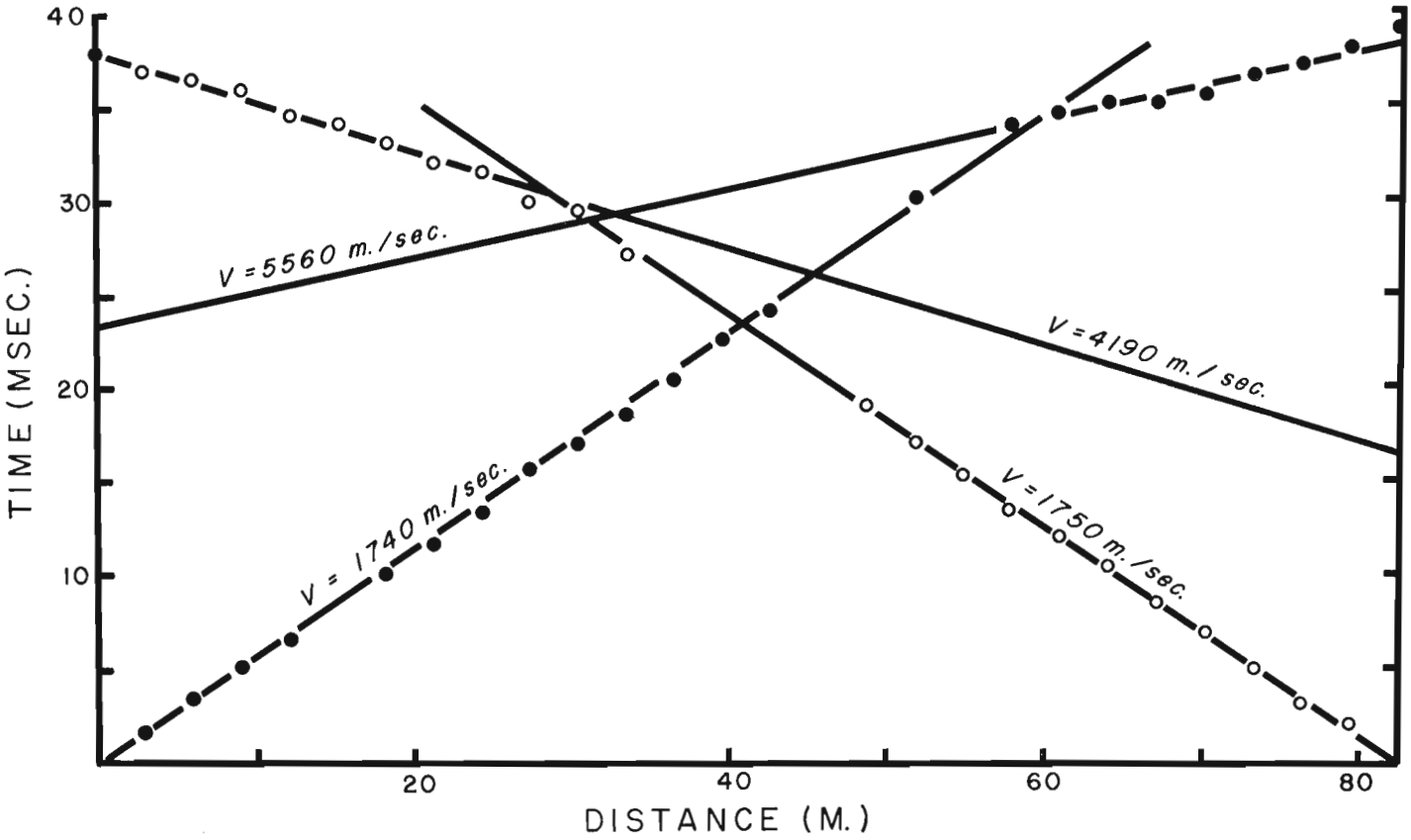

Figure 32.4. *Reversed refraction profile shot perpendicular to line 2 at the position marked E in Figure 32.3. Interpreting this as a case of a uniform overburden (v = 1745 m/sec) above a dipping bedrock (v = 4770 m/sec) the depth to bedrock varies from 22 m at the left end of the profile to 15 m at the right end.*

extensive flats at the outlet of the Duval River. Approximately 30 m of sediment lie above this bedrock platform along most of the survey line. A bedrock high (a knob? or ridge?) was mapped at approximately 150-200 m inside the boulder barricade shoreward of the steep drop-off into the fiord. There is evidence of considerable topography on the bedrock surface perpendicular to the survey lines, so the bedrock profiles presented here can only be considered to be representative ones in a most general sense. It is thought that there are boulders or groups of boulders buried in the sediments, but the density of these in comaprison to those observed on the surface of the flats cannot be estimated.

Acknowledgments

R. Gilbert was supported by a grant from the Natural Sciences and Engineering Research Council of Canada.

References

Aitken, A.E. and Gilbert, R.
1981: Biophysical processes on intertidal flats at Pangnirtung Fiord, Baffin Island, N.W.T.; Final contract report to Petro-Canada Exploration Inc., 92 p.

Dyke, A.S.
1979: Glacial and sea-level history of southwestern Cumberland Peninsula, Baffin Island, N.W.T., Canada; Arctic and Alpine Research, v. 11, p. 179-202.

Gilbert, R.
1978: Observations on oceanography and sedimentation at Pangnirtung Fiord, Baffin Island; Maritime Sediments, v. 14, p. 1-9.

Gilbert, R. and Aitken, A.E.
1981: The role of sea ice in biophysical processes on intertidal flats at Pangnirtung (Baffin Island), N.W.T.; in Workshop on the Action of Ice on Shoreline Evolution, ed. J.C. Dionne, National Research Council of Canada, Associate Committee for Research on Shoreline Erosion and Sedimentation, Proceedings 89-103.

McCann, S.B., Dale, J.E., and Hale, P.B.
1981: Subarctic tidal flats in areas of large tidal range, southern Baffin Island, eastern Canada; Géographie physique et Quaternaire, v. 35, p. 183-204.

Hunter, J.A., Burns, R.A., and Good, R.L.
1980: Mating the digital engineering seismograph with the small computer – some useful techniques; Society of Exploration Geophysicists, 1980 Annual Meeting, Preprint Series.

Hunter, J.A., Burns, R.A., Gagné, R.M., Good, R.L., MacAulay, H.A., and Pullan, S.E.
1982: Field experience with the "optimum window" hammer seismic reflection technique; Society of Exploration Geophysicists, 1982 Annual Meeting, Technical Abstracts Series.

33.

DISTRIBUTION AND LOCALIZATION OF GOLD IN MEGUMA GROUP ROCKS, NOVA SCOTIA. PART 1: STRUCTURAL EFFECTS AND PRESSURE SOLUTION – PRELIMINARY RESULTS[1]

DSS Contract Serial OSU 82-00077

P.M. Clifford[2], J.H. Crocket[2], and F. Fueten[2]
Precambrian Geology Division

Clifford, P.M., Crocket, J.H., and Fueten, F., Distribution and localization of gold in Meguma Group rocks, Nova Scotia. Part 1: structural effects and pressure solution – preliminary results; in Current Research, Part B, Geological Survey of Canada, Paper 83-1B, p. 279-283, 1983.

Also in Mines and Minerals Branch, Report of Activities, 1982, Nova Scotia Department of Mines and Energy, Report 83-1, 1983.

Abstract

Greywackes of the Meguma Group are host to quartz veins, many of which are gold-bearing. Field, petrographic and chemical analyses of the greywackes in the Liscomb Mills area of Nova Scotia show that much quartz has been removed from what are now cleavage zones; that some of this quartz has been reprecipitated as "beards" on quartz grains in lithons between cleavage planes; but that much quartz appears to have been lost from the immediate system. It is clear that pressure solution-transfer was the mechanism involved in generating cleavage and mobilizing quartz. We tentatively suggest that the "missing" quartz now appears as quartz veins, and that perhaps gold was mobilized by the same pressure solution-transfer mechanism.

Résumé

Les grauwackes du groupe de Meguma renferment des filons de quartz, dont certains sont aurifères. L'étude sur le terrain et l'analyse pétrographique et chimique des grauwackes de la région de Liscomb Mills (Nouvelle-Écosse) montrent qu'une grande partie du quartz a été enlevée de ce qui sont maintenant des zones de clivage; qu'une partie de ce quartz a été reprécipitée sous forme d'excroissances sur les grains de quartz dans les microlithons et que le système immédiat aurait perdu une importante quantité de quartz. Il est évident qu'un processus de dissolution-transfert sous pression aurait provoqué le clivage et la mobilisation du quartz. Il est suggéré provisoirement que le quartz "perdu" apparaît maintenant sous forme de filons et que l'or aurait peut-être été mobilisé par le même processus de dissolution-transfert sous pression.

Introduction

We are concerned with possible structural controls on the transfer and location of gold in rocks of the Meguma Group in Nova Scotia. Field and laboratory studies reveal abundant signs of pressure solution and related precipitation associated with mesoscopic cleavage. Chemical analyses suggest that silicate material has been moved within, and out of, the system; other analyses imply comparable transfer of Au and associated metal species.

Faribault (1899) suggested that in Nova Scotia gold is hosted by quartz veins which occur in anticlinal crests as saddle reefs, after the fashion of the vein deposits of Bendigo and Ballarat in Australia. If true, this implies a regular structural control of gold deposits. More recently (Boyle, 1959; Henley et al., 1976) there have been suggestions that gold may be derived from the rock pile in which it is now found, being mobilized by pressure solution, and redeposited in relatively high concentrations elsewhere. In the Nova Scotia case, this translates to mobilization of gold from the Meguma Group rocks, and subsequent precipitation of the gold, with quartz, in quartz veins. This inference carries with it the implication that some of the quartz now in the veins has been extracted from the rock pile generally.

Acknowledgments

It is a pleasure to acknowledge the continuous interest and judicious advice of J.R. Henderson; also conversations with U. Kretschmar and P.I. Wallace.

General Geology

Attention has been concentrated on the Ruth Falls syncline, and adjacent smaller folds. These structures are exposed in the Liscomb Mills area of Nova Scotia, about 140 km east-northeast of Halifax (Fig. 33.1). The 1:10 000 orthophoto map 11 E/01-T1 shows the outcrop very well, and all our maps have been based on it.

The rocks in these folds are of the Goldenville Formation, which, with the Halifax Formation, makes up the Meguma Group. These Goldenville rocks are now metamorphosed high-rank greywackes, at chlorite grade.

The greywackes are cyclically bedded, although this is not always readily apparent. Incomplete Bouma sequences are common. Of particular interest are water escape structures. Sand volcanoes can be seen on some bedding surfaces and are particularly well displayed beyond the Ruth Falls Syncline, on some islands a few kilometres offshore (see Henderson, 1983). In a few cases, these can be seen to be connected to zones oriented at a high angle to bedding. Such zones, seen in thin section, are devoid of phyllitic minerals, are better sorted than the general greywacke, and have a higher median grain size. They are clearly elutriation zones up which water travelled to build a sand volcano at the surface, the material of the sand volcano being the elutriated material. Such escape "pipes" are now at a high angle to, but not perpendicular to, bedding.

---

[1] Contribution to Canada-Nova Scotia Co-operative Mineral Program 1981-84. Project carried by Geological Survey of Canada

[2] Department of Geology, McMaster University, Hamilton, Ontario

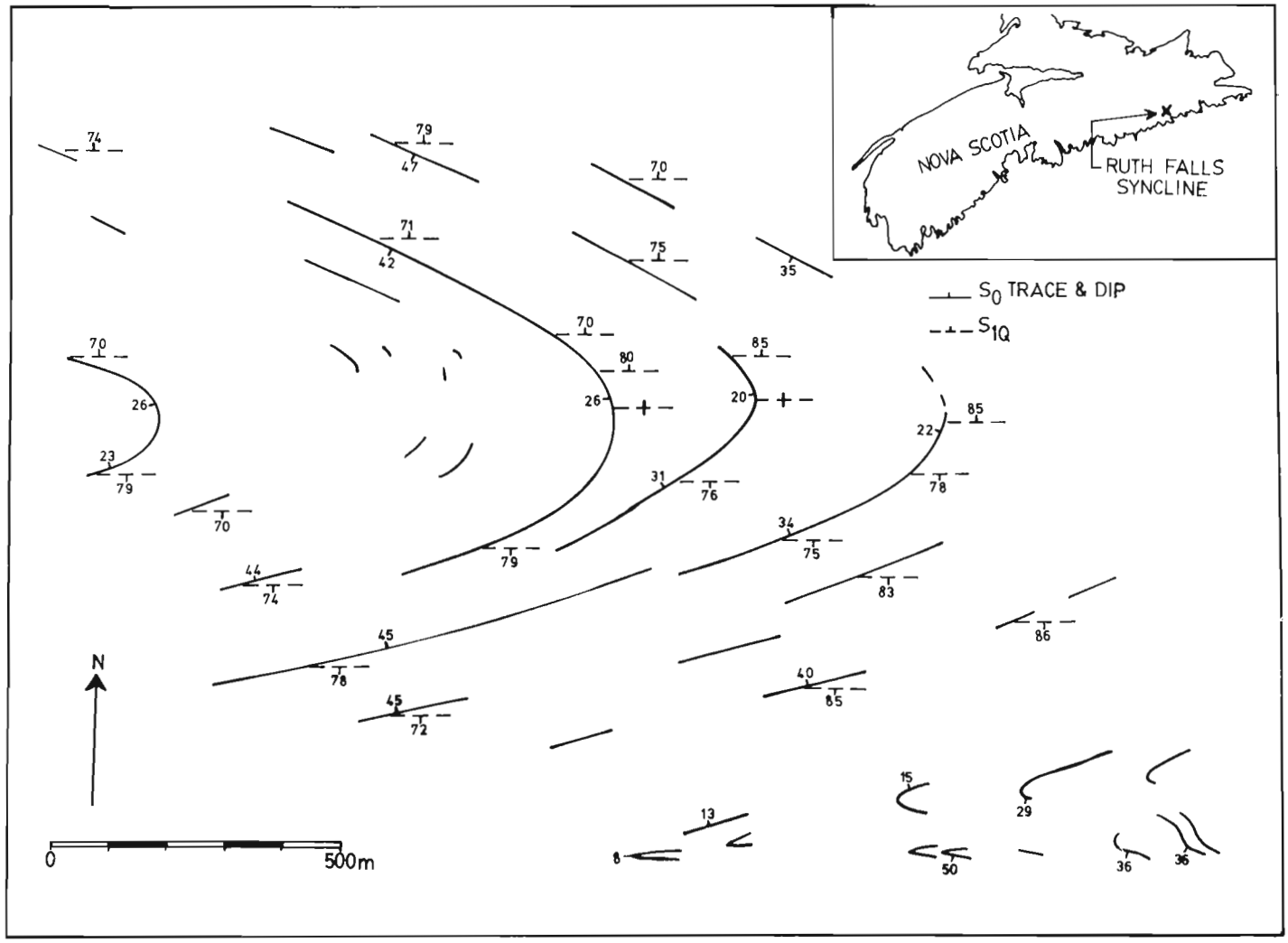

Figure 33.1. *Map showing generalized trends and dip values of bedding and cleavage, Ruth Falls Syncline. Inset: location of area.*

Water escape must have occurred prior to consolidation. Further, pipes without sand volcanoes may mean that after a bed or group of beds dewatered, the next passage of a turbidity current across the basin floor planed away any still-exposed sand volcanoes just prior to deposition of a new layer of sediment. Pipes were presumably perpendicular to bedding. It is significant that the traces of cleavage zones on ac planes are parallel to these "pipes", in that this implies that cleavage was initiated as planar zones perpendicular to bedding (see below).

Structures

These rocks are now disposed in the Ruth Falls Syncline and an attendant smaller anticline (Fig. 33.1). These folds have axial surfaces which strike east and are approximately vertical; they plunge at about 10° to the west. No parasitic folds have been seen.

The most conspicuous structural feature is an array of cleavage zones (CZ). Each cleavage zone is at a high, but oblique, angle to bedding, except in the axial zone where the angle is 90°. Cleavage therefore diverges systematically from parallelism to the axial surface, proceeding from axial zone to limb. Each cleavage zone is marked by a high concentration of micas and chlorite, with a strong preferred orientation of individual mineral grains subparallel to the general attitude of the cleavage zone. Widths of cleavage zones are normally in the range 1-5 mm. Cleavage zones separate lithons of "normal" rock, the lithons being, on average, from 1 to 5 cm wide, although variation in dimensions is considerable.

In the limbs, on ac planes, cleavage zones are anastomosing at a wavelength of 0.1-1.0 m. (It should be pointed out that few outcrops present an ac face more than 0.5 m high.) On ab surfaces, or surfaces nearly parallel to ab, cleavage zones anastomose at a wavelength of 0.1 to 1.0 m. Thus each lithon is actually a triaxial ellipsoid. The overall fabric is domainal at the metre scale.

The intensity of the cleavage in the greywackes varies with position in the fold. To quantify this in the field the number of cleavage zones per metre (CZm^{-1}) identifiable along a line perpendicular to the lineation produced by intersection of cleavage and bedding, was measured. Measurements for rocks of roughly the same grain size ranged from 75 ± 20 CZm^{-1} in the limbs to 130 ± 20 CZm^{-1} in the core of the fold. In a single bed, increases of 40-50 cleavage zones per metre can be detected.

In thin section, cleavage zones are marked by an abundance of micas and chlorite, with their basal planes conspicuously aligned subparallel to the trend of the cleavage. Some zones appear as very narrow "seams" totally

composed of phyllitic minerals; however, the typical zone has a higher concentration of mica in the zone centre (approximately 40 per cent), decreasing more or less symmetrically to the zone margin, which is not very well defined. The other major phase in the CZ is quartz, which is less abundant there than in the lithons. The CZ quartz grains have very sharp, rectiplanar boundaries against phyllosilicates; boundaries of the same grains not in contact with phyllosilicates are irregular. The two-dimensional form of these quartz grains is quite inequant, with long axes aligned parallel to cleavage, but the grains display little or no undulatory extinction or other signs of ductile deformation (Fig. 33.2a). We conclude that the form of the grains, and the nature of their boundaries imply pressure solution of quartz during creation of the cleavage in its present form.

A sample calculation, taking lithon width as 10x CZ width, with 95:5 and 70:30 percentage ratios of quartz and phyllosilicates in lithons and cleavage zones respectively, and assuming that phyllosilicates in cleavage are residual, chemically and perhaps mineralogically, suggests a loss of about 85 per cent quartz by volume from the rock volumes now represented by CZ. This represents a bulk loss of quartz from the system of about 33 per cent by volume. These values are very probably too high.

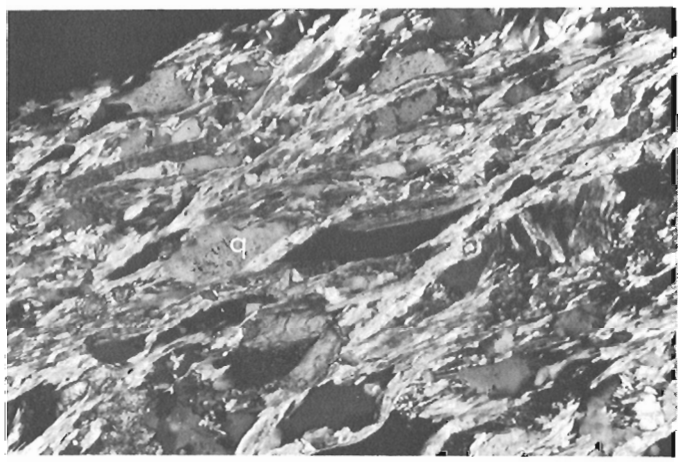

Figure 33.2a. *Photomicrograph of fabric in cleavage zones. Note sharp boundaries of inequant quartz (q) against phyllosilicates, and the more ragged terminations of the quartz generally. Long dimension of photograph is 1.5 mm.*

Figure 33.2b. *Photomicrograph of lithon fabric. Note substantial development of quartz "beards" (b) on subequant quartz. Long dimension of photograph is 1.5 mm.*

Within the lithons, there are clear signs of localized deposition of quartz, in the form of "beards" attached to sundry original quartz grains (Fig. 33.2b). But the amount of such deposited quartz is less than 5 per cent by volume, or no more than 25 per cent of the loss calculated above. We conclude that the process of pressure-solution plus deposition acting on these rocks has induced a net loss of quartz as a dispersed mineral phase of about 40 per cent.

Quartz Veins

Virtually all of the quartz veins seen in the Ruth Falls Syncline are in, or near, an ac position. They contain quartz, with minor amounts of chlorite. The veins are clearly post-folding, but pre-kink band development (see Henderson, 1983, for a more detailed discussion of quartz veins in these rocks).

King Folds

Kink folds have been observed and measured at 13 stations in the axial zone. All kink folds have layering abruptly inflected across the kink band boundary. Very little of the area is actually affected by these folds which are the last structural items to be impressed on the rocks, and make a trivial contribution to the total strain in these rocks.

In summary, the kink bands usually are small, with aspect ratios (width/length) of about 0.01, and widths up to 12 cm. The majority of folds show a sinistral sense of rotation. A majority of folds are also underrotated. The very few conjugate kink bands imply a stress field of:

$$\sigma_1\ 286/06;\ \sigma_2\ 028/78;\ \sigma_3\ 177/10.$$

If all kink bands are treated as if they are conjugate arrays (box folds), the stress field is:

$$\sigma_1\ 277/16;\ \sigma_2\ 097/74;\ \sigma_3\ 186/00.$$

The second stress field is based upon a wide scatter of data. We can safely say that σ_1 was oriented roughly E-W with a 10°(±) plunge to the west, and that σ_3 was horizontal, about N-S (Fig. 33.3).

The very sharp inflection of laminae and the equally sharp inflection of ac quartz veins caught up in kink bands, suggests that they are the latest structural event. About 75 per cent of all folds measured are underrotated, that is, geometrically they can be viewed as having positive dilation preserved (Clifford, 1969). This suggests production at shallow depths.

One peculiarity is the presence of "aborted" kink bands. These have clear boundaries oblique to layering, accentuation of layering within the band, but no rotation of layers in the band. Values of α for such bands are invariably high. We have no explanation for these structures.

Rock Chemistry

If we are justified in our conclusion that cleavage developed via pressure solution processes, there should be some chemical trace of this, as a chemical difference between core and limb areas, which have markedly different cleavage densities, and between CZ and lithon anywhere.

We have analyzed six pairs of samples from correlatable layers to compare limb with core. Other samples have been split into lithon and CZ portions. For such samples, however, it has proved impossible to keep the CZ samples free of "contamination" by attached lithon material. Consequently, the contrasts between lithons and CZ are diminished somewhat from their actual levels.

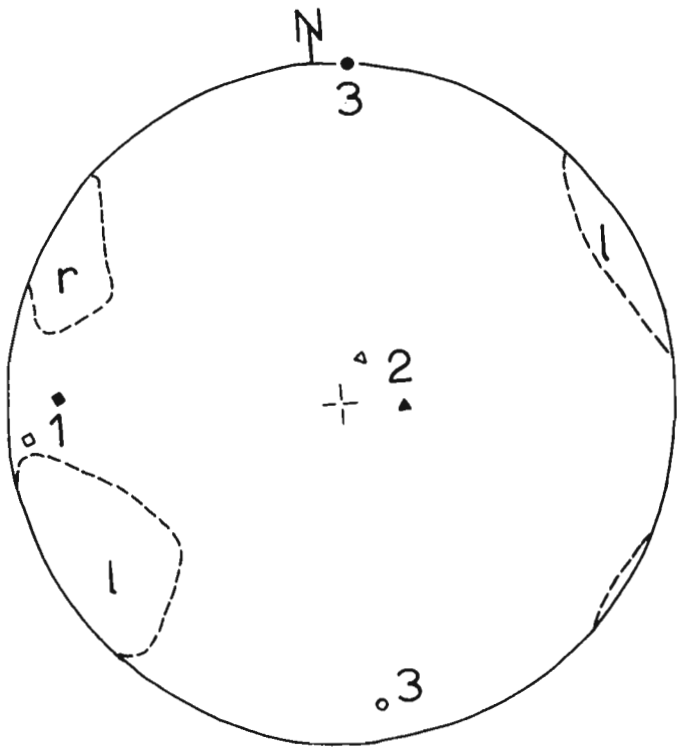

Figure 33.3. *Principal axes of stress (1 = σ_1, 2 = σ_2, 3 = σ_3) determined from kink bands. Open symbols – inferred from conjugate sets; closed symbols – inferred from all kink bands. Fields are of poles to kink band boundaries: l – left-hand rotation, r – right-hand rotation. Total poles: 97.*

Dealing first with bulk differences between axial zone and limbs (Table 33.1), it can be seen that, for six pairs, core versus limb, four show a loss and two show a gain of SiO_2, Fe_2O_3 and K_2O. Other components very nonsystematically. We conclude that, overall, there is indeed differential removal of material from the core in relation to the limbs, associated with the higher density of CZ in the core.

The picture is a little different when we look at CZ versus lithons (Table 33.2). SiO_2 and Na_2O are depleted in CZ in every case. Always the CZ showing highest relative loss of SiO_2 also show highest relative loss of Na_2O. Al_2O_3, Fe_2O_3 and K_2O are augmented in CZ relative to lithons. Again, other components vary nonsystematically. There is little doubt that the process of cleavage generation in these rocks involves relative loss of SiO_2 and Na_2O from the rock volumes which we now recognize as CZ.

Generally, there has been removal of material to give CZ, and a broader scale transfer and loss of material from core to limb and out of the local system. Presumably the pathways for these transfers were along the CZ or at the CZ-lithon interface; it is not likely that material was transferred across CZ. The most plausible mechanism for this chemical readjustment is pressure solution with some local reprecipitation, a view supported by petrographic evidence.

Suggested History

The overall sequence of events envisaged for the generation of cleavage and the production of the folds is as follows:

1. Unconsolidated sediment lost water, via water escape structures in particular.

Table 33.1

Normalized composition, including loss of ignition, whole-rock

Sample	SiO_2	Al_2O_3	Fe_2O_3	MgO	CaO	Na_2O	K_2O	TiO_2	MnO	P_2O_5	Loss on Ign.	Total	Core/Limb
A8	78.27	10.38	2.76	1.98	.68	2.13	2.35	.35	.04	.05	1.06	100.00	Core
A1	78.95	10.10	2.70	1.33	.87	2.18	2.27	.50	.05	.04	1.00	100.00	Limb
B92	83.06	8.63	1.95	1.03	.64	1.91	1.48	.38	.05	.04	.83	100.00	Core
F18	81.08	9.16	2.37	1.42	.94	2.18	1.40	.44	.06	.06	.89	100.00	Limb
F15	79.29	9.96	2.82	.87	.95	2.81	1.44	.46	.05	.10	1.23	100.00	Core
F5A	77.30	11.28	3.69	1.30	.84	1.88	1.62	.51	.06	.09	1.43	100.00	Limb
F14	75.91	11.58	4.00	1.33	1.02	2.08	1.87	.55	.08	.09	1.48	100.00	Core
A45	77.77	10.35	2.67	1.23	1.76	2.80	1.32	.41	.07	.06	1.54	100.00	Limb
A55	81.32	9.41	2.52	.95	1.07	1.92	1.13	.44	.07	.07	1.11	100.00	Core
A54	82.32	8.93	2.34	1.03	.73	1.98	1.08	.50	.04	.07	.94	100.00	Limb
A50	79.71	9.80	2.74	1.35	1.14	1.97	1.34	.53	.07	.08	1.26	100.00	Core
A49	79.52	9.37	2.64	1.55	1.03	2.83	1.22	.49	.09	.07	1.18	100.00	Limb
A47	80.76	9.06	2.42	1.35	.75	2.66	1.14	.48	.03	.07	1.28	100.00	Limb
F12	80.02	9.86	2.81	1.14	.82	2.23	1.30	.55	.06	.07	1.14	100.00	0
A53	80.32	9.68	2.86	1.06	.78	2.15	1.34	.51	.06	.08	1.18	100.00	0
A52	81.61	9.19	2.37	1.09	1.18	1.67	1.01	.46	.01	.06	1.35	100.00	0
A50A	80.22	8.72	2.36	2.21	1.12	2.76	.93	.46	.06	.07	1.07	100.00	x
A50C	79.46	9.90	2.76	1.35	1.11	2.02	1.35	.53	.07	.08	1.36	100.00	x
A50E	79.64	9.52	2.68	.77	1.81	2.22	1.31	.54	.08	.09	1.35	100.00	x
A50D	64.47	7.67	1.95	1.26	13.00	1.63	1.04	.40	.26	.33	8.00	100.00	x
A50F	77.74	10.94	3.27	.96	1.07	2.23	1.67	.60	.06	.08	1.39	100.00	x
A50B	81.03	9.31	2.42	1.06	1.09	1.94	1.24	.51	.05	.08	1.26	100.00	x

x – Samples used to check composition of different flow units in one bed.

0 – Bed cannot be properly correlated.

Table 33.2

Normalized composition, including loss on ignition, cleavage (c) versus lithon (l)

Sample	SiO_2	Al_2O_3	Fe_2O_3	MgO	CaO	Na_2O	K_2O	TiO_2	MnO	P_2O_5	Loss on Ign.	Total
F5AC	70.80	14.01	4.97	2.03	1.02	2.16	2.44	.64	.09	.12	1.73	100.00
F5AL	74.73	12.21	4.46	1.37	1.05	1.94	1.94	.59	.08	.09	1.53	100.00
	74.29	12.28	4.55	1.38	1.06	2.19	1.95	.58	.09	.11	1.53	100.00
F5AC	70.22	13.87	5.32	2.08	1.13	2.08	2.76	.67	.09	.11	1.67	100.00
F5AL	74.71	11.87	4.48	1.83	.99	1.95	1.90	.55	.07	.11	1.54	100.00
F5A1C	75.10	11.85	4.13	1.23	1.08	1.70	2.74	.63	.07	.09	1.38	100.00
F5A1L	79.89	9.58	2.96	1.26	.84	2.04	1.86	.49	.07	.06	.95	100.00
F5A50C	67.83	16.08	4.58	1.42	1.33	1.89	3.59	.83	.08	.13	2.24	100.00
F5A50L	78.74	9.88	3.19	.97	1.47	2.19	1.35	.49	.07	.08	1.57	100.00
F14C	70.31	13.46	5.61	2.22	.98	2.09	2.51	.63	.12	.08	2.00	100.00
F14L	74.35	12.22	4.46	1.41	1.04	2.19	2.07	.56	.10	.09	1.51	100.00
A49C	72.54	13.66	4.03	1.37	1.15	2.12	2.50	.71	.07	.12	1.72	100.00
A49L	78.48	9.89	3.00	1.39	1.72	1.87	1.26	.50	.08	.08	1.74	100.00

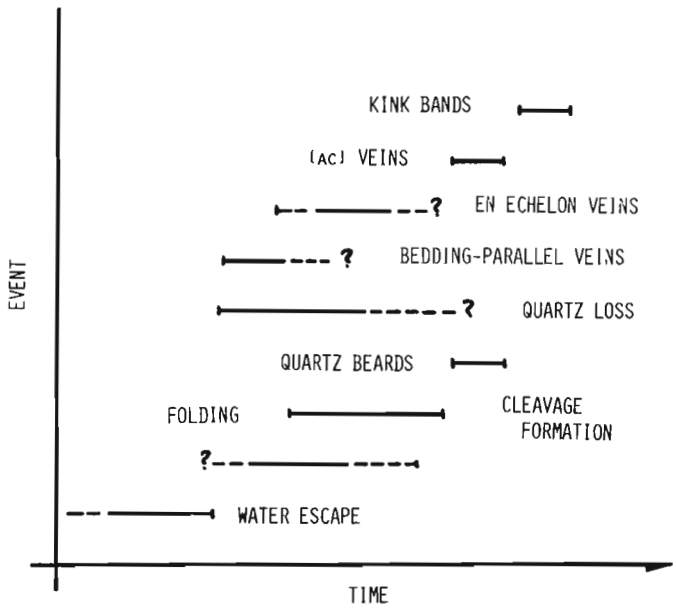

Figure 33.4. *Proposed sequence of events in the Ruth Falls Syncline. Position of bedding-parallel and en echelon veins are based upon coastal data, and are not locally inferrable.*

2. CZ developed, post-dewatering, and continued into the folding episode. CZ are now parallel to water-escape channels, and so were initially bedding-normal. Development of CZ has involved removal of silica, so an episode of pressure solution, with maximum pressure exerted parallel to bedding, occurred prior to, and perhaps during, the early stages of fold formation.

3. Subsequent growth of the fold led to the present structure, with fanning cleavage. Cleavage now fans symmetrically about the axial plane but is not generally normal to bedding. There is no sign of slippage in or on CZ, so the rotation of CZ from bedding-normal to bedding-oblique positions may be ascribed to an episode of flattening superimposed on a simple deflection geometry. (Preliminary estimates suggest a flattening of 20-25 per cent, but this is based upon only two data sets.)

4. Quartz beards attached to quartz grains in the lithons are composed of rectilinear fibres. It follows that during the period of growth of such beards the strain was irrotational. The alignment of fibres parallel to cleavage traces, without any sign of distortion suggests a late stage growth.

Figure 33.4 shows, schematically, the sequence of events, against an arbitrary time scale.

Discussion

It is apparent that pressure solution was largely responsible for the production of the cleavage zones; chemically, such zones are consistently depleted in SiO_2 and Na_2O. But there is an apparent substantial loss from the system of SiO_2; the reprecipitated "beards" do not represent more than 25 per cent of the mobilized SiO_2. We suggest that the mobilized SiO_2 which is not now seen as "beards" actually appears as the quartz veins of the area. If pressure solution mobilized SiO_2, it is conceivable that it also mobilized the gold which occurs in some veins. It is this possibility that is the focus of continuing work.

References

Boyle, R.W.
1959: The geochemistry, origin and role of carbon dioxide, water, sulfur and boron in the Yellowknife gold deposit, Northwest Territories, Canada; Economic Geology, v. 54, p. 1506-1524.

Clifford, P.M.
1969: Kink band development in the Lake St. Joseph area, NW Ontario; Geological Survey of Canada, Paper 68-52, p. 229-241.

Faribault, E.R.
1899: The gold measures of Nova Scotia and deep mining; Journal of the Mining Society of Canada, Vol. 2, p. 119-128.

Henderson, J.R.
1983: Analysis of structure as a factor controlling gold mineralization in Nova Scotia; in Current Research, Part B, Geological Survey of Canada, Paper 83-1B, Report 2.

Henley, R.W., Norris, R.J., and Paterson, C.J.
1976: Multistage ore genesis in the New Zealand geosyncline: a history of post-metamorphic lode emplacement; Mineralium Deposita, v. 11, p. 180-196.

DISTRIBUTION AND LOCALIZATION OF GOLD IN MEGUMA GROUP ROCKS, NOVA SCOTIA. PART 2: IMPLICATIONS OF BACKGROUND GEOCHEMISTRY AND CLEAVAGE DEVELOPMENT- A PRELIMINARY REPORT[1]

DSS Contract Serial OSU 82-00077

J.H. Crocket[2], P.M. Clifford[2], F. Fueten[2] and A. Kabir[2]
Precambrian Geology Division

Crocket, J.H., Clifford, P.M., Fueten, F., and Kabir, A., Distribution and localization of gold in Meguma Group rocks, Nova Scotia. Part 2: implications of background geochemistry and cleavage development – a preliminary report; in Current Research, Part B, Geological Survey of Canada, Paper 83-1B, p. 285-290, 1983.

Also in Mines and Minerals Branch, Report of Activities, 1982, Nova Scotia Department of Mines and Energy, Report 83-1, 1983.

Abstract

Gold and arsenic were determined by radiochemical neutron activation analysis in metagreywacke and slates from Meguma Group rocks. Averages for 22 greywackes from the Ruth Falls syncline are 1.19 ppb gold and 2.30 ppm arsenic. Averages for 38 slates from Liscomb Point and nearshore islands are 1.72 ppb gold and 2.54 ppm arsenic. These values are background levels as the sampled areas are unmineralized.

A study of gold and arsenic distribution between limb and axial zone domains of the Ruth Falls syncline suggested that no consistent redistribution of these metals on a scale of hundreds of metres has occurred in response to deformation associated with the folding. The partition of gold and arsenic between cleavage and lithon domains in Ruth Falls metagreywackes is usually characterized by higher metal content in cleavage domains. Pressure solution of quartz is an important factor in cleavage domain upgrading of gold content.

Résumé

La teneur en or et en arsenic des métagrauwackes et des schistes du groupe de Meguma a été déterminée grâce à l'analyse par activation radiochimique des neutrons. Vingt-deux échantillons de grauwackes provenant du synclinal de Ruth Falls ont une teneur moyenne en or de 1,19 ppb et en arsenic de 2,30 ppm. Trente-huit échantillons de schistes provenant de Liscomb Point et des îles près du littoral ont une teneur moyenne en or de 1,72 ppb et en arsenic de 2,54 ppm. Ces chiffres sont des valeurs de fond puisque les régions échantillonnées ne sont pas minéralisées.

L'étude de la répartition de l'or et de l'arsenic entre les flancs et la zone axiale de synclinal de Ruth Falls suggère qu'il n'y a pas eu répartition uniforme de ces métaux sur des centaines de mètres en réponse à la déformation associée au plissement. La répartition de l'or et de l'arsenic entre les zones de clivage et les microlithons des métagrauwackes de Ruth Falls est généralement caractérisée par une teneur plus élevée en métaux dans les zones de clivage. La dissolution sous pression du quartz est un facteur important dans l'accroissement de la teneur en or des zones de clivage.

Introduction

Native gold and arsenopyrite are concentrated in quartz veins hosted by the flysch-type Cambro-Ordovician sedimentary rocks of the Meguma Group in eastern Nova Scotia. Most of the productive veins are bedding parallel and commonly localized at the centre of elliptical domes along anticlinal crests according to Faribault (1899). Some studies including those of Faribault (1899) and Keppie (1976) argue that folding and vein formation are essentially synchronous whereas others, for example Graves and Zentilli (1982), would have vein formation predate folding. It is therefore of interest to determine the distribution of gold and arsenic with respect to both small and large scale features related to deformational history. One facet of this study has been an evaluation of gold and arsenic distribution in cleavage and adjacent lithon domains in metagreywacke on a hand specimen scale. A companion study has been carried out on the gold and arsenic variation in fold limb and axial zone domains in single beds of metagreywacke. The structure on which these studies were conducted was the Ruth Falls syncline, Ecum Secum area (see Clifford et al., 1983).

The ultimate origin of gold in Meguma Group quartz veins is enigmatic. Boyle (1966), McBride (1978) and Graves and Zentilli (1982) argue that the Meguma Group rocks represent an adequate source for the mineralization, and stress the importance of regional greenschist metamorphism as an effective process to mobilize and concentrate metals. Glasson and Keays (1978), on the other hand, do not believed the host rocks of the Clunes field in Victoria, Australia, represent a sufficient reservoir to account for the gold mineralization. Their study is relevant to the Meguma zone in view of the very similar geological history and mineralization characteristics of the Victoria gold fields. To evaluate the potential of the Meguma Group as a source domain, an evaluation of the background levels of the metals of interest is of importance. Thorpe and Thomas (1976) have carried out such a study on drill core from the Oldham district. We have determined the backgroupd levels of gold and arsenic at two locations in the Ecum Secum area to increase the data base, evaluate regional variation, compare metal levels in greywacke and slate, and to gain insight into the mineralogical siting of gold in unmineralized environments.

Acknowledgments

We are grateful for the logistic and financial support of the Geological Survey of Canada. Jack Henderson, GSC, offered advice on sampling site selection and we are indebted to him for much thoughtful discussion and encouragement.

[1] Contribution to Canada – Nova Scotia Co-operative Mineral Program 1981-84 Project carried by Geological Survey of Canada

[2] Department of Geology, McMaster University, Hamilton, Ontario

Sampling and Analytical Procedure

Samples were collected from two localities in the Ecum Secum area including the Ruth Falls syncline (see Clifford et al., 1983) and Liscomb Point and nearshore islands (see Fig. 34.1). In the Ruth Falls syncline metagreywacke outcrops were sampled from the limb and axial zone domains of individual beds with a spacing of approximately 100 m between samples. Several samples of the same bed were collected at one site to establish metal variation on a local scale (A50 series). At Liscomb Point and on Barren, Crook's and Goose islands (Fig. 34.1) slate outcrops were sampled across approximately 2500 m of stratigraphy. Both sites are in unmineralized localities in the Goldenville Formation.

Greywacke and slate hand specimens of approximately 0.5 kg were passed through a jaw crusher and disk grinder to obtain fragments of about 0.5 mm. Final reduction of 100 gm of this material to -200 mesh was done in a ceramic shatter box. Slabbing of greywacke samples to obtain cleavage-lithon slices is described in Clifford et al. (1983) and subsequent reduction was carried out as above. About 300 mg of -200 mesh powder was taken for analysis.

Gold and arsenic determinations were carried out by radiochemical neutron activation analysis using a procedure similar to that described by Kronborg and Steinnes (1975). Briefly, samples were irradiated for 12 h in a neutron flux of 1×10^{13} neutrons/cm^2/sec in the McMaster University reactor. Following a 3 to 4 day decay period samples and appropriate gold and arsenic carriers were dissolved by an alkali peroxide fusion and subsequently dissolved in HCL. Thioacetamide solution was added and precipitated by heating. Gold and arsenic coprecipitate with the liberated sulphide which is filtered, washed and then counted.

The composite gamma ray spectrum of ^{198}Au and ^{76}As was taken on a 4000 channel gamma spectrometer coupled to an intrinsic coaxial germanium detector. Chemical yields of gold and arsenic are determined by a one minute re-irradiation of the recovered carrier. The sensitivity limits are approximately 0.1 ppb for gold and 200 ppb for arsenic. The gold and arsenic levels in the samples are sufficiently high that no samples were below the sensitivity limits.

Results

Analytical results for the Ruth Falls syncline rocks are tabulated in Tables 34.1 and 34.2, together with the arithmetic mean and standard deviation for the entire whole rock suite. In Table 34.1 the A8, A1 to A55, A54 pairs represent two samples from the same bed, one from the core or axial zone and the other from the fold limb. Samples A49 and A47 are from the limb domain of the same bed and are

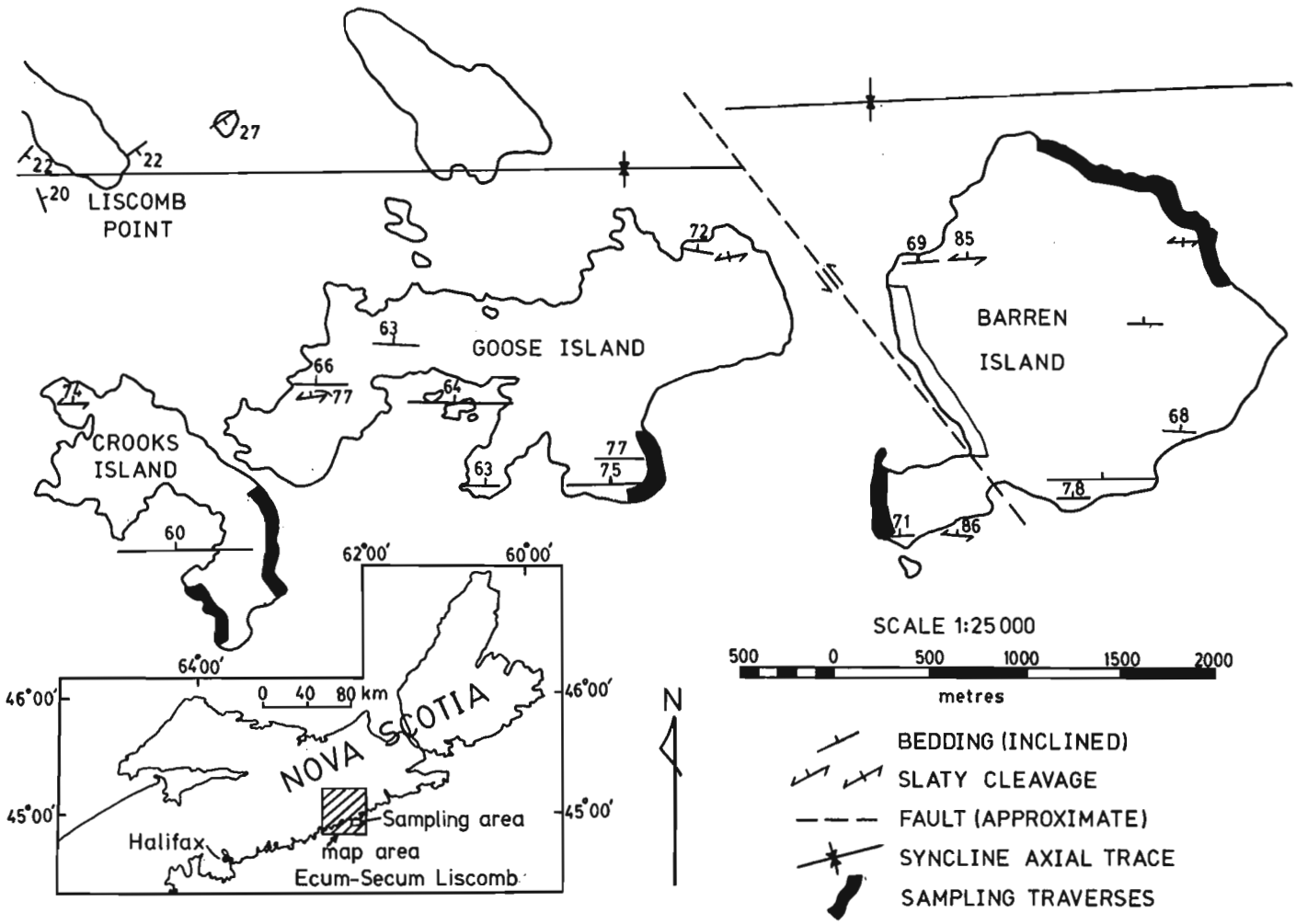

Figure 34.1. Location map showing sampling traverses for collection of slate samples from Goose, Crook's and Barren islands, and Liscomb Point.

separated by tens of metres. The series F12, A53, A52 are from the axial zone domain but probably are not from the same bed. The A50 series are samples representing a 250 cm stratigraphic thickness of amalgamated beds, and are briefly described in the footnote to Table 34.1

The cleavage-lithon data are presented in Table 34.2 and a summary of the gold and arsenic contents of 38 slate samples from four sites is given in Table 34.3.

Discussion

Heavy metals in Ruth Falls syncline metagreywacke

Background metal levels. The Ruth Falls syncline rocks represent an unmineralized environment lacking auriferous bedding parallel quartz veins. The gold and arsenic contents are regarded as background values thought to represent mainly the metal content inherited at sedimentation, but subject to redistribution during structural evolution of the syncline. Comparison of the statistics on the Ruth Falls suite with comparable bodies of data is severely limited as available compilations usually include arenaceous rocks representative of several depositional enrivonments. However, the study of Thorpe and Thomas (1976) provides comparable data for gold obtained by a similar analytical technique. Thorpe and Thomas (1976) report a maximum likelihood value for the mean gold content of 39 greywacke samples from a drill core taken near Oldham as 0.62 ppb. The hole is apparently several hundred metres from the nearest known auriferous vein in the district. The arithmetic mean for Ruth Falls metagreywacke is 1.19 ± 1.05 ppb gold for 22 samples. Both averages should provide an estimate of the background gold content of Meguma Group greywackes. The difference in the two estimates is approximately a factor of two. This may reflect real regional variation or may arise because the maximum likelihood value is a better estimator of true mean value than the arithmetic mean. Alternatively, difference in the neutron activation analytical technique employed in the two studies may introduce a bias. Both the Oldham and Ruth Falls averages indicate that Meguma Group greywackes are not significantly higher in gold than sandstone in general. Estimates of average gold in sandstone, siltstones, greywacke and subgreywacke compiled by Boyle (1979) and Croclet (1974) are 13 and 3.0 ppb respectively. These estimates, although not specifically relevant to sandstones deposited by turbidity mechanisms, suggest that Meguma Group greywackes carry a normal or slightly depleted compliment of gold.

Table 34.1

Gold and arsenic contents of metagreywacke, Ruth Falls syncline, Meguma Group, N.S.: comparison of metal distribution in the axial zone and limbs of the fold

Sample	Code	Au, ppb	As, ppm
A8	Core	0.85	2.1
A1	Limb	0.79	2.2
B92	Core	0.36	1.7
F18	Limb	1.2	2.5
F15	Core	1.2	1.2
F5A	Limb	3.6	1.25
F14	Core	3.2	3.2
A45	Limb	0.83	2.1
A55	Core	0.22	1.0
A54	Limb	0.34	3.6
A50	Core	0.75	2.9
A49	Limb	1.15	1.9
A47	Limb	0.56	1.7
F12	Core	3.5	1.5
A53	Core	0.91	3.8
A52	Core	2.7	1.5
A50A		0.39	2.1
A50B		0.54	2.7
A50C	Core	0.47	2.1
A50D		0.45	2.6
A50E		1.4	1.9
A50F		0.71	5.0
Average for A50 series		0.66 ± 0.38	2.28 ± 0.35
Aggregate statistics	$\bar{X}$	1.19	2.30
	r r	0.22-3.6	1.0-5.0
	σ	1.05	0.96
	n=22		

Note:

The A50 series are from one outcrop consisting of approximately 2.5 m of amalgamated greywacke beds. Five beds are A unit Bouma sequence rocks and one A50D represents a B unit. The arsenic value for A50F is not included in the series average.

The background level for arsenic suggested by the Ruth Falls data is 2.30 ppm. Unfortunately, it cannot be established by comparison with lithogeochemical data if this average arsenic content is representative of sandstones in general. According to Onishi (1969) 1 ppm may be taken as an average arsenic content for sandstone, but the data base is extremely limited and no significance is attached to the difference between Ohishi's estimate and the Ruth Falls average.

One comparative aspect of the arsenic and gold distribution may be noted. Arsenic and gold concentrations do not correlate significantly on a sample-to-sample basis. The gold-arsenic correlation coefficient is r=0.23, a value which is not significant at a 10 per cent probability level when tested against a Student's t distribution. This behaviour is in contrast to the strong association of these metals characteristic of mineralized quartz veins in Meguma Group rocks. A tentative inference from this observation is that the gold-arsenic association in quartz veins is established by and during the mineralization process. This in turn suggests that the inherent availability of the metals to ore solutions, a factor which is probably more dependent on mineralogical siting of the metal than on absolute concentration, is an important factor in the generation of ore fluids.

Distribution of metals in fold limbs and axial zone An early generalization from studies of gold vein distribution in the Nova Scotia fields was that veins were preferentially sited in the axial zones of folds (Faribault, 1899). Clifford et al. (1983) cite evidence that pressure solution processes have caused considerable mobilization of silica. To test the possibility that gold and arsenic were redistributed on a large scale by such processs, a series of Ruth Falls metagreywacke beds were sampled in limb and axial zone domains. In general the lateral separation of samples along strike was about 100 m. Six sets of samples, A8-A1 to A50-A49-A47 as listed in Table 34.1 were collected for this purpose.

The major element data (Clifford et al., 1983, Table 33.1) do not suggest consistent compositional trends related to sample location on the fold limb or axial zone.

Table 34.2

A comparison of gold and arsenic contents of cleavage plane-lithon pairs from Ruth Falls syncline metagreywackes

Sample		Au, ppb	As, ppm
F5A 1	cleavage	2.1	4.3
	lithon		
F5A(i)	cleavage	5.8	2.0
	lithon	1.3	1.6
F5A(ii)	cleavage	7.3	2.0
	lithon	1.6	1.6
A49	cleavage	1.2	2.6
	lithon	0.62	1.7
F14	cleavage	1.5	2.2
	lithon	6.1	2.9
F5A50	cleavage	0.61	2.4
	lithon	1.3	2.1

Note:

F5A(i) and F5A(ii) are two different cleavage-lithon pairs from the same hand specimen.

Gold and arsenic concentrations are also inconsistent with respect to fold geometry, tentatively suggesting that no unidirectional migration of metals on a scale of hundreds of metres has occurred in response to regional stress gradients in the Ruth Falls structure. This assessment is necessarily qualitative because, in addition to redistribution of metals induced by deformation, other factors probably contribute to metal heterogeneity within the same bed. In particular, some variation is probably inherited from sedimentation.

To assess such variation six samples A50A to A50F (Table 34.1) were taken from a single outcrop representing a 250 cm stratigraphic thickness consisting mainly of a series of amalgamated A unit Bouma sequence greywackes. Rather consistent gold and arsenic results were obtained suggesting that relatively uniform metal contents are inherited from sediment deposition and lithification processes. A basis for recognizing variation in excess of that expected of such processes can be established by comparing the differences in metal content of core-limb pairs with differences between samples in the A50 series. Specifically, the average difference between an individual sample and the A50 series average is calculated for each metal. This average difference is 40 per cent for gold and 27 per cent for arsenic. Differences between core and limb values in excess of 40 and 27 per cent are interpreted as greater variations than those expected from processes of sediment deposition and lithification. On this basis it is suggested that in four cases the differences in gold and arsenic contents of core and limb samples exceed the variation expected from sedimentation also. These pairs are B92-F18, F15-F5A, F14-A45 and A55-A54 for gold and B92-F18, F14-A45, A55-A54 and A50-A49-A47 for arsenic. Presumably the gold and arsenic contents of these samples have been affected by postdepositional processes which may be related to the structural history of the Ruth Falls syncline. Three of the four core-limb pairs which are significantly different in gold content are characterized by high gold in the limb while the fourth pair shows the opposite trend. Two pairs are characterized by higher arsenic in the core and two by higher arsenic in the limb. Therefore, it does not appear that clear and consitent metal trends related to the regional structural fabric are evident in the Ruth Falls syncline, although there is a tendency for a specific bed to carry more gold in the limb then in the axial zone.

Distribution of metals between cleavage planes and lithon A prominent anisotropy developed during deformation of the Ruth Falls rock is cleavage. As shown in Part 1 (Clifford et al., 1983) systematic and consistent compositional differences between cleavages and adjacent lithons characterize Ruth Falls greywackes with lower SiO_2 contents and higher Al_2O_3, Fe_2O_3, K_2O and TiO_2 contents in cleavage domains compared with the adjacent lithon. Gold and arsenic also vary between cleavage and lithon domains. In a given sample the two elements vary sympathetically in that both are always higher in the same domain. Cleavage-lithon pairs differ much more in gold content that in arsenic. On average the difference for gold is a factor of 3.2 compared with 1.3 for arsenic. Thus cleavage represents a major anisotropy with respect to gold in that adjacent layers of rock within 2 to 3 mm of each other may differ in gold content by up to 4.5 times (e.g. sample F5A).

Unlike the very consitent compositional trends found for the major elements, gold and arsenic are not always partitioned between cleavage and lithon domains in the same sense. In four of six cases, all of which are samples from the fold limbs, the cleavage domains are higher in metal than the adjacent lithons. This relationship appears consistent on a hand specimen scale in that two different cleavage-lithon pairs from the same sample, F5A, give nearly identical results for both metals. In the remaining two cases which are samples from the axial zone, gold and arsenic are higher in the lithon. Whether any significance can be attached to the differing sense of metal concentration in limb and axial zone settings is difficult to assess. The dominant trend is the gold-arsenic enrichment in cleavage domains on the fold limb which may result, in part, from pressure solution of quartz.

The essential mineral components of the greywackes are quartz, feldspar, chlorite and mica. One process thought to be involved in cleavage development is pressure solution of quartz. As loss of silica is suggested by the comparative SiO_2 contents of cleavage-lithon paris, such loss must be reflected in a proportionate increase in other minerals in the cleavage domain as reflected in increases in Al_2O_3, K_2O and other components. This process would increase the gold and arsenic contents of the cleavage domain if quartz is significantly lower in gold than chlorite, micas or any accessory minerals not attacked in the pressure solution process. Based on a compilation of literature data Crocket (1974) found an average gold content of quartz and feldspar of 1.7 and 2.0 ppb which is significantly lower than averages for mica of 6.0 ppb and magnetite-ilmenite of 6.7 ppb. If was also noted that accessory minerals, for example sphene, zircon and apatite are extremely variable in gold content and often very high compared to the parent whole-rock. While accessories and minerals of low modal abundance such as the micas or iron oxides are usually minor contributors to the total gold compliment of igneous rocks, their importance as gold contributors to the very quartz-rich Ruth Falls greywackes may be significantly enhanced if these rocks are subject to selective removal of gold-poor quartz. In samples such as F5A 1 or A49 where the gold enhancement of the cleavage domain is approximately twice that of the lithon, an increase in the proportion of phyllosilicate through quartz removal may well be sufficient to account for the observed difference. Where a marked gold increase in the cleavage domain is found, such as the 4.5-fold enrichment in F5A (i, ii), upgrading of the proportion of some accessory

Table 34.3

Gold and arsenic contents of Meguma Group slates, Ecum Secum ares, N.S.

Locality	n[1]	Au, ppb			As, ppm			CO_2, wt.%		
		$\bar{X}$[1]	σ[1]	r[1]	$\bar{X}$	σ	r	$\bar{X}$	σ	r
Barren Island	17	1.87	3.35	0.40-14	2.16	1.16	0.95-5.3	0.15	0.14	0.01-0.50
Crook's Island	14	1.38	0.64	0.65-2.5	1.96	0.36	1.5-2.9	0.07	0.04	0.01-0.14
Goose Island	5	0.96	0.44	0.42-1.5	1.69	1.06	0.75-3.1	0.06	0.04	0.02-0.12
Liscomb Point[2]		2.1			18					0.09
		7.2			6.0					0.07
Aggregate statistics	38	1.72	2.44	0.40-14	2.54	2.80	0.75-5.3	0.11	0.11	0.01-0.50

[1] n-number of samples; $\bar{X}$-arithmetic mean; σ-one standard deviation; r-range
[2] Two samples were analyzed from this locality. Data for each sample are given.

gold concentrator mineral in addition to phyllosilicates may be required. Two tentative generalizations are drawn from these considerations. Cleavage development is often accompanied by the formatin of localized domains enriched in gold in comparison with the immediate host rock. Secondly, the pressure-temperature regime necessary to generate an ore fluid from the indigenous gold in Meguma Group greywackes, presumably must break down or recrystallize the phyllosilicate minerals.

Gold and Arsenic Contents of Meguma Group slates

Slates are the second major lithology of Meguma Group rocks. Background gold and arsenic levels were evaluated by sampling an area in the Ecum Secum-Liscomb Point district with no known mineralization. The sampling was carried out on Barren, Crook's and Goose islands, as well as Liscomb Point (see Fig. 34.1). These localities consist of Goldenville Formation rocks and offer superb exposures of slate units. The stratigraphy includes a few quartz veins, mainly en echelon type, but no auriferous veins have been reported.

The averages reported in Table 34.3 are the simple arithmetic means of all analyses – 1.72 ppb and 2.54 ppm for gold and arsenic respectively. In comparison with the greywacke averages of 1.19 ppb gold and 2.30 ppm arsenic, the shales are higher in gold by a factor of 1.4 and higher in arsenic by a factor of 1.1. As is characteristic of many background gold distributions, however, the simple arithmetic average is strongly biased by a few samples of unusually high gold content, so that the arthmetic mean is greater than the true mean. This situation applies to the Ecum Secum slate data where one sample from Goose Island contains 14 ppb gold. If this sample, which exceeds the arithmetic mean by greater than 2σ is excluded, the remaining 37 samples average 1.39 ppb gold. The arsenic data are also subject to the same consideration in that one sample (Liscomb Point) exceeds the 2σ range. The recalculated arsenic average, excluding the value of 18 ppm is 2.12 ppm arsenic. These constrained averages are regarded as better estimators of the true mean metal content of the slates.

Literature compilations yield rather variable estimates of the average gold content of shale. Crocket (1974) reported an average of 2.5 ppb, and Boyle (1979) an average of 8 ppb gold. Onishi (1969) noted that arsenic is highly variable in shales and recommends an average for shales of 13 ppm arsenic. The most directly comparable data are those of Thorpe and Thomas (1976) who consider 2.0 ppb gold as the best mean for slates from the Oldham drillhole.

Factors commonly cited as important in concentration of metals in shales are adsorption on clay minerals, coprecipitation on diagenetic iron sulphide and reduction by organic matter (Boyle, 1979; Onishi, 1969). Total carbon was determined as a measure of the significance of organic matter. The average carbon content expressed as CO_2 equivalent is 0.11 weight per cent. By comparison with an average for clays and shales of 0.67 per cent C or 2.45 per cent CO_2 (after Ronov, 1958), the Meguma Group slates very low in carbon. Deformation has probably affected the carbon content significantly with some attendant loss; nevertheless, the lack of any significant positive correlation of gold or arsenic with carbon content, and the very low carbon contents, suggest that concentration of metals by organic carbon was probably not a significant factor in controlling the primary gold and arsenic contents of Meguma Group slates.

The sampling area represents approximately 2500 m of stratigraphy with a coverage along strike of about 6000 m. Within this area no significant regional trends in gold or arsenic content are evident. The Barren Island gold average of 1.87 ppb is considerably higher than that of Goose Island, but is strongly biased by one sample with 14 ppb gold. This sample contains 1.1 ppm arsenic and 0.13 weight per cent CO_2, and is therefore not unusual with respect to either of these constituents. If this sample is neglected, the Barren Island gold average is 1.12 ppb which is probably a better estimate of the true mean. The most anomalous locality is Liscomb Point where two high arsenic values and one high gold value were obtained. Unfortunately, the Liscomb Point data base is currently too small to evaluate the signifance of these two samples.

Two comparative aspects of this study and that of Thorpe and Thomas (1976) are worth comment. Similar average gold contents were obtained in both studies – 1.4 in this study compared with 2.0 in Thorpe and Thomas' study. Our samples were obtained from outcrop. Metal loss as a result of weathering is a potential problem. However, the relatively close agreement with the result of Thorpe and Thomas which was obtained on drill core, suggests that no major bias has been introduced by weathering. Secondly, Thorpe and Thomas' data suggest that the slates are significantly higher in gold than greywackes, in that their average gold contents are 2.0 and 0.62 ppb respectively. Our averages are 1.4 and 1.2 ppb gold for slate and greywacke respectively, and it is suggested that these differences are statistically insignificant. This difference may result from real differences in the gold content of the various areas sampled or may be caused by other factors briefly noted in previous discussion. In genetic modelling which envisages a source of gold within Meguma host rocks, the relative potential of greywacke and slate as gold sources is probably essentially independent of the actual background gold levels if our averages are accepted. Factors such as differences in the mineralogical siting of gold in the two lithologies or differences in permeability of the rocks to fluids are probably of greater significance in controlling the relative contribution of metal from greywacke and slate to ore fluids.

Conclusions

The principal findings of the study are that cleavage development in Meguma Group greywacke resulted in redistribution of gold, usually with an increase in gold content in the cleavage domain. A similar trend is found for arsenic. A second finding is that slate and greywacke from unmineralized areas differ little in gold or arsenic contents, and are not unusually high in these metals.

Pressure solution of quartz is probably a very important factor in the redistribution of gold in cleavage domains and may upgrade the average gold content of the rock if remobilized silica is removed.

References

Boyle, R.W.
1966: Origin of the gold and silver in the gold deposits of the Meguma Series, Nova Scotia; Canadian, Mineralogist, v. 8, p. 662.

1979: The geochemistry of gold and its deposits; Geological Survey of Canada, Bulletin 280, 584 p.

Clifford, P.M., Crocket, J.H., and Fueten, F.
1983: Distribution and localization of gold in Meguma Group rocks, Nova Scotia. Part 1: structural effects and pressure solution-preliminary results; in Current Research, Part B, Geological Survey of Canada, Paper 83-1B, Report 33.

Crocket J.H.
1974: Gold; in Handbook of Geochemistry, v. II/5, ed. K.H. Wedepohl; Springer-Verlag, Berlin, chapter 79, sections B-O.

Faribault, E.R.
1899: The gold measures of Nova Scotia and deep mining; Journal of the Mining Society of Canada, v. II, p. 119-128.

Glasson, M.H. and Keays, R.R.
1978: Gold mobilization during cleavage development in sedimentary rocks from the auriferous slate belt of central Victoria, Australia: Some important boundary conditions; Economic Geology, v. 73, p. 496-511.

Graves, M.C. and Zentili, M.
1982: A review of the geology of gold in Nova Scotia; in Geology of Canadian Gold Deposits; Canadian Institute of Mining and Metallurgy, Special Paper 24, p. 233-242.

Keppie, J.D.
1976: Structural model for the saddle reef and associated gold veins in the Meguma Group, Nova Scotia, Nova Scotia Department of Mines, Paper 76-1, 34 p.

Kronborg, O.J. and Steinnes, E.
1975: Simultaneous determination of arsenic and selenium in soil by neutron-activation analysis; Analyst (London), v. 100, p. 835-837.

McBride, D.E.
1978: Geology of the Ecum Secum area, Halifax and Guysborough counties, Nova Scotia; Nova Scotia Department of Mines, Paper 78-1, 12 p.

Onishi, H.
1969: Arsenic; in Handbood of Geochemistry, v. II/3, ed. K.H. Wedepohl; Springer-Verlag, Berlin, chapter 33, sections B-M.

Ronov, A.B.
1958: Organic carbon in sedimetnary rocks (in relation to the presence of petroleum); Geochemistry, v. 5, p. 510-536.

Thorpe, R.I. and Thomas, G.M.
1976: Gold content of greywacke and slate of the Goldenville Formation, Nova Scotia, as determined by neutron activation analysis, in Report of Activities, Part A, Geological Survey of Canada, Paper 76-1A, p. 319-326.

35. AGE AND ORIGIN OF PITCHBLENDE FROM THE GUNNAR DEPOSIT, SASKATCHEWAN

Project 770024

S.S. Gandhi
Economic Geology Division

Gandhi, S.S., Age and origin of pitchblende from the Gunnar deposit, Saskatchewan; in Current Research, Part B, Geological Survey of Canada, Paper 83-1B, p. 291-297, 1983.

Abstract

The host rock of the Gunnar uranium deposit is an Aphebian granite gneiss which is strongly albitized near the ore zone. Albitization, fracturing and brecciation of the albitized rocks and initial uranium deposition from alkaline carbonate-rich solutions occurred most probably during late Aphebian time. The U-Pb isotopic dates on pitchblendes from the Gunnar deposit, however, are close to 1000 Ma, and are interpreted to represent a substantial modification of the older uranium mineralization by supergene processes.

Résumé

La roche encaissante du gisement d'uranium Gunnar est un gneiss granitique aphébien fortement albitisé gisant près de la zone minéralisée. L'albitisation, la formation de fissures et de brèches dans les roches albitisées et l'accumulation initiale d'uranium à partir de solutions alcalines riches en carbonate ont probablement eu lieu vers la fin de l'Aphébien. Toutefois, la datation isotopique à l'U/Pb des pechblendes provenant du gisement Gunnar donne un âge de 1 000 millions d'années, et représenterait une modification importante de la minéralisation en uranium plus ancienne par des processus secondaires.

Introduction

The Gunnar deposit produced 7500 t of uranium metal. The host granite gneiss is part of an Aphebian gneiss complex derived from predominantly sedimentary and subordinate mafic volcanic rocks of the Tazin Group. Similar rocks occur to the north in the District of Mackenzie near the Saskatchewan border. Evaluation of the uranium potential of this area involves consideration of the possibility of discovery of Gunnar-type deposits. The present study was thus undertaken to review the geological features of the deposit that may serve as guides to exploration and evaluation, and have a bearing on the genesis of the deposit.

The deposit was mined by open pit and underground methods (Fig. 35.1). The pit is now flooded, and little detectable uranium mineralization was noted at the property by the writer during a visit in 1981. The U-Pb isotopic systematics were determined for a high grade pitchblende sample provided by C.M. Trigg of Trigg, Woollett Consulting Ltd., and yield a date of 966 Ma from the $^{207}Pb/^{206}Pb$ ratio (Table 35.1). This is essentially in agreement with a date of 989 Ma previously reported by Koeppel (1967). A somewhat younger date of 865 Ma was reported earlier by Robinson (1955). Results of the first two dates (Table 35.1) are plotted on a concordia diagram in Figure 35.2. They lie very close to a line from zero passing between them, within the range of analytical error.

Geology of the Gunnar Deposit

The deposit was discovered in 1952 and produced 5 million tonnes of ore averaging 0.15 per cent U metal during the period 1956 to 1964 (Lang et al., 1962, p. 158; Griffith, 1967, p. 270). The orebody was pipe-like in form with a maximum diameter of 150 m at the surface. It plunged from surface at 45° in a direction 10-15° east of south for more than 425 m (Fig. 35.1). In detail, it was composed of several smaller bodies elongated in the direction of plunge with well-defined foot- and hanging-walls, but with extremely irregular terminations in an east-northeast direction (Staff, Gunnar Mining Limited, 1963). It was located within 310 m of the north shore of Lake Athabasca; it surfaced beneath a swampy area.

The host rock is a coarse- to medium-grained granite gneiss which at the mine was highly brecciated on both megascopic and microscopic scale and altered to an albite-rich calcite-veined, syenite-like rock (Jolliffe and Evoy, 1957; Evoy, 1961). The granitic gneiss is one of a number of two-mica granite bodies mapped as 'Gunnar granite', in the paragneisses of the Tazin Group (Bell, 1961); the granite is believed to be the product of granitization of quartzo-feldspathic sedimentary rocks. The average of 14 modal analyses given by Evoy (1961, p. 25), in volume percentage, is: quartz, 34.3; feldspars, 57.9; calcite, 0.7; chlorite, 3.5; biotite, 1.2; muscovite, 1.2; opaque, 1.0 and other 0.2. Feldspars include microcline, microcline perthite and albite (An_5-An_8), with the ratio of potash feldspar to soda feldspar 2 to 1. The foliation of the granite gneiss and paragneiss, and their contact, trend east-northeast and dip moderately to the south. The orebody was at the north contact of a large granite gneiss body.

A pegmatite sample from the 5th level of the mine gave a K-Ar age of 1815 Ma (Lowdon, 1961, p. 39), and it defines the minimum age of the host granite gneiss. The pegmatite was reported to be post-ore (Lowdon, 1961) but this interpretation has not been substantiated. In the Beaverlodge Lake area, 30 km northeast of the Gunnar mine, pegmatite dykes cutting the Tazin gneisses yielded a Rb-Sr isochron date of 1975 ± 20 Ma (Sassano et al., 1972) and the 'epigenetic' pitchblende veins were formed, according to Koeppel (1967), 1780 ± 20 Ma ago. There is no evidence to suggest that pitchblende in the Gunnar deposit formed earlier than the pitchblende in veins in the Beaverlodge Lake area, hence it is most probable that the pegmatite at the Gunnar mine is pre-ore and was probably close in age to the pegmatite dykes in the Beaverlodge Lake area. The post-ore appearance of the pegmatite probably stems from its unaltered character; conceivably, pegmatites locally may have escaped alteration (L.P. Tremblay, personal communication, 1982).

The rocks of Tazin Group near Beaverlodge Lake (Tremblay, 1972), have been dated by the Rb-Sr method which yielded a minimum age of 2100 Ma (Sassano et al., 1972) and by the zircon U-Pb method. The latter gave a date

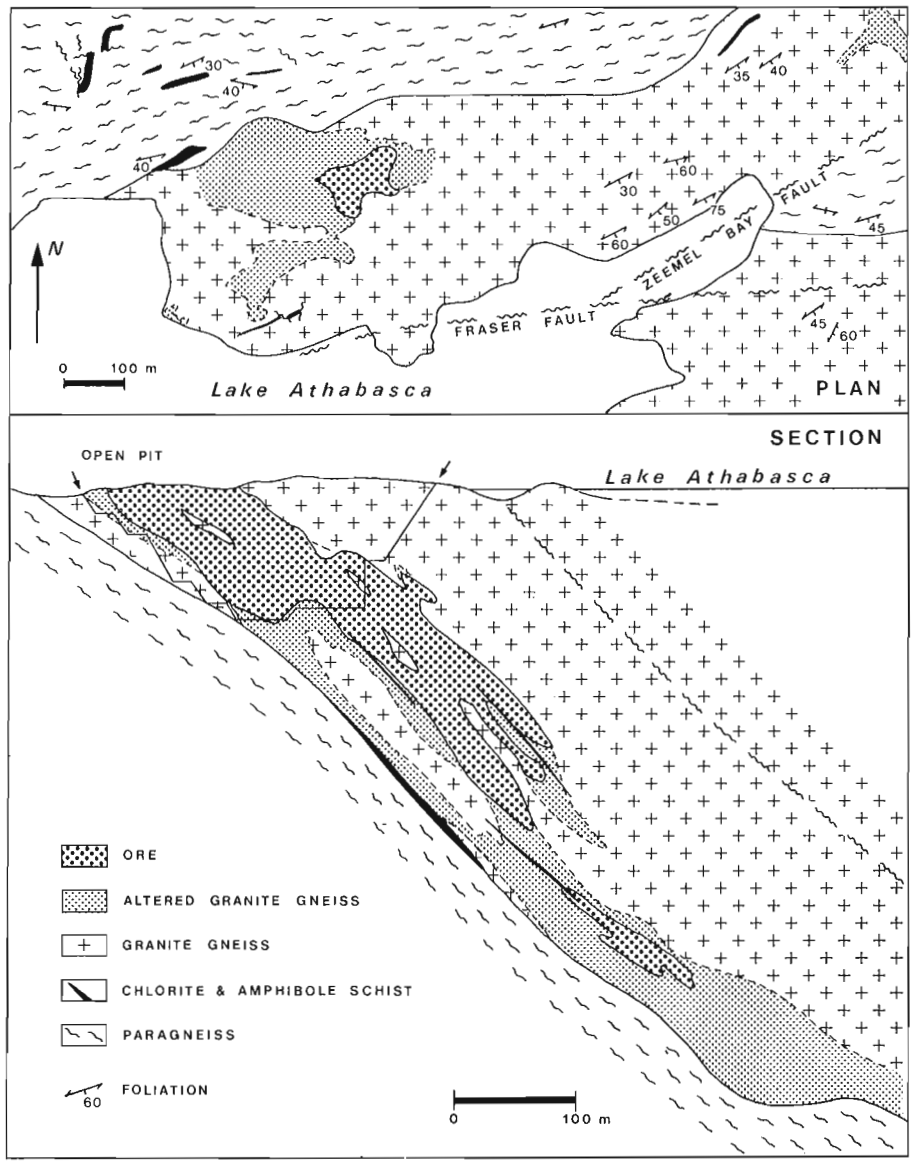

Figure 35.1

Geological plan and longitudal section of the Gunnar uranium deposit, Saskatchewan (from the Staff, Gunnar Mining Limited, 1963, p. 57).

of 2179 ± 12 Ma for a part of the group referred to as Donaldson Lake gneiss and 2513 + 34/-22 Ma for the stratigraphically lower Foot Bay gneiss (Tremblay et al., 1981). The Donaldson Lake gneiss is overlain by the Fay Complex which in turn is followed by the Murmac Bay Formation in the Tazin Group succession (Tremblay, 1972, 1978). The Fay Complex is a mixture of metapelites, quartzites, basaltic metatuffs, quartzo-feldspathic gneisses and granite, and is host to a majority of the pitchblende veins in the district. The Tazin Group rocks in the vicinity of the Gunnar deposit are interpreted by Sassano (1975) as equivalent to the Fay Complex.

The ore at the Gunnar deposit was exclusively in the altered rock referred to as 'syenite'. Jolliffe (1956) from his microscopic studies recognized that the feldspar in the granitic gneiss and syenite adjacent to the mine is predominantly albite, and reported textures showing replacement of quartz by calcite. The alteration of the granite gneiss to syenite and the uranium mineralization were studied by Evoy (1961) and more recently, Hoeve (1982) obtained additional chemical data. Evoy recognized two stages: (i) albitization of granite, involving replacement of microcline and perthite, and then of quartz, leading to albite syenite, and (ii) carbonatization, involving abundant calcite veining of fractured and brecciated albitized rocks, and accompanied by deposition of uranium minerals. Carbonatization may have continued after the ore deposition stage. There are several tabular syenite bodies at the mine, subparallel to the granite gneiss-paragneiss contact and rarely to they transgress this contact. They range in size from small to large, up to 500 m long, measured parallel to strike or dip and up to 130 m thick. They commonly have irregular terminations, although the boundary is sharply defined within a few centimetres (Evoy, 1961). They appear to have been localized along a set of shear planes subparallel to the paragneiss contact and dipping approximately 65° to the south, and less markedly along a set of subvertical north-striking shears. Several major faults occur in the vicinity of the Gunnar deposit, e.g. the Zeemel Bay Fault (Fig. 35.1) and these have been explored at the surface and by diamond drilling, but none of them are ore-bearing (Evoy, 1961; Sassano, 1975). Their age relation to the mineralization at the Gunnar deposit is not known.

The uranium minerals in the ore were pitchblende and uranophane (Robinson, 1955; Evoy, 1961), mostly finely disseminated through syenite and invisible to the naked eye. Pitchblende occurred in two varieties: a massive to botryoidal, black, lustrous variety commonly in microscopic

cavities and filling interstices in breccia, and less commonly as veinlets, and a soft, dull, sooty variety forming heavy coatings on the lustrous variety and films on fracture faces, and also filling vugs. Uranophane and its dimorph beta-uranophane, accounted for less than 10 per cent of uranium, and near the surface formed acicular and prismatic crystals as an encrustration on massive pitchblende and veneers on joint faces, and at depth as disseminated flecks and crystals in porous parts of the ore down to the deepest part of the orebody (Evoy, 1961). The orebody, however, had fairly uniform grade throughout indicating a lack of supergene enrichment or impoverishment (Jolliffe, 1956). This uniformity of grade, however, may be more apparent than real in view of the bulk mining method adopted, and does not necessarily imply uniform distribution of uranium in the deposit. The sample dated for this study (Table 35.1) for example, was very high grade.

The associated gangue minerals were calcite, hematite, quartz, chlorite, orthoclase, kaolin, dolomite, titanates, barite, pyrite, chacopyrite, and galena (Robinson, 1955; Evoy, 1961). The paragenetic sequence is complex and poorly defined due to overlaps in formation of these minerals. Abundant fine hematite dustings imparted a red colouration to the ore. It is noteworthy that calcite was abundant throughout the orebody, along with minor dolomite, and the total carbonate content, from hundreds of assays and acid consumption of mill feed, was about 8 per cent. At places

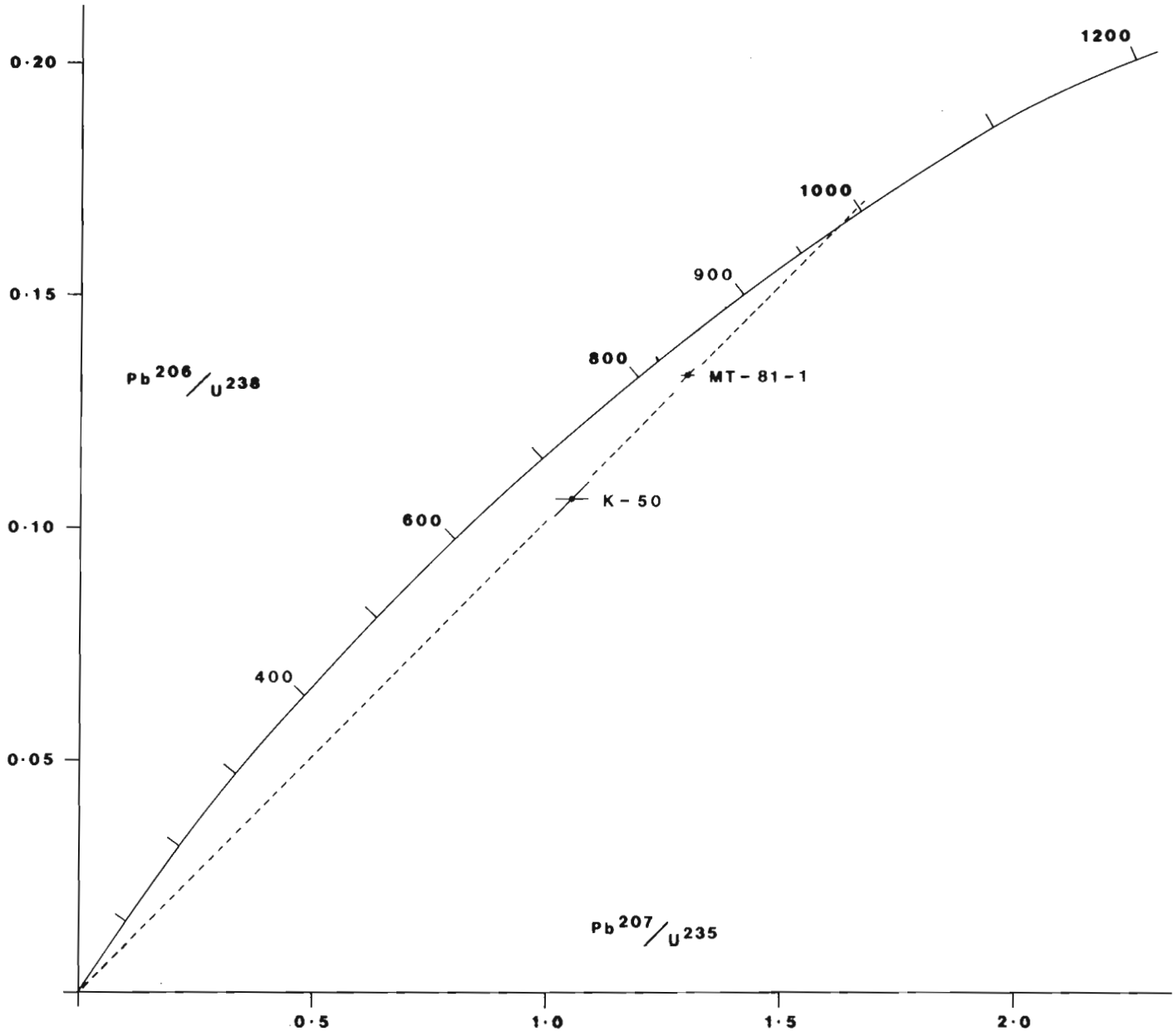

Figure 35.2. *Concordia plot of the Pb/U isotopic ratios of pitchblende samples from the Gunnar uranium deposit, Saskatchewan (Table 35.1).*

Note: Error bars for K-50 from Koeppel, 1967, p. 64 and for MT-81-1 based on measurement precision of U/Pb ratios within 1 per cent at 95 per cent confidence limit.

Table 35.1

Pb-U isotopic analyses on pitchblende samples from the Gunnar uranium deposit, Saskatchewan

Sample Number	Sample Weight mg	U Weight per cent	Pb Weight per cent	Pb Atomic Weight Per Cent Measured				Isotopic Ratio			Age in Million Years		
				^{204}Pb	^{206}Pb	^{207}Pb	^{208}Pb	$^{206}Pb/^{238}U$	$^{207}Pb/^{235}U$	$^{207}Pb/^{206}Pb$	$^{206}Pb/^{238}U$	$^{207}Pb/^{235}U$	$^{207}Pb/^{206}Pb$
MT-81-1[1]	1.100	87.65	10.79	0.0121	92.712	6.782	0.494	0.1325	1.3024	0.07315	802.1	846.8	965.9
K-50[2]	0.4555[3]	91.11	8.89	0.031	91.40	7.03	1.535	0.10604	1.054	0.07211	650	731	989
R-753[4]	-	-	-								730	755	865

NOTES:

([1]) Sample MT-81-1 provided by C.M. Trigg, of Trigg, Woollett Consulting Ltd., Edmonton, and analyzed by Geospec Consultants Limited, Edmonton.
The sample, measuring approximately 3x2x2 cm, contains coarse black vein-like pitchblende aggregates in a pinkish red matrix. A polished thin section cut from it shows several coarse elongate grains of massive pitchblende and calcite, with irregular boundaries and up to 10 mm long and 5 mm wide, set in a matrix of irregular coarse to fine grains of calcite, which predominates, and hematite, quartz, chlorite and clay minerals, and minor pitchblende as grains and along the cleavage of coarse calcite. The coarse pitchblende has sinuous thin veins or syneresis cracks filled with the calcareous and hematitic fine matrix. Red hematitic dusting is most intense near the coarse pitchblende. Parts of the matrix have small aggregates of opaque minerals, mostly hematite, thinly rimmed by clear calcareous material. No feldspar was detected in the section, despite a careful search, including use of energy dispersive spectra at the Geological Survey of Canada, Ottawa. Precise location of the sample is not available, but it represents a very high grade vein-like concentration of pitchblende rather uncommon in the deposit.

([2]) Sample K-50 analyzed and reported by Koeppel (1967, p. 101, Table 6 and photomicrograph Fig. 21). Ratios and ages recalculated, using 1800 Ma lead, by 'concord' program developed by R.I. Thorpe at the Geological Survey of Canada.
The sample is from a 1 m wide lens that cuts across a diabase dyke. Pitchblende is massive to colloform and forms poorly defined, approximately parallel bands several millimetres wide separated by altered wall-rock containing quartz, hematite and nests of pitchblende. Specular hematite also cements pitchblende. In places, the pitchblende is separated from the altered wall-rock by a zone of finely disseminated pitchblende in a gangue matrix. Minor specks of pyrite were observed in pitchblende.

([3]) Total of U and Pb only, viz. excluding impurities; the analyzed material of sample K-50 consisted of massive pitchblende with some hematite.

([4]) Sample R-753 reported by Robinson (1955, Table IX, p. 86), as massive pitchblende with trace sulphides, from a 1.2 m trench.

the calcite was weathered out leaving a pitted, vuggy rock, referred to as 'sponge rock', which was encountered sporadically to a depth of 500 m (Griffith, 1967, p. 272).

The analyses of three massive pitchblende samples show that the last time of isotopic homogenization was at a little less than 1000 Ma ago (Table 35.1; Fig. 35.2).

Discussion

Evoy (1961) concluded that uranium was transported in carbonate-rich alkaline hydrothermal solutions and was precipitated by a drop in pressure and temporary change to an acid environment. A similar process of hydrothermal deposition of uranium is also postulated for the vein-type uranium deposits in Hercynian granites in France (Cuney, 1978; Leroy, 1978) and in Nova Scotia (Chatterjee et al., 1981). In these areas, alteration of the host granite, including albitization, and fracturing, preceded uranium deposition as in the case of the Gunnar deposit. Evoy (1961) suggested that fracturing and brecciation at the Gunnar deposit was localized in the massive albitized rocks due to their greater competency relative to the foliated unaltered granite. All these events may represent a single protracted period of mineralization as visualized by the Staff, Gunnar Mining Limited (1963), but a significant time interval between albitization and uranium deposition cannot be ruled out.

The formation of the Gunnar deposit and the ages of pitchblende from it may be considered in the context of other uranium deposits in northern Saskatchewan. These deposits can broadly be grouped into the older Beaverlodge-type and the younger unconformity-type, primarily on the basis of isotopic dates on the contained pitchblende and supported by their regional geological setting and other features, following Tremblay (1978), but without implying a genetic distinction. Some features such as structural control and aspects of mineralogy are common to both groups. The Beaverlodge-type vein deposits were formed, according to Koeppel (1967), 1780 ± 20 Ma ago, and underwent episodic loss of radiogenic lead at 1100 ± 50 Ma and from 230 to 0 Ma. The unconformity-type deposits occur at the base of the virtually undeformed, predominantly continental clastic sedimentary rocks of the Helikian Athabasca Group, which unconformably overlie the crystalline basement that was affected by the Hudsonian orogeny (Tremblay, 1982). They are commonly very long, narrow and carrot-shaped in cross-section. Some of the deposits extend into the Athabasca Group. Rocks of the Athabasca Group were deposited approximately 1500 Ma ago (Ramaekers, 1981; Tremblay, 1982). The isotopic ages of pitchblende from the deposits are in the range of 1050 to 1350 Ma as sumamrized by Tremblay (1982, p. 11).

The Gunnar deposit resembles the major vein deposits of the Beaverlodge-type (Robinson, 1955; Dawson, 1956; Tremblay, 1972, 1978) in terms of the age of the host-rocks, mineralogy and wall-rock alteration, including albitization and hematization. There is however, apparently more extensive albitization of the host-rock and greater abundance of carbonate at the Gunnar deposit. The sequence of distinct events observed at the Gunnar deposit, viz. albitization, fracturing and brecciation, and carbonatization and uranium deposition, is not apparent in the case of the Beaverlodge-type deposits. In any case, albitization is a common feature, although it is variable in extent and intensity due in part to the variations in wall-rock lithology. It is probable that albitization occurred more or less contemporaneously at the Gunnar and the Beaverlodge deposits. It was accompanied by, or followed closely in time by, uranium deposition at 1780 ± 20 Ma in the case of the Beaverlodge-type deposits, and it is reasonable to suggest that a similar situation prevailed at the Gunnar deposit and the initial uranium deposition occurred there at about the same time. The pitchblende ages close to 1000 Ma then may be interpreted as indicating either a substantial reconstitution of the deposit, possibly involving addition of uranium from an outside source, or merely a major loss of radiogenic lead from the pitchblende. As mentioned earlier, Koeppel (1967) has interpreted loss of radiogenic lead from the Beaverlodge deposits to have occurred at 1100 ± 50 Ma and from 230 to 0 Ma. However a substantial reconstitution of the Gunnar deposit at or close to the time of formation of major uranium deposits of unconformity-type, cannot be ruled out. It is apparent that the Athabasca Group most probably covered the Gunnar deposit at one time. This leads to a further possibility that the Gunnar deposit is of unconformity-type.

Various hydrothermal and supergene hypotheses of mineralization that have been invoked for the Beaverlodge-type and unconformity-type deposits were outlined by Langford (1978) and Tremblay (1978, 1982). Regarding the hypotheses of hydrothermal origin, it may be noted that the source of mineralizing solutions is obscure or conjectural. A direct link to a discrete pluton was not established. The host granite at the Gunnar deposit is a product of in situ granitization of the Tazin Group metasedimentary rocks. Judging from the isotopic dates on pegmatite dykes and pitchblende veins in the Beaverlodge Lake area, as mentioned earlier, it is more than 200 Ma older than the initial mineralizing event. It is thus an unlikely source of the mineralizing solutions. Hence it is necessary to postulate that the hydrothermal solutions were generated at depth, either by anatexis or by crystallization of an unexposed granitic pluton, or during retrograde metamorphism after granitization. Generation of metamorphic-hydrothermal solutions, as proposed by Tremblay (1970), appears unlikely during a retrograde metamorphic stage when water is likely absorbed rather than released by the rocks (F.F. Langford, personal communication, 1983). In the case of the postulated unexposed pluton, the solutions generated may be magmatic or heated meteoric waters or a mixture of the two. The presence of pegmatites in the vicinity of the Gunnar deposit suggests that such a pluton may be close. Anatexis was favoured by Hoeve (1982) from his study of comparable uranium deposits in southeastern Sweden. In any case, the hydrothermal activity probably represents the final stages of Aphebian orogeny. This is in agreement with the hypothesis presented by Beck (1970) who regarded the uranium deposits of the Beaverlodge area, including the Gunnar deposit, as mesothermal, formed during the final states of the Hudsonian orogeny from 1950 to 1750 Ma. They were formed after the crystallization of syngenetic uraninite in pegmatite, a phenomenon regarded as transitional to the mesothermal uranium deposition. Albitization and uranium mineralization may have been brought about by the same hydrothermal solution as suggested by Hoeve (1982) or by separate phases of an evolving hydrothermal solution.

Most of the vein deposits of the Beaverlodge-type are in Tazin gneisses, but some cut the younger Martin Formation. The latter is an unmetamorphosed continental calstic sequence unconformably overlying the Tazin gneisses (Lang et al., 1962; Tremblay, 1972). The age of the Martin Formation, indicated by K-Ar dates on one of the intercalated tholeiitic basalt flows and a gabbro dyke, is between 1830 and 1630 Ma (Fraser et al., 1970; Tremblay, 1972), and on the basis of the pitchblende dates by Koeppel (1967) it is greater than 1780 ± 20 Ma. Many of the Beaverlodge-type deposits are located close to the Tazin-Martin unconformity. The Martin Formation may have extended over the Gunnar deposit area at one time. These and other considerations, led Langford (1977, 1978) to propose that initial concentration of uranium in these deposits and in the younger unconformity-type deposits, occurred by supergene processes at the sub-Martin Formation and sub-Athabasca Group unconformities. In the case of the

Gunnar deposit, Robinson (1955) had earlier proposed that it is at least in part supergene on the basis of the presence of uranophane and sooty pitchblende, which he considered as secondary minerals, and uranium enriched artesian waters from diamond-drill holes. This, however, was countered by Jolliffe (1956) who pointed out a lack of supergene enrichment near the surface and a remarkable uniformity of grade considering the size of the ore body. He regarded uranophane to have formed in situ by alteration of primary pitchblende, without a marked migration of uranium, and to be attributable to the scarcity of sulphides and an abundance of calcite, the two factors which inhibited the development of an acidic environment. Evoy (1961) also rejected a supergene enrichment, citing in addition a lack of any textural evidence of uranophane replacing pitchblende. He also noted corrosion of well-formed prismatic crystals of uranophane by calcite. Regardless of the debated secondary enrichment of the deposit, the formation of secondary uranophane at a later date from the older pitchblende is compatible with the formation of pitchblende by surficial processes as postulated in the supergene model. Because of their near-surface position, deposits so formed are likely to undergo further modifications by meteoric waters.

The main features of the Gunnar deposit as discussed above can be best explained, in the writer's opinion, by a multi-stage genetic model as follows. Initial uranium mineralization by carbonate-rich low-temperature hydrothermal solutions occurred at about 1780 Ma, at the time of initial formation of pitchblende veins in the Beaverlodge district. Uranium deposition was preceded by albitization of the host granite at higher temperature, and a structural event that caused fracturing and brecciation of the albitized rocks. Subsequent modification of the primary deposit occurred a little less than 1000 Ma ago. This may have involved either a substantial reconstitution of the deposit, possibly involving addition of uranium from an outside source, or merely a major loss of radiogenic lead from the pitchblende. Open structures common in the deposit permitted circulation of meteoric waters which were instrumental in the modification, and have remained open since to permit the formation of uranophane, sooty pitchblende and younger calcite. This is undoubtedly a simplistic view of the history of the deposit, because the posibility exists for other modifications, particularly at the times of deposition of the Martin Formation and of the Athabasca Group, which may have covered the deposit at one time, and of the remobilization and lead-loss events that also affected the other deposits in northern Saskatchewan.

Further research is needed to answer a number of problems related to the origin and geological history of this very interesting but inadequately studied deposit, particularly in view of its potential usefulness as a model on which to base exploration of abundant granites of the Gunnar type elsewhere in the Canadian Shield.

Acknowledgments

C.M. Trigg of Trigg, Woollett Consulting Ltd., Edmonton, kindly provided a suitable sample for age determination; he also read the manuscript. Much encouragement in the present study was received from F.F. Langford of the University of Saskatchewan, Saskatoon, and D. Thomas, Resident Geologist at Uranium City, Saskatchewan Geological Survey, and both of them also gave valuable guidance for the writer's visit to the Gunnar mine site in 1981. The writer benefitted greatly from discussions with L.P. Tremblay and R.I. Thorpe of the Geological Survey of Canada, Ottawa, and personal communication with J. Hoeve of the Saskatchewan Research Council, Saskatoon, and D.E. Jiricka of the Saskatchewan Mining Development Corporation, Saskatoon. The opinions expressed here, however, are the writer's own.

Luc Plante provided field assistance during 1981. The paper was read critically by S.M. Roscoe and R.I. Thorpe of the Geological Survey of Canada.

References

Beck, L.S.
1970: Genesis of uranium in the Athabasca region and its significance in exploration; Canadian Institute of Mining and Metallurgy Bulletin, v. 63, p. 367-377.

Bell, C.K.
1961: Millikan Lake, Sheet 2, Saskatchewan; Geological Survey of Canada, Map 33-161, scale 1:9,600.

Chatterjee, A.K., Robertson, J., and Pollock, D.
1981: A summary on the petrometallogenesis of the uranium mineralization at Millet Brook, South Mountain Batholith, Nova Scotia; Geological Association of Canada, Field Trip: Appalachian Minerals, Fredericton: October 1981.

Cuney, M.
1978: Geologic environment, mineralogy, and fluid inclusions of the Bois Noirs-Limouzat uranium vein, Forez, France; Economic Geology, v. 73, no. 8, p. 1567-1610.

Dawson, K.R.
1956: Petrology and red colouration of wall-rocks, radioactive deposits, Goldfields region, Saskatchewan; Geological Survey of Canada, Bulletin 33, 46 p.

Evoy, E.F.
1961: Geology of the Gunnar uranium deposit, Beaverlodge area, Saskatchewan; unpublished Ph.D. thesis, University of Wisconsin, Madison, Wisconsin, 80 p.

Fraser, J.A., Donaldson, J.A., Fahrig, W.F., and Tremblay, L.P.
1970: Helikian basins and geosynclines of the Northwestern Canadian Shield; in Symposium on Basins and Geosynclines of the Canadian Shield; Geological Survey of Canad,a Paper 70-60, p. 213-238.

Griffith, J.W.
1967: The Uranium Industry – Its History, Technology and Prospects; Minerals Resources Division, Department of Energy, Mines and Resources, Ottawa, Mineral Report 12, 335 p.

Hoeve, J.
1982: Perspective on uranium mineralization at Beaverlodge; Saskatchewan Research Council Publication no. G-745-1-E-82, 23 p.

Jolliffe, A.W.
1956: The Gunnar 'A' orebody; Transactions of the Canadian Institute of Mining & Metallurgy, v. 59, p. 181-185.

Jolliffe, A.W. and Evoy, E.F.
1957: Gunnar mine; in Structural Geology of Canadian ore deposits, Volume II, Canadian Institute of Mining & Metallurgy, p. 240-246.

Koeppel, V.
1967: Age and history of uranium mineralization of the Beaverlodge area, Saskatchewan; Geological Survey of Canada, Paper 67-31, 111 p.

Lang, A.H., Griffith, J.W., and Steacy, H.R.
1962: Canadian deposits of uranium and thorium, Geological Survey of Canada, Economic Geology Report 16, 324 p.

Langford, F.F.
1977: Surficial origin of North American pitchblende and related uranium deposits, American Association of Petroleum Geologists, Bulletin, v. 61, no.1, p. 28-42.

1978: Origin of Unconformity-type Pitchblende deposits in the Athabasca Basin of Saskatchewan; in Uranium Deposits: their Mineralogy and Origin, ed. M.M. Kimberly, Short Course, Minterlogical Association of Canada, University of Toronto, p. 485-499.

Leroy, J.
1978: The Margnac and Fanay uranium deposits of the La Crouzille district (western Massif Central, France): geologic and fluid inclusion studies; Economic Geology, v. 73, no. 8, p. 1611-1634.

Lowdon, J.A. (compiler)
1961: Age determinations by the Geological Survey of Canada, Report 2: Isotopic ages; Paper 61-27, 127 p.

Ramaekers, P.
1981: Hudsonian ad Helikian basins of the Athabasca region, northern Saskatchewan; in Proterozoic Basins of Canada, ed. F.H.A. Campbell, Geological Survey of Canada, Paper 81-10, p. 219-233.

Robinson, S.C.
1955: Mineralogy of uranium deposits, Goldfields, Saskatchewan; Geological Survey of Canada, Bulletin 31, 128 p.

Sassano, G.P.
1975: Reinterpretation of Gunnar geology provides new clues for uranium search; Canadian Mining Journal, v. 96, no. 3, p. 47-57.

Sassano, G.P., Baadsgaard, H., and Morton, R.D.
1972: Rb-Sr isotopic systematics of the Foot Bay gneiss, Donaldson Lake gneiss, and pegmatite dikes from the Fay Mine, NW Saskatchewan; Canadian Journal of Earth Sciences, v. 9, no. 11, p. 1368-1381.

Staff, Gunnar Mining Limited
1963: The Gunnar story; Canadian Mining Journal, v. 84, no. 7, p. 47-119.

Tremblay, L.P.
1972: Geology of the Beaverlodge mining area, Saskatchewan; Geological Survey of Canada; Memoir 367, 265 p.

1978: Geologic setting of the Beaverlodge-type of vein-uranium deposit and its comparison to that of the unconformity-type; in Uranium Deposits: their Mineralogy and Origin, ed. M.M. Kimberley; Short Course, Mineralogical Association of Canada, University of Toronto, p. 431-456.

1982: Geology of the uranium deposits related to the sub-Athabasca unconformity, Saskatchewan; Geological Survey of Canada, Paper 81-20, 56 p.

Tremblay, L.P., Loveridge, W.D., and Sullivan, R.W.
1981: U-Pb ages of zircon from the Foot Bay gneiss and the Donaldson Lake gneiss, Beaverlodge area, northern Saskatchewan; in Rb-Sr and U-Pb Isotopic Age studies, Report 4, in Current Research, Part C, Geological Survey of Canada, Paper 81-1C, p. 123-126.

36.

PARTICLE-SIZE DISTRIBUTIONS OF THE SURFACE OF ALLUVIAL CHANNEL BEDS

Project 750077

T.J. Day[1] and P. Egginton
Terrain Sciences Division

Day, T.J. and Egginton, P., Particle-size distributions of the surface of alluvial channel beds; in Current Research, Part B, Geological Survey of Canada, Paper 83-1B, p. 299-302, 1983.

Abstract

Flume experiments show that the size distribution of particles on the surface of a channel bed formed after the general transport of all grain sizes is essentially the same as that of the underlying bed material. This is contrary to some recently published works. On the basis of our work, where a coarser surface exists in natural channels, it results from non-equilibrium transport.

Résumé

Des expériences menées au moyen de chambres d'eau montrent que la granulométrie des particules à la surface d'un lit de chenal formé après le transport général des grains de toutes dimensions est essentiellement la même que celle du matériel sous-jacent. Ces résultats contredisent certains rapports récemment publiés. À la suite de leurs travaux, les auteurs sont en mesure d'avancer que lorsque les chenaux naturels présentent une surface plus grossière, cette dernière résulte d'un transport non équilibré.

Introduction

In several recent articles attention has been drawn to the grain-size characteristics and inferred processes associated with mobile bed deposits (Parker, 1980; Parker et al., 1982; Parker and Klingeman, 1982). According to their work the median grain size of the pavement (surface layer to the depth of the largest particle) formed under equilibrium conditions is 1.6 to 2.4 times coarser than the subpavement (underlying bed material).

The terms armour and pavement both are used to describe only the surface (one grain thick) of a gravel river. In essence the terms are used to describe two distinct surface conditions where (1) the surface is substantially coarser than the underlying bed material such that it is rarely if ever transported and (2) the surface and subsurface material are essentially the same and both materials are commonly transported. In the literature the terms armour and pavement are used interchangeably. Bray and Church (1980), in an attempt to clarify usage, suggested that pavement be used to describe condition 1 and armour be used to describe condition 2 (as given above); however, Parker (1980), Parker et al. (1982), and Parker and Klingeman (1982) used the term pavement to describe condition 2 but applied it to a layer of sediment as thick as the largest particle.

According to Parker and Klingeman (1982, p. 1409), this pavement "is in place during typical transport events capable of moving all available sizes... and... this pavement acts as a regulator that enables a stream to transport the coarse half and the fine half of its bedload supply at equal rates". If correct, this interpretation has significant implications.

In reviewing these papers we noted a problem in the compatability of the sampling procedures used. In describing the procedure used to sample the surface layer, Parker et al. (1982, p. 1400) stated that "pressure was applied to a clay-coated plate so as to cause the clay to impregnate the pores down to a level roughly corresponding to the bottom of one of the largest grains exposed on the pavement. All grains between the plate and this level were removed and defined to be pavement". Since Parker (1980) used this same procedure, it can be assumed that penetration also occurred.

As described by Parker et al. (1982) their procedure should produce a sample that is volumetric. The important issue, however, is that in the case where the surface size distribution is coarser than the underlying sediment, Parker's surface layer sample would contain two separate populations of particles. Parker's samples were compared directly with bulk, sieve-by-weight samples of the bed material and found to be different. The surface layers were all coarser than the bed material. Our disagreement with Parker's interpretation of these results is that we feel his surface layer sample (volumetric) is essentially a surface sample (areal), and cannot be directly compared to the bed material (Kellerhals and Bray, 1971).

From our own experience in using adhesive sampling methods (wax and grease), we have noted penetration below the first layer (one grain thick) of particles. We feel that uniform penetration to the depth of the largest particle was most unlikely, as the consistency of wet clay at room temperature would inhibit penetration. We would expect that only the surface was sampled by Parker. By sieving the particles, Parker should end up with an area-by-weight sample whose size distribution is not directly comparable to that of the bed material.

To test this supposition, the surface layer samples of Parker (1980) and Dhamotharn et al. (1980), on which Parker et al. (1982) is based, were treated as area-by-weight samples (of the surface only) and were converted to be equivalent to the sieve-by-weight samples of the bed materials. As defined by Kellerhals and Bray (1971), this conversion requires an adjustment of the weight of each size fraction made by its division by the geometric mean size of the size fraction.

The data pertinent to Run 2 (Parker, 1980) are shown in Figure 36.1. The grain-size distribution of the pavement before and after conversion is shown. When the conversion is performed there is little difference between his surface "layer" (pavement) and the underlying bed material and the bed load. Similar results can be shown for the remaining pavement-bed material plots in Parker (1980) and in Dhamotharn et al. (1980) on which Parker et al. (1982) is based.

[1] Water Resources Branch, Environment Canada, Ottawa, Ontario, K1A 0E7

Parker and Klingeman (1982) have attempted to explain differences between surface layer and bed material size distributions by the loss of fine particles from the surface layer to the underlying bed material. Even by removing all sizes below the median grain size, however, an areal sampling bias can be identified in the particle sizes coarser than D_{50}.

Parker's (1980) Run 2 data are replotted in Figure 36.1 showing only those sizes above 2 mm. Again the area-by-weight conversion to sieve-by-weight results in a surface layer size distribution similar to that of the original truncated bed material. If only the fines were being selectively lost from the surface layer, then the coarser size fraction would not be altered. We interpret this observation again to mean that the coarseness of Parker's surface layer is due to sampling procedures rather than any hiding or burrowing process of the fines.

We had hoped to resolve this issue of the surface layer by more experimentation and sampling. The results presented here refer to comparisons of surface and bed material size distributions for particles greater than the D_{50} of the bed material. The inference in Parker and Klingeman (1982) is that these size fractions are unaltered by the loss of fines. As pointed out in the preceding paragraph, however, their surface layers do show differences for these sizes. Even though we believe these differences are due to sampling problems, we also feel that their use of an adhesive sampling medium could have produced a biased sample. Our experiments were directed to clarify this issue of the coarser size fractions.

Experimental Design

Under natural conditions sediment supply and discharge rarely, if ever, stop simultaneously. Natural channels, because of possible modification of the surface after equilibrium transport, cannot be used to support the concept of pavement formation during equilibrium transport. The concept can only be tested in a flume.

Our experiments were designed with the objective of creating equilibrium transport conditions such that all grain sizes on the bed are capable of motion. The experiments were simply to determine the relationship between the surface and the underlying bed material. The laboratory experiments reported by Parker et al. (1982) were of two types: (1) sediment feed and (2) sediment recirculating. Our experiments were run using a sediment feed and the flume at the Geological Survey of Canada which is described in detail by McDonald (1972).

Sampling Procedures

A grid-by-number procedure is the most suitable for sampling the surface as it is equivalent to the sieve-by-weight procedure (Kellerhals and Bray, 1971), and only surface particles are sampled.

Sediment Characteristics

A graded sediment ($\sqrt{D_{84}/D_{16}} = 3.3$) with a D_{50} of 2.2 mm was used (Fig. 36.2); the distribution of size fractions greater than 2 mm is also shown. This portion of the bed material is the most important for our experiments as 2 mm was determined to be the practical lower limit for the collection of surface particles for grid-by-number analysis.

Experimental Procedures

Before each run the initial bed sediment layer was remixed thoroughly and was levelled with a template. For all runs the flume slope was fixed at 0.0044, and the discharge set at 48 L/s. Once the discharge stabilized, sediment feed commenced. The continuity of the sediment feed was evaluated by periodic samplings of the sediment at its outlet.

Bed and water surface profiles were taken along the centreline of the flume at 50 cm intervals over a length of 6 m. Bed load samples were collected by positioning a collector at the end of the flume for periods of 5 to 20 minutes, depending upon the transport rate. The experiments continued until bed and water surface profiles

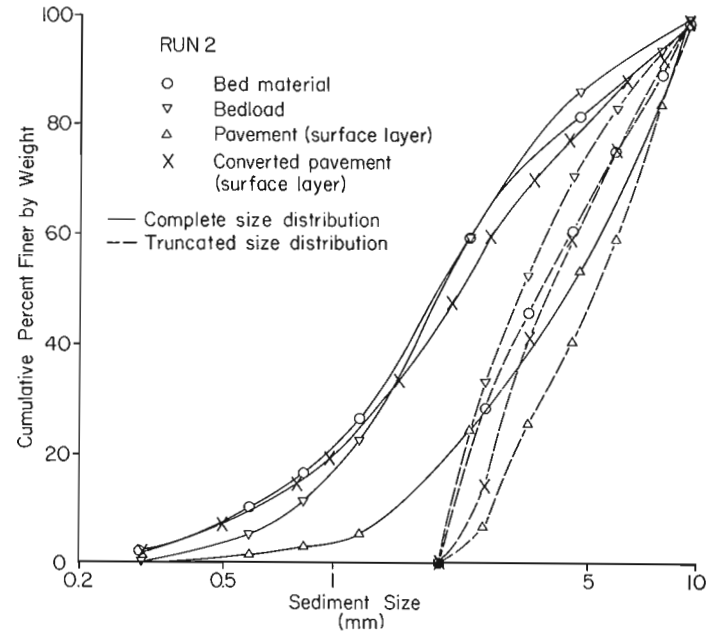

Figure 36.1. *Data pertinent to Run 2 in Parker (1980). The grain-size distribution of the pavement (before conversion) is significantly coarser than the bed material and bed load; however, after proper conversion to allow for differences in sampling technique there is little difference between the grain-size curves.*

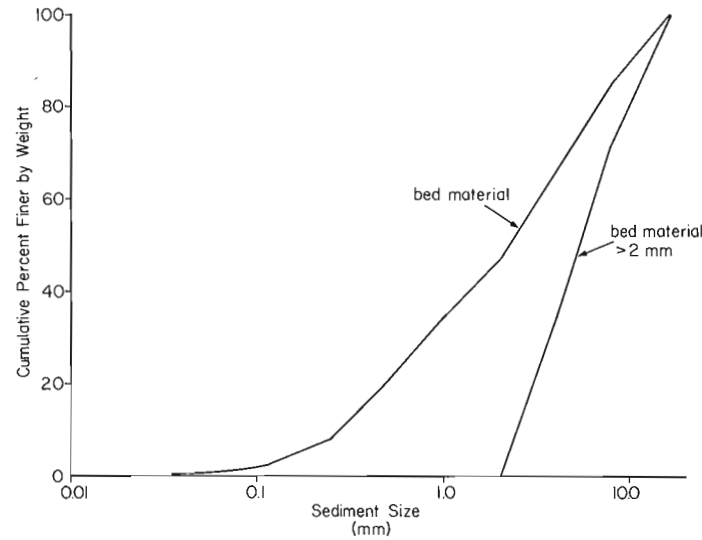

Figure 36.2. *Grain-size distributions of sediment used in this study. Both the total sediment distribution and the distribution of the sediment greater than 2 mm are shown.*

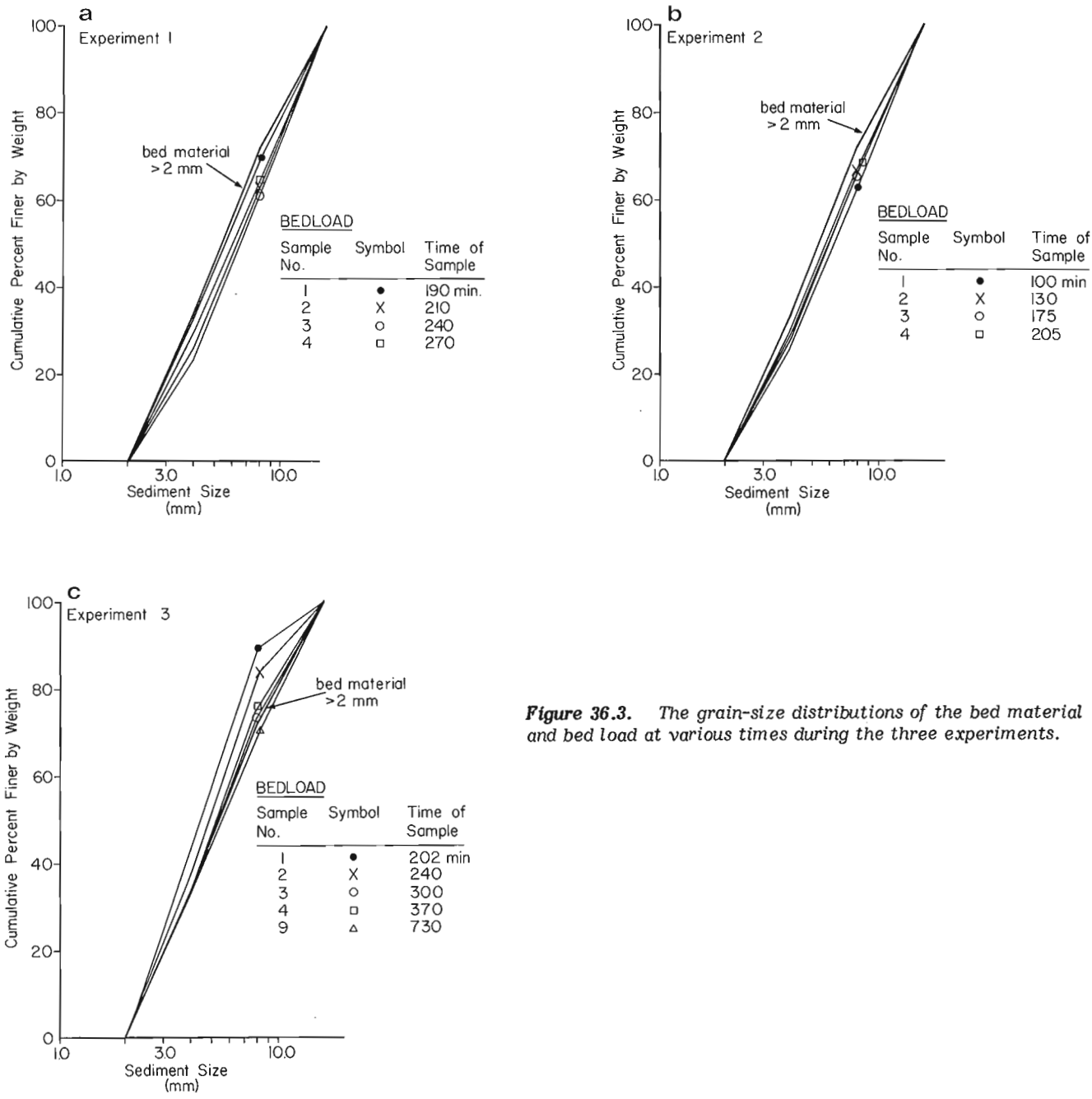

Figure 36.3. *The grain-size distributions of the bed material and bed load at various times during the three experiments.*

Table 36.1

Data summary of experiments

Experiment No.	Discharge (L/s)	Sediment Feed Mean (g/s)	Sediment Feed Coefficient of Variation	Experiment Duration (min)	Final Water Surface Slope
1	48	70.5	15.5%	270	0.00347
2	48	131.9	3.9%	205	0.00597
3	48	20.0	10.6%	730	0.00282

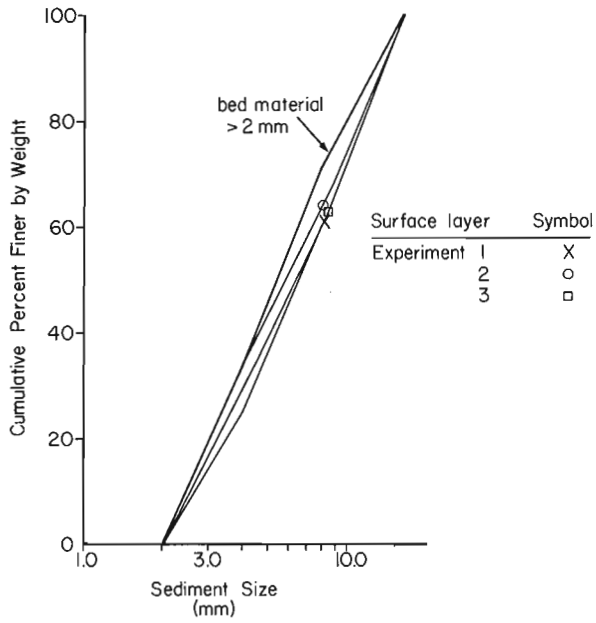

Figure 36.4. *The grain-size distributions of the surface (pavement) and bed material for three experiments. Note that the bed material is the same in all experiments.*

stabilized at which time equilibrium conditions were assumed to have been reached. This was later verified by comparing the grain-size characteristics of the sediment input and bed load samples (output).

Surface sampling of the dried flume bed was limited to a 3 m section in the middle of the 6 m transport reach. A grid 10 by 10 cm was established and the particles lying under each grid intersection were removed; between 85 and 95 particles were collected. These particles were then sieved to establish axis dimensions, and then the individual particles in each fraction were counted.

Results and Discussion

Three experiments were run with different sediment feed rates. Table 36.1 shows a summary of data from the experiments. In each experiment equilibrium transport, as defined by stability of the water surface slope, was obtained.

The grain size distributions of the bed material and bed load at various times during the three experiments are presented in Figure 36.3a, b, c.

The size distributions of the three pavement surfaces and of the bed material are presented in Figure 36.4. Clearly little difference exists between the surface and bed material. In experiment 1 the pavement is slightly coarser than the bed material (ratio of bed material D_{50} to pavement D_{50} is 1.20), and both have the same grain size distribution as the bed load. In experiment 2 the D_{50} ratio is only 1.07, and again the grain-size distributions of the pavement, bed load, and bed material are similar. In experiment 3 the pavement is slightly coarser than both the bed material (D_{50} ratio of 1.18) and the final bed load sample (Fig. 36.3, 36.4).

Although there are consistent differences between the coarser sizes in the two distributions, they are much smaller than those found in Parker's truncated distributions. These results indicate that the coarser size fractions are not altered during equilibrium transport. This much is in agreement with Parker and Klingeman (1982).

We submit, however, that it has been proven here that the differences in the coarse size fractions of Parker's truncated distributions are due to the non-equivalence of his sampling procedures. Therefore, it is argued that what is true for the coarse half of the size distribution must be true for the complete distribution, i.e. Parker's surface layer samples are truly areal samples. As has been shown in Figure 36.1, the sieve-by-weight equivalent of Parker's surface layer (all sizes) is essentially the same as the bed material.

We conclude that a distinct surface layer as described by Parker and Klingeman (1982), which acts as a regulating mechanism to prevent preferential transport of the smaller size fractions, does not exist. The regulating mechanism must be found elsewhere. Finally, where coarser bed surfaces (coarser by the magnitudes described by Parker and Klingeman, 1982) are found in natural channels, they result from non-equilibrium transport, for example as studied by Proffitt and Sutherland (1980).

Acknowledgment

We thank M. Church for his comments on an earlier version of this paper.

References

Bray, D.I. and Church, M.
1980: Armored versus paved gravel beds; American Society of Civil Engineering, Journal of the Hydraulics Divisions, v. 106, no. HY11, p. 1937-1940.

Dhamotharn, S., Wood, A., Parker, G., and Stefan, H.
1980: Bedload transport in a model gravel stream; St. Anthony Falls Hydraulic Laboratory, University of Minnesota, Minneapolis, Project Report No. 190.

Kellerhals, R. and Bray, D.I.
1971: Sampling procedures for coarse fluvial sediments; American Society of Civil Engineering, Journal of the Hydraulics Division, v. 97, no. HY8, p. 1165-1180.

McDonald, B.C.
1972: The Geological Survey of Canada sedimentation flume; Geological Survey of Canada, Paper 71-46, 12 p.

Parker, G.
1980: Experiments on the formation of mobile pavement and static armor; Department of Civil Engineering, University of Alberta, Technical Report, 57 p.

Parker, G. and Klingeman, P.C.
1982: On why gravel bed streams are paved; Water Resources Research, v. 18, no. 5, p. 1409-1423.

Parker, G., Dhamotharan, S., and Stefan, H.
1982: Model experiments on mobile, paved gravel bed streams; Water Resources Research, v. 18, no. 5, p. 1395-1408.

Proffitt, G.T. and Sutherland, A.J.
1980: Self armouring of non-uniform alluvial sediments; Proceedings 7th Australasian Hydraulics and Fluid Mechanics Conference (Brisbane), p. 225-228.

37.

URANIUM AND BASE METAL CONCENTRATIONS IN TILL SAMPLES FROM NORTHERN MANITOBA

Project 800024

L.A. Dredge
Terrain Sciences Division

Dredge, L.A., Uranium and base metal concentrations in till samples from northern Manitoba; in Current Research, Part B, Geological Survey of Canada, Paper 83-1B, p. 303-307, 1983.

Abstract

Histograms and a summary map show regional background, mean, and anomalous concentrations of uranium and ten base metals in the Late Wisconsin till sheet of northern Manitoba. Isolated anomalies occur in tills overlying all rock types, but clusters of associated elemental anomalies are found in granodiorites at Caribou River, gneisses at Snyder Lake and Ballantyne Lake, and volcanics at Great Island. Anomalies in sandy till (northern provenance) indicate nearby bedrock characteristics; those in silty till (eastern provenance) apparently are unrelated to the underlying bedrock.

Résumé

Des histogrammes et une carte sommaire montrent les concentrations en uranium et en dix métaux communs dans une nappe de till du Wisconsinien supérieur du Nord du Manitoba. Le bruit de fond régional, la moyenne et les anomalies sont indiqués. Des anomalies éparses se retrouvent sur tous les types lithologiques; cependant, des groupements d'anomalies d'éléments associés se manifestent sur des granodiorites à la rivière Caribou, sur des gneiss aux lacs Snyder et Ballantyne et sur des roches volcaniques à l'île Great. Les anomalies du till sablonneux, d'origine nordique, réflètent les caractéristiques de la roche en place environnante. Par ailleurs, les anomalies dans le till silteux, provenant de l'est, n'ont aucun lien apparent avec la roche en place sous-jacente.

Introduction

This report presents the results of base metal and uranium analyses of till samples from northern Manitoba. About 400 samples were collected over an area of 125 000 km^2. Because these samples were collected during the course of surficial geological mapping (Dredge and Nixon, 1981; Dredge et al., 1982), and not solely for geochemical prospecting, the sampling density is much too low for detailed geochemical interpretation of the data. The results do, however, show the range of background values characteristic for the region, point out variations related to different bedrock types and ice flow directions, and indicate a few areas where more detailed geochemical sampling may be warranted. Drift sampling is especially important in northern Manitoba because extensive areas are drift-mantled; only 2% of the area is rock outcrop.

Acknowledgments

I would like to thank A.S. Dyke and R.N.W. DiLabio for their comments on the manuscript.

Methods

Till samples were collected at depths of about 50 cm from hand-dug pits in unfrozen ground, or at depths of 0.5 to 2 m from power auger cores in frozen terrain. Most sample sites were well drained. The samples were centrifuged, and the <2 µm fractions were analysed for copper, lead, zinc, cobalt, nickel, chromium, molybdenum, manganese, iron, arsenic and uranium[1]. Analytic procedures follow the style and rationale of previous geochemical studies at the Geological Survey of Canada (Shilts, 1975). Base metals were analyzed using atomic absorption techniques after LaForte reverse aqua regia extraction; arsenic values were derived using colorimetric standards; and uranium values were determined by fluorometric methods after nitric acid extraction.

Bedrock, Till, and Ice Flow Directions

The two main types of bedrock in the area are widespread igneous and metamorphic (metasedimentary and metavolcanic) rocks of Precambrian age, and calcareous sedimentary rocks of Paleozoic age. Principal bedrock types are shown on the map of base metal anomalies (Fig. 37.1). A thin blanket of till covers the Precambrian rocks; the Paleozoic rocks are commonly covered by thick drift.

Crosscutting striae, glacial bedforms, and the textural and lithologic composition of the till in northern Manitoba (Dredge and Nixon, 1981; Dredge et al., 1982) indicate that the uppermost till sheet was emplaced by two ice masses flowing in different directions (Fig. 37.2). One ice mass was centred in Keewatin, the other over Hudson Bay. Keewatin ice flowed southwards for much of the last glaciation, although flow directions shifted somewhat during ice recession. During deglaciation, ice from Keewatin centres flowed both southwestwards and southeastwards across this area, radial to an outflow centre lying in central District of Keewatin. As deglaciation proceeded, the centre of outflow migrated southwards and eastwards. Final flow in northern Manitoba therefore, was radial to, and came from, an remnant ice centre lying about 80 km west of Hudson Bay, just north of the Manitoba-Keewatin border. Tills associated with these Keewatin flow patterns are sandy because of their incorporation of medium textured Precambrian rock components. They are also generally thin (1-4 m). Many samples from areas within this Keewatin ice flow regime were taken from rib moraine, which is composed of drift that was carried by glaciers for very short distances. Consequently, base metal concentrations from these sites reflect those in the bedrock underlying the sites or directly up glacier from them. Sandy till sampled from other landforms has been transported, on average, 0 to 5 km (Dredge, 1981).

In contrast, Hudsonian ice flowed westwards across the southeastern part of the area during the last glaciation. It deposited a blanket of till 2 to 20 m thick. The till derives

[1] Samples were analyzed by Bondar-Clegg and Co. Ltd., Ottawa.

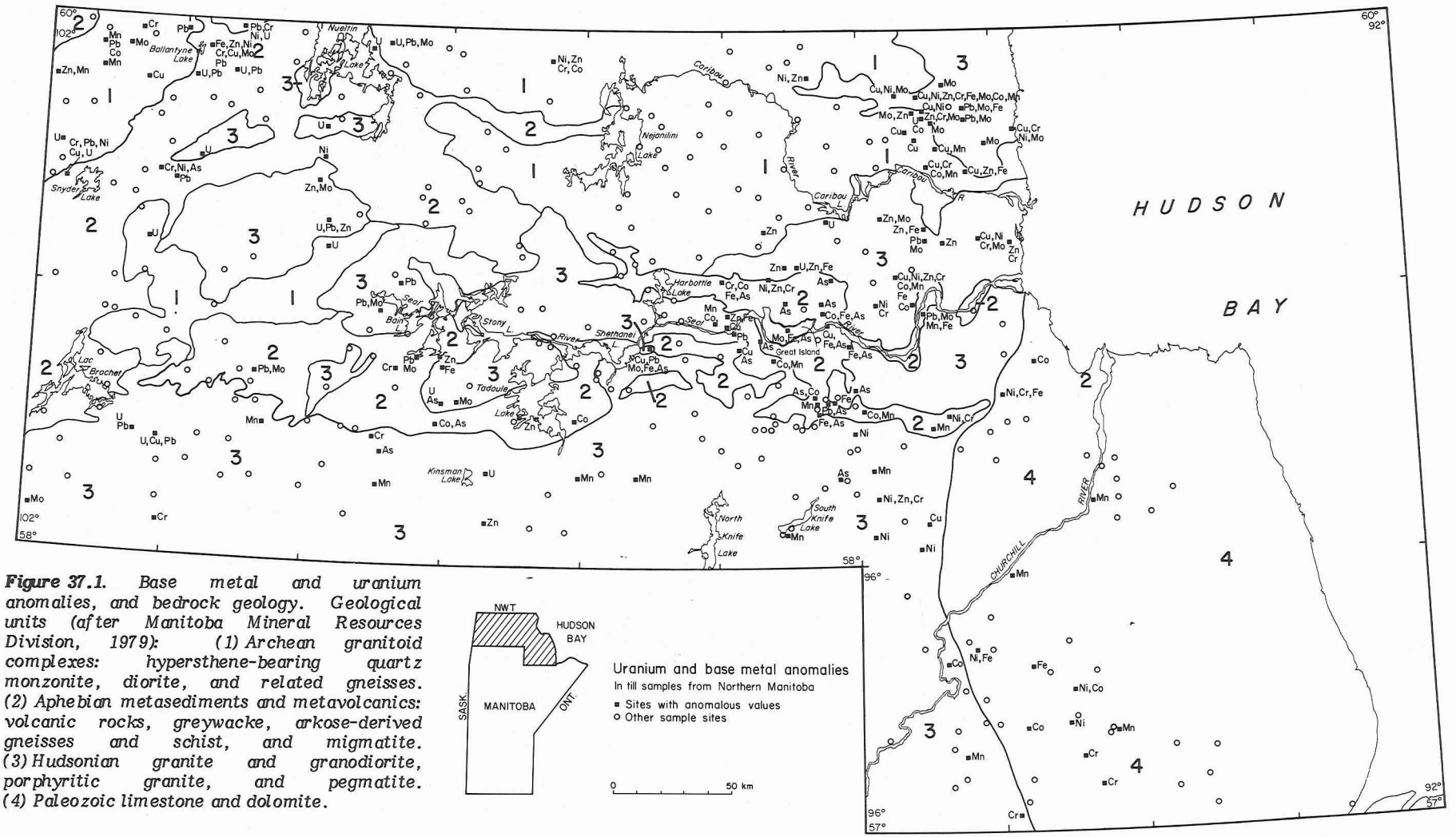

Figure 37.1. *Base metal and uranium anomalies, and bedrock geology. Geological units (after Manitoba Mineral Resources Division, 1979): (1) Archean granitoid complexes: hypersthene-bearing quartz monzonite, diorite, and related gneisses. (2) Aphebian metasediments and metavolcanics: volcanic rocks, greywacke, arkose-derived gneisses and schist, and migmatite. (3) Hudsonian granite and granodiorite, porphyritic granite, and pegmatite. (4) Paleozoic limestone and dolomite.*

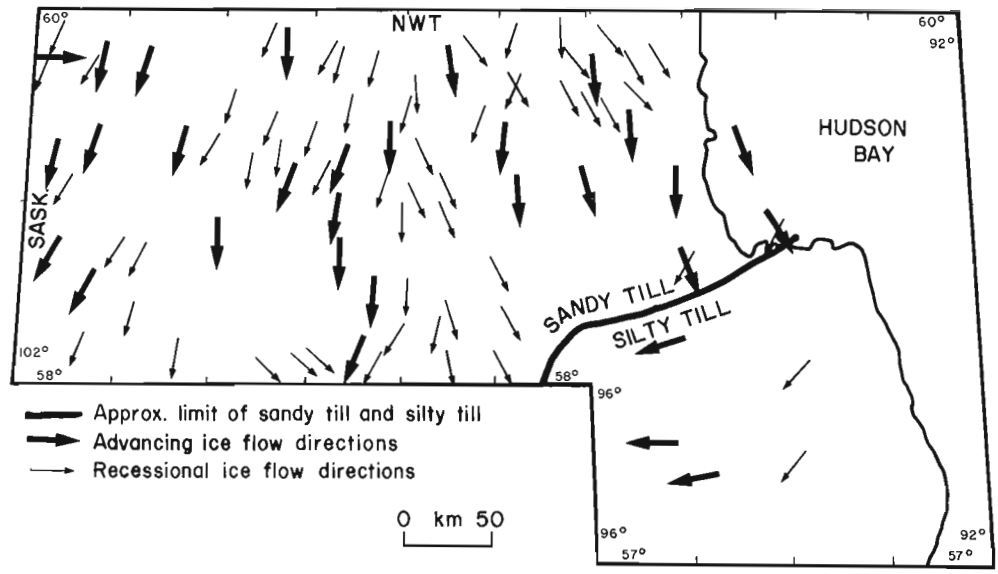

Figure 37.2

Main and recessional ice flow patterns, and approximate limit of silty till (eastern provenance) and sandy till (northern provenance).

mainly from carbonate and related sedimentary rocks of the Hudson Bay Basin, but minor amounts of far-travelled Precambrian metasediments from easterly sources are also present. In addition, a substantial fraction of the uppermost part of the till may have been produced from the reworking of older till sheets which were deposited by earlier flows of Hudsonian, and to a lesser extent Keewatin, ice across the region. The silty till that was sampled is homogenized and has a mixed origin; hence, base metal concentrations reported from the silty till do not necessarily reflect characteristics of the underlying or nearby bedrock, although they do ultimately relate to eastern, rather than to northern sources.

Base Metal and Uranium Concentrations

Figure 37.3 shows the frequency distribution of concentrations for each base metal and for uranium. Anomalies, or elevated background values, are defined as those lying at or beyond the 95th centile of the distribution. The boundary between background and "anomalous" values is 10 ppm for uranium, 80 ppm for copper, 60 ppm for nickel, 85 ppm for chromium, 32 ppm for lead, 6 ppm for molybdenum, 22 ppm for cobalt, 132 ppm for zinc, 6% for iron, 850 ppm for manganese, and 16 ppm for arsenic. Class mean value for each histrogram is shown by a vertical arrow in Figure 37.3. Frequency distributions of metal contents of the sandy till and silty till, plotted separately, show that in some cases these two till types form significantly different subgroups within the population of samples from northern Manitoba. The average concentrations (Table 37.1) for uranium and cobalt are significantly higher in the sandy till than in the silty till, whereas average levels of nickel, zinc, chromium, manganese, and iron are higher in the silty till. Mean levels for arsenic, copper, molybdenum, and lead are similar. Despite the commonly higher average levels in silty tills, most anomalous values come from samples of sandy till.

Location of Anomalies

Contour maps of metal concentrations, and values for each sample site, are presented in Dredge (1983). Figure 37.1 shows the distribution of sampling sites and the locations of anomalies. Almost 25% of the sites are enriched in some element, and 10% of the sites are enriched in two or more. Each element shows anomalous values over more than one

Table 37.1

Mean values for base metal and uranium concentrations for northern Manitoba (in ppm)

Element	Mean		
	Regional	Sandy Till	Silty Till
U	3.4	4	1.7
As	6	7	6
Cu	36	36	35
Pb	18	18	16
Ni	41	38	51
Zn	86	80	103
Cr	58	55	69
Mo	3.2	3.3	2.9
Mn	499	463	621
Fe(%)	3.6	3.5	4.1
Co	15	22	16

rock type, and in different combinations with other elements. The densest clusters of multiple anomalies lie near Hudson Bay north of Caribou River, in till that appears to be underlain by, and associated with, porphyritic granites and pegmatites (Manitoba Mineral Resources Division, 1979) intruded into nearby Archean basement rocks. Multiple anomalies are also common in till overlying tonalite-granodiorite south of Caribou River, overlying the metasedimentary gneisses and migmatites between Snyder Lake and Ballantyne Lake, and near the volcanics and related metasediments in the vicinity of Great Island and lower Seal River. Arsenic anomalies are concentrated in till near the Great Island Group of volcanics and related metasediments. Uranium anomalies are most commonly encountered in the western third of the area, particularly in the Wollaston Metasedimentary Belt and its extensions. Manganese and limited combinations of other elements are scattered throughout the areas underlain by granites, granodiorites, and tonalites in the southern part of the study area; isolated high concentrations may come from weathered samples. Those anomalies or elevated background values mentioned above in

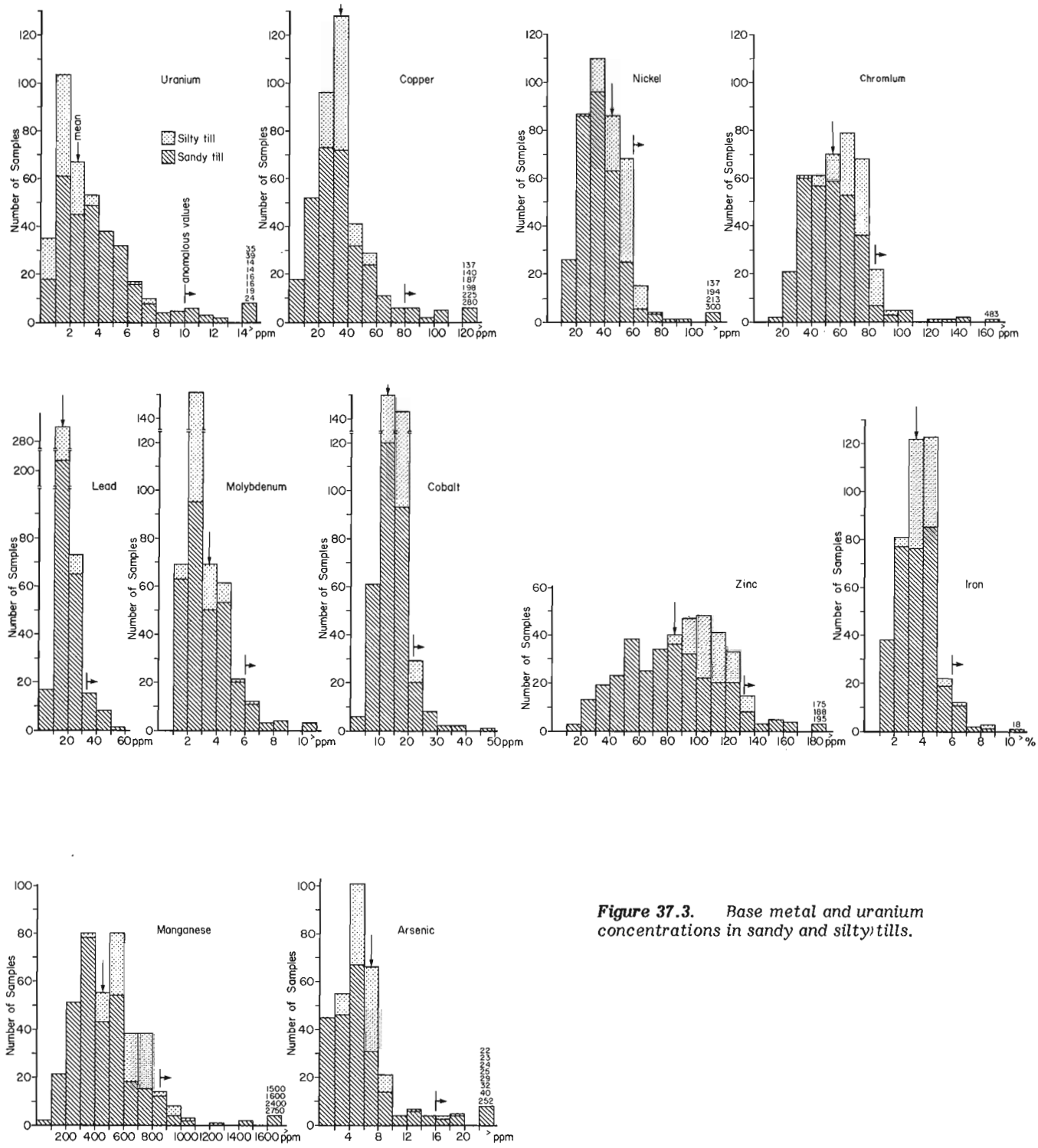

Figure 37.3. *Base metal and uranium concentrations in sandy and silty till.*

sandy till probably reflect base metal contents in the nearby bedrock and thus indicate those areas where further investigations are warranted. Manganese and iron-nickel-cobalt combinations are found in anomalous quantities in the silty tills overlying both Paleozoic and Precambrian rocks, but probably do not reflect the characteristics of the underlying bedrock. They do suggest, however, that pedogenic coprecipitation of cobalt and nickel by manganese may occur preferentially in till derived from the Paleozoic marine formations lying beneath and around Hudson Bay.

References

Dredge, L.A.
1981: Trace elements in till and esker sediments in northwestern Manitoba; in Current Research, Part A, Geological Survey of Canada, Paper 81-1A, p. 377-381.

1983: Uranium and base metal concentrations in till, northern Manitoba; Geological Survey of Canada, Open File 931.

Dredge, L.A. and Nixon, M.F.
1981: Surficial geology, northeastern Manitoba; Geological Survey of Canada, Map 1-1980 (Herchmer), Map 2-1980 (York Factory), Map 3-1980 (Cape Churchill), Map 4-1980 (Churchill), Map 5-1980 (Caribou River), Map 6-1980 (Shethanei Lake), Map 7-1980 (Nejanilini Lake), scale 1:250 000.

Dredge, L A., Nixon, M.F., and Richardson, R.J.
1982: Surficial geology, northwestern Manitoba; Geological Survey of Canada, Map 17-1981 (Tadoule Lake), Map 18-1981 (Whiskey Jack Lake), Map 19-1981 (Kasmere Lake), Map 20-1981 (Munroe Lake), scale 1:250 000.

Manitoba Mineral Resources Division
1979: Geological Map of Manitoba; Manitoba Mineral Resources Division, Map 79-2, scale 1:1 000 000.

Shilts, W.W.
1975: Principles of geochemical exploration for sulphide deposits using shallow samples of glacial drift; Canadian Mining and Metallurgical Bulletin, May 1975, p. 1-8.

38. GEOLOGICAL INVESTIGATIONS OF BAFFIN ISLAND SHELF IN 1982

Project 760015

B. MacLean and G.L. Williams
Atlantic Geoscience Centre, Dartmouth

MacLean, B. and Williams, G.L., Geological investigations of Baffin Island shelf in 1982; in Current Research, Part B, Geological Survey of Canada, Paper 83-1B, p. 309-315, 1983.

Abstract

Marine geological and geophysical studies of the Baffin Island continental shelf, carried out from ***CSS Hudson*** *in 1982, were concerned primarily with the collection of bedrock samples. Biostratigraphic and lithostratigraphic analyses of the samples permitted identification of units previously only observed on seismic profiles.*

Palynological studies indicate the presence of Upper Cretaceous strata at Home Bay, and Lower Cretaceous strata off Padloping Island and in the outer part of Cumberland Sound. Cores obtained from Hudson Strait are lithologically similar to Lower Paleozoic rocks outcropping on Coats and Southampton islands in northern Hudson Bay.

Surficial sediment samples were taken to define correlations and depositional history of Quaternary sediments on the southeastern Baffin shelf.

Résumé

Des études géologiques et géophysiques marines du plateau continental de l'île Baffin, effectuées en 1982 à partir du ***CSS Hudson*** *ont porté surtout sur l'échantillonnage du socle rocheux. L'analyse biostratigraphique et lithostratigraphique des échantillons a permis d'identifier des unités qui, auparavant, avaient seulement été observées sur des profils sismiques.*

L'étude palynologique indique la présence de couches du Crétacé supérieur à Home Bay et du Crétacé inférieur au large de l'île Padloping et de la partie extérieure du détroit de Cumberland. Des carottes prélevées dans le détroit d'Hudson ont une lithologie semblable à celle des roches du Paléozoïque inférieur qui affleurent dans les îles Coats et Southampton dans le nord de la baie d'Hudson.

Des échantillons de sédiments de surface ont été prélevés afin de corréler les sédiments quaternaires de la partie sud-est du plateau de Baffin et de déterminer leur histoire stratigraphique.

Introduction

A program to extend geological knowledge of the Baffin Island shelf was undertaken from **CSS Hudson** between September 24 and October 18, 1982 (cruise 82-034). The prime objective of the cruise was the collection of bedrock samples for lithostratigraphic and biostratigraphic information for geological mapping. Surficial sediment sampling was also carried out on the southeastern Baffin shelf. The stations occupied and survey tracks are indicated in Figures 38.1 and 38.2. Satellite navigation and rho-rho Loran C (groundwave and skywave) systems and radar were used for navigational positioning.

The bedrock studies included collection of both samples and geophysical data. The sampling program was undertaken with a prototype version of the BIO underwater electric rock core drill extended to 10 m penetration capability to cope with the thick overburden found in this region. We were thus able to obtain samples beyond the reach of the regular 6 m drill. Most drill locations were selected on the basis of previously acquired data. All were resurveyed to ensure best possible site conditions. Drilling was hampered by mechanical and electrical problems with the drill, by the presence of gravel, and by the nature of the substrate.

Geophysical data were obtained using a conventional single channel seismic reflection system (655 cm^3 compressed air source), Huntec high resolution deep tow seismic system, and Varian magnetometer. Acoustic information from a Nova Scotia Research Foundation 6 m hydrophone in addition to that obtained with a SE 30 m hydrophone and the Huntec system proved very helpful in carrying out the drill site surveys.

Samples of sedimentary bedrock were recovered from Home Bay, Padloping Island, Cumberland Sound, and Hudson Strait areas (Fig. 38.1, Table 38.1). Preliminary results of laboratory studies are outlined for each of these areas.

Home Bay Area

Short cores of semiconsolidated sediments including mudstone, siltstone, and sandstone were recovered from two main localities 24 km apart (Stations 3, 8, 10). Figure 38.3 illustrates a seismic reflection profile across the station 8 and 10 locality. Station 3 in the northern part of the bay contained abundant dinoflagellates which show affinities with Bylot Island assemblages dated as Campanian. Station 8 and 10 in the southern part of the bay also contained dinoflagellates of Late Cretaceous age, possibly coeval with assemblages from station 3. Mudstone samples from station 8 (Figure 38.4) had a petroliferous odour and are organic rich. They appear to represent promising petroleum source rocks.

Bedrock samples recovered previously from the northeastern Baffin shelf included Upper Cretaceous (Campanian) marine strata from Buchan Trough and upper Eocene-lower Oligocene strata from Scott Trough, 425 km and 315 km north of Home Bay, respectively (MacLean et al., 1981; MacLean and Williams, 1980; Levy and MacLean, 1981).

Our highest priority for sampling on the cruise was Home Bay as it is the only area between Scott Trough and Padloping Island where overburden is thin enough to be penetrated by the drill. The acoustic stratigraphy also suggested that pre-Tertiary strata would be accessible.

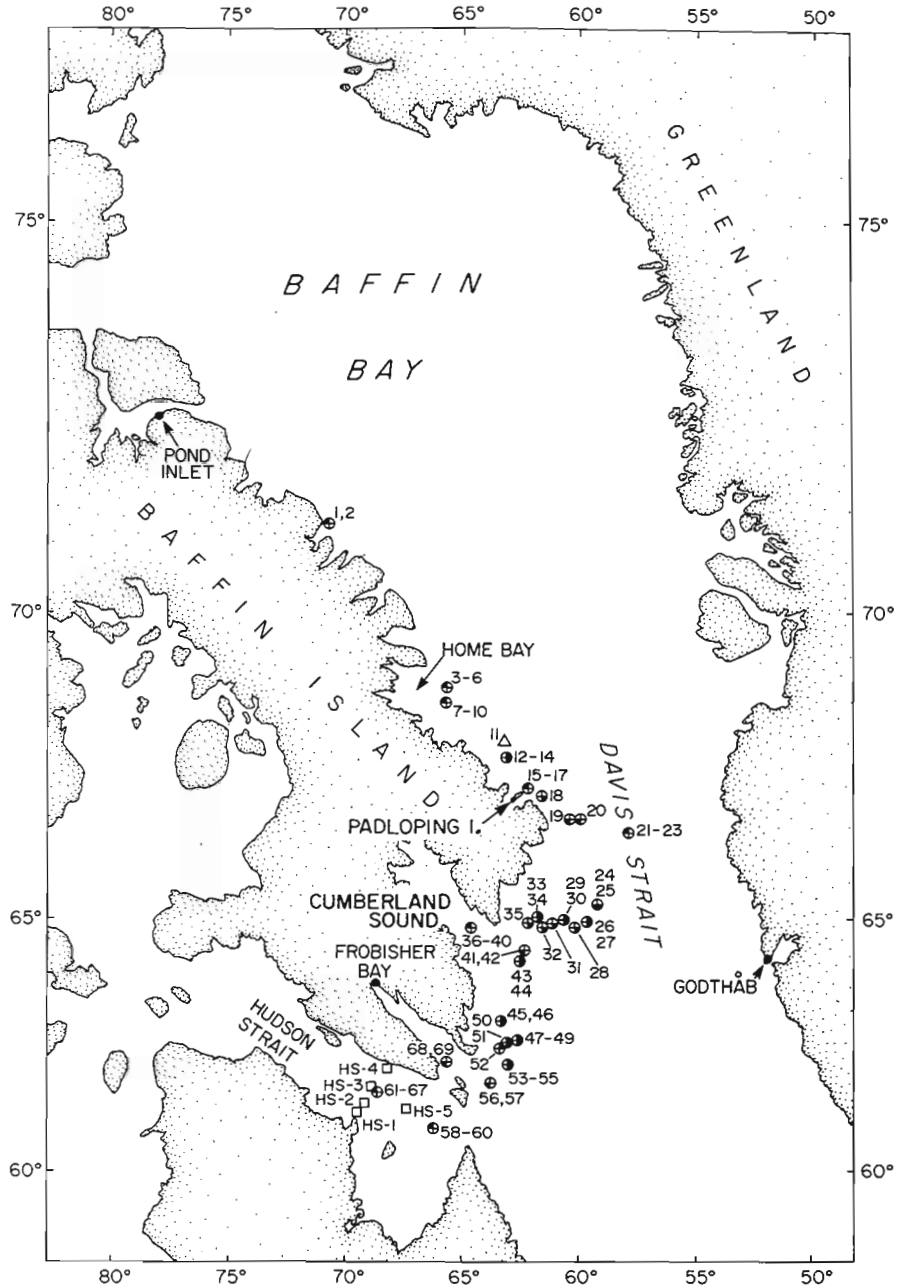

Figure 38.1. *Station locations – Cruise 82-034.*

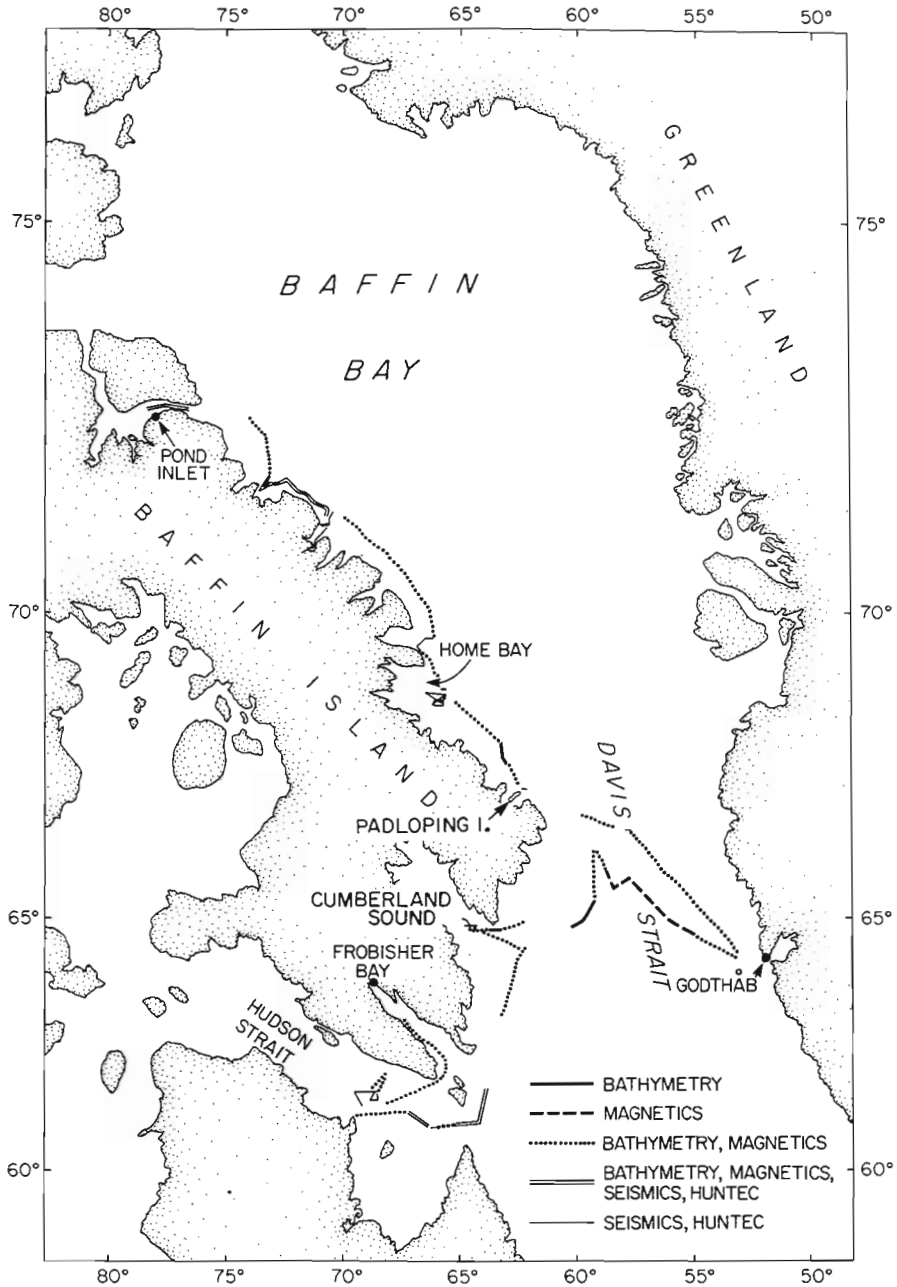

Figure 38.2. *Survey tracks – Cruise 82-034.*

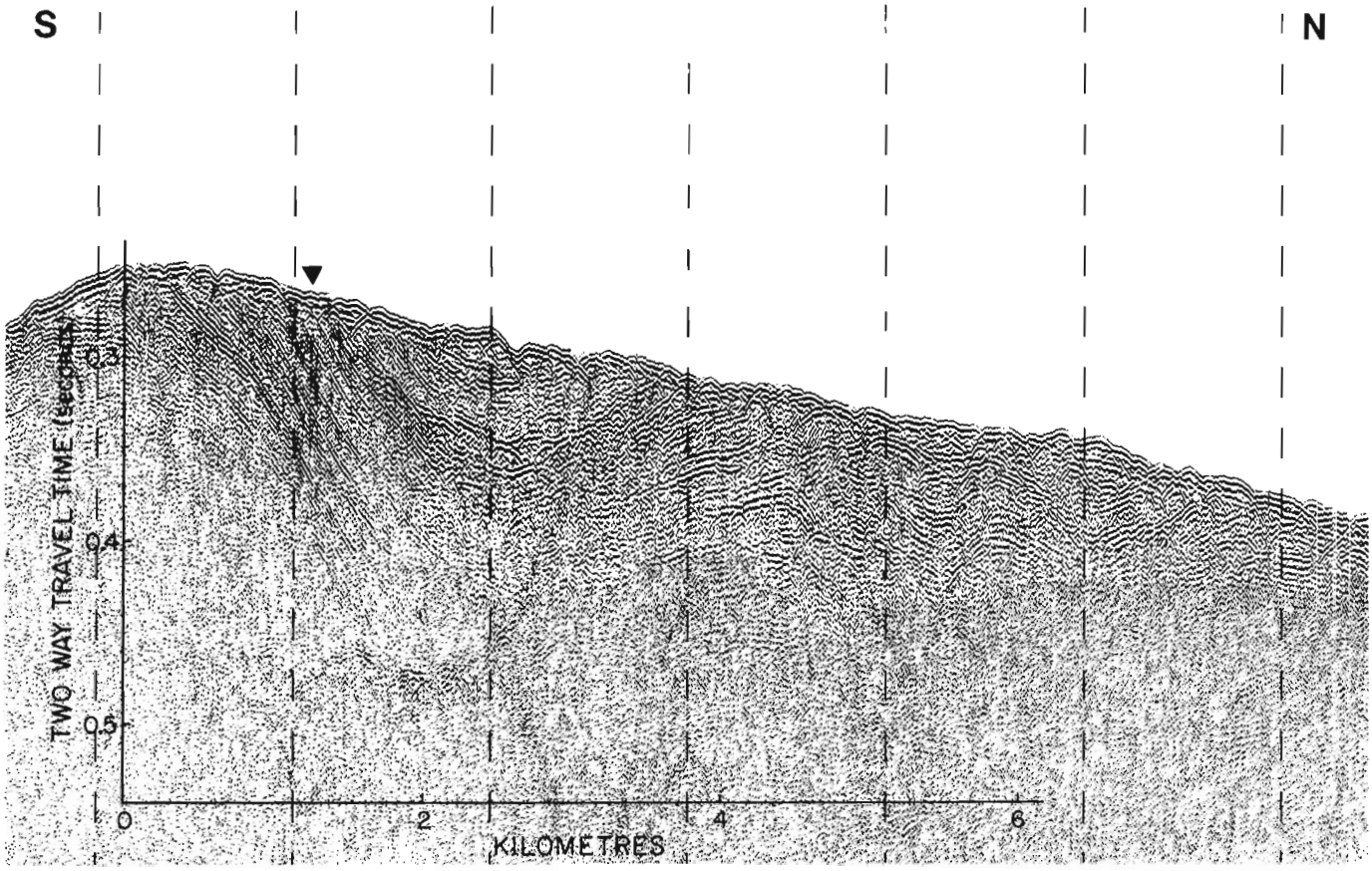

Figure 38.3. *Seismic reflection profile showing northward dipping Upper Cretaceous strata at sample locality in southern part of Home Bay. Solid triangle designates the station 8 and 10 locality (see Fig. 38.1 for location).*

Results from the 1982 Home Bay samples together with those obtained earlier from Buchan and Scott areas indicate that Upper Cretaceous marine strata occur extensively on the northeast shelf beneath a variable cover of Tertiary and Quaternary sediments. The existence of the natural submarine oil seep at Scott Trough and the apparent promising source rock characteristics of Upper Cretaceous strata at Home Bay suggest that the northeast Baffin shelf is a potential area for hydrocarbon resources.

Padloping Island Area

The single core (station 16) recovered from a locality 13 km northeast of Padloping Island (Fig. 38.1, 38.5) was of semiconsolidated fine grained clastic sediment containing coaly fragments. Palynological analyses of the sediment indicated a mixed Cretaceous spore assemblage with no dinoflagellates being seen. It is therefore believed that the sample represents nonmarine deposition. Coaly fragments processed separately contained rich spore assemblages with known Albian affinities (E.H. Davies, personal communication, 1983). Onshore coals of this age are unknown in the region although there are coals in the Bjarni Formation in Labrador Shelf wells (Umpleby, 1979). According to palynological studies referenced in Umpleby (1979), the Bjarni Formation is of Berremian-Aptian age. The only known outcrops of coal on Baffin Island other than those near Pond Inlet far distant to the north, are contained in sediments of Paleocene age underlying volcanic rocks on the coastal islands adjacent to station 16 (Clarke and Upton, 1971).

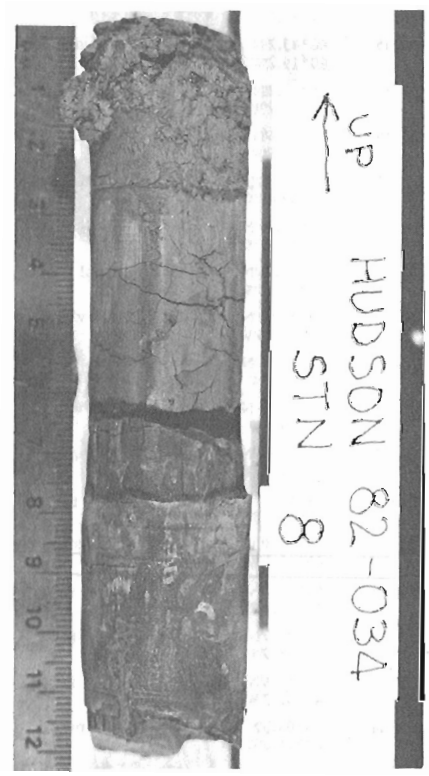

Figure 38.4. *A section of semiconsolidated Upper Cretaceous mudstone core recovered from southern Home Bay locality (station 8) illustrated in Figure 38.3.*

Table 38.1

Stn. no.	Time	Position	Depth (m)	Type and results
1	271/1637	71°15.3'N 70°41.4'W	752	Drill – No sample
2	271/2212	71°15.38'N 70°41.45'W	752	Drill – No sample
3	273/1606	68°52.0'N 65°39.6'W	659	Drill – Recovery: 19 siltstone core (bedrock) 3 cm gravel
4	273/1746	68°52.0'N 65°39.0'W	659	Drill – No Sample
5	273/2045	68°51.74'N 65°40.74'W	674	Drill – Recovery: gravel and small amount of bedrock as at stn. 3
6	273/2319	68°51.87'N 65°40.27'W	530	Drill – Recovery: gravel and small amount of bedrock as at stn. 3
7	274/1248	68°38.3'N 65°40.3'W	457	Drill – Recovery: 17 cm gravel
8	274/2035	68°38.8'N 65°40.2'W	460	Drill – Recovery: 15 cm bedrock (mudstone) 4 cm gravel
9	275/1052	68°38.8'N 65°42.5'W	461	Drill – Recovery: Few pebbles and a mud sample from legs
10	275/1548	68°38.2'N 65°42.0'W	460	Drill – Recovery: 17 cm bedrock (sandstone)
11	275/2300	68°00.0'N 63°13.0'W	795	CTD
12	276/0049	67°48.7'N 63°11.5'W	256	Camera
13	276/0120	67°45.6'N 63°11.0'W	230	Camera
14	275/0311	67°43.6'N 63°02.1'W	129	Van Veen grab
15	276/1310	67°15.5'N 62°11.1'W	274	Drill – No recovery
16	276/1652	67°15.6'N 62°11.3'W	368	Drill – Recovery: 6 cm bedrock (mudstone) 22 cm gravel
17	276/1830	67°15.3'N 62°11.0'W	366	Drill – Recovery: small amount of gravel
18	276/2105	67°08.0'N 61°36.0'W	156	Van Veen grab
19-1	277/0005	66°45.2'N 60°19.2'W	550	Gravity core
19-2	277/0025	66°45.2'N 60°19.2'W	550	Gravity core
20	277/0139	66°44.6'N 59°59.9'W	690	Gravity core
21	277/1205	66°30.38'N 57°53.08'W	569	Drill – Recovery: 14 cm bedrock (basalt) 5 cm gravel
22	277/1300	66°29.94'N 57°52.57'W	569	Drill
23	277/1423	66°30.28'N 57°52.75'W	564	Drill – Recovery: 15 cm gravel
24	282/0914	65°15.05'N 59°13.10'W	428	Gravity core
25	282/0940	65°15.36'N 59°12.6'W	428	Van Veen grab
26	282/1227	64°56.54'N 59°39.5'W	275	Camera
27	282/1325	64°56.67'N 59°39.74'W	377	IKU grab
28	282/1626	64°50.1'N 60°10.5'W	311	IKU grab
29	282/1811	64°59.8'N 60°41.2'W	288	Camera
30	282/1839	64°58.7'N 60°42.9'W	288	IKU grab
31	282/2005	64°55.0'N 61°08.0'W	265	IKU grab
32	282/2127	64°50.6'N 61°32.7'W	247	IKU grab
33	282/2301	65°01.0'N 61°46.0'W	275	Camera
34	282/2325	65°01.18'N 61°48.24'W	274	IKU grab
35	283/0044	64°55.18'N 62°09.48'W	275	IKU grab
36	283/1542	64°50.54'N 64°40.70'W	750	Drill – Mud sample from leg only
37	284/1127	64°48.9'N 64°34.4'W	724	Drill – No sample (lost flushing at 329 cm)
38	284/1157	64°48.99'N 64°34.9'W	724	Drill – Recovery 6 cm bedrock (mudstone)
39	284/1524	64°48.9'N 64°35.7'W	713	Drill – No sample
40	284/1747	64°48.9'N 64°35.7'W	720	Drill – No sample
41	284/2330	64°25.22'N 62°26.38'W	340	Piston core
42	285/0051	64°24.7'N 62°13.0'W	340	Piston core
43	285/0247	64°12.48'N 62°32.48'W	148	Camera
44	285/0305	64°12.6'N 62°32.4'W	148	Van Veen grab
45	285/1038	63°02.45'N 63°19.26'W	148	Van Veen grab
46	285/1048	63°02.06'N 63°19.29'W	148	Camera
47	285/1317	62°39.6'N 62°39.73'W	201	Camera
48	285/1336	62°39.38'N 62°40.16'W	201	IKU grab
49	285/1357	62°39.38'N 62°40.16'W	201	IKU grab
50	285/1457	62°36.90'N 63°02.65'W	214	Camera
51	285/1520	62°36.62'N 63°03.15'W	214	IKU grab
52	285/1607	62°31.72'N 63°15.54'W	220	Camera
53	285/1810	62°10.65'N 63°00.98'W	350	Camera
54	285/1825	62°10.45'N 63°01.91'W	350	IKU grab
55	285/1845	62°10.45'N 63°02.74'W	350	IKU grab
56	285/2055	61°51.01'N 63°39.3'W	523	Piston core
57	285/2200	61°46.75'N 63°49.7'W	512	Piston core
58	286/1901	60°53.24'N 66°11.81'W	690	Drill – No sample
59	286/2105	60°52.0'N 66°11.7'W	710	Drill – No sample
60	286/2232	60°52.83'N 66°12.02'W	710	Drill – No sample
61	288/1940	61°36.7'N 68°32.86'W	295	Drill – Recovery: fragments of core (limestone)
62	288/2045	61°36.8'N 68°33.26'W	295	Drill – No sample
63	288/2248	61°37.0'N 68°36.7'W	295	Drill – No sample
64	289/1220	61°37.79'N 68°41.86'W	293	Drill – No sample
65	289/1524	61°37.56'N 68°40.75'W	293	Drill – Recovery: 8 cm bedrock (limestone)
66	289/1612	61°37.52'N 68°41.02'W	293	Drill – Recovery: 50 cm bedrock (limestone)
67	289/1816	61°36.92'N 68°33.35'W	285	Drill – Recovery: 155 cm bedrock (limestone)
68	290/0734	62°13.3'N 65°40.2'W	311	Piston core
69	290/0905	62°14.9'N 65°35.0'W	315	Piston core

Current meter recovery locations:

HS 1	61°08.6'N 69°28.8'W	HS 4	62°00.5'N 68°09.7'W
HS 2	61°18.1'N 69°07.5'W	HS 5	61°12.3'N 67°22.1'W
HS 3	61°36.8'N 68°50.0'W		

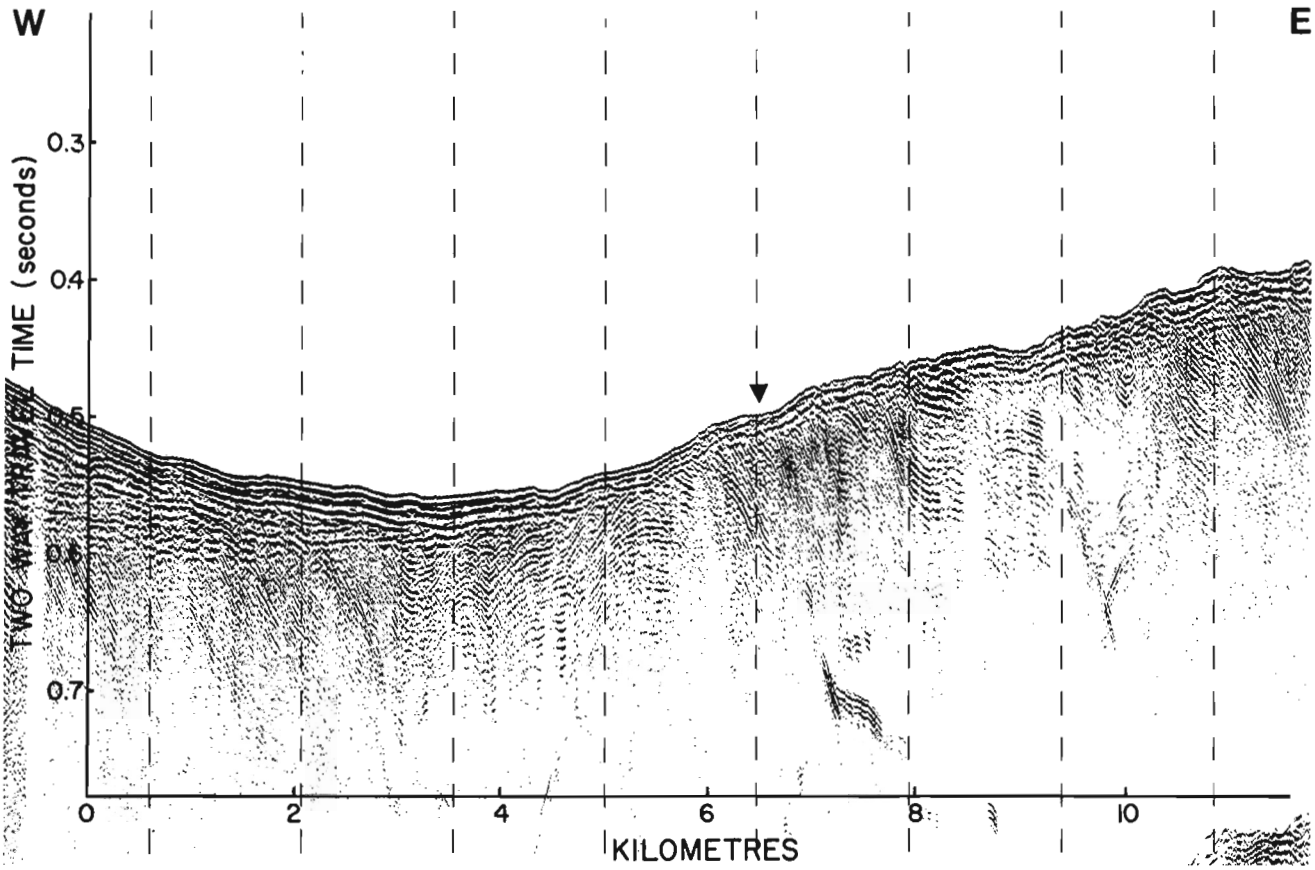

Figure 38.5. *Seismic reflection profile west to east across station 16 off Padloping Island.*

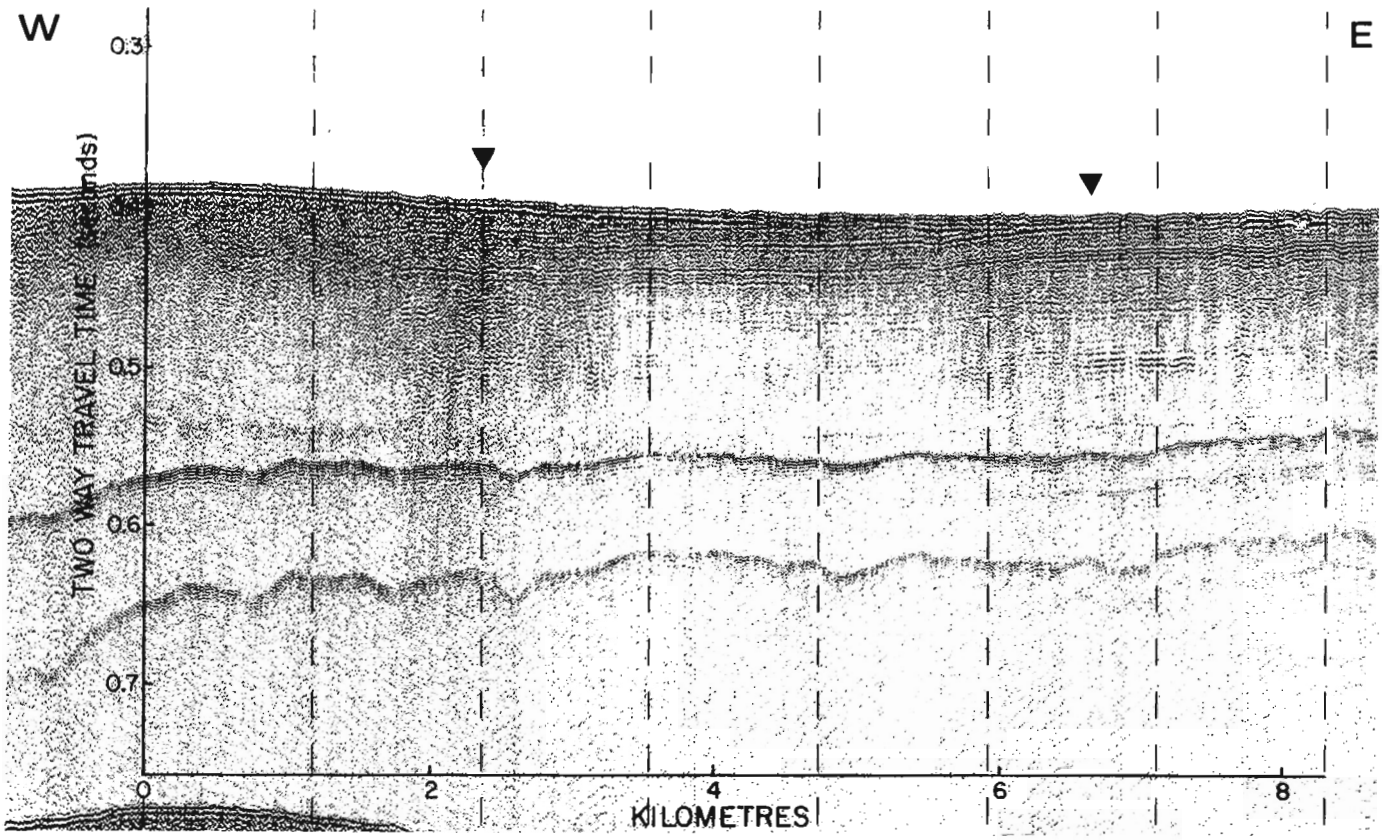

Figure 38.6. *Seismic reflection profile from west to east through sample localities in Hudson Strait, northeast of Cape Hopes Advance (see Fig. 38.1 for location). The profile lies approximately along strike of the strata which dip gently southward at this locality. Triangles indicate locations of stations 66 and 67 to the left and right, respectively.*

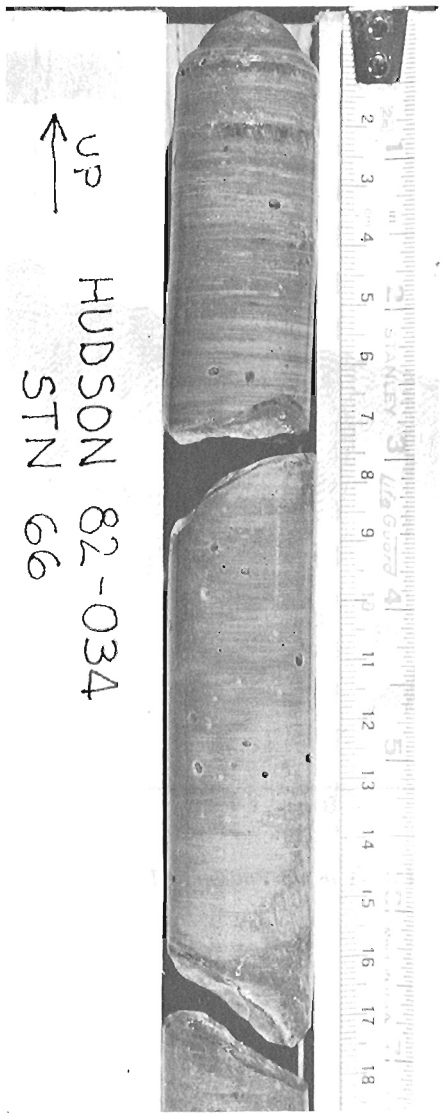

Figure 38.7. Section of core of massive limestone from Station 66 in Hudson Strait.

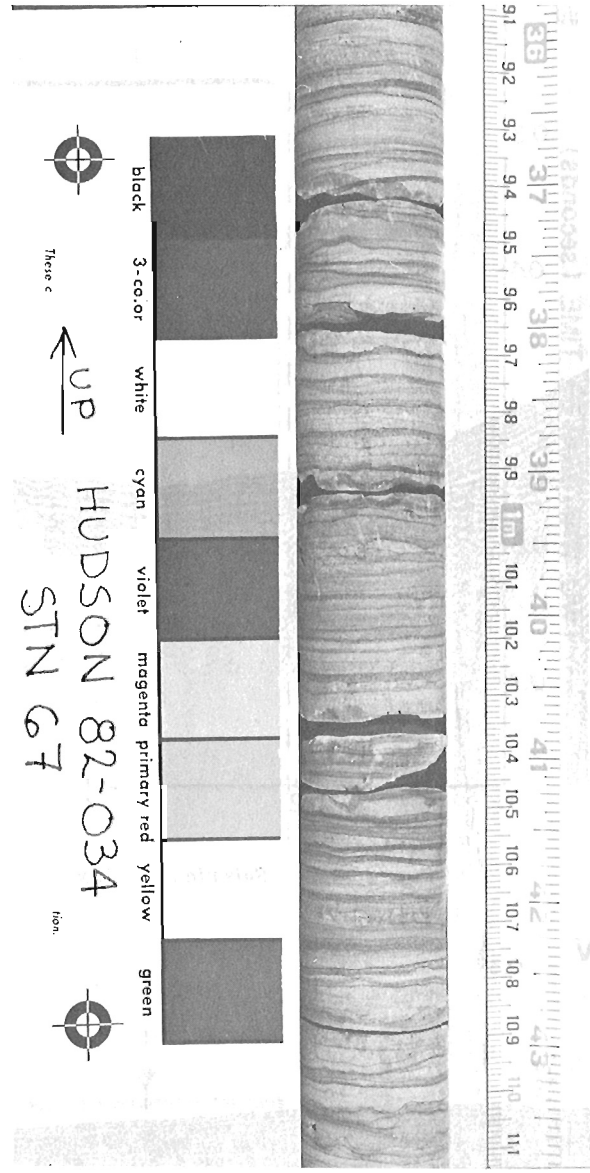

Figure 38.8. Section of core of finely laminated limestone from Station 67 in Hudson Strait.

Cumberland Sound

One short bedrock core of semiconsolidated mudstone was recovered from beneath 8 m of overburden in Cumberland Sound (station 38). The material has been assigned an Aptian-Cenomanian age on the basis of palynomorph assemblages. The core appears to be rich in organic matter, all of which is from a terrestrial source.

Strata underlying Cumberland Sound previously were considered by Grant (1975) to be of Paleozoic-Mesozoic age on the basis of acoustic resemblance to rocks in other east coast offshore areas. Middle-upper Ordovician strata subsequently identified on the adjacent shelf were also thought by MacLean et al. (1982) to be present in Cumberland Sound. The present age assignment indicates that Cretaceous strata are included in the Cumberland Sound succession. This suggests that the Cumberland Sound graben existed in the Cretaceous.

Hudson Strait

Two limestone cores, presumed to be of Early Paleozoic age, were recovered from two localities 4 km apart near the middle of Hudson Strait, northeast of Cape Hopes Advance (stations 66 and 67). Figure 38.6 illustrates a seismic reflection profile through the sample localities. One core was a massive limestone; the other was a finely laminated limestone (Fig. 38.7, 38.8). Paleontological studies of the material are as yet incomplete. Lithologically the samples appear similar to rocks included in the Upper Ordovician Red Head Rapids Formation, described by Heywood and Sanford (1976) from Coats and Southampton islands. These two islands lie 630 km to the west in the northern part of Hudson Bay. Sample and seismic reflection and magnetic data from cruise 82-034, geophysical data acquired by Grant and Manchester (1970), and data from the Premium Homestead Akpatok L-26 drillhole on Akpatok Island in Ungava Bay (Workum et al., 1976) indicate that lower Paleozoic rocks underlie much of eastern Hudson Strait and Ungava Bay.

Surficial Sediments

In addition to the bedrock investigation, surficial sediment samples were recovered using a piston corer and a large IKU clamshell sampler at several localities on the southeastern Baffin shelf. The samples were required for textural and paleontological study to clarify correlations, and to determine depositional environments. Sediments sampled included apparent glacial till, possible proglacial, and postglacial sediments.

Acknowledgments

We are grateful to Captain F.W. Mauger, Officers and Crew of **CSS Hudson** for their excellent co-operation and assistance in carrying out this program. We extend special thanks to F. Learning and D. Wilson of Geomarine Associates Ltd. and to all members of the scientific staff for their dedicated efforts and tremendous support. We are also grateful to A.C. Grant and R.F. Macnab for reviewing the manuscript.

References

Clarke, D.B. and Upton, B.G.J.
1971: Tertiary basalts of Baffin Island: field relations and tectonic setting; Canadian Journal of Earth Sciences, v. 8, p. 248-258.

Grant, A.C.
1975: Geophysical results from the continental margin off southern Baffin Island in Canada's Continental Margins and Offshore Petroleum Exploration, ed. C.J. Yorath, E.R. Parker, and D.J. Glass; Canadian Society of Petroleum Geologists, Memoir 4, p. 411-431.

Grant, A.C. and Manchester, K.S.
1970: Geophysical investigations in the Ungava Bay-Hudson Strait region of northern Canada; Canadian Journal of Earth Sciences, v. 7, p. 1062-1076.

Heywood, W.W. and Sanford, B.V.
1976: Geology of Southampton, Coats, and Mansel Islands, District of Keewatin, Northwest Territories; Geological Survey of Canada, Memoir 382, 35 p.

Levy, E.M. and MacLean, B.
1981: Natural hydrocarbon seepage at Scott Inlet and Buchan Gulf, Baffin Island shelf: 1980 update; in Current Research, Part A, Geological Survey of Canada, Paper 81-1A, p. 401-403.

MacLean, B. and Williams, G.L.
1980: Upper Cretaceous rocks in Baffin Bay; Geological Association of Canada, Program with Abstracts, v. 5, p. 69.

MacLean, B., Falconer, R.K.H., and Levy, E.M.
1981: Geological, geophysical and chemical evidence for natural seepage of petroleum off the northeast coast of Baffin Island; Bulletin of Canadian Petroleum Geology, v. 29, p. 75-95.

MacLean, B., Srivastava, S.P., and Haworth, R.T.
1982: Bedrock structures off Cumberland Sound, Baffin Island shelf: core sample and geophysical data; in Arctic Geology and Geophysics, ed. A.F. Embry and H.R. Balkwill; Canadian Society of Petroleum Geologists, Memoir 8, p. 279-295.

Umpleby, D.C.
1979: Geology of the Labrador Shelf; Geological Survey of Canada, Paper 79-13, 34 p.

Workum, R.H., Bolton, T.E., and Barnes, C.R.
1976: Ordovician geology of Akpatok Island, Ungava Bay, District of Franklin; Canadian Journal of Earth Sciences, v. 13, p. 157-178.

39.

ORIGIN OF PITCHBLENDE VEINS IN THE UNION ISLAND AREA, GREAT SLAVE LAKE, NORTHWEST TERRITORIES

Project 770024

S.S. Gandhi
Economic Geology Division

Gandhi, S.S., Origin of pitchblende veins in the Union Island area, Great Slave Lake, Northwest Territories; in Current Research, Part B, Geological Survey of Canada, Paper 83-1B, p. 317-326, 1983.

Abstract

Pitchblende veins are sparsely distributed in an 8x1 km zone of northeast-trending, steeply dipping Aphebian sedimentary rocks deposited on Archean granitic basement and affected by complex faulting. They occur in brecciated dolomite of the Union Island Group on the east shore of Union Island, and along fractures subsidiary to a nearly vertical, northeast-trending fault between phyllites of this group and arkosic quartzite of the younger Sosan Group, which is exposed for a distance of 4 km on Opener Island to the east. The veins are close to the unconformity between the host rocks and the younger, gently dipping clastic redbeds of the Late Aphebian Et-Then Group, which most probably covered the mineralized zone at one time.

A supergene origin for the veins is proposed on the basis of geological setting, mineralogy, presence of Ag, Se and V, isotopic dates on pitchblende, and lack of evidence for alternative magmatic or metamorphic hydrothermal sources.

Résumé

Des filons épars de pechblende sont répartis dans une zone de 8 sur 1 km de roches sédimentaires aphébiennes à orientation nord-est et fortement inclinées, qui ont été déposées sur le socle granitique archéen et sont parcourues par un réseau de failles complexes. Ces filons se manifestent dans la dolomie bréchique du groupe de Union Island sur le littoral est de l'île Union et le long de fissures secondaires d'une faille presque verticale, à orientation nord-est, située entre les phyllites de ce groupe et le quartzite feldspathique du groupe de Sosan plus récent, qui affleure sur une distance de 4 km dans l'île Opener, à l'est. Les filons se trouvent près de la discordance entre les roches encaissantes et les formations rouges clastiques plus récentes, à pendage faible, du groupe de Et-Then de l'Aphébien récent, qui auraient déjà recouvert la zone minéralisée.

Le milieu géologique, la minéralogie, la présence d'Ag, de Se et de V, les dates isotopiques de la pechblende et l'absence d'indices d'autres sources magmatiques ou métamorphiques hydrothermales semblent indiquer que les filons sont d'origine secondaire.

Introduction

High grade pitchblende veins were discovered in 1967 on the DM-MDM and TEL claim groups[1] at the east end of Union Island and at the southwest end of Opener Island[2], respectively (Fig. 39.1, 39.2). Other high grade pitchblende veins, containing significant silver values, were discovered in 1978 on the SHUM claims at the northeast end of Opener Island.

The present study summarizes results of exploration, of the writer's geological observations made in 1980 and 1982, and of mineralogical and isotopic studies. The uranium occurrences on the three claim groups are briefly described, and a supergene origin proposed for them.

General Geology

The study area is in the west-central part of a structural trough along the 200-km length of the east arm of Great Slave Lake (Fig. 39.1), in which a thick sequence of Aphebian sedimentary and volcanic rocks is preserved (Stockwell, 1932, 1936a, b; Hoffman, 1969; Hoffman et al., 1974, 1977).

The Aphebian rocks were deposited on a granitic basement of Archean age (Reinhardt, 1969). The basement is well exposed in the study area (Fig. 39.2) and a quartz monzonite sample from it (61°59'20"N, 111°48'00"W) yielded a muscovite K-Ar date of 2575 Ma (Lowdon et al., 1963, p. 46). It is overlain unconformably by the Union Island Group. This group comprises basal quartzite-quartz pebble conglomerate in topographic lows of the basement, overlain successively by lower massive dolomite, black carbonaceous mudstone, basaltic lavas and tuffs and gabbro, upper bedded dolomite, and red and green laminated mudstone (Hoffman et al., 1977, p. 120).

The Sosan Group includes four formations (Hoffman, 1968, 1969), all of which are exposed in the study area:

i) the basal Hornby Channel Formation of pebbly feldspathic arkose or granule-stone;

ii) Duhamel Formation of stromatolitic dolomite;

iii) Kluziai Formation of white to pink quartzite; and

iv) Akaitcho Formation of red micaceous sandstone.

The Et-Then Group is the youngest Aphebian sequence in the study area, and is a redbed sequence divided into the lower Murky Formation and the upper Preble Formation (Stockwell, 1932, 1936 a, b). The Murky Formation is fanglomeratic, with cobbles and pebbles of predominantly sedimentary rocks in a red oxidized matrix. It was deposited as alluvial fans growing northwestwards from fault scarps trending northeast, and includes intercalated tholeiitic basalt flows (Hoffman, 1968; Hoffman et al., 1974, 1977). The flows yielded a Rb-Sr isotopic date of 1969 ± 82 Ma (Gandhi and Loveridge, 1982). Preble Formation is predominantly red feldspathic sandstone, and in some localities it directly overlies rocks older than the Et-Then Group.

[1] Claim group names at the time of original discovery are used here.
[2] Unofficial name, used by Chevron Standard Limited during its 1978-80 exploration.

Structure

The structural history is complex. Regional folding involving some nappes in the axial parts of the east arm trough preceded deposition of the Et-Then Group (Hoffman et al., 1977). The study area is located at the eastern extremity of a wedge-shaped basement block, bound by regional strike slip faults along Preble and Wilson islands (Fig. 39.1). These faults belong to the McDonald Fault system of northeast-trending right-lateral transcurrent faults, which have some vertical displacements. Movements along this fault system initiated the deposition of the Et-Then Group, and some of the movements also occurred during and after the deposition (Reinhardt, 1969, 1972; Hoffman et al., 1974). A number of subsidiary faults in the study area trend at moderate to high angles to the major faults (Fig. 39.2).

The Union Island Group in the study area is moderately to tightly folded, with local minor folds and crenulations in incompetent mudstone beds. The beds of the Sosan Group dip steeply to the southeast, and those of the Et-Then Group gently to moderately, commonly to the southeast.

The contact between the Union Island Group and Sosan Group is well exposed on Opener Island (Fig. 39.2) where it is sharp, nearly vertical, and trends northeast. The argillaceous beds of the Union Island Group on the north side of the fault show nearly vertical bedding and foliation, and numerous minor folds and crenulations plunging shallowly to the northeast. The arkosic quartzite of the Sosan Group to the south is massive, with bedding seen only locally in a few lenses. The contact was mentioned by Hoffman et al. (1977, p. 120) who considered it to represent an unconformity between the Union Island Group and Sosan Group. It is interpreted here as a fault, close to the unconformity, following Walton (1979, p. 5). The direction and amount of displacement along it, however, are not known, nor is its relation to the McDonald Fault system. It may be an older reverse fault, subparallel to the unconformity between the Union Island and Sosan groups, later reactivated by movements related to the system. The fault is offset by steeply dipping cross faults trending eastwards and commonly having right lateral displacement. A few of the cross faults are shown in Figure 39.2, but there are a number of other small faults and fractures subparallel to them, and several others at high angles to them.

The Preble Fault (Fig. 39.1, 39.2) is interpreted to extend in the DM-MDM claim area along the topographic low that separates the basement granite to the northwest and the dolomite and mudstone units of the Union Island Group to the southeast, as indicated by Stockwell (1936a, b). It then follows the shore of Union Island to the northeast. To the southwest of the claim area, a fault subparallel to the Preble Fault and located close to the north shore of Union Island (Hoffman, 1977), is here regarded as a splay of the Preble Fault. There are several minor faults and breccia zones in the claim area, some of which are known only from drillholes. They are probably related to the McDonald Fault System, but the relationship is not certain in some cases. The main mineralized dolomite breccia zone (Fig. 39.3) may predate the fault system.

A breccia body containing large angular blocks of Sosan Group rock is present at the northeast end of Opener Island. It was mapped as Murky Formation by Hoffman (1977) and was described as 'diatreme' by Walton (1979). Some of the blocks near the contact are close to their source beds and a few of them can be recognized as only slightly moved from their original position with respect to unbrecciated

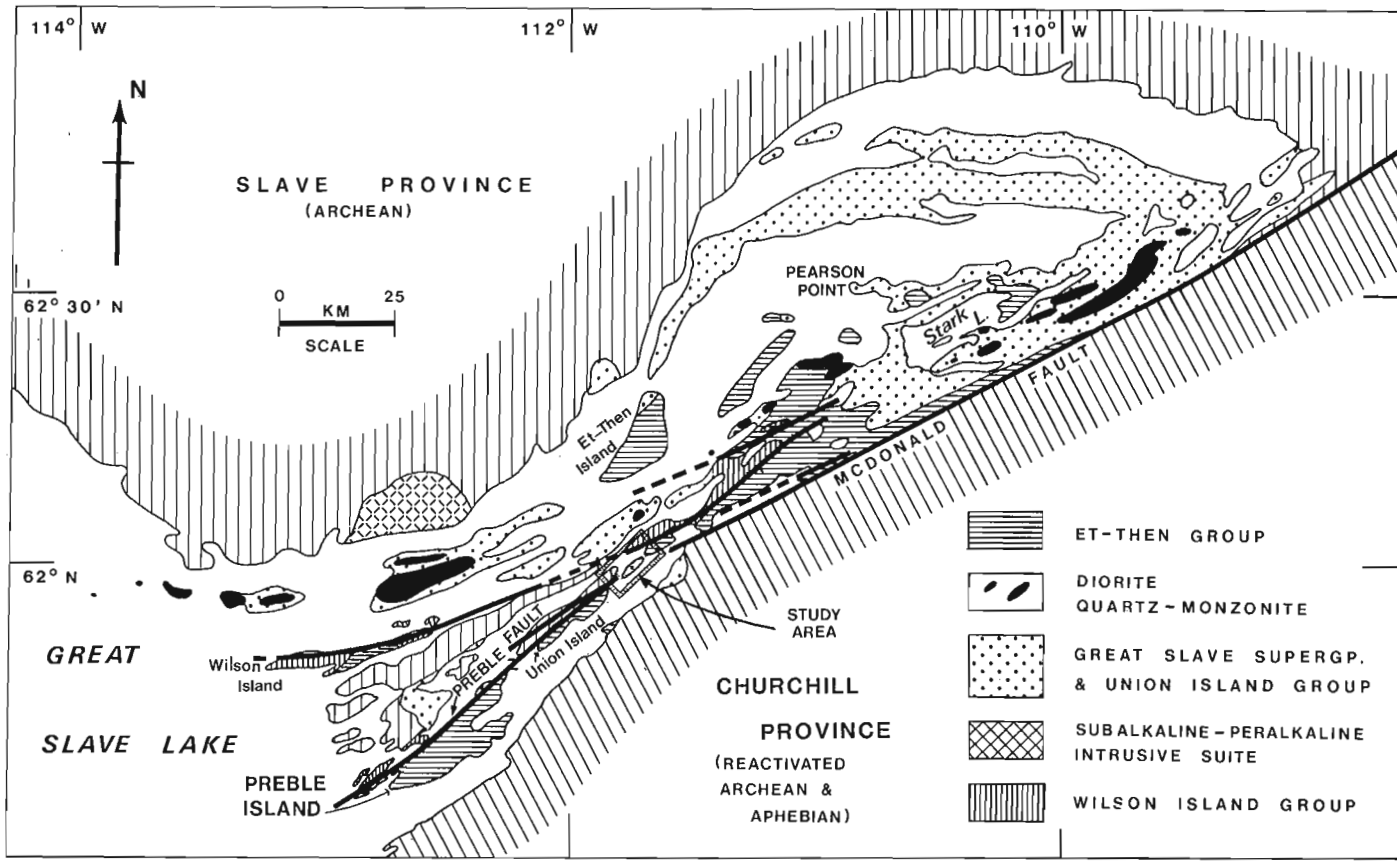

Figure 39.1. *Generalized geological map of the east arm of Great Slave Lake, District of Mackenzie.*

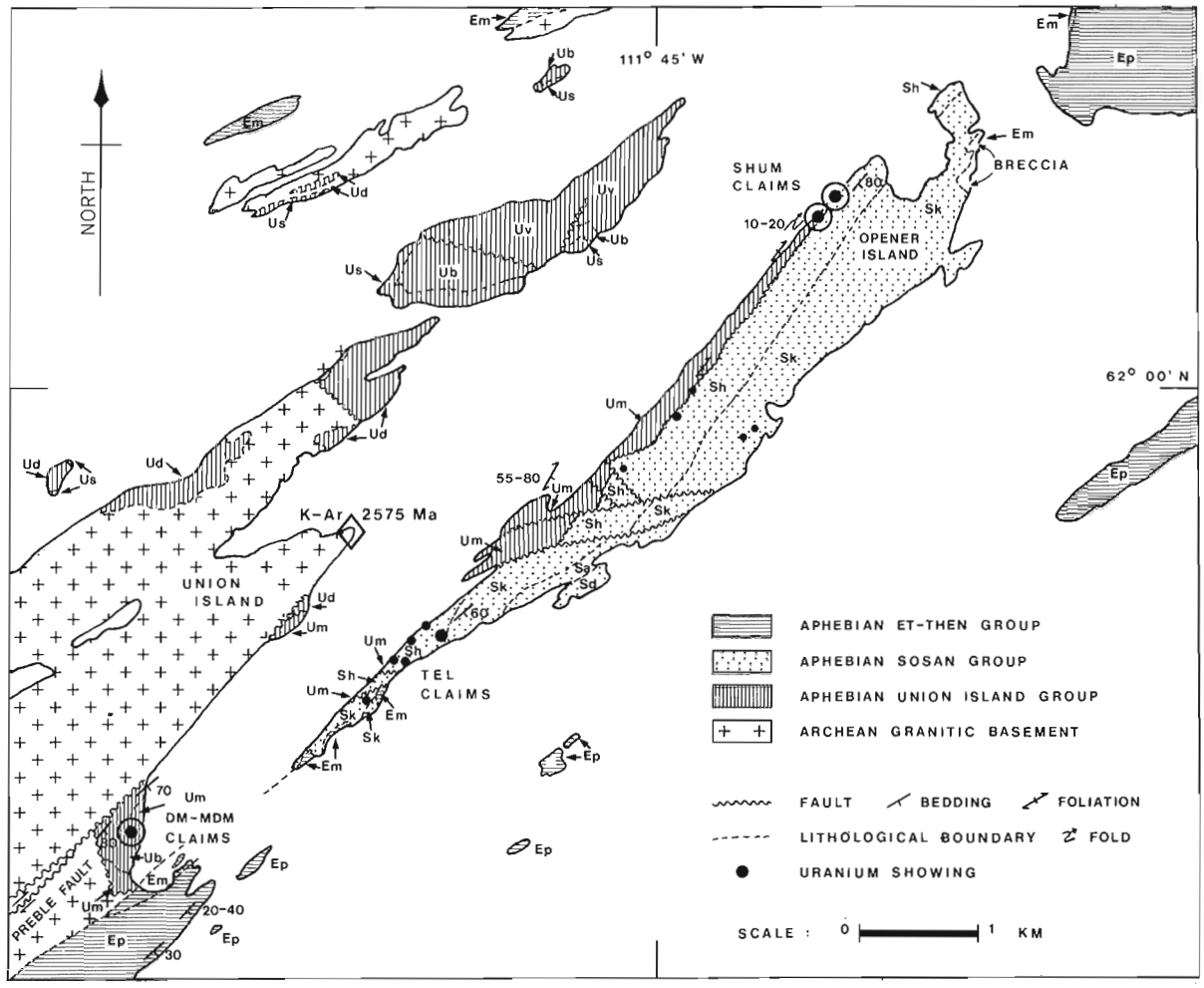

Figure 39.2. *Geology and uranium occurrences of the eastern part of Union Island and Opener Island, east arm of Great Slave Lake, District of Mackenzie.*

Union Island Group: Ud: lower dolomite, Us: black shale, Ub: upper dolomite, Um: laminated mudstone, Uv: basalt flows.

Sosan Group: Sh: Hornby Channel Fm., Sd: Duhamel Fm., Sk: Kluziai Fm., Sa: Akaitcho Fm.

Et-Then Group: Em: Murky Fm., Ep: Preble Fm.

(Modified after Hoffman, 1977, sheets 75E/13 and L/4).

source beds. The matrix of the breccia is red hematitic and sandy, like that of the fanglomerate of the Murky Formation. It is apparent that this type of breccia is a source of large cobbles in the fanglomerate of the Murky Formation.

Exploration History

The first uranium discoveries in the study area were made during 1967, on the DM-MDM claims on Union Island by prospectors P. D'Aoust and H. Miron, and on the TEL claims on Opener Island by E. Carmody, all of whom were prospecting under the Federal Government Prospectors Assistance Program (Thorpe, 1972, p. 15-18). The DM-MDM claims were explored by Northwest Explorers in 1967 and by Union Island Uranium Limited in 1968. The TEL claims were explored by Cominco Limited during the same period. The work included mapping and trenching, and two drill holes on the DM-MDM claims.

In 1978, Chevron Standard Limited discovered uranium showings on the SHUM claims on Opener Island, and in 1979 carried out mapping, ground geophysical surveys, extensive trenching and diamond drilling totalling 500 m in 4 holes. Also in 1979, Scurry-Rainbow Oil Limited, a subsidiary of Home Oil Limited, optioned the DM-MDM claims (restaked as the PD and Juniper claims) and staked additional claims on Union Island (Kelly, 1981). Following mapping and EM surveys in 1979 and 1980, the DM-MDM property was drilled in late 1980 and early 1981. A total of 1492 m was drilled in 10 holes.

Uranium Occurrences

DM-MDM claims

Pitchblende occurs in brecciated upper dolomite of the Union Island Group as irregular veins and fracture-linings and local high grade pockets. The dolomite is massive to thinly laminated and contains quartz, in places comprising up to 10 per cent of the rock, as thin siliceous laminae, suggestive of stromatolitic character at some places and as more abundant irregular veins and patches (Johnson, 1980, p. 9). Mineralization is exposed on the side of a south facing cliff. Assays from 3 trenches (Fig. 39.3), as determined

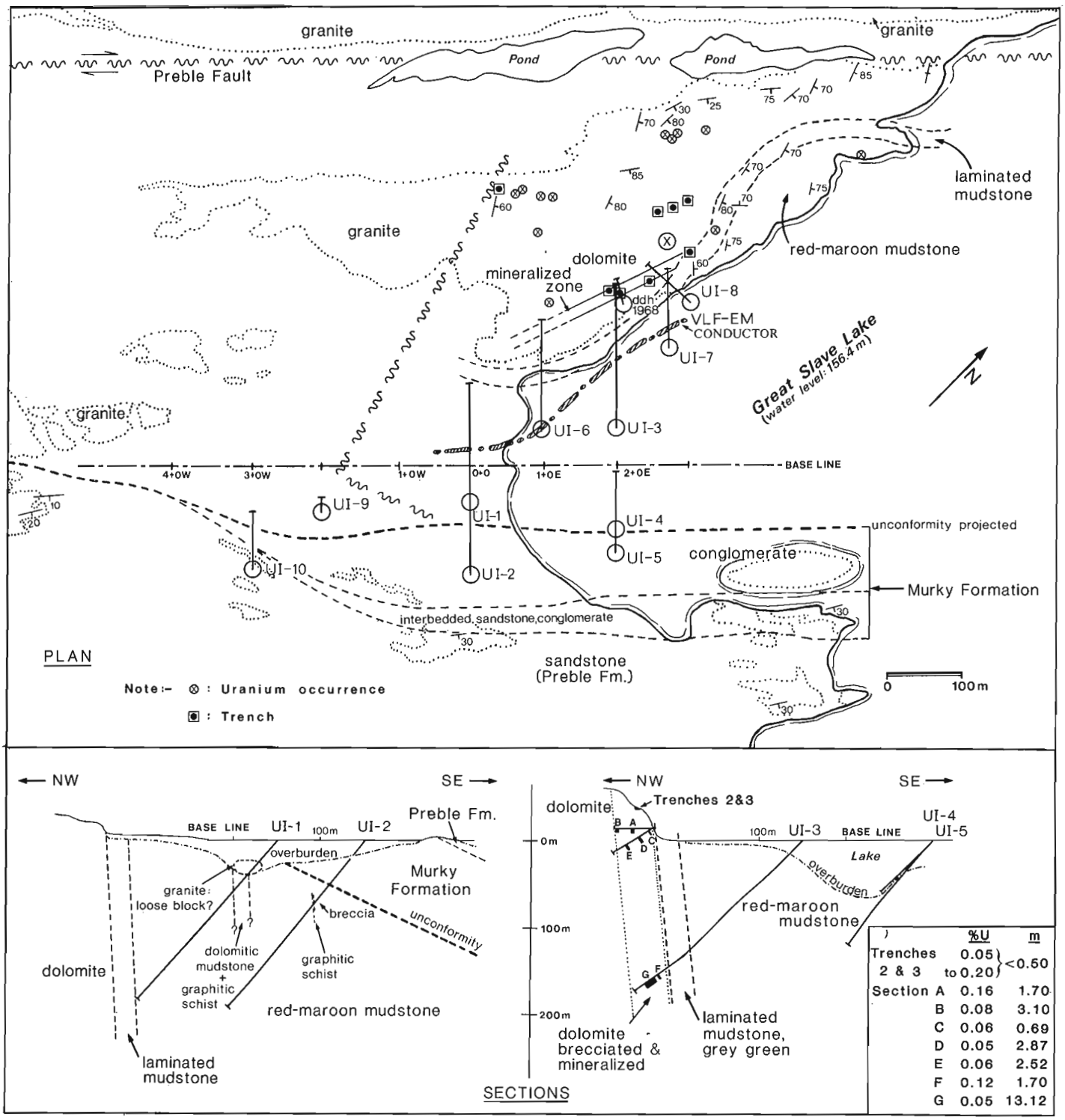

Figure 39.3. *Plan and sections of the DM-MDM claims uranium prospect, Union Island, east arm of Great Slave Lake, District of Mackenzie. (After unpublished surface geology maps by W. Johnson and J.A. Kelly, 1980, for Scurry-Rainbow Oil Limited; drill data from Kelly, 1981).*

radiometrically, ranged between 0.025 and 1.33 per cent U over sample widths of several centimetres to 2.4 m. However, chemical assays were much lower, none exceeding 0.17 per cent U (Taylor, 1968, 1969; Thorpe, 1972, p. 16). Two holes drilled in 1968 were collared at one spot on the cliff face below the trenches, and both of them intersected values as shown in a drill section (Fig. 39.3). Their location indicates irregular distribution of pitchblende veins. Below them, in hole no. UI-3 drilled during 1981 in the same section, a 13.12 m intersection averaging 0.05 per cent U included a 2.3 m length grading 0.095 per cent U (Kelly, 1981). The adjacent drillholes, UI-6 to the southwest and UI-8 to the northeast, interesected the dolomitic breccia, but encountered very weak radioactivity in breccia and in laminated mudstone at the contact with breccia, respectively. The pitchblende veins are thus distributed irregularly in a steeply dipping zone of brecciated dolomite approximately 150 m long, 40 m wide and over 200 m deep. The full extent of the zone is not known because the other seven drillholes did not reach its projected extensions. To the southwest, it may extend for 350 m from the trenches to a north-northwest trending fault that has brought the basement granite against the upper units of the Union Island Group. To the northeast it may follow the contact of upper dolomite with the laminated mudstone.

Northwest of the main zone, moderately to weakly anomalous radioactivity due to pitchblende-bearing fractures is encountered at several surface exposures of the brecciated or faulted upper dolomite and trenching has been done on some of them (Fig. 39.3; Johnson, 1980). These occurrences, however, are apparently much less significant than the main zone. A radiometric ground survey carried out using an exploranium GRS-101A scintillometer showed 75 to 90 counts per second over the dolomite area and 100 to 300 counts per second over the mudstone area. This led Johnson (1980) to suggest that the mudstones contain syngenetic uranium mineralization. These count levels, however, are normal for these lithologic units, and relatively higher counts in the mudstone reflect higher average contents of potassium and uranium, and do not indicate significant syngenetic uranium enrichment. Although the environment of a stagnant basin in which they were deposited (Hoffman et al., 1977, p. 120) is favourable for such syngenetic uranium mineralization, the graphite- and pyrite-bearing beds present in the mudstone unit, which are most likely to be enriched in uranium during deposition, do not show anomalously high radioactivity.

The drilling has defined a 25-m thick laminated mudstone, with grey and green laminae, stratigraphically above the dolomite unit, and this is overlain by a red to maroon coloured, rather massive mudstone unit with an apparent thickness of over 150 m. The true thickness is difficult to estimate because of minor folding as indicated by rapid variations in the core angle of the bedding. There are a few graphitic and dolomitic mudstone horizons in the red-maroon mudstone. A VLF-EM anomaly is located south of the main zone (Fig. 39.3), and is due to the graphitic layers. Drillholes UI-2 and UI-10 intersected the unconformity at the base of the Et-Then Group. In UI-2, some brecciation is seen in red mudstone for 1.5 m beneath the conglomerate of the group. The contact between them is obscure and appears gradational. In UI-10, the basement granite is overlain by 8 m of sandstone, which grades upwards into 21 m of interbedded conglomerate and sandstone, followed by 40 m of sandstone. The medium to coarse muscovite granite is highly oxidized for 8 m below the unconformity as indicated by red colouration. A red regolithic material, approximately 7 cm thick, is present at the unconformity. The sandstone immediately above is red with buff and white leached patches and specks that are kaolinitic.

The high grade samples from the trenches of the main zone contain pitchblende veinlets up to 2 mm thick, which irregularly cut across dolomite fragments and dolomite matrix. Calcite, quartz, and hematite are closely associated with pitchblende. Pyrite occurs locally as aggregates up to 2 cm wide in the trenches (Johnson, 1980, p. 13). Weathering has produced rusty surfaces, and secondary uranium minerals are seen on high grade parts of the pitchblende veins (Thorpe, 1972, p. 15-16). Bloy (1979, p. 21-24, 28-29) noted the ooloid or colloform nature of pitchblende in the samples he studied, and reported significant enrichment in V and Zn, moderate contents of Co and Ni, low contents of Mo, Be, Cu and Cr, traces of Ag, and variable Ba and TiO_2 (25037 ppm U, 4668 ppm Pb, 2740 ppm V and 29 ppm Zn in sample 45-4, and 85 ppm U, 204 ppm Pb, 50 ppm V and 50 ppm Zn in sample 45-3). In the mineralized section of hole UI-3, the writer recognized four types of veins: 1) graphitic veinlets and patches, 2) coarse carbonate veins with chalcopyrite, 3) veins rich in pyrite and galena, and 4) quartz veins with minor hematite. Cross-cutting relations show that vein types 2, 3 and 4 are in the order of older to younger in age. High radioactivity is closely associated with the quartz-hematite veins.

TEL Claims

Pitchblende veins occur along fractures in the Hornby Channel Formation of the Sosan Group, a predominantly massive, coarse arkose-pebbly arkose carrying quartz pebbles 2 to 10 cm in diameter. The formation includes heavy mineral concentrations in thin layers and lenses which are up to a few centimetres thick and a few metres long. They indicate that the formation strikes north-northeast and dips about 65° to the southeast. They are rich in hematized magnetite and show weak radioactivity due mainly to thorium.

The mineralized fractures are vertical or subvertical; the majority of them strike in a 325° to 340° direction, but some are at right angles to this. They are widely distributed over an area about 750 x 200 m. Individual fractures are anomalously radioactive for lengths of a few metres to a maximum of 20 m, but visible pitchblende occurs commonly only over lengths of less than a metre and over widths of less than a millimetre. Some fractures subsidiary to these are also mineralized. Seven trenches on clusters of veins with very high radioactivity yielded samples containing up to 0.18 per cent U over 73 cm and appreciable silver. The highest silver analysis reported was 1.86 oz/t Ag in a channel sample 30 cm long (Nichols, 1968; Thorpe, 1972). The samples were analyzed for gold, but no values greater than 0.01 oz/t were obtained. Rare visible pitchblende is intimately associated with hematite and rarely specularite. Secondary uranium minerals are present at some high grade spots. A characteristic feature associated with the radioactive veins or fracture-fillings is a zone of intense hematization of the host arkosic quartzite. The hematized zones range in width from a few centimetres to 3 m. Their boundaries are irregular but sharply defined against the buff-white host arkosic quartzite. A few anomalously radioactive localities away from the trenches are associated with rusty weathering, but no visible pyrite was observed by the writer. The arkosic quartzite is locally brecciated. The matrix of the breccia is hematitic and weakly radioactive.

One reported pitchblende vein is at the northern contact of the arkose of the Hornby Channel Formation with the green and red-purple phyllites of the Union Island Group (Nichols, 1968). Thorpe (1972, p. 17) reported that along the north edge of the island, brecciated red shale appears to be in fault contact with the arkosic quartzite. The uranium

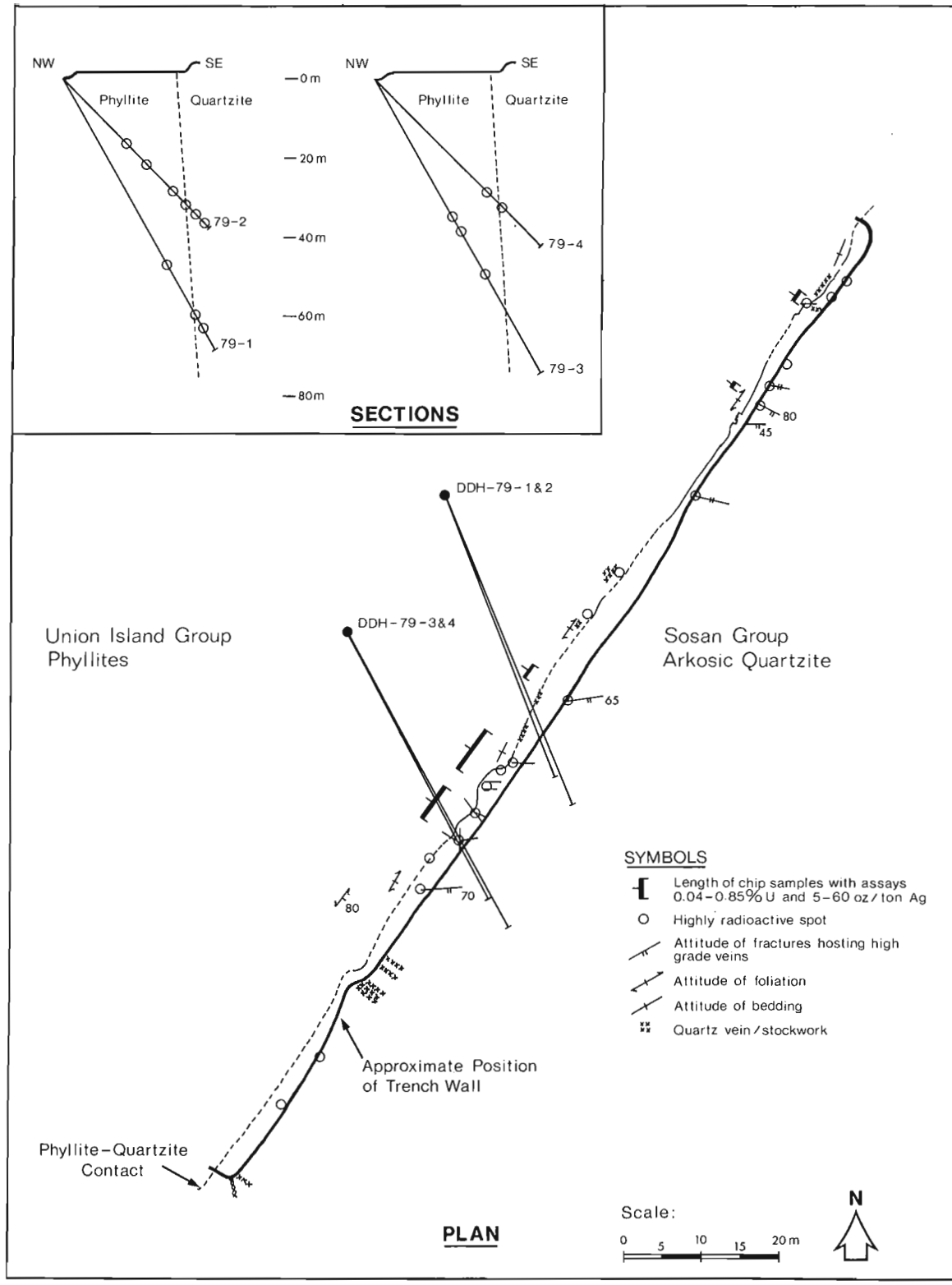

Figure 39.4. *Plan and sections of the main trench on SHUM claims, northeastern part of Opener Island, east arm of Great Slave Lake, District of Mackenzie (Modified after Walton, 1979).*

occurrence at the contact contains pitchblende and associated chalcopyrite. It is lens-shaped, approximately 60 cm wide by 120 cm long, and grades 0.118 per cent U.

SHUM Claims

Uranium mineralization is localized in steeply dipping fractures in arkosic quartzite of the Hornby Channel Formation at its north contact with the phyllites of the Union Island Group. The fractures trend at high angles to the sharply defined contact, and some of them extend for a few metres into the phyllite. Some mineralization occurs in the phyllites along these fractures, and in addition along fractures subparallel to and near the phyllite-quartzite contact.

The contact between the arkosic quartzite and phyllites is sharp and nearly vertical as observed at many localities along its 4 km length on Opener Island and from drill sections (Fig. 39.4), and is marked by a north-facing escarpment due to differential erosion of the phyllites. The mineralized fractures are most numerous at the northeast end of the island. They are well exposed in a 150 m long bulldozed trench that has a northwest facing wall 4 to 8 m high in the arkosic quartzite, and a level floor 10 to 30 m wide. The phyllite-quartzite contact is located within 0.5 to 5 m from the base of the wall (Fig. 39.4). Pitchblende veins in the quartzite are exposed in another trench situated approximately 150 m to the northeast along the contact. This trench is 75 m long, but here the contact is largely covered by arkosic quartzite blast debris on the ground sloping northeastwards to the shore. A few isolated pitchblende veins, present several hundred metres to the southwest, are similar to those found in the two trenches.

The individual fracture-fillings, like those on the TEL claims, are no more than a few metres long, but at some places the pitchblende veins are thicker and range up to 5 mm in width. At a few localities several fractures at low angles to each other are concentrated and here high grade pitchblende concentrations are observed and some secondary uranium minerals are present, as in the drilled zone shown in Figure 39.4. Channel samples from this zone yielded a few high U and Ag values, such as 0.65 per cent U, 217 oz/t Ag and 0.012 oz/t Au over a 1.2 m sample length, and 1 per cent U, 43 oz/t Ag and 0.086 oz/t Au over a 1 m sample length (Walton, 1979). High silver values were noted in some other samples. Gold content, on the other hand, is negligible in most of the samples. Green malachite stain is observed at a few highly radioactive veins in the second long trench to the east, but elsewhere copper appears to be scarce or absent. Drillholes encountered some radioactivity at depths of as much as 60 m vertically below the surface samples, but the assays were generally considerably lower than those of the surface samples (Walton, 1979).

Mineralogical studies, including microprobe analyses by energy dispersive spectra, were undertaken by the writer at the Geological Survey of Canada on two high grade grab samples provided by Chevron Standard Limited (Samples EA-80-2 and EA-81-1, located at the phyllite-quartzite contact near the surface projection of drillholes 79-3 and 4, Fig. 39.4). These showed the presence of the following minerals: Pitchblende, pyrite, chalcopyrite, galena, clausthalite (PbSe), glaucodot (Co,Fe)AsS and skutterudite ($CoAs_{2-3}$) (A.L. Littlejohn, personal communication, 1982). The skutterudite contains minor nickel and traces of silver. Silver occurs in the form of Ag-Hg amalgam, often mixed with small grains of clausthalite. Walton (1979, p.14) reported that a small sample of native silver from a high grade vein in the trench contained 600 ppm bismuth and 8 per cent mercury.

Hematite is commonly present in intimate association with pitchblende, as evident at the surface exposures. Locally, the hematization is intense. In phyllites, red colouration at highly radioactive veins is due to hematization related to mineralization rather than to the inherent colour of the phyllites, which are commonly green and grey in the northeastern part of Opener Island. In the arkosic quartzite, some hematized fractures cut massive quartz veins and are in turn cut by coarse crystalline vuggy quartz veins showing specularite encrustations on the quartz crystals, as observed by the writer at the southwest end of the 150 m long trench (Fig. 39.4).

The phyllites, including some calcareous beds and some pyritic and graphitic layers, show background radioactivity in the range of 25 to 110 counts per second, similar to that shown by the arkosic quartzite, according to the ground radiometric survey done with Saphymo Stel SPP2NF scintillometer held at waist level (Walton, 1979). Thus there is little evidence for syngenetic stratiform uranium mineralization. The writer's observations made with a McPhar TV-1 scintillometer are in agreement with the survey results. Pyrite and graphite are present in drill core as disseminations but no significant amount of uranium is associated with them.

U-Pb Isotopic Studies

Isotopic analyses of three trench samples, one from the DM-MDM property and two from the drilled zone of the SHUM property, are given in Table 39.1. They show considerable discordance on a concordia plot (Fig. 39.5), due to either Pb loss or U gain. The three points however lie close to a straight line which intersects the concordia curve at its upper end at 1605 Ma. This relationship could be interpreted as indicating an initial period of mineralization approximately 1605 Ma ago, followed by an episodic loss of radioactive decay products at approximately 100 Ma ago as indicated by the lower intercept. The isotopic history however, is probably much more complex than suggested by this simple interpretation. The open structures in which the mineralization is localized are also readily available channels for circulation of meteoric waters that may have affected the mineralization unevenly through the ages. Thus more data points would likely show a greater scatter. The 1605 Ma date, however, may be regarded as the minimum age for the initial mineralization.

Origin of Pitchblende Veins

For the veins in the study area, a supergene origin at the time of deposition of the Et-Then Group is postulated here. This is similar to the hypothesis proposed by Langford (1977, 1978) for the deposits in Saskatchewan and elsewhere, and that proposed by Walton (1979) and Kelly (1981) for the veins in the study area. Such an interpretation is supported by the following observations.

1. The mineral assemblage of the veins, in particular the presence of colloform pitchblende, selenide, silver and other minerals, indicates a low temperature of deposition.
2. The proximity to the unconformity at the base of the Late Aphebian Et-Then Group, which most probably covered the mineralized zone at one time.
3. The presence of open fractures in folded and faulted, but little metamorphosed, Aphebian sedimentary rocks below the unconformity.
4. The fluvial clastic and highly oxidized character of the Et-Then Group, indicating environments favourable for mobilization of uranium from source rocks and its transportation by circulating meteoric waters.

Table 39.1

U-Pb isotopic analyses of 3 pitchblende samples from the Union Island-Opener Island area, east arm of Great Slave Lake

Sample numbers	Location	Sample Weight mgm.	U Weight per cent	Pb weight per cent	Common Pb per cent	Pb isotopic ratios			$\frac{^{206}Pb}{^{238}U}$	$\frac{^{207}Pb}{^{235}U}$	Age in million years		
						$\frac{^{207}Pb}{^{206}Pb}$	$\frac{^{208}Pb}{^{206}Pb}$	$\frac{^{204}Pb}{^{206}Pb}$			$\frac{^{206}Pb}{^{238}U}$	$\frac{^{207}Pb}{^{235}U}$	$\frac{^{207}Pb}{^{206}Pb}$
Chevron 1	SHUM claims 1050 S on Base line	0.08	97.71	2.758	4.03	0.0810549	0.0321182	0.0006369	0.02916	0.2892	185.3	258.0	984.2
Chevron 2	SHUM claims 1050 S on Base line	0.96	24.44	1.444	14.16	0.1061272	0.1261855	0.0024825	0.05326	0.5179	334.5	423.5	943.8
Bloy-45-4	DM-MDM claims		2.5037	0.4668		0.09841			0.1956	2.6546	1152	1316	1590

Notes: Analyses of samples Chevron 1 and 2 by Geospec Consultants Limited, Edmonton, Alberta, for Chevron Standard Limited, Vancouver, British Columbia (Walton, 1979, p. 13-14).

Analyses of sample Bloy-45-4 from Bloy, 1979, p. 28 and p. 43.

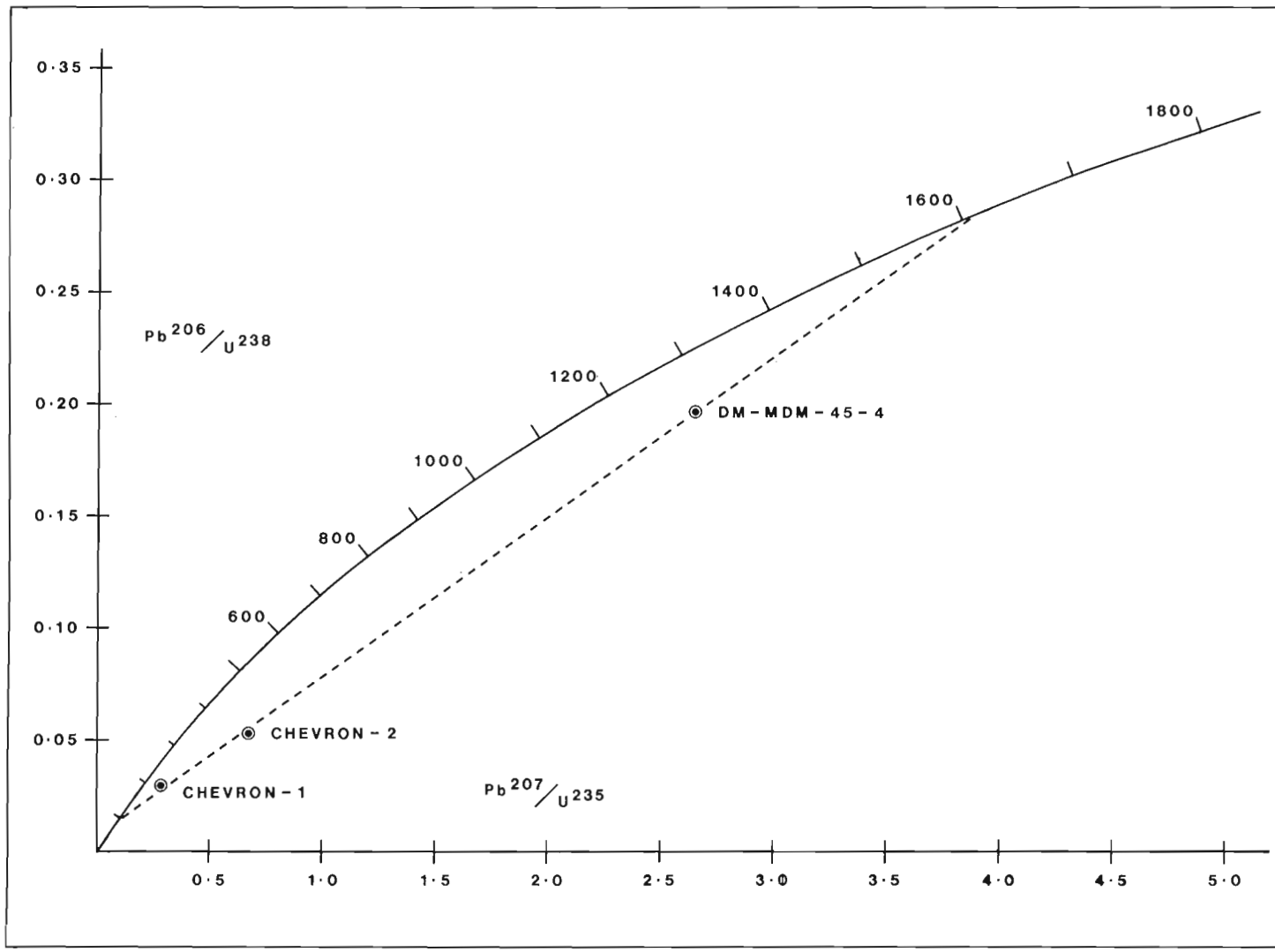

Figure 39.5. *Concordia plot of pitchblendes from the Union and Opener islands, east arm of Great Slave Lake, District of Mackenzie (Table 39.1).*

5. The presence of shale beds below the Et-Then Group – including some pyritic and carbonaceous horizons – in the vicinity of the veins, providing reducing environments favourable for precipitation of uranium.
6. The probable Late Aphebian age of mineralization suggested by the isotopic dates on pitchblende.
7. The lack of evidence for magmatic or metamorphic hydrothermal sources, as no intrusions cut the host rocks in the vicinity of the veins, and metamorphic grade of the host rocks is very low.

The distribution of the fracture controlled veins along a zone 8 km long would be difficult to reconcile from a localized hydrothermal source. A possibility exists, however, that the mudstones of the Union Island Group may have been enriched in uranium at the time of deposition, and that the uranium migrated to the fractures during deformation. There is, on the other hand, no field evidence for a significant syngenetic enrichment of uranium in the mudstones, and it is unlikely that evidence for such enrichment would be destroyed by subsequent deformation. The sulphide-rich and graphitic beds, which are most likely to be enriched in uranium, also show radioactivity at the background level of the mudstones, except at several spots in surface exposures and drill core, where anomalously high radioactivity is probably due to a later epigenetic mineralizing episode rather than to syngenetic concentration of uranium. If the rocks were initially enriched in uranium, and the metal was remobilized during deformation, it would likely be reprecipitated locally due to the reducing effect of sulphides and graphite, and the highest concentrations would be expected to occur in the source beds. This is not the case for the prospects described. It is possible that mudstones may have contributed some uranium to the oxidizing meteoric waters, as visualized in the supergene hypothesis, but they are more likely to have provided a barrier to circulation of the waters and a chemical environment that led to precipitation of uranium from the waters at the contact with the arkosic quartzite. Another possible source of uranium is the Sosan Group sandstones which host small occurrences elsewhere in the east arm of the Great Slave Lake. The occurrences were interpreted by Morton (1974) to have formed during burial metamorphism, with uranium derived from the heavy minerals in sandstones. Walker (1977), however, favoured a supergene deposition for some of these occurrences located on Simpson Islands north of Preble Fault, and postulated their formation at the time of sub-Et-Then Group unconformity. In any case, the supergene process postulated here does not require a concentrated source of uranium, and some rocks with normal uranium contents e.g. the basement granite, are adequate sources. The critical factor is a highly oxidizing environment to mobilize uranium in surface waters, and intense oxidation observed in the Et-Then Group and in granite at its base, is an evidence for such an environment. It may be noted that Walton (1979) suggested the possibility of a separate stage of silver-mercury mineralization. More mineralogical studies, however, are needed to establish a paragenetic sequence.

The above interpretation of the origin of the pitchblende veins has an important bearing on the exploration potential and evaluation of uranium resources not only of the study area, but also the whole area of the east arm of Great Slave Lake, viz. the Et-Then basin. The Et-Then Group probably covered a larger part of east arm of Great Slave Lake area than its present exposures (Fig. 39.1) which are commonly fault bounded. Uranium deposits, if present at its base, would be preserved in the down-faulted blocks. In the adjacent upthrown blocks, erosion has probably partly or wholly removed any deposit that may have formed at the unconformity. The veins in the study area may thus represent only the roots of pre-existing larger deposits or they may extend for a considerable depth. Further exploration in the area is therefore warranted, not only for uranium but also for silver, which may be associated with uranium or may occur in deposits containing little or no uranium.

Conclusions

Pitchblende deposition in the Aphebian sedimentary rocks of the study area was controlled by fractures that are subsidiary to major faults and close to the unconformity with an overlying late Aphebian redbed clastic sequence. A supergene model for concentration of uranium and associated silver and selenium, at the time of deposition of the sequence, is favoured, and provides encouragement and guides for further exploration.

Acknowledgments

The writer is thankful to Chevron Standard Limited and Scurry-Rainbow Oil Limited for permission to present unpublished exploration data incorporated in this paper. He also extends thanks to exploration staff of the companies for their help and guidance in his field work in the study area during 1978, 1980 and 1982, in particular J.A. Kelly, M. Trapnell, and D. Dole of Scurry-Rainbow Oil Limited, consulting geologists W. Johnson and M. Senkiew working for the company in 1978, and H.H. Wober and G.J. Walton of Chevron Standard Limited. The writer also benefitted during fieldwork in the east arm of Great Slave Lake from contact with S.M. Roscoe of the Geological Survey of Canada, and K. Kwan of SERU Nucléaire Canada Limited. R. Stevenson assisted the writer in fieldwork during 1982. The paper was critically read by S.M. Roscoe and R.I. Thorpe of the Geological Survey of Canada.

The writer benefitted considerably from discussions with the persons named above, but the responsibility for the opinions and ideas expressed in this paper are the writer's own.

References

Bloy, G. R.
1979: U-Pb geochronology of uranium mineralization in the east arm of Great Slave Lake, N.W.T.; unpublished M.Sc. thesis, University of Alberta, Edmonton, Alberta, 64 p.

Gandhi, S.S. and Loveridge, W.D.
1982: A Rb-Sr study of the Et-Then Group basalts, Great Slave Lake, District of Mackenzie; in Rb-Sr and U-Pb Isotopic Age Studies, Report 5; in Current Research, Part C, Geological Survey of Canada, Paper 82-1C, p. 155-160.

Hoffman, P.F.
1968: Stratigraphy of the lower Proterozoic (Aphebian) Great Slave Supergroup, East Arm of Great Slave Lake, District of Mackenzie; Geological Survey of Canada, Paper 68-42, 93 p.

1969: Proterozoic paleocurrents and depositional history of the East Arm fold belt, Great Slave Lake, Northwest Territories; Canadian Journal of Earth Sciences, v. 6, no. 3, p. 441-462.

1977: Preliminary geology of Proterozoic formations in the East Arm of Great Slave Lake, District of Mackenzie; Geological Survey of Canada, Open File 475 – Sheets A to L, scale 1:50 000.

Hoffman, P.F., Dewey, J.F., and Burke K.
1974: Aulacogens and their genetic relation to geosynclines, with a Proterozoic example from Great Slave Lake, Canada; in Modern and Ancient Geosynclinal Sedimentation, ed. R.H. Dott, Jr. and R.H. Shaver; Society of Economic Paleontologists and Mineralogists, Special Publication 19, p. 38-55.

Hoffman, P.F., Bell, I.R., Hildebrand, R.S., and Thorstad, L.
1977: Geology of the Athapuscow Aulacogen, East Arm of Great Slave Lake, District of Mackenzie; in Report of Activities, Part A, Geological Survey of Canada, Paper 77-1A, p. 117-129.

Johnson, W.
1980: Geological mapping, geochemical and scintillometer surveys on the PD, Juniper, Tim, Dief and Chief claims, 75 E-13, 111°51'W, 61°57'N; Target Exploration Services Ltd. unpublished report to Scurry-Rainbow Oil Ltd., 23 p.

Kelly, J.A.
1981: Report on the diamond drilling programme, Union Island uranium project: PD-1, PD-2, Juniper, Tim, Mike, Steve, Haf, Dief & Chief Claims, N.T.S. sheet 75-E-13, East Arm Area, Mackenzie Mining District, Northwest Territories; Scurry-Rainbow Oil Limited; Assessment Files, Document No. 081318, Department of Indian and Northern Affairs, Ottawa, 7 p.

Langford, F.F.
1977: Surficial origin of North American pitchblende and related uranium deposits; American Association of Petroleum Geologists Bulletin, v. 61, no. 1, p. 28-42.

1978: Origin of unconformity-type pitchblende deposits in the Athabasca Basin of Saskatchewan; in Uranium Deposits: their Mineralogy and Origin, ed. M.M. Kimberly, Short Course, Mineralogical Association of Canada, University of Toronto, p. 485-499.

Lowdon, J.A., Stockwell, C.H., Tipper, H.W., and Wanless R.K.
1963: Age determinations and geological studies: Geological Survey of Canada, Paper 62-17, 140 p.

Morton, R.D.
1974: Sandstone-type uranium deposits in Proterozoic strata of northwestern Canada; in Formation of Uranium Ore Deposits, International Atomic Energy Agency, Vienna, Ser. No. STI/PUB/374, p. 255-273.

Nichols, R.F.
1968: Report on a geological and radiometric survey done by Cominco Limited on the TEL claims owned by Rudy Steiner, northeast of Union Island in the east arm of Great Slave Lake; Assessment Report No. N018779 (NTS 075E/NW), Department of Indian and Northern Affairs, Ottawa.

Reinhardt, E.W.
1969: Geology of the Precambrian rocks of Thubun Lakes map-area in relationship to the McDonald Fault system, District of Mackenzie; Geological Survey of Canada, Paper 69-21, 29 p.

1972: Occurrence of exotic breccias in the Petitot Islands and Wilson island map-areas, East Arm of Great Slave Lake, District of Mackenzie; Geological Survey of Canada, Paper 72-25, 43 p.

Stockwell, C.H.
1932: Great Slave Lake – Coppermine River area, Northwest Territories, Geological Survey of Canada, Summary Report 1932, Part C, p. 37-63.

1936a: Eastern portion of Great Slave Lake (west half); Geological Survey of Canada, Map 377A (with marginal notes).

1936b: Eastern portion of Great Slave Lake (east half); Geological Survey of Canada, Map 378A (with marginal notes).

Taylor, R.S.
1968: Report on ground radiometric survey, DM-MDM claim groups, Union island, east arm of Great Slave Lake; Assessment Files Document No. N 018780, Department of Indian and Northern Affairs, Ottawa.

1969: Report on geology, trenching, drilling and radiometric survey, DM-MDM-DML claim groups, Union Island, east arm of Great Slave Lake, Assessment Files Document No. N 019974, Department of Indian and Northern Affairs, Ottawa.

Thorpe, R.I.
1972: Mineral exploration and mining activities, mainland Northwest Territories, 1966 to 1968; Geological Survey of Canada Paper 70-70, 204 p.

Walker, R.R.
1977: Geology and uranium deposits of Proterozoic rocks, Simpson Islands, Northwest Territories; unpublished M.Sc. thesis, University of Alberta, Edmonton, 193 p.

Walton, G.J.
1979: East Arm Report: Property – Opener Island; Unpublished Report to Chevron Standard Limited, Vancouver, 17 p.

40.

SHIPAC: A SOFTWARE PACKAGE FOR THE SHIPBOARD PROCESSING OF MARINE GEOPHYSICAL SURVEY DATA

Project 730081

Ron Macnab
Atlantic Geoscience Centre, Dartmouth

Macnab, R., SHIPAC: a software package for the shipboard processing of marine geophysical survey data; in Current Research, Part B, Geological Survey of Canada, Paper 83-1B, p. 327-330, 1983.

Abstract

SHIPAC has been developed as part of an effort to rationalize computer procedures for the handling and management of navigational, bathymetric, and potential fields data collected on multiparameter surveys. The package is interactive and highly modularized, consisting of nearly 14 000 lines of FORTRAN code in over 50 programs and subprograms. The main product of these programs is a set of digital files containing clean data that are ready for further processing ashore after cruise end. The package executes on HP1000 minicomputers, and has been used on two major survey operations to date.

Résumé

SHIPAC a été mis au point afin de rationaliser les procédures informatisées utilisées pour la manipulation et la gestion des données de navigation, de bathymétrie et de champs potentiels prélevées lors d'études à paramètres multiples. Il s'agit d'un ensemble interactif et très modularisé de près de 14 000 lignes de code FORTRAN dans plus de 50 programmes et sous-programmes. Le produit principal de ces programmes est une série de fichiers numériques contenant des données nettoyées, prêtes à être traitées davantage sur terre à la fin de la croisière. SHIPAC s'exécute sur des miniordinateurs HP1000 et a déjà été utilisé au cours de deux projets de levés importants.

Introduction

As part of the East Coast multiparameter mapping project (Macnab, 1983), a major effort is underway to rationalize and to restructure procedures for handling and managing digital survey data. These data are collected on a round-the-clock basis by ships executing a pattern of well controlled survey lines, and consist of: navigation (latitude, longitude, course, speed, and Eotvos correction), bathymetry, gravity, and total field magnetics.

Fundamental to this process of rationalization is the recognition that survey data are handled and managed in two distinct stages. The first stage involves processing in the field, where shipboard minicomputers are used to detect and to correct errors in the data, to convert raw instrument output to meaningful physical parameters, to display data in preliminary form, and to archive data files for later processing ashore. Under ideal conditions, these shipboard operations should be completed within twenty-four hours of data acquisition.

The second stage involves processing back in the laboratory, where the cruise data set may be further corrected prior to merging with pre-existing data sets in a master data base. Data may then be subjected to an adjustment process that is designed to achieve good agreement between all cruise data sets in the data base. This second stage can take much longer to complete, and in fact can go on as long as new cruise sets are being added to the data base.

Reflecting these two stages of operations, the restructuring of our data handling and management procedures is taking place in two phases that are concerned, respectively, with ship and shore processes. The aim in both phases is to end up with sets of procedures and computer software that will ensure the accuracy and integrity of the data, and to do so in a manner that makes efficient use of human and computer resources. Especially important is the need for an overall strategy that will integrate ship and shore procedures in order to promote a smooth transfer of data and data processing functions from field to laboratory environments.

Over the past two years, there has been progress in both phases of this rationalization. Phase one, the restructuring of shipboard procedures and software, has been essentially completed in the form of a package known as SHIPAC. It is the subject of the remainder of this report. Phase two, the restructuring of shore procedures for post-processing, merging, adjustment, and archival/retrieval, has begun.

System Concept

The main purpose of processing multiparameter survey data in the field is to prepare a cruise data set that is free of errors and ready for further manipulation and interpretation after the cruise is over.

To meet this objective, the SHIPAC system has been designed as a collection of programs, file structures, and data manipulation protocols that handle, edit, merge, and process the various types of digital survey data. Central to the concept is the provision for performing various operations, such as display and edit, on specific subsets of the data without affecting related data sets that are coresident in the system. These operations can be performed once, or as many times as necessary on a given data set until the data are in a desired condition.

The ability to process iteratively has been facilitated through the implementation of modular and specialized programs that operate on restricted portions of the data. Thus an operator can repeat a procedure over and over on a specific data subset with different input parameters, until he is satisfied with the results.

A modular approach also caters to the inevitable demand for software modification and expansion. It is usually easier to change and to maintain a small program than a big one, and the compartmentalization of processes that characterizes SHIPAC software is expected to minimize the impact of program changes.

All SHIPAC procedures are carried out with a high degree of user interaction, e.g. the operator has immediate control over what is being done, and can view the outcome of

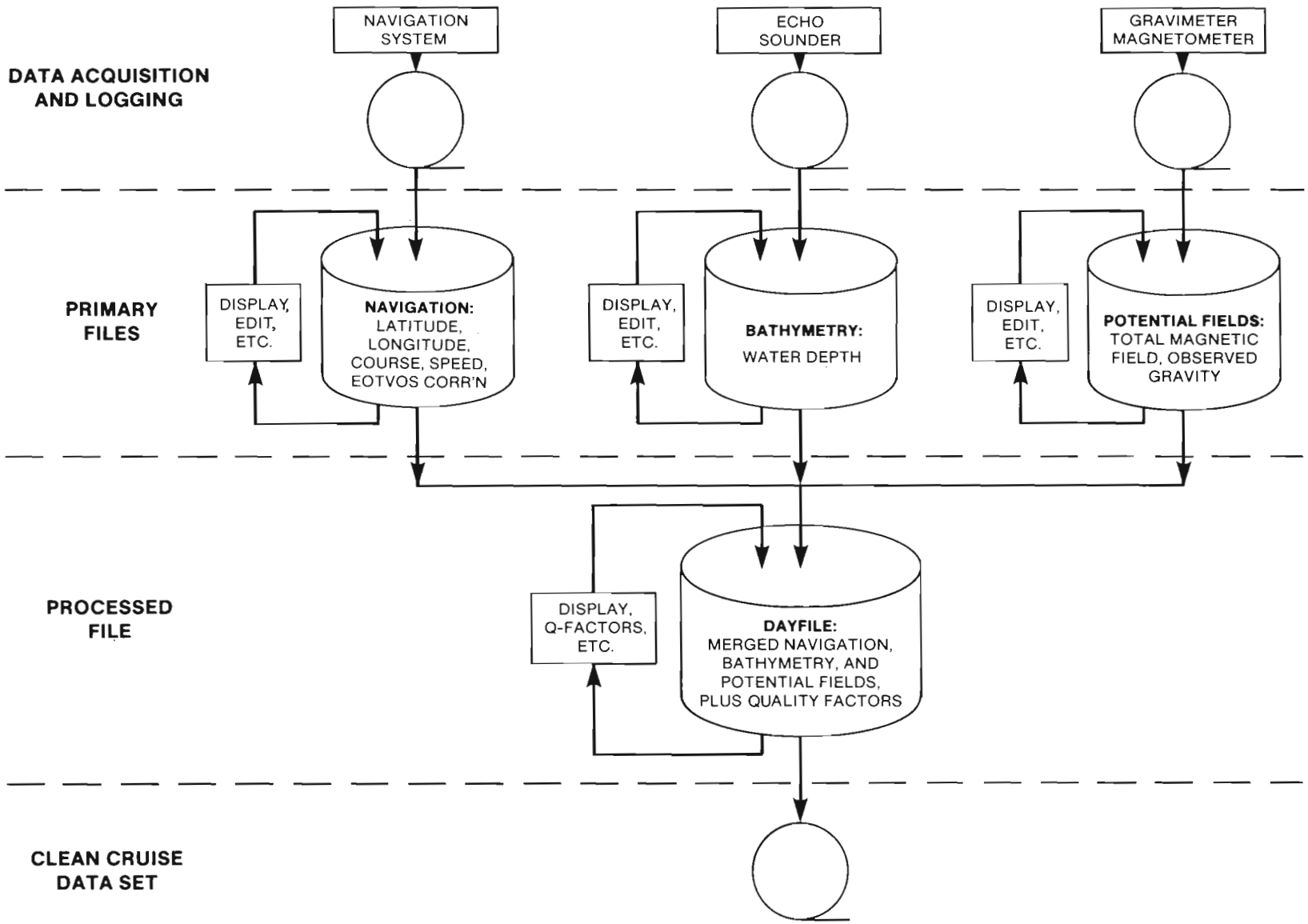

Figure 40.1. *Block diagram illustrating the general flow of marine geophysical survey data through the SHIPAC processing package.*

a particular process at any time. To this end, the package makes heavy use of graphics CRT terminals, so that an operator can see immediately how the data are affected by different actions.

A typical session with SHIPAC consists largely of a dialogue where the computer asks questions and the operator supplies answers. Blunder-induced errors are eliminated to a certain degree through comprehensive checking of operator input for reasonable answers. Wherever possible, a standard dialogue format and standard error messages are used, so that operators do not have to cope with a great diversity of styles.

System utilities, which are general-purpose programs that handle a range of common tasks such as editing, file management, and input-output, complement the SHIPAC software. For the most part, these utilities are supplied by the computer manufacturer; they tend to be reliable and well documented. Using this software which is readily avilable not only eliminates the need to develop it locally, but also reduces the amount of training required for operators who have learned to use the same utilities while engaged in other kinds of data processing tasks.

Programs and Data Organization

At present, SHIPAC software consists of over 50 programs and subprograms with an aggregate of nearly 14 000 lines of FORTRAN code. Four to six person-months were required to develop most of this code, with nearly all the work done at sea.

For the most part, SHIPAC routines perform specific operations on data stored in three different types of disc files: primary, processed, and auxiliary. Figure 40.1 illustrates the general flow of data. Initially, separate measuring and logging systems record the primary data on 9-track magnetic tapes, which are the main input media for shipboard processing.

Primary and processed files each contain one day's worth of data stored in 1440 one-minute records. In addition to data records, the files contain header records that hold file identification information, time stamps that log execution dates and times of various operations, operator comments, and miscellaneous constants.

There are three primary files associated with each day, for the separate storage of the three classes of survey data: navigation, bathymetry, and potential fields (gravity and magnetics). These files are ASCII-coded and sequentially accessible to permit the use of standard system utilities for edit, display and simple manipulation. All verity/edit procedures are performed on the data while they are still in the primary files.

There is one processed file per day. It is binary coded and randomly accessible, to achieve data compaction and efficiency of storage/retrieval. The processed file serves as a "collector file" for merging data from the three primary files. This facilitates the collective handling of daily data, and simplifies further combinations. For instance, the Bouguer gravity anomaly is not stored per se in the processed file, but can be easily derived from information that has been transferred into that file from the three primary files: observed gravity, Eotvos correction, position-dependent theoretical gravity, and depth-dependent density correction. In this case, subsequent discovery of an error, say in navigation, will necessitate corrective action only in the primary navigation file; the bathymetry and potential fields files will remain unaffected.

An important cofunction of the processed file is to store codes that describe data quality: a quality factor code is assigned to each data type for every minute of the day, based on an operator assessment of measurement conditions and instrument performance. The assignment of quality factor codes is the last operation affecting the processed file, other than backup to magnetic tape. Also, it is the only procedure that permits an operator to modify the contents of the processed file directly through keyboard action.

Auxiliary files contain information used by SHIPAC to operate on certain kinds of data. Typically, they contain information such as gravimeter calibration constants, or coefficients for calculating the reference magnetic field.

Output Products

SHIPAC output consists of a variety of plots, listings, notes, and digital files. Profile plots and listings are produced routinely as part of the daily display/edit cycle. The plots are generally of the small-format X-Y variety, and show data versus time in order to facilitate the detection of spikes and other abnormalities.

All plots and listings are annotated and inserted in a processing logbook, which also contains daily operator notes that chronicle the occurrence of problems, unusual features, etc., and the corrective steps that have been taken where applicable. The processing logbook therefore serves as a valuable document for tracing the history of operations on the cruise data set.

Large-format geographic displays of multiparameter survey data have been produced on a trial basis by a companion package produced by USGS workers at Woods Hole: MAPGEN (Evenden, 1982). This collection of programs reads SHIPAC files for the production of annotated ship's track plots and data plots at a variety of scales and projections, complete with detailed coastlines. Some specialized software, mainly in the line of data reformatting, will be necessary before the full range of MAPGEN's graphics capabilities is available to us.

The most important SHIPAC product, of course, is the digital data itself, in the form of magnetic tape files that are ready for post-cruise processing. These files hold the entire cruise data set. This includes not only raw and processed data, but also constants used in the shipboard processing, and quality factor codes that give some preliminary assessment of how good, or how poor, the data are.

Operating Environment and Documentation

SHIPAC runs on Hewlett-Packard model 1000 (HP1000) minicomputers executing under the control of the RTE-4B operating system. This is a standard, supported installation at the Bedford Institute of Oceanography, both ashore and in the ships that are based there. The same kind of installation also supports other important functions and packages that are closely allied to SHIPAC, such as real-time navigation, bathymetric processing by the Canadian Hydrographic service, and MAPGEN graphics.

To execute SHIPAC, a minimal HP1000 configuration must include the following: 256 kilobytes of user-addressable memory, 8 to 10 megabytes of dedicated disc storage, magnetic tape tansports, a graphics CRT terminal, and a hard-copy graphics device. Loading of the package on an HP1000 installation is simplified through the use of comprehensive procedure files that automatically handle the relocating and linking of all routines.

System documentation consists of a two volume manual and numerous comment lines embedded in the source code (typically, comment lines comprise 30 to 40 per cent of the source code in all SHIPAC routines). Documentation is organized in two levels: one for operators who just want to use the package, the other for programmers who want to modify existing code or to develop new routines. In addition to a conventional version in printed form, the complete manual is maintained in digital form for easy updating and printing.

Applications and Other Developments

SHIPAC has been used as a primary processing package on two major survey cruises to date. On both cruises, the entire responsibility for the package was assumed by operators after a hands-on training period lasting two weeks.

SHIPAC will continue to evolve with the development of software for:

a. handling output from a third gravimeter (AGC's new model KSS-30);

b. improved processing of navigation data to yield better Eotvos corrections;

c. improving the interface to the Hydrographic Service's bathymetric processing system;

d. automatically detecting and tabulating track crossovers in order to determine the internal consistency of a given cruise data set;

e. reformatting data preparatory to MAPGEN geographic display.

Acknowledgments

I am indebted to Julian Goodyear and Mike Hughes for helpful comments and feedback while operating SHIPAC software at sea. Steve Grant, John Halpenny, and Dave Halliday contributed ideas and codes for handling navigation data, LaCoste and Romberg gravimeter output, and crossover checks. Keh-Gong Shih and Ford Doherty devised procedures and software for the more efficient calculation of magnetic anomalies. Herman Varma and Paul Conrad installed the MAPGEN package for evaluation, and developed software drivers for additional graphics devices.

References

Evenden, G.I.
1982: MAPGEN: An interactive, flexible, expandable software system for generation of publication-quality maps; First Annual Conference on the Management, Analysis, and Display of Geoscience Data, Mathematical Geologists of the United States, Golden, Colorado.

Macnab, R.F.
1983: Multiparameter mapping off the east coast of Canada; in Current Research Part A, Geological Survey of Canada, Paper 83-1A, p. 163-171.

41.

CANADIAN EAST COAST MULTIPARAMETER SURVEYS, 1982

Projects 730081, 730072, and 800036

Robert O. Miller, Ron Macnab, C.L. Amos, and Gordon B. Fader
Atlantic Geoscience Centre, Dartmouth

Miller, R.O., Macnab, R., Amos, C.L., and Fader, G.B., Canadian East Coast multiparameter surveys, 1982; in Current Research, Part B, Geological Survey of Canada, Paper 83-1B, p. 331-334, 1983

Abstract

Preliminary results are presented from a multiparameter integrated geophysical cruise with collaboration among the Canadian Hydrographic Service, the Gravity, Geothermics and Geodynamics Division of the Earth Physics Branch and the Atlantic Geoscience Centre of the Geological Survey of Canada. This cruise obtained data from the continental shelf, slope and rise off southwestern Nova Scotia and Georges Bank, the outer continental shelf around Sable Island and the Grand Banks of Newfoundland. Interpretation of the data from the Sable Island area indicates the presence of sand ribbons, megaripples and sand ridges. Numerous areas of shell deposits occur across the study area from Sable Island Bank to the Grand Banks of Newfoundland. Thick deposits of glacial till and glaciomarine sediments provide evidence for the extension of glacial ice across the Grand Banks of Newfoundland.

Résumé

Les auteurs présentent les résultats préliminaires d'une croisière géophysique intégrée à paramètres multiples entreprise en collaboration avec le Service hydrographique canadien (PO) et les divisions de la gravité, de la géothermique et de la géodynamique de la Direction de la physique du globe (EMR). Des données ont été prélevées sur le plateau et le talus continentaux et la pente océanique au large de la côte sud-ouest de la Nouvelle-Écosse et du banc Georges et sur le plateau continental extérieur autour de l'île de Sable et des Grands Bancs de Terre-Neuve. L'interprétation des données provenant de la région de l'île de Sable indique la présence de rubans de sable, de mégarides et de crêtes de sable. La région à l'étude comporte de nombreuses zones d'accumulation de coquillages du banc de l'île de Sable aux Grands Bancs de Terre-Neuve. Des dépôts épais de till glaciaire et de sédiments glaciomarins indiquent que la glace avait recouvert les Grands Bancs de Terre-Neuve.

Introduction

In the fall of 1982, the Canadian Scientific Ship **Baffin** sailed from the Bedford Institute of Oceanography on a two-month mapping expedition (Cruise 82-039). This cruise was the most recent in the East Coast multiparameter mapping project (Macnab, 1983) and its objectives were:

a. to extend regional multiparameter coverage to the west and east of previously surveyed areas on the Scotian Margin and the Grand Banks of Newfoundland;

b. to obtain detailed data on sedimentary bedforms in the vicinity of Sable Island; and

c. to contribute to an ongoing surficial and bedrock geological mapping project of the Grand Banks of Newfoundland.

The ship's track is shown in Figure 41.1. The cruise was divided into two phases: the first to work in the western Scotian Margin – Georges Bank area where gravity, magnetic and bathymetric data were collected; the second on Sable Island Bank and the Grand Banks of Newfoundland where, in addition, seismic reflection and sidescan sonar data were collected.

In keeping with the collaborative nature of the multiparameter mapping project, survey personnel on **CSS Baffin** represented three federal agencies: the Atlantic Region of the Canadian Hydrographic Service (DFO); the Gravity, Geothermics and Geodynamics Division of the Earth Physics Branch (DEMR); and the Atlantic Geoscience Centre of the Geological Survey of Canada (DEMR).

Methods

Navigation

Ship's positions were derived through an integration of data from various navigation aids: Doppler satellite, rho-rho Loran C, speed log, and gyrocompass. Navigation processing was performed automatically and in real time by the BIO Integrated Navigation System – BIONAV (Wells and Grant, 1981). Fixes were calculated and logged once a minute with a positional accuracy estimated at better than 150 m, and manually plotted on a 1:150 000 boatboard once every ten minutes.

Seismic Reflection and Sidescan Sonar

High resolution seismic reflection data on the surficial sediments and near-surface bedrock were obtained with the Huntec Deep Towed High Resolution Seismic Reflection System (DTS) (Hutchins et al., 1976). The DTS was equipped with an Acoustic Reflectivity Unit (ARU) that produced on-line acoustic reflectivity values used to provide an interpretation of seabed lithologies (Parrott et al., 1980). The reflected energy of the DTS was measured in two time windows, r_1 and r_2: r_1, a measure of the energy which is coherently reflected from the seabed and r_2 a measure of the scattered energy from the top metre of sediment. For deeper seismic penetration, a 655 cm^3 (40 cubic inch) airgun reflection system together with the Nova Scotia Research Foundtion Mark 5A oil filled seismic streamer was deployed. A Klein K-map sidescan sonar with a range of 250 m to each side of the ship provided sonograms of the seabed.

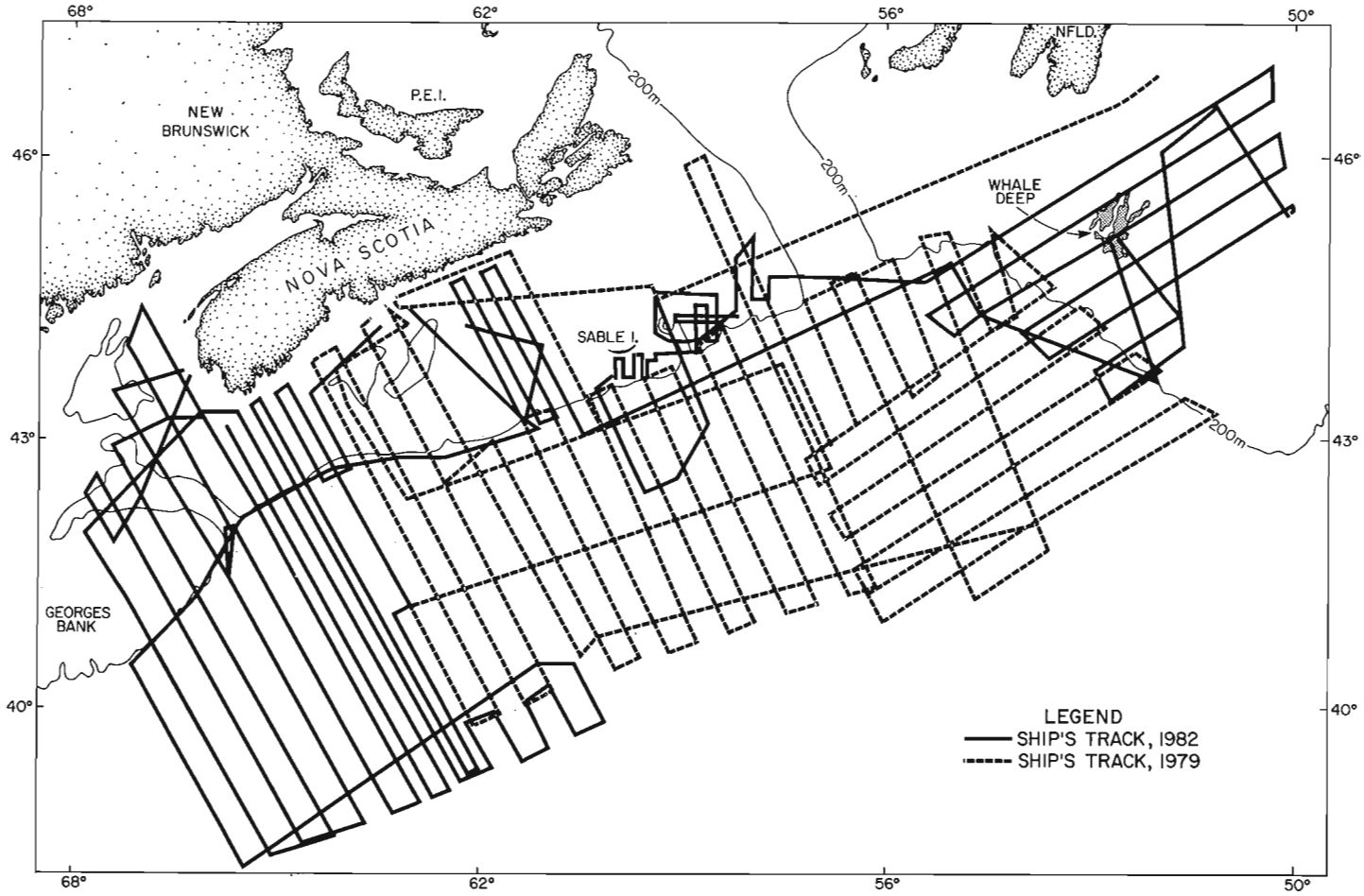

Figure 41.1. *Ship's track, off southeastern Canada.*

Bathymetry, Magnetics and Gravity

Water depth was measured with a 12 kHz ram-mounted transducer. Soundings were scaled manually every five minutes, and in addition at highs, lows, and inflection points, then stored in computer-readable form for subsequent processing. No sound velocity corrections were applied, however tidal corrections were applied in depths of less than 100 m.

Total magnetic field was measured with a Geometrics proton precession magnetometer connected to a Barringer sensor towed approximately 250 m astern of the ship. Magnetic anomaly values were calculated with reference to the 1980 International Geomagnetic Reference Field.

Gravity was measured by two meters provided by the Earth Physics Branch. One was a standard LaCoste and Romberg model, the other a prototype "straight line" system undergoing field tests. The straight line system was a LaCoste and Romberg instrument with digital controller and a sensor re-designed to eliminate cross-coupling effects (Valliant, 1983; LaCoste, 1983). Both meter outputs were converted to observed gravity, compared for performance assessment, and then corrected for the Eotvos effect (using data provided from BIONAV).

All bathymetric and potential field data were processed on board, generally within twenty-four hours of acquisition. Processing at sea served three purposes: quality control, preliminary display and analysis and preparation for post-cruise processing.

Interpretation of High Resolution Seismic and Sidescan Data

The high resolution seismic reflection data and sidescan sonograms collected during this cruise help to provide a regional data base for a numerical model of sediment transport and stability on Sable Island Bank and Banquereau. The geophysical data will also assist in model calibration and sample location.

Preliminary interpretation of the 1982 data indicates that much of eastern Sable Island Bank and Banquereau is covered with a continuous layer of sand which varies in thickness from a thin veneer to over 10 m. Sand waves (sensu stricto) were not found on any of the banks contrary to previously published reports (Evans-Hamilton, 1975); however, sand ribbons, megaripples and sand ridges were frequently observed. Numerous circular areas (10-20 m in diameter) of high intensity reflections interpreted on the sonograms occur on Sable Island Bank, and are thought to represent shell deposits at the seabed (Parrott et al., 1980). Shell beds also occur on the Eastern Shoal area of Banquereau.

The geophysical data collected from the Grand Banks of Newfoundland form part of a regional data base for mapping the surficial and bedrock geology. Previous studies have concentrated on areas to the north and east (Hibernia discovery area) (Fader and King, 1981). The 1982 study extends the regional coverage to the south and east.

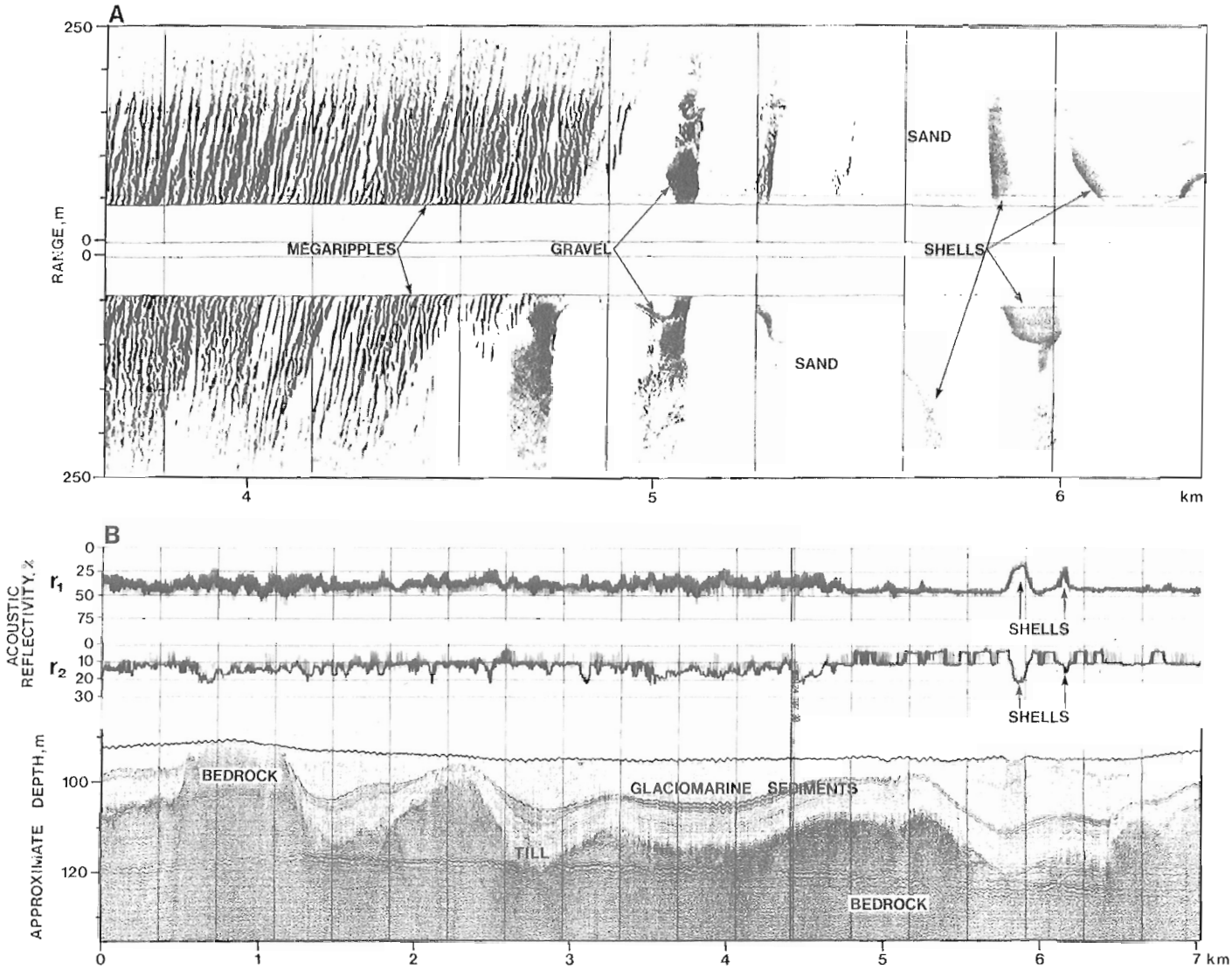

Figure 41.2. *Sidescan sonogram (A) and Huntec deep towed seismic reflection profile (B) collected in Whale Deep, Grand Banks of Newfoundland. The seismic profile shows Cretaceous – Tertiary bedrock overlain by glacial till, glaciomarine sediment and a thin veneer of sand, gravel and shells. The sonogram, which ranges from the 3.7 to 6.3 km marks along the seismic profile, shows a field of low megaripples, a featureless sand sheet and gravel and shell deposits at the seabed.*

Preliminary interpretation of the data indicates a large number of erosional bedrock channels, up to 100 m in depth, which have been infilled with glacial till and glaciomarine sediments (Fig. 41.2). The presence of these glacial materials in this area of the Grand Banks provides the first evidence for glacial ice extending across the Grand Banks.

Overlying the glacial sediments are thin veneers of sand and gravel which exist in a complex pattern of sand ribbons, sand ridges, megaripples and featureless sand sheets (Fig. 41.2). Shell deposits, as interpreted from the sonogram and Huntec DTS data, are widespread and range in shape from more or less circular deposits to complex linear bodies. Sampling of these features is necessary for a complete interpretation. Also interpreted on the sidescan sonograms are iceberg furrows which appear concentrated in the northwestern area of the survey coverage on the Grand Banks of Newfoundland.

Acknowledgments

We thank members of the Canadian Hydrographic Service for their valuable support in the field, particularly M.G. Swim, S.S. Dunbrack and H.P. Varma. D. Halliday, J. Halpenny, and R. Cooper of EPB operated the LaCoste and Romberg meters and processed the gravity data. M. Hughes was senior AGC technician and data processor. G. Standen was the Huntec (DTS) operator. Excellent co-operation was received from Captain Neil Norton and the officers and crew of **CSS Baffin.**

References

Evans-Hamilton, Inc.,
1975: Study of sand waves on Sable Island Bank. Phase 1. Report prepared for Mobil Oil Canada, Ltd., by Evans-Hamilton, Inc., Houston.

Fader, Gordon B. and King, Lewis, H.
1981: A reconnaissance study of the surficial geology of the Grand Banks of Newfoundland; in Current Research, Part A, Geological Survey of Canada, Paper 81-1A, p. 45-56.

Hutchins, R.W., McKeown, D.L., and King, L.H.
1976: A deep tow high resolution seismic system for continental shelf mapping; Geoscience Canada, v. 3, p. 95-100.

LaCoste, L.
1983: LaCoste and Romberg straight line gravity meter; Geophysics, v. 48.

Macnab, R.F.
1983: Multiparameter mapping off the east coast of Canada; in Current Research, Part A, Geological Survey of Canada, Paper 83-1A, p. 163-171.

Parrott, D.R., Dodds, D.J., King, L.H., and Simpkin, P.G.
1980: Measurement and evaluation of the acoustic reflectivity of the sea floor; Canadian Journal of Earth Sciences, v. 17, p. 722-737.

Valliant, H.D.
1983: Field trials with the LaCoste and Romberg straight line gravimeter; Geophysics, v. 48.

Wells, D.E. and Grant, S.T.
1981: An adaptable integrated navigation system: BIONAV; Proceedings of Colloquim III on Petroleum Mapping and Surveys in the 80's, the Canadian Petroleum Association, Banff, Alberta.

42.

NEW DEVONIAN RUGOSE CORALS OF PROBABLE LATE DALEJAN AGE FROM THE BIRD FIORD FORMATION OF SOUTHWESTERN ELLESMERE ISLAND, NORTHWEST TERRITORIES

Project 680093

A.E.H. Pedder and Q.H. Goodbody[1]
Institute of Sedimentary and Petroleum Geology, Calgary

Pedder, A.E.H. and Goodbody, Q.H., New Devonian rugose corals of probable late Dalejan age from the Bird Fiord Formation of southwestern Ellesmere Island, Northwest Territories; in Current Research, Part B, Geological Survey of Canada, Paper 83-1B, p. 335-352, 1983.

Abstract

The Bird Fiord Formation, between Blubber Point and the area north of Muscox Fiord, is divided into four lithological units, informally designated Units 1 to 4. Unit 3 contains a rich benthic, marine fauna, including the corals described in this paper. Its age is deduced to be probably late Dalejan (late Early Devonian), on the basis of conodonts, brachiopds and corals.

The genera ***Spongophylloides, Actinocystis, Grypophyllum, Dubrovia, Salairophyllum, Tonkinaria*** *and* ***Neogrypophyllum*** *are discussed in preparation for the proposal of a new ptenophyllid genus, named* ***Ellesmerelasma.*** *Four new species and a new subspecies are introduced. They are* ***Lekanophyllum foliatum, Ellesmerelasma pumile, Mansuyphyllum uyenoi avernale, M. versicularium*** *and M.* ***comsolum.***

Résumé

La formation de Bird Fiord, située entre la pointe Blubber et la région au nord du fjord Muscox, est divisée en quatre unités lithologiques, appelées officieusement unités 1 à 4. L'unité 3 contient une riche faune marine de nature benthique qui comprend les coraux décrits dans le présent rapport. Les conodontes, les brachiopodes et les coraux qu'elle contient permettent d'établir qu'elle date probablement du Dalejan récent (fin du Dévonien ancien).

Les auteurs décrivent les genres ***Spongophylloides, Actinocystis, Grypophyllum, Dubrovia, Salairophyllum, Tonkinaria*** *et* ***Neogrypophyllum*** *avant de présenter le nouveau genre proposé de ptenophyllidés,* ***Ellesmerelasma.*** *Ils présentent quatre nouvelles espèces et une nouvelle sous-espèce, soit* ***Lekanophyllum foliatum, Ellesmerelasma pumile, Mansuyphyllum uyenoi avernale, M. versicularium*** *et* ***M. comsolum.***

Introduction

Devonian corals that were collected by Per Schei, while he was on the Second Norwegian Arctic Expedition in the "Fram" (1898-1902), were described originally by Loewe (1913). Many of them came from beds that are now referred to the Bird Fiord Formation. Pedder is revising Loewe's work, and Goodbody is studying the Bird Fiord Formation. The corals described in this work are specimens, collected by Goodbody, of species that are not represented in the Per Schei Collection (Fig. 42.1).

Previous work

Exposures of the Bird Fiord Formation were examined by Schei, at Blubber Point (known to members of the second "Fram" expedition as Spaekkassen or Spaekodden) and around Goose Fiord (Gasse Fjorden). Schei (1903a, b; 1904) divided the Devonian of this part of Ellesmere Island into three series, designated C, D and E. Of these, C was considered to be partly Silurian. Series D was further divided into nine divisions, designated D(a) to D(i). Because of his death, soon after the return of the "Fram", Schei was unable to elaborate his sketchy preliminary account of the stratigraphy of the area. Descriptions of his fossils by other workers, and recent field work, suggest that the Bird Fiord Formation, as it is currently recognized in the Blubber Point and Goose Fiord region, closely approximates to Schei's divisions D(d) to D(i) combined.

Tolmachoff (1926, p. 10-20) collated the early paleontological works on Schei's Devonian units, and reiterated Holtedahl's (1917, p. 12-13) summary of the opinions of the ages of these units. In this summary, the poorly fossiliferous units D(d), D(e) and D(f) were said to point towards uppermost Lower Devonian and lower Middle Devonian; D(g) was assigned to the Middle Devonian; D(h), the most fossiliferous division, was said to be transitional between Middle and Upper Devonian; and D(i) was considered to be Upper Devonian.

The next publication to appear, concerning the Bird Fiord Formation of southwestern Ellesmere Island, was authored by McLaren (1963, p. 324-328). The formation was named and first described in this work. Faunas listed by McLaren came mostly from that part of the formation that corresponds to Schei's division D(h) and to our Unit 3. McLaren considered that the faunas indicate a Givetian (late Middle Devonian) age.

The current phase of paleontological work on faunas from the Bird Fiord Formation, south of Schei Syncline, began with Ormiston's (1967, p. 94-96, Pl. 12, figs. 9, 10) revision of the holotype of **Dechenella (D.) spaekkassensis** (Tolmachoff), from Schei's D(h) division at Blubber Point, and continued with Brice's (1982) and Jones' (1982) works on brachiopods from Goose Fiord, and Pedder's (1982b) description of corals from Blubber Point.

Stratigraphy

Along the southern limb of Schei Syncline, the Bird Fiord Formation is divisible into four units. The basal unfossiliferous unit of dolostones and interbedded gypsum, varies in thickness from about 150 to 295 m. It is succeeded by a resistant, bluff-forming unit of very bioturbated,

[1] Department of Geology, University of Alberta, Edmonton, Alberta, T6G 2E3

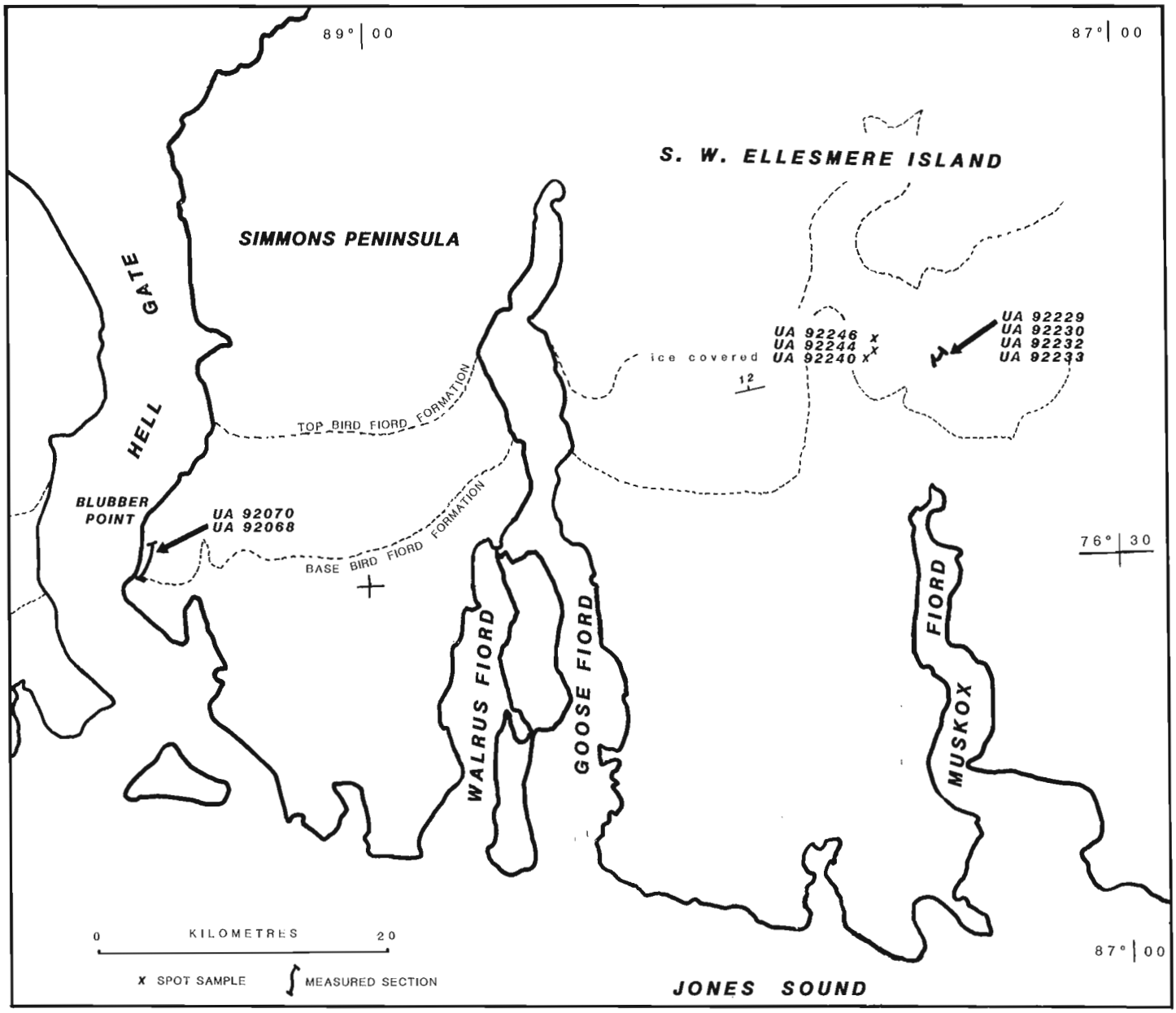

Figure 42.1. *Sketch map of southwestern Ellesmere Island showing localities that have provided fossil material used in this paper. Stratigraphic details and faunal lists are given in the Locality Register.*

calcareous sandstones and sandy limestones, varying in thickness from about 55 to 113 m. The third unit consists of repetitive shale-calcareous sandstone couplets, and includes biostromal beds at Goose Fiord and north of Muskox Fiord. It varies from about 60 to 100 m in thickness, and is easily identified in outcrop and on air photographs by its striped weathering pattern and recessive profile above the bluffs of Unit 2. The highest division, Unit 4, comprises crossbedded micaceous sandstones, estimated to be in the order of 150 m thick.

The corals described in this paper were collected from calcareous sandstones and biostromes in Unit 3. The accompanying fauna includes heteractinid sponges, stromatoporoids, tabulate corals, brachiopods, bryozoa, trilobites and crinoidal debris, all in variable abundance. It is evidently a shallow marine benthic assemblage that was able to tolerate a substantial influx of clastic material.

The change from the high intertidal/supratidal environment, in which Unit 1 was deposited (Jones, 1982, p. 1397), to the deeper, open marine environment represented in Unit 3, holds high promise for future event correlations on Ellesmere and nearby islands.

Age of the Unit 3 Coral Fauna

Conodont studies (Uyeno and Klapper, 1980; Uyeno, 1981) have demonstrated that the Blue Fiord and overlying Bird Fiord formations of the Arctic Islands are diachronous, so that any discussion of the ages of these formations must be specific in both geographic and stratigraphic detail. Here, we are discussing the age of Unit 3 of the Bird Fiord Formation, on the southern limb of Schei Syncline. Sections and spot locations, from which the corals of this work were collected, lie along present

structural strike (believed to be close to Devonian sedimentological strike), within 25 km in both directions from Goose Fiord.

Chatterton is quoted by Smith and Stearn (1982, p. 153) as having identified **inversus** Zone (Zlichovian) conodonts 200 m above the base of the Blue Fiord Formation at Goose Fiord. Figures 4 and 5 of these authors show the Blue Fiord Formation to be about 450 m thick at this locality. Chatterton has also identified **Steptotaxis glenisteri** (Klapper), **Pelekysgnathus** sp. n. of Uyeno and Klapper (1980) and **Panderodus** spp. from a sample taken by Jones from near the base of Unit 2 of the Bird Fiord Formation in Jones' (1982) section J at Goose Fiord. The age indicated by this assemblage is early Dalejan, equivalent to the age of either the upper **inversus** Zone or lower **serotinus** Zone. Efforts to obtain conodonts from Unit 3 have been unsuccessful, however, the coral-bearing horizons of Unit 3 are only about 100 m above the upper **inversus** Zone or lower **serotinus** Zone assemblage in Unit 2.

Brachiopods described by Jones (1982) from Goose Fiord are from Units 2 and 3 of the Bird Fiord Formation. **"Elythina" sverdrupi** Brice is known to occur with Dalejan **serotinus** Zone conodonts in other places on southwestern Ellesmere Island, but the remaining forms studied by Jones are not known from other datable occurrences.

Brice (1982) described three species of brachiopods from beds at Goose Fiord that pertain to Unit 3 of our divisions of the Bird Fiord Formation. Eleven brachiopod taxa have been identified by Jones from Unit 3 collections made by Goodbody, and in all, there are seven recognizable species in the unit. On the basis of ages established by conodonts at other arctic island localities, four species, **Cupularostrum** (?) **ellesmerense** Brice, **Atrypa** sp. B of Jones (1982), **Perryspirifer scheii** (Meyer) and **"Elythina" sverdrupi** Brice, are not known to range higher than the Dalejan **serotinus** Zone. The other three species, **Schizophoria sulcata** Johnson and Perry, **Spinatrypa borealis** (Warren) and **Costacranaena marlenae** Johnson and Perry, are known from an assemblage that occurs repetitively from 355 to 579 m below the top of a 765 m section, just south of South Dundee Bight, Bathurst Island (Johnson and Perry, 1976). The section was assigned to the Bird Fiord Formation in Johnson and Perry's paper, but it lies directly on the Eids Formation, and is evidently partly equivalent to the Blue Fiord Formation of Uyeno (1981). Raasch (1982, p. 165) has since identified **Dechenella (D.) neotesca** Ormiston and, 72 m higher, **D. (D.) bathurstensis** Ormiston from the same section. Johnson and Perry (1976, p. 618) reported that Klapper had identified a specimen of **Polygnathus parawebbi** Chatterton from the 579 m level in the South Dundee Bight section. The earliest recorded occurrence of this Eifelian and Givetian conodont in western Canada is in the Funeral Formation, near Mount Dahadinni, in the front range of the Mackenzie Mountains (Chatterton, 1979, Fig. 6, section 12). This occurrence is presumably below the **pedderi** conodont faunal unit, and possibly correlates with part of the **costatus costatus** Zone of other regions. If the **Polygnathus parawebbi** occurrence in the South Dundee Bight section were as old as the **costatus costatus** Zone, it would be consistent with Uyeno's (1981) claim that the highest Devonian carbonate unit on central Bathurst Island ranges from the **patulus** to **costatus costatus** Zones. In summary, it is suggested, by four of the seven brachiopod species, that Unit 3 is no younger than middle Dalejan (**serotinus** Zone), and by the three remaining species, that it is no older than early Eifelian (**costatus costatus** or **partitus** Zone).

As it is presently known, the rugose coral fauna of Unit 3 comprises twelve species. One of these belongs to the genus **Taimyrophyllum**, and may be a subspecies of **T. nolani** Merriam, which was first described from possible Dalejan age (Pedder, 1982a, p. 73) rocks in Nevada. Another is a subspecies of **Mansuyphyllum uyenoi** (Pedder), which occurs in Zlichovian beds on the northern flank of Schei Syncline. The remaining corals in Unit 3 are known only from their type localities. There is no species of either **Spongonaria** or **Digonophyllum** in the Unit 3 fauna. The significance of this is possibly that **Spongonaria** (a genus known to include species that were tolerant of clastic-rich environments) became extinct near the top of the **serotinus** Zone, and **Digonophyllum**, which is the most abundant rugose coral genus in many early and later Eifelian faunas of western and arctic Canada, is extremely rare below the **partitus** Zone.

Although none of the foregoing arguments is unassailable, independent lines of evidence from conodonts, brachiopods and corals consistently point to a late or post-**serotinus** Zone, and a pre-**partitus** Zone age for the corals of Unit 3. That is, they point to a late **serotinus** Zone or **patulus** Zone age, which is the age of the upper part of the Dalejan stratotype in Czechoslovakia (Chlupáč, 1982, Table 1).

Systematic Paleontology

Type specimens and locality numbers referred to in this paper are registered in the Paleontological Collections, Department of Geology, The University of Alberta, Edmonton, Alberta, Canada, T6G 2E3. UA and PCC are abbreviations for the University of Alberta and Paleontological Collections Catalogue.

Family CYSTIPHYLLIDAE Milne Edwards and Haime, 1850

Subfamily DIGONOPHYLLINAE Wedekind, 1923

Genus **Lekanophyllum** Wedekind, 1924

Lekanophyllum Wedekind, 1924, p. 29-34 [in part, includes a species of **Mesophyllum**].

Type species. **Lekanophyllum punctatum** Wedekind, 1924, p. 30, 34, figs. 36-38. Junkerberg Formation, Eifelian; Auberg, Gerolsteiner Mulde, Germany (Birenheide, 1968, p. 23).

Remarks. A synonymy and diagnosis of the genus **Lekanophyllum** was given by Pedder and McLean (1982, p. 75). The sixty-four species currently assigned to the genus are listed in McLean (1976, p. 19) and Pedder (1982b, p. 84).

Lekanophyllum foliatum sp. n.

Plate 42.1, figures 1-7; Plate 42.1, figures 8-15

Type series. Holotype, UA 7029, UA locality PCC 92246. Paratypes, UA 7030-7034, UA locality PCC 92246; UA 7035, 7036, UA locality PCC 92229; UA 7037, 7038, UA locality PCC 92233; UA 7039, UA locality PCC 92240; UA 7040, UA locality PCC 92244.

Diagnosis. Solitary species of **Lekanophyllum** with known maximum mean diameter of 40 mm. Major septal crests unequally long, some entirely lamellar from outer wall to axial region, and only slightly fusiform. Typically, at maturity, they number 35 to 52 and are arranged in a crudely bilateral fashion. Minor septal crests suppressed. Dissepiments and less numerous presepiments form inwardly inclined dissepimentarial surfaces. Lateral dissepiments absent.

Description. Corallum solitary, trochoid or less commonly ceratoid in early stages, subsequently becoming erect and subcylindrical. Rejuvenescences generally do not reduce the diameter of the corallum significantly. Before sectioning, one paratype (UA 7032) displayed a steady contraction in diameter during late growth. Most specimens of the type series would have been 55 to 65 mm long, and have had a maximum mean diameter of 25 to 35 mm. One paratype

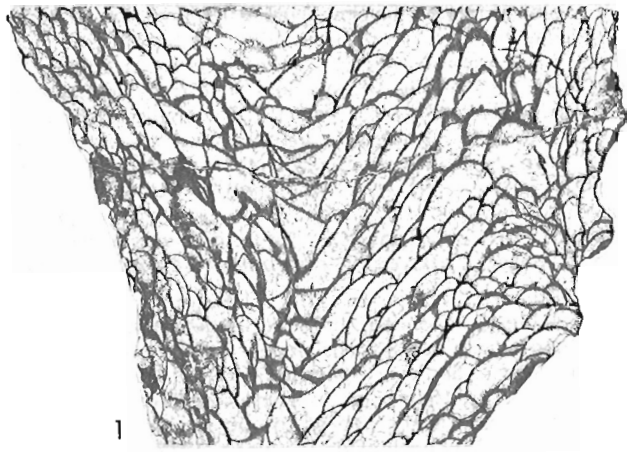

1

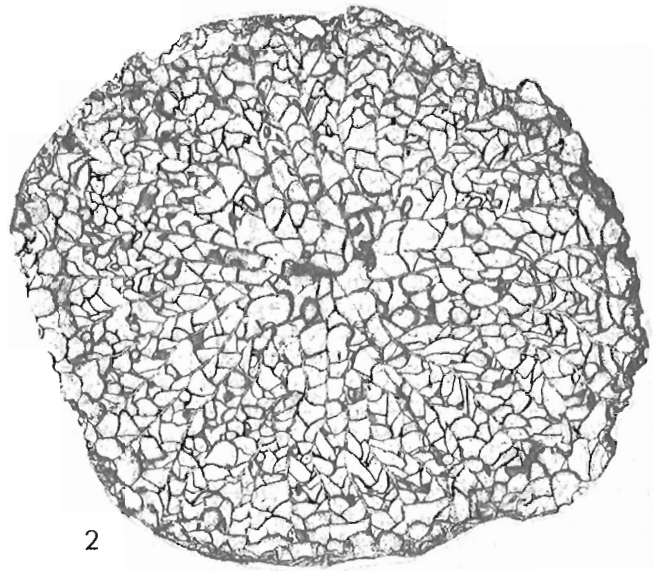

2

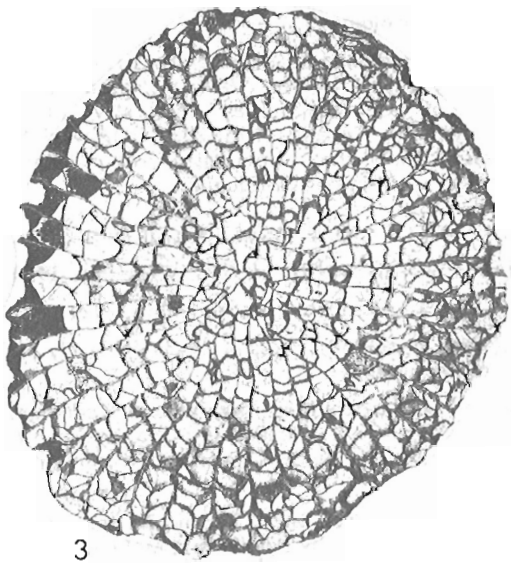

3

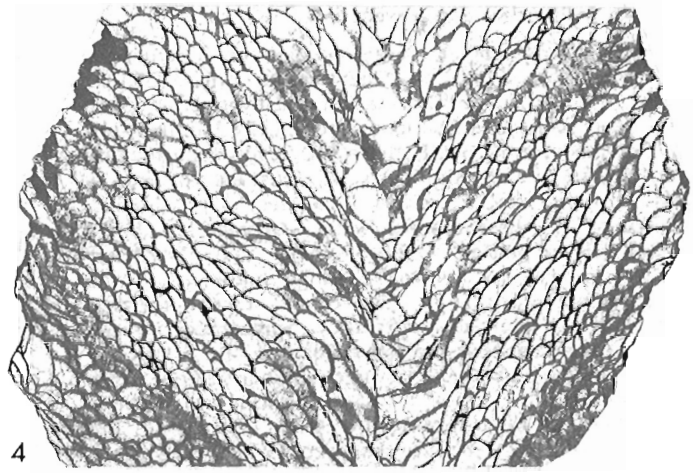

4

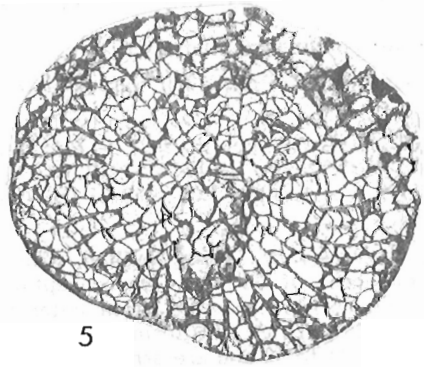

5

6

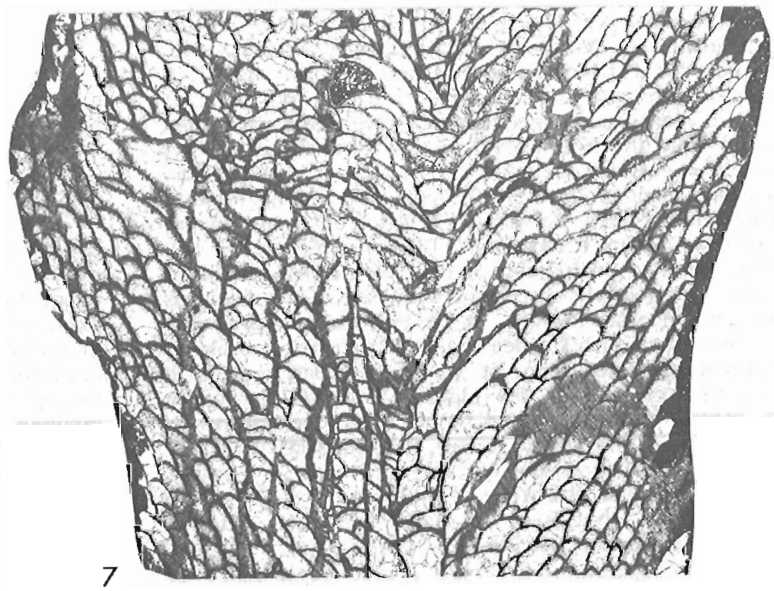

7

(UA 7039) has a maximum mean diameter of 40 mm; another (UA 7038) was at least 95 mm long, even though its diameter was only about 29 mm. The calice is shallow, typically less than 10 mm deep, and has gently sloping sides. Calices lack distinct platforms, although some developed temporarily everted marginaria. Cardinal fossula variable, commonly shallow and more prominent in the tabularial, than in the dissepimentarial region. Dissepimented radiciform process are typically present; some were formed after the corallum had acquired its adult diameter.

The periphery of most of the type specimens is damaged by abrasion and crushing; where preserved, the outer wall generally has a thickness of 0.2 to 0.5 mm in early stages, and 0.1 to 0.2 mm in later stages. In adult stages, especially, the septal apparatus is highly differentiated and commonly crudely bilateral in arrangement, although fossulae are not present consistently. About half of the major septal crests extend, unbroken, from the outer wall to the axial or periaxial region; many of the remaining major septal crests are separated from the outer wall by only one to three presepiments. In the inner dissepimentarium, major septal crests are somewhat wavy, weakly to moderately carinate and slightly fusiform. Adaxially, they are thin to slightly dilated, smooth to weakly carinate; they may also be conspicuously bent so as to abut each other locally. Where there is a well developed cardinal fossula, the cardinal septum is short, but if the cardinal fossula is not well developed, the cardinal septum is not necessarily the shortest of the major septal crests, and may not be identifiable. Microstructure of the major septal crests is not well preserved, but appears to comprise fine contiguous monacanths. At corallite diameters of 9 to 21 mm, there are 25 to 35 major septal crests; adult corallites with diameters of 25 to 40 mm have 35 to 52 major septal crests. In early stages, major septa are withdrawn from the axis relatively more than they are at maturity. UA 7041, from PCC 92070, retains this juvenile feature to a diameter of at least 31 mm, and for this reason, is excluded from the type series. Minor septal crests are either entirely suppressed, or occur as short strands or discrete trabeculae.

Commonly, the adult dissepimentarium consists of about 8 to 14 rows of dissepiments and less numerous presepiments, but longitudinal sections that cut the plane of bilateral symmetry at right angles, may reveal as many as 25 rows of plates on both sides of a narrow tabularium. Dissepimentarial surfaces slope inwards without forming a platform, except at levels from which peripheral dissepimented radiciform processes protrude, where the inner dissepimentarium is everted. Most dissepiments fail to cross the wide interseptal loculi, but lateral dissepiments are not normally present. The tabularium is variable, although it is usually narrow. An irregular tabular fossula is present in some specimens. Sclerenchyme may cover the horizontal elements around the fossula, and commonly coats the dissepiments and walls of the radiciform processes. It is absent essentially from other regions of the corallum.

Plate 42.1

Figures 1-7. **Lekanophyllum foliatum** sp. n.

1, 2. Holotype, UA 7029, longitudinal and transverse thin sections, x3; UA locality PCC 92246.
3-5. Paratype, UA 7032, two transverse and a longitudinal thin section, x3; UA locality PCC 92246.
6. Paratype, UA 7035, longitudinal thin section showing a radiciform process, on right side, reaching out over the old calicinal rim, following a rejuvenescence, x3; UA locality PCC 92229.
7. Paratype, UA 7040, longitudinal thin section, x3; UA locality PCC 02244.

Remarks. The very long, thin and crudely bilaterally arranged major septal crests, suppressed minor septal crests, wide interseptal loculi, and absence of lateral dissepiments make this a highly distinctive species of **Lekanophyllum.** A poorly ilustrated specimen, named **Dialythophyllum astraeiforme kerlegeshicum** by Ivaniya (1965, p. 74, 75, Pl. 1, figs. 3-5), from the Givetian Safonov Beds of the Kuznets Basin, is perhaps, morphologically, the closest of previously named species or subspecies. However, it has dilated major septal crests, less reduced minor septal crests, is not strongly bilaterally symmetrical, and should not be confused with the new species.

The trivial name, which is the Latin adjective for leafy or leaved, is chosen to draw attention to the strongly lamellar septal crests.

Family PTENOPHYLLIDAE Wedekind, 1923

Remarks. Birenheide (1978, p. 122-151) and Pedder (1982a, p. 72) recognized the Spongophyllinae and Ptenophyllinae as subfamilies of the Spongophyllidae. Hill (1981, p. 231-246) separated the Ptenophyllidae from the Spongophyllidae and split the Ptenophyllidae into the Ptenophyllinae and Actinocystinae. Both classifications are acceptable, but since Hill's 1981 work is the current standard treatise on the Rugosa, we are also elevating the Ptenophyllidae to full family rank.

The Actinocystinae closely resemble the Ptenophyllinae. Hill diagnosed them as "solitary Ptenophyllidae with septa strongly flexuous to zigzag and flanged in inner parts of dissepimentarium and in tabularium, thickened in some". However, the three most typical genera-**Actinocystis** (=? **Spongophylloides**), **Cymatelasma** and **Cymatella**-are characterized by having fully dilated septa in early stages. This feature should be stressed in the diagnosis more than the flexing and flanging of the septa.

Difficulties in recognizing a solitary versus colonial growth form, as a generic criterion in the Ptenophyllidae, have been discussed by Strusz (1968, p. 16). Strusz advocated a separation between species that are exclusively fasciculate, forming colonies by repeated budding, and those that either never bud, or do so only occasionally to form small clumps of a few radiating corallites. A similar position is taken in this work, although it is recognized that the distinction is difficult to draw in practice, because many of the named species have not been fully described.

No less than 33 generic names have been proposed for solitary and fasciculate ptenophyllinid and actinocystinid corals of Silurian and Devonian age. It is not possible to review fully the problems arising from this profusion of names, but a limited discussion of some of the genera is necessary to justify yet another genus that we are proposing.

Subfamily ACTINOCYSTINAE Wedekind, 1927

Genus **Spongophylloides** Meyer, 1881

Spongophylloides Meyer, 1881, p. 109.

Type species. **Spongophylloides schumanni** Meyer, 1881, p. 109, 110, Pl. 5, figs. 12a-c. Drift; East Prussia.

Remarks. **Spongophylloides schumanni** is too poorly described and illustrated to act as a type species in modern taxonomic work. Unfortunately, the type specimen is lost, and since it is, or was, a poorly located drift specimen, there is no possibility of recollecting authentic material. Authors have circumvented the need for a neotype by assuming **Spongophylloides schumanni** to be synonymous with **Cystiphyllum grayi** Milne Edwards and Haime, which is a comparatively well known species. This may be the case, but now that Soviet workers have combined two seemingly

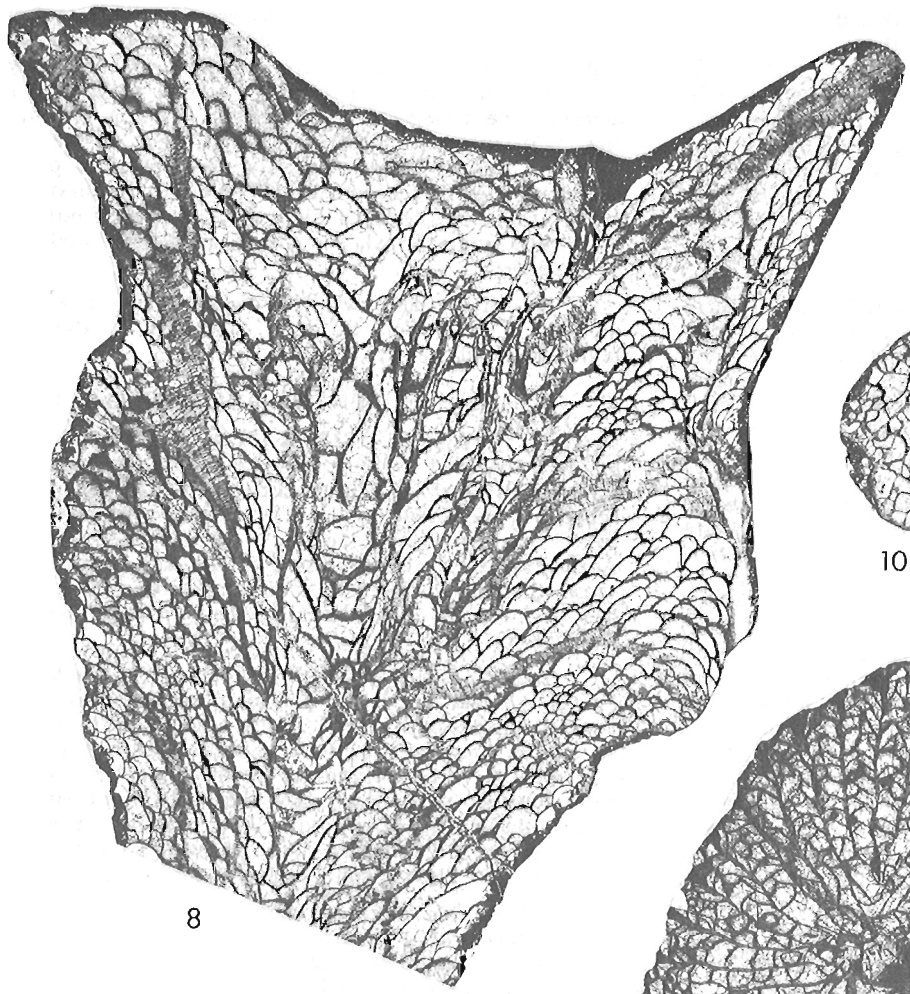

8

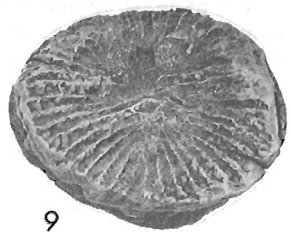

9

10

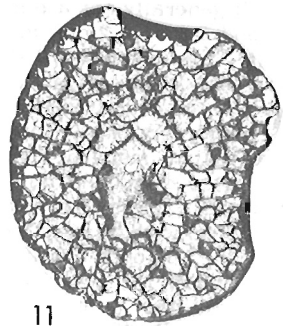

11

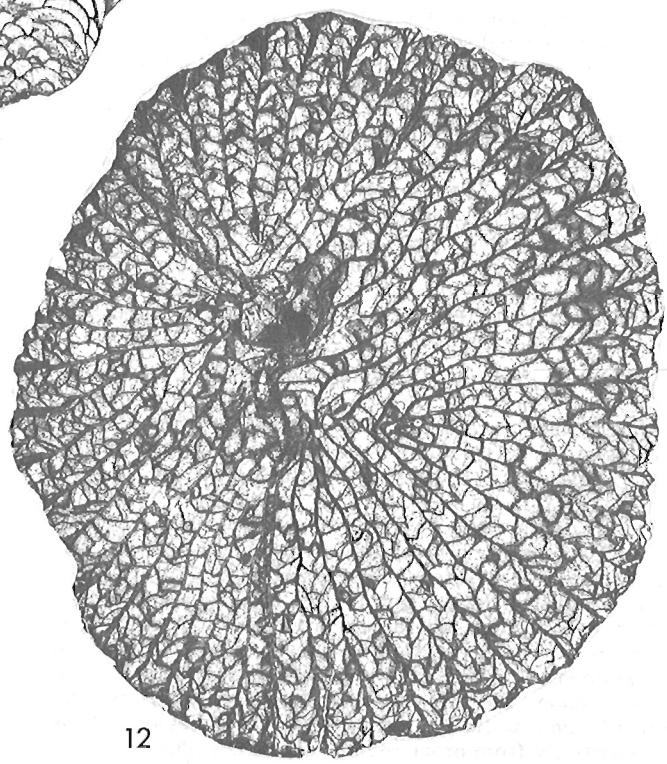

12

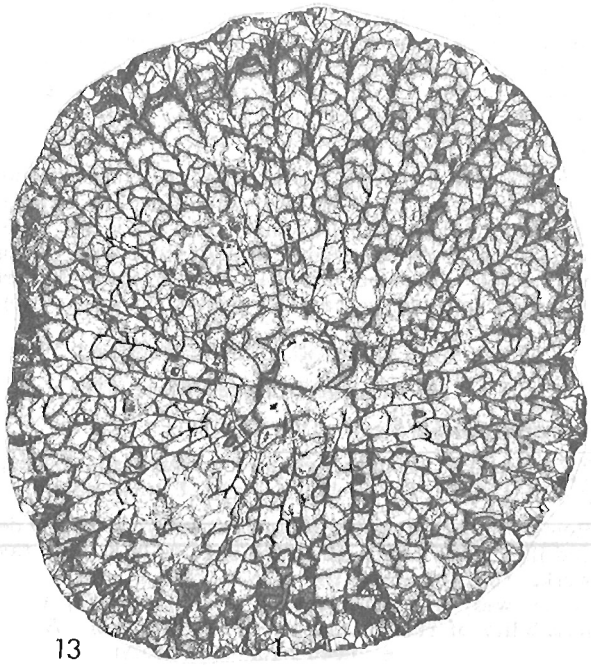

13

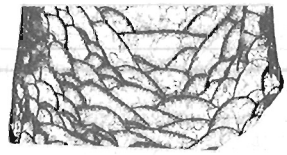

14

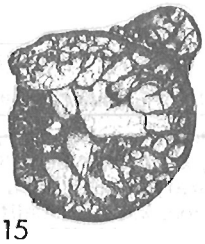

15

different junior genera -**Actinocystis** Lindström, 1882, and **Dubrovia** Zheltonogova, 1961- under the name **Spongophylloides**, it is essential to clarify and make known the morphology of **Spongophylloides schumanni**. This could be done by designating and sectioning a neotype, but it would be better to make a formal application for **Cystiphyllum grayi** to become the type species of **Spongophylloides**. In this way **Actinocystis** would become an absolute synonym of **Spongophylloides**.

Genus **Actinocystis** Lindström, 1882

Actinocystis Lindström, 1882, p. 21.

Type species. **Cystiphyllum grayi** Milne Edwards and Haime, 1851, p. 465; 1855, p. 297, 298, Pl. 72, fig. 3 (not ? fig. 3a). Silurian, "supérieur", Dudley, England. Topotypic material of this species has been monographed by Lang and Smith (1927, p. 480-482, Pl. 37, figs. 1, 2), who chose the original specimen illustrated in figure 3 of Milne Edwards and Haime's 1855 plate 72 as lectotype, and by Butler (1934, p. 541-545, Pl. 17, figs. 1a-2e; Pl. 18, figs. 1, 2). Butler noted that all the English specimens known to him came from the Wenlock Limestone of Dudley Castle Hill or Wren's Nest, Worcestershire.

Assigned species. In addition to the type species, the following belong to the genus: **Actinocystis cylindrica** Wedekind (1927, p. 45, Pl. 1, figs. 14, 15), Klinteberg Beds (equivalent to Wenlock to lower Ludlow Series), Gotland; **A. spinosa** Wedekind (1927, p. 45, Pl. 21, fig. 12), a synonym of **A. grayi** from the Klinteberg Beds, Gotland; **A. perfecta** Wedekind (1927, p. 45, Pl. 26, figs. 15-18), Klinteberg Beds, Gotland; **Spongophylloides pusillus** Butler (1934, p. 545-548, Pl. 17, figs. 3a-e; Pl. 18, figs. 3-8), Wenlock Limestone (upper Wenlock Series), Wenlock Edge, Shropshire, England; **Spongophylloides cockei** Sutherland (1965, p. 16-18, Pl. 4, figs. 1a-2e; Pl. 5, figs. 1a-4c; Pl. 6, figs. 2a-6b), Henryhouse Formation (equivalent to the lower Ludlow Series), southern Oklahoma, U.S.A.

Diagnosis. Solitary, ceratoid to subturbinate genus of actinocystinid corals with a deep, conical calice. In early stages, the septa are strongly dilated and commonly in lateral contact. Subsequently, the septa attenuate in the tabularium, although a variable marginarial stereozone may be retained. In mature stages, the major septa are unequally long, reaching, or almost reaching the axis; peripherally, they are typically well withdrawn from a weak outer wall. Septa of both orders are zigzag and flanged, or waved parallel to their upper edges. The dissepimentarium comprises numerous small presipiments and dissepiments, but these may be, in part, displaced by a marginarial stereozone, or obscured by secondary sclerenchyme.

Remarks. Lindström (1896, p. 48) believed **Actinocystis** to be synonymous with **Spongophylloides**, and was aware that **Spongophylloides** had priority. However, he considered **Spongophylloides** to be invalid, on the grounds that Linnaeus reserved generic names ending in **-oides** for botanical nomenclature. Later workers, who correctly have rejected this argument, may, nevertheless, have been incorrect in assuming the type species of the two genera to be congeneric.

Subfamily PTENOPHYLLINAE Wedekind, 1923

Genus **Grypophyllum** Wedekind, 1922

Grypophyllum Wedekind, 1922, p. 13 [in part, includes the type species of **Parasociophyllum**].

Hooeiphyllum Taylor, 1951, p. 173, 174.

Type species of **Grypophyllum**. **Grypophyllum denckmanni** Wedekind, 1922, p. 13, 14, text-figs. 13, 14. Bücheler Schichten (Givetian); Hand near Bergisch-Gladbach, Paffrath Syncline, Rhenish Mountains, Germany. This species has been redescribed by Engel and von Schouppé (1958, p. 103-107, Pl. 9, figs. 18-25) and by Birenheide (1978, p. 136, text-figs. 80a-c). Wedekind's (1925, p. 14) subsequent designation of **Grypophyllum isactis** (Frech) as the type species of **Grypophyllum** is invalid.

Type species of **Hooeiphyllum**. **Grypophyllum normale** Wedekind, 1925, p. 22, Pl. 5, figs. 25, 26. Upper Middle Devonian (Givetian); Hand near Bergish-Gladbach, Paffrath Syncline, Rhenish Mountains, Germany. This species has approximately the same type stratum (Bücheler Schichten) and locality as **Grypophyllum denckmanni** Wedekind, and is considered to be conspecific with it (Engel and von Schouppé, 1958, p. 103).

Assigned species. Most of the species listed by Pedder (1973, p. 100).

Diagnosis. See Birenheide (1972, p. 407) and Hill (1981, p. 236-238).

Remarks. **Grypophyllum** is currently restricted to solitary ptenophyllinid species having a conical calice and thin septa formed of fine, well-aligned trabeculae.

Genus **Dubrovia** Zheltonogova, 1961

Dubrovia Zheltonogova, 1961, p. 80, 81.

Type species. **Dubrovia dubroviensis** Zheltonogova, 1961, p. 81, Pl. S-19, figs. 3a, b. Tom'chumysh Beds (according to plate legend), "Upper Silurian"; River Baskuskan, near Dubrovo, Salair, Soviet Union. Topotypic material has been redescribed by Besprozvannykh (1968, p. 112, Pl. 49, figs. 5a-6b). The Tom'chumysh and underlying Sukhaya Beds are both now known to be Lochkovian (Elkin and others, 1982).

Assigned species. The type species is interpreted to be congeneric with the following species and forms: **Grypophyllum vilvense** Spasskiy (1955, p. 131, 132, Pl. 20, figs. 3a-4), Koyva Beds (Dalejan or early Eifelian), western slope of the southern Urals; **Grypophyllum salairicum** Bul'vanker (1958, p. 145, 146, Pl. 51, figs. 1a-2), Upper Shanda Beds (late Dalejan), Kuznets Basin; **Grypophyllum carinatum** of authors (Soshkina, 1949, Pl. 52, figs. 3a-4b; Pl. 53, figs. 1a-c. Degtyarev, 1951, Pl. 1, figs. 3a, b. Spasskiy, 1955, Pl. 20, figs. 2a-v), Dalejan or Eifelian, western slope (Koyva, Kosva, Tanchikha and Vilva Rivers) of the central Urals; **Grypophyllum mirabile** Sytova (1968, p. 65, 66, Pl. 4, figs. 1a-v) lower and middle subhorizons of the Borshchov Horizon (Lochkovian), Podolia.

The holotype of **Astrophyllum carinatum** Soshkina (1936, p. 60-62, figs. 68-70), from Malyj Patok River in the northern Urals, and specimens, identified as **Grypophyllum carinatum** (Soshkina, 1949, Pl. 52, figs. 6-8), from Katav River in the southern Urals, are unrecognisable.

Plate 42.1

Figures 8-15. **Lekanophyllum foliatum** sp. n.

8, 10, 11. Paratype, UA 7031, two transverse and a longitudinal thin section, x3; UA locality PCC 92246.
9, 12. Paratype, UA 7037, exterior calicular view, x1, and a transverse thin section, x3; UA locality PCC 92233.
13. Paratype, UA 7036, transverse thin section, x3; UA locality PCC 92229.
14. Paratype, UA 7033, longitudinal thin section, x3; UA locality PCC 92246.
15. Paratype, UA 7035, transverse thin section showing radiciform process on upper right side, x3; UA locality PCC 92229.

Diagnosis. Solitary, predominantly ceratoid to subcylindrical genus of ptenophyllinid corals with a deep, conical calice. Early stages of topotypic specimens of type species not known; specimens from the Guby Belush'ya Beds (probably equivalent to the upper Ludlow series) on Vaigach Island, western Soviet Arctic, that have been identified as being conspecific with **Dubrovia dubroviensis** by Sytova (1970, Pl. 8, figs. 1a, b), do not show early septal dilation. In late stages, the septa are sinuous, locally strongly flanged, and are commonly disrupted peripherally by a few presepiments. Dissepiments are mostly elongate, but vary in size. Outer wall thin. Dissepimentarial surfaces are invariably inwardly sloping. Tabulae closely spaced, forming weakly to strongly axially depressed tabularial surfaces.

Remarks. In addition to occurrences in Lochkovian strata of Salair and the Upper Silurian on Vaigach Island, western Soviet Arctic, the type species has been identified in the Borovushkin Suite (Pridolian?) of the Rudnyy Altay (Sytova, 1966, p. 99, Pl. 3, figs. 4a, b), and in the Lower Tagil Beds (Lochkovian) of the eastern Urals (Shurygina, 1968, p. 127, Pl. 54, figs. 1a, b).

Two interpretations of the genus **Dubrovia** are possible. The one given by Hill (1981, p. 246), which is tentatively followed here, assumes that it is differentiated from **Actinocystis** (=? **Spongophylloides**) by lacking strong septal dilation in early stages. The other interpretation, which is advocated by Soviet workers, including, now, Zheltonogova (1973, p. 119, 120) herself, is that **Dubrovia** is synonymous with **Spongophylloides.**

Genus **Salairophyllum** Besprozvannykh, 1968

Salairophyllum Besprozvannykh, 1968, p. 111.

Type species. **Pilophyllum angustum** Zheltonogova, 1961, p. 78, Pl. S-17, fig. 5; Pl. S-18, fig. 1. Tom'chumysh Beds, "Upper Silurian"; River Tom'chumysh below Tomsk, Salair, Soviet Union. Topotypic specimens have been monographed by Besprozvannykh, 1968, p. 111, 112, Pl. 49, figs. 4a, b. The Tom'chumysh Beds are known now to be Lochkovian (Early Devonian) (Elkin and others, 1982).

Diagnosis. Solitary subcylindrical genus of ptenophyllinid corals. Septa flanged adaxially; dilated peripherally, locally forming a dense stereozone. Dissepimentarium inwardly sloping, in places largely displaced by the sterozone. Presepiments very rare or absent. Tabulae closely spaced. Tabularial surfaces mostly weakly depressed in figured topotypic material of the type species, but more strongly depressed in specimens, identified as **Salairophyllum angustum,** from the Lower Podotdel Beds (Lochkovian) of the eastern Urals (Shurygina, 1968, Pl. 55, figs. 2, 3b).

Remarks. The type species is possibly the only named species that should be referred to the genus, although the holotype of **Briantelasma mainense** Oliver (1960, Pl. 1, figs. 6, 7) appears to conform to the diagnosis of **Salairophyllum,** given above.

Specimens identified as **Salairophyllum** sp. e, from the Upper Silurian of Kuiu Island, southeastern Alaska (Merriam in Oliver and others, 1975, Pl. 22, figs. 13-16), may be fasciculate. Furthermore, they have septa that are strongly carinate in the marginarium, as well as marginally elevated and moderately spaced tabularial surfaces. They are unlikely to be ptenophyllids. A specimen identified as **Salairophyllum** ? sp., from the Lochkovian coral zone E of Nevada (Merriam, 1974, Pl. 12, figs. 6-8), has a ptenophyllid tabularium. It may be a species of **Salairophyllum,** but has exceptionally carinate septa and a few presepiments.

Genus **Tonkinaria** Merriam, 1974

Tonkinaria Merriam, 1974, p. 51, 52.

Type species. **Tonkinaria simpsoni** Merriam, 1974, p. 52, Pl. 7, figs. 1-8. "Late Silurian", coral zone D; upper beds of Unit 3 of the Roberts Mountains Formation; type section of the Roberts Mountains Formation, northwestern side of Roberts Creek Mountain, Roberts Creek Mountains Quadrangle, Nevada, U.S.A. Johnson and Oliver (1977, p. 1464) have shown that the type horizon is Lochkovian (Early Devonian) age.

Assigned species. The species founded under the name of **Grypophyllum antiquum** by Sytova (1968, p. 65, Pl. 5, figs. 4-5b), from the Lower Borschov Subhorizon (Lochkovian) of Podolia, is assigned tentatively to the genus.

Diagnosis. Solitary, and possibly parricidally budding (apparently seen in only one unsectioned specimen, provisionally assigned to the type species by Merriam), subcylindrical to turbinate genus of ptenophyllinid corals. The calice may become flared at maturity. Outer wall narrow. Major septa long, thin, somewhat wavy but not noticably flanged; minor septa reduced, represented by short lamellae inside the outer wall and possibly, also, by discontinuous interior fragments. Relatively large, elongate dissepiments predominate over presepiments in the unexpanded part of the corallum; less inwardly inclined presepiments predominate in flared parts. Tabulae closely spaced, forming concave tabularial surfaces.

Remarks. **Tonkinaria simpsoni** is based on about 20 silicified specimens from two localities in Nevada. Transverse and longitudinal thin sections of a topotypic paratype have been illustrated, but the holotype has not been sectioned. The diagnosis, given here, is based primarily on the sectioned paratype of **T. simpsoni** and the published figure of **T.** (?) **antiqua.** In these circumstances it must be regarded as provisional.

The septal and calicular morphology of **Tonkinaria** appear to relate it to the fasciculate Pridolian (late Silurian) genus **Imennovia** Shurygina (1968, p. 133).

Genus **Neogrypophyllum** Jia, 1977

Neogrypophyllum Jia in Jia and others, 1977, p. 163.

Type species. **Neogrypophyllum zhongguoense** Jia in Jia and others, 1977, p. 163, Pl. 55, figs. 5a, b. Upper part of the Donggangling Formation, Middle Devonian; holotype from either Bohong or Waituo, Tianyang County, Guangxi, China. The upper part of the Donggangling Formation (formerly transliterated as Tungkanling Formation) is Givetian age.

Original description. Solitary cylindrical corallum. The septa are thin, their peripheral ends are separated from the outer wall by presepiments. Major septa reach the centre of the corallum. Minor septa are rather long. The zone of presepiments is wide, with many rows of large, vertically arranged, hemielliptical presepiments. Tabulae incomplete, small, inwardly sloping, forming concave tabularial surfaces (edited version of a translation from the original Chinese, provided by the Translation Bureau of the Department of the Secretary of State, Canada).

Remarks. According to Jia, **Neogrypophyllum** is distinguished from **Grypophyllum** by its large presepiments that completely dominate the marginarium, and it is separated from **Neomphyma** by its better developed septa, especially minor septa, and by its concave tabulae. In addition to the type species, **Grypophyllum salairicum** Bul'vanker, from the late Dalejan Upper Shanda Beds of the Kuznets Basin, was referred to **Neogrypophyllum** by Jia. However, Bul'vanker's species has wavy septa and inconsistently developed presepiments, and is better referred to **Dubrovia.**

Neogrypophyllum must be regarded as nomen dubium, until its type species is more fully described and illustrated. Hill (1981, p. 236) considered it be questionably synonymous with **Grypophyllum.**

Genus **Ellesmerelasma** nov.

Type species. **Ellesmerelasma pumile** sp. n.

Assigned species. The only species placed in the genus, other than the type, is **Lyrielasma pinghuangshanense** Kong (in Kong and Huang, 1978, p. 123, Pl. 40, figs. 9a, b), from the Longdonshui Formation (Eifelian), Dushan region of Guizhou, southern China.

Diagnosis. Solitary ceratoid to subcylindrical genus of ptenophyllinid corals with a deep, conical calice. Septa moderately flexuous and flanged, weakly rhopaloid, peripherally discontinuous but forming a narrow, irregular septal stereozone. Inwardly sloping dissepimentarium comprises both dissepiments and presepiments. Tabulae closely spaced, incomplete, arranged to form axially depressed tabularial surfaces.

Remarks. Prior to Birenheide's (1972) revision of **Grypophyllum,** species of **Ellesmerelasma** might have been placed in that genus. Now, they are distinguished from species of **Grypophyllum** by having a broader, less regular stereozone and relatively much coarser and less well aligned trabeculae. According to Hill's (1981) concept of **Dubrovia,** that genus is distinguished from **Ellesmerelasma** by lacking a septal stereozone. **Salairophyllum** has a septal stereozone, but lacks presepiments. **Tonkinaria** has a flared calice, and in **Neogrypophyllum,** both the septa and outer wall are thin.

The name is compounded from Ellesmere (Island), and the Greek noun **elasma,** meaning a plate. The elision is deliberate.

Ellesmerelasma pumile sp. n.

Plate 42.1, figures 16-30

Type series. Holotype, UA 7042, and paratypes UA 7043-7048, all from UA locality PCC 92246.

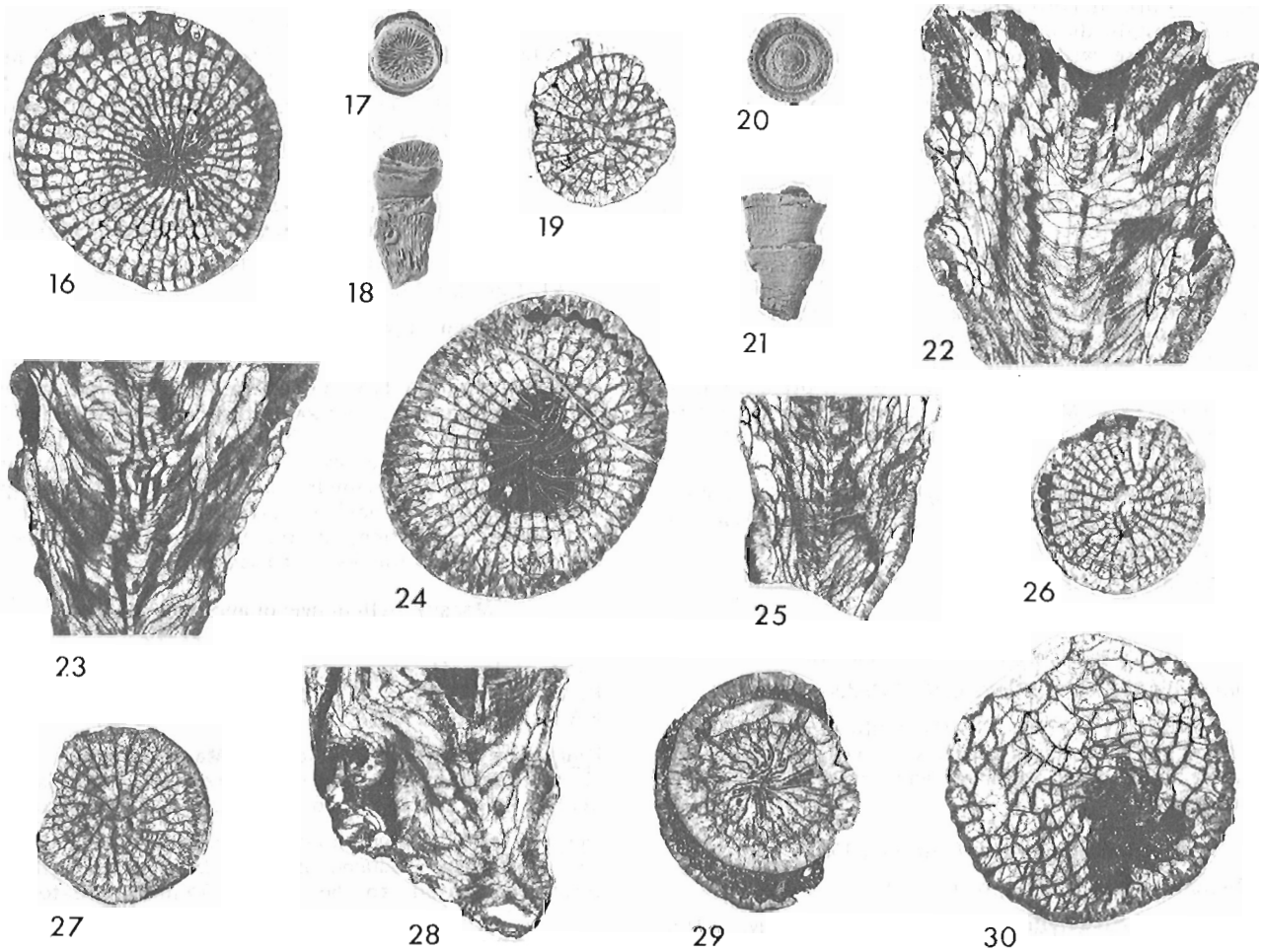

Plate 42.1

Figures 16-30. **Ellesmerlasma pumile** gen. et sp. n.

16-18, 23. Holotype, UA 7042, transverse and longitudinal thin sections, x4, and two exterior views before sectioning, x1; UA locality PCC 92246.
19. Paratype, UA 7046, transverse thin section, x4; UA locality PCC 92246.
20-22, 26. Paratype, UA 7043, two exterior views before sectioning, x1, and longitudinal and transverse thin sections, x4; UA locality PCC 92246.
24, 28. Paratype, UA 7044, transverse and longitudinal thin sections, x4; UA locality PCC 92246.
25, 29. Paratype, UA 7045, longitudinal and transverse thin sections, x4; UA locality PCC 92246.
27. Paratype, UA 7047, transverse thin section, x4; UA locality PCC 92246.
30. Paratype, UA 7048, transverse thin section, x4; UA locality PCC 92246.

Diagnosis. Small (maximum length and mean diameter about 25 and 10 mm) species of **Ellesmerelasma** with 19x2 to 23x2 septa at maturity, and a dissepimentarium that includes some exceptionally elongate dissepiments and presepiments.

Description. Corallum solitary, growth form ceratoid, tending towards subcylindrical, with relatively prominent rejuvenescences. When complete, probably none of the specimens in the type series exceeded 25 mm in length, or 10 mm in maximum mean diameter. Upper edges of the flexuous and flanged septa are much higher than the most distal tabularial surface, so that the calice of unprepared specimens appears to be considerably shallower than it would be in longitudinal section. In longitudinal section, the calice appears to be almost as deep as it is wide and to have the form of an upside-down cone. There is no calicular platform. Growth rings, septal furrows and interseptal ridges are not prominent.

The outer wall, which is abraided, to some extent, in all the type specimens, varies in thickness. The maximum thickness is 1.3 mm; the mean thickness is estimated to be about 0.7 mm. Along its thickest parts, the wall is a septal stereozone. Septa of both orders are well developed. Over most of their length, they are flexuous and moderately thick, and, in places, are withdrawn from the periphery. Major septa are unequally long; the longest terminate near the axis. They are commonly somewhat dilated adaxially, but show almost no tendency to rotate. Most minor septa are a half to three quarters of the length of the major septa. At diameters of 5.5 to 6.5 mm, there are 18x2 to 20x2 septa; at the maximum mean diameter of 9.0 to 10.0 mm, the septal count is 19x2 to 23x2.

In early stages, that is when the diameter is less than 5.0 mm, dissepiments may be absent, or limited to one or two rows. At maturity, there are normally four to six rows of elongate to very elongate, steeply inwardly inclined dissepiments and presepiments. Tabulae are closely spaced, incomplete and form typical axially depressed, ptenophyllinid tabularial surfaces. Many of the outermost tabulae are inwardly inclined almost as much as the dissepiments and presepiments.

Remarks. **Ellesmerelasma pinghuangshanense** is a slightly smaller species and has smaller dissepiments, as well as considerably fewer presepiments.

The trivial name is the Latin adjective **pumilis,** meaning dwarfish, little, etc.

Family CYATHOPHYLLIDAE Dana, 1846

Subfamily STERICTOPHYLLINAE Pedder, 1965

Diagnosis. Subfamily of the Cyathophyllidae distinguished principally by its trabeculae, which are contiguous, forming dilated septa, in at least the inner and central parts of the dissepimentarium.

Genus **Mansuyphyllum** Fontaine, 1961

Mansuyphyllum Fontaine, 1961, p. 100, 101.

Type species. **Cyathophyllum annamiticum** Mansuy, 1913, p. 9, 10, Pl. 1, fig. 11; Pl. 2, fig. 2. "Dévonien supérieur", region of Mui Ron, Qui-Dat area, Viet-Nam. This species was redescribed by Fontaine (1961, p. 101, 102, Pl. 17, figs. 1a-2). Fontaine (1961, p. 19) stated that its age is not known, but on page 101 of the same work, gave the stratigraphic range of **Mansuyphyllum** as Middle Devonian.

Diagnosis. Genus of sterictophyllinid corals in which the trabeculae are directed upwards and inwards at high angles (typically 55° to 80°) near the periphery.

Description. Corallum solitary, trochoid to ceratoid. Calice with narrow platform and cup-shaped pit that is generally not as deep as it is wide. Septa well developed in two orders, variably carinate with zigzag or offset carinae; they are also variably fusiform. Arrangement of septa radial, to just bilateral about a shortened cardinal septum and elongate counter septum. Trabeculae monacanthate, directed at high angles (typically 55° to 80°) near the periphery, flattening and flexing in the charactophylloid manner adaxially. Dissepiments numerous, small, well inflated, forming more or less horizontal surfaces around the calicular platform, becoming more elongate and inwardly inclined towards the tabularium. Tabulae, in species having abaxially withdrawn septa (includes the type species), are broad and tend to form flat tabularial surfaces. Species having well developed septa generally have incomplete tabulae and concave tabularial surfaces.

Remarks. **Mansuyphyllum** was proposed by Fontaine (1961, p. 100; 1966, p. 58) for solitary corals that, he believed, have the internal morphology of **Disphyllum.** The interpretation given to the genus here is similar to Hill's (1981, p. 302), but must remain tentative until the trabecular structure of the type species is adequately known.

Mansuyphyllum uyenoi (Pedder, 1982a) was at first referred to **Cavanophyllum** Pedder (1965, p. 215, 216). Now it is recognized that true species of **Cavanophyllum** have flatter (inclined at 45° or less at the periphery) and less divergent trabeculae.

Mansuyphyllum uyenoi (Pedder, 1982)
Mansuyphyllum uyenoi uyenoi (Pedder, 1982)

Cavanophyllum sp.; Pedder in Jackson et al., 1978, p. 152, Pl. 41, figs. 2, 4.

Cavanophyllum uyenoi Pedder, 1982a, p. 76, Pl. 9.1b, figs. 5-10.

Remarks. The holotype and one of the paratypes came from the **Polygnathus** aff. **perbonus** conodont unit (Zlichovian) of the Blue Fiord Formation in the Sor Fiord section on the northern limb of the Schei Syncline. The other paratype came from a spot sample collected from the **Polygnathus dehiscens** Zone (Zlichovian part), near or at the base of the Blue Fiord Formation, on the northern limb of the Schei Syncline, close to the Sor Fiord section.

Mansuyphyllum uyenoi avernale subsp. n.
Plate 42.1, figures 31-40

Type series. Holotype, UA 7049, UA locality PCC 92068. Paratypes, UA 7050, 7051, UA locality PCC 92068; UA 7052, UA locality PCC 92070.

Diagnosis. Subspecies of **Mansuyphyllum uyenoi** characterized by its small size (maximum mean diameter of 26.0 mm) and low septal count (31x2 or 32x2 at maturity).

Description. Corallum solitary, trochoid to ceratoid, not known to have produced offsets. Maximum length in type series estimated to be about 45 mm; greatest mean

---

Plate 42.1

Figures 31-40. **Mansuyphyllum uyenoi avernale** subsp. n.

31, 36, 40. Holotype, UA 7049, transverse and longitudinal thin sections, x3, and part of transverse thin section, x10; UA locality PCC 92068.
32, 33, 38, 39. Paratype, UA 7050, two exterior views before sectioning, x1, and longitudinal and transverse thin sections, x3; UA locality PCC 92068.
34, 35, 37. Paratype, UA 7052, two transverse and a longitudinal thin section, x3; UA locality PCC 92070.

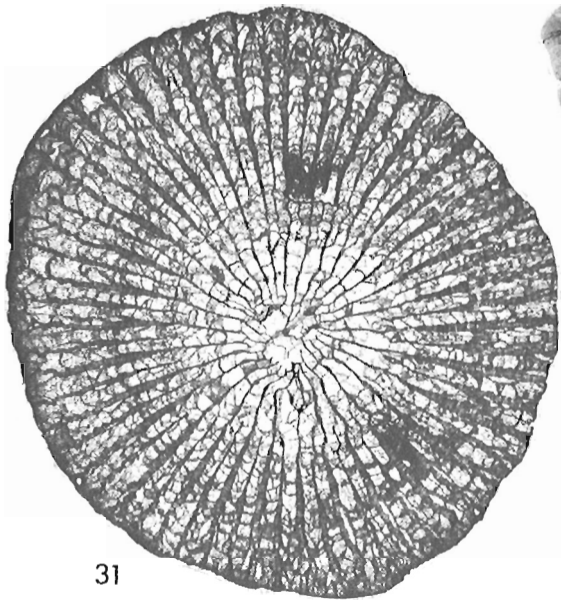

31

32

33

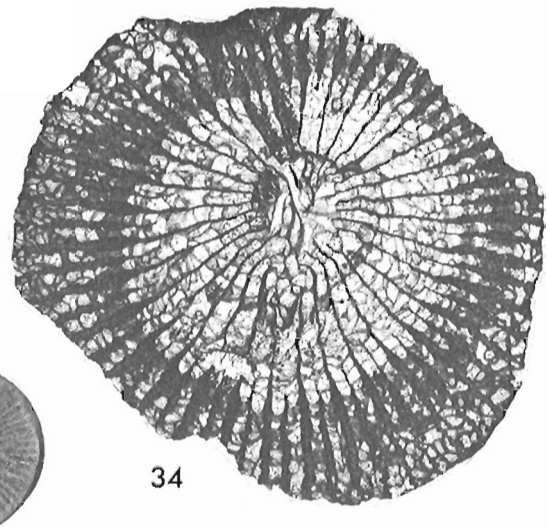

34

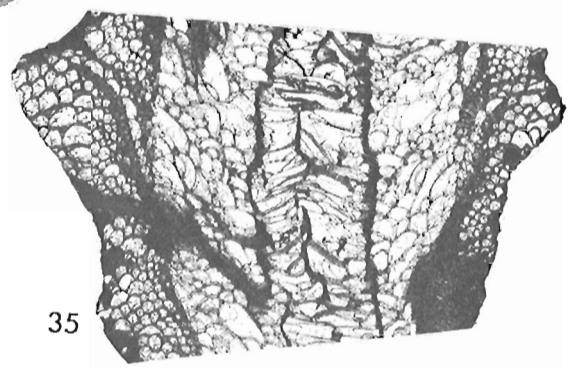

35

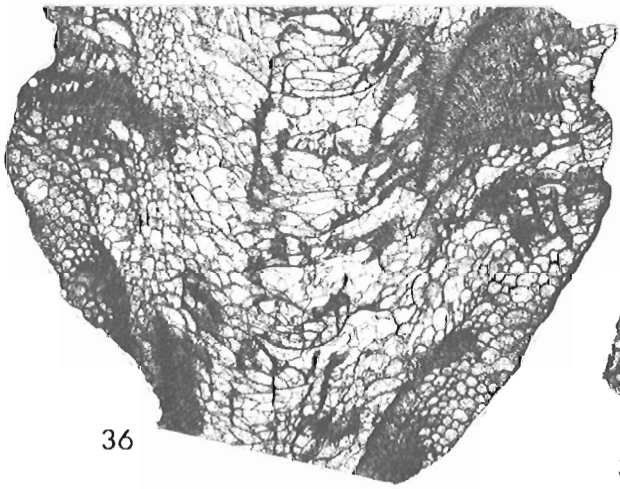

36

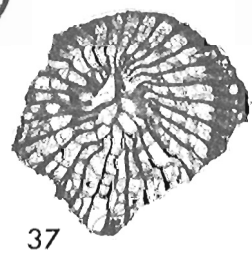

37

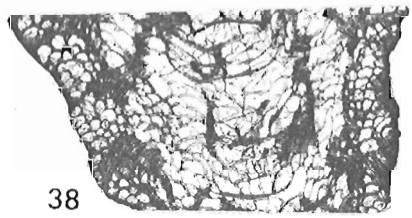

38

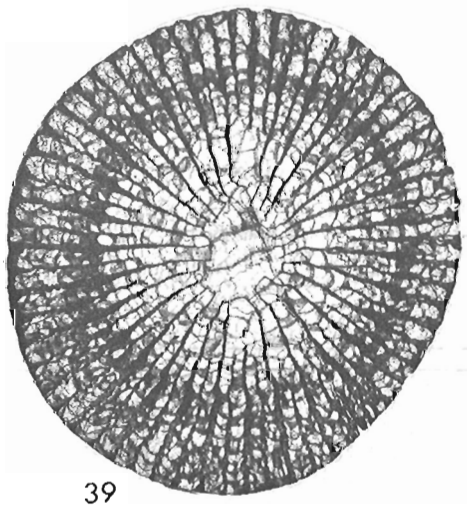

39

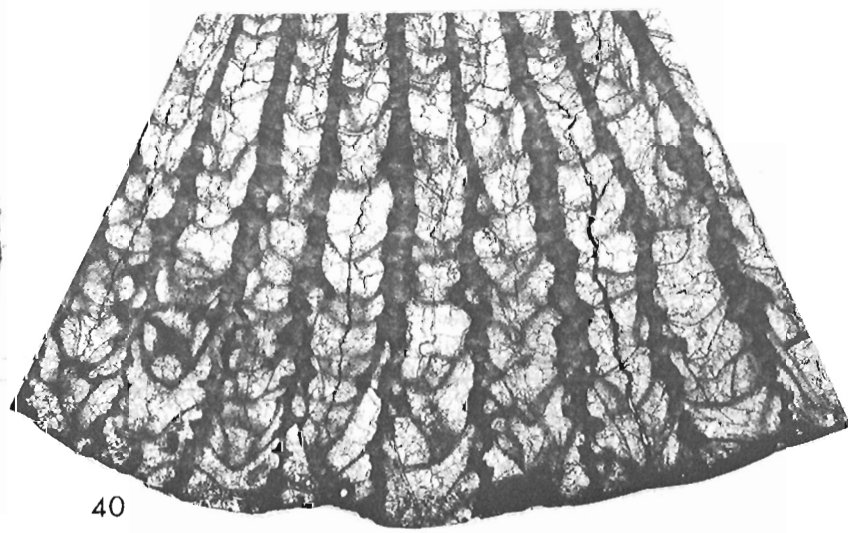

40

diameter 26.0 mm. Calice shallow, about 12.0 mm deep; base of calicular pit gently concave, sides not clearly differentiated from the narrow calicular platform. Where preserved, the outer wall is 0.1 to 0.3 mm thick, and bears prominent septal furrows and broad interseptal ridges.

Septa radially arranged around the marginarium, very weakly bilateral, in the tabularium, about a slightly shortened cardinal septum and a typically elongated counter septum. The septal count increases from 29x2 at a diameter of 13.0 mm, to 31x2 or 32x2 at full size. Between prominent zigzag and offset carinae, septa are thin in the peripheral region; in the inner dissepimentarium the septa are thickened, appearing fusiform in transverse section. Major septa project well into the tabularium, but leave an axial region, of about 3.0 mm diameter, that is virtually free of septa. Minor septa terminate in the outer tabularium. Both orders of septa progressively attenuate adaxially from the inner margin of the dissepimentarium. Trabeculae poorly preserved in type material, probably monacanthate, certainly coarse, with diameters mostly of 0.1 to 0.3 mm. Immediately inside the periphery, the trabeculae are commonly not in contact and are directed upwards at angles of 55° to 80°; towards the axis they become contiguous and their angle of inclination decreases. At and near the transition from dissepimentarium to tabularium, they are flexed in the charactophylloid manner. In the paratypes, variable inner walls are formed by sclerenchymal investment of certain inner dissepimentarial surfaces.

Dissepiments vary in size and shape. Towards the periphery, most are small, but strongly inflated; towards the axis many are elongate and not easily differentiated from marginal tabellae. At maturity, there are typically 12 to 15 rows of dissepiments. Dissepimentarial surfaces, which are more or less horizontal near the periphery, become increasingly more inwardly inclined towards the axis. Tabulae incomplete, concave to convex, typically forming gently concave tabularial surfaces, that may, however, be upturned against the elongated counter septum. Periodically the tabularial surfaces carry a coating of sclerenchyme.

Remarks. The trivial name of this subspecies, which is the Latin adjective **avernalis**, meaning of Avernus, the nether world, refers to the proximity of the type locality to Hell Gate.

Mansuyphyllum versicularium sp. n.

Plate 42.1, figures 41-56

Type series. Holotype, UA 7053, UA locality PCC 92246. Paratypes UA 7054-7057, UA locality PCC 92246; UA 7058, UA locality PCC 92240; UA 7059, UA locality PCC 92230.

Diagnosis. Small (maximum length and mean diameter about 32 and 24 mm respectively) species of **Mansuyphyllum** with deeply incised septal furrows and as many as 36x2, thin, slightly fusiform and distinctly carinate septa. Tabulae incomplete, forming predominantly gently concave tabularial surfaces.

Description. Corallum solitary, trochoid to ceratoid; no evidence of budding in the type series. Maximum known length, measured along the convex side of the corallum, 32 mm; transverse sections elliptical rather than circular, maximum mean diameter 24 mm, but normally less than 22 mm. Calice shallow, about 9 mm deep; base of calicular pit weakly concave, walls grading to a calicular platform, about 4 mm wide. Outer wall mostly 0.1 to 0.2 mm thick between adjacent septal bases; locally, thickness decreases to as little as 0.05, or increases to as much as 0.3 mm. Convex interseptal ridges and deep setal furrows, such as those shown in figures 44 and 45, are characteristic of the species. Fine growth rings are well preserved on some specimens.

Normally, one septum, situated on the convex side of the corallum, is longer than the other septa. It is assumed to be the counter septum. Another septum, situated more or less opposite the long septum, is shorter than most of the other major septa, and is assumed to be the cardinal septum. The remaining major septa are commonly just bilaterally symmetrical about the assumed cardinal/counter plane, which usually corresponds to the greatest diameter of the corallum at a given level. The septal count increases from about 24x2 at 7.5 mm diameter, to about 33x2 at 19.0 mm, and about 35x2 at 22.0 mm. The largest type has 36x2 septa at its greatest mean diameter of 24.0 mm. Zigzag and offset carinae are weakly to strongly developed. Septa tend to be thinner and more strongly carinate near the periphery than in the inner dissepimentarium, where they are generally slightly fusiform. Major septa leave an axial space, usually 2.0 to 2.2 mm in mean diameter, that is free of septa, except for the elongated counter septum. Minor septa are confined to the dissepimentarium in early stages, subsequently they lengthen, but terminate near the transition from dissepimentarium to tabularium. Trabeculae, which are believed to be monacanthate and to have diameters of 0.05 to 0.2 mm, are mostly in contact, even at the periphery, where they are directed upwards and inwards at angles of 50° to 85°; adaxially, their angle of inclination decreases, and they flex in the charactophylloid manner.

There are about eight or nine rows of dissepiments in fully grown coralla. The outer five or six rows comprise small globular dissepiments, arranged to form a more or less horizontal surface, that corresponds to the calicular platform. Interior dissepiments are more elongate and inwardly inclined than the outer ones, and merge with lateral tabellae. Tabulae vary in shape; a few are almost complete, most are not. Tabularial surfaces are flat in places, but, overall, are concave. Very thin, sclerenchymal layers coat a few of the tabularial surfaces.

Remarks. Although **Mansuyphyllum versicularium** is slightly smaller than **M. uyenoi avernale**, it has more septa. Other distinctions between the two species are that the septa and trabeculae are finer in **M. versicularium**, its trabeculae are mostly contiguous near the periphery, and it has deeper septal furrows and a shallower calice than **M. uyenoi avernale.**

The form named **Mansuyphyllum** cf. **pseudosociale** (Soshkina) by Fontaine (1966, p. 60, 61, Pl. 8, fig. 6; Pl. 9, fig. 9), from the Middle Devonian of Yunnan, is similar to **M. versicularium.** It differs in having reduced minor septa, convex tabularial surfaces, and trabeculae that are said to be "fortement inclinées vers l'extérieur". **Tabulophyllum**

Plate 42.1

Figures 41-56. **Mansuyphyllum versicularium** sp. n.

41-43, 50, 54. Holotype, UA 7053, two transverse and a longitudinal thin section, x3, and two exterior views before sectioning, x1; UA locality PCC 92246.
44. Paratype, UA 7054, exterior view before sectioning, x1; UA locality PCC 92246.
45. Paratype, UA 7056, exterior calicular view before sectioning, x1; UA locality PCC 92246.
46, 49, 56. Paratype, UA 7058, transverse and longitudinal thin sections, x3, and part of longitudinal thin section, x10; UA locality PCC 92240.
47, 52. Paratype, UA 7055, longitudinal and transverse thin sections, x3; UA locality PCC 92246.
48, 51, 55. Paratype, UA 7059, transverse and longitudinal thin sections, x3, and part of a transverse thin section, x10; UA locality PCC 92230.
53. Paratype, UA 7057, transverse thin section, x3; UA locality PCC 92246.

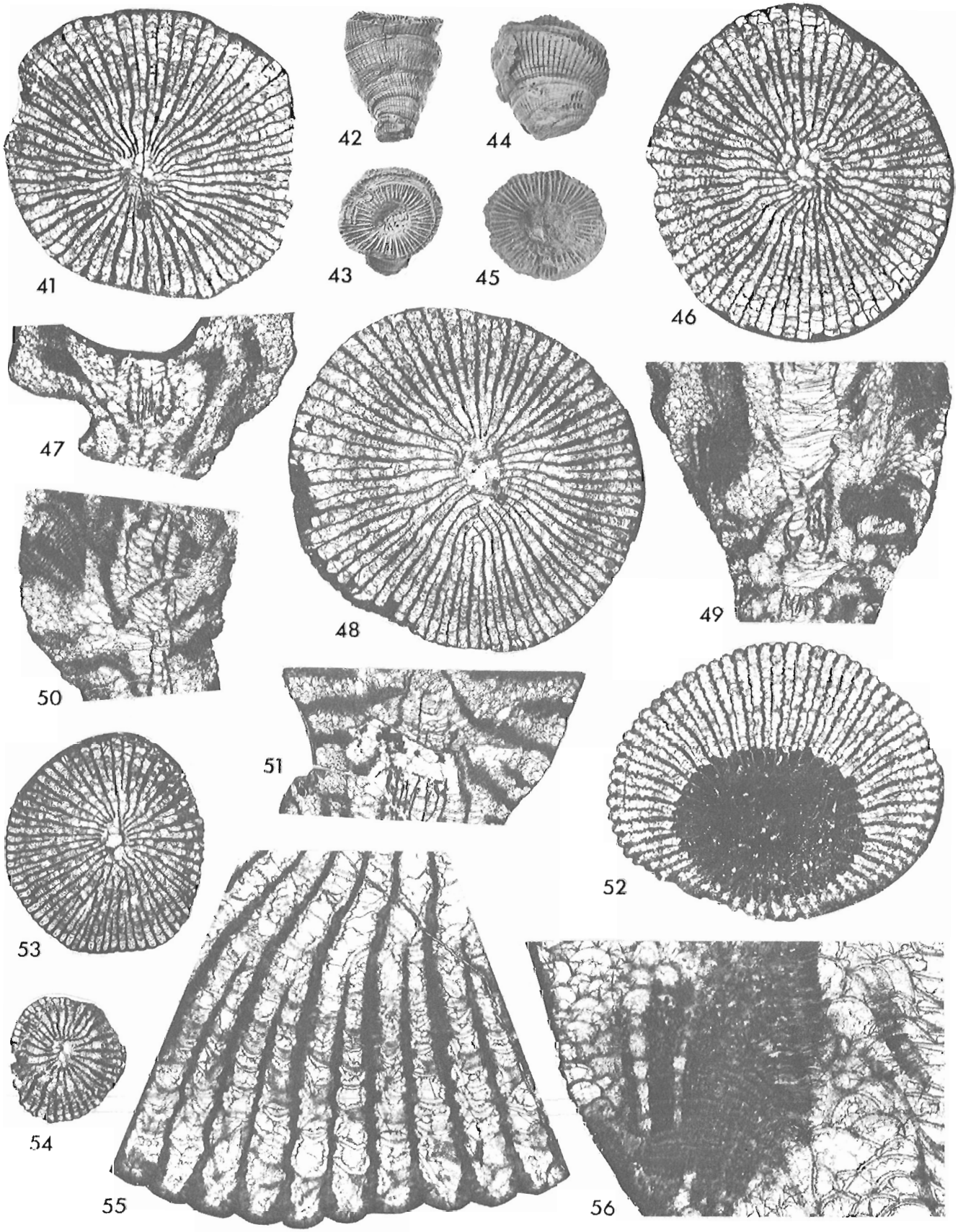
41
42
43
44
45
46
47
48
49
50
51
52
53
54
55
56

pseudosociale Soshkina (1952, p. 71, text-fig. 100, Pl. 3, fig. 18), strict sense, is an Upper Devonian species from the Russian Platform, that is weakly colonial, and has the interior morphology of **Mictophyllum.**

The trivial name **versicularius** comes from the Latin **versiculus,** meaning a small furrow, and the suffix **-arius.** It refers to the strong septal furrows of the species.

Mansuyphyllum comsolum sp. n.

Plate 42.1, figures 57-63

Type series. Holotype, UA 7060, UA locality PCC 92232. Paratype, UA 7061, UA locality PCC 92246.

Diagnosis. Small (maximum mean diameter about 18.5 mm) species of **Mansuyphyllum,** with about 32x2 abaxially withdrawn septa, that leave an axial region, of about 4.0 mm diameter, free of septa. Dissepimentarium narrow, generally with six, or less, rows of dissepiments. Tabulae broad, forming tabularial surfaces that tend to be flat periaxially and downturned marginally.

Description. Corallum solitary, trochoid to ceratoid, not known to have produced offsets. Maximum mean diameter 18.5 mm; full length unknown, at least 30 mm. Calice not preserved, but longitudinal sections indicate that it would have a narrow calicular platform and a wide, more or less flat bottomed calicular pit. The outer wall is 0.1 to 0.3 mm thick, and bears deep septal furrows and variably convex interseptal ridges.

Septa radially arranged. In the holotype, the septum that is assumed to be the cardinal septum is slightly shorter than the other major septa; a slightly elongated septum is assumed to be the counter septum. In the paratype, a slightly shortened major septum is assumed to be the cardinal septum; the counter septum does not appear to be differentiated. At a diameter of 13.0 mm, the paratype has 23x2 septa. The holotype has 32.2 septa at 16.5 and 18.4 mm diameter. Septa are variably, but on the whole, moderately carinate in the dissepimentarium; the carinae being of both the zigzag and offset types. Near the periphery, septa are either thin or thick; in the inner dissepimentarium and outer tabularium they are fusiform. Major septa are withdrawn from the axis, leaving an axial region, of about 4.0 mm mean diameter, that is completely free of septa. Minor septa just project into the tabularium. Trabeculae are directed upwards and inwards, mostly at angles of 50° to 60° near the periphery. Adaxially, their angles of inclination decrease, and they become flexed in the charactophylloid manner. Diameters of the trabeculae are about 0.08 to 0.13 mm; their fine structure is not preserved.

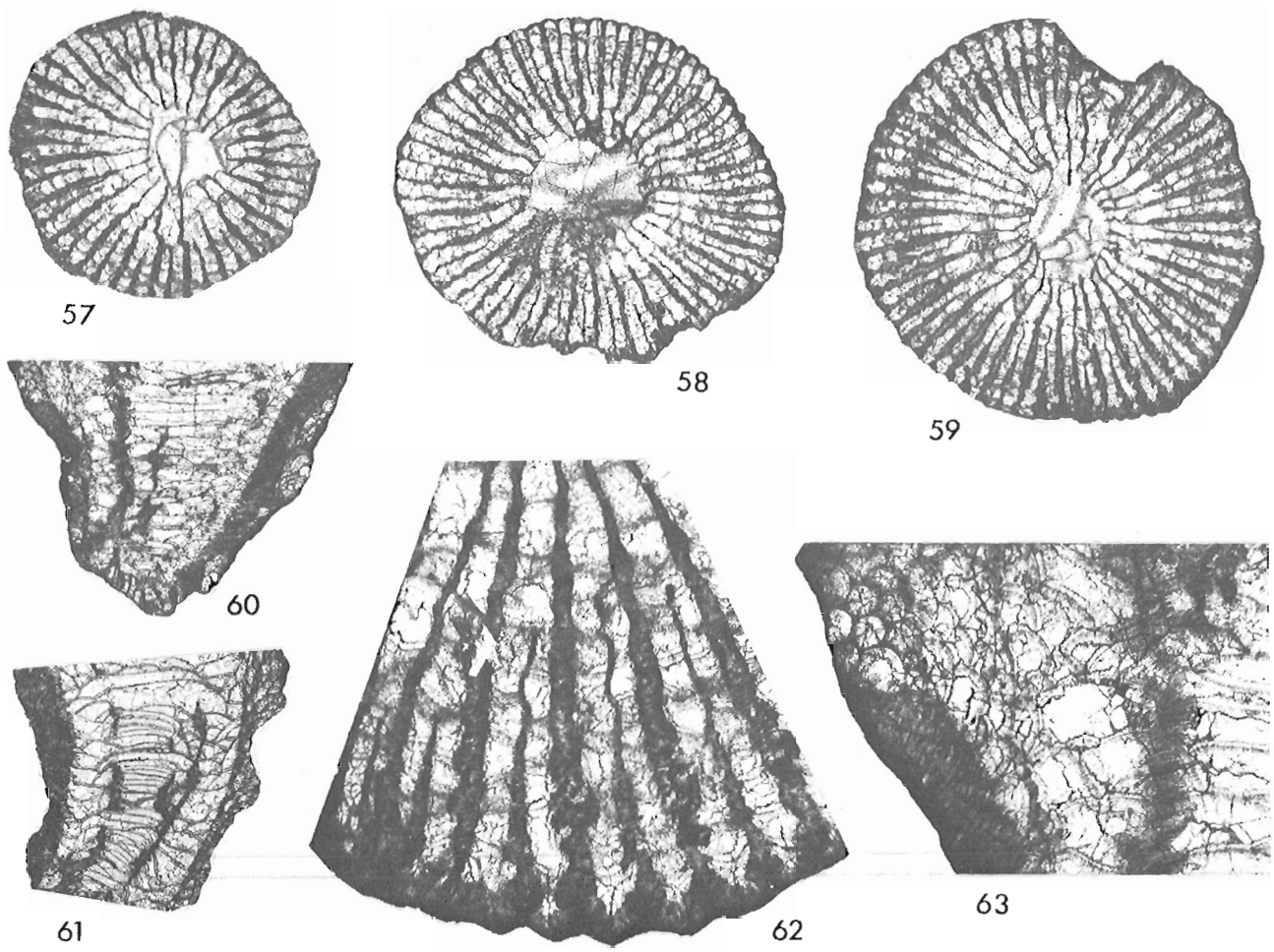

Plate 42.1

Figures 57-63. **Mansuyphyllum comsolum** sp. n.

57, 61. Paratype, UA 7061, transverse and longitudinal thin sections, x3; UA locality PCC 92246.
58-60, 62, 63. Holotype, UA 7060, two transverse and a longitudinal thin section, x3, and parts of transverse and longitudinal thin sections, x10; UA locality PCC 92232.

The dissepimentarium is narrow, usually comprising only four to six rows of dissepiments in adult stages. Dissepiments in the outer rows tend to be small and well inflated. Interior dissepiments are more elongate and are steeply inclined. Tabulae are broad, some are quite complete. Tabularial surfaces are commonly more or less flat periaxially, and downturned marginally. Thin layers of sclerenchyme cover many of the more proximally situated tabularial surfaces.

Remarks. **Mansuyphyllum comsolum** resembles **M. versicularium,** and the two species are presumed to be closely related. **M. comsolum** is distinguished by having shorter major septa, a much narrower dissepimentarium, and broad tabulae that tend to form periaxially flat tabularial surfaces.

The trivial name **comsolum** is formed from the Latin noun **solum,** meaning bottom, floor etc., and the prefix **com-**, meaning with. It refers to the relatively wide, almost flat tabularium of the species.

Acknowledgments

Brian Jones, University of Alberta, identified the brachiopods listed in the Locality Register and supervised Goodbody's field work. B.D.E. Chatterton, University of Alberta, isolated and identified conodonts from a sample of Bird Fiord Formation collected by Brian Jones and Goodbody. The age significance of this fauna was also discussed with T.T. Uyeno, Institute of Sedimentary and Petroleum Geology. David Worsley, University Paleontological Museum, Oslo, provided copies of some of Schei's unpublished field notes. The photography is the work of B.C. Rutley and W.B. Sharman, both of the Institute of Sedimentary and Petroleum Geology. R.D. Michie, of the same Institute, assisted in preparing thin sections. Goodbody's field work was supported logistically by the Polar Continental Shelf Project, and financially by the National Sciences and Engineering Research Council of Canada (grant no. A6090 to Brian Jones), the Boreal Institute for Northern Studies, the Arctic Institute of North America, the Geological Society of America and the American Association of Petroleum Geologists.

We are grateful to these individuals and organizations for their considerable aid.

Locality Register

All localities are on southwestern Ellesmere Island in the District of Franklin. Brachiopods of the faunal lists were identified by Brian Jones. UA and PCC are abbreviations for the University of Alberta and Paleontological Collections Catalogue.

UA locality PCC 92068. Bird Fiord Formation, 375.5 m above base, and 125.5 m above the top of the gypsiferous dolostone unit in the lower part of the formation at this locality. Blubber Point; 76°36'N latitude, 89°35'W longitude. Collected by Q.H. Goodbody, 1981. **Favosites** sp., **Cladopora** sp., **Oculipora** ? sp., **Lekanophyllum retiforme** Pedder, **L. rugulosum** Pedder, **Taimyrophyllum** sp., **Mansuyphyllum uyenoi avernale** Pedder and Goodbody, **Schizophoria sulcata** Johnson and Perry, indeterminate strophomenid brachiopod, **Minutostropheodonta** ? sp., **Trigonirhynchia** ? sp., **Spinatrypa** sp., **Perryspirifer scheii** (Meyer), **"Elythina" sverdrup** Brice, indeterminate bivalves.

UA locality PCC 92070. Bird Fiord Formation, 385 m above base, and 135 m above the top of the gypsiferous dolostone unit in the lower part of the formation at this locality. Same section and collection data as UA locality PCC 92068. **Cladopora** sp., **Alveolites** sp., **Oculipora** ? sp., **Syringopora** sp., **Lekanophyllum foliatum** Pedder and Goodbody, **L. retiforme** Pedder, **L. rugulosum** Pedder, **Taimyrophyllum** sp., **Mansuyphyllum uyenoi avernale** Pedder and Goodbody, **M.** sp., **Schizophoria sulcata** Johnson and Perry, indeterminte strophomenid brachiopod, **Minutostropheodonta** ? sp., **Spinatrypa** sp., **Perryspirifer scheii** (Meyer), **"Elythina" sverdrupi** Brice.

UA locality PCC 92229. Bird Fiord Formation, approximately 350 m above base, and 58 m above the top of the gypsiferous dolostone unit in the lower part of the formation at this locality. Top of the northeastern wall of a cirque, north fork of valley, 9 km north-northwest of the head of Muskox Fiord; 76°42'26"N latitude, 87°28'W longitude. Collected by Q.H. Goodbody, 1982. **Favosites** sp., **Oculipora** ? sp., **Lekanophyllum foliatum** Pedder and Goodbody, **L. rugulosum** Pedder, **Schizophoria sulcata** Johnson and Perry, **Atrypa** sp. B of Jones (1982), **Perryspirifer scheii** (Meyer), **"Elythina" sverdrupi** Brice.

UA locality PCC 92230. Bird Fiord Formation, approximately 352 m above base, and 60 m above the top of the gypsiferous dolostone unit in the lower part of the formation at this locality. Same section and collection data as UA locality PCC 92229. **Alveolites** sp., **Oculipora** ? sp., **Lekanophyllum foliatum** Pedder and Goodbody, **L. retiforme** Pedder, **Mansuyphyllum versicularium** Pedder and Goodbody, **Schizophoria sulcata** Johnson and Perry, **Atrypa** sp. B of Jones (1982), **Perryspirifer scheii** (Meyer), **"Elythina" sverdrupi** Brice, biaxial crinoid ossicles.

UA locality PCC 92232. Bird Fiord Formation, approximately 368 m above base, and 76 m above the top of the gypsiferous dolostone unit in the lower part of the formation at this locality. Same section and collection data as UA locality PCC 92229. **Alveolites** sp., undetermined sponge, **Lekanophyllum foliatum** Pedder and Goodbody, **Mansuyphyllum comsolum** Pedder and Goodbody, **Minutostropheodonta** ? sp., **Atrypa** sp. B of Jones (1982), **Spinatrypa borealis** (Warren), **Perryspirifer scheii** (Meyer).

UA locality PCC 92233. Bird Fiord Formation, approximately 374 m above base, and 82 m above the top of the gypsiferous dolostone unit in the lower part of the formation at this locality. Same section and collection data as UA locality PCC 92229. **Cladopora** sp., **Alveolites** sp., **Oculipora** ? sp., **Syringopora** sp., **Lekanophyllum foliatum** Pedder and Goodbody, **L. retiforme** Pedder, **L. rugulosum** Pedder, **Taimyrophyllum** sp., **Atrypa** sp. B of Jones (1982), **Spinatrypa borealis** (Warren), **"Elythina" sverdrupi** Brice, biaxial crinoid ossicles.

UA locality PCC 92240. Bird Fiord Formation, spot sample from approximately 375 m above base, and 90 m above the top of the gypsiferous dolostone unit in the lower part of the formation at this locality. Eastern side of main valley, 10 km north of the head of Muskox Fiord; 76°42'33"N latitude, 87°42'15"W longitude. Collected by Q.H. Goodbody, 1982. Caunopore consortium, **Oculipora** ? sp., **Aulopora** sp., **Lekanophyllum foliatum** Pedder and Goodbody, **L. retiforme** Pedder, **Taimyrophyllum** sp., **Mansuyphyllum versicularium** Pedder and Goodbody, **Schizophoria sulcata** Johnson and Perry, indeterminate strophomenid brachiopod, **Trigonirhynchia** ? sp., **Atrypa** sp. B of Jones (1982), **Spinatrypa borealis** (Warren), **Emanuella** sp., **"Elythina" sverdrupi** Brice.

UA locality PCC 92244. Bird Fiord Formation, spot sample from approximately 400 m above base, and 115 m above the top of the gypsiferous dolostone unit in the lower part of the formation at this locality (UA locality PCC 92244 is 25 m stratigraphically above UA locality PCC 92240). Eastern side of main valley, 10 km north of the head of Muskox Fiord; 76°42'45"N latitude, 87°42'W longitude. Collected by

Q.H. Goodbody, 1982. Caunopore consortium, **Favosites** sp., **Cladopora** sp., **Alveolites** sp., **Oculipora** ? sp., **Syringopora** sp., **Lekanophyllum foliatum** Pedder and Goodbody, **L. retiforme** Pedder, **L. rugulosum** Pedder, **Taimyrophyllum** sp., **Atrypa** sp. B of Jones (1982), **Spinatrypa borealis** (Warren), **Howellella** ? sp. **Perryspirifer scheii** (Meyer).

UA locality PCC 92246. Bird Fiord Formation, spot sample from approximately 420 m above base, and 135 m above the top of the gypsiferous dolostone unit in the lower part of the formation at this locality (UA locality PCC 92246 is 20 m stratigraphically above UA locality PCC 92244, and 45 m stratigraphically above UA locality PCC 92240). Eastern side of main valley, 10 km north of the head of Muskox Fiord; 76°42'45"N latitude, 87°42'W longitude. Collected by Q.H. Goodbody, 1982. **Cladopora** sp., **Alveolites** sp., **Oculipora** ? sp., **Syringopora** spp. (2), **Lekanophyllum foliatum** Pedder and Goodbody, **L. retiforme** Pedder, **L. rugulosum** Pedder, **Ellesmerelasma pumile** Pedder and Goodbody, **Taimyrophyllum** sp., **Mansuyphyllum comsolum** Pedder and Goodbody, **M. versicularium** Pedder and Goodbody, **Schizophoria sulcata** Perry and Johnson, indeterminate strophomenid brachiopod, **Trigonirhynchia** ? sp., **Atrypa** sp. B of Jones (1982), **Spinatrypa borealis** (Warren), **Emanuella** sp., **Perryspirifer scheii** (Meyer), **Costacranaena marlenae** Johnson and Perry.

References

Besprozvannykh, N.I.
1968: Rugozy Tom'chumyshskikh sloev Salaira; in Korally pogranichnykh sloev silura i devona Altae-Sayanskoy gornoy oblasti i Urala, ed. A.B. Ivanovskiy; Akademiya Nauk SSSR, Sibirskoe Otdelenie, Institut Geologii i Geofiziki, Izdatel'stvo "Nauka", Moskva, p. 110-116, 160, 161.

Birenheide, R.
1968: Die Typen der Sammlung Wedekind aus der Gattung **Plasmophyllum** (Rugosa; Mitteldevon); Senckenbergiana lethaea, Band 49, p. 1-37.

1972: Ptenophyllidae (Rugosa) aus dem W-deutschen Mitteldevon; Senckenbergiana lethaea, Band 53, p. 405-437.

1978: Leitfossilien. No. 2. Rugose Korallen des Devon; Gebrüder Borntraeger, Berlin, Stuttgart, 265 p.

Brice, D.
1982: Brachiopodes du Dévonien inférieur et moyen des formations de Blue Fiord et Bird Fiord des îles arctiques Canadiennes; Geological Survey of Canada, Bulletin 326, 175 p.

Bul'vanker, E.Z.
1958: Devonskie chetryrekhluchevye korally okrani Kuznetskoy basseya; Vsesoyuznyy Nauchno-Issledovatel'skiy Geologicheskiy Institut (VSEGEI), Leningrad, text 212 p. and atlas.

Butler, A.J.
1934: On the Silurian corals **Spongophylloides grayi** (Edwards & Haime) and **Spongophylloides pusillus,** sp. n.; The Annals and Magazine of Natural History, ser. 10, v. 13, p. 540-549.

Chatterton, B.D.E.
1979: Aspects of late Early and Middle Devonian conodont biostratigraphy of western and northwestern Canada; in Western and Arctic Canadian biostratigraphy, eds. C.R. Stelck and B.D.E. Chatterton; Geological Association of Canada, Special Paper 18, p. 161-231 (imprint 1978).

Chlupáč, Ivo
1982: The Bohemian Lower Devonian stages; in On Devonian stratigraphy and palaeontology of the Ardenno-Rhenish Mountains and related Devonian matters, ed. Willi Ziegler and Rolf Werner; Courier Forschungsinstitut Senckenberg, 55, p. 345-400h.

Degtyarev, D.D.
1951: Fauna korallov izvestnyakov, vklyuchayushchikh Pashiyskuyu rudonosnuyu tolshchu v Chusovskom rayone; Ural'skiy Gosudarstvennyy Universitet imeni A.M. Gor'skogo, Sverdlovsk, 40 p.

Elkin (Yolkin), E.A., Gratsianova, R.T., Zheltonogova, V.A., and Kim, A.I.
1982: Osnovnye biostratigraficheskie rubezhi i podrazdeleniy nizhnego i srednego devona na zapade Altae-Sayanskoy oblasti i ikh korrelyatsiya; in Biostratigrafiya pogranichnykh otlozheniy nizhnego i srednego devona. Trudy polevoy sessii Mezhdunarodnoy podkomissii po stratigrafii devona. Samarkand, 1978, ed. B.S. Sokolov and M.A. Rzhonsnitskaya; Vsesoyuznyy Nauchno-Issledovatel'skiy Geologicheskiy Institut (VSEGEI), Leningrad, p. 65-80.

Engel, G. and Schouppé A. von
1958: Morphogenetisch-taxionomische Studie zu der devonischen Korallengruppe **Stringophyllum, Neospongophyllum** und **Grypophyllum;** Paläontologische Zeitschrift, Band 32, p. 67-114.

Fontaine, H.
1961: Les Madréporaires paleozoiques du Viêt-Nam, du Laos et du Cambodge; Archives Géologiques du Viêt-Nam, no. 5, 276 p. and atlas.

1966: Quelques Madréporaires dévoniens du Musée du Service Géologique de Saigon (collections du Yunnan); Archives Géologiques du Viêt-Nam, no. 9, p. 52-95.

Hill, D.
1981: Treatise on invertebrate paleontology. Part F. Coelenterata. Supplement 1. Rugosa and Tabulata, ed. Curt Teichert; Geological Society of America and the University of Kansas Press, Boulder and Lawrence, v. 1, p. 1-378; v. 2, p. 379-762.

Holtedahl, O.
1917: Summary of geological results; in Report of the Second Norwegian Arctic Expedition in the "Fram" 1898-1902; Videnskabs-Selskabet i Kristiania, v. 4, no. 36, 27 p.

Ivaniya, V.A.
1965: Devonskie korally Rugosa Sayano-Altayskoy gornoy oblasti; Izdatel'stvo Tomskogo Universiteta, Tomsk, 398 p.

Jackson, D.E., Lenz, A.C. and Pedder, A.E.H.
1978: Late Silurian and Early Devonian graptolite, brachiopod and coral faunas from northwestern and arctic Canada; Geological Association of Canada, Special Paper 17, 159 p.

Jia Hui-zhen, Xu Shou-yong, Kuang Guo-dun, Zhang Bu-fei, Zuo Zi-bi, and Wu Jin-shu
1977: Anthozoa; in Atlas of the paleontology of central and southern China, v. 2. Late Paleozoic Era (in Chinese), ed. Geological Science Research Institute, Hubei, and other institutions; Geological Publishing House, Peking, p. 109-270, 764-789.

Johnson, J.G. and Oliver, W.A., Jr.
1977: Silurian and Devonian coral zones in the Great Basin, Nevada and California; Geological Society of America, Bulletin, v. 88, p. 1462-1468.

Johnson, J.G. and Perry, D.G.
1976: Middle Devonian brachipods from the Bird Fiord Formation of Bathurst Island, Arctic Canada; Canadian Journal of Earth Sciences, v. 13, p. 615-635.

Jones, B.
1982: Devonian brachiopods from the Bird Fiord Formation of the Goose Fiord area, southern Ellesmere Island, Arctic Canada; Journal of Paleontology, v. 56, p. 1397-1409.

Kong, Lei and Huang, Yun-ming
1978: Tetracoralla; in Atlas of the paleontology of the southwestern regions of China, v. 1. Cambrian to Devonian (in Chinese), ed. Guizhou Stratigraphy and Paleontology Work Team; Geological Publishing House, Peking, p. 35-161, 739-759.

Lang, W.D. and Smith, S.
1927: A critical revision of the rugose corals described by W. Lonsdale in Murchison's 'Silurian System'; The Geological Society, Quarterly Journal, v. 83, p. 448-491.

Lindström, G.
1882: Anteckningar om silurlagren på Carlsöarne; Öfversigt of Kongliga Vetenskaps-Akademiens Förhandlingar, v. 39, no. 3, p. 5-30.

1896: Beschreibung einiger Obersilurische Korallen aus der Insel Gotland; Bihang till Kongliga Svenska Vetenskaps-Akademiens Handlingar, v. 21, no. 7, p. 1-50.

Loewe, S.
1913: Die devonischen Korallen von Ellesmereland; in Report of the Second Norwegian Arctic Expedition in the "Fram" 1898-1902, Videnskabs-Selskabet i Kristiania, v. 4, no. 30, 23 p.

Mansuy, H.
1913: Paléontologie de l'Annam et du Tonkin; Service Géologique de l'Indochine, Mémoirs, v. 2, fasc. 3, 48 p.

McLean, R.A.
1976: Middle Devonian cystiphyllid corals from the Hume Formation, northwestern Canada; Geological Survey of Canada, Bulletin 274, 80 p.

McLaren, D.J.
1963: Southwestern Ellesmere Island between Goose Fiord and Bjorne Peninsula; in Y.O. Fortier and others, Geology of the north-central part of the Arctic Archipelago Northwest Territories (Operation Franklin); Geological Survey of Canada, Memoir 320, p. 310-338.

Merriam, C.W.
1974: Silurian rugose corals of the central and southwest Great Basin; United States Geological Survey, Professional Paper 777, 66 p. (imprint 1973).

Meyer, G.
1881: Rugose Korallen als ost- und westpreussische Diluvialgeschiebe; Physikalisch- Oekonomische Gesellschaft zu Königsberg, Schriften, Band (Jahrg) 22, Abt. 1, p. 97-110.

Milne Edwards, H. and Haime, J.
1851: Monographie des polypiers fossiles des terrains palaeozoïques; Archives du Muséum d'Histoire Naturelle, tome 5, 502 p.

1855: A monograph of the British fossil corals. Part 5. Corals from the Silurian Formation; The Palaeontographical Society, London, p. 245-299 (imprint 1854).

Oliver, W.A., Jr.
1960: Devonian rugose corals from northern Maine; United States Geological Survey, Bulletin 1111-A, 23 p.

Oliver, W.A., Jr., Merriam, C.W., and Churkin, M., Jr.
1975: Ordovician, Silurian, and Devonian corals of Alaska; United States Geological Survey, Professional Paper 823-B, p. i-iv, 13-44.

Ormiston, A.R.
1967: Lower and Middle Devonian trilobites of the Canadian Arctic Islands; Geological Survey of Canada, Bulletin 153, 148 p.

Pedder, A.E.H.
1965: A revision of the Australian Devonian corals previously referred to **Mictophyllum**; Royal Society of Victoria, Proceedings, v. 78, p. 201-220.

1973: Description and biostratigraphical significance of the Devonian coral genera **Alaiophyllum** and **Grypophyllum** in western Canada; Geological Survey of Canada, Bulletin 222, p. 93-127.

1982a: New Zlichovian (Early Devonian) rugose corals from the Blue Fiord Formation of Ellesmere Island; in Current Research, Part C, Geological Survey of Canada, Paper 82-1C, p. 71-82.

1982b: Probable Dalejan (Early Devonian) cystiphyllid corals from Bird Fiord Formation of Ellesmere Island; in Current Research, Part C, Geological Survey of Canada, Paper 82-1C, p. 83-90.

Pedder, A.E.H. and McLean, R.A.
1982: Lower Devonian cystiphyllid corals from North America and eastern Australia with notes on the genus **Utaratuia**; Geologica et Palaeontologica, 16, p. 57-110.

Raasch, G.O.
1982: Lower and Middle Devonian faunal zones in the Canadian Arctic Archipelago; in Arctic geology and geophysics. Proceedings of the Third International Symposium on Arctic Geology, ed. A.F. Embry and H.R. Balkwill; Canadian Society of Petroleum Geologists, Memoir 8, p. 155-170.

Schei, P.
1903a: Preliminary report on the geological observations made during the Second Norwegian Polar Expedition of the "Fram"; Royal Geographical Society, London, 9 p.

1903b: Forelobig Redegjorelse for de geologiske lagttagelser anstillede under den 2den Norske Polarfaerd med "Fram"; Aktie-Bogtrykkeriet, Kristiania, 16 p.

1904: Preliminary account of the geological investigations made during the Second Norwegian Polar Expedition in the 'Fram'; Appendix I, in Otto Sverdrup (translated from the Norwegian by E.H. Hearn); New Land. Four years in the arctic regions, v. 2; Longmans, Green, and Co., London, New York and Bombay, p. 455-466.

Shurygina, M.V.
1968: Pozdnesiluriyskie i rannedevonskie rugozy vostochnogo sklona severnogo i srednego Urala; in Korally pogranichnykh sloev silura devona Altae-Sayanskoy gornoy oblasti i Urala, ed. A.B. Nanovskiy; Akademiya Nauk SSSR, Sibirskoe Otdelenie, Institut Geologii i Geofiziki, Izdatel'stvo "Nauka", Moskva, p. 117-150, 161-164.

Smith, G.P. and Stearn, C.W.
1982: The Devonian carbonate-clastic sequence on southwest Ellesmere Island, arctic Canada; in Arctic geology and geophysics. Proceedings of the Third International Symposium on Arctic Geology, ed. A.F. Embry and H.R. Balkwill; Canadian Society of Petroleum Geologists, Memoir 8, p. 147-154.

Soshkina, E.D.
1936: Korally Rugosa srednego devona severnogo Urala; Akademiya Nauk SSSR, Polyarnoy Komissii, Trudy, vyp 28, p. 15-76.

1949: Devonskie korally Rugosa Urala; Akademiya Nauk SSSR, Paleontologicheskogo Instituta, Trudy, tom 15, vyp. 4, 160 p.

1952: Opredelitel' devonskikh chetyrekhluchevykh korallov; Akademiya Nauk SSSR, Paleontologicheskogo Instituta, Trudy, tom 39, 127 p.

Spasskiy, N.Ya.
1955: Korally Rugosa i ikh znachenie dlya stratigrafii srednego devona zapadnogo sklona Urala; in Stratigrafiya paleozoyskikh otlozheniy Timna i zapadnogo sklona Urala (sbornik statey), ed. M.V. Kulikov; Vsesoyuznogo Neftyanogo Nauchno-Issledovatel'skogo Geologo-Razvedochnogo Instituta (VNIGRI), Trudy, nov. ser., vyp. 90, p. 91-224.

Strusz, D.L.
1968: On **Cyathophyllum mansfieldense** Dun 1898: Lower Devonian, Loyola, Victoria; Royal Society of Victoria, Proceedings, v. 81, p. 11-18.

Sutherland, P.K.
1965: Henryhouse rugose corals; Oklahoma Geological Survey, Bulletin 109, 92 p.

Sytova, V.A.
1966: Rugozy borovushkinskoy svity (verkhniy silur) Rudnogo Altaya; Voprosy Paleontologii, tom 5, p. 93-100.

1968: Tetrakorally skal'skogo i borshchovskogo gorizontov Podolii; in Siluriysko-devonskaya fauna Podolii, ed. E.G. Balashov; Leningradskiy Ordena Lenina Gosudarstvennyy Universitet im A.A. Zhdanova, Izdatel'stvo Leningradskogo Universeteta, p. 51-71.

1970: Tetrakorally grebenskogo gorizonta vaygacha; in Stratigrafiya i fauna siluriyskikh otlozheniy Vaygacha (sbornik statey), ed. S.V. Cherkesova; Nauchno-Issledovatel'skiy Institut Geologii Arktiki, Leningrad, p. 65-86.

Taylor, P.W.
1951: The Plymouth Limestone; The Royal Geological Society of Cornwall, Transactions, v. 18, p. 146-214.

Tolmachoff, I.P.
1926: On the fossil faunas from Per Schei's Series D from Ellesmere Land with exception of brachiopods, corals and cephalopods; in Report of the Second Norwegian Arctic Expedition in the "Fram" 1898-1902, no. 38, Det Norskie Videnskaps-Akademi i Oslo, 106 p.

Uyeno, T.T.
1981: Lower and Middle Devonian conodont biostratigraphy of the Franklinian Miogeosyncline and arctic Platform, Canadian Arctic Archipelago (Abstract); Third International Symposium on Arctic Geology, Calgary, Canadian Society of Petroleum Geologists, p. 126.

Uyeno, T.T. and Klapper, G.
1980: Summary of conodont biostratigraphy of the Blue Fiord and Bird Fiord Formations (Lower-Middle Devonian) at the type and adjacent areas, southwestern Ellesmere Island, Canadian Arctic Archipelago; in Current Research, Part C, Geological Survey of Canada, Paper 80-1C, p. 81-93.

Wedekind, R.
1922: Zur Kenntnis der Stringophyllen des oberen Mitteldevon; Gesellschaft zur Beförderung der gesamten Naturwissenschaften zu Marburg, Sitzungsberichte, 1921, no. 1, p. 1-16.

1924: Das Mitteldevon der Eifel. Eine biostratigraphische Studie. 1. Teil. Die Tetrakorallen des unteren Mitteldevon; Gesellschaft zur Beförderung der gesamten Naturwissenschaften zu Marburg, Schriften, Band 14, Heft 3, 93 p.

1925: Das Mitteldevon der Eifel. Eine biostratigraphische Studie II. Teil. Materialien zur Kenntnis des mittleren Mitteldevon; Gesellschaft zur Beförderung der gesamten Naturwissenschaften zur Marburg, Schriften, Band 14, Heft 4, 85 p.

1927: Die Zoantharia Rugosa von Gotland (bes. Nordgotland); Sveriges Geologiska Undersökning, Ser. Ca, No. 19, 95 p.

Zheltonogova, V.A.
1961: Siluriyskaya sistema. Podklass Tetracoralla (Rugosa). Tetrakorally; in Biostratigrafiya paleozoya Sayano-Altayskoy gornoy oblasti. Tom II. Sredniy paleozoy, ed. L.L. Khalfin; Sibirskogo Nauchno-Issledovatel'skogo Instituta Geologii, Geofiziki i Mineral'nogo Syr'ya (SNIGGIMS), Trudy, vyp. 20, p. 33-36, 74-78, 152-169 (imprint 1960).

1973: Kompleksy rugoz nizhnego i srednego devona Salaira; in Stratigrafiya nizhnego i srednego devona. Trudy III Mezhdunarodnogo simpoziuma po granitse silura i devona i stratigrafii nizhnego i srednego devona (Leningrad, 1968 g.), tom 2, ed. D.V. Nalivkin and others; Akademiya Nauk SSSR, Otdelenie Geologii Geofiziki i Geokhimii, Izdatel'stvo "Nauka", Leningrad, p. 118-127.

43.

LATE EARLY CAMBRIAN AND EARLY MIDDLE CAMBRIAN ACRITARCHS FROM MANUELS RIVER, EASTERN NEWFOUNDLAND

Project 500029

F. Martin[1] and W.T. Dean[2]
Institute of Sedimentary and Petroleum Geology, Calgary

Martin, F. and Dean, W.T., Late Early Cambrian and early Middle Cambrian acritarchs from Manuels River, eastern Newfoundland; in Current Research, Part B, Geological Survey of Canada, Paper 83-1B, p. 353-363, 1983.

Abstract

*Late Early Cambrian (**Catadoxides** Zone) and early Middle Cambrian (**Paradoxides bennettii** Zone) acritarch assemblages from Manuels River, eastern Newfoundland, are discussed. New taxa described are: **Peramorpha manuelsensis** gen. et sp. n., and **Retisphaeridium howellii** sp. n. Previously described species which occur in this section are known principally from the Lower and/or Middle Cambrian of Europe (from the Cantabrian Mountains to the Russian Platform) and from the Middle Cambrian of Canada (southern Alberta; Random Island, eastern Newfoundland) and southeastern Turkey.*

Résumé

*Le présent rapport décrit des assemblages d'acritarches de la fin du Cambrien ancien (zone de **Catadoxides**) et de la base du Cambrien moyen (zone de **Paradoxides bennettii**) provenant de Manuels River dans l'est de Terre-Neuve. Les auteurs décrivent les nouveaux taxons suivants: **Peramorpha manuelsensis** gen. et sp. n. et **Retisphaeridium howellii** sp. n. Les caractéristiques des espèces déjà décrites dans cette coupe stratigraphique ont principalement été observées dans le Cambrien inférieur ou moyen, ou les deux, d'Europe (des monts Cantabriens jusqu'au Plateau russe) et dans le Cambrien moyen du Canada (sud de l'Alberta; île Random, l'Est de Terre-Neuve) et de la partie sud-est de la Turquie.*

Introduction

In the course of the 1981 field season, three hundred and thirteen Cambrian and Lower Ordovician samples, mostly dated by means of trilobites and intended for acritarch and chitinozoan study, were collected by the authors from Random Island and Manuels River (part of the Avalon Platform, eastern Newfoundland), and from Wilcox Pass (in the southern Canadian Rocky Mountains). Late Early Cambrian and early Middle Cambrian acritarchs from strata along Manuels River, on the southeastern side of Conception Bay, 10.25 km south of Bell Island (Fig. 43.1), are the subject of the present preliminary report. All come from the west bank of Manuels River, 360 m west-northwest of the road bridge at Manuels (Fig. 43.2). The section was measured and described in detal by Howell (1925, p. 35, Pl. 1, fig. 2), whose account has formed the basis of all subsequent stratigraphic work. Type specimens illustrated on Plates 43.1 and 43.2 are in the GSC type collection, Ottawa.

Acknowledgments

We thank the Geological Survey of Canada for financial support of our field-work; Professor C. Downie, University of Sheffield, for critically reading the manuscript and loaning us a relevant, then unpublished manuscript; R. Turner and R.K. Stevens for critically reading the manuscript; and Patrick Grootaerts, Institut royal des Sciences naturelles de Belgique, Bruxelles, for taking the SEM photographs.

Stratigraphic Review
(W.T. Dean)

The most comprehensive account of upper Lower and Middle Cambrian rocks and faunas at the classic section in the banks of Manuels River (previously Manuels Brook) is still that by Howell (1925), who gave a full review of earlier work. Lithostratigraphic units relevant to the present paper are the Brigus Formation and the succeeding Chamberlains Brook Formation, the contact between which is exposed in the west bank of Manuels River about 360 m west-northwest of the road bridge at Manuels.

Named by Van Ingen (1914) for the type locality in Conception Bay, the Brigus Formation was said by him to comprise "red shales with nodular limestone" containing the index fossils **Callavia broggeri** (sic) (now **broeggeri** (Walcott) and **Sternuella** (sic) (=**Strenuella**) **strenua** (Billings). Van Ingen showed Brigus Formation B2 as the second of three formations constituting the Etcheminian Series, underlain by Bonavista Formation B1 and overlain by Smith Point Formation B3. The type section, 121 m (396 ft) thick, at Brigus South Point, on the west side of Conception Bay and 35 km west of Manuels, was described by Hutchinson (1962, p. 128) who demonstrated that the Brigus Formation overlies, and is not overlain by, the Smith Point Formation.

Chamberlin's (sic) Brook Formation was named by Howell (1925, p. 58) for the section "in the banks of Chamberlin's Brook, a mile or two northeast of Manuels". The present day 1:50,000 scale topographic map shows two streams which run north-northwest into Conception Bay in the vicinity of the settlement of Chamberlains, approximately 5 km northeast of Manuels. The larger stream, situated on the southwest side of Chamberlains, is named Fowlers Brook; the smaller, to the northeast, is unnamed. Howell gave no details of the section at "Chamberlin's Brook" and Hutchinson (1962, p. 18, 19) subsequently modified, without comment, the formational name to Chamberlain's Brook Formation and accepted Manuels River as the type section. The spelling was changed yet again, to the Chamberlains Brook Formation, by the Geological Survey of Canada (Poole et al., 1970, p. 240) whose usage is followed here.

The Cambrian succession at Manuels begins with the well known basal conglomerate, approximately 5.5 m (18 ft) thick, which rests unconformably on Precambrian rocks in the bed and banks of Manuels River by the north side

[1] Département de Paléontologie, Institut Royal des Sciences Naturelles de Belgique, rue Vautier 29, B-1040 Bruxelles, Belgium.
[2] Department of Geology, University College, P.O. Box 78, Cardiff CF1 1XL, U.K.

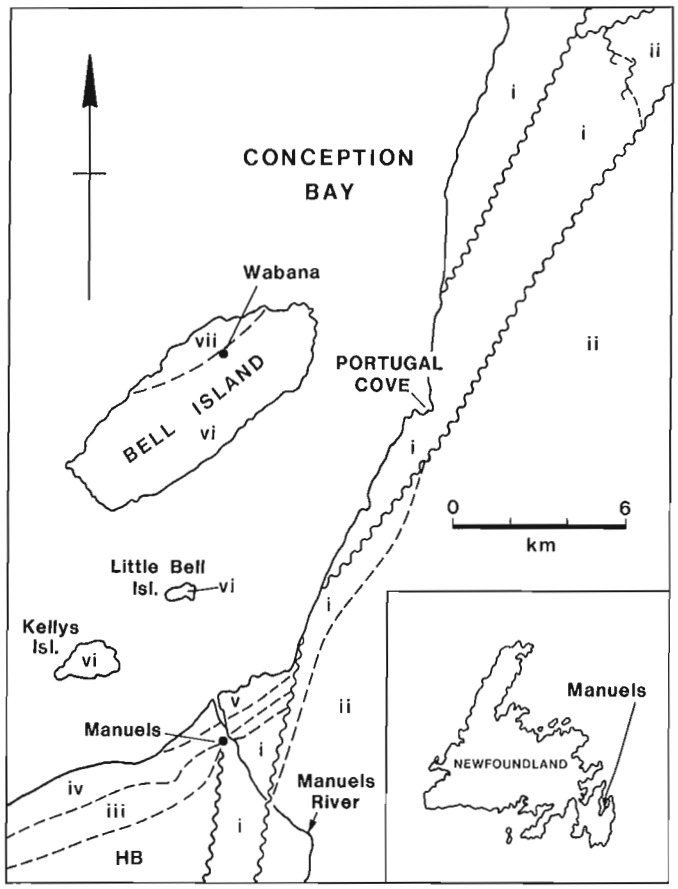

Figure 43.1. *Outline map (after Rose, 1952) showing location of Manuels River and principal outcrops in south-eastern part of Conception Bay, eastern Newfoundland. Key: i = Harbour Main Group (Precambrian); ii = Conception Group (Precambrian); iii = Brigus Formation and Chamberlains Brook Formation; iv = Manuels River Formation, and v = Elliott Cove Formation (Cambrian); vi = Bell Island Group and vii = Wabana Group (L. Ordovician); HB = Holyrood Batholith (intrusive).*

of the road bridge. Between the base of the conglomerates and the base of what he termed the "**Paradoxides** Beds", Howell (1925, p. 24) noted a sequence containing grey and red shales, nodular limestone and sandstone. Even in 1925 this part of the succession was not fully exposed, and, as some units are relevant to the present discussion, details given by Howell are as follows (the letters a, b, etc. are added here for convenience): a. conglomerate 5.5 m (18 ft); b. limy sandstone, 91 cm (3 ft); c. shaly, pyritic, pink and blue limestone containing pteropod shells (no thickness given); d. almost unexposed olive-grey shales (no thickness given); e. red shales, 76 cm (2 ft, 6 in); f. red and green limy shale, 15 cm (6 in); g. nodular and pebbly, reddish blue limestone, 46 cm (1 ft, 6 in); h. hard, olive-grey shale with occasional small manganiferous nodules, 10.36 m (34 ft); i. dark, blue-grey shale full of flattened manganiferous nodules, 10 to 13 cm (4-5 in); j. so-called "Cryptozoon shale" full of manganiferous nodules (said to be "thin", but no thickness given); k. hard, green shale with manganiferous nodules in upper part, 91 cm (3 ft); l. manganiferous, red and green shales, some with small nodules, 3.3 m (10 ft, 10 in). The trilobite **Catadoxides magnificus** (Matthew, 1899a) was recorded from unit h near Manuels railway station, and from unit k in the valley of Manuels River (Howell, 1925, p. 25, 26).

The last of the above units is overlain by what Howell (1925, p. 56) described as a 15 cm (6 in) bed of tough, nodular, manganiferous, argillaceous dolomite, with uneven lower and upper surfaces. The bed formed the base of Howell's **Paradoxides** Beds, the base of his **Paradoxides bennettii** Zone, and the base of the Chamberlains Brook Formation as interpreted by him (Howell, 1925, p. 60). No trilobites were found by Howell in Bed l but the unit, then as now, formed a convenient datum, and from the shales immediately above it he recorded "**Paradoxides**? sp. undet. (probably **Paradoxides bennettii** Salter)".

Although numerous formational names were proposed by Van Ingen (1914), Howell did not use any of them for strata below the Chamberlains Brook Formation at Manuels, but chose (1925, Table 1) to refer the "manganiferous beds" (probably unit l) to an "Unnamed formation", underlain by "Unnamed beds (**Catadoxides** Zone)", the exact age of which was unknown. Hutchinson (1962, p. 19) modified slightly Howell's interpretation of the Chamberlains Brook Formation and extended the base downwards to include 3.3 m (10 ft, 10 in) of manganiferous shale (unit l), on the grounds that the same beds at Brigus South Head, 35 km west of Manuels, contained **Paradoxides bennettii**; he referred (1962, p. 17) the whole of the underlying succession, including Cambrian basal conglomerates, to the Brigus Formation, said by him to be 18.3 m (60 ft) thick at this section. The contact of the Chamberlain Brook Formation with the Brigus Formation was held by Hutchinson (1962, p. 19) to be probably disconformable, indicated by lithological change, faunal break, and local development of a very thin (1.2 cm) basal conglomerate, though not at Manuels; positive evidence was, however, said to be lacking. Jenness (1963, p. 70) also postulated a disconformity near Burgoyne's Cove, on Smith Sound, 113 km northwest of Manuels, but the evidence, based on "a pronounced faunal change, without a corresponding lithological change", appears inconclusive.

In the stratigraphic succession for eastern Newfoundland adopted by Hutchinson (1962) the upper part of the Brigus Formation was correlated with a **Protolenus** Zone, topmost Lower Cambrian, said to occupy the same position as the **Protolenus** Zone of New Brunswick, which corresponds to what Cowie et al. (1972, p. 10) termed the Protolenid – Strenuellid Zone in the Welsh Borders of the British Isles. The Chamberlains Brook Formation in its entirety was correlated by Hutchinson with the **Paradoxides bennetti** (sic; more correctly **P. bennettii**) Zone, lowest Middle Cambrian. Provided the appearance of **Paradoxides** is accepted as marking the base of the Middle Cambrian (see Robison et al., 1977 for a discussion of the subdivision of the Cambrian) then the latter boundary at Manuels River must be drawn below unit l, the 3.3 m of manganiferous shales which underlie Bed 1 of Howell (1925, p. 56). During the present work a thickness of 5 m rather than 3.3 m was measured. **Paradoxides bennettii** Salter (1859, p. 552, Fig. 1) (based on a specimen from Branch, on the west side of St. Mary's Bay, on the south coast of Avalon Peninsula) was chosen by Howell (1925, p. 60) as the index fossil for the lowest zone of the Middle Cambrian and was subsequently reported from the same level over much of southeastern Newfoundland (Hutchinson, 1962, p. 118). In terms of the Middle Cambrian subdivisions in Sweden proposed by Westergård (1946, p. 8), the **P. bennettii** Zone was correlated by Sdzuy (1971, Table 2) with the lowest part of the **Paradoxides paradoxissimus** "Stage" plus an unspecified portion of the underlying **P. oelandicus** "Stage".

Catadoxides, though employed by Howell as a zonal index, was not mentioned by Hutchinson (1962) and has not yet been recorded outside eastern Newfoundland. Proposed by Matthew (1899b, p. 87) as a subgenus of **Metadoxides** Bornemann, 1891, **Catadoxides** was founded on

Metadoxides magnificus Matthew (1899a, p. 137, Pl. 3; see also Matthew, 1899b, p. 83, Pl. 8, figs. 1a-e) from outcrops (since removed) at the railway cutting near Manuels station, and was said by its author to belong to the "Protolenus Fauna". Published assessments of the age of the genus vary, and some rely on its supposed affinities with Sardinian Lower Cambrian trilobites once assigned to **Metadoxides**, but shown by Nicosia and Rasetti (1970) and by Rasetti (1972, p. 59) to be better referred to **Anadoxides** Matthew, 1899. Lochman-Balk and Wilson (1958, Fig. 4) considered **Catadoxides** to occupy a stratigraphic position in the lowest Middle Cambrian, below **Paradoxides oelandicus**, but in the Treatise on Invertebrate Paleontology (C. Poulsen in Moore, 1959, p. 0214, Fig. 156, 2) the genus was placed in the Subfamily Metadoxidinae and stated to be of upper Lower Cambrian age. V. Poulsen (1964, p. 70, 71) argued for the Lower Cambrian age of **Catadoxides** and for a disconformity at the base of the Chamberlains Brook Formation. More recently Bergstrom and Ahlberg (1981, Fig. 2) listed "**Catadoxides, Strenuella** and others" from the uppermost Lower Cambrian of Atlantic North America, strata equivalent to the upper part of the Protolenid – Strenuellid Zone of Comley, Shropshire. Trilobites indicative of the **Protolenus** Zone have been described from the Brigus Formation of Manuels River (Matthew, 1899b, p. 75-82; Hutchinson, 1962, p. 50-51) but so far none appear to have been recorded in association with **Catadoxides**. The highest record of **Catadoxides** at Manuels (Howell, 1925, p. 26) is from unit k, topmost Brigus Formation, and for present purposes we follow Hutchinson (1962) in considering these strata as topmost Lower Cambrian.

Location of Palynological Samples
(W.T. Dean and F. Martin)

Acritarchs from the Brigus Formation belong to the **Catadoxides** Zone of Howell (1925, p. 16); those from the Chamberlains Brook Formation belong to the **Paradoxides bennettii** Zone of Howell (1925, p. 60).

a. Fossiliferous Samples. Only the compact, grey-green shales yielded acritarchs. The latter, although flattened, are generally well preserved, yellow-brown in colour, and number some tens of specimens per gramme of rock.
GSC loc. C-98028. Brigus Formation, 6.1 m below Bed 1 of Howell (1925, p. 56).
GSC loc. C-98032. Chamberlains Brook Formation, 15 cm above Bed 1.
GSC loc. C-98033. Chamberlains Brook Formation, 2 m above Bed 1.

b. Barren Samples. All are from red shales, with or without manganiferous nodules, in the Chamberlains Brook Formation.

GSC loc. C-98029, 5 m below Bed 1.
GSC loc. C-98030, 4 m below Bed 1.
GSC loc. C-98031, 1.9 m below Bed 1.

Stratigraphic Significance of the Arcritarchs
(F. Martin)

For each of the three samples, the acritarch taxa present and their abundance are shown in Table 43.1, together with their stratigraphic ranges according to published records and the present work. Questionable stratigraphic occurrences, though discussed in the text, are omitted from the table.

The abundance of **Nucellosphaeridium** sp. A and **Peramorpha manuelsensis** gen. et sp. n. at GSC loc. C-98028, their only occurrence, marks at least locally the clearest difference between the uppermost Lower

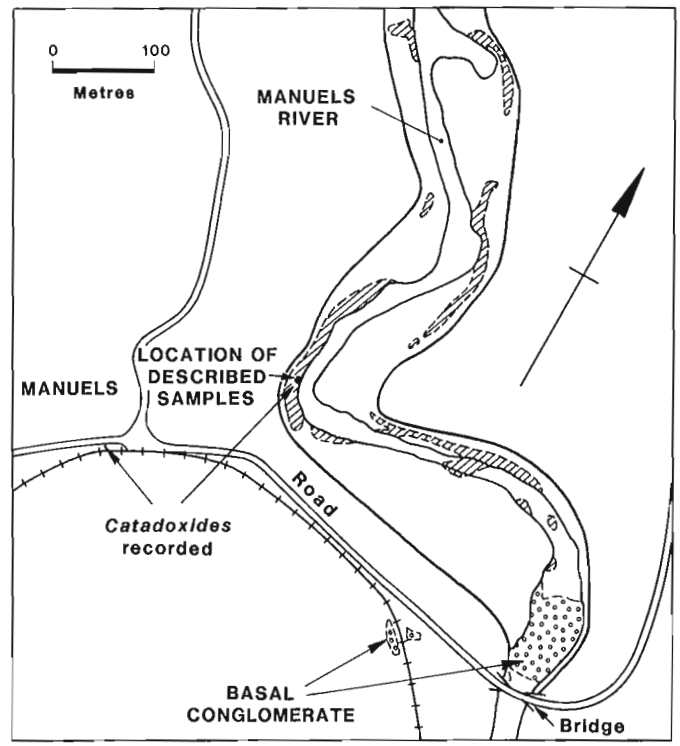

Figure 43.2. Outline map (after Howell, 1925) showing principal exposures (shaded) of Cambrian rocks in the section in the Manuels River valley, north of the road bridge at Manuels.

Cambrian (**Catadoxides** Zone) and the lowest Middle Cambrian (**Paradoxides bennettii** Zone). **Pterospermopsimorpha** Timofeev, 1962 ex Timofeev, 1966 is rare at the same level. Judging from the work of Timofeev (1973) and of Jankauskas (1976), the genus ranges from Riphean (late Precambrian) at least to the end of the Lower Cambrian on the Russian Platform. **Annulum squamaceum** (Volkova, 1968) emend., **Retisphaeridium dichamerum** Staplin, Jansonius and Pocock, 1965 and **R. howellii** sp. n. are common to all three samples, though of variable frequency. The stratigraphic range of **Annulum squamaceum** is from the base of the Lower Cambrian (below the **Holmia** "stage") to lowest Middle Cambrian (**Paradoxides oelandicus** Zone). Volkova (1968, 1969a, b) described the species from the Lower Cambrian of Estonia (Lomonosov Beds and Lontova Beds) and of northeastern Poland (Radzyn "Series" and Kaplonosy "Series"). **A. squamaceum** was recorded from the Lontova Beds to the Kibartai Beds (early Middle Cambrian) of the Russian Platform by Volkova et al. (1979), and from the **Platysolenites** Zone, **Mobergella** Zone and **Holmia** Zone of the Lower Cambrian in Podlasia by Moczydlowska (1980). According to Tynni (1978) it is found at Soderfjarden, western Finland, in strata assigned to the Lower Cambrian on palynological evidence. Downie (1982) describes **Annulum squamaceum** in or among Lower Cambrian acritarch assemblages from the Fucoid Beds in northwest Scotland, the Holmia Shales in Norway, the Bastion Formation in east Greenland, the Gog Formation in the southern Canadian Rockies, Alberta, and an unnamed formation on the Burin Peninsula, southeastern Newfoundland. The species is often cited from the Lower Cambrian, and has been recorded from the Glauconite Sandstone and Lower Shelly Limestone of East Greenland by Downie (1974, p. 58, 59); from the Booley Bay

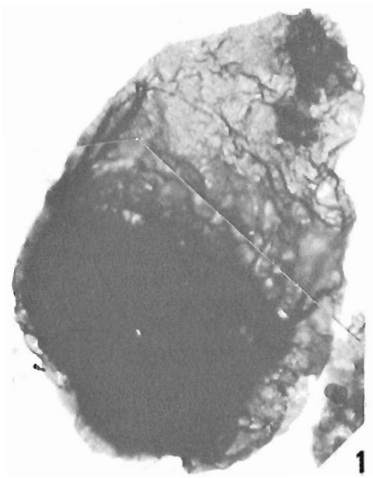
1

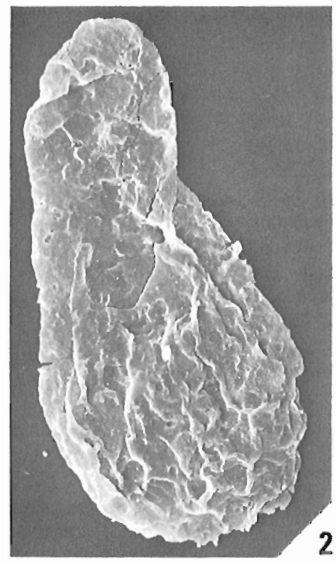
2

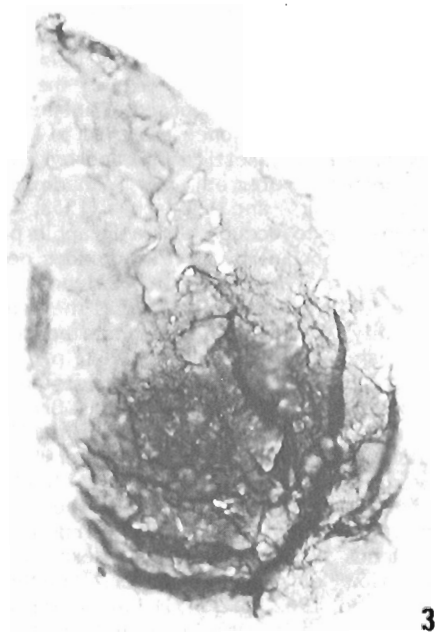
3

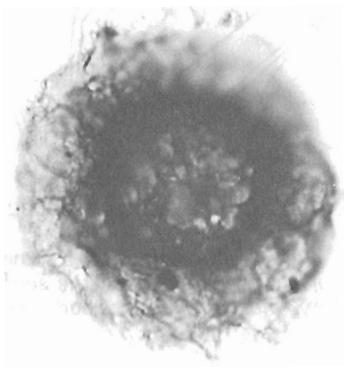
4

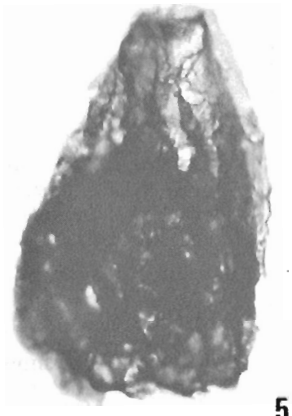
5

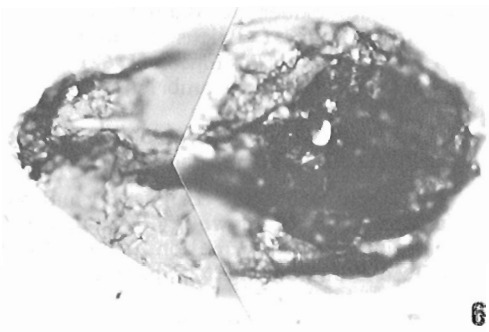
6

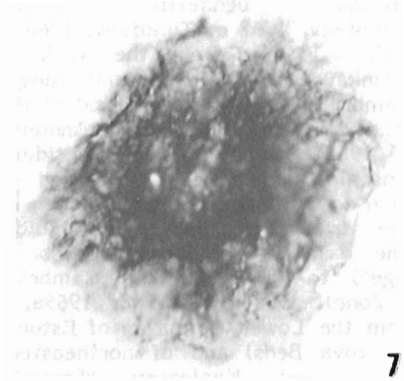
7

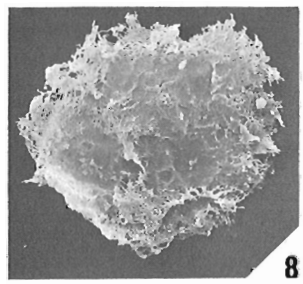
8

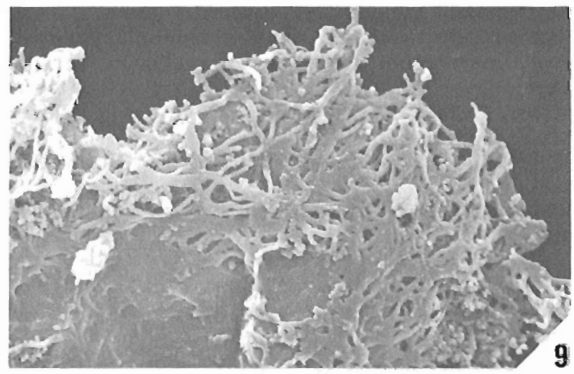
9

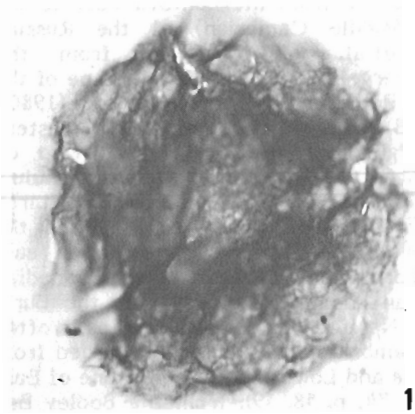
10

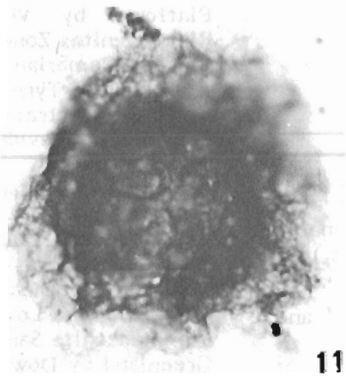
11

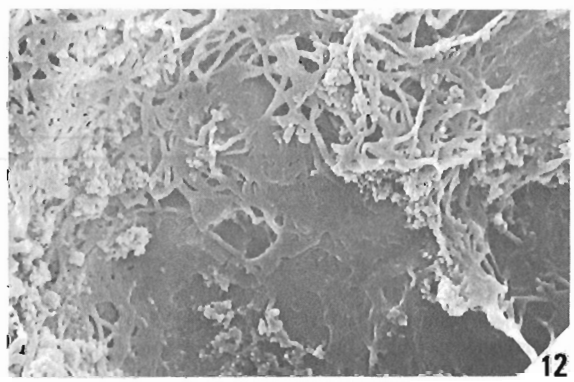
12

Table 43.1

Distribution of acritarchs

ACRITARCHS FROM MANUELS RIVER. NUMBER OF SPECIMENS PER SAMPLE : rr=1 ; r=2-19 ; c=20-100 ; cc=>100	Late Lower Cambrian	Early Middle Cambrian		RANGE OF ACRITARCHS
	Catadoxides Zone	*Paradoxides bennettii* Zone		
	BRIGUS FM. (in part)	CHAMBERLAINS BROOK FM. (in part)		
	GSC Loc.C-98028	GSC Loc.C-98032	GSC Loc.C-98033	
Nucellosphaeridium sp. A	c	—	—	Known only at Manuels River
Peramorpha manuelsensis gen. et sp. nov.	c	—	—	
Pterospermopsimorpha sp.	r	—	—	Pre-Camb. (Riphean) - L.Camb.
Kildinella sp.	r	—	—	Pre-Camb. (Riphean) - early M. Camb.
Leiosphaeridia sp.	c	c	r	Pre-Camb. -Tertiary
Annulum squamaceum (VOLKOVA, 1968) comb. nov.	cc	r	cc	Early L.Camb. - early M. Camb.
Retisphaeridium dichamerum STAPLIN, JANSONIUS & POCOCK,1965.	c	c	c	Late L. Camb. - early M.Camb.
Retisphaeridium howellii sp. nov.	c	c	c	
Eliasum llaniscum FOMBELLA, 1977.	—	c	—	Middle Camb.
Cymatiosphaera crameri SLAVÍKOVÁ, 1968.	—	—	rr	
Stictosphaeridium brayense GARDINER & VANGUESTAINE,1971.	—	—	r	Late L. Camb., M. Camb., ? U. Camb.

Plate 43.1

*Figures 1-3, 5, 6. **Peramorpha manuelsensis** gen. et sp. n. Fig. 1, holotype, GSC 69624. Fig. 2, GSC 69625. Fig. 3, GSC 69626. Fig. 5, GSC 69627. Fig. 6, GSC 69628. All from GSC loc. 98028. All x500.

*Figures 4, 7-12. **Annulum squamaceum** (Volkova, 1968) comb. n.
Fig. 4, GSC 69618, GSC loc. C-98033, x1000. Fig. 7, GSC 69619, GSC loc. C-98028, x1000. Fig. 8, GSC 69620, GSC loc. C-98028, x1100. Figs. 9, 12, detail of, respectively, upper right and lower central portions of Fig. 8, x7000. Fig. 10, GSC 69621, GSC loc. C-98033, x1000. Fig. 11, GSC 69622, GSC loc. C-98033, x1000.

*Described in text.

Formation of southeast Ireland by Smith (1981, p. 140); and from the **Holmia** Zone of northern and southern Sweden, southeastern Denmark, and Norway (Vidal, 1981a, b). It was noted by Vanguestaine (1978, p. 271) in the Devillian of the Franco-Belgian Ardennes, rocks attributed to the Lower Cambrian on palynological evidence. Owing to the absence of precise location data for samples from northern Spain, and to the methodology employed by Fombella (1978, 1979), the precise range of **A. squamaceum, Retisphaeridium dichamerum** Staplin, Jansonius and Pocock, 1965 and **R. howellii** sp. n. within the Oville Formation (the age of which extends from early Middle Cambrian to late Late Cambrian-Tremadoc), cannot be ascertained. In western Canada, **R. dichamerum** was described by Staplin et al. (1965) from the early Middle Cambrian (**Albertella** Zone) in a borehole in southern Alberta. Elsewhere in Alberta the species is figured by Downie (1982) from the Gog Formation, Lower Cambrian, at the Lookout section on Mount Eisenhower (Castle Mountain), Banff National Park; according to Downie, it is known also from the Fucoid Beds in northwest Scotland and the Holmia Shales in Norway. **R. howellii** was figured, as **Retisphaeridium** n. sp., by Slavíková (1968) from the upper part of the Middle Cambrian (**Ellipsocephalus hoffi** Subzone) in the Jince Formation of Czechoslovakia.


1

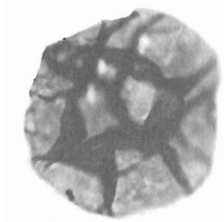
2

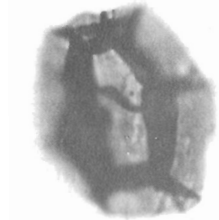
3

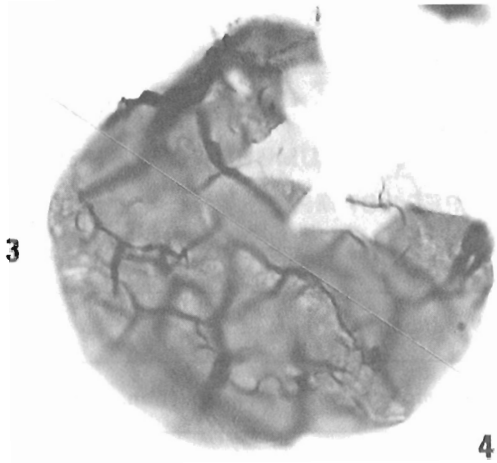
4


5

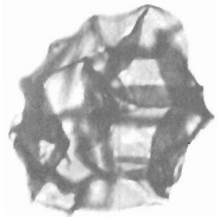
6

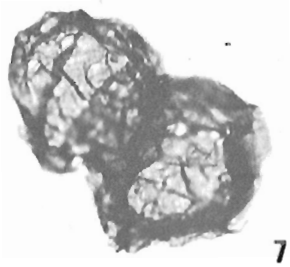
7

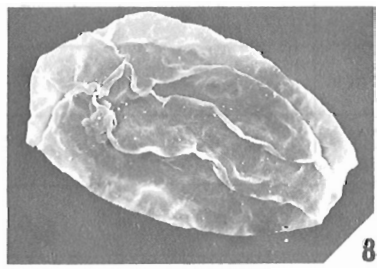
8

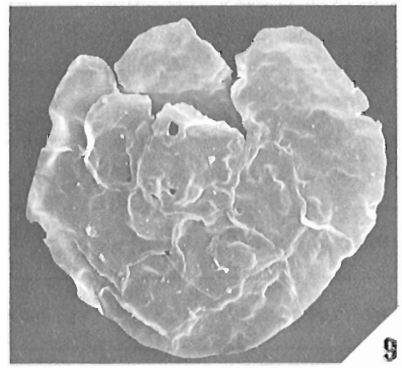
9

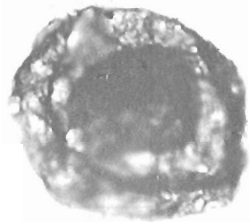
10

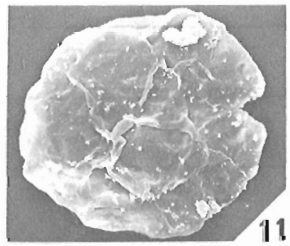
11

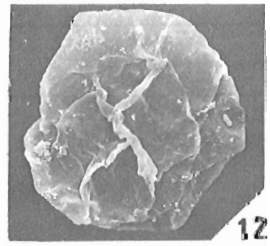
12

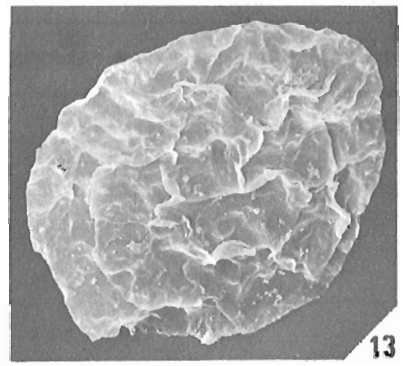
13

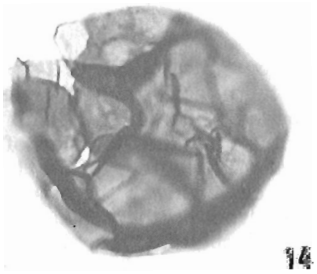
14

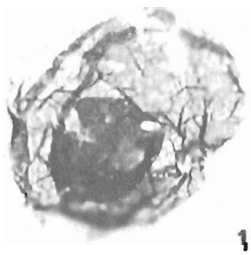
15

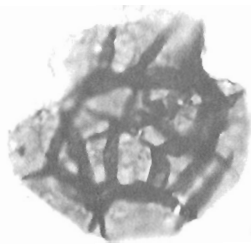
16

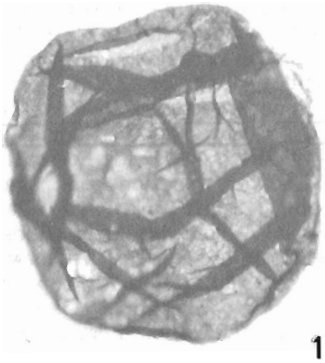
17

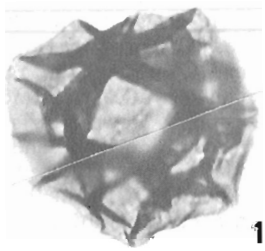
18

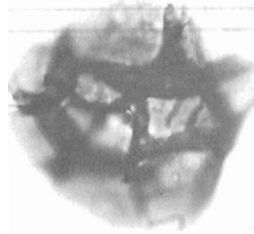
19

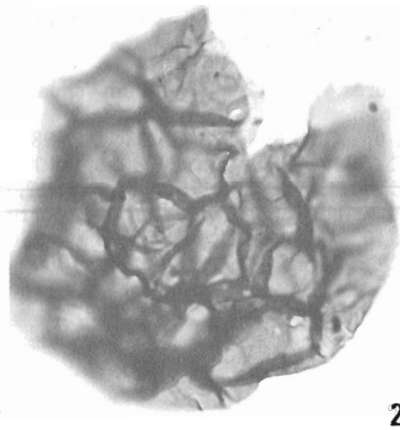
20

On the whole, the Sphaeromorphitae are relatively abundant in the samples from Manuels River. Representatives of **Leiosphaeridia** Eisenack, 1958 emend. Downie, Evitt and Sarjeant, 1963, clearly predominate by comparison with those of **Kildinella** Shepeleva and Timofeev, 1963 ex Timofeev, 1966. In view of the paucity of diagnostic characters and the consequent lack of stratigraphic value of these taxa, no specific attribution is proposed. The first genus is widely distributed in the Northern Hemisphere; it is known from rocks as old as Precambrian (Timofeev, 1973) and according to Combaz (1967) may extend from the Palaeozoic to the Tertiary. **Kildinella** has been found from the Riphean to the Lower Cambrian on the Russian Platform (Timofeev, 1973; Vidal, 1979).

Eliasum llaniscum Fombella, 1977, abundant at GSC loc. C-98032, is known from the higher Middle Cambrian (upper part **Paradoxides hicksii** Zone and **Paradoxides davidis** Zone in the Manuels River Formation) at Random Island, eastern Newfoundland (Martin and Dean, 1981, p. 19), and from the early Middle Cambrian (**Eccaparadoxides pusillus** Zone) in the Jince Formation of Czechoslovakia (Vavrdová, 1976). In southeastern Turkey, Erkmen and Bozdoğan (1981) have illustrated the species from the Sosink Formation; trilobites from the lower member of the formation indicates a late Middle Cambrian age but are absent from the highest beds (Dean, 1982). Smith (1981) recorded **E. llaniscum** from the type section of the Booley Bay Formation (Ribband Group) in southeastern Ireland, and cited the unpublished doctoral thesis of Potter (1974) in reporting the species from the Middle Cambrian of England and Wales. Judging from these records, the species appears to be restricted to the Middle Cambrian, although Fombella (1978, 1979; see also above) showed it ranging from Middle Cambrian to Upper Cambrian-Tremadoc.

Cymatiosphaera crameri Slavíková, 1968 and **Stictosphaeridium brayense** Gardiner and Vanguestaine, 1971 are represented by only a few specimens at GSC loc. C-98033. The first is known (Slavíková, 1968, p. 200) from the upper Middle Cambrian (**Ellipsocephalus hoffi** Subzone) in the Jince Formation of Czechoslovakia. According to Gardiner and Vanguestaine (1971, p. 193) the second is common in four samples, the age of which, based on acritarch evidence, extends from middle Early Cambrian to early or middle Middle Cambrian, from the Thulla Formation (Bray Group) and the Booley Bay Formation (Ribband Group) in southeastern Ireland. **Stictosphaeridium brayense** is present in the upper Lower Cambrian of northeastern Spain according to Vanguestaine (in Gardiner and Vanguestaine, 1971, p. 194), who also (Vanguestaine, 1974, p. 78; 1978, p. 272) determined the species in palynological Zones 2, 3 and 4 of the Revinian in the Franco-Belgian Ardennes, subdivisions which, on the basis of acritarch evidence, range from Lower to probably Upper Cambrian.

Systematic Paleontology
(F. Martin)

Genus **Annulum** Fombella, 1978

Type species. **Annulum squamaceum** (Volkova, 1968) comb. n., here emended, originally designated as **Annulum difuminatum** Fombella, 1978.

Emended diagnosis. Central internal body of flattened form, with more or less circular outline. Numerous fine, tangled, anastomosing filaments are arranged radially over the whole surface of the central body; they form a continuous median layer which appears spongy and fluffy in transmitted light and "vermicelli-like" under the scanning electron microscope. This intermediate layer is itself surrounded by a very fine, transparent, external membrane.

Discussion. **Annulum** is here emended to incorporate new data obtained by means of the scanning electron microscope. These indicate that an intermediate layer and a fine external membrane enclose the internal central body; gold coating of the fine external membrane masks obervation of the intermediate layer which, in transmitted light, is always visible and has rather the appearance of an equatorial border. Neither the schematic illustration nor the brief diagnosis of **Granomarginata** Naumova, 1961 (identical with those of **G. prima** Naumova, 1961, the type species by original designation) indicates the presence of an intermediate envelope of spongy appearance and of a fine external membrane. For this reason Downie, Evitt and Sarjeant (1963, p. 8) and Norris and Sarjeant (1965, p. 11) classed **Granomarginata** with the Sphaeromorphitae; on the other hand **G. squamacea** Volkova, 1968, for reasons given below, is here transferred to **Annulum** emend.

Annulum squamaceum (Volkova, 1968) comb. n.
Plate 43.1, figures 4, 7-12

Granomarginata squamacea sp. n. Volkova, 1968, p. 25, Pl. 4, figs. 14-19; Pl. 10, figs. 4, 5; Pl. 11, fig. 11.
Granomarginata squamacea Volkova, 1969b, p. 231, Pl. 47, figs. 5, 17; Pl. 49, fig. 12.
Granomarginata squamacea Volkova, Tynni, 1978, p. 48, Pl. 6, figs. 47, 48.
Annulum difuminatum sp. n. Fombella, 1978, p. 249, Pl. 3, figs. 18, 19.
Granomarginata squamacea Volkova, 1968; Fombella, 1979; Pl. 1, fig. 2; Pl. 3, fig. 40.

Plate 43.2

Figure 1. **Cymatiosphaera crameri** Slavikova, 1968. GSC 69643. GSC loc. C-98033, x1000.

*Figures 2, 3, 5, 6, 11, 12, 16, 18, 19. **Retisphaeridium howellii** sp. n.
Fig. 2, holotype, GSC 69634. Fig. 3, GSC 69635. Fig. 5, GSC 69636. Fig. 6, GSC 69637. Fig. 11, GSC 69638. Fig. 12, GSC 69639. Fig. 16, GSC 69640. Fig. 18, GSC 69641. Fig. 19, GSC 69642. All from GSC loc. C-98033, x1000.

*Figures 4, 9, 13, 14, 20. **Retisphaeridium dichamerum** Staplin, Jansonius and Pocock, 1965. Fig. 4, GSC 69629, GSC loc. C-98033. Fig. 9, GSC 69630, GSC loc. C-98032. Fig. 13, GSC 69631, GSC loc. C-98033. Fig. 14, GSC 69632, GSC loc. C-98028. Fig. 20, GSC 69633, GSC loc. C-98033. All x1000.

Figure 7. **Stictosphaeridium brayense** Gardiner and Vanguestaine, 1971. GSC 69647, GSC loc. C-98033, x700.

Figure 8. **Eliasum llaniscum** Fombella, 1977. GSC 69644, GSC loc. C-98032, x700.

Figure 10. **Pterospermopsimorpha** sp. GSC 69646, GSC loc. C-98028, x700.

*Figure 15. **Nucellosphaeridium** sp. A. GSC 69623, GSC loc. C-98028, x700.

Figure 17. **Kildinella** sp. GSC 69645, GSC loc. C-98028, x500.

*Described in text.

Granomarginata squamacea Volkova; Volkova et al., 1979, p. 198, Pl. 18, figs. 6-9.
Granomarginata squamacea Volkova, 1968; Moczydlowska, 1980, p. 472, Pl. 2, figs. 5-7.
?non **Granomarginata squamacea** Volkova, 1968; Volkova, 1981, p. 71, Pl. 1, figs. 1, 2.
Granomarginata squamacea Volkova, 1968; Downie, 1982, Figs. 13k, m.

Figured specimens. GSC 69618 (Pl. 43.1, fig. 4); GSC 69619 (Pl. 43.1, fig. 7); GSC 69620 (Pl. 43.1, figs. 8, 9, 12); GSC 69621 (Pl. 43.1, fig. 10); GSC 69622 (Pl. 43.1, fig. 11).

Emended diagnosis. Based on five hundred specimens. Central internal body more or less discoidal, with circular equatorial outline and entirely covered with fine, radial filaments which form a tangled, anastomosing network of irregular meshes. The width of the intermediate layer, enclosed by a fine, transparent, fragile membrane, which has often disappeared locally, equals one third to two thirds the diameter of the internal body. The superposition of the irregular meshes gives the microfossil a spongy or fluffy appearance in transmitted light. Under the scanning electron microscope, and when the peripheral membrane has disappeared, the interlacing filaments have a "vermicelli-like" appearance. Following compression of the radiating filaments, the equatorial periphery of the internal body sometimes appears darker than the remainder of the acritarch, which is light yellow brown.

Dimensions. Based on fifty specimens. Diameter of central body from 20 to 37 µm; width of the intermediate layer and of the filaments forming it, from 11 to 15 µm and less than 0.3 µm respectively; thickness of external wall less than 0.3 µm.

Discussion. In the original diagnosis of the species, the relatively thick median layer and the fine external membrane were not recognized, and were described as an "equatorial border". However, certain of Volkova's illustrations, including that of the holotype (Volkova, 1968, Pl. 4, fig. 14), are identical with those obtained here using transmitted light. Fombella (1979) illustrated under the name **Granomarginata squamacea** specimens identical with others that she had earlier (Fombella, 1978) identified as **Annulum difuminatum.** Specimens from the late Precambrian of Siberia, though inadequately illustrated by Volkova (1981), appear to differ from the species in having a much narrower intermediate layer and the determination is not accepted here.

Occurrence. Very common in the highest Brigus Formation (GSC loc. C-98028) and rare to abundant in the lowest Chamberlains Brook Formation (GSC locs. C-98032 and C-98033).

Genus **Nucellosphaeridium** Timofeev, 1963 ex Timofeev, 1966
Type species. **Nucellosphaeridium deunffii** Timofeev, 1966, by original designation.

Nucellosphaeridium sp. A
Plate 43.2, figure 15

Figured specimen. GSC 69623.

Description. Based on fifty specimens. External envelope light yellow brown, thin, very finely granulate, with circular outline, secondarily crumpled and deformed, and commonly incomplete. Central internal body globular, opaque, with diameter approximately one third that of the external envelope.

Dimensions. Based on twenty specimens. Diameter of central body from 17 to 22 µm; diameter of external envelope from 50 to 65 µm.

Discussion. Following Timofeev (1966, p. 41; 1969, p. 16, 23), **Nucellosphaeridium** is distinguished arbitrarily from **Pterospermopsimorpha** Timofeev, 1962 ex Timofeev, 1966, by having a relatively smaller central body, one fifth to one third of the diameter of the external envelope in the former genus compared with two thirds in the latter. The specimens differ from **Nucellosphaeridium deunffii,** from the Lower Silurian of the U.S.S.R., in having a relatively large internal body and a more fragile, crumpled external membrane. **Nucellosphaeridium** sp. A has a diameter which varies little and corresponds to the smallest recorded by Timofeev (1966, p. 42, Pl. 8, fig. 10). **Nucellosphaeridium** sp. A differs from **Archaeodiscina umbonulata** Volkova, 1968 in having an internal body with smooth outline.

Occurrence. Common in highest Brigus Formation (GSC loc. C-98028).

Genus **Peramorpha** gen. n.
Type species. Here designated. **Peramorpha manuelsensis** sp. n. No other species known.

Diagnosis. External envelope pyriform to variably elongated oviform with fine membrane smooth or slightly ornamented, and secondarily folded; its widest part contains a spherical, more or less opaque, internal body. No opening observed.

Discussion. The non-circular form of the external envelope in **Peramorpha** clearly distinguishes the new genus from **Megasacculina** Naumova, 1961, **Nucellosphaeridium** Timofeev, 1966 and **Pterospermopsimorpha** Timofeev, 1962 ex Timofeev, 1966. The three times larger dimensions of **Peramorpha** and the preferential position of the internal body, the outline of which is not star-shaped, separate the genus from **Archaeodiscina** Naumova, 1961.

Peramorpha manuelsensis gen. et sp. n.
Plate 43.1, figures 1-3, 5, 6

Holotype. GSC 69624 (Pl. 43.1, fig. 1).

Paratypes. GSC 69625 (Pl. 43.1, fig. 2); GSC 69626 (Pl. 43.1, fig. 3); GSC 69627 (Pl. 43.1, fig. 5); GSC 69628 (Pl. 43.1, fig. 6).

Type locality. GSC loc. C-98028, west bank of Manuels River, in upper part of Brigus Formation (as interpreted by Hutchinson, 1962, p. 19) and 6.10 m below Bed 1 of Chamberlains Brook Formation as described by Howell (1925, p. 56). Age is late Early Cambrian (see discussion earlier).

Diagnosis. Based on one hundred specimens. External envelope pyriform to variably elongated oviform, one and a half times to twice as long as wide, with finely granulate surface, transparent light yellow brown, and commonly shows longitudinal folds due to compression. The external envelope contains an internal central body which is more or less spherical, generally dark brown, and is localised within the wider pole of the microfossil. The diameter of the internal body varies between two thirds and nine tenths of the maximum width of the external envelope. No opening attributable to an excystment mechanism has been observed.

Dimensions. Based on thirty specimens. Length and maximum width of external envelope, from 96 to 170 µm and from 55 to 96 µm respectively; diameter of internal body from 43 to 84 µm.

Discussion. The original form of the taxon is relatively constant, but may appear to vary, depending on the orientation and degree of compression of specimens.

Occurrence. Common in highest Brigus Formation (GSC loc. C-98028).

Genus **Retisphaeridium** Staplin, Jansonius and Pocock, 1965
Type species. **Retisphaeridium dichamerum** Staplin, Jansonius and Pocock, 1965 by original designation.

Retisphaeridium dichamerum Staplin, Jansonius and Pocock, 1965
Plate 43.2, figures 4, 9, 13, 14, 20

Retisphaeridium dichamerum sp. n. Staplin, Jansonius and Pocock, 1965, p. 187, Pl. 19, figs. 1-7.
non **Retisphaeridium dichamerum** Staplin et al.; Fombella, 1978, Pl. 1, fig. 15.
Retisphaeridium dichamerum Staplin et al.; Fombella, 1979, Pl. 1, fig. 11?; Pl. 4, fig. 57 only, non figs. 58, 59, 62.
Retisphaeridium dichamerum Staplin et al.; Downie, 1982, figs. 13o, p.

Figured specimens. GSC 69629 (Pl. 43.2, fig. 4); GSC 69630 (Pl. 43.2, fig. 9); GSC 69631 (Pl. 43.2, fig. 13); GSC 69632 (Pl. 43.2, fig. 14); GSC 69633 (Pl. 43.2, fig. 20).

Description. Based on two hundred specimens. Central body with outline more or less circular, sometimes locally polygonal. The membrane is smooth, and fine external ribs divide the surface into a network of numerous (more than twenty-five) fields which tend to be polygonal and are commonly incompletely delimited. The fine ribs are commonly masked by folds with tapered extremities; both are generally absent at the equatorial margin. Some specimens are partly broken along the sides of the polygonal fields.

Dimensions. Based on one hundred specimens. Diameter of central body from 35 to 49 µm.

Discussion. Specimens figured as **R. dichamerum** by Fombella (1978, Pl. 1, fig. 15; 1979, Pl. 4, fig. 62) differ from the species in having much thicker folds and a smaller number of polygonal fields; they are assigned to **Retisphaeridium howellii** sp. n. Other specimens illustrated as **R. dichamerum** by Fombella (1979, Pl. 4, figs. 58, 59) exhibit folds with little or no taper and are identified here as **Cymatiosphaera** sp.

Occurrence. Common in the highest Brigus Formation (GSC loc. C-98028) and lowest Chamberlains Brook Formation (GSC locs. C-98032 and C-98033).

Retisphaeridium howellii sp. n.
Plate 43.2, figures 2, 3, 5, 6, 11, 12, 16, 18, 19

Retisphaeridium n. sp. Slavíková, 1968, Pl. 2, fig. 8.
Retisphaeridium dichamerum Staplin et al. Fombella, 1978, Pl. 1, fig. 15.
Retisphaeridium dichamerum Staplin et al. (in part). Fombella, 1979, Pl. 4, fig. 62 only.

Holotype. GSC 69634 (Pl. 43.2, fig. 2).

Paratype. GSC 69635 (Pl. 43.2, fig. 3); GSC 69636 (Pl. 43.2, fig. 5); GSC 69637 (Pl. 43.2, fig. 6); GSC 69638 (Pl. 43.2, fig. 11); GSC 69639 (Pl. 43.2, fig. 12); GSC 69640 (Pl. 43.2, fig. 16); GSC 69641 (Pl. 43.2, fig. 18); GSC 69642 (Pl. 43.2, fig. 19).

Type locality. GSC loc. C-98033, west bank of Manuels River, in shales of the Chamberlains Brook Formation, 2 m above Bed 1 described by Howell (1925, p. 56). **Paradoxides bennettii** Zone, early Middle Cambrian.

Diagnosis. Based on one hundred and fifty specimens. Central body globular to polyhedral; membrane smooth with few external ribs. Surface of central body is divided by relatively thick, tapered folds into a network of polygonal fields (generally about fifteen) which are sometimes incompletely delimited; folds generally not seen at the equatorial margin. No opening observed.

Dimensions. Based on sixty specimens. Diameter of central body from 25 to 35 µm.

Discussion. **R. howellii** is distinguished from the smallest specimens of **R. dichamerum** by its longer, wider and less numerous folds, and fewer external ribs and polygonal fields.

Occurrence. Common in the highest Brigus Formation (GSC loc. C-98028) and lowest Chamberlains Brook Formation (GSC locs. C-98032 and C-98033).

References

Bergström, J. and Ahlberg, P.
1981: Uppermost Lower Cambrian biostratigraphy in Scania, Sweden; Geologiska Föreningens i Stockholm Förhandlingar, v. 103, p. 193-214.

Combaz, A.
1967: **Leiosphaeridiaceae** Eisenack, 1954, et **Protoleiosphaeridae** Timofeev, 1959 -Leurs affinités, leur rôle sédimentolgique et géologique; Review of Palaeobotany and Palynology, v. 1, p. 309-321.

Cowie, J.W., Rushton, A.W.A., and Stubblefied, C.J.
1972: A correlation of Cambrian rocks in the British Isles; Geological Society of London, Special Report No. 2, 40 p.

Dean, W.T.
1982: Middle Cambrian trilobites from the Sosink Formation, Derik - Mardin district, southeastern Turkey; British Museum (Natural History), Geology, Bulletin 36 (1), p. 1-38.

Downie, C.
1974: Acritarchs from near the Precambrian-Cambrian boundary - a preliminary account; Review of Palaeobotany and Palynology (Special issue on acritarchs), v. 18, p. 57-60.

1982: Lower Cambrian acritarchs from Scotland, Norway, Greenland and Canada; Transactions of the Royal Society of Edinburgh, v. 72, p. 257-285.

Downie, C., Evitt, W.R., and Sarjeant, W.A.S.
1963: Dinoflagellates, hystrichospheres, and the classification of the acritarchs; Stanford University Publications, Geological Sciences, v. 7, 16 p.

Erkman, U. and Bozdogan, N.
1981: Cambrian acritarchs from the Sosink Formation in southeast Turkey; Revista Española de Micropaleontologia, v. 13, p. 47-60.

Fombella, M.A.
1977: Acritarchs de Edad Cambrico Medio-Inferior de la Provincia de León, España; Revista Española de Micropaleontologia, v. 9, p. 115-124.

1978: Acritarchs de la Formación Oville, Edad Cambrico Medio-Tremadoc, Provinica de León, España; Palinologia, Número extraordinario 1, p. 245-261.

1979: Palinologiá de la Formación Oville al Norte y Sur de la Cordillera Cantábrica, España; Palinologia, v. 1, p. 1-16.

Gardiner, P.R.R. and Vanguestaine, M.
1971: Cambrian and Ordovician microfossils from southeast Ireland and their implications; Geological Survey of Ireland, Bulletin, v. 1, p. 163-210.

Howell, B.F.
1925: The faunas of the Cambrian **Paradoxides** beds at Manuels, Newfoundland; Bulletin of American Paleontology, v. 11, no. 43, 140 p.

Hutchinson, R.D.
1962: Cambrian stratigraphy and trilobite faunas of southeastern Newfoundland; Geological Survey of Canada, Bulletin 88, 156 p.

Jankauskas, T.V.
1976: Révision de l'âge des formations "cambro-ordoviciennes" des régions baltiques par l'analyse micropaléontologique (Acritarches, Chitinozoaires); Société Géologique de France, Compte Rendu Sommaire, fasc, 2, p. 47-49.

Jenness, S.E.
1963: Terra Nova and Bonavista map-areas, Newfoundland (2D E½ and 2C); Geological Survey of Canada, Memoir 327, 184 p.

Lochman-Balk, C. and Wilson, J.L.
1958: Cambrian biostratigraphy in North America; Journal of Paleontology, v. 32, p. 312-350.

Martin, F. and Dean, W.T.
1981: Middle and Upper Cambrian and Lower Ordovician acritarchs from Random Island, eastern Newfoundland; Geological Survey of Canada, Bulletin 343, 43 p.

Matthew, G.F.
1899a: A new Cambrian trilobite; Bulletin of the Natural History Society of New Brunswick, no. 17, p. 136-142.

1899b: Studies on Cambrian faunas, No. 4. Fragments of the Cambrian faunas of Newfoundland; Transactions of the Royal Society of Canada, Ser. 2, v. 5, Sec. 4, p. 67-95.

Moczydlowska, M.
1980: Acritarcha from the Cambrian of the borehole Okuniew IG 1; Kwartalnik Geologiczny, v. 24, p. 461-479 (in Polish).

Moore, R.C. (ed.)
1959: Treatise on invertebrate paleontology; Part O: Arthropoda 1; Lawrence, Kansas, and Meriden, Conn.; Geological Society of America and University of Kansas Press.

Naumova, S.N.
1961: Spore-pollen complexes of the Riphean and Lower Cambrian in USSR (in Russian); Mezhdunarodnii Geologitcheskii Kongress, XXI Sessija, 1960, Problema 6, p. 109-117.

Nicosia, M.L. and Rasetti, F.
1970: Revisione dei trilobiti del Cambriano dell'Iglesiente (Sardegna) descritti da Meneghini; Accademia Nazionale dei Lincei. Memoire. Roma. Classe di Scienze Fisische, Matematiche e Naturali, Ser. 8, v. 10, p. 1-20.

Norris, G. and Sarjeant, W.A.S.
1965: A descriptive index of genera of fossil Dinophyceae and Acritarcha; New Zealand Geological Survey; Paleontological Bulletin 40, 72 p.

Poole, W.H., Sanford, B.V., Williams, H., and Kelley, D.G.
1970: Geology of southeastern Canada; in Geology and economical minerals of Canada, R.J.W. Douglas, ed.; Geological Survey of Canada, Economic Geology Report No. 1, p. 228-304.

Potter, T.L.
1974: The stratigraphic palynology of some Cambrian successions in North Wales, England and northwest Spain. Unpublished Ph.D. thesis. University of Sheffield.

Poulsen, V.
1964: Contributions to the Lower and Middle Cambrian palaeontology and stratigraphy of northwest Greenland; Meddelelser om Grønland, v. 164, no. 6, p. 1-105.

Rasetti, F.
1972: Cambrian trilobite faunas of Sardinia; Atti della Academia Nazionale dei Lincei. Memorie. Roma. Classe di Scienze Fisische, Matematiche e Naturali, Ser. 8, v. 11, p. 1-100.

Robison, R.A., Rosova, A.V., Rowell, A.J., and Fletcher, T.P.
1977: Cambrian boundaries and divisions; Lethaia, v. 10, p. 257-262.

Rose, E.R.
1952: Torbay map-area, Newfoundland; Geological Survey of Canada, Memoir 265, 64 p.

Salter, J.W.
1859: On the fossils of the **Lingula**-Flags or "Zone Primordiale"; Quarterly Journal of the Geological Society of London, v. 15, p. 551-555.

Sdzuy, K.
1971: La subdivisión biostratigráfica y la correlación del Cámbrico medio de España; Publication I, Congress hisp.-luso.-America, Geol. econ., v. 2, 1, p. 769-782.

Slavíková, K.
1968: New finds of acritarchs in the Middle Cambrian of the Barrandian (Czechoslavakia); Vestnik Ustredního ústavu geologického, v. 43, p. 199-205.

Smith, D.G.
1981: Progress in Irish Lower Palaeozoic palynology; Review of Palaeobotany and Palynology, v. 34, p. 137-148.

Staplin, F.L., Jansonius, J., and Pocock, S.A.J.
1965: Evaluation of some acritarchous Hystrichosphere genera; Neues Jahrbuch für Geologie and Paläontologie, v. 123, p. 167-201.

Timofeev, B.V.
1966: Micropaleophytological investigations of the ancient suites (in Russian); Akademiia a Nauk SSSR, Laboratorija Geologii Dokembrija, 147 p.

1969: Proterozoic Sphaeromorphida (in Russian); Akademiia a Nauk SSSR, Institut Geologii i Geokhronologii Dokembrija, 144 p.

1973: Proterozoic and Early Paleozoic microfossils (in Russian); in Mikrofossilii drenejshikh otlozhenii, Trudy III Mezhdunarodnoj palinologitcheskoj konferentsii, Akademiia Nauk SSSR, Sibirskoe otdelenie, Institute Geologii i Geofiziki, p. 7-12.

Tynni, R.
1978: Lower Cambrian fossils and acritarchs in the sedimentary rocks of Söderfjärden, western Finland; Geological Survey of Finland, Bulletin 297, p. 39-81.

Vanguestaine, M.
1974: Espèces zonales d'acritarches du Cambro-Trémadocien de Belgique et de l'Ardenne française; Review of Palaeobotany and Palynology, v. 18, p. 63-82.

1978: Critères palynostratigraphiques conduisant à la reconnaissance d'un pli couché revinien dans le sondage de Grand-Halleux; Annales de la Société Géologique de Belgique, v. 100, p. 249-276.

Van Ingen, G.
1914: Table of the geological formations of the Cambrian and Ordovician systems about Conception and Trinity bays, Newfoundland and their northeastern American and western European equivalents, based upon the 1912-1913 field-work; Princeton University Contributions to Geology, Newfoundland, No. 4.

Vavrdová, M.
1976: Excystment mechanism of Early Paleozoic acritarchs; Časopis pro Mineralogii a Geologii, v. 21, p. 55-64.

Vidal, G.
1979: Acritarchs from the Upper Proterozoic and Lower Cambrian of East Greenland; Grønlands Geologiske Undersøgelse, Bulletin 134, 40 p.

1981a: Lower Cambrian acritarch stratigraphy in Scandinavia; Geologiska Föreningens i Stockholm Förhandlingen, v. 103, p. 184-192.

1981b: Micropalaeontology and biostratigraphy of the Lower Cambrian sequence in Scandinavia; in Short Papers from the Second International Symposium on the Cambrian System 1981, M.E. Taylor, ed.; U.S. Geological Survey, Open File Report 81-743, p. 232-235.

Volkova, N.A.
1968: Acritarchs of Precambrian and Cambrian deposits of Estonia (in Russian); in Problematiki pogranitchnikh sloev Rifeja u Kembrija russkoj platformi Urala i Kazakhstana, Trudy 188, Geologitcheskii Institut, Akademiia Nauk SSSR, p. 1-37.

1969a: Distribution of acritarchs in sequence of north-eastern Poland (in Russian); in Tommotskij jarus i problema nizhnej granitsi Kembrija, Trudy 206, Geologitcheskii Institut, Akademiia Nauk SSSR, p. 74-76.

1969b: Acritarchs of the northwest of the Russian Platform (in Russian); in Tommotskij jarus i problema nizhnej granitsi Kembrija, Trudy 206, Geologitcheskii Institut, Akademiia Nauk SSSR, p. 224-236.

1981: Upper Precambrian acritarchs of southeastern Siberia (Ustkirbinsk Suite); Biulleten Moskovskovo Obshesteva Ispitatelei Prirodi, Otdel geologitcheskii 56, p. 66-75.

Volkova, N.A., Kirjanov, V.V., Piskun, L.V., Pashkyavichene, L.T., and Jankauskas, T.V.
1979: Microflora (in Russian); in Paleontologija Verkhedokembriiskikh i Kembriiskikh otlozhenii Vostotchno-Evropeiskoj platformi, B.M. Keller and A.Yu. Rozonov, eds.; Geologitcheskii Institut, Akademiia Nauk SSSR, p. 4-38.

Westergård, A.H.
1946: Agnostidea of the Middle Cambrian of Sweden; Avhadlingar Sveriges Geologiska Undersökning, Ser. C, 477, 140 p.

44. STRATA AND TRACE FOSSILS NEAR THE PRECAMBRIAN-CAMBRIAN BOUNDARY, MACKENZIE, SELWYN, AND WERNECKE MOUNTAINS, YUKON AND NORTHWEST TERRITORIES

Project 650024

EMR Research Agreement 227/4/82

W.H. Fritz, G.M. Narbonne[1], and S.P. Gordey[2]
Institute of Sedimentary and Petroleum Geology, Ottawa

Fritz, W.H., Narbonne, G.M., and Gordey, S.P., Strata and trace fossils near the Precambrian-Cambrian boundary, Mackenzie, Selwyn, and Wernecke mountains, Yukon and Northwest Territories; in Current Research, Part B, Geological Survey of Canada, Paper 83-1B, p. 365-375, 1983.

Abstract

Uppermost Precambrian and lowermost Cambrian strata and trace fossils were examined in and near the Wernecke Mountains (4 sections), in the Mackenzie Mountains (3 sections), and in the Selwyn Mountains (1 section). In the first two regions, fine clastics containing the Precambrian-Cambrian boundary are overlain by the Lower Cambrian Sekwi Formation and underlain by a regional dolomite unit. In the third region, strata containing the boundary are overlain by shale that is, at least in part, correlatable with the Sekwi Formation, and underlain by a limestone that may be a physical extension of the regional dolomite unit. Trace fossils are the best indicators used thus far for locating the Precambrian-Cambrian boundary in the study area.

In the Wernecke Mountains, the zinc-bearing karst(?) breccias of the Goz Creek deposit are within the regional dolomite unit.

Résumé

Les auteurs ont examiné des couches et des empreintes fossiles du Précambrien supérieur et du Cambrien inférieur gisant à proximité ou au sein des monts Wernecke (4 profils), des monts Mackenzie (3 profils) et des monts Selwyn (1 profil). Dans les deux prémières régions, des sédiments clastiques fins renfermant la limite précambrienne et cambrienne sont sousjacents à la formation de Sekwi du Cambrien inférieur et reposent sur une unité régionale de dolomie. Dans la troisième région, des couches contenant la limite sont recouvertes de schiste argileux pour lequel il est possible d'établir une corrélation partielle avec la formation de Sekwi et reposent sur un calcaire qui pourrait être une prolongation physique de l'unité régionale de dolomie. Les empreintes fossiles sont les meilleurs indicateurs utilisés jusqu à présent pour situer la limite du Précambrien et du Cambrien dans la région à l'étude.

Dans les monts Wernecke, les brèches karstiques(?) zincifères du gisement de Goz Creek gisent au sein de l'unité régionale de dolomie.

Introduction

During the 1982 field season, strata directly underlying the Lower Cambrian Sekwi Formation were measured in four areas near the Yukon-Northwest Territories border (Fig. 44.1, sections 7-14). The objective was to correlate uppermost Precambrian and lowermost Cambrian strata using a combination of trace fossil ranges and lithological characteristics. Previous work (Fritz, 1982) had suggested that lithological correlations might be enhanced by utilizing the persistance of a regional dolomite unit (map unit 11 of Blusson, 1971). Optimism concerning the application of trace fossils came after their successful use by other workers in tentatively locating the Precambrian-Cambrian boundary at a section near June Lake in the Mackenzie Mountains (Fig. 44.1, section 11). At that section, the boundary was located by the International Precambrian-Cambrian Boundary Working Group, in 1979, at a level that is approximately 360 m above the top of map unit 11 (Fritz, 1980).

The most northwesterly area visited (sections 7-10) is in and near the southeastern margin of the Wernecke Mountains and is here referred to as the Goz Creek area. This area contains the thinnest sections and several disconformities. The June Lake area in the Mackenzie Mountains (sections 11, 12) contains the thickest stratigraphic succession and the greatest range of lithologies. Only a small percentage of the original strata are believed to have been removed by erosion. In the South Nahanni Anticline area in the Mackenzie Mountains (section 13), no evidence of erosion was seen in what have been recognized as predominantly slope deposits (Fritz, 1982). In the Selwyn Mountains, in the Gull Lake area (section 14), erosion is even less likely, as the strata there comprise a thick succession of basinal deposits.

This paper provides only a brief outline of the strata and trace fossils examined during the 1982 field season. A more detailed description is being prepared by Fritz and Narbonne. Microfossil samples and Ediacaran megafossils collected from levels shown in Figure 44.2 were sent to H.J. Hofmann and small shelly fossils were submitted to G.S. Nowlan.

Acknowledgments

The writers wish to express their appreciation to T.J. Frakes for assisting with trace fossil collecting at section 9, to H. McLaughlin for drafting figures, and to D.F. Marino for sharing supply aircraft in the Goz Creek area.

Trace Fossils and Biostratigraphic Control

Most of the trace fossils observed in the present study are simple horizontal traces such as **Planolites** (Pl. 44.1, fig. 4), **Gordia** (Pl. 44.1, fig. 3), **Helminthopsis** (Pl. 44.1, fig. 6), **Palaeophycus, Torrowangea, Cochlichnus,**

[1] Department of Geological Sciences, Queen's University, Kingston, Ontario, K7L 3N6
[2] Cordilleran Geology Division, Vancouver

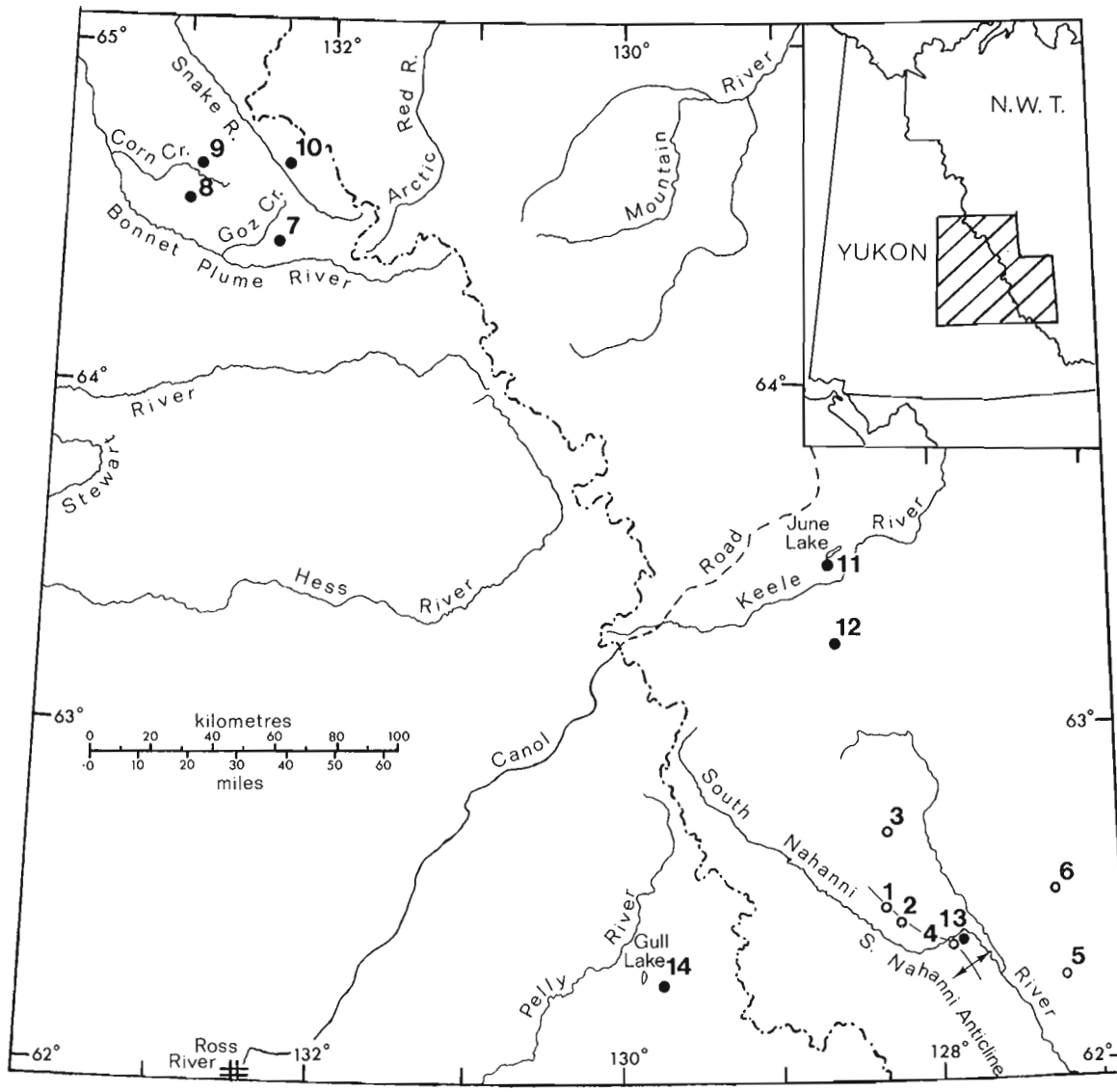

Figure 44.1. *Locality map. Stratigraphic sections discussed in text and illustrated in Figure 44.2 are located with solid circles. Open circles 1 (Fritz, 1979), 2, 3 (Fritz, 1981), and 4 through 6 (Fritz, 1982) locate sections described in previous reports.*

Plate 44.1

Trace fossils from Upper Precambrian and lowermost Cambrian strata. All specimens are natural size.

1. **Phycodes pedum** Seilacher. GSC 73056. Map unit 12, 349 m below top (GSC loc. 99155) section 11, June Lake area.
2. **Rusophycus** sp. A. GSC 73057. Vampire Formation, local float 64 m above base (GSC loc. 99069), section 10. Goz Creek area.
3. **Gordia** sp. GSC 73058. Unnamed siltstone unit 1, local float 53.5 m above base (GSC loc. 99098), section 8, Goz Creek area.
4. **Rusophycus** sp. B (centre) GSC 73059. **Planolites montanus** Richter (upper left) GSC 73060. Vampire Formation, local float 11 m below top (GSC loc. 99057), section 9, Goz Creek area.
5. **Treptichnus** sp. GSC 73061. Vampire Formation, float from unknown horizon (GSC loc. 99124), section 8, Goz Creek area.
6. **Helminthopsis** sp. GSC 73062. Vampire Formation, local float 90 m below top (GSC loc. 99120), section 8, Goz Creek area.
7. **Diplichnites** sp. and arthropod scratch marks. GSC 73063. Vampire Formation, local float 11 m below top (GSC 99057), section 9, Goz Creek area.


1

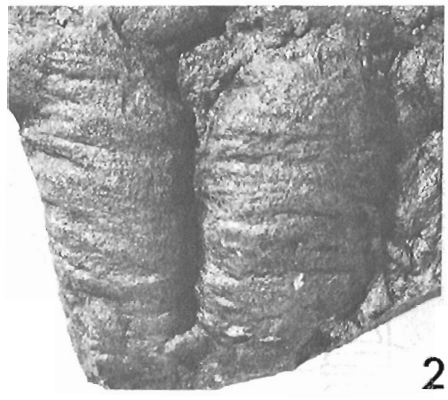
2


5


3

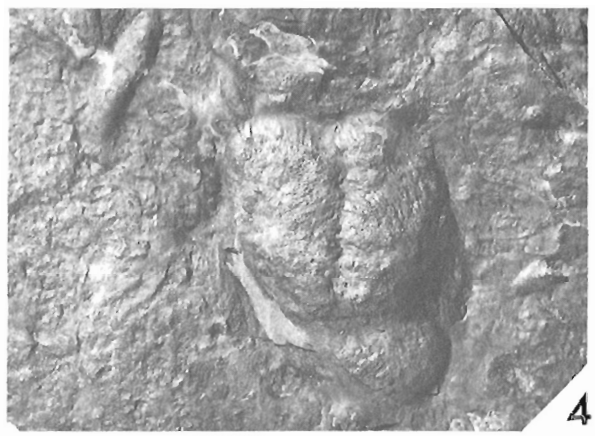
4


6

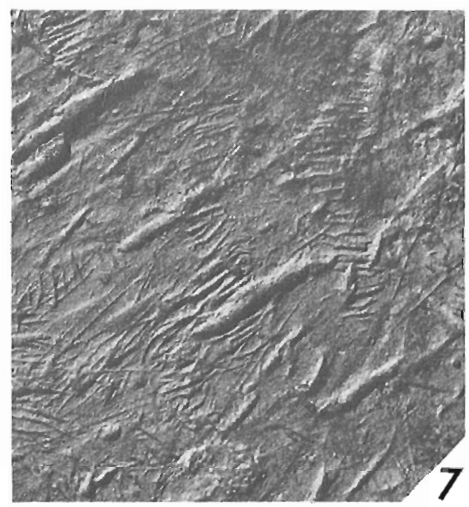
7

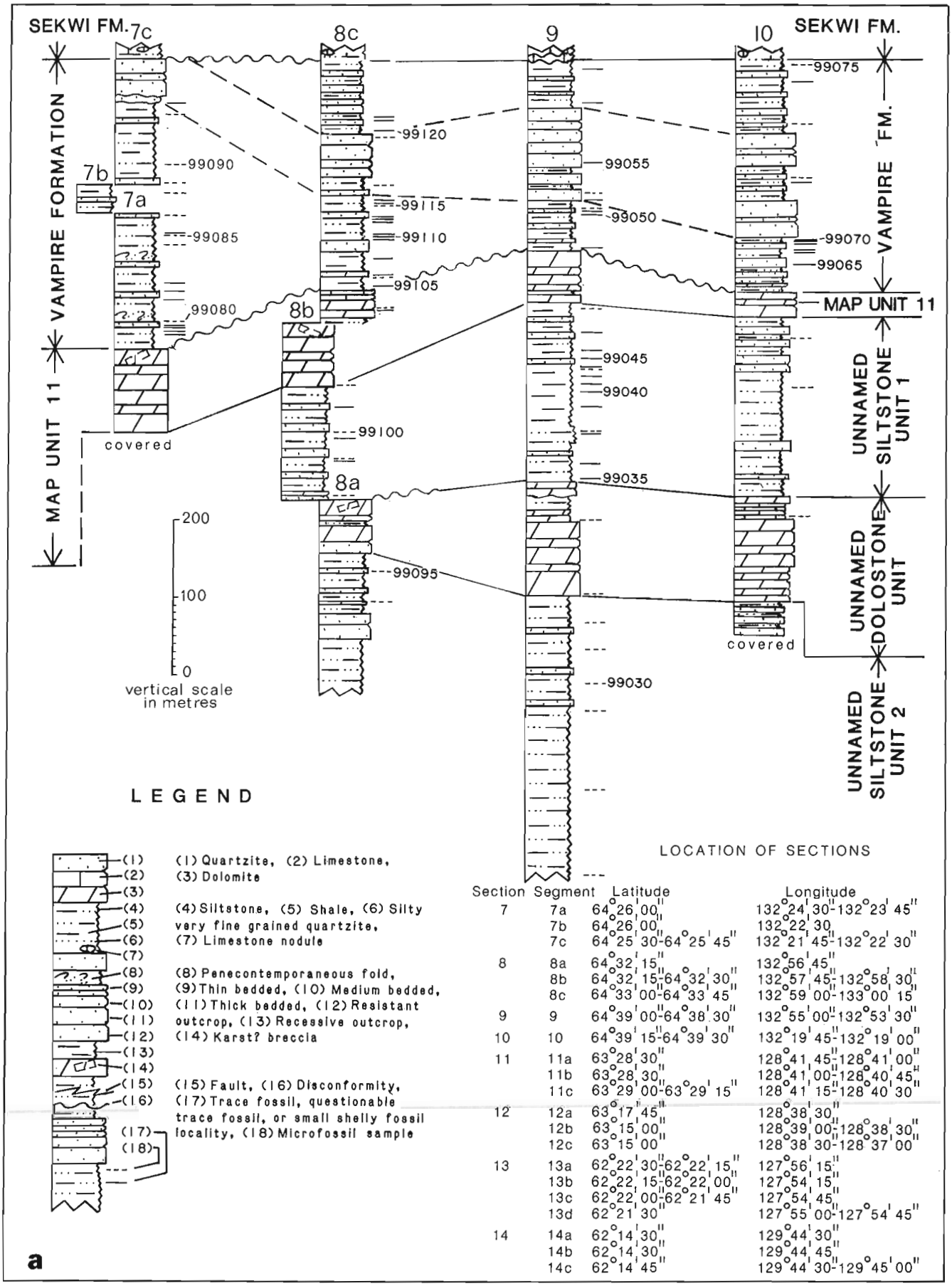

LOCATION OF SECTIONS

Section	Segment	Latitude	Longitude
7	7a	64°26'00"	132°24'30"-132°23'45"
	7b	64°26'00"	132°22'30"
	7c	64°25'30"-64°25'45"	132°21'45"-132°22'30"
8	8a	64°32'15"	132°56'45"
	8b	64°32'15"-64°32'30"	132°57'45"-132°58'30"
	8c	64°33'00"-64°33'45"	132°59'00"-133°00'15"
9	9	64°39'00"-64°38'30"	132°55'00"-132°53'30"
10	10	64°39'15"-64°39'30"	132°19'45"-132°19'00"
11	11a	63°28'30"	128°41'45"-128°41'00"
	11b	63°28'30"	128°41'00"-128°40'45"
	11c	63°29'00"-63°29'15"	128°41'15"-128°40'30"
12	12a	63°17'45"	128°38'30"
	12b	63°15'00"	128°39'00"-128°38'30"
	12c	63°15'00"	128°38'30"-128°37'00"
13	13a	62°22'30"-62°22'15"	127°56'15"
	13b	62°22'15"-62°22'00"	127°54'15"
	13c	62°22'00"-62°21'45"	127°54'45"
	13d	62°21'30"	127°55'00"-127°54'45"
14	14a	62°14'30"	129°44'30"
	14b	62°14'30"	129°44'45"
	14c	62°14'45"	129°44'30"-129°45'00"

Figure 44.2a, b. *Stratigraphic sections from localities shown in Figure 44.1. Fossil localities are numbered in sequence with every fifth number showing opposite the section.*

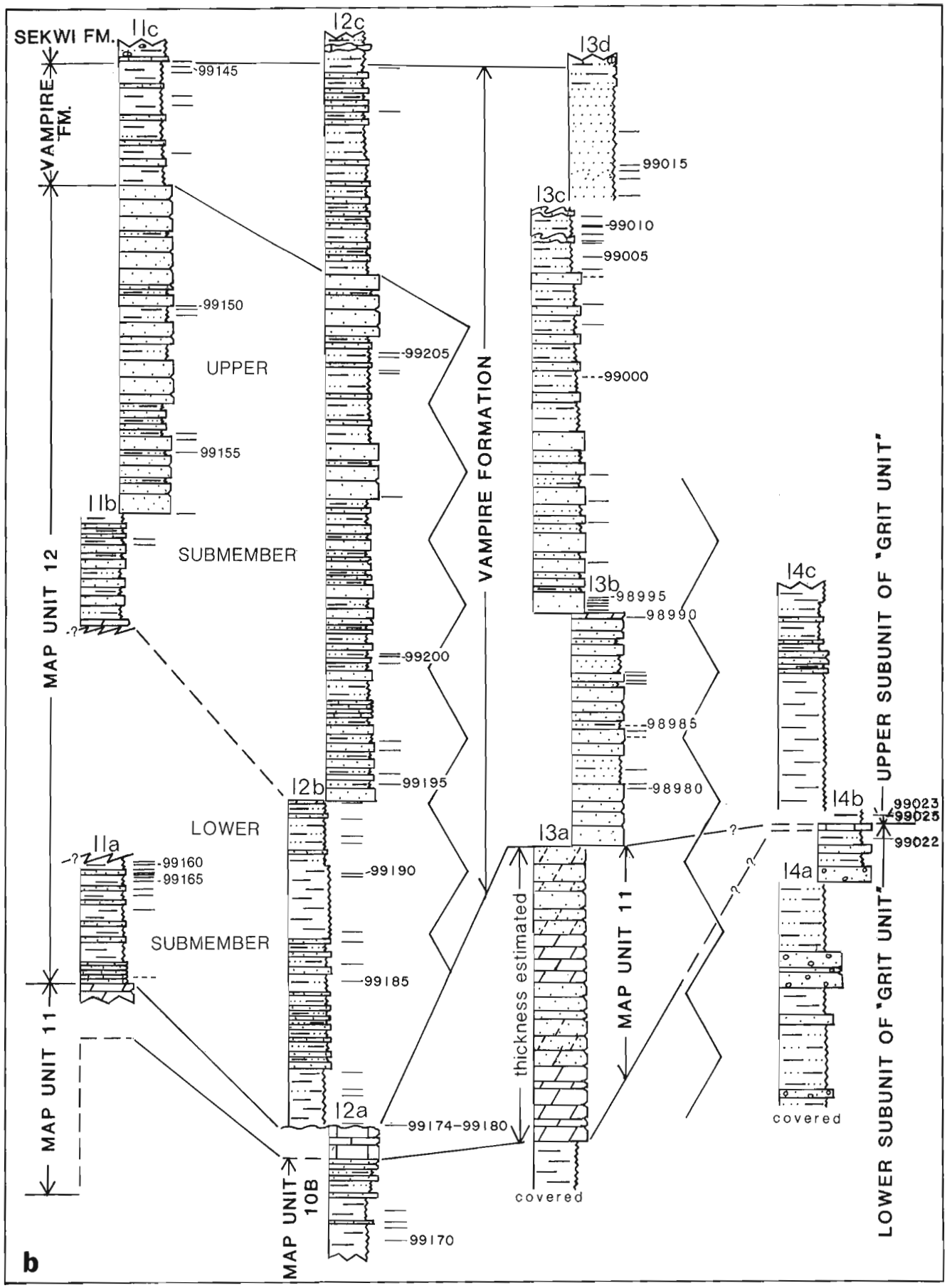
SEKWI FM.
VAMPIRE FM.
MAP UNIT 12
MAP UNIT 11
MAP UNIT 10B
VAMPIRE FORMATION
UPPER SUBUNIT OF "GRIT UNIT"
LOWER SUBUNIT OF "GRIT UNIT"
11c
12c
13d
13c
13b
13a
14c
14b
14a
12b
12a
11b
11a
UPPER
SUBMEMBER
LOWER
SUBMEMBER
99145
99150
99155
99205
99200
99195
99190
99185
99174-99180
99170
99015
99010
99005
99000
98995
98990
98985
98980
99023
99025
99022
99160
99165
thickness estimated
covered
covered
b

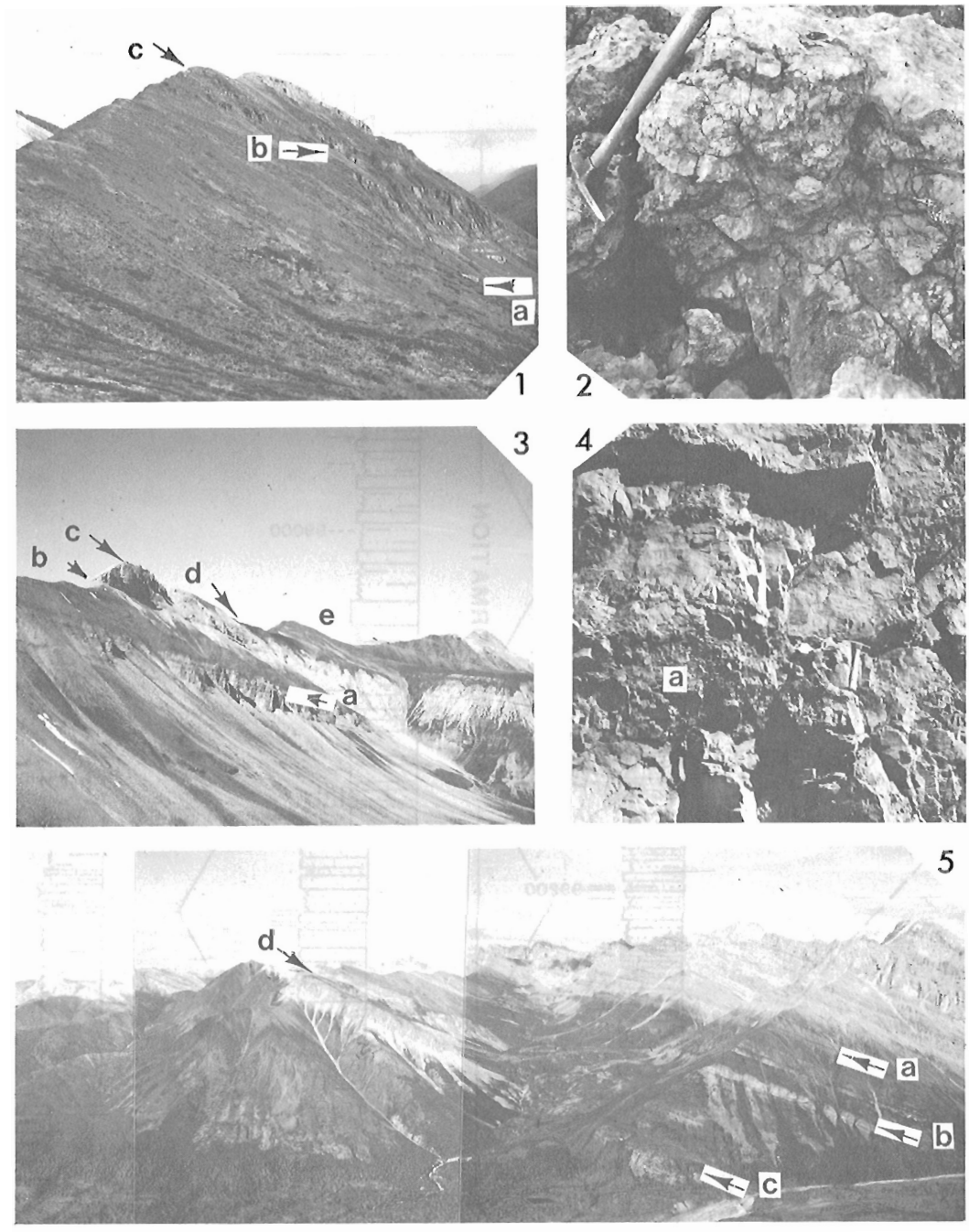

Plate 44.2

Figures

1. View east showing upper segment (7c) in section 7. Base of segment is at "a"; base of quartzite unit within Vampire Formation is at "b"; and contact between Vampire and Sekwi formations is at "c". GSC photo. 203852-V.
2. Karst(?) breccia in map unit 11 at section 7. GSC photo. 203852-U.
3. View northwest, showing section 8. Top of unnamed dolostone unit is at "a"; base and top of map unit 11 are at "b" and "d" respectively; karst(?) breccia shown in Figure 4 is located at "c"; and contact between Vampire and Sekwi formations is at "e". GSC photo. 203852-T.
4. Karst(?) breccia ("a") in map unit 11, section 8 (locality on section is at "c" in Figure. 3). GSC photo. 203852-0.
5. View northwest from section 9. Contact between Sekwi and Vampire formations is at "a"; top of map unit 11 is at "b"; top of unnamed dolostone unit is at "c" and "d"; long, dark southwest slope below unnamed dolostone at "d" is underlain by unnamed siltstone unit 2 (mapped here by Eisbacher, 1981, and in the vicinity by Blusson, 1974, as Sheepbed Formation). Figure is composite of GSC photos. 203853-H, 203853-I, and 203853-N.

Didymaulichnus and **Neonereites.** These ichnogenera are common in both Upper Precambrian and Cambrian deposits, and therefore cannot be used as biostratigraphic indicators. Approximately thirty collections of definite Cambrian trace fossils were made during the study. Arthropod traces including **Rusophycus** (Pl. 44.1, figs. 2, 4), **Diplichnites** (Pl. 44.1, fig. 7), **Monomorphichnus** and **Cruziana**?; complex feeding burrows such as **Phycodes** (Pl. 44.1, fig. 1), **Treptichnus** (Pl. 44.1, fig. 5) and **Teichichnus;** and the spreiten dwelling burrow **Diplocraterion** are restricted to Cambrian and younger rocks. Trace fossils are the best indicators used thus far for locating the Precambrian-Cambrian boundary in the study region.

Goz Creek Area

In this area the strata of major interest are underlain by three unnamed map units (Fig. 44.2a, sections 7-10). The oldest, here termed unnamed siltstone unit 2, is very thick (Pl. 44.2, fig. 5), and its upper part comprises medium brownish grey to medium grey weathering siltstone and a subordinate amount of very fine grained quartzite. It is overlain by an unnamed light grey dolostone unit. The carbonate unit is in turn overlain by unnamed siltstone unit 1 comprising siltstone and interbedded quartzite. Ediacaran megafossils are present in unnamed siltstone unit 2, and simple trace fossils, such as **Gordia** sp. (Pl. 44.1, fig. 3) occur in unnamed siltstone unit 1.

A local disconformity is suspected between unit 1 and the dolostone unit. Near section 7, and at section 8, unit 1 is much thinner than at sections 9 and 10. At the former two localities there are possible karst breccias that are overlain by basal white quartzite of unit 1. At sections 9 and 10 no karst breccia was identified, and the basal beds of siltstone unit 1 contain maroon siltstone (section 9, in basal 48.5 m; section 10, in basal 57 m).

The next two higher map units, map unit 11 and the Vampire Formation, include strata that are either close to or contain the Precambrian-Cambrian boundary. Map unit 11 comprises orange weathering dolostone with karst(?) breccias at various levels (Pl. 44.1, figs. 2, 4). At section 7 there is an abundance of white quartz in veins and cavity fillings. Map unit 11 at section 10 differs from that at the other three sections in its high content of very fine grained quartz sand (Pl. 44.3, fig. 2). At section 8, simple, horizontal trace fossils were found within map unit 11 (GSC locs. 99103, 99064), and all forms are tentatively placed in the Upper Precambrian.

The Vampire Formation in the Goz Creek area contains recessive siltstone and shale in its upper and lower parts, and has a more resistant medial part comprising very fine to fine grained quartzite. (Pl. 44.2, figs. 1, 3, 5; Pl. 44.3, fig. 1). The upper siltstone part at section 7 is absent, and was likely removed by pre-Sekwi erosion, as the Sekwi Formation rests directly on the resistant quartzite member. At section 8 the Sekwi Formation begins with 10 cm of conglomerate comprised of reworked Vampire strata, suggesting that some pre-Sekwi erosion has taken place there as well.

At an outcrop 1.5 km north of section 8, a limestone breccia is present in the basal few metres of the Vampire Formation. The breccia contains phosphate nodules and small shelly fossils, such as **Anabarites trisulcatus** Missarzhersky, and **Protohertzina anabarica** Missarzhersky (G.S. Nowland, personal communication). The Cambrian trace fossils **Rusophycus** sp., **Cruziana** sp. and arthropod scratch marks were found 1 m above the base of the Vampire Formation at the same locality. At the site of section 8 no fossils, phosphate nodules, or breccia were found at the base of the Vampire Formation, and the lowest Cambrian trace fossil, **Phycodes** sp., was located (GSC loc. 99106) 17 m above base of the formation. At sections 9 (GSC loc. 99060, located 150 m east of section) and 10 (GSC loc. 99066), the lowest Cambrian trace fossils were found 50 m above the base of the Vampire Formation. The abundance, diversity and large size of trace fossils (GSC locs. 98976-98979), near the base of the Vampire Formation at section 7, suggest a Cambrian age. None of the traces, however, can unquestionably be dated as Cambrian. These observations, plus correlations to be made later, indicate that a disconformity exists at the map unit 11-Vampire Formation contact in the Goz Creek area.

June Lake Area

Of the two sections measured in this area (Fig. 44.2b, sections 11, 12; Pl. 44.3, figs. 3, 5), section 12 is the better exposed, and therefore offers the best stratigraphic and trace fossil control. Section 12 starts in the upper part of map unit 10B (Blusson, 1971), which is composed of dark grey shale with some light brown quartzite near the top. The overlying map unit 11 comprises cream weathering, fine- to coarse-grained limestone, at the top of which are 3 m of limestone breccia that is locally scoured to a depth of 30 cm (Pl. 44.3, fig. 4) and is immediately overlain by basal dark shales of map unit 12 (Blusson, 1971). Breccia similar to those at the top of the unit is also present at various horizons within unit 11.

The next overlying unit, map unit 12, is divided into two submembers. At section 12 a lower, greenish grey and maroon weathering shale submember (423.5 m in thickness) is overlain by a submember (682.5 m in thickness) comprising white, light brown, and rust weathering quartzite with abundant interbedded siltstone.

Dark brownish grey weathering, recessive strata of the Vampire Formation, at the top of sections 11 and 12 (Pl. 44.3, fig. 5), are readily distinguished from lighter coloured strata in map unit 12 below and in the Sekwi Formation above. Silty shale predominates in the Vampire at section 11, whereas in the thicker Vampire exposure at section 12 shaly siltstone predominates. At both sections, dark brownish grey siltstones of the Vampire Formation grade upward through an interval of several metres into the light brown weathering, limy siltstone of the overlying Sekwi Formation.

The simple, small, trace fossils **Gordia** sp. and **Planolites** sp. are common in the upper part of map unit 10B and in the lower submember of map unit 12. No small, shelly fossils or phosphate nodules were noted in the breccias at the top of map unit 11. Numerous rock samples from map unit 11 are being processed in an attempt to supplement the small shelly fossil collection reported (Conway Morris and Fritz, 1980) from an outcrop of this unit between sections 11 and 12. The collection contains **Protohertzina** cf. **P. anabarica** Missarzhevsky and several small fossils of uncertain systematic position, and was tentatively placed in the upper Upper Precambrian. **Phycodes** sp., the lowest definite Cambrian trace fossil found (GSC loc. 99198) in section 12, is 76.5 m above the base of the upper submember (500 m above the base of map unit 12). The International Precambrian-Cambrian Boundary Working Group had previously placed the Precambrian-Cambrian boundary in an interval 350 to 370 m above the base of map unit 12 (Fritz, 1980, p. 45), at a section that partially overlaps section 11.

South Nahanni Anticline

Section 13 in this area was measured 2 km east of the type section for the Vampire Formation (Fritz, 1982, section 4) and near sections 1 and 2 on the South Nahanni Anticline. The latter two sections and section 3, located 42 km northwest of section 13, extend down into the upper strata of the Vampire Formation (see Fig. 44.1 for locations; Fritz, 1979, 1981). Section 13 lies near the point where

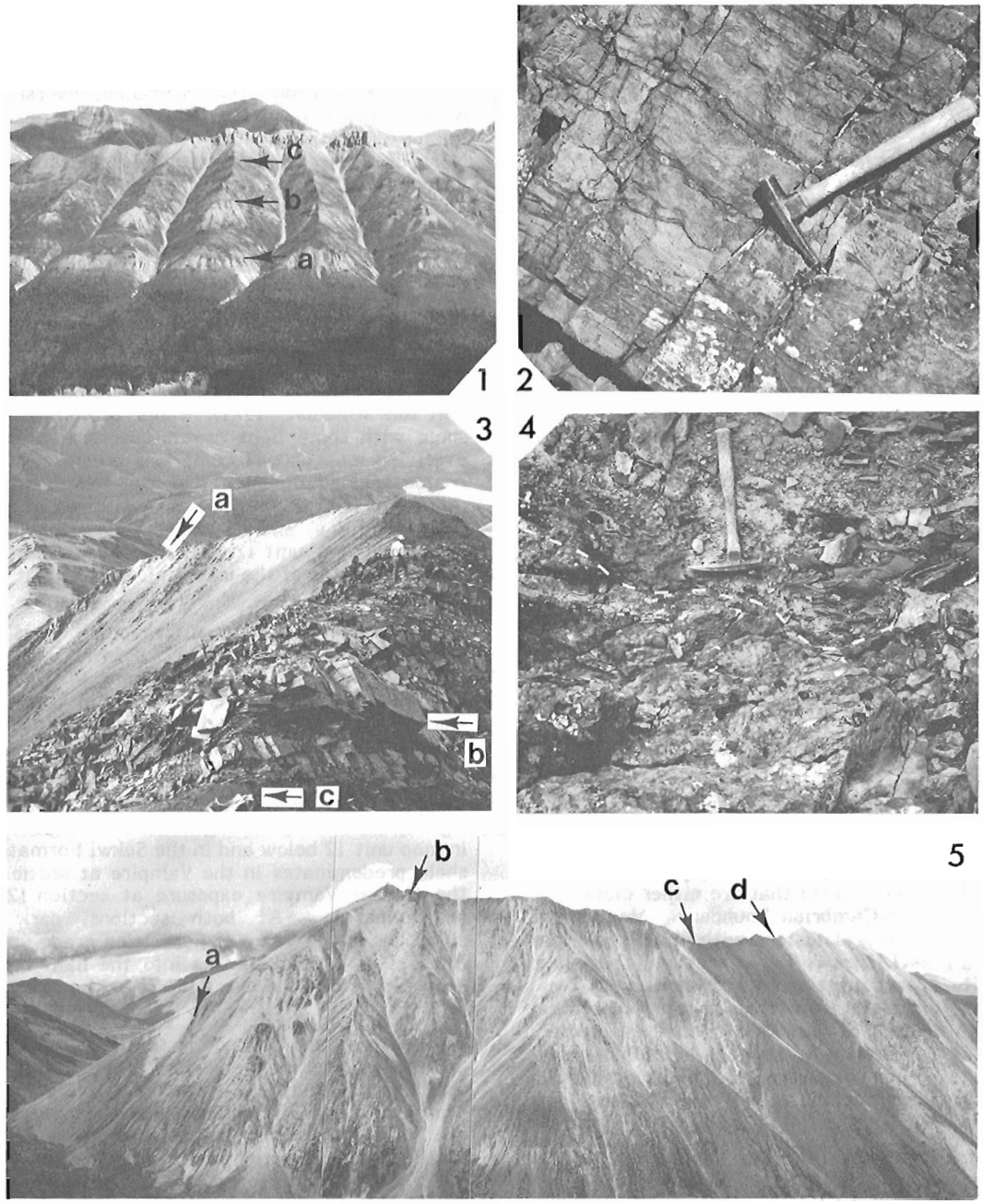

Plate 44.3

Figures

1. View from helicopter looking northeast at section 10. Top of unnamed dolostone unit is at "a"; top of map unit 11 is at "b"; and contact between Vampire and Sekwi formations is at "c". GSC photo. 203853-G.
2. Thin to medium bedded dolomite in map unit 11 at section 10. Light rock is dolomite. Dark laminae are layers of very fine grained quartz sand. GSC photo. 203852-J.
3. View west of overturned map unit 12 in section 11. Rough outcrop in foreground belongs to segment 11b. Pack in immediate foreground ("c") gives scale. The top of thick quartzite bed "b" is 302 m stratigraphically above base of member. Smooth slope in middle ground (between level of top of man's head and "a") belongs to lower segment (11a) of section 11. Contact between map unit 11 and map unit 12 is at "a". GSC photo. 203852-K.
4. Erosional relief located by dashed line at contact between map units 11 and 12 in section 12. Below line is limestone conglomerate at top of map unit 11. Above line is black shale of map unit 12, partially covered by float. GSC photo. 203853-E.
5. Section 12 viewed from south. Contact between map units 11 and 12 is at "a"; contact between map unit 12 and Vampire Formation is at "c"; and contact between Vampire and Sekwi formations is at "d". Section was measured along ridge crest between points "b" and "d" (segment 12c), and high on south flank between points "b" and "a" (segment 12b). Figure is composite of GSC photos. 203852-L, 203852-M, and 203853-D.

either map unit 11, or the middle member of the Backbone Ranges Formation, are appropriate names for the same lithological unit (Fritz, 1982, Figs. 12.3, 12.4); in this report we use map unit 11.

At section 13 an unnamed, highly sheared, silvery shale underlies map unit 11. Map unit 11 comprises medium and thick bedded, sandy dolostone and quartzite that weather light grey, cream, and light orange. The overlying Vampire Formation (Pl. 44.4, fig. 1) is composed of rust weathering siltstone and very fine grained quartzite that alternate with rust to medium brownish grey weathering, very fine- and fine-grained quartzite in thin to thick beds. Penecontemporaneous folds (Pl. 44.4, fig. 2) and ball and pillow structures are common at various horizons within the Vampire Formation. At the top of the formation, silty, very fine grained Vampire sandstone grades upward within a few metres into limy siltstone of the Sekwi Formation.

No trace fossils were found in the sheared shales at the base of the section, nor within map unit 11. Trace fossils are sparse in the lower part of the Vampire Formation, and the first definite Cambrian traces, **Rusophycus** sp. (GSC loc. 99015), were located 860.5 m above the base of the formation. This horizon is clearly well above the base of the Cambrian, as the Cambrian traces cf. **Rusophycus** sp., and other arthropod scratch marks, have been reported (Fritz, 1982, p. 87) from a horizon 301 m above the base of the formation at the nearby type section.

Gull Lake Area

In this area the Upper Precambrian and part of the Lower Cambrian are within a regionally widespread map unit termed the "grit unit" (Gabrielse, 1967, p. 275). The lower subunit of the "grit unit" comprises alternating thick successions of quartzite, that locally bear clasts up to pebble size (Pl. 44.4, fig. 3), and thick successions of shale and/or siltstone. At section 14, and elsewhere in the Gull Lake area, the top of the lower subunit is the top of a thin limestone member (8.5 m in thickness at section 14). Most of the upper subunit comprises maroon shale. At section 14, at least 40 m of similar shale is present, 251 m below the top of the lower subunit (Pl. 44.4, fig. 4), but this is a rare occurrence of maroon shale within the lower subunit. Higher strata in the upper subunit were not measured at section 14 because of strong cleavage and folding. However, in this area the upper subunit is known to be overlain by brown shale that locally contains an archaeocyathid-bearing limestone conglomerate near its base (Gordey, 1980). The archaeocyathids suggest that the brown shale is, at least in part, the lateral equivalent of the Sekwi Formation, and that the contact between the "grit unit" and the brown shale is well within the Lower Cambrian (assuming no disconformity).

The trace fossil **Gordia**? sp. was collected from the interval 8.5 to 54 m below the top of the lower subunit (GSC loc. 99022), and trace fossils **Gordia** sp., **Palaeophycus** sp., and **Planolites** sp., were collected from the interval between the base and 20 m above the base of the upper subunit. No diagnostic Cambrian trace fossils are present in these collections, and they are tentatively placed in the uppermost Precambrian.

Elsewhere, near the headwaters of the Hess River, the Lower Cambrian trace fossil **Oldhamia radiata** Forbes was found at a horizon high in the upper subunit of the "grit unit" (Hofmann and Cecile, 1981).

Correlations

Correlations for the four study areas are given in Figure 44.3. The two map units found to be the most useful for regional lithologic correlations are the Sekwi Formation, located at the top of most sections, and map unit 11 near the base. A tentative correlation of map unit 11 with the limestone member in the "grit unit" is based upon the latter unit's stratigraphic position and general age.

Strata below map unit 11 in the Goz Creek and June Lake areas, and below the limestone member at the top of the lower subunit of the "grit unit" in the Gull Lake area,

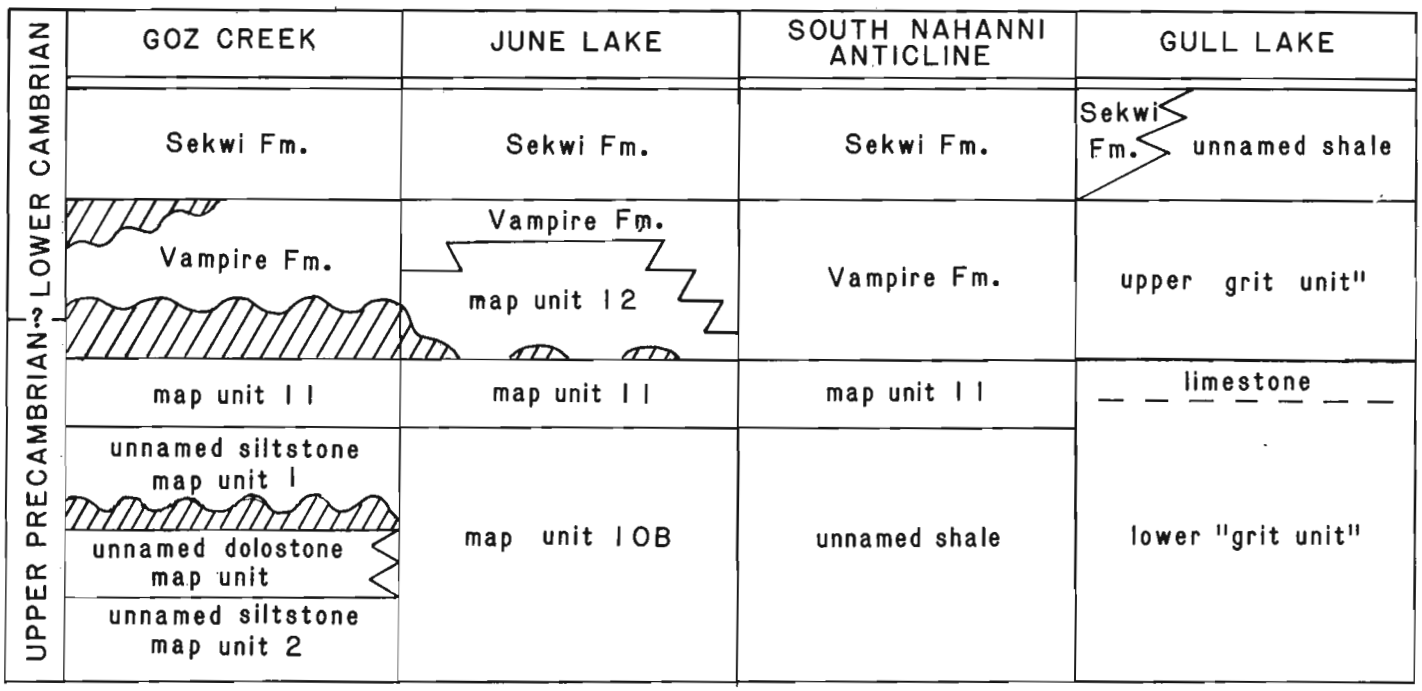

Figure 44.3. *Correlation chart for Upper Precambrian and Lower Cambrian strata in the Mackenzie Mountains and adjacent areas.*

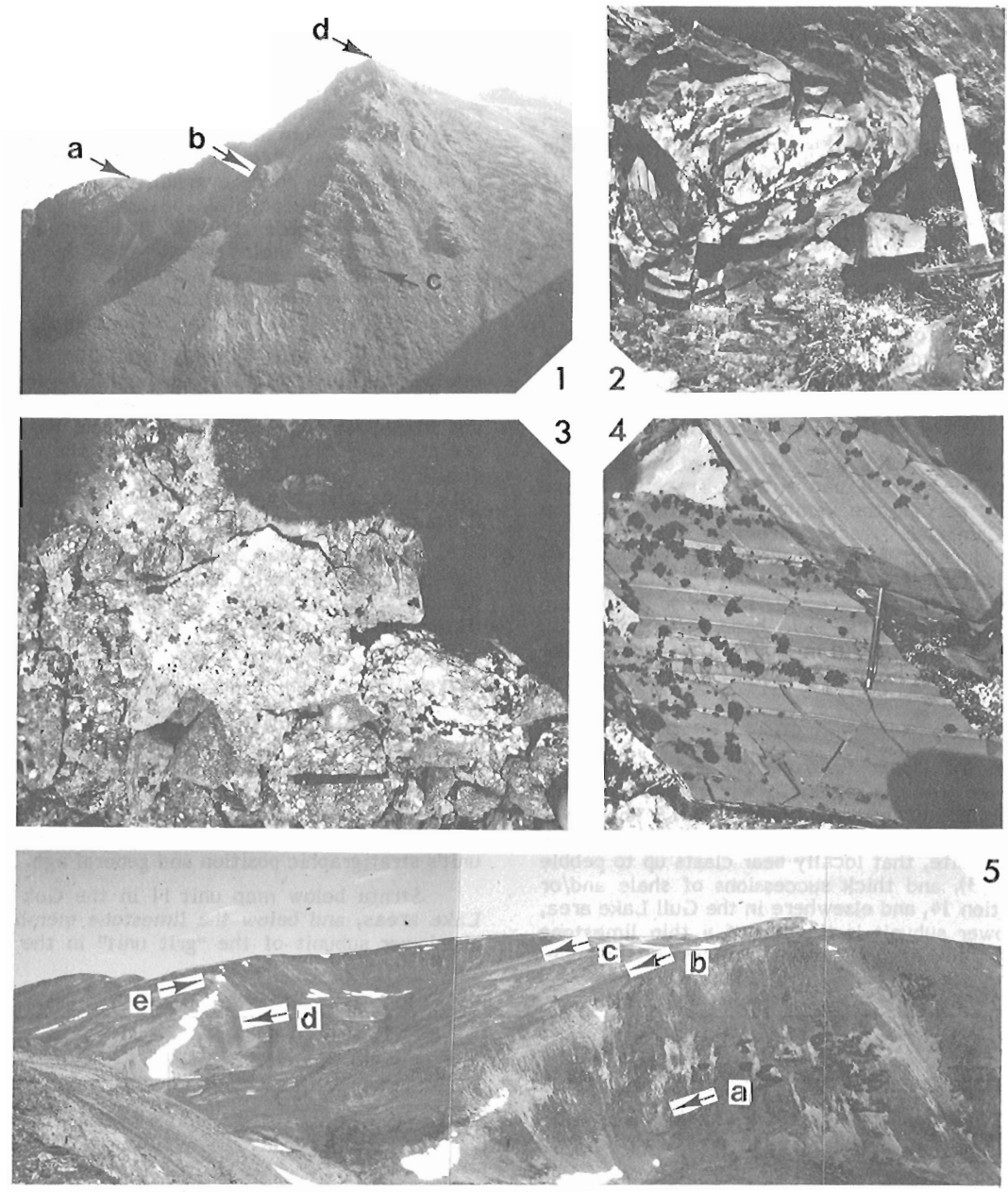

Plate 44.4

1. View east, looking at Vampire Formation in section 13. Top of segment 13c is at "a". Contact between units 5 and 6 (Fritz, 1982, p. 87) was located at "b" and projected to 10.5 m above point "a". Upper segment starts between points "c" and "d" and terminates on ridge beyond point "d". GSC photo. 203853-Q.
2. Penecontemporaneous fold, 92.5 m below top of Vampire Formation and located 1 km east of segment 13d. GSC photo. 203853.
3. Quartz pebble conglomerate (in local float) from lower subunit of "grit unit". Location is 160 m above base at section 14. White quartzite pebbles in this part of section range up to 2 cm in diameter. GSC photo. 203853-M.
4. Maroon weathering siltstone with apple green (light coloured) laminae, from "grit unit" in section 14. Siltstone blocks shown are from lower subunit of "grit unit" and originate from an interval 66 to 97.5 m above base of section. Maroon siltstone like this is rare in lower subunit, whereas shale with an almost identical appearance comprises most of the upper subunit. GSC photo. 203853-0.
5. View north-northwest of "grit unit" in section 14. Lower member was measured in lower segment (14a) between points "a" and "c", and in middle segment (14b) between points "d" and "e". Point "b" is 113.5 m above base of section. Top of lower subunit of "grit unit" is at top of limestone at "e". Remainder of section (14c) was measured westward from base of upper subunit (locally covered) above (but near) point "c" and down far side of ridge. Figure is composite of GSC photos. 203853-L, 203853-R and 203853-S.

contain Precamrian trace fossils that do not provide close correlation; but they do at least indicate a lack of a major erosion beneath this regional map unit. Ediacaran fossils reported from map unit 10B near the June Lake area (Hofmann, 1981), and from siltstone map unit 2 in the Goz Creek area (H.J. Hofmann, personal communication) lend weight to this observation. Strata below map unit 11 in the Nahanni Anticline area are too strongly sheared for the preservation of trace or body fossils, and correlation to these strata is, therefore, based purely on lithology.

Map unit 11 was found to lie close to, but below, the Precambrian-Cambrian boundary. In the June Lake and South Nahanni Anticline areas, trace fossils suggest the boundary is well above map unit 11. The boundary's position at the map unit 11-Vampire Formation contact at section 8 (and probably at sections, 7, 9, and 10 as well) in the Goz Creek area, is attributed to a disconformity in that area.

Earlier correlations (Fritz, 1982) of the strata described herein with the Backbone Ranges Formation are consistent with the present data. In those correlations, the Vampire Formation, map unit 12, and the upper subunit of the "grit unit" were correlated with the upper member of the Backbone Ranges Formation, and map unit 11 was correlated with the middle member of the Backbone Ranges Formation.

Economic considerations

At the Goz Creek zinc deposit, located 5 km west of section 7, in what is here considered map unit 11, 10 drill intersections have proven 1.75 million metric tons of zinc in 18 per cent ore, and a total potential of 5 million tons in 13 per cent or better ore has been estimated (Reeve, 1977, p. 14). Reeve (*op. cit.*) has noted the association of ore with breccias, and that the breccias may be the product of a karst environment. He suspected, but was unable to prove, the existence of an unconformity at the top of the dolostone, as was made clear in his statement (*op. cit.*, p. 8), "While specific evidence of an unconformity....is lacking; it seems unlikely that such breccias could have developed in any other way...."

During the present study similar breccias were noted in map unit 11 at section 7 and near section 8. Breccias were not seen at sections 9 and 10, but the extensive outcrops along strike from these sections were not explored. Karst(?) breccias in the lateral extenstion of map unit 11 (middle member of the Backbone Ranges Formation) were noted by Fritz (1982) at sections 5 and 6 (Fig. 44.1) east of the South Nahanni Anticline area. Slope breccias or rip-up breccias in map unit 11 at section 12 may be of less economic interest than the mentioned karst(?) breccias.

References

Blusson, S.L.
1971: Sekwi Mountain map-area, Yukon Territory and District of Mackenzie; Geological Survey of Canada, Paper 71-22, 17 p.

1974: Geology, Northern Selwyn Basin (Operation Stewart), Yukon and NWT; Geological Survey of Canada, Open File 205.

Conway Morris, S. and Fritz, W.H.
1980: Shelly microfossils near the Precambrian-Cambrian boundary, Mackenzie Mountains, northwestern Canada; Nature, v. 286, no. 5771, p. 381-384.

Eisbacher, G.H.
1981: Sedimentary tectonics and glacial record in the Windermere Supergroup, Mackenzie Mountains, northwestern Canada; Geological Survey of Canada, Paper 80-27, 40 p.

Fritz, W.H.
1979: Cambrian stratigraphic section between south Nahanni and Broken Skull rivers, southern Mackenzie Mountains; in Current Research, Geological Survey of Canada, Paper 79-1B, p. 121-125.

1980: International Precambrian-Cambrian Boundary Working Group's 1979 field study to Mackenzie Mountains, Northwest Territories, Canada; in Current Research, Part A, Geological Survey of Canada, Paper 80-1A, p. 41-45.

1981: Two Cambrian stratigraphic sections, eastern Nahanni map area, Mackenzie Mountains, District of Mackenzie; in Current Research, Part A, Geological Survey of Canada, Paper 81-1A, p. 145-156.

1982: Vampire Formation, a new Upper Precambrian(?)/Lower Cambrian formation, Mackenzie Mountains, Yukon and Northwest Territories; in Current Research, Part B, Geological Survey of Canada, Paper 82-1B; p. 83-92.

Gabrielse, H.
1967: Tectonic evolution of the northern Canadian Cordillera; Canadian Journal of Earth Sciences, v. 4, p. 271-298.

Gordey, S.P.
1980: Stratigraphic cross-section, Selwyn Basin to Mackenzie Platform, Nahanni map area, Yukon Territory and District of Mackenzie; in Current Research, Part A; Geological Survey of Canada, Paper 80-1A, p. 353-355.

Hofmann, H.J.
1981: First record of a Late Proterozoic faunal assemblage in the North American Cordillera; Lethaia, v. 14, p. 303-310.

Hofmann, H.J. and Cecile, M.P.
1981: Occurrence of **Oldhamia** and other trace fossils in Lower Cambrian(?) argillites, Niddery Lake map area, Selwyn Mountains, Yukon Territory; in Current Research, Part A, Geological Survey of Canada, Paper 81-1A, p. 281-290.

Reeve, A.F.
1977: The Goz Creek zinc prospect, Yukon Territory, Canada; Barrier Reef Resources, Limited, Internal Report, 19 p.

45. UPPER PROTEROZOIC AND PALEOZOIC STRATIGRAPHY, DELPHINE CREEK AREA, SOUTHEASTERN BRITISH COLUMBIA: IMPLICATIONS FOR THE PURCELL ARCH

Project 810010

Kevin G. Root[1]
Institute of Sedimentary and Petroleum Geology, Calgary

Root, K.G., Upper Proterozoic and Paleozoic stratigraphy, Delphine Creek area, southeastern British Columbia: implications for the Purcell Arch; in Current Research, Part B, Geological Survey of Canada, Paper 83-1B, p. 377-380, 1983.

Abstract

Eocambrian and Lower Paleozoic strata in the Purcell Anticlinorium are anomalously thin, compared to coeval strata to the east in the Main Ranges and to the west in the Kootenay Arc, as a result of deposition on the tectonically positive Purcell Arch. A previously unrecognized exposure of Eocambrian Hamill Group and Upper Devonian Starbird Formation strata in the Purcell Anticlinorium at Delphine Creek, constitutes the most condensed section of Eocambrian and Paleozoic strata deposited on the Purcell Arch. Stratigraphic relationships at Delphine Creek, and within the northern portion of the Purcell Anticlinorium, demonstrate activity of the Purcell Arch from Late Proterozoic to at least Upper Devonian time. Local variations in the thicknesses of Upper Proterozoic and Paleozoic strata at Delphine Creek are the result of deposition in north-northwesterly trending sub-basins which were probably formed by west-side-down movement on listric normal faults. Stratigraphic relationships suggest that the Mount Forster thrust fault follows the locus of a Late Proterozoic to Paleozoic normal fault which formed the western boundary of the Purcell Arch.

Résumé

Les couches de l'Eocambrien et du Paléozoïque inférieur de l'anticlinorium de Purcell sont anormalement minces lorsqu'on les compare aux couches contemporaines des chaînons Main à l'est et de l'arc de Kootenay à l'ouest, et ce, parce qu'elles ont été déposées dans l'arche de Purcell tectoniquement positive. Un affleurement auparavant inconnu des couches du groupe de Hamill (Éocambrien) et de la formation de Starbird (Dévonien supérieur) dans l'anticlinorium de Purcell au ruisseau Delphine constitue la section la plus condensée de couches éocambriennes et paléozoïques déposées dans l'arche de Purcell. Les liens stratigraphiques au ruisseau Delphine et au sein de la partie nord de l'anticlinorium de Purcell témoignent de l'activité continue de l'arche de Purcell du Protérozoïque récent au moins jusqu'au Dévonien supérieur. Les variations locales de l'épaisseur des couches du Protérozoïque et du Paléozoïque supérieurs au ruisseau Delphine résultent de l'accumulation dans des bassins secondaires orientés nord-nord-ouest qui avaient probablement été formés par le mouvement descendant des compartiments ouest de failles normales listriques. Les liens stratigraphiques suggèrent que la faille chevauchante du mont Forster suit la ligne d'une faille normale datant du Protérozoïque récent au Paléozoïque, responsable de la formation de la limite ouest de l'arche de Purcell.

Introduction

The Delphine Creek study area is situated in the Purcell Anticlinorium (Fig. 45.1), which is located in the southern portion of the Canadian Cordillera. Strata exposed within the Purcell Anticlinorium are dominantly Proterozoic sedimentary rocks of the Purcell and Windermere supergroups. Within the northern portion of the Purcell Anticlinorium, Eocambrian and Paleozoic strata are present in a few outliers, and are anomalously thin compared to coeval strata to the east and to the west.

Douglas et al. (1970) suggested that the Purcell Arch was a north-northwesterly trending structure which formed the southwestern flank of the early Paleozoic shale basin that is presently situated within the Main Ranges of the Rocky Mountains. Cambrian and Ordovician strata, consisting largely of calcareous mudstone and argillaceous limestone, accumulated in this basin to the southwest of an abrupt facies change from a shallow water carbonate platform (Cook, 1975; Aitken, 1971). The basin was bounded to the south by the Dibble Creek Monocline (Benvenuto and Price, 1979).

The Lower Paleozoic succession attains a thickness of approximately 8 km in the western Main Ranges (Price, 1981), and becomes progressively condensed southwestward toward the Purcell Arch. At the east side of Mount Forster (Fig. 45.2), approximately 800 m of Lower Paleozoic strata (Reesor, 1973) and 476 m of Middle Devonian strata (Norford, 1981) are present beneath the Upper Devonian Starbird Formation. At Law Ridge, only 135 m of Lower Paleozoic strata are present between the Upper Proterozoic Horsethief Creek Group and the Middle Devonian Mount Forster Formation (Reesor, 1973). This southwestward thinning of Paleozoic strata records the northeasterly tilting of large blocks, possibly resulting from the activity of down-to-the-basin listric normal faults (Price, 1981).

To the west of the axial region of the Purcell Anticlinorium, Lower Paleozoic strata thicken dramatically; at Jumbo Pass (Fig. 45.2) about 1900 m of Eocambrian and Lower Cambrian strata are exposed (Reesor, 1973).

Prior to the recognition of Eocambrian and Paleozoic strata at Delphine Creek, the outlier at Law Ridge was the most condensed Paleozoic section known to have been deposited on the Purcell Arch; the section at Law Ridge demonstrates activity of the Purcell Arch through early Paleozoic time.

Paleozoic Strata at Delphine Creek

An outcrop of Upper Devonian Starbird Formation was recognized at Delphine Creek by the author in 1980, while employed by Trigg, Woollett Consulting Ltd. Fieldwork in

[1] Department of Geology and Geophysics, University of Calgary, Calgary, Alberta

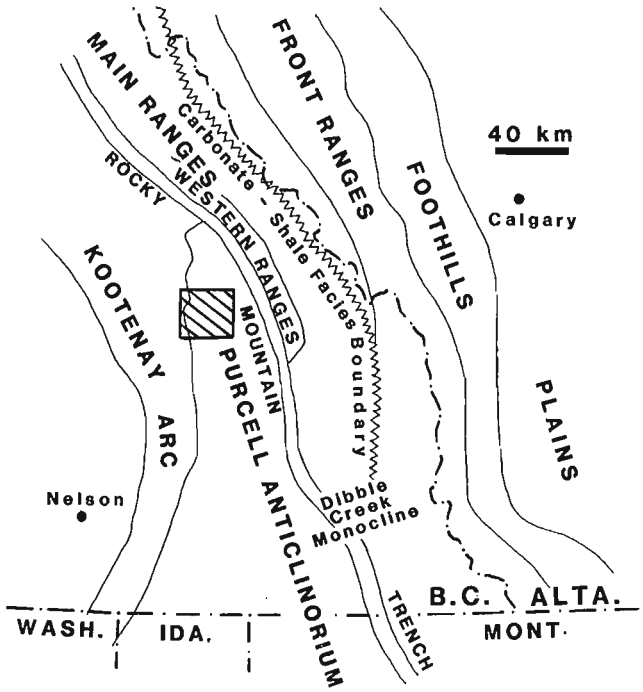

Figure 45.1. Geological provinces of the southern Canadian Cordillera. The age of the facies boundary is Early Paleozoic. The location of Figure 45.2 is indicated by the cross-hatched area.

1982 has demonstrated that strata of the Eocambrian Hamill Group are present between the Upper Proterozoic Horsethief Creek Group and the Upper Devonian Starbird Formation, in all but the westernmost exposures of the Starbird Formation (Fig. 45.2). These strata were not recognized in reconnaissance mapping by Walker (1926) and were included with the Horsethief Creek Group; later reports by Reesor (1957, 1973) incorporated Walker's mapping at Delphine Creek with no modification.

Stratigraphy

Strata of the Horsethief Creek Group, Hamill Group, and Starbird Formation at Delphine Creek have significant implications concerning the timing of activity and the tectonic processes active at the crest of the Purcell Arch.

Horsethief Creek Group

The Upper Proterozoic Horsethief Creek Group consists of argillite, quartz-pebble conglomerate, sandstone, limestone, and dolomite. Well developed graded beds of pebble conglomerate, and both complete and incomplete Bouma sequences, suggest that much of the Horsethief Creek Group was deposited by submarine mass flows in a deep water environment. Coarse clastic content decreases rapidly upwards; near the top of the sequence, beds of dolomite and limestone locally contain mud cracks and structures of presumed algal origin, indicating deposition in a peritidal setting.

The Horsethief Creek Group is a minimum of 950 m thick at Law Ridge, 12 km northeast of Delphine Creek, and over 1600 m thick at Jumbo Pass, 15 km southwest of Delphine Creek (Reesor, 1973). At both locations the Horsethief Creek Group comprises argillite, pebble conglomerate, and minor carbonate, similar to strata present below the shallow water carbonates at Delphine Creek. In contrast to exposures to the northeast and southwest, the

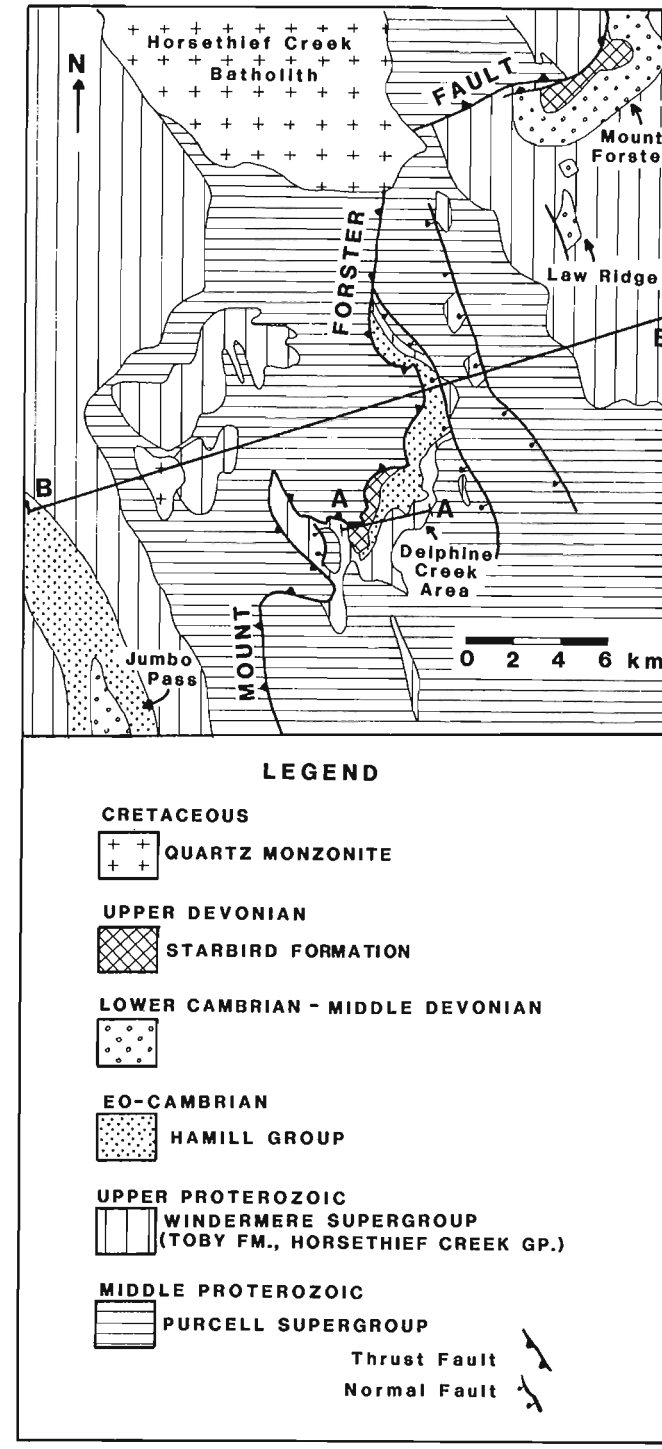

Figure 45.2. Generalized geological map compiled from Reesor (1973), G. Freiholz (personal communication, 1983), and work of the writer, to illustrate the distribution of Paleozoic strata in the northern portion of the Purcell Anticlinorium. A-A denotes the line of stratigraphic section in Figure 45.3; B-B denotes the line of schematic stratigraphic section in Figure 45.4.

thickness of the Horsethief Creek Group at Delphine Creek varies from 100 m to 400 m. Erosion prior to deposition of the Hamill Group accounts for some thinning of the Horsethief Creek Group, but comparison of depositional facies at Delphine Creek with exposures to the northeast and southwest indicates that the thinning is largely due to depositional attenuation. Deep water Horsethief Creek Group strata at Delphine Creek are overlain by shallow water carbonates and are much thinner than coeval deep water strata to the northeast and southwest.

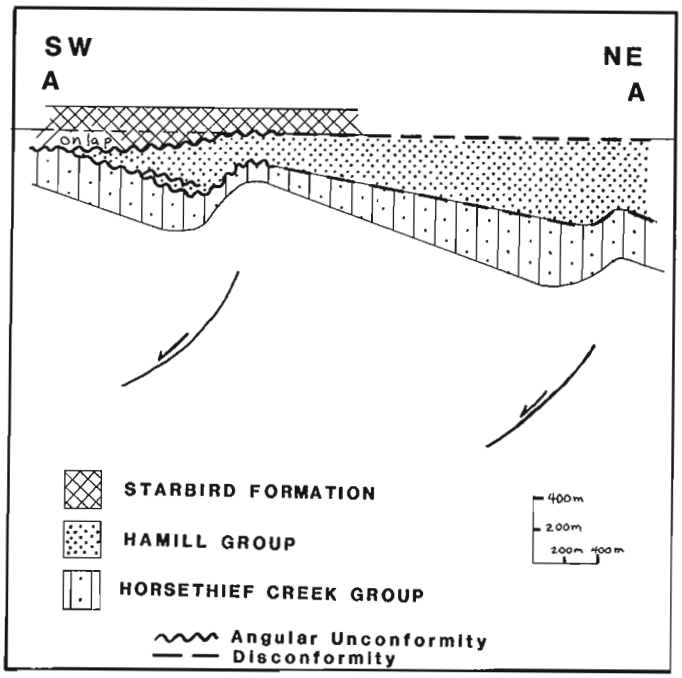

Figure 45.3. *Stratigraphic section illustrating the asymmetric wedges of strata developed in subbasins, probably as a result of movement on listric normal faults. The horizontal datum is the base of a dolomitic siltstone in the Upper Devonian Starbird Formation. Section location is shown in Figure 45.2.*

Hamill Group

Strata of the Eocambrian Hamill Group unconformably overlie the Horsethief Creek Group. The Hamill Group consists of friable sandstone, quartzite, pebble and granule conglomerate, and minor argillite and dolomite. Basic volcanic flows are present at two stratigraphic levels. Medium and large scale trough and planar cross-stratification and crudely developed fining-upward sequences in much of the sandstone suggest a fluvial depositional environment; planar bedding and small scale multidirectional crossbeds in the remainder of the Hamill Group are suggestive of shallow marine deposition.

The strata are assigned to the Hamill Group because of their dissimilarity in lithology to the Horsethief Creek Group, both at Delphine Creek and regionally, and their similarity to Hamill Group strata at Jumbo Pass, 15 km southwest of Delphine Creek.

The Hamill Group is a minimum of about 600 m thick at easternmost exposures at Delphine Creek, where it is faulted against strata of the Middle Proterozoic Purcell Supergroup; it thins rapidly westward to a zero edge due to depositional thinning, an internal unconformity, and erosional truncation at the base of the Upper Devonian Starbird Formation (Fig. 45.3). Horsethief Creek Group strata underlie westernmost exposures of the Starbird Formation.

Starbird Formation

Dolomite, dolomitic siltstone, quartzite, and minor argillite, which unconformably overlie the Hamill Group and Horsethief Creek Group at Delphine Creek, are considered correlative with the Upper Devonian Starbird Formation. This correlation is based on a probable Middle or Late Devonian age assigned to fossils collected from a dolomite unit at the base of the sequence (B.S. Norford, personal communication, 1981). The Mount Forster Formation, which is exposed at Mount Forster and Law Ridge, is Middle Devonian in age (Norford, 1981), but is lithologically dissimilar to the Devonian strata at Delphine Creek. The lowermost strata of the Devonian sequence at Delphine Creek consist of dolomite in which stromatoporoids, **Amphipora**, corals, and crinoid debris are locally abundant; this unit is lithologically similar to the exposure of Starbird Formation at Mount Forster.

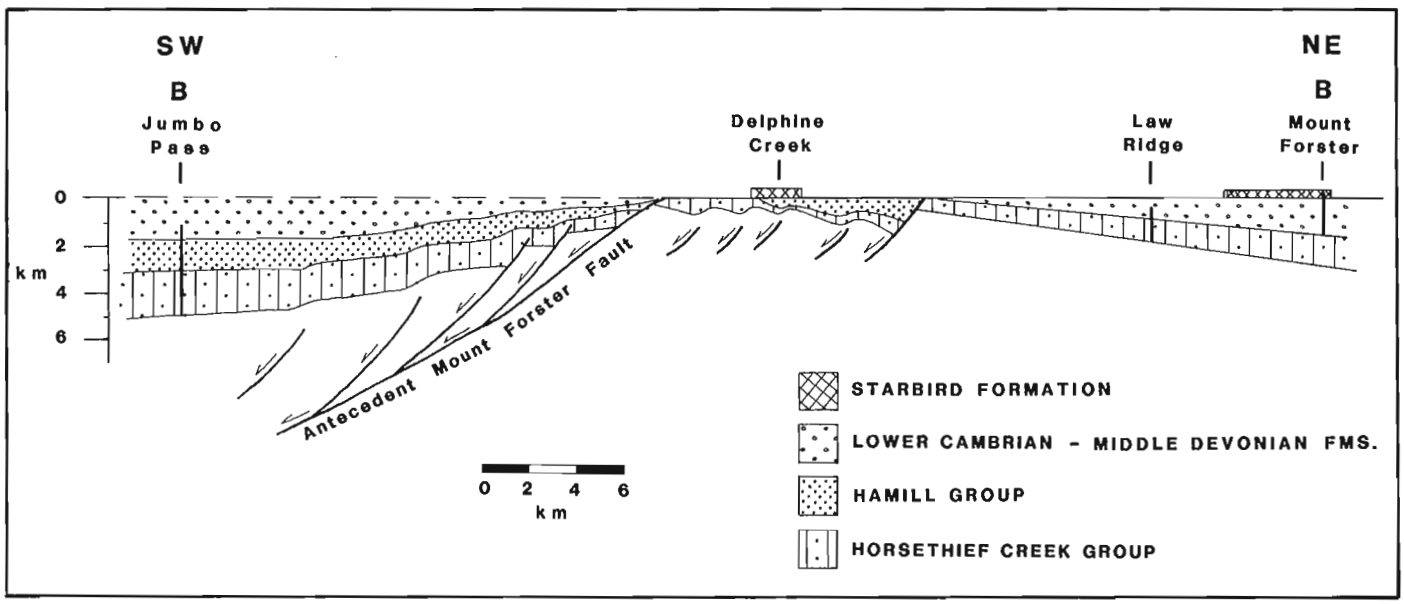

Figure 45.4. *Schematic stratigraphic section across the crest of the Purcell Arch. The base of the Upper Devonian is the horizontal datum. Section location is shown in Figure 45.2. Thickness of strata at Law Ridge and Jumbo Pass from Reesor (1973), and at Mount Forster from Reesor (1973) and Norford (1981).*

The basal dolomite unit of the Starbird Formation onlaps Horsethief Creek Group and Hamill Group strata from the west; the thickness varies from about 120 m in western exposures to zero in eastern exposures (Fig. 45.3).

Strata overlying the lowermost dolomite unit include: dolomitic siltstone, dolomite, quartzite, and minor argillite. The aggregate thickness of these strata is about 150 m.

Syndepositional Tectonics

Rapid thickness variations in Upper Proterozoic, Eocambrian, and Upper Devonian strata at Delphine Creek are a record of the tectonic processes active during their deposition. Detailed studies demonstrate that strata of the Horsethief Creek Group, Hamill Group, and Starbird Formation were deposited in north-northwest trending, asymmetric sub-basins about 2 or 3 km in width. Each sequence of strata was deposited as an eastwards thickening wedge, which abruptly thins at the east flank of each sub-basin (Fig. 45.3). This suggests the sub-basins were formed by drape folding over west-side-down, listrict, normal faults. Movement on the faults caused eastward rotation of the fault blocks, thereby creating the asymmetry of the sub-basins.

Angular unconformities of local extent are present at Delphine Creek between the Horsethief Creek Group and the Hamill Group, within the Hamill Group, and between the Hamill Group and the Starbird Formation (Fig. 45.3). Truncation relationships at each unconformity record eastward tilt prior to deposition of the overlying sequence.

An apparent contradiction exists between the dramatic eastward thickening of the Eocambrian Hamill Group strata at Delphine Creek (Fig. 45.3) and the lack of Eocambrian to the east at Law Ridge (Fig. 45.3). The eastward thickening of the Hamill Group, the eastward rotation of the depositional basin, as recorded by unconformities below, within, and above the Hamill Group, and west-side-down normal faults inferred to have been active during the deposition of the Hamill Group, suggest deposition of the Hamill Group in a half graben, bounded to the east by one or more normal faults (Fig. 45.4). Two major normal faults with west-side-down motion are present between the outlier of Paleozoic strata at Law Ridge and the exposures of Hamill Group strata at Delphine Creek (Fig. 45.2); it is possible that one or both of these faults were active during the Eocambrian.

Conclusions

Dramatic variations in the thickness of Upper Proterozoic to Upper Devonian strata across the Purcell Arch are the result of the eastward tilting of the depositional basin by contemporaneous, listric, normal faulting, with westward thinning of strata due to depositional attenuation and inter-sequence erosional truncation. Local reversals in the westward pattern of thinning at Delphine Creek are probably the result of west-side-down movement on north-northwesterly trending normal faults.

Horsethief Creek Group strata are anomalously thin at Delphine Creek in comparison to exposures to the northeast and southwest. Comparison of depositional facies indicates that the abbreviated section at Delphine Creek is primarily a result of depositional attenuation. The thinning of Horsethief Creek Group strata is analogous to the thinning of Paleozoic strata over the Purcell Arch (Fig. 45.4) and thus demonstrates that the Purcell Arch was already active during Late Proterozoic time.

The Starbird Formation overlies Upper Proterozoic and Eocambrian strata at Delphine Creek; the Upper Cambrian to Middle Devonian strata present at Mount Forster and Law Ridge are absent. This implies that Upper Devonian strata overlapped Upper Cambrian through Middle Devonian strata between Law Ridge and Delphine Creek and demonstrates that the Purcell Arch continued to be active until at least Late Devonian time (Fig. 45.4).

The condensed sections of Upper Proterozoic and Paleozoic strata deposited on the Purcell Arch are located in the footwall of the Mount Forster thrust fault (Fig. 45.2); Upper Proterozoic and Paleozoic strata in the hanging wall are significantly thicker. The dramatic increase in the thickness of strata between Delphine Creek and Jumbo Pass implies that the western boundary of the Purcell Arch was a major normal fault, which had the west side downthrown during the Late Proterozoic and Paleozoic (Fig 45.4). The juxtaposition of the thick hanging wall succession with the condensed section at Delphine Creek suggests that the older normal fault was reactivated during the Mesozoic to form the Mount Forster thrust fault.

Acknowledgments

This manuscript has benefited from the comments and suggestions of D.G. Cook, M.E. McMechan, B.S. Norford, P.S. Simony, and D.H. Root. Many thanks to B.S. Norford for his fossil identifications.

References

Aitken, J.D.
1971: Control of Lower Paleozoic sedimentary facies by the Kicking Horse Rim, southern Rocky Mountains, Canada; Bulletin of Canadian Petroleum Geology, v. 19, p. 557-569.

Benvenuto, G.L. and Price, R.A.
1979: Evolution of the Hosmer thrust sheet, southeastern British Columbia; Bulletin of Canadian Petroleum Geology, v. 27, p. 360-394.

Cook, D.G.
1975: Structural style influenced by lithofacies, Rocky Mountain Main Ranges, Alberta-British Columbia; Geological Survey of Canada, Bulletin 233, 73 p.

Douglas, R.J.W., Gabrielse, H., Wheeler, J.O., Stott, D.F., and Belyea, H.R.
1970: Geology of western Canada; in Geology and Economic Minerals of Canada, R.J.W. Douglas, ed.; Geological Survey of Canada, Economic Geology report no. 1, p. 365-488.

Norford, B.S.
1981: Devonian stratigraphy of the margins of the Rocky Mountain Trench, Columbia River, southeastern British Columbia; Bulletin of Canadian Petroleum Geology, v. 29, no. 4, p. 540-560.

Price, R.A.
1981: The Cordilleran foreland thrust and fold belt in the southern Canadian Rocky Mountains; in Thrust and Nappe Tectonics, K.R. McClay and N.J. Price, eds., Geological Society of London, Special Publication no. 9, p. 427-448.

Reesor, J.E.
1957: Lardeau (east half) map area, British Columbia; Geological Survey of Canada, Map 12-1957.

1973: Geology of the Lardeau map area, east half, British Columbia; Geological Survey of Canada, Memoir 369, 129 p.

Walker, J.F.
1926: Geology and mineral deposits of the Windermere map area, British Columbia; Geological Survey of Canada, Memoir 148, 69 p.

46. THE HEIBERG GROUP, WESTERN SVERDRUP BASIN, ARCTIC ISLANDS

Project 750083

Ashton F. Embry
Institute of Sedimentary and Petroleum Geology, Calgary

Embry, A.F., The Heiberg Group, western Sverdrup Basin, Arctic Islands; in Current Research, Part B, Geological Survey of Canada, Paper 83-1B, p. 381-389, 1983.

Abstract

The Heiberg, a prominent formation in the eastern and central Sverdrup Basin, is given group status in the western Sverdrup. The Heiberg Group comprises five formations which, in ascending order are: Skybattle, Grosvenor Island, Maclean Strait, Lougheed Island and King Christian. These new formations are formally defined herein. The Skybattle, Maclean Strait and King Christian formations are sandstone-dominant and consist of delta front, distributary mouth bar and delta plain deposits. The sandstone-dominant units are separated from each other by shale-siltstone formations (Grosvenor Island and Lougheed Island). These argillaceous formations represent prodelta and offshore shelf deposits.

Three formal members are recognized in the King Christian Formation. The Drake Point (lowest) and Whitefish members are sandstone-dominant and are separated by the Stupart Member, which consists of shale and siltstone.

Résumé

La formation de Heiberg, formation importante dans les parties est et centrale du bassin de Sverdrup, devient un groupe dans la partie ouest du bassin. Le groupe de Heiberg comprend cinq formations soit, en ordre ascendant: Skybattle, Grosvenor Island, Maclean Strait, Lougheed Island et King Christian. Ces nouvelles formations sont décrites officiellement dans le présent rapport. Les formations de Skybattle, de Maclean Strait et de King Christian sont dominées par des grès et composées de sédiments provenant d'un front de delta, d'une flèche à l'embouchure d'un effluent et d'une plaine deltaique. Des formations de schiste-argileux et de pélite (Grosvenor Island et Lougheed Island) séparent ces unités les unes des autres. Ces formations argilleuses représentent des sédiments déposés en avant d'un delta et sur un plateau au large des côtes.

On a divisé la formation de King Christian en trois niveaux officiels. Les niveaux de Drake Point (niveau inférieur) et de Whitefish sont dominés par des grès et séparés par le niveau de Stupart, lui-même composé de schiste argileux et de pélite.

Introduction

The Heiberg Formation/Group of the Sverdrup Basin is an Upper Triassic-Lower Jurassic, sandstone-dominant interval, which occurs between two shale-siltstone formations, the Barrow below and the Jameson Bay above. The Heiberg was originally defined as a formation by Souther (1963) from exposures at Buchanan Lake on eastern Axel Heiberg Island. I have recently described the Heiberg Formation in the eastern and central Sverdrup Basin and recognized three members within it (Embry, 1982, 1983). In the western Sverdrup the Heiberg interval is still clearly recognizable, but is divisible into five units, three sandstone-dominant and two shale-siltstone dominant. Consequently, the Heiberg in this area is raised to group status and five component formations, Skybattle, Grosvenor Island, Maclean Strait, Lougheed Island and King Christian are formally named herein .

The type sections for these new formations are in the Sun Skybattle Bay C-15 well, which is located on southwestern Lougheed Island (77°14'12"N, 105°05'57"W) (Fig. 46.1). The Skybattle Bay C-15 well was spudded on April 1, 1971 and was abandoned on November 23, 1971 at a total depth of 3658 m (12 000 ft). The elevation of the K.B. is 33.5 m. Chip samples taken at 3 m intervals from these strata can be examined at the Institute of Sedimentary and Petroleum Geology in Calgary, Alberta.

Figure 46.1 illustrates the distribution of the Heiberg Group in the western Sverdrup Basin and the available control points. Surface exposures occur on northwestern Ellef Ringnes Island, Borden Island, Prince Patrick Island and Melville Island. Over most of the area the Heiberg Group is in the subsurface and it has been penetrated by 66 wells.

Previous Work

The first study of strata now included in the Heiberg Group was done by Tozer and Thorsteinsson (1964) on basin margin outcrops on Borden and Melville Islands. On Borden Island they designated 60 m of poorly exposed, ferruginous sand and sandstone as the Borden Island Formation. At the type section the strata rest unconformably on sandstone of the Upper Triassic Schei Point Formation and are overlain conformably by the Wilkie Point Formation. The Borden Island Formation was dated as Sinemurian (Early Jurassic) on the basis of an ammonite collected from the scree. Tozer and Thorsteinsson (1964) also assigned 12 m of red and green sand and sandstone, outcropping on northwestern Melville Island, to the Borden Island Formation.

The type section of the Borden Island Formation was again examined and described by Rahmani and Tan (1978). They recognized two subdivisions in the formation, a lower unit (50 m) of shale and siltstone with interbeds of argillaceous, very fine grained sandstone in the upper portion and a poorly exposed, upper unit (23 m), which was assumed to consist mainly of sandstone.

In 1967, Stott (1969) mapped Ellef Ringnes Island and referred 60 m of fine grained, quartzose sandstone, present on the northwestern portion of the island, to the Borden Island Formation. Stott (1969) collected Sinemurian ammonites from the lower portion of the formation. In this area the base of the Borden Island is not exposed and it is conformably overlain by shales of the Savik Formation.

Subsurface studies of the Heiberg Group began with Reinson (1975) who described the Borden Island Formation in two wells on Sabine Peninsula, Melville Island. He divided

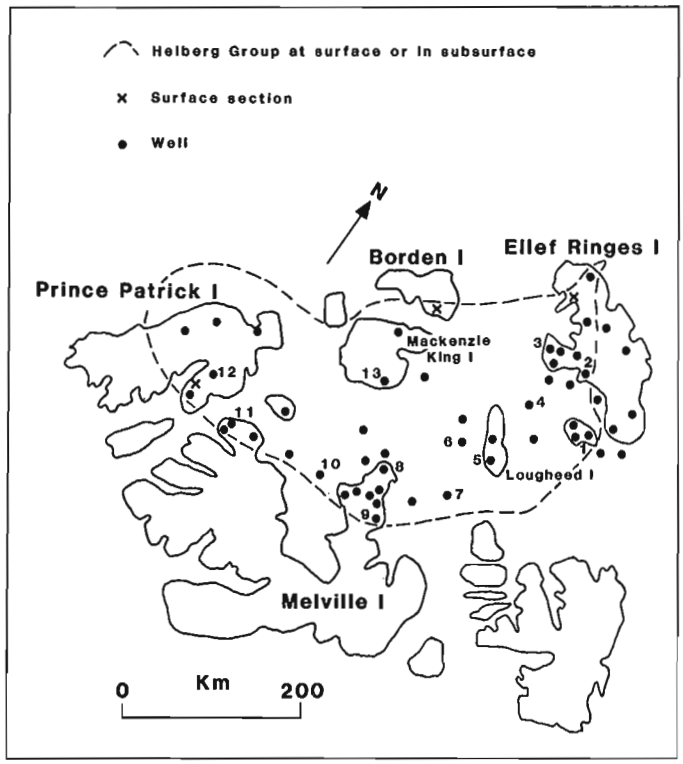

Figure 46.1. *Distribution of Heiberg Group in western Sverdrup Basin and available control points. Key to wells listed in appendix: 1. King Christian N-06; 2. Kristoffer Bay B-06; 3. Mocklin Point D-23; 4. Skate L-80; 5. Skybattle Bay C-15; 6. Whitefish 2H-63; 7. Desbarats B-73; 8. North Sabine H-49; 9. Drake Point F-16; 10. N.W. Hecla M-25; 11. Sandy Point L-46; 12. Jameson Bay C-31; 13. Cape Norem A-80.*

the formation into three units, a lower oolitic ironstone (10 m), a cyclic sandstone-siltstone (30 m), and an upper unit of interbedded shale, siltstone and glauconitic sandstone. Reinson (1975) interpreted unconformities between the units. Douglas (1977) and Douglas and Oliver (1979) described the Borden Island Formation in the Sabine Peninsula area and recognized Reinson's three informal units throughout that area.

Meneley (1977), in a review of the hydrocarbon exploration prospects in the Arctic Islands, presented a stratigraphic cross-section of the Drake Point gas field on Sabine Peninsula where the Borden Island Formation contains the main reservoir strata. He restricted the name Borden Island Formation to the lower two units of Reinson (1975) and referred to the upper glauconitic unit as the "lower Wilkie Point". Significantly, he demonstrated that a regional unconformity occurs beneath the glauconitic unit.

Henao-Londono (1977) illustrated subsurface stratigraphic correlations in the Lougheed, King Christian, and Ellef Ringnes area. In the interval now designated as Heiberg Group, he proposed four informal stratigraphic units: Heiberg (sensu stricto), Upper Triassic sandstone and shale; Borden Island, Sinemurian, sandstone-dominant unit; Lower Savik, Pliensbachian shale and siltstone; King Christian Sand, Pliensbachian to Toarcian sandstone. Henao-Londono (1977) interpreted regional unconformities beneath the Borden Island and Lower Savik units.

Balkwill and Roy (1977), and Balkwill et al. (1982) also described the subsurface stratigraphy of the King Christian and Lougheed Island areas. In both papers strata of the Heiberg Group are divided into two units: Heiberg Formation (lower member); Heiberg Formation (upper member) – Borden Island Formation (undivided). This nomenclatural scheme follows that used by Balkwill (in press) in the central Sverdrup Basin.

Present Work

The previous studies of the Heiberg Group strata were mainly of a local nature and this fact, in combination with the presence of facies changes and regional unconformities, led to a complicated and confusing stratigraphic nomenclature for the strata. For this study a regional approach has been taken and all available surface and subsurface sections have been correlated. Both the Barrow and Jameson Bay formations can be recognized over almost the entire western Sverdrup, so that the Heiberg interval can be objectively delineated and mapped in the area. As previously mentioned, the Heiberg is given group status in the area because five mappable formations can be recognized within the interval and because, in some areas, unconformities separate some of the formations.

The stratigraphic relationships of the five formations of the Heiberg Group are portrayed on Figure 46.2. The reader is referred to Embry (1982) for a more detailed stratigraphic and sedimentologic study, which includes stratigraphic cross-sections and maps for these units.

Figure 46.3 illustrates the correspondence between these new stratigraphic units and the nomenclature used by previous workers. Note that the term Borden Island, as used by previous workers, had a variety of stratigraphic meanings. Ironically, the term was applied mainly to sandstone-dominant units when in fact we now know that the type section consists predominantly of shale and siltstone. To avoid confusion the term Borden Island has been abandoned.

The tops for Heiberg Group units from 13 selected wells throughout the western Sverdrup Basin (Fig. 46.1) are listed in the appendix.

Skybattle Formation

Definition

The Skybattle Formation consists of interbedded, very fine- to fine-grained sandstone, siltstone and shale with sandstone being the dominant component. The type section is in the Sun Skybattle Bay C-15 well, between 2105 m (6905 ft) and 2159 m (7082 ft), and is 54 m thick (Fig. 46.4). The formation is named after Skybattle Bay which is 7 km south of the C-15 well.

Synonyms

1. Heiberg (sensu stricto) of Henao-Londono (1977).
2. Lower portion of Heiberg Formation (lower member) of Balkwill et al. (1982).
3. Heiberg/Blaa Mountain transition zone (informal name commonly used in petroleum industry).

Boundaries

The Skybattle Formation conformably overlies the Barrow Formation and the contact is placed at the base of the first sandstone unit which exceeds 4 m in thickness, and above which sandstone is relatively common (Fig. 46.4). The upper contact with the Grosvenor Island Formation varies

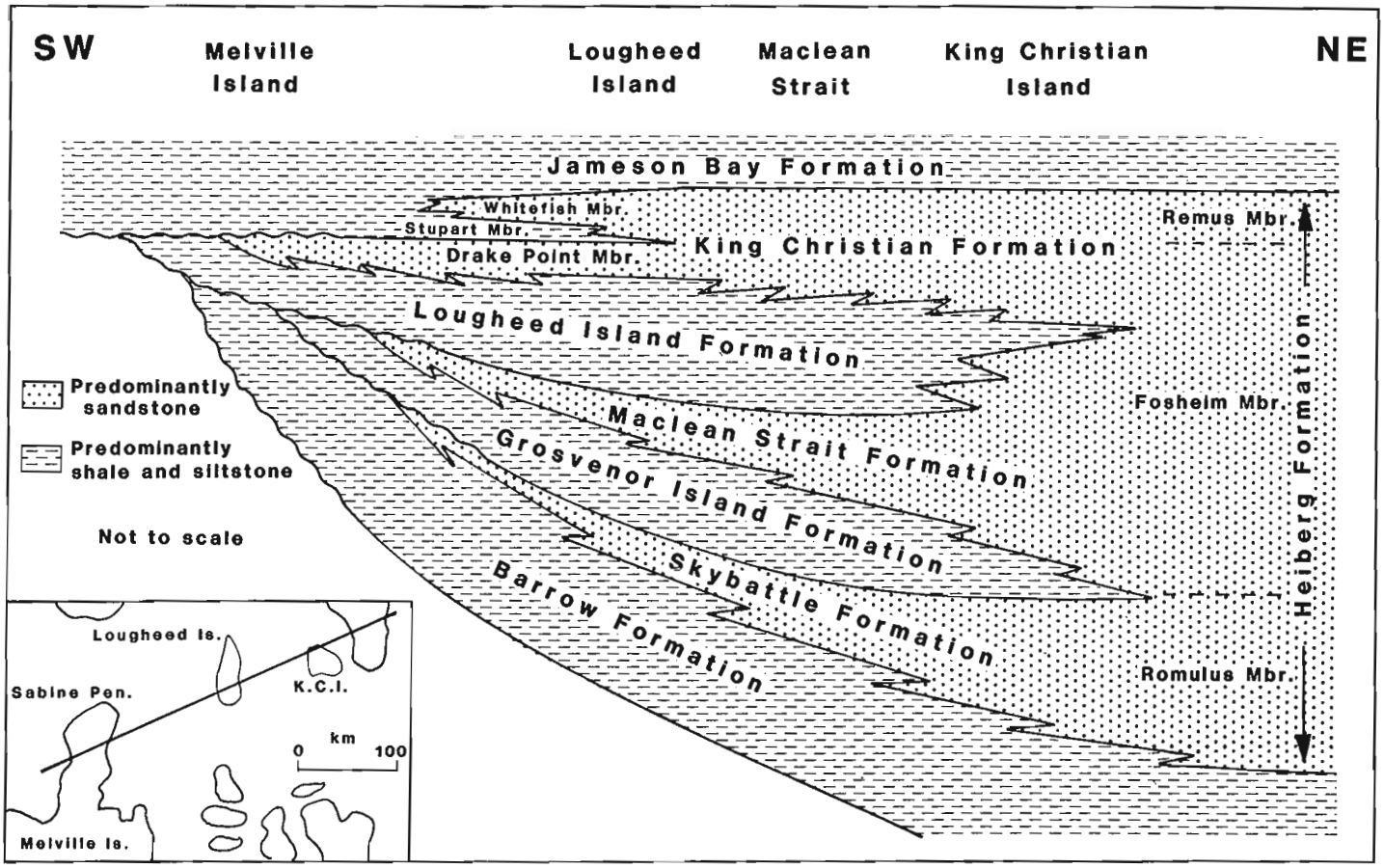

Figure 46.2. *Schematic stratigraphic cross-section, Heiberg Group, western Sverdrup Basin.*

from conformable to unconformable. The contact is placed at the top of the highest sandstone unit above which shale and siltstone become the predominant lithologies. A distinctive oolitic ironstone bed occurs directly above the contact in the Lougheed Island area.

Lithology

The formation consists of interbedded very fine- to fine-grained sandstone, siltstone and shale with the lithologies arranged in coarsening-upward cycles 10-35 m thick. Sandstone units are usually 5-15 m thick. The sandstone is quartzose with variable amounts of quartz, calcite and clay cements. Porosity ranges from 5 to 15 per cent.

Thickness and Distribution

The Skybattle Formation thins westward from King Christian Island, where it is up to 160 m thick, to a shale-out edge just west of Lougheed Island. East of King Christian Island the Skybattle merges with the Romulus Member of the Heiberg Formation (Fig. 46.2). A narrow band of Skybattle Formation may occur along the southern and northwestern margins of the basin (e.g. Jameson Bay C-31).

Age

The Skybattle Formation is dated as Norian (Late Triassic) on the basis of its intertonguing relationship with the Barrow Formation, which contains Norian pelecypods (Tozer, 1973) and palynomorphs (unpublished GSC paleontology reports).

Environment of Deposition

The lithologies, cyclicity and stratigraphic relationships of the Skybattle Formation indicate a delta front to shallow marine shelf origin for the formation (Embry, 1982).

Grosvenor Island Formation

Definition

The Grosvenor Island Formation consists mainly of shale and siltstone and is the lower of two shale-siltstone units which occur in the Heiberg Group. The type section is in the Sun Skybattle Bay C-15 well, between 2081 m (6828 ft) and 2105 m (6905 ft), and is 24 m thick (Fig. 46.4). The member is named after Grosvenor Island which lies 15 km south of Lougheed Island.

Synonyms

1. Oolitic ironstone unit, Borden Island Formation (Reinson, 1975).
2. Unit A, Borden Island Formation (Douglas, 1977; Douglas and Oliver, 1979).
3. Basal portion of Borden Island unit, in Panarctic Pat Bay A-72 well (Henao-Londono, 1977).
4. Uppermost Heiberg Formation (lower member) (Balkwill and Roy, 1977; Balkwill et al., 1982).

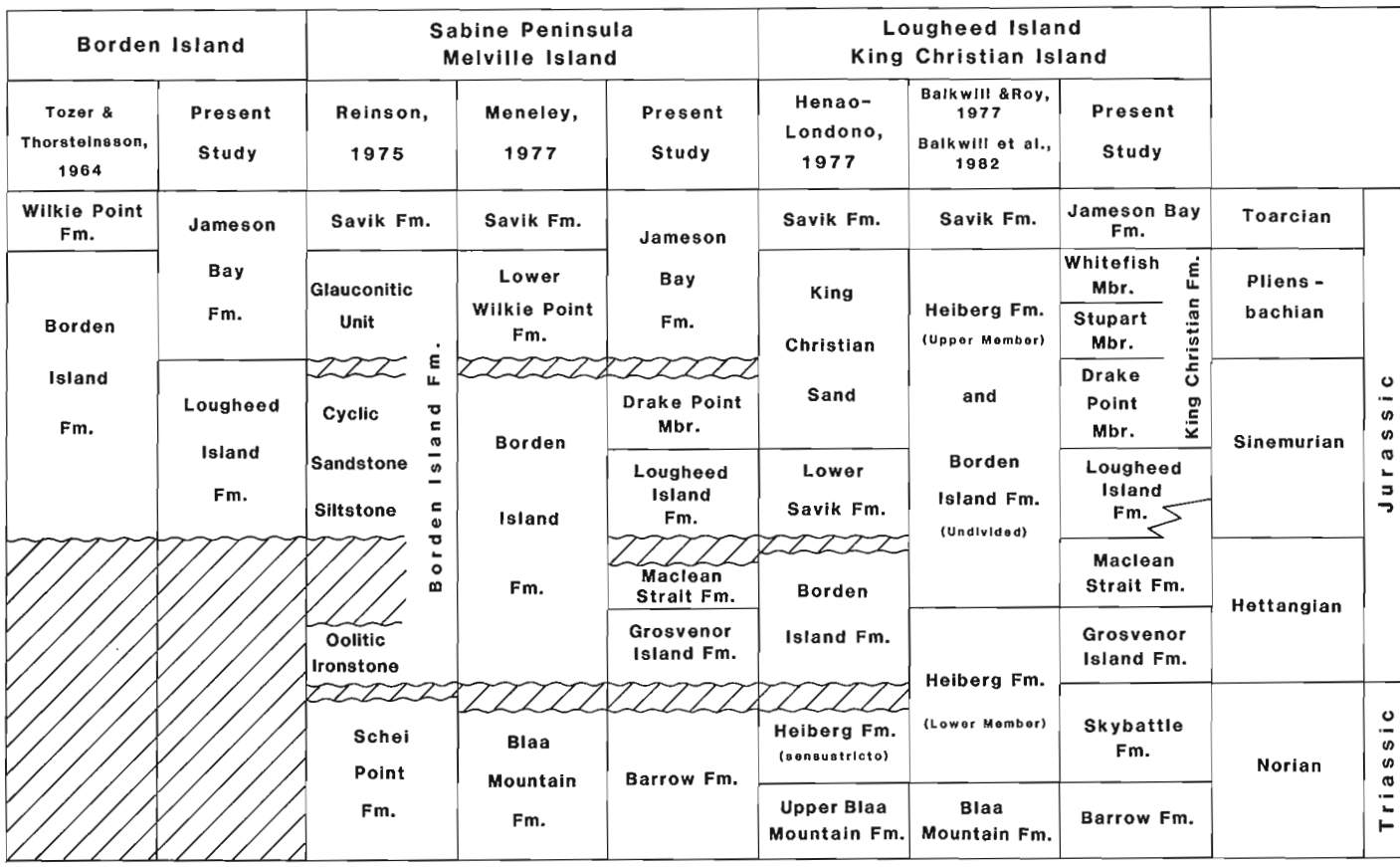

Figure 46.3. *Past and present stratigraphic nomenclature for Heiberg Group, western Sverdrup Basin.*

Boundaries

The Grosvenor Island Formation rests on the Skybattle Formation with the contact varying from conformable to unconformable (Fig. 46.2). The upper contact with the Maclean Strait Formation is conformable and is placed at the base of the first sandstone unit greater than 4 m in thickness and above which sandstone is the predominant lithology. On the basin margin the Grosvenor Island is bounded by unconformities (Fig. 46.2).

Lithology

The Grosvenor Island consists mainly of shale and siltstone with thin, very fine grained sandstone units near the top of the formation. Overall, the formation coarsens upward into the overlying sandstone-dominant Maclean Strait Formation. In the King Christian – Ellef Ringnes area the shales are medium grey and silty. Westward, red shales occur in the lower portion of the formation and on northwestern Melville Island such shales comprise almost all of the formation. In the Lougheed Island area and westward an oolitic ironstone unit occurs at the base of the formation and is up to 10 m thick on Sabine Peninsula.

Thickness and Distribution

The formation is present over most of the western Sverdrup Basin, being absent only on the extreme margins of the basin, where it is overstepped by the Lougheed Island Formation (Fig. 46.2). East of King Christian Island The Grosvenor Island Formation merges with the Romulus Member of the Heiberg Formation (Fig. 46.2). The greatest recorded thickness of the formation is 120 m (western Ellef Ringnes Island), but it is less than 50 m thick over much of its extent.

Age

The Grosvenor Island Formation is dated as Hettangian by palynomorphs (unpublished GSC paleontology report).

Environment of Deposition

The lithologies, fossil contact (dinoflagellates), and stratigraphic relationships suggest an offshore shelf environment of deposition for the formation. The basal oolitic ironstone unit is interpreted to be a shallow, shelf deposit, which formed when clastic supply to the western Sverdrup was drastically reduced due to an earliest Jurassic transgression (Embry, 1982).

Maclean Strait Formation

Definition

The Maclean Strait Formation consists of interbedded, very fine- to coarse-grained sandstone, siltstone and shale with sandstone the dominant lithology. The type section is in the Sun Skybattle Bay C-15 well, between 2043 m (6702 ft) and 2081 m (6828 ft), and is 38 m thick (Fig. 46.4). The name is taken from Maclean Strait, which separates Lougheed Island from King Christian and Ellef Ringnes islands.

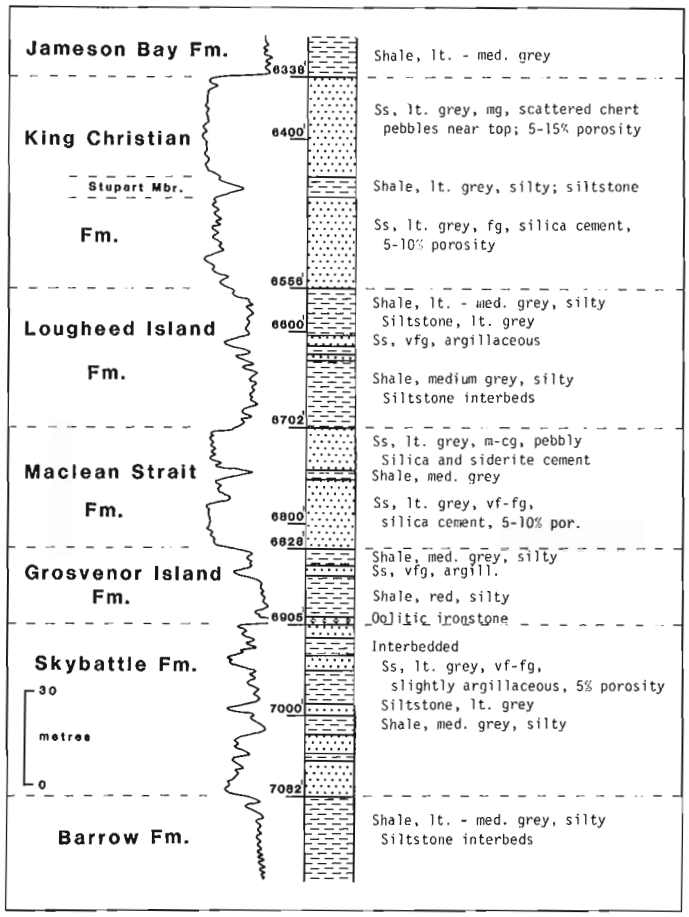

Figure 46.4. *Lithology (from samples) and gamma ray curve for type sections of Skybattle, Grosvenor Island, Maclean Strait, Lougheed Island and King Christian formations, and Stupart Member; Skybattle Bay C-15 well.*

Synonyms

1. Lowermost portion of Unit B, Borden Island Formation, North Sabine H-49 well (Douglas, 1977; Douglas and Oliver, 1979).
2. Various portions of Borden Island unit of Henao-Londono (1977).
3. Lower portion of the Heiberg Formation (upper member) – Borden Island Formation (undivided) (Balkwill and Roy, 1977; Balkwill et al., 1982).

Boundaries

The Maclean Strait Formation gradationally overlies the Grosvenor Island Formation. Over most of its extent the Maclean Strait is conformably overlain by the Lougheed Island Formation, with the contact placed at the top of the uppermost sandstone unit above which shale and siltstone predominate. On the basin margins the contact becomes unconformable and the Lougheed Island oversteps the Maclean Strait (Fig. 46.2).

Lithology

In the King Christian – Ellef Ringnes area the Maclean Strait Formation consists of three lithologic intervals: a lower interval of interbedded, very fine- to fine-grained sandstone, siltstone and shale with the lithologies arranged in coarsening-upward cycles; a middle interval of massive, fine- to coarse-grained sandstone with rare interbeds of carbonaceous siltstone and shale; and an upper interval of interbedded, fine- to coarse-grained sandstone, siltstone and shale also arranged in coarsening-upward cycles. To the west, in the Lougheed Island area, the entire formation consists of coarsening-upward cycles. The sandstones are quartzose, with varying amounts of quartz, calcite and clay cement. Porosity ranges from 5 to 15 per cent.

Thickness and Distribution

The Maclean Strait Formation thins westward from a maximum of 370 m on western Ellef Ringnes Island to a shale-out edge west of Lougheed Island. Eastwards it merges with the Fosheim Member of the Heiberg Formation (Fig. 46.2). A narrow band of Maclean Strait Formation may occur along the southwestern and northwestern basin margins.

Age

The age of the Maclean Strait Formation ranges from Hettangian to Sinemurian. In the King Christian – Ellef Ringnes area the lower two intervals of the formation are dated as Hettangian on the basis of their stratigraphic equivalence with the Grosvenor Island Formation. The upper interval is dated as Sinemurian on the basis of its intertonguing relationship with the Lougheed Island Formation, which contains Sinemurian palynomorphs and ammonites. In the Lougheed Island area the formation is considered to be almost entirely Hettangian on the basis of stratigraphic relationships.

Environment of Deposition

The Maclean Strait Formation is of deltaic origin, with the coarsening-upward cycles originating as delta front sediments and the massive, continuous sandstone intervals as distributary channel and distributary mouth bar deposits (Embry, 1982).

Lougheed Island Formation

Definition

The Lougheed Island Formation mainly consists of shale and siltstone, with interbeds of very fine grained sandstone in the upper portion. The type section is in the Sun Skybattle Bay C-15 well, between 1998 m (6556 ft) and 2043 m (6702 ft), and is 45 m thick (Fig. 46.4). The name is taken from Lougheed Island on which the C-15 well was drilled.

Synonyms

1. Lower portion of type Borden Island Formation (Rahmani and Tan, 1978).
2. Lower portion of the cyclic sandstone-siltstone unit, Borden Island Formation (Reinson, 1975).
3. Lower portion of unit B, Borden Island Formation (Douglas, 1977; Douglas and Oliver, 1979).
4. Lower Savik unit (Henao-Londono, 1977).
5. Middle portion of the Heiberg Formation (upper member) – Borden Island Formation (undivided) Balkwill et al., 1982).

Boundaries

The Lougheed Island Formation both conformably and unconformably overlies the Maclean Strait Formation (Fig. 46.2). On the basin margins the Lougheed Island

Formation unconformably overlies various stratigraphic units of Triassic to Early Jurassic age and a basal conglomerate or oolitic ironstone unit commonly occurs directly above the unconformity. The Lougheed Island Formation is conformably overlain by the King Christian Formation and the contact is drawn at the base of the first sandstone unit greater than 4 m in thickness, above which sandstone is the dominant lithology.

Thickness and Distribution

The Lougheed Island Formation occurs over the entire western Sverdrup Basin, except for the extreme southwest margin where it is overstepped by the Jameson Bay Formation (Fig. 46.2). The Lougheed Island is very thin (5 m) and silty along its eastern margin, thickens rapidly westward, mainly at the expense of the underlying Maclean Strait Formation, to a maximum recorded thickness of 140 m on western Ellef Ringnes Island, and then gradually thins westward toward the basin margins.

Age

The age of the Lougheed Island Formation is Sinemurian, on the basis of ammonites (Rahmani and Tan, 1978; unpublished paleontology report) and palynomorphs (Tan, 1979). This age assignment is corroborated by the occurrence of Sinemurian ammonites in basal King Christian Formation strata (Stott, 1969), which are stratigraphically equivalent to Lougheed Island strata farther west.

Environment of Deposition

The Lougheed Island Formation is interpreted as representing prodelta and offshore shelf deposits, on the basis of lithology, fossil content and stratigraphic relationships (Embry, 1982).

King Christian Formation

Definition

The King Christian Formation consists of interbedded very fine- to coarse-grained sandstone, siltstone, shale and minor coal. Sandstone is the dominant lithology. The type section is in Sun Skybattle Bay C-15 well, between 1932 m (6338 ft) and 1998 m (6556 ft), and is 66 m thick (Fig. 46.4). The formation is named after King Christian Island, which lies 100 km northwest of the C-15 well.

Synonyms

1. Borden Island Formation (Stott, 1969).
2. Upper portion of the cyclic sandstone-siltstone unit, Borden Island Formation (Reinson, 1975).
3. Upper portion of unit B, Borden Island Formation (Douglas, 1977; Douglas and Oliver, 1979).
4. King Christian sand (Henao-Londono, 1977).
5. Upper portion of the Heiberg Formation (upper member) – Borden Island Formation (undivided) (Balkwill and Roy, 1977; Balkwill et al., 1982).

Boundaries

The King Christian Formation conformably overlies the Lougheed Island Formation. The upper contact with the Jameson Bay Formation is conformable over much of the area, but becomes unconformable on the southwestern basin margin where the Jameson Bay oversteps the King Christian. The contact is placed at the top of the uppermost sandstone unit, above which siltstone and shale become the predominant lithologies.

Lithology

East of Lougheed Island the King Christian Formation consists of a lower interval of interbedded, very fine- to fine-grained sandstone, siltstone and shale, arranged in coarsening-upward cycles; a middle interval of fine- to coarse-grained sandstone with thin intervals of carbonaceous siltstone, shale and coal; and an upper interval of fine- to coarse-grained sandstone which is commonly pebbly and glauconitic. The sandstones are quartzose with chert the dominant pebble type. Quartz, calcite, and clay cements occur throughout, and sideritic cement is common in the uppermost portion of the formation. Porosity ranges from 5 to 25 per cent.

On Lougheed Island and westward the King Christian has been subdivided into three formal members, Drake Point, Stupart and Whitefish, which are formally named and described herein.

Thickness and Distribution

The King Christian Formation is thickest (180 m) on western Ellef Ringnes Island. Westwards the formation gradually thins by facies change into shale and siltstone of the Lougheed Island Formation and finally disappears at a poorly-defined shale-out edge between Lougheed and Mackenzie King islands. A band of the Drake Point Member extends along the southwestern margin of the basin.

Age

The King Christian Formation is Sinemurian and Pliensbachian in age. Both Early and Late Sinemurian ammonites have been collected from the formation (Stott, 1969; Frebold, 1975). The upper portion of the formation (Whitefish Member) is laterally equivalent to the basal strata of the Jameson Bay Formation, which have yielded Late Pliensbachian ammonites (Frebold, 1975).

Environment of Deposition

The King Christian Formation is interpreted to be deltaic in origin with the lower portion representing delta front deposits, the middle portion distributary mouth bar and delta plain deposits, and the upper portion delta-destructional deposits (Embry, 1982).

Drake Point Member

Definition

The Drake Point Member of the King Christian Formation mainly consists of very fine- to medium-grained sandstone with minor interbeds of siltstone and shale. The type section is in the Panarctic Drake Point F-16 well, which is located on Sabine Peninsula (76°25'15"N, 108°35'39"W) (Fig. 46.1). The Drake Point F-16 well was spudded on May 10, 1972, and was completed on June 16, 1972 at a total depth of 1478 m. The elevation of the K.B. is 33 m. The member occurs between 1093 m (3586 ft) and 1114 m (3654 ft), and is 21 m thick (Fig. 46.5). It is named after Drake Point, which is on the east coast of Sabine Peninsula, 4 km north of the F-16 well.

Synonyms

1. Upper portion of the cyclic sandstone-siltstone unit, Borden Island Formation (Reinson, 1975).
2. Upper portion of unit b, Borden Island Formation (Douglas, 1977; Douglas and Oliver, 1979).
3. Upper portion of Borden Island Formation, Sabine Peninsula (Meneley, 1977; Henao-Londono, 1977).
4. Lower portion of the King Christian sand, Pat Bay A-72 well (Henao-Londono, 1977).

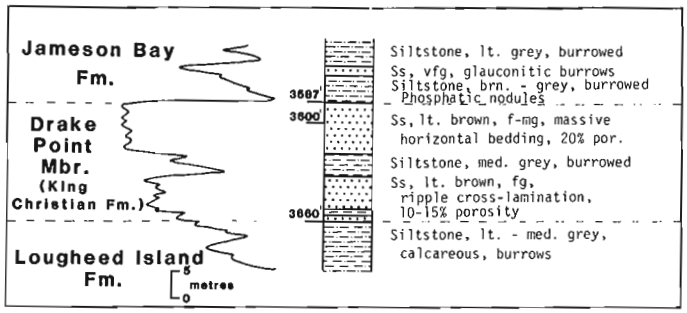

Figure 46.5. Lithology (from core) and gamma ray curve for type section of Drake Point Member of the King Christian Formation; Drake Point F-16 well.

Boundaries

The Drake Point Member conformably overlies the Lougheed Island Formation. The member is overlain by either the Stupart Member of the King Christian Formation or the Jameson Bay Formation, with the contact placed at the top of the uppermost sandstone, above which shale and siltstone become predominant. This contact is conformable except on the southwestern basin margin where the Jameson Bay Formation disconformably overlies the Drake Point Member.

Lithology

In the Lougheed Island - Sabine Peninsula area, the Drake Point Member consists of coarsening-upward cycles of very fine- to medium-grained sandstone, siltstone and shale. In the lower portion of the cycles, sandstone units are commonly argillaceous and highly burrowed, but are clay-free and horizontally bedded to massive in the upper portion. Sandstone dominates the member and the shale-siltstone units are thin. The sandstones are quartzose and porosity ranges from 10 to 25 per cent. Westwards, in the Prince Patrick area, the Drake Point Member mainly consists of very fine- to fine-grained, glauconitic, burrowed sandstone with porosity ranging from 5 to 12 per cent.

Distribution and Thickness

In the Lougheed Island area the member is up to 29 m thick. Eastwards it merges with the lower portion of the undivided King Christian Formation. A shale-out edge for the member occurs a few kilometers west of Lougheed Island. The member also occurs along the southwestern margin of the Sverdrup Basin, between Sabine Peninsula and Prince Patrick Island, where it is up to 40 m thick.

Age

Ammonites from outcrops of the member on Prince Patrick Island indicate a Sinemurian age (Frebold, 1975).

Environment of Deposition

The Drake Point Member is of delta front origin in the Lougheed Island area and of beach to nearshore shelf origin along the southwestern basin margin (Embry, 1982).

Stupart Member

Definition

The Stupart Member of the King Christian Formation mainly consists of grey siltstone and shale. The type section is in the Sun Skybattle Bay C-15 well, between 1963 (6440 ft) and 1969 m (6460 ft), and is 6 m thick (Fig. 46.4). The member is named after Stupart Island which lies 1 km south of Lougheed Island.

Synonyms

This stratigraphic unit was not recognized as a significant unit by previous workers and was included within various sandstone-dominant units such as the King Christian sand (Henao-Londono, 1977) and the Heiberg Formation (upper member) – Borden Island Formation (undivided) (Balkwill et al., 1982).

Boundaries

The Stupart Member conformably overlies the Drake Point Member as described above. West of Lougheed Island, where the Drake Point is no longer recognizable, the Stupart Member conformably overlies the Lougheed Island Formation. The contact is placed at the base of a clay-rich shale unit, which rests on argillaceous sandstone or siltstone of the uppermost Lougheed Island Formation. The Stupart Member is conformably overlain by the Whitefish Member of the King Christian Formation. The contact is placed at the base of the first sandstone unit greater than 4 m in thickness, above which sandstone is the dominant lithology.

Lithology

The member consists of interbedded, medium grey, silty shale and light to medium grey siltstone.

Thickness and Distribution

The member has been recognized in the Lougheed Island area and east of Sabine Peninsula. The maximum recorded thickness is 10 m. To the west it loses its identity when the overlying Whitefish sandstone shales out and it merges with the basal Jameson Bay Formation. It thins eastward, becomes more arenaceous, and grades laterally into the lower portion of the undivided King Christian Formation.

Age

The Stupart Member is assigned a Pliensbachian age on the basis of its stratigraphic equivalence with the basal Jameson Bay Formation, which contains Pliensbachian ammonites (Frebold, 1975) and palynomorphs (unpublished GSC paleontology reports).

Environment of Deposition

The lithologies and stratigraphic relationships suggest an offshore, shelf environment of deposition for the member (Embry, 1982).

Whitefish Member

Definition

The Whitefish Member is the uppermost member of the King Christian Formation and mainly consists of very fine- to medium-grained sandstone. The type section is in the Whitefish 2H-63 well, which is in the offshore area west of Lougheed Island (77°12'24"N, 106°53'26"W) (Fig. 46.1). The Whitefish 2H-63 well was spudded on December 3, 1979, and was completed on May 15, 1980 at a total depth of 3003 m. The K.B. of the well is 9.8 m. The member occurs between 2076 m and 2107 m and is 31 m thick (Fig. 46.6). The name is taken from the well in which the type section occurs.

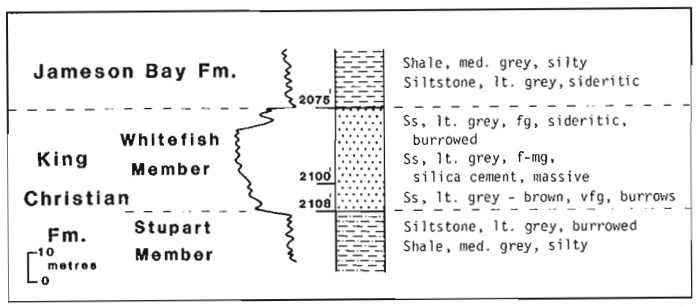

Figure 46.6. *Lithology (from core) and gamma ray curve for type section of Whitefish Member of the King Christian Formation; Whitefish 2H-63 well.*

Synonyms

1. Upper portion of the King Christian sand in Pat Bay A-72 well (Henao-Londono, 1977).
2. Upper portion of Heiberg Formation (upper member) – Borden Island Formation (undivided) (Balkwill et al., 1982).

Boundaries

The Whitefish Member conformably overlies the Stupart Member. The upper contact with the Jameson Bay Formation is also conformable and is placed at the top of the uppermost sandstone unit, above which shale and siltstone are predominant.

Lithology

The lower portion of the Whitefish Member consists of very fine grained, bioturbated sandstone, which contains shale-siltstone partings. The main upper portion is fine- to medium-grained sandstone which is usually massive in appearance. The uppermost sandstones are commonly glauconitic, burrowed and slightly argillaceous. Sandstones are quartzose with silica and clay cements. Porosity ranges from 7 to 20 per cent.

Thickness and Distribution

The Whitefish Member is recognized on Lougheed Island and offshore to the west and southwest. Recorded thicknesses range between 20 m and 45 m. The member shales-out between Lougheed Island and Mackenzie King Island to the west and between Lougheed Island and Sabine Peninsula to the southwest.

Age

The Whitefish Member is dated as Pliensbachian on the basis of its lateral equivalence with the basal Jameson Bay Formation (Fig. 46.2), which contains Pliensbachian ammonites (Frebold, 1979).

Environment of Deposition

The Whitefish Member is interpreted to be of deltaic origin with the lower strata consisting of delta front deposits, the massive upper portion being of distributary mouth bar origin, and the uppermost glauconitic sandstones representing delta destructional deposits.

References

Balkwill, H.R.
– Geology of Amund Ringnes, Cornwall and Haig-Thomas islands, District of Franklin; Geological Survey of Canada, Memoir 390. (in press)

Balkwill, H.R. and Roy, K.J.
1977: Geology, King Christian Island, District of Franklin; Geological Survey of Canada, Memoir 386.

Balkwill, H.R., Hopkins, W.S., Jr., and Wall, J.H.
1982: Geology, Lougheed Island, District of Franklin; Geological Survey of Canada, Memoir 388.

Douglas, T.R.
1977: Environments of deposition of the Borden Island Gas Zone in the subsurface of the Sabine Peninsula area, Melville Island, Arctic Archipelago; unpublished MSc. thesis, Department of Geology, University of Calgary.

Douglas, T.R. and Oliver, T.A.
1979: Environments of deposition of the Borden Island Gas Zone in the subsurface of the Sabine Peninsula area, Melville Island, Arctic Archipelago; Bulletin of Canadian Petroleum Geology, v. 27, p. 273-313.

Embry, A.F.
1982: The Upper Triassic-Lower Jurassic Heiberg Deltaic Complex of the Sverdrup Basin; in Arctic Geology and Geophysics, eds. A.F. Embry and H.R. Balkwill; Canadian Society of Petroleum Geologists, Memoir 8, p. 189-217.

1983: Stratigraphic subdivision of the Heiberg Formation, eastern and central Sverdrup Basin; in Current Research, Part B; Geological Survey of Canada, Paper 83-1B, report 24.

Frebold, H.
1975: The Jurassic faunas of the Canadian Arctic. Lower Jurassic ammonites, biostratigraphy and correlations; Geological Survey of Canada, Bulletin 243.

Henao-Londono, D.
1977: Correlation of producing formations in the Sverdrup Basin; Bulletin of Canadian Petroleum Geology; v. 25, p. 969-980.

Meneley, R.
1977: Exploration Prospects in the Canadian Arctic Islands; Panarctic Oils Limited, Calgary, 16 p.

Rahmani R.A. and Tan, J.T.
1978: The type section of the Lower Jurassic Borden Island Formation, Borden Island, Arctic Archipelago, Canada; in Current Research, Part A; Geological Survey of Canada, Paper 78-1A, p. 538-540.

Reinson, G.E.
1975: Lithofacies analysis of cores from the Borden Island Formation, Drake Point, Melville Island; in Report of Activities, Part B; Geological Survey of Canada, Paper 75-1B, p. 297-301.

Souther, J.G.
1963: Geological traverse across Axel Heiberg Island from Buchanan Lake to Strand Fiord; in Y.O. Fortier et al., Geology of the north central part of the Arctic Archipelago, Northwest Territories (Operation Franklin); Geological Survey of Canada, Memoir 320, p. 426-448.

Stott, D.F.
1969: Ellef Ringnes Island, Canadian Arctic Archipelago; Geological Survey of Canada, Paper 68-16.

Tan, J.T.
1979: Late Triassic-Jurassic dinoflagellate biostratigraphy, western arctic Canada; unpublished PhD. thesis, Department of Geology, University of Calgary.

Tozer, E.T.
1973: Triassic Assemblages (macrofossils); in B.S. Norford et al., Biostratigraphic determinations of fossils from the subsurface of the Yukon Territory and the District of Franklin, Keewatin and Mackenzie; Geological Survey of Canada, Paper 72-38, p. 18-19.

Tozer, E.T. and Thorsteinsson, R.
1964: Western Queen Elizabeth Islands, Arctic Archipelago; Geological Survey of Canada, Memoir 332.

Appendix

Selected well tops, Heiberg Group, western Sverdrup Basin. Location of wells shown on Figure 46.1.

Panarctic King Christian N-06		
King Christian Formation	613 m	(2010 ft)
Lougheed Island Formation	703 m	(2305 ft)
Maclean Strait Formation	716 m	(2350 ft)
Grosvenor Island Formation	956 m	(3136 ft)
Skybattle Formation	971 m	(3186 ft)
Barrow Formation	1103 m	(3260 ft)
Panarctic Kristoffer Bay B-06		
King Christian Formation	1418 m	(4652 ft)
Lougheed Island Formation	1559 m	(5115 ft)
Maclean Strait Formation	1588 m	(5210 ft)
Grosvenor Island Formation	1863 m	(6112 ft)
Skybattle Formation	1976 m	(6482 ft)
Barrow Formation	2039 m	(6688 ft)
Panarctic Mocklin Point D-23		
King Christian Formation	1567 m	(5140 ft)
Lougheed Island Formation	1713 m	(5620 ft)
Maclean Strait Formation	1853 m	(6080 ft)
Grosvenor Island Formation	1955 m	(6414 ft)
Skybattle Formation	2047 m	(6715 ft)
Barrow Formation	2141 m	(7025 ft)
Panarctic AIEG Skate L-80		
King Christian Formation	867 m	(2844 ft)
Lougheed Island Formation	983 m	(3225 ft)
Maclean Strait Formation	1102 m	(3615 ft)
Grosvenor Island Formation	1141 m	(3743 ft)
Skybattle Formation	1188 m	(3898 ft)
Barrow Formation	1267 m	(4157 ft)
Sun Skybattle Bay C-15		
Whitefish Member	1932 m	(6338 ft)
Stupart Member	1963 m	(6440 ft)
Drake Point Member	1969 m	(6460 ft)
Lougheed Island Formation	1998 m	(6556 ft)
Maclean Strait Formation	2043 m	(6702 ft)
Grosvenor Island Formation	2081 m	(6828 ft)
Skybattle Formation	2105 m	(6905 ft)
Barrow Formation	2159 m	(7082 ft)
Panarctic AIEG Whitefish 2H-63		
Whitefish Member	2076 m	(6811 ft)
Stupart Member	2107 m	(6913 ft)
Lougheed Island Formation	2129 m	(6985 ft)
Maclean Strait Formation	2175 m	(7136 ft)
Grosvenor Island Formation	2213 m	(7260 ft)
Barrow Formation	2222 m	(7290 ft)
Panarctic Desbarats B-73		
Whitefish Member	505 m	(1657 ft)
Stupart Member	525 m	(1722 ft)
Drake Point Member	535 m	(1755 ft)
Lougheed Island Formation	552 m	(1811 ft)
Grosvenor Island Formation	561 m	(1841 ft)
Barrow Formation	567 m	(1860 ft)
Panarctic North Sabine H-49		
Drake Point Member	3014 m	(9887 ft)
Lougheed Island Formation	3038 m	(9968 ft)
Maclean Strait Formation	3062 m	(10 047 ft)
Grosvenor Island Formation	3072 m	(10 080 ft)
Barrow Formation	3092 m	(10 145 ft)
Panarctic Drake Point F-16		
Drake Point Member	1093 m	(3586 m)
Lougheed Island Formation	1114 m	(3654 ft)
Grosvenor Island Formation	1124 m	(3688 ft)
Barrow Formation	1132 m	(3715 ft)
Panarctic N.W. Hecla M-25		
Drake Point Member	1020 m	(3346 ft)
Lougheed Island Formation	1046 m	(3432 ft)
Grosvenor Island Formation	1065 m	(3493 ft)
Barrow Formation	1073 m	(3520 ft)
Panarctic Sandy Point L-46		
Drake Point Member	707 m	(2320 ft)
Lougheed Island Formation	719 m	(2360 ft)
Grosvenor Island Formation	732 m	(2400 ft)
Barrow Formation	760 m	(2494 ft)
Elf Jameson Bay C-31		
Drake Point Member	855 m	(2805 ft)
Lougheed Island Formation	895 m	(2937 ft)
Grosvenor Island Formation	940 m	(3083 ft)
Skybattle Formation	981 m	(3220 ft)
Barrow Formation	992 m	(3255 ft)
Elf Cape Norem A-80		
Lougheed Island Formation	1467 m	(4812 ft)
Grosvenor Island Formation	1563 m	(5130 ft)
Skybattle Formation	1591 m	(5220 ft)
Barrow Formation	1599 m	(5246 ft)

47. TINDIR GROUP LIMESTONES FROM CATHEDRAL CREEK, WEST-CENTRAL YUKON

Project 770047

B.D. Ricketts
Institute of Sedimentary and Petroleum Geology, Calgary

Ricketts, B.D., Tindir Group limestones from Cathedral Creek, west-central Yukon; in Current Research, Part B, Geological Survey of Canada, Paper 83-1B, p. 391-395, 1983.

Abstract

Stromatolitic limestone and grainstone exposed on Cathedral Creek are correlated with the lower Tindir Group of late Precambrian age. Four rock units are recognized:

1. *A lower, tabular bedded, Fine Grained Dolostone unit which grades upward into unit 2.*
2. *A Limestone-Grainstone unit consisting of grainstone, pisolite, and cryptalgal laminates, that represent deposition in shallow water.*
3. *A Stromatolitic Limestone unit containing interbedded grainstone and limestone, including stromatolites with digitate-dendroid style branching (cf. **Baicalia**) and a few bulbous, dendroid stromatolites. A shallow water environment is inferred here also.*
4. *An upper Thinly Bedded Mudstone unit, probably representing somewhat deeper water conditions.*

Résumé

Les calcaires stromatolitiques et les "grainstones" (roches carbonatées) affleurant au ruisseau Cathedral sont corrélés avec le groupe inférieur de Tindir qui date du Précambrien récent. On y reconnaît quatre unités lithologiques:

1. *Une unité inférieure de dolomie à grains fins, stratifiée et tabulaire, qui se transforme progressivement vers le haut en l'unité 2.*
2. *Une unité de calcaire et "grainstone" composée de "grainstone", de pisolite et de sédiments lamellaires algaires, résultats d'une mise en place ayant eu lieu en eau peu profonde.*
3. *Une unité de calcaire stromatolitique qui contient des "grainstones" et des calcaires interstratifiés, y compris des stromatolites à ramifications de type digité-dendroïde (cf. **Baicalia**) et quelques stromatolites dendroïdes bulbeux. Ces sédiments auraient également été mis en place en eau peu profonde.*
4. *Une unité supérieure de "mudstone" finement stratifiée, probablement le résultat d'une mise en place en eau un peu plus profonde.*

Introduction

The Precambrian Tindir Group (Cairnes, 1914) is found in a number of areas in southeastern Alaska and west-central Yukon, including one area which straddles the Yukon-Alaska border. In Yukon Territory, west of Tatonduk River, Tindir rocks occur in the upper thrust plate above the Yukon Fault, with folded Mesozoic and Paleozoic strata in the footwall.

Work on the Tindir Group by D.D. Cairnes of the Geological Survey of Canada was part of an international investigation in 1911 (with the United States Geological Survey) of the geology adjacent to the 141 st. Meridian, between Porcupine and Yukon rivers. Subsequent investigations by Mertie (1930, 1933) resulted in a sevenfold lithostratigraphic subdivision of the Tindir Group. This subdivision was modified by Brabb and Churkin (1969) who mapped the Tindir in east-central Alaska. On the Yukon side of the border, the Tindir Group was mapped by Norris (1979), while more recently Young (1982) studied a number of stratigraphic sections on both sides of the border.

During the field season of 1982, a section of Tindir strata was examined while conducting a brief survey along a south-flowing reach of Cathedral Creek, 7 km east of the international boundary (Fig. 47.1). The sequence outcrops about 100 m north of the junction with a small tributary, is approximately 230 m thick, and dips 30-35° northeast. A thin, vertical, diabase dyke cuts the sequence along the east bank of the creek and strikes almost due north, parallel to the regional dyke trend in this area.

Exposure of the Tindir is relatively poor in this area and, therefore, a report of this section was considered to be worthwhile. Furthermore, little published information is available on the Tindir Group on the Canadian side of the border. Of additional interest here is the presence of stromatolitic and clastic limestones with well preserved sedimentary structures. It is hoped that, in the near future, a more detailed investigation of this important group of rocks will be undertaken.

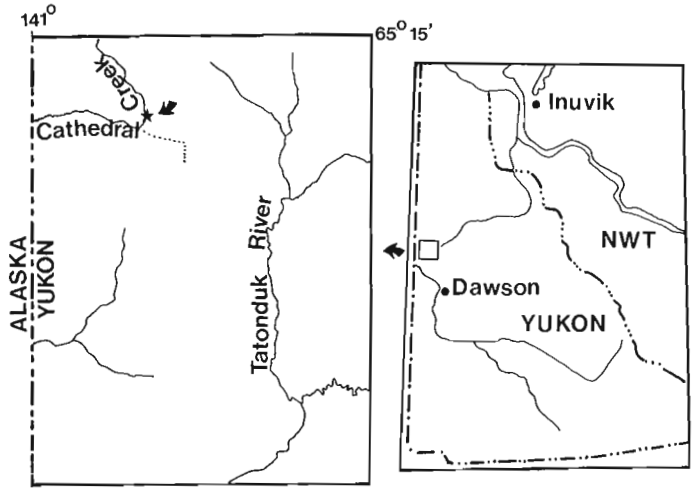

Figure 47.1. *Location of the Cathedral Creek section.*

Acknowledgments

The author thanks D.W. Morrow for his critical review of this paper and is grateful to P. Zalenka for his capable assistance in the field.

Sedimentology and Petrology

Some 230 m of almost continuous stratigraphic section is exposed along Cathedral Creek at this locality, and is summarized in Figure 47.2. The sequence is subdivided into four informal lithologic units based on composition and sedimentary structures. Both the base and top of this section are covered.

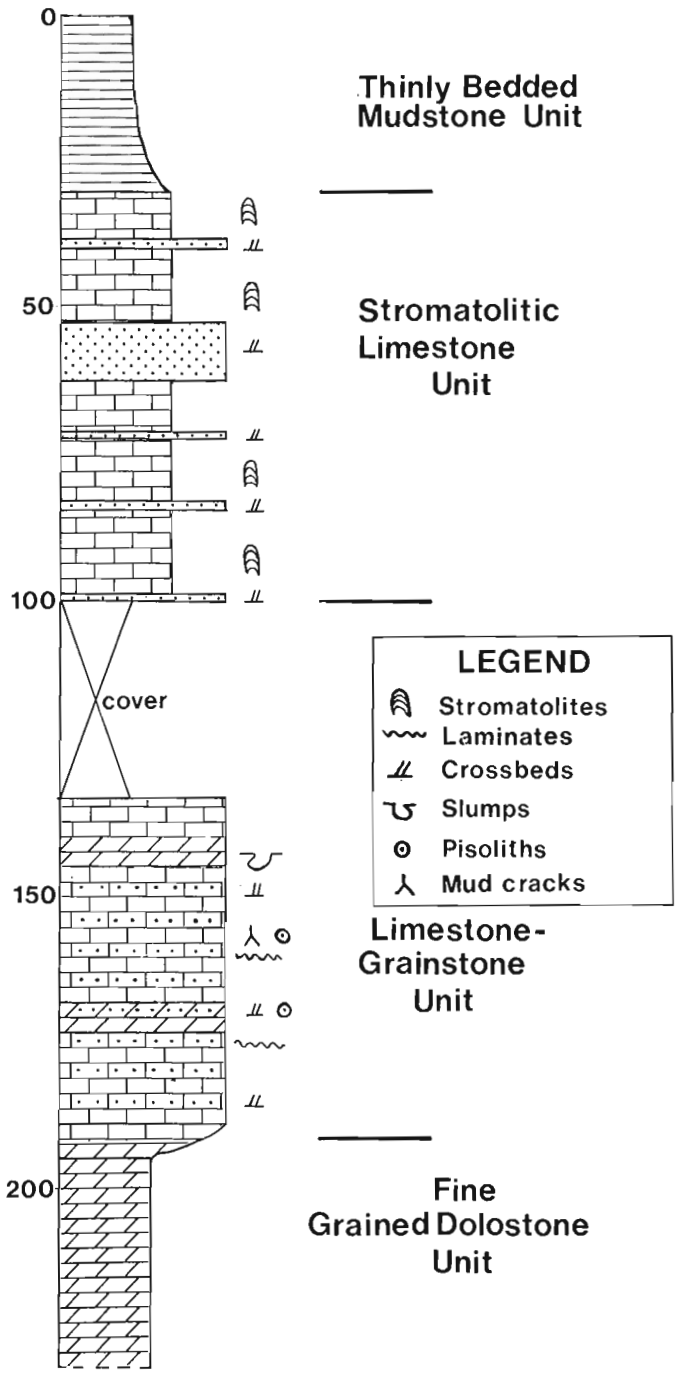

Figure 47.2. *Schematic representation of the measured section at Cathedral Creek. Depths in metres.*

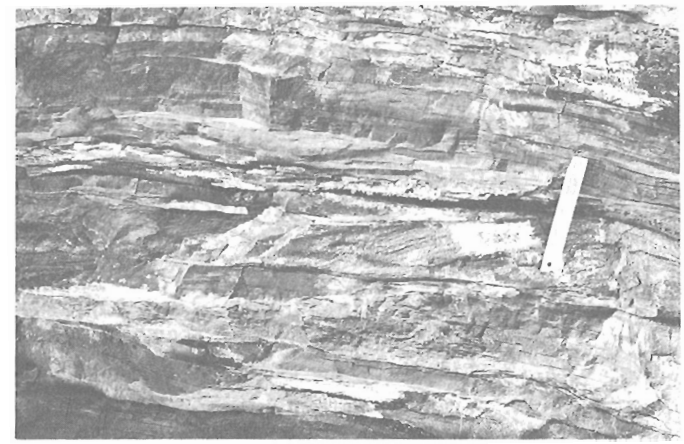

Figure 47.3. *Laminated and crossbedded grainstone of unit 2. Scale is 15 cm long.*

Figure 47.4. *Pisolitic grainstone from unit 2, containing thin wavy cryptalgal laminates. A few large mud chips have been enveloped by cryptalgal mats in the interval above the scale. The calcitic pisoliths have weathered recessively. Scale is 11 cm long.*

1. Fine Grained Dolostone Unit (lowest exposed unit).

Forty-two metres of parallel, tabular bedded, fine grained dolostone occur near the base of the section. Beds at the base are 50-60 cm thick and superficially appear rather massive, although on close examination they are seen to contain vague parallel and wavy laminae, and occasional small scours and truncation surfaces. The scours are filled with mud chips a few millimetres in length. Higher in this unit, small, starved, current ripples and thin lenses of dolomitic grainstone appear, becoming more abundant toward the top of the unit. The increase in the clastic carbonate component is accompanied by an overall decrease in bed thickness to about 10-20 cm.

These rocks consist of relatively equant dolomite crystals up to 50 μm in size. Small decamicron-sized patches of micritic dolomite are present locally, but it is difficult to determine whether these are relict peloids or relict laminae. Intercrystal boundaries are highly irregular, suggesting some recrystallisation that may have been induced by local diabase intrusion. The argillaceous component of these rocks is small.

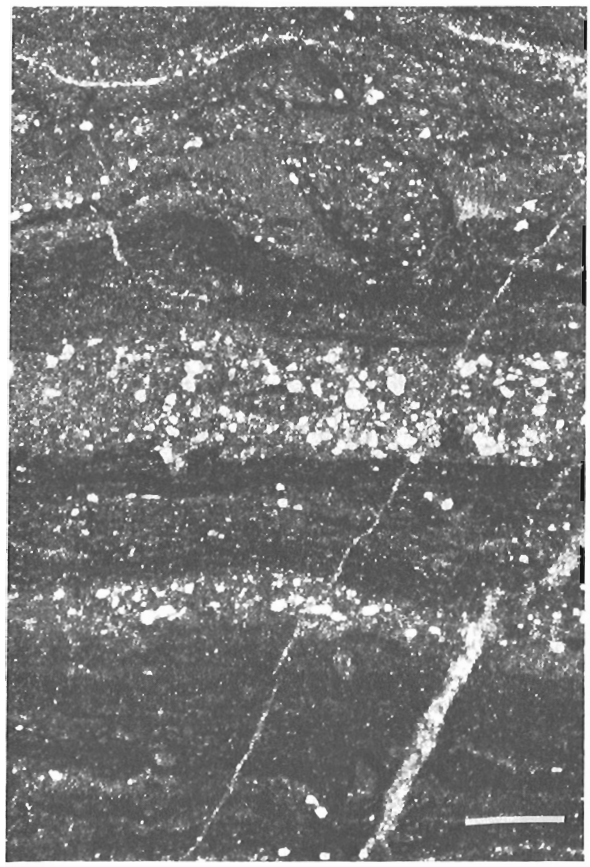

Figure 47.5. *Photomicrograph of cryptalgal laminated limestone (dark layers), alternating with lighter coloured, silty layers containing abundant detrital quartz. The small fractures are filled with dolomite. Plane polarized light. Bar scale represents 1 mm.*

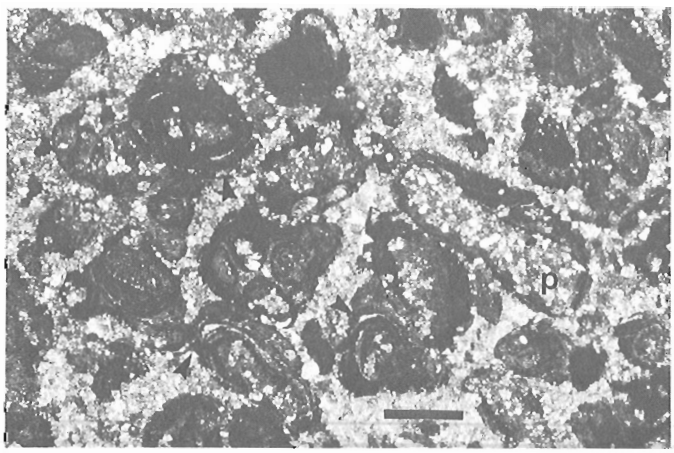

Figure 47.6. *Photomicrograph of pisolitic limestone. Dolomite has replaced much of the interpisolith cement, and also occurs between detached pisolith laminae (arrows). Pisolith cores generally are composed of micritic limestone; the elongate form (p) contains abundant silt-sized detrital quartz. Plane polarized light. Bar scale represents 1 mm.*

2. Limestone-Grainstone Unit.

Tabular bedded, grey limestones of this unit range in thickness from a few centimetres to one metre, and contain a variety of sedimentary and cryptalgal structures. Grainstones consist of intraformational lutite clasts, and bed forms such as ripples and small scale, planar crossbeds are common (Fig. 47.3). Ball-and-pillow structures are found locally where thin lime mudstones are interbedded with grainstone. Some beds contain abundant pisoliths that constitute a clast-supported framework; they may be crossbedded, and most are associated with simple cryptalgal laminates (Fig. 47.4). The dark grey, lutitic limestones form a relatively minor proportion of this unit but contain distinctive, mud-filled, desiccation cracks with curled tops similar to mud cracks. Bird's-eye structures and calcite-filled, compacted desiccation cracks, similar to molar tooth structures, were found in some of the mudstones.

Wavy and parallel laminated cryptalgal laminates usually occur in the grainstone and pisolitic lithologies. A few small domal structures appear to have grown over mud rip-up clasts. Erosion and regrowth of mats also is common; some exhibit desiccation features. In places, cryptalgal laminae form small protuberances suggesting initiation of some sort of columnar structure. Like many other stromatolite buildups that have been reported from Precambrian rocks, the Tindir laminates exhibit a light-dark colour alternation. Darker laminae generally consist of fine calcite (commonly less than 10 μm) with varying degrees of replacement by sucrosic dolomite (crystals 20-50 μm); terrigenous detritus is rare (Fig. 47.5). The lighter coloured laminae are made up of clastic carbonate debris (grains of micritic calcite) and angular quartz grains, again with varying degrees of dolomite replacement. All of these fabrics are cut by dolomite-filled fractures.

Pisoliths, 1-3 mm in diameter, exhibit well preserved concentric growth laminae which are composed mainly of very fine calcite. Individual laminae range from 10-25 μm thick and consist of micritic calcite crystals 3-5 μm in size. Pisolith cores vary in composition and include coarse grains of microcrystalline calcite, cemented peloid grains and some detrital quartz. In some cases, multiple growth patterns are evident where concentric rinds envelop two or more smaller pisoliths (Fig. 47.6). Dolomitisation of pisolitic lithologies is ubiquitous but selective, and has replaced most of the interstitial calcite cement, leaving pisolith rims relatively intact. Dolomite rhombs (up to 300 μm) also fill zones between detached pisolith laminae.

3. Stromatolitic Limestone Unit.

This unit consists of alternating grainstone and stromatolitic limestone in beds 40-200 cm thick. The clastic lithologies are similar to grainstones in the subjacent unit, wherein planar crossbeds, shallow scours, pisoliths and oncolites are found. However, desiccation structures are rare.

Two types of stromatolite were observed in this Tindir section; stromatolites having digitate to slightly dendroid branching patterns, and bulbous, branched stromatolites. Where individual beds can be traced laterally for 10-20 m, discrete biohermal structures can be discerned in which the bulk of the stromatolites are digitate, the bulbous forms having developed on the bioherm flanks.

Digitate Forms. In most cases, growth was initiated from simple domal structures, giving rise to parallel or slightly divergent columns up to 25 cm high, and 3-5 cm wide (Fig. 47.7). Some columns thicken slightly toward their tops.

Figure 47.7

Columnar stromatolites having parallel and locally divergent branching. Note the paucity of lateral linking between columns. The alternation of resistant and recessive laminae is a function of dolomite content in the former. The vertical fractures have been filled by dolomite. Scale is 5 cm long.

Figure 47.8

Examples of small, bulbous stromatolites with divergent branching. To the right of this photograph, and in the same bed, the bulbous forms grade into parallel, digitate branching stromatolites.

Figure 47.9

Photomicrograph of the crestal zone of a digitate stromatolite, showing alternating micritic limestone (dark layers), and light coloured laminae consisting of sucrosic dolomite. The limestone fabrics are cut by dolomite-filled fractures. Plane polarized light. Bar scale represents 1 mm.

Individual laminae are moderately to highly convex and terminate abruptly at column margins; thus the columns lack wall structure. Lateral linking between columns also is poorly developed, although locally they coalesce to form thick bridges of wavy or parallel laminae, which provide a substrate for subsequent column growth.

Bulbous forms. This category includes a few isolated, bulbous stromatolites with a highly divergent branching style (Fig. 47.8). Laminae usually are moderately convex and are tangential to column margins, providing some degree of wall structure. The margins are relatively smooth compared to the digitate forms described above. In some cases these bulbous structures are similar to the initial growth style of the digitate stromatolites and may well be gradational with those forms.

Stromatolites from Lower Tindir Group strata located in eastern Alaska, were identified as **Baicalia** by M.A. Semikhatov (in Churkin, 1973, p. 8). The forms illustrated here are consistent with this identification.

Petrographically, the stromatolitic carbonates are quite different from the grainstone and cryptalgal laminated lithologies in the subjacent unit. Here, the laminated fabric is an expression of fine micritic calcite layers (0.1-3 mm thick, and showing only minor dolomite replacement) alternating with layers of relatively coarse, sparry dolomite (crystals up to 200 μm, see Fig. 47.9). On a sub-millimetre scale,individual laminae cannot be traced more than a few millimetres because of dolomitization. Detrital quartz is rare in stromatolite-bearing rocks, although it does occur in the interbedded grainstone lithologies. The poor definition of cryptalgal fabrics in these rocks, compared to those found in the limestone-grainstone unit, is a result of dolomite replacement and crystal growth. A similar trend in dolomite fabrics has been observed in stromatolitic carbonates belonging to the Aphebian Belcher Group (Ricketts, in press). The differences in the degree of fabric preservation are, in part, a function of the differences in original mineralogy between stromatolitic and non-stromatolitic carbonates, and subsequent selective dolomitization. If the dolomite in these fabrics is the same generation as the fracture-filling dolomite, then the replacement process must have occurred after lithification.

4. Thinly Bedded Mudstone Unit.

Grainstones of the subjacent unit grade over an interval of two to three metres into a 30 m thick section of thinly bedded (1-5 cm), fine grained, calcareous dolosiltite and argillaceous dolostone. Some beds contain parallel or wavy laminae, but in general there is little evidence for bed load transport of sediment. The top of this unit is not exposed.

Interpretation

The two middle units, the Limestone-Grainstone and Stromatolitic-Limestone, contain evidence of shallow water conditions of sedimentation, including crossbedding, stromatolites and cryptalgal laminates, pisoliths, and coarse clastic debris. The grainstone unit in particular also shows some evidence of subaerial exposure, although there are no indications that evaporitic conditions ever developed. In contrast to these relatively high-energy conditions, the lowermost, Fine Grained Dolostone unit, and the upper, Thinly Bedded Mudstone unit, are representative of environments in which bed load transport of sediment was minimal; in addition, there is no evidence of exposure. However, a more specific interpretation of the upper and lower units is difficult, because of the limited stratigraphic and lateral extent of the Cathedral Creek section. For example, the sequence of units 1 through 4 could represent a phase of transgression in which fine grained dolostone in the lowest unit formed in a backwater or lagoonal setting, whereas the upper Thinly Bedded Mudstone unit formed in a muddy, outer platform environment; the Limestone-Grainstone and Stromatolitic Limestone units would then represent transitional shallow water deposits. Alternatively, units 1 to 3 might indicate a regressive phase of sedimentation with progressively shallower water carbonates being deposited, whereas unit 4 would represent a return to deeper water conditions.

Correlation

A lenticular body of grey stromatolite-bearing limestone, up to 150 m thick, has been mapped in eastern Alaska as part of the Dolomite and Shale unit of Brabb and Churkin (1969); according to Churkin (1973), this limestone contains the form genus **Baicalia.** Young (1982) also has examined stromatolitic limestone and dolostone in sections of the lower Tindir, near Tindir Creek, some 10 km north of the Cathedral Creek locality. Within the Tindir Group, the branched stromatolites have been observed only in the lower, and not the upper part of the group. Therefore, it is reasonable to correlate the Cathedral Creek section with the lower Tindir Group.

References

Brabb, E.E. and Churkin, M.Jr.
1969: Geologic map of the Charley River Quadrangle, east-central Alaska; United States Geological Survey, Map I-573.

Cairnes, D.D.
1914: The Yukon-Alaska International boundary, between Porcupine and Yukon Rivers; Geological Survey of Canada, Memoir 67.

Churkin, M., Jr.
1973: Paleozoic and Precambrian rocks of Alaska and their role in its structural evolution; United States Geological Survey, Professional Paper 740.

Mertie, J.B.
1930: Geology of the Eagle-Circle District, Alaska; United States Geological Survey, Bulletin 816.

1933: The Tatonduk-Nation district, Alaska; United States Geological Survey, Bulletin 836E.

Norris, D.K.
1979: Ogilvie River, Yukon Territory; Geological Survey of Canada, Map 1526A.

Ricketts, B.D.
– The evolution of a Middle Precambrian dolostone sequence - A spectrum of dolomitization regimes; Journal of Sedimentary Petrology. (in press)

Young, G.M.
1982: The late Proterozoic Tindir Group, east-central Alaska: Evolution of a continental margin; Geological Society of America, Bulletin, v. 93, p. 759-783.

SCIENTIFIC AND TECHNICAL NOTES
NOTES SCIENTIFIQUES ET TECHNIQUES

PETROGRAPHY OF FEED COALS AND RESIDUAL MATERIALS FROM LIQUEFACTION EXPERIMENTS

Project 810015

A. Cameron, W. Kalkreuth and D. Marchioni[1]
Institute of Sedimentary and Petroleum Geology, Calgary

Cameron, A., Kalkreuth, W., and Marchionil, D., Petrography of feed coals and residual materials from liquefaction experiments; in Current Research, Part B, Geological Survey of Canada, Paper 83-1B, p. 397-400, 1983.

Abstract

Three feed coals and a hydrogenation residue from one of them were analysed petrographically. According to ASTM standards these coals are subbituminous in rank. Reflectances determined on huminite ranged from 0.36 to 0.42. Petrographic analyses were made using reflected "white light" and blue light irradiation. The use of the latter technique revealed that in these low rank coals a considerable amount of the liptinite components is overlooked under "white light" observation. Consequently, results on maceral composition were adjusted to data obtained by using blue light irradiation. The liquefaction residue was found to consist of two phases, namely reacted and unreacted materials. Within the former, vitroplast, granular residue, mesophase-spheres, and semi-coke were identified, while unreacted material comprises inertinite particles, pyrite and other minerals. The granular residue may also contain a significant amount of unreacted material.

Résumé

Les auteurs ont analysé la pétrographie de trois charbons d'alimentation et du résidu de l'hydrogénation d'un de ces charbons. Selon les normes de l'ASTM, il s'agit de charbons subbitumineux. Les réflectances déterminées à partir de l'huminite variaient de 0,36 à 0,42. Les analyses pétrographiques ont été effectuées à l'aide de la lumière blanche réflechie et de l'irradiation en lumière bleue. L'utilisation de la lumière bleue a révélé que ces charbons de bas rang contiennent une importante quantité de liptinite non aperçue à la lumière blanche. Les résultats sur la teneur en éléments macéraux ont donc été rajustés en fonction des données obtenues par le procédé d'irradiation en lumière bleue. Les analyses ont établi que le résidu de liquéfaction se compose de deux phases, soit des matériaux ayant réagi et des matériaux n'ayant pas réagi. Parmi les matériaux ayant réagi, on a identifié du vitroplaste, un résidu granulaire, des sphères de mésophase et du semi-coke tandis que les matériaux n'ayant pas réagi contenaient des particules d'inertite, de la pyrite et d'autres minéraux. Le résidu granulaire peut aussi contenir une quantité importante de matériel qui n'a pas réagi.

Introduction

A suite of four samples was submitted by the Alberta Research Council to the Coal Technology Section of ISPG, Calgary, for microscopic analyses. The suite consisted of three feed coals: identified as 207/80, 208/80, and 209/80, and the hydrogenation residue from one of them. The latter is identified as sample 89/80 and is the residue from feed coal 207/80. The results of the analyses, and studies made of the samples, are contained in this report. Sample numbers are those of the Alberta Research Council.

Petrography of Feed Coals

The coal samples were ground to minus 20 mesh (850 microns), made into pellets with a cold-setting epoxy resin and polished according to commonly accepted practice (ASTM Standard D 2797, 1981). Microscopic examination was carried out with a Leitz MPV-2 instrument using oil immersion (n oil = 1.518 at 546 nm) at a magnification of x675. Fifty reflectance measurements per sample were made on the maceral huminite B (Stach et al., 1982; International Committee for Coal Petrology, 1971/1975). Means and standard deviations were calculated and are reported in Table 1. Maceral determinations were carried out initially with "white" light using a quartz halogen lamp as a light source. A second examination was carried out using fluorescent light in order to better distinguish the liptinite macerals. Maceral data are reported in volume per cent and are based on a count of 500 points per sample. The maceral data on a mineral-free basis are shown in Table 1.

The reflectance data for samples 207/80 and 209/80 are indicative of subbituminous coals, the mean value for 208/80 appears somewhat low and may represent a coal close to the boundary between lignite and subbituminous. With regard to maceral content, 208/80 and 209/80 are somewhat similar with relatively low huminite content and relatively high inertinite. In comparision, sample 207/80 is relatively rich in huminite. Huminite is the low rank precursor of vitrinite in higher rank coals (Stach et al., 1982).

As mentioned above the initial maceral counts were made under white light. It is now well established that those constituents relatively rich in hydrogen tend to be underestimated under such optical conditions, particularly in low rank coals. With a few exceptions, these contituents comprise the group maceral liptinite. The main problem is that such constituents are difficult to distinguish from mineral matter because of their very low reflectance. The use of fluorescence techniques helps to resolve this problem. Under blue light or ultra violet irradiation the liptinitic components flouresce in distinctive fashion with colours ranging from light yellow to orange or orange red, while most other constituents do not fluoresce. Some of the huminite in lower rank coals will also fluoresce, but normally with much weaker intensity than the associated liptinite.

In order to better delineate the liptinitic constituents, the three coal samples of this study were examined microscopically using blue light excitation. The samples were point counted, with two categories of materials being distinguished, namely fluorescing and non-fluorescing. The fluorescent material was identified mainly as sporinite and resinite with minor amounts of exudatinite. Some examples of weakly fluorescing huminite were noted in sample 209/80. A second set of liptinite values based on the fluorescence observations are included in Table 1 and the other maceral data are adjusted accordingly. Note that for each sample the fluorescence technique has identified more liptinite than was detectable with normal light.

[1] D.L. Marchioni & Associates, 33 Kingsway Avenue, Rankin Park, Newcastle 2287, NSW, Australia.

Table 1

Summary of Petrographic Data

Maceral[1] Group	Maceral	207/80		208/80		209/80	
		Maceral Content (volume %)					
		White[2]	Fluor.	White	Fluor.	White	Fluor.
Huminite	Ulminite A	10	9	5	5	10	10
	Ulminite B	40	38	27	27	34	33
	Densinite	21	20	28	27	17	16
	Gelinite	7	6	2	2	2	2
	Corpohuminite	7	7	7	7	2	2
Total Huminite		85	80	69	68	65	63
Inertinite	Semifusinite & Fusinite	7	7	9	9	15	14
	Other Inerts	4	4	9	9	14	13
Total Inertinite		11	11	18	18	29	27
Total Liptinite		4	9	13	14	6	10
Reflectance[3]	Mean	0.40		0.36		0.42	
	Std. Dev.	0.04		0.05		0.02	

[1] For maceral descriptions see Stach et al. (1982) or International Committee for Coal Petrology (1971/1975)
[2] White = white light; Fluor. = fluorescent light
[3] Random reflectance

Petrography of Hydrogenation Residue

Considerable difficulty was experienced in preparing a specimen of the residue for microscopic examination. The problems involved partial solution of the residue particles in the bonding resin and a tendency for the pellet to remain soft beyond a normal curing time. An adequate specimen was finally prepared using uncrushed particles of residue bonded with Buehler epoxide resin in a cold-setting process.

The solid residues from the hydrogenation process consist mainly of two types of materials, vitroplast and granular matrix. The term vitroplast comes from Mitchell et al. (1977) and was discussed by Diessel (in press), who suggested "coagulant" as an alternative term. It refers to material, derived from huminite, and possibly other macerals as well, which has likely become plastic and converted to some extent to liquids and gases during the hydrogenation process. The areas of vitroplast encountered in residue 89/80 are large in size, greyish in colour and isotropic. The vitroplast also serves as a matrix for unreacted inertinite, mesophase spheres, and semi-coke (see Pl. 1, Fig. 1, 2). Reflectance measurements show a mean value of 0.74 (random reflectance). This in agreement with data reported by Diessel (in press). He analysed a number of residues from a variety of coal ranks and showed reflectance values ranging from 0.70 to 1.20 for the vitroplast or coagulant.

The "granular matrix" phase consists mainly of an aggregate of sub-microscopic particles, so far unidentified, though it is suspected many of them may be mineral matter. A qualitative examination of this matrix by scanning electron microscope revealed an abundance of aluminum, silicon, chlorine, sulphur, calcium and iron, with smaller amounts of potassium and magnesium. Iron was detected in two modes of occurrences: combined with sulphur as pyrite, and without sulphur (possibly as an oxide). Even under the SEM the matrix still appeared granular.

With the petrographic microscope, the granular matrix is seen to be relatively rich in pyrite and inclusions of unreacted inertinite, (see Pl. 1, Fig. 3). In contrast to the vitroplast, mesophase and semicoke are rare in the granular matrix. The overall composition of the hydrogenation residue, as determined by point count and expressed in per cent, is as follows:

vitroplast	36
granular matrix	47
mesophase	7
inertinite	6
semi-coke	1
pyrite	3

Discussion

Although some literature on the subject is beginning to accumulate, research on the relationship of conversion yields, petrographic composition, and hydrogenation residues, is still at a relatively early stage. Given et al. (1975), Guyot (1976), Guyot and Diessel (1979), Wakeley et al. (1979), and Grey et al. (1980) are among those who have published on the subject. The conclusions reached by these workers are still of a general nature and in part contradictory. For example Given et al. (1975) reported their best yields from high volatile bituminous coals with lower yields from ranks both above and below high volatile. On the other hand Diessel (in press) suggested that conversion decreases as rank increases. Most seem to agree that increase in reactives, that is huminite (vitrinite) plus liptinite, gives increased yields on conversion. However, this conclusion must be treated with some caution, because not all "reactives" are equally reactive. Even within the liptinite group it is quite possible that alginite for instance may give different yields than sporinite and cutinite. In addition there is the problem of inertinite; most likely not all constituents grouped under this general label are totally inert in a hydrogenation process.

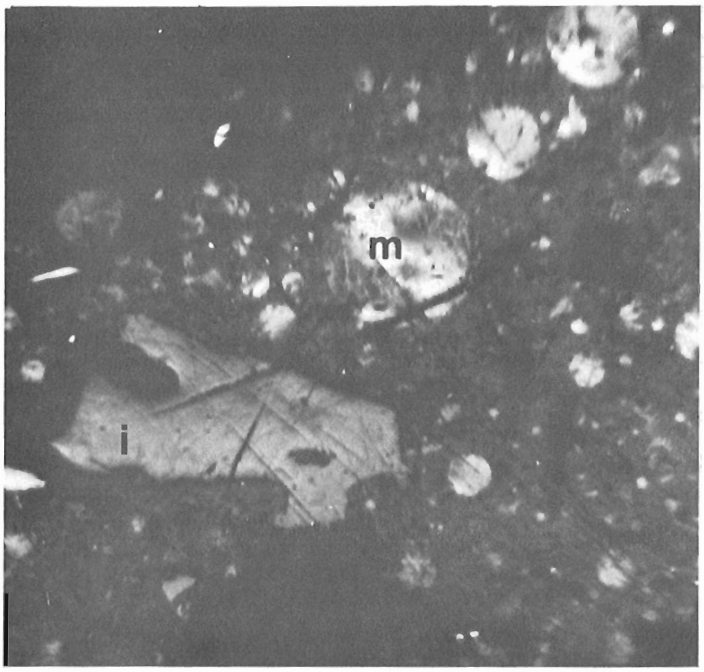

1

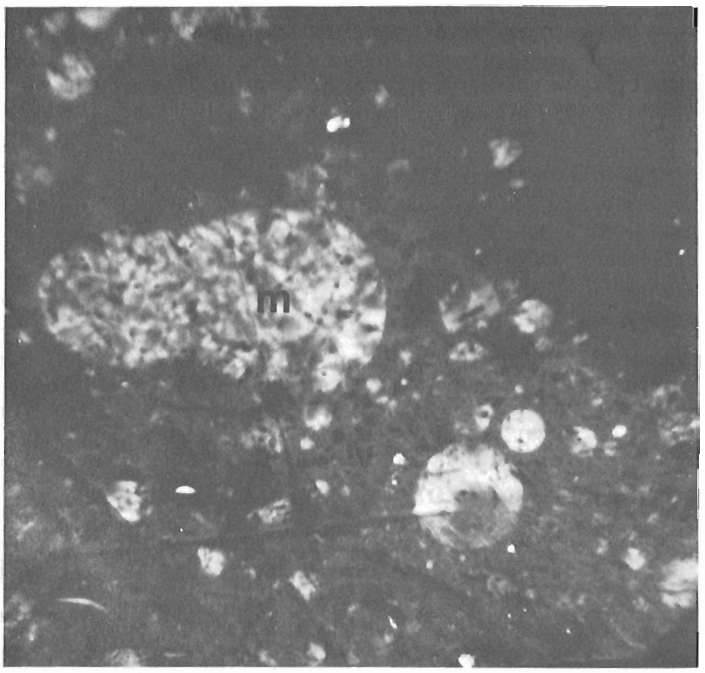

2

40 um

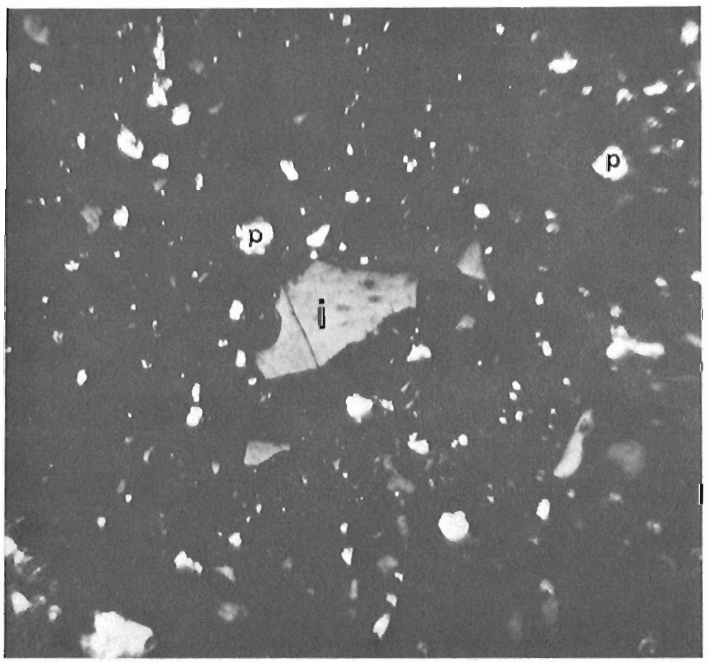

3

Plate 1

Figures

1. Mesophase-spheres (m) of various sizes and unreacted inertinite (i) in vitroplast matrix. Reflected light, oil immersion, partially crossed polars.
2. Coalesced mesophase-spheres (m) in vitroplast matrix. Reflected light, oil immersion, partially crossed polars.
3. Unreacted inertinite particles (i) and pyrite (p) in granular matrix. Reflected light, oil immersion, plane polarised light.

Finally, there is the matter of differences in the experimental conditions of the various hydrogenation processes, coupled with the catalytic and anticatalytic effects of the particular suite of minerals and trace elements which a given coal may contain.

Acknowledgments

The authors wish to thank S. Parkash of the Alberta Research Council for the samples, and are also grateful to F. Goodarzi (ISPG) for his critical review of the manuscript.

References

Diessel, C.F.K.
– Petrographic studies on solid residue derived from the hydrogenation of some Australian coals; Paper given at IX International Carboniferous Congress, Urbana, Illinois, May, 1979. (in press)

Given, P.H., Cronauer, D.C., Spackman, W., Lovell, H.L., Davis, A., and Biswas, B.
1975: Dependence of coal liquefaction on coal characteristics; Fuel, v. 54, pt. 1, p. 34-39; pt. 2, p. 40-49.

Gray, D., Barrass, B., Jezko, J., and Kershaw, J.R.
1980: Relations between hydroliquefaction behaviour and the organic properties of a variety of South African coals; Fuel, v. 59, p. 146-150.

Guyot, R.E.
1976: Production of synthetic oil and chemicals from coal - Part 3 -Relationships between coal properties and hydroliquefaction potential; Australian Coal Industry Research Laboratories, Ltd., Progress Report 76-8.

Guyot, R.E., and Diessel, C.F.K.
1979: The application of coal petrography to hydrogenation research; Australian Coal Industry Research Laboratories, Ltd., Progress Report 79-3.

International Committee for Coal Petrology
1971/ 1975: International Handbook of Coal Petrography (supplement to 2nd edition); also 2nd supplement, 1975; Centre National de la Recherche Scientifique 15, Quai Anatole-France, Paris, France.

Mitchell, G.D., Davis, A., and Spackman, W.
1977: A petrographic classification of solid residue derived from the hydrogenation of bituminous coals; in Liquid Fuels from Coal, R.T. Ellington, ed.; Academic Press Inc., New York, San Francisco, London, p. 255-270.

Stach, E., Taylor, G.H., Mackowsky, M.T., Chandra, D., Teichmuller, M., and Teichmüller, R.
1982: Coal Petrology; 3rd edition, Gebruder Borntraeger, Berlin, Stuttgart, p. 535.

Wakeley, L.D., Davis, A., Jenkins, R.G., Mitchell, G.D., and Walker, P.L.
1979: The nature of solids accumulating during solvent refining of coals; Fuel, v. 58, p. 379-385.

FLUORESCENT MINERALS FROM THE FORT SMITH AREA, DISTRICT OF MACKENZIE, N.W.T.

H.H. Bostock and D.L. Thompson

Bostock, H.H. and Thompson, D.L., Fluorescent minerals from the Fort Smith area, District of Mackenzie, N.W.T.; in Current Research, Part B, Geological Survey of Canada, Paper 83-1B, p. 401-402, 1983.

Abstract

Two new occurrences of scheelite ($CaWO_4$), two of fluorescent potash feldspar, and one of yellow fluorescent andalusite are reported.

Résumé

Deux nouvelles venues de scheelite ($CaWo_4$), deux de feldspath potassique fluorescent et une d'andalousite jaune fluorescente sont signalées.

Introduction

During 1:250 000 scale mapping of the Fort Smith map sheet (Bostock, 1982) in 1979-81, several thousand hand specimens were collected for petrographic reference. Each specimen was routinely examined in ultraviolet light and reports of fluorescence recorded in field notes. Computer sorting of field notes at the end of the project suggested further examination of some dozen specimens, the most interesting of which are listed with ancilliary data in Table 1. None of these occurrences were recognized in the field as being of particular interest and hence no special care was taken in preparation of the original description. The identification of each fluorescent mineral has been confirmed by X-ray powder pattern. Feldspars and andalusite were analyzed by electron probe in polished thin section, and concentrates of these minerals are being analyzed by spectrographic and energy dispersive methods. The principal mineral occurrences are plotted on Figure 1.

Geological Setting

The Fort Smith area (75D and part of 85A) encompasses a region of well exposed Precambrian Shield east of Slave River (Fig. 1). The basement plutonic rocks within this area include an extensive north-south oriented, uplifted region of high grade (granulite facies) ortho- and paragneiss of probable Archean age that has been abundantly intruded by early Hudsonian (1944 ± 16 Ma, U/Pb zircon) megacristic granite. This region is flanked by gneisses and plutonic rocks which have undergone variable to severe greenschist facies retrogression, and is separated from them by zones of mylonitization and faulting. Supracrustal rocks of the Nonacho and Tazin groups lie unconformably upon retrograded gneisses in the eastern part of the area where at least the Tazin and probably the Nonacho as well have been locally intruded by granites. All of these rocks are intruded by minor diabasic to gabbroic bodies which include the west-northwest trending Sparrow Dykes (1700 Ma, McGlynn et al., 1974).

Discussion

The two scheelite occurrences are in the northern part of the map area as veins near the contact between Hudsonian megacrystic granite and its host rocks. Cassiterite and

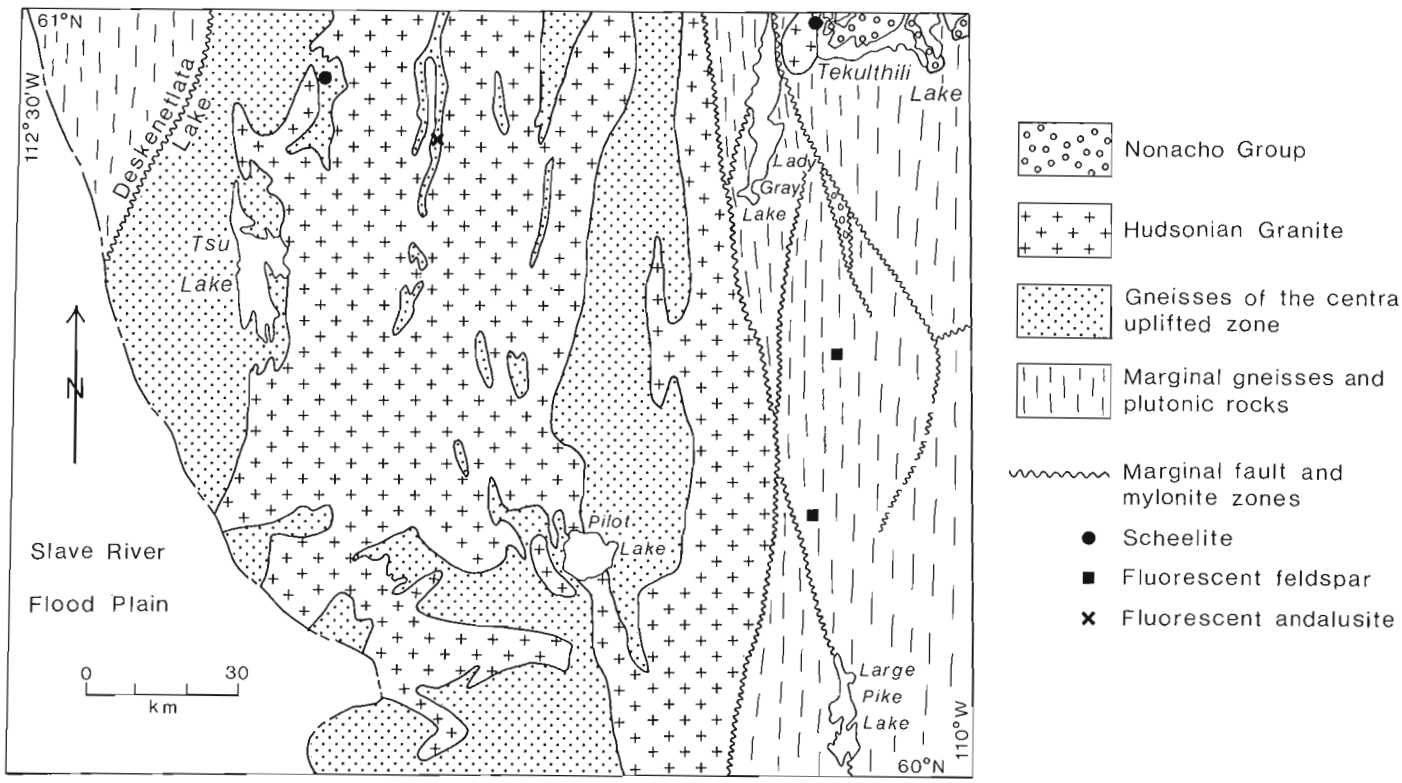

Figure 1. *General geology of the Fort Smith area.*

Table 1

Fluorescent mineral occurrences, Fort Smith area

Sample	Easting (zone 12)	Northing (zone 12)	Host Lithology	Fluorescent Mineral	Colour of Fluorescence	Elements** Reported	Remarks
79BK115A	533010	6761400	Pink, medium grained granite	scheelite ($CaWO_4$)	strong blue-white	Ca, W	Small granite apophyse intrudes laminated calcareous siltstone near contact of granite stock. Scheelite occurs as tiny grey-white veins (2 mm) with local purple fluorite in granite near shore of Thekulthili Lake.
80BK770A	460730	6753150	Fractured, fine grained amphibolite band ~3 m thick in pelitic granulite	scheelite ($CaWO_4$)	strong blue-white	Ca, W	Amphibolite is located on east-facing slope near bottom of valley about 100 m west of coordinates given. Scheelite occurs as local finely crystalline fracture coatings.
79BK1108B	477190	6744520	Dark grey pelitic granulite	andalusite (Al_2SiO_5)	moderate yellow (diminished on crushing)	Al_2O_3 63.16 SiO_2 37.10 FeO 0.26	Andalusite-orthoclase-cordierite-bearing gneiss from screen within Hudsonian batholith. Fluorescence reported in field was dark green, changing after 3 years to yellow*
81BKF56A	532960	6690470	melanocratic gneiss-breccia	potash feldspar ($KAlSi_3O_8$)	pale white (diminished on crushing)	CaO 0.27 BaO 0.32 FeO 0.04 Pb 23 ppm	Feldspathic matrix from melanocratic gneiss breccia band 5 m thick in mesocratic gneiss.
81BKF182A	536200	6713600	quartz-rich gneiss with feldspathic interbeds	potash feldspar ($KAlSi_3O_8$)	pale white (diminished on crushing)	CaO 0.26 BaO 0.46 FeO 0.02 Pb 23 ppm	Intruded by granitic veins.
79BK160A	534920	6764500	Sandstone bed in Nonacho conglomerate	Calcite ($CaCO_3$)	deep red		Calcite cement between sand grains. Fluorescence reported in field was pink, changing to deep red 3 years later.

* Change in fluorescence may be due to low humidity conditions of storage?
** Elements reported in weight per cent except where parts per million indicated.

native gold have been reported farther north at MacInnis Lake in heavy mineral sands within Nonacho Group (Maurice et al., 1979) which may have been deposited before or essentially contemporaneously with emplacement or uplift of the megacrystic granite. These occurrences suggest that prospecting for this group of related minerals along the contacts of the Hudsonian batholith in the northern Fort Smith (75D) and Taltson Lake (75E) map sheets might prove rewarding.

References

Bostock, H.H.
1982: Geology of the Fort Smith map area, District of Mackenzie, Northwest Territories (NTS 75D); Geological Survey of Canada, Open File 859, p. 1-53.

McGlynn, J.C., Hanson, G.N., Irving, E., and Park, J.K.
1974: Paleomagnetism and age of Nonacho Group Sandstones and associated Sparrow Dykes, District of Mackenzie; Canadian Journal of Earth Sciences, v. 11, p. 30-42.

Maurice, Y.T. and Plant, A.G.
1979: Some mineralogical and geochemical characteristics of uranium occurrences in the Nonacho Lake area; in Current Research, Part B, Geological Survey of Canada, Paper 79-1B, p. 179-188.

NOTES ON THE DEGLACIATION OF SOUTHEASTERN QUEBEC

Project 780017

Nelson R. Gadd
Terrain Sciences Division

Gadd, N.R., Notes on the deglaciation of southeastern Quebec; in Current Research, Part B, Geological Survey of Canada, Paper 83-1B, p. 403-412, 1983.

Abstract

Recent observations of some ice contact features and drainage patterns in southeastern Quebec are the basis for re-evaluation of the pattern of deglaciation. In contrast to the earlier concept of regular retreat of an active ice margin, these features may be interpreted in terms of downwasting of the ice mass, leaving significant ice lobes in preglacial depressions while Champlain Sea entered the lowland in the form of a calving bay through the ice sheet. Remnant ice masses on the west flank of Monts Sutton controlled drainage and marine invasion of that area; thus ice marginal drainage systems and glacial lakes formed at levels below the marine limit established by earlier workers. Marine invasion of the area between Mont Yamaska, Lac Champlain, and Monts Sutton occurred at a much lower level than previously indicated and at a time after the maximum phase of Champlain Sea that is represented by the ***Mya*** *biotic phase of the late-glacial sea.*

Résumé

Des observations récentes de certaines formes de relief dues au contact glaciaire et de la configuration des réseaux hydrographiques dans le sud-est du Québec ont mené à une réévaluation du modèle de déglaciation. Contrairement à la notion antérieure du recul régulier de la marge glaciaire active, on peut interpréter ces éléments en fonction de la fonte de la glace qui aurait laissé d'importants lobes glaciaires dans des creux pré-glaciaires tandis que la mer de Champlain aurait inondé les basses-terres sous forme d'une baie de vêlage ayant traversé la calotte glaciaire. Des masses résiduelles de glace sur le flanc ouest des monts Sutton ont contrôlé le drainage et l'invasion marine de la région; des réseaux hydrographiques proglaciaires et des lacs glaciaires se sont donc formés sous la limite marine établie antérieurement par d'autres chercheurs. L'invasion marine de la région entre le mont Yamaska, le lac Champlain et les monts Sutton a eu lieu à un niveau beaucoup plus bas que celui qui avait été identifié antérieurement et ce, suivant la phase maximale de la mer de Champlain qui est représentée par la phase biotique de ***Mya*** *de la mer glaciaire tardive.*

Introduction

A review of surficial geology has been carried out during the 1981 and 1982 field seasons in southeastern Quebec. This report deals with the area from Drummondville, Quebec, south to 45°N and from Rivière Richelieu east to approximately Lac Mégantic (Fig. 1). Reconnaissance mapping was carried out in previously unmapped areas, and selected areas were studied in order to gain a clearer understanding of the regional deglaciation pattern. New stratigraphic observations deal only with very late Wisconsinan, mainly deglacial, events. Since new data modify the picture of deglaciation of southern Quebec as it was presented by Gadd et al. (1972), this report summarizes that earlier picture and discusses the impact of new observations on the pattern of deglaciation.

According to Gadd et al. (1972) the late Wisconsinan Laurentide Ice Sheet in southeastern Quebec terminated at or near the International Boundary, and its meltwater escaped southward into New England (Fig. 2). One such ice margin position was defined as the Frontier Moraine (Gadd et al., 1972; Shilts, 1981). Regular retreat towards the northwest of the active Laurentide Ice Sheet margin was marked by halts at, or readvances to, positions marked by the Cherry River Moraine and Highland Front morainic complex. As the ice margin was retreating down the regional drainage divide, ice marginal lakes of broad extent were formed more or less continuously between the ice and the deglaciated terrain. Lakes occupied levels between approximately 610 and 160 m a.s.l. When the ice-dammed lakes were at this lower level, ice barriers in St. Lawrence Lowland were destroyed and the Champlain Sea occupied all southern regions of the Lowland, i.e. all regions north and west of the Sutton-Notre Dame range (Green Mountains of Vermont) lying below about 160 m a.s.l.

The time-frame for the above events was provided by radiocarbon dates. Lake-bottom sediments from Unknown Pond, which lies within an early meltwater channel, gave a minimum age of 14 900 ± 220 BP (GSC-1339; Mott, 1977) for deglaciation of the International Boundary region. The events described above predate the Champlain Sea (i.e. before 12 500 BP); the Laurentide Ice Sheet continued to exist during Champlain Sea time, but only on the north shore of the St. Lawrence where the St. Narcisse Moraine was deposited.

This report deals with an area in southeastern Quebec along the International Boundary and no attempt is made to discuss the pattern of deglaciation in the context of the larger region of southern Ontario-northwestern United States. Figures 2-6 show the pattern of deglaciation and the development of postglacial drainage in southeastern Quebec. New observations are used to demonstrate a need to modify some previous interpretations.

Discussion

Radiocarbon Dates vs. Pollen Stratigraphy

Mott (1977) established a reference pollen diagram for comparison of radiocarbon-dated lacustrine deposits of southern Quebec. The Unknown Pond stratum dated 14 900 ± 220 BP (GSC-1339; Mott, 1977) was found to fall in a stratigraphic zone whose true age probably lies between 11 000 and 12 000 BP; the older date is considered anomalous due to the presence of marl in the sample.

Hence, the minimum date for deglaciation of southeastern Quebec could be between 11 000 and 12 000 BP rather than ca. 15 000 BP. Therefore, it is possible that regional deglaciation may not have begun until somewhat later than previously considered, even though an earlier timing is not ruled out.

High-Level Drainage of the International Boundary Zone

Figure 2 shows outwash systems in northern New England that originated at high-level cols along the Canadian side of the International Boundary. As an example, east of Lac Lindsay, headwater pond of Rivière Ascot, a minor moraine occurs at approximately 490 m a.s.l. that heads an outwash valley train, which is tributary to and confluent with a larger valley train in Hall River valley (Quebec-New Hampshire border). Hall River is part of the headwater of Connecticut River, other branches of which have similar valley trains. The outwash deposits observed in Hall River terraces and in tributaries on the Canadian side of the border are regularly bedded, gently dipping gravels and sands

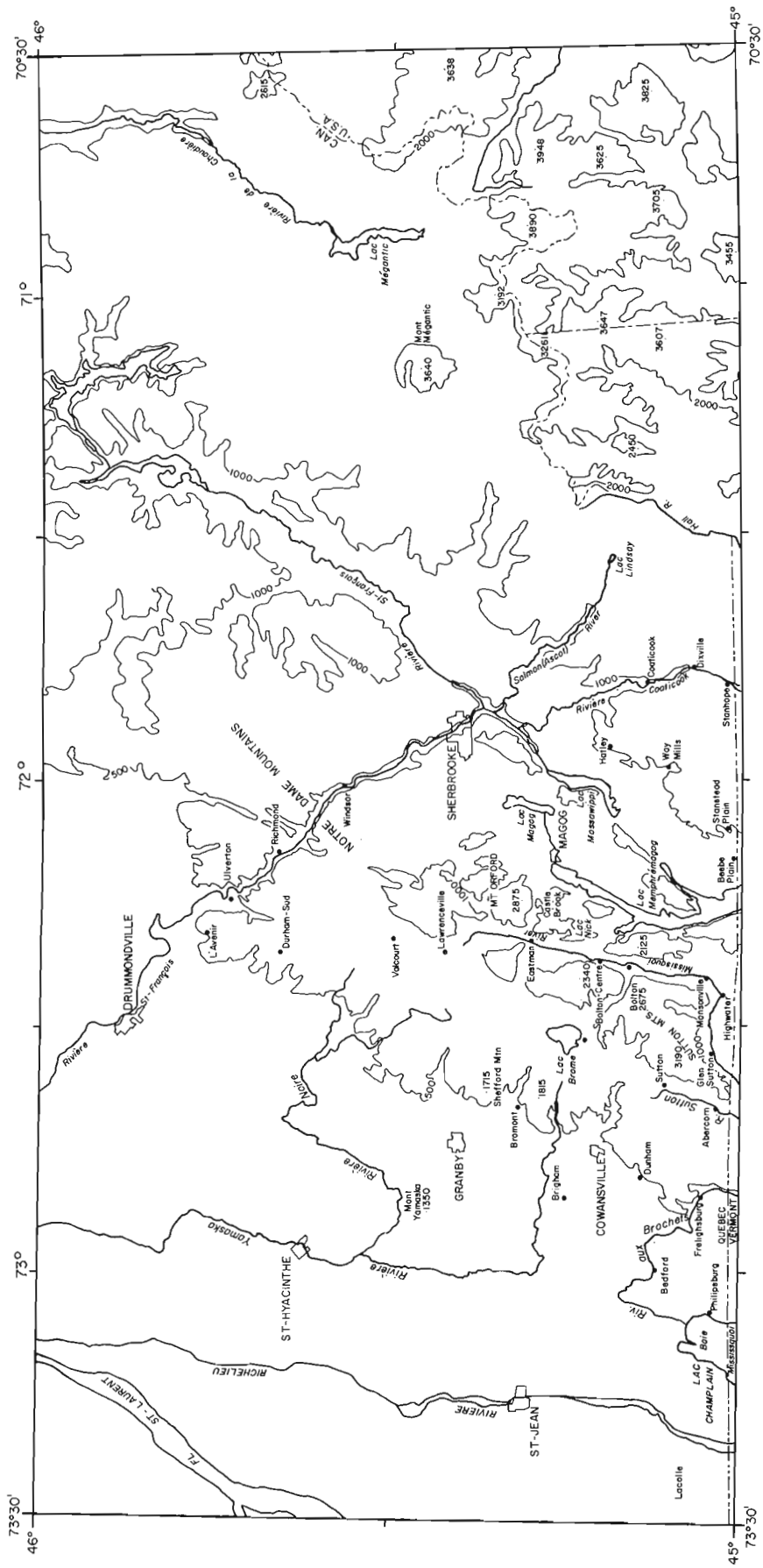

Figure 1. Study area in southeastern Quebec (Fig. 2-6 show the pattern of deglaciation).

showing no evidence of collapse due to melt-out of ice blocks. It is assumed, therefore, that these systems were ice free at a time when the ice margin in southeastern Quebec stood at an elevation of approximately 490 m.

West and southwest of Lac Lindsay, kame terraces, whose westerly flow direction is shown by dips and crossbedding of their sediments, are indicated by ice marginal arrows (Fig. 2). These are parallel to slopes in the interfluve as well as to the walls of Coaticook valley at elevations between 425 and 365 m. These ice marginal features were integrated into an outwash system that lies mainly south of the International Boundary and that terminates in a major outwash plain in the vicinity of Island Pond, Vermont (25 km south of the border).

Early Lake Development in Coaticook Valley

In Coaticook valley between Dixville and Stanhope, Quebec, ice contact deposits, kame terraces, and other outwash gravels and some associated ponded silts are found on the valley walls at elevations between 380 and 425 m (Fig. 2). In the same area, the valley bottom contains till, ablation moraine, and alluvium, but no erosional remnants of lacustrine deposits. This is interpreted to indicate that an ice lobe was present in the valley bottom while ice marginal drainage and lacustrine deposits were confined to the valley walls; drainage was southward. Under the same lobe, meltwater flowed southward to form an esker west of Coaticook and a delta at 410 m.

Later Lacustrine and Outwash Systems in Coaticook Valley

Figure 3 shows a hypothetical ice margin position when a moraine was formed at the town of Coaticook. A glacial lake was ponded in Coaticook valley between Coaticook and Dixville and its water level probably stood near 370 m a.s.l. At least part of the drainage of this small water body flowed southwestward across the interfluve between Coaticook and Massawippi valleys, producing deltas at Way Mills and Hatley at elevations near 300 m.

McDonald (1967a) recognized a series of lakes at lower levels in both valleys. These drained southwesterly via progressively lower outlets until the system had expanded westward and occupied the basin of Lac Memphrémagog. This system drained via the Lac Nick outlet (approximately 265 m) into an outwash system in Missisquoi valley. It seems implied by

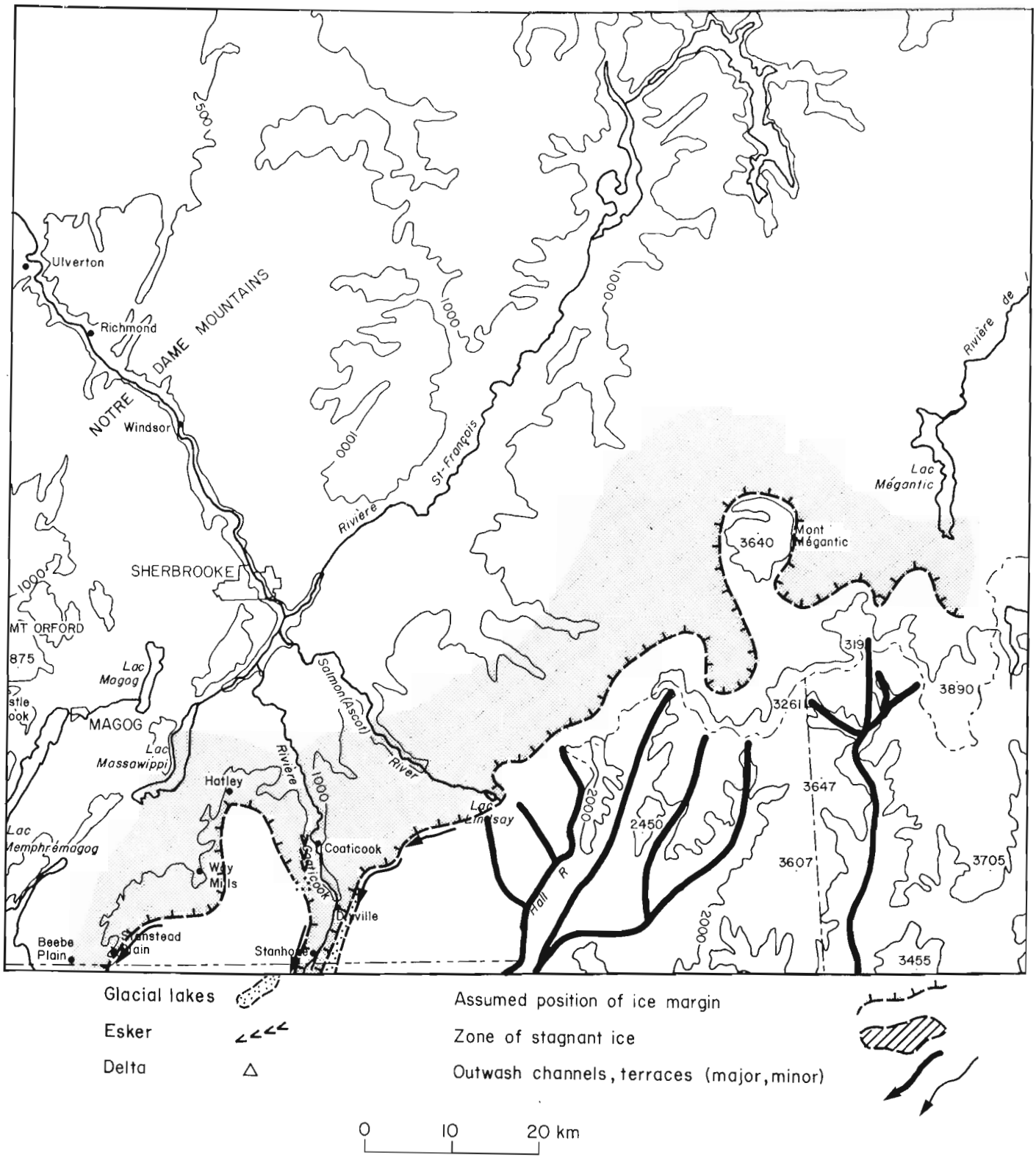

Figure 2. *Early southward drainage, eskers developing beneath ice, hypothetical ice margins.*

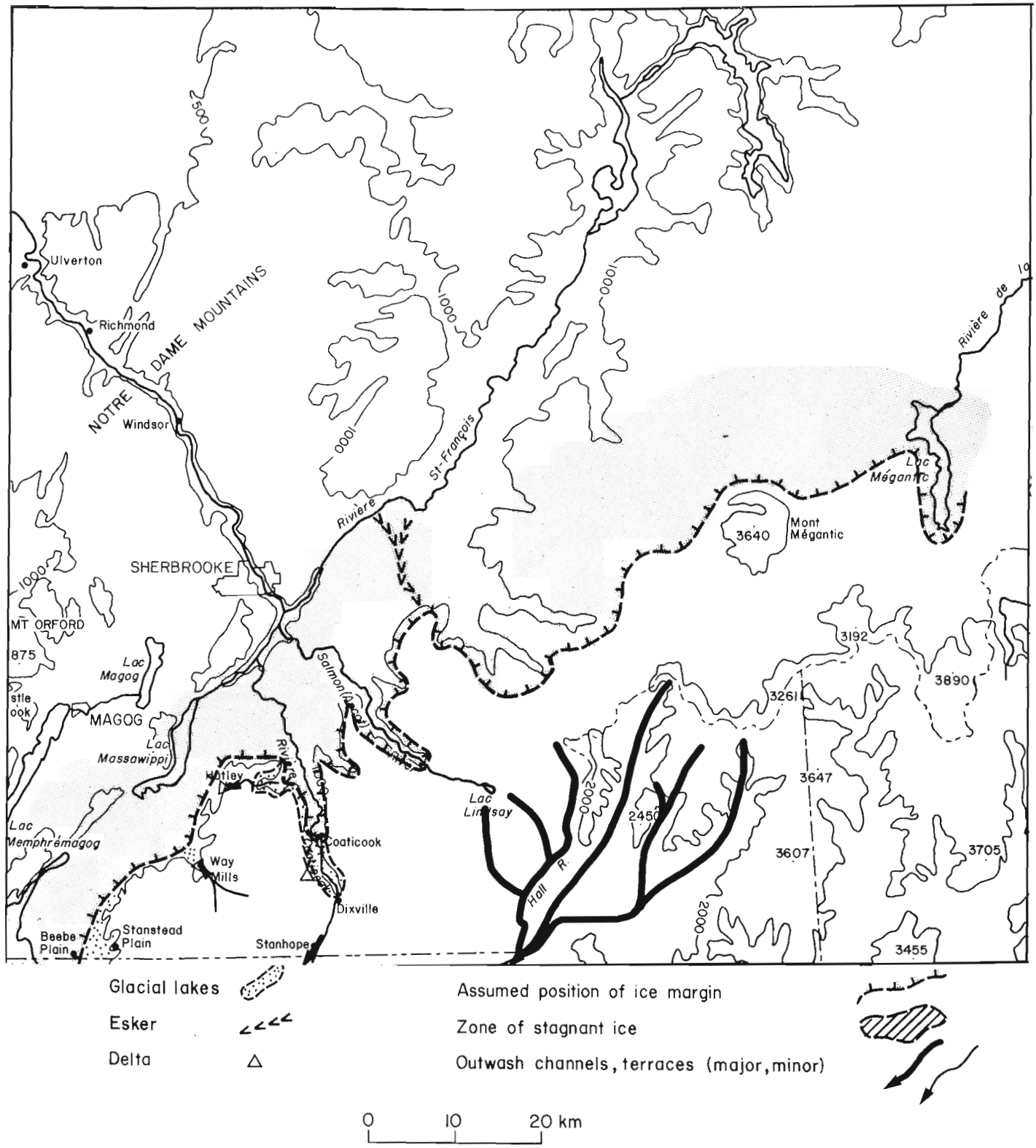

Figure 3. *Hypothetical ice marginal position at Coaticook; drainage southward via Coaticook valley and westward across interfluve to deltas at Hatley and Way Mills.*

McDonald (1967a, p. 110-114) that lake level below the Lac Nick outlet may have drained northward to Champlain Sea mainly via Saint-François valley.

The Coaticook-Saint-François river system presently flows northward to St. Lawrence River. Esker systems, terminating in glacial lakes along Saint-François valley in the vicinity of Richmond and Sherbrooke were part of south-flowing meltwater systems controlled by ice lying north of Sherbrooke and Richmond (e.g. Banerjee and McDonald, 1975, and references therein; Fig. 4). In addition, it has been noted during 1982 reconnaissance surveys that outwash systems at and below 200 m, e.g. terrace gravels at the northern limit of Coaticook, also flowed southward. These latter outwash terraces have been incised in the basins of pre-existing glacial lakes and now rest on older materials such as till and bedrock. This, of course, indicates that drainage control, in the form of ice blocking the valley of Rivière Saint-François in the region north of Sherbrooke and Richmond, continued to exist during the formation of, and following the drainage of, one or more systems of ice marginal lakes in the Saint-François and Memphrémagog basins. These lakes, therefore, drained southward and southwestward to levels near the maximum level of marine submergence, rather than northward into the sea as implied earlier (e.g. Antevs, 1925; McDonald, 1967a).

Contrasting Outwash Systems of Missisquoi and Memphrémagog Valleys

McDonald (1967a, p. 51) noted a "well-developed 'valley train' ... in the upper reaches of the North Missisquoi River". He recognized that the train extended a few kilometres north of Lac d'Argent (at Eastman) but 1982 reconnaissance in areas not mapped by McDonald shows that the valley train heads in the vicinity of Lawrenceville, about 15 km north of the lake (Fig. 4). At and just north of Lawrenceville it is clear that the head of the valley train is associated with parts of the Highland Front morainic system. The gravel-sand outwash system is continuous along Missisquoi valley for some 50 km from Lawrenceville to Mansonville and Highwater (Fig. 4). At Mansonville an early phase of the system consists of an esker interfingering with and partly buried by reddish brown glaciolacustrine silts that occupy a clay plain at 190 m elevation or higher. A delta surface within this system at South-Bolton suggests a water level of about 245 m, at least locally. The lake plain and the delta surface were later incised and outwash was inset in terraces as the lake drained southward and westward via Missisquoi valley (Fig. 5).

In the immediately adjacent Memphrémagog valley, the only outwash feature stemming from ice in highland areas to the north is the esker-outwash complex (Fig. 5) at Rivière Cherry (4 km north of Magog) that is a principal element of the Cherry River Moraine (McDonald, 1967a,b; Gadd et al., 1972). Little if any outwash or lacustrine sediment exists in the entire Lake Memphrémagog basin at <240 m elevation; however, on both sides of the north end of Lac Memphrémagog, ice contact features at 275 m a.s.l., which dip westerly and easterly away from the lake basin, both in the ridge extending north from downtown Magog and at the southeast toe of Mont Orford, show that ice stood in the lake basin. Similarly, near the south end of the lake, at the border towns of Beebe-Plain the Stanstead-Plain, southeasterly dipping ice contact features and lacustrine sediments ponded on their distal side (Fig. 4) at 240-275 m indicate that ice stood in the Memphrémagog basin during their formation.

From this evidence it appears that part of the Cherry River Moraine, as interpreted by McDonald (1967a) and by Gadd et al. (1972), was built at a higher level, and therefore perhaps earlier, than the Cherry River esker-outwash complex by ice standing in Memphrémagog basin (Fig. 4) and not by ice standing on higher ground fringing the north end of the basin. Because deltaic sediments at Rivière Cherry have not been mapped as extending into Lac Memphrémagog basin (McDonald, 1967b), it is assumed here that the basin retained some ice during formation of the Cherry River complex and the glaciofluvial drainage of the Rivière Cherry area was mainly westward into the Missisquoi outwash system (Fig. 5).

Evidence seemingly contradictory to the above interpretation was presented by McDonald (1967a,b). McDonald (1967b) showed glaciolacustrine sediments at the north end of Lac Memphrémagog that might be interpreted as the distal facies of the esker-delta complex at Rivière Cherry. However, in sections along Castle Brook, which flows into the nowthwest tip of Lac Memphrémagog, the indistinctly laminated sandy silt at the surface, probably the material mapped by McDonald as glaciolacustrine, rests on coarse gravel containing tree trunks. Because the wood in one of the logs has been identified as **Tsuga canadensis**, eastern hemlock (GSC Wood Identification Report 82-36 by R.J. Mott), it was first estimated to have a maximum age of 7000-8000 years at this latitude; the wood was subsequently ^{14}C dated at 1940 ± 50 BP (GSC-3531). This clearly indicates that the overlying silts are relatively modern alluvium. Although during fieldwork in 1982 silts and silty sands were observed in several excavations within the area north of Lac Memphrémagog that had been mapped by McDonald (1967b) as glaciolacustrine sediment, there were no exposures of well laminated, varve-like sediments; all may be alluvial.

Outwash and Marine Sequences From Monts Sutton Westward to Granby, Cowansville, and Lac Champlain

A system of ice marginal drainage channels in the area west of Monts Sutton has been identified by Prichonnet et al. (1982) and has been extended over a larger area as a result of my fieldwork.

On the west flank of Monts Sutton at elevations of at least 400-425 m, individual kame deposits with undisturbed planar glaciofluvial gravel and sand beds dipping southeasterly (i.e. into the slope of the mountain), and kame terraces parallel to the slope with stream channel beds and crossbeds indicating flow of meltwater towards south and southwest, are fairly common. The most conspicuous geomorphic form is an esker chain (shown beneath ice cover, Figure 4), whose north end lies about 3 km east of Lac Brome, continues southerly and southeasterly into Bolton Pass and terminates in an outwash fan at 265 m a.s.l. at Étang Sallys. This connects via an outwash valley train to the above-mentioned delta at 245 m at South-Bolton (Fig. 4), which constitutes a part of the Missisquoi valley train of outwash. This occurrence represents an ice margin against the west flank of Monts Sutton at probably greater than 300 m a.s.l. simultaneously with that at Lawrenceville (Fig. 4). It is implied above that at the same time an ice mass was stagnating in the basin of Lac Memphrémagog as well as in the Saint-François valley area designated by McDonald (1967a, Fig. 12) as a "zone of stagnant ice". Below 300 m along the west flank of Monts Sutton, small remnants of fine rhythmite deposits indicate that glacial lakes were ponded against the mountain by ice standing to the northwest, all drainage being directed southerly. One such deposit of varved lake silt on the flank of the mountain slope, about 1.5 km due south of Sutton, is at about 200 m elevation. This occurrence probably is part of a varved silt deposit found at similar elevation in Missisquoi valley near Glen Sutton, Mansonville, and Highwater (Fig. 4). These occurrences may represent a significant glacial lake in Missisquoi valley, e.g. a large ice-marginal basin possibly extending into Lac Champlain basin via Missisquoi valley.

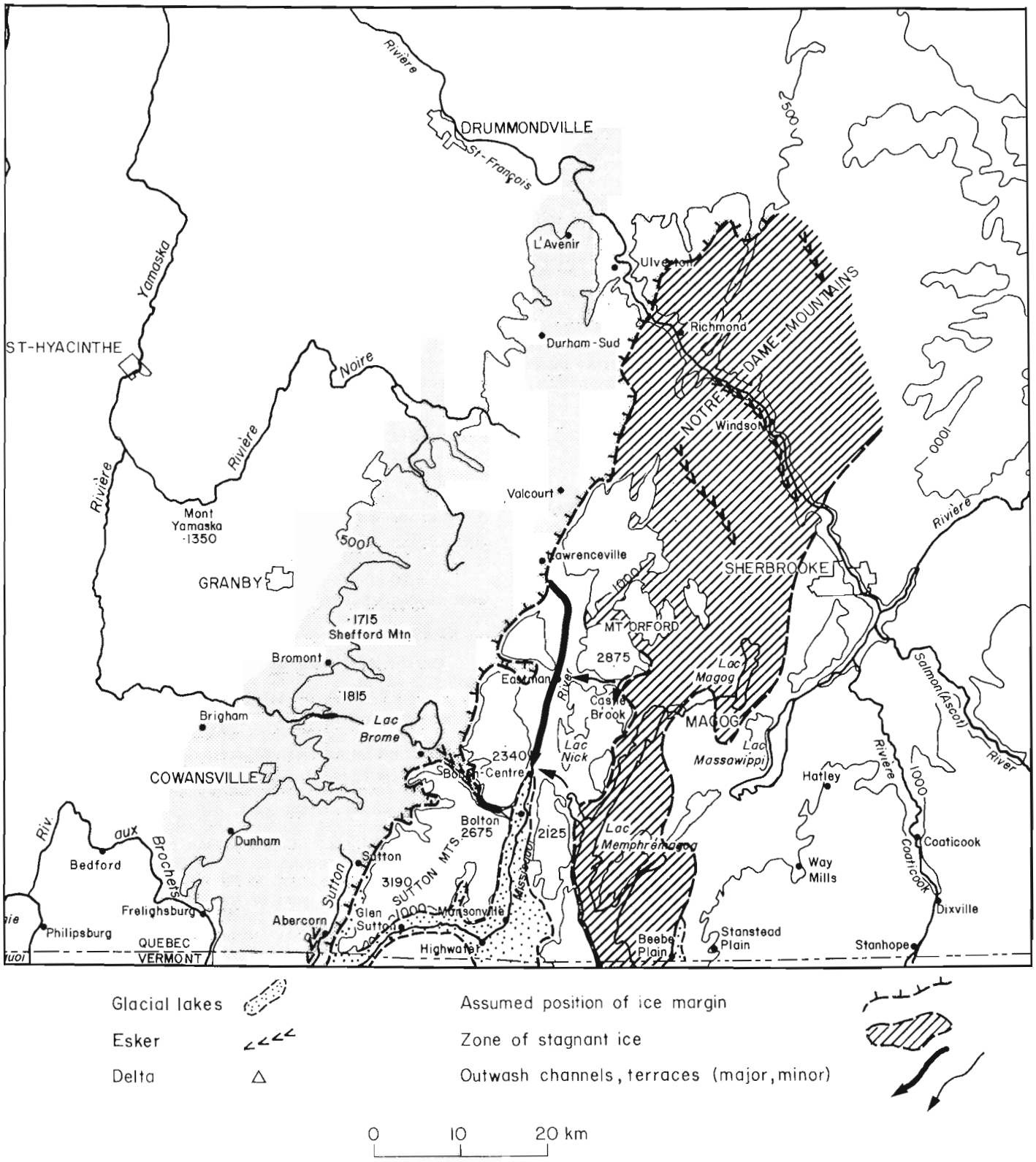

Figure 4. *Initial development of Missisquoi valley outwash and lacustrine systems with major (active?) ice mass on the northwest flank of Sutton – Notre Dame mountain range and stagnant ice masses in Saint-François and Memphrémagog valleys.*

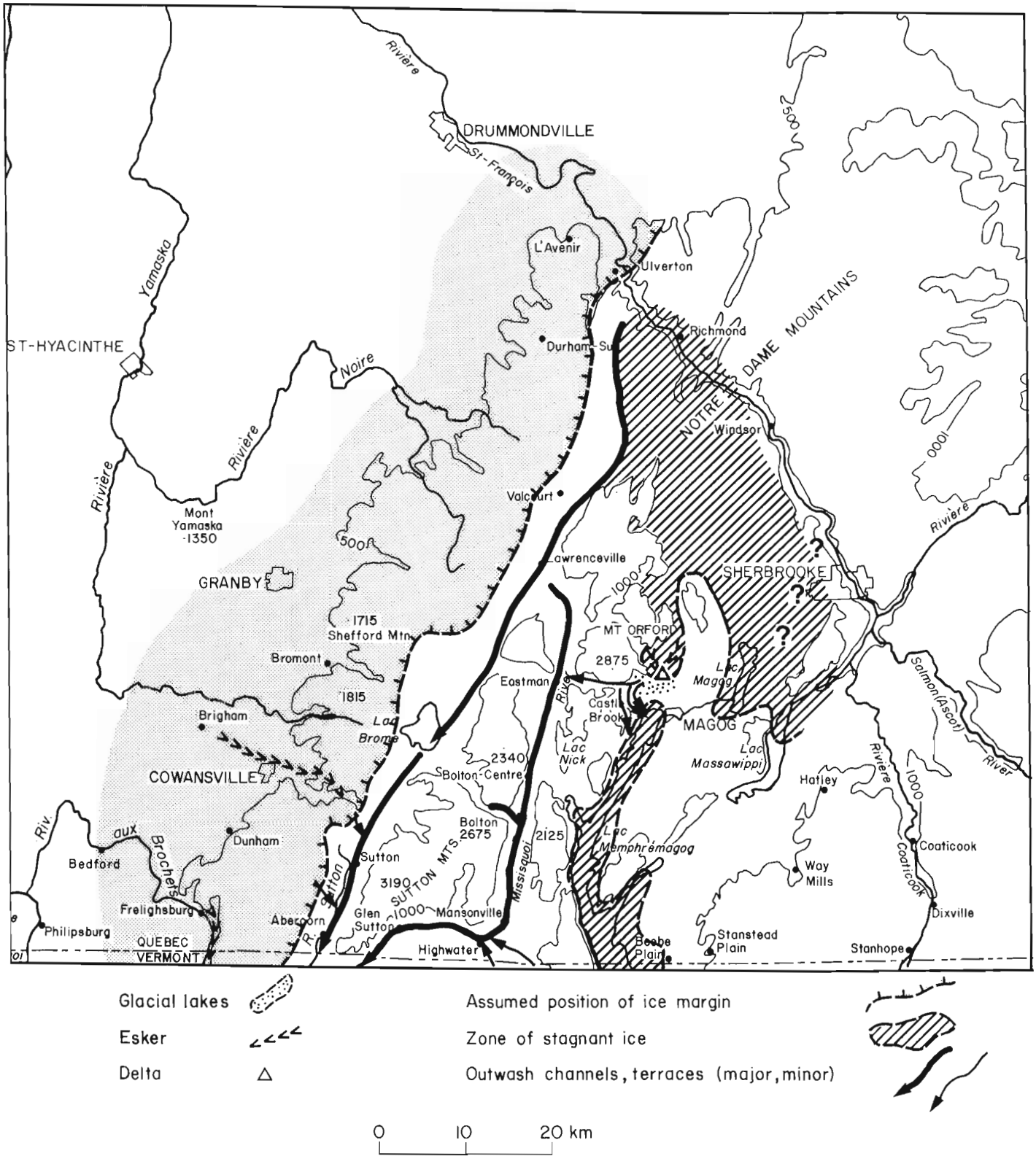

Figure 5. *Later development of Missisquoi valley outwash incised in older lacustrine sediments and confluent with new ice marginal drainage along the northwest margin of the Sutton – Notre Dame mountain range and reduced stagnant ice areas within the highland.*

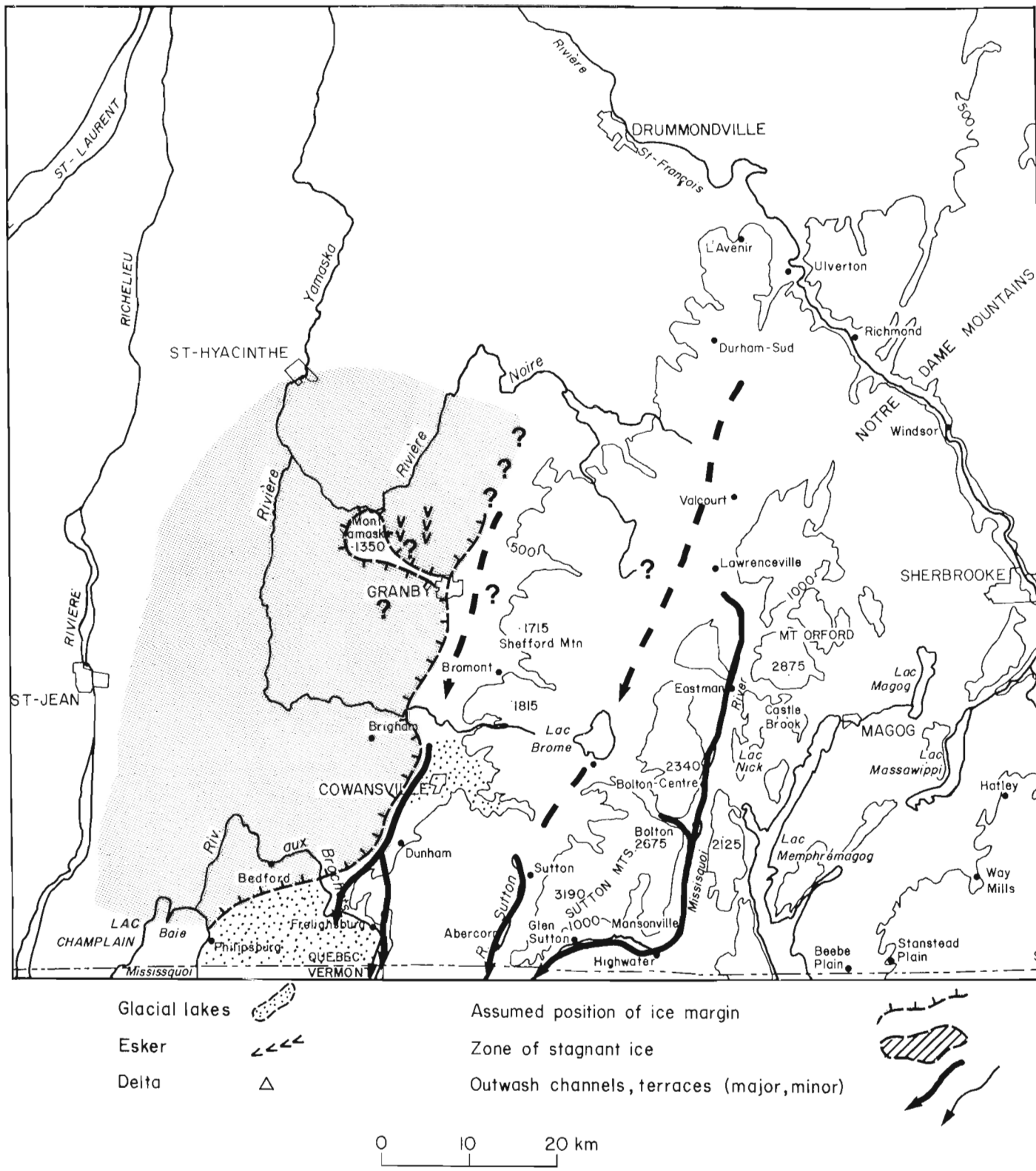

Figure 6. *Ice marginal drainage below 150 m in the vicinity of Mont Yamaska, Cowansville, and Dunham, that is, in areas previously considered to be below marine limit.*

Rivière Sutton, which flows southward to join Missisquoi River in Vermont, occupies a broad valley of considerable significance. An esker extends from Abercorn to and beyond the U.S. border (Fig. 4). Its gravels and sands grade into and interfinger with lacustrine silt. The lacustine silt, in turn, forms a broad plain in Sutton valley that covers most of the esker. The lacustrine plain was later incised, resulting in glaciofluvial terraces that are associated with outwash fans and minor eskers produced by ice along the north and west flanks of Sutton valley; outwash terraces without ice contact features occur at matching elevations on the southeast flank of Sutton valley. Identical conditions occur north of the town of Sutton and have been traced through Lac Brome, Valcourt, and southeast of Durham-Sud to the vicinity of Ulverton in Saint-François valley (Fig. 5). In short, a broad meltwater channel system exists on the southeast flank of what was the original trace of the Highland Front morainic complex (Gadd et al., 1972). This well developed glacial drainage system flowed southwesterly and southerly and appears to have been confluent with glacial lakes in the vicinity of Missisquoi valley.

A similar parallel system occurs farther west in the valley of Rivière aux Brochets. Eskers (shown forming beneath the ice in Figure 5) in the valley south of Frelighsburg are associated with varved lacustrine sediment and south-flowing younger outwash terraces, similar to those described above at Abercorn in Sutton valley. It appears that ice, with its margin more or less parallel to Monts Sutton, retreated towards the northwest, producing eskers beneath the ice and ponding sediments and outwash at the free ice margin. Several subparallel valleys in the area were subject to a similar sequence of events (also noted by Prichonnet et al., 1982).

A series of gravel deposits following one of these former ice margins (Fig. 6) passes through the towns of Dunham, Cowansville, and Granby. Goldthwait (1913, Fig. 10A) described some of these deposits as beaches of the "South shore-line of the Ancient Champlain Sea"; marine limit was given elevations of "516+ feet (157.2 m)" for a feature at Granby and "509 feet (155.2 m)" for one at Dunham. At these localities new exposures in gravel pits show moderately to poorly sorted gravels in stream-channelled and crossbedded structures, as well as ice contact beds, all dipping towards southeast, south, and southwest; high-angle faults around the margins of collapse basin in gravels and sands indicate melt-out of ice blocks from ice contact and outwash sediments. Ice stood to the northwest of these features. No fossils have been found in these localities. It is therefore concluded that the presence of ice contact features in these places not only refutes the earlier interpretation as marine beaches, but also precludes the existence of sea water at those places and elevations.

Eskers and associated lacustrine sediments in deposits parallel to Rivière Yamaska extend from about 4.8 km northwest of Cowansville to the vicinity of the village of Brome-Ouest (Fig. 5). These eskers and kame terraces range from 100 m elevation in the northwest to about 160 m in the southeast. Bedding and crossbedding in these features indicate that the meltwater flowed easterly and southeasterly along the esker chain and interstratification with lacustrine sediments indicates that the esker system was engulfed progressively from southeast towards northwest by expanding lacustrine waters.

Only about 1 km farther west of the apparent beginning of this esker system (1 km southeast of Brigham), uniform grey sand overlies grey calcareous till. The upper surface of the till and about 1 m of overlying sands are fossiliferous at about 95 m a.s.l.; fossils present include **Hiatella** sp., **Macoma** sp., **Balanus** sp., **Mya arenaria,** and **Mya truncata.** The presence of the **Mya** species in the assemblage is characteristic of a middle to late phase of Champlain Sea since they are absent from early phase assemblages. A radiocarbon date of 10 700 ± 100 BP (GSC-3574) was obtained from a sample of these shells and one of 10 300 ± 90 BP (GSC-3539) for a similar deposit 3.2 km northwest of Granby.

Conclusions

Although much remains to be learned and discussed concerning the regional significance of these and other observations, it is possible to draw some tentative conclusions:

1. Re-interpretation of pollen stratigraphy and radiocarbon dates allows consideration of a younger minimum age (about 11 000-12 000 rather than 15 000 BP) for deglaciation of the boundary area of southern Quebec. Open southward-draining systems in northern New England seem more compatible with a younger time-frame.
2. Melt-down of an irregular ice surface with the resultant isolation of large masses and lobes of ice from time to time is a proposed hypothesis more in keeping with new observations, and possible new chronology, than is the former concept of regional retreat of an active ice margin taking place before Champlain Sea time.
3. Ice standing within and on the northwest flank of the Sutton – Notre Dame chain of highlands had two fundamental effects: 1) it confined all drainage between 600 to 150 m into a southerly to southwesterly flow pattern that is opposed in large degree to the modern north-northwest drainage pattern and 2) for some time it prevented the invasion by Champlain Sea of a large area, i.e. much of the area lying between Mont Yamaska, Baie Missisquoi of Lac Champlain, and Monts Sutton, and perhaps more. Marine invasion there took place, apparently, only after a considerable amount of regional isostatic uplift had occurred and after the **Mya** biotic phase of Champlain Sea had developed. These data support the concept of a calving bay mechanism (Gadd, 1980) for submergence of the area.
4. Figures 2 to 6, depict a pattern and a chronological sequence of events in the deglaciation of southeastern Quebec, regardless of the age of those events.

Acknowledgments

Thanks are extended to R.J. Fulton and D.R. Sharpe for their comments on this report.

References

Antevs, A.
1925: Retreat of the last ice sheet in Eastern Canada; Geological Survey of Canada, Memoir 146.

Banerjee, I. and McDonald, B.C.
1975: Nature of esker sedimentation; in Glaciofluvial and Glaciolacustrine Sedimentation, ed. A.V. Jopling and B.C. McDonald; Society of Economic Paleontologists and Mineralogists, Special Publication 23, p. 132-154.

Gadd, N.R.
1980: Late-glacial regional ice-flow patterns in eastern Ontario; Canadian Journal of Earth Sciences, v. 17, no. 11, p. 1439-1453.

Gadd, N.R., McDonald, B.C., and Shilts, W.W.
1972: Deglaciation of southern Quebec; Geological Survey of Canada, Paper 71-47; Map 10-1971.

Goldthwait, J.W.
1913: The upper marine limit at Montreal; in Excursions in the Neighbourhood of Montreal and Ottawa; Geological Survey of Canada, Guide Book No. 3, p. 117-122.

McDonald, B.C.
1967a: Pleistocene events and chronology in the Appalachian region of southeastern Quebec, Canada; unpublished Ph.D. dissertation, Department of Geology, Yale University, 161 p.

1967b: Surficial geology, Sherbrooke-Orford-Memphrémagog, Quebec; Geological Survey of Canada, Map 5-1966.

Mott, R.J.
1977: Late Pleistocene and Holocene palynology in southeastern Quebec; Géographie physique et Quaternaire, vol. XXXI, n° 1-2, p. 139-149.

Prichonnet, G., Doiron, A., et Cloutier, M.
1982: Le mode de retrait glaciaire tardi-Wisconsinien sur la bordure Appalachienne au sud du Québec; Géographie physique et Quaternaire, vol. XXXVI, n° 1-2, p. 125-137.

Shilts, W.W.
1981: Surficial geology of the Lac Mégantic area, Québec; Geological Survey of Canada, Memoir 397.

A NEW PROCEDURE FOR EXTRACTING FORAMINIFERA FROM INDURATED ORGANIC SHALE

Project 500029

D.R. Then and B.J. Dougherty
Institute of Sedimentary and Petroleum Geology, Calgary

Then, D.R. and Dougherty, B.J., A new procedure for extracting foraminifera from indurated organic shale; in Current Research, Part B, Geological Survey of Canada, Paper 83-1B, p. 413-414, 1983.

Abstract

A time saving method for extracting foraminifera from indurated organic shale is described. Organic material contained in indurated shale may be effectively oxidized by successive application of hydrogen peroxide (H_2O_2) and bleach (NaC1O), leading to rapid sample disaggregation and increased efficiency in recovery of foraminifers.

Résumé

Le présent rapport décrit une méthode rapide d'extraire les foraminifères des schistes argileux durcis. Il est possible d'oxyder le matériel organique contenu dans les schistes argileux durcis grâce à des applications successives de peroxyde d'hydrogène (H_2O_2) et de décolorant (NaC1O), ce qui mène à la désagrégation rapide de l'échantillon et à une récupération plus efficace des formainifères.

Introduction

The recovery of microfossils is often hampered by difficulties in disaggregating indurated samples. Duffield and Warshauer (1979) proposed a method of breaking down indurated shale containing organic matter by prolonged immersion in a bleach and base solution. This method is effective, but requires weeks for sample disintegration. A modification of the bleach treatment described below, makes it possible to process numerous samples in a relatively short time.

Procedure

1. One hundred and fifty grams of crushed sample is dry sieved through a 10 mesh (2000 micron) screen. The sieved sample is then placed in a glass beaker and barely covered with 30 per cent hydrogen peroxide (H_2O_2). Effervescence is usually evident in a matter of seconds. The sample should be closely monitored, and water added to dampen any violent reactions. Once the reaction is under control, it is allowed to continue for approximately one hour, or until bubbling is no longer evident.
2. The sample is wet sieved with a 200 mesh (75 micron) screen, placed in a beaker, and covered with 300 mL of a 50 per cent solution of water and standard household bleach (active ingredient NaC1O, 5-6%). A 0.3M solution of base (10 g NaOH pellets to 750 mL H_2O) should be substituted for the water when working with highly indurated material. The beaker is placed on an oscillating hot plate for one to two hours. Oxidation of organic material will produce a colour change from grey-brown to yellow.
3. The sample is wet sieved, placed in a beaker with 20 mL of stock Quaternary O and 300 mL of water (Quaternary O stock is approximately a 5 % solution). After soaking for a few hours, overnight if possible, the samples are oscillated for one to two hours, then wet sieved. Most samples are sufficiently disaggregated to allow picking at this stage. More resistent samples are treated with bleach-base and Quaternary O a second time to enhance disaggregation.

Reactions

Hydrogen peroxide is a strong oxidizing agent which penetrates the rock matrix and initiates the oxidation of organic compounds. This reagent causes chemical and physical disintegration of the rock. Bleach is also a strong oxidizing agent that facilitates the disaggregation of the rock by destroying the organic material. Base may be added to enhance the effectiveness of the bleach. The application of hydrogen peroxide and bleach is essential for sample breakdown. Without initial penetration of hydrogen peroxide, the bleach will oxidize only the surface of the sample.

Removal of clastic material is facilitated by the use of Quaternary O, a wetting agent that penetrates the matrix and disperses clastic particles so that they are in suspension and can easily pass through the sieve (Zingula, 1968).

Volume reduction of the sample after the use of Quaternary O, and colour change during bleach treatment, are the two physical changes that result from the reactions.

Controls

Comparative tests were run on fractions of a shale sample from the Upper Cretaceous Wapiabi Formation, collected from the quarry at Seebe in the southern Alberta Foothills (GSC loc. C-60380). All possible combinations of

Table 1

Test breakdown of samples using various reagents and combinations (GSC Loc. C-60380)

Test No.	Reagent(s) used on each test	Weight (grams) of original sample	Weight (grams) after treatment
1.	Quaternary O	150	62
2.	Hydrogen Peroxide (H_2O_2)	150	123
3.	Bleach/Base	150	122
4.	H_2O_2 and Quaternary O	150	57
5.	Bleach/Base and Quaternary O	150	63
6.	H_2O_2 and Bleach/Base	150	129
7.	H_2O_2, Bleach/Base and Quaternary O	150	3

the reagents were tested and equal oscillation time was allotted for each run. It was found that breakdown was greatly increased when all three reagents were used and all steps of the procedure outlined above were followed (see Table 1).

The residues of the test samples, with the exception of test run 7, all had large fragments of sample which had not been broken down. Material from test run 7 was granular in appearance and was totally disaggregated, with no large fragments remaining, dramatically increasing the chance of fossil recovery. Time at the microscope is reduced by having a small sample to pick.

To assess the possibility of excess damage to foraminifers caused by our procedure, tests were run on richly fossiliferous samples from the Upper Cretaceous Kemp and Corsicana Clays of Texas. Specimens obtained by the standard method (Zingula, 1968) were compared with those obtained by the modified bleach method described above. No appreciable differences in preservation were observed.

Safety

All work should be done in a fumehood, or a well ventilated area, as any sample containing sulfides will produce noxious fumes when bleach is used (Merrill, 1980). Rubber gloves and a face shield are strongly recommended when handling peroxide and NaOH to prevent severe burns that may result from exposure.

References

Duffield, S. and Warshauer, S.M.
1979: Two-step process for extraction of microfossils from indurated organic shales; Journal of Paleontology, v. 53, no. 3, p. 746-747.

Merrill, G.K.
1980: Removal of pyrite from microfossil samples by means of sodium hypochlorite; Journal of Paleontology, v. 54, no. 3, p. 633-634.

Zingula, R.P.
1968: A new breakthrough in sample washing; Journal of Paleontology, v. 42, p. 1092.

RELICT ICEBERG SCOURS, KING WILLIAM ISLAND, NORTHWEST TERRITORIES

Project 810044

R.G. Hélie
Terrain Sciences Division

Hélie, R.G., Relict iceberg scours, King William Island, Northwest Territories; in Current Research, Part B, Geological Survey of Canada, Paper 83-1B, p. 415-418, 1983.

Abstract

Emerged relict iceberg scours occur on King William Island, Northwest Territories. These long, shallow troughs are similar to those found in the Lake Agassiz basin, and they represent the presence of a body of water adjacent to a calving ice front.

Résumé

Des marques résiduelles émergées de creusement par les icebergs ont été trouvées dans l'île Roi-Guillaume (T.N.-O.). Ces auges longues et peu profondes ressemblent à celles qui ont été trouvées dans le bassin du lac Agassiz et indiquent la présence d'une masse d'eau adjacente à un front glaciaire vêlant.

Introduction

In recent years, numerous example of ice scouring in the Beaufort Sea (Pelletier and Shearer, 1972; Shearer and Blasco, 1975; Wahlgren, 1979) and in the northwest Atlantic (Balderson et al., 1973) have been described. The origin of the long, sometimes curved and intersecting lineaments has been attributed to iceberg or pressure ridge keels ploughing the seafloor. Photographic documentation on the morphology of ice scours on the seafloor was obtained by McLaren (1975). His work provided additional information on these features; previously, only sonar images were available.

The floating ice origin of similar lineations on land was first suggested by Webber (1958) for features in the Great Slave Lake area, Northwest Territories. Clayton et al. (1965) suggested a similar origin for lineations in the Lake Agassiz basin. Recent analysis of lineations in the northern part of glacial Lake Agassiz by Dredge (1982) has confirmed the floating ice origin.

King William Island Ice Scours

King William Island is located in the Victoria Lowland of Bostock (1967), between Boothia Peninsula and Victoria Island (Fig. 1). The ice scours on King William Island are similar in size and morphology to those in the Lake Agassiz basin (Dredge, 1982). The greatest concentration of ice scours is located in the coastal area west of Gjoa Haven (Fig. 2). The scours are mostly in thick marine silts but also cut across minor till hummocks. Isolated scours can also be found elsewhere on the island and on Adelaide Peninsula to the south (Fig. 3).

The ice scours are from a few metres to a few tens of metres wide and generally a few hundred metres long, although some large scours reach lengths of 5 km. They show no particular orientation, many are slightly curved, and many cross (Fig. 2). Although the scours are conspicuous on aerial photographs, they are difficult to recognize on the ground because of their low relief: most scours are no more than 1 to 3 m deep. From the air they appear as long straight bands of poorly drained, well vegetated ground, containing ovoid and rectangular ponds (Fig. 4).

Ice scours can be formed in two ways: by erosion by sea ice pressure ridges or by iceberg keels. In the first case, the ice scours would be expected to occur as belts of parallel or subparallel lineations, at more or less right angles to the existing coastline. Such scour marks would be of moderate width and length because pressure ridges attain vertical development of only a few metres. Scours formed by single icerbergs, as is the case in the study area, would not necessarily show any particular orientation, and the single tracks formed by the different icebergs at different times would be expected to intersect. Furthermore, an individual track could curve as a partially grounded iceberg responded to wind action or other factors. The width and length of the ice scour produced by an iceberg can reach great dimensions, since these parameters are controlled only by the size of the iceberg keel and slope of the bottom. The presence of icebergs in any abundance demands the presence of a calving ice front nearby. Very few icebergs penetrate this area today because most Greenland and Canadian icebergs exit to the North Atlantic via Baffin Bay. Pressure ridge fragments are common today in the Arctic, but relict scours formed this way have not been recognized perhaps because their limited size inhibits their preservation. Iceberg scours are deeper and larger so that they survive most subaerial surface processes.

The first aerial reconnaissance of King Willaim Island was carried out by Fortier (1948). Although his flight plan took him over the scour field, he did not recognize the long, shallow lineations. Fraser and Henoch (1954), in discussing the surficial materials and glacial history of King Willaim Island, described and mapped the lineations, referring to them as "trenches"; they interpreted the relict ice scours as the surface expression of linear bedrock joints – the same conclusion reached by Mollard (1957) and Elson (1961) for glacial Lake Agassiz basin – and mapped them as such. During later mapping of King William Island, Craig (1964) made no mention of the iceberg scours.

Discussion

Only two large fields of emerged iceberg scours have been identified in Canada – in the Lake Agassiz basin and on the south coast of King William Island. Dredge (1982) indicated the proximity of calving Keewatin ice and Hudsonian ice in glacial Lake Agassiz to the north and east, respectively. On King William Island, the calving M'Clintock ice model suggested by Dyke (in press), is supported by the

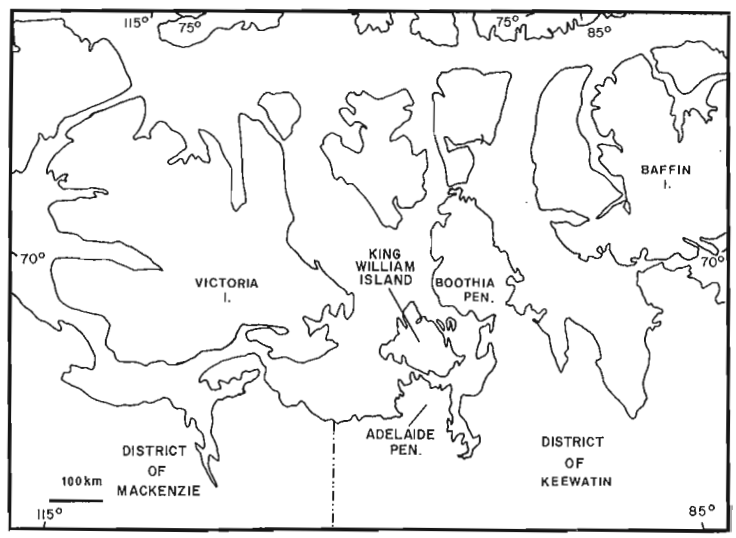

Figure 1. *Location map showing King William Island and Adelaide Peninsula.*

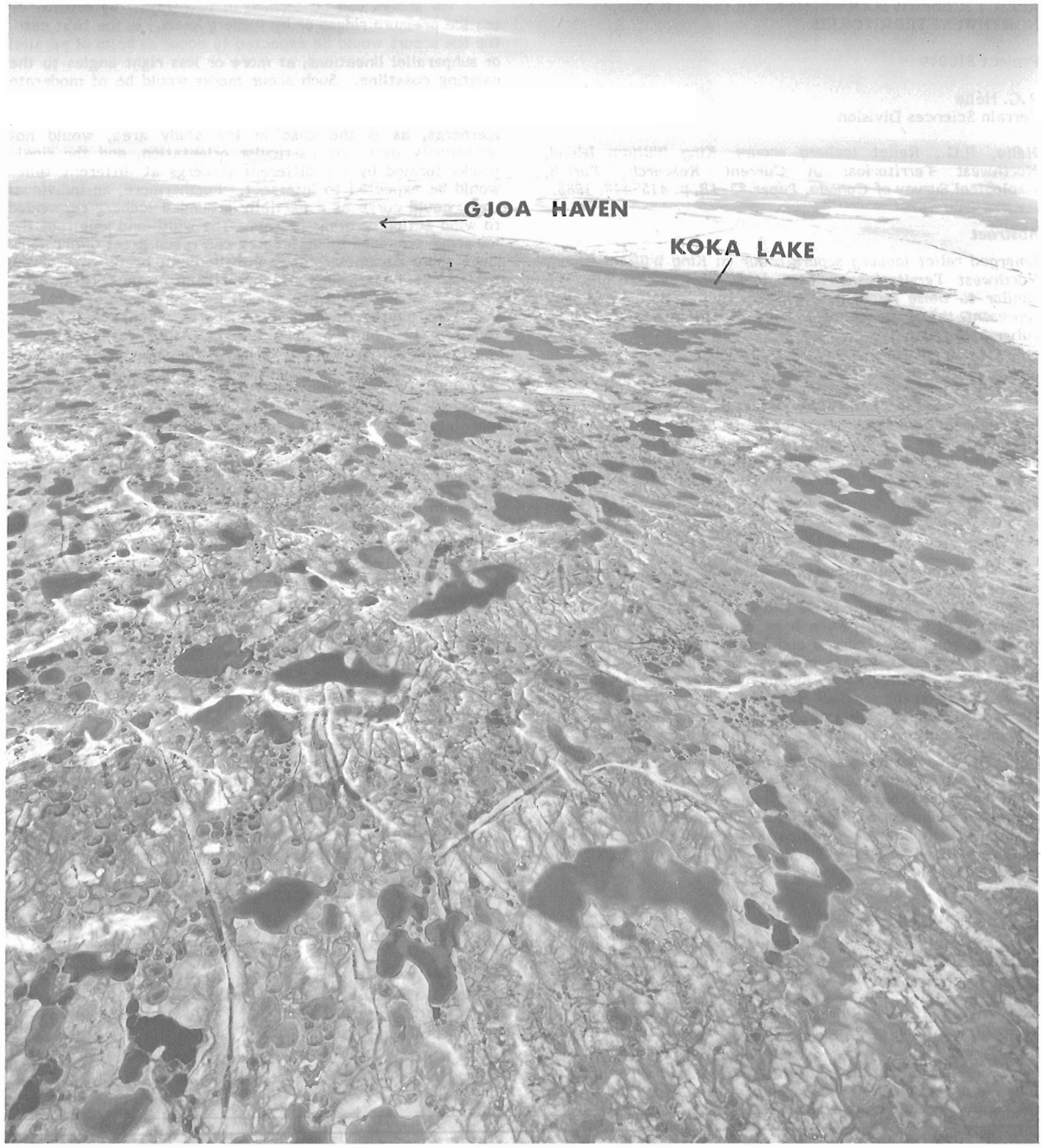

Figure 2. *Aerial photograph looking east across the south coast of King William Island, showing the large iceberg scour field west of Gjoa Haven (cf. Fig. 3). Many scour marks are curved and intersect each other. Note the esker trending across the photograph. (NAPL T434L-205)*

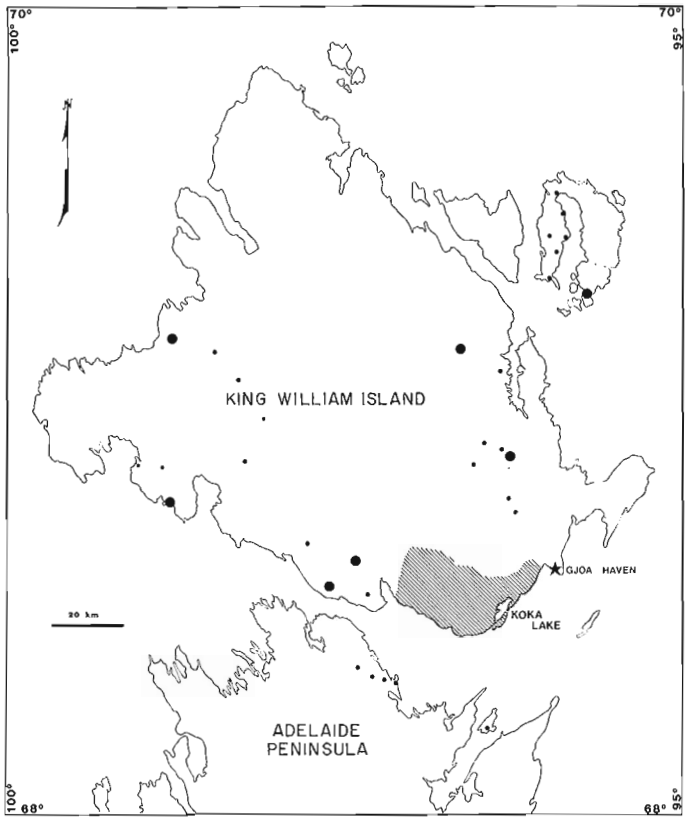

Figure 3. *Distribution of relict iceberg scours on King William Island and northern Adelaide Peninsula. Small dots indicate the location of less than four scour marks, large dots indicate clusters of more than four scour marks. Shaded area corresponds to the large iceberg scour field west of Gjoa Haven.*

presence or iceberg scours on the south coast of King William Island. King William Island was deglaciated between 8800 and 8600 years ago, based on dated ice margins on Boothia Peninsula and northern District of Keewatin (Dyke, in press). At that time, the sea in Rasmussen Lowland (northernmost District of Keewatin), about 100 km east of King William Island, was approximately 180 m higher than at present. The sea over King William Island during deglaciation probably was between 150 m and 200 m above present level. Since the large iceberg scour field lies at about 30 m above sea level, and assuming that this corresponds to the maximum depth reached by the majority of icebergs, we can estimate the thickness of the icebergs. Nine-tenths of the iceberg thickness would correspond to the depth of water – 120 m if the more conservative value for sea level during deglaciation is used. Thus the total thickness the scouring iceberg would be 132 m, which also estimates the thickness of the ice at the front of the calving ice sheet.

Conclusion

Ice scours are well known from the present marine environment; however, emerged relict scours are known only from the glacial Lake Agassiz basin and the south coast of King William Island. These iceberg scour fields indicate a water body adjacent to a calving ice front.

Figure 4. *Low level oblique aerial photograph, showing a single iceberg scour. The poor drainage of this broad, very shallow trough makes it conspicuous from the air. Koka Lake is in the background, near the coast. (GSC 203846-D)*

References

Balderson, R.H., Kenyon, N.H., and Wilson, J.B.
1973: Iceberg plough marks in the northwest Atlantic; Palaeogeography, Palaeoclimatology, Palaeoecology, v. 13, p. 215-224.

Bostock, H.S.
1967: Physiographic regions of Canada; Geological Survey of Canada, Map 1254A.

Clayton, L., Laird, W.M., Klassen, R.W., and Kupsch, W.D.
1965: Intersecting minor lineations on Lake Agassiz plain; Journal of Geology, v. 73, p. 652-656.

Craig, B.G.
1964: Surficial geology of Boothia Peninsula and Somerset, King William, and Prince of Wales Islands, District of Franklin; Geological Survey of Canada, Paper 64-44, 10 p.

Dredge, L.A.
1982: Relict ice-scour marks and late phases of Lake Agassiz in northernmost Manitoba; Canadian Journal of Earth Sciences, v. 19, p. 1079-1087.

Dyke, A.S.
– Quaternary geology of Boothia Peninsula and northern District of Keewatin; Geological Survey of Canada, Memoir 407. (in press)

Elson, J.A.
1961: Soils of the Lake Agassiz region; in Soils in Canada, ed. R.F. Legget; Royal Society of Canada, Special Publication 3, p. 51-79.

Fortier, Y.O.
1948: Flights in 1947 over the region of the north magnetic pole and the mainland between the Arctic coast, Great Slave Lake, and Hudson Bay, Northwest Territories; Geological Survey of Canada, Paper 48-23.

Fraser, J.K. and Henoch, W.E.S.
1959: Notes on the glaciation of King William Island and Adelaide Peninsula, Northwest Territories; Geographical Branch, Canada Department of Mines and Technical Surveys, Geographical Paper 22, 39 p.

McLaren, P.
1975: Under-ice diving observation in the coastal environments of southeastern Melville and western Byam Martin Islands; in Current Research, Part A, Geological Survey of Canada, Paper 75-1A, p. 475-477.

Mollard, J.D.
1957: A study of aerial mosaics in southern Saskatchewan and Manitoba; Oil in Canada, v. 9, no. 40, p. 26-50.

Pelletier, B.R. and Shearer, J.M.
1972: Seabottom scouring in the Beaufort Sea of the Arctic Ocean; 24th International Geological Congress (Montréal), Section 8, p. 251-261.

Shearer, J.M. and Blasco, S.M.
1975: Further observations on the scouring phenomena in the Beaufort Sea; in Current Research, Part A, Geological Survey of Canada, Paper 75-1A, p. 483-493.

Wahlgren, R.V.
1979: Ice-scour tracks in eastern Mackenzie Bay and north of Pullen Island, Beaufort Sea; in Current Research, Part B, Geological Survey of Canada, Paper 79-1B, p. 51-62.

Webber, J.N.
1958: Recent grooving in the lake bottom sediments at Great Slave Lake, Northwest Territories; Journal of Sedimentary Petrology, v. 28, p. 333-341.

FOURFOLD SIGNIFICANCE OF AN EARLY SILURIAN U-Pb ZIRCON AGE FROM RHYOLITE IN REDBEDS, SOUTHWEST NEWFOUNDLAND

Project 760027

F.W. Chandler and G.R. Dunning[1]
Precambrian Geology Division

Chandler, F.W. and Dunning, G.R., Fourfold significance of an early Silurian U-Pb zircon age from rhyolite in redbeds, southwest Newfoundland; in Current Research, Part B, Geological Survey of Canada, Paper 83-1B, p. 419-421, 1983.

Abstract

$^{207}Pb/^{206}Pb$ dating of zircons from a rhyolite flow in redbeds in southwest Newfoundland yielded a preliminary age of 431 ± 5 Ma. The age, besides dating the redbeds, establishes that they are about 55 Ma older than a closely associated grey sedimentary sequence and should not be correlated with the Billiards Brook Formation and the Windsor Point Group that lie to the southwest. Because it has close lithological similarity with the redbeds, the Springdale Group to the northeast may also be of early Silurian age. The Annieopsquotch ophiolite, unconformably overlain by the redbeds, was emplaced before the extrusion of the dated rhyolite.

Résumé

La datation au Pb^{207} et Pb^{206} de zircons provenant d'une coulée de rhyolite dans des couches rouges du sud-ouest de Terre-Neuve donne un âge préliminaire de 431 ± 5 millions d'années. En plus de dater les couches rouges, l'âge indique que la formation de ces couches a eu lieu environ 55 millions d'années avant celle d'une séquence sédimentaire grise à laquelle elles sont étroitement associées, et qu'il ne faut pas les mettre en corrélation avec la formation de Billiards Brook et le groupe de Windsor Point, gisant au sud-ouest. Puisque sa lithologie s'apparente beaucoup à celle des couches rouges, le groupe de Springdale, au nord-est, pourrait également dater du Silurien ancien. Les ophiolites Annieopsquotch, recouvertes en discordance par les couches rouges, ont été mises en place avant l'extrusion de la rhyolite en question.

Zircons separated from a flow-banded quartz-feldsparphyric rhyolite flow that lies within redbeds near the northern boundary of the King George IV Lake area (NTS 12A/4; see Fig. 1) were analyzed by G.R. Dunning in T. Krogh's laboratory at the Royal Ontario Museum, Toronto. Abraded and unabraded fractions have identical $^{207}Pb/^{206}Pb$ ages indicating that grains are a single age population with no evidence of older cores. A preliminary age of 431 ± 5 Ma was determined, based on projection of the discordia line through a lower intercept of 50 ± 50 Ma.

The significance of the age is fourfold. First, it settles the question of the age of the redbeds; second, it resolves the problem of their local stratigraphic correlation; third, it suggests the age of the possibly correlative Springdale Group, a major undated redbed sequence that lies to the northeast; and fourth, it sets an upper limit on the timing of emplacement of an Ordovician ophiolite, the Annieopsquotch Complex.

The redbeds themselves are unfossiliferous, but are part of sequence of basalt and rhyolite-bearing redbeds and grey sediments that occupies a narrow southwest-striking belt in the King George IV Lake map area (Chandler, 1982; Kean and Jayasinghe, 1981a, b). Riley (1957) compared the sequence with the Baie du Nord Group that had been mapped as Devonian. De Grace (1974) noted a "pronounced resemblance" with Carboniferous sandstones elsewhere in Newfoundland, an assessment quoted by Herd and Dunning (1979, p. 308). Kean and Jayasinghe (1981a) considered them Devonian or older, also noting an earlier report of early Devonian plant fossils in grey shale in the sequence. Dunning and Herd (1980, p. 230) suggested a Silurian age for the redbeds, drawing attention to the similarity between the redbeds and strata to the northeast, the undated Springdale Group, and to redbeds in the Botwood Group which contain Silurian fossils. The new data establish the age of the redbeds as early Silurian.

The unmetamorphosed, commonly steeply dipping, but otherwise little deformed, strata of the King George IV Lake area strike into a strongly deformed, metamorphosed sequence to the southwest in the LaPoile River area (NTS 11 0/16). Chorlton (1980, p. 32), noting an earlier record of Devonian plant fossils in strata at Billiards Brook, assumed that the sequence there was Devonian. Wilton (in press) obtained a Rb-Sr whole-rock isochron date of 377 ± 21 Ma for a rhyolitic ignimbrite of the Windsor Point Group, the presumed along-strike equivalent of the Billiards Brook Formation to the southwest, confirming its Devonian age. Citing the recovery of Devonian fossils from grey beds in the King George IV Lake area, Chorlton and Dingwell (1981, p. 64) correlated the sequences in the Billiards Brook and King George IV Lake areas, strongly implying a Devonian age for the entire sequence at King George IV Lake.

Chandler (1982) mapped the sedimentary sequence in the King George IV Lake area in detail, concluding that it consisted of two different parts. A grey sequence, devoid of volcanic rocks except in the form of sedimentary clasts, consists of grey conglomerate and interbedded grey sandstone and black shale. The sequence overlies a feldsparphyric granite that is mantled by a grey regolith. The grey sandstone and shale, interpreted by Chandler (1982) as deposited under a meandering fluvial regime, are the rocks bearing the Devonian plant fossils mentioned above.

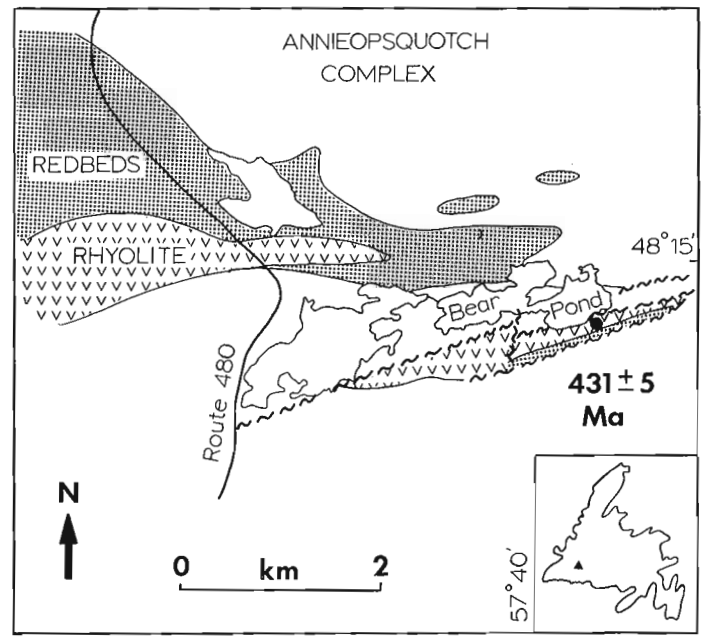

Figure 1. *Location of Silurian redbeds after Kean and Jayasinghe (1981b) and Dunning and Herd (1980) and dated rhyolite sample at "Bear Pond" (informal name).*

[1]Department of Earth Sciences, Memorial University of Newfoundland, St. John's, Newfoundland, A1B 3X5

The second part of Chandler's (1982) sequence, red conglomerate and finer grained clastics with intercalated felsic and mafic volcanic rocks, unconformably overlies the unweathered Ordovician Annieopsquotch Complex. Also two outliers of red basal conglomerate outcrop on the ophiolite. At location 29 of Chandler (1982) the grey and red sequences appear to be conformable, but close inspection shows that the two face in opposite directions. Because of the lack of separation of the finer sediments into in-channel and overbank facies Chandler (1982) interpreted the red sequence to reflect a different, braided fluvial to alluvial-fan sedimentary regime of dry climate and/or of pre-Devonian age. The new zircon age vindicates the suggestion that there are two sequences of significantly different age in the King George IV Lake area. Although the grey sequence may be correlative with Chorlton's (1979, 1980) Windsor Point Group, i.e. Billiards Brook Formation, the redbeds certainly are not and are about 50 Ma older.

The Springdale Group is a sequence of redbeds with felsic volcanic rocks interlayered in its lower part that lies about 200 km to the northeast near Hall's Bay (Kean, 1981). Espenshade (1937) noting a similarity with a ?Silurian conglomerate, the Goldson Formation, gave it a Silurian age. Twenhofel (1947) thought the group to be Devonian or perhaps Mississippian and correlated it with a sequence to the east known as the Botwood Group. Williams (1963) and Neale and Nash (1963) cited William's discovery of Silurian fossils in the Botwood Group and again suggested a Silurian age for the Springdale Group.

As noted above, Dunning and Herd (1980) noted a similarity between the redbeds of King George IV Lake area and redbeds of the Botwood Group. The similarity is more marked between the redbeds at King George IV Lake and the rhyolite-bearing lower part of the Springdale Group. Admittedly these lithological comparisons are no better than some used above to assign an age to the Springdale Group, but they are no worse, and the early Silurian age of the rhyolite at King George IV Lake area can be said to support a Silurian age for the Springdale Group. It should be added that zircons separated from a rhyolite collected by F.W. Chandler in the Springdale Group near the village of Springdale are with the geochronology laboratory of the Geological Survey of Canada in Ottawa.

Formation of the Bay of Islands ophiolite complex of the west coast of Newfoundland has been dated by the U-Pb (zircon) method by Dunning and Krogh (1983) at 485.7 + 1.9, -1.2 Ma. According to Rodgers (1965) and Stevens (1970), the complex was overlain after obduction by the middle Caradocian Long Point Formation (Fahraeus, 1973). Taking the number 445 Ma as representative of the middle of the Caradocian (van Eysinga, 1975) yields an interval of 40 Ma between formation of the complex and its final emplacement.

The Annieopsquotch Complex (Dunning and Herd, 1980) 80 km to the southeast (NTS 12A/5) was also dated by Dunning and Krogh (1983) at 477.5 + 1.3, -1.0 Ma and 481.4 + 4.0, -1.9 Ma. A maximum period of about 48 Ma is indicated between formation of the ophiolite and deposition of the unconformably overlying rhyolite-bearing redbeds at 431 Ma. This is an interval similar to that cited above for the Bay of Islands complex.

Thanks are due to R.K. Herd and T. Krogh for constructive discussion, and to Bohdan Podstawskyj of the Geochronology Laboratory, Royal Ontario Museum, for technical assistance.

References

Chandler, F.W.
1982: Sedimentology of two Middle Paleozoic terrestrial sequences, King George IV Lake area, Newfoundland, and some comments on regional paleoclimate; in Current Research, Part A, Geological Survey of Canada, Paper 82-1A, p. 213-219.

Chorlton, L.B.
1979: La Poile River map area (110/16), Newfoundland; in Report and Activities for 1978, Newfoundland, Department of Mines and Energy, Mineral Development Division, Report 79-1, p. 43-53.

1980: Geology of the La Poile River Area (110/16), Newfoundland; Newfoundland Department of Mines and Energy, Mineral Development Division, Report 80-3, 86 p.

Chorlton, L.B. and Dingwell, D.B.
1981: Grandys Lake (110/15), Newfoundland; in Current Research, Newfoundland Department of Mines and Energy, Mineral Development Division, Report 81-1, p. 57-69.

De Grace, J.R.
1974: Notes on the geology of the King George IV Lake area, southwest central Newfoundland; in Report of Activities, 1973, Newfoundland Department of Mines and Energy, Mineral Development Division, Report 74-1, p. 43-49.

Dunning, G.R. and Herd, R.K.
1980: The Annieopsquotch ophiolite complex, southwest Newfoundland and its regional relationships; in Current Research, Part A, Geological Survey of Canada, Paper 80-1A, p. 227-234.

Dunning, G.R. and Krogh, T.E.
1983: Tightly-clustered precise U/Pb (Zircon) ages of ophiolites from the Newfoundland Appalachians; in Abstracts with Programs, 1983, Geological Society of America, Northeastern Section, p. 136.

Espenshade, G.A.
1937: Geology and Mineral deposits at the Pilleys Island area, Newfoundland; Department of Natural Resources of Newfoundland, Geology Section, Bulletin 6.

Fahraeus, L.E.
1973: Depositional environments and conodont-based correlation of the Long Point Formation (Middle Ordovician), western Newfoundland; Canadian Journal of Earth Sciences, v. 10, p. 1822-1833.

Herd, R.K. and Dunning, G.R.
1979: Geology of Puddle Pond map area, southwestern Newfoundland; in Current Research, Part A, Geological Survey of Canada, Paper 79-1A, p. 305-310.

Kean, B.F.
1981: Geological compilation of the Newfoundland central volcanic belt, in The Buchans Ore Bodies: Fifty Years of Geology and Mining, ed. E.A. Swanson, D.F. Strong, and J.G. Thurlow, Geological Association of Canada, Special Paper 22.

Kean, B.F. and Jayasinghe, N.R.
1981a: Geology of the King George IV Lake Map area (12A/14), Newfoundland; in Current Research, Newfoundland Department of Mines and Energy, Mineral Development Division, Report 81-1, p. 32-39.

1981b: King George IV Lake, Grand Falls District, Newfoundland, NTS 12A/4; Newfoundland Department of Mines and Energy, Mineral Development Division, Map 81-119.

Neale, E.R.W. and Nash, W.A.
1963: Sandy Lake (East Half), Newfoundland, 12H E½; Geological Survey of Canada, Paper 62-28, 40 p.

Riley, G.C.
1957: Red Indian Lake (West Half), Newfoundland; Geological Survey of Canada, Map 8-1957.

Rodgers, J.
1965: Long Point and Clam Bank Formations, western Newfoundland; Geological Association of Canada, Proceedings, v. 16, p. 83-94.

Stevens, R.K.
1970: Cambro-Ordovician flysch sedimentation and tectonics in west Newfoundland and their possible bearing on a proto-Atlantic; Geological Association of Canadian Special Paper 7, p. 165-178.

Twenhofel, W.H.
1947: The Silurian of eastern Newfoundland with some data relating to physiography and Wisconsin glaciation of Newfoundland; American Journal of Science, v. 245, p. 65-122.

van Eysinga, F.W.B. (Compiler)
1975: Geological Time Table, 3rd Edition; Elsevier Scientific Publishing Company, Amsterdam.

Williams, H.
1963: Botwood, Newfoundland, E½; Geological Survey of Canada, Map 60-1963.

Wilton, D.H.C.
– The geology and structural history of the Cape Ray Fault Zone in southwestern Newfoundland; Canadian Journal of Earth Sciences. (in press)

THE ENDERBY CLIFFS LANDSLIDE, BRITISH COLUMBIA

EMR Research Agreement 117-4-79

S.G. Evans
Terrain Sciences Division

Evans, S.G., The Enderby Cliffs landslide, British Columbia; in Current Research, Part B, Geological Survey of Canada, Paper 83-1B, p. 423-427, 1983.

Abstract

The Enderby Cliffs landslide (estimated volume 1.7 x 10^8 m^3) is located 4.8 km northeast of Enderby, British Columbia. The complex slope movement involves rocks of Eocene age. The boundaries are determined by structural lineaments which also controlled the boundaries of major blocks involved in the landslide. Secondary flow is currently active within the debris. The landslide is postglacial in age and did not take place in direct response to valley excavation.

Résumé

Le glissement de terrain d'Enderby Cliffs (volume estimatif de 1,7 sur 10^8 m^3) est situé à 4,8 km au nord-est d'Enderby (Colombie-Britannique). Des roches de l'Eocène ont été touchées par le mouvement complexe de la pente. Des linéaments structuraux marquent les limites du glissement et ont également contrôlé les marges des plus grands blocs touchés par le mouvement. Un écoulement secondaire au sein des débris a présentement lieu. Le glissement de terrain est d'origine postglaciaire et ne s'avère pas le résultat direct de l'excavation de la vallée.

Introduction

A reconnaissance of the Enderby Cliffs landslide was carried out as part of a regional landslide study of slope movements in Tertiary volcanic rocks in the southern interior of British Columbia (Evans and Cruden, 1981; Evans, 1983). The landslide is on the eastern margin of the Hunters Range Eocene outlier (Okulitch, 1979), 4.8 km northeast of Enderby (Fig. 1,2).

The volume of the landslide is estimated to be of the order of 1.7 x 10^8 m^3. Debris has spread out over a bench above the floodplain of Shuswap River and the movement appears to have combined sliding and flowage. According to Varnes' (1978) classification, the landslide is a complex slope movement. Traverses were made along the scarp and parts of the debris. This report examines the stratigraphic and structural controls on the landslide, its morphology, and its occurrence in relation to valley development.

Acknowledgments

Field work was carried out under Energy, Mines and Resources Research Agreement 117-4-70 to D.M. Cruden, University of Alberta. R.J. Fulton critically read the manuscript.

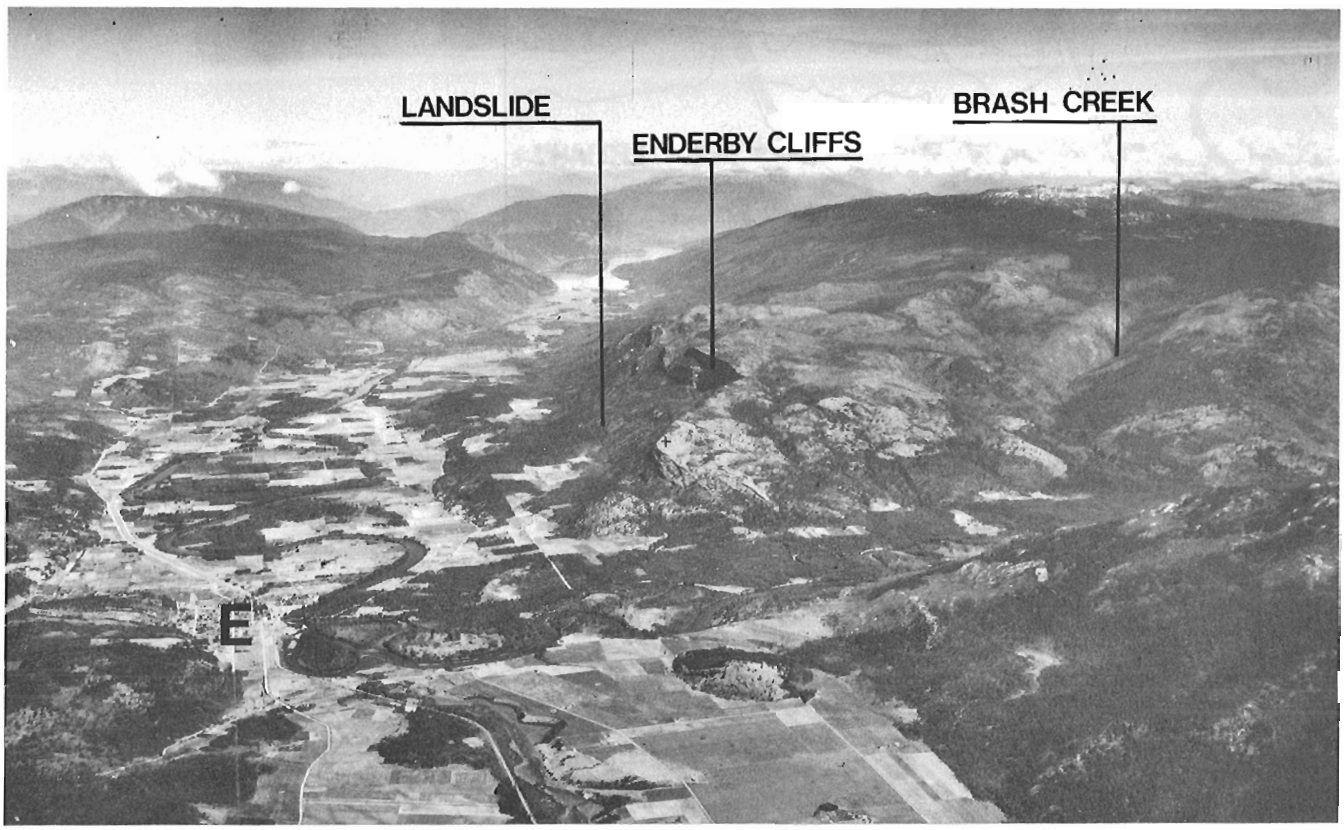

Figure 1. *Oblique aerial photograph looking north down Shuswap River valley. E = Enderby. NAPL A2425-78.*

Stratigraphy of Valleyside Slope

The regional geology setting of the landslide is given in Figure 2. The geology of the outlier has been examined by Cairnes (1932) and in detail by Mathews (1981) who distinguished three Eocene units in Enderby Cliffs. These are as follows:

Unit 1: a basal unit consisting of thinly bedded shales, sandstone, and conglomerates with local development of coal seams;

Unit 2: a coarse intermediate unit consisting of conglomerate and fanglomerate-clastic breccia which in part appears to be an Eocene age landslide deposit;

Unit 3: an upper unit of lava flows and volcanic breccia which is exposed in a scarp of the landslide.

The Eocene rocks are underlain by metamorphic rocks of the Shuswap Assemblage. Figure 3 shows the reconstructed pre-movement slope profile and approximate stratigraphy. The rupture zone appears to have been located in the upper part of the clastic breccia (Unit 2), just below the base of the lava-volcanic breccia cap. The dip of the strata is into the slope.

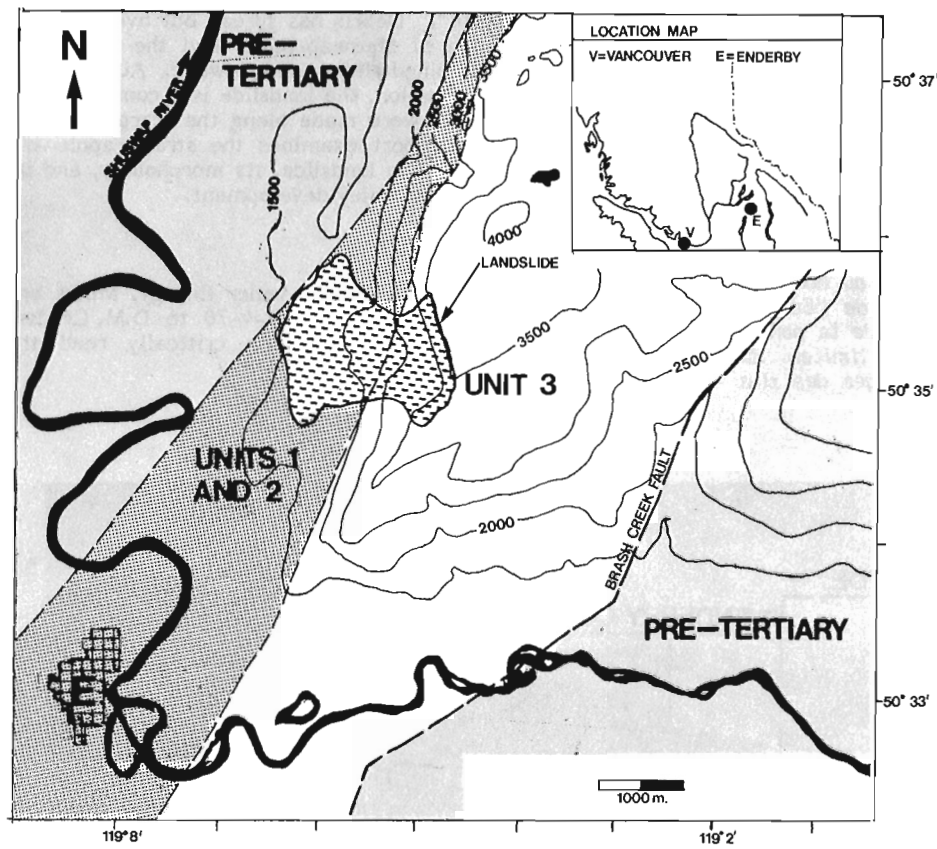

Figure 2

Location and geological setting of the Enderby Cliffs landslide. Geology based on Mathews (1981). Tertiary units are numbered as discussed in text.

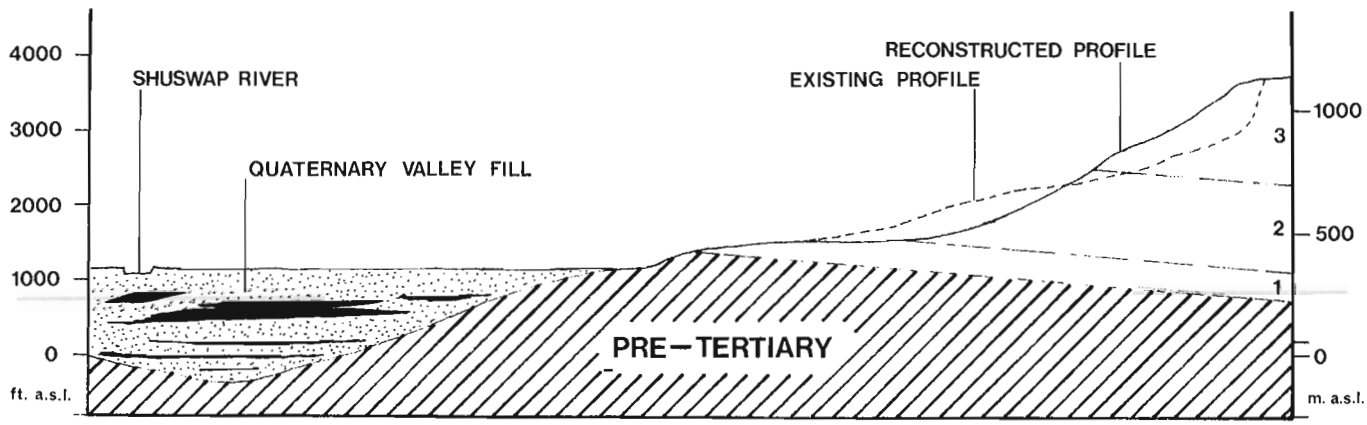

Figure 3. Cross-section of Shuswap valley at Enderby Cliffs landslide. Bedrock profile in Shuswap valley drawn from bedrock contours in McAulay and Hobson (1972). Tertiary units are numbered as discussed in text. Bedrock geology inferred from Mathews (1981) and field observations by the writer. Pre-movement profile based on reconstructed contours.

Figure 4. *A. Aerial photograph of Enderby Cliffs; landslide is outlined. (BC 5190-158) 1 = active flow lobe; 2 = North Block; 3 = glaciolacustrine deposits.*

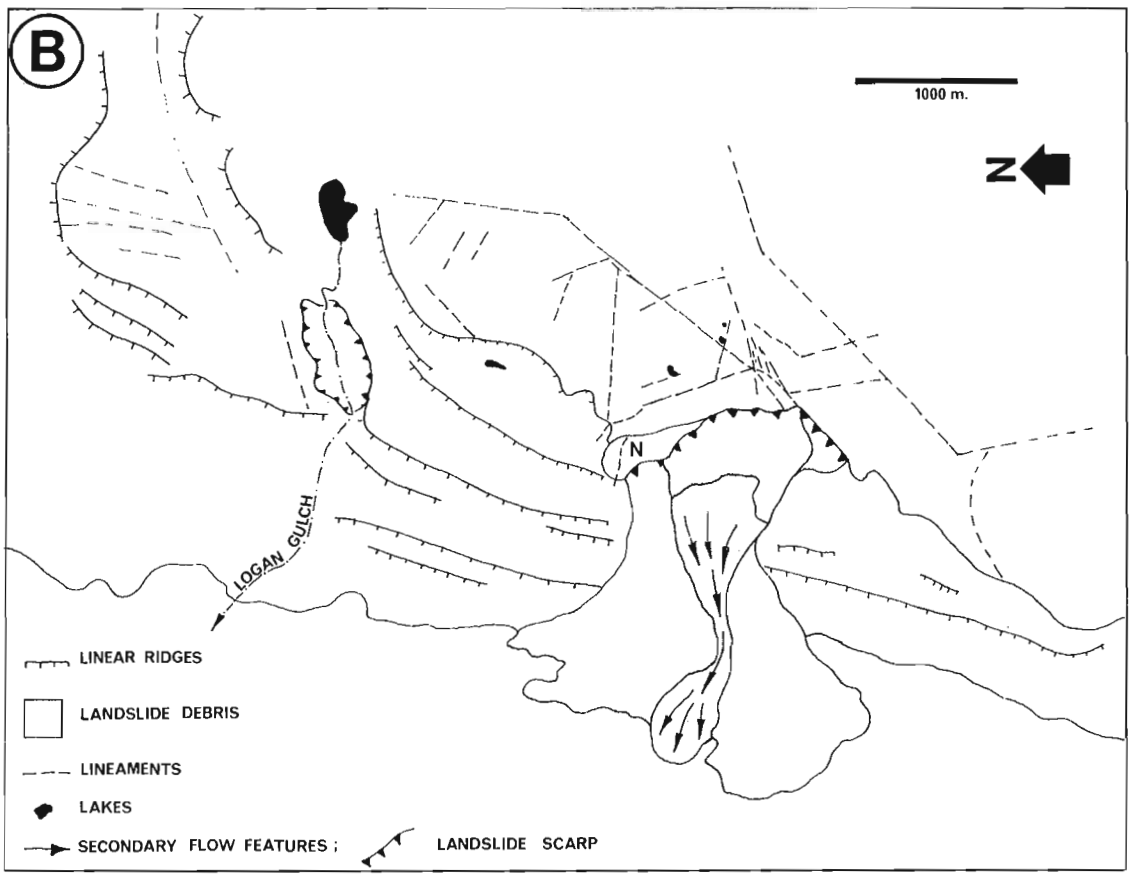

Figure 4. *B. Interpretation of Figure 4A showing landslide morphology and structural lineaments in the vicinity of the landslide. N = North Block.*

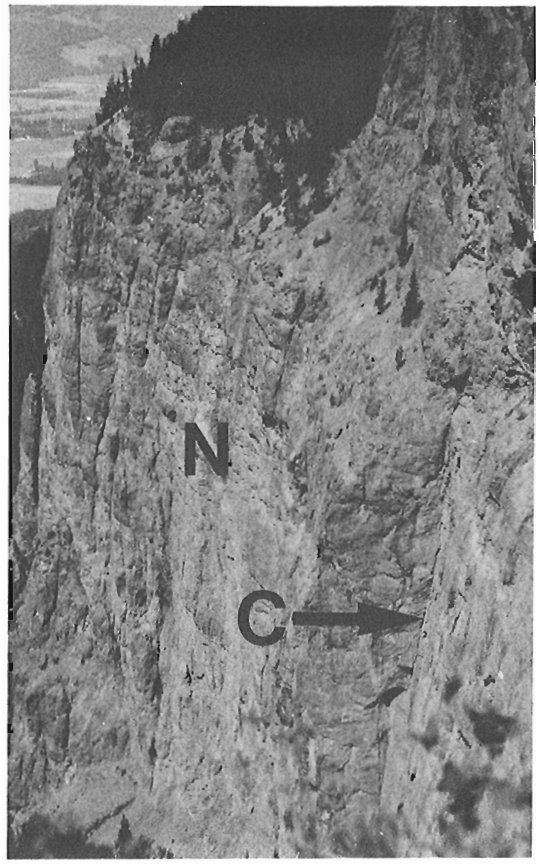

Figure 5. *Discontinuities in lava-volcanic breccia cap, north scarp of Enderby Cliffs landslide. Note crack (C) separating North Block (N) from main headscarp.*

Structural Factors

The outlier is an eastward tilted fault block within which the dips of the various strata are erratic, a structural style characteristic of other outcrops of Eocene volcanic rocks in southern British Columbia (cf. Campbell and Tipper, 1971; Ewing, 1981). Lineament patterns are evident on the aerial photograph in Figure 4A and an interpretation of this photograph is seen in Figure 4B. The face of the cliffs south of the landslide, and the south scarp of the landslide itself have developed along a near vertical fracture trace which trends 041°, changing to 006° northeast of the landslide (Fig. 4B). This trend mirrors the inferred trace of the Brash Creek fault (Fig. 1) which forms the eastern margin of the outlier (Mathews, 1981).

Discontinuities in the lava-breccia cap are near vertical, persistent joints with apertures up to 0.5 m (Fig. 5); these controlled the boundaries of five major blocks which are thought to have moved sequentially as the landslide developed (Fig. 6). A sixth block, termed the North Block (Fig. 4A,B), is separated from the main north scarp by a crack up to 1.5 m in width (Fig. 5). Although the crack extends from the top of the block to the lowest part of the exposed rock slope, very little, if any, vertical displacement has occurred. It appears that the block is buttressed by landslide debris at its foot.

Landslide Morphology

The morphology of the landslide is seen in Figures 4A and 4B. As noted above, the scarp is near vertical and displays prominent vertical jointing. Beneath the scarp, a zone of irregular blocks is currently undergoing degradation by weathering and secondary flow. The centre of the debris is the site of an active flow, the lobe of which is encroaching on farmland at its toe (Fig. 4A). The flow appears to be related to groundwater discharge near the base of the lava-breccia cap, a factor which may have been important in the initial slope movement. The remainder of the debris surface is irregular and blocky and supports a dense vegetation cover.

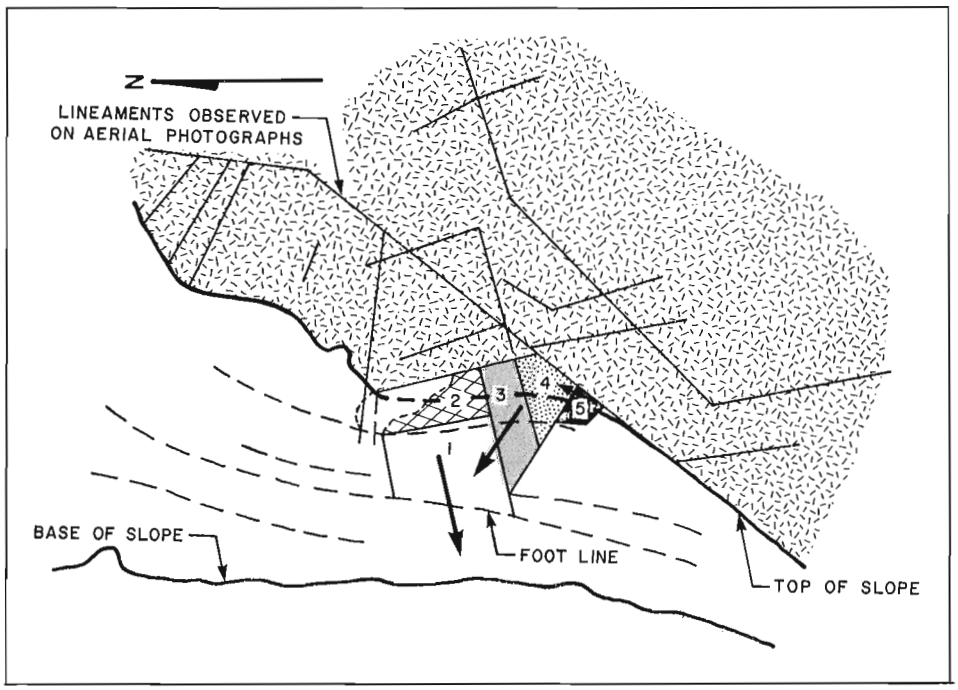

Figure 6

Hypothetical sequence of block movement at Enderby Cliffs landslide.

Relationship to Valley Development

The position of the landslide rupture surface in the valleyside slope presents several problems in establishing the relationship between landslide occurrence and valley development. It daylights approximately 213 m above the existing Shuswap River floodplain (Fig. 3). Thus, recent oversteepening or erosion at the slope base is not a factor. It is also above the highest level of proglacial lakes (~533 m) which occupied the North Okanagan-Shuswap valley during deglaciation (R.J. Fulton, personal communication, 1983).

In addition, the preservation of older Quaternary valley fill in Shuswap valley was used as evidence by Fulton (1972) that the valley was not extensively modified during the Fraser Glaciation or possibly in the previous two or three.

Materials for absolute dating have not been recovered to date. A postglacial age for the landslide is indicated, however, by the fact that landslide debris covers glaciolacustrine deposits on the bench above Shuswap valley (Fulton, 1975).

The landslide has clearly not taken place in direct response to valley excavation. It may be viewed as a delayed slope movement in relation to the process of slope geometry change and as a response to other factors which may include time-dependent changes in the strength of the material in Unit 2, groundwater conditions, or seismic forces.

These observations raise the general question of the timing of landslides in the Tertiary volcanic rocks of the Interior Plateau and reflect the uncertainty about the precise conditions necessary for slope movement in this geological environment, a fact which adds to the difficulty of making an assessment of slope hazard adjacent to existing landslides.

References

Cairnes, C.E.
1932: Mineral resources of northern Okanagan Valley, British Columbia; Geological Survey of Canada, Summary Report 1931, Part A, p. 66-109.

Campbell, R.B. and Tipper, H.W.
1971: Geology of the Bonaparte Lake map-area, British Columbia; Geological Survey of Canada, Memoir 363, 100 p.

Evans, S.G.
1983: Landslides in layered volcanic successions with particular reference to the Tertiary rocks of South Central British Columbia; unpublished Ph.D. thesis, University of Alberta, Edmonton, 340 p.

Evans, S.G. and Cruden, D.M.
1981: Landslides in the Kamloops Group in south-central British Columbia: A progress report; in Current Research, Part B, Geological Survey of Canada, Paper 81-1B, p. 170-177.

Ewing, T.E.
1981: Regional stratigraphy and structural setting of the Kamloops Group, south-central British Columbia; Canadian Journal of Earth Sciences, v. 18, p. 1464-1477.

Fulton, R.J.
1972: Stratigraphy of unconsolidated fill and Quaternary development of North Okanagan Valley; Geological Survey of Canada, Paper 72-8, Part B, p. 9-17.

1975: Quaternary geology and geomorphology, Nicola-Vernon area, British Columbia; Geological Survey of Canada, Memoir 380.

McAulay, H.A. and Hobson, G.D.
1972: A seismic refraction survey of the North Okanagan and South Shuswap Valleys; Geological Survey of Canada, Paper 72-8, Part A, p. 1-8.

Mathews, W.H.
1981: Early Cenozoic resetting of potassium-argon dates and geothermal history of north Okanagan area, British Columbia; Canadian Journal of Earth Sciences, v. 18, p. 1310-1319.

Okulitch, A.V.
1979: Geology and mineral occurrences of the Thompson-Shuswap-Okanagan region, south-central British Columbia; Geological Survey of Canada, Open File 637.

Varnes, D.J.
1978: Slope movement types and processes; in Landslides: Analysis and Control, ed. R.L. Schuster and R.J. Krizek; Transportation Research Board, National Research Council, Special Report 176, p. 11-33.

A GRAVITY MAP OF THE CANADIAN EAST COAST OFFSHORE: A DEMONSTRATION OF COMPUTER TECHNIQUES FOR THE CONSTRUCTION OF REGIONAL CONTOUR MAPS FROM LARGE DATA SETS

Project 730081

K.G. Shih and Ron Macnab
Atlantic Geoscience Centre, Dartmouth

Shih, K.G. and Macnab, Ron, A gravity map of the Canadian east coast offshore: a demonstration of computer techniques for the construction of regional contour maps from large data sets; in Current Research, Part B, Geological Survey of Canada, Paper 83-1B, p. 429-431, 1983.

Abstract

An automatic contouring package has been used to produce a regional contour map from a data set consisting of 1.1 million marine gravity measurements. The final product compares well with a hand-contoured version. A by-product is a master gridded data set, which will facilitate the production of other contour maps at different scales and in different projections.

Résumé

Un programme automatique de traçage des courbes de niveau a déjà été utilisé pour produire une carte régionale en courbes de niveau à partir d'une série de données comprenant 1,1 million d'observations gravimétriques marines. Le produit final se compare favorablement à la carte tracée à la main. Un sous-produit, à savoir une série-maître de données quadrillées, facilitera la production d'autres cartes en courbes de niveau dans des projections différentes et à diverses échelles.

Map Construction by Computer

When used intelligently and with an appreciation of their limitations, automated contouring packages can yield plots of a quality and accuracy comparable to hand-drawn versions. Where large data sets are involved, they can do this in a fraction of the time it would take to do the job manually.

Automated contouring methods are especially valuable for earth scientists who want to present data on a geographic base, i.e. in map form. For a number of quite valid reasons, earth scientists tend to construct their maps in a great variety of scales and projections. Clearly, this has the potential for creating difficulties at later stages, when data displayed on incompatible map bases have to be compared, correlated, or amalgamated. It is possible to transform data from one map to another, but this is a tedious and time-consuming process. Where feasible, it is far more efficient to maintain the data in digital form, and to assign map construction tasks to a computer. The same data can then be displayed easily and quickly on a variety of map bases to suit any number of special purposes.

There are other advantages to this approach. For one, digital data sets are easy to modify through correction, deletion, or addition; automated contouring techniques simplify the task of producing updated maps that reflect modifications to the data sets. Automated techniques also facilitate the merging and display of more than one type of data on a single map. A simple example, which we shall return to later in this report, is the inclusion of geographic features such as coastlines on a geopotential field contour map. In this case, coastline coordinates and spot values of the potential field are maintained as separate data sets, but are merged in a common display.

East Coast Gravity Data

The marine gravity data used in this demonstration were collected on over thirty multiparameter survey cruises operating out of the Bedford Institute of Oceanography during the period 1964-1982 (Macnab, 1983). Some 1.1 million data points are involved, representing over 462 000 km of survey tracks.

Two types of device were used to measure gravity on these surveys: the Graf-Askania Model GSS-2, and the LaCoste and Romberg Air-Sea Gravity Meter. From an analysis of discrepancies at track crossover points, data accuracy is estimated to be within 5 milligals for 75 per cent of the data points.

During 1964-1973, navigation was accomplished by Decca Lambda in the range-range mode. As technology improved, a methodology was developed to combine satellite navigation and rho-rho Loran-C; this technique has been employed since 1974. Regardless of the method used, positioning accuracy in the entire survey area is estimated to be better than 200 m.

Data Preparation and Techniques for Map Construction

The objective of this demonstration was to produce a regional map for publication at a small scale. A certain degree of generalization was therefore deemed acceptable, in that only the main features of the offshore gravity field would be portrayed. This influenced the choice of techniques described below.

Data points were first assembled and sorted geographically in a sequence based on ascending latitude-longitude coordinates. These points were pseudo-randomly located, i.e. they were positioned at more or less regular intervals along parallel and intersecting ships' tracks; throughout the map area, spacing between parallel lines ranged from less than five nautical miles to twenty miles.

Generally, contouring algorithms require input data that are distributed over a uniform matrix. (While many contouring packages accept randomly-positioned data, most perform some kind of internal gridding before initiating the contouring procedures.) For this reason, and to reduce the number of data points to a manageable quantity for further manipulation, the data were averaged to create a master gridded set. This entailed the calculation of mean gravity values within cells measuring 0.1° latitude by 0.1° longitude, with the mid-point of each cell designated as the position of the cell's mean gravity value.

The resulting master gridded data set contained 29 000 data points. While this was a substantial reduction from the original 1.1 million points, it still represented an unwieldy quantity of data and would have entailed prohibitive execution times for the software at our disposal, the CalComp GPCP-II (California Computer Products, 1973).

Previous investigations (Shih and Macnab, 1983) showed that we could expect a fair trade-off between reasonable resolution of the gravity field and acceptable computation time by re-averaging the master gridded set over large cells: 0.5° latitude by 0.5° longitude. This step reduced the number of data points to something like 1600. With this data set, GPCP contour generation on a Cyber Model 171 took about five minutes.

Contour lines were drawn at a scale of 1:5 000 000 on a UTM projection. For geographic reference, landforms were drawn to the same scale and projection by a separate program reading from a digital file of coastline coordinates. The contour and coastline maps were produced on a drum plotter, then superimposed to produce a combined plot.

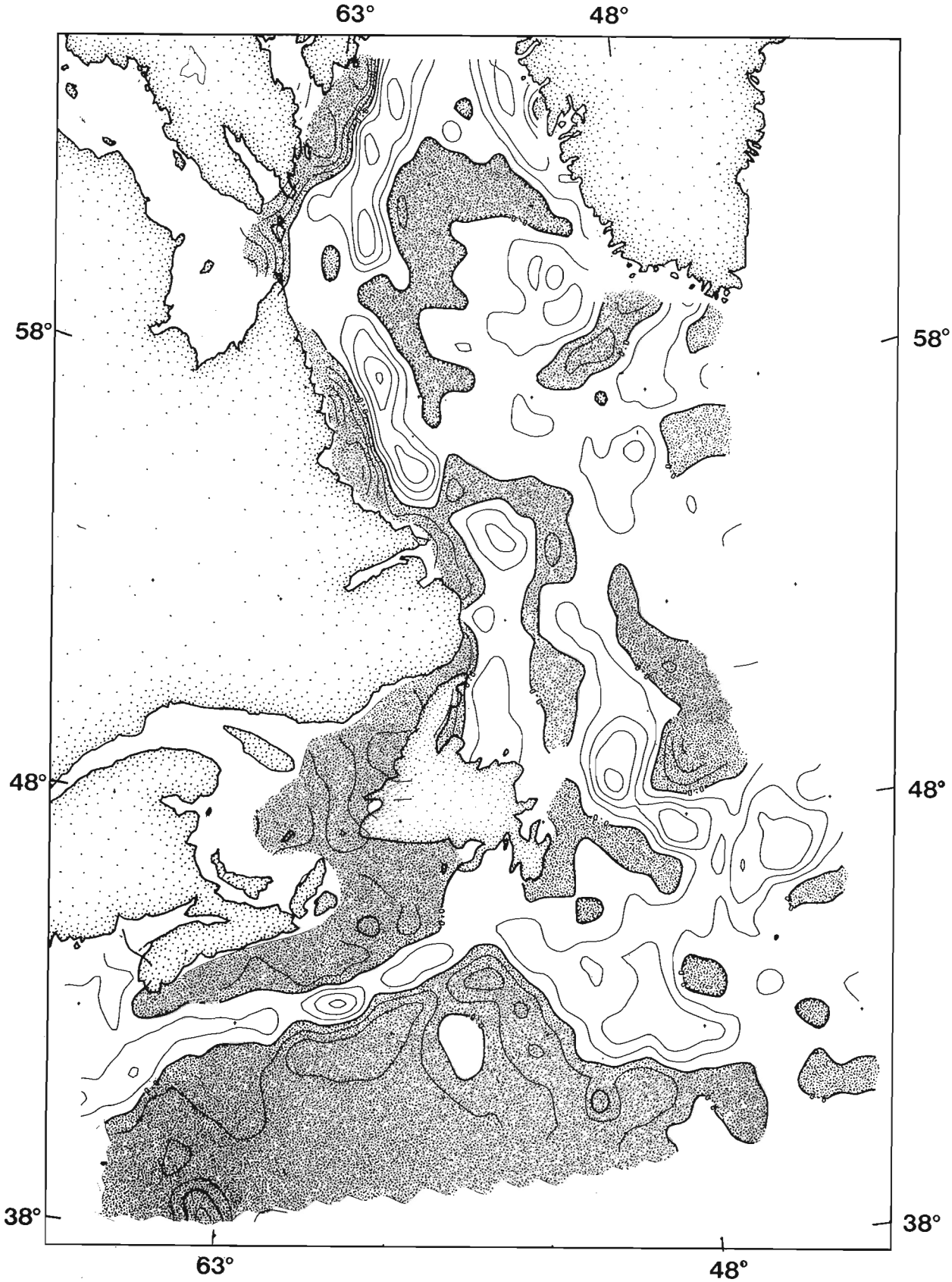

Figure 1. *Contour map of the regional free-air gravity anomaly, produced by computer from a data set containing 1.1 million sea-surface measurements. Contour interval: 20 miligals. Negative areas are stippled. This is a reduced copy; the original was produced at a scale of 1:5 000 000.*

Although the aim was to create a map suitable for black and white reproduction, the original contour lines were drawn in colour to facilitate visual inspection. Cosmetic touches such as stippling and co-ordinate labelling were added manually.

The Finished Map: Some Comments

The final product (reduced copy in Fig. 1) displays the free air gravity anomaly from Davis Strait in the north to the Scotian Margin in the south. In general shape and amplitude, the computer-drawn contours are a fair match to those portrayed on the hand-drawn, 1:5 000 000 Gravity Map of Canada (Department of Energy, Mines, and Resources, 1980). The gravity highs trending along the shelf edge off Nova Scotia and Labrador are well represented, as is the positive nature of the field over the Labrador Sea and the Grand Banks of Newfoundland.

To produce this map, we developed techniques and software for the manipulation of a large data set, and for the subsequent display of that data set in contour form. The satisfactory conclusion of this project increases our confidence in the data set, and in our ability to manipulate it. Moreover, the availability of the 0.1° by 0.1° master gridded set will facilitate the production of other gravity contour maps at different scales and projections.

The lessons learned from the production of this map will be applied to the preparation of a similar regional contour map of the magnetic anomaly off the east coast of Canada. The particular challenge in that undertaking will be to see whether an automatic contouring package can portray accurately the magnetic lineations that exist in mid-ocean.

Acknowledgments

Harvey Slade of the BIO Drafting and Illustrations Section did the cosmetic artwork that transformed raw computer output into Figure 1. We thank Andy Sherin of the AGC Data Section for reviewing the manuscript.

References

California Computer Products, Inc.
1973: GPCP-II: A general-purpose contouring program; Anaheim, California.

Department of Energy, Mines, and Resources
1980: Gravity Map of Canada; Earth Physics Branch, Ottawa.

Macnab, R.F.
1983: Multiparameter mapping off the east coast of Canada; in Current Research, Part A, Geological Survey of Canada, Paper 83-1A, p. 163-171.

Shih, K.G. and Macnab, R.F.
1983: Computer contouring of marine survey data: choosing the best technique for gridding input data; in Current Research, Part A, Geological Survey of Canada, Paper 83-1A, p. 173-178.

DISCUSSIONS AND COMMUNICATIONS
DISCUSSIONS ET COMMUNICATIONS

A STUDY OF THE HEAVY MINERAL DISTRIBUTION IN THE BOTTOM SEDIMENTS OF HUDSON BAY: DISCUSSION

Arthur S. Dyke
Terrain Sciences Division

In her recent paper Henderson (1983) presented information on the distribution of siderite, hematite, pyrite, and augite in 41 samples of Hudson Bay bottom sediments and commented on their interpretation in terms of ice flow direction. Although not specified in the paper, the ice flow patterns in question presumably date from the Late Wisconsin and this is implied by reference to Late Wisconsin features such as the Dubawnt dispersal train.

Currently some disagreement exists regarding the pattern of Late Wisconsin ice flow in the southern half of Hudson Bay with two contrasting interpretations presented by Shilts (1980) and Dyke et al. (1982). Henderson's interpretations appear to be totally congruent with those of Shilts, and while her conclusions may be entirely correct, is it worth pausing to examine them less we too hastily reject the alternative model.

The first concern is that although resolution of the problem of the Late Wisconsin flow direction in the Hudson Bay region may be resolved most unambiguously by determining the composition of the Late Wisconsin till at the bottom of the bay through studies such as Henderson has undertaken, we must be careful to ensure that the samples scrutinized are in fact till. This does not seem to be known in Henderson's study. We must proceed with the admission that glaciomarine sediment with abundant ice-rafted debris is likely to be encountered on the seafloor. It is generally agreed that the entirety of the Tyrrell Sea was deglaciated by the process of calving of icebergs into the sea. The area of ice involved means that there must have been an immense number of icebergs and a considerable amount of debris dispersed by them. Even the present seasonal sea ice cover accomplishes a large amount of debris dispersal, transporting debris several hundred kilometres along shore and more than 100 km offshore. Ice-rafted particles are strewn over the entire floor of Hudson Bay by this process and constitute more than 20% of the surficial sediment over several large areas (Pelletier, 1969, Fig. 12). It seems reasonable to assume that the amount of debris dispersed by icebergs during deglaciation was several orders of magnitude more than that being dispersed now. We cannot assume, however, that current directions in the Tyrrell Sea, whose shape, depth, and perhaps wind field were changing rapidly, followed patterns similar to today's currents. In summary, without knowing that we are looking at till rather than glaciomarine or marine sediment we cannot infer direction of glacier flow.

This problem of unknown sediment origin also applies to data from the same sample sites presented by Shilts (1982, Fig. 5-8).

The second concern is the way in which the data were contoured. Only the augite map could be said to indicate a distinct ribbon shaped dispersal train so comments will be restricted to that figure. The 3% and 5% contours, which define the train, pass twice between data points that have less than 3% augite. When I recontoured the data using the same contour interval, the pattern was much less suggestive of a westward flow of ice from the Belcher Islands (Fig. 1). Another relevant point here is that at concentrations of 4% and less the probable error of the method is ± 100% (Paré, 1982), so it could be argued that contouring values of less than 5% is not justified. Even if all the samples in question are from till, no unequivocal interpretation is possible.

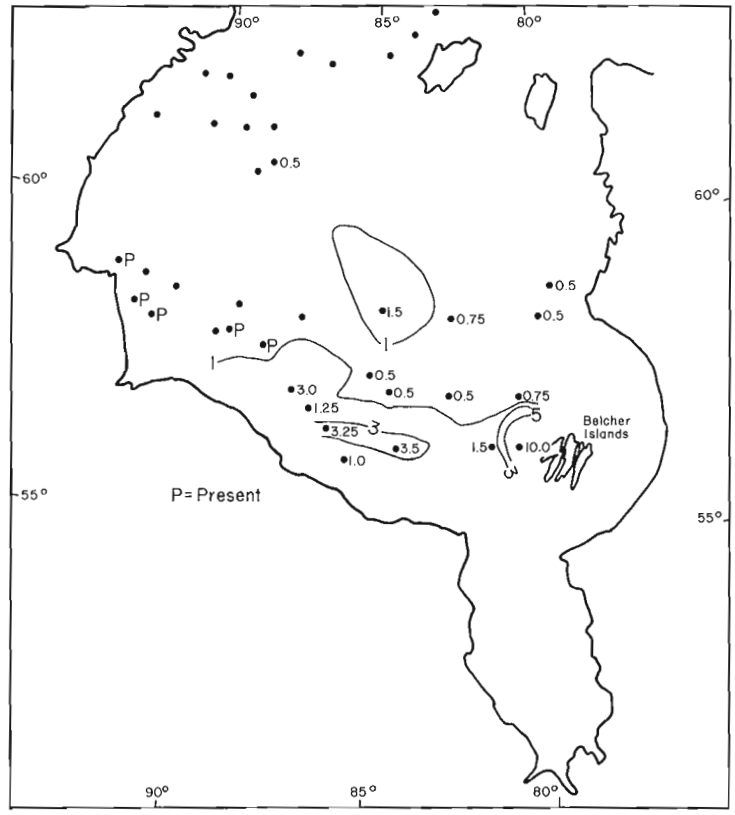

Figure 1. *Distribution of augite in bottom sediments of Hudson Bay. Compare with Figure 48.4 of Henderson (1983).*

A third concern is that it may be premature to assume that these heavy minerals have such narrowly restricted source areas. For example, although siderite cavity fillings have been known for a long time (Bell, 1877) from the Devonian Stooping River and Kwataboahegan formations where they are exposed above sea level in the Hudson Bay Lowlands, this does not preclude much more widespread distribution of siderite at lower concentrations in other formations. In fact, siderite probably occurs in all post-Ordovician rocks of the Hudson Basin – throughout 90% of the basin (B.V. Sanford, personal communication, 1982) – and Paré (1982), quoting S. Averill (personal communication), noted that siderite had been observed in concentrations of up to 25% in several samples of mature Cretaceous sediments south of James Bay. Furthermore, siderite and other heavy minerals are probably widespread in pre-Late Wisconsin Quaternary sediments throughout Hudson Bay Lowlands and

possibly beneath the bay itself. In the face of this problem, dispersal trains will have to be exceptionally well defined before they are positively identified.

However, if the high concentrations (>10%) of siderite in the southwestern part of the bay do originate from subaerial coastal exposures of Stooping River and Kwataboahegan formations, why does the distribution not indicate offshore glacier flow rather than fluvial transport? Although neither Shilts (1980) nor Dyke et al. (1982) suggest offshore ice flow in that area during the last glacial maximum, such a flow could have occurred at several times during the Wisconsin if Hudson Bay opened two or more times as suggested by Andrews et al. (1983) and if remnants of ice were isolated south of the bay during these openings. Similarly, why do the slightly elevated siderite concentrations in the southeastern part of the bay not indicate southeastward flow across the Kwataboahegan and Stooping River formations, rather than westward flow from the Belcher Islands? Or is there any way at present to distinguish between the various possible flow directions or the various possible transporting agents?

References

Andrews, J.T, Shilts, W.W., and Miller, G.H.
1983: Multiple deglaciations of the Hudson Bay Lowlands, since deposition of the Missinaibi (Last-interglacial?) Formation; Quaternary Research, v. 19, p. 18-37.

Bell, R.
1877: Report on an exploration in 1875 between James Bay and Lakes Superior and Huron; Geological Survey of Canada, Report of Progress, 1875-1876, p. 294-342.

Dyke, A.S., Dredge, L.A., and Vincent, J-S.
1982: Configuration and dynamics of the Laurentide Ice Sheet during the late Wisconsin maximum; Géographie physique et Quaternaire, v. 36, p. 5-14.

Henderson, P.J.
1983: A study of the heavy mineral distribution in the bottom sediments of Hudson Bay; in Current Research, Part A, Geological Survey of Canada, Paper 83-1A, p. 347-351.

Paré, D.
1982: Application of heavy mineral analysis to problems of till provenance along a transect from Longlac, Ontario to Somerset Island; unpublished M.A. thesis, Carleton University, Ottawa, 76 p.

Pelletier, B.R.
1969: Submarine physiography, bottom sediments, and models of sediment transport in Hudson Bay; in Earth Science Symposium on Hudson Bay, ed. P.J. Hood; Geological Survey of Canada, Paper 68-53, p. 100-135.

Shilts, W.W.
1980: Flow patterns in the central North American Ice Sheet; Nature, v. 286, no. 5770, p. 213-218.

1982: Quaternary evolution of the Hudson/James Bay region; Le naturaliste canadien, v. 109, p. 309-332.

A STUDY OF THE HEAVY MINERAL DISTRIBUTION IN THE BOTTOM SEDIMENTS OF HUDSON BAY: REPLY

Penny J. Henderson
Terrain Sciences Division

Dyke (1983) makes some interesting points regarding the interpretation of the heavy mineral distribution in Hudson Bay. Since at least part of the sediment distribution was interpreted as the result of Quaternary glacial flow (Henderson, 1983), he questions whether or not any of the sedimentary material studied is truly till, suggesting ice-rafted debris as an alternative source of sand and coarser debris. Dyke also questions the significance of contouring specific mineral species with so few sample points and expresses concern with the reported distribution of augite. He also questions the interpreted sources of the heavy minerals, specifically siderite.

This pilot study was carried out to determine whether heavy minerals could yield information on the sources of Hudson Bay bottom sediments. Certainly this preliminary work and Shilts' (1982) study of the granules (2-6 mm) from the same sample locations (plus others) show that some types of pebbles and minerals are most abundant in specific areas within the bay. This distribution pattern is not random but is due most likely to a combination of specific processes.

The bottom sediments are no doubt of varied origin depending on their proximity to the shoreline, their relationship to major rivers, and on the bathymetry of the bay. There is some evidence to suggest, however, that most of the samples used in this study are till, or sediment derived from till.

Hudson Bay, as it appears today, is really a remnant of the postglacial Tyrrell Sea which has been reduced to its present size by continued glacio-isostatic uplift of the region. Much of the terrain on the western and southern sides of Hudson Bay was sea bottom and sea shore at some time during the past. The only major difference between the marine sedimentary processes and environments of the emerged terrain and the present floor of Hudson Bay is the length of submergence. Probably more than half of the terrain below the maximum limit of the Tyrrell Sea west and south of Hudson Bay, was submerged for several thousand years. One can gain a great deal of insight, therefore, about the probable nature of the present floor of Hudson Bay by studying maps and descriptions of the surficial deposits of its emerged floor.

Onshore observations of material deposited below the limit of the Tyrrell Sea have been reported from the District of Keewatin on the west side of Hudson Bay (Shilts, 1973; Ridler and Shilts, 1974; Aylsworth et al., 1981, for example) and the southern Hudson Bay and James Bay region (Skinner, 1973; Vincent, 1977). In these areas, no significant ice-rafted material has been reported in the offshore facies of the Tyrrell Sea. In the District of Keewatin, west of Hudson Bay, the retreating glacier front stood in deep marine water, presumably shedding icebergs. In this region ice-rafted debris is rare and makes up a small volume (<5%) of the identifiable marine muds, which are themselves rare. In fact, most of the terrain of that area comprises till with little modification by marine nearshore processes and virtually no burial by marine muds. The latter observation is important and is confirmed by more than 6000 observations made during sampling of 14 000 km^2 of typical terrain below marine limit (Shilts, 1973; Ridler and Shilts, 1974; Klassen and Shilts, 1977). Marine mud was observed at fewer than 5% of the sample sites and occurred mainly in depressions and adjacent to major rivers. Little if any ice-rafted debris was recognized within the sediment. Glacial landforms with little or no marine sediment cover are also preserved in the La Grande Rivière region, Québec, below the limit of the Tyrrell Sea (Vincent, 1977).

Pelletier (1969), reporting the distribution of sediment types on the floor of Hudson Bay, noted coarse sediment on the crests and flanks of major topographic highs, and finer material (perhaps marine muds) in lows. Although he suggested ice rafting as a source for the coarser material, it is not unreasonable, in the light of the above discussion of the emerged seafloor, to suggest that till has not been submerged by marine muds on these slopes. A situation analogous to Hudson Bay exists in the Bothnian Sea (Scandinavia) – a shallow, epeiric sea subjected to continental glaciation. In a study of the submarine geology using acoustic and seismic reflection profiles, bottom samples, diving observations and seafloor photography, Winterhalter (1972) described till shoals, drumlinoid fields, and eskers interspersed with modern marine clays on the seabed. He identified glacial erosion and deposition as the major influences on seabed morphology and sediment composition with no significant contribution by ice-rafted debris.

Because there is very little evidence of ice-rafted debris in the marine sequences observed on land adjacent to Hudson Bay, the possibility of ice-rafting, although originally considered, was rejected as a major contributing mechanism. If, as Dyke (1983) has suggested, there had been "an immense number of icebergs and considerable amount of debris dispensed by them" one would expect an almost random distribution of indicator lithologies. This study and that of Shilts (1982) show definite concentrations in specific areas. Therefore, if the sediments do represent ice-rafted material, it must not have travelled far in icebergs before deposition.

Present day sea-ice rafting may play some role in nearshore sediment redistribution; however, studies on samples from river mouths and several kilometres into the southern part of Hudson Bay by Adshead (1983a) show that in these areas at least, the sediment composition is more strongly controlled by recent fluvial processes. This influx of sediment overrides anything that might be deposited by ice rafting in that area. The effect of recent ice rafting due to seasonal ice is unknown in the central part of Hudson Bay but is likely minimal due to the lack of contact of the ice with the seabed, and the fact that the more sediment-rich nearshore ice does not move great distances before melting (Pelletier, 1969).

The problems of objectivity in contouring are well known, particularly when the data are derived from a limited number of sample points as in this study. In responding to Dyke's criticism it was found that the percentage of augite reported at station L-5 (Fig. 48.4, Henderson, 1983) should have been reported as 0.5% rather than 2.0%. This changes any contouring slightly but surely does not change the observation that, even with such widely spaced samples, augite can be seen to be concentrated in the southeastern part of the bay. The interpretation that the distribution of augite and hematite was related to southwesterly glacial flow from the Belcher Islands (Henderson, 1983) is justified when considered in conjunction with the provenance studies of Shilts (1982) and Adshead (1983b) who arrived at similar conclusions. Those authors examined sediment from Hudson Bay, as well as glacial and nonglacial material from the Hudson Bay Lowlands.

Dyke (1983) has implied that a Late Wisconsin age for glacial flow patterns in Hudson Bay was suggested by Henderson (1983). This is not the case; no age for the glacial pattern (other than Quaternary) was stated in the paper.

With reference to siderite, the provenance of this mineral is unclear; however, its euhedral form and common

limonitic stain is similar to that reported in the Paleozoic Devonian sequences (Skinner, 1973). The interpretation by Henderson (1983) is based on the close association of siderite concentration in Hudson Bay with the outcrop of Devonian formations which are known to have high siderite content where they outcrop on land in the Moose River Basin. Other or additional sources may well be available in pre-Quaternary sediments. It should be kept in mind, however, that the author made no reference to glacial dispersal trains of siderite.

Dyke (1983) has suggested offshore glacial flow from the Stooping River and Kwataboahegan formations to explain high concentrations of siderite in the southwestern part of the bay. It should be noted, however, that siderite has been reported in till west of Hudson Bay along the proposed Polar Gas Pipeline route (Shilts, 1980; Paré, 1982; see Henderson, 1983, Fig. 48.2). Therefore, if a Devonian source is assumed, westerly glacial flow must also have predominated at some time during the Quaternary.

As stated in Henderson (1983), the study was undertaken to determine whether any trends in heavy mineral distribution could be recognized from a sampling of the few bottom samples available from Hudson Bay. It was hoped that these trends could be related to fluvial or marine processes, to bedrock lithologies, or to glacial processes affecting the bay. Patterns were found that indicate further detailed work is in order. These patterns are not inconsistent with glacial dispersal trends proposed by Shilts (1982) and Adshead (1983a, b).

References

Adshead, J.D.
1983a: Hudson Bay river sediments and regional glaciation: I. Comparision of carbonate dispersal trains southwest of Hudson and James Bay, Canadian Journal of Earth Science, v. 20, p. 290.

1983b: Hudson Bay river sediments and regional glaciation: III. Implications of mineralogical studies for Wisconsin and earlier ice-flow patterns. Canadian Journal of Earth Science, v. 20, p. 322.

Aylsworth, J.M., Boydell, A.N., and Shilts, W.W.
1981: Surficial geology, Tavani, District of Keewatin; Geological Survey of Canada, Map 9-1980, 1:125 000 scale.

Dyke, A.S.
1983: A study of the heavy mineral distribution in the bottom sediments of Hudson Bay: Discussion; in Current Research, Part B, Geological Survey of Canada, Paper 83-1B.

Henderson, P.J.
1983: A study of the heavy mineral distribution in the bottom sediments of Hudson Bay; in Current Research, Part A, Geological Survey of Canada, Paper 83-1A, p. 347-351.

Klassen, R.A. and Shilts, W.W.
1977: Glacial dispersal of uranium in the District of Keewatin, Canada; in Prospecting in Areas of Glaciated Terrain, 1977; Institute of Mining and Metallurgy, London, p. 80-88.

Paré, D.
1982: Application of heavy mineral analysis to problems of till provenance along a transect from Longlac, Ontario to Somerset Island; unpublished M.A. thesis, Carleton University, Ottawa.

Pelletier, B.R.
1969: Submarine physiography, bottom sediments and models of sediment transport; in Earth Science Symposium on Hudson Bay, ed. P.J. Hood; Geological Survey of Canada, Paper 68-53, p. 100-136.

Ridler, R.H. and Shilts, W.W.
1974: Exploration for Archean polymetallic sulphide deposits in permafrost terrains: an integrated geological/geochemical technique, Kaminak Lake Area, District of Keewatin; Geological Survey of Canada, Paper 73-34.

Shilts, W.W.
1973: Drift prospecting, geochemistry of eskers and till in permanently frozen terrain: District of Keewatin, Northwest Territories; Geological Survey of Canada, Paper 72-45, 34 p.

1980: Geochemical profile of till from Longlac, Ontario to Somerset Island, Canadian Mining and Metallurgical Bulletin, v. 73, p. 85-94.

1982: Quaternary evolution of the Hudson/James Bay region; Le naturaliste canadien, v. 109, p. 309-332.

Skinner, R.G.
1973: Quaternary stratigraphy of the Moose River basin, Ontario; Geological Survey of Canada, Bulletin 225, p. 38.

Vincent, J.
1977: Le Quaternaire recent de la région du cours inferieur de La Grande Rivière, Québec; Commission géologique du Canada, Étude 76-19.

Winterhalter, B.
1972: On the geology of the Bothnian Sea, an epeiric sea that has undergone Pleistocene glaciation; Geological Survey of Finland, Bulletin 258.

CANADA-NOVA SCOTIA CO-OPERATIVE MINERAL PROGRAM 1981-84

CANADA-NOUVELLE-ÉCOSSE: PROGRAMME COOPÉRATIF SUR LES MINÉRAUX 1981-84

CONTENTS/TABLES DES MATIÈRES

Camera-ready copy was provided by:/Le texte prêt à être photographié a été fournir par:
Nova Scotia Department of Mines and Energy.

GEOLOGY OF THE COCHRANE HILL GOLD DEPOSIT, GUYSBOROUGH COUNTY, NOVA SCOTIA*

P. K. Smith**

ABSTRACT

The Cochrane Hill gold deposit is located within the Cambro-Ordovician Meguma Group of southeastern Nova Scotia. A detailed examination of this turbidite-hosted deposit indicates a polygenetic origin for the vein mineralization. The Meguma Group sediments probably represent the original source for much of the gold in this deposit. At least six different vein types occur at Cochrane Hill (type A to type F). These include, from oldest to youngest, type-A stratiform micro-crosslaminated veins, type-B stratiform/stratabound veins, type-C bedding-parallel veins, type-D flat angular veins, type-E crosscutting pegmatoid veins and type-F crosscutting high angle stringers. The relative age range of these veins is from late syn-sedimentation to post-Hercynian Orogeny. The relative ages of veins and gold mineralization is based on crosscutting relationships with (i) the Acadian and Hercynian structures, (ii) porphyroblastic mineral growth during the Acadian amphibolite grade static metamorphism, and (iii) with subsequent Devono-Carboniferous plutonism. Although much of the gold is associated with the earlier veins, remobilization and/or secondary enrichment has occurred not less than four times during the geological history.

Regional, amphibolite grade, static metamorphism is presumed to be an Acadian event. Index porphyroblasts include muscovite, biotite, garnet, staurolite and andalusite. In the area of the mine these porphyroblasts are observed to overgrow poorly preserved Acadian structures. Fabrics which deform and augen the index porphyroblasts are regarded as Hercynian. Hercynian structures are generally dominant over the northern domain, adjacent to the Minas Geofracture. The early structural history is preserved in strain windows where locally, competent units preserve Acadian structures. In less competent metapelites these structures have been destroyed or strongly deformed by the Hercynian Orogeny.

---

*Contribution to Canada-Nova Scotia Co-operative Mineral Program 1981-84. Project carried by Nova Scotia Department of Mines and Energy

Full paper printed in Mines and Minerals Branch, Report of Activities, 1982; Nova Scotia Department of Mines and Energy, Report 83-1

**Nova Scotia Department of Mines and Energy, Halifax, Nova Scotia

GEOLOGICAL HISTORY OF THE ISAACS HARBOUR AREA

PARTS OF 11F/3 AND 11F/4, GUYSBOROUGH COUNTY, NOVA SCOTIA*

J. D. Keppie**

ABSTRACT

The Meguma Group of the Isaacs Harbour area consists of the predominantly sandy turbidites of the Goldvenville Formation overlain by slates of the Halifax Formation. Deposition of the Meguma Group appears to have been accompanied by the formation of monoclinal faults over postulated high angle basement faults. These faults are believed to have formed in response to the transpression which produced the graben or trough in which the Goldenville Formation was deposited. These faulted monoclines also appear to have formed the locus of fissures which formed the conduits for hot springs producing auriferous veins.

Deposition of the Meguma Group was followed by three phases of (?)Acadian deformation accompanied by greenschist facies metamorphism. The first, D_s, produced a low angle foliation induced by mass sliding on bedding plane shears. The second and main phase of deformation, D_g, produced the major folds, pressure solution and slaty cleavage. These F_g folds appear to have nucleated at the steep limbs of the early monoclinal folds. Gold appears to have been remobilized into tight cylindrical and conical F_g fold hinges. The F_g folds were produced by oblique flexural folding and tangential longitudinal strain with the X-axis of the finite strain ellipsoid approximately horizontal and east-west. It is postulated that these structures were induced by dextral transcurrent movements on the faulted monoclines. This is consistent with the dextral movements inferred to have taken place on the Minas Geofracture during the Acadian Orogeny. The third phase of deformation, D_c, produced a subhorizontal crenulation cleavage as a result of gravitational collapse induced by the relaxation of the D_g stresses.

This was closely followed by amphibolite facies, low pressure regional metamorphism in the northern part of the area, characterized by porphyroblasts of biotite, garnet, staurolite, andalusite and cordierite. This was followed by intrusion of the Sherbrooke pluton yielding a whole rock Rb/Sr isochron age of 369 ± 2 Ma.

Further deformation followed correlated with the Hercynian Orogeny. This produced shear and flattening foliations which transposed earlier fabrics and rotated the porphyroblasts which are most intense north of the Stormont and Waternish Synclines. Gold appears to have been remobilized along Hercynian shear zones. This deformation becomes less intense southwards. Kinematic interpretation suggests that these structures resulted from dextral movements on the Minas Geofracture.

Finally, the area was cut by a series of northwest-southeast sinistral transcurrent faults associated with kink bands. These are inferred to be the result of sinistral movements on the Minas Geofracture during the early Mesozoic as the Bay of Fundy Rift formed.

---

*Contribution to Canada-Nova Scotia Co-operative Mineral Program 1981-84. Project carried by Nova Scotia Department of Mines and Energy
Full paper printed in Mines and Mineral Branch, Report of Activities, 1982; Nova Scotia Department of Mines and Energy, Report 83-1.

**Nova Scotia Department of Mines and Energy, Halifax, Nova Scotia

THE STRUCTURE OF THE MEGUMA GROUP BETWEEN GEGOGAN HARBOUR AND COUNTRY HARBOUR, GUYSBOROUGH COUNTY*

B. H. O'Brien**

ABSTRACT

A multiphase history of Acadian deformation is proposed for Meguma Group rocks between Gegogan Harbour and Country Harbour, Guysborough County. Three episodes of coaxially superimposed deformation are recognized on the basis of regionally developed, minor structures. In ascending order they are here defined as the Sherbrooke deformation (D_s), the Guysborough deformation (D_g) and the Country Harbour deformation (D_c). Cleavages, folds, lineations and vein-filled fractures were produced during successive increments of a progressive deformation. These minor structures are developed on only one group of major, east-west trending folds. They record the various effects of the D_s, D_g and D_c deformations in producing the present shape and orientation of the regional folds. The latest movements on the major faults postdate the formation of the major folds and the intrusion of the 369 ± 2 Ma Sherbrooke pluton.

*Contribution to Canada-Nova Scotia Co-operative Mineral Program 1981-84. Project carried by Nova Scotia Department of Mines and Energy and by Geological Survey of Canada.
Full paper printed in Mines and Minerals Branch, Report of Activities, 1982; Nova Scotia Department of Mines and Energy, Report 83-1.

**Nova Scotia Department of Mines and Energy, Halifax, Nova Scotia.

TYPOMORPHISM OF TURBIDITE-HOSTED AURIFEROUS QUARTZ VEINS, SOUTHERN GUYSBOROUGH COUNTY*

S. J. Haynes**

ABSTRACT

Field studies were concentrated in the greenschist facies Meguma Terrane of southern Guysborough County at Wine Harbour (chlorite zone) and Isaacs Harbour-Goldboro-Seal Harbour (biotite zone). Eleven different quartz-vein polytypes have been distinguished on the basis of form, characteristic mineralogy, wall-rock alteration and crosscutting relationships to each other and regional structures. Gold is only present in stratiform, stratabound and side veins and as rare disseminations in the host rock slates. These predate the main period of Acadian deformation, dynamo-thermal metamorphism and granite intrusion. Most of the gold is contained within stratiform veins which exhibit crosslamination and columnar structures similar to modern geyserites observed in active geothermal areas. Gold is preferentially enriched in those zones where high angle K-feldspar ± muscovite bearing "feeders" (step and side veins) are abundant. These feeders often display marked arsenopyritization and/or sericitization of the wall rocks. The gold districts are preferentially located near the hinge zone of asymmetric Acadian folds. Although true "saddle reefs" are present, many vein systems are located on the limbs of folds often adjacent to monoclinal flexures. It is postulated that these monoclinal zones represent tectonic reactivation of original fault systems. The mineralogy and form of the veins, and their attendant wall-rock alteration effects, suggest that gold was deposited initially from hydrothermal solutions, that passed upward through the fault systems, as they were ejected into seawater as low density plumes from submarine hot springs. This resulted in aprons of siliceous sinter being deposited at the spring orifices and a flanking mat of siliceous chemical sediment being deposited from the plume. Phase relations and the composition of fluid inclusions suggest that CO_2 boiled off from low-salinity hydrothermal solutions to yield potassium silicate assemblages in the feeders and carbonate assemblages in the sediments (stratiform veins). The origin of these solutions is as yet unknown, but may be related to dewatering of the lower Meguma Group or the basement. Although hydrothermal mobilization of gold and silica during early Acadian dynamo-thermic events cannot be discounted, syn-deformational quartz veins emplaced during the main period of Acadian deformation and metamorphism (discordant, radial and vertical veins) are devoid of gold. This casts doubt on those previous theories that invoked deposition of the auriferous quartz veins during Acadian dynamo-thermal metamorphism and deformation.

---

*Contribution to Canada-Nova Scotia Co-operative Mineral Program 1981-84. Project carried by Nova Scotia Department of Mines and Energy

Full paper printed in Mines and Mineral Branch, Report of Activities, 1982; Nova Scotia Department of Mines and Energy, Report 83-1.

**Nova Scotia Department of Mines and Energy, Halifax, Nova Scotia

LOCH LOMOND BASIN, CAPE BRETON ISLAND, WINDSOR GROUP PROJECT - AN UPDATE*

R. C. Boehner**

INTRODUCTION

Field activities continued in the Loch Lomond Basin (Fig. 1) first outlined in a preliminary report by Boehner (1981). This outline summarized previous work and results up to the 1980 field season. Field mapping and logging of a series of diamond-drill hole controlled cross-sections has been completed in the area between Head of Loch Lomond and Terra Nova-Big Glen (Fig. 2). The project area is planned to be extended into the Salmon River area through to the southern part of the Sydney Basin project area (see Giles, this volume).

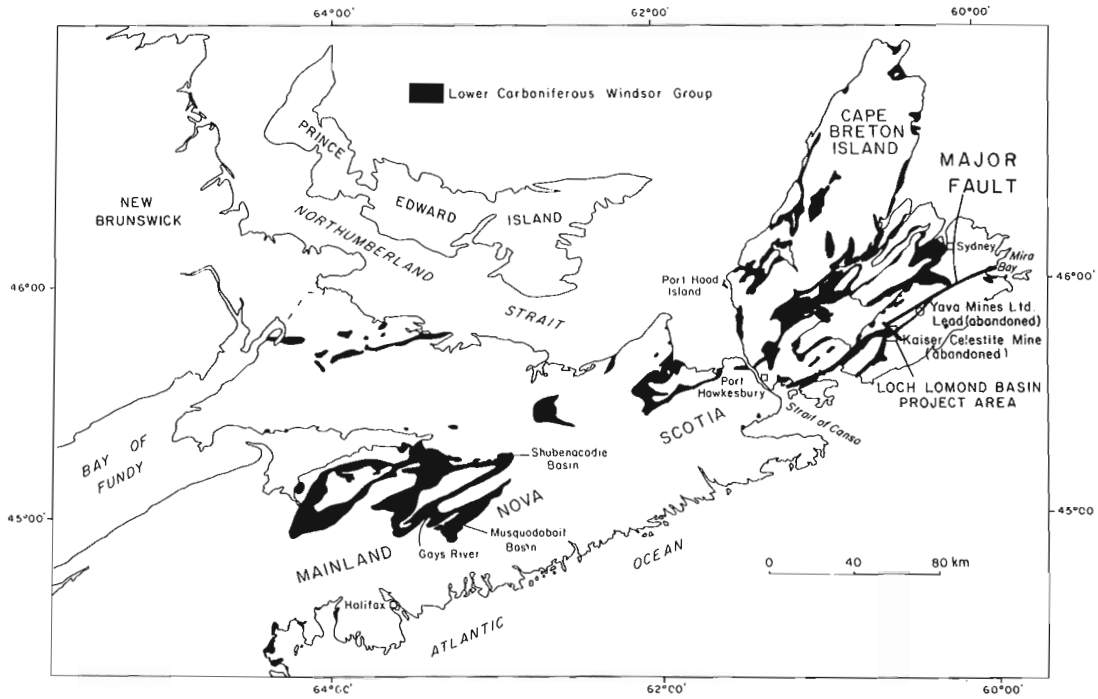

Figure 1. Location map of the Loch Lomond project area.

Mining activity and mineral exploration in the Loch Lomond area have had a fluctuating history. Coal was mined to limited extent near Glengarry and manganese was produced in small amounts near Enon and McCuish Brook in the early 1900's. Enon was the site of a celestite mine operated by Kaiser Celestite Mining Ltd. between 1970 and 1976 when poor markets forced the operation to close (Forgeron, 1977). Between 1979 and 1981 the

*Contribution to Canada-Nova Scotia Co-operative Mineral Program 1981-84 Project carried by Nova Scotia Department of Mines and Energy.
Also in Mines and Minerals Branch, Report of Activities, 1982, Nova Scotia Department of Mines and Energy, Report 83-1.

**Nova Scotia Department of Mines and Energy, Halifax, Nova Scotia.

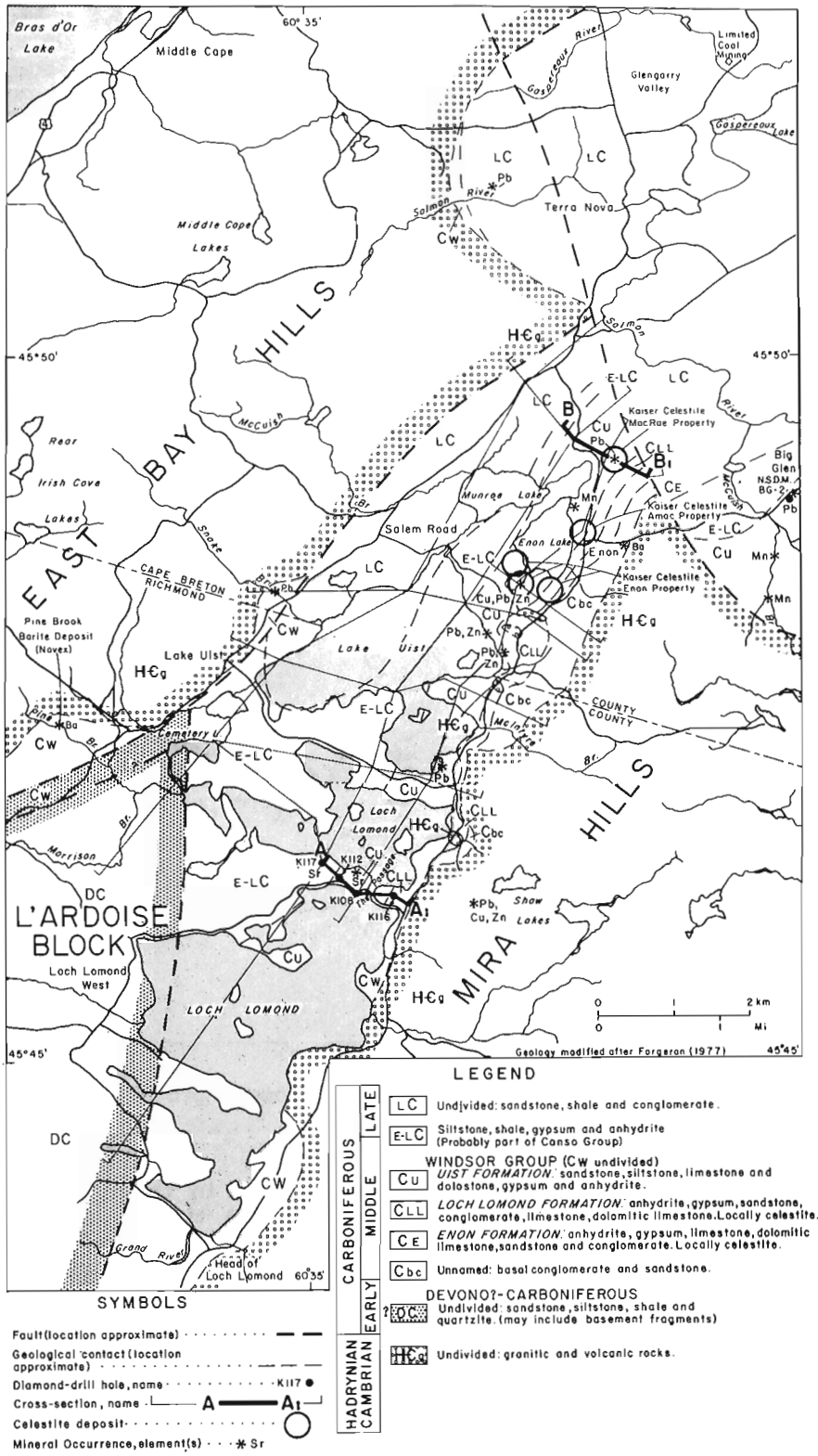

Figure 2. Preliminary geological map of the Loch Lomond Basin, Cape Breton Island.

mill at Enon was used by Yava Mines Ltd. to produce lead concentrate from the Salmon River lead deposit located 14 km to the northeast. Declining metal prices and difficult economic conditions were major contributors to the premature closing of the Yava Mine. More recently Novex Mining and Exploration Ltd. is reactivating the mill at Enon to beneficiate barite from the Pine Brook deposit on the northwestern border of the Loch Lomond Basin (Fig. 2).

The Loch Lomond Project was undertaken to document the stratigraphic onlap of Windsor Group rocks in an area of high paleotopographic relief in a marginal basin setting. Within this framework the distribution and origin of the area's numerous mineral occurrences and deposits (Sr, Ba, Pb, Cu, Zn, Mn and Fe) could be evaluated and predictive models developed. Economic minerals are believed to be closely related to paleogeography (topography), and sedimentation history especially unconformities and stratigraphic onlap-overstep. The possible inherited relationship of the geochemistry of the underlying basement to adjacent sediment hosted mineral deposits remains to be determined.

STRUCTURE

The Loch Lomond Basin is an asymmetric structural basin and contains up to 800+ m of Viséan to Namurian age rocks. It has the form of a northeasterly-southwesterly trending half graben bounded on the northwest by a high angle fault (Fig. 2). This fault is inferred to have up to 800 m of dip slip and uncertain, but potentially kilometres of strike slip. It is a major fault that extends from the Strait of Canso to Mira Bay (Figs. 1 and 2). The Basin is bordered on the northwest by Hadrynian Fourchu Group volcanic-sedimentary rocks and plutonic rocks of the East Bay Hills. The major unconformable contact to the southwest is with similar rocks of the East Bay Hills (largely the Loch Lomond pluton). To the southwest, the basin pattern is complicated by the L'Ardoise Block consisting of deformed Devono-Carboniferous sediments. This block although originally considered to be a thrust (Weeks, 1954) is presently interpreted to be bounded by high angle strike slip faults and is allochthonous to the area. The continuity of the northwestern border fault is broken by a high angle transverse fault near Terra Nova and Big Glen. Small scale faults (displacement <2 m) related to this fault are found in the MacRae property celestite open-pit.

Faulting which is suspected to occur locally along the southeastern border of the Basin has probably been obscured by solution collapse and the highly irregular basement topography. Present basement slopes, as interpolated from drillhole data range from 10°-15° in the intermediate to central part of the Basin to 20°-35° along parts of the margin. The steeper dips may be related to early basin block faulting and erosion.

STRATIGRAPHY AND SEDIMENTATION

The Loch Lomond Basin contains a mixed Carboniferous succession dominated by continental alluvial-fluvial and marine evaporite-carbonate sediments. The Carboniferous generally represents molassic deposition in a complex wrench fault basin system. The Loch Lomond Basin area is one of the few areas where data are available to document the details of progressive onlap of coarse and fine grained siliciclastics and carbonates onto basement. Major rock packages recognized (Fig. 3) are comparable

(with a few exceptions) with those in other parts of Nova Scotia and include in ascending order: Windsor Group comprising interstratified evaporite, fine to coarse redbeds and marine carbonate of the Enon, Loch Lomond and Uist Formations (up to 350 m); fine grained Canso Group (up to 200 m); and upper Canso Group (dominantly grey sandstone up to 250+ m).

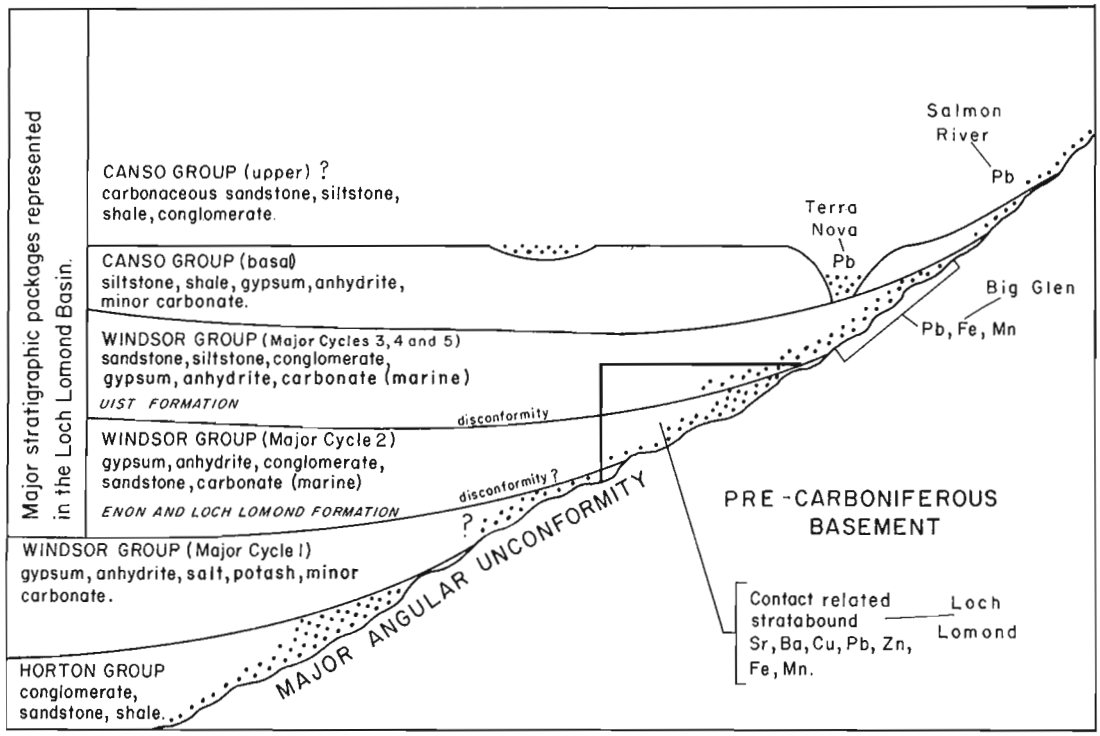

Figure 3. Schematic stratigraphy, onlap-overstep and mineral occurrences, Loch Lomond Basin and vicinity, Cape Breton Island.

Progressive onlap and overstep of stratigraphic packages with accompanying facies changes are well documented both parallel and perpendicular to the strike of the Loch Lomond Basin (Fig. 3). Similar changes are also present in the Salmon River-Glengarry Basin. Details of these features remain to be fully documented (1982-1983).

The typical basal Windsor Group evaporite section (Major Cycle 1) and Horton Group rocks are absent in the Loch Lomond Basin because of onlap and overstep (Fig. 3). Some of the coarse conglomerate breccia at the base of the section, especially in the Head of Loch Lomond area southwest to Grand River, may be a marginal fanglomerate facies of Major Cycle 1. Major Cycles 2 through 5 (Subzone B and Subzones C to E) display rapid facies variation, but are typical of mixed continental and evaporitic marine Windsor Group lithology. The Enon and Loch Lomond Formations (Major Cycle 2) are interstratified sections dominated by gypsum and anhydrite, with redbeds, conglomerate-breccia, sandstone, siltstone and fossiliferous marine carbonate. This package is disconformably overlain by the Uist Formation.

The Uist Formation (Major Cycles 3, 4 and 5) is a generally similar package, but is dominated by redbeds, siltstone-sandstone and minor

conglomerate with interbedded fossiliferous marine carbonate and minor gypsum and anhydrite.

Conformably overlying fine grained Canso Group rocks are dominantly grey and red siltstone-shale with minor gypsum and anhydrite, and rare algal limestone. This sequence is inferred to represent the transition from marine to continental sedimentation in residual evaporitic lacustrine environment that followed the retreat of Windsor seas. A thick fluvial section of grey sandstone with minor red to grey siltstone-shale concordantly to disconformably overlies the fine grained Canso and is tentatively assigned to the upper part of the Canso Group.

Windsor Group sections representing all or parts of Major Cycles 2 through 5 (Subzone B and Subzones C to E) display rapid facies change ranging over a distance of several kilometres from evaporite dominated (ie. Passage Bridge Section, Fig. 4a) to terrigenous (conglomerate breccia) dominated (ie. MacRae Property, Fig. 4b). Marine carbonate members locally exhibit rapid facies change especially in the terrigenous dominated sections. In these sections the carbonate has undergone severe recrystallization, has been reworked to form calcirudites or has been completely removed by erosion. In some areas shelly carbonate banks are preferentially developed on, or surrounding, protruding paleotopographic basement highs. Facies change is particularly dramatic where redbeds change basinward to evaporites. This change is masked and complicated in part by karstification and solution collapse features.

Within the Windsor Group formations, the carbonate members pinchout marginally (Fig. 5). The major members record widespread and sustained marine invasions trangressing further up the margin of the basin. Thinner carbonate members representing less widespread marine transgressions pinchout and are not represented in areas such as Big Glen and Terra Nova. These areas which are structurally preserved by faulting, may represent facies which formerly were present updip (southeast) from the Loch Lomond area. A similar facies relationship may also be inferred to occur parallel to the basin strike (to the northeast).

Paleotopography and tectonism greatly influenced sedimentation in the Loch Lomond Basin especially in the early stratigraphic units. The importance of paleotopography decreased with time as erosion and deposition of onlapping strata buried the basement topography. The sequence to the top of the fine grained Canso Group displays overall fining upward and basinward trends. Coarse fanglomerates occur as marginal facies of the Windsor Group at all stratigraphic levels.

The Windsor Group has been complicated by karstification and solution collapse of subcropping evaporite sections along the southeastern border of the Basin (Fig. 4a). The age(s?) of this feature are as yet unclear, but appear to postdate the celestite deposits which are collapsed and redistributed to some extent. Diagenetic and weathering processes may have been important in the preparation of porosity-permeability within host rocks.

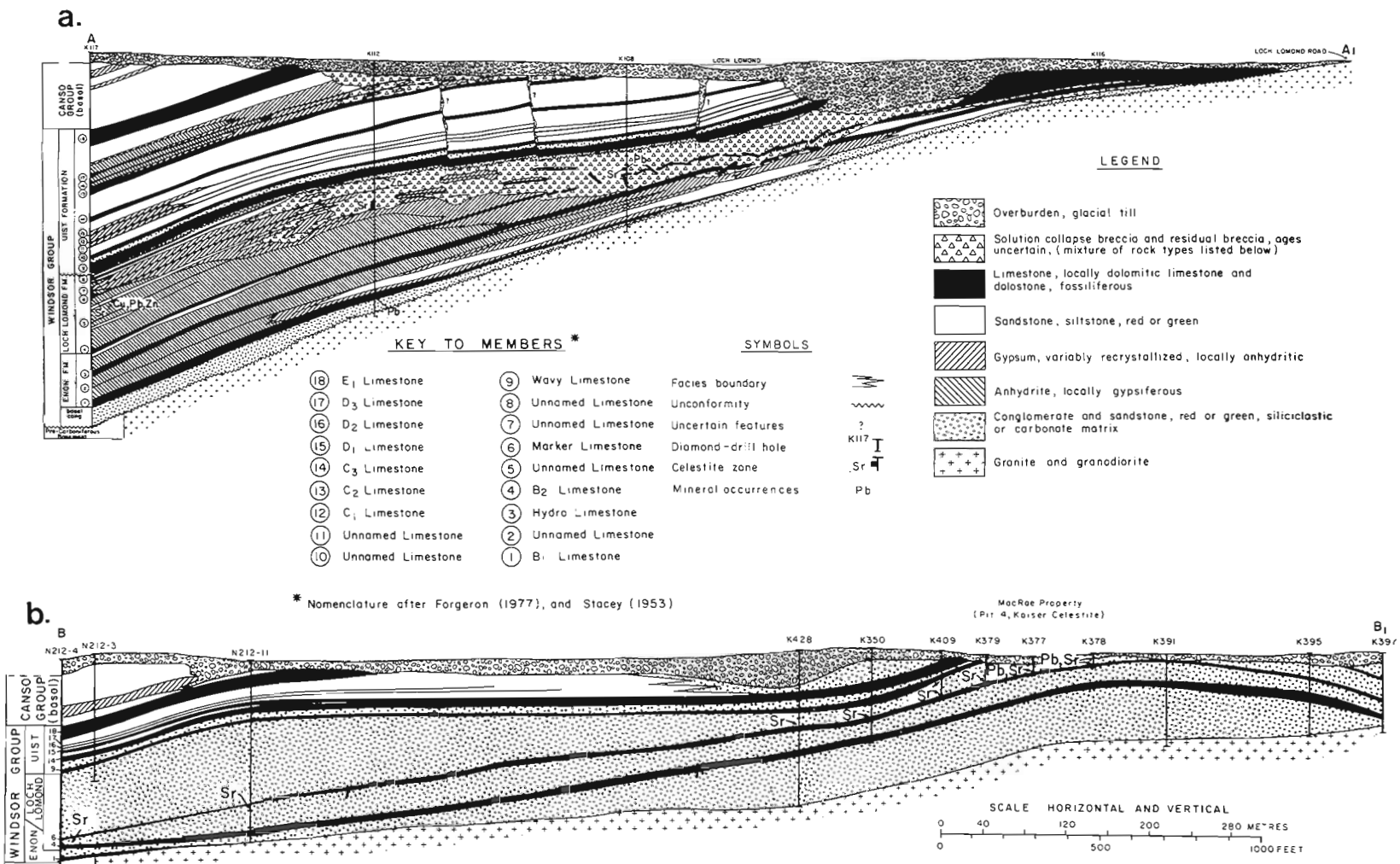

Figure 4a. Geological cross-section A-A_1, Passage Bridge, Loch Lomond Basin, Cape Breton Island.

4b. Geological cross-section B-B_1, MacRae Property, Loch Lomond Basin, Cape Breton Island.

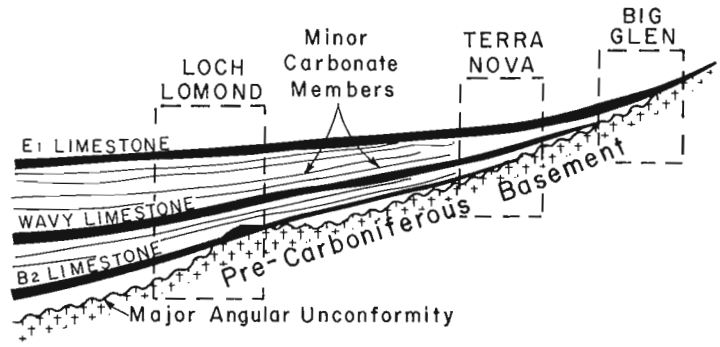

Figure 5. Windsor Group onlap relations in the vicinity of Loch Lomond, Terra Nova and Big Glen.

MINERAL DEPOSITS

Mineral development in the Loch Lomond Basin has occurred primarily in the celestite deposits at Lake Enon with very minor exploitation of manganese at McCuish Brook. Substantial celestite resources are presently economically unattractive due to lack of markets. Mineral exploration has been directed at base metal deposits of several types: 1) the Salmon River type, galena in sandstone, e.g. Terra Nova; 2) carbonate hosted onlap facies Pb-Zn similar to the Gays River type, e.g. E_1 limestone at Big Glen, B_2 limestone; and 3) contact oriented, Macumber Formation Horton-Windsor contact type Cu ± Pb ± Zn, e.g. B_1 limestone.

Base metals ± celestite ± Fe-Mn occurrences are contact related and localized at or near unconformity pinchouts at all stratigraphic levels (Fig. 3) where suitable chemistry, hydrology, lithology and geometry were present. Pinchout areas are inferred to have provided the necessary geometric conditions trapping and mixing metal-mineralizing fluids. Pyrite and/or organic material (coal debris and possibly liquid hydrocarbons) within a suitably porous and permeable host may have been important precipitating agents for base metals. However, the details of base metal deposition are unclear. The weathering or diagenetic alteration of silicate minerals in the continental sediments is a possible source of metals within tectonically active evaporitic arid molassic basins.

Tectonism, high angle faults and possibly increased thermal activity related to tectonism may have been important as the driving mechanism for large scale movement of mineralizing fluids.

Barite and celestite ± Pb ± Fe are dominantly stratabound, nodular to irregular replacement deposits. Carbonate rocks and redbeds are the major hosts. Celestite bodies are localized at or near facies changes particularly in carbonate rocks at carbonate-gypsum contacts and in redbeds at gypsum contacts. Sr is a common minor element in marine evaporites and may be released during gypsum/anhydrite dehydration/hydration. Shallow subaqueous and diagenetic nodular sulphates (modern sabkhas) often have celestite as an accessory mineral, but never in the large amounts present

at Loch Lomond. Dissolution of Sr-enriched evaporites maybe a source for Loch Lomond celestite, but a working hypothesis is yet to be tested. Dissolution of updip evaporites may have occurred during regression and redbed progradation (fanglomerate) may have provided a preconcentrated source for a large quantity of strontium. This could have migrated downdip in continental waters within the redbeds. Deposition of celestite from solutions subsequently occurred as replacement of suitable (sulphate enriched) host redbeds and carbonate. Base metals, especially Pb, are sometimes closely associated with the celestite. Fe may also be present as hematite with or without manganese especially in redbed hosts. Barite and celestite $\pm$ Pb $\pm$ Fe may represent early diagenetic replacement during, or soon after sedimentation.

Barite occurs as replacement of limestone in a stratabound deposit at Pine Brook (Fig. 2). Although details of the setting and origin of this deposit are not clear, it appears to be similar in character to the celestite bodies at Enon.

REFERENCES

Boehner, R. C.
1981: Preliminary report on the geology and mineral deposits of the Loch Lomond Basin, Cape Breton Island; in Mineral Resources Division, Report of Activities, 1980; Nova Scotia Department of Mines and Energy, Report 81-1, p. 153-165.

Forgeron, S.
1977: The Kaiser Celestite mining operation and mineral potential of the Loch Lomond Basin, Cape Breton, Nova Scotia; Nova Scotia Department of Mines, Open File Report 328.

Stacey, M. C.
1953: Stratigraphy and paleontology of the Windsor Group (Upper Mississippian) in parts of Cape Breton Island, Nova Scotia; Nova Scotia Department of Mines, Memoir 2, 143 p.

Weeks, L. J.
1954: Southeast Cape Breton Island, Nova Scotia; Geological Survey of Canada, Memoir 277, 112 p.

SEDIMENTARY FEATURES OF THE GOLDENVILLE FORMATION, SHERBROOKE AREA, NOVA SCOTIA*

J. W. F. Waldron**

The Goldenville Formation in eastern Nova Scotia resembles other Lower Paleozoic greywacke terranes in consisting of monotonous alternations of sandstone and slate, which have so far resisted attempts at stratigraphic subdivision. Several unique features indicate peculiarities of both the depositional environment and the source area.

Goldenville sandstone beds range from less than 1 cm to several metres in thickness. They commonly show sharp scoured basal surfaces against underlying slate, with abundant grooves and flutes. Top surfaces of sandstone beds may be gradational or sharp. Depositional sedimentary structures within beds include parallel and ripple crosslamination, and locally abundant slate intraclasts. Syn-sedimentary deformation and water-escape produced convolute lamination, load casts and pseudonodules, dish, pipe and sheet structures, and abundant small sand volcanoes. Sandstone dykes penetrate upwards into overlying slate at some horizons.

Sandstone beds may be classified into two groups according to the nature of the top surfaces. **Beds with gradational tops** correspond well with those described from submarine fan environments elsewhere (Walker, 1979). Three intergradational types are recognized (Fig. 1).

1) **Massive sandstones** are typically 50 cm to 3 m thick, but frequently occur in amalgamated packets, within which distinct depositional events are difficult to distinguish. Grading is usually confined to the top few centimetres, in which parallel or ripple crosslamination may be present.

2) **Proximal turbidites** are usually 10 cm to 50 cm thick, and grade into overlying slates. They show complete (T_{abcde}) or partial (T_{abe} or T_{ae}) Bouma sequences.

3) **Distal turbidites** are generally thinner and lack the basal structureless "a" division of the Bouma sequence. Thinner beds lack the "b" division also. Distal turbidites are largely confined to slate dominated intervals in the Goldenville Formation.

Types 2 and 3 represent classical turbidites and type 1 massive sandstones were probably deposited by currents intermediate between true turbidity flow and grain flow; massive sandstones are common in channelled parts of many ancient submarine fan deposits.

Beds with sharp upper surfaces do not correspond with classical turbidites, but are believed to represent modifications of types 1-3 above. Two processes were responsible for this modification (Fig. 1).

---

*Contribution to Canada-Nova Scotia Co-operative Mineral Program 1981-84. Project carried by Nova Scotia Department of Mines and Energy

Also in Sixth Annual Open House and Review of Activities, Program and Summaries, Nova Scotia Department of Mines and Energy, Information Series No. 5.

** Department of Geology, Saint Mary's University, Halifax, Nova Scotia.

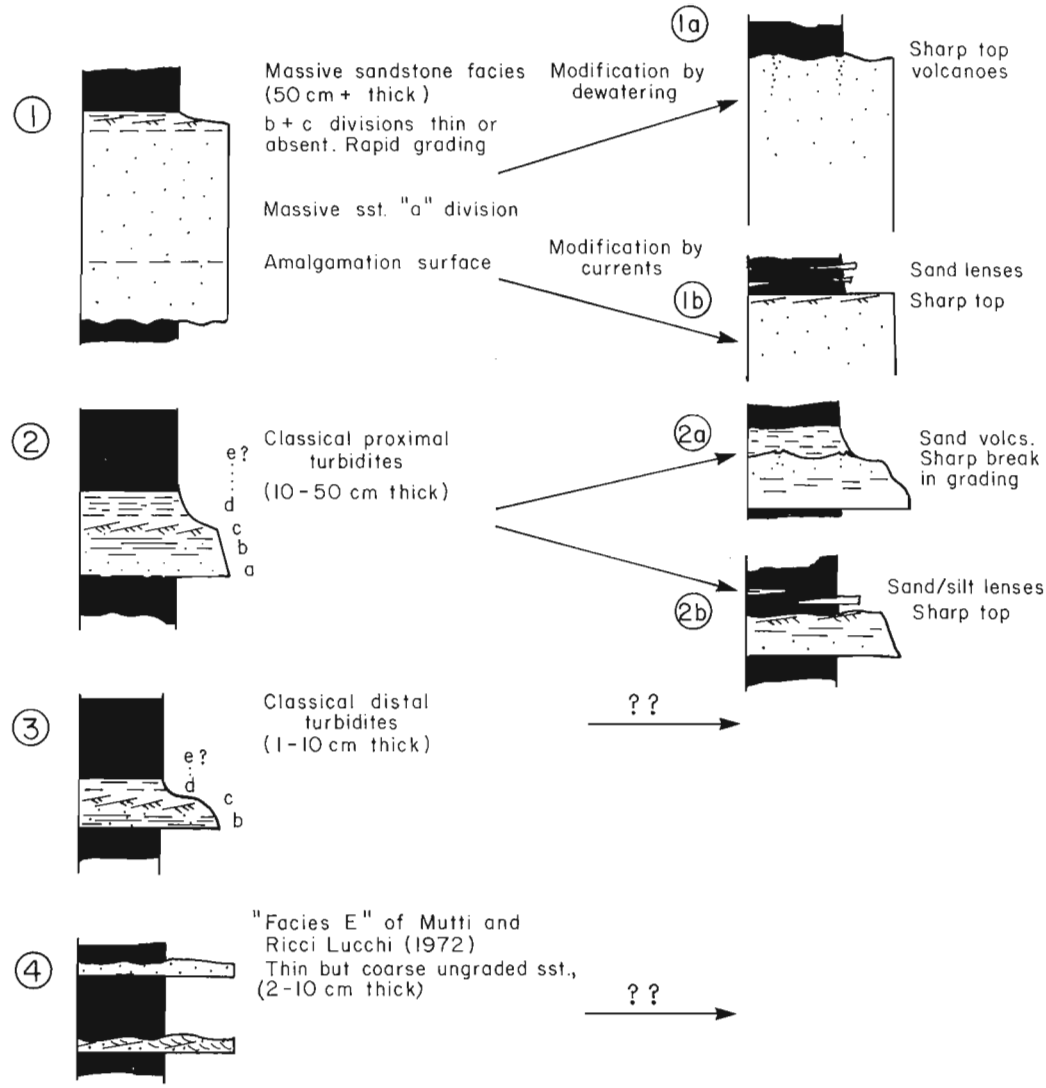

Figure 1. Diagram to show typical Goldenville Formation sandstone layer types.
Left: Layers typical of submarine-fan turbidite deposits generally.
Right: Layers modified by dewatering and current reworking.

a) **Dewatering:** water escaped from rapidly deposited sands, transporting sand grains upwards through the layers and sometimes depositing them in small (5-20 cm diameter) sand volcanoes on the upper surface. Graded silt and mud (now slate) were deposited above this surface.

b) **Reworking by bottom currents** produced sharp, rippled top surfaces overlain by slates containing isolated starved ripples and discontinuous laminae of reworked sand and silt. Tectonic deformation of the commonly lingnoid ripples precludes systematic measurement of the current direction.

Occasional very thin (2-5 cm) beds of medium to coarse rather well sorted crosslaminated sandstone (Fig. 1) cannot be explained by either of the above processes, but appears similar to "facies E" turbidites of Mutti and Ricci Lucchi (1972), believed to represent overbank or mouth bar deposits associated with submarine fan channels.

Direct observation of the geometry of Goldenville sandstone bodies is not generally possible, owing to the difficulty of correlating along strike between sections. Current directions have low plunge, so that channels, if present, are unlikely to show up in the outcrop pattern. Correlation across an anticline at Indian Harbour suggests that considerable across strike variation occurs in the overall thickness of sandstone packets.

Further indications of channelling are:

i) lenticular and crosscutting relationships at erosive bases of massive sandstones,
ii) abundance of intraclasts at some horizons,
iii) presence of "facies E" sandstones (see above)

Petrographic study of the sandstones is at an early stage. The sandstones are "sublitharenites" containing abundant metamorphic chlorite probably representing original clay matrix. Detrital components include quartz, alkali, and plagioclase feldspar, muscovite, tourmaline, sphene, pyroxene and ?epidote. A number of samples show a strongly bimodal grain-size distribution, with a conspicuous well-sorted component of coarse, well rounded "millet seed" sand. The presence of sedimentary rock fragments as well as quartz grains in this component suggests that the rounded grains are unlikely to have been derived by erosion of an older sandstone; rounding therefore possibly occurred in an eolian environment in the Goldenville source area.

REFERENCES

Mutti, E and Ricci Lucchi, F.
1972: Le torbiditi dell'Appennino settentrionale: introduzione all'analisi di facies; Memoir Societa Geologica Italiana, v. 11, p. 161-199.

Walker, R. G.
1979: Turbidites and associated coarse clastic deposits; in Facies Models, ed. R. G. Walker; Geoscience Canada, Reprint Series 1, p. 91-103.

Author Index

Erratum

Geological Survey of Canada Paper 83-1A
Current Research Part A, Report 47, p. 344-346

DPTA should read DTPA

NOTE TO CONTRIBUTORS

Submissions to the *Discussion* section of *Current Research* are welcome from both the staff of the Geological Survey and from the public. Discussions are limited to 6 double-spaced typewritten pages (about 1500 words) and are subject to review by the Chief Scientific Editor. Discussions are restricted to the scientific content of Geological Survey reports. General discussions concerning branch or government policy will not be accepted. Illustrations will be accepted only if, in the opinion of the editor, they are considered essential. In any case no redrafting will be undertaken and reproducible copy must accompany the original submissions. Discussion is limited to recent reports (not more than 2 years old) and may be in either English or French. Every effort is made to include both *Discussion* and *Reply* in the same issue. *Current Research* is published in January, June and November. Submissions for these issues should be received not later than November 1, April 1, and September 1 respectively. Submissions should be sent to the Chief Scientific Editor, Geological Survey of Canada, 601 Booth Street, Ottawa, Canada, K1A 0E8.

AVIS AUX AUTEURS D'ARTICLES

Nous encourageons tant le personnel de la Commission géologique que le grand public à nous faire parvenir des articles destinés à la section discussion *de la publication* Recherches en cours. *Le texte doit comprendre au plus six pages dactylographiées à double interligne (environ 1500 mots), texte qui peut faire l'objet d'un réexamen par le rédacteur en chef scientifique. Les discussions doivent se limiter au contenu scientifique des rapports de la Commission géologique. Les discussions générales sur la Direction ou les politiques gouvernementales ne seront pas acceptées. Les illustrations ne seront acceptées que dans la mesure où, selon l'opinion du rédacteur, elles seront considérées comme essentielles. Aucune retouche ne sera faite aux textes et dans tous les cas, une copie qui puisse être reproduite doit accompagner les textes originaux. Les discussions en français ou en anglais doivent se limiter aux rapports récents (au plus de 2 ans). On s'efforcera de faire coincider les articles destinés aux rubriques* discussions *et réponses dans le même numéro. La publication* Recherches en cours *paraît en janvier, en juin et en novembre. Les articles pour ces numéros doivent être reçus au plus tard le 1er novembre, le 1er avril et le 1er septembre respectivement. Les articles doivent être renvoyés au rédacteur en chef scientifique: Commission géologique du Canada, 601, rue Booth, Ottawa, Canada, K1A 0E8.*

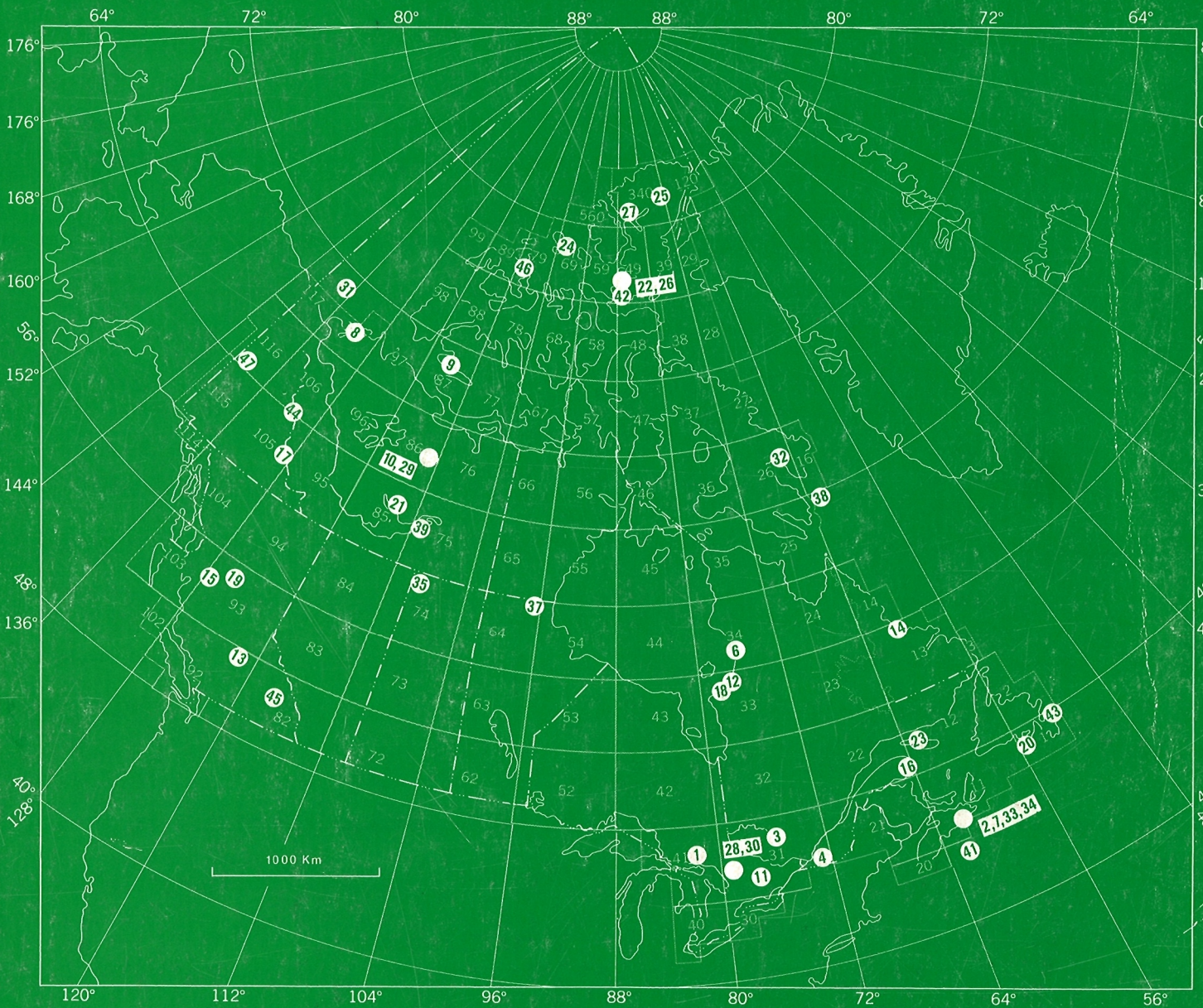

Energy, Mines and Resources Canada

Énergie, Mines et Ressources Canada